

THE JOURNAL OF PHYSICAL CHEMISTRY

(Registered in U. S. Patent Office)

CONTENTS

Symposium on Applications of Quantum Mechanics in Chemistry, Washington, D. C., March 21-23, 1962

Thomas L. Allen and Harrison Shull: Electron Pairs in the Beryllium Atom	2281	Benzene, Butadiene, and Naphthalene	2310
Oktay Sinanoğlu: Some Aspects of the Quantum Theory of Atoms, Molecules, and their Interactions	2283	A. Streitwieser, Jr., and I. Schwager: A Molecular Orbital Study of the Polarographic Reduction in Dimethylformamide of Unsubstituted and Methyl-Substituted Aromatic Hydrocarbons	2316
J. de Heer: A Refined Alternant Molecular Orbital Treatment of the Ground State of Benzene	2288	Harrison Shull: The Nature of the Two-Electron Chemical Bond. II. The Heteropolar Case	2320
Frank O. Ellison: Some Applications of Semi-empirical Valence Bond Theory to Small Molecules	2294	Peter G. Lykos: The Present Status of π -Electron Calculations	2324
Lawrence C. Snyder: A Simple Molecular Orbital Study of Aromatic Molecules and Ions Having Orbitally Degenerate Ground States	2299	Leland C. Allen and Arnold M. Karo: Electronic Structure of Simple Molecules	2329
Robert S. Mulliken: π -Delocalization in Butadiene and Cyanogen	2306	F. A. Matsen and J. C. Browne: In Defense of the Use of Atomic Orbital Configuration Wave Functions for Small Molecules	2332
Michael J. S. Dewar and Nora L. Sabelli: The Split p-Orbital (S.p.o.) Method. III. Relationship to Other M.o. Treatments and Application to		Richard L. Hummel and Klaus Ruedenberg: Electronic Spectra of Catacondensed and Pericondensed Aromatic Hydrocarbons	2334

Symposium on Photographic Processes, Washington, D. C., March 22-24, 1962

J. W. Mitchell: Some Aspects of the Theory of Photographic Sensitivity	2359	W. West: Some Recent Trends in the Theory of Spectral Sensitization	2398
Frederick C. Brown: Electronic Properties and Band Structure of the Silver Halides	2368	James E. LuValle, Asa Leifer, P. H. Dougherty, and M. Koral: Investigation of Spectral Sensitization. I. Some Properties of Sensitizing and Desensitizing Dyes	2403
Roland C. Hanson: Hall Mobility of Holes in Silver Bromide	2376	E. Klein: The Theory of the Photographic Sensitivity	2407
Robert J. Friauf: Ionic Transport Processes in the Silver Halides	2380	P. A. Faelens and B. H. Tavernier: On the Mechanism of the Antifogging and Sensitizing Action of Noble Metal Salts on Photographic Emulsion	2411
J. F. Hamilton and L. E. Brady: The Role of Mobile Silver Ions in Latent-Image Formation	2384	T. H. James: Some Views on the Mechanism of Development	2416
Howard Layer and Lawrence Slifkin: Studies of Point Defects in Silver Chloride	2396		

International Symposium on Reversible Photochemical Processes, Durham, North Carolina, April 16-18, 1962

Robert L. Strong: The Presence of Transient Charge-Transfer Complexes in Halogen Atom Recombination and Photohalogenation Processes	2423	M. D. Cohen and G. M. J. Schmidt: Photochromy and Thermochromy of Anils	2442
Glenn H. Brown, Setty R. Adishes, and Jay E. Taylor: Kinetic Studies of Phototropic Reactions. I. Evidence for an Ion-Pair Intermediate in the Reaction of Methyl Violet with Cyanide Ion	2426	F. I. Metz, W. C. Servoss, and F. E. Welsh: Photochromic Behavior of Sydnones	2446
E. Lippert and W. Lüder: Photochemical <i>cis-trans</i> Isomerization of <i>p</i> -Dimethylaminocinnamic Acid Nitrile	2430	G. Scheibe and F. Feichtmayr: The Phototropy of Tetrachloro- <i>ortho</i> -dihydronaphthalene as a Reversible Photochemical Reaction	2449
J. D. Margerum, L. J. Miller, E. Saito, Melancthon S. Brown, Harry S. Mosher, and R. Hardwick: Phototropism of <i>ortho</i> -Nitrobenzyl Derivatives	2434	J. N. Pitts, Jr., H. W. Johnson, Jr., and T. Kuwana: Structural Effects in the Photochemical Processes of Ketones in Solution	2456
G. Kortum, M. Kortum-Seiler, and S. D. Bailey: Optical Properties of 2-(2',4'-Dinitrobenzyl)-pyridine in the Adsorbed State	2439	G. D. Thaxton, R. C. Jarnagin, and M. Silver: Band Structure and Transport of Holes and Electrons in Homologs of Anthracene	2461
		Rahel Heiligman-Rim, Yehuda Hirshberg, and Ernst Fischer: Photochromism in Spiropyrans. Part IV. Evidence for the Existence of Several Forms of the Colored Modification	2465

Contents continued on page 1A

THE JOURNAL OF PHYSICAL CHEMISTRY

(Registered in U. S. Patent Office)

W. ALBERT NOYES, JR., EDITOR

WALTER J. MOORE, ASSISTANT EDITOR

ALLEN D. BLISS, SENIOR PRODUCTION EDITOR

EDITORIAL BOARD

A. O. ALLEN
C. E. H. BAWN
J. BIGEISEN
F. S. DAINTON

D. D. ELEY
D. H. EVERETT
S. C. LIND
F. A. LONG

J. P. McCULLOUGH
K. J. MYSELS
J. E. RICCI
R. E. RUNDLE

W. H. STOCKMAYER
E. R. VAN ARTSDALEN
M. B. WALLENSTEIN
W. WEST

Published monthly by the American Chemical Society at 20th and Northampton Sts., Easton, Pa. Second-class postage paid at Easton, Pa.

The Journal of Physical Chemistry is devoted to the publication of selected symposia in the broad field of physical chemistry and to other contributed papers.

Manuscripts originating in the British Isles, Europe, and Africa should be sent to F. C. Tompkins, The Faraday Society, 6 Gray's Inn Square, London W. C. 1, England.

Manuscripts originating elsewhere should be sent to W. Albert Noyes, Jr., Department of Chemistry, University of Rochester, Rochester 20, N. Y.

Correspondence regarding accepted copy, proofs, and reprints should be directed to Senior Production Editor, Allen D. Bliss, ACS Office, Mack Printing Company, 20th and Northampton Sts., Easton, Pa.

Advertising Office: Reinhold Publishing Corporation, 430 Park Avenue, New York 22, N. Y.

Articles must be submitted in duplicate, typed, and double spaced. They should have at the beginning a brief Abstract, in no case exceeding 300 words. Original drawings should accompany the manuscript. Lettering at the sides of graphs (black on white or blue) may be pencilled in and will be typeset. Figures and tables should be held to a minimum consistent with adequate presentation of information. Photographs will not be printed on glossy paper except by special arrangement. All footnotes and references to the literature should be numbered consecutively and placed in the manuscript at the proper places. Initials of authors referred to in citations should be given. Nomenclature should conform to that used in *Chemical Abstracts*, mathematical characters be marked for italic, Greek letters carefully made or annotated, and subscripts and superscripts clearly shown. Articles should be written as briefly as possible consistent with clarity and should avoid historical background unnecessary for specialists.

Notes are similar to articles in every way except as to length and are subjected to the same editorial appraisal. In their preparation particular attention should be paid to brevity and conciseness. Material included in Notes must be definitive and may not be republished subsequently.

Communications to the Editor are designed to afford prompt preliminary publication of observations or discoveries whose value to science is so great that immediate publication is imperative. The appearance of related work from other laboratories is in itself not considered sufficient justification for the publication of a Communication, which must in addition meet special requirements of timeliness and significance. Their total length may in no case exceed 1000 words or their equivalent. They differ from Articles and Notes in that their subject matter may be republished.

Symposium papers should be sent in all cases to Secretaries of Divisions sponsoring the symposium, who will be responsible for their transmittal to the Editor. The Secretary of the Division by agreement with the Editor will specify a time after which symposium papers cannot be accepted. The Editor reserves the right to refuse to publish symposium articles, for valid scientific reasons. Each symposium paper may not exceed four printed pages (about sixteen double spaced typewritten pages) in length except by prior arrangement with the Editor.

Remittances and orders for subscriptions and for single copies, notices of changes of address and new professional connections, and claims for missing numbers should be sent to the Subscription Service Department, American Chemical Society, 1155 Sixteenth St., N. W., Washington 6, D. C. Changes of address for *The Journal of Physical Chemistry* must be received on or before the 30th of the preceding month. Please include an old address label with the notification.

Claims for missing numbers will not be allowed (1) if received more than sixty days from date of issue (because of delivery hazards, no claims can be honored from subscribers in Central Europe, Asia, or Pacific Islands other than Hawaii), (2) if loss was due to failure of notice of change of address to be received before the date specified in the preceding paragraph, or (3) if the reason for the claim is "missing from files."

Subscription rates (1962): members of American Chemical Society, \$12.00 for 1 year; to non-members, \$24.00 for 1 year. Postage to countries in the Pan-American Union \$0.80; Canada, \$0.40; all other countries, \$1.20. Single copies, current volume, \$2.50; foreign postage, \$0.15; Canadian postage \$0.10; Pan-American Union, \$0.10. Back volumes (Vol. 56-65) \$30.00 per volume; foreign postage, per volume \$1.20, Canadian, \$0.40; Pan-American Union, \$0.80. Single copies: back issues, \$3.00; for current year, \$2.50; postage, single copies: foreign, \$0.15; Canadian, \$0.10; Pan-American Union, \$0.10.

The American Chemical Society and the Editors of *The Journal of Physical Chemistry* assume no responsibility for the statements and opinions advanced by contributors.

The American Chemical Society also publishes *Journal of the American Chemical Society*, *Chemical Abstracts*, *Industrial and Engineering Chemistry*, International Edition of *Industrial and Engineering Chemistry*, *Chemical and Engineering News*, *Analytical Chemistry*, *Journal of Agricultural and Food Chemistry*, *Journal of Organic Chemistry*, *Journal of Chemical and Engineering Data*, *Chemical Reviews*, *Chemical Titles*, *Journal of Chemical Documentation*, *Journal of Medicinal and Pharmaceutical Chemistry*, *Inorganic Chemistry*, *Biochemistry*, and *CA—Biochemical Sections*. Rates on request.

Contents continued

Rabel Heiligman-Rim, Yehuda Hirshberg, and Ernst Fischer: Photochromism in Spiropyrans. Part V. On the Mechanism of Phototransformation..	2470	Melvin Calvin: The Effect of Light on Oxidation and Reduction Reactions Involving Phthalocyanine and Etioporphyrin I Manganese Complexes.....	2517
Gavrielah Gabor and Ernst Fischer: Tautomerism and Geometrical Isomerism in Arylazophenols and Naphthols. Part II. 2-Phenylazo-3-naphthol. The Effect of Internal Hydrogen Bonds on Photoisomerization. Part I.....	2478	D. Mauzerall: The Photoreduction of Uroporphyrin: Effect of pH on the Reaction with EDTA..	2531
Shmuel Malkin and Ernst Fischer: Temperature Dependence of Photoisomerization. Part II. Quantum Yields of <i>cis</i> \rightleftharpoons <i>trans</i> Isomerizations in Azo-Compounds.....	2482	Robert Livingston and David Stockman: A Further Study of the Phototropy of Chlorophyll in Solution.....	2533
Dietrich Schulte-Frohlinde, Hartwig Blume, and Hans Güsten: Photochemical <i>cis</i> - <i>trans</i> -Isomerization of Substituted Stilbenes.....	2486	Eugene Rabinowitch: Reversible Photochemical Reactions of Chlorophyll in Photosynthesis.....	2537
E. J. Bowen, N. J. Holder, and G. B. Woodger: Hydrogen Bonding of Excited States.....	2491	William Dawson and E. W. Abrahamson: Population and Decay of the Lowest Triplet State in Polyenes with Conjugated Heteroatoms: Retinene.....	2542
G. A. Crosby, R. E. Whan, and J. J. Freeman: Spectroscopic Studies of Rare Earth Chelates.....	2493	W. Berends and J. Posthuma: Energy Transfer in Aqueous Solution.....	2547
S. P. McGlynn, M. J. Reynolds, G. W. Daigre, and N. D. Christodouleas: The External Heavy-Atom Spin-Orbital Coupling Effect. III. Phosphorescence Spectra and Lifetimes of Externally Perturbed Naphthalenes.....	2499	Sterling B. Hendricks, Warren L. Butler, and H. W. Siegelman: A Reversible Photoreaction Regulating Plant Growth.....	2550
C. A. Parker and C. G. Hatchard: Triplet-Singlet Emission in Fluid Solution.....	2506	Horst Stegemeyer: On the Mechanism of Photochemical <i>cis</i> \rightleftharpoons <i>trans</i> Isomerization.....	2555
Gisela Kallmann Oster, Gerald Oster, and Cecily Dobin: Stepwise Photoreversible Dye Systems.....	2511	Gunnar Wettermark: Light-Induced Isomerization of <i>o</i> -Nitrotoluene in Water Solution.....	2560
Gerald Oster, Gisela Kallmann Oster, and Gerhart Karg: Extremely Long-Lived Intermediates in Photochemical Reactions of Dyes in Non-viscous Media.....	2514	A. Shepp, S. Chaberek, and R. MacNeil: Thionine-Sensitized Photopolymerization of Acrylamide....	2563
G. Engelsma, Akio Yamamoto, E. Markham, and		F. Wilkinson: Transfer of Triplet State Energy and the Chemistry of Excited States.....	2569
		Henry Linschitz, Colin Steel, and Jerry A. Bell: The Uncatalyzed Decay of Anthracene and Porphyrin Triplets in Fluid Solvents.....	2574
		Colin Steel and Henry Linschitz: The Catalysis of Anthracene Triplet Decay by Copper Complexes.....	2577

Ralph A. Zingaro, Raymond E. McGlothlin, and Edward A. Meyers: Phosphine Oxide, Sulfide, and Selenide Complexes with Halogens: Visible and Ultraviolet Studies.....	2579	S. Toby and B. H. Weiss: The Photolysis of Azomethane at Higher Pressures: A Second Ethane-Producing Reaction.....	2681
Benjamin Carroll and Herbert C. Cheung: On the Interaction of Dyes and Polysaccharides.....	2585	L. R. Dawson, J. W. Vaughn, M. E. Pruitt, and H. C. Eckstrom: Solvents Having High Dielectric Constants. X. Solutions of Acetic Acid and its Derivatives in <i>N</i> -Methylacetamide at 40°.....	2684
Jack H. Lunsford and Thomas W. Leland, Jr.: Effects of Neutron and Ultraviolet Irradiation on the Catalytic Activity of Magnesium Oxide.....	2591	Donald Rosenthal and James S. Dwyer: Acid-Base Equilibria in Concentrated Salt Solutions. I. Potentiometric Measurements, Indicator Measurements, and Uncharged Bases in Dilute Acid Solutions.....	2687
George Blyholder and Edwin A. Richardson: Infrared and Volumetric Data on the Adsorption of Ammonia, Water, and Other Gases on Activated Iron(III) Oxide.....	2597	Ituro Uhara, Sadao Yanagimoto, Kazuo Tani, Gin-Ya Adachi, and Shōsuke Teratani: The Structure of Active Centers in Copper Catalyst.....	2691
Daniel W. Brown, Roland E. Florin, and Leo A. Wall: Formation and Decay of Atoms and Small Free Radicals at Low Temperatures.....	2602	Shozo Kishimoto: Studies on Thermoelectric Force and Lattice Defects as Active Centers in Metallic Catalysts.....	2694
Nicholas J. Stevens, Jr., Edward A. Mason, and Robert C. Reid: The Effect of Electron Irradiation Prior to Reaction on the Activity of a Semiconductor Catalyst.....	2613	Hannah B. Hetzer, R. A. Robinson, and Roger G. Bates: Dissociation Constant of <i>t</i> -Butylammonium Ion and Related Thermodynamic Quantities from 5 to 35°.....	2696
Edward K. C. Lee and F. S. Rowland: The Reactions of Recoil Tritium Atoms with Cyclopropane Platinous Chloride.....	2622	Robert S. Moore and John D. Ferry: Diffusion of Radioactively Tagged Cetane in Polyisobutylene-Cetane Mixtures and in Three Methacrylate Polymers.....	2699
H. P. Schwan, G. Schwarz, J. Maczuk, and H. Pauly: On the Low-Frequency Dielectric Dispersion of Colloidal Particles in Electrolyte Solution.....	2626		
Gerhard Schwarz: A Theory of the Low-Frequency Dielectric Dispersion of Colloidal Particles in Electrolyte Solution.....	2636	NOTES	
H. E. Ungnade, E. D. Loughran, and L. W. Kissinger: Hydrogen Bonding in β -Nitro Alcohols. II. Association in Solution.....	2643	Ram Gopal and Ramay Kumar Srivastava: Studies on Solutions of High Dielectric Constant. Part I. Partial Molal Volumes of Some Uni-Univalent Electrolytes in Formamide at 25°.....	2704
John Zinn and R. N. Rogers: Thermal Initiation of Explosives.....	2646	Nobuyuki Tanaka, Eishin Kyuno, Gen Satō, and Reita Tamamushi: Specific Adsorption of Isothiocyanatochromium(III) Complex Ions at the Mercury-Aqueous Solution Interface.....	2706
W. G. Schneider: Directed Solute-Solvent Interactions in Benzene Solutions.....	2653	R. P. Rastogi, Parmjit S. Bassi, and S. L. Chadha: Kinetics of Reaction between Naphthalene and Picric Acid in the Solid State.....	2707
S. Gilman: A Study of the Adsorption of Carbon Monoxide and Oxygen on Platinum. Significance of the "Polarization Curve".....	2657	E. Fischer, I. Laulich, and S. Pinchas: Dipole Moment Measurements of O ¹⁸ -Labeled X=O Compounds.....	2708
L. A. Errede and F. DeMaria: The Chemistry of Xylylenes. XV. The Kinetics of Fast Flow Pyrolysis of <i>p</i> -Xylene.....	2664	Akiko Aramata and Paul Delahay: Influence of the Alkali Metal Cations on the Reduction of Iodate Ion on Mercury in Alkaline Solution.....	2710
Roland E. Florin, Daniel W. Brown, and Leo A. Wall: γ -Irradiation of Small Molecules at 4 and 77°K....	2672	Stanley Cantor and Terry S. Carlton: Freezing Point	
Ralph Klein and Milton D. Scheer: Matrix Effects in the Gaseous H Atom-Condensed Olefin System; Surface Reaction—Olefin Diffusion Model.	2677	<i>Contents continued on page 2A</i>	

Contents continued

Depressions in Sodium Fluoride. II. Effect of Trivalent Fluorides.....	2711	R. L. Hickok, J. A. Parodi, and W. G. Segelken: Electronic Paramagnetic Resonance of Manganous Ion in Calcium Pyrophosphate and Calcium Fluoride.....	2715
COMMUNICATIONS TO THE EDITOR			
Donald R. Scott and Ralph S. Becker: Extended Calculations of the Electron Affinities of Polynuclear Aromatic Hydrocarbons by the LCAO-MO ω -Technique.....	2713	R. Mills: The Effect of the Ionization of Water on Diffusional Behavior in Dilute Aqueous Electrolytes.....	2716
Robert R. Hentz: Isopropylbenzene Conversion on Pre-irradiated Silica-Alumina.....	2714	Additions and Corrections.....	2719
		Author Index.....	2721
		Subject Index.....	2738

AUTHOR INDEX

Abrahamson, E. W., 2542	Dewar, M. J. S., 2310	Karo, A. M., 2329	Mosher, H. S., 2434	Siegelman, H. W., 2550
Adachi, G.-Y., 2691	Dobin, C., 2511	Kishimoto, S., 2694	Mulliken, R. S., 2306	Silver, M., 2461
Adisesb, S. R., 2426	Dougherty, P. H., 2403	Kisinger, L. W., 2643	Oster, G., 2511, 2514	Sinanoglu, O., 2283
Allen, L. C., 2329	Dwyer, J. S., 2687	Klein, E., 2407	Oster, G. K., 2511, 2514	Slifkin, L., 2396
Allen, T. L., 2281	Eckstrom, H. C., 2684	Klein, R., 2677	Parker, C. A., 2506	Snyder, L. C., 2299
Aramata, A., 2710	Ellison, F. O., 2294	Koral, M., 2403	Parodi, J. A., 2715	Srivastava, R. K., 2704
Bailey, S. D., 2439	Engelsma, G., 2517	Kortum, G., 2439	Pauly, H., 2626	Steel, C., 2574, 2577
Bassi, P. S., 2707	Errrede, L. A., 2664	Kortum-Seiler, M., 2439	Pinchas, S., 2708	Stegeneyer, H., 2555
Bates, R. G., 2696	Faelens, P. A., 2411	Kuwana, T., 2456	Pitts, J. N., Jr., 2456	Stevens, N. J., Jr., 2613
Becker, R. S., 2713	Feichtmayr, F., 2449	Kyuno, F., 2706	Posthuma, J., 2547	Stockman, D., 2533
Bell, J. A., 2574	Ferry, J. D., 2699	Laulicht, I., 2708	Pruitt, M. E., 2684	Streitwieser, A., Jr., 2316
Berends, W., 2547	Fischer, E., 2465, 2470, 2478, 2482, 2708	Laver, H., 2396	Rabinowitch, E., 2537	Strong, R. L., 2423
Blume, H., 2486	Florin, R. E., 2602, 2672	Lee, E. K. C., 2622	Rastogi, R. P., 2707	Tamamushi, R., 2706
Blyholder, G., 2597	Freeman, J. J., 2493	Leifer, A., 2403	Reid, R. C., 2613	Tanaka, N., 2706
Bowen, E. J., 2491	Friauf, R. J., 2380	Leland, T. W., Jr., 2591	Reynolds, M. J., 2499	Tani, K., 2691
Brady, L. E., 2384	Gabor, G., 2478	Linschitz, H., 2574, 2577	Richardson, E. A., 2597	Tavrelier, B. H., 2411
Brown, D. W., 2602, 2672	Gilman, S., 2657	Lippert, E., 2430	Robinson, R. A., 2696	Taylor, J. E., 2426
Brown, F. C., 2368	Gopal, R., 2704	Livingston, R., 2533	Rogers, R. N., 2646	Taylor, S., 2691
Brown, G. H., 2423	Güsten, H., 2486	Loughran, E. D., 2643	Rosenthal, D., 2687	Thaxton, G. D., 2461
Brown, M. S., 2434	Hamilton, J. F., 2384	Lüder, W., 2430	Rowland, F. S., 2622	Toby, S., 2681
Browne, J. C., 2332	Hanson, R. C., 2376	Lunsford, J. H., 2591	Ruedenberg, K., 2334	Uhara, I., 2691
Butler, W. L., 2550	Hardwick, R., 2434	LuValle, J. E., 2403	Sabelli, N. L., 2310	Ungnade, H. E., 2643
Calvin, M., 2517	Hatchard, C. G., 2506	Lykos, P. G., 2324	Saito, E., 2434	Vaughan, J. W., 2684
Cantor, S., 2711	Heiligman-Rim, R., 2465, 2470	MacNeil, R., 2563	Satō, G., 2706	Wall, L. A., 2602, 2672
Carlton, T. S., 2711	Hendricks, S. B., 2550	Maczuk, J., 2626	Scheer, M. D., 2677	Weiss, B. H., 2681
Carroll, B., 2585	Hentz, R. R., 2714	Malkin, S., 2482	Scheibe, G., 2449	Welsch, F. E., 2446
Chaberek, S., 2563	Hetzer, H. B., 2696	Margerum, J. D., 2434	Schmidt, G. M. J., 2442	West, W., 2398
Chadha, S. L., 2707	Hickok, R. L., 2715	Markham, E., 2517	Schneider, W. G., 2653	Wettermark, G., 2560
Cheung, H. C., 2585	Holder, N. J., 2491	Mason, E. A., 2613	Schulte-Frohlinde, D., 2486	Whan, R. E., 2493
Christodoyless, N. D., 2499	Hummel, R. L., 2334	Matsen, F. A., 2332	Schwager, I., 2316	Wilkinson, F., 2569
Cohen, M. D., 2442	James, T. H., 2416	Mauzerall, D., 2531	Schwan, H. P., 2626	Woodger, G. B., 2491
Crosby, G. A., 2493	Jarnagin, R. C., 2461	McGlothlin, R. E., 2579	Schwarz, G., 2626, 2636	Yamamoto, A., 2517
Daigre, G. W., 2499	Johnson, H. W., Jr., 2456	McGlynn, S. P., 2499	Scott, D. R., 2713	Yanagimoto, S., 2691
Dawson, L. R., 2684	Karg, G., 2514	Metz, F. I., 2446	Segelken, W. G., 2715	Zingaro, R. A., 2579
Dawson, W., 2542		Meyers, E. A., 2579	Servoss, W. C., 2446	Zinn, J., 2646
de Heer, J., 2288		Miller, L. J., 2434	Shepp, A., 2563	
Delabay, P., 2710		Mills, R., 2716	Shull, H., 2281, 2320	
DeMaria, F., 2664		Mitchell, J. W., 2359		
		Moore, R. S., 2699		

THE JOURNAL OF PHYSICAL CHEMISTRY

Volume 66

January—June, 1962

Pages 1—1216

W. ALBERT NOYES, JR., EDITOR

A. B. F. DUNCAN, ASSISTANT EDITOR

ALLEN D. BLISS, SENIOR PRODUCTION EDITOR

EDITORIAL BOARD

A. O. ALLEN
C. E. H. BAWN
J. BIGEISEN
F. S. DAINTON

D. D. ELEY
D. H. EVERETT
S. C. LIND
F. A. LONG

J. P. McCULLOUGH
K. J. MYSELS
J. E. RICCI
R. E. RUNDLE

W. H. STOCKMAYER
E. R. VAN ARTSDALEN
M. B. WALLENSTEIN
W. WEST

EASTON, PA.
MACK PRINTING COMPANY
1962

THE JOURNAL OF PHYSICAL CHEMISTRY

Volume 66

July—December, 1962

Pages 1217—2754

W. ALBERT NOYES, JR., EDITOR

A. B. F. DUNCAN, ASSISTANT EDITOR

ALLEN D. BLISS, SENIOR PRODUCTION EDITOR

EDITORIAL BOARD

A. O. ALLEN
C. E. H. BAWN
J. BIGEISEN
F. S. DAINTON

D. D. ELEY
D. H. EVERETT
S. C. LIND
F. A. LONG

J. P. McCULLOUGH
K. J. MYSELS
J. E. RICCI
R. E. RUNDLE

W. H. STOCKMAYER
E. R. VAN ARTSDALEN
M. B. WALLENSTEIN
W. WEST

EASTON, PA.
MACK PRINTING COMPANY
1962

THE JOURNAL OF PHYSICAL CHEMISTRY

(Registered in U. S. Patent Office) (© Copyright, 1962, by the American Chemical Society)

VOLUME 66

DECEMBER 28, 1962

NUMBER 12

ELECTRON PAIRS IN THE BERYLLIUM ATOM¹

BY THOMAS L. ALLEN²

Department of Chemistry, University of California, Davis, California

AND HARRISON SHULL

Chemistry Department, Indiana University, Bloomington, Indiana

Received May 19, 1962

The electron-pair approximation in the beryllium atom is investigated using a properly antisymmetrized product function over geminals (electron-pair wave functions). A wave function of this relatively simple type is obtained having an overlap of 0.9998886 with one of the best published functions, a superposition of 37 configurations. As a consequence of the separation into electron pairs, some of the coefficients in the configuration interaction treatment are found to be interrelated.

A major problem connected with wave functions of high accuracy is the difficulty of comprehending their significance in physical terms, and in fact the Hartree-Fock approximation has been described recently as "the last hardhold for elementary physical intuition."³ A very promising approach to this problem is the method of electron-pair wave functions or geminals.⁴ It should be much more accurate than the Hartree-Fock approximation, and yet a rather high degree of visuality is retained. Thus far specific applications include the water⁵ and formaldehyde⁶ molecules.

We felt that it would be useful to test the accuracy of the method on a much simpler electronic system, where the results could be compared with the highly accurate "superposition of configurations" or "configuration interaction" method. In the beryllium atom the electrons are thought to form two fairly distinct pairs, and therefore it should be an especially favorable case for this approach. A number of configuration interaction studies of this system have been published. The most recent and accurate are those of Watson⁷

and Weiss.⁸ Watson calculated a 37-configuration function using an orthogonal basis set, and obtained a total energy which included 89.4% of the correlation energy. Weiss calculated a 55-configuration function using a non-orthogonal basis, and obtained a total energy containing 93.1% of the correlation energy. Because of its orthogonal basis, the former function

$$\Phi = \sum_{n=1}^{37} K_n \Psi_n \quad (1)$$

provides a convenient starting point for calculating a good approximation to an accurate geminal product function.

The geminal product will be most easily handled if the geminals are one-electron orthogonal

$$\int \Lambda_K^*(1,2) \Lambda_L(1,4) d\tau_1 = 0 \quad (2)$$

where Λ_K and Λ_L designate the K-shell geminal and the L-shell geminal, respectively. This condition is fulfilled when each geminal is constructed from different orthogonal orbitals. An examination of Φ shows that most of the orbitals can be classified as strictly K-shell or L-shell orbitals. Only three (s_I , p_I , and p_{II}) are used in both shells. The s_I and p_{II} orbitals are mainly used in the K shell (except for configurations 10, 11, 36, and 37), while the p_I orbital appears in the L shell except for configurations 8, 21, and 35. Therefore s_I and p_{II} are assigned to the K shell, p_I is assigned to

(1) Supported in part by grants from the National Science Foundation to each of the authors and in part by a contract with Indiana University by the Air Force OSR.

(2) On leave from the University of California, Davis, for 1959-1960.

(3) R. K. Nesbet, *Rev. Modern Phys.*, **33**, 28 (1961).

(4) T. L. Allen and H. Shull, *J. Chem. Phys.*, **35**, 1644 (1961), and references therein.

(5) R. McWeeny and K. A. Ohno, *Proc. Roy. Soc. (London)*, **A255**, 367 (1960).

(6) J. M. Parks and R. G. Parr, *J. Chem. Phys.*, **32**, 1657 (1960).

(7) R. E. Watson, *Phys. Rev.*, **119**, 170 (1960).

(8) A. W. Weiss, *ibid.*, **122**, 1826 (1961).

the L shell, and the configurations mentioned are omitted from the geminal product function. The resulting classification of orbitals is shown in Table I.

TABLE I
CLASSIFICATION OF ORBITALS

K shell	L shell
1s, s _I , s _{II} , s _{III} , s _{IV}	2s
p _{II} , p _{III} , p _{IV}	p _I , p _V
d _{II} , d _{III} , d _{IV}	d _I
f _{II} , f _{III}	
g _{II} , g _{III}	

It also is convenient to omit configuration 14 from the geminal product because of the vector coupling problem. (It could be included at a later stage in the calculations by applying a ¹S projection operator to the resulting geminal product function.)

We can now write first approximations to Λ_K and Λ_L

$$\begin{aligned} \Lambda_K(1,2) = & N_K(K_1 1s^2 + K_3 p_{II}^2 + K_4 s_I^2 + \\ & K_6 d_{II}^2 + K_7 p_{III}^2 + K_{12} p_{II} p_{III} + K_{15} f_{II}^2 + \\ & K_{16} s_{III}^2 + K_{17} d_{III}^2 + K_{18} p_{IV}^2 + K_{20} s_{IIV} + \\ & K_{22} g_{II}^2 + K_{23} p_{III} p_{IV} + K_{24} s_{III} s_{IV} + \\ & K_{25} s_{IIV} + K_{26} p_{II} p_{IV} + K_{29} d_{II} d_{III} + K_{30} f_{III}^2 + \\ & K_{31} d_{IV}^2 + K_{33} s_{IV}^2 + K_{33} g_{III}^2)/K_1 \quad (3) \end{aligned}$$

$$\begin{aligned} \Lambda_L(3,4) = & N_L(K_1 2s^2 + K_2 p_I^2 + K_{13} d_I^2 + \\ & K_{27} p_V^2 + K_{28} p_{IPV}) \quad (4) \end{aligned}$$

In each configuration the functions with different m_l and m_s values are vector coupled to form a ¹S function. The K_n 's are taken from Table III of reference 7, and the normalization constants N_K and N_L are 1.0008179 and 0.9991075, respectively.

The geminal product function⁹ $\Lambda = [\Lambda_K(1,2)\Lambda_L(3,4)]$ consists of 105 configurations. These include 29 of the 37 configurations in Φ , of which 25 (1-5, 7, 12, 13, 15-18, 20, 22-31, 33, and 34) appear with reasonable coefficients because the corresponding K_n 's have been used in writing Λ_K and Λ_L . The other 4 configurations (6, 9, 19, and 32) appear automatically, and a comparison of their coefficients with the corresponding K_n 's provides a test of the validity of this approach. For example, the coefficient of configuration 6 is $K_2 K_3 / K_1$ (disregarding $N_K N_L$, which is almost unity). In this way the following approximate relationships are derived

$$\begin{aligned} K_6 &\simeq K_2 K_3 / K_1, & K_9 &\simeq K_2 K_4 / K_1, \\ K_{19} &\simeq K_2 K_5 / K_1, & K_{32} &\simeq K_3 K_{13} / K_1 \end{aligned} \quad (5)$$

The numerical values (shown in Table II) are in reasonably good agreement. Thus the electron pair method is able to predict correctly the sign and approximate magnitude of four coefficients in Φ from six other coefficients.¹⁰

(9) Brackets denote the partial antisymmetrization operator. It should be emphasized that the geminal product function is a completely antisymmetric wave function satisfying the Pauli exclusion principle.

TABLE II
COMPARISON OF COEFFICIENTS IN Φ AND Λ ^a

Configuration	Φ	Λ
$p_I^2(^1S) p_{II}^2(^1S)$	$K_6 = 0.0071$	$K_2 K_3 / K_1 = 0.0078$
$p_I^2(^1S) s_I^2(^1S)$	$K_9 = .0057$	$K_2 K_4 / K_1 = .0069$
$p_I^2(^1S) d_{II}^2(^1S)$	$K_{19} = .0016$	$K_2 K_5 / K_1 = .0018$
$p_{II}^2(^1S) d_I^2(^1S)$	$K_{32} = .00046$	$K_3 K_{13} / K_1 = .00050$

^a Rounded off to two significant figures.

This method predicts that five of the new configurations will have coefficients of magnitude larger than 0.001: $p_I^2(^1S) s_I s_{II} (^1S)$, -0.0031; $p_I^2(^1S) s_{III} s_{IV} (^1S)$, 0.0017; $p_I^2(^1S) p_{III}^2 (^1S)$, 0.0015; $p_I^2(^1S) p_{II} p_{III} (^1S)$, 0.0015; $p_I^2(^1S) s_I s_{IV} (^1S)$, 0.0015.

The overlap integral of the geminal product function with the 37-configuration function, $\int \Lambda^* \Phi d\tau$, is easily calculated because of the orthogonal basis. Its value is 0.9998886. (Variation of the coefficients to maximize the overlap integral did not give any significant improvement.) Therefore the two functions are almost identical, and they should have closely similar energies. This result is to be contrasted with the overlap integral of the SCF function with Φ , which has a value of $K_1 = 0.9575824$.

The energy contribution of each configuration when added to the configuration interaction function may be obtained from Table III of ref. 7. For the configurations omitted from the geminal product function (8, 10, 11, 14, 21, 35, 36, and 37) the total energy increments are 0.00347 a.u., or 3.7% of the total correlation energy. Since a configuration usually contributes less to the energy of the final function than it does when first included, in the 37-configuration function these configurations probably account for somewhat less than 3.7% of the correlation energy. The slight differences in the coefficients of configurations 6, 9, 19, and 32 undoubtedly have a negligible effect on the energy. The new configurations introduced by the geminal product function also must have nearly optimum coefficients, as indicated by the coefficient test in Table II, and therefore they should improve the energy significantly. Thus we estimate that $89.4 - 3.7 = 85.7\%$ is a lower limit to the correlation energy of this geminal product function.

In a geminal product wave function, electrons in different geminals affect one another by their average distribution only. Therefore inter-shell correlation cannot be included in a geminal product function, and in some systems this limitation may be of importance. For the beryllium atom, the inter-shell correlation energy has been variously found to be negligible,¹¹ and amounting to about 5% of the correlation energy incorporated into Φ (plus an unknown amount from the remaining correlation energy).⁷ The latter estimate is based on the correlation energy introduced by 1s2sxy and quadruple substitution configurations (that is, configurations using neither 1s nor 2s orbitals), although it was pointed out that this interpretation is not strictly realistic. Since Λ , which cannot have any inter-shell correlation, has a large num-

(10) Similar results have been obtained independently by O. Sinanoglu, *Proc. Natl. Acad. Sci. U. S.*, **47**, 1217 (1961) and *J. Chem. Phys.*, **36**, 708 (1962).

(11) J. Linderberg and H. Shull, *J. Mol. Spectry.*, **5**, 1 (1960).

ber (80) of quadruple substitution configurations, such configurations do not represent inter-shell effects. Configurations of the $1s2sxy$ type also could be included in Λ , and therefore they do not necessarily contribute inter-shell correlation. The particular configurations of this type in Φ (10, 11, 14, and 21) were excluded from Λ to obtain orthogonal 1S geminals.

Inter-shell correlation energy might be most suitably defined as the difference between the energy of the optimum geminal product function (where the geminals are not subject to any orthogonality or symmetry conditions) and the exact non-relativistic energy. In the transition from the optimum geminal product to the exact function the energy improves, not because any new configurations are introduced, but because the constraints on the coefficients are removed.

There does not seem to be any reason to revise

the earlier conclusion that the inter-shell correlation energy in the beryllium atom is negligible. Thus the energy of the optimum geminal product function should be considerably lower than the energies obtained thus far by configuration interaction.

NOTE ADDED IN PROOF.—The total energy of the beryllium atom may be decomposed into the separate contributions from the two electron pairs.⁴ In the SCF approximation, the energies of the K and L electron pairs are found to be 13.571 and 1.002 a. u., respectively. The former result may be compared with the corresponding energy in Be^{+2} , 13.61130 a. u. [C. C. J. Roothaan, L. M. Sachs, and A. W. Weiss, *Rev. Mod. Phys.*, **32**, 186 (1960)].

Acknowledgments.—T. L. A. wishes to express his appreciation to Professor Harry G. Day and the members of the Chemistry Department at Indiana University for the generous hospitality extended to him and his family during their stay in Bloomington.

SOME ASPECTS OF THE QUANTUM THEORY OF ATOMS, MOLECULES, AND THEIR INTERACTIONS¹

BY OKTAY SINANOĞLU

Sterling Chemistry Laboratory, Yale University, New Haven, Connecticut

Received May 28, 1962

A quantitative and systematic basis for semi- and non-empirical theories of (a) atomic and π -electron spectra, (b) heats of formation, relative energies of the different isomers or conformations of large molecules, and (c) intermolecular forces at all R is developed. Various effects in the exact wave function and energy of a many-electron system are examined. The major effects are the properties including electron correlation of separate shells or molecular orbital pairs. Effects of correlation on Hartree-Fock SCF orbitals are found to be negligible. The simple transformation of MO's into localized ones transforms the correlation energy of a saturated molecule exactly into the sum of bond correlation energies and non-bonded attractions. This allows the energy of, *e.g.*, a C-C bond or a lone pair to be obtained separately in the same way as in H_2 . Also the effects of molecular environment on localized correlations are studied. They are within the constancy of experimental bond energies.

Among the properties that quantum chemistry must deal with are: (a) electronic spectra, (b) thermodynamic quantities such as heats of formation, relative energies of different isomers or conformations of a molecule, and (c) intermolecular forces.

Semi-empirical theories of both atomic and π -electron spectra are based on orbital pictures (Hartree-Fock or approximations to it such as simple MO). In these, cores and their instantaneous polarizations by valence electrons are left out. In the π -electron case, an empirical " π -electron Hamiltonian", \mathcal{H}_π , is used.²

The expressions for the energies obtained on these orbital theories are parametrized, in atomic spectra F and G integrals; in the π -electron case α, β and one or two center coulombic integrals are left to be determined empirically. The empirical values give quite good agreement with experiment, but values calculated directly from orbitals lead to large errors which are known to be due to electron correlation.²⁻⁴

Relative energies of saturated molecules also are calculated well empirically. Pitzer⁵ assumed constant bond energies and considered zero point vibrational energies and van der Waals attractions between non-bonded regions. In this way, the heats of formation and isomerization of saturated hydrocarbons were obtained to within 0.01 e.v. (0.2 kcal./mole).

Intermolecular forces are given quite well around the equilibrium configuration by Hartree-Fock MO as shown, for example, by Ransil⁶ on He-He interaction. At large separations van der Waals forces are due mainly to correlations in the motions of electrons.⁵ In the usual London dispersion theory the complete basis set for the composite system of interacting molecules which occurs in the usual infinite sum of the second-order perturbation energy is taken as all products $\psi_a^k \psi_b^l$ of the eigenfunctions of separate atoms. This, of course, assumes not only that there is no overlap between the ground state wave functions of the atoms but also none for all the virtual excited states.

Consider, for example, two hydrogen atoms 3 Å. apart both with the same spin. There is no

(1) This work was supported by a grant from the National Science Foundation.

(2) (a) M. G. Mayer and A. L. Sklar, *J. Chem. Phys.*, **6**, 645 (1938); (b) R. Pariser and R. G. Parr, *ibid.*, **21**, 466 (1953).

(3) W. Kolos, *ibid.*, **27**, 591, 592 (1957).

(4) M. J. S. Dewar and C. E. Wulfman, *ibid.*, **29**, 158 (1958).

(5) K. S. Pitzer, *Advan. Chem. Phys.*, **2**, 59 (1959); K. S. Pitzer and E. Catalano, *J. Am. Chem. Soc.*, **78**, 4844 (1956).

(6) B. J. Ransil, *J. Chem. Phys.*, **34**, 2109 (1961).

overlap between the ground state orbitals. However, since Bohr radii are proportional to n^2 , even the next virtually excited state $(2p_z)_a(2p_z)_b$ that would contribute to London dispersion energy shows very large overlap. Thus, the usual theories of long range van der Waals forces even at considerable distances are not on a sound basis. The situation is certainly worse in non-bonded intramolecular attraction.

In all these semi-empirical theories use is made of "the chemical picture." Separate groups such as inner and outer shells or localized bonds are assumed; only interactions within or between some groups are evaluated, often semi-empirically.

Such quantum chemical problems can be separated into an orbital part and the remaining electron correlation part.⁷ The framework of the above semi-empirical theories is based on orbitals. But both large errors in non-empirical calculations and some important effects such as the non-bonded attractions are due mainly to electron correlation. Therefore, the semi-empirical theory should be based not on orbital pictures but on a theory that considers electron correlation in a detailed way.

Non-empirical Theories.—The configuration interaction (CI) method is meant for the removal of actual or near degeneracies. However, non-empirical calculations on more than two-electron systems usually are done by CI too, even though many configurations may have to be mixed in as for He atom.⁹

In extending the Hylleraas' " r_{12} -coordinate method"⁸ that deals successfully with such correlations in He to n -electron systems difficult integrals¹⁰ arise if all r_{ij} 's are introduced into trial functions in the usual manner.¹¹ In addition to the computational difficulties, these methods treat each atom or molecule as a different numerical problem without making use of the physical distinctness of various correlation effects and the existence of separate groups of electrons.

In the orbital picture, concentric shells such as σ , π already are separated. For saturated molecules, Lennard-Jones¹² showed that an MO determinant already contains localization of electrons of the same spin with respect to one another. One goes to such a localized description by a simple unitary transformation that leaves the original determinant unchanged.

There have been attempts to put electron correlation into these localized groups directly.¹³

(7) The best orbitals that give good electron densities and simplify the remaining electron-electron effects are those of Hartree-Fock method. This will be taken here as the standard starting point. Following Löwdin (ref. 8) the remaining non-relativistic error will be defined as "electron correlation."

(8) P. O. Löwdin, *Advan. Chem. Phys.*, **2**, 207 (1959).

(9) See, e.g., J. C. Slater, "Quantum Theory of Atomic Structure," McGraw-Hill Book Co., Inc., New York, N. Y., 1961, Vol. II, p. 48.

(10) L. Szasz, *J. Chem. Phys.*, **35**, 1072 (1961).

(11) For "correlation factor" methods see Löwdin (ref. 8), also R. E. Peirls, "Lectures in Theoretical Physics, Boulder, 1958," Vol. I, p. 265 (discussion of trial function of Lenz (1929)), and R. Jastrow, *Phys. Rev.*, **28**, 1479 (1955), for the type of trial function discussed by Szasz (ref. 10).

(12) J. E. Lennard-Jones, *Proc. Roy. Soc. (London)*, **A198**, 1, 14 (1949); *Ann. Rev. Phys. Chem.*, **4**, 167 (1953).

(13) (a) A. C. Hurley, J. E. Lennard-Jones, and J. A. Pople, *Proc. Roy. Soc. (London)*, **A220**, 446 (1953); (b) P. G. Lykos and R. G. Parr,

These assume a pair function with correlation for each bond and antisymmetrize their product to get the total wave function. The pair functions Λ_K are assumed to satisfy the arbitrary and strong orthogonality condition

$$\langle \Lambda_A(i,j), \Lambda_B(i,l) \rangle_{\mathbf{x}_i} = 0 \quad (1)$$

where $\langle \rangle_{\mathbf{x}_i}$ means integration over electron \mathbf{x}_i only. This condition is equivalent to assuming the separability of bonds to start with. In addition the method does not allow for non-bonded correlations to be put in in a natural way. Limitations of this method have been discussed previously.¹⁴

The "Chemical Picture" and Quantitative Theory.—The "chemical" facts have been with us for a long time. Early quantum chemistry started with intuitive pictures based on these facts, but because it introduced many unexamined assumptions to force the theory into these pictures, it almost fell into disrepute. It is now desirable to formulate the quantitative theory such that one starts with an exact but detailed form of a wave function and energy, from this systematically isolates the important correlation effects, but allows adequate means for estimating everything that is left over. Below, such a theory is outlined which provides a common basis for both semi- and non-empirical theory. The semi-empirical theory differs from the non-empirical mainly in the evaluation of the major quantities empirically.

Theory is not based on infinite basis set expansions so that other methods such as " r_{12} -coordinate," "open-shell," etc., can be used. A basic point of the theory, however, is to separate first the various correlation effects, then apply a different suitable method to each part of an atom or molecule. For example in Be atom one would use " r_{12} -coordinate" for $1s^2$, $(2s^2 - 2p^2)2 \times 2$ CI for $2s^2$, and the core polarization method (see reference 28 below) for $1s2s$. There is no one method best for all the electrons.

Parts of this theory have been developed in a series of articles.¹⁵ We summarize the over-all picture here as well as giving some previously unreported results.

On Hartree-Fock Methods.—The Hartree-Fock method is a very good starting point. It gives the charge distributions well, since it takes out the long-range part of the coulomb repulsions between electrons.¹⁵ Also for this reason the remaining electron correlation effects are simplest if one starts with the Hartree-Fock method.

Even though it is difficult to obtain Hartree-Fock orbitals for large systems, it is still desirable to start a "framework" theory with the Hartree-Fock method and then to put on the remaining corrections. Any further approximations such as

J. Chem. Phys., **24**, 1166 (1956); **25**, 1301 (1956), have based σ , π separation on this work. For later references discussing this type of trial function, see, e.g., T. L. Allen and H. Shull, *J. Chem. Phys.*, **35**, 1644 (1961).

(14) P. O. Löwdin, *ibid.*, **35**, 78 (1961); P. G. Lykos and R. G. Parr, *ibid.*, **25**, 1301 (1956); O. Sinanoglu, *ibid.*, **33**, 1212 (1960); R. McWeeny, Preprint No. 59, Quant. Chem. Group, Uppsala Univ., Uppsala, Sweden, 1961; L. Szasz, *Phys. Rev.*, **126**, 169 (1962).

(15) O. Sinanoglu, *J. Chem. Phys.*, **36**, 706, 3198 (1962); *Proc. Natl. Acad. Sci. U. S. A.*, **47**, 1217 (1961), and earlier papers cited there.

the use of LCAO MO instead of Hartree-Fock orbitals then may be examined in regard to their effects on the more general theory.

For a closed-shell system there is a unique Hartree-Fock method. With non-closed shells, however, about 9 variants of Hartree-Fock methods have been discussed. There are many possibilities because one can vary the energy of different combinations of degenerate determinants that arise from a given non-closed configuration or make different approximations to get around complications such as the off-diagonal energy parameters that do not come up for a closed-shell system. All these methods give energies within often less than 0.01 e.v. of one another. The simplest theory both for getting the orbitals and for putting on correlations later is one based on the average energy of a configuration,¹⁶ but with each Hartree-Fock potential modified so as to make it the same acting on all electrons and as symmetric as possible.¹⁷ (For instance, in carbon $1s^2 2s^2 2p^2$ configuration, the orbitals obtained this way are the same for all the terms 3P , 1D , 1S ; there are no off-diagonal energy parameters λ_{ij} and the Hartree-Fock potentials are the same for all the electrons.)

Even in large saturated molecules the Hartree-Fock method is a valid starting point. The Hartree-Fock wave function for such a molecule is expected to show regional properties quite unaffected in going from one molecule to another. This is because electrons move in the Hartree-Fock potentials of all the electrons and also in the field of the nuclei. The net potential of one end of a molecule is a shielded one and therefore of short range.¹⁸ For example, in ethane the average potential of a hydrogen atom on one carbon dies off before it reaches a hydrogen atom on the other carbon. Attempts to build molecular Hartree-Fock orbitals from localized and invariant orbitals have been and are being made.¹⁹

Clusters of Electrons in the Hartree-Fock "Sea."—In the Hartree-Fock method each electron moves in the average field of all the other electrons. Consider now all the remaining effects that the residual instantaneous repulsions between electrons will introduce. For simplicity, let us take a closed-shell system. Theory for a non-closed shell is quite similar.

It was shown previously that the exact wave function of a many-electron system¹⁵ is

$$\psi = \phi_0 + X; \langle \phi_0, X \rangle = 0 \quad (2)$$

$$\phi_0 = \alpha(123 \dots k \dots N); 1 \equiv 1(\mathbf{x}_1) \equiv 1s_{\alpha}, \text{ etc.}$$

$$X = \sum_{i=1}^N \{f_i\} + \sum_{i>j}^N \{\hat{u}'_{ij}\} + \sum_{ijk}^N \{\hat{U}'_{ijk}\} + \dots + \hat{U}'_{123-N} \quad (3a)$$

(16) See, e.g., J. C. Slater, "Quantum Theory of Atomic Structure," Vol. I, McGraw-Hill Book Co., Inc., New York, N. Y., 1960.

(17) A. J. Freeman, *Rev. Mod. Phys.*, **32**, 273 (1960). This combines the advantages of methods discussed by R. K. Nesbet (*Proc. Roy. Soc. (London)*, **A230**, 312 (1955)) and by Slater (ref. 9). See also K. Ruedenberg (ref. 18) for a similar starting point for π -electron systems.

(18) K. Ruedenberg, *J. Chem. Phys.*, **34**, 1861 (1961).

(19) For example, W. H. Adams, *ibid.*, **34**, 89 (1961); T. L. Gilbert

$$\{f_i\} = \phi_0 \left(\frac{f_i}{i} \right); \{\hat{u}'_{ij}\} = \phi_0 \frac{\hat{u}'_{ij}}{(ij)}, \text{ etc.} \quad (3b)$$

$$\langle f_i, k \rangle = 0, \langle \hat{u}'_{ij}, k \rangle = 0, \dots, \langle \hat{U}'_{ijk-N}, k \rangle = 0 \quad (4)$$

$$\text{for } k = 1, 2, 3, i, \dots, j, \dots, N$$

ϕ_0 is the Hartree-Fock determinant. Note that this exact expression contains only a finite number of terms for a finite many-electron system. The functions f_i , \hat{u}'_{ij} , etc., are not expanded in any basis set; they are in closed forms and are rigorously orthogonal (eq. 4) to all the individual Hartree-Fock orbitals occupied in ϕ_0 .

The successive terms in X correct for the effects of progressively larger numbers of interacting electrons. For convenience, one may speak of "collisions" of successive numbers of electrons in analogy with imperfect gas theory. The "collisions" are caused by the instantaneous repulsions that remain after the average parts have been taken out in the Hartree-Fock orbitals.

Equation 3 can be written in a much more detailed fashion. It is easily shown that each term \hat{U}' containing a certain number of electrons at a time actually consists of all possible antisymmetrized products of previous terms and an additional new term \hat{U} representing the "collisions" of that many electrons all at once. For example

$$\begin{aligned} \hat{u}'_{ij} &= \mathcal{B}(f_i f_j) + \hat{u}_{ij} \\ \hat{U}'_{ijk} &= \alpha \{f_i f_j f_k + f_i \hat{u}_{jk} + \dots + \hat{U}_{ijk}\} \quad (5) \\ \hat{U}'_{ijkl} &= \alpha \{f_i f_j f_k f_l + f_i f_j \hat{u}_{kl} + \dots + f_i \hat{U}_{ijk} + \dots + \hat{u}_{ij} \hat{u}_{kl} + \dots + \hat{U}_{ijkl}\} \end{aligned}$$

The product terms represent correlations taking place at the same time but in different regions of space, whereas a non-separable term such as \hat{U}_{ijkl} accounts for the correlations of all four electrons at once (a four-body "collision"). Again, by analogy to imperfect gas theory the latter are "linked clusters," whereas products are referred to as "unlinked clusters."

Corrections to the Hartree-Fock energy which represent various physical correlation effects can be obtained explicitly by substituting X, eq. 3, in the variational expression.¹⁵ The explicit evaluation of the energy in this manner is greatly facilitated by the use of diagrams as in imperfect gas theory.

Many different theories can now be derived from this detailed variational energy expression by minimizing different portions of it.²⁰

If only the first two terms of eq. 3a are retained and the energy varied so as to obtain optimum f_i and \hat{u}_{ij} , one gets essentially a Brueckner theory for finite systems. This is also similar to a method discussed by Fock, *et al.*²¹

(to be published; this work was pointed out to us by P. G. Lykos). See also S. F. Boys, *Rev. Mod. Phys.*, **32**, 296 (1960).

(20) A most systematic way of using the variation method is to get trial functions by minimizing the physically significant or large portions of $\langle \psi, H \psi \rangle / \langle \psi, \psi \rangle$, then using these in the complete expression. Various perturbation theories come out as special cases of this approach. O. Sinanoğlu, *J. Chem. Phys.*, **34**, 1237 (1961).

(21) V. Fock, M. Veselov, and M. Petrashen, *J. Exptl. Theor. Phys., USSR*, **10**, 723 (1940).

If all the terms are retained, coupled equations are obtained which make f_i self-consistent with the remaining effects. This is similar to Slater's generalized SCF method.²² These theories are unnecessarily complicated and stress the part of X which is not physically the most important.

We examine below all the different effects in X and in the energy and then take out the most significant parts, but estimate the remaining effects.

Effect of Correlation on Orbitals.—Since the average coulombic field of all the electrons on a given one are implicit in the Hartree-Fock orbitals of ϕ_0 , the f_i in eq. 3 represents corrections to the Hartree-Fock orbital, i , due to the residual, instantaneous repulsions, *i.e.*, due to electron correlation. If X is approximated by perturbation theory, the first-order X_1 rigorously does not contain²³ any f_i . Since X_1 gives both the second and third-order energies, any effect of f_i on energy would show up in the fourth and higher orders.

Without being limited to perturbation theory nor to an infinite summation of single excitations, f_i for a closed shell system can be obtained easily.

A strong test of how much correlation would modify a Hartree-Fock orbital would be on He atom where the two electrons are quite tightly packed. Any trial function such as one of Hylleraas' with r_{12} for He atom can be rewritten as in eq. 2 and then a further Schmidt orthogonalization (see ref. 23) splits the correlation part into f_i and the two-electron parts as in eq. 3. Thus, just by simple integrations from the known wave functions of helium, one obtains the f_i completely. This was done²⁴ using the simple trial function of Löwdin and Redei²⁵ for He and the f_i was found to be about 4% of the Hartree-Fock orbital where it is largest. This f_i however is due to the inadequacy of the trial function. If it is subtracted out, a better trial function is obtained as evidenced by an energy lowering of 0.019 e.v. Similarly when a more accurate trial function, a Hylleraas' six-term one, is used, one obtains an f_i everywhere considerably smaller than in the previous case.

In other types of correlation effects which give large energy errors, f_i may be unimportant, too. For example, the main part of the correlation error in the outer shell of the Be atom is due to the new degeneracy of $2s^2$ with $2p^2$. But this is a double excitation and does not give any f_i (for a study of f_i in H_2 near dissociation see ref. 24).

Hartree-Fock orbitals give good electron densities. This supplemented by the above results leads one to drop f_i from eq. 3 for closed shells. This eliminates all the products in eq. 5 that involve f_i . The resulting energy expressions are much simpler than they would have been otherwise.

Many-Electron Correlations.—Any three electrons picked out in a many-electron system will have at least two spins alike. These will stay away from each other's Fermi hole. Now, the repulsion, $1/r_{ij}$, that an electron i exerts on another one, say

j , deviates any instant from the average value (the i, j part of the total Hartree-Fock potential). This "fluctuation potential" is what causes "electron correlation,"²⁶ and is of short range in going from orbital to orbital.¹⁵ Thus, only at the most two electrons can "see" each other at once. Others remain outside the Fermi hole which is larger than the range. This causes more than two electron correlations, \hat{U}_{ijk} , etc., in eq. 5 to be small.

The angular potential shown in ref. 15 for boron is similar to those that act between the p-electrons also in C, N, O, F, and Ne. In neon there are two separate tetrahedra of like spins which in ϕ_0 move uncorrelated with one another. But only two electrons of opposite spins can come together at one point, so even here pair correlations are the significant ones. These considerations also are supported by the recent values of correlation energies of first row atoms estimated empirically.²⁷

In large systems when electrons get delocalized near-degeneracies arise just as the energy levels of a particle-in-a-box get closer together as the box gets larger. Even in such delocalized cases the molecular orbital pair correlations are the significant ones due to the orthogonality $\langle \hat{u}_{ij,k} \rangle = 0$, eq. 5. Electrons i, j while correlating cannot go into the already occupied orbital k .

For example, the $(\sigma_{1g})^2$ correlation in H_2 is about 7.7 e.v. near dissociation. This reduces to 0.5 to 1 e.v. in He-He, because now (σ_{1u}) is occupied and the \hat{u}_{12} for $(\sigma_g)^2$ no longer contains $(\sigma_{1u})^2$ as its main part. This also has the effect of making the correlation between any three (in He_2^+) or four electrons at a time (in He-He) small. These arguments apply also to the many-electron terms that arise in energy even when just u_{ij} 's and their products are taken into account in X (see ref. 15).

Main Correlation Effects.—Then the energy of a closed shell system reduces to the sum of the variational expressions of independent two-electron systems in the Hartree-Fock medium.¹⁵ This allows calculations to be made on all the first row atoms and their ions with essentially 11 distinct pair functions of which only 5 or 6 are significant. These now provide the new building blocks to be used with slight changes in parameters in many atoms and molecules. Such calculations, also with estimates of the many-electron terms, etc., that are neglected, are in progress in this writer's Laboratory. Once the coupling terms are shown to be small, these results also provide a basis for semi-empirical methods.

Inner, Outer Shells.—The above theory naturally separates inner and outer shells in atoms and molecules without concealing what the neglected terms are. In a π -electron system if just that portion of the total energy corresponding to π -electrons is minimized according to the theory,¹⁵ one derives

(26) Note the definition in ref. 7. This should not be confused with, *e.g.*, J. W. Linnett's use of the word. His usage does not distinguish between all the "orbital average polarization" and Fermi hole effects, already contained in the Hartree-Fock ϕ_0 , and the residual charge fluctuations.

(27) E. Clementi, *J. Chem. Phys.*, in press. The $2p_x\alpha 2p_y\alpha$ correlation in nitrogen atom is only 0.1 e.v.

(22) J. C. Slater, *Phys. Rev.*, **91**, 528 (1953).

(23) O. Sinanoglu, *Proc. Roy. Soc. (London)*, **A260**, 379 (1961). In CI language, this means there are no single excitations which mix with ϕ_0 (Brillouin theorem).

(24) O. Sinanoglu and D. Tuan, *J. Chem. Phys.*, to be published.

(25) P. O. Löwdin and L. Redei, *Phys. Rev.*, **114**, 752 (1959).

rigorously the semi-empirical " π -electron Hamiltonian."

The form of the energy including correlation is now just the same^{15,28} as in the Hartree-Fock approximation: $\sum_{i>j}^N (J_{ij} - K_{ij} + \epsilon_{ij})$ instead of just $\sum_{i>j}^N (J_{ij} - K_{ij})$. These ϵ_{ij} 's are independent of one another. They do not depend on \hat{U}_{ijk} , f_i , etc., of X, but only on \hat{u}_{ij} . This justifies the parametrization of spectra mentioned above.

Note also that the above theory not only introduces correlations into each shell, but also contains the correlations (instantaneous core polarizations) between different shells. These are analogous to van der Waals' attractions.²⁸

Localized Groups.—The determinantal function ϕ_0 was so far expressed in terms of molecular orbital pairs. How are these related to the localized electron-pair bonds or lone pairs of a saturated molecule?

It is not necessary now to start anew with arbitrary assumptions to discuss localized groups. The transformation of Lennard-Jones¹² which took ϕ_0 from the molecular to the localized orbital description also translates the correlation energy and X from one picture to the other. It has been shown rigorously that *the exact correlation energy of a saturated molecule is given by the sum of bond or lone pair correlation energies and non-bonded van der Waals' attractions.*²⁹

The same transformation applies also to the variational expression¹⁶ involving sums of correlation energies of molecular orbital pairs. The latter then becomes the sum of variational expressions for individual bonds or lone pairs and for just the individual van der Waals attractions. Some simple coupling terms arise too. These have been estimated³⁰ to be about 0.1 e.v. in CH₄ by making the transformation²⁹ on the configuration interaction (MO CI) wave function of Nesbet.³¹

This means²⁰ that each of these energy terms can be minimized independently. For instance, one can obtain the energy including correlation of just a CH bond or a lone pair by taking a trial function, e.g., containing r_{12} just as in the H₂ molecule. On the other hand, the part of the energy which corresponds to a van der Waals attraction between bonds also can be obtained by itself. Since this theory does not make any of the assumptions about the independence of basis functions of groups or about the range of the internuclear separations as in the usual theories discussed at the beginning of this article, one now also has a theory of intermolecular forces applicable at all R. Such applications are being carried out on He-He and hydrocarbons.³⁰

How sensitive are these transformed localized functions and energies to the rest of the molecular environment?

Just the orbital part of this question has been investigated by Lennard-Jones and co-workers. Hall³² correlated the ionization potentials of the hydrocarbons ethane to decane assuming constant localized orbitals. Ionization potentials are not much influenced by electron correlation.

In heats of formation and conformations of molecules on the other hand, correlation is all important.⁵ Detailed theory²⁸⁻³⁰ shows that the correlation energy of a bond depends on the rest of the molecule through (a) the Hartree-Fock potential of the whole molecule and (b) by exclusion effects as in eq. 4. The localized correlation functions²⁹ are still orthogonal in the sense of eq. 4 to the *entire molecular orbitals*. However, in this orthogonality the only significant contribution from an MO is from the localized orbital part for just that bond.

The parts of the Hartree-Fock potentials from other regions are shielded by the nuclei. Moreover, "tight correlation energies" as in helium and H₂ (similar to those in inner-shells, C-H, C-C single bonds, lone pairs, etc.) are remarkably insensitive to the over-all potential. The 1s² correlation⁸ changes only by 0.012 e.v. in going from Li⁺ to Be⁺². Thus the effect of Hartree-Fock potential changes on localized correlations are expected to be a good deal less than 0.01 e.v.

The exclusion effects from other orbitals also are expected to be small. We had already estimated the exclusion effect of 2s on the Li⁺ correlation energy to be about 0.004 e.v.²⁸

Thus, the theory enables one to put such well established empirical facts as additivity and constancy of bonds on a quantitative basis with the inclusion of many-electron effects.

Another potential use of the transformations of correlation energy described above is in relating correlation shifts of the levels based on Hartree-Fock MO theory in the electronic spectra of molecules to the correlation energies of localized groups which can be estimated much more readily. In $n-\pi^*$ transitions, for instance, one could estimate the correlation energy in lone pairs, then by the transformation make estimates of correlation energies between delocalized molecular orbitals.

Finally, the theory described above also can be formulated in very much the same way relativistically. Once shells are separated, relativistic effects can be left in the inner shells where they are known to be important.^{27,33} One then deals with non-relativistic results for the outer shells obtained upon further approximation.

Thus one finds a quantitative and systematic basis for the "simple quantum chemistry" as well as a "chemical" simplification in "molecular quantum mechanics."

(28) O. Sinanoğlu, *J. Chem. Phys.*, **33**, 1212 (1960).

(29) O. Sinanoğlu, *ibid.*, **37**, 191 (1962).

(30) O. Sinanoğlu and V. McKoy, *ibid.*, to be published.

(31) R. K. Nesbet, *ibid.*, **32**, 1114 (1960).

(32) G. G. Hall, *Proc. Roy. Soc. (London)*, **A205**, 541 (1951).

(33) A. Fröman, *Rev. Mod. Phys.*, **32**, 317 (1960).

A REFINED ALTERNANT MOLECULAR ORBITAL TREATMENT OF THE GROUND STATE OF BENZENE

BY J. DE HEER

Department of Chemistry, University of Colorado, Boulder, Colorado

Received May 28, 1962

In the refined alternant molecular orbital (AMO) method we allow for different variable parameters for each MO pair which is coupled. Application to the ground state of benzene reveals this method to be extremely powerful: The AMO wave function, involving two variable parameters only, has a lower energy than the nine-term configuration interaction (CI) wave function which was obtained by Parr, Craig, and Ross. A further numerical analysis reveals that the relative improvement of the refined over the simple method is independent of any reasonable choice of core potential and electron interaction integral approximation. A detailed comparison of the AMO and CI wave functions is given.

Introduction

Dewar¹ has discussed a way in which to treat the "vertical correlation" in conjugated systems. The alternant molecular orbital (AMO) method concerns itself with the more conventional "horizontal correlation" which, in quantum chemistry, usually is treated by means of configuration interaction (CI) techniques.² As such, the AMO method is by no means confined to π -electrons; it pertains to all systems of alternant character, *i.e.*, consisting of a set of identical atomic centers which can be divided into two sub-sets in such a way that no two atoms of the same sub-set are neighbors to each other. In fact, when Löwdin proposed the use of alternant molecular orbitals to treat electron correlation,³ he primarily envisaged applications to solid state problems, and it is quite possible that here they may ultimately find their most useful domain. To date, however, the more interesting applications have been in the field of conjugated systems⁴⁻⁶ and it appears appropriate to give a first application of a *refined* AMO method within this framework. More specifically, we shall treat the ground state of the π -electron sextet in benzene. Not only has this been the initial test case for the AMO method in its original form,⁴ but it also has been the subject of a most extensive CI treatment,⁷ so that all relevant data are available for comparison.

The Simple and Refined AMO Method.—The effectiveness of the AMO method is due to the fact that a major portion of the correlation between electrons with different spins can be taken into account by assigning these to different, "semilocalized" orbitals so that they can avoid each other as much as possible.⁸ In alternant systems, this is achieved by taking suitable linear combinations of sets of "paired" bonding and antibonding MO, ψ_k and $\psi_{\bar{k}}$, to yield the AMO, a_K and \bar{a}_K , thus

$$a_K = \cos \theta_k \psi_k + \sin \theta_k \psi_{\bar{k}} \quad (1)$$

$$\bar{a}_K = \cos \theta_k \psi_k - \sin \theta_k \psi_{\bar{k}}$$

with

$$0 < \theta_k < \pi/4$$

[For a system with $2n$ equivalent atomic centers and $2n$ electrons, $k = 1, 2, \dots, n$, hence $K = I, II, \dots, N$.] As illustrated schematically in Fig. 1, the a_K and \bar{a}_K have the desired semilocalized property. The AMO wave function takes the form

$${}^1\Psi_0(\theta_1, \dots, \theta_n) \equiv \Psi = \mathcal{O}_{00}\mathcal{A}\Phi T_0 \quad (2)$$

where \mathcal{O}_{00} is the projection operator selecting the proper singlet spin state

$$\mathcal{O}_{00} = \sum_{\nu=0}^n (-1)^\nu \frac{S_-^\nu S_+^\nu}{\nu! (\nu+1)!} \quad (3)$$

\mathcal{A} is the antisymmetrization operator

$$\mathcal{A} = [(2n)!]^{-1/2} \sum_P (-1)^P P \quad (4)$$

$$\Phi = a_I(1) \dots a_N(n) \bar{a}_I(n+1) \dots \bar{a}_N(2n) \quad (5)$$

and

$$T_0 = \alpha(1) \dots \alpha(n) \beta(n+1) \dots \beta(2n) \quad (6)$$

Thus, in a loose way of speaking, we have assigned all electrons with α spin to the a_K and all those with β spin to the \bar{a}_K . It is important to note that unless all θ_k equal $\pi/4$, the AMO do not form an orthonormal set; while

$$\int a_K^*(1) a_L(1) dv_1 = \int \bar{a}_K^*(1) \bar{a}_L(1) dv_1 = \delta_{KL} \quad (7a)$$

one also has

$$\int a_K^*(1) \bar{a}_L(1) dv_1 = \lambda_K \delta_{KL} \quad (7b)$$

with

$$\lambda_K \equiv \cos 2\theta_K \quad (8)$$

As in our earlier work,^{6,9} we shall find it convenient to carry out all algebraical manipulations in terms of the λ_K rather than in terms of the θ_K .

The energy associated with the wave function ${}^1\Psi_0$ of eq. 2 is

(9) R. Pauncz, J. de Heer, and P. O. Löwdin, *J. Chem. Phys.*, **36**, 2247 (1962).

(1) M. J. S. Dewar and N. L. Sabelli, *J. Phys. Chem.*, **66**, 2310 (1962).

(2) For a review of the correlation problem in quantum chemistry, see P. O. Löwdin, *Advan. Chem. Phys.*, **2**, 209 (1959).

(3) P. O. Löwdin, "Symposium on Molecular Physics," Nikko, Japan, 1953, p. 13; *Phys. Rev.*, **97**, 1509 (1955).

(4) T. Itoh and H. Yoshizumi, *J. Phys. Soc. Japan*, **10**, 201 (1955).

(5) R. Lefebvre, H. H. Dearman, and H. M. McConnell, *J. Chem. Phys.*, **32**, 176 (1960).

(6) R. Pauncz, J. de Heer, and P. O. Löwdin, *ibid.*, **36**, 2257 (1962).

(7) R. G. Parr, D. P. Craig, and I. G. Ross, *ibid.*, **18**, 1561 (1950).

(8) Electrons with the same spin are correlated through the Pauli antisymmetrization principle. See, *e.g.*, P. O. Löwdin, ref. 2.

$${}^1E_0(\theta_1, \dots, \theta_n) \equiv E = \int \Psi^* H_{op} \Psi d\tau / \int \Psi^* \Psi d\tau \quad (9)$$

Corresponding to the usual splitting of H_{op} into a "one-electron Hamiltonian," $\sum_i h_1(i)$, comprising

kinetic energy and potential energy due to the "core," and the electron interaction terms, e^2/r_{ij} ,¹⁰ the energy E is written as the sum of a "one-electron energy," E_1 , and an electron interaction energy, E_{12} .

In what we shall henceforth refer to as the *simple* AMO method, we impose the restriction that all mixing parameters θ_k (or λ_k) have to take on the same value. The corresponding one-parameter energy expressions, $E_1(\theta)$, $E_{12}(\theta)$, and $E(\theta)$, for an arbitrary alternant system with closed-shell structure, have been given elsewhere.⁹ The typical behavior of these quantities, referred to the energies of the relevant single ASMO determinant (denoted by 2ε , U , and $U + 2\varepsilon$, respectively), as a function of θ , is illustrated in Fig. 2. Note the characteristic monotonic increase in E_1 and the decrease in E_{12} , resulting in a single minimum in E . For any particular system, a numerical analysis will have to yield the optimum value of θ , θ^0 , and the corresponding energy depression, ΔE_{rel} . The latter quantity denotes the improvement of the AMO energy over that of the single ASMO determinant, relative to the condition that all θ_k^0 are equal. The ground state of the π -electron sextet in benzene has been treated in this fashion by Itoh and Yoshizumi⁴ and by Pauncz, de Heer, and Löwdin.⁶ The relevant results will be referred to below.

Both the strength and the limitations of the simple AMO method reside in the circumstance that only one variable parameter is used. In the *refined* AMO method the restriction of equal θ_i is dropped and we obtain a more flexible, many-parameter wave function. General expressions for $E_1(\theta_1, \dots, \theta_n)$, $E_{12}(\theta_1, \dots, \theta_n)$, and $E(\theta_1, \dots, \theta_n)$ will be given elsewhere.¹¹ For any particular system an energy minimization procedure will have to give us a set of optimum mixing parameters, $\theta_1^0, \theta_2^0, \dots, \theta_n^0$, and an energy depression, $|\Delta E|$. The latter quantity reflects the improvement of the energy obtained with the refined AMO wave function over that of the single ASMO determinant. While the possibility of developing the AMO method in this fashion has been apparent since its inception, and it is intuitively clear that a MO pair, ψ_k and $\bar{\psi}_k$, will mix the stronger the smaller the energy gap between them, only actual computations can reveal whether the degree of improvement of the results justifies the complications which of necessity are introduced as the simpler scheme is abandoned. As far as we know, the present investigation is the first numerical analysis of this type. Reasons for selecting the benzene molecule to this purpose already have been given in the Introduction.

Wave Function and Energy Expression for Benzene.—It is most convenient to write the benzene MO, ψ_j , in terms of the carbon $2p_z$ AO, u_μ , as

$$\psi_j = (6N_j)^{-1/2} \sum_{\mu=0}^5 \omega^{\mu j} u_\mu \quad (j = 0, \pm 1, \pm 2, 3) \quad (10)$$

with

$$\omega = \exp(\pi i/3) \quad (11a)$$

and

$$N_j = \sum_{\mu=0}^5 \omega^{\mu j} S_\mu \quad (11b)$$

where

$$S_\mu = \int u_0^*(1) u_\mu(1) dv_1 \quad (11c)$$

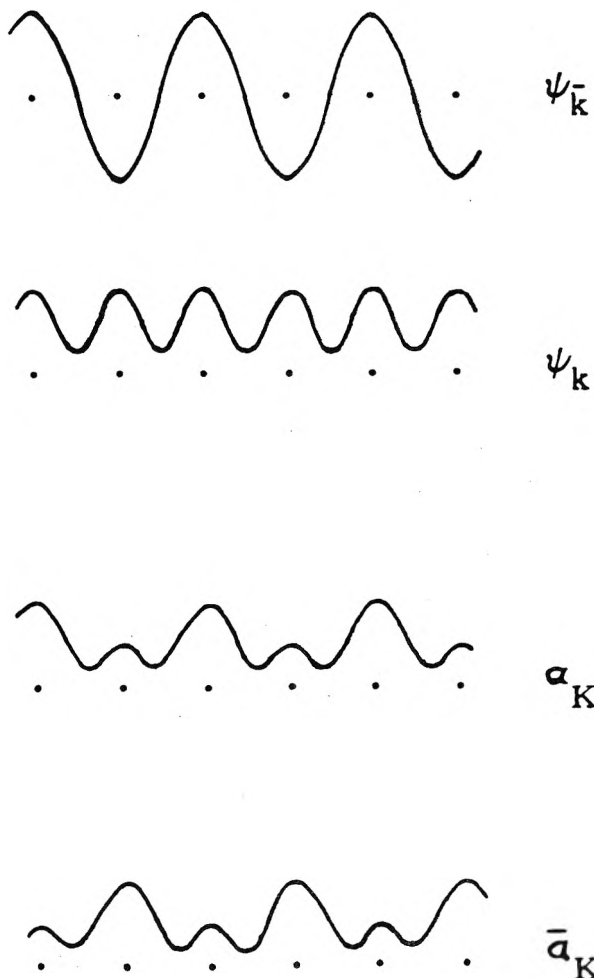


Fig. 1.—Hückel-Wheland MO and AMO.

The AMO will have to be of the type formally denoted by eq. 1 above. However, it is readily verified that, in order to get the required A_{1g} symmetry for the total wave function, the two degenerate MO pairs must be transformed into AMO with the same mixing parameter. Hence, in the special case under consideration, even although we are dealing with an electron sextet, we get a two- rather than a three-parameter problem and the six AMO become

$$a_0 = \cos \theta_0 \psi_c + \sin \theta_0 \psi_3$$

$$\bar{a}_0 = \cos \theta_0 \psi_c - \sin \theta_0 \psi_3$$

(10) See, e.g., P. G. Lykos, *J. Phys. Chem.*, **66**, 2324 (1962).

(11) J. de Heer, *J. Chem. Phys.*, in press.

$$a_I = \cos \theta_{12} \psi_1 + \sin \theta_{12} \psi_{-2} \quad (12) \quad \text{with}$$

$$\bar{a}_I = \cos \theta_{12} \psi_1 - \sin \theta_{12} \psi_{-2}$$

$$a_{II} = \cos \theta_{12} \psi_{-1} + \sin \theta_{12} \psi_2$$

$$\bar{a}_{II} = \cos \theta_{12} \psi_{-1} - \sin \theta_{12} \psi_2$$

$\Phi(\theta_0, \theta_{12})$ is the simple product of these six AMO and

$$\begin{aligned} \mathcal{O}_{00} T_0 = & 1/4 \alpha(1) \alpha(2) \alpha(3) \beta(4) \beta(5) \beta(6) - \\ & 1/12 [\beta(1) \alpha(2) \alpha(3) + \alpha(1) \beta(2) \alpha(3) + \\ & \alpha(1) \alpha(2) \beta(3)] \cdot [\alpha(4) \beta(5) \beta(6) + \beta(4) \alpha(5) \beta(6) + \\ & \beta(4) \beta(5) \alpha(6)] + 1/12 [\alpha(1) \beta(2) \beta(3) + \\ & \beta(1) \alpha(2) \beta(3) + \beta(1) \beta(2) \alpha(3)] \cdot [\beta(4) \alpha(5) \alpha(6) + \\ & \alpha(4) \beta(5) \alpha(6) + \alpha(4) \alpha(5) \beta(6)] - \\ & 1/4 \beta(1) \beta(2) \beta(3) \alpha(4) \alpha(5) \alpha(6) \quad (13) \end{aligned}$$

Thus, by eq. 2, ${}^1\Psi_0(\theta_0, \theta_{12})$ is a linear combination of twenty Slater determinants, which establishes the connection between the AMO and the CI methods (see the discussion below).

The desired energy expressions may be obtained either from the general equations given elsewhere¹¹ or by direct derivation using the techniques described by Pauncz, de Heer, and Löwdin.⁹ It is convenient to express these energies immediately with reference to those of the single ASMO determinant. Define \mathfrak{N} as

$$\mathfrak{N} = 1 + 1/3(\lambda_0^2 + 2\lambda_{12}^2) + 1/3(2\lambda_0^2\lambda_{12}^2 + \lambda_{12}^4) + \lambda_0^2\lambda_{12}^4 \quad (14)$$

Then the one-electron energy becomes

$$E_1(\lambda_0, \lambda_{12}) - E_1(1, 1) = \Delta W -$$

$$\frac{4}{3\mathfrak{N}} [\lambda_0(1 + \lambda_{12}^2 + \lambda_{12}^4)\Delta w_0 + \lambda_{12}(2 + \lambda_0^2 + \lambda_{12}^2 + 2\lambda_0^2\lambda_{12}^2)\Delta w_{12}] \quad (15)$$

$$\begin{aligned} \Gamma(\gamma) \equiv & [5 + 2\lambda_{12} + 2\lambda_{12}^2 + \lambda_0^2(2 + 2\lambda_{12} + 5\lambda_{12}^2)](1 + \lambda_{12})^2\gamma_{11}/4 + [5 - 2\lambda_{12} + 2\lambda_{12}^2 + \lambda_0^2(2 - 2\lambda_{12} + 5\lambda_{12}^2)](1 - \lambda_{12})^2\gamma_{22}/4 + [4 - \lambda_{12}^2 + \lambda_0^2(1 - 4\lambda_{12}^2)](1 - \lambda_{12}^2)\gamma_{12}/2 + (1 - \lambda_{12}^4)(1 - \lambda_0^2)\gamma_{03}/4 + (1 + \lambda_{12}^2 + \lambda_{12}^4)[(1 + \lambda_0^2)\gamma_{00}/4 + (1 - \lambda_0^2)\gamma_{33}/4] + [3 + \lambda_0 + \lambda_{12} + \lambda_0\lambda_{12} + \lambda_{12}^2(1 + \lambda_0 + \lambda_{12} + 3\lambda_0\lambda_{12})] \times \\ & (1 + \lambda_0)(1 + \lambda_{12})\gamma_{01}/2 + [3 + \lambda_0 - \lambda_{12} - \lambda_0\lambda_{12} + \lambda_{12}^2(1 + \lambda_0 - \lambda_{12} - 3\lambda_0\lambda_{12})](1 + \lambda_0)(1 - \lambda_{12})\gamma_{02}/2 + \\ & [3 - \lambda_0 + \lambda_{12} - \lambda_0\lambda_{12} + \lambda_{12}^2(1 - \lambda_0 + \lambda_{12} - 3\lambda_0\lambda_{12})](1 - \lambda_0)(1 + \lambda_{12})\gamma_{13}/2 + [3 - \lambda_0 - \lambda_{12} + \lambda_0\lambda_{12} + \lambda_{12}^2(1 - \lambda_0 - \lambda_{12} + 3\lambda_0\lambda_{12})](1 - \lambda_0)(1 - \lambda_{12})\gamma_{23}/2 \quad (20a) \end{aligned}$$

$$\begin{aligned} \Delta(\delta) \equiv & (1 - \lambda_0^2\lambda_{12}^2)(1 - \lambda_{12}^2)\delta_{1,-2}/2 + (3 + 2\lambda_{12}^2 + \lambda_{12}^4)(1 - \lambda_0^2)\delta_{03}/4 + [1 + \lambda_0 + \lambda_{12} + \lambda_{12}^2(\lambda_0 + \lambda_{12} + \lambda_0\lambda_{12})](1 + \lambda_0)(1 + \lambda_{12})\delta_{01}/2 + [1 - \lambda_0 - \lambda_{12} + \lambda_{12}^2(-\lambda_0 - \lambda_{12} + \lambda_0\lambda_{12})](1 - \lambda_0)(1 - \lambda_{12})\delta_{-2,3}/2 + \\ & [1 + 2\lambda_{12} + \lambda_0^2(2\lambda_{12} + \lambda_{12}^2)](1 + \lambda_{12})^2\delta_{1,-1}/4 + [1 - 2\lambda_{12} + \lambda_0^2(-2\lambda_{12} + \lambda_{12}^2)](1 - \lambda_{12})^2\delta_{2,-2}/4 + \\ & [1 + \lambda_0 - \lambda_{12} + \lambda_{12}^2(\lambda_0 - \lambda_{12} - \lambda_0\lambda_{12})](1 + \lambda_0)(1 - \lambda_{12})\delta_{02}/2 + [1 - \lambda_0 + \lambda_{12} + \lambda_{12}^2(-\lambda_0 + \lambda_{12} - \lambda_0\lambda_{12})](1 - \lambda_0)(1 + \lambda_{12})\delta_{13}/2 + [3 + \lambda_0^2 + \lambda_{12}^2 + \lambda_0^2\lambda_{12}^2](1 - \lambda_{12}^2)\delta_{12}/2 \quad (20b) \end{aligned}$$

$$\begin{aligned} Z(\zeta) \equiv & [2 + \lambda_0^2 - \lambda_{12}^2 - 2\lambda_0^2\lambda_{12}^2](1 - \lambda_{12}^2)\zeta_{1,-1}/2 + [(2 + \lambda_{12}^2)(\zeta_{01} + \zeta_{13}) - \lambda_0\lambda_{12}(1 + 2\lambda_{12}^2)(\zeta_{01} - \zeta_{13})][(1 - \lambda_0^2)(1 - \lambda_{12}^2)]^{1/2} + [2 + \lambda_0^2 + \lambda_{12}^2 + 2\lambda_0^2\lambda_{12}^2](1 - \lambda_{12}^2)\zeta_{1,-2}/2 \quad (20c) \end{aligned}$$

Here

$$\Delta W = \Delta w_0 + 2\Delta w_{12} \quad (16)$$

$$\Delta w_0 = h_{33} - h_{00}; \quad \Delta w_{12} = h_{22} - h_{11} \quad (17)$$

with

$$h_{kk} \equiv \int \psi_k^*(1) h_1(1) \psi_k(1) dv_1 \quad (18)$$

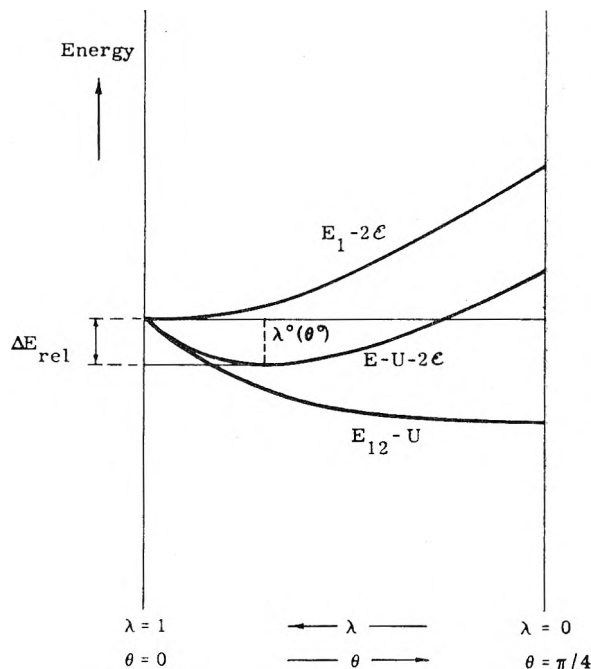


Fig. 2.—Energies as a function of a single mixing parameter.

The one-electron operator energies, h_{kk} , frequently are referred to as “orbital energies” and usually are denoted by ϵ_k .^{4,7} For the electron interaction energy we obtain

$$E_{12}(\lambda_0, \lambda_{12}) - E_{12}(1, 1) = \frac{4}{3\mathfrak{N}} [\Gamma(\gamma) - \Delta(\delta) - Z(\zeta)] - U \quad (19)$$

where we have introduced the shorthands

and

$$U \equiv \gamma_{00} + 6\gamma_{11} + 8\gamma_{01} - 4\delta_{01} - 2\delta_{1,-1} \quad (21)$$

In eq. 20a and 20b the γ_{ij} and δ_{ij} are the Coulomb-

and exchange integrals, involving the MO ψ_i and ψ_j . The ζ_{ij} are defined as

$$\zeta_{ij} \equiv \iint \psi_i^*(1) \psi_j(1) \frac{e^2}{r_{12}} \psi_j^*(2) \psi_i(2) dv_1 dv_2 \quad (22)$$

The use of these ζ_{ij} allows for a systematic notation of all electron interaction integrals needed in our investigation. For reference purposes, we give below the corresponding, partially of an *ad hoc* nature, symbols introduced by Parr, Craig, and Ross,⁷ as also used by Itoh and Yoshizumi,⁴ for the four relevant integrals in benzene

$$\begin{aligned} \zeta_{1,-2} &= \eta; & \zeta_{1,-1} &= \xi \\ \zeta_{01} &= \zeta_{23}^{10}; & \zeta_{13} &= \zeta_{13}^{02} \end{aligned} \quad (23)$$

Using the identification (8), one may readily check that in the limiting case $\lambda_0 = \lambda_{12} = \lambda$ (hence $\theta_0 = \theta_{12} = \theta$), our energy expressions reduce to the ones given by Itoh and Yoshizumi,⁴ when the latter are referred to those of the single ASMO determinant. The drastic simplifications to which their formulas can be subjected in this limiting case^{6,9} are, on the whole, no longer applicable in the refined scheme.

One further point arises with respect to eq. 19. If one uses an integral approximation in which all Coulomb integrals between MO, γ_{ij} , are equal ($= \gamma$ say), as is the case if the Mulliken or Parr-Pariser approximation is used to determine all electronic interaction integrals,¹² we have¹¹

$$\frac{4}{3\pi} \Gamma(\gamma) = U + 4\delta_{01} + 2\delta_{1,-1} = 15\gamma \quad (24)$$

so that, in effect, we can eliminate all γ_{ij} -containing terms from the electron interaction energy expression. This also shows a real advantage of computing $E_{12}(\lambda_0, \lambda_{12}) - E_{12}(1,1)$ rather than $E_{12}(\lambda_0, \lambda_{12})$ as such.

Numerical Analysis.—To carry out a numerical analysis, we have to (i) select a specific form of the one-electron Hamiltonian, h_1 , and (ii) adopt an approximation for the evaluation of the electron interaction integrals. These matters have been extensively discussed in the literature¹⁰ and we merely wish to justify our choices concerned within the context of the aims of the present investigation. As we outlined in the Introduction, these aims are twofold: to determine the improvement over the simple AMO method and to give a comparison with the best available CI treatment. With the former goal in mind, we have carried out computations with the same set of integrals as used in our earlier work.^{6,3,12,13} That is, we used Ruedenberg's values of the one-electron integrals and a combined Mulliken-tight-binding approximation for all electronic interaction integrals. To make the desired comparison with the CI wave function of Parr, Craig, and Ross,⁷ we have repeated the calculations with the integrals used by these investigators and used also by Itoh and Yoshizumi

(12) J. de Heer and R. Pauncz, *J. Mol. Spectry.*, **5**, 326 (1960).

(13) K. Ruedenberg, *J. Chem. Phys.*, **34**, 1861 (1961).

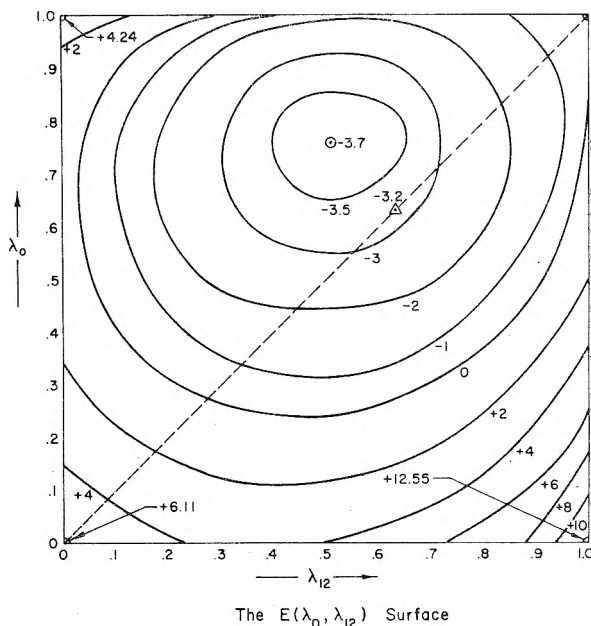


Fig. 3.—The $E(\lambda_0, \lambda_{12})$ surface: Δ , relative minimum ($\lambda_0 = \lambda_{12}$); \odot , absolute minimum.

in their simple AMO study of benzene.⁴ Here one-electron integrals were obtained according to the original Goepfert-Mayer-Sklar approximation, two center electronic repulsion integrals were computed directly, using Slater-type orbitals, and three- and four-center integrals were evaluated with the Sklar-London approximation. Finally, we carried out a third set of calculations following the method of neglecting differential overlap, with empirically selected, much reduced, electron interaction integrals, actual values of which were taken from Pariser.¹⁴ Our chief purpose here was to check whether a correspondingly much reduced electron correlation would essentially alter the relative merits of the refined over the simple method.

While in our earlier work⁶ we were primarily concerned with total electronic energies, it is of interest in the current investigation not only to obtain $E(\lambda_0, \lambda_{12})$, but also $E_1(\lambda_0, \lambda_{12})$ and $E_{12}(\lambda_0, \lambda_{12})$ separately. After computing the three energy surfaces concerned over the entire range of λ_0 and λ_{12} , that is from zero to unity, we ascertained that in each case $E(\lambda_0, \lambda_{12})$ is simply concave. Figure 3 shows a projection of the latter surface on the λ_0, λ_{12} -plane for the results obtained with the first of the three integral approximations referred to above (compare the first column of numerical data in Table I). With the other two integral approximations, the general appearance of this surface remains the same.

The important numerical results are collected in Table I; after each optimum 3 value the corresponding θ value is given in parentheses.

Discussion

The immediate conclusions to be drawn from the data summarized in Table I are that our refinement of the AMO method results in a sizable improvement in energy and that the optimum values of the mixing parameters are distinctly different

(14) R. Pariser, *ibid.*, **24**, 250 (1956).

TABLE I
ENERGIES AND OPTIMUM λ VALUES

		Mulliken-tight binding approximation ^a	Parr-Craig-Ross (Itoh-Yoshizumi) integrals ^b	Neglect of differential overlap; empirical integrals ^c
Simple method ($\lambda_0 = \lambda_{12} = \lambda$)	$\lambda^0(\theta^0)$	0.631 (25° 26')	0.691 (23° 9')	0.837 (16° 35')
	$E_1(\lambda^0) - E_1(1)$, e.v.	3.993	2.915	0.671
	$E_{12}(\lambda^0) - E_{12}(1)$, e.v.	-7.171	-5.317	-1.236
	ΔE_{rel} , e.v.	-3.178 ^d	-2.402 ^e	-0.565
Refined method	$\lambda_0^0(\theta_0^0)$	0.762 (20° 11')	0.808 (18° 3')	0.911 (12° 11')
	$\lambda_{12}^0(\theta_{12}^0)$	0.510 (29° 40')	0.590 (26° 55')	0.767 (19° 57')
	$E_1(\lambda_0^0, \lambda_{12}^0) - E_1(1,1)$, e.v.	4.167	3.136	0.780
	$E_{12}(\lambda_0^0, \lambda_{12}^0) - E_{12}(1,1)$, e.v.	-7.863	-5.928	-1.449
	ΔE , e.v.	-3.696	-2.792	-0.669
Comparison	$ \Delta E - \Delta E_{rel} $, e.v.	0.518	0.390	0.104
	$\frac{100(\Delta E - \Delta E_{rel})}{\Delta E}$	16.3%	16.2%	18.4%

^a See ref. 6, 9, 12, 13. ^b See ref. 4, 7. ^c Numerical values from Pariser, ref. 14. ^d Identical with the value obtained by Pauncz, de Heer, and Löwdin, ref. 6. ^e This number differs by 0.05 e.v. from the value published by Itoh and Yoshizumi, ref. 4.

TABLE II
COMPARISON OF AMO AND CI TREATMENTS

¹ A _{1g} Configuration functions	Expansion coefficient in the AMO wave function ^a	Numerical expansion coefficients		Same coefficients in the nine-term CI wave function of Parr, Craig, Ross ^c
		$\lambda^0 = 0.691^b$	$\lambda_{12}^0 = 0.590$	
$\phi_1 = (\psi_0^2 \psi_1^2 \psi_{-1}^2)$	$\sigma(\lambda)(1 + \lambda_0)(1 + \lambda_{12})^2$	0.897	0.871	0.910
$\phi_2 = (\psi_0^2 \psi_1 \psi_{-1} \psi_2 \psi_{-2})$	$\sigma(\lambda)(1 + \lambda_0)(1 - \lambda_{12})^2$.164	.225	.210
$\phi_3 = \frac{1}{[3]^{1/2}} [2(\psi_0^2 \psi_1 \psi_{-1} \psi_2 \psi_{-2}) - (\psi_0^2 \psi_1 \psi_{-1} \psi_2 \psi_{-2})]$	$[3]^{-1/2} \sigma(\lambda)(1 + \lambda_0)(1 - \lambda_{12})^2$.095	.130	.142
$\phi_4 = (\psi_0^2 \psi_1 \psi_{-1} \psi_2^2)$	0	0	0	.052
$\phi_5 = (\psi_1^2 \psi_{-1}^2 \psi_2 \psi_{-2})$	0	0	0	-.056
$\phi_6 = (\psi_1^2 \psi_{-1}^2 \psi_2^2)$	$-\sigma(\lambda)(1 - \lambda_0)(1 + \lambda_{12})^2$	-0.164	-0.093	-.059
$\phi_7 = \frac{1}{[2]^{1/2}} [(\psi_0^2 \psi_1^2 \psi_2^2) + (\psi_0^2 \psi_{-1}^2 \psi_2^2)]$	$-[2]^{1/2} \sigma(\lambda)(1 + \lambda_0)(1 - \lambda_{12})^2$	-.232	-.318	-.227
$\phi_8 = \frac{1}{[2]^{1/2}} [(\psi_0 \psi_1^2 \psi_{-1} \psi_2 \psi_2) + (\psi_0 \psi_{-1} \psi_{-1}^2 \psi_2 \psi_2)]$	$\sigma(\lambda)(1 + \lambda_{12})[2(1 - \lambda_0^2)(1 - \lambda_{12}^2)]^{1/2}$.232	.204	.204
$\phi_9 = \frac{1}{[6]^{1/2}} [2(\psi_0 \psi_1^2 \psi_{-1} \psi_2 \psi_2) + 2(\psi_0 \psi_{-1} \psi_{-1}^2 \psi_2 \psi_2) - (\psi_0 \psi_1^2 \psi_{-1} \psi_2 \psi_2) - (\psi_0 \psi_{-1} \psi_{-1}^2 \psi_2 \psi_2)]$	$\sigma(\lambda)(1 + \lambda_{12})[2(1 - \lambda_0^2)(1 - \lambda_{12}^2)/3]^{1/2}$.134	.118	.069
$\phi_{10} = (\psi_0^2 \psi_2^2 \psi_{-2}^2)$	$\sigma(\lambda)(1 + \lambda_0)(1 - \lambda_{12})^2$.030	.058	Not included
$\phi_{11} = \frac{1}{[2]^{1/2}} [(\psi_0^2 \psi_{-1}^2 \psi_2^2) - (\psi_2^2 \psi_1^2 \psi_2^2)]$	$[2]^{1/2} \sigma(\lambda)(1 - \lambda_0)(1 - \lambda_{12})^2$.042	.034	Not included
$\phi_{12} = (\psi_2^2 \psi_1 \psi_{-1} \psi_2 \psi_{-2})$	$-\sigma(\lambda)(1 - \lambda_0)(1 - \lambda_{12})^2$	-.030	-.024	Not included
$\phi_{13} = \frac{1}{[3]^{1/2}} [2(\psi_2^2 \psi_1 \psi_{-1} \psi_2 \psi_{-2}) - (\psi_2^2 \psi_1 \psi_{-1} \psi_2 \psi_{-2})]$	$-[3]^{-1/2} \sigma(\lambda)(1 - \lambda_0)(1 - \lambda_{12})^2$	-.017	-.014	Not included
$\phi_{14} = \frac{1}{[2]^{1/2}} [(\psi_0 \psi_{-1} \psi_2^2 \psi_{-2} \psi_2) + (\psi_0 \psi_1 \psi_2^2 \psi_{-2} \psi_2)]$	$\sigma(\lambda)(1 - \lambda_{12})[2(1 - \lambda_0^2)(1 - \lambda_{12}^2)]^{1/2}$.042	.053	Not included
$\phi_{15} = \frac{1}{[6]^{1/2}} [2(\psi_0 \psi_{-1} \psi_2^2 \psi_{-2} \psi_2) + 2(\psi_0 \psi_1 \psi_2^2 \psi_{-2} \psi_2) - (\psi_0 \psi_1 \psi_2^2 \psi_{-2} \psi_2) - (\psi_0 \psi_{-1} \psi_2^2 \psi_{-2} \psi_2)]$	$\sigma(\lambda)(1 - \lambda_{12})[2(1 - \lambda_0^2)(1 - \lambda_{12}^2)/3]^{1/2}$.024	.030	Not included
$\phi_{16} = (\psi_2^2 \psi_2^2 \psi_{-2}^2)$	$\sigma(\lambda)(1 - \lambda_0)(1 - \lambda_{12})^2$.006	.006	Not included

^a $\sigma(\lambda) \equiv 1/4 [1 + 1/3(\lambda_0^2 + 2\lambda_{12}^2) + 1/3(\lambda_{12}^4 + 2\lambda_0^2 \lambda_{12}^2) + \lambda_0^2 \lambda_{12}^4]^{-1/2} = 1/[4\sqrt{\mathcal{N}}]$. ^b The first nine already given by Itoh and Yoshizumi (ref. 4). ^c As communicated to Itoh and Yoshizumi (ref. 4).

for different MO pairs. This is true even in the case where the correlation is greatly reduced by the use of empirical two-center electron interaction

integrals¹⁴; the relative improvement in energy remains of the same order.

As the result of an extensive CI calculation, in-

volving a nine-term wave function with nine variable parameters, Parr, Craig, and Ross¹⁵ obtained an energy depression, $|\Delta E_{CI}|$, of 2.7 e.v. It is extremely gratifying that, with exactly the same integrals, we get an energy depression of 2.8 e.v., using two variable parameters only.

Independent of our choice of integral approximation, in going from the simple to the refined method, there always is a slight increase in one-electron energy, which is more than offset by an accompanying decrease in electron interaction energy. It is of interest to analyze this further by splitting up the former in its kinetic and potential energy parts. We have done this for the results obtained with the Mulliken-tight-binding approximation, where the relevant data are readily available^{9,13}; those with alternative integrals should give us essentially the same picture since the same underlying principles are involved. We readily compute that the 3.993 e.v. one-electron energy rise of the simple scheme is due to an increase of 11.167 e.v. in kinetic energy and a decrease of 7.624 e.v. in potential energy. When we break down the corresponding amount, 4.167 e.v., in the refined method we get +12.124 e.v. kinetic energy and -7.957 e.v. potential energy. While the electron interaction energy depressions reflect the main portion of the correlation effect the AMO method aims at, it is no surprise that with the accompanying "semi-localization" process, one obtains a rather steep rise in kinetic energy. The sizable decrease in the potential energy part of the one-electron energy is, at first sight, somewhat of a surprise. It is due to the fact that as more of the antibonding MO, which have more nodes between the atoms than the bonding MO, are mixed into the wave function, the electrons are concentrated more "on" than "between" the (positively charged) atomic centers. In going from the simple to the refined method, the kinetic energy increases by 0.507 e.v. while the potential energy decreases by 1.025 e.v. to yield the resultant lowering of 0.518 e.v. listed in Table I. The near-validity of the virial theorem is fortuitous here, as is evident from an inspection of the data pertaining to either the simple or the refined scheme separately.

In order to compare the AMO and CI wave functions, we have expanded the former in terms of a set of orthonormal configuration functions given in the first column of Table II. The expansion coefficients, in terms of λ_0 and λ_{12} , are given in the second column of this table.¹⁶ In the third and fourth

columns, numerical values of these coefficients are given in terms of the optimum λ 's with the simple and refined AMO method, respectively. In the last column we have listed the nine coefficients of the CI wave function obtained by Parr, Craig, and Ross.¹⁵ As a measure of the "resemblance" of the AMO and CI wave functions, Itoh and Yoshizumi⁴ considered the "inner product integral"

$$\mathcal{I} \equiv \int \Psi^*_{AMO} \Psi_{CI} d\tau \quad (25)$$

With the simple and refined AMO function, we readily compute $\mathcal{I} = 0.983$ and $\mathcal{I} = 0.986$, respectively. Since these two wave functions are markedly different, as an inspection of the third and fourth columns of Table II shows, the quantity \mathcal{I} can hardly be considered very revealing. We note that, while both AMO treatments exclude ϕ_4 and ϕ_6 , the coefficients of ϕ_{10} and ϕ_{14} , in particular those of the refined AMO wave function, are of the same order of magnitude as those of ϕ_4 , ϕ_6 , and ϕ_8 in the CI wave function. Here, as elsewhere, it is evident that it is difficult to decide *a priori* what configurations to include and which to exclude from a conventional CI treatment. This difficulty increases of course with the size of our system, whence the AMO method will become increasingly attractive. We plan to investigate such systems within the framework of the refined method described in this paper.

Recently, Pauncz has computed the lowest triplet state in benzene using the simple AMO method.¹⁷ We hope to obtain the same, using the refined method. This will not only allow for a further comparison between AMO methods and the CI treatment, but also will give us a first direct check against experimental data. Research to obtain singlet excited states also is in progress.

Acknowledgment.—The author is indebted to Professor Per-Olov Löwdin, the originator of the AMO method, for his encouragement in the course of this investigation. This work has been supported in part by a grant from the Council on Research and Creative Work at the University of Colorado. The computations were carried out on the CDC 1604 computer at the National Bureau of Standards, Boulder, Colorado, with financial support of the Numerical Analysis Center of the Applied Mathematics Department at the University of Colorado. The assistance of Mr. Hans M. Roder in programming the problem is gratefully acknowledged.

(15) As communicated to Itoh and Yoshizumi; see ref. 4.

(16) The first nine of these coefficients already were obtained by Itoh and Yoshizumi in the limiting case of the simple method; see

ref. 4. By substituting $\cos 2\theta$ for both λ_0 and λ_{12} , it is readily verified that these two sets of coefficients become identical.

(17) R. Pauncz, to be published.

SOME APPLICATIONS OF SEMI-EMPIRICAL VALENCE BOND THEORY TO SMALL MOLECULES¹

BY FRANK O. ELLISON

Department of Chemistry, Carnegie Institute of Technology, Pittsburgh 13, Pennsylvania

Received May 28, 1962

A semi-empirical theory of the low-lying electronic states of diatomic molecules is described and applied to H₂, LiH, BeH, and BH. Ionic and covalent valence bond structures are utilized as a basis; the atoms-in-molecules method, modified to account for intra-atomic energy changes on deflation or inflation of atoms and ions in molecules, is employed. Coulomb parts of the interatomic energy are obtained theoretically using integrals over Slater orbitals. A new approach is proposed for estimating exchange integrals in terms of overlap and empirical atomic properties. In the over-all theory, all empirical quantities admitted are strictly atomic; no calibration parameters dependent on molecular properties are present. Encouraging results for dissociation and excitation energies, especially for H₂, LiH, and BeH, indicate that this rather simple model is fairly sound. However it is concluded that further applications will require molecular parameters in order to obtain semiquantitative predictions.

One of the major devices which chemists have long been seeking through quantum mechanics is a scheme for the quantitative theoretical analysis of known molecular energies and for the quantitative theoretical synthesis of unknown molecular energies. Although the universal reagent (the Schrödinger wave equation) is known, only dilute solutions (molecular orbital and valence bond theories) have been practicable to any extent. The yield of qualitative understanding of molecular stabilities has been impressive; unfortunately, quantitative successes have been few.

One main obstacle in the way toward obtaining and interpreting accurate values is the profound effect of electron correlation, especially of the intra-atomic kind, on molecular energies. Really theoretical accounting of this correlation energy requires an extremely large set of configurational functions in the conventional variational calculation. However, Moffitt² has shown that it is possible to allow for intraatomic correlation by admitting experimental energies of atomic and ionic states in a particular way.

The wave function ψ for a diatomic molecule is expanded in terms of functions $(\alpha\psi_n)$, where ψ_n is a product of eigenfunctions for the two atoms involved and α is the normalized antisymmetrization operator applied to assure satisfaction of the Pauli principle

$$\psi = \sum_n c_n (\alpha\psi_n), \quad \psi_n = \psi_i^A \psi_j^B \quad (1)$$

In practice, appropriate products of ion states also are included in the expansion; *i.e.*, ψ_i^A and ψ_j^B may be eigenfunctions for A⁺ and B⁻, etc. To find the minimum expectation value for the total energy, the secular equations $Hc = ScE$ must be solved. In the atoms-in-molecules approach, the total Hamiltonian operator H is first rigorously divided into two main parts

$$H\psi_n = (H_A^0 + H_B^0 + V_n)\psi_n = [W_i^0(A) + W_j^0(B) + V_n]\psi_n \quad (2)$$

H_A^0 and H_B^0 contain all intraatomic terms, V_n all remaining interatomic terms (the particular division of H used depends upon ψ_n whether it in-

volves eigenfunctions for neutral atoms, or for A⁺ and B⁻, etc.). The elements of the H -matrix turn out to be

$$H_{nm} = 1/2[S_{nm}(W_n^0 + W_m^0) + V_{nm} + V_{mn}] \quad (3)$$

where $W_n^0 = W_i^0(A) + W_j^0(B)$ are experimental atomic state energies

$$S_{nm} = \int (\alpha\psi_n)\psi_m d\tau, \quad V_{nm} = \int (\alpha\psi_n)V_m\psi_m d\tau \quad (4)$$

Moffitt suggested that the V_{nm} and S_{nm} could be satisfactorily assessed using approximate wave functions of the orbital type.

Now it is well known that the effective nuclear charges for valence electrons in atoms and ions often must be modified in order to yield good approximations of interaction energies. Assuming that such modifications do not appreciably affect intra-atomic correlation energies, Hurley³ has developed a new and quite successful method for correcting *ab initio* orbital-type calculations for their neglect of correlation energy.

As molecules become more and more complex, *ab initio* calculations become correspondingly difficult to carry through, to correct, and indeed to interpret physically. Until such time that this situation is improved, simpler approaches containing additional empirical elements are of value in providing at least semiquantitative answers to chemical questions. Some attempts at building such methods on more or less fundamental theoretical grounds are typified by the Magic Formula for the structure of bond energies developed by Mulliken⁴ and by studies of hydrides of first-row elements by Longuet-Higgins⁵ and by Companion and Ellison.^{6,7}

Description of Method and Application to H₂.—The work reported here represents an attempt to extend the Magic Formula by explicit inclusion of the coulomb energy, of ionic-covalent resonance, and by possible theoretical improvement of methods for estimating VB exchange integrals.

(3) (a) A. C. Hurley, *Proc. Phys. Soc. (London)*, **A69**, 49 (1956); (b) A. C. Hurley, *J. Chem. Phys.*, **28**, 532 (1958).

(4) R. S. Mulliken, *J. Phys. Chem.*, **56**, 295 (1952).

(5) P. C. H. Jordan and H. C. Longuet-Higgins, *Mol. Phys.*, **5**, 121 (1962).

(6) A. L. Companion and F. O. Ellison, *J. Chem. Phys.*, **32**, 1132 (1960).

(7) F. O. Ellison, *ibid.*, **36**, 3112 (1962).

(1) Supported in part by a grant from the National Science Foundation.

(2) W. Moffitt, *Proc. Roy. Soc. (London)*, **A210**, 245 (1951).

The starting formula is eq. 3 with the important qualification that the effective nuclear charges for all orbitals comprising ψ_i^A and ψ_i^B are subject to modification. We shall make the simplification that a given atomic orbital will possess the same effective nuclear charge throughout all ψ_n . From here on in this paper, the ψ_n in eq. 1 and 4 will be considered to be in the VB basis.³ Thus, the ground state of H_2 is approximated using covalent and ionic functions

$$\begin{aligned}\psi_1 &= 2^{-1/2} [|a\bar{b}] - |\bar{a}b|] \\ \psi_2 &= 2^{-1/2} [|a\bar{a}] + |b\bar{b}|] \quad (5)\end{aligned}$$

these are given here in terms of determinantal wave functions, in which a represents a $1s$ orbital with arbitrary effective nuclear charge ζ situated on atom A ; a bar over the orbital indicates β -spin, no bar indicates α -spin.

In general, eq. 3 is rewritten

$$H_{nm} = 1/2[S_{nm}'(W_n + W_m) + V_{nm}' + V_{mn}'] \quad (6)$$

where the primes on S_{nm}' and the V_{nm}' indicate that these are evaluated using approximate orbital wave functions. The absence of the 0-superscripts on the W_n (cf. eq. 3) means that these now represent semi-empirical valence state energies of component hypothetical atoms or ions which have had their valence shells "inflated" or "deflated" to yield a best fit to the molecular eigenfunction.

It has been shown⁸ that if all electron coordinates in an exact atomic eigenfunction are multiplied by a factor γ , the energy $W_i(A)$ of the modified eigenfunction is related to the true energy $W_i^0(A)$ as

$$W_i(A) = W_i^0(A)\gamma(2 - \gamma) \quad (7)$$

For example the energy of a modified H-atom is $W(H) = -(13.61 \text{ e.v.})\zeta(2 - \zeta)$. For H^- , the orbital exponent in the best $(1s)^2$ wave function is 0.6875; to modify this function so that it is of the same "size" as an H-atom with orbital exponent ζ , the electron coordinates in H^- need to be multiplied by $\gamma = \zeta/0.6875$. Assuming that the best orbital description is in close correspondence to the true electron density of H^- , the "true" energy of modified H^- is $W(H^-) = W^0(H^-)\gamma(2 - \gamma)$, where $\gamma = \zeta/0.6875$. Thus in eq. 6

$$\begin{aligned}W_1 &= 2W(H) = -(27.21 \text{ e.v.})\zeta(2 - \zeta) \\ W_2 &= W(H^-) = -(14.35 \text{ e.v.})\gamma(2 - \gamma) \quad (8)\end{aligned}$$

$W^0(H^-) = -14.35 \text{ e.v.}$ is the exact energy of H^- .⁹

Using eq. 5 it is easy to show that $S_{11}' = S_{22}' = (1 + S^2)$ and that $S_{12}' = 2S$, where S is the $1s_a-1s_b$ overlap integral. Elements in the V' -matrix can be expressed as

$$\begin{aligned}V_{11}' &= (aa:V_1:bb) + (ab:V_1:ab), \\ V_{22}' &= (aa:V_2:aa) + (ab:V_2:ab), \quad (9) \\ V_{ij}' &= 2(aa:V_i:ab), \quad i \neq j\end{aligned}$$

where

$$\begin{aligned}(ab:V_i:cd) &= \int a(1)b(1)V_i c(2)d(2) dv(1)dv(2) \\ V_1 &= -1/r_{2a} - 1/r_{1b} + 1/r_{12} + 1/R \quad (10) \\ V_2 &= -1/r_{1b} - 1/r_{2b} + 1/R\end{aligned}$$

The two coulomb-type integrals may be expressed in terms of the basic two-center nuclear attraction integral $(A:bb)$ and electron repulsion integral $(aa:bb)$ as well as the nuclear repulsion term $1/R$,¹⁰ or alternatively in the forms

$$\begin{aligned}(aa:V_1:bb) &= 2\alpha - \beta \\ (aa:V_2:aa) &= 2\alpha - 1/R \quad (11)\end{aligned}$$

where $\alpha = 1/R - (A:bb)$ and $\beta = 1/R - (aa:bb)$.

The Mulliken approximation¹¹ for overlap distributions is utilized in estimating exchange- and hybrid-type integrals; that is, we assume

$$a(1)b(1) = 1/2S[a(1)a(1) + b(2)b(2)] \quad (12)$$

Thus

$$\begin{aligned}(ab:V_i:ab) &= 1/4S^2[(aa:V_i:aa) + (aa:V_i:bb) + \\ & (bb:V_i:aa) + (bb:V_i:bb)] \quad (13)\end{aligned}$$

In addition to two-center interactions α , β , and $1/R$, there appear in these new integrals additional interactions of the one-center variety; e.g.

$$(aa:V_1:aa) = -(A:aa) + (aa:aa) - \alpha \quad (14)$$

But $(A:aa) - (aa:aa)$ can be associated with the change in potential energy accompanying the process

$$H^- = H + 1e^-, \Delta V = (A:aa) - (aa:aa) \quad (15)$$

We shall denote this particular ΔV by the symbol $I_h(h^2)$ hereafter. Since all orbitals being used are assumed to contain the same effective charge, it would be improper to associate $I_h(h^2)$ with twice the electron affinity (the electron affinity being ΔE for the process, which according to the virial theorem is equal to one-half ΔV). Rather, this ΔV is for the reaction involving hypothetical species which have been appropriately rescaled. It can be shown⁸ that if all electron coordinates in an exact atomic eigenfunction are multiplied by a factor γ , the potential energy $V(A)$ of the modified eigenfunction is related to the actual potential energy $V^0(A)$ as

$$V(A) = V^0(A)\gamma = 2W^0(A)\gamma \quad (16)$$

Using $\gamma = \zeta/0.6875$ for H^- , we obtain $I_h(h^2) = (14.54 \text{ e.v.})\zeta$. Similarly, for the process $H = H^+ + 1e$, $\Delta V = (A:aa) = I_h(h) = (27.21 \text{ e.v.})\zeta$.

In these ways, elements of the V' -matrix (eq. 9) can be expressed in terms of the overlap integral S , the two-center coulomb interactions α , β , and $1/R$, and the semi-empirical one-center terms $I_h(h^2)$ and $I_h(h)$. The final expressions are

(8) F. O. Ellison, *J. Chem. Phys.*, to be published.

(9) L. R. Henrich, *Astrophys. J.*, **99**, 59 (1944).

(10) S. Fraga and R. S. Mulliken, *Rev. Mod. Phys.*, **32**, 254 (1960).

(11) R. S. Mulliken, *J. chim. phys.*, **46**, 497 (1949).

$$V_{11}' = 2\alpha - \beta + \frac{1}{2}S^2[2\alpha - \beta + 1/R - I_h(h^2) - I_h(h)]$$

$$\frac{1}{2}(V_{12}' + V_{21}') = \frac{1}{2}S[6\alpha - \beta - I_h(h) - I_h(h^2) - 1/R] \quad (17)$$

$$V_{22}' = 2\alpha - 1/R + \frac{1}{2}S^2[2\alpha - 2I_h(h^2)]$$

The evaluation of $I_h(h^2)$ and $I_h(h)$ already has been noted. The integrals α and β are computed theoretically.^{10,12} Final results are shown in Table I.

TABLE I
ELECTRONIC ENERGY OF GROUND STATE H₂

R (Å.)	ρ	Dissociation energy (kcal.) ^a	
		Calcd.	Obsd. ^b
0.65	1.14	96.6	103.2
.74	1.07	105.7	109.3
.82	1.07	109.2	
.89	1.07	108.6	103.2
1.06	1.00	99.2	89

^a Energy of ground state atoms minus molecular energy for nuclei fixed at distance R . ^b J. O. Hirschfelder and J. W. Linnett, *J. Chem. Phys.*, **18**, 130 (1950).

Agreement with observed energies is quite remarkable, even more so if the calculated results are displaced by about 0.1 Å. to smaller R . It should be remembered, however, that the approximations utilized in this model are not few: only two VB functions are admitted (eq. 5), the basic eq. 6 is approximate,¹³ the Mulliken approximation is used,¹⁴ semi-empirical W_i (eq. 8) and one-center potential energies (eq. 16) are employed. Coefficients for *normalized* covalent and ionic structures, ψ_1 and ψ_2 , are $c_1 = 0.7174$ and $c_2 = 0.0963$ at $R = 0.74$ Å. The structure projections or occupation numbers^{3,15}

$$n_i = c_i \sum_j S_{ij}c_j \quad (18)$$

are $n_1 = 0.886$ and $n_2 = 0.114$ (i.e., 11.4% ionic character).

Application to LiH, BeH, and BH.—The ground and lower excited states of diatomic hydrides for first row elements can be classified according to the number of lone-pair σ -electrons (having principal quantum number 2) in their associate covalent structures. For example, for ground state LiH, BeH, and BH, this number is 0, 1, and 2, respectively. These shall be referred to as case 0, case 1, and case 2. For each such case, we consider five VB basis wave functions

for case 0

$$\begin{aligned} A(\text{sh})\text{H} & \quad \psi_1 = 2^{-1/2} [|s\bar{h}| - |\bar{s}h|] \\ A(\text{zh})\text{H} & \quad \psi_2 = 2^{-1/2} [|z\bar{h}| - |\bar{z}h|] \\ A^+(\text{h})^2\text{H}^- & \quad \psi_3 = |h\bar{h}| \\ A^-(\text{s})^2\text{H}^+ & \quad \psi_4 = |s\bar{s}| \\ A^-(\text{sz})\text{H}^+ & \quad \psi_5 = 2^{-1/2} [|s\bar{z}| - |\bar{s}z|] \end{aligned}$$

(12) C. C. J. Roothaan, *J. Chem. Phys.*, **19**, 1445 (1951).

(13) For an analogous exact approach, see T. Arai, *ibid.*, **26**, 451 (1957).

(14) For a discussion of its errors, see R. S. Barker, H. Eyring, C. J. Thorne, and D. A. Baker, *ibid.*, **22**, 699 (1954).

(15) J. C. Browne, *ibid.*, **36**, 1814 (1962).

for case 1

$$\begin{aligned} A(\text{s})(\text{zh})\text{H} & \quad \psi_1 = 2^{-1/2} [|s\bar{z}h| - |s\bar{z}h|] \\ A(\text{z})(\text{sh})\text{H} & \quad \psi_2 = 2^{-1/2} [|s\bar{z}h| - |\bar{s}zh|] \\ A^-(\text{s})^2(\text{z})\text{H}^+ & \quad \psi_3 = -|s\bar{s}z| \\ A^+(\text{s})(\text{h})^2\text{H}^- & \quad \psi_4 = |sh\bar{h}| \\ A^+(\text{z})(\text{h})^2\text{H}^- & \quad \psi_5 = -|zh\bar{h}| \end{aligned}$$

for case 2

$$\begin{aligned} A(\text{s})^2(\text{zh})\text{H} & \quad \psi_1 = 2^{-1/2} [|s\bar{s}z\bar{h}| - |s\bar{s}z\bar{h}|] \\ A(\text{z})^2(\text{sh})\text{H} & \quad \psi_2 = 2^{-1/2} [|s\bar{s}z\bar{h}| - |\bar{s}z\bar{z}h|] \\ A^-(\text{s})^2(\text{z})^2\text{H}^+ & \quad \psi_3 = |s\bar{s}z\bar{z}| \\ A^+(\text{sz})(\text{h})^2\text{H}^- & \quad \psi_4 = 2^{-1/2} [|s\bar{z}h\bar{h}| - |s\bar{z}h\bar{h}|] \\ A^+(\text{s})^2(\text{h})^2\text{H}^- & \quad \psi_5 = |s\bar{s}h\bar{h}| \quad (19) \end{aligned}$$

In these equations, s and z represent the 2s and 2p σ orbitals on the heavier atom and h represents a 1s-orbital on hydrogen. The various excited states of these hydrides are obtained by interjecting appropriate numbers of 2p π -electrons, with proper pairing of spins, into the above expressions. For example, the ³Π excited state of BH belongs to case 1, the first structure being

$$B(\pi)(\text{s})(\text{zh})\text{H} \quad \psi_1 = 2^{-1/2} [|\pi s\bar{z}h| - |\pi s\bar{z}h|] \quad (20)$$

The 1s electrons on the heavier atom have not been written into the wave functions; however, effects of exchange repulsion between these electrons and those on hydrogen have been included.

In addition to the above, two rather unusual cases are considered, namely, the a³Π and A¹Π states of LiH. For each of these, only one VB structure was found to be significant, Li(π)(h)H and Li(π h)H, respectively.

Since theoretically computed overlap and coulomb integrals over orbitals containing Slater effective nuclear charges were the only ones readily available for these systems, variations of effective charges were not attempted. The first step, therefore, was to estimate the hypothetical valence state energies W_n appearing in eq. 6.

To obtain the energy of say B⁻(s)²(z)² in which the effective charges of s and z are not optimized with respect to energy but rather are given by Slater's rules for neutral B, one cannot use eq. 7 directly since the factor γ rescales the total wave function, including the inner 1s-shell. We use an approach based upon Hurley's hypothesis² that correlation energy is independent of effective nuclear charge. Let W' be the calculated energy of an atom or ion state using orbital wave functions, in which W' has been minimized with respect to all Z_{eff} 's. Let W'' be a similarly calculated energy using all Slater Z_{eff} 's for the neutral atom. We then assume that

$$W'' - W' = W - W^0$$

$$\text{or } W = W'' - W' + W^0 \quad (21)$$

The W' and W'' for all required stationary states of Li, Be, and B and their positive and negative ions

were calculated¹⁶ using energy expressions similar to those given by Roothaan.¹⁷ Corresponding observed W^0 values were obtained using data given by Moore.¹⁸ Values of W and W^0 for states of Li, Li⁻, Be⁺, Be, and B⁺, given relative to the ground states of the neutral atom, are listed in Table II (corresponding values for Li⁺, Be⁻, B, and B⁻ furnished on request). From these energies, valence state energies W_n for the various VB structures were obtained in the conventional manner.¹⁹

TABLE II

RESCALED ENERGIES OF ATOMS AND IONS (e.v.) ^a						
Electronic state	Li		Be ⁺		W^0	W
	W^0	W	W^0	W		
1s ² s, ² S	0	0	9.32	9.54		
1s ² p, ² P	1.85	2.03	13.28	13.37		
	Li ⁻		Be		B ⁺	
1s ² s ² , ¹ S	-0.54	0.32	0	0	8.30	8.64
1s ² s ² p, ³ P	(0.16)	1.89	2.72	2.81	12.92	13.39
1P	(0.26)	4.78	5.28	6.21	17.40	17.77
1s ² p ² , ³ P	(1.66)	4.03	7.40	7.64	20.56	20.83
1D	(0.46)	3.19	6.99	7.36	20.99	21.15
1S	(1.46)	4.79	8.86	9.47	24.12	24.18

^a W^0 and W are observed and rescaled energies, respectively, relative to ground state of neutral atom. Values in parentheses are extrapolated.

Expressions for elements of the S' -matrix in terms of basic overlap integrals are easily obtained using eq. 19. Diagonal elements of the V' -matrix may be expressed first in terms of coulomb and exchange integrals using the conventional VB perfect pairing energy formula.²⁰ The coulomb energy¹⁰ and the complete S' -matrices are calculated using theoretically computed integrals.²¹

The method for evaluating exchange integrals is essentially the same as for H₂. For example, in ψ_1 (LiH) the integral $K(h,s)$ obtained on electron exchange between s and h is

$$\int k_1 k_2 s_4 h_3 V_1 k_1 k_2 s_3 h_4 dv = (k^2, k^2, h s; V_1: h s) = \\ \frac{1}{4} S_{hs}^2 [(k^2, k^2, h^2; V_1: h^2) + (k^2, k^2, h^2; V_1: s^2) + \\ (k^2, k^2, s^2; V_1: h^2) + (k^2, k^2, s^2; V_1: s^2)] \quad (22)$$

in which

$$V_1 = -3/r_{4Li} - 1/r_{1H} - 1/r_{2H} - 1/r_{3H} + \\ 1/r_{14} + 1/r_{24} + 1/r_{34} + 3/R \quad (23)$$

The numerical subscripts on orbitals in eq. 22 and on distances r in eq. 23 refer to electrons, 1-3 assigned to Li, 4 to H; similarly in the symbolic

(16) The author gratefully acknowledges the assistance of Mr. Norman T. Huff in programming and executing these calculations.

(17) C. C. J. Roothaan, Technical Report, Laboratory of Molecular Structure and Spectra, Department of Physics, University of Chicago, 1955, p. 24.

(18) C. E. Moore, "Atomic Energy Levels," Natl. Bur. Standards (U. S.) Circular 467, Vol. 1.

(19) A. L. Companion and F. O. Ellison, *J. Chem. Phys.*, **28**, 1 (1958); F. O. Ellison, *ibid.*, **36**, 3107 (1962).

(20) H. Eyring, J. Walter, and G. E. Kimball, "Quantum Chemistry," John Wiley and Sons, Inc., New York, N. Y., 1944, p. 248. Single exchange integrals are the only type which arise in the diagonal elements except in the last two structures for case 2. Exchange integrals involving simultaneous exchange of two electron pairs occur here and have been included (see footnote 7).

(21) For LiH, these were obtained from ref. 3; for BeH from I. Fischer, *Arkiv Fysik*, **5**, 349 (1952); and for BH from R. C. Sahni, *J. Chem. Phys.*, **25**, 332 (1956).

representations of integrals, the three orbitals to the left of the operator V_1 contain electrons 1-3, the orbitals to the right electron 4. Equation 22 involves the Mulliken approximation, eq. 12, of electron distributions 3 and 4. Just as in H₂, one-center potential energy terms appear. For example, the first integral within brackets contains the term $-I_h(h^2)$, the potential energy change when one electron is removed from a hypothetical hydride ion of appropriate size; in this case $I_h(h^2) = 14.54$ e.v. The last integral contains the term $-I_s(k^2s^2)$, associated with the process

$$\text{Li}^-(k^2s^2) = \text{Li}(k^2s) + 1e, \Delta V = I_s(k^2s^2) \quad (24)$$

where again, the ΔV used is not simply twice the electron affinity of Li, but rather the ΔV obtained by first adjusting potential energies of Li⁻ and Li for change in effective nuclear charges from their optimum values to their neutral atom Slater values. As in eq. 21, we assume that for each atom or ion state, $V = V'' - V' + V^0 = V'' - 2W' + 2W^0$, the last step being due to the virial theorem.

Other one-center interactions appearing in the LiH problem are

$$I_s(k^2s), I_s(k^2sz), I_z(k^2z^2), I_z(k^2sz), I_z(k^2z), I_k(k^2s^2), \\ I_k(k^2sz), I_k(k^2z^2)$$

It was found that the final results were not appreciably affected by using an average I_s , average I_z , and average I_k .²²

Expansion of the integrals in eq. 22 yields not only one-center potential energies already discussed, but also two-center terms like $1/R$, α_h , and β_h (equivalent to α and β in eq. 11), and α_t and β_t , where $\alpha_t = 1/R - (A/tt)$, $\beta_t = 1/R - (hh:tt)$, and $t = s, z, \text{ or } k$. All of the α 's and β 's are small compared with the one-center potential energies with which they are combined inside of the exchange integrals (*cf.* eq. 17); they therefore were neglected in calculating exchange integrals for LiH, BeH, and BH.²³ All $1/R$ terms left over were retained, however.

Final expressions for $K(h,s)$, $K(h,z)$, and $K(h,k)$ are of the form

$$K(h,t) = -\frac{1}{4} S_{ht}^2 \sum_i c_i X_i \quad (25)$$

where the X_i are $I_h(h)$, $I_h(h^2)$, I_s , I_z , I_k , $(kk:kk)$, and $1/R$; the c_i are coefficients. These are given in Table III.

Off-diagonal elements in the V' -matrix can be treated in precisely the same way as the $K(h,t)$. They may be expressed in the form

$$\frac{1}{2}(V_{nm}' + V_{mn}') = -\frac{1}{4} S_{nm}' \sum_i c_i X_i \quad (26)$$

Coefficients are given in Table III.

(22) These average values are, respectively, as follows (in e.v.): for LiH, 7.42, 5.70, and 167.56; for BeH, 18.41, 14.72, and 312.67; for BH, 34.72, 26.22, and 499.37. In the exchange integral $K(h,k)$, there also appear two-electron repulsion integrals $(kk:kk)$; exact values for these obtained from experimental energies of two-electron ions are 42.7, 59.7, and 76.6 e.v. for Li, Be, and B, respectively.⁸

(23) For H₂, neglect of the α and β inside of the brackets in eq. 17 would cause the binding energy to increase by about 20 kcal. Change is particularly noticed in the off-diagonal element containing $6\alpha - \beta$. In molecules other than H₂, these coulomb terms may take on even greater importance.¹⁰

TABLE III

COEFFICIENTS IN EQUATIONS 25 AND 26 FOR EXCHANGE INTEGRALS AND OFF-DIAGONAL ELEMENTS OF V' -MATRIX

(nm) Case ^a	$I_h(h)$ ^b	$I_h(h)$	I_s	I_x	1/R
(12)0, (12)2	1	1	1	1	-2
(12)1	1	1			-2
(13)0, (15)1, (25)1, (14)2	1		1		1
(14)0, (25)0, (13)1, (23)1, (23)2		1	1		1
(15)0, (13)2		1	1		1
(23)0, (24)1, (14)1, (15)2, (24)2	1		1		1
(34)0, (35)1		2	2		
(35)0, (34)1, (34)2		2	1	1	
(45)1, (45)2	2		1	1	
(35)2		2		2	
$K(hs)$	1	1	2		-2
$K(hz)$	1	1		2	-2
$K(hk) - 2I_k + (kk:kk)$	1	1			-2

^a Numbers in parentheses give nm in V_{nm} , number following gives case number. For (24)0, (45)0, and (25)2, $V_{nm}' = 0$.

Results for LiH, BeH, and BH.—The calculated ground state dissociation energies D_0 and vertical excitation energies T_v are compared with observed values in Table IV. Results are good for LiH²⁴ and BeH except for the one excitation energy in the latter. The high dissociation energy calculated for BH may be due in part to the neglect of coulomb terms in calculating off-diagonal V_{nm}' ²³; the diagonal coulomb energy for BH has been estimated to be almost twice as large as for LiH.¹⁰ Inasmuch as these calculations have admitted only

TABLE IV

RESULTS FOR LiH, BeH, AND BH^a

Molecular state	$-D_0$ (kcal.)		$-T_v$ (cm. ⁻¹)		T_0 (cm. ⁻¹)
	Calcd.	Obsd.	Calcd.	Obsd.	Obsd.
LiH, X ¹ Σ ⁺	55.1	58.0			
A ¹ Σ ⁺			27360	27223	26516
a ³ Π			34210		
A ¹ Π			37114	37485	34912 ^b
BeH, X ² Σ ⁺	42.2	(53.6)			
A ² Π			11239		20028
A ² Σ ⁺			61464		
B ³ Π			59000		(50934)
BH, X ¹ Σ ⁺	106.9	(81.6) ^c			
a ³ Π			12127		(8956) ^d
A ¹ Π			23446	23105	23105
b ³ Σ ⁻			24447		(36307) ^d

^a All observed values from G. Herzberg, "Molecular Spectra and Molecular Structure," D. Van Nostrand Co., Inc., New York, N.Y., 1950, except where otherwise noted. ^b R. Velasco, *Can. J. Phys.*, **35**, 1204 (1957). ^c A. C. Hurley, *Proc. Roy. Soc. (London)*, **A261**, 237 (1961). ^d Reference 28.

The structure projections or occupation numbers (eq. 18) and gross atomic populations^{26,27} are listed in Table V and compared with those of some other workers. General agreement is somewhat lacking. Omitted from Table V are Hurley's predictions²⁸ for n_3 in the ³Π and ¹Π states of BH, 0.30 and 0.31, respectively (our values: 0.23 and 0.27), and for $n_4 + n_5$ in the ³Σ⁻ state, 0.39 (our value, 0.24).

We calculate for ground state LiH a dipole mo-

TABLE V
ANALYSIS OF LiH, BeH, BH WAVE FUNCTIONS

	Occupation numbers					Gross atomic populations					Source
	n_1	n_2	n_3	n_4	n_5	1s	2s	2p	2p _x	h	
LiH, X ¹ Σ ⁺	0.56	0.16	0.26	0.04	-0.02	2	0.63	0.14		1.23	a
	.42	.17	.41								b
	.58	.29	.20	-.03	-.01	2	.50	0.24		1.27	c
						2	.39	.26		1.35	d
						2	.44	.25		1.31	e
A ¹ Σ ⁺	.24	.61	.05	.09	.01	2	.43	.62		0.96	a
						2	.74	.62		0.64	f
BeH, X ² Σ ⁺	.28	.46	.09	.10	.06	2	1.03	.90		1.07	a
A ² Π	.71	.10	.06	.11	.02	2	0.95	.12	1.00	0.93	a
B ³ Π	.06	.63	.05	.17	.09	2	.49	.72	1.00	0.79	a
A ² Σ ⁺	.01	.13	-.02	.41	.47	2	.51	.59		1.89	a
BH, X ¹ Σ ⁺	.49	.32	.13	.01	.04	2	1.66	1.41		0.93	a
						2	1.81	1.17		1.02	f
						2	1.84	1.13		1.04	g
a ³ Π	.25	.43	.23	.07	.02	2	1.22	0.93	1.00	0.85	a
A ¹ Π	.11	.44	.27	.10	.08	2	1.20	.90	1.00	.90	a
b ³ Σ ⁻	.71	.06	.00	.23	.01	2	1.18	.06	2.00	.76	a

^a This work. ^b Atoms-in-molecules with intraatomic correlation correction, ref. 3. ^c Theoretical VB results, ref. 15. ^d Best limited MO SCF, S. Fraga and B. J. Ransil, *J. Chem. Phys.*, **34**, 727 (1961). ^e SCF MO using Hartree-Fock AO's, ref. 30. ^f Same as e, ref. 31. ^g Same as b, ref. 27.

empirical atomic data and no empirical calibration parameters dependent upon molecular data, the energy results seem encouraging. It is anticipated that further development will require the introduction of molecular parameters in much the same way as is being done in π -electron theory.²⁵

(24) For the LiH ground state, structure 1 by itself gives a binding energy of 30.6 kcal. Mixing in structure 3 gives 46.9, adding structure 2 gives 52.2, adding structure 4 gives 53.2, and finally with 5 yields 51. This type of convergence was found in all cases.

ment of 5.46 D.(Li⁺H⁻), which may be compared with the best limited MO²⁹ value 5.92 D., the modified atoms-in-molecules result³ 6.26 D., and the SCF MO value using Hartree-Fock atomic orbitals,³⁰ 6.05 D. The latter method³¹ yields

(25) P. G. Lykos, *J. Chem. Phys.*, **35**, 1249 (1961).

(26) R. S. Mulliken, *ibid.*, **23**, 1833 (1955).

(27) A. C. Hurley, *Proc. Roy. Soc. (London)*, **A249**, 119 (1958).

(28) A. C. Hurley, *ibid.*, **A249**, 402 (1959).

(29) B. J. Ransil, *Rev. Mod. Phys.*, **32**, 239 (1960).

-4.91 D. (Li-H^+) for excited $A^1\Sigma^+$ LiH and 3.065

(30) A. M. Karo, *J. Chem. Phys.*, **31**, 182 (1959).

(31) A. M. Karo, *ibid.*, **32**, 907 (1960).

D. for the electric transition moment connecting $A^1\Sigma^+$ and $X^1\Sigma^+$; we obtain -4.25 and 4.30 D. for these quantities.

A SIMPLE MOLECULAR ORBITAL STUDY OF AROMATIC MOLECULES AND IONS HAVING ORBITALLY DEGENERATE GROUND STATES

BY LAWRENCE C. SNYDER

Bell Telephone Laboratories, Inc., Murray Hill, New Jersey

Received May 31, 1962

Modifications of simple Hückel molecular orbital theory have been employed to describe the static Jahn-Teller geometrical instability of symmetrical aromatic molecules having orbitally degenerate π electronic ground states in the Hückel approximation. The parameterization of Hückel theory by Longuet-Higgins and Salem has been applied in iterative computations to describe cyclobutadiene (C_4H_4), C_4H_4^+ , tetraphenylcyclobutadiene ($\text{C}_4(\text{C}_6\text{H}_5)_4$), $\text{C}_4(\text{C}_6\text{H}_5)_4^+$, cyclooctatetraene (C_8H_8), and C_8H_8^- . The magnitude of distortion energies and properties of the distorted molecule are estimated. It is noted that the rectangular form of cyclobutadiene is an unstable planar geometry under the parameterization by Lennard-Jones. For the neutral molecules, whose ground states are pseudo-degenerate, the effect of approximate introduction of electron repulsion is shown to be a reduction of the Jahn-Teller instability found by the simpler theory for the lowest energy singlet state. The results of applications of the modified Hückel theory to several other molecules are summarized.

Introduction

In 1937 Jahn and Teller¹ stated that symmetrical molecular systems having an orbitally degenerate ground state may be geometrically unstable with respect to a displacement of atoms which removes that degeneracy. Orbital degeneracy of the π electrons can occur in a simple Hückel² description of planar aromatic systems having a threefold or greater axis of rotational symmetry. It occurs when the highest occupied pair of orbitals is degenerate and contains 1, 2, or 3 electrons. In this case, there is more than one way allowed by the Pauli principle to assign the electrons to these orbitals, and all are degenerate in the Hückel approximation. A list of observed and hypothetical molecules, which if planar would have orbitally degenerate ground states in the Hückel approximation, occurs in Fig. 7 and 8 along with references reporting their experimental properties.

One can anticipate for these molecules unusual phenomena associated with the fact that a small perturbation can remove the apparent degeneracy and cause large fluctuations in properties computed from the wave function. The perturbation may be an interaction with the medium containing the molecule, as has been assumed in an explanation³ of the unusually great electron spin resonance (e.s.r.) line width exhibited by benzene⁻, coronene⁻, and triphenylene⁻.⁴ Displacements of C-C bond lengths also may act as the perturbation.⁵⁻⁹ A strong interaction can cause the molecule to behave as having a distorted geometry. Weaker interac-

tions can lead to effects in Raman and infrared spectra.

This study is a computational exploration of the importance of bond length displacements as a perturbation removing the π electronic orbital degeneracy. Results of detailed calculations are given for cyclobutadiene (C_4H_4), C_4H_4^+ , tetraphenylcyclobutadiene ($\text{C}_4(\text{C}_6\text{H}_5)_4$), $\text{C}_4(\text{C}_6\text{H}_5)_4^+$, cyclooctatetraene (C_8H_8), and C_8H_8^- . A modification of simple Hückel molecular orbital theory is adopted to obtain an estimate of the change in energy when the hypothetical symmetrical molecule of minimum energy is distorted to that set of bond lengths which minimize the total energy. Bond lengths and orders together with charge and spin densities are computed for the distorted molecule. The electronic energy is taken to depend parametrically upon the bond lengths. This is a static Jahn-Teller calculation. The potential energy surfaces obtained for nuclear motion probably can be safely used, with some caution, in classical thinking about the nuclear motions. These calculations are a convenient preliminary to the more complex dynamic description which bears more direct interpretation.^{3,10} Approximate introduction of electron repulsion is made for the neutral molecules to explore its effect on the estimated magnitude of the energy changes upon distortion in the lowest singlet state.

A Simple Molecular Orbital Description.—To attain an approximate description of the interaction of the π electrons with bond length displacements, we adopt a well known model used earlier by Lennard-Jones¹¹ and later by Longuet-Higgins and Salem.¹² The total energy E is taken to be the sum of the π electron energy E_π computed in a modified Hückel approximation plus an energy E_σ taken to be a sum of independent σ bond energies $V(r_{kl})$.

(1) H. A. Jahn and E. Teller, *Proc. Roy. Soc. (London)*, **A161**, 220 (1937).

(2) A. Streitwieser, "Molecular Orbital Theory for Organic Chemists," John Wiley and Sons, New York, N. Y., 1961.

(3) H. M. McConnell and A. D. McLachlan, *J. Chem. Phys.*, **34**, 1 (1961).

(4) M. G. Townsend and S. I. Weissman, *ibid.*, **32**, 309 (1960).

(5) J. E. Lennard-Jones and J. Turkevich, *Proc. Roy. Soc. (London)*, **A158**, 297 (1937).

(6) A. D. Liehr, *Z. physik. Chem. (Frankfurt)*, **9**, 338 (1956).

(7) L. C. Snyder, *J. Chem. Phys.*, **33**, 619 (1960).

(8) W. D. Hobey and A. D. McLachlan, *ibid.*, **33**, 1695 (1960).

(9) C. A. Coulson and A. Golebiewski, *Mol. Phys.*, **5**, 71 (1962).

(10) A. D. Liehr, *Ann. Rev. Phys. Chem.*, **13** (1962).

(11) J. E. Lennard-Jones, *Proc. Roy. Soc. (London)*, **A158**, 280 (1937).

(12) H. C. Longuet-Higgins and L. Salem, *ibid.*, **A251**, 172 (1959).

$$E = E_\pi + E_\sigma \quad (1)$$

$$E_\sigma = \sum_{k>l} V(r_{kl}) \quad (2)$$

A π electron wave function ψ_π is taken to be a simple product of molecular orbitals φ_i with occupation numbers ν_i and which are linear combinations of the π atomic orbitals χ_l .

$$\psi_\pi = \prod_i \varphi_i^{\nu_i} \quad (3)$$

$$\varphi_i = \sum_l C_{il}\chi_l \quad (4)$$

$$E_\pi = \sum_i \nu_i W_i = \sum_j \nu_j W_j + \nu_m W_m + \nu_n W_n \quad (5)$$

$$= E_\pi^{cs} + \nu_m W_m + \nu_n W_n \quad (6)$$

The energy of the π electrons is conveniently expressed as the energy of those in lower closed shells E_π^{cs} plus the energy of those in the degenerate orbitals φ_m and φ_n . The molecular orbital energies W_i are conveniently expressed in this approximation as the sum over all bonds, which join pairs of atoms k and l , of the i th orbital contribution to the bond order p_{kl}^i multiplied by the resonance integral $\beta(r_{kl})$.

$$W_i = \sum_{k>l} 2p_{kl}^i \beta(r_{kl}) \quad (7)$$

$$p_{kl} = C_{ik}C_{il} \quad (8)$$

The qualitative origin of Jahn-Teller geometrical instability in this approximate description may be seen in eq. 7. For the symmetrical molecule, the sum of the partial bond orders of a single chemical type of bond is equal in the degenerate orbitals φ_m and φ_n . A perturbation which shortens one bond and thus increases β in that bond causes a mixing of φ_m and φ_n , removes the degeneracy, and lowers the energy of the π electrons.

The presentation of computational results is conveniently made in terms of the Coulson bond orders p_{kl} and charge densities q_l .²

$$p_{kl} = \sum_i p_{kl}^i \nu_i \quad (9)$$

$$q_l = \sum_i C_{il}^2 \nu_i \quad (10)$$

Properties of the hypothetical symmetrical molecule are computed with the assumption that its wave function is composed of equal components of functions corresponding to the ways allowed by the Pauli principle for $\nu_n + \nu_m$ electrons to be assigned to the degenerate pair of orbitals. The corresponding expression for the π electron energy E_π^{sym} is written

$$E_\pi^{sym} = E_\pi^{cs} + \bar{\nu}W_m + \bar{\nu}W_n \quad (11)$$

where

$$\bar{\nu} = (\nu_m + \nu_n)/2$$

and

$$E_\pi^{sym} = E_\pi^{sym} + E_\sigma$$

In computations of bond orders, and charge densities for the symmetrical molecule, one replaces ν_m and ν_n by $\bar{\nu}$ in eq. 9 and 10.

Parameterization and Computations.—Computations with the expressions of the previous section require the dependence of the resonance integral β and the σ bond potential V on bond length. Several pairs of functions have been developed. Two have been used in this study: the recent expressions by Longuet-Higgins and Salem,¹² and those originated by Lennard-Jones.¹¹

Longuet-Higgins and Salem fitted the A_{1g} and B_{2u} stretching force constants of benzene and a linear bond order-bond length relation to obtain the constants a and β_0 of the equations

$$\beta(r_{kl}) = \beta_0 e^{-(r_{kl}-1.40)/a} \quad (12)$$

$$V(r_{kl}) = 2(6.667)(r_{kl} - 1.50 + a)\beta \quad (13)$$

$$a = 0.3106 \text{ \AA.}$$

$$\beta_0 = -25.56 \text{ kcal.}$$

These equations imply that with a bond order p_{kl} , the energy of a bond is minimum when

$$p_{kl} = 6.667(1.500 - r_{lm}) \quad (14)$$

Several qualitative features of this parameterization are attractive for this study in which bond lengths may exceed the usual small range of lengths found in unsaturated compounds. First, the resonance integral β is approximately proportional to the overlap between two π atomic orbitals on interacting neighbor atoms. Second, the second derivative of β and of the negative of the overlap have the same sign over the interesting range of bond lengths. Third, the σ bond potential has a minimum of about 75 kcal. with respect to the separated atoms; this is approximately the dissociation energy of a carbon-carbon single bond. Finally, the stretching force constant for a bond of zero π bond order is only about 10% greater than the stretching force constant for the C-C bond of ethane.

A classical parameterization is due to Lennard-Jones. It was applied by Lennard-Jones and Turkevich,⁵ by Liehr,^{6,13} and by Snyder⁷ to study the interaction of π electrons with bond length displacements in cyclobutadiene. It is basic in many papers on π electron theory.

$$2\beta(r_{kl}) = \frac{1}{2}K_d(r_{kl} - 1.33)^2 - \frac{1}{2}K_s(r_{kl} - 1.54)^2 - 54.4 \text{ kcal.} \quad (15)$$

$$V(r_{kl}) = \frac{1}{2}K_s(r_{kl} - 1.54)^2 \quad (16)$$

$$K_d = 1410.906 \text{ kcal./\AA.}^2 \quad K_s = 714.091 \text{ kcal./\AA.}^2$$

The constant -54.4 kcal. is added here to give β the magnitude which Coulson and Altman¹⁴ found satisfactory in a study of the resonance energy of benzene. These equations imply that a bond of bond order p_{kl} will have minimum energy at the length r_{kl} given by the equation

(13) A. D. Liehr, *Z. Naturforsch.*, **16a**, 641 (1961).

(14) C. A. Coulson and S. L. Altman, *Trans. Faraday Soc.*, **48**, 293 (1952).

$$r_{k1} = \frac{1.54 + p_{k1}(1.0878225)}{1 + p_{k1}(0.9758064)} \text{ \AA} \quad (17)$$

This parameterization is less satisfactory in several ways. First, the quadratic form of V must be incorrect at large bond distances. Second, the resonance integral β changes sign at large bond lengths. Finally, its second derivative is opposite in sign to that of the negative of the overlap of two π atomic orbitals.

The author believes that the parameterization by Longuet-Higgins and Salem is superior for this study of geometrical instability. Unless otherwise noted, all computations reported here have used those assumptions.

Computations to seek that set of bond lengths which minimizes E^{sym} for the symmetrical molecule or E for the distorted molecule were performed iteratively on an I.B.M. 7090 computer. The following sequence of steps is common to both calculations: (a) The resonance integrals β are given initial values. (b) The eigenvalue problem is solved. (c) The total energy, bond orders, and charge densities are computed from the roots and vectors obtained in b. (d) Bond lengths are computed from eq. 14 with the bond orders obtained in c. (e) The resonance integrals β are revised with eq. 12 and the bond lengths obtained in d. (f) Control is returned to b until the total energy does not change upon iteration.

In the iterations to seek an energy minimum for the symmetrical molecule, all β are initially taken equal. In step c, $\bar{\nu}$ is substituted for ν_m and ν_n in eq. 6, 9, and 10 for energy, bond order, and charge density.

To seek an energy minimum for the distorted molecule, the initial bond lengths are taken to be those computed to minimize E^{sym} , plus an arbitrary small displacement of any or all bond lengths. The initial β values are computed from these displaced bond lengths. The electrons are now assigned to orbitals φ_m and φ_n computed in b so as to fill the lower energy orbital first.

Early in this study, a subroutine was written to generate a complete set of C-C bond length displacements having the character of the symmetry group of the π electron Hamiltonian. The change in E upon adding or subtracting each of this complete set of bond length displacements to the bond lengths found for the symmetrical molecule was studied. It was found for molecules with a 3-, 5-, 6-, or 7-fold axis of rotation that only a *single* degenerate pair of bond length displacements gave a stabilizing Jahn-Teller interaction with the π electrons. This was found for all such molecules in Fig. 7 and 8. Only a single displacement was found to give a stabilizing interaction for molecules with a 4- or 8-fold axis of rotation. That displacement alternately lengthens and shortens the bonds around the central ring of the six molecules of this study.¹⁵

Results

The computed changes in energy upon distortion for $C_4H_4^+$, $C_4(C_6H_5)_4^+$, and $C_8H_8^-$ are collected in Table I. The stabilization upon distortion is

(15) M. S. Child, *Mol. Phys.*, **3**, 601 (1960).

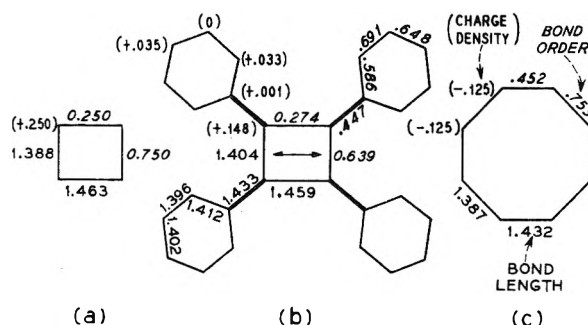


Fig. 1.—Computed Hückel description of distorted (a) $C_4H_4^+$, (b) $C_4(C_6H_5)_4^+$, and (c) $C_8H_8^-$. Spin density equals absolute value of charge density.

TABLE I
DISTORTION ENERGIES IN MOLECULES HAVING DEGENERATE GROUND STATES

Energy change ^a	$C_4H_4^+$	$C_4(C_6H_5)_4^+$	$C_8H_8^-$
ΔE	-2.851	-1.219	-1.804
ΔE_π	-6.397	-3.084	-4.503
ΔE_σ	+3.546	+1.865	+2.699

^a $\Delta E = E_{\text{min}} - E_{\text{sym}}$ in kcal.

about 2 kcal. for each. Computed properties for the distorted molecules are shown in Fig. 1.

It is convenient to discuss the energy of these molecules as a function of a coordinate X , which is a linear combination of displacements of all nearest neighbor bond lengths. We define $X \equiv 0$ for that set of bond lengths which minimizes E^{sym} , and $X \equiv 1$ for that set of bond length displacements which minimizes E of eq. 1.

If the bond length displacements in Fig. 1 are taken to correspond to $X \equiv 1$, then there is a second energy minimum at $X \equiv -1$. Indeed, according to the analysis of McLachlan and Snyder,¹⁶ the ground states of these molecules are doubly degenerate, with the two states corresponding qualitatively to the geometries at $X \equiv 1$ and $X \equiv -1$. Also according to that analysis, these three molecules are expected to have smaller spin density fluctuations and e.s.r. line widths than were exhibited by the negative ions of benzene, coronene, and triphenylene.

The computed stabilization energies for the neutral molecules having pseudo-degenerate ground states are summarized in Table II. The gain in

TABLE II
DISTORTION ENERGIES IN MOLECULES HAVING PSEUDO-DEGENERATE GROUND STATES

Energy change ^a	C_4H_4	$C_4(C_6H_5)_4$	C_8H_8
ΔE	-11.445	-6.83	-7.213
ΔE_π	-25.764	-20.092	-17.975
ΔE_σ	+14.319	+13.258	+10.762

^a $\Delta E = E_{\text{min}} - E_{\text{sym}}$ in kcal.

energy upon distortion is computed to be about four times as large as in the ions. The 6 to 11 kcal. of stabilization would suggest that these hypothetical molecules would exist in a rectangular stable geometry. The computed bond lengths and

(16) A. D. McLachlan and L. C. Snyder, *J. Chem. Phys.*, **36**, 1159 (1962).

แผนกห้องสมุด กรมวิทยาศาสตร์

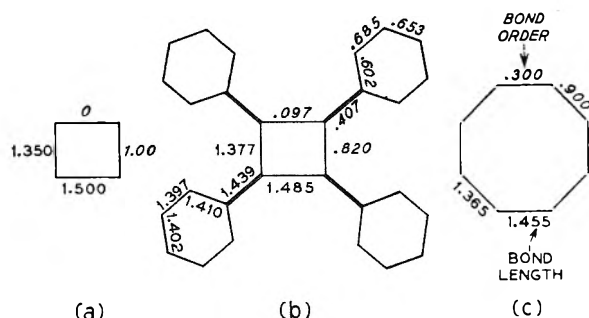


Fig. 2.—Computed Hückel description of distorted (a) C_4H_4 , (b) $C_4(C_6H_5)_4$, and (c) C_8H_8 .

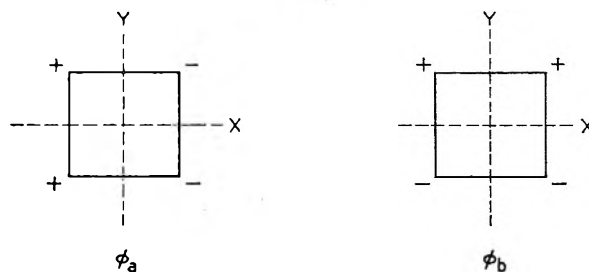


Fig. 3.—Basic molecular orbitals convenient for study of effect of introduction of electron repulsion.

bond orders are shown in Fig. 2. This approximation suggests almost alternating double and single bonds in the ground state. The long bonds have a mobile π order almost zero in C_4H_4 and $C_4(C_6H_5)_4$, suggesting instability with respect to decomposition to acetylene and stilbene. In contrast, the long bonds of distorted $C_4H_4^+$ and $C_4(C_6H_5)_4^+$ have bond orders 0.25 and 0.27. This suggests that these ions may be more stable and easy to prepare than the neutral molecules. The bond length alternation shown in Fig. 2 for cyclooctatetraene⁵ recalls its actual boat form with alternating double and single bonds. In this modified Hückel approximation, the energy required to change distorted C_8H_8 to a planar form with alternating double and single bond lengths and orders is 24.39 kcal. This suggests that the strain relieved upon buckling to non-planarity is of that magnitude.

The present calculations show that in an expression for the potential energy as a function of the bond lengths in the central cyclic ring, for all six molecules, the bonds will be strongly interacting. Evidence for this in Raman spectra of cyclobutadiene derivatives will be an unusually low antisymmetric stretching frequency relative to the symmetrical stretching frequency of the central ring.¹⁷ In the infrared spectra, evidence of this interaction is a tendency of the degenerate E stretching mode to split toward double and single C-C bond stretching frequencies.

Under the assumptions of Lennard-Jones, symmetrical cyclobutadiene is unstable by 20.9 kcal. with respect to a rectangular configuration.⁵⁻⁷ If the stability of this rectangular form with respect to a complete set of bond length displacements is examined, it is found not to correspond to a minimum of the energy.¹⁸ Instead iterative computa-

tions, in which an initial displacement lengthens one single bond and shortens the other, indicate geometrical instability, as shown in Table III. This novel behavior is not, however, to be interpreted as having much chemical meaning. It is a reflection of the cited basic inadequacies of that parameterization. It is true, however, that under both parameterizations E_π decreases under this displacement of the rectangular form.

TABLE III

INSTABILITY OF RECTANGULAR CONFIGURATION OF CYCLOBUTADIENE UNDER LENNARD-JONES PARAMETERIZATION

Iteration	ΔE^a	r_{12}	r_{23}	r_{34}	r_{41}
0	0.0	1.330	1.540	1.330	1.540
1	-26.8	1.330	1.547	1.330	1.533
2	-82.7	1.330	1.533	1.330	1.528
3	-255.9	1.330	1.563	1.330	1.519
4	-803.9	1.330	1.582	1.330	1.505
5	-2645.0	1.331	1.620	1.331	1.482
6	-9997.8	1.335	1.705	1.335	1.447

^a In cal.

Approximate Introduction of Electron Repulsion.—If one introduces electron repulsion, then the three singlet and single triplet functions of the neutral hydrocarbons, which are degenerate in the Hückel approximation, are no longer degenerate: these compounds therefore are said to have pseudo-degenerate ground states. It is of interest to explore the effect of the introduction of electron repulsion on the Jahn-Teller interactions. Elaborate computations have been made to describe the electronic structure of square cyclobutadiene.¹⁹⁻²² Complete configuration calculations indicate that its ground state is a singlet and that the lowest excited state is a triplet. There has been only qualitative discussion of the relation of the introduction of electron repulsion to the Jahn-Teller stabilization of the lowest singlet state.^{23,24}

It is convenient to adopt basis functions like Φ_a and Φ_b in Fig. 3 for the degenerate pair of molecular orbitals. The function Φ_a is antisymmetric with respect to the line $x = 0$. With these orbitals one may write the following functions and approximate expressions for their energy

$${}^1\Psi_{aa} = \{\varphi_a(1) \varphi_a(2)\} \quad E_\pi = E_\pi^{cs} + 2W_a + J_{aa}$$

$${}^1\Psi_{bb} = \{\varphi_b(1) \varphi_b(2)\} \quad E_\pi = E_\pi^{cs} + 2W_b + J_{bb}$$

$${}^1\Psi_{ab} = \frac{1}{\sqrt{2}} \{\varphi_a(1) \varphi_b(2) + \varphi_b(1) \varphi_a(2)\} \\ E_\pi = E_\pi^{cs} + W_a + W_b + J_{ab} + K_{ab}$$

$${}^3\Psi_{ab} = \frac{1}{\sqrt{2}} \{\varphi_a(1) \varphi_b(2) - \varphi_b(1) \varphi_a(2)\} \\ E_\pi = E_\pi^{cs} + W_a + W_b + J_{ab} - K_{ab}$$

(19) G. W. Wheland, *Proc. Roy. Soc. (London)*, **A164**, 397 (1938).

(20) D. P. Craig, *ibid.*, **A202**, 498 (1950).

(21) R. McWeeny, *ibid.*, **A227**, 288 (1955).

(22) D. P. Craig, in "Nonbenzenoid Aromatic Compounds," D. Ginsburg, Ed., Interscience Publishers, Inc., New York, N. Y., 1959, p. 1.

(23) S. Shida, *Bull. Chem. Soc. Japan*, **27**, 243 (1954).

(24) C. A. Coulson, Contribution "The Fundamentals of Conjugation in Ring Systems," to the Chemical Society (London) Symposium, Bristol, 1958, Special Publication No. 12.

(17) T. P. Wilson, *J. Chem. Phys.*, **11**, 369 (1943).

(18) L. C. Snyder, "Symposium on Molecular Structure and Spectroscopy," Ohio State University, Columbus, Ohio, June, 1960, Paper B4, and June, 1961, Paper B7.

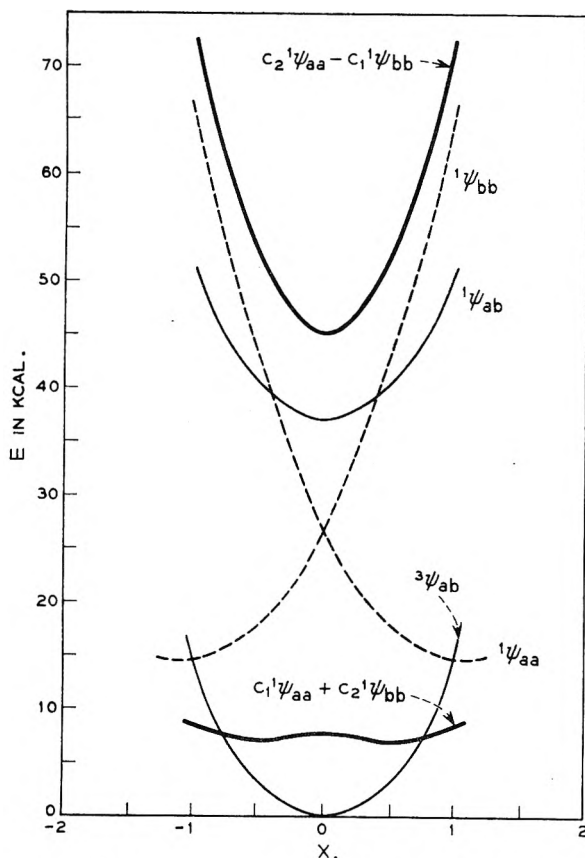


Fig. 4.—Geometrical stability of C_4H_4 states after configuration interaction.

The function ${}^1\Psi_{aa}$ corresponds to the bond length and order alternation depicted in Fig. 2, while ${}^1\Psi_{bb}$ corresponds to the opposite alternation. Of the listed four functions for the symmetrical molecule, only this pair interacts through electron repulsion.

$$({}^1\Psi_{aa} | 1/r_{12} | {}^1\Psi_{bb}) = K_{ab} \quad (18)$$

For the symmetrical molecule the functions ${}^1\Psi_{aa}$ and ${}^1\Psi_{bb}$ interact to form the highest and lowest singlet states, separated by $2K_{ab}$. This important integral contains no contribution of overlap charge distributions. It was computed with the approximations of Parr and Pariser,²⁵ and with the following integrals over atomic orbitals: $(pp|pp) = 10.98$ e.v., $(pp|qq) = 7.1$ e.v. for nearest neighbors, and a classical electrostatic model which places one half π electron 0.82 Å. above and below interacting atoms more distant than nearest neighbors.

After configuration interaction, the lowest singlet is $J_{aa} - J_{ab}$ above the lowest triplet function. This separation depends mainly on overlap charge distributions. Although $J_{aa} - J_{ab}$ has been computed approximately and is listed in Table III, its magnitude is not critical in this study of the effect of the interaction ${}^1\Psi_{aa}$ and ${}^1\Psi_{bb}$ on Jahn-Teller geometrical instability. The qualitative consequence of this interaction is that the minimization of electron repulsion requires an equal mixture of ${}^1\Psi_{aa}$ and ${}^1\Psi_{bb}$, yet the maximization of the interaction with

(25) R. G. Parr and R. Pariser, *J. Chem. Phys.*, **23**, 711 (1955).

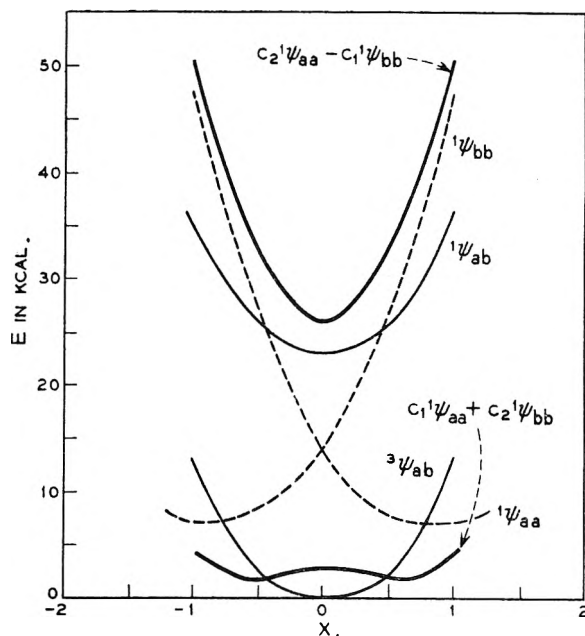


Fig. 5.—Geometrical stability of $C_4(C_6H_5)_4$ states after configuration interaction.

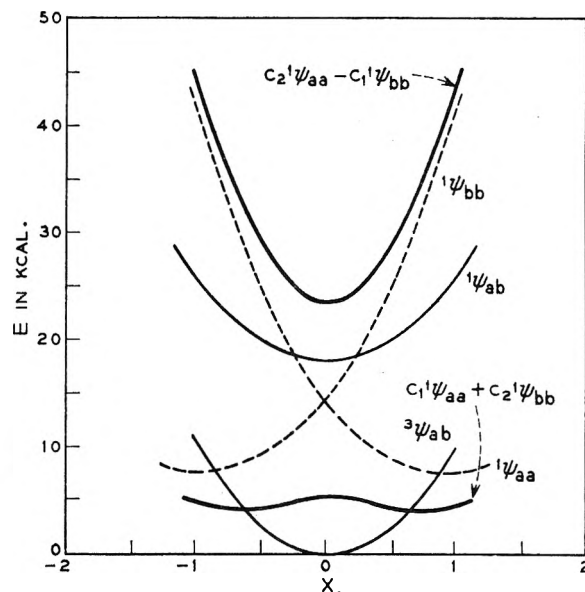


Fig. 6.—Geometrical stability of C_8H_8 states after configuration interaction.

the changing bonds of the core requires ${}^1\Psi_{aa}$ or ${}^1\Psi_{bb}$ alone. Thus, no wave function can achieve maximum Jahn-Teller interaction and minimum electron repulsion simultaneously.

To afford an approximate description of this situation, the following approximations have been made.²⁶ It is assumed that the electron interaction integrals are independent of the bond length displacement X and have values appropriate for $X = 0$. It is assumed that

$$E_{\pi}({}^1\Psi_{aa}; X) = E_{\pi}({}^1\Psi_{aa}; 0) - K_{\pi}X \quad (19)$$

(26) Subsequent to this lecture, a paper has been published which introduces electron repulsion in a similar way to describe large conjugated polyenes: M. Gouterman and G. Wagniere, *J. Chem. Phys.*, **36**, 1188 (1962).







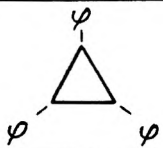
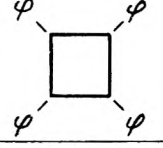
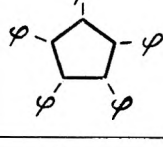
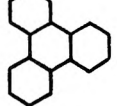
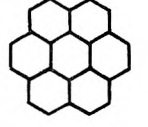
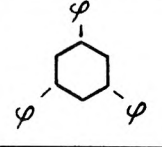
MOLECULE	STRUCTURE	MINIMAL WAVE FUNCTION	$E_{SYM}-E_{MIN}$ (KCAL/MOLE)	$E_{SYM}-E_{SAD}$ (KCAL/MOLE)
C_3H_3		Θ_x Θ_y	2.077(L-S) 4.463(L-J)	2.046(L-S) 3.079(L-J)
$C_4H_4^\pm$		Θ_x OR Θ_y	2.851 4.794	— —
C_5H_5		Θ_x Θ_x	1.459 2.080	1.459 2.053
$C_6H_6^\pm$ ^a		Θ_x Θ_y	1.095 1.615	1.085 1.381
C_7H_7 ^b		Θ_x Θ_y	1.178 1.534	1.178 1.534
$C_8H_8^\pm$ ^c		Θ_x OR Θ_y	1.804 2.356	— —
C_3Ph_3		Θ_x	0.611	0.561
$C_4Ph_4^\pm$		Θ_x OR Θ_y	1.219	—
C_5Ph_5		Θ_x	0.493	0.493
TRIPHENYLENE ^a		Θ_x	0.503	0.495
CORONENE ^a		Θ_y	0.404	0.402
SYM-TRIPHENYL-BENZENE ^a		Θ_x	0.425	0.384

Fig. 7.—Summary of modified Hückel description of geometrical instability of molecules having orbitally degenerate ground states. Parameterizations of Longuet-Higgins and Salem (L-S) and of Lennard-Jones (L-J) are employed. If the last electron enters a molecular orbital with a vertical nodal plane for the distorted molecule of minimum energy, Θ_y is entered; otherwise Θ_x . Experimental observation of these or closely related molecules has been reported: (a) ref. 4, (b) ref. 27, (c) ref. 28.

$$E_\pi(^1\Psi_{bb};X) = E_\pi(^1\Psi_{bb};0) + K_\pi X \quad (20)$$

$$E_\pi(^3\Psi_{ab};X) = E_\pi(^3\Psi_{ab};0) \quad (22)$$

$$E_\pi(^1\Psi_{ab};X) = E_\pi(^1\Psi_{ab};0) \quad (21) \quad \text{where}$$






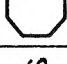
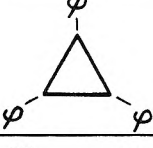
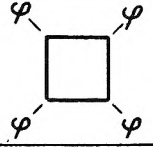
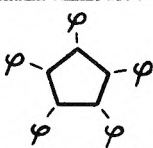
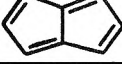
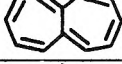
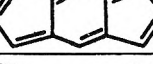
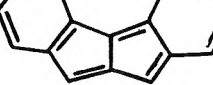
MOLECULE	STRUCTURE	MINIMAL WAVE FUNCTION	E _{SYM} -E _{MIN} (KCAL/MOLE)	E _{SYM} -E _{SAD} (KCAL/MOLE)
C ₃ H ₃ ⁻		A ₁ (C _{2v})	7.429(L-S) DISSOC(L-J)	7.295(L-S) 15.650(L-J)
C ₄ H ₄		¹ ψ _{aa} OR ¹ ψ _{bb}	11.445 DISSOC	— 20.909
C ₅ H ₅ ⁺		A ₁ (C _{2v})	5.249 DISSOC	5.246 9.540
C ₇ H ₇ ⁻ ^a		A ₁ (C _{2v})	4.202 6.550	4.202 6.400
C ₈ H ₈		¹ ψ _{aa} OR ¹ ψ _{bb}	7.213 9.832	— —
C ₈ H ₈ ⁼ ^b		A _{1g} (D _{8h})	0 0	0 0
C ₃ Ph ₃ ⁻		A ₁ (C _{2v})	2.399 DISSOC	2.058 4.638
C ₄ Ph ₄ ^c		¹ ψ _{aa} OR ¹ ψ _{bb}	6.834 DISSOC	— 11.207
C ₅ Ph ₅ ⁺ ^d		A ₁ (C _{2v})	1.838 4.048	1.834 3.761
PENTALENE ^e		A _g (C _{2h})	0.090 0.495	— —
HEPTALENE ^f		A _g (C _{2h})	0.298 0.585	— —
BENZODICYCLO-PENTADIENE		A _g (D _{2h})	0 0	— —
1,2:5,6-DIBENZO-PENTALENE		A ₁ (C _{2v}) A'(C _s)	0 0.008	— —

Fig. 8.—Summary of modified Hückel description of geometrical instability of molecules having pseudo-degenerate ground states. Parameterizations of Longuet-Higgins and Salem (L-S) and of Lennard-Jones (L-J) are employed. Experimental observation of these or closely related molecules has been reported: (a) ref. 27, (b) ref. 28, (c) ref. 29, (d) ref. 30, (e) ref. 31, (f) ref. 32. The lowest four molecules in this table are pseudo-aromatic but not pseudo-degenerate: molecular orbital discussions of their geometric stability have been given in ref. 33 and the second paper of ref. 18.

$$K_{\pi} = -\Delta E_{\pi} \quad (23)$$

Moreover, the average bond length has been found to be almost independent of X in many computations. Thus, we take

$$E_{\sigma} = +K_{\sigma}X^2 \quad (24)$$

$$K_{\sigma} = \Delta E_{\sigma} \quad (25)$$

The values of ΔE_{π} and ΔE_{σ} in eq. 23 and 25 are taken from Table II. Under these assumptions, the energies of the four states after configuration interaction have been computed at $X = 0$, $X = 1$, and X_{\min} , which minimizes the energy of the lowest singlet state.

$$X_{\min}^2 = \left(\frac{K_{\pi}}{2K_{\sigma}} \right)^2 - \left(\frac{K_{ab}}{K_{\pi}} \right)^2 \quad (26)$$

$$E_{\min} = E_{\pi} (\Psi_{aa} : 0) - \frac{K_{\pi}^2}{4K_{\sigma}} - \frac{K_{\sigma} K_{ab}^2}{K_{\pi}^2} \quad (27)$$

The resulting description of the interacted states and their energy dependence on the displacement X are summarized in Fig. 4 to 6 and Table IV. The important observation to make is that whereas the lowest singlet of the neutral molecules is stabilized on distortion by 6 to 11 kcal. in the simpler approximation; with the introduction of electron repulsion, a shallow minimum of only 1.3 kcal. or less occurs. For these pseudo-degenerate neutral molecules, the simple Hückel theory almost certainly greatly overestimates the Jahn-Teller stabilization on distortion.

TABLE IV
GEOMETRICAL INSTABILITY WITH CONFIGURATION
INTERACTION

	C ₄ H ₄	C ₄ (C ₆ H ₆) ₄	C ₆ H ₆
$E_{\min} - E_{\text{sym}}^a$	-0.46	-0.46	-1.27
X_{\min}	± 0.53	± 0.49	± 0.67
$C_1^2 \min^b$	0.91	0.93	0.95
K_{ab}	18.5	11.4	9.0
K_{π}	25.8	20.1	17.9
K_{σ}	14.4	13.3	10.8
$J_{aa} - J_{ab}$	7.85	2.54	5.54

^a All energies in kcal. ^b See Fig. 4-6.

Summary

Molecules having orbitally degenerate ground states usually are chemically labile and difficult to separate and study by classical chemical methods. The advent of electron spin resonance, nuclear magnetic resonance, and other advances in chemical technology have made these molecules suitable for scientific study. The vigorous efforts of organic chemists are daily adding to the list of observed

species having orbitally degenerate ground states in a Hückel description of a hypothetical planar state.²⁷⁻³⁰ The iterative modified Hückel calculations described here have been applied to study the possible geometrical stability of many molecules. A partial summary of the computed results is made in Fig. 7 and 8. This summary should provide a qualitative picture of the importance of the interaction of π electrons with bond length displacements in these molecules. As was noted, in molecules with a 3-, 5-, 6-, or 7-fold axis, a degenerate pair of bond length displacements interacts with the π electrons. As has been shown by Liehr¹³ and by Coulson and Golebiewski,⁹ there may occur both minima and saddle-points in the total energy as a function of these displacements. In Fig. 7 and 8, energy minima are referred to by E_{\min} , and energy saddle-points are referred to by E_{sad} . More detailed discussions of the results for some of the aromatic negative ions and for the pseudo-aromatic molecules are planned.

It is the author's hope that these computations, while admittedly approximate, will stimulate research in this area.

Acknowledgments.—The author wishes to thank Dr. A. D. Liehr for introducing him to the study of molecules having orbitally degenerate ground states, and Professor R. Breslow and Dr. H. H. Freedman for discussions of some of their experimental findings.

(27) R. Breslow and H. W. Chang, *J. Am. Chem. Soc.*, **84**, 1484 (1962).

(28) T. J. Katz and H. L. Strauss, *J. Chem. Phys.*, **32**, 1873 (1960); T. J. Katz, *J. Am. Chem. Soc.*, **82**, 3784, 3785 (1960).

(29) H. H. Freedman, *ibid.*, **83**, 2195 (1961).

(30) R. Breslow and H. W. Chang, *ibid.*, **83**, 3727 (1961).

(31) T. J. Katz and M. Rosenberger, *ibid.*, **84**, 865 (1962).

(32) H. J. Dauben and D. J. Bertelli, *ibid.*, **83**, 4558 (1961).

(33) P. C. Den Boer-Veenendaal and D. H. W. Den Boer, *Mol. Phys.*, **4**, 33 (1961).

π -DELOCALIZATION IN BUTADIENE AND CYANOGEN¹

BY ROBERT S. MULLIKEN

Departments of Physics and Chemistry, University of Chicago, Chicago 37, Illinois

Received June 8, 1962

An examination of Coulson bond orders and of overlap populations obtained from Clementi and McLean's all-electron SCF-LCAO-MO calculations on C₂N₂ shows a close parallelism to corresponding quantities obtained from π -electron-only SCF-LCAO-MO calculations on 1,3-butadiene, thus giving support to the validity of the latter. Comparisons of overlap populations for the hypothetical unconjugated butadiene or cyanogen, for the related molecules C₂H₄ or HCN, and for the actual conjugated molecules, show a consistent picture of the effects of π -electron delocalization. This picture is more instructive than that which is seen in similar comparisons of Coulson bond orders.

Introduction

As is well known from π -electron-only LCAO-MO calculations on conjugated π -electron systems, conjugation is accompanied by π -electron delocalization which increases the Coulson bond order from zero to a finite value for a single bond located between two double bonds, at the same time slightly decreasing the bond orders of the double bonds. When the self-consistent-field (SCF) form of the

method including overlap is used, the computed effects, which are much smaller than when the simple Hückel method is used, are of reasonable magnitude. However, the calculated results still involve the assumption that the effects of the numerous non- π electrons present can be adequately represented by the usual simplified model for the σ -electron core.

Recent *all-electron* SCF-LCAO-MO calculations by Clementi and McLean² on one of the simplest

(1) This work was assisted by the Office of Naval Research under Contract Nonr-2121(01).

(2) E. Clementi and A. D. McLean, *J. Chem. Phys.*, **36**, 563 (1962).

conjugated systems, cyanogen ($\text{N}\equiv\text{C}-\text{C}\equiv\text{N}$), taken in connection with all-electron calculations by McLean on HCN,³ now tend strongly to remove possible doubts about the validity of the assumption mentioned, since with respect to π -electron delocalization the results closely parallel those of the π -electron-only SCF method on butadiene. To be sure, the conjugation in C_2N_2 is between somewhat polar triple bonds, whereas that in the otherwise similar case of 1,3-butadiene is between non-polar double bonds. However, probably the only really important difference involved is the presence of twice as many π -electrons in cyanogen, which should affect only the absolute, not the relative, bond orders of the middle and outer bonds.

In connection with both sets of calculations, it should be pointed out (as is true of most calculations to date) that only the simplest LCAO expressions (one π -atomic orbital per atom) were used. Hence accurate SCF MO's, to obtain which several AO's per atom must be used, were not found in either case. Nevertheless the expressions used were equally flexible in the two cases, and there is no particular reason to suppose that with accurate SCF MO's their parallelism would be upset. However, it is conceivable that calculations with accurate SCF MO's might lead to different results in both cases.

Here it should be noted also that with accurate SCF MO's, constructed from several AO's per atom, there is difficulty⁴ in maintaining the simple concepts of bond order and of overlap population which are easily set up when only one AO per atom is used.

Bond Order Changes in Conjugation.—The parallelism between butadiene and cyanogen is shown in Fig. 1, where bond orders for "unconjugated" are compared with those for actual, conjugated, butadiene, and for unconjugated with those for conjugated cyanogen. Comparisons of butadiene with two C_2H_4 , and of C_2N_2 with two HCN, systems with the same numbers of double or triple bonds in each respective case, also are given.

To obtain the Coulson bond orders for actual C_2N_2 and HCN, the coefficients in the occupied π MO's of these molecules as determined by McLean and Clementi have been renormalized to correspond to assuming all overlap integrals to be zero. The product $c_k c_l$ of the LCAO coefficients c_k and c_l of the atomic orbitals of any pair of neighboring atoms, k and l , times two because each MO is occupied by two electrons, then is formed in the usual way. The resulting number is the contribution of the MO to the π -bond order for the bond between atoms k and l . The total kl bond order p then is obtained by summing over all occupied π MO's: $p = 2\sum(\text{MO's})c_k c_l$.

In LCAO approximation, the occupied π MO's in C_2H_4 or HCN, or in butadiene or cyanogen, are of the forms

$$\text{C}_2\text{H}_4 \text{ or HCN: } \phi = c_a \pi_a + c_b \pi_b \quad (1)$$

$$\text{Butadiene or C}_2\text{N}_2:$$

$$\phi_1 = c_{1a} \pi_a + c_{1b} \pi_b + c_{1c} \pi_c + c_{1d} \pi_d$$

$$\phi_2 = c_{2a} \pi_a + c_{2b} \pi_b - c_{2c} \pi_c - c_{2d} \pi_d \quad (2)$$

In HCN and C_2N_2 , eq. 1 and 2 refer to both π_x and π_y electrons.

In C_2H_4 , $c_a = c_b = [2(1 + S)]^{-1/2}$, where S is the overlap integral $\int \pi_a \pi_b dv$. If S is neglected, $c_a = c_b = 2^{-1/2}$, hence the Coulson π -bond order is $(2)(2^{-1/2})(2^{-1/2}) = 1$.

For "unconjugated" butadiene, $c_{1a} = c_{1b} = c_{2a} = c_{2b}$, with values determined by requiring $\int \phi_1^2 dv = 1 = \int \phi_2^2 dv$, namely⁴

$$c_{1a} = c_{1b} = 1/2(1 + S_{ab})^{-1/2}(1 + S_{bc})^{-1/2};$$

$$c_{2a} = c_{2b} = 1/2(1 + S_{ab})^{-1/2}(1 - S_{bc})^{-1/2}$$

The overlap integrals are $S_{ab} = 0.2785$, $S_{bc} = 0.2328$.⁵ If S is neglected, $c_{1a} = c_{1b} = c_{2a} = c_{2b} = 1/2$, and the Coulson π -bond order is 1 for the C=C and 0 for the C-C bond.

In the π -electron-only-SCF solution for butadiene (*i.e.*, the actual conjugated case), the coefficients which minimize the energy are $c_{1a} = 0.3540$, $c_{1b} = 0.4687$, $c_{2a} = 0.5081$, $c_{2b} = 0.4229$.⁵ Renormalized to correspond to neglect of overlap, these values become $c_{1a} = 0.423$, $c_{1b} = 0.564$, $c_{2a} = 0.543$, $c_{2b} = 0.452$, and the Coulson bond orders are $p_{ab} = p_{cd} = 0.972$, $p_{bc} = 0.227$.

In HCN, $c_a = 0.6048$, $c_b = 0.6293$ according to McLean,³ where a and b refer to the C and N atoms, respectively. Because of the polarity of the π MO in HCN, the correct way to obtain the forms of the MO's for "unconjugated" cyanogen is less obvious than in the case of butadiene. However, the most reasonable procedure seems to be to choose the coefficients in eq. 2 in such a way that $c_{1b}/c_{1a} = c_{2b}/c_{2a} = c_b/c_a$. This procedure taken in connection with the normalization requirement $\int \phi_1^2 dv = 1 = \int \phi_2^2 dv$ yields the values $c_{1a} = 0.404$, $c_{1b} = 0.420$, $c_{2a} = 0.457$, $c_{2b} = 0.475$ for "unconjugated" cyanogen.

In the all-electron SCF solution for cyanogen (*i.e.*, the actual conjugated case), the coefficients which minimize the energy are $c_{1a} = 0.3513$, $c_{1b} = 0.4599$, $c_{2a} = 0.4855$, $c_{2b} = 0.4378$.² The relevant overlap integrals⁶ are $S_{ab} = 0.3130$, $S_{bc} = 0.2736$, $S_{ac} = 0.0185$, $S_{ad} = 0.0004$. (In the case of butadiene, S_{ac} and S_{ad} were neglected, but in the calculations on C_2N_2 they were used.) When renormalized to correspond to neglect of all overlaps, the coefficients become $c_{1a} = 0.429$, $c_{1b} = 0.562$, $c_{2a} = 0.525$, $c_{2b} = 0.474$. The corresponding Coulson bond orders are $p_{ab} = p_{cd} = 1.959$, $p_{bc} = 0.366$; values for p_{ac} also can be obtained, but these are very small.

Overlap Population Shifts as Mirrors of Conjugation.—Some time ago⁷ the writer called attention to the fact that overlap populations give a more instructive picture of the nature of π -

(5) From R. G. Parr and R. S. Mulliken, *ibid.*, **18**, 1338 (1950). Slightly improved values are now available (see R. S. Mulliken, *Tetrahedron*, **6**, 68 (1959), Table 1 for references and discussion), but the changes are too small to make it worthwhile to revise the numbers quoted here.

(6) Overlap integrals from private communication from the authors of ref. 2.

(7) R. S. Mulliken, *J. Chem. Phys.*, **23**, 2343 (1955).

(3) A. D. McLean, *J. Chem. Phys.*, in press.

(4) Cf. R. S. Mulliken, *ibid.*, **36**, 3428 (1962).

$$\text{Two Lone Pairs : } p = 0.000 ; \quad n = -[4s^2/(1-s^2)]$$

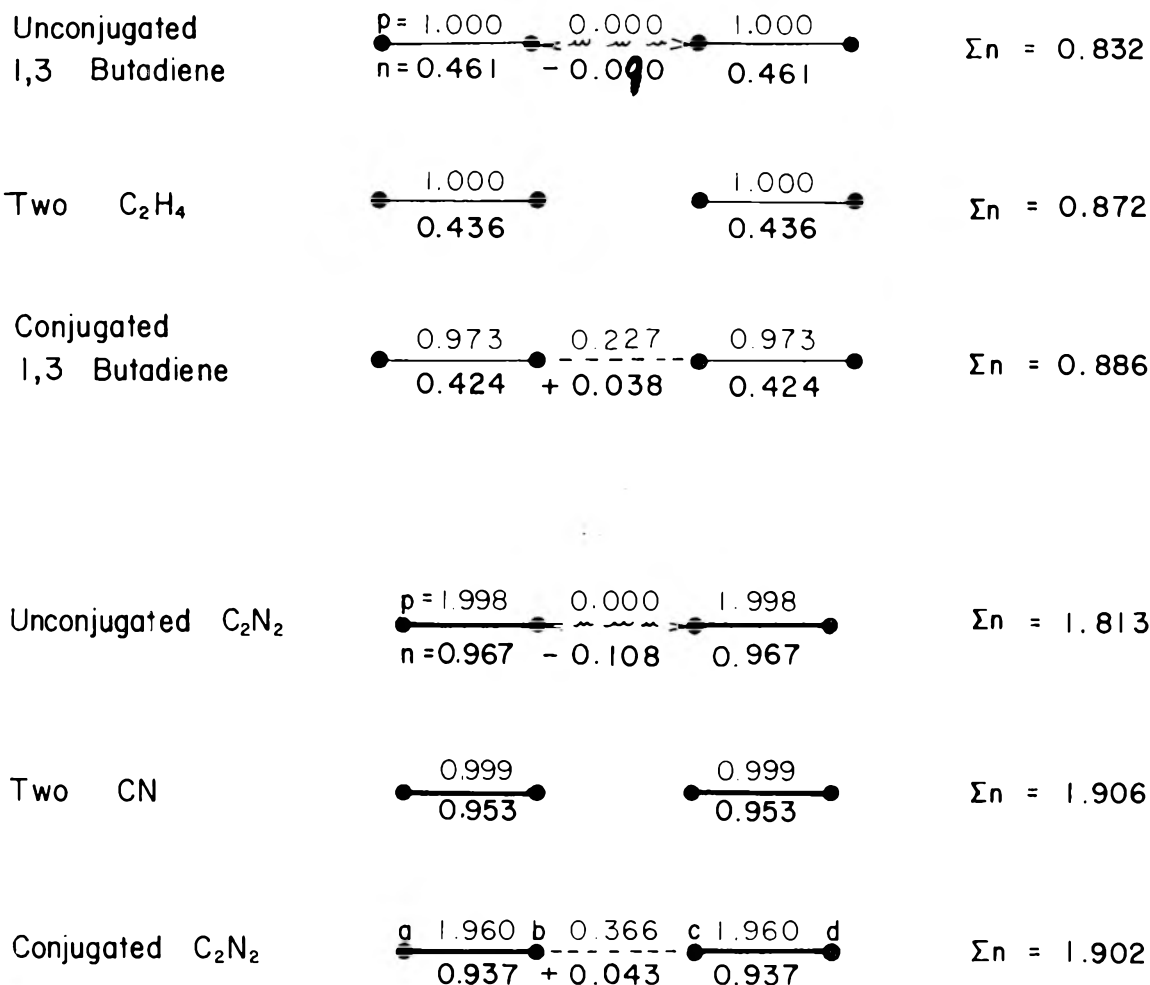


Fig. 1.—Electronic overlap populations (n_{kl}) are given below and Coulson bond orders (p_{kl}) above each bond. The four atoms are labeled a, b, c, d from left to right. In addition to the numbers given, there are small overlap populations between non-adjacent atoms. These were not computed for butadiene, but for cyanogen they are $n_{ac} = n_{bd} = -0.0070$ for the unconjugated case, -0.0075 for the conjugated case, while $n_{ad} = -0.0001$ and -0.0004 in the two respective cases. In Fig. 1 these non-adjacent populations are included in the totals Σn given at the right in the case of cyanogen, but *not* in that of butadiene.

electron delocalization in butadiene than do Coulson bond orders. The same fact should be equally true for cyanogen and for other conjugated systems. In the case of butadiene, it was shown that the computed overlap populations n behave in the following way. For the double bonds, $n_{ab}(\text{unconj.}) > n_{ab}(C_2H_4) > n_{ab}(\text{conj.})$; for the middle bond, $n_{bc}(\text{unconj.}) < 0 < n_{bc}(\text{conj.})$; while for the total π overlap population (summed over all the bonds) $n(\text{unconj.}) < n(2C_2H_4) < n(\text{conj.})$.

It is now found that analogous relations exist for C_2N_2 , where now HCN plays the same role that C_2H_4 did for butadiene. However, the difference $\Sigma n(\text{conj.}) - \Sigma n(\text{unconj.})$ for the total overlap population is now approximately twice as great as before (see Fig. 1), as is reasonable since there are twice as many π electrons. (The

fact that this difference is a *little less* than twice as great may be due to a greater accuracy of the all-electron results, or perhaps to a slight real difference between conjugation in the two cases.) One valuable conclusion, already noted in the opening paragraph, is the confirmation which the all-electron SCF calculations on C_2N_2 give to the essential rightness of the picture of conjugation which is obtained from π -electron-only SCF calculations like those on butadiene.

Before commenting further, a brief reminder on the computation of overlap populations will be helpful. For the two-center LCAO MO as in eq. 1, when occupied by two electrons, the overlap population n_{ab} is merely $2(2c_a c_b S_{ab})$.⁸ For a molecule with two four-center MO's (eq. 2) each oc-

(8) R. S. Mulliken, *J. Chem. Phys.*, **23**, 1833 (1955).

cupied by two electrons (butadiene) or by four (cyanogen), one has several overlap populations $n_{ab} = n_{cd}$, n_{bc} , $n_{ac} = n_{bd}$, and n_{ad} , of which only the first three are important. In (actual, *conjugated*) cyanogen

$$n_{ab} = 4S_{ab}(2c_{1a}c_{1b} + 2c_{2a}c_{2b}) = 0.937 = n_{cd}$$

$$n_{bc} = 4S_{bc}(2c_{1b}^2 - 2c_{2b}^2) = 0.044$$

$$n_{ac} = 4S_{ac}(2c_{1a}c_{1b} - 2c_{2a}c_{2b}) = -0.0075 = n_{bd}$$

$$n_{ad} = 4S_{ad}(2c_{1a}^2 - 2c_{2a}^2) = -0.0004$$

$$n = 2n_{ab} + n_{bc} + 2n_{ac} + n_{ad} = 1.916$$

Now commenting on the results displayed in Fig. 1, we note first (as already discussed in an earlier paper⁷) that the overlap populations for the bonds are rather good counterparts of energy terms which appear in VB (valence-bond) theory. In particular for the *unconjugated* cases, one has in VB theory a bonded attraction between each end atom (a or d) and the adjacent middle atom (b or c, respectively), while in LCAO MO theory one finds positive overlap populations. Then in VB theory there is a moderate NBR (non-bonded repulsion) between the two middle atoms b and c whose counterpart in LCAO theory is a negative overlap population n_{bc} between them.

The creation of an NBR or of a negative overlap population when two double or triple bonds each with a pair or quartet of π electrons are brought together without any change in the ratio c_b/c_a (cf. eq. 1), as in the hypothetical unconjugated butadiene or cyanogen, is precisely analogous to the NBR, or the corresponding negative overlap population, which arises when two He atoms are forced together, or when lone pairs of electrons in two atoms (as, e.g., in N_2 or F_2) are forced together as a result of the formation of bonds by bonding electrons.⁷ For two such lone pairs, one on atom a and one on b, the overlap population n is $-4S^2/(1 - S)$, whereas the Coulson bond order, since there is no bond, is by definition

zero. The π pairs or quartets in the double or triple bond in unconjugated butadiene or cyanogen are interacting in essentially the same way.

In actual, conjugated, butadiene or cyanogen, the mechanism of resonance in VB theory or of π -electron delocalization in LCAO theory acts to increase the stability of the middle bond. The resulting small positive n_{bc} population in butadiene, now confirmed by that in cyanogen, indicates that this stabilization has proceeded to the extent of somewhat more than canceling out the NBR, or its negative n_{bc} counterpart, which would otherwise be present.

Here it should be clearly noted that the true measure of the effect of conjugation in LCAO theory is not the value of n_{bc} , but that of the *change* in n_{bc} from the unconjugated to the conjugated case. The fact that n_{bc} turns out to be slightly positive in actual conjugated cases, and that the *total* overlap population is somewhat larger for butadiene than for two C_2H_4 , though slightly smaller for cyanogen than for two HCN, probably should be regarded as more or less accidental.

Comparing the overlap population changes in Fig. 1 (e.g., from unconjugated butadiene to two C_2H_4 to conjugated butadiene) with corresponding Coulson bond order changes, it seems evident that the former give a more realistic picture of what is happening.⁹ Conversely, the bond order changes may be said to give a distorted picture, especially in the comparison between, e.g., unconjugated butadiene and two C_2H_4 . However, the rather considerable bond order p_{bc} in the conjugated as compared with $p_{bc} = 0$ in the unconjugated cases does seem to be a fair and rather direct measure of the effect of conjugation. The value of p_{bc} in the conjugated case parallels the *change* in n_{bc} from the unconjugated to the conjugated case.

Acknowledgment.—The writer is indebted to Dr. E. Clementi and Dr. A. D. McLean for information about their calculations.

(9) See also R. S. Mulliken, *J. Chem. Phys.*, **23**, 1841 (1955).

THE SPLIT p-ORBITAL (S.P.O.) METHOD. III. RELATIONSHIP TO OTHER M.O. TREATMENTS AND APPLICATION TO BENZENE, BUTADIENE, AND NAPHTHALENE¹

BY MICHAEL J. S. DEWAR AND NORA L. SABELLI

George Herbert Jones Laboratory, University of Chicago, Chicago, Illinois

Received June 8, 1962

Previous papers of this series have described a modification of the l.c.a.o. m.o. method designed to allow for the effects of vertical correlation in unsaturated molecules. Here the relationship of the *split p-orbital* (s.p.o.) method to other m.o. treatments is discussed; it appears to differ from these only in the values ascribed to the individual two-electron integrals. A s.p.o. treatment of benzene is described, both with and without configuration interaction and with and without differential overlap. The results seem better than those given by other treatments, except for the semi-empirical method of Pariser and Parr. The simplest s.p.o. calculation, using single configurations with neglect of overlap, gives much better results than any other treatment using single configurations. The s.p.o. method also is applied successfully to butadiene and naphthalene.

I. Introduction

Previous papers of this series² have described a modification of the usual m.o. procedure designed to allow for vertical correlation³ of electrons in orbitals of p- or π -type symmetry. Before describing the application of this s.p.o. (split p-orbital) approximation to several polyatomic molecules we will first show its relationship to existing m.o. treatments.

Consider a conjugated system of n atoms. In the simple Hückel treatment the corresponding π -m.o.'s ψ_m are written as linear combinations of the n $2p_z$ a.o.'s φ_i of the individual atoms taking part

$$\psi_m = \sum_{i=1}^n a_{mi} \varphi_i \quad (1)$$

The energies (E) of the m.o.'s are given by the secular equation

$$\det |H_{ij} - ES_{ij}| = 0 \quad (2)$$

where

$$H_{ij} = \int \varphi_i H \varphi_j d\tau; S_{ij} = \int \varphi_i \varphi_j d\tau \quad (3)$$

The Hamiltonian H is not very clearly defined in this treatment so the H_{ij} usually are treated as empirical parameters (see, however, Ruedenberg⁴).

The coefficients a_{mi} in eq. 1 are given by the set of linear equations

$$\sum_j a_{mj} (F_{ij} - E_m S_{ij}) = 0 \quad (i = 1, 2, \dots, n) \quad (4)$$

where E_m is one of the roots of eq. 2. In the s.c.f. m.o. treatment⁵ the orbital energies and coefficients are given by equations of the same form as (2) and (4) but the matrix elements F_{ij} are now functions of the coefficients a_{mi} . The equations for the coefficients a_{mi} are therefore non-linear and must be solved by an iterative procedure, the F_{ij} being calculated with the values for the a_{mi} found from the previous iteration. In the case of a closed

shell configuration, where the $2n$ π -electrons occupy in pairs the n m.o.'s of lowest energy

$$F_{ii} = \int \varphi_i H^C \varphi_i d\tau + \sum_{p=1}^n \sum_{k=1}^{2n} \sum_{l=1}^{2n} a_{pk} a_{pl} [2(ii,kl) - (ik,il)] \quad (5)$$

$$F_{ij} \quad (i \neq j) = \int \varphi_i H^C \varphi_j d\tau + \sum_{p=1}^n \sum_{k=1}^{2n} \sum_{l=1}^{2n} a_{pk} a_{pl} [2(ij,kl) - (ik,jl)] \quad (6)$$

where H^C is the core Hamiltonian and the (ij,kl) are the usual two-electron repulsion integrals.

In the m.o. treatment the wave function Ψ for the set of $2n$ π -electrons is written (neglecting the normalizing factor) as the determinant

$$\Psi = \det |\psi_1 \bar{\psi}_1 \psi_2 \bar{\psi}_2 \dots \psi_n \bar{\psi}_n| \quad (7)$$

In the s.p.o. treatment, where it is assumed that the two electrons occupying a given π -m.o. are kept in separate lobes by their mutual repulsion, the corresponding (unnormalized) wave function Ψ' is given by

$$\Psi' = \Psi \prod_i (U(z_i \bar{z}_i)) \quad (8)$$

where z_i, \bar{z}_i are the z -coordinates of the electrons occupying the spin orbitals $\psi_i \bar{\psi}_i$ and U is a step function defined by

$$U(x) = 0 \text{ if } x > 0 \\ = 1 \text{ if } x < 0 \quad (9)$$

If the m.o.'s ψ_i are expressed in terms of s.p.o.'s $\bar{\Xi}_i, H_i$

$$\psi_i = (2)^{-1/2} (\bar{\Xi}_i + H_i) \quad (10)$$

eq. 8 becomes

$$\Psi' \sum_i P_i \det |\bar{\Xi}_1 \bar{H}_1 \bar{\Xi}_2 \bar{H}_2 \dots \bar{\Xi}_n \bar{H}_n| \quad (11)$$

where P_i is a permutation operator which inverts the spins of the pair of spin orbitals $\bar{\Xi}_i, \bar{H}_i$, i.e.

$$P_i(\bar{\Xi}_i, \bar{H}_i) = (\bar{\Xi}_i, H_i) \quad (12)$$

and the sum in eq. 11 is over all such permutations. Now it is easily shown that the individual de-

(1) This work has been supported by a grant from The National Science Foundation.

(2) M. J. S. Dewar and N. L. Hojvat, *J. Chem. Phys.*, **34**, 1232 (1961); *Proc. Roy. Soc. (London)*, **A264**, 431 (1961).

(3) M. J. S. Dewar and H. N. Schmeising, *Tetrahedron*, **5**, 166 (1959); **11**, 96 (1960).

(4) K. Ruedenberg, *J. Chem. Phys.*, **34**, 1861 (1961).

(5) C. C. J. Roothaan, *Rev. Mod. Phys.*, **23**, 69 (1961).

terminants in eq. 11 are not only orthogonal to one another but also that all matrix elements between them must vanish; this is due to the fact that one or the other of the pair of s.p.o.'s Ξ_i , H_i vanishes in every region of space. The energy calculated for the complete wave function of eq. 11 is therefore a mean of those calculated for the individual determinants. The total energy E corresponding to one single determinant can be shown to be given by

$$E = 2 \sum_{i=1} \int \psi_i H^C \psi_i d\tau + \sum_{(i\bar{k}j\eta)} J_{ij} + \sum_{(i\bar{k})(j\bar{\epsilon})} (J_{ij} - K_{ij}) \quad (13)$$

where $\sum_{(i\bar{k}j\eta)}$ implies a summation over the "upper" s.p.o.'s Ξ_i and "lower" s.p.o.'s H_j while $\sum_{(i\bar{k})(j\bar{\epsilon})}$ implies summation over pairs of upper or pairs of lower s.p.o.'s. Here J_{ij} , K_{ij} are the corresponding coulomb and exchange integrals between s.p.o.'s.

Now K_{ij} vanishes unless the spin-orbitals i , j have similar spins; the total energy E is therefore less, the more electrons in the set of s.p.o.'s Ξ have like spin. The energy will be least for the two determinants in which all the electrons of one spin are in the s.p.o.'s Ξ , and all the electrons in s.p.o.'s H have opposite spin.⁶ It is reasonable to suppose that correlation effects will make the actual wave function correspond more closely to this limiting case than eq. 11 implies; we therefore may take this single determinant as an approximation to the actual wave function. We therefore write the normalized 2n-electron s.p.o. wave function Ψ' as

$$\Psi' = (2n!)^{-1/2} \det |\Xi_1 \bar{H}_1 \Xi_2 \bar{H}_2 \Xi_3 \bar{H}_3 \dots \Xi_n \bar{H}_n| \quad (14)$$

If this wave function is substituted into the Roothaan⁶ equations we obtain a set of equations for the coefficients of the s.p.o.'s in the s.p.o.'s similar to eq. 2 and 4 with

$$F_{ii} = \int \varphi_i H^C \varphi_i d\tau + \sum_{p=1}^n \sum_{k=1}^{2n} \sum_{l=1}^{2n} a_{pk} a_{pl} [2(i\bar{i},kl) - (\bar{i}k,\bar{i}l)] \quad (15)$$

$$F_{ij} (i \neq j) = \int \varphi_i H^C \varphi_j d\tau - \sum_{p=1}^n \sum_{k=1}^{2n} \sum_{l=1}^{2n} a_{pk} a_{pl} [2(ij,kl) - (\bar{i}k,\bar{i}l)] \quad (16)$$

where $(\bar{i}j,\bar{k}l)$ is a repulsion integral between s.p.o.'s all of the same type (i.e., all upper or all lower), the core integrals are the same as in the usual treatment.¹

Comparison of eq. 15, 16 with eq. 5, 6 shows them to be identical except that the exchange-type integrals in eq. 15, 16 are of "upper-upper" type whereas in the usual s.c.f. treatment all the electron repulsion integrals are "normal."

This throws a new light on the s.p.o. treatment. Vertical correlation cannot in itself alter the

coulomb terms in the Roothaan equations, for these appear as coupled interactions between a given electron and the pair of electrons occupying some other m.o. The total electron density of a pair of electrons occupying a given π -m.o. is the same in the s.p.o. treatment as in the usual s.c.f. approach. The main effect of vertical correlation appears in a somewhat different form to that previously envisaged³; it lowers the energy of the molecule by increasing the exchange energy rather than by decreasing the coulombic repulsion. The exchange energy will be greatest when all the α -spin electrons occupy s.p.o.'s of one set and all the β -spin electrons those of the other; for all the integrals in the expression for the exchange energy are then "upper-upper" integrals $(\bar{i}j,\bar{k}l)$ —and these are larger than the "normal" integrals (ij,kl) calculated for normal p-a.o.'s.

This provides an alternative view of the s.p.o. approximation. It could be regarded as a semi-empirical way of allowing for vertical correlation in the s.c.f. treatment. In this approach there would be no need to take the extreme step of assigning "upper-upper" values to the integrals appearing in the exchange terms of the Roothaan equations; one can indeed envisage a series of intermediate approximations in which the exchange-type integral $(\bar{i}i,\bar{j}j)$ ¹ is written in the form

$$(\bar{i}i,\bar{j}j)^1 = C_1(i\bar{i},j\bar{j}) + C_2(\bar{i}\bar{i},\bar{j}\bar{j}) \quad (17)$$

The usual s.c.f. approximation corresponds to the values $C_1 = C_2 = 0.5$ for the parameters C_1 , C_2 , while the pure s.p.o. approximation is given by $C_1 = 0$, $C_2 = 1$.

Pariser and Parr⁷ have described a modification of the s.c.f. treatment in which allowance is made for correlation effects by an empirical adjustment of the repulsion integrals. They replace the "normal" integrals (ij,kl) everywhere by the "upper-lower" values $(\bar{i}j,kl)$ corresponding to interactions between electrons on opposite sides of the nodal plane of the π -electron system. They further simplify the treatment by neglecting differential overlap.

If differential overlap is neglected, so that

$$S_{ij} = \delta_{ij} \quad (18)$$

the Roothaan equations adopt a rather simple form.⁸

The matrix elements F_{ij} in the secular equation then are given by

$$F_{ii} = \int \varphi_i H^C \varphi_i d\tau + \sum_{p=1}^n \left[\sum_k a_{pk}^2 (i\bar{i},kk) - 1/2 a_{pi}^2 (i\bar{i},i\bar{i}) \right] = \int \varphi_i H^C \varphi_i d\tau + \sum_k q_k (i\bar{i},kk) - 1/2 q_i (i\bar{i},i\bar{i}) \quad (19)$$

$$F_{ij} (i \neq j) = \int \varphi_i H^C \varphi_j d\tau - \sum_{p=1}^n a_{pi} a_{pj} (i\bar{i},j\bar{j}) = \int \varphi_i H^C \varphi_j d\tau - 1/2 p_{ij} (i\bar{i},j\bar{j}) \quad (20)$$

(6) In our previous papers we stated incorrectly that the various determinantal wave functions correspond to states of similar energy.

(7) R. Pariser and R. G. Parr, *J. Chem. Phys.*, **21**, 466, 767 (1953).

(8) J. A. Pople, *Trans. Faraday Soc.*, **49**, 1375 (1953).

where q_i is the π -electron charge density at atom i and p_{ij} is the bond order between atoms i, j .

The corresponding equations for the s.p.o. method, with neglect of differential overlap, are

$$F_{ii} = \int \varphi_i H^C \varphi_i d\tau + \sum_k q_k(\bar{i}i, k\bar{k}) - 1/2 q_i(\bar{i}i, \bar{i}i) \quad (21)$$

$$F_{ij} (i \neq j) = \int \varphi_i H^C \varphi_j d\tau - 1/2 p_{ij}(\bar{i}i, \bar{j}j) \quad (22)$$

Here again the only difference lies in the exchange-type integrals which in the s.p.o. treatment have the "upper-upper" values $(\bar{i}i, \bar{j}j)$.

Now eq. 21 can be written in the equivalent form

$$F_{ii} = \int \varphi_i H^C \varphi_i d\tau + \sum_{k \neq i} q_k(\bar{i}i, k\bar{k}) + 1/2 q_i(\bar{i}i, \bar{i}i) \quad (23)$$

Here the integral in the last term is of "upper-lower" type, being a difference between the normal integral $(\bar{i}i, \bar{i}i)$ and $1/2(\bar{i}i, \bar{i}i)$. This is the most important electron repulsion term in the expression; for each of the other terms $q_k(\bar{i}i, k\bar{k})$ represents the repulsion between electrons attached to atom i and electrons attached to some other atom k —and this is balanced by the attraction between the k th nucleus and the electrons on atom i (cf. Pople⁸). The expression for F_{ii} is therefore very similar to that in the Pariser-Parr treatment where all integrals are of "upper-lower" type. The exchange integrals are, however, different in the two treatments; in the s.p.o. approach these integrals have values *greater* than those in the usual s.c.f. treatment whereas in the Pariser-Parr approach their values are less. The analysis given here suggests that the Pariser-Parr approach is logically self-inconsistent; for the correlation effects that make it necessary to use a smaller value for the $(\bar{i}i, \bar{i}i)$ integral in the expression for F_{ii} also require the integrals $(\bar{i}i, \bar{j}j)$ in F_{ij} to be larger than usual.

II. Results for Benzene

The integrals over a.o.'s were calculated as in part I² for a bond length of 1.397 Å. The one-electron integrals have the same value as in the conventional s.c.f. treatment.⁹ The (ij, kl) integrals were obtained by interpolation from the tables of Parr and Crawford¹⁰ and the $(\bar{i}j, k\bar{l})$ integrals by the uniformly charged sphere approximation, except for the $(\bar{11}, 11)$ integral for which we used the more precise value of Parr and Snyder.¹¹ The integrals $(\bar{i}j, k\bar{l})$ were derived from the relation

$$1/2\{(\bar{i}j, k\bar{l}) + (\bar{i}j, kl)\} = (ij, kl) \quad (24)$$

The values for the integrals are listed in Table I. Table II shows the orbital energies for the various m.o.'s.

Table III compares the results of calculations by the s.p.o. method for single configurations, with and without overlap, with the results of other m.o. treatments. The first three columns show the sym-

TABLE I
VALUES OF INTEGRALS OVER ATOMIC ORBITALS FOR A C-C
BOND LENGTH OF 1.397 Å.

Integral	Designation	Value (e.v.)	
Overlap	S ₁₂	0.2583	
	S ₁₃	.0382	
	S ₁₄	.0173	
		.8448	
Penetration	(1:22)	.0129	
	(1:33)	.0026	
	(1:44)	.8662	
	(1:12)	.1090	
	(1:13)	.0370	
	(1:14)	.0038	
	(1:23)	.0057	
	(1:24)	.0125	
	(1:25)	.3143	
	(1:26)	.0027	
	(1:34)	.0019	
	(1:35)		
	Repulsion	($\bar{i}j/k\bar{l}$)	($\bar{i}j/k\bar{l}$)
(11/11)		10.980	22.900
(11/22)		7.286	10.718
(11/33)		4.736	6.598
(11/44)		4.207	5.741
(11/12)		2.381	4.196
(11/13)		0.300	0.454
(11/14)		.126	0.194
(12/12)		.688	1.190
(13/13)		.015	0.037
(14/14)		.003	0.006
(11/23)		1.605	1.885
(11/24)		0.237	0.279
(11/25)		.126	.186
(11/26)		.352	.672
(11/34)		1.291	1.531
(11/35)		0.218	0.278
(12/13)		.078	.187
(12/14)		.037	.053
(12/15)		.062	.116
(12/16)		.546	.789
(12/34)		.315	.546
(12/35)		.053	.081
(12/36)	.037	.053	
(12/45)	.344	.412	
(13/14)	.005	.013	
(13/15)	.012	.016	
(13/24)	.013	.026	
(13/25)	.005	.013	
(13/46)	.011	.016	
(14/25)	.003	.007	

TABLE II
ENERGIES OF INDIVIDUAL M.O.'S IN THE S.P.O. APPROXIMATION

M.o.	Orbital energy (e.v.)
ψ_0	$W_{2p} - 40.156$
$\psi_1; \psi_{-1}$	$W_{2p} - 36.778$
$\psi_2; \psi_{-2}$	$W_{2p} - 31.937$
ψ_3	$W_{2p} - 31.346$

metry designations of the states and the s.p.o. values. The fourth column gives the results of a very complete a.s.m.o.c.i. calculation by Parr, Craig, and Ross.⁹ The fifth and sixth columns list results obtained by the semi-empirical methods of Pariser and Parr⁷ (P-P) and Moffitt and Scan-

(9) R. G. Parr, D. P. Craig, and I. G. Ross, *J. Chem. Phys.*, **18**, 1561 (1950).

(10) R. G. Parr and B. L. Crawford, *ibid.*, **16**, 1049 (1948).

(11) L. C. Snyder and R. G. Parr, *ibid.*, **28**, 1250 (1958).

lan¹² (a.i.m.c.i.). The last column gives the results obtained by Kolos¹³ using a wave function in which the interelectronic distances were explicitly included.

TABLE III

EXCITATION ENERGIES (E.V.) OF STATES OF BENZENE CALCULATED BY (a) S.P.O. METHOD, SINGLE CONFIGURATION WITH OVERLAP; (b) S.P.O. METHOD, SINGLE CONFIGURATION AND NO OVERLAP; (c) PARR, CRAIG, AND ROSS; (d) MOFFITT AND SCANLAN; (e) PARISER AND PARR; (f) KOLOS

State	—S.p.o.—		A.s.m.- o.c.i. ^a	A.i.m.c.i. ^b	P-P ^c	Kolos ^d
	a	b	c	d	e	f
¹ E _{1u}	8.03	8.16	9.9	7.60	7.0	8.3
¹ B _{1u}	4.68	5.00	9.0	4.06	5.3	5.9
¹ B _{2u}	5.05	5.24	4.4	5.13	(4.9)	4.5
¹ E _{2g}	8.17	7.98	7.7	9.18	..	9.2
³ E _{1u}	5.13	5.32	4.7	4.88	4.45	..
³ B _{1u}	3.06	3.88	4.1	4.50	4.0	5.6
³ B _{2u}	5.35	5.24	8.2	5.36	4.9	..
³ E _{2g}	6.96	6.92	6.4	7.50

^a See ref. 9. ^b See ref. 12. ^c See ref. 7. ^d See ref. 13.

Tables IV and V show the results of s.p.o. calculations including configuration interaction (s.p.o.c.i. method). The second and third columns of Table IV list excitation energies calculated with and without overlap, respectively. The number of configurations included in the calculation is shown in the fourth column. Table V gives the coefficients of the ground state configuration in various c.i. wave functions for the ground state, together with the lowering of the ground state by configuration interaction. In addition to the a.s.m.o.c.i. and a.i.m.c.i. values, a value obtained by Itoh and Yoshizumi¹⁴ using the alternating orbital method (a.o.m.c.i.) is listed.

TABLE IV

EXCITATION ENERGIES CALCULATED BY THE S.P.O. METHOD (a) WITH AND (b) WITHOUT OVERLAP, TOGETHER WITH THE NUMBERS OF CONFIGURATIONS USED AND EXPERIMENTAL VALUES

State	—S.p.o.c.i.—		No. of configurations	Exptl.
	a	b		
¹ A _{1g}	0	0	4	0
¹ E _{1u}	7.78	7.92	5	7.0
¹ B _{1u}	4.31	4.61	4	6.2
¹ B _{2u}	4.00	4.45	3	4.9
¹ E _{2g}	7.42	6.99	5	..
³ E _{1u}	5.29	5.40	5	4.9
³ B _{1u}	2.24	3.29	4	3.6
³ B _{2u}	5.64	5.56	3	..

III. Discussion of Results for Benzene

The electron spectrum of benzene has been extensively studied and reviewed.¹⁵⁻¹⁸ The assignment of the band at 7.0 e.v. to the ¹E_{1u} ← ¹A_{1g} transition and of the band at 4.9 e.v. to the ¹B_{2u}

(12) W. Moffitt and J. Scanlan, *Proc. Roy. Soc. (London)*, **A220**, 530 (1953).

(13) W. Kolos, *J. Chem. Phys.*, **27**, 592 (1957).

(14) T. Itoh and H. Yoshizumi, *J. Phys. Soc. Japan*, **10**, 201 (1955).

(15) C. C. J. Roothaan and R. S. Mulliken, *J. Chem. Phys.*, **16**, 118 (1948).

(16) D. P. Craig, *Rev. Pure Appl. Chem. (Australia)*, **3**, 207 (1953).

(17) J. W. Potts, *J. Chem. Phys.*, **23**, 73 (1955).

(18) N. S. Ham and K. Ruedenbe'g, *ibid.*, **25**, 1 (1956).

TABLE V

COEFFICIENT OF THE GROUND STATE CONFIGURATION IN THE GROUND STATE WAVE FUNCTION OF BENZENE FOR (a) S.P.O.C.I. WITH OVERLAP; (b) S.P.O.C.I. WITHOUT OVERLAP; (c) PARR, CRAIG, AND ROSS; (d) ITOH AND YOSHIKUMI; (e) MOFFITT AND SCANLAN

	—S.p.o.c.i.—		A.s.m.- o.c.i. ^a	A.m.o.- c.i. ^b	A.i.m.- c.i. ^c
	a	b	c	d	e
Coefficients of ground state configuration	0.967	0.974	0.910	0.900	...
Lowering of ground state (e.v.)	0.42	0.36	2.72	2.35	0.694

^a See ref. 9. ^b See ref. 14. ^c See ref. 12.

← ¹A_{1g} transition remain undisputed. The lowest singlet-triplet band at 3.6 e.v.¹⁹ probably corresponds to the ³B_{2u} ← ¹A_{1g} transition; this assignment is supported by all theoretical calculations, using either the valence bond or the molecular orbital methods.^{20,21} Ham²² found evidence for a second singlet-triplet transition coinciding with the singlet-singlet transition of 4.9 e.v. The bands observed by him may merely be part of the ¹B_{2u} ← ¹A_{1g} transition but the evidence that they are not is strong. Ham ascribed them to the transition ³E_{1u} ← ¹A_{1g}. If the bands do indeed correspond to an independent transition, this seems the most likely assignment; for there is certainly no observable transition between 3.6 and 4.9 e.v. (an earlier observation by Pitts²³ having proved incorrect) and all theories agree that the order of ascending energy of the triplets is ³B_{2u}, ³E_{1u}, ³B_{1u}. Since ³E_{1u} ← ¹A_{1g} certainly must be the strongest of the singlet-triplet transitions, this seems to eliminate the alternative possibility¹⁸ that the "Ham bands" are due to the transition ³B_{2u} ← ¹A_{1g}. The origin of the remaining strong singlet-singlet band at 6.2 e.v. is still uncertain. This originally was assigned to the transition ¹B_{1u} ← ¹A_{1g} by Goepfert-Mayer and Sklar²⁴ on the basis of a one-configuration a.s.m.o. calculation, an assignment supported by the semi-empirical treatments of Pariser and Parr⁷ and Moffitt and Scanlan,¹² by the correlated method of Kolos,¹³ and by calculations with the free electron model.^{18,20} However, calculations by the valence bond method^{25,26} and by the complete a.s.m.o.c.i. treatment⁹ favor the assignment ¹E_{2g} ← ¹A_{1g} and recently Dunn and Ingold²⁷ have claimed in a preliminary note that their experimental work supports this. Bloor, Lee, and Garside²⁸ also have described a calculation supporting the ¹E_{2g} ← ¹A_{1g} assignment based on a m.o. treatment in which certain molecular integrals are treated as variation parameters.

However the evidence put forward by Dunn and

(19) D. F. Evans, *J. Chem. Soc.*, 3885 (1957).

(20) H. Schull, *J. Chem. Phys.*, **17**, 295 (1949).

(21) R. Pariser, *ibid.*, **24**, 250 (1956).

(22) J. Ham, *ibid.*, **21**, 756 (1953).

(23) A. Pitts, *ibid.*, **18**, 1416 (1950).

(24) M. Goepfert-Mayer and A. L. Sklar, *ibid.*, **6**, 645 (1938).

(25) A. L. Sklar, *ibid.*, **5**, 669 (1937).

(26) D. P. Craig, *Proc. Roy. Soc. (London)*, **A200**, 474 (1950).

(27) T. M. Dunn and C. K. Ingold, *Nature*, **176**, 65 (1955).

(28) J. E. Bloor, J. Lee, and S. Garside, *Proc. Chem. Soc.*, 413 (1960).

Ingold is certainly not conclusive and there are reasons for preferring the original assignment of Goeppert-Mayer and Sklar. All the theoretical treatments agree in placing the states ${}^1B_{2u}$, ${}^1B_{1u}$, ${}^1E_{1u}$ in that order of ascending energies and all agree that the intensity of the transition ${}^1B_{1u} \leftarrow {}^1A_{1g}$ should be much greater than that of ${}^1B_{2u} \leftarrow {}^1A_{1g}$. Since there is only one region of strong absorption between the ${}^1B_{2u} \leftarrow {}^1A_{1g}$ transition at 4.9 e.v. and the ${}^1E_{1u} \leftarrow {}^1A_{1g}$ transition at 7.0 e.v., it is difficult to escape from the conclusion that the transition ${}^1B_{1u} \leftarrow {}^1A_{1g}$ must lie there. It is of course possible that there may be two transitions superimposed in this region—but that seems unlikely.

The calculations reported here agree closely with experiment for the singlet bands at 4.9 and 7.0 e.v. and for the triplet bands at 3.6 and 4.9 e.v.; the agreement is indeed better than for any other treatment except the semi-empirical treatment of Pariser and Parr⁷—in which the parameters were chosen to fit the experimental data for benzene. Although the agreement is less good for the third singlet, our calculations very strongly support its assignment to the ${}^1B_{1u} \leftarrow {}^1A_{1g}$ transition. It is interesting that the treatments which support this assignment are the ones which give the best absolute estimates of the transition energies for the other bands.

Tables IV and V show that the simplest s.p.o. treatment, in which both overlap and configuration interaction are neglected, is also the most successful. This is very encouraging; for calculations of this kind can be carried out very easily with digital computers using simpler modifications of existing programs. As we have seen the treatment differs from the Pople approximation only in the values assigned to the basic integrals.

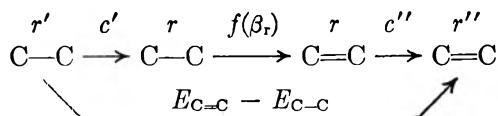
This is further emphasized by the data in Table V for the contributions of excited structures to the ground state in a configuration interaction treatment. Their contribution is significantly less in the s.p.o. treatment than in the Pariser-Parr or atoms-in-molecules methods. This provides further support for our contention than the use of reduced values for the coulomb integrals as suggested by Pariser and Parr logically requires the use of increased values for the exchange integrals.

IV. Results for Butadiene and Naphthalene

The calculations for butadiene were carried out by the standard s.c.f. procedure, as indicated in section I, using a modification of a program written by Dr. L. C. Snyder for the I.B.M. 7090 computer at Bell Telephone Laboratories. The values assumed for integrals of the type $(\bar{i}\bar{i}, \bar{i}\bar{i})$ and $(\bar{i}\bar{i}, \bar{i}\bar{i})$ were 10.98 e.v.¹¹ and 22.88 e.v., respectively; the remaining repulsion integrals were computed automatically, using the uniformly charged sphere approximation.²⁹ All bond angles were assumed equal (120°). The bond lengths for butadiene (1.337, 1.483 Å.) were taken from the paper by Almenningen, Bastiansen, and Traetteberg.³⁰ Cal-

culations for naphthalene were carried out for equal bond lengths (1.40 Å).

The value of β (the one-electron resonance integral) was estimated as a function of bond length by the method of Dewar and Schmeising³ from the cycle



Here c' is the energy required to stretch a C-C single bond between sp^2 carbon atoms from its equilibrium length r' to a length r ; $f(\beta_r)$ is the energy of a C-C π -bond calculated by the s.p.o. method for bond length r . The only unknown in the expression for the energy is the value (β_r) of the one-electron resonance integral; c'' is the energy required to stretch a C=C double bond from its equilibrium length r'' to length r ; and $E_{C=C}$, E_{C-C} are the bond energies of carbon-carbon double and single bonds, respectively, between sp^2 carbon atoms. The values obtained are shown in Table VI.

TABLE VI

β AS A FUNCTION OF BOND LENGTH	
Bond length (Å.)	β (e.v.)
1.338	2.143
1.348	2.073
1.358	2.006
1.368	1.941
1.378	1.880
1.388	1.818
1.398	1.767
1.408	1.713
1.418	1.662
1.428	1.614
1.438	1.569
1.448	1.524
1.458	1.481
1.468	1.439
1.478	1.402
1.488	1.358

Table VII compares the observed transition energies for the first two singlet excited states and first two triplet excited states of *trans*-1,3-butadiene with values calculated by the s.p.o. method and by various other methods. Here f.e.m.o. refers to calculations by the free electron m.o. approximation.³¹ Three sets of s.p.o. values are shown, one using different values for β_{12} and β_{23} , corresponding to the values listed in Table VI for the experimental bond lengths, one using the same value (-2.39 e.v.) for both β 's as the value assumed by Pariser and Parr⁷ for benzene, and one using for both bonds the value (-1.77 e.v.) deduced from Table VI for an average "aromatic" bond length of 1.40 Å.

Table VIII shows a comparison of the transition energies for *cis*- and *trans*-1,3-butadiene calculated by the s.p.o. method ($\beta_{12} = \beta_{23} = -2.39$ e.v.) and by the Pariser-Parr method.

(29) R. Pariser, *J. Chem. Phys.*, **21**, 568 (1953).

(30) A. Almenningen, O. Bastiansen, and M. Traetteberg, *Acta Chem. Scand.*, **12**, 1221 (1958).

(31) S. Olzewski, *Acta Phys. Polon.*, **14**, 419 (1955).

TABLE VII

EXCITATION ENERGIES (E.V.) OF STATES OF *trans*-BUTADIENE (a) OBSERVED AND CALCULATED BY (b) S.P.O. METHOD, DIFFERENT β^a ; (c) S.P.O. METHOD, $\beta = -2.39$ E.V.; (d) S.P.O. METHOD, $\beta = -1.77$ E.V.; (e) PARISER AND PARR; (f) ATOMS-IN-MOLECULES; (g) F.E.M.O.; (h) S.C.F.; (i) S.C.F.C.I.; (j) S.C.F.C.I. (SEMI-EMPIRICAL)

State	Exp. a	S.p.o.			P-P ^b e	A.i.m. + c.i. ^g f		F.e.m.o. ^d g	h	S.o.f. ^e	
		b	c	d		i	j				
¹ B _u	6.0	6.06	5.39	5.97	6.2	7.0	6.0	5.4	8.1	9.6	6.3
¹ A _g	7.2	6.71	7.32	7.65	7.9	8.0	6.1	7.3	10.1	7.1	7.9
³ B _u	3.2	4.00	3.60	3.78	3.9	4.4	2.1	3.9	3.1	2.5	3.4
³ A _g	3.9	3.00	4.00	4.12	4.6	7.2	6.0	3.7	4.4

^a See discussion in text. ^b See ref. 7. ^c See ref. 32. ^d See ref. 31. ^e See ref. 33-35.

TABLE VIII

EXCITATION ENERGIES FOR *cis*- AND *trans*-BUTADIENE, CALCULATED BY (a) S.P.O. METHOD; (b) PARISER AND PARR

State	S.p.o.		Pariser and Parr	
	<i>cis</i> -	<i>trans</i> -	<i>cis</i> -	<i>trans</i> -
¹ B _u	5.62	5.93	5.91	6.20
¹ A _g	7.78	7.32	8.29	7.87
³ B _u	3.64	3.60	3.96	3.92
³ A _g	4.79	4.00	4.61	4.62

Table IX lists the coefficients of the a.o.'s in the m.o.'s of *trans*-1,3-butadiene, and the corresponding bond orders, calculated by the s.p.o. method with equal β 's (-1.77 e.v.) and with β 's corresponding to the experimental bond lengths.

TABLE IX

COEFFICIENTS OF A.O. IN S.C.F. M.O.'S; AND BOND ORDERS FOR *trans*-BUTADIENE CALCULATED USING (a) DIFFERENT β ; (b) $\beta_{12} = \beta_{23}$

	a	b
C ₁₁	0.457	0.463
C ₁₂	.539	.534
P ₁₂	.986	.975
P ₂₃	.164	.222

Table X compares the observed transition energies for naphthalene with those calculated by various methods. As indicated, the assignment of the third and fourth transitions is uncertain. The s.p.o. calculations were carried out with $\beta = -1.77$ e.v. for all bonds, the value corresponding to a mean bond length of 1.40 Å. (Table VI).

TABLE X

EXCITATION ENERGIES (E.V.) OF STATES OF NAPHTHALENE (a) OBSERVED; AND CALCULATED BY (b) S.P.O., $\beta = -1.77$ E.V.; (c) POPLE; (d) PARISER; (e) F.E.M.O.; (f) S.C.F.C.I.

State	Exp. a	S.p.o. b	Pople ^c c	P-P ^b d	F.e.m.o. ^e e	S.c.f.c.i. ^d f
¹ B _{2u}	3.99 ^g	3.95	4.40	4.02	3.74	7.11
¹ B _{2u}	4.27 ^g	4.86	4.65	4.49	4.54	8.37
¹ B _{3u}	{ 5.63 ^{e,f} }	6.10	6.13	5.94	5.83	10.30
¹ B _{2u}		5.52	6.20	6.31	5.84	9.31
³ B _{2u}	2.60 ^g	3.27	3.09	2.18		
³ B _{3u}		3.91	4.09	3.64		
³ B _{3u}		3.95	4.40	4.02		
³ B _{2u}		4.06	4.83	4.42		

^a See ref. 40. ^b See ref. 21. ^c See ref. 18. ^d See ref. 41. ^e See ref. 16, 42, 43. ^f This assignment remains undecided. ^g See ref. 44, 45.

(32) R. S. Berry, *J. Chem. Phys.*, **26**, 1660 (1957).
 (33) R. G. Parr and R. S. Mulliken, *ibid.*, **18**, 1338 (1950).
 (34) A. Pullman, *J. chim. phys.*, **51**, 188 (1954).
 (35) J. W. Sidman, *J. Chem. Phys.*, **27**, 429 (1957).
 (36) W. C. Price and A. D. Walsh, *Proc. Roy. Soc. (London)*, **A174**, 220 (1940).

V. Discussion of Results for Butadiene and Naphthalene

Table VII shows that the s.p.o. method gives excellent results for butadiene. It is at least as good as any other method that has been tried and very much better than the standard s.c.f.m.o. treatment, with or without configuration interaction. The only methods that compete are those which involve configuration interaction as well as the empirical adjustment of integrals. The only empirical value that enters the s.p.o. treatment is that of the one-electron resonance integral β , Table VII shows that the results are surprisingly insensitive to the value chosen and that the best results are given by values estimated independently from thermochemical data by the method indicated above.

Table VIII shows that the s.p.o. one-configuration treatment gives very much the same result for the relationship between *cis*- and *trans*-butadiene as that given by the Pariser-Parr treatment.

Table IX shows that the bond order for the central bond in butadiene is less than that given by other s.c.f. treatments,⁴⁶ a very striking result since we have neglected differential overlap—and inclusion of this in the case of butadiene is known to lower the bond order of the central bond. Thus the Pople treatment (s.c.f. with neglect of differential overlap) gives a bond order for the central bond of 0.34, with $\beta_{12} = \beta_{23} = -2.39$ e.v. This shows that vertical correlation has a pronounced effect on the alternation of bond character in butadiene.³ The bond order is still further reduced if different β 's are used for the central and terminal bonds.

Table X shows that the s.p.o. method is equally successful in the case of naphthalene, the agreement with experiment being very satisfactory. Whether the method is slightly better than, or slightly worse than, the Pariser-Parr and Pople treatments depends on the assignment of the transitions at 5.63 and 6.30 e.v. According to the s.p.o. results the assignment of these is opposite to that given by the other methods, though the difference predicted by the Pople method is very small (0.07 e.v.). The

(37) J. R. Platt and H. B. Klevens, *Rev. Mod. Phys.*, **16**, 182 (1944).
 (38) R. S. Mulliken, *ibid.*, **14**, 265 (1942).
 (39) D. F. Evans, *J. Chem. Soc.*, 1735 (1960).
 (40) J. A. Pople, *Proc. Phys. Soc. (London)*, **A68**, 81 (1955).
 (41) S. Kolboe and A. Pullman, "Calcul des Fonctions d'onde Moleculaire," Ed. CNRS, Paris, 1958.
 (42) H. B. Klevens and J. R. Platt, *J. Chem. Phys.*, **17**, 470 (1949).
 (43) H. Spomer and C. D. Cooper, *ibid.*, **23**, 646 (1955).
 (44) M. Kasha, *Chem. Rev.*, **41**, 401 (1947).
 (45) D. F. Evans, *J. Chem. Soc.*, 1351 (1957).
 (46) R. S. Mulliken, *Tetrahedron*, **6**, 68 (1959).

f.e.m.o. method predicts a still smaller difference in energy (0.01 e.v.) between these states. It is interesting that the s.p.o. treatment agrees with the usual s.c.f. m.o. method (including configuration interaction) as regards the assignment of the transitions; the results given by the latter method are, however, greatly in error.

VI. Summary

The main conclusions of this paper can be summarized as follows.

(1) The s.p.o. treatment can be regarded as a modification of the usual s.c.f. method in which allowance is made for vertical correlation by adjustment of integrals. It could be regarded in this sense as a semi-empirical extension of the s.c.f. treatment along the lines pioneered by Pariser and Parr,⁷ but with the integrals modified in a logical and self-consistent manner. The approach provides a further justification for the use of the s.p.o. method and further support for our contention² that the neglect of non-orthogonality between s.p.o. functions and the core may not in practice have any serious consequences.

(2) The results in this and the two preceding papers² suggest that the s.p.o. method is a very promising one for calculating the properties of conjugated systems.

(3) The only one-configuration treatment that can compare with the s.p.o. method is the Pople⁸ approximation. In the case of hydrocarbons the two methods would be expected to give very similar results, for the following reason. Using a Goepfert-Mayer-Sklar potential and neglecting penetration integrals, eq. 19 becomes⁸

$$F_{ii} = W_{2p} + \frac{1}{2}q_i(\bar{ii}, \bar{ii}) + \sum_{j \neq i} (q_j - 1)(\bar{ij}, \bar{ij}) \quad (25)$$

The corresponding s.p.o. equation (21) becomes

$$F_{ii} = W_{2p} + \frac{1}{2}q_i(\bar{ii}, \bar{ii}) + \sum_{j \neq i} (q_j - 1)(\bar{ij}, \bar{ij}) \quad (26)$$

Pople assumes, following Pariser and Parr,⁷ that all the repulsion integrals have reduced values, corresponding in our system to "upper-lower" integrals. Since $q_i = 1$ for all atoms in an alternant hydrocarbon, if differential overlap is neglected,⁸ the Pople and s.p.o. expressions for the diagonal elements in the F -matrix are identical for such compounds. The expressions for the off-diagonal elements differ, being given by

$$(\text{Pople}) \quad F_{ij} = \beta_{ij} - \frac{1}{2}p_{ij}(\bar{ii}, \bar{jj}) \quad (27)$$

$$(\text{s.p.o.}) \quad F_{ij} = \beta_{ij} - \frac{1}{2}p_{ij}(\bar{ii}, \bar{jj}) \quad (28)$$

However, since bond orders do not vary much in aromatic compounds, and since the elements F_{ij} are small for non-bonded atoms, the values for the two methods can be brought into near coincidence by using different values for β . The value appropriate to the s.p.o. treatment should of course be numerically smaller—as in fact it is.

However this correspondence between the Pople and s.p.o. treatments applies only to alternant hydrocarbons; in the case of non-alternant hydrocarbons, or of compounds containing heteroatoms, the charge densities q_i are no longer unity and the expressions for the diagonal elements of the F -matrix differ. Preliminary results suggest that the s.p.o. method is significantly superior for heteroaromatic systems.

Acknowledgment.—We are very grateful to Dr. L. C. Snyder of Bell Telephone Laboratories for helpful discussions and for his Molecular Orbital Program, to Bell Telephone Laboratories for computational facilities, and to the National Science Foundation for support. N. L. S. thanks the Consejo Nacional de Investigaciones Cientificas de Argentina for a Fellowship, for part of the period covered by this work.

A MOLECULAR ORBITAL STUDY OF THE POLAROGRAPHIC REDUCTION IN DIMETHYLFORMAMIDE OF UNSUBSTITUTED AND METHYL-SUBSTITUTED AROMATIC HYDROCARBONS¹

BY A. STREITWIESER, JR.,² AND I. SCHWAGER

Department of Chemistry, University of California, Berkeley, Cal.

Received June 20, 1962

The half-wave potentials of a number of aromatic compounds have been determined and are found to fit the same type of correlation with the energies of the lowest vacant molecular orbitals in the HMO approximation established in other solvents. The deviation of biphenylene from this correlation can be accounted for in terms of "long bonds" but this explanation fails when applied to 2,3-benzobiphenylene. Azulene and acepleiadylene do not obey the simple theory. The effect of methyl substituents is accounted for successfully in terms of a combination of conjugative (hyperconjugation) and inductive influences.

Laitinen and Wawzonek found that phenyl-substituted olefins and acetylenes and aromatic polynuclear hydrocarbons are reduced at the dropping mercury electrode in aqueous dioxane and

give reproducible half-wave potentials. The first reduction wave of these compounds corresponds to the approximately reversible addition of one or two electrons to the compound.³⁻¹⁰ Hence, the half-

(1) This research was supported in part by an Air Force Grant, AF-AFOSR-62-175.

(2) Alfred P. Sloan Fellow, 1958-1962.

(3) H. A. Laitinen and S. Wawzonek, *J. Am. Chem. Soc.*, **64**, 1765 (1942).

(4) S. Wawzonek and H. A. Laitinen, *ibid.*, **64**, 2365 (1942).

wave potential for this reduction corresponds to an electron affinity of the hydrocarbon. Such half-wave potentials have been found to give excellent correlations with the lowest lying molecular orbital in simple MO theory.¹¹ These correlations provide an important means of comparing theoretical predictions with quantitative experimental results.

2-Methoxyethanol also has been used as a solvent for polarographic studies of polycyclic aromatic hydrocarbons¹² and more recently Given¹³ has shown the advantages of dimethylformamide for such studies. We have extended the measurements of Given in dimethylformamide and have established the same type of correlation of half-wave potentials with the energies of the lowest vacant MO's shown previously in other solvents. This correlation then has been used to examine departures from the simple polycyclic aromatic hydrocarbons. Several non-alternant hydrocarbons have been included and we have studied the effect of the "long bonds" in biphenylene systems. Finally, we have looked at the effects of methyl substituents and the explanation of the effects in terms of molecular orbital theory.

Experimental

Instrumentation.—Current-potential curves were recorded with a Sargent Model XV polarograph. All potentials were measured with reference to an internal mercury pool anode in 0.1 *N* tetra-*n*-butylammonium iodide in dimethylformamide (which was -0.55 v. *vs.* s.c.e.). The Hg pool cell was thermostated at $25.0 \pm 0.2^\circ$. A commercial conductance bridge obtained from Electromer Inc., Portland, Oregon (Model 250-DA) was used to measure solution resistance. An average value for resistance in the supporting solution was 700 ± 50 ohms.

Materials.—Dimethylformamide was purified by distillation in a sixteen-plate Oldershaw column. The fraction used distilled in the range $152\text{--}153^\circ$. Polarograph grade tetra-*n*-butylammonium iodide was supplied by Southwestern Analytical Chemicals, Austin, Texas. The majority of the aromatic hydrocarbons were obtained from various commercial sources, and purified when necessary by chromatography on neutral alumina, gas chromatography on a carbowax column, or by repeated crystallization from suitable solvents. The authors wish to express their gratitude to Dr. W. C. Langworthy, who supplied samples of several methyl-substituted aromatic hydrocarbons, and to Dr. F. R. Jensen, who supplied a sample of 2,3-benzbiphenylene. Acepleiadylene was the kind gift of Dr. V. Boekelheide; biphenylene was prepared by Dr. R. M. Williams.

Experimental Procedure.—Solutions of the hydrocarbons (about 0.001 *M*) were prepared with previously deoxygenated dimethylformamide and were further degassed for 10 min. Cylinder nitrogen, used for degassing, was purified according to Fieser.¹⁴

Experimental System.—Dimethylformamide, as reported previously,¹³ proved to be an excellent solvent for the polarographic investigation of aromatic compounds. Its ease of

purification, dissolving power, and the excellent character of the observed current-voltage curves demonstrate that it compares very favorably with 2-methoxyethanol¹² as a useful aprotic solvent for polarography. The decomposition potential of the supporting solution is approximately -2.40 v. *vs.* Hg pool anode. No maxima were observed at the concentration range studied. The solution resistance of 700 ± 50 ohms caused, at a 1 *mM* concentration of aromatic hydrocarbon, an *IR* drop of 1 or 2 mv. The values reported have not been corrected for this small *IR* drop since it is less than the experimental uncertainty, and remains constant for similar concentrations of substrate.

Many of the aromatic and methyl aromatic compounds also run *vs.* s.c.e. in an H-cell separated by an agar-saturated potassium chloride bridge, and were found to give good agreement with the results observed *vs.* the internal Hg pool reference electrode. The Hg pool electrode was preferred because both KCl and water diffused through the agar bridge into the sample compartment of the s.c.e. cell, and were potential sources of difficulty. Potassium ion is itself reduced in dimethylformamide at approximately -2.05 v., and the addition of a proton source such as water to dimethylformamide has been shown^{15,16} to cause small shifts in the half-wave potentials of aromatic hydrocarbons.

Experimental Results and Uncertainties.—For representative compounds such as naphthalene and anthracene, the diffusion current was found to be proportional to concentration over the range 0.5 to 5 *mM*, and the standard deviation of the half-wave potential over this range for ten different concentrations, and over a period of several days, was ± 0.010 v. However, the reproducibility was ± 0.005 v. for successive runs at similar concentrations.

The values reported for the methyl-substituted and parent compounds are the average of three such consecutive runs made at similar concentrations.

Discussion

The half-wave potentials for the benzenoid aromatic hydrocarbons (Table I) plotted against the energies of the lowest vacant MO's give a good linear correlation (Fig. 1) as expressed by the equation¹⁶

$$-E_{1/2} = (2.407 \pm 0.182)m_{m+1} - 0.396 \pm 0.093 \quad (1)$$

This correlation is amazingly close to that in 2-methoxyethanol¹¹

$$-E_{1/2} = (2.414 \pm 0.092)m_{m+1} - 0.435 \pm 0.065 \quad (2)$$

It is noteworthy that the slopes and intercepts in the two solvents are so similar and show again the unexpected similarity of solvation energies of hydrocarbon anions in different solvents.

Several hydrocarbons deviate markedly from the correlation line. In one of these cases, biphenylene, it has been reported recently, on the basis of X-ray structure analysis, that the central bonds are virtually single bonds (1.52 ± 0.03 Å.)¹⁷ and that the remaining six-membered ring bonds are almost normal benzene bonds. One of the assumptions made in the simple Hückel MO theory is the equality of bond integral terms for nearest neighbors. This assumption is equivalent to assuming an equality of all bond distances. The effect that a change in β of bond *r*-s has on the energy, ϵ_j ,

(15) G. J. Hoijtink, *Ricerca Sci.*, **30**, Suppl. No. 5, 217 (1960).

(16) The "unusual" compounds, biphenylene, 2,3-benzobiphenylene, azulene, and acepleiadylene were omitted.

(17) T. C. W. Mak and J. Trotter, *J. Chem. Soc.*, 1 (1962).

(5) S. Wawzonek and J. W. Fan, *J. Am. Chem. Soc.*, **68**, 2541 (1946).

(6) G. J. Hoijtink and J. van Schooten, *Rec. trav. chim.*, **71**, 1089 (1952).

(7) G. J. Hoijtink and J. van Schooten, *ibid.*, **72**, 691 (1953).

(8) G. J. Hoijtink, J. van Schooten, E. de Boer, and W. I. Aalbersberg, *ibid.*, **73**, 355 (1954).

(9) G. J. Hoijtink, *Rec. trav. chim.*, **73**, 895 (1954).

(10) A. C. Aten, C. Büthker, and G. J. Hoijtink, *Trans. Faraday Soc.*, **55**, 324 (1959); K. Schwabe and E. Schmidt, *Z. physik. Chem. (Leipzig)*, Sonderheft, 278 (1958); K. Schwabe, *ibid.*, 289 (1958); H. J. Gardner, *Nature*, **183**, 320 (1959).

(11) For a summary see A. Streitwieser, Jr., "Molecular Orbital Theory for Organic Chemists," John Wiley and Sons, Inc., New York, N. Y., 1961.

(12) I. Bergman, *Trans. Faraday Soc.*, **50**, 829 (1954).

(13) P. H. Given, *J. Chem. Soc.*, 2684 (1958).

(14) L. F. Fieser, *J. Am. Chem. Soc.*, **46**, 2639 (1924).

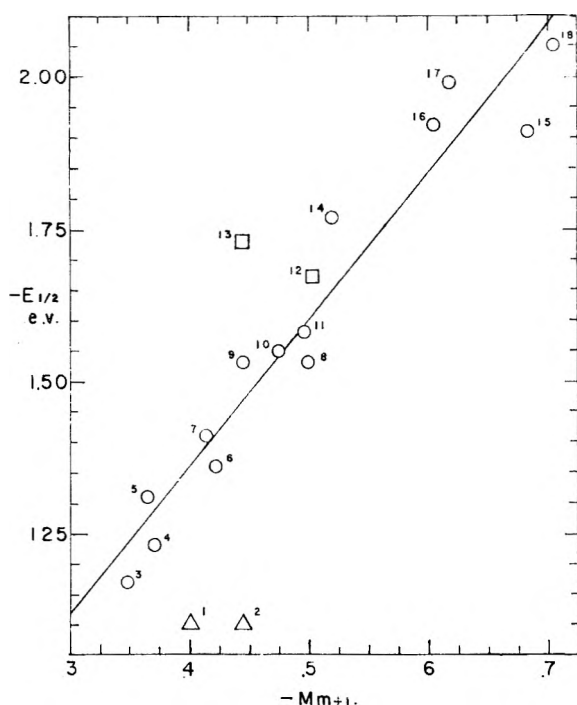


Fig. 1.—Half-wave potentials of aromatic hydrocarbons in dimethylformamide vs. energy coefficient of lowest vacant MO in the HMO approximation.

TABLE I
HALF-WAVE REDUCTION POTENTIALS FOR AROMATIC
HYDROCARBONS IN DIMETHYLFORMAMIDE

No. in Fig. 1	Hydrocarbon	$-m_{m+1}^a$	$-E_{1/2}$ vs. Hg pool Dimethyl- formamide
1	Azulene	0.400	1.10
2	Acepleiadylene	.445	1.10
3	Perylene	.347	1.17
4	Fluoranthene	.371	1.23
5	1,2-Benzopyrene	.365	1.31
6	1,2,4,5-Dibenzopyrene	.422	1.36
7	Anthracene	.414	1.41 ^b
8	1,2,3,4-Dibenzanthracene	.499	1.53
9	Pyrene	.445	1.53 ^b
10	1,2,5,6-Dibenzanthracene	.474	1.55
11	4,5-Benzopyrene	.497	1.58
12	2,3-Benzobiphenylene	.502	1.67
13	Biphenylene	.445	1.73
14	Chrysene	.520	1.77
15	Triphenylene	.684	1.91
16	Phenanthrene	.605	1.92 ^b
17	Naphthalene	.618	1.99 ^b
18	Biphenyl	.705	2.05

^a Energy coefficient of lowest vacant MO in the HMO method (see ref. 11). ^b Given¹² reports: naphthalene, 1.99; anthracene, 1.41; phenanthrene, 1.93; pyrene, 1.56.

of molecular orbital, ψ_j , is given to a first approximation as¹⁸

$$\delta\epsilon_j = \frac{\partial\epsilon_j}{\partial\beta_{rs}} \delta\beta_{rs} = 2p_{rs}^j \delta\beta_{rs} \quad (3)$$

in which p_{rs}^j is the partial mobile bond order [$p_{rs}^j = c_{jr}c_{js}$, in which c_{jr} is the coefficient of the r th

(18) C. A. Coulson and H. C. Longuet-Higgins, *Proc. Roy. Soc. (London)*, **A191**, 39 (1947).

atomic orbital in the j th molecular orbital]. If we assume that β is proportional to overlap integral, $\delta\beta$ for each of the central bonds in biphenylene is $-0.20\beta_0$,¹¹ and $\delta\epsilon_{m+1} = (2)(0.3685)^2(-0.20) = -0.054\beta$. Because there are two such bonds the corrected m_{m+1} is -0.553 , which yields a calculated $-E_{1/2} = 1.73$ v., in excellent agreement with the experimental value, 1.73 v.

Unfortunately, the success of this method does not appear to be general. A similar correction may be made to 2,3-benzobiphenylene assuming that the bonds joining the benzene and naphthalene rings are also 1.52 Å. in length. The corrected m_{m+1} corresponds to $-E_{1/2} = 1.85$, in poor agreement with the experimental value, 1.67 v. Actually 2,3-benzobiphenylene agrees rather well with the correlation line without any corrections.

The behavior of the non-alternant hydrocarbons merits comment. Fluoranthene behaves as a typical benzenoid hydrocarbon in fitting the correlation. Azulene, however, has a lower reduction potential by 0.25 v. than that predicted by the correlation of other hydrocarbons. The half-wave potential of acepleiadylene, -1.10 v., has not been reported before and is lower by almost 0.4 v. than the predicted value. These serious deviations are not corrected by allowing for "long bonds." Instead, the enhanced oxidizing power of these hydrocarbons probably is associated with more serious limitations of simple MO theory. The compounds are calculated to have greater stability than they actually possess; their resonance energies are lower than expected on the basis of calculated delocalization energies.¹¹

The effect of methyl groups on ionization potentials has been shown previously to be accounted for satisfactorily in terms of an inductive effect alone.¹⁹ A similar treatment has been suggested for the effect of methyl groups on polarographic half-wave potentials but the data available for testing the method were rather meager.^{11,20} In this method the π -carbon attached to the methyl group is made more electropositive by the assignment of a negative h in the definition

$$\alpha_r = \alpha_0 + h_r\beta_0 \quad (4)$$

The effect that such a change in the coulomb integral has on the energy, ϵ_{m+1} , of the lowest vacant MO is given by

$$\delta\epsilon_{m+1} = c_{m+1,r}^2 \delta\alpha_r = c_{m+1,r}^2 h_r\beta_0 \quad (5)$$

As a test of this model we have determined the half-wave potentials of a number of methyl-substituted aromatic compounds (Table II). Methyl groups invariably render the hydrocarbons somewhat harder to reduce, in agreement with the qualitative predictions of the simple model. The quantitative prediction that the energy change is proportional to $c_{m+1,r}^2$ (eq. 5) is tested in Fig. 2 and is found to be unsuccessful. Inspection of this figure reveals that methyl groups at β -naphthyl type positions (triangles in Fig. 2) give a good linear correlation among themselves but that α -methyl substituted compounds fall generally below this line.

(19) A. Streitwieser, Jr., *J. Phys. Chem.*, **66**, 368 (1962).

(20) L. E. Lyons, *Research*, **2**, 587 (1949).

TABLE II
EFFECT OF METHYL OR METHYLENE SUBSTITUENTS ON HALF-WAVE POTENTIALS

No. in Fig. 2, 3	Subst. pos.	$-E_{1/2}$ (v.)	$-\Delta E_{1/2}$ (v.)	$\bar{\nu}^b$ (cm. ⁻¹)	$\Delta \nu$ (v.)	$-\Delta E_{1/2}$ corr.	$\sum c_{r,m+1}^2$
		1.994		35010			
1	1	2.022	0.028	34220	0.098	0.126	0.180
2	2	2.042	.048	35010	.000	.048	.069
3	1,2	2.046	.052	34180	.103	.155	.249
4	1,4	2.023	.029	33500	.187	.216	.360
5	1,6	2.055	.061	33940	.133	.194	.249
6	1,7	2.056	.062	34250	.094	.156	.249
7	2,3	2.090	.096	34720	.036	.132	.138
8	2,6	2.070	.076	34950	.007	.083	.138
		1.920		34130			
9	2	1.942	.022	34070	.007	.029	.002
10	3	1.980	.060	33670	.057	.117	.099
11	9	1.969	.049	33560	.071	.120	.172
		1.405		26740			
12	2	1.450	.045	26530	.026	.071	.048
13	9	1.417	.012	25910	.103	.115	.194
		1.526		29960			
14	1	1.549	.023	29210	.093	.115	.135
15	2	1.541	.015	29750	.026	.041	.000
16	4	1.555	.029	29750	.026	.055	.087
		1.228					
	3	1.267	.039				
	7	1.273	.045				
	8	1.304	.076				
		2.050					
		2.170	.120				
		2.200	.206				
		1.946	.026				

^a These compounds were not included in the correlations. Fluoranthene is a non-alternant hydrocarbon; the other compounds are not methyl-substituted. ^b Values were obtained from D. Peters, *J. Chem. Soc.*, 646 (1957), and American Pet. Inst. Project 44; Natl. Bur. Standards.

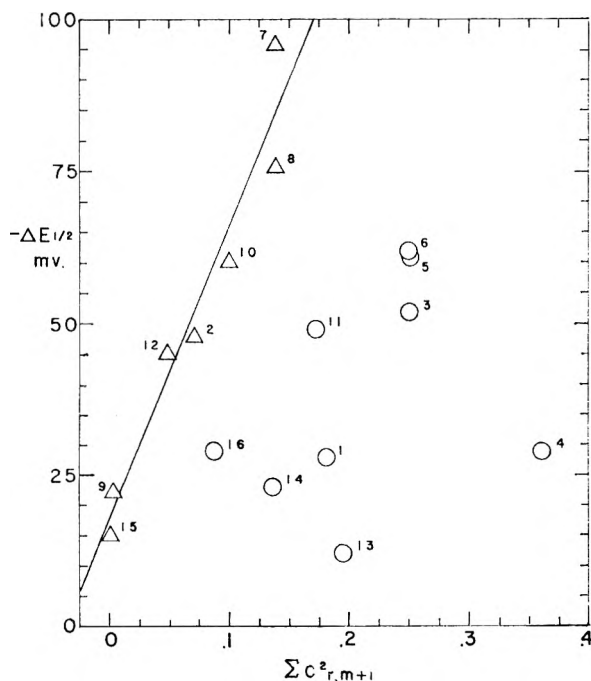


Fig. 2.—Attempted correlation of the effect of methyl groups on half-wave potentials using an inductive model only.

The inductive model of the methyl group alone is inadequate for the present purpose. The conjugative ability of the methyl group has been ig-

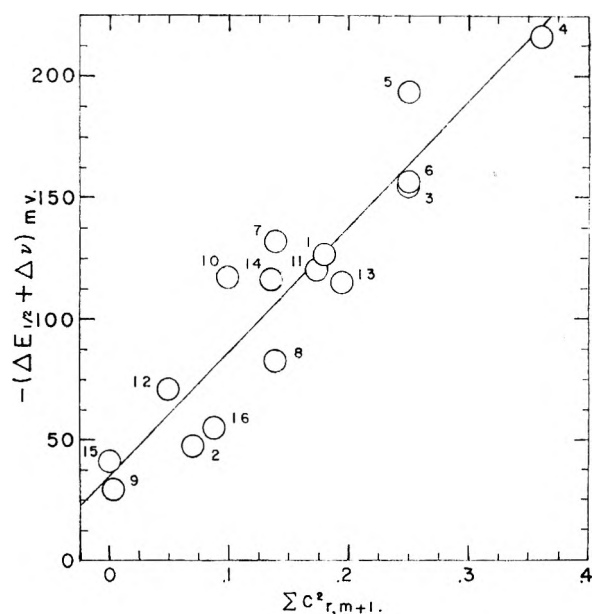


Fig. 3.—Correlation of the effect of methyl groups on half-wave potentials corrected for conjugation effects using the inductive model.

nored in this model. For the evaluation of this effect we turn to absorption spectra. The p-band of aromatic hydrocarbons may be associated with transition of an electron from the highest occupied to the lowest vacant π -MO. The effect of a

methyl substituent on this band for alternant hydrocarbons is determined essentially entirely by the conjugation effect and not by inductive effects.²¹ This analysis suggests the use of the bathochromic shift given by a methyl substituent as a means to correct the shift in reduction potential for conjugation by the methyl group. Actually, the bathochromic shift results from changes in energies of both the highest occupied and lowest vacant orbitals and only a part of the spectral shift should be associated with the change in one orbital alone. Nevertheless, the simple MO interpretation of spectra is highly approximate; hence, the entire bathochromic shifts accompanying methyl substitution as listed in Table II have been converted to volts and added to the observed $\Delta E_{1/2}$ values to give an estimate of the reduction potential in the absence of conjugation effects. The new values, $\Delta E_{1/2, \text{corr}}$, should now be dependent only on the inductive effect as in eq. 5. A plot of

$\Delta E_{1/2, \text{corr}}$ against $c_{m+1, r}^2$ in Fig. 3 shows a greatly improved correlation; the correlation coefficient is 0.94 despite the fact that both types of shifts are of comparatively small magnitude and contain rather substantial experimental errors. For $\beta_0 = -2.4$ e.v. (the slope of Fig. 1), the slope of Fig. 3 corresponds to $h_X = -0.21$. This correlation provides evidence for the importance of both conjugative and inductive influences in the effect of methyl groups on reduction potentials. The inductive effect decreases the electron affinity and is generally more important than the conjugation effect which tends to increase the electron affinity; conjugation is clearly more important at α -naphthyl than at β -naphthyl-type positions. Both effects are undoubtedly also important in ionization potentials but in this case the two effects operate in the same direction and probably to comparable extents. Hence, consideration of the inductive effect alone suffices to a reasonable approximation. It is undoubtedly for this reason that the effective h_X for the inductive model in ionization potentials, -0.54 ,¹⁹ is numerically greater than that for reduction potentials in Fig. 3, -0.21 .

(21) C. A. Coulson, *Proc. Phys. Soc. (London)*, **A65**, 933 (1952); H. C. Longuet-Higgins and R. G. Sowden, *J. Chem. Soc.*, 1404 (1952). An illuminating graphic analysis is given by E. Heilbronner, Chapt. 5 of "Non-benzenoid Aromatic Hydrocarbons," Interscience Publishers, New York, N. Y., 1959; see also ref. 11.

THE NATURE OF THE TWO-ELECTRON CHEMICAL BOND. II. THE HETEROPOLAR CASE¹

BY HARRISON SHULL

Chemistry Department, Indiana University, Bloomington, Indiana

Received June 20, 1962

By using the artifice of dividing space into two parts by means of a plane perpendicular to the internuclear axis and passing through its mid-point, it is shown that there is possible a division of a two-configuration two-electron wave function into three orthogonal parts each of which has optimum properties associated with the plane intuitively corresponding to the names "ionic" and "atomic." In this paper, the heteropolar case is considered, and it is shown that there arises a natural mathematical quantity, θ , which is a function of three integrals over natural orbitals over half space. The quantity, θ , seems to bear a considerable resemblance to electronegativity difference. An example is given for the simple diatomic hydride two-electron system, $\text{HZ}^{(Z-1)+}$, at a fixed internuclear distance. Finally it is pointed out that the treatment is a special case of the use of a much more general weight factor. Suitable choices of the latter may make it possible to relate functionally the large number of different electronegativity scales.

I. Introduction

In a previous paper² we have developed a treatment of the two-electron bond in the homopolar case which seems to avoid some of the pitfalls of the typical textbook version. In particular, by starting from the natural orbital expansion,³ we avoid completely the arbitrary features of previous treatments which depend upon a very particular choice of basis set. The natural expansion is uniquely determined⁴ from the exact wave function, which is obviously quite independent of the particular basis set chosen. In actual practice it has been shown that even fairly crude approximations to the exact wave function lead to very similar

approximate natural expansions.⁵ At an early stage in the calculation, therefore, the use of the natural expansion frees one from the arbitrary nature of the approach.

A second pitfall that has been pointed out previously^{2,6} is the identification of chemical concepts with non-orthogonal wave mechanical functions. Thus the rather generally used "covalent" function of Wang for the hydrogen molecule and the "ionic" terms introduced in the Weinbaum function had an overlap of about 0.95. One might have said that the addition of "ionic" terms in this case was 95% utilized in improving the "covalent" representation, or indeed that the original "covalent" function was 95% ionic in the first place. One can easily show that if one is not particular about the precise nature of the "covalent"–"ionic" criterion, that there exists almost any degree of ionic character that one chooses.

(1) Supported by contracts and grants from the U. S. Air Force OSR and from the National Science Foundation.

(2) H. Shull, *J. Am. Chem. Soc.*, **82**, 1287 (1960). We refer to this paper as I.

(3) (a) P.-O. Löwdin and H. Shull, *Phys. Rev.*, **101**, 1720 (1956); (b) H. Shull and P.-O. Löwdin, *J. Chem. Phys.*, **30**, 617 (1959).

(4) Excepting, of course, certain cases of degeneracy which are not of importance here.

(5) H. Shull, *J. Chem. Phys.*, **30**, 1405 (1959).

(6) J. Braunstein and W. T. Simpson, *ibid.*, **23**, 174, 176 (1955).

In the homopolar case, it was shown that a crude and rather naive division of space into two parts by a plane passing through the mid-point of and perpendicular to the hydrogen molecule bond could be utilized to *define* a criterion for an optimum "atomic" and an optimum "ionic" function in the space of hydrogen molecule wave functions of rank two. The optimum atomic function and the optimum ionic function were attained with precisely the same choice of variable parameters, and this choice furthermore led to the highly desirable and satisfying result that these two functions were orthogonal to each other.

We can summarize the philosophy of this treatment. We desire that theoretical counterparts of intuitive chemical concepts be exactly and precisely defined in the framework of a mathematical approximation to the exact wave function. This approximation on the one hand should itself be precisely defined and in addition, of course, it should bear as close a relation as possible to the exact wave function. We should finally remind the reader that the natural orbital expansion satisfies this count ideally in the two-electron case, for the truncated ordered natural expansion is term-by-term that function of corresponding rank with optimum representation of the electron density of the exact function.^{3a}

II. Extension to the Heteropolar Case

If one attempts to apply the general theory to the heteropolar case, one soon finds that what has been an interesting exercise in trigonometric identities becomes a nightmare. We rationalize our unwillingness to pursue this more general problem in its complete form by falling back on the desiderata mentioned in the Introduction. Namely, the solutions in which we are primarily interested are those which maintain the orthogonality of Ψ_A , Ψ_+ , and Ψ_- defined by

$$\Psi_A = [u(1)v(2) + v(1)u(2)]/\sqrt{2} \quad (1a)$$

$$\Psi_+ = [u(1)u(2) + v(1)v(2)]/\sqrt{2} \quad (1b)$$

$$\Psi_- = [u(1)u(2) - v(1)v(2)]/\sqrt{2} \quad (1c)$$

The restriction to the orthogonal case implies that we can expand u and v in terms of the natural orbitals χ_1 and χ_2 with a single variable parameter α

$$u = \chi_1 \cos \alpha + \chi_2 \sin \alpha \quad (2a)$$

$$v = \chi_1 \sin \alpha - \chi_2 \cos \alpha \quad (2b)$$

We then still have the general expansion for the optimum function of rank 2

$$\Psi = c_1\chi_1(1)\chi_1(2) + c_2\chi_2(1)\chi_2(2) \quad (3)$$

which may be expressed as

$$\Psi = \lambda_A\Psi_A + \lambda_+\Psi_+ + \lambda_-\Psi_- \quad (4)$$

In the orthogonal case considered here⁸

(7) Ψ_+ and Ψ_- are identical with Ψ_{I+} and Ψ_{I-} of I in the orthogonal case.

$$\lambda_A = [(c_1 - c_2) \sin 2\alpha]/\sqrt{2} \quad (5a)$$

$$\lambda_- = [(c_1 - c_2) \cos 2\alpha]/\sqrt{2} \quad (5b)$$

$$\lambda_+ = (c_1 + c_2)/\sqrt{2} \quad (5c)$$

As in I, we can introduce a plane perpendicular to and bisecting the internuclear line in the heteropolar bond under discussion. We reserve for later discussion the question of the validity of such an arbitrary division in the first place, placing it at the mid-point of the bond in the heteropolar molecule in the second, and in the third place, ways of circumventing this division in its entirety. At this point we note that the division is used merely as a criterion of optimum functional *form* of Ψ_A , Ψ_+ , Ψ_- . It plays no direct role in the evaluation of λ_A , λ_+ , and λ_- . Of course, it plays an indirect role. But if some other criterion should lead to the same choice of Ψ_A , Ψ_+ , Ψ_- , then the arbitrary division of space would be completely unnecessary and indeed irrelevant.

Continuing as in part IV of I, we define

$$A_A = \int \Psi_A^2 d\tau_{1R} d\tau_{2L} + \int \Psi_A^2 d\tau_{1L} d\tau_{2R} \quad (6a)$$

$$A_+ = \int \Psi_+^2 d\tau_{1R} d\tau_{2L} + \int \Psi_+^2 d\tau_{1L} d\tau_{2R} \quad (6b)$$

$$A_- = \int \Psi_-^2 d\tau_{1R} d\tau_{2L} + \int \Psi_-^2 d\tau_{1L} d\tau_{2R} \quad (6c)$$

and correspondingly

$$I_A = \int \Psi_A^2 d\tau_{1R} d\tau_{2R} + \int \Psi_A^2 d\tau_{1L} d\tau_{2L} \quad (7a)$$

$$I_+ = \int \Psi_+^2 d\tau_{1R} d\tau_{2R} + \int \Psi_+^2 d\tau_{1L} d\tau_{2L} \quad (7b)$$

$$I_- = \int \Psi_-^2 d\tau_{1R} d\tau_{2R} + \int \Psi_-^2 d\tau_{1L} d\tau_{2L} \quad (7c)$$

We note, of course, that $A_A + I_A = 1$. Similar relations hold for the other pairs. We introduce the definitions (1) and (2) into (6) and (7) to arrive at general expressions for A_A , etc., as a function of the variable parameter α and of three independent integrals over the natural orbitals (several others occur but are easily related to these three)

$$R_{11} = \int \chi_1^2 d\tau_R \quad (8a)$$

$$R_{22} = \int \chi_2^2 d\tau_R \quad (8b)$$

$$R_{12} = \int \chi_1\chi_2 d\tau_R \quad (8c)$$

In the homopolar case, $R_{11} = R_{22} = 1/2$, but these relations do not apply in the heteropolar bond.

Performing the substitution and rearranging

(8) We note that eq. 10a-10c of I contain errors. The correct general formulas are

$$\lambda_A = [(n_1^{1/2} + n_2^{1/2}) \sin(\alpha + \beta) + (n_1^{1/2} - n_2^{1/2}) \sin(\alpha - \beta)]/2N_+ \cos^2(\alpha - \beta) \quad (10a)$$

$$\lambda_{I+} = [(n_1^{1/2} - n_2^{1/2}) + (n_1^{1/2} + n_2^{1/2}) \sin(\alpha + \beta) \times \sin(\alpha - \beta)]/2N_+ \cos^2(\alpha - \beta) \quad (10b)$$

$$\lambda_{I-} = [(n_1^{1/2} + n_2^{1/2}) \cos(\alpha + \beta)]/2N_- \cos(\alpha - \beta) \quad (10c)$$

It is easy to verify that these corrected equations lead to eq. 5 above for the case $\alpha = \beta$, $n_1^{1/2} = c_1$, and $-n_2^{1/2} = c_2$. There is an additional small error in I where erroneous limits are given for the variable λ_{I+}/λ_A on p. 1289. This variable can easily be shown to lie between the limits -1 (for $S = +1$) and +1 (for $S = -1$). These changes inadvertently introduced in the preparation of the manuscript do not affect any of the remaining equations or data given in I.

somewhat, we arrive at the following general expressions for the orthogonal heteropolar case

$$A_A = 1/2 - 1/2(\epsilon_1 + \epsilon_2)^2 + 2R_{12}^2 [(\theta^2 - 1) \cos 4\alpha + 2\theta \sin 4\alpha] \quad (9a)$$

$$I_- = 1/2 + 1/2(\epsilon_1 + \epsilon_2)^2 + 2R_{12}^2 [(\theta^2 - 1) \cos 4\alpha + 2\theta \sin 4\alpha] \quad (9b)$$

$$I_+ = 1/2 + \epsilon_1^2 + \epsilon_2^2 + 2R_{12}^2 \quad (9c)$$

where

$$\theta = (R_{11} - R_{22})/2R_{12} \quad (10)$$

and

$$\epsilon_1 = R_{11} - 1/2, \quad \epsilon_2 = R_{22} - 1/2 \quad (11)$$

The expressions 9a-9c may be formulated in a number of alternative ways, but the above seems most convenient for our purpose. Another convenient variable to use in place of ϵ_1 and ϵ_2 may be $\epsilon_1/2R_{12}$ and $\epsilon_2/2R_{12}$ analogous to the definition of θ . It should be noted that there is a simple relation between θ and ϵ_1, ϵ_2 ; namely

$$\theta = (\epsilon_1 - \epsilon_2)/2R_{12}$$

We now proceed to find the optimum choices of α ; that is, the respective choices which maximize A_A and I_- . Since I_+ is independent of α , no maximization is possible in this case. Inspection of (9a) and (9b) shows that the dependence of A_A and of I_- upon α is identical. Hence the same choice of α which maximizes A_A also will make I_- a maximum. It should be pointed out that the identity in dependence upon α is by no means obvious at the outset, since the functions Ψ_A and Ψ_- are different and independent, and in addition the respective integrations are over different regions of two-electron space.

Proceeding with the differentiation of A_A and I_- with respect to α , setting the result to zero, and rearranging, we arrive immediately at the equation for optimum α

$$\tan 4\alpha = 2\theta/(\theta^2 - 1) \quad (12)$$

Finally we can express the coefficients, λ , in eq. 4 in terms of this new parameter θ

$$\lambda_A = (c_1 - c_2)/[2(\theta^2 + 1)]^{1/2} \quad (13a)$$

$$\lambda_- = (c_1 - c_2)\theta/[2(\theta^2 + 1)]^{1/2} \quad (13b)$$

$$\lambda_+ = (c_1 + c_2)/[2]^{1/2} \quad (13c)$$

This completes the formal analysis of the problem utilizing this naïve division of space into two parts. We see that it leads to a division of the wave function into parts which have optimum identification with the particular criterion for the intuitive concepts which we have chosen. Furthermore these functions are orthogonal, and the final parameters are a function of a single variable, here labeled θ .

III. Application to a Simple Heteropolar System

In order to obtain some feel for the nature of the above results, we have applied these equations to the

simple case of a two-electron heteropolar diatomic hydride $ZH^{(Z-1)+}$ of which H_2, HeH^+ are particular examples. For the present purpose there was no reason to restrict the calculations to integral Z , and in fact the nuclear charge of atom Z was taken over the range 0.5 (0.5) 5.5. A simple energy calculation was carried out using "covalent" and "ionic" terms derived from 1s atomic orbitals of appropriate orbital exponent on each center without scaling. Thus

$$\Psi = \mu_a 1s_a(1)1s_a(2) + \mu_b 1s_b(1)1s_b(2) + \mu_c N_+ [1s_a(1)1s_b(2) + 1s_b(1)1s_a(2)] \quad (14)$$

This is, of course, a rank two wave function, and it is a relatively simple matter to express the resultant function, with coefficients μ_a, μ_b , and μ_c chosen for optimum energy, in the functional form of eq. 3, and *via* eq. 8, 10, 12, and 5 in the functional form of eq. 4. The coulomb integrals required were obtained by five-point Lagrangian interpolation from tables published by the Chicago group. The hybrid and exchange integrals were evaluated using the Mulliken approximation. Typical results for a fixed internuclear distance, $R = 1.0B$, are given in the accompanying table for a selected set of charges. Although the integral approximations may have introduced small errors into the quantitative results, the figures should be qualitatively correct.

Some comments on these results seem pertinent at this point. Looking at the homopolar case ($Z = 1.0$) we find a relatively low fraction of atomic character, λ_A^2 , as was noted in I. In this case, λ_A^2 is even lower than found for the properly scaled Wang and Weinbaum functions for which λ_A^2 was 0.680, 0.615, respectively (0.579 in the present calculation). It is to be noted that λ_A^2 does reach a maximum in the homopolar case as would be hoped. Furthermore it falls rapidly toward zero as the nuclear charge of the atom Z is raised. This corresponds to a rapid dominance of the term with coefficient μ_b in eq. 14 as Z is raised. This dominance also is reflected in the rising value of n_1 , the occupation number of $\chi_1 (= c_1^2)$ as Z increases. In the limit of large Z , $n_1 = 1, n_2 = 0$ for the approximation we are using here.

Finally, some mention should be made of λ_+ and λ_- . The square of the former, with its value of 0.421 for the homopolar case, represents the "ionic character" present in a homopolar bond, if indeed one wishes to attribute any such non-observable quantity to the homopolar case. It is to be recognized that the function Ψ_+ with its orthogonality constraints does not necessarily bear a very close relationship to the actual function for, say, H^+H^- . It would be interesting to explore this relationship, but we have not done this as yet. The fraction λ_+^2 increases gradually with increasing Z , obviously approaching in the limit of very large Z the value of $1/2$. The function Ψ_- , on the other hand, does not contribute to the homopolar molecule at all since its coefficient is zero for that case. The magnitude of λ_-^2 rises rapidly with increasing Z , approaching again the expected limit of $1/2$ at very large Z values.

TABLE I

PARAMETERS CALCULATED FOR THE TWO-ELECTRON HYDRIDE SYSTEM $HZ^{(Z-1)+}$ AS A FUNCTION OF Z AT THE FIXED INTERNUCLEAR DISTANCE OF $R = 1.0B$ (SEE TEXT FOR DEFINITION OF PARAMETERS)

	Z 0.5	1.0 ^a	1.5	2.0 ^b	3.0	4.0	5.0
λ_A	0.721	0.761	0.713	0.644	0.387	0.216	0.122
λ_-	.285	.000	-.254	-0.380	-.613	-.680	-.699
λ_+	.632	.649	.653	.664	.689	.701	.705
λ_A^2	.519	.579	.509	.414	.150	.047	.015
R_{11}	.362	.500	.651	.756	.896	.960	.984
R_{22}	.563	.500	.380	.325	.265	.250	.252
R_{12}	-.254	-.437	-.380	-.316	-.199	-.113	-.064
θ	.396	.000	-.357	-.590	-1.585	-3.141	-5.741
c_1	.99489	.99683	.99728	.99827	0.99967	0.99996	0.99999
c_2	-.10097	-.07952	-.07368	-.05874	-.02552	-.00923	-.00366
n_1	.98980	.99367	.99458	.99655	.99935	.99992	.99999
n_2	.01020	.00632	.00543	.00345	.00065	.00008	.00001
$(\lambda_+ + \lambda_-)/\sqrt{2}$.648	.458	.283	.201	.054	.014	.004
$(\lambda_+ - \lambda_-)/\sqrt{2}$.246	.458	.642	.738	.921	.976	.993

^a This is an approximation to H_2 . E for this function at $R = 1.0$ is $-1.99766H$. ^b This is an approximation to HeH^+ .

The behavior of these coefficients is a little more understandable if we relate them to u and v character since u and v may be considered as analogs of the atomic orbitals we started with. The coefficient of the term $u(1)u(2)$ in the wave function is just $(\lambda_+ + \lambda_-)/\sqrt{2}$, and the coefficient of $v(1)v(2)$ is $(\lambda_+ - \lambda_-)/\sqrt{2}$. The latter increases toward 1 as the Z value grows very large.

IV. Electronegativity Difference

One of the aims of the present work is to find, if possible, mathematical quantities which correspond fairly closely to chemically intuitive concepts. Thus we are interested in finding quantities corresponding to "ionic character" and to its closely related but apparently more fundamental concept, electronegativity. One of the quantities which came naturally from the calculation, namely θ as defined in eq. 10, seems to have many of the properties one might associate with electronegativity difference. It was very pleasing that the three integral parameters, R_{11} , R_{12} , and R_{22} merged into a single parameter, θ , in the calculation. This parameter has been defined in such a way as to be zero for the homopolar case (when $R_{11} = R_{22} = 1/2$ and in general $R_{12} \neq 0$) and to become large in magnitude as we approach an extreme ionic case (where, say, $R_{11} \rightarrow 1$, $R_{22} \rightarrow 0$, and $R_{12} \rightarrow 0$). The sign of θ is not of particular concern since it reflects merely an arbitrary choice of coordinate direction. But it is interesting to note that the magnitude of θ is in the very same range of numbers that are entailed in the Pauling definition of electronegativity difference.

It is impossible to make a very good comparison between the values of θ given here and Pauling's scale because all the former are at a fixed R far from the equilibrium value, and the latter scale is chosen from data on a variety of molecules at their respective equilibrium configurations. There is an implicit variable of internuclear separation present in evaluations of electronegativities since these can be expected to vary considerably with R . One can easily convince oneself that this is so by considering the simple (normal) case of a diatomic molecule dissociating into two different

atoms. Although the atoms have different tabulated electronegativities, at $R = \infty$ the amount of ionic character will have decreased to zero. More extensive calculations as a function of R are in process, and it may prove possible to find a simple more direct relationship between θ for the configuration of minimum energy and the Pauling scale.

V. A More General Treatment

The principal defect in the above treatment is the arbitrary and naive use of a plane to divide space into two equal parts. Even if one were willing to accept this in the homopolar case, there seems little reason for using it in the heteropolar one other than mathematical convenience. One alternative would be to use a plane perpendicular to the bond but placed, say, at the minimum of the electron density along the axis between the two nuclei. By searching for the optimum placement of the plane, one might be led to a relationship which involves constancy of atomic radius as well.

A more satisfying way of looking at the problem, however, is to consider the use of a generalized weight factor, $g(1, 2)$, which expresses inherently the concept of "ionicness" or "alternant character" to the satisfaction of the reader.⁹ Then the problem becomes that of maximizing A_A , for example, where

$$A_A = \int \Psi_A^2 g \, d\tau_1 \, d\tau_2 \quad (15)$$

Here g would be that weight factor which expresses the alternant concept. It is straightforward to show that under this more general condition one arrives at a condition for optimum α very similar to that of eq. 12, with θ explicitly written out as in eq. 10. Two-electron integrals over the weight-factor and the natural orbitals, however, replace R_{11} , R_{22} , and R_{12} .

The use of the arbitrary plane then corresponds to a particular choice of $g(1, 2)$ which is unity for volume elements with electrons on opposite sides of the dividing plane and zero otherwise. We are happily led to the point suggested in I that the naive use of the plane only as a criterion of definition of Ψ_A , etc., can be replaced by some more sophisticated

(9) This was first suggested to the author by Dr. Eugene Helfand.

derivation which leads to essentially the same choice of function without affecting the general conclusions.

A number of other possible weight factors suggest themselves. One involving directly the inter-electronic distance or at least its component along the molecular axis seems not unreasonable from some points of view. In addition one can think of operator forms of $g(1, 2)$ of which the most obvious choice is the Hamiltonian operator itself. In this case, the parameter θ becomes identical with a parameter introduced empirically by Löwdin¹⁰ to discuss some bond length perturbations. This is probably not a lucky accident, although the interpretation of, say, A_A using this operator formulation is none too clear.

Indeed, it is well known that roughly comparable

(10) P.-O. Löwdin, communicated at an early morning (1:30 a.m.) lecture at the Sanibel Island Winter School, January, 1962.

electronegativity scales can be derived from such diverse phenomena as bond energies, ionization potentials, force constants, nuclear quadrupole coupling constants, and the like. We would like to suggest that these diverse scales may be brought together by the suggestion that they refer to a well defined mathematical approximation to the optimum geminal function in which slightly different but nevertheless potentially well defined weight factors are used. Further work needs to be done to ascertain the possible validity of this very general viewpoint.

Acknowledgments.—This work has been carried out in spurts over a long span of time. The author is particularly indebted to P.-O. Löwdin for his hospitality at the time of origin of this program and for his enthusiastic interest.

THE PRESENT STATUS OF π -ELECTRON CALCULATIONS¹

BY PETER G. LYKOS²

Department of Chemistry, Illinois Institute of Technology, Chicago 16, Illinois

Received June 25, 1962

New results for electron distribution in a typical ground state, a lowest triplet state, and lowest double states are presented as examples of kinds of π -electron calculations that can be performed. Also some actual elapsed computer running times are cited for a variety of specific examples. Recent advances in our understanding of the π -electron approximation in terms of quantum mechanics, together with the advent of electronic digital computers, make it possible for π -electron theory to become a powerful tool for the chemist. On one hand the quantum chemist can proceed systematically in his testing of the various approximations which are made and also to study the problem of the meaning of the best values for the critical parameters which must be known. On the other hand, other chemists can use existing techniques and computer programs with chemistry-oriented input and output as an aid in planning and evaluating their research.

Introduction

The idea that some electrons in a molecule can be studied separately is one of the oldest notions of quantum chemistry. That idea has seen widest application in dealing with so-called π -electron³ or conjugated systems such as ethylene and benzene, either as neutral molecules or as ions, substituted and unsubstituted, in their ground and excited states.

A wide variety of physical and chemical phenomena relating to conjugated systems are being observed⁴ and π -electron theory, in various forms

and to varying degrees of approximation, is being used as a basis for "understanding" what is going on in each case. A number of the approximations that are made are based on chemical and physical intuition brought to bear on the particular problem at hand.

After a number of correlative-type successes have been achieved, however, it is a natural development to take an overview of the various kinds of π -electron theory with the realization that in order that one be able to extract information from a study of one phenomenon involving π -electron systems that might be used with some confidence in a study of another phenomenon involving them, the meanings of the various π -electron approximations need to be well understood on the basis of the underlying quantum mechanics.

π -Electron Theory.—In the evolution of π -electron theory, the simple model system of the type used for benzene (where six non-interacting electrons are constrained to move in a wire loop) first clearly brought out the essential quality of π -electron molecules; *i.e.*, (1) that the π -electrons are relatively free to move over the entire molecular framework and (2) that the detailed structure of the core does not play a significant role in determining the gross properties of such molecules. For example, the position of the lowest lying ultra-

(1) There are a number of other laboratories where there is a more or less comprehensive activity involving π -electron theory and its applications. The different relative emphasis placed on different aspects of the approach together with ingrained biases all tend to lead to rather unique situations. The intent here is to describe what has been going on in one laboratory rather than to attempt an overview of a variety of experiences.

(2) Presented at the 141st National Meeting of the American Chemical Society, Washington, D. C., March, 1962.

(3) Strictly speaking, the terminology σ and π is borrowed from the designation used for the line-of-centers component of the orbital angular momentum of an electron moving in the field of a linear array of nuclei. In non-linear systems, so-called σ -bonds will not in general have cylindrical symmetry nor will the π -bonds in general be symmetric to reflection in a plane normal to the plane of the molecule and passing through any two atoms in the non-linear conjugated system. The fact that σ -bonds may have structure has been recognized in dealing with cyclopropane, for example, where bent C-C bonds are proposed and also may play a role in the assessment of the barrier to internal rotation in ethane.

(4) P. G. Lykos, *J. Chem. Phys.*, **35**, 1249 (1961). An erratum is to be published in *J. Chem. Phys.* with regard to the interpretation of α

as defined in eq. 2 in that paper which is inconsistent with how it is used in some of the energy formulas also given there.

the coordinates of the π -electrons while E_{Σ}^0 depends on (Σ) only. A more explicit form for H_{π} is

$$H_{\pi} = \sum_{i=n\sigma+1}^{n\sigma+n\pi} \left(H_{\text{core}}(i) + \sum_{j>i}^{n\sigma+n\pi} \frac{1}{r_{ij}} \right)$$

where $H_{\text{core}}(i) = -\frac{1}{2}\nabla_i^2 - \sum_{\alpha} \frac{Z_{\alpha}}{r_{\alpha i}} + G_{\Sigma}(i)$. $G_{\Sigma}(i)$ is the operator which couples the σ -electrons and the π -electrons, *i.e.*, which contains the coulomb and exchange effect of the σ -electrons on the π -electrons and is the term in H_{π} which gives $E_{\Sigma\Pi}$ when one takes the expectation value of H_{π} and gets $E_{\pi} \equiv E_{\Sigma\Pi} + E_{\pi}^0$. In a little more detail $G_{\Sigma}(i) = J_{\Sigma}(i) - K_{\Sigma}(i)$, where the coulomb operator $J_{\Sigma}(i)$ is defined as

$$J_{\Sigma}(i)(\Pi) = \int (\Sigma)^* \left(\sum_{j=1}^{n\sigma} \frac{1}{r_{ij}} \right) (\Sigma) dv(\Pi)$$

and the exchange operator $K_{\Sigma}(i)$ is defined as

$$K_{\Sigma}(i)(\Pi) = \int (\Sigma)^* \left(\sum_{j=1}^{n\sigma} \frac{1}{r_{ij}} (\Sigma)_{\text{ex}}^i(\Pi)_{\text{ex}}^j \right) dv$$

Thus we may conclude that we can define a quantum mechanically meaningful H_{π} for the π -electrons alone such that the expectation value of that operator over a wave function for the π -electrons alone gives us the π -electron contribution to the total energy including σ - π coulomb and exchange interaction.

One additional point can be made. Whereas we collected

$$E_{\Sigma\Pi} + E_{\pi}^0 \text{ into } E_{\pi} \text{ by}$$

defining the operators $H_{\text{core}}(i)$ and $G_{\Sigma}(i)$, by formal symmetry it is clear we could have just as well collected $E_{\Sigma}^0 + E_{\Sigma\Pi}$ into E_{Σ} , say, by defining the operators $H_{\text{peel}}(i)$ and $G_{\pi}(i)$. This suggests that one might proceed iteratively as follows: assume some (Σ) in order to define $G_{\Sigma}(i)$, and hence $H_{\text{core}}(i)$, and then optimize (Π) with respect to any variational parameters which may enter (such as linear coefficients); then use that optimized (Π) in order to define $G_{\pi}(i)$, and hence $H_{\text{peel}}(i)$, and proceed to determine an improved (Σ) ; and so on. As the π -electron approximation is ordinarily used, (Σ) is assumed not to change significantly when π -electrons are excited. The effect of such excitation on (Σ) can be assessed, however, by this iteration technique.

With regard to the one-electron spin orbitals σ_i and π_i which were used, what usually is done is to assume that they are elements of mutually exclusive subsets of a complete set of orthonormal one-electron functions, that they are space-spin factored, and that the space parts in the closed shell part of the system are doubly occupied by electrons with opposite spin.⁷ The π_i are further

(7) The freedom of different space orbitals for electrons with different spins is sometimes invoked, especially in dealing with paramagnetic molecules. The misnomer "Unrestricted Hartree-Fock" was at one time used to describe that approach when applied to paramagnetic molecules which is better referred to as "Spin Polarized Hartree-Fock." The difficulty in using different orbitals for different spins in a single determinantal wave function is that the approximate wave

approximated as linear combinations of atomic orbitals, $\pi_i = \sum_j c_{ij}\chi_j$, the χ_j being π -type atomic orbitals at each nucleus in the conjugated system.

Thus, in the final analysis, E_{π} as defined here depends on three things:

(1) The assumed form of (Σ) , which has not been given much attention since the pioneering work of Goepfert-Mayer and Sklar.⁸

(2) The linear coefficients c_{ij} , which are taken as variational parameters and are conveniently determined by the beautiful self-consistent matrix formalism worked out for ground and for excited states by Roothaan⁹ (the self-consistent molecular orbitals thus defined are found by solving by an iterative method an eigenvalue problem where the eigenfunctions are needed to generate the operator they are eigenfunctions of).

(3) Integrals over the atomic orbitals which depend on the assumed form of (Σ) and also on the assumed form of the χ_j . For example, if one computes the overlap integral between two π -type atomic orbitals which are 1.4 Å. apart, one gets 0.25 or 0.33 according to whether Slater orbitals¹⁰ or Hartree-Fock orbitals¹¹ are used, respectively; and these are orbitals found appropriate for free undistorted atoms! Since there is yet some uncertainty about the best form for (Σ) as well as for the χ_j , it would seem that it would be best to treat the integrals over atomic orbitals as empirical parameters. The saving feature here is that the number of such parameters is probably smaller than the number of properties and molecules to be studied.¹²

The foregoing is a summary of the theoretical framework which is the basis of a program for studying π -electron systems. In the following sections a brief description of a particular computer program and some new results obtained should serve to indicate something of what can be done in assessing the properties of π -electron systems. In all of this no mention has been made of classical or Hückel π -electron theory. In an attempt to understand Hückel theory, it was established that for some systems, Hückel molecular orbitals may be interpreted as maximum overlap molecular orbitals,¹³ and it may someday develop that for closed shell systems (but probably not for open shell systems) one can come to know when Hückel results are reliable—and when they are not. At the present time, however, we take the view that Hückel theory presents an interesting enigma in that sometimes it works even though it involves

function is no longer an eigenfunction of S^2 . If an appropriate linear combination of such determinants is taken to meet that objection, the fact that the (space) orbitals are not orthogonal can lead to a complicated energy expression although expansion techniques are being used in an attempt to overcome that problem.

(8) M. Goepfert-Mayer and A. Sklar, *J. Chem. Phys.*, **6**, 645 (1938).

(9) C. C. J. Roothaan, *Rev. Mod. Phys.*, **32**, 179 (1960).

(10) H. Eyring, J. Walter, and G. E. Kimball, "Quantum Chemistry," John Wiley and Sons, Inc., New York, N. Y., 1944.

(11) R. S. Mulliken, C. A. Rieke, D. Orloff, and H. Orloff, *J. Chem. Phys.*, **17**, 1248 (1949).

(12) See ref. 4 where an attempt has been made to outline the problem.

(13) P. G. Lykos and H. N. Schmeising, *J. Chem. Phys.*, **35**, 288 (1961).

some apparently serious quantum mechanical errors. However, since the advent of electronic digital computers makes it possible to erect a structure correctly based on quantum mechanical foundations, we need not concern ourselves with that problem.

A Program for Studying π -Electron Systems.—The projected development of a program for studying π -electron systems involves three distinct steps:

(1) The evolution of the theoretical framework and the programming of it for a large, fast electronic digital computer. The programming needs to be done in a flexible fashion so that revisions dictated by experience and by advances in the theory can be implemented easily and also so that a number of different options can be exercised conveniently.

(2) An intensive study of a variety of prototype conjugated systems which have been well characterized with respect to both chemical as well as physical properties. In this way the basic integrals-over-atomic-orbitals parameters may be assessed empirically and also a variety of properties may be studied within the same theoretical framework in order to check its adequacy.

(3) The calibrated truly semi-empirical theory then should be used not only to assess similar properties of more complicated systems but also to be the basis for computing various reactivity criteria and thus to provide a starting point for a theoretical assessment of chemical reactivity for π -electron systems in ground and excited states.

It should be clear from the foregoing that such a program is materially aided by access to a large, fast computer for two main reasons. First, large molecules with low symmetry may be approached directly without being limited to Hückel-type and/or perturbation techniques. Second, the search for best parameters is one which involves making repeated calculations on any given molecule or series of molecules in order to get best fits for a given set of data, and redoing the job when better and/or more data come along. In fact, it may very well develop that computers will turn out to be relatively more important for semi-empirical approaches to complicated molecules than for *ab initio* approaches to simple molecules.

The first plateau has been reached in evolving a flexible automatic computer program. Roothaan's⁹ open shell Hartree-Fock matrix method has been implemented for π -electron systems¹⁴ and programmed for the Univac 1105. The program has been carefully organized such that a simplified chemistry-oriented input format is made available to a user. Only the minimum number of bond lengths and bond angles need to be supplied for, in a preliminary step, the program "steps around" the molecular framework and computes all the unique internuclear distances which are needed for calculation of integrals.

The program may be supplied with a starting set of molecular orbitals or it may be asked to generate its own, in which case it produces maximum overlap molecular orbitals¹³ or Hückel orbitals as starting orbitals.

Also it may be supplied with values for the integrals-over-atomic-orbitals or the user can elect to use those already stored in the program.

In solving the eigenvalue problem, the program iterates toward a normalized solution until the largest change in any linear coefficient on one iteration is less than some preset convergence criterion, usually one ten thousandth. In Table I are listed some typical runs showing the number of iterations and approximate total elapsed times to convergence. It should be noted that the elapsed times increase rapidly with the size of the molecule being studied.

When the program has converged to a solution the user has several options with regard to what information can be extracted and also with regard to the format of the output. Where appropriate the program can produce charge densities, spin densities, orbital energies, and/or frontier electron densities. Already operational at a primitive stage is an auxiliary program whereby the data comes out of the computer in the form of a molecular diagram as shown in Fig. 1.

As part of a research program to examine reactivity criteria, Miller and Schmeising¹⁵ have produced a computer program for computing self-consistent localization energies for conjugated systems and these can be requested as well.

Two Illustrations.—In order to illustrate something of the range and power of the computer program briefly described in the foregoing section we have selected two kinds of systems for presentation here involving phenomena which are becoming quite important in chemistry. The first is the lowest triplet state of a conjugated system and the question of the electron distribution in it. This is currently of interest because of the e.s.r. studies being made on such systems and also because the chemical reactivity of molecules in excited states also is receiving an increasing amount of attention. The second is the ground state of an odd electron system and the question of the electron distribution in it. This is of interest both because these systems are being examined extensively by e.s.r. techniques and also because some of the more casual π -electron approaches have proven to be unsatisfactory when applied to this problem.

We selected a substituted butadiene (substituted in order to destroy the highly restrictive molecular symmetry of butadiene itself) as an illustration of what happens when one approaches an excited state directly as is possible with the open-shell Hartree-Fock method rather than use the same set of molecular orbitals for the ground state and for the excited state as well. We see in Table II that the electron density distribution can assume distinctly different characteristics depending on what course is followed.

We can make two observations. First, the electron distribution in the excited state is quite different from that in the ground state. This is an example of an *intramolecular charge transfer* phenomenon. Insofar as charge density is a basis for assessing the relative reactivity to electrophil-

(15) Presented at the 140th National Meeting of the American Chemical Society, Chicago, Ill., Sept., 1961; submitted for publication to *J. Chem. Phys.*

PROTONATED IMIDAZOLE, RUN NUMBER 6. NITROGENS AT POSITIONS 3 AND 5.

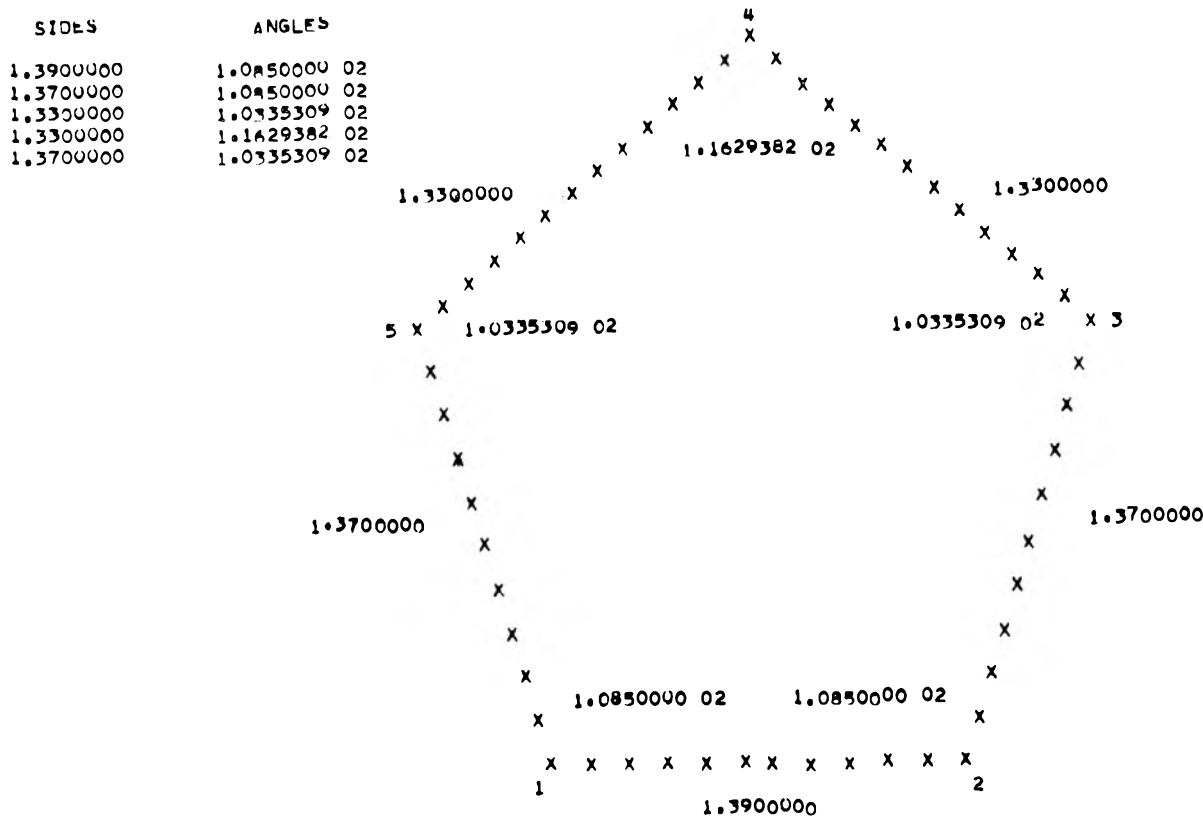


Fig. 1.—A sample of molecular diagram output as it comes directly from the high-speed printer associated with the Univac 1105 computer. In this particular sample the geometry of protonated imidazole was being studied. The tables in the upper left hand corner contain the nearest neighbor distances and the bond angles. These numbers are also superposed in the appropriate places on the Univac's sketch of the molecular framework.

TABLE I
SOME TYPICAL UNIVAC 1105 LCAO-SCMO RUNS^a

State	Molecule	No. of iterations	Time, min.
Singlet	Butadiene	11	1/2
Triplet	Benzene	10	1
Singlet	Naphthalene	13	6
Triplet	Pyridine	6	1
Singlet	Purine	8	2
Doublet	Tetraphenyl pyrrol	11	88

^a An IBM 1620 computer would take 25 or 30 times as long while an IBM 7090 computer would take 1/10 as long.

TABLE II
PERTURBED *cis*-BUTADIENE CHARGE DENSITIES^{a,b}

How obtained	Q(N)	Q(C1)	Q(C2)	Q(C3)
Ground state singlet	1.217	0.799	1.036	0.947
Lowest triplet using ground state orbitals	1.149	0.979	0.942	0.932
Lowest triplet obtained directly	1.007	1.004	0.994	0.995

^a From the Ph.D. Thesis submitted to the Graduate School of Illinois Institute of Technology by Fr. O. W. Adams. ^b The system is perturbed by replacing a terminal carbon by a pyridine-type nitrogen. The carbons are numbered serially starting with the carbon adjacent to the nitrogen.

lic, nucleophilic, or radical attack, it is quite clear that the relative reactivities of the unique positions in conjugated systems in the excited states are likely to be quite different from the pattern

in the ground state. Second, the charge distribution in the excited state obtained by direct calculation on the excited state⁹ may be quite different from that which is obtained by using ground state orbitals to compute excited state charge densities.

Another research program underway is a study of the reactivities of the various polymethyl-substituted benzenes. The parameters used were obtained from an analysis of benzene itself and certain radicals not directly related to benzene nor to any molecules in the methylbenzene series. As an aside to that program, the same basic parameters were used to compute spin densities for the corresponding negative ions of some of the methyl-substituted benzenes. It should be noted that in a sense these latter were *ab initio* calculations in that

TABLE III
DOUBLET STATE ELECTRON SPIN DENSITIES

Compound	Position	Obsd. ^a	Calcd. ^b
Toluene negative ion	2	0.228	0.247
	3	.242	.253
	4	.026	.000
<i>m</i> -Xylene negative ion	2	.304	.324
	4	.065	.075
	5	.343	.373
<i>p</i> -Xylene negative ion	2	.237	.250

^a J. R. Bolton and A. Carrington, *Mol. Phys.*, **4**, 497 (1961). ^b From some unpublished work by Dr. R. L. Flurry, Jr., Postdoctoral Research Associate, Illinois Institute of Technology.

no data from any member of the methyl-substituted benzenes were used. The results of the spin density work are summarized in Table III and the good agreement is gratifying indeed.

Conclusions

It seems quite clear that π -electron theory: (1) can be conveniently used in a form which is properly based on quantum mechanics; (2) has been given considerable impetus by the advent of the large fast electronic digital computer; (3) is sufficiently profound that a variety of molecular properties can be understood within a single theoretical framework while at the same time sufficiently simple that it is tractable; (4) already has brought into new prominence and provided the theoretical basis for the chemistry of conjugated molecules

in their excited states; (5) has become an established tool for the chemist.

Acknowledgments.—The implementation for the Univac 1105 of the π -electron program was in the main due to Dr. H. N. Schmeising, who, in the process, produced a comprehensive matrix interpretive for the Univac 1105. Dr. O. W. Adams and Mr. R. L. Miller played a significant role in the evolution of the program. We also were aided by Dr. R. L. Flurry, Jr., and Mr. R. Blomquist was responsible for the "molecular diagram" computer output program. We received material support from the following: generous grants of Univac 1105 computer time from IIT; a grant from the National Science Foundation; and a grant from the National Institutes of Health, for all of which we are grateful.

ELECTRONIC STRUCTURE OF SIMPLE MOLECULES¹

BY LELAND C. ALLEN

Department of Chemistry, Princeton University, Princeton, N. J.

AND ARNOLD M. KARO

Department of Chemistry, Lawrence Radiation Laboratory, Livermore, Calif.

Received June 25, 1962

Recent theoretical and computational developments in the direct solution of Schrödinger's equation are reviewed. The relationship between direct solutions of Schrödinger's equation and semi-empirical calculations also is discussed.

I. Introduction

Direct solutions of Schrödinger's equation are defined as those attempts to solve the non-relativistic many-electron problem without approximation. Although most of the theoretical framework was worked out in the decade from 1930 to 1940, intensive efforts to explore, extend, and test the theory date from about 1951. The present article is concerned primarily with developments in the last two years and with systems of more than two electrons.²

A tabulation of molecular calculations reported during the last two years was to have been included but is omitted due to circumstances beyond our control. It will be published in *J. Phys. Chem.* in the near future and will bring a previous tabulation up to date.

II. General Formulations.—During the past two years there have been numerous papers devoted purely to the theory of many-electron systems.

Perturbation Theory.—Many-particle perturbation theory for electronic problems has been actively pursued by Löwdin^{3a} and Sinanoglu.^{3b} This work follows the field theoretic approach developed by Brueckner, Pines, Gell-Mann, Hubbard, Bogolubov, Goldstone, Hugenholtz, and others.⁴

Pair Correlations.—The high percentage of the total energy achieved by a Hartree-Fock solution (approximately 99.5%) and the stability of this solution as expressed by Brillouin's theorem plus the exclusion effects of the Pauli principle and a wide variety of numerical calculations over a period of years has led us to believe that correlation corrections to Hartree-Fock solutions, adequate for chemical problems, can be obtained with correlations between rather localized, independent pairs of electrons only. Recent treatments by Nesbet,⁵ Sinanoglu,⁶ and Löwdin⁷ have formalized these ideas. Although arising basically from a valence bond description, recent many-electron formulations using two-electron basis functions are closely related to the pair correlation problem. Much of this work derives from the classic paper of Hurley, Lennard-Jones, and Pople.⁸ Parks and Parr,⁹ Allen and Shull,¹⁰ and McWeeny and Ohno¹¹ have made contributions to this area in the last two years. None of this work nor that on pair correlations and the many-particle perturbation theory has led to improved computational methods, but expres-

(1) A. M. K. wishes to acknowledge the support of the U. S. Atomic Energy Commission. L. C. A. wishes to acknowledge the financial assistance of the Petroleum Research Fund of the American Chemical Society.

(2) L. C. Allen and A. M. Karo, *Rev. Mod. Phys.*, **32**, 275 (1960).

(3) (a) P.-O. Löwdin, Technical Notes 47 and 48, "Quantum Chemistry Group," Uppsala University, Uppsala, Sweden; (b) O. Sinanoglu, *Proc. Roy. Soc. (London)*, **A260**, 379 (1961).

(4) D. Pines, "The Many-Body Problem," W. A. Benjamin, Inc., New York, N. Y., 1961.

(5) R. K. Nesbet, *Rev. Mod. Phys.*, **32**, 275 (1960).

(6) O. Sinanoglu, *J. Chem. Phys.*, **36**, 706 (1962).

(7) P.-O. Löwdin, *Phys. Rev.*, **97**, 1509 (1955); *Advan. Chem. Phys.*, **2**, 207 (1959); preprint No. 1, July, 1960, Quantum Theory Project, University of Florida, Gainesville, Florida.

(8) A. C. Hurley, J. E. Lennard-Jones, and J. A. Pople, *Proc. Roy. Soc. (London)*, **A220**, 446 (1953).

(9) J. M. Parks and R. G. Parr, *J. Chem. Phys.*, **28**, 335 (1958); **32**, 1657 (1960).

(10) T. L. Allen and H. Shull, *ibid.*, **35**, 1644 (1961).

(11) R. McWeeny and K. A. Ohno, *Proc. Roy. Soc. (London)*, **A255**, 367 (1960).

sing the results in a variety of ways has led us to a clearer understanding of the many-electron problem.

A good deal of our thinking about the correlation problem comes from the unrestricted and extended Hartree-Fock methods and the *alternant molecular orbital scheme* is one practical result of these concepts. Originating with Coulson and Fischer,¹² the scheme has been generalized by Löwdin¹³ and applied to several molecular systems by Itoh and Yoshizumi,¹⁴ Lefebvre, Dearman, and McConnell,¹⁵ and Pauncz, de Heer, and Löwdin.¹⁶ Although the recent calculations have been restricted to π -electrons, the results are of general significance. The calculations present fairly good evidence that the alternant molecular orbital scheme for introducing different orbitals for different spins accounts for perhaps half the correlation energy and leads to improvement in such quantities as the unpaired spin density in certain free radicals.

Hypervirial Theorem.—Hirschfelder and Coulson¹⁷ have generalized the virial theorem and have shown that the resultant hypervirial theorem is a consequence of the Heisenberg equation of motion. As pointed out by the authors, this generalization may help in the determination of average values of dynamical variables and in providing criteria for improving wave functions.

Density Matrices.—The subject of density matrices continues to receive a considerable amount of attention. McWeeny¹⁸ and Löwdin¹⁹ have been prominent in this endeavor. However, the well known and great problem of ascertaining the necessary and sufficient conditions that must be satisfied to make density matrices correspond to solutions of Schrödinger's equation still is unsolved. Coleman²⁰ has made some progress on conditions for first-order density matrices but the realization of a complete set of requirements for the first and second-order density matrices seems very remote. Nevertheless, it is quite likely that density matrices and perhaps Löwdin's natural spin orbitals will provide the best *canonical form* for comparing wave functions calculated by different methods. Shull has demonstrated how this may be done for the two-electron problem.²¹ Even a cursory survey of the existing *ab initio* wave functions reveals that except in a very few cases, we have not abstracted the information and knowledge available nor do we have a systematic method (other than the total energy) for comparing spacial distributions

and other theoretically interesting quantities. This seems particularly unfortunate since the principal utility of direct solutions for simple systems has been and remains the testing of theories rather than the prediction of chemically interesting properties.

III. Parametric Methods and Models.—There is another aspect to the general formulations mentioned above which is quite encouraging and this is our greatly increased understanding of why the highly successful Hückel model and the Pariser and Parr method actually work. In addition to the papers noted above, Parr and Lykos²² have comprehensively analyzed these schemes and Ruedenberg²³ has written a definitive set of articles on the problem. The increasing interest of organic chemists in simple electronic structure models and our more extensive knowledge concerning them leads one to believe that there will be a greater interchange between groups of people working at different levels of approximation and a greater impact of *a priori* methods on chemical problems.

IV. Wave Functions for Simple Molecules.—By 1960 there were approximately 80 molecular wave functions that could be classed as direct solutions to Schrödinger's equation. During the past two years 80 more have been carried out. In spite of their inability to aid in the interpretation of current chemical problems, these calculations provide by far the best guide to a detailed understanding of the electronic structure of molecules. Almost all existing calculations have constructed a many-electron wave function from one-electron spin-orbitals and almost all have adopted a molecular orbital approach carried out *via* the Roothaan procedure. Within this framework the wave functions have been expressed either as LCAO or one-center expansions. One-center calculations for methane and hydrogen fluoride have been quite successful but the potential singularities for atoms other than hydrogen are so severe that the LCAO expansion is almost certainly the more efficient. All but about 25 of the existing wave functions use the LCAO expansion.

Two Four-Electron Calculations.—A Be atom wave function calculated by Watson²⁴ and an LiH wave function determined by Ebbing²⁵ have considerably enhanced our knowledge of many-electron effects and deserve special mention. The important feature of these calculations is the extensive configuration interaction that was carried out and the detailed analysis and testing of particular configurations. They form the best confirmation of our qualitative ideas about pair-correlations.

A Molecular Hartree-Fock Solution.—Probably the most exciting development in the past two years has been the achievement of the first true *molecular Hartree-Fock* solution. The calculations were performed independently by Clementi²⁶

(12) C. A. Coulson and I. Fischer, *Phil. Mag.*, **40**, 386 (1949).

(13) P.-O. Löwdin, *Nikko Symp. Mol. Phys.*, **13** (Maruzen, Tokyo, 1954), Technical Note 67, Quantum Chemistry Group, Uppsala University, Oct., 1961.

(14) T. Itoh and H. Yoshizumi, *J. Phys. Soc. Japan*, **10**, 201 (1955); *J. Chem. Phys.*, **23**, 412 (1955).

(15) R. Lefebvre, H. H. Dearman, and H. M. McConnell, *ibid.*, **32**, 176 (1960).

(16) R. Pauncz, J. de Heer, and P.-O. Löwdin, Technical Notes 55 and 56, Quantum Chemistry Group, Uppsala University, 1960; *J. Chem. Phys.*, to be published.

(17) J. O. Hirschfelder and C. A. Coulson, *J. Chem. Phys.*, **36**, 941 (1962).

(18) R. McWeeny, *Proc. Roy. Soc. (London)*, **A232**, 114 (1955).

(19) P.-O. Löwdin, *Phys. Rev.*, **97**, 1474 (1955); *Ann. Rev. Phys. Chem.*, **11**, 107 (1960).

(20) A. J. Coleman, *Can. Math. Bull.*, **4**, 209 (1961).

(21) H. Shull, *J. Am. Chem. Soc.*, **82**, 1287 (1960).

(22) R. G. Parr and P. G. Lykos, *Texas J. Sci.*, **8**, 135 (1956); R. G. Parr, *J. Chem. Phys.*, **33**, 1184 (1960). See this latter article for discussion and references to previous work on the justification of semi-empirical models.

(23) K. Ruedenberg, *ibid.*, **34**, 1861, 1878, 1884, 1892, 1897, 1907, (1961).

(24) R. E. Watson, *Phys. Rev.*, **119**, 170 (1960).

(25) D. D. Ebbing, *J. Chem. Phys.*, **36**, 1361 (1962).

(26) E. Clementi, *ibid.*, **36**, 33 (1962).

and Nesbet²⁷ with identical results. Hydrogen fluoride was chosen because we have more extensive theoretical knowledge on this molecule than any other. The results obtained were quite unexpected and have far-reaching significance for our understanding of molecular correlation energy and binding energy. This wave function predicts force constant, equilibrium separation, dipole moment, and the derivative of the dipole moment to within a few per cent of the experimental results and reasonable values for excitation energies—all improvements over previous calculations carried out by diverse methods. And, of greatest interest, the predicted binding energy is $2/3$ of the experimental value, in sharp contrast to the figure $1/4$ which has become almost a cliché for the typical LCAO wave function. This molecular Hartree-Fock wave function is not, of course, an LCAO expansion and the improvement is achieved through polarization of the atomic orbitals (obtained by adding σ and π basis functions of one higher l -value to the outer orbitals). Since the molecular wave function is a Hartree-Fock solution and since the separated atoms are Hartree-Fock solutions, the error in the binding energy is the molecular correlation energy and these calculations are our first accurate estimate of this important quantity. The value is only 1.8 e.v., although it frequently has been assumed to be 2.5 times as much, and is close to the value yielded by typical simple configuration interaction calculations, although these have not started with molecular Hartree-Fock solutions. On the other hand, there has been very little exploration of the appropriate excited basis orbitals to use for configuration interaction and it is possible that accurate wave functions may be obtainable by simple, rapidly converging configuration interaction treatments.

V. Molecular Integrals.—Mounting one-electron basis orbitals at the various nuclear sites in a molecule still seems to be the most efficient and readily interpretable procedure for setting up molecular wave functions, even though this leads to the formidable many-center, two-electron integral problem. It is still true, as it has been for the past decade, that multi-center integrals are by far the greatest problem in the direct solution of Schrödinger's equation. It also is well known that

(27) R. K. Nesbet, *J. Chem. Phys.*, **36**, 1518 (1962).

the difficulty arises through use of the exponential basis function form $r^n e^{-ar} Y_l^{lm}(\theta, \varphi)$ where n , l , m are integral, $a > 0$, and Y is a spherical harmonic. Because exponentials form natural solutions to the atomic central field problem, single or linear combinations of this type of function are the most widely employed basis orbitals (about 95% of all existing wave functions) and four different techniques for their evaluation are under continuing development by workers at four institutions.

Massachusetts Institute of Technology.—The Barnett-Coulson expansion²⁸ about a single center is employed by Barnett and co-workers.

University of Chicago.—The two-dimensional integration technique developed by McLean and Roothaan²⁹ is used by Roothaan and co-workers.

Columbia University-IBM Watson Laboratory.—A scheme exploiting the analytic integral transform between exponential and gaussian functions ($r^n e^{-ar^2} Y_l^{lm}(\theta, \varphi)$) has been worked out by Shavitt.³⁰ This is the newest and in some ways the most promising method.

Cambridge University.—Boys and co-workers³¹ use a direct gaussian expansion of the exponentials.

The first three groups are now writing the majority of their computer programs for the IBM 7090 while Boys employs the Cambridge University Edsac II. At present it is possible to obtain for exponential basis functions all integrals to the required accuracy for a set of several first row atoms on a line or a first row atom surrounded by any number of hydrogen atoms.

Because all integrals over gaussian basis functions may be expressed analytically, these are the most attractive alternative to exponentials. There has been only a small amount of experimentation with gaussian orbitals but it generally has been thought that the number of gaussians required for an adequate representation of molecular wave functions was prohibitively large. New evidence³² indicates that this viewpoint probably is incorrect and a revival of interest in this approach is taking place.

(28) M. P. Barnett and C. A. Coulson, *Phil. Trans. Roy. Soc. (London)*, **A243**, 221 (1951).

(29) A. D. McLean, *J. Chem. Phys.*, **32**, 1595 (1960).

(30) I. Shavitt and M. Karplus, *ibid.*, **36**, 550 (1962).

(31) S. F. Boys and G. B. Cook, *Rev. Mod. Phys.*, **32**, 285 (1960).

(32) L. C. Allen, *J. Chem. Phys.*, **37**, 200 (1962).

IN DEFENSE OF THE USE OF ATOMIC ORBITAL CONFIGURATION WAVE FUNCTIONS FOR SMALL MOLECULES¹

BY F. A. MATSEN AND J. C. BROWNE

Departments of Chemistry and Physics, University of Texas, Austin, Texas

Received July 23, 1962

The merits of the SCF-MOC and atomic orbital configuration (AOC) methods of computing wave functions and energies for small molecules are compared. New AOC results for LiH and He₂⁺ are presented in support of our views.

Discussion

Most recent quantum mechanical calculations of small molecules have been made with self-consistent field molecular orbital configuration (SCF-MOC) wave functions.² An alternate, but less popular, approach is to use atomic orbital configuration (AOC) wave functions. For a given basis set of atomic orbitals and with complete configuration interaction both of these approaches yield identical results. It has, however, been found that the use of large basis sets is necessary to secure meaningful results in molecular calculations. With these large basis sets complete configuration interaction is not practical and the configuration interaction must be limited. It does not appear to be widely appreciated that with large basis sets and limited configuration interaction the AOC approach has several advantages over the SCF-MOC approach for the calculation of ground state energies and wave functions for small molecules.

1. The AOC wave function for the molecule goes smoothly into the atomic wave functions of correct symmetry as $R \rightarrow 0$ and as $R \rightarrow \infty$. This is not, in general, true for an SCF-MOC wave function.

2. As a consequence of (1) the choice of optimum orbital exponents is easier in the AOC approach than in the SCF-MOC approach since they can be followed from the easily computed separated atomic cases.

3. Irrespective of the size of the basis set of atomic orbitals each AOC wave function term for an N electron system contains N or less different orbitals while each SCF-MOC contains all of the atomic orbitals in the set. As a consequence the number of integrals which must be calculated (or stored) and hence the amount of computer time (or computer storage) required for the AOC approach is less than for the SCF-MOC approach.

4. In the AOC approach there is greater flexibility in the choice of configuration interaction terms since in the SCF-MOC approach the investigator must use the molecular orbitals obtained by the minimization of the single configuration energy. There is no guarantee that these SCF-MO's are optimum choices for limited configuration interaction. In fact, there appears to be growing evidence to the contrary.³

5. The AOC approach does not require the pre-

liminary self-consistent step that is required for the SCF-MOC approach.

6. States with $S \neq 0$ cause no difficulty in the AOC approach but may in the SCF-MOC approach.

7. Molecules with an odd number of electrons cause no difficulty in the AOC approach but may in the SCF-MOC approach.

8. The use of an "open shell" configuration for the primary configuration causes no difficulty in the AOC approach but does in the SCF-MOC approach.

Moreover, it does not seem to be widely appreciated that a number of the alleged advantages of the SCF-MOC approach do not exist at the level of the computation we are discussing.

1. The fact that a single closed shell SCF-MOC is superior to a single closed AOC configuration is irrelevant since significant improvement can be obtained by "opening the shell" on the AOC configuration or by configuration interaction.

2. The fact that the SCF-MO's are orthogonal and therefore easier functions with which to compute matrix elements is not of significance since the problems raised by the use of non-orthogonal functions are readily solved by means of linear processes which are highly efficient on a large scale digital computer. Nor is it necessarily true that the SCF orthogonalization gives MO's which are optimal choices for configuration interaction (see preceding discussion).

3. The Koopmans theorem⁴ states that as a result of cancellation of errors the ionization energies are given with relatively high accuracy by the single SCF-MO configuration. Configuration interaction, however, can give no improvement in Koopmans theorem ionization energies.

There is at least one advantage to the SCF-MOC approach: The SCF-MO's are eigenfunctions of an independent particle Hamiltonian and as such are theoretically more attractive. For example, they lend themselves to perturbation theory development.⁵ However, it has not yet been proved that these developments lead to better quantitative results for molecules than does the AOC approach.

A graphical comparison of the two approaches is given in Fig. 1.

Two examples of atomic orbital configuration calculations are presented and are compared with results obtained with SCF molecular orbital calculations. Our first example is LiH. Here we

(1) This research was supported by the Robert A. Welch Foundation of Houston, Texas, and the Air Force Office of Scientific Research.

(2) With SCF-LCAO-MO's, self-consistent field-linear combinations of atomic orbitals—molecular orbitals. See, for example, C. C. J. Roothaan, *Rev. Mod. Phys.*, **23**, 67 (1951), **32**, 179 (1960).

(3) S. Fraga and B. J. Ransil, *J. Chem. Phys.*, **36**, 1127 (1962).

(4) T. Koopmans, *Physica*, **1**, 104 (1933).

(5) See, for example, O. Sinanoglu, *J. Chem. Phys.*, **36**, 706 (1962), and earlier papers; also, R. K. Nesbet, *Proc. Roy. Soc. (London)*, **A230**, 312 (1955). Perturbation theory treatment of configuration interaction for SCF wave functions suggests that single excitation contributions to one-electron properties are small.

TABLE I
LiH WAVE FUNCTION^a

$$\psi = c_1(1s^2, 2s1h) + c_2(1s1s', 2s1h) + c_3(2p_+2p_-, 2s1h) + c_4(2p_0^2, 2s1h) + c_5(1s1s', 2p_0'1h) + c_6(1s^2, 1h^2) + c_7(1s^2, 2p_0h^2) + c_8(1s^2 2p_{+h} 2p_{-h}) + c_9(1s^2, 2p_+' 2p_-') + c_{10}(1s^2, 2p_0'^2) + c_{11}(1s^2, 2s^2) + c_{12}(1s^2, 2s2p_{0h}) + c_{13}(1s^2, 2s2s_h) + c_{14}(1s^2, 1h2s_h) + c_{15}(1s^2, 1h2p_{0h}) + c_{16}(1s^2, 3s1h) + c_{17}(1s^2, 1h, h') + c_{18}(1s1s', 2s1h') + c_{19}(3d^2, 1h2s) + c_{20}(1s^2, 3d_01h)$$

^a Orbitals (other than 1s) centered on the H atom nucleus are given a subscript h, e.g., 2p_{0h}.

TABLE II

	SCF-MOC				
	AOC This research	Fraga and Ransil ^{3,7}	Ebbing ⁸	Nesbitt and Kahalas ⁹	Exptl. ¹⁰⁻¹²
Equil. R (a.u.)	3.075	2.9195		3.0581	3.0132
Total E (a.u.)	8.04379	7.99145	8.04127	8.01711	8.0703
Binding E (e.v.)	1.793	0.014	1.725	1.067	2.514
Dipole mom. (D.)	-5.57	-5.84	-5.96		-5.882
ω_e (cm. ⁻¹)	1602	1973			1406
$\omega_e x$ (cm. ⁻¹)	28.19	336			23.20
α_e (cm. ⁻¹)	0.0867	0.7279			0.2132
$(q/2e)_{el}$ (a.u.)	-0.0495			-0.0571	

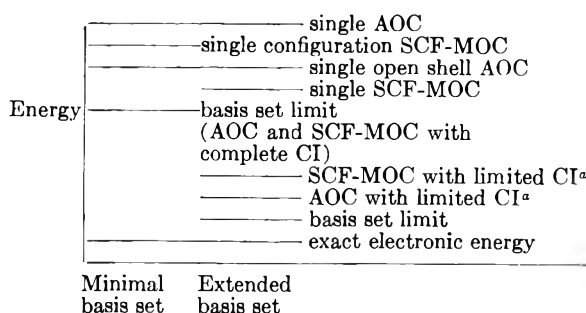
TABLE III

He₂⁺ WAVE FUNCTION

$$\psi = c_1(1s_a 1s_a 1s_b') + c_2(2s_a 2s_a 1s_b') + c_3(3s_a 3s_a 1s_b') + c_4(1s_a 2s_a 1s_b') + c_5(1s_a 3s_a 1s_b') + c_6(2s_a 3s_a 1s_b') + c_7(1s_a 2s_a 1s_b') + c_8(1s_a 1s_a' 2s_a) + c_9(1s_a 1s_a' 3s_a) + c_{10}(2p_{0a} 2p_{0a} 1s_b') + c_{11}(2p_{+a} 2p_{-a} 1s_b') + c_{12}(1s_a 1s_a' 2p_{0a}) + c_{13}(1s_a 2p_{0a} 1s_b') + c_{14}(2s_a 2p_{0a} 1s_b') + c_{15}(3p_{0a} 3p_{0a} 1s_b') + c_{16}(3p_{+1a} 3p_{-1a} 1s_b') + c_{17}(3d_{0a} 3d_{0a} 1s_b') + c_{18}(3d_{+1a} 3d_{-1a} 1s_b') + c_{19}(3d_{+2a} 3d_{-2a} 1s_b') + c_{20}(1s_a 3p_{0a} 1s_b') + c_{21}(1s_a 3d_{0a} 1s_b') + c_{22}(2s_a 3p_{0a} 1s_b') + c_{23}(2p_{0a} 3p_{0a} 1s_b') + c_{24}(1s_a 1s_a' 3p_{0a})$$

have constructed a 20-term wave function from 21 atomic orbitals (see Table I). The orbital exponents for the lithium core were taken from an atomic calculation, and the remaining exponents were originally chosen by Slater's rules and improved by a single pass of a technique described elsewhere.⁶ The calculation of the energy and the configuration coefficients as a function of the internuclear distance, the exponent improvement, and the calculation of properties required less than two hours on the Control Data Corporation 1604. This includes some compiling time for Fortran programs. Some results are listed in Table II together with results from self-consistent field molecular orbital configuration calculations and from experiment.⁷⁻¹¹ It is seen that the AOC energy is the best calculated energy and that the results, with the exception of the dipole moment,¹² for other properties are of comparable quality to those obtained from SCF-MOC calculations of approximately comparable size.

Our second example is the helium molecule ion. With the 24-atomic orbital configuration function listed in Table III we obtain for the rigorous lower bound of the dissociation energy $E(\text{exptl., atoms}) - E(\text{calcd., molecule}) = 2.14$ e.v., a value which is equal to or greater than two of the three published



^a Estimated improvement for a given amount of computing time.

Figure 1.

experimental determinations^{10,13,14} of the dissociation energy. This is an odd electron problem and as a consequence has not been attacked by the SCF-MOC approach; however, if it is attacked it is difficult to imagine that a result of comparable quality can be obtained by the SCF-MOC procedure with a lesser amount of effort.

In conclusion we submit that the AOC approach is not without merit for small molecules and may in certain cases be superior to the SCF-MOC approach.

Acknowledgments.—We wish to acknowledge helpful conversations with Dr. C. W. Scherr and with Messrs. Joe D. Stuart and Pat N. Reagen. We also thank the University of Texas Computation Center for time on the Control Data 1604 and Mr. Charles Earhart for help with the computations.

- (6) R. P. Hurst, *et al.*, *Mol. Phys.*, **1**, 189 (1958).
- (7) S. Fraga and B. J. Ransil, *J. Chem. Phys.*, **35**, 669 (1961).
- (8) D. D. Ebbing, *ibid.*, **36**, 1361 (1962).
- (9) S. L. Kahalas, Doctoral Dissertation, Boston University, Boston, Mass., 1961, unpublished.
- (10) G. Herzberg, "Spectra of Diatomic Molecules," D. Van Nostrand Co., Inc., Princeton, N. J., 1950, 2nd Ed., Table 39.
- (11) R. Velasco, *Can. J. Phys.*, **35**, 1024 (1957).
- (12) L. W. Wharton, L. P. Gold, and W. Kemperer, *J. Chem. Phys.*, **33**, 1255 (1960).

- (13) J. A. Hornbeck and J. P. Molnar, *Phys. Rev.*, **84**, 621 (1951).
- (14) E. A. Mason and J. T. Vanderslice, *J. Chem. Phys.*, **29**, 361 (1958).

ELECTRONIC SPECTRA OF CATACONDENSED AND PERICONDENSED AROMATIC HYDROCARBONS¹

BY RICHARD L. HUMMEL² AND KLAUS RUEDENBERG^{2a}

Institute for Atomic Research,³ Department of Chemistry, Department of Physics, Iowa State University, Ames, Iowa

Received July 23, 1962

The electronic spectra arising from the excitations of π -electrons in homonuclear conjugated bond systems are calculated for 37 aromatic hydrocarbons. The theoretical approach used takes into account overlap effects between different atoms, correlation between different electrons, variations in internuclear distances, and the influence of non-conjugated neighbors, hydrogen, and carbon. Four types of approximations are carried through for the molecules in order to obtain an estimate of the inadequacies of the theory. From the calculated transition energies and oscillator strengths, theoretical spectra are synthesized and compared with observed spectra. In order to help the interpretation, a decomposition of the transition dipoles into atomic contributions is introduced. The spectra of alternant molecules are successfully predicted, but the limits of the underlying assumptions appear to be exceeded in the applications to non-alternant systems. The calculations are markedly successful for the pericondensed systems, which had presented an obstacle to previous treatments. It is found that the calculated spectra are sensitive to small variations in interatomic distances. Calculations with exact atomic positions, where available, give considerably better agreement with experimental spectra. The calculations lead to an understanding of the general spectral pattern found in all aromatic hydrocarbons. On this basis the possibility of a general nomenclature of electronic transitions is examined.

Introduction

The quantum mechanics of aromatic molecules has continued to attract interest for several reasons. The molecules themselves are important, and their chemical and physical properties have been studied fairly extensively by experiment. Their spectra exhibit distinctive regularities which have permitted early empirical classification. Even relatively simple theoretical work can correlate reasonably well with various observed properties of at least a number of molecules. However an equal interest arises from the possibility of testing and proving more rigorous methods in molecular theory. For this purpose conjugated systems are exceptionally well suited, since attention can be focused upon interatomic molecular aspects with a minimum of purely atomic complications. This is so because, to a good approximation, each atom contributes but one atomic orbital and at most one electron, and, in hydrocarbons, all of the atomic orbitals are essentially identical. On the other hand, due to the variety in geometrical patterns, series can be formed which display systematic and often subtle relationships whose qualitative reproduction frequently provides a more reliable and sensitive test for the theory than isolated comparisons for individual molecules.

For some of the catacondensed molecules treated here, there have been carried out comparable calculations under certain simplifying assumptions, such as neglect of differential overlap between all atomic orbitals, neglect of the hydrogen atoms in the potential energy, neglect of the difference between joint and non-joint carbon atoms, assumption of constant neighbor-distance and semi-empirical framework integrals, and, in some cases, limitation of the configuration interaction. These

are the calculations of Parr, Pariser, Pople, Ham, and Ruedenberg.⁴ The objective of the present study is neither to account for the observed spectra of conjugated hydrocarbons with a minimum of theoretical effort, nor to achieve a maximum of agreement with experimental values; such objectives can obviously be better pursued by less rigorous, semi-empirical approaches. Rather the objective is the development and testing of a theory sufficiently rigorous and flexible so that (1) it can be extended to more complex systems, *e.g.*, involving heteroatoms; (2) it can give a realistic and sensitive indication of inadequacies in the assumptions, in particular of those errors which, in the semi-empirical treatments, are masked by compensation effects; (3) it might give a reasonably reliable indication of such unobservable quantities as molecular electronic wave functions.

The assumptions and approximations underlying the present work are those developed recently by one of the authors.⁵ Without full theoretical analysis, this treatment adopts the usual purely π -electronic approach, omitting specific interaction with the σ -electrons. However, in contrast to all previous work, the overlap-dependent contributions are taken realistically, though not completely, into account; two alternative approximations for the small elements of the overlap and one-electron energy-matrices are followed through: the "tight-binding" approximation and the "intra-ring approximation." Extensive, though not exhaustive, configuration interaction allows for electron correlation in the excited states. The choice of atomic orbitals involved gaging the short-range electron interaction and the atomic framework contributions by reference to the benzene spectrum and the carbon valence state.

The calculations permit an evaluation of the validity of these hypotheses. Limits of error for

(1) Research supported by the National Science Foundation (Grant G-10351).

(2) Part of a thesis submitted to the graduate faculty of Iowa State University in partial fulfillment of the requirements for the degree of Doctor of Philosophy.

(2a) Dept. of Chemistry, Johns Hopkins University, Baltimore 18, Md.

(3) Contribution No. 1184.

(4) R. G. Parr and R. Pariser, *J. Chem. Phys.*, **21**, 767 (1953); **23**, 711 (1955); R. Pariser, *ibid.*, **24**, 250 (1956); **25**, 1112 (1956); J. A. Pople, *Proc. Phys. Soc. (London)*, **A68**, 81 (1955); N. S. Ham and K. Ruedenberg, *J. Chem. Phys.*, **25**, 13 (1956). A more detailed historical bibliography is given in the first paper of ref. 5.

(5) K. Ruedenberg, *ibid.*, **34**, 1861, 1878, 1884, 1892, 1897, 1907 (1961).

the tight-binding approximation and the intra-ring approximation should be found by comparing the calculations made under the two assumptions. For the tight-binding approximation underestimates the smaller-than-neighbor matrix elements, whereas the intra-ring approximation appears to overestimate the smaller-than-neighbor energy elements. Any error due to either approximation should be smaller than that introduced, but hidden, in the studies based on the neglect of neighbor elements. Furthermore, the inclusion of at least neighbor overlap renders the calculations responsive to the actual bond lengths. The effect of the latter on the spectra will be demonstrated in those, all too few, cases where the true bond lengths are well established and comparative calculations possible. Another effect traced by the present calculations is the corrections which arise by taking into account the differences between non-joint and joint atoms in the diagonal elements of the framework potential matrix.

The inadequacies due to the neglect of interactions with σ -electrons and those inherent in the gaging of atomic orbitals could not be determined by comparative calculations. However, as there is no reason for consistent compensation between them in all molecules, an absence of sizable unexplained disagreements between experiment and calculations would seem to imply that such errors are small. None the less, a bona fide analysis of the corresponding corrections would contribute valuable insights.

1. Description of Method

Outline of Calculations.—The calculations were performed on an IBM-704 computer with a 32K core memory at the Midwest Universities Research Association, Madison, Wisconsin, by a completely automatic program. In the following, the course of the calculations executed is briefly described. For the mathematical details the reader must be referred to the derivations in ref. 5.

The *required input* consists of the name of the molecule, the number of conjugated carbon atoms, and the cartesian coordinates of each of these. The non-conjugated neighbors are assumed to be hydrogens unless additional input specifies otherwise. Further, if there are symmetry planes perpendicular to the plane of the molecule or a center of symmetry, a list of symmetrically placed atoms may be added for the program's use.

From this input are computed all interatomic distances and, from these, the overlap integrals for the intra-ring approximation are calculated. The overlap matrix is diagonalized by Jacobi's procedure, the eigenvalues are ordered according to decreasing size, and the symmetries of the eigenvectors are determined if the previously mentioned symmetry input data had been supplied. In general the diagonalization procedure does not produce symmetrical and antisymmetrical eigenvectors for degenerate eigenvalues; such eigenvectors are constructed by a subsequent transformation. The overlap eigenvectors then are converted to eigenvectors of the neutral framework Hamiltonian matrix.

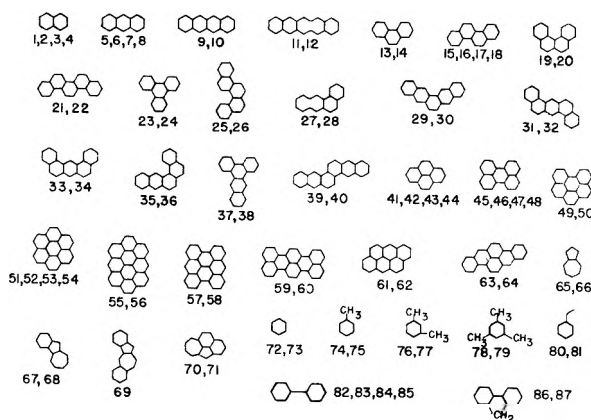


Fig. 1.—Chemical formulas of molecules treated. The numbers refer to the entries in Tables I to VI.

After determining the joint atoms, end atoms, and non-joint atoms, the program determines the applicable resonance integral, γ , and the joint correction, $\delta\alpha$, to the coulomb integral. Then the ground state bond order matrices, p and p' , are computed. Furthermore, from the interatomic distances, the interatomic two-electron interaction integrals $[PP|QQ] = G(PQ)$, are calculated.

Next, in preparation for the configuration interaction calculation, the one-electron excitations are examined as to transition energy and symmetry, if present. Discarded are those having transition energy in excess of 60,000 wave numbers or not having a dipole moment in transition with the ground state for symmetry reasons. If there is at least one perpendicular plane of symmetry, the remaining excitations split into two non-interacting groups with mutually perpendicular dipole moments. For each group, the configuration matrices are now constructed and then diagonalized giving the energies and compositions of the excited singlets and triplets and the oscillator strengths for the singlets. From these results a theoretical spectrum is synthesized by a procedure to be discussed in the next section.

The calculations are carried out first for the intra-ring approximation, thereafter the procedure is repeated for the tight-binding approximation. In Fig. 1, there are given the formulas for all 37 molecules which are treated in the present investigation. As indicated, 87 molecular calculations are carried through for these systems.

Outline of Results.—The machine printed results are divided into two parts. The first contains the material pertaining directly to the spectra and aiding in their interpretation or assignment. The second part consists of basic information concerning the atomic contributions, which is needed for the calculation or estimation of molecular properties, including, among others, spectra.

Spectral Data.—In the first spectral part it is assumed that in a molecule of N atoms there exist N molecular orbitals, well ordered according to increasing energies and numbered 1 to N . The excited wave functions then are characterized merely by their composition in terms of one-electron excitations ($n \rightarrow \nu$). For each of these jumps ($n \rightarrow \nu$), the printed output follows the de-

velopment of the energy, from the one-electron jump, through the diagonal elements of the configuration interaction matrix (with and without joint correction), to the final state energy. The oscillator strength and the transition moment components are given for the transitions, and the moments also are supplied for the one-orbital excitations. A table containing this detailed information will be published elsewhere.⁶ Machine-printed tables which abstract transition energies and oscillator strengths for the major transitions are given in the sequel for the various groups of molecules to be discussed.

In these tables as well as elsewhere in the paper, the following abbreviations are used to denote the four types of calculations carried out for a given molecule: TBX \equiv tight-binding approximation (neighbors only) using exact internuclear distances, and IRX \equiv intra-ring approximation using exact internuclear distances (if exact distances are known); TBM and IRM \equiv tight-binding approximation and intra-ring approximation using the constant bond length of 1.395 Å. and the constant bond angle of 120°, both "aromatic mean-values."

Synthetic Spectra.—In order to permit direct comparison with experimental spectra, without the somewhat subjective intermediary of interpretive assignments, the program finally calculates, and automatically plots, theoretically predicted spectra. Smoothed vibrational-rotational broadening is simulated by assuming, for each transition, a triangular band shape in the ϵ vs. λ^{-1} spectrum. In accordance with the empirically observed average half width of 2 kK., a base of 4 kK. is chosen for this triangle. Its height, ϵ (max.), is found from the relationship between oscillator strength, f , and band area, $v\lambda z$.

$$f = (\pi r_0)^{-1} \int d(\lambda^{-1}) \kappa(\lambda^{-1}) \quad (1)$$

where

$$r_0 = e^2/mc^2 = 2.81784 \times 10^{-13} \text{ cm.}$$

is the classical "electron radius" and the "absorption coefficient" κ is related to the usual extinction coefficient,⁷ ϵ , by

$$\kappa = \epsilon(10^3 \ln 10)/N \quad (2)$$

with $N =$ Avogadro number. One obtains

$$\epsilon(\text{max}) = (6.82188 \times 10^{-7}/Nr_0)f$$

$$\epsilon(\text{max}) = 115,813f \text{ (l./mole cm.)} \quad (3)$$

whence

$$\log \epsilon(\text{max}) \approx \log f + 5 \quad (4)$$

After superposing all bands, a plot of $\log \epsilon$ vs. λ is made and printed. Since the logarithm is plotted, in accordance with the usual spectral tracings, the initial choice of the individual band shapes is practically irrelevant.

(6) R. L. Hummel and K. Ruedenberg, "Pi-Electronic Excitations in Aromatic Molecules," U.S.A.E.C. Report I.S. 450, Ames Laboratory, Ames, Iowa, 1962.

(7) The intensity attenuation over the path length of x cm. is given by the formula $I(x)/I(0) = e^{-\kappa x} = 10^{-\epsilon x}$, where $n =$ number of molecules per cm.³ and $c =$ number of moles per liter.

The spectra which are synthesized from calculated transitions and oscillator strengths are compared with the experimental ones in several figures to be discussed later on (Fig. 3, 4, 7, 8, 10, 11, 13, 14, 15, 18). In these figures the arrangement for each molecule is as follows: experimental spectra in the center, tight-binding approximation above, intra-ring approximation below. Three kinds of abscissas are used. For the experimental spectra taken from Clar,⁸ the abscissa is in Å., increasing from right to left; for the spectra taken from Friedel and Orchin,⁹ the abscissa is in Å., increasing from left to right; for the spectra taken from Klevens and Platt,¹⁰ the abscissa is in kK. (1 kK. = 1000 cm.⁻¹), increasing from left to right. The synthetic spectra are plotted accordingly. In comparing theoretical and experimental spectra, it must be kept in mind that strong transitions are in general subject to a red shift of about 1 kK. in liquid or solid solution.

Dipole Maps.—In order to trace similarities between individual transitions for a variety of different molecules, decompositions of the transition-dipole moments were machine plotted for all transitions with oscillator strength greater than 0.0005 in the following manner.

If, in the state function of a given excited state, the one-electron transitions ($n \rightarrow \nu$) occur with coefficients $C(n\nu)$, the transition dipole to the ground state is given by¹¹

$$\vec{Q} = \sum_P \vec{R}_P \sum_{(n)} C(n\nu) c_{Pn} c_{P\nu}' (s_n + s_\nu) / \sqrt{2} \quad (5)$$

In order to exhibit the relative importance of the individual atomic contributions to the total moment, the scaled quantities

$$\sigma \bar{5} [N \sum_{(n)} C(n\nu) c_{Pn} c_{P\nu}']^{1/2} \quad (6)$$

(where σ is the sign of the sum before taking the absolute value) were considered optimal for display. They are printed, in map form, at the atomic positions. The $(s_n + s_\nu)/2$ are omitted because they are essentially constant, close to 2. Since the $c_{Pn}, c_{P\nu}'$ are subject to a normalization involving summation over N atoms, the chosen quantities exhibit variation from -9 to $+9$. For the mapping they are truncated to integers.

For our more complex wave functions these dipole maps replace the nodal arguments used by Platt, in analogy to atomic spectra, for the perimeter model. It will be seen that there are interesting agreements as well as significant disagreements between the present analysis and the pattern of perimeter nodes.

Molecular Orbital Data.—A second table of machine printed results consists of basic information concerning the molecular orbitals. Reference to their component atomic orbitals is based on a molecular map printed out to scale with the atomic numbering in the appropriate positions. The cartesian coordinates of these are printed beneath in units of $D = 1.395$ Å.

(8) A. Clar, "Aromatische Kohlenwasserstoffe," Springer, Berlin, 1952.

(9) R. A. Friedel and M. Orchin, "Ultraviolet Spectra of Aromatic Compounds," John Wiley and Sons, Inc., New York, N. Y., 1951.

(10) H. B. Klevens and J. R. Platt, "Survey of Vacuum Ultraviolet Spectra of Organic Compounds in Solution. Laboratory of Molecular Structure and Spectra," Technical Report 1953-1954, Part I (Department of Physics, University of Chicago, 1954).

(11) See eq. (3.18) and (4.12) of the first paper in ref. 5.

Next are printed the eigenvalues and eigenvectors of the overlap matrix and those of the neutral framework-Hamiltonian matrix. The molecular orbitals are numbered in order of increasing one-electron energy and characterized by their symmetry properties with respect to symmetry planes and centers of symmetry. Finally the Coulson-type bond order matrix, p , as well as the Mulliken-type bond order matrix, p' , are printed out. These tables will be published elsewhere.¹²

Comparison between Theory and Experiment.—Before comparing the results of the calculation with experiment, it might be well to consider the limitations in the experimental spectra themselves. The most obvious is the limitation of the available spectral range. Measurements must in general be made in solution, a solid solution in some cases, which restricts them to the range of transmission of the solvent and precludes measurement of the many short wave transitions. Consequently, except for certain molecules for which special pains have been taken, the available spectra are limited to a few of the lower transitions.

The interpretation is complicated by solvent shifts, dependent upon the transition involved as well as upon the solvent. A more serious problem is that of vibrational interactions with electronic transitions¹³ to create broad, poorly defined maxima and to introduce peaks often indistinguishable from electronic transitions.

On the theoretical side the comparison is made difficult by the fact that the number of transitions that can be calculated is proportional to the square of the number of atoms and the fraction in the observable region increases for larger molecules. Thus, except for small molecules and except for the two or three lowest transitions and the strongest transition, which remain clearly distinguishable for all molecules, experimental as well as theoretical spectra lose more and more of their distinctiveness with increasing molecular size.

Therefore the simpler hydrocarbons which have been the primary object of previous investigations will provide the more sensitive test of the present method in that their spectra are more characteristic and more thoroughly measured and assigned. The most critical test will lie in the still smaller subgroup for which atomic positions have been determined with precision, since correct positions alone allow the present theory full scope.

The more complex molecules, which are not well treated by the semi-empirical theories, also are included to test the theory, to provide theoretical information on these molecules, and to provide a fairer comparison¹⁴ between the present method

(12) R. L. Hummel and K. Ruedenberg, "Topological Molecular Orbitals in Aromatic Molecules," U.S.A.E.C. Report I.S. 449, Ames Laboratory, Ames, Iowa, 1962.

(13) As an illustration of the difficulties, consider the low transitions 1L_a and 1L_b in the standard sequence of the linear polyacenes. Platt's earlier assignment of the stronger one (1L_a) differs from Ham's later assignment by more than 2000 wave numbers in two cases. The weaker one can be picked out of the spectra only for the first and the last member of the sequence. In anthracene it was located by polarized light in a carefully prepared solution crystal, but in naphthalene it has not been experimentally located to date.

(14) Semi-empirical methods may be expected to show up more favorably relative to a more theoretically restricted theory for a

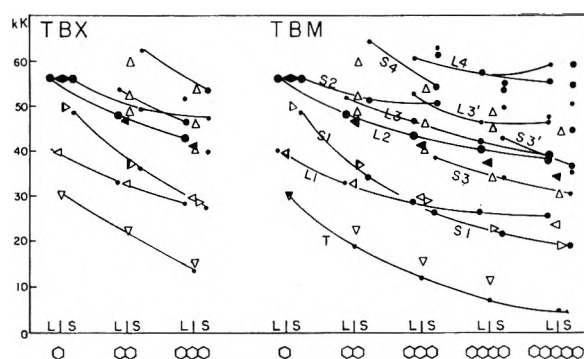


Fig. 2.—Assigned and calculated transitions in the linear polyacenes. Explanation: Calculated transitions connected by solid lines. Points above L: long-axis polarized; points above S: short-axis polarized. Oscillator strengths: $f < 0.1$ for light dots; $0.1 < f < 1$ for medium dots; $f > 1$ for heavy dots. Observed transitions indicated by triangles: downward pointing for triplets; upward for singlets of unknown polarization; left-pointing for singlets long-axis polarized; right-pointing for short-axis polarized singlets. Filled triangles: $f > 1$.

and the semi-empirical methods. As for these molecules plots of assigned transitions *vs.* calculated transitions tend to become rather arbitrary in the assignments, it was found more illuminating to compare the synthetic spectra for each molecule directly with a reproduction of the actual experimental spectrum.

2. Linear Polyacenes

Transition Energies.—Although the present study includes many molecules, the first five of the linear polyacenes remain a backbone of comparison with experiment for two reasons, both experimental. First of all, the experimental spectra for all but pentacene are more complete than usual and have been carefully studied and assigned to electronic transitions. In particular, measurements have been extended to shorter wave lengths, and for several transitions the polarizations have been determined and can be reasonably extended to the entire group. The second reason is that, of the *four* aromatic molecules whose atomic positions are known *with confidence*, three are members of this group, namely, benzene, naphthalene, and anthracene.

The results of the calculations for the linear polyacenes are presented in Table I. For the TBX and TBM cases, calculated and assigned transition energies are shown in Fig. 2. Polarizations and relationships between transitions in different molecules are indicated only when considered justifiable. For the purpose of discussion it is convenient to divide the transitions into three groups; (1) the strongest and sharpest transition named 1B_b by Platt, (2) the families of transitions below 1B_b in energy, and (3) the remaining transitions with energies greater than or, in pentacene, comparable to 1B_b .

For the transitions below 1B_b , use of exact atomic positions yields a perfect fit between calculated and experimental energies and polarizations regardless of which approximation (TBX or IRX) is used.

family of molecules used in fitting the parameters. This advantage fades as the molecules differ more and more from those used in the gaging.

TABLE I
 CALCULATED TRANSITIONS OF THE LINEAR POLYACENES

Explanation: One set of data occupies two lines. The first two entries on the first line are a counting integer referring to the chemical formula in Fig. 1 and the name of the molecule. The first two entries on the second line give the method of approximation (TBX, IRX, TBM, IRM) and the transition energy of the lowest triplet. The remaining entries on both lines consist of pairs of numbers of which the first gives the transition energy of a singlet transition and the second its oscillator strength.

If the molecule possesses a symmetry plane perpendicular to the molecular plane, the first line contains the singlets of S symmetry and the second line contains the singlets of A symmetry.

If the molecule possesses two planes of symmetry perpendicular to the molecular plane, the first line contains the singlet of SA symmetry and the second contains the singlets of AS symmetry, where the first symmetry specification refers to the long axis and the second to the short axis.

If the molecule possesses a center of symmetry, only the A states are listed (since the S states are symmetry forbidden), and they occupy both lines. In the absence of any symmetry, too, the second line is merely a continuation of the first.

ELECTRONIC TRANSITIONS FOR THE LINEAR POLYACENES											
1	NAPHTHALENE	33.004	0.050	47.789	2.002	53.998	0.323	72.693	0.036		
	TBX TRIPLET= 21.253	35.992	0.201	49.504	0.742	62.616	0.003	67.641	1.007		
2	NAPHTHALENE	33.685	0.029	48.857	2.396	62.039	0.131	74.006	0.005		
	IRX TRIPLET= 21.977	36.534	0.186	49.171	0.710	66.491	1.013	70.030	0.004		
3	NAPHTHALENE	32.547	0.073	48.086	1.961	52.544	0.346	72.680	0.032		
	TBM TRIPLET= 18.643	33.827	0.263	51.246	0.641	64.536	0.	68.094	1.083		
4	NAPHTHALENE	33.354	0.039	49.097	2.462	61.065	0.080	73.694	0.003		
	IRM TRIPLET= 19.213	34.135	0.251	50.964	0.600	66.873	1.082	72.218	0.010		
5	ANTHRACENE	28.312	0.116	42.599	2.982	46.876	0.199	51.526	0.095		
	TBX TRIPLET= 12.844	27.728	0.283	39.357	0.009	47.387	0.385	53.835	0.474		
6	ANTHRACENE	29.093	0.063	43.299	3.556	50.075	0.019	56.561	0.125		
	IRX TRIPLET= 13.406	27.751	0.265	43.311	0.005	46.897	0.355	49.575	0.201	59.746	1.140
7	ANTHRACENE	28.283	0.162	43.157	2.818	46.462	0.348	52.747	0.026	60.629	0.089
	TBM TRIPLET= 11.882	26.058	0.359	38.213	0.018	50.513	0.222	54.208	0.670	61.140	0.614
										62.760	0.035
										69.050	0.006
										71.758	0.003
										65.270	0.023
8	ANTHRACENE	29.284	0.087	43.888	3.631	51.552	0.036	57.162	0.033	67.848	0.
	IRM TRIPLET= 11.218	25.399	0.290	42.518	0.011	48.200	0.002	50.574	0.350	59.987	1.227
										71.611	0.008
										61.531	0.059
										72.320	0.027
9	NAPHTHALENE	26.041	0.312	40.013	3.285	41.689	0.512	46.164	0.057	57.198	0.169
	TBM TRIPLET= 6.747	21.449	0.366	33.932	0.036	42.522	0.079	49.544	0.067	53.438	0.952
										54.729	0.408
										62.874	0.021
										62.216	0.030
10	NAPHTHALENE	26.829	0.149	39.935	4.586	46.156	0.016	53.000	0.022	60.111	0.145
	IRM TRIPLET= 6.581	20.387	0.331	36.758	0.043	40.928	0.030	48.875	0.036	52.465	0.872
										56.672	0.664
										64.445	0.061
11	PENTACENE	25.232	0.495	37.651	2.125	38.742	2.223	45.977	0.027	47.107	0.009
	TBM TRIPLET= 4.316	18.835	0.414	30.047	0.069	35.261	0.038	36.307	0.116	44.374	0.181
										50.531	0.026
										58.952	0.086
										54.236	0.878
12	PENTACENE	25.671	0.268	37.380	5.384	42.022	0.017	49.836	0.016	55.542	0.
	IRM TRIPLET= 3.914	17.186	0.357	32.086	0.099	35.865	0.036	39.763	0.010	44.417	0.212
										46.263	0.017
										59.190	0.066
										53.276	0.686

However since exact distances are not known for the two largest molecules, the assumption of constant bond lengths and angles is unavoidable if all molecules are to be treated. With these incorrect distances, the results for the same transitions are not nearly as good. In particular, the lowest triplets fall three to five kK. below the experimental values. The remaining three transitions per molecule already are well fitted by TBM and reasonably well fitted by IRM. It seems not unreasonable to expect that the use of correct distances would bring all transitions into close agreement with experiment.

The very prominent 1B_b transition shows a beginning of error even when exact distances are used. For TBX the calculated value is slightly high at anthracene and for the intra-ring approximation, IRX, the error begins at naphthalene and is greater than 1 kK. at anthracene. Use of the incorrect, average distances gives results that are a bit poorer for these two molecules and probably the same would hold for the two larger molecules. Even so the average error for all molecules and methods is roughly 2 kK., which is still considered fairly good.

Presumably, the higher transitions are not predicted as accurately, since the calculations are subject to increasing error as larger one-electron jumps are involved. It is, however, difficult to prove this disagreement for the larger molecules

because of the increasing number of transitions predicted above 1B_b . This spectral region becomes crowded and rather confused for the larger molecules; for still larger ones this "barrage" of transitions presumably would appear more and more continuous. Under these circumstances, the synthetic spectra become the most straightforward means of comparing theory with experiment. For the linear polyacenes, they are given in Fig. 3 and 4.

Only two of the higher transitions can be observed in naphthalene and both are reasonably but not closely predicted by the TBX method. The results of the IRX approximation are for once quite a bit higher, resulting in errors of 4 and 8 kK., respectively.

While two high experimental transitions also are experimentally assigned in anthracene, all calculations place at least three theoretical transitions nearby. The synthetic spectrum shows, however, that some of these are underlying and, as a whole, it exhibits a reasonable similarity to the actual spectrum.

Intensities.—For all four methods of approximation, the intensities of a given transition are usually quite similar, and there is even greater resemblance between the two tight-binding or the two intra-ring methods. As in the previous semi-empirical calculations, the intensities of the strongest transitions are a bit too strong. The weaker ones suffer

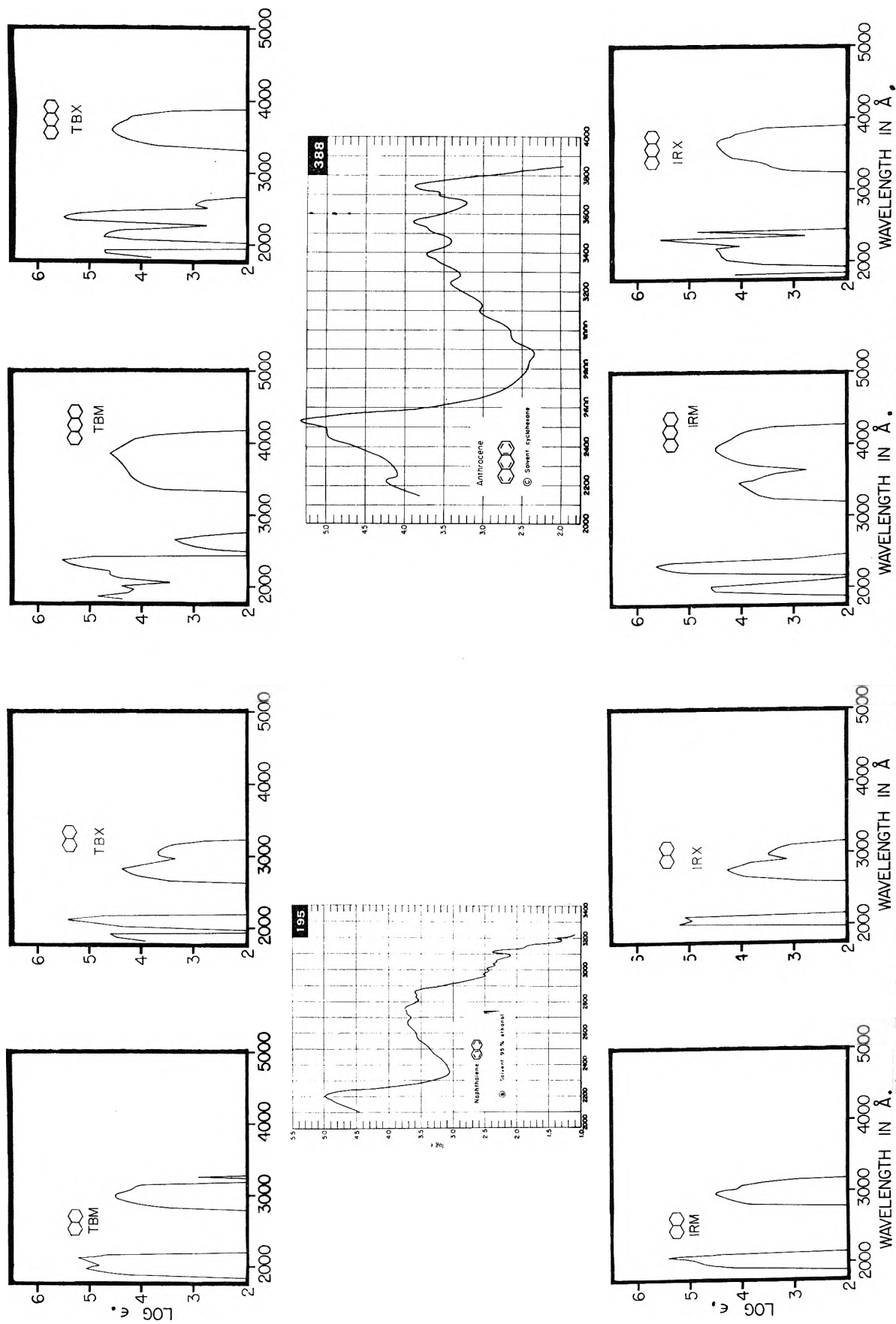


Fig. 3.—Experimental and synthetic spectra for linear polyacenes. I. For explanation see section 1, after eq. 4.

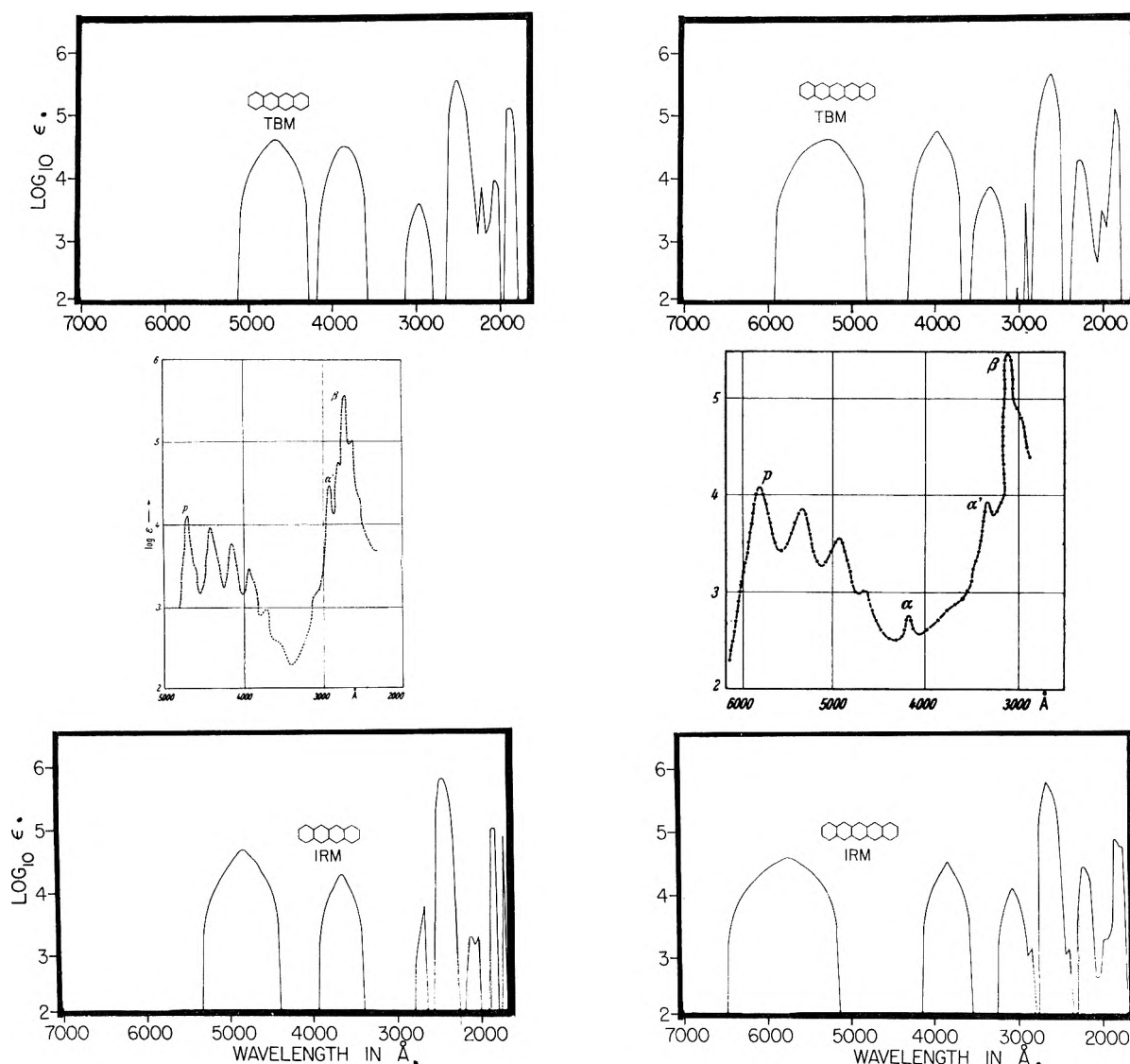


Fig. 4.—Experimental and synthetic spectra for linear polyacene. II. Explanation in section 1, after eq. 4.

from this fault to a greater degree. For example the intensity of 1L_b in naphthalene is calculated $1/50$ as strong as 1B_b , whereas it should be $1/500$ as strong as that (Pariser gives 1L_b zero intensity; Ham and Ruedenberg, however, obtain the correct intensity ratio).

These observations are also verified by reference to the synthetic spectra in which the intensity results are incorporated as described earlier.

Comparison between Different Approximations.

—Both of the present approximations using exact distances clearly fit the experimental energies better than the semi-empirical methods,⁴ but these in turn are better than the present approximations when constant bond lengths are assumed. These results imply rather strongly that the actual positions of the atoms are not negligible parameters.

Both approximations using exact distances yield equally perfect fits for the lower transitions, but the higher transitions seem to indicate, particularly in naphthalene, that TBX fits the experimental energy levels considerably better than IRX.

(Pariser also calculated these transitions, but the energies obtained were even higher than IRX.)

The somewhat unexpected conclusion would seem to be that neglect of the smaller-than-neighbor elements in the overlap and one-electron energy matrices, implicit in TBX, results in less error than taking them into account in the manner of IRX. To a large extent the explanation must lie in the particular manner in which the small matrix elements are approximated in IRX.

Another possible factor may be a greater sensitivity of the intra-ring approximation to the neglect of σ -electrons. Whereas TBX gives a constant value of unity for all gross atomic populations, the latter are usually unequal, in the IRX approximation (greater than unity for one and less than unity for the other of two neighbors). The σ -electrons in the bond between the atoms, were they taken into account, perhaps would tend to compensate for this charge disparity.

Criteria for Forming Families of Transitions. Previous Approaches.—(1) Several criteria have

been used in the past for classifying the electronic transitions into families whose members can be traced through all polyacenes. On the basis of regularities concerning energies, intensities, and vibronic structure found empirically in the actual spectra, Clar⁸ pointed out that, usually, three distinct and characteristically different bands could be recognized in each aromatic hydrocarbon. These he called the α -band, the β -band, and the p-band.

(2) Later theoretical calculation led to the grouping of the excited states according to irreducible representations of the molecular symmetry group. The linear polyacene singlets fall into four groups. Only two of these, however, ${}^1B_{2u}$ (A \perp , S \parallel) and ${}^1B_{3u}$ (S \perp , A \parallel) have a dipole transition with the ground state and thus may contribute to the observable spectra. Each group has a specific polarization, which can be experimentally determined. As two main directions of polarization also are found for but approximate symmetry, the two classes of characteristic polarizations are indeed fundamental. They alone, however, do not furnish sufficient subdivision for a satisfactory classification.

(3) Platt¹⁵ stressed that, in view of Clar's observations, these molecules must exhibit certain quantum mechanical similarities in addition to the symmetry properties just mentioned. Basing his arguments on the perimeter model and drawing analogies to the use of angular momentum in simple atomic spectra, he characterized the transitions by the nodal behavior of their one-electron jumps and proposed a system of classification which accounted for the families of Clar and moreover suggested additional families frequently hidden under stronger transitions or in an optically inaccessible region. His classification retained the division according to polarization.

(4) Moffitt¹⁶ and Pariser⁴ developed a different explanation for Clar's relationships, based on the fact that, in the neighborhood of the highest occupied orbital, *viz.*, the $(N/2)^{th}$ orbital, the one-electron energies are fairly evenly spaced. Consequently, the four lowest transitions fall roughly into the order: $[N/2 \rightarrow ((N/2) + 1)] < [((N/2) - 1) \rightarrow ((N/2) + 1)] \approx [N/2 \rightarrow ((N/2) + 2)] < [((N/2) - 1) \rightarrow ((N/2) + 2)]$. The first yields essentially 1L_a , the second and third are known as "paired excitations" and interact to form 1B_b and 1L_b , while the fourth essentially becomes 1B_a . In the neglect-of-differential-overlap approximation used by these authors, these paired excitations, as well as other, higher excitation pairs, are degenerate and the resulting states are 1:1 mixtures, *viz.*, the + and - combinations. Since the minus combinations interact only with each other, Pariser suggested a division of the actual transitions into + and - states as a subclassification within the group theoretical species.

Unfortunately this subdivision is limited to alternants, and even there the + combinations are much more numerous and but two of them,

${}^1B_{2u}^+$ and ${}^1B_{3u}^+$, account for almost all observable transitions in the linear polyacenes. Hence this subdivision is not too helpful.

In the present, more accurate calculation, it is still true that the lowest three transitions arise from the first three excitations mentioned above; but Pariser's \pm -classification loses its meaning. On the other hand, the essence of Platt's classification was seen as a structural analysis of the transition moments. For the trigonometric wave functions of the perimeter model, his analysis of nodes alone provided a complete description. For the present, more complicated wave function, a more thorough analysis of the transition dipole structure is needed to establish clearly kinships between different molecules.

Present Approach.—(1) It proved possible to determine such finer features with the help of the graphical dipole decomposition described earlier. The transitions on which Clar's and Platt's identifications agree are clearly related by common characteristics and so are a number of additional transitions. In some molecules, it is found that a relationship is disrupted by extensive configuration interactions which had been absent in smaller molecules. These relationships can be seen from the dipole maps reproduced in Fig. 5. The numerical values are truncated to one figure, they have sufficient variation for good resolution, but not so much as to create confusion. The relationships between transitions in different molecules are exhibited by connecting lines, bearing the corresponding label, in Fig. 2.

(2) Consider first the four low transitions, 1L_a , 1L_b , 1B_a , and 1B_b in Platt's nomenclature. The dipole maps reflect, of course, the well known symmetry properties: 1L_a and 1B_a are symmetrical about the short axis, antisymmetrical about the long axis, while 1L_b and 1B_b are antisymmetrical about the short axis, symmetrical about the long.

The 1L_a is characterized by having a node in every bond just as Platt suggested. The values at the atoms alternate in sign, but are not uniform as they would be in the perimeter model. The two largest magnitudes are found in the short axis; succeeding values of the same sign diminish toward the outside within one quadrant. The values of opposite sign have their smallest magnitude next to the short axis and increase away from this axis. The envelopes of the two groups are essentially parallels.

The dipole map of 1B_a , too, exhibits the nodal properties suggested by Platt, *viz.*, one single node only along the short axis. In addition the following details occur consistently. The atomic contributions increase gradually from the central node, but after a short inflection peak they increase suddenly to a high value at the end atoms. This is the origin of the very strong intensity of 1B_b .

In contrast, the 1L_b dipole does not have the multiple nodes derived by Platt from the perimeter model; instead it has a single node like 1B_b . The resemblance to 1B_b is in fact very close in all particulars, except that the magnitudes involved are much smaller, resulting in the very small transition moment. Indeed, to the extent that 1L_b ,

(15) J. R. Platt, *J. Chem. Phys.*, **17**, 484 (1949).

(16) W. Moffitt, *ibid.*, **22**, 1820 (1954); see also M. J. S. Dewar and H. C. Longuet-Higgins, *Proc. Phys. Soc. (London)*, **A67**, 795 (1954).

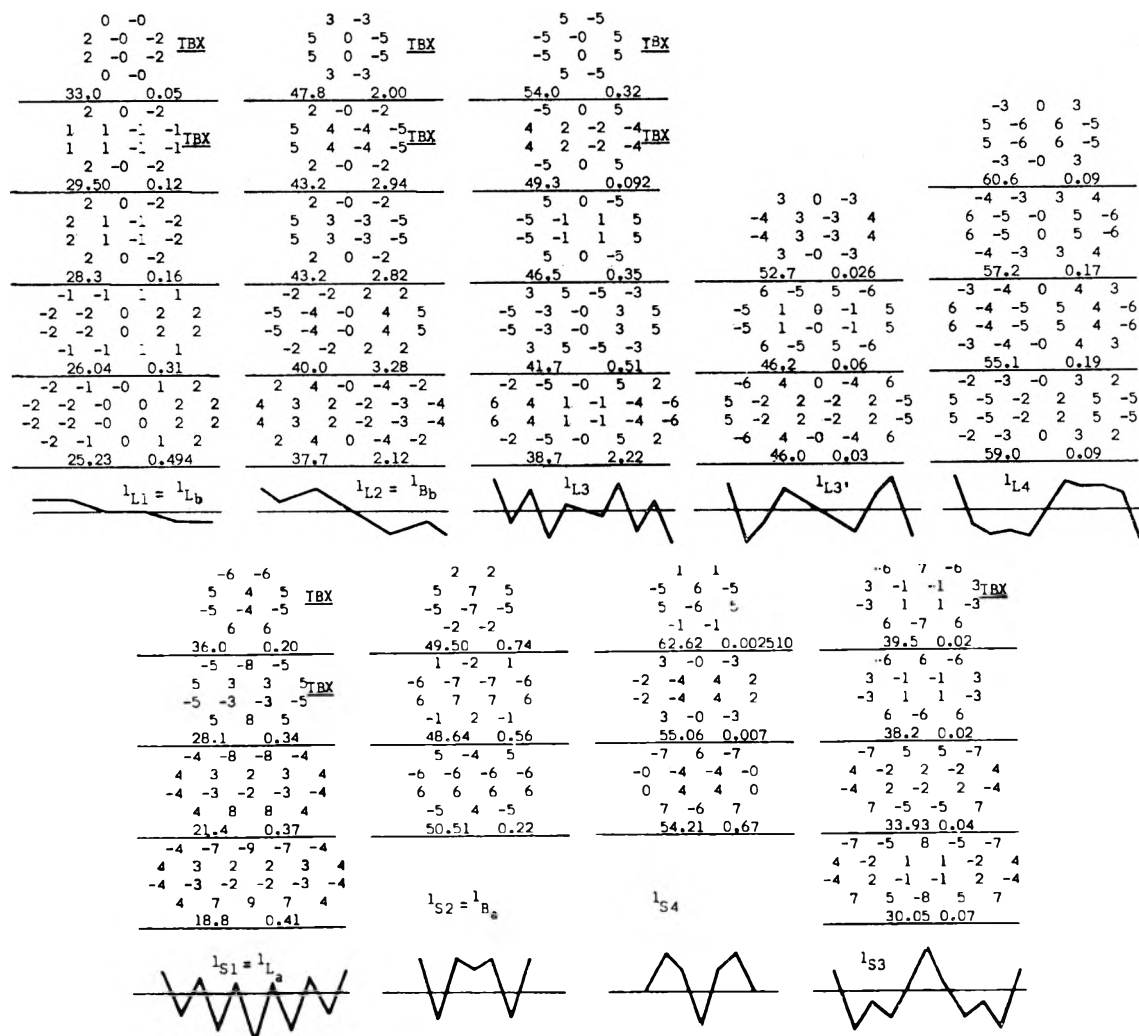


Fig. 5.—Dipole maps for electronic transitions of linear polyacenes. Under each map is given the transition energy and the oscillator strength, so that reference can be made to Table I.

and 1B_b arise from paired transitions, the atomic dipole contributions of 1L_b must be proportional to those of 1B_b in any calculation—not just the present. Our result for 1L_b is not in complete disagreement with Platt's picture: the simple perimeter model produces nodes at all atoms, and the present atomic contributions are small. They would indeed vanish if, instead, the results of Pariser's approximation would be plotted in like manner. The major differences from Platt's diagrams lie in the dipole contributions assigned to the bond regions. While the free-electron perimeter model suggests antinodal behavior, the actual bond contributions are smaller than those from the atoms. Similar limitations of the free-electron model are found whenever the number of nodes equals or exceeds the number of atoms.

The " 1B_a " transition differs from the previous ones in that there exists no characteristic dipole pattern for it which would persist to the higher molecules of the polyacene series. This is a consequence of the increasing amounts of configuration interaction to which 1B_a is subject because of its constantly high one-electron excitation energy. In naphthalene it has the single node along the long axis that Platt proposed. The dipole struc-

ture is similar to that of 1L_a , however, in that for both it fluctuates strongly, although the fluctuations in 1B_a are not strong enough to produce nodes through all bonds. In anthracene, however, eight additional nodes are produced—only four short of 1L_a . In naphthalene two additional transitions have moved down to interact very strongly (>50%) with the $[(N/2 - 1) \rightarrow (N/2 + 2)]$ one-electron jump to form transitions with new and varying characteristics. Conclusions concerning this transition are further complicated since it is one where the differences between TBM and the more nearly correct TBX are greatest and the fine details provided by the dipole analysis are sensitive to such considerations. The correct distances needed for TBX are not available for the very molecules in which the complications arise.

(3) In order to describe the relationships for the remaining transitions, it is convenient to have short state labels. Since the nomenclature derived from the perimeter model does not really fit, and since it seemed premature to promulgate another general scheme on the basis of the present work alone, the following simple nomenclature is used in the following discussion. The long axis polarized states are labeled $L1, L2, L3, L4, \dots$. The short

axis polarized are labeled S1, S2, S3, S4, . . . Naturally in larger molecules, additional transitions arise. If some appear to resemble those of an already existing family, such branching is brought out by using symbols like L1', S2', L3', L3'', etc.

In particular the previously discussed states are now denoted as

$$L_b = L1, B_b = L2, L_a = S1, B_a = S2$$

On the whole it is surprising how many of the transitions can be placed into families with quite consistent characteristics. This is indicated by the many connecting curves in Fig. 2. The only case where such correlations are really hopeless and therefore omitted in this figure is the group of heavily interacting states into which ${}^1B_a = {}^1S2$ disappears from naphthacene on.

Best characterized are the long axis polarized transitions. In fact all L transitions below 55 kK. except L1 and L2 seem to belong to one clan denoted by L3, L3'. The main branch, L3, has almost the identical structure as S1(1L_a) except that there is a node rather than a maximum on the short axis. It has nodes in every bond. The next branch, L3', is characterized by maintaining the total numbers of nodes and the general appearance of L3 in anthracene through the larger molecules, and hence does not have nodes in every bond. The remaining long axis polarized transitions all seem to be characterized by being flat and of one sign from the central nodes to the next to end atom and then changing sign strongly to attain the maximum magnitude. Thus these transitions are all classed together as L4.

The remaining short axis polarizations do not carry a rigid pattern from the first member of a family to the last, but must be followed from molecule to molecule. The lower energy S3 has a considerable resemblance to S4 but the considerable difference in energy led to their being assigned to separate families. S4 is one of the transitions which enter into interaction with S2 (1B_a) and its characteristics can be partially found in several of the highly mixed S states of naphthacene and pentacene. The S transition at 35.26 kK. in pentacene is an almost pure state of new characteristics hatched in this molecule.

3. Non-Linear Polyacenes

Criteria for Grouping.—Because of their great number, the non-linear polyacenes must be divided into groups for calculation and display. Under the influence of the perimeter model it has been customary to form groups of molecules having the same number of carbon atoms. However, the strong variations in energy found in such a group both experimentally and theoretically indicate considerable distortions from the perimeter model. In contrast we observed that the following *general rule* seems to hold:

Similarities in the positions of the lower transition energies exist between these aromatics which agree as to the largest linear polyacene contained in the molecular structure.

Within such a group, energy variations are

much finer and present therefore a greater challenge to theoretical calculation than the larger variations found in the aforementioned grouping. They therefore are chosen for the present work. Representative members of two groups will be considered: one based on naphthalene and one based on anthracene.

Naphthalene Group.—The numerical results for the naphthalene group are reproduced in Table II. The experimental and theoretical transition energies are compared in Fig. 6, for the TBM approximation. The agreement between the lower assigned and calculated transitions is reasonable and comparable with the results for the linear polyacenes and better than what Ham and Ruedenberg have obtained previously for several of the present molecules. Note that the TBX approximation again improves the triplet value for chrysene.

The spectra of the non-linear polyacenes are more complicated than those for the linear polyacenes, since they have at most one symmetry plane (not including the molecular plane). The presence of one plane will create two sets of transitions with mutually perpendicular polarizations, but none of them will be dipole forbidden. The only exception is chrysene, which has a point of symmetry, so that the symmetric states are dipole forbidden. But the remaining states, all antisymmetric, are all mutually interacting and without limitation as to the polarization directions.

Thus many excited states are to be expected in the present group, and it is rather surprising that most of them seem to fall in the region around the strong transition, where they are hidden, or higher, where observation is difficult. The lowest two singlets are remarkably separate. It is still true that their polarizations are mutually orthogonal except for chrysene, which has the lowest state polarized along the long axis of the molecule and the next at an angle of less than 30° with it. These similarities in polarization, intensity, dipole map, etc., are expressed by the connecting lines in the figures.

In the 40 kK. region, all molecules typically show a strong transition, long axis polarized, with a fairly strong satellite less than 2 kK. higher. The latter is short axis polarized except in chrysene, where both transitions are almost equally strong and bracket the long axis between them. These two transitions resemble 1L2 (1B_b) and 1S2 (1B_a) in naphthalene. This similarity appears to support the present grouping. The discussed relationships again are indicated by connecting lines on the figures.

While the appearance of the two low weak transitions and the strong higher transitions in all molecules is quite similar to naphthalene, the situation is more complicated as regards symmetry and pairing properties. In all cases, except naphthalene, the long axis is orthogonal to that symmetry plane which is perpendicular to the molecular plane (if existing). If this perpendicular symmetry plane contains atoms, "the paired excitations" are long axis polarized; if it bisects a bond, then the "paired excitations" are short axis polarized. In fact, it emerges that *the pairing*

TABLE II
CALCULATED TRANSITIONS OF THE NON-LINEAR POLYACENES. NAPHTHALENE GROUP
See Table I for explanations.

ELECTRONIC TRANSITIONS FOR THE NON - LINEAR POLYACENES I									
13 PHENANTHRENE TBM TRIPLET= 20.272	30.786 0.017 32.529 0.352	39.992 0.394 38.830 0.087	42.327 0.466 42.102 1.177	48.998 0.010 43.630 0.614	51.612 0.083 49.408 0.059	53.829 0.701 53.348 0.106	54.566 0.029 54.218 0.548		
14 PHENANTHRENE IRM TRIPLET= 21.000	31.741 0.005 33.273 0.268	40.411 0.622 40.329 0.197	46.230 0.026 42.606 1.411	48.342 0.385 47.137 0.403	55.666 0.684 51.523 0.709	57.204 0.111 54.003 0.133	54.602 0.038		
15 CHRYSENE TBX TRIPLET= 20.371	30.388 0.411 46.907 0.025	30.764 0.405 51.812 0.352	40.969 0.890 53.010 0.224	42.436 1.205 55.110 0.295	43.423 1.462 58.082 0.368				
16 CHRYSENE IRX TRIPLET= 21.223	31.156 0.153 49.959 0.078	31.410 0.551 53.298 0.407	41.934 1.996 56.247 0.719	43.039 1.205 60.410 0.227	44.799 0.623 65.186 0.132				
17 CHRYSENE TBM TRIPLET= 22.220	30.247 0.291 42.979 1.222	30.606 0.495 46.759 0.038	40.895 0.651 52.808 0.304	41.768 1.511					
18 CHRYSENE IRM TRIPLET= 21.187	31.059 0.235 49.808 0.053	31.330 0.466 53.285 0.424	41.830 2.052 56.134 0.676	42.853 1.167 59.763 0.265	44.694 0.529				
19 3,4 BENZPHENANTHRENE TBM TRIPLET= 21.367	31.285 0.022 28.601 0.005	38.870 0.052 35.706 1.392	39.969 1.274 37.852 0.408	42.136 0.169 43.964 0.336	47.735 0.486 44.948 0.003	51.317 0.002 46.620 0.002	47.313 0.		
20 3,4 BENZPHENANTHRENE IRM TRIPLET= 22.006	31.161 0.038 28.654 0.019	37.442 0.033 36.421 1.438	39.633 0.791 38.207 0.284	45.084 0.112 44.909 0.349	48.594 0.298 46.799 0.262	49.283 0.011 48.104 0.100	52.999 1.731 49.985 0.408		
21 PICENE TBM TRIPLET= 19.045	30.288 0.105 28.626 0.968	35.890 0.296 35.285 0.105	39.027 0.696 39.693 0.244	42.424 0.004 40.300 2.138	48.756 0.208 43.219 0.064	49.639 0.017 44.859 0.230	46.833 0.305		
22 PICENE IRM TRIPLET= 20.337	31.567 0.149 36.441 0.117	36.695 0.532 40.152 2.244	40.215 0.364 42.372 0.649	45.850 0.007 45.064 0.405	51.839 0.182 46.645 0.108	55.430 0.042 49.923 0.231	50.838 0.060		
23 TRIPHENYLENE TBM TRIPLET= 28.961	31.433 0. 32.937 0.	40.458 0.428 39.159 0.008	41.191 1.780 40.840 2.085	44.914 0. 42.887 0.098	49.695 0.013 45.052 0.013	49.952 0. 46.593 0.027	56.507 0.047 49.698 0.010		
24 TRIPHENYLENE IRM TRIPLET= 29.415	32.137 0. 33.507 0.	41.740 2.046 39.479 0.129	42.051 0.230 41.530 1.908	48.770 0. 42.726 0.187	53.780 0.003 46.357 0.	53.958 0. 49.200 0.049	63.933 0.027 52.136 0.002		
25 5,6 BENZCHRYSENE TBM TRIPLET= 21.550	29.704 0.025 45.559 0.071	30.795 0.297 46.747 0.015	34.483 1.802 50.233 0.013	37.441 1.118 53.504 0.005	39.091 0.359 54.527 0.032	39.605 0.058 59.841 0.	42.780 0.158		
26 5,6 BENZCHRYSENE IRM TRIPLET= 22.356	30.232 0.012 49.874 0.217	31.264 0.155 52.139 0.005	35.151 1.923 56.360 0.010	37.520 1.521 61.219 0.002	40.322 0.215 64.329 0.011	40.773 0.032 68.090 0.002	46.745 0.263		

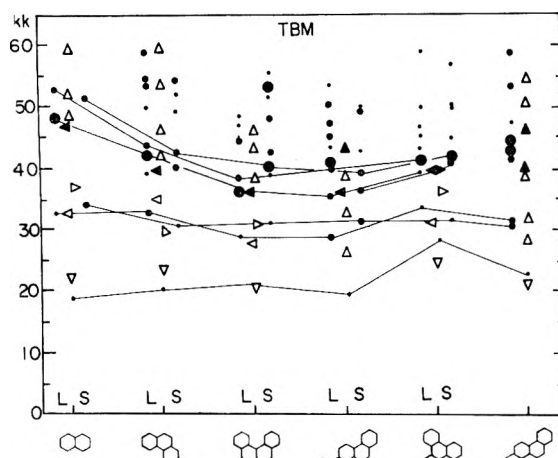


Fig. 6.—Assigned and calculated transitions for naphthalene group. Chrysenes is TBX. For explanations, see Fig. 2.

properties play a negligible role in the make-up of the wave functions. Also the dipole maps do not show the same structure as in the linear polyacenes. Almost absent, for instance, is the picture with a single node found there for 1B_b , 1B_a , and 1L_b and predicted generally by the perimeter model for the 1B_b and 1B_a states. Also the present dipole maps are more difficult to systematize.

In spite of all these considerable complications and differences the spectra display remarkable uniformity in certain features: a low lying triplet, two low lying weak transitions some 8 kK. higher, and two stronger transitions some 5 kK. higher yet. On these points there is agreement between

calculations and experiment. Consequently, a gratifying correspondence exists between experimental and synthetic spectra, as shown in Fig. 7 and 8.

Anthracene Group.—The numerical results for the anthracene group are given in Table III. They are compared with the assigned transitions in Fig. 9. The principle of grouping seems to be justified inasmuch as the energies of the transitions remain generally constant throughout the group and are consistently lower than those of the naphthalene group. Moreover the non-linear members appear to have acquired a third, low lying, weak transition in addition to the two found in the naphthalene group.

These results are reproduced in the calculations, which are, however, somewhat high on these transitions. Also in 1,2,3,6-dibenzanthracene, one of the three is dipole forbidden according to the calculation and its observation must be justified by vibrational interactions similar to 1L_b in benzene and coronene. The experimental spectrum of pentaphene has a rather unique appearance in that the single strong peak seems to be replaced by two or three fairly strong peaks. Calculations reproduce this rather peculiar feature.

A comprehensive comparison of all calculated singlet transitions with experiment is given in Fig. 10 and 11 by reproducing together experimental and simulated theoretical spectra. Again reasonable agreement is found. The general analogy to the naphthalene group is close enough to make further discussion unnecessary.

It would be valuable to have measurements on the triplets of these molecules.

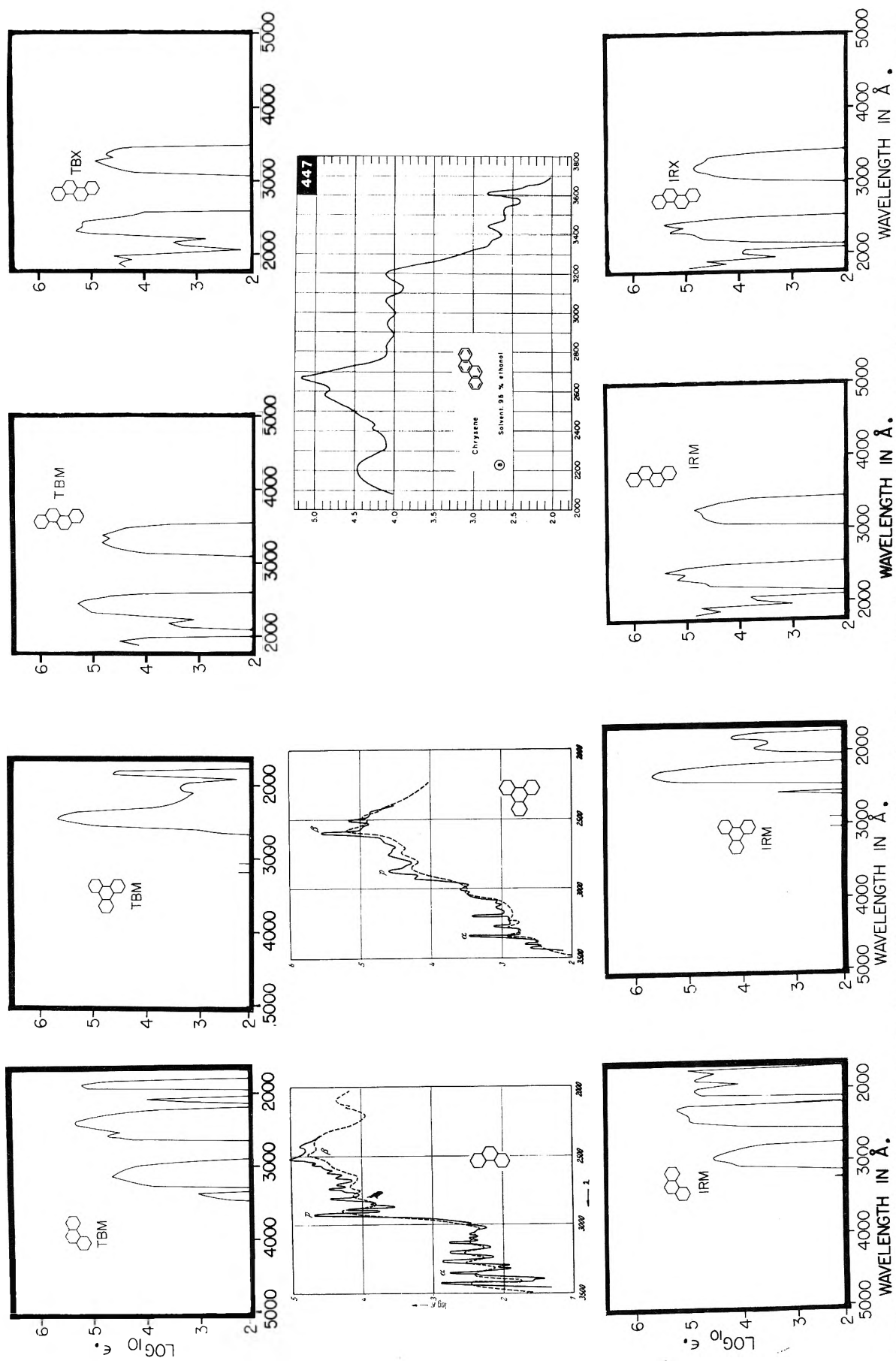


Fig. 7.—Experimental and synthetic spectra for naphthalene group. I. Explanation in section 1, after eq. 4. In triphenylene the two lowest electronically symmetry-forbidden transitions, which become weakly allowed *via* vibrational interactions, are indicated by short perpendicular marks.

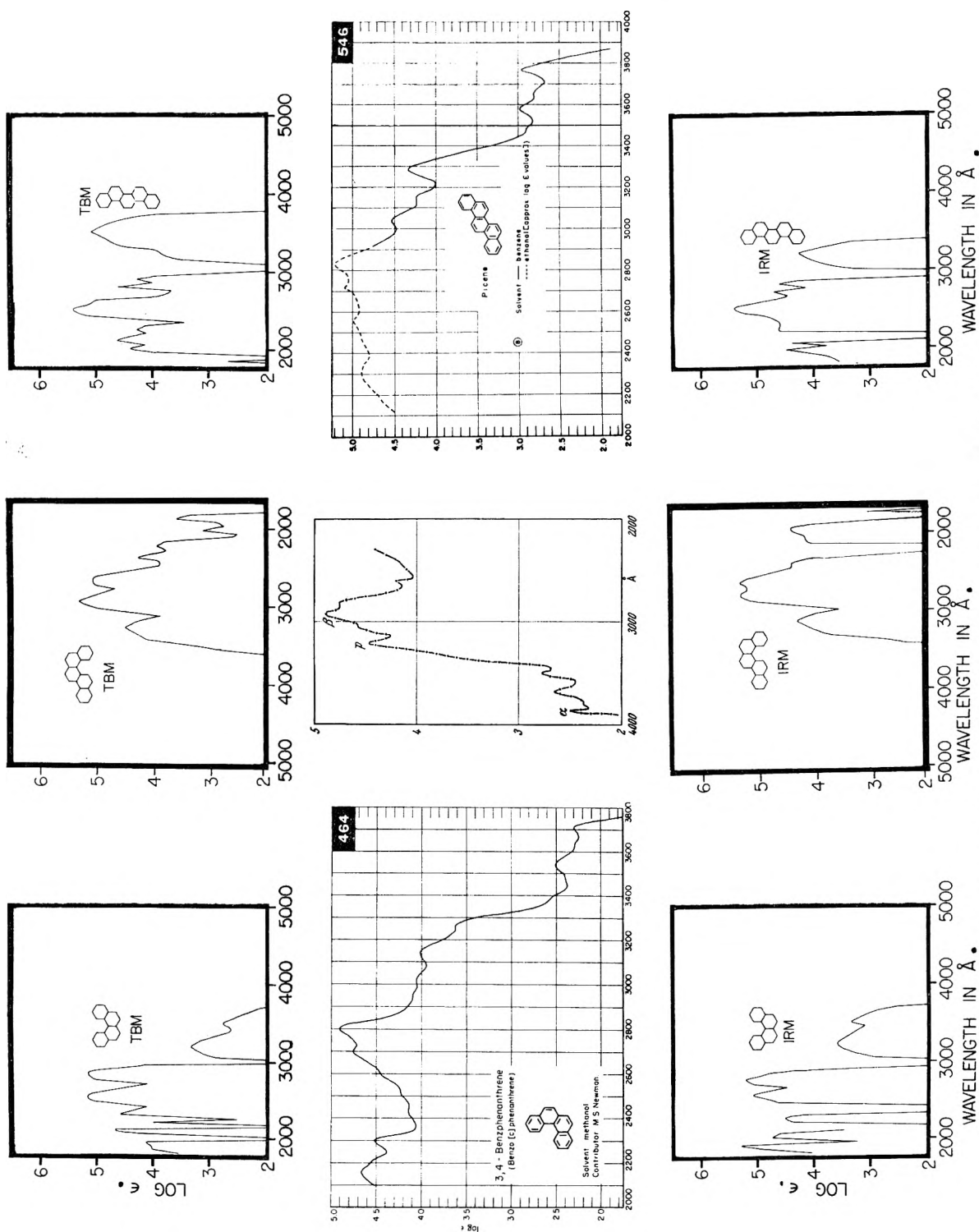


Fig. 8.—Experimental and synthetic spectra for naphthalene group. II. Explanation in section I, after eq. 4.

4. Pericondensed Molecules

General Considerations.—The pericondensed aromatic hydrocarbons have long been a stumbling block for theoretical understanding. Unlike the catacondensed systems, they have resisted attacks based on simple models as well as on more rigorous calculations.^{17a} Not only have their spectra special characteristics, but in some cases even the extent of the conjugation over the molecular framework

(17a) J. R. Platt, *J. Chem. Phys.*, **22**, 1448 (1954).

has been the object of controversy. It therefore is very gratifying that the present work leads to results remarkably close to experiment.

To be sure, the calculations were handicapped by the lack of information on the exact nuclear positions. While X-ray measurements are available for all molecules, it is presently recognized that, so far, their degree of analysis is inadequate. Indeed, in perylene and 1,12-benzperylene many of the atomic positions are not located by experiment. Nevertheless, these measured distances were used

TABLE III
CALCULATED TRANSITIONS OF NON-LINEAR POLYACENES. ANTHRACENE GROUP
See Table I for explanations.

ELECTRONIC TRANSITIONS FOR THE NON - LINEAR POLYACENES II										
27	TETRAPHENE TBM TRIPLET= 15.539	27.822 0.423 43.709 0.287	29.457 0.199 47.291 0.311	34.487 0.475 48.145 0.091	37.088 1.465 49.780 0.121	38.672 0.106 50.685 0.049	39.774 0.258 55.121 0.003	40.276 0.284		
28	TETRAPHENE IRM TRIPLET= 16.159	27.610 0.349 43.704 0.164	30.299 0.143 47.568 0.367	35.973 1.203 50.281 0.096	38.429 1.422 51.999 0.240	39.484 0.312 55.055 0.057	42.005 0.014 59.150 0.008			
29	PENTAPHENE TBM TRIPLET= 14.819	28.310 0.123 27.294 0.539	30.172 0.373 32.245 1.259	36.624 0.115 35.088 0.316	40.209 0.465 36.539 0.624	46.649 0.160 40.218 0.078	48.597 0.038 45.033 0.024	46.230 1.032		
30	PENTAPHENE IRM TRIPLET= 15.016	28.579 0.137 27.304 0.362	29.756 0.348 33.144 2.318	38.711 0.085 36.087 0.448	43.309 0.681 39.002 0.215	47.482 0.065 43.713 0.014	49.285 0.099 45.335 0.113	54.085 0.016 49.324 0.012		
31	DIBENZANTHRACENE TBX TRIPLET= 18.089	28.448 0.418 43.569 0.086	28.532 0.088 43.939 0.238	34.568 1.826 46.378 0.039	37.608 1.997 48.093 0.063	41.726 0.406 50.006 0.103				
32	DIBENZANTHRACENE IRX TRIPLET= 18.806	28.263 0.048 44.837 0.336	28.671 0.261 46.302 0.517	34.408 1.939 49.847 0.025	37.235 2.530 52.018 0.659	43.420 0.059 56.214 0.053				
33	1,2,7,8-DIBENZANTHRACENE TBM TRIPLET= 18.239	29.257 0.287 27.910 0.017	36.984 0.166 33.238 1.991	38.719 0.096 37.422 0.972	40.609 0.585 39.335 0.073	43.459 0.228 42.241 0.002	47.310 0.319 45.004 0.005	50.022 0.107 48.486 0.017		
34	1,2,7,8-DIBENZANTHRACENE IRM TRIPLET= 19.012	29.164 0.257 28.475 0.017	37.498 0.291 34.333 2.431	39.812 0.087 38.591 0.644	43.450 0.631 40.226 0.232	47.812 0.256 44.923 0.013	50.162 0.221 46.530 0.001	53.898 0.126 50.407 0.024		
35	1,2 BENZOTETRAPHENE TBM TRIPLET= 15.081	26.613 0.258 42.530 0.160	29.023 0.280 43.295 0.385	32.257 0.543 46.860 0.037	34.989 1.233 50.190 0.017	37.372 0.099 51.342 0.003	39.902 0.948 56.090 0.003	38.160 0.205		
36	1,2 BENZOTETRAPHENE IRM TRIPLET= 15.598	26.026 0.215 41.909 0.999	29.671 0.256 46.545 0.035	32.900 0.778 47.548 0.267	35.240 1.078 52.905 0.008	39.435 0.023 57.690 0.013	40.177 0.855 59.619 0.004			
37	1,2,3,4-DIBENZANTHRACENE TBM TRIPLET= 17.773	29.884 0.100 28.897 0.193	37.480 2.744 34.995 0.001	39.039 0.027 38.880 0.126	44.153 0.001 39.513 0.344	46.737 0. 40.696 1.067	48.416 0.024 42.896 0.265	50.579 0.109 45.895 0.282		
38	1,2,3,4-DIBENZANTHRACENE IRM TRIPLET= 18.219	30.827 0.082 28.699 0.161	37.905 2.979 36.100 0.007	40.521 0.045 38.095 0.011	46.509 0.010 40.357 1.139	51.159 0.017 41.883 0.421	51.598 0.138 44.911 0.535	56.364 0.025 47.493 0.128		
39	1,2,1,2 DIANTHRACENE TBM TRIPLET= 17.788	25.588 0.360 42.266 0.320	31.338 1.013 44.024 0.537	33.547 0.226 50.087 0.157	36.866 0.057 54.575 0.045	39.057 0.009 55.738 0.004				
40	1,2,1,2 DIANTHRACENE IRM TRIPLET= 15.670	23.033 0.424 45.437 0.217	29.409 0.726 48.658 0.005	35.494* 1.262 56.664 0.086	38.998 0.306 58.437 0.035	41.428 0.153				

in the present calculation in the hope that on the average they would represent an improvement over the use of mean distances.

The numerical results are given in Table IV and V. For some of the molecules, the assigned transitions are compared with the calculated TBX (where X indicates measured, not necessarily exact distances) values in Fig. 12. For all molecules experimental spectra are compared with the synthesized singlet spectra in Fig. 13, 14, 15, and 16.

Lowest Triplet and Lowest Singlets.—Unfortunately only two triplets have been assigned. The theoretical value is 4 kK. low in pyrene, but only 1 kK. off (high) in coronene. The error in pyrene is reminiscent of those found in the polyacenes when average, rather than exact, distances were used.

As in the polyacenes, two transitions follow between 15 and 32 kK. in all molecules, weak in the pyrene group, but one of them strong in the perylene group. Agreement between theory and experiment is near perfect for most of these. The remaining two, both perpendicularly polarized, are 3 kK. low.

While the polarizations for perylene are in agreement with the experimental observations,^{17b} a discrepancy exists as regards the polarizations in pyrene. While Williams and Hochstrasser^{17c} conclude from crystal measurements that the lowest two transitions are both parallel to the short molecular axis, our results indicate, as did those of Ham and Ruedenberg,⁴ that the second transition is long-axis polarized. While the present calculations

(17b) R. M. Hochstrasser, *Can. J. Chem.*, **39**, 451 (1961).

(17c) R. Williams, *J. Chem. Phys.*, **26**, 1186 (1956); R. M. Hochstrasser, *ibid.*, **33**, 459 (1960).

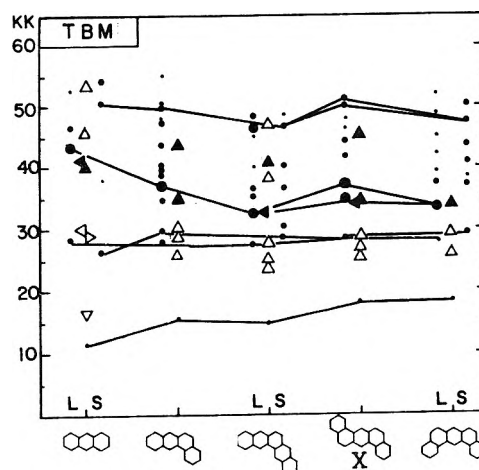


Fig. 9.—Assigned and calculated transition for anthracene group. Dibenzanthracene is TBX. For explanations, see Fig. 2.

are of course far from perfect, it is nevertheless very difficult simply to discount the theoretical result on this matter. For one thing, the *over-all* agreement between experiment and theory is so consistent as regards spectral locations, that no specific unambiguous theoretical prediction can be ignored. For another thing, it is readily seen that no calculation based on linearly combining $2p\pi$ atomic orbitals will yield the 3 or 4 lowest states all polarized in the same direction. As regards a possible reconciliation of experiment and theory, it should be pointed out that our results place the two lowest transitions within 1 kK. of each other, with the long-axis polarized one more than twenty times more intense and, also, that several assumptions

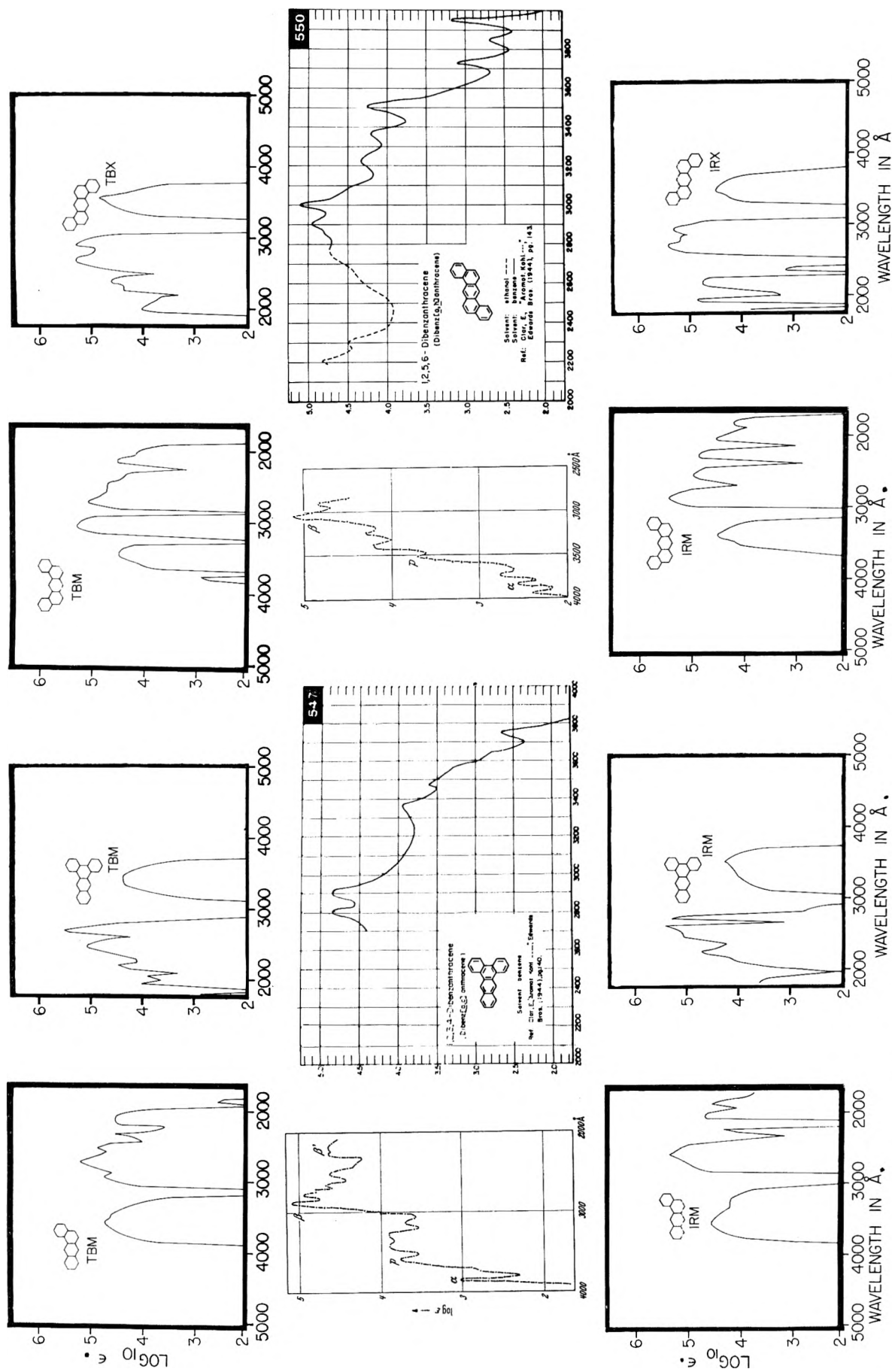


Fig. 10.—Experimental and synthetic spectra for anthracene group. I. Explanations in section 1, after eq. 4.

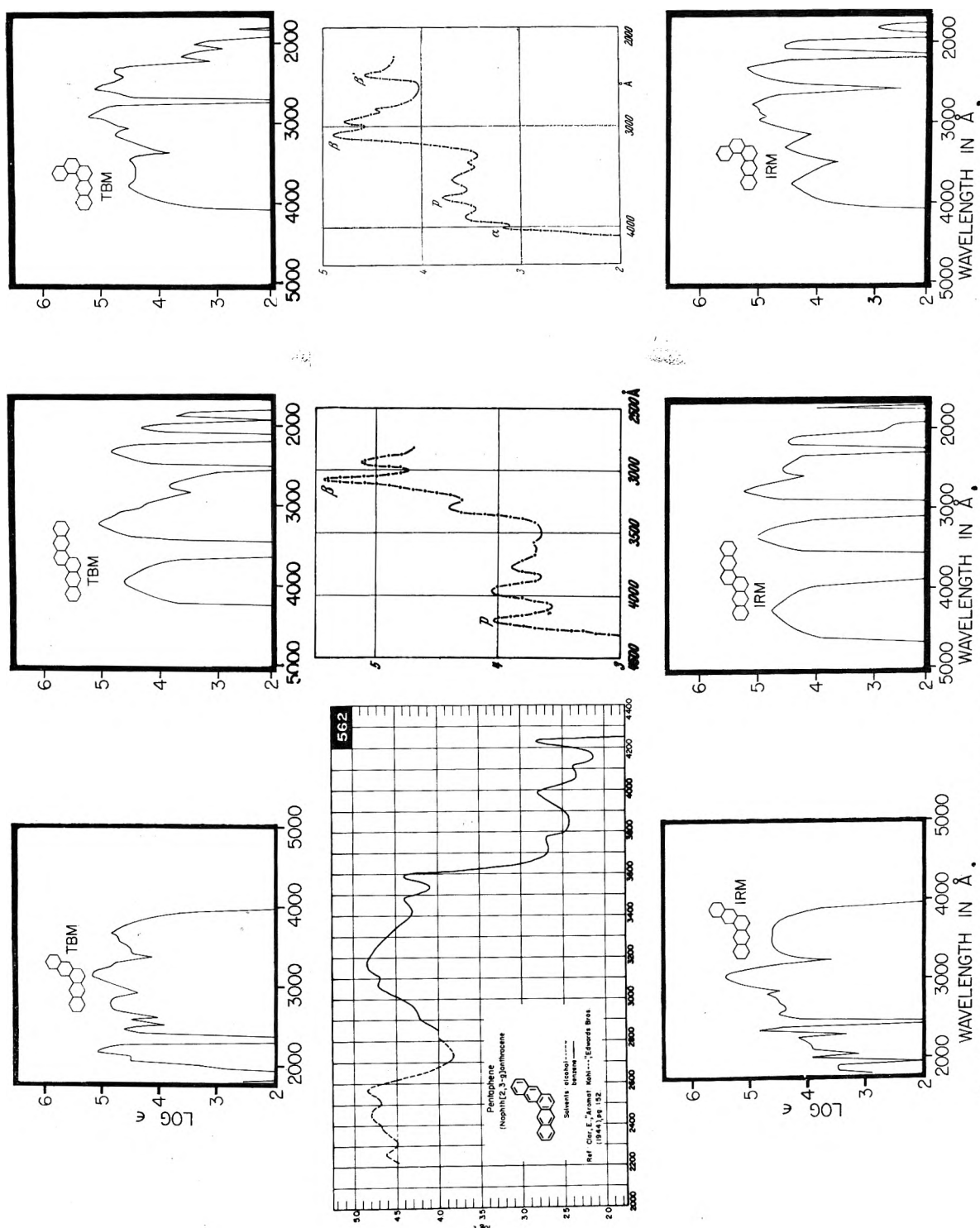


Fig. 11.—Experimental and synthetic spectra for anthracene group. II. Explanations in section 1, after eq. 4.

are necessary in extrapolating from the crystal spectrum to the molecule spectrum.

Pyrene Group. Pyrene.—Toward higher energies, where the polyacenes exhibit one strong band, the pyrene spectrum is distinguished by having three rather intense peaks of nearly equal strength. The characteristic feature is satisfactorily reproduced by the present study.

The lower two of these correspond to what has been known as 1B_u (the lower) and 1B_a (the higher) in the polyacenes, the former containing the paired

excitations and being parallel to the horizontal axis in Fig. 12. In contrast to the polyacenes this axis is not the longest in pyrene, but the one perpendicular to it is somewhat longer. This circumstance is the origin of the comparable strength of the two bands, with the 1B_u -like transition a bit stronger.

Between these two transitions and the third strong band at higher energy with its accompanying barrage of weaker transitions lies a clear gap of 7 kK., free of transitions both weak and strong.

TABLE IV
 CALCULATED TRANSITION ENERGIES OF PERICONDENSED AROMATICS. I.

For explanations see Table I; but note the following specification: In cases with two symmetry places perpendicular to the molecular plane, the first symmetry specification in "SA" and "AS", respectively, refers to the axis indicated in the perylene structure in Fig. 12.

ELECTRONIC TRANSITIONS FOR THE PERI-CONDENSED AROMATICS I

41 PYRENE TBX TRIPLET= 13.466	27.380 0.031 28.335 0.794	39.373 0.873 43.592 0.330	45.974 0.001 45.450 1.093	51.234 0.049 53.538 1.972	55.744 0.264 58.091 0.004	59.089 1.878 59.861 0.044	64.247 0.030 60.267 0.007
42 PYRENE IRX TRIPLET= 14.182	28.076 0.010 29.010 0.766	39.097 0.857 45.228 1.396	48.750 0.012 50.859 0.005	55.771 0.046 53.858 2.365	58.232 1.653 57.281 0.001	60.806 0.656 60.592 0.001	64.562 0.057 64.762 0.001
43 PYRENE TBM TRIPLET= 12.193	26.818 0.034 27.409 0.796	39.024 0.909 43.877 0.183	46.113 0.002 45.613 1.170	52.944 0.161 53.933 2.135	56.875 0.209 58.445 0.	61.707 1.855 60.149 0.039	67.692 0.047 64.241 0.013
44 PYRENE IRM TRIPLET= 13.021	27.700 0.013 28.181 0.768	38.806 0.897 45.745 1.307	50.750 0.033 51.802 0.001	60.374 1.678 54.270 2.559	62.785 0.747 59.329 0.039	68.409 0.011 62.569 0.003	65.839 0.012
45 PERYLENE TBX TRIPLET= 10.720	29.130 0.122 23.206 1.194	39.657 0.122 41.708 0.086	41.937 1.351 49.995 0.234	49.512 0.048 50.957 1.318	51.770 0.926 52.058 0.244	52.628 0.170 55.153 0.070	53.116 0.040 56.529 0.066
46 PERYLENE IRX TRIPLET= 9.675	29.980 0.024 22.291 0.977	43.198 1.629 44.333 0.	45.527 0.150 48.409 0.245	52.748 0.173 48.564 0.293	55.742 0.486 52.646 0.441	51.123 0.004 54.199 1.967	56.154 2.066 54.989 0.077
47 PERYLENE TBM TRIPLET= 13.372	26.103 0.905 29.029 0.051	41.935 0.027 41.801 0.096	44.673 1.073 43.180 1.574	47.803 0.077 59.590 0.006	52.355 0.070 51.668 0.015	53.920 0.001 52.502 0.243	54.988 1.530 53.731 2.004
48 PERYLENE IRM TRIPLET= 11.957	25.842 0.857 30.000 0.006	44.534 0.879 43.612 1.625	44.534 0.184 46.604 0.001	49.782 0.030 49.783 0.235	51.996 0.143 52.703 0.040	54.551 0.354 54.071 2.941	54.682 0.224 56.705 0.
49 1,12 BENZPERYLENE X TBX TRIPLET= 18.174	26.847 0.008 27.077 0.525	35.767 0.161 31.393 0.013	37.239 2.084 36.240 0.378	39.664 0.002 37.683 1.490	43.604 0.354 40.926 0.151	44.736 0.096 45.986 0.054	45.194 0.117 48.540 0.002
50 1,12 BENZPERYLENE X IRX TRIPLET= 16.887	27.301 0. 26.882 0.549	37.541 2.048 33.651 0.005	38.173 0.183 37.303 1.367	42.224 0.042 39.251 0.502	46.312 0.716 43.109 0.059	47.743 0.004 46.257 0.076	50.096 0.007 50.422 0.006
51 CORONENE TBX TRIPLET= 22.109	24.507-0. 26.254 0.	34.669 2.219 34.669 2.274	43.856 0.052 43.856 0.085	44.935 0.062 46.486 0.014	45.940 0. 48.844 0.	49.550 0. 49.519 0.001	53.124 0.180 54.170 1.955
52 CORONENE IRX TRIPLET= 20.948	24.985-0. 27.144 0.	35.027 2.134 35.012 2.135	45.474 0. 48.239 0.001	48.271 0. 48.349 0.	48.822 0.245 48.857 0.242	53.856 1.158 53.825 1.190	54.351 1.673 54.350 1.610
53 CORONENE TBM TRIPLET= 22.219	24.880-0. 26.602-0.	35.050 2.275 35.059 2.273	43.853 0.066 44.331 0.080	46.947 0.007 47.061 0.003	47.417-0. 49.467-0.	50.247-0. 50.964-0.	55.526 0.750 55.637 1.788
54 CORONENE IRM TRIPLET= 22.485	25.569-0. 27.724-0.	35.553 2.129 35.553 2.129	47.222-0. 49.476 0.003	49.477 0.003 49.971-0.	50.426 0.238 50.426 0.238	55.207 0.197 55.207 0.199	55.547 2.414 55.547 2.412
55 OVALENE TBX TRIPLET= 13.030	23.009 0.041 22.727 0.567	33.014 3.354 32.183 0.052	37.979 0.404 35.281 1.664	40.741 0.001 40.950 0.003	43.147 0.184 45.614 0.001	45.206 0.949 46.049 1.847	48.719 0.101 47.917 0.261
56 OVALENE IRX TRIPLET= 13.800	23.569 0.025 23.161 0.556	33.788 3.670 33.891 0.690	42.155 0.597 36.482 1.047	44.214 0.019 44.834 0.051	46.231 0.942 45.714 1.129	47.636 0.164 47.909 0.340	51.452 0.087 50.152 0.470

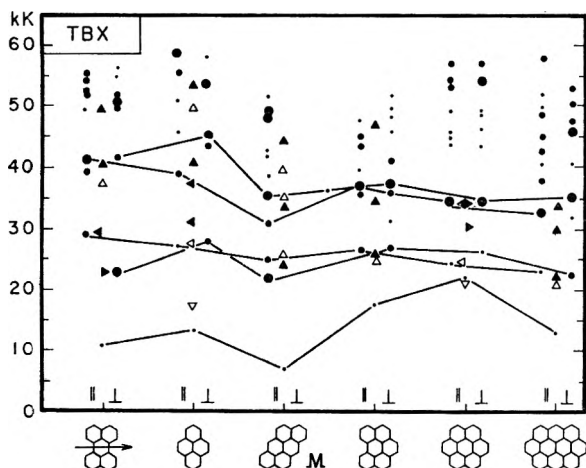


Fig. 12.—Assigned and calculated transitions for pericondensed molecules. Anthanthrene is TBM. For explanations, see Fig. 2.

This theoretically predicted gap is clearly apparent in the observed spectrum.

The predictions of the intensities in the two highest bands, which are also the two strongest, are not completely satisfactory. Whereas experimentally the highest is slightly weaker, theory gives it slightly stronger than the second highest.

Benzperylene.—The calculations in 1,12-benzperylene are not as successful in the upper energy

region as they were for the preceding molecule. The energies fit experiment reasonably well in its prominent features. The gap referred to previously has, however, been filled in by fairly weak transitions, whereas it is still shown by experiment. True it is less prominent and may cover weak absorptions. As noted earlier, agreement is very good in the placement of the two low transitions.

The intensities are unsatisfactory. The experimental spectrum again has three comparably strong bands, but, unlike in pyrene and perylene, theory fails to provide adequate intensity for two of these (at 25 and 47 kK.) and provides possibly a bit too much for the strongest (at 35 kK.), which according to theory is a pair of almost degenerate strong transitions. The experimental peak possibly supports this latter prediction.

On the whole it is consoling that, in reporting the measured distances, Robertson indicated that the benzperylene distance was the least reliable and that several of the important distances could not be determined. The comparison of transitions is after all reasonably good, but suffers from comparison with other molecules of the sequence.

Anthanthrene.—Anthanthrene differs from pyrene by the addition of two benzene rings; it differs from benzperylene merely in the location of one of these two additional rings. Yet there are distinct differences in the spectra of these molecules. These differences are reproduced by the

TABLE V
CALCULATED TRANSITIONS OF PERICONDENSED AROMATICS, II, AND OF AZULENE DERIVATIVES
See Table IV for explanations.

ELECTRONIC TRANSITIONS FOR THE PERI-CONDENSED AROMATICS II															
57	BISANTHRENE	27.069	0.957	32.436	0.006	40.789	0.028	43.519	0.002	46.205	0.975	49.318	0.098	53.118	1.802
	TBM TRIPLET= 2.105	16.616	1.235	27.183	0.178	34.769	0.011	41.591	1.008	43.525	0.181	44.672	0.015	48.979	0.614
58	BISANTHRENE	29.885	1.071	36.704	0.001	42.193	0.002	46.506	0.799	49.512	0.003	52.550	2.677	53.374	0.148
	IRM TRIPLET= 54.673	15.426	1.134	30.060	0.168	38.360	0.001	42.528	0.947	45.489	0.002	48.048	0.217	50.119	0.628
59	TERRYLENE	28.054	0.002	30.863	0.968	33.706	0.007	43.461	0.089	44.512	0.011	47.856	0.251	49.041	0.055
	TBM TRIPLET= 7.051	18.808	2.333	32.870	0.100	41.515	0.002	49.061	2.533	52.548	0.006	55.081	0.027	57.236	0.024
60	TERRYLENE	29.826	0.028	34.361	1.253	37.550	0.026	44.025	0.033	47.398	0.360	50.899	0.415	53.478	0.053
	IRM TRIPLET= 6.166	17.904	2.156	35.976	0.077	44.362	0.030	47.886	0.886	49.343	1.221	52.625	0.011	54.603	1.840
61	ANTHANTHRENE	22.067	1.180	25.163	0.128	31.391	0.149	35.699	1.451	38.866	0.026				
	TBM TRIPLET= 6.962	41.844	0.017	42.901	0.042	48.258	1.923	49.084	3.204	51.655	0.011				
62	ANTHANTHRENE	22.491	1.130	26.214	0.056	35.190	0.226	35.643	1.556	42.900	0.006				
	IRM TRIPLET= 7.870	45.208	0.098	49.509	4.432	47.928	0.401	51.336	0.721	54.249	0.122				
63	3,4,8,9CIBENZOPYRENE	22.753	1.652	25.288	0.248	34.559	0.068	36.504	2.415	41.155	0.067				
	IRM TRIPLET= 8.794	42.521	0.041	48.865	0.215	49.809	0.321	49.498	0.076	54.656	0.018				
64	3,4,8,9CIBENZOPYRENE	22.684	1.455	26.331	0.178	36.186	2.569	37.971	0.412	47.749	0.164				
	IRM TRIPLET= 9.616	48.710	0.045	50.317	0.077	52.132	0.457	56.606	0.065						
ELECTRONIC TRANSITIONS FOR THE NON-ALTERNANTS															
65	AZULENE	10.902	0.013	30.311	0.053	39.262	0.537	46.906	0.280	56.772	0.172	68.897	0.299		
	TBM TRIPLET= 8.899	21.768	0.011	32.254	1.130	32.472	0.340	36.244	0.041	45.780	0.045	46.330	0.043	50.175	0.894
66	AZULENE	24.244	0.001	36.818	1.660	45.189	0.030	52.388	0.537	55.142	0.202	68.734	0.258		
	IRM TRIPLET= 10.462	12.376	0.013	33.077	0.092	43.665	0.569	54.770	0.275	58.090	0.043	62.128	0.048	66.525	0.720
67	1,2 BENZAZULENE	9.618	0.023	20.043	0.018	28.163	0.142	28.928	0.737	30.968	0.842	35.448	0.047	37.215	0.073
	TBM TRIPLET= 6.628	39.842	0.588	41.787	0.134	42.440	0.016	46.398	0.047	46.689	0.116	50.317	0.827	52.971	0.045
68	1,2 BENZAZULENE	10.544	0.016	21.279	0.043	31.486	0.339	32.475	0.076	33.803	1.957	38.794	0.020	39.500	0.055
	IRM TRIPLET= 7.268	43.698	0.362	44.450	0.097	48.934	0.362	50.058	0.453	52.548	0.321	53.865	0.267	56.514	0.878
69	1,2,4,5 DIBENZAZULENE	5.336	0.012	18.514	0.047	26.021	0.080	27.050	1.553	31.486	0.021	32.568	0.257	38.085	0.555
	IRM TRIPLET= 1.936	40.869	0.475	45.304	0.884	46.482	0.099	47.892	0.099	51.025	0.534	55.244	0.023		
70	NAPHTHAZULENE	10.122	0.032	15.979	0.218	24.521	0.064	25.472	0.123	30.426	0.287	31.884	0.974	35.111	0.057
	TBM TRIPLET= 5.170	36.826	0.135	38.588	1.412	41.066	0.440	41.977	0.130	44.056	0.067	45.656	0.361	48.950	0.245
71	NAPHTHAZULENE	9.180	0.017	14.494	0.211	25.559	0.030	26.843	0.089	30.808	0.221	31.906	0.284	36.240	1.117
	IRM TRIPLET= 4.196	39.440	0.196	41.040	0.707	44.611	0.813	46.813	0.482	47.561	0.175	49.700	0.606	51.021	0.190

calculations, as can best be seen by comparing the experimental with the synthetic spectra. In fact, the agreement between the TBM spectrum and the experimental one in anthanthrene is almost too good to be true. We consider it significant, however, and proof of the basic validity of the theoretical approach that the remarkable differences between the isomers benzopyrene and anthanthrene are so clearly reproduced.

Coronene and Ovalene.—The lower transitions of coronene have been discussed previously. The doubly degenerate very strong transition is matched perfectly by the calculated energies. Above this transition the experimental absorption curve falls monotonically up to the cut-off at 39 kK., forming the first part of a gap in complete agreement with theory which predicts the next peak at 44 kK. It would be helpful to have the experimental spectra extended to higher wave lengths.

Ovalene apparently is particularly difficult to dissolve, for its experimental spectrum is restricted to wave lengths longer than 3000 Å. To the extent that the experimental spectrum has been observed it seems to agree with the theoretical values. For this molecule a more complete experimental spectrum would be even more desirable.

Perylene Group. Perylene.—Perylene differs from the other molecules of this study in that negligible conjugation is indicated by the consideration of Kekulé structures for the two central bonds joining the two naphthalene groupings. Support

for this conclusion has been seen by some in the large measured length of 1.50 Å. for the bonds in question. Undoubtedly the existence or non-existence of such conjugation should be reflected in the spectrum. But so far the latter has presented a puzzle, even to qualitative understanding, because of certain unique features to be discussed. All of these aspects seem to have contributed to the feeling that perylene would be a tough nut to crack.

In the present work the central bonds were treated no differently than the other conjugated bonds, and with this assumption excellent agreement was found between theoretical and experimental spectra. In view of the fact that, even in the TBX calculation(!), the LCAO-MO bond order in the central bond is only 35% lower than the average perylene bond order, it is indeed very hard to see why there should not be appreciable conjugation over the central bond. The excessive length of this bond is very likely due in part to steric hindrance,¹⁸ as has been fairly well proven for a similar, unquestionably conjugated bond¹⁹ in chrysene.

(18) Singly bonded carbons normally are able to stagger their hydrogens and reduce steric interaction. Rotational activation energies of the order of 3 cal. are therefore a lower limit for the increased energy of the unstaggered hydrogens in perylene-type geometry.

(19) The bonds in the two concave sections of well measured chrysene are 0.04 Å. longer than predicted by bond order. The final refinement of the determination indicates confirming displacements of the hydrogen atoms. D. W. Cruickshank and R. A. Sparks, *Proc. Roy. Soc. (London)*, **A268**, 270 (1960).

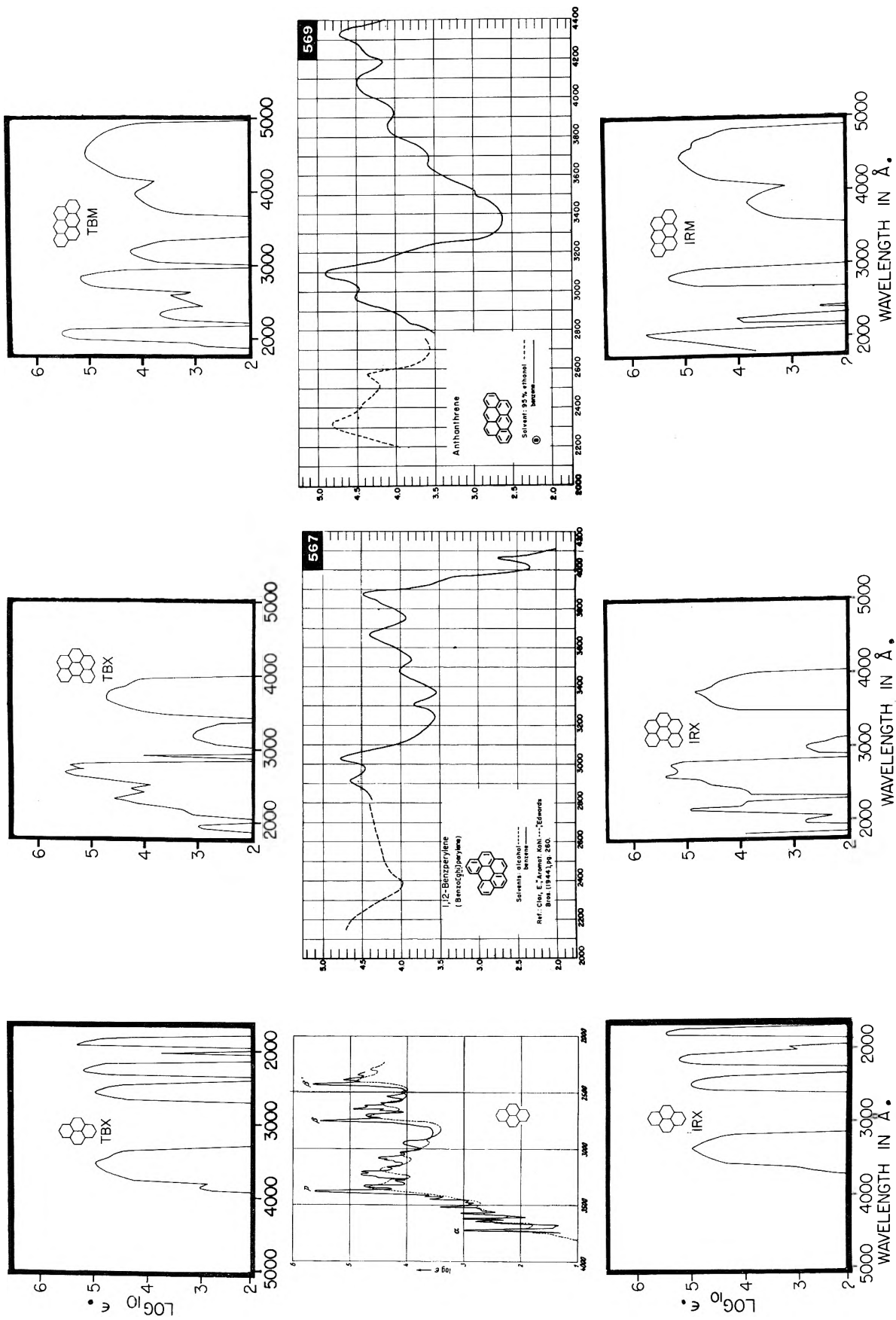


Fig. 13.—Experimental and synthetic spectra for pericondensed systems. I. Explanations in section 1, after eq. 4.

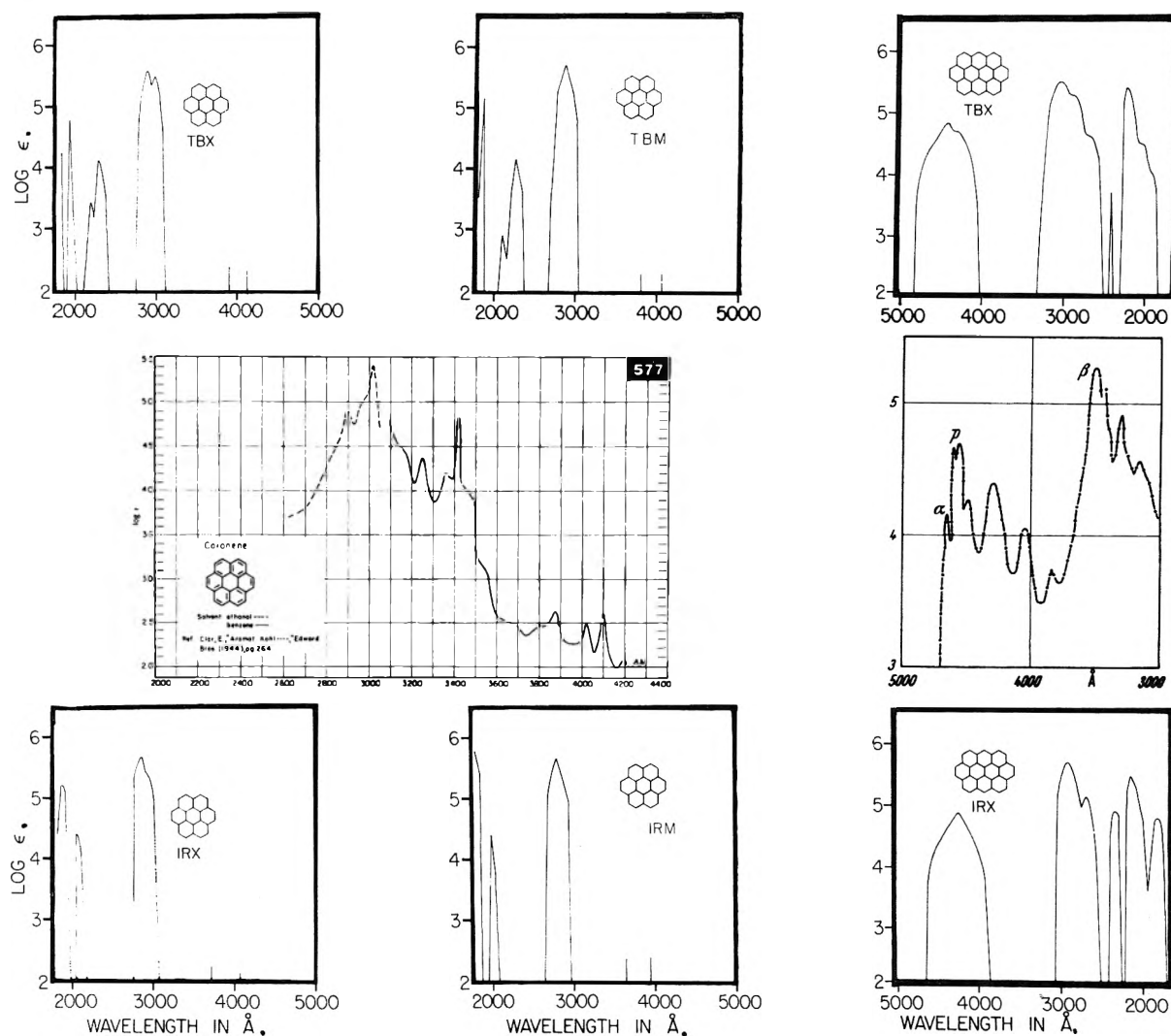


Fig. 14.—Experimental and synthetic spectra for pericondensed systems. II. Explanation in section 1, after eq 4. In coronene the two lowest electronically symmetry-forbidden transitions, which become weakly allowed *via* vibrational interactions, are indicated by short perpendicular marks.

The spectrum of perylene is very distinctive indeed. The lowest singlet, weak in all other molecules, is here the strongest peak. Also the two low transitions are separated by an unusually wide spacing between them. Unlike pyrene, only one of the transitions around 40 kK. (B_b) is fairly strong. But, similar to pyrene, there follows another band of about equal strength some 8 kK. higher.

These spectral features are matched by the excellent fit between theoretical and experimental energies and the good fit (subject to the usual empirical scaling factor) of the strong intensities. Also there is again a gap at high energy, in the calculated transitions, before the onslaught of the barrage. This distinctive gap is found in experiment.

Terrylene and Bisanthene.—Terrylene and bisanthene differ from perylene in that both have three additional rings. Both molecules preserve the two typical central bonds of perylene; but whereas terrylene has altogether four bonds of this type, bisanthene has only two of them.

The appearances of the spectra of perylene, ter-

rylene, and bisanthene are remarkably alike, and the characterization of the perylene spectrum applies equally to the other two molecules. The distinctive difference between them is that corresponding parts of their spectra stretch over larger and larger wave length regions. The perylene spectrum between 2400 and 4400 Å. corresponds to the terrylene spectrum between 2800 and 5400 Å., and to the bisanthene spectrum between 2900 and 7100 Å.²⁰ All these experimental observations are excellently reproduced by the calculations, as is shown by the synthetic spectra in Fig. 14 and 15.

We conclude that conjugation *does* extend over the "long" bonds in these molecules. It just so happens that, *in the ground state, these bonds lie in regions of strong destructive interference* of the electron waves.

Dipole Maps.—The dipole maps are very interesting and display, as expected, radial as well

(20) The shift to long wave length in bisanthene is presumably related to the fact that the "building block" increases from naphthalene to anthracene. Note however that anthracene itself has its longest transition below 4000 Å.

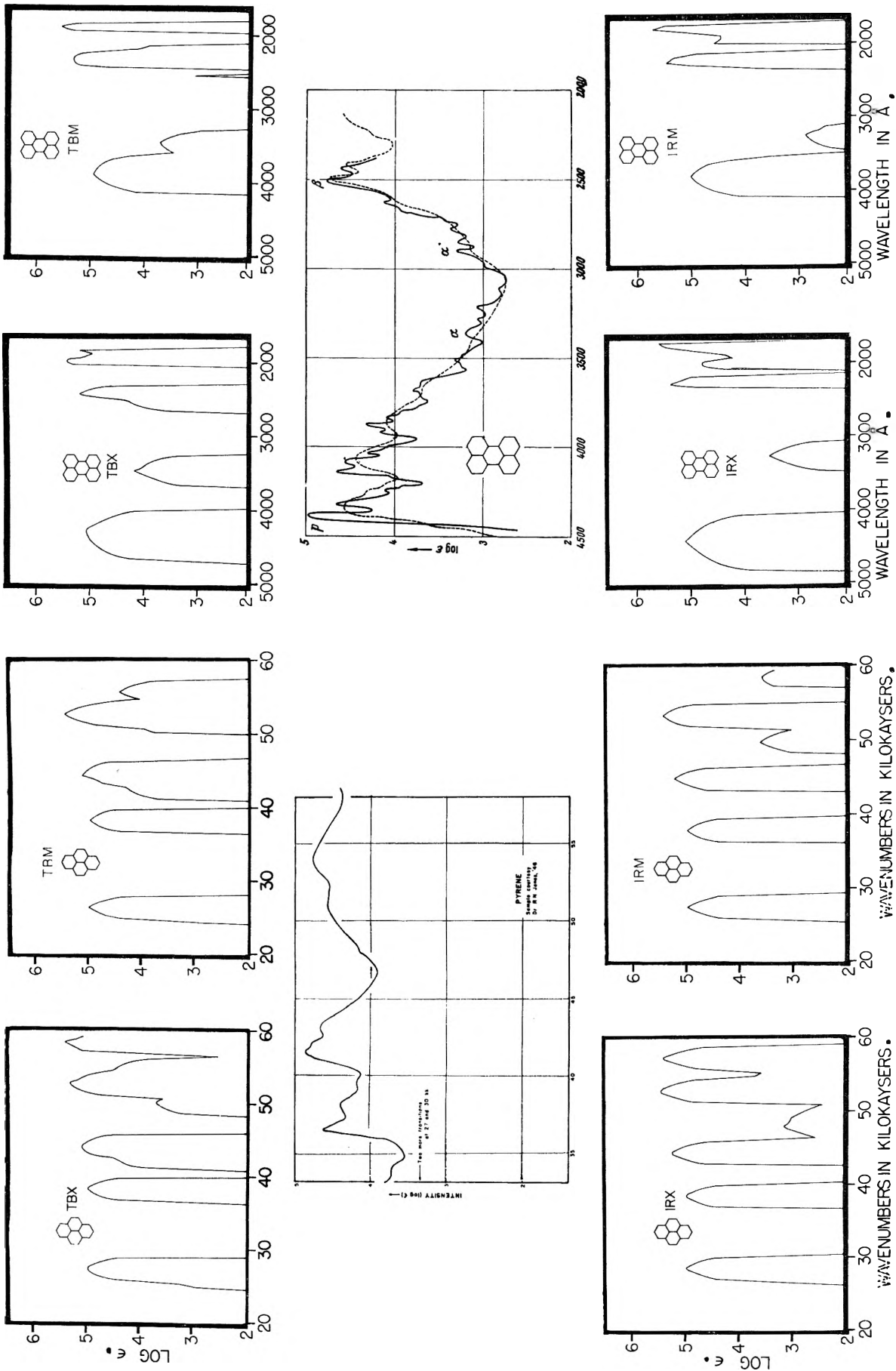


Fig. 15.—Experimental and synthetic spectra for pericondensed systems. III. Explanation in section 1, after eq. 4.

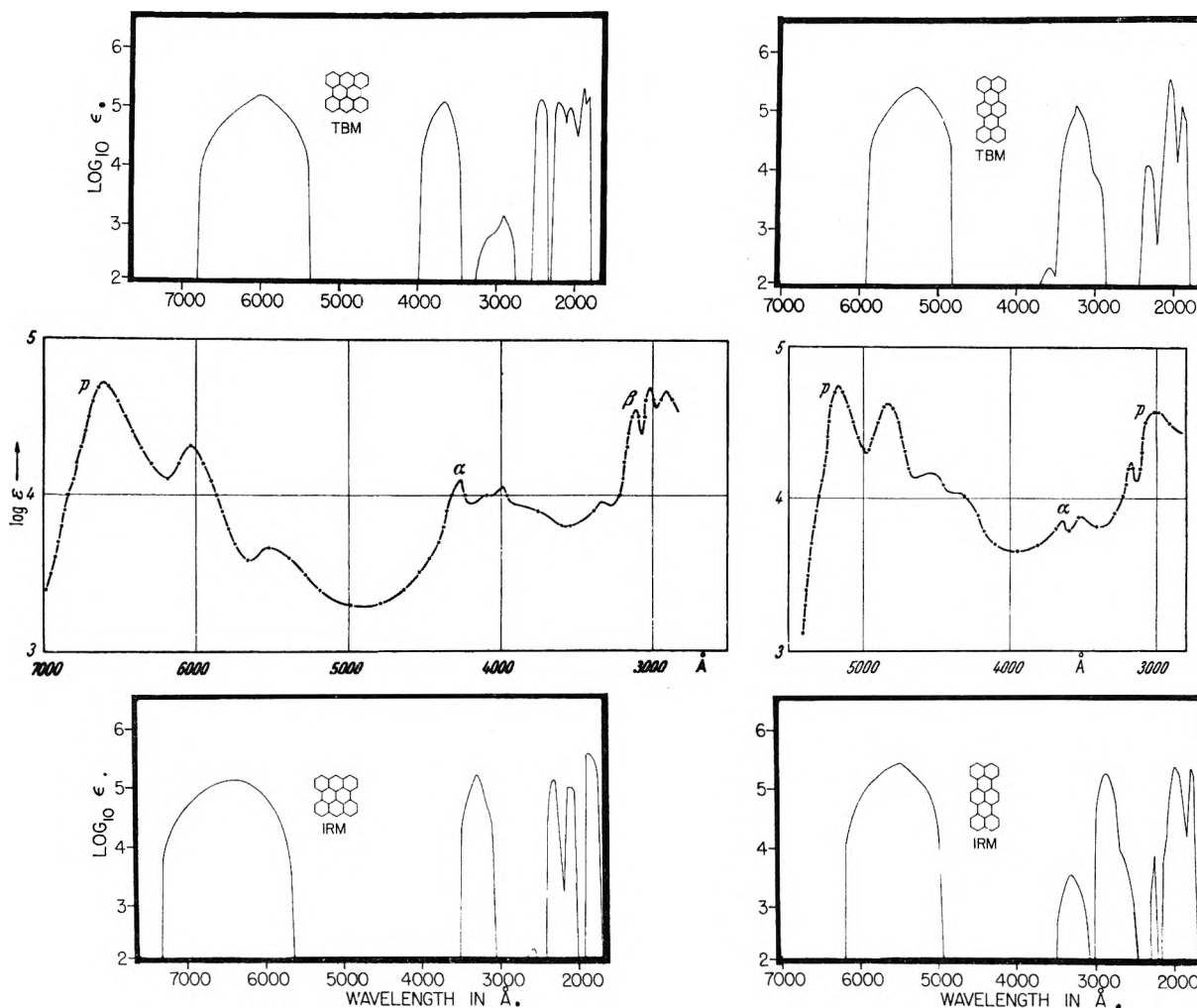


Fig. 16.—Experimental and synthetic spectra for pericondensed systems. IV. Explanation in section 1, after eq. 4.

as angular nodes, although the structure is more complex than indicated by nodes alone. The parallel transitions have dipole regularities even more striking than were observed in the linear polyacenes, which makes it easy to trace the transitions. The regularity is such that the patterns can be adequately recognized by the first and last members of the sequence, which are displayed in Fig. 17. As in the linear polyacenes naphthalene and pentacene transitions of the perpendicular polarization have much less regularity. The reason is presumably that the parallel excitations contain the paired excitations.

5. The Azulene Family

The results for the non-alternant, azulene family compare very poorly indeed with experiment. Particularly in view of the good results that have been obtained for the alternant aromatics, this failure may be quite illuminating with regard to the assumptions of the underlying theory. The results, which also are listed in Table V, are considerably too low, most notably for the lower two.²¹ Only the TBM and IRM approximations were carried through. While use of exact distances

(21) The experimental assignments are taken from E. M. Layton, *J. Mol. Spectry.*, **5**, 181 (1960).

might yield some improvement, it is unlikely to remedy the basic deficiency.

Azulene itself also has been treated by Ham and Ruedenberg and their results have been somewhat, but not significantly, closer to experiment than the present one. The best calculation to date is that of Pariser due to the inclusion of configuration interaction in the ground state. It falls 3 kK. below the peak of 1L_b and more than 5 kK. below the peak of 1L_a . Since our really drastic discrepancies occur in the higher members of the azulene family, it is difficult to say, at this point, whether configuration interaction in the ground state will in general be an adequate remedy. It may be that, in all treatments carried out so far, some fundamental physical effect has been given inadequate consideration.

The basic reason for the failure seems to be related to the fact that the atomic populations in non-alternants differ greatly from unity in all approximations. In some higher azulenes they go even up to 1.3, as can be seen from the Coulson bond order matrix. As a consequence, the average potential needed to determine adequate molecular orbitals must be composed of contributions from non-neutral atoms and hence have long range, coulombic components. Such adequate molecular

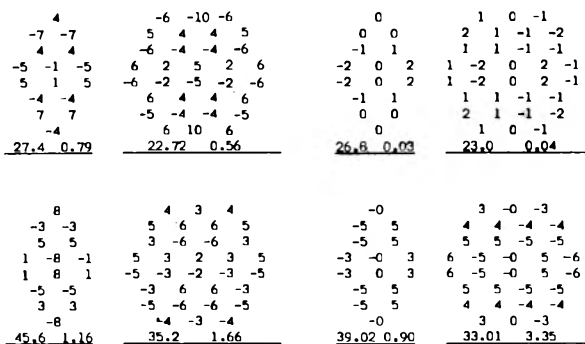


Fig. 17.—Dipole maps for electronic transitions of pericondensed systems. For explanation see Fig. 5.

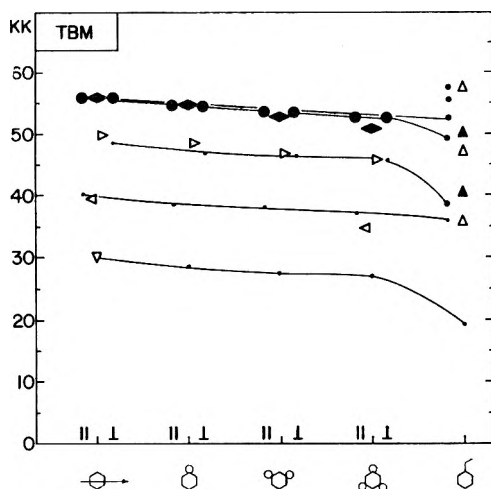


Fig. 18.—Assigned and calculated transitions for substituted benzenes. For explanation see Fig. 2.

orbitals therefore must be different from the Hückel-type eigenvectors of the overlap matrix.

This inadequacy of the present molecular orbitals is more serious for the ground state, which by hypothesis has been taken as a single determinant, than for the excited states, which have been subjected to extensive configuration interaction. There is in fact evidence that the ground state configuration as presently used may interact appreciably with the excited configurations. This is indicated by the fact that, for the lowest transition in azulene, electron interaction *decreases* the one-electron jump energy of 16.4 kK. by 3 kK., whereas in alternants it consistently introduces an increase of 6–20 kK. The inference may be drawn that, in contrast to the situation in alternants, certain excited states now may contain less internal electronic repulsion than the ground state, and this can indeed be related to the charge accumulations indicated by the atom populations. Admitting configuration interaction to the ground state would not be the only, or necessarily a sufficient, remedy (Pariser lowered the ground state 2.44 kK. by this means); proper modification of the molecular orbitals would be another possibility.

If it should be necessary to use slightly different atomic orbitals for the different atoms, this would lead to further, but not insurmountable, complications.

Finally, it is not unlikely that the interplay with

σ -electrons is considerably more important in the non-alternants than in the alternants. Neglect of σ -electrons has been justified on the basis that they are localized in a bond between two atoms and thus their ability to correlate with the mobile π -electrons is severely restricted. However, they are free to move within a bond, and, if the bonded atoms have an unequal charge due to the π -electrons, the σ -electrons may be expected to shift within the bond to partially neutralize the inequality. This would lower the energy of those states having the greatest electron interaction energies, which in the present case would include the ground state.

6. Influence of Substituents

Benzene Homologs.—After having treated so many large molecules it appeared tempting to consider several small homologs of benzene characterized by conjugated and unconjugated substituents.

The methyl-substituted derivatives toluene, xylene, and mesitylene were dealt with by changing the framework potential, *i.e.*, the contribution of one neutral hydrogen atom was replaced by that of a neutral carbon atom. Hence for the conjugated carbon atom next to the methyl group, the *neutral* framework potential was assumed to be the same as that of a joint atom. Thus the treatment can be said to include the inductive effect in its most general form, but to omit hyperconjugation.

On the basis of the theory developed in the earlier papers,⁵ this change of the framework potential does not affect the molecular orbitals, but enters the calculation in two ways: the resonance integral γ is lowered, and certain joint correction contributions enter the configuration interaction matrix.

The numerical results are listed in Table VI. The comparison with the experimental assignments is shown in Fig. 18. The trend to longer wave lengths is reasonably reproduced. In Table VII, the change of each transition is decomposed, for each molecule, into two contributions; the first arising from the modification of the resonance integral, γ , the second from the joint correction mentioned in the preceding paragraph. Contrary to assumptions popular in some simple models, the former is the greater of the two.

Figure 18 also contains the result for styrene as an example of a conjugated substitution. Although the free ending chain must give rise to certain effects not properly accounted for by the present treatment, the agreement between theory and experiment is relatively satisfactory.

Diphenyl and Fluorene.—Another simple case where the influence of unconjugated substituents could be tested was the comparison between diphenyl and fluorene. The results, also given in Table VI, give rise to the synthetic spectra in Fig. 19. The shift of the lower diphenyl band in fluorene is given incorrectly, the shift of the upper band, though in the right direction, is too small. However, the split of the lower band in fluorene, due to increasing separation of the involved transitions, is reasonably reproduced. The ap-

TABLE VI
CALCULATED TRANSITIONS OF BENZENE AND DIPHENYL DERIVATIVES
See Table I for explanations.

ELECTRONIC TRANSITIONS FOR THE BENZENE HOMOLOGUES										
72	BENZENE	40.233 0.	56.126 1.271							
	TBX TRIPLET= 30.043	48.659 0.	56.126 1.271							
73	BENZENE	40.234 0.	56.050 1.264							
	IRX TRIPLET= 30.043	48.592 0.	56.049 1.264							
74	TOLUENE	38.950 0.	54.830 1.234							
	TBM TRIPLET= 28.618	47.330 0.	54.790 1.235							
75	TOLUENE	38.946-0.	54.827 1.229							
	IRM TRIPLET= 28.617	47.332-0.	54.796 1.231							
76	m - XYLENE	38.232 0.002	54.123 1.217							
	TBM TRIPLET= 27.906	46.619 0.001	54.082 1.219							
77	m - XYLENE	38.232 0.002	54.113 1.217							
	IRM TRIPLET= 27.901	46.619 0.001	54.082 1.219							
78	MESITYLENE	37.560 0.	53.453 1.210							
	TBM TRIPLET= 27.193	45.986 0.	53.453 1.210							
79	MESITYLENE	37.554 0.	53.370 1.204							
	IRM TRIPLET= 27.188	45.912 0.	53.370 1.204							
80	STYRENE	36.255 0.015	38.578 0.743	46.971 0.068	49.599 0.781	52.780 0.537				
	TBM TRIPLET= 19.373	55.887 0.263	57.359 0.109	63.269 0.018	66.238 0.212	68.850 0.572				
81	STYRENE	36.673 0.	38.397 0.705	47.988 0.420	51.299 0.863	54.033 0.243				
	IRM TRIPLET= 19.648	59.395 0.054	60.843 0.477	63.610 0.013	65.761 0.575	69.721 0.023				
82	DIPHENYL	35.149 0.006	50.453 1.359	55.415 0.178	60.702 0.030	64.523 0.904				
	TBX TRIPLET= 22.905	37.265 0.838	48.242 1.461	54.299 0.247	57.708 0.001	69.309 0.021				
83	DIPHENYL	35.696 0.	50.768 1.338	56.455 0.256	62.994 0.794	66.088 0.093				
	IRX TRIPLET= 22.722	37.265 0.853	48.318 1.639	57.561 0.021	59.940 0.103	69.408 0.001				
84	DIPHENYL	36.069 0.010	51.293 1.311	57.137 0.208	62.836 0.043	67.891 0.886				
	TJM TRIPLET= 23.237	37.312 0.897	49.942 1.378	54.845 0.299	59.171 0.003	73.196 0.020				
85	DIPHENYL	36.926 0.	51.691 1.296	58.324 0.295	66.162 0.769	68.740 0.100				
	IRM TRIPLET= 23.010	37.303 0.922	50.088 1.617	59.101 0.022	61.331 0.101	73.154 0.001				
86	FLUCRENE	35.497 0.002	45.463 0.004	50.832 1.233	52.472 0.053	54.631 0.144	56.222 0.053	57.702 0.028		
	TBX TRIPLET= 23.992	36.068 0.	38.172 0.615	46.551 0.160	47.535 1.435	56.386 0.006	54.728 0.	55.387 0.160		
87	FLUORENE	36.175 0.001	46.513 0.002	51.388 0.979	53.759 0.257	55.092 0.100	56.791 0.159	58.678 0.257		
	IRX TRIPLET= 23.313	35.181 0.009	36.927 0.444	45.156 0.608	47.494 1.300	56.389 0.001	57.260 0.			

TABLE VII
ENERGIES OF THE BENZENE HOMOLOGS

		¹ B _b	¹ B _a	¹ L _b	¹ L _a
Benzene		56.05	56.05	40.23	48.59
Toluene	No joint corn.	54.62	54.62	38.81	47.16
	Joint corn.	54.83	54.79	38.95	47.33
m-Xylene	No joint corn.	53.91	53.91	38.09	46.45
	Joint corn.	54.11	54.08	38.23	46.61
Mesitylene	No joint corn.	53.19	53.19	37.37	45.74
	Joint corn.	53.37	53.37	37.55	45.91

plication of the present method, presupposing a planar molecule, seems much more justified for fluorene than for diphenyl, which is known to twist around the central bond. It therefore is gratifying that, between the two, the agreement between theoretical and experimental spectra is better in fluorene.

7. Conclusions

Assessment of Theory.—While the present approach is more rigorous than past π -electronic work, it does involve approximations without which molecules as big as the one considered here would be untractable. The calculations therefore represent a test of their validity.

The calculations have proved successful, as judged by comparison with experiment, for the alternant hydrocarbons investigated. There are aspects, to be sure, which are in need of serious improvements, in particular as regards the intensities. The lack of contrast in allowed intensities, encountered in all calculations to date, as well

as the polarization puzzle in pyrene, remain disconcerting. Notable achievements were the markedly successful treatment of the pericondensed systems, the first of its kind, and the even better results for those catacondensed molecules whose exact atomic positions were available. It was established that the calculated spectra are fairly sensitive to variations in the atomic positions.

The synthetic spectra have proved to be very helpful, and they compare encouragingly with the experimental ones. There are in fact cases of isomers (*e.g.*, tetraphene and anthracene, or more interestingly, anthanthrene and 1,12-benzperylene) where a decision regarding the molecular structure could be made by comparing the experimental spectrum with the calculated synthetic spectrum. To be sure, in certain cases the proper choice of an appropriately simplified model can explain, or at least rationalize, such differences without an elaborate calculation. There is something to be said, however, for a computer program which automatically establishes the synthetic spectra as soon as it is supplied with the cartesian coördinates of the atoms.

The limits of the assumptions and approximation are clearly over-stepped in the applications to the non-alternant systems.

Review of Spectra.—In comparing so many experimental spectra with their reasonably corresponding theoretical counterparts, one is struck by certain features common to all molecules. Consistently one finds, above the lowest triplet,

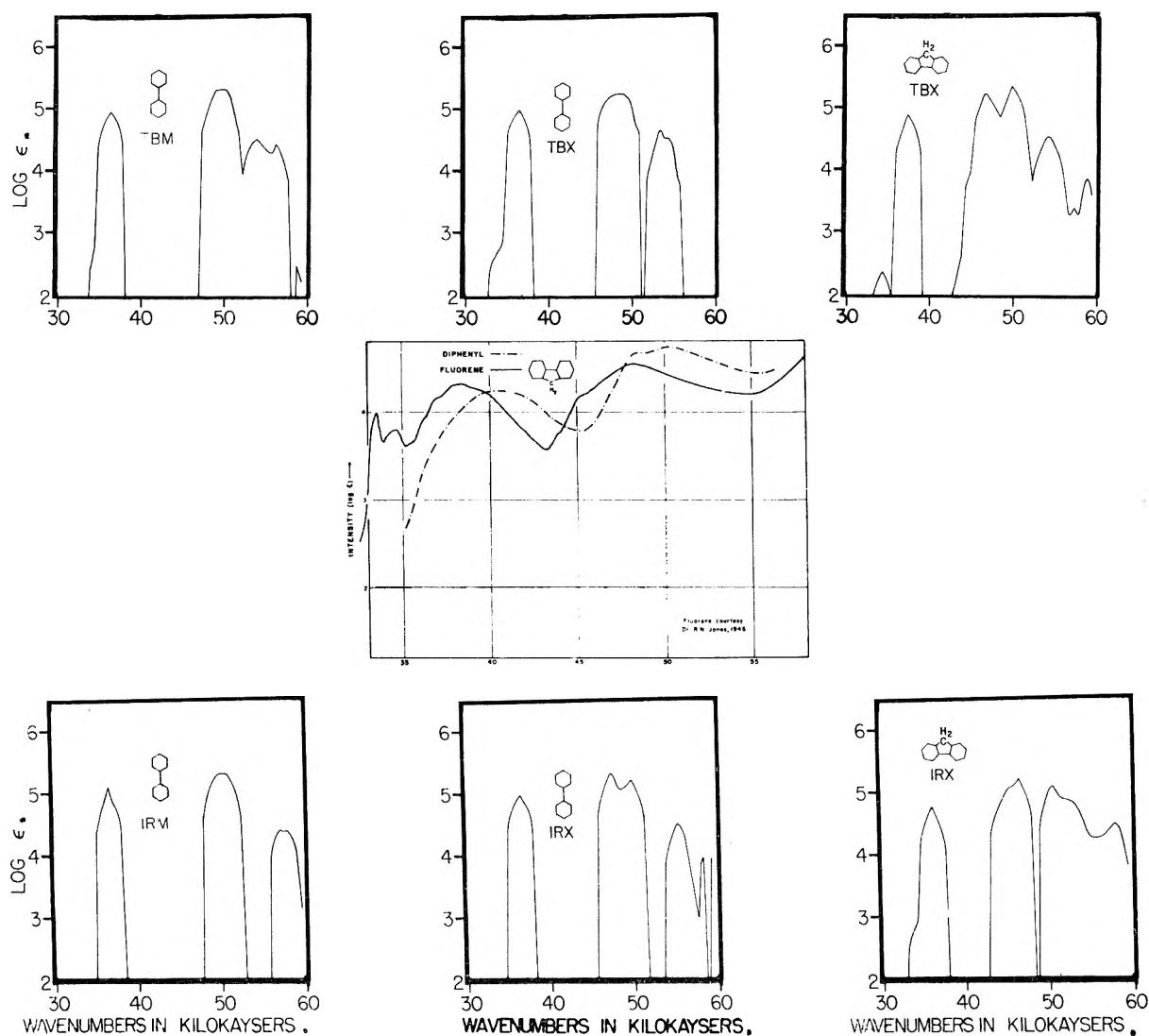


Fig. 19.—Experimental and synthetic spectra for diphenyl and fluorene. Explanation in section 1, after eq. 4.

two, or in a few cases three, low lying singlets. This theoretical result agrees with the empirical observation that the considerable broadness of these bands is clearly recognizable as vibrational fine structure. Toward shorter wave lengths, there follow in general one or two much stronger absorption bands and, traditionally, their fine structure, too, is interpreted as vibrational, although this hardly can be inferred from the line shapes and little of it is found in the simple molecules. The theoretical calculations furnish in general as many strong transitions as are observed. In larger molecules, these are accompanied, however, by varying numbers of medium or weak transitions which extend from this vicinity to higher energies, resembling a barrage and presumably going into the Rydberg transitions. The existence of such a multitude of states cannot be a surprise from quantum mechanical considerations. It is remarkable rather that they do not extend into lower regions. In view of these results, we feel that the majority of the fine structure of the strong bands at higher energies is presumably not vibrational but electronic in character. This

conclusion seems to be supported by the synthetic spectra. Although the calculations of the very high transitions (above 60 kK.) are of course much less reliable, we predict an almost continuous fairly strong absorption in the short wave length region, which presently is unobserved due to technical difficulties.

Classification of Transitions.—Is it possible, within this general spectral pattern, to relate specific transitions in different molecules to each other?

In addition to symmetry, we used the transition-dipole maps to trace kinships of this kind. In families of molecules with enough symmetry throughout the series, they provided indeed a sensitive fingerprint of particular transitions. In more irregular sequences, formed by less closely related molecules, they proved rather too sensitive to the molecular variations for establishing connections.

We therefore see no basis for a nomenclature which could express intimate similarities in the transitions of *all* aromatics. The most practical convention would be to take over, from the linear

polyacenes, the symbols 1L_a , 1L_b for the generally observed lower transitions and the symbols 1B_a , 1B_b for the higher and generally strong transitions, without, however, associating with them the characteristics of the dipole structures found in the polyacenes or the original model concepts of Platt. In those few cases where there are more than two transitions of one kind, they may be denoted by ${}^1L_a'$, ${}^1B_b'$, etc. If a clear gap does exist above the B-bands, then the next strong transitions following at shorter wave length should receive different names, say C_a , C_b , etc. In alternants the indices a,b indicate behavior with respect to symmetry planes, "b" states being polarized parallel to a plane intersecting bonds and "a" states polarized parallel to a plane containing atoms, regardless of the length of the corresponding molecular axes. In unsymmetric molecules, these subscripts

can be used if there is a clear enough relationship to states in closely related symmetric molecules. It appeared unnecessary to invent a special nomenclature for the many moderate transitions in the high energy region. These practices have been followed in the present investigation, since they do justice to the observed spectra as well as to the theoretical results with a minimum amount of complication.

Acknowledgments.—The authors wish to acknowledge many helpful discussions with Mr. E. Miller Layton concerning spectroscopic questions as well as assignments. They furthermore thank him for his help in preparing the manuscript. The assistance of Dr. D. R. Fitzwater and of the Midwest Universities Research Association in aiding the computations also is appreciated.

SOME ASPECTS OF THE THEORY OF PHOTOGRAPHIC SENSITIVITY

By J. W. MITCHELL

Department of Physics, University of Virginia, Charlottesville, Va.

Received June 20, 1962

This paper reviews the Mitchell theory of photographic sensitivity. The experimental evidence upon which the theory was based is summarized and the essential features of the theory are discussed. Recent experimental evidence which appears, at first sight, to be inconsistent with the theory and has led to its rejection by a number of authors is outlined. Further consideration of this evidence shows that it is not inconsistent with the theory. The conclusion is reached that there is, as yet, no justification for the rejection of the theory. It does indeed provide the only clear explanation which has so far been given of the recently established fact that the absorption of four light quanta is sufficient to render developable the most sensitive grains of photographic emulsions.

1. Introduction

Five years have now elapsed since the theory of photographic sensitivity which was worked out by the author on the basis of experimental work done in the H. H. Wills Physics Laboratory of the University of Bristol was presented essentially in its final form. Although the theory, taken as a whole, is acknowledged to have stimulated experimental research and theoretical discussion, many aspects of it have been criticized by different authors and rejected by them. It may therefore be not inappropriate at this time to ask what, if anything, remains of the theory which depended upon experimental observations made over the course of ten years. The purpose of this paper is to review the experimental evidence upon which the theory was founded, to discuss the essential features of the theory, and to consider whether its final rejection on account of the new experimental evidence is fully justified.

The main aim of the experimental work at Bristol was to prepare large thin single crystals of silver halides which would serve as models for the silver halide grains of photographic emulsions and allow physical and chemical experiments on chemical sensitization and on the nature and distribution of the latent image and of photolytic silver to be carried out. At the time when the work was begun, little was known of the nature and distribution of the internal latent image.¹ There was also much

discussion as to whether or not the surface latent image consisted of groups of silver atoms or was formed by the action of light on a complex of silver ions and gelatin.² It therefore appeared desirable to study the physical and chemical properties of crystals of silver halides in the absence of gelatin. Unless it could be shown that crystals of silver halides could be chemically sensitized for the formation of a surface latent image in the absence of gelatin, the validity of the physical theories of the formation of the latent image in which gelatin is assumed to play an effectively inert role in chemical sensitization and exposure would be seriously in doubt.

The outcome of the Bristol work was that a systematic body of experimental knowledge of physical and chemical properties of single crystals of silver halides was built up. This provided a sound basis for the formulation of a theory of photographic sensitivity with a number of new and distinctive features.³⁻⁵ The method of using thin sheet crystals of silver halides for experimental

(2) E. E. Loening, "Fundamental Mechanisms of Photographic Sensitivity," Butterworths, London, 1951, p. 126.

(3) J. W. Mitchell, "Wissenschaftliche Photographie, Proceedings of International Conference," Köln, 1956, (Verlag Dr. Othmar Helwich: Darmstadt), 29 (1958).

(4) J. W. Mitchell, *Sci. Ind. Photogr.*, [2] 1, 41 (1958).

(5) J. W. Mitchell, *J. Phot. Sci.*, 6, 57 (1958).

(6) J. W. Mitchell, *ibid.*, 9, 328 (1961).

(7) J. W. Mitchell, "Die Photographische Empfindlichkeit," *Phot. Korr. Sonderheft* (1957).

(8) J. W. Mitchell, *Rept. Progr. Phys.*, 20, 433 (1957).

(1) W. F. Berg, *Rept. Progr. Phys.*, 11, 248 (1948).

work on photographic sensitivity which was developed at Bristol by the author and his co-workers^{7,9-11} led to the first observations of dislocations in crystals.¹² It has since been very effectively applied to establish further physical and chemical properties of silver halide crystals by West and Saunders of the Kodak Research Laboratories in Rochester³⁻¹⁵ and by research workers in many European laboratories.

2. Experimental

2.1 Thin Sheet Single Crystals of Silver Halides.—All the experimental work which will be described in this section was carried out with single crystals of silver halides with a thickness between 100 and 500 μ . They were prepared by the controlled crystallization of molten silver halide between plates. After separation from the plates, the disk-shaped crystals were cut into square pieces with a side of about 0.6 cm. which were then mounted on 3×1 in. glass microscopic slides. The crystals were not reduced to silver immediately upon immersion in normal surface and internal developers if they had not previously been exposed to light. Crystals which were, therefore, in the photographic sense, free from surface and internal fog could be reliably prepared for experimental studies of chemical sensitization and latent image formation.^{5,10,11}

2.2 Annealed Thin Sheet Crystals of Silver Halides.—The experiments which will be described in section 2.4 showed that the unannealed thin sheet crystals had a high density of small dislocation loops and of dislocation lines. The number of internal dislocation loops was reduced greatly when the crystals were annealed in an atmosphere of the corresponding halogen at a temperature between 150 and 250°. During the anneal, the density of dislocation lines decreased and the remaining dislocations arranged themselves in well defined sub-boundaries.¹⁶ Both the internal sensitivity and the capacity of the crystals for chemical sensitization were reduced when the crystals were annealed in this way.^{10,17} The dislocation lines were eliminated by annealing the thin sheet crystals for a long period at 400° in an atmosphere of the corresponding halogen. The crystals then had a remarkably low internal photochemical sensitivity and chemical sensitization of their surfaces for the formation of a surface latent image which would initiate chemical development was not possible.^{10,18} These observations showed that crystal imperfections play an important role in determining the chemical and photochemical behavior of the thin sheet crystals.

2.3 The Deposition of Silver on the Surfaces of Silver Halide Crystals.—The surfaces of the crystals were reduced to silver immediately upon immersion in a chemical developer after the deposition on their surfaces by evaporation in a high vacuum of 10^{16} silver atoms per cm.². A dense deposit of silver was also produced on the surfaces when the same crystals were immersed in a physical developer.^{7,9} The distribution of silver atoms produced by evaporation had the same reactivity toward a dilute solution of chromic acid containing silver nitrate¹⁹ as the surface latent image formed on a sulfur sensitized sheet crystal by the action of light. This was, moreover, the same as the reactivity of a surface latent image formed in a sulfur sensitized pure silver bromide emulsion.¹⁰ From this we conclude that it is very

probable that the surface latent image consists of a distribution of groups of silver atoms.

Crystals on which 10^{14} silver atoms per cm.² had been condensed were not reduced to silver when they were immersed in surface chemical developers of low activity immediately after the deposition of the silver atoms. They became developable after periods of storage of several hours at room temperature. This indicates that, in the absence of gelatin, silver atoms can diffuse over the surfaces of silver halide crystals and form aggregates with the same properties as those formed directly during the deposition of 10^{16} silver atoms per cm.². The aggregation process could be accelerated by exposing the crystals to light.^{7,9,10}

Internal fog appeared when crystals with either 10^{14} or 10^{16} silver atoms per cm.² on their surfaces were stored in the dark for several hours at room temperature. The residual surface silver was destroyed with a solution of chromic acid and the crystals then were treated with an internal developer. Discrete development centers appeared which were distributed along the elements of a two-dimensional network on the surface.^{6,7,10}

These experiments show that silver atoms can diffuse over the external surface of a gelatin-free silver halide crystal and that they can diffuse away from the external surface on to internal surfaces. These diffusion processes occur slowly if the crystals are stored in the dark at room temperature; they are greatly accelerated if the crystals are exposed to light.⁹ By both the thermal and the photochemically accelerated diffusion and aggregation of the silver atoms, latent images are formed which have the same chemical properties as the surface and internal latent images formed by the action of light on chemically sensitized crystals. These latent images are destroyed when the crystals are exposed to the corresponding halogen at a very low vapor pressure. We believe that these experiments provide strong evidence to support the view that the surface and internal images consist of a distribution of groups of silver atoms.

2.4 The Exposure of Silver Halide Crystals to Light.

A surface latent image is not formed when the thin fog-free non-chemically sensitized sheet crystals are exposed to light for short or long periods at high or low intensities. When they are immersed in a physical or chemical surface developer for a normal period after exposure, no silver is deposited on their surfaces and there is no reduction of the silver halide to silver. This is true of the fog-free crystals whether they are exposed in the unannealed state or after annealing for short or long periods at high or low temperatures.^{7,9,10,17}

The most probable interpretation of this important observation is that any silver which separated at the surface of a pure silver halide crystal during exposure would either trap positive holes, react with halogen which was being liberated there, or else dissociate into silver ions and electrons and diffuse away from the external surface. That reaction with positive holes or liberated halogen provides the most likely reason why a surface latent image was not formed is shown by the observation that a thin fogging film of silver with more than 10^{15} silver atoms per cm.² disappeared rapidly during exposure to light leaving a fog-free surface in the exposed region. A strong internal latent image was formed beneath the surface.⁹

When the exposed crystals were treated with an internal developer, it was found that specks of silver were produced along the elements of the same two-dimensional surface network as was made visible by the diffusion of silver from the surface into the interior and subsequent internal development.^{9,10} From this observation, it was concluded that the internal image was formed during exposure by the separation of silver atoms on the internal surfaces of a polyhedral sub-structure in the crystals.

This sub-structure was made visible by exposing the crystals to light for a sufficiently long period to cause the separation of visible particles of internal photolytic silver. The boundaries of the sub-structure then were seen with the optical microscope to be formed by arrays of dislocations and these were, in fact, the first observations ever to be made of the internal sub-structure of a crystal.^{12,16} It thus appeared that the silver atoms which diffused away from the surface in the experiments of section 2.3 became concentrated along dislocation lines near the surface where silver atoms of the internal latent image also separated during exposure. These experiments provided the first definite information about the nature and distribution of the internal latent image.

(9) J. M. Hedges and J. W. Mitchell, *Phil. Mag.*, **44**, 357 (1953).

(10) T. Evans, J. M. Hedges, and J. W. Mitchell, *J. Phot. Sci.*, **3**, 73 (1955).

(11) P. V. McD. Clark and J. W. Mitchell, *ibid.*, **4**, 1 (1956).

(12) J. M. Hedges and J. W. Mitchell, *Phil. Mag.*, **44**, 223 (1953).

(13) W. West and V. I. Saunders, "Wissenschaftliche Photographie, Proceedings of International Conference," Köln, 1956 (Verlag Dr. Othmar Helwich: Darmstadt), 47 (1958).

(14) W. West and V. I. Saunders, *J. Phys. Chem.*, **63**, 45 (1959).

(15) W. West and V. I. Saunders, *Phot. Sci. Eng.*, **3**, 258 (1959).

(16) J. W. Mitchell, "Dislocations and Mechanical Properties of Crystals," John Wiley, New York, N. Y., 1957, p. 69.

(17) J. W. Mitchell, *Z. Elektrochem.*, **60**, 557 (1956).

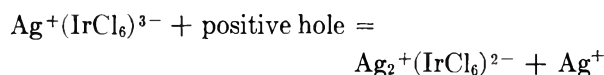
(18) J. W. Mitchell, "Growth and Perfection of Crystals," John Wiley, New York, N. Y., 1958, p. 386.

(19) G. W. W. Stevens, "Fundamental Mechanisms of Photographic Sensitivity," Butterworths, London, 1951, p. 227.

2.5 The Sensitization of Silver Halide Crystals for the Formation of a Surface Latent Image. **2.5.1 Silver Chloroiodide.**—The observations of the previous section led to the conclusion that small groups of silver atoms would not survive on the surface of a silver halide crystal to serve as nuclei for the formation of a surface latent image because they would trap positive holes diffusing to the surface with the formation of silver ions which then could diffuse away from the surface and combine with electrons to form silver atoms on internal surfaces. The surface groups of silver atoms also would react with atoms and molecules of halogen liberated there.

On the basis of this conclusion, the author looked for a substance which would be strongly adsorbed to the surfaces of silver halide crystals, provide a much higher surface density of effective traps for positive holes than the groups of silver atoms of the surface latent image, and react with both atoms and molecules of halogens. It appeared that the substance should form a sparingly soluble silver compound in order that it should be strongly adsorbed and that it should be able to trap a positive hole by an electron transfer mechanism. Silver chloroiodide was found to fulfill these requirements; it is adsorbed to the surfaces of silver halide crystals and the octahedral chloroiodide ion can transfer an electron to an electron acceptor such as a positive hole to form an octahedral chloroiodate ion.

The surfaces of thin sheet crystals of silver halides were, in fact, strongly sensitized for the formation of a surface latent image by immersion in a weak solution of potassium or ammonium chloroiodide.¹⁰ This treatment also greatly increased the exposure required for the removal of a fogging layer of 10^{15} silver atoms per cm^2 from the surface. It appears to the author that there can be little doubt that the adsorbed silver chloroiodide functions as a chemical sensitizer by trapping positive holes which would otherwise be trapped by the silver atoms of the surface latent image. The trapping of a positive hole releases a silver ion according to the scheme



West and Saunders¹⁵ have shown that a sensitizing layer of silver chloroiodide will trap positive holes but not conduction electrons. In the Bristol experiments,¹⁰ a strong surface latent image was formed when crystals sensitized with silver chloroiodide were exposed to light. It must therefore be concluded that the trapping of conduction electrons at the surface by the chemical sensitizer is not an essential prerequisite for effective surface sensitization.

2.5.2 Silver Sulfide.—The sheet crystals of silver halides were most conveniently sensitized with silver sulfide by immersion in a dilute solution of sodium thiosulfate followed by washing, or by immersion in a dilute solution of allyl thiourea followed by a hydrogen ion cycle according to the method of James and Vanselow.²⁰ Fog-free sulfur sensitization was achieved more readily with sodium thiosulfate than with allyl thiourea so that this was the method generally employed.¹⁰

A surface latent image was formed when the sulfur sensitized crystals were exposed to light and this was made visible by either physical or chemical development. The gelatin-free crystals were fogged by depositing 10^{15} silver atoms per cm^2 on their sulfur sensitized surfaces by vacuum evaporation of silver. A dense black image was then formed; immediately they were immersed in a chemical or physical surface developer.⁷ The fogging distribution was rapidly removed by a dilute solution of chromic acid containing silver ions which appeared to leave the silver sulfide layer unchanged. The surface latent image formed by exposing the sensitized crystal to light was removed in the same time by the same chromic acid solution. This indicates that the surface latent image formed during the exposure of sulfur sensitized crystals also probably consists of groups of silver atoms.

Further experimental work showed that silver sulfide, adsorbed in the form of a monomolecular layer on the surfaces of the crystals, probably has two functions in the formation of the surface latent image. It can trap positive holes in the same way as silver chloroiodide and it undergoes a chemical change in the process.

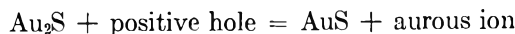


It also can adsorb silver atoms and stabilize a surface distribution of silver atoms preventing them from diffusing away from the surface into the interior of the crystal.^{3,5,7}

The fact that the adsorbed monolayer of silver sulfide plays an active chemical role in the formation of the surface latent image was demonstrated by exposing a silver bromide crystal sensitized with sodium thiosulfate through a slit which was 1 mm. wide. When the crystal was developed in a surface developer a dense black image of the slit appeared. Another similarly sensitized piece of the same crystal then was exposed and treated with the dilute chromic acid solution to destroy the surface latent image without affecting the sensitizing silver sulfide layer in the unexposed regions. It was washed and dried and after this uniformly exposed to the same source and developed in a surface developer. A clear reversed image of the slit appeared on a black ground showing that the silver sulfide was no longer effective as a chemical sensitizer in the area which had received the first exposure. No image appeared when the crystal was developed after the chromic acid treatment without receiving the second uniform exposure and only a very weak internal image was formed in the exposed region by the first exposure. The developed internal image was not significantly increased in density by the second exposure. We therefore concluded that the silver sulfide was involved in a chemical reaction during the first exposure and that the most probable reaction was the trapping of positive holes with the formation of diatomic molecules and the release of silver ions. The diatomic molecules might then dissociate into silver atoms and sulfur atoms and any of these products would be oxidized by the chromic acid solution at a higher rate than the silver sulfide.²¹

The second role of the silver sulfide was clearly demonstrated when the diffusion experiments described in section 2.3 were repeated with silver halide crystals sensitized with a monolayer of silver sulfide by treatment with a dilute solution of sodium thiosulfate. Between 10^{14} and 10^{15} silver atoms per cm^2 were deposited on the surfaces by vacuum evaporation and the crystals then were stored in the dark for several days at room temperature. No internal fog could be detected when the crystals were developed with an internal developer after treatment with the chromic acid solution. From this we conclude that the potential energy of a silver atom is less when it is adsorbed to a monolayer of silver sulfide than when it is present on the free surface of the crystal and that groups of silver atoms are stabilized by adsorption to a monolayer of silver sulfide.⁷

2.5.3 Gold Sensitization.—The sheet crystals of silver halides were sensitized for the formation of a surface latent image by immersion in a dilute solution of sodium aurous dithiosulfate even more effectively than by immersion in a solution of sodium thiosulfate.^{10,11} The sensitizing layer contained both gold and sulfur and in the case of this particular sensitizer was probably an adsorbed monomolecular layer of aurous sulfide. As far as the trapping of positive holes and the adsorption of silver atoms was concerned, it had properties which were similar to those of a monolayer of silver sulfide. A considerably longer first exposure was, however, required before a reversed image was formed in the double exposure experiment. We have



Both the surface latent image formed during exposure and fogging layers produced by the vacuum deposition of silver atoms were much more resistant to attack by dilute chromic acid solutions than corresponding crystals sensitized with silver sulfide. The stable surface latent image specks probably consist of groups of silver and gold atoms in this case. No diffusion of silver atoms away from a vacuum deposited fogging layer on the surface of a crystal sensitized with aurous sulfide could be detected by the appearance of internal fog even after long periods of storage. From these experimental observations, we concluded that silver atoms and groups of silver atoms were stabilized even more by adsorption to a monolayer of aurous sulfide than by adsorption to silver sulfide.

2.5.4 Silver Chloroiodide and Aurous Sulfide.—A solution

(20) T. H. James and W. Vanselow, *J. Phys. Chem.*, **57**, 725 (1953); *J. Phot. Sci.*, **1**, 133 (1953).

(21) J. W. Mitchell, "Proceedings of a Conference on Photographic Sensitivity," Liege, 1959, Butterworths, London, 1962, p. 226.

containing low concentrations of both potassium or ammonium chloroiridite and sodium aurous dithiosulfate proved to be a particularly effective sensitizer for the sheet crystals of silver halides in the absence of gelatin.^{10,11,15} This solution probably produces a composite sensitizing layer in which monolayer islands of aurous sulfide are associated with adsorbed molecules of silver chloroiridite. The experimental observations which have been described suggest that the most important function of the silver chloroiridite is to trap positive holes while that of the aurous sulfide is to facilitate the combination of silver ions and conduction electrons by adsorbing the resulting silver atoms. Long exposures were required before silver halide crystals sensitized with this combination showed any evidence of solarization.¹⁰

3. The Mitchell Theory of the Formation of the Latent Image

3.1 The Model of a Sensitized Silver Bromide Crystal.—For the presentation of the theory, the grains of a photographic emulsion are assumed to consist of microcrystals of silver bromide with imperfections in which the internal latent image is formed.^{5,17,22–24} A more detailed model and a more detailed role for the crystal imperfections is not necessary for the discussion which will be given here. The chemical sensitizer which is responsible for the formation of the surface latent image is assumed to be present on the surface in the form of discrete monolayer islands of silver or aurous sulfide which may be nucleated at sites where internal imperfections meet the surface.⁵ The hypothesis that the sensitizing silver or aurous sulfide is present on the surfaces of the crystals in the form of adsorbed monomolecular layer islands was introduced into the theory of photographic sensitivity for the first time by the author.^{3,10} It previously had been assumed that the silver sulfide was present on the surface as a discrete speck and this concept led to the concentration speck theory of Sheppard²⁵ for which the Gurney–Mott theory provided a physical mechanism.²⁶ The importance of the introduction of the concept of a sensitizing monolayer of silver sulfide lies in the fact that it allows the chemical sensitizer to have two functions. It may trap positive holes or react with liberated halogen atoms or molecules at one part of the monolayer and it may adsorb silver atoms which then can aggregate to groups of silver atoms in another part. Because of this, the groups of silver atoms of the surface latent image can be protected from regression so long as adsorbed silver sulfide is present on the immediately surrounding surface.^{3,5–7,21}

3.2 The Formation of the Latent Image and of Photolytic Silver.—The Mitchell theory of photographic sensitivity was worked out so that it would be consistent with the experimental observations of Berg and Burton¹ on the formation of the latent image in photographic emulsions and with the experimental work on chemically sensitized large single crystals which has been described in section 2. These observations, taken together, show that there are two clearly distinguishable stages in the formation of the latent image and of

particles of photolytic silver in silver halide crystals. In the first stage, a latent sub-image is formed which will initiate physical or chemical development only with low efficiency. Immediately after deposition, a distribution of 10^{14} silver atoms per cm^2 on the surface of a silver halide sheet crystal sensitized with silver sulfide has the same chemical properties as a latent sub-image formed in a sulfur sensitized emulsion by the action of light.⁷ In the second stage, stable surface and internal latent image specks, which initiate chemical development with a much shorter induction period than latent sub-image specks, and internal particles of photolytic silver are formed. The stable surface latent image specks have the same chemical properties as the aggregates of silver atoms in a surface distribution with 10^{15} silver atoms per cm^2 .^{2,7}

To avoid any possibility of confusion and misunderstanding, the successive steps which the author proposes for the two stages of the photochemical process in chemically sensitized silver bromide crystals will be enumerated in the two following sections.

3.3 The First Stage in the Formation of the Latent Image.—(1) The discussion given here is based on the assumption that the first step in the formation of photochemical products consists in the absorption of energy within the silver halide crystals which results in the liberation of conduction electrons and positive holes. Other primary processes are considered elsewhere.^{3,5,7,8}

(2) The experimental evidence is consistent with the postulate that, at the beginning of this stage, there are no deep irreversible traps for conduction electrons in fog-free, previously unexposed, chemically sensitized silver bromide crystals at room temperature.

(3) There are, however, deep irreversible traps for positive holes which are provided by adsorbed molecules of chemical sensitizers.

(4) The positive holes therefore are trapped finally and irreversibly before the conduction electrons are so trapped and a positive ionic charge in the form of a mobile silver ion appears at the trapping site.

(5) The shallow traps for conduction electrons which are associated with silver or aurous sulfide monolayer islands and with silver ions on the external and internal surfaces of the crystals are not effective at room temperature. The potential energy wells associated with these traps must first be deepened by the proximity of a mobile silver ion. The probability for finding a conduction electron in the potential energy well during exposure steadily increases as the silver ion approaches nearer to the trap. This situation leads to attractive interaction and results in the combination of the mobile silver ion with the conduction electron at the trap. A silver atom is formed which is adsorbed at the site of the trap and constitutes a latent pre-image speck.^{4,5,7,21}

(6) The silver atoms are formed and adsorbed (a) in interstices and around the edges of the monolayer islands of aurous sulfide, (b) at equivalent sites associated with monolayer islands of silver sulfide, (c) at jogs occupied by silver ions along

(22) J. W. Mitchell, *J. Phot. Sci.*, **1**, 110 (1953).

(23) J. W. Mitchell, *Z. Physik*, **138**, 381 (1954).

(24) T. Evans and J. W. Mitchell, "Defects in Crystalline Solids," (London, Physical Society), 1955, p. 409.

(25) S. E. Sheppard, *Photogr. J.*, **68**, 397 (1928).

(26) R. W. Gurney and N. F. Mott, *Proc. Roy. Soc. (London)*, **A164**, 151 (1938).

edge components of dislocation lines, and (d) at kink sites occupied by silver ions on the external surfaces of the crystals. These sites are arranged in order of increasing potential energy and decreasing stability and lifetime for the adsorbed silver atom. This order is based on the observations on the diffusion of silver atoms away from the surface which have been described in section 2.^{4,5,7}

(7) At this stage in the formation of the latent image, the isolated silver atoms or latent pre-image specks can dissociate again into mobile silver ions and conduction electrons and diffuse away from the sites at which they were formed and adsorbed.^{4,5,7,8}

(8) As a consequence of the relative lifetimes of silver atoms adsorbed at different sites, which decrease with increasing potential energy of the adsorbed atom, silver atoms will be associated with higher probability with interstices in aurous and silver sulfide monolayers on the surface than with sites occupied by silver ions at surface and internal imperfections. The silver atoms will be concentrated in regions where they have the lowest potential energy in accordance with the Boltzmann principle.

(9) Associated pairs of silver atoms are next produced, either by the successive formation and adsorption of silver atoms at the same site or by the slower processes of thermal diffusion of silver atoms as mobile silver ions and electrons and aggregation. These constitute latent sub-image specks and, on account of (8), they will be produced with higher probability, when successive events occur at a low rate, in association with sensitizing layers of aurous or silver sulfide than elsewhere in the crystals. They have a longer lifetime than latent pre-image specks but still do not provide, in the absence of a silver ion in close proximity, effective traps for conduction electrons at room temperature. They will, however, initiate chemical development after a relatively long induction period.^{4,5,7,8}

According to this theory, the first stage in the formation of the latent image in chemically sensitized crystals is distinguished by the fact that no effective deep traps for conduction electrons are available at room temperature in fog-free chemically sensitized silver bromide crystals in a fully stabilized photographic emulsion. If such traps were available, as is assumed in the Gurney-Mott theory, they would, in the opinion of the author, constitute fog specks, as they would accept electrons from reducing molecules in solution during physical and chemical photographic development. It is the absence of such traps in unexposed crystals and their formation either during the development of crystals which carry a surface latent sub-image or at the beginning of the second stage of a longer exposure which allows the photographic developer to distinguish between exposed and unexposed grains.

3.4 The Second Stage in the Formation of the Latent Image.—The distinguishing feature of the second stage in the formation of the latent image according to the Mitchell theory is that irreversible traps are available for conduction electrons which

are not inherently associated with the chemical sensitizer. These traps are provided by positively charged groups of silver atoms which are formed by the absorption of light or other forms of energy in the crystals. The depth and effectiveness of the traps is determined by their positive charge, which is conferred by the absorption of a silver ion to the groups of silver atoms. There are no irreversible traps for positive holes either in chemically non-sensitized crystals or in chemically sensitized crystals which have been given sufficiently long exposures to solarize the surface latent image. The sequence of photochemical processes in the second stage is as follows.

(1) The first stage in the formation of the latent image in which no deep traps are available for conduction electrons is terminated when groups of three silver or of gold and silver atoms have been formed by a succession of the events of the first stage which have been enumerated above or by the mechanism proposed by Burrow and Mitchell.²⁷ According to this mechanism, the diatomic AgS or AuS molecules dissociate into silver and gold atoms, which can contribute to the surface latent image, and sulfur atoms. The planar groups of three silver atoms may be associated with monolayer islands of chemical sensitizer on the surface or with internal imperfections.

(2) In 1954, the author proposed, for the first time, that such planar groups can become transformed into positively charged tetrahedral groups of four silver atoms by adsorbing silver ions when they are in thermal equilibrium with crystals of silver halides at room temperature.^{3,5,7,27} The compensating negative charge is provided by a surface halide ion or by a vacant silver ion lattice site. The experimental evidence is consistent with the hypothesis that groups of three or more silver atoms adsorb silver ions to become positively charged groups of four or more silver atoms which are associated with very much deeper potential energy wells than smaller uncharged groups of silver atoms and provide irreversible traps for conduction electrons. The positively charged groups also exert some long range attraction upon a conduction electron. The charge is neutralized by the electron and then restored by the adsorption of a further silver ion. The author first introduced this idea that, in the second stage of the formation of the latent image, the adsorption of a silver ion by a group of silver atoms precedes the trapping of a conduction electron by the group. This reverses the sequence of events of the Gurney-Mott theory.

(3) The positive holes are repelled by the positively charged groups of silver atoms. They have to diffuse thermally to adsorbed molecules of chemical sensitizer with which they react with the liberation of silver ions.

(4) At this stage, the lifetime of the positive hole, which diffuses to and reacts with uncharged molecules of chemical sensitizer, is greater than that of the conduction electron which is attracted to and captured by a positively charged group of silver atoms.

(5) The chemical sensitizer which is adsorbed

(27) J. H. Burrow and J. W. Mitchell, *Phil. Mag.*, **45**, 208 (1954).

on the surface is progressively consumed, partly through the trapping of positive holes and partly by reaction with atoms and molecules of halogen formed at the surface. The number of irreversible traps for positive holes therefore steadily decreases with increasing exposure.

(6) Although the positively charged groups of silver atoms repel positive holes, they can react with neutral molecules of halogen which are formed at the surface. As a result of this, unless an external halogen acceptor is present, the surface groups of silver atoms are gradually reduced in size.

(7) The positively charged internal groups of silver atoms repel positive holes and are not exposed to halogen molecules. So long as halogen molecules formed at the surface can diffuse away from the surface, the internal groups continue to increase in size with the result that a visible image of internal particles of photolytic silver is formed. These particles are distributed along dislocations and other internal imperfections in the crystals and render these imperfections visible.

(8) When the stage is reached at which the adsorbed molecules of the chemical sensitizer have been completely exhausted, no irreversible traps for positive holes remain in the crystals. The positive holes then are trapped reversibly by halide ions on surface and internal sites to form halogen atoms which are adsorbed to halide ions. A second positive hole must now be trapped by a halide ion adjacent to a halogen atom adsorbed at the surface before a halogen molecule can be formed which can diffuse away from the surface.^{5,7} The positive charge of each positive hole is represented by the positive charge of an excess silver ion after trapping. An amount of halogen which is chemically equivalent to the amount of silver which separates to form the internal image of photolytic silver must be liberated at the surface at this stage of the exposure and either diffuse away or react with molecules in the surroundings. This condition must always be satisfied, even for an internal latent image, when chemically non-sensitized crystals are exposed to light.^{4,5,7}

(9) At this stage of the exposure of chemically sensitized crystals, deep irreversible traps are provided for conduction electrons by positively charged internal groups of silver atoms. There are now no irreversible traps for positive holes either at the surface or in the interior of the silver halide crystals. The positive holes therefore must be trapped reversibly at room temperature by halide ions on external and internal surfaces and by vacant lattice sites. The conduction electrons therefore are finally trapped before the positive holes. This will also be the situation with chemically non-sensitized silver halide microcrystals in which positively charged stable internal latent image specks have been formed by a previous exposure or by the earlier part of a prolonged exposure.

(10) When silver halide crystals are exposed in the circumstances of (9) in the absence of an external halogen acceptor, the molecules of halogen which are liberated may accumulate at the inter-

face between the silver halide and the gelatin. The dark electrical conductivity of the crystals then will be greater than that of unexposed crystals on account of the contribution from the positive holes which then will be present at room temperature in thermal equilibrium within the crystals.²⁸

4. Discussion

4.1 Experimental Evidence which Appears to be Inconsistent with the Mitchell Theory.—The theory of photographic sensitivity which has been outlined in the previous section has been criticized or rejected during the past few years by a number of authors on account of different experimental observations which have been made.²⁹ The following experimental evidence which appears at first sight to be inconsistent with the theory has been brought forward:

(1) From experimental work in which silver bromide sols sensitized with silver sulfide were exposed in aqueous suspension, Sutherns and Loening³⁰ concluded that silver sulfide does not disappear during exposure if a halogen acceptor such as phenol is present in the medium. This is quite inconsistent with the author's conception of one of the important roles of silver sulfide in the formation of the surface latent image and with the experimental results which have been described in section 2.5.2.

(2) Hamilton and Brady³¹ have described experiments in which they have found the lifetime of positive holes to be greater than the lifetime of the conduction electrons. They have rejected the Mitchell theory on the basis of these experiments.

(3) In experiments in which a layer of silver sulfide has been sandwiched between two thin sheets of silver bromide, West and Saunders¹⁵ have shown that this sulfide layer traps both conduction electrons and positive holes. The observed trapping of conduction electrons by a sensitizing silver sulfide layer would appear to be inconsistent with the mechanism proposed for the first stage in the formation of the latent image by the author.

(4) West and Saunders¹⁵ have described an interesting series of experiments in which sensitized silver bromide crystals were exposed to light flashes with synchronized voltage pulses applied normal to their surfaces. The surface near the negative electrode was covered with a layer of silver sulfide to trap positive holes. The opposite surface near the positive electrode was partially immersed in a solution of sodium aurous dithiosulfate, which probably forms a layer of aurous sulfide on it. When the crystals were exposed, a latent image which could be developed was produced on the area near the positive electrode which was covered with the layer of aurous sulfide but not on the adjacent untreated silver bromide surface. They point out that they eliminated any possible reaction between positive holes and the sensitizing layer near the positive electrode in this experiment but

(28) G. W. Luckey and W. West, *J. Chem. Phys.*, **24**, 879 (1956).

(29) A. L. Kartuzhanskii, *Soviet Physics, Uspekhi*, **4**, 205 (1961).

(30) E. A. Sutherns and E. E. Loening, *J. Phot. Sci.*, **4**, 154 (1956).

(31) J. F. Hamilton and L. E. Brady, *J. Appl. Phys.*, **30**, 1893 (1959).

that a developable latent image nevertheless was formed on the aurous sulfide sensitized surface. It appears that they may believe this to be inconsistent with the author's theory.

4.2 The Original Gurney-Mott Theory and the Mitchell Theory.—The general impression which must be gained from reading some of the discussion in the papers referred to in the previous section and other related papers which deal with the interpretation of experimental results is that the recent experimental work favors the original Gurney-Mott theory and is inconsistent with the Mitchell theory. This appears to be the conclusion reached by Kartuzhanskii²⁹ in his recent review article.

The author has himself pointed out in a recent note⁶ that the Gurney-Mott theory and the Mitchell theory are two alternative theories of the formation of the latent image and of particles of photolytic silver and that knowledge will best be advanced if they are considered side by side as alternative working hypotheses in the designing of experimental work and in the interpretation of experimental results. It is only in this way that it will be possible to arrive at a critical assessment of their relative merits.

In the Gurney-Mott theory, the trapping of positive holes is considered to be unimportant and is not discussed. The sensitizing silver sulfide is assumed to play an entirely passive role during exposure as would appear to be established by the experimental work of Sutherns and Loening referred to above.³⁰ This is inconsistent with the experimental work of the author and his co-workers.

According to the original Gurney-Mott theory, the only function of the silver sulfide, which is assumed to be present as a speck on the surface, is to provide traps for electrons which are deeper than any present in the chemically non-sensitized crystals. According to this theory, the traps are uncharged when they are in thermal equilibrium with the silver halide at room temperature. They become negatively charged when they trap conduction electrons released during exposure. The negative charge then is neutralized by the drift of interstitial silver ions to the traps and the formation of silver atoms. The fact that the silver sulfide sensitivity specks provide the deepest traps for conduction electrons in the sulfur sensitized crystals is held to account fully for the role of silver sulfide in the formation of the surface latent image.

In the opinion of the author, the whole body of experimental evidence forces one to accept an active as well as a passive role for the chemical sensitizer during exposure; the sensitizer is chemically involved in the formation of the surface latent image. The adsorbed molecules of the chemical sensitizer trap positive holes and release a chemically equivalent number of mobile silver ions or react with halogen atoms. As a consequence of this active role, and also as a result of reaction with liberated molecules of halogen, the chemical sensitizer is consumed during prolonged exposures.

The author believes that a product of chemical sensitization which would trap electrons in the

manner postulated by Gurney and Mott would initiate spontaneous reduction if the unexposed silver halide crystal were immersed in a chemical developer. On the basis of the Gurney-Mott theory, there appears to be no satisfactory way of explaining both the non-developability of unexposed crystals and the fact that the most sensitive grains of photographic emulsions are made developable by the absorption of four quanta.^{32,33} There is also no satisfactory way of fitting the formation and properties of latent pre-image specks and latent sub-image specks into the theory.

In the Mitchell theory, it is postulated that deep traps for conduction electrons are not associated with non-fogging products of chemical sensitization. With this hypothesis, no difficulty is encountered in explaining the non-developability of unexposed crystals, the inefficiency of the first stage in the formation of the latent image, and the long induction period required for the initiation of development by a latent sub-image.⁵

An essential feature of the theory, which distinguishes it from all other theories, is the further hypothesis that the deep electron traps which are responsible for developability are first formed during exposure. The discontinuous increase in the depth of the traps which occurs at a certain critical size is determined, not by a simple increase in the number of silver atoms associated with a very small group, but by a change from a state in which the group is, on the average, uncharged to a state in which it is positively charged. This critical change occurs when a group of three silver atoms has been produced. A group of this size adsorbs a silver ion and becomes a positively charged group of four silver atoms when it is in equilibrium with the silver halide crystal. This and larger positively charged groups provide the deep traps which capture conduction electrons and accept electrons from reducing molecules during development.

It appears at the present time that the most sensitive grains of photographic emulsions are made developable by the absorption of not more than four light quanta.^{32,33} This is fully consistent with the theoretical model of the stable latent image speck of minimum size, according to the Mitchell theory. The size of this speck was worked out at a time when it was generally believed that the formation of a stable latent image speck required the absorption of between ten and a hundred quanta in a silver halide emulsion grain.²⁷

4.3 Discussion of the Experimental Results of Section 4.1.—We return now to the discussion of the evidence which appears to be inconsistent with the Mitchell theory and we will consider each group of observations.

(1) In their experiments, Sutherns and Loening determined the amount of silver sulfide remaining after exposure by boiling with hydroquinone and hydrobromic acid and displacing the hydrogen sulfide formed from the system with a stream of nitrogen. With this method, they might have produced the same amount of hydrogen sulfide from diatomic Ag₂S molecules and from

(32) A. Marriage, *J. Phot. Sci.*, **9**, 93 (1961).

(33) E. Klein, *ibid.*, **10**, 26 (1962).

atomic sulfur as from the equivalent amount of Ag₂S. In this case, their experimental work could give no information on whether or not positive holes were trapped by adsorbed molecules of silver sulfide. Their conclusions that silver sulfide plays a passive role during exposure and that positive holes are not trapped by it²⁹ therefore may require revision. In the experiments of section 2.5.2, the active role of silver sulfide during a latent image exposure was established by treating the exposed crystals with a dilute solution of chromic acid.

(2) In the experiments which have been carried out by Hamilton and Brady³¹ single grain layer coatings of a large grained chemically non-sensitized pure silver bromide emulsion have been used. These coatings have been exposed for many hours at the rate of 1000 flashes per second to light flashes with thousands of quanta per flash while voltage pulses have been applied which have been synchronized with the light flashes. In these circumstances, it would be surprising if, in accordance with the Mitchell theory, stable internal latent image specks, positively charged by the adsorption of silver ions, were not formed during the early part of the exposure. These provide deep irreversible traps for conduction electrons. In the chemically non-sensitized crystals, there are no irreversible traps for positive holes and, in the absence of an external halogen acceptor, halogen molecules are likely to accumulate at the interface between the silver halide microcrystals and the gelatin. So long as such molecules are present, there will therefore be a certain concentration of positive holes within the crystals in thermal equilibrium.²⁸ These conditions correspond with those postulated by Mitchell to hold during the second stage in the formation of the latent image (see section 3.4 above). The theory predicts that, at this stage of the exposure with chemically non-sensitized crystals, the lifetime of the conduction electrons will be less than the lifetime of the positive holes⁸ and this is what Hamilton and Brady have observed. Their observations appear to be fully consistent with the theory.

The hypothesis that the lifetime of the positive hole is less than the lifetime of the conduction electron refers particularly to the first stage in the formation of the latent image during the exposure of an unfogged fully chemically sensitized emulsion at room temperature. It appears that Hamilton and Brady have not yet carried out experiments with chemically sensitized silver halide microcrystals in which they have demonstrated that the lifetimes of the positive holes in these microcrystals are greater than the lifetimes of the conduction electrons, which is what they will have to do to sustain their rejection of the Mitchell theory. When these experiments are carried out, the exposure should be limited to the number of flashes which is required for the production of not more than a latent sub-image on the surfaces and in the interior of the silver halide crystals. The experiments of the author and his co-workers have shown that four flashes with synchronized voltage pulses are sufficient to produce displaced stable

latent image specks on the sensitized surface of a large crystal of silver bromide.¹⁰

It does not appear to be altogether reasonable that an important hypothesis relating to the first stage in the formation of the latent image in chemically sensitized emulsions should be rejected²⁹ on the basis of experiments carried out with one particular chemically non-sensitized emulsion under the conditions of the second stage in which this hypothesis, according to the theory itself, is no longer applicable.

It also appears to be desirable that the experimental work which Hamilton and Brady have done with the chemically non-sensitized silver bromide emulsions to establish that the ionic dark conductivity of emulsion microcrystals is orders of magnitude greater than the ionic conductivity of silver bromide macrocrystals should be repeated.

They first proposed that the greatly enhanced conductivity of the microcrystals which they observed was due to interstitial silver ions in excess of the concentration which would be expected to be in thermal equilibrium in a large silver bromide crystal at room temperature.³⁴ They now propose that the enhanced conductivity is due to mobile surface silver ions.³⁵ It would be surprising if this interpretation were correct in view of the observations of West on the suppression of the negative photoconductive effect in silver bromide crystals by gelatin.³⁶ It appears that this experimental work should be repeated either with chemically sensitized emulsions or with chemically non-sensitized emulsions to which potassium or ammonium chloroiridite has been added to form a layer of silver chloroiridite on the surfaces of the silver bromide microcrystals. This will react with both atoms and molecules of halogen which are liberated at the surfaces of the microcrystals of the otherwise chemically non-sensitized emulsion during exposure. It is difficult to accept the conclusion of Hamilton and Brady that the concentration of either surface or interstitial silver ions in the grains of a fully stabilized photographic emulsion, particularly in one stabilized by the addition of divalent cadmium ions, is orders of magnitude greater than in a single crystal of silver bromide of the type used for the experiments on photographic sensitivity described in section 2.²¹

In view of the considerations presented in this section, it seems desirable to reserve judgment upon the rejection by Hamilton and Brady of the two hypotheses which the author advanced in his discussion of the theory of photographic sensitivity.²¹ The first, which has been discussed in this paper, is that during the first stage of the formation of the latent image in chemically sensitized silver halide crystals when latent pre-image and latent sub-image specks are being formed, irreversible traps are provided for positive holes by adsorbed molecules of the sensitizer, but there are no deep irreversible traps for conduction electrons. The

(34) J. F. Hamilton and L. E. Brady, *J. Appl. Phys.*, **30**, 1902 (1959).

(35) J. F. Hamilton and L. E. Brady, "Proceedings of Conference on Photographic Sensitivity," Zurich, 1959.

(36) W. West, "Fundamental Mechanisms of Photographic Sensitivity," Butterworths, London, 1951, p. 99.

second, which is that there is a negligible concentration of mobile surface silver ions and of interstitial silver ions associated with the grains of a fully stabilized photographic emulsion containing divalent cations, has been discussed elsewhere.²¹ This second hypothesis is, however, not an essential feature of the Mitchell theory.³

(3) The intermediate layers of silver sulfide used by West and Saunders¹⁵ in their sandwich experiments were fogging layers which would initiate chemical development without exposure to light. The fact that such fogging layers acted as barriers to the diffusion of conduction electrons is not surprising. Observations made with such fogging layers cannot be used as evidence for the rejection²⁹ of the author's hypothesis that deep traps for conduction electrons are not present in fog-free unexposed chemically sensitized crystals but are first formed during exposure. It is desirable that these interesting sandwich experiments should be repeated with non-fogging intermediate layers of silver sulfide, but it is doubtful if an unequivocal observation can, even then, be made by this method. Can the experiment establish that a non-fogging silver sulfide layer does not provide deep traps for conduction electrons at the beginning of the exposure when no effect of exposure can be seen until such traps have been formed by the action of light?

(4) This group of experiments of West and Saunders¹⁵ appears to provide a convincing demonstration of the validity of items (5), (6), and (7) of section 3.3. Since it was observed experimentally⁷ that the presence of a monolayer of silver sulfide on the surface of a silver bromide crystal would prevent silver atoms deposited from an atomic beam from diffusing into the interior of the crystal, the author always has supposed that one function of the sensitizing silver sulfide monolayer was to adsorb silver atoms.³ Since then, he has never stated that the *only* function of the silver sulfide was to trap positive holes as seems to be assumed in many discussions of his theory.²¹ It appears that it will be possible to establish the dual role of the silver or aurous sulfide in a particularly striking way by experiments of the type which have been carried out by West and Saunders. The surface of a thin sheet crystal which is near the negative electrode can be sensitized with a non-fogging monomolecular layer of silver sulfide and that near the positive electrode with a non-fogging monomolecular layer of silver or aurous sulfide. If the crystal then is exposed to light flashes with

synchronized voltage pulses, the silver sulfide should react and disappear at the surface toward which the positive holes are attracted and silver atoms should be formed and adsorbed at the surface toward which the conduction electrons are attracted. This experiment will provide no evidence for the trapping of conduction electrons by an uncharged sensitizing layer of silver or aurous sulfide during the first latent sub-image stage of an ordinary exposure when the crystals are exposed in the absence of an applied electric field. It only will demonstrate that silver atoms have been formed and that they are stabilized by adsorption to the silver or aurous sulfide layer. In the author's view, the two functions of the sulfide monolayer which would be performed at separated surfaces in this experiment are performed at separated sites within the silver or aurous sulfide monolayer islands when a sensitized emulsion microcrystal is exposed to light in the normal way.

As far as the adsorption of silver atoms is concerned, the difference between the author's theory and Sheppard's earlier theory is that Sheppard assumed that the silver sulfide which adsorbed silver atoms was present on the surface in the form of a discrete speck and rejected any suggestion that a reaction between silver sulfide and halogen (positive holes in current terminology) could play an essential role in the formation of the latent image. The author believes that the experimental evidence which is at present available supports the view that the silver sulfide or aurous sulfide is present on the surface in the form of adsorbed monolayer islands.³ He introduced the idea that one of the functions of the silver sulfide was to trap positive holes and liberate silver ions, the other function being the adsorption of silver atoms formed at the silver or aurous sulfide monolayer by the combination of silver ions and electrons.

4.4 Conclusion

The role of any theory is to stimulate creative thinking and new experimental work. It appears that this role has not yet been exhausted for the theory of photographic sensitivity with which the author's name has been associated and that the time has not yet come when this theory should be rejected and discarded.

Acknowledgment.—This paper has been prepared with support from the Office of Naval Research, Contract NONR 474(05), Project NRO 17-615, which is gratefully acknowledged.

ELECTRONIC PROPERTIES AND BAND STRUCTURE OF THE SILVER HALIDES¹

BY FREDERICK C. BROWN

Department of Physics, University of Illinois, Urbana, Illinois

Received June 20, 1962

The band structure of AgCl and AgBr is discussed with emphasis on recent experiments which bear on our understanding of the solid state. These include external photo-emission, magneto-resistance at low temperature, and optical absorption. Certain additional phenomena are mentioned such as luminescence, electron-hole pair production by ionizing radiation, and the temperature dependence of electron mobility. The importance of high purity material such as is produced by zone refining is pointed out.

I. Introduction

Several recent articles have reviewed the silver halides from the point of view of solid state physics.²⁻⁵ It is not our intention to go over the ground covered in these earlier papers at this time. Rather we will discuss some new developments and make a few suggestions for future investigations. Our remarks will apply mainly to fundamental processes in large single crystals but it is hoped that they will bear in part on what goes on in the photographic process. For information on conduction phenomena in emulsion type material, one can turn to other papers of this conference as well as to a recent review, "Elementary Photographic Processes in an Electric Field," by A. L. Kartuzhanskii.⁶

The new developments referred to above are some optical absorption and magnetoconductivity experiments which bear upon the band structure of AgBr and AgCl. In addition, progress has been made recently in the preparation of crystals of high purity. Pure materials are needed in the study of the mobility of electrons, especially at low temperature. The factors which control the mobility of carriers at room temperature and below are now at least qualitatively understood.

II. Band Properties

A. Band Structure and Electron Affinity.—

It has been pointed out by Taft, Phillip, and Apker⁷ that the silver halides are a particularly intriguing case compared to other non-metallic photo-emitters. These workers and an earlier investigator⁸ have published results on the photo-yield of electrons from AgBr into a vacuum. Photo-emission begins at a photon energy of about $\varphi' = 6.1$ e.v. at 300°K. Apparently this is the energy required to excite an electron from the top of the filled or valence band and remove it to infinity. On the

other hand, optical absorption and photo-conductivity data (discussed below) show that the band gap of AgBr is $E_g = 2.6$ e.v. This means that the electron affinity, the energy to remove an electron from the bottom of the conduction band at E_c to infinity, is $\chi = 3.5$ e.v. for AgBr. This is of the same order of magnitude as the energy gap. The situation is midway between two extremes, as shown in Fig. 1. Cesium iodide⁹ belongs to the alkali halides, a class of substances which have electron affinities less than their band gaps. Actually CsI is an extreme case in that it has a very low affinity, $\chi = 0.3$ e.v., and a rather high yield or quantum efficiency. Other alkali halides have affinities of the order of one electron volt.¹⁰ On the other hand, semiconductors such as Ge and Si have affinities much larger than band gaps. The sketch for Si in Fig. 1 is drawn from new data taken on cleaved surfaces under ultra high vacuum.¹¹ It is also true in the case of Si and Ge but not the alkali halides that the threshold for emission, φ' , is larger than the energy above which a conduction electron will scatter appreciably with valence band electrons as deduced from breakdown phenomena. It may be that this scattering threshold occurs about 8 e.v. above the valence band in the case of AgBr.⁷

The energies of Fig. 1 are estimated assuming little or no bending of the bands at the surface due to space charge or a dipole layer.¹² This assumption may be checked in the case of AgBr by considering the emission from silver directly into AgBr. It is reasonable^{13,14} to assume that the threshold of this process is just given by the difference in the vacuum work function of Ag metal, $\varphi = 4.7$ e.v.,¹⁵ and χ . Emission from deposited silver into AgBr has not been reported, but the threshold of the Herschel effect in both AgBr and AgCl emulsions is near $h\nu = \varphi - \chi = 1.2$ e.v.,¹⁶ which would give $\chi = 3.5$ e.v. Moreover, Gilleo has given a value of $\varphi - \chi = 1.1$ e.v. for photo-emission from silver into large crystals of AgCl

(1) (a) Presented at a Symposium on Photographic Processes sponsored by the ACS Division of Physical Chemistry, Washington, D. C., March 22-24, 1962; (b) Supported in part by the U. S. Air Force Office of Scientific Research.

(2) F. Seitz, *Rev. Mod. Phys.*, **23**, 328 (1951).

(3) (a) F. Seitz, "Photographic Sensitivity," Vol. I, Maruzen, Tokyo, 1956, p. 5; (b) F. C. Brown and F. Seitz, "Photographic Sensitivity," Vol. II, Maruzen, Tokyo, 1958, p. 11.

(4) F. C. Brown and F. Seitz, "Conference on Scientific Photography," Liege, 1960 (to be published).

(5) J. W. Mitchell, in A. F. Gibson, F. A. Kroger, and R. E. Burgess, "Progress in Semiconductors," Vol. 3, Heywood & Co., 1958, p. 55.

(6) A. L. Kartuzhanskii, *Soviet Phys.-Uspekhi*, A.I.P. translation, **4**, 205 (1961).

(7) E. A. Taft, H. R. Phillip, and L. Apker, *Phys. Rev.*, **110**, 876 (1958).

(8) R. Fleischmann, *Ann. Physik*, **5**, 73 (1930).

(9) H. R. Phillip and E. A. Taft, *J. Phys. Chem. Solids*, **1**, 159 (1956).

(10) E. A. Taft and H. R. Phillip, *ibid.*, **3**, 1 (1957).

(11) F. G. Allen and G. W. Gobelli, *Bull. Am. Phys. Soc.*, **II**, **6**, 421 (1961), paper E3.

(12) J. Bardeen, *Phys. Rev.*, **71**, 717 (1947).

(13) N. F. Mott and R. W. Gurney, "Electronic Processes in Ionic Crystals," Oxford, 1940.

(14) W. T. Turner, *Phys. Rev.*, **101**, 1653 (1956).

(15) H. E. Farnsworth and R. P. Winch, *ibid.*, **58**, 812 (1940).

(16) O. Bartlett and H. Klug, *Z. Physik*, **89**, 779 (1934); B. H. Carroll and C. M. Kretschmann, *J. Res. Natl. Bur. Std.*, **10**, 449 (1933).

so that again $\chi \simeq 4.7 - 1.1 = 3.6$ e.v.¹⁷ His experiments were carried out at 80°K. in order to freeze out ionic conductivity. The band gap in AgCl is 3.225 e.v. at 80°K. (see below), so one would expect external photo-emission to set in at $\phi' = 6.8$ e.v., in rough agreement with the results of Fleischmann⁸ for AgCl. Because thermal vibrations have a large effect in smearing out the band edges of these ionic crystals it would be better if the photo-emission experiments were carried out at low temperature.

The width of the valence band of CsI, shown in Fig. 1, is estimated from the kinetic energy of emitted electrons.¹⁸ No experimental data of this type are yet available for the silver halides. On the other hand, theoretical calculations using the tight binding method have been carried out for the valence band of NaCl¹⁹ and KCl²⁰ neglecting spin-orbit interaction. Casella starts with the 3p wave function of the Cl⁻ ion, which is assumed to be on a face-centered cubic lattice of appropriate lattice spacing but neglecting the effect of the metal ion (estimated to be small). He obtains a band width of the order of 1 e.v. Howland's calculations are more detailed but give similar band widths and show that a branch of the valence band bends upward toward a maximum not at $k = 0$ in at least one crystallographic direction. This effect may be more prominent in the case of AgCl due to the 4d states of the silver ion as discussed below.

B. Magnetoconductivity.—One expects that the higher lying energy bands, that is, the empty conduction bands, of the alkali and silver halides are of standard form with a minimum at $k = 0$. Still other possibilities exist such as a multi-valley situation and it seemed worthwhile to carry out experiments which bear upon this point. Electrical conductivity, $\sigma(0)$, in the absence of a magnetic field may have a higher symmetry than the band structure. For example, it can be easily shown that one need specify only one value of conductivity in the case of a cubic conductor. The application of a magnetic field lifts this requirement and permits the observation of more symmetry elements consistent with the crystal class. Experiments on the direction of current flow for photoelectrons in AgBr and AgCl in the presence of both electric and magnetic fields have recently been completed by Tippins.²¹

The observations were carried out on crystals of very high purity at liquid helium temperatures. Samples were cut from ingots which were zone refined in halogen²² and then were annealed in a clean atmosphere of helium gas. They were mounted in a cryostat between plane parallel blocking electrodes and illuminated by light in the absorption edge, either between the electrodes or through one electrode which was transparent.

(17) M. A. Gilleo, *Phys. Rev.*, **91**, 534 (1953).

(18) H. Phillip, E. A. Taft, and L. Apker, *ibid.*, **120**, 49 (1960).

(19) R. C. Casella, *ibid.*, **104**, 1260 (1956).

(20) L. P. Howland, *ibid.*, **109**, 1927 (1958).

(21) H. H. Tippins, "Magnetoconductance of the Silver Halides," Ph.D. thesis, University of Illinois, Feb., 1962; H. H. Tippins and F. C. Brown, *Bull. Am. Phys. Soc.*, [II] **7**, 221 (1962).

(22) F. Moser, D. C. Burnham, and H. H. Tippins, *J. Appl. Phys.*, **32**, 48 (1961).

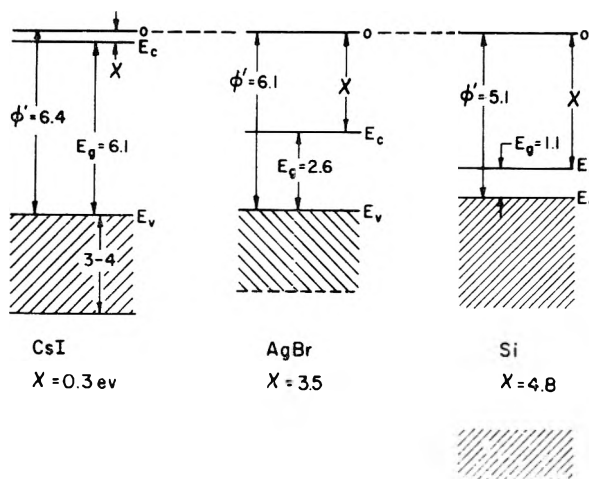


Fig. 1.—Simple energy band diagrams for three different types of solids shown relative to the zero level at infinity. The electron affinity, χ , is much less than the band gap energy, E_g , for an alkali halide such as CsI, about the same for the silver halides, and considerably greater than the band gap for an elemental semiconductor such as Si.

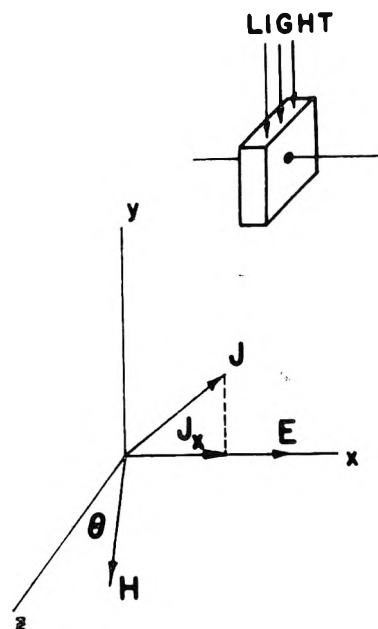


Fig. 2.—Showing the coordinates used in the transient magnetoconductivity experiments. The electric field is applied along the x -axis. The magnetic field makes an angle θ with the z -axis and can be rotated in the yz -plane (see Fig. 3). It is also possible to study transverse magnetoconductivity, keeping H perpendicular to E but allowing it to rotate in the yz -plane and thus make various angles with respect to the crystallographic axes.

Currents of the order of 10^{-14} amp. were recorded by a vibrating reed electrometer. The experiments were transient in the sense that space charge fields were not allowed to build up.²³ The direction of

the electric field in the sample $\vec{E} = (E, 0, 0)$ is determined by the electrodes and applied voltage whereas the current depends in direction and magnitude upon the applied magnetic field (see Fig. 2). The current can be described in terms of

(23) R. S. Van Heyningen and F. C. Brown, *Phys. Rev.*, **111**, 402 (1958).

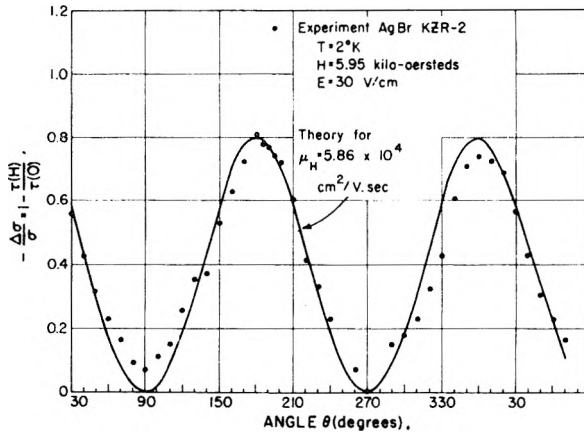


Fig. 3.—Magnetoconductivity $(-\Delta\sigma/\sigma) = 1 - J(H)/J(0)$ as a function of the angle between H and the transverse or z -axis. A longitudinal effect occurs at $\theta = 90$ and 270° , a transverse at 180 and 0° . The points are experimental data, the solid curve is according to theory, eq. 7 of the text, for a Hall mobility of $58,600$ $\text{cm}^2/\text{volt sec}$.

the well known conductivity coefficients.²⁴ In the case of cubic symmetry, standard band shape, and isotropic scattering, the current is given by²⁵

$$\vec{J} = \sigma\vec{E} + \alpha\vec{E} \times \vec{H} + \gamma(\vec{E} \cdot \vec{H})\vec{H} \quad (1)$$

In a conductivity experiment with \vec{E} along the x -axis one observes the component

$$J_x(H) = (\sigma + \gamma H^2 \sin^2 \theta)E \quad (2)$$

where σ and γ are functions of H and θ is the angle between \vec{H} and the transverse or z -axis. In the absence of a magnetic field

$$J_x(0) = \sigma(0)E \quad (3)$$

Experimentally one observes the ratio $J_x(H)/J_x(0)$. Therefore, the effect of the magnetic field is conveniently given by the magnetoconductivity defined as

$$-\frac{\Delta\sigma}{\sigma(0)} = \frac{J_x(0) - J_x(H)}{J_x(0)} = 1 - \frac{J_x(H)}{J_x(0)} \quad (4)$$

a number which is observed to vary between zero and $+1$. Substitution of eq. 2 and 3 yields

$$-\frac{\Delta\sigma}{\sigma} = 1 - \frac{\sigma + \gamma H^2 \sin^2 \theta}{\sigma(0)} \quad (5)$$

The coefficients σ and γ can be evaluated for a particular scattering mechanism in terms of standard semiconductor integrals. Further it can be shown that the following relation applies independent of the scattering mechanism assumed

$$\sigma + \gamma H^2 = \sigma(0) \quad (6)$$

This last relation permits us to simplify eq. 5 with the result

$$-\frac{\Delta\sigma}{\sigma(0)} = \frac{\gamma H^2 \cos^2 \theta}{\sigma(0)} \quad (7)$$

The quantity $-\Delta\sigma/\sigma$ is more convenient than

(24) F. Seitz, *Phys. Rev.*, **79**, 372 (1950).

(25) D. C. Burnham, F. C. Brown, and R. S. Knox, *ibid.*, **119**, 1560 (1960).

the magneto-resistance $\Delta\rho/\rho$ as normally defined because the coefficients which are dependent upon H appear in the numerator of the theoretical expressions. It is closest to the quantity actually measured in the present case. Notice that here

one observes the component of \vec{J} in the direction of \vec{E} and not the component of \vec{E} in the direction of \vec{J} —there is no Hall potential developed across the sample.

The theoretical expression eq. 7 is compared with experimental points in Fig. 3. Notice that there is little or no observable longitudinal magnetoconductivity ($\theta = 90^\circ$), a result in agreement with simple band structure. Furthermore the observed transverse magnetoconductivity ($\theta = 0$) is nearly constant as the angle of the magnetic field is changed with respect to the crystal axis. From these experiments the value of Hall mobility defined as

$$\mu_H \equiv \frac{c\alpha(H)}{\sigma(H)} \quad (8)$$

in the limit of small H turns out to be in excess of $50,000$ $\text{cm}^2/\text{volt sec}$. at 2°K . in the case of at least one sample of AgBr.

The results of magnetoconductivity measurements on AgCl are similar to those for AgBr. Since holes appear to have a shorter drift range than electrons, especially at the very low temperatures of these experiments, we assume that the above results bear on the symmetry of the conduction band. It is likely that the conduction band is of standard, or nearly standard, form, with a minimum centered at $k = 0$. Further details will be published elsewhere.

C. Optical Absorption.—The absorption spectra of silver chloride and silver bromide have been investigated from wave lengths in the visible to the vacuum ultraviolet below 100 $\text{m}\mu$. Thin films have been prepared in various ways to provide values of the extinction coefficient in the ultraviolet where the absorption is characteristically very strong. In the absorption edge at longer wave lengths one may use large single crystals, but it is necessary to be careful about purity.

As shown in Fig. 4, one notes a remarkable similarity between the structure in the ultraviolet for AgCl²⁶ and an alkali halide such as NaCl.²⁷ There seems little doubt that the first strong absorption peak near 250 $\text{m}\mu$ (4.9 e.v.) in AgCl corresponds to direct excitation of the electron on the Cl^- ion.^{2a} An exciton state is formed in which the electron is still bound to the halogen atom with a binding energy of the order of a few tenths of an electron volt. The exciton peak is split into a so-called halogen ion doublet.^{13,28} Similar remarks apply to AgBr.

Unlike the alkali halides, the silver halides have a relatively low level absorption tail which extends to long wave lengths near the visible. Light absorbed in this region produces photoconductivity

(26) Y. Okamoto, *Nachr. Akad. Wiss. Göttingen*, [IIa] **14**, 275 (1956).

(27) J. E. Eby, K. J. Teegarden, and D. B. Dutton, *Phys. Rev.*, **116**, 1099 (1959).

(28) R. S. Knox and N. Inchauspé, *ibid.*, **116**, 1093 (1959).

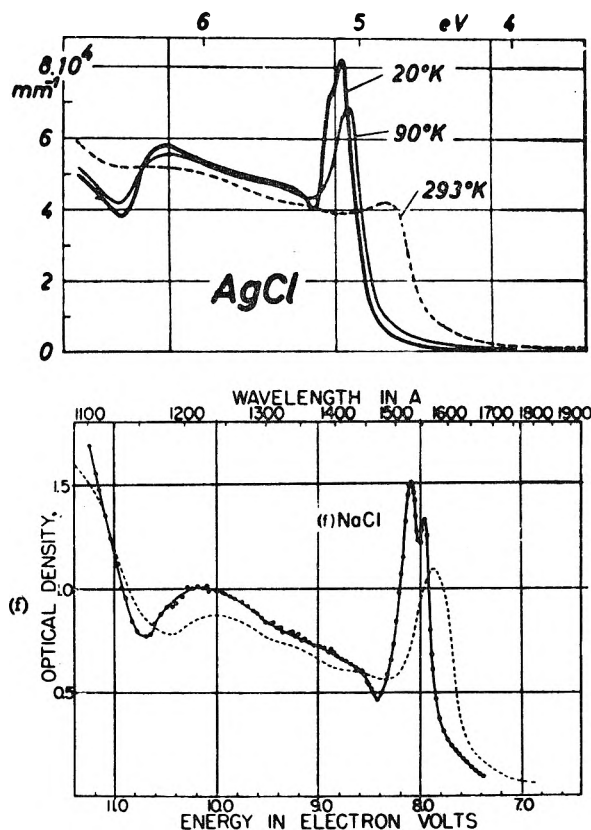


Fig. 4.—Showing the similarity in the fundamental absorption of thin films of AgCl and of NaCl. The curves for AgCl are due to Okamoto²⁹ and the data on NaCl is from the work of Eby and Teegarden.²⁷ In the latter case the solid curve, drawn through the experimental points, is for 80°K., whereas the dotted curve applies at room temperature. The effect of thermal vibrations in smearing out structure appears to be much more prominent for AgCl than NaCl. In addition, the silver halides possess a low level absorption tail (not clearly visible in this plot) which extends out to about 3 e.v.

with high efficiency and under certain conditions is responsible for photolysis. Recent observations on the edge at very low temperatures²⁹ indicate the presence of indirect transitions involving phonons to conserve wave numbers. Although the conduction band is simple the valence band is relatively complex in that it contains a branch which turns upward in at least one crystallographic direction to a maximum near the zone boundary.^{28,20} The situation is just the inverse of that for Ge and Si³⁰ where the valence band has a maximum at $k = 0$ but the conduction band bends downward to a minimum away from $k = 0$. The absorption edge spectrum of semiconductors is reviewed in detail by McLean.³¹

Fine structure associated with the emission and absorption of phonons of different energy is found in the case of the silver halides when measurements are made at sufficiently low temperature. Figure 5 shows the optical density *vs.* wave length of a

(29) F. C. Brown, T. Masumi, and H. H. Tippins, *J Phys. Chem. Solids*, **22**, 101 (1961).

(30) G. G. MacFarland, T. P. McLean, J. E. Quarrington, and V. Roberts, *Phys. Rev.*, **108**, 1377 (1957); **111**, 1245 (1958).

(31) T. P. McLean in A. F. Gibson, F. A. Kroger, and R. E. Burgess, "Progress in Semiconductors," Vol. 5, Heywood and Company, 1960, p. 55.

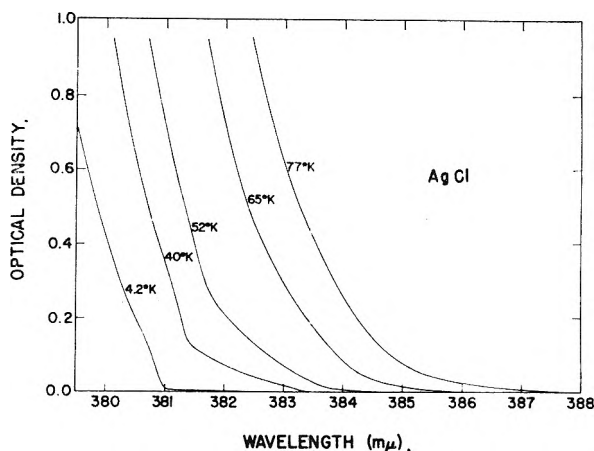


Fig. 5.—Spectrophotometer tracings for a AgCl crystal of thickness 0.208 cm. From reference 29, courtesy of *J. Phys. Chem. Solids*.

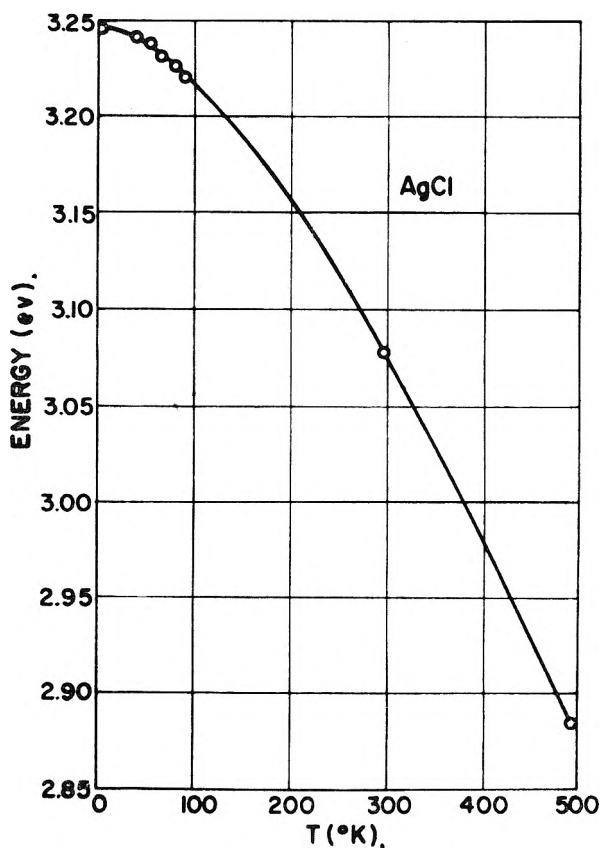


Fig. 6.—Showing the band gap energy as a function of temperature for AgCl as determined from optical absorption data and an analysis of the indirect transitions. The quantity actually plotted is $E_g - E_{ex}$, where E_{ex} is the exciton binding energy, a few tenths of an electron volt.

pure AgCl crystal, thickness 0.208 cm., as recorded on a Cary Model 14R spectrophotometer using a specially designed liquid helium cryostat.³² Note that a very narrow range of wave lengths is covered near the threshold of an absorption edge which shifts to higher energies as the temperature is lowered. The shift reflects the change in band gap with temperature due to dilation of the lat-

(32) Designed by Professor R. Wild after a cryostat described by H. M. Herab, *Phys. Rev.*, **105**, 1158 (1957).

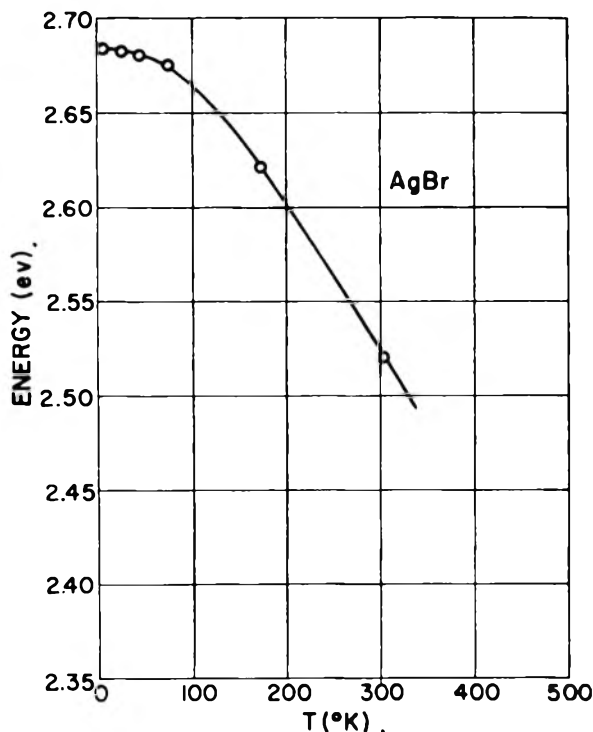


Fig. 7.—The band gap energy minus the exciton binding energy for AgBr as a function of temperature. Similar to the data for AgCl shown in Fig. 6.

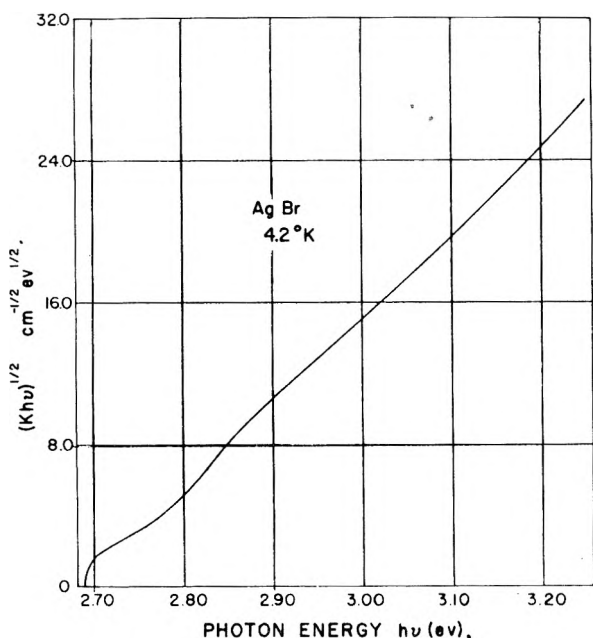


Fig. 8.—The basic shape of the absorption edge of AgBr at liquid helium temperature. The theory of indirect-allowed transitions shows that the absorption constant times photon energy $Kh\nu$ should eventually rise as the square of photon energy measured from a threshold. Therefore, we plot $(Kh\nu)^{1/2}$ vs. $h\nu$. A transition involving the emission of a single phonon ($\theta = 75^\circ\text{K.}$) is presumably taking place. The curve covers the onset of absorption corresponding to excitation to the $n = 1$ states of the indirect exciton as well as the $n = 2$ and higher states above the slight bump at $h\nu = 2.85$ e.v.

tion. A plot of the band gap energy, E_g (minus a small correction E_{ex} for exciton binding energy)

is shown for AgCl and AgBr in Fig. 6 and 7. At temperatures below liquid nitrogen E_g can be determined by an analysis of the direct processes which take place in the edge.

Certain characteristic features of indirect or phonon assisted processes can be seen in Fig. 5. Consider first the abrupt threshold beginning at $381 \text{ m}\mu$ (3.254 e.v.) for AgCl at 4.2°K. This is a threshold corresponding to the formation of indirect excitons ($Kh\nu \propto \Delta E^{1/2}$) with emission of a phonon whose energy turns out to be $k\theta_1$, where $\theta_1 \simeq 90^\circ\text{K.}$ As the temperature is increased a tail is seen to arise which is due to transitions involving phonon absorption. Phonon emission still occurs at higher energy and the difference between the thresholds for these two processes is $2k\theta_1$. Values of θ_1 determined in this way can be compared with an analysis of the magnitude of the absorption at different temperatures and some degree of internal consistency is found in assigning phonon energies. When the vibrational spectrum is complicated additional phonons of higher energies become important. Another phonon of $\theta_2 \simeq 250^\circ\text{K.}$ may be important in the case of AgCl and also two phonon processes may have to be considered.

A rather low level tail extending to quite long wave lengths is seen to appear at 65 and 77°K. and higher temperatures in Fig. 5. This probably is due to the effect of thermal vibrations in smearing out the density of states near a band edge.^{33,34} Notice also that the kinks and structure are lost at high temperature, an effect more important for these ionic crystals than for Ge and Si. The data of Fig. 5 at 4.2°K. reflect the basic shape of the indirect process (phonon emission only). It can be readily extended to higher absorption constant using thin samples and is found to begin as $Kh\nu \propto (\Delta E)^{1/2}$ but eventually to rise more nearly as $Kh\nu \propto (\Delta E)^2$. In addition, structure appears which reflects transitions to different exciton levels as well as the possible involvement of different phonon energies.

AgBr should have a simpler vibration spectrum than AgCl—the ions are of nearly equal mass. Therefore, let us turn to AgBr in discussing the basic shape of the 4.2°K. data. Figure 8 plots $(Kh\nu)^{1/2}$ vs. $h\nu$. A broad bump is seen about 0.13 e.v. above the first shoulder. It may be that the shoulder and this higher energy bump correspond to excitation to the $n = 1$ and $n = 2$ states of the exciton, respectively.³⁵ Assuming a hydrogen-like model, the reduced mass of the exciton can be deduced from the formula

$$\Delta E = \frac{13.6}{\epsilon^2} \left(\frac{m}{m_e} \right) \left(\frac{1}{1} - \frac{1}{4} \right) \quad (9)$$

with the result that $m \simeq 0.27m_e$. We use the optical dielectric constant for $\epsilon = n^2 = 4.6$ since the radius of the exciton satisfies the criterion of Haken.³⁶ If the hole is somewhat heavier than

(33) D. L. Dexter, *Nuovo Cim.*, Suppl. No. 2 to Vol. VII, 245 (1958).

(34) F. Urbach, *Phys. Rev.*, **92**, 1324 (1953).

(35) R. J. Elliot, *ibid.*, **108**, 1384 (1957).

(36) H. Haken, *J. Phys. Chem. Solids*, **8**, 166 (1959).

the electron the above mass may be close to the electron mass and is in reasonable agreement with other results.²⁵

The basic shape of the chloride data is a little more complicated as shown in Fig. 9 in that three bumps, B, C, and D, follow the first threshold separated by energies of the order of 0.02 to 0.03 e.v. We previously suggested²⁹ that the first and third of these "knees," A and C, correspond to $n = 1$ and $n = 2$ excitations involving the 90°K. phonon, whereas the peaks B and D require a higher energy phonon. This is highly speculative. The structure in region D is quite broad as befits $n = 2$ and higher states. It may be that A, B, and C correspond to $n = 1$ and phonons of different energy starting with $\theta_1 = 90^\circ\text{K.}$, which is probably an acoustic-phonon, whereas B and C may belong to other branches, including the optical, or to two phonon processes.

Further analysis and assignment of phonon energies awaits new work on (1) the vibration spectrum of AgCl and AgBr, possibly by neutron scattering (an analysis of X-ray scattering data and the elastic spectrum of AgCl has been given by Cole³⁷); (2) theoretical work on the band structure, possibly along new lines³⁸; and (3) a study of the absorption edge at low temperatures with high resolution in a magnetic field. Magneto-optic data should be capable of distinguishing direct from indirect processes and should give much more detail.

A guess as to the band structure of AgCl in the absence of spin orbit interaction is shown for the reduced zone scheme in Fig. 10. Here electron energy is sketched as a function of the wave vector, $k = 2\pi/\lambda$, for two of the three principal directions, the [110] and [100]. The uppermost band indicated by Γ_1 at $k = 0$ is the empty conduction band drawn to be of nearly standard shape ($\epsilon = \hbar^2 k^2 / 2m$) near $k = 0$. One does not know how high the points x_1 and k_1 lie above Γ_1 , or for that matter the band shape away from $k = 0$. As indicated in section II-A the minimum of the conduction band at Γ_1 lies about $\chi = 3.5$ e.v. below the zero level and about $E_g = 3.2$ e.v. above the maximum of the valence band. The filled valence bands bear the designations Γ_{15} , Γ_{12} , and Γ_{25}' at $k = 0$. The first relates to 3p states of the Cl^- ion and the last two to 4d states of the Ag^+ ion. The strong exciton absorption in the ultraviolet is due to vertical transitions near $k = 0$. Therefore the point Γ_{15} is about 5.1 e.v. below Γ_1 , as shown. To a first approximation the relative position of Γ_{25} , can be arrived at from ionization energies and the Madelung potentials.^{2a}

In general a single ϵ vs. k curve must intersect perpendicular to the vertical lines at the zone boundary for the [100] and [111] directions. For these directions the intersection occurs on a face of the surface bounding the first Brillouin zone (the points marked X in the [100] direction, Fig. 10). On the other hand, intersection with the boundary of the zone occurs at an edge in the [110] direction so that the slopes may be finite at the points marked

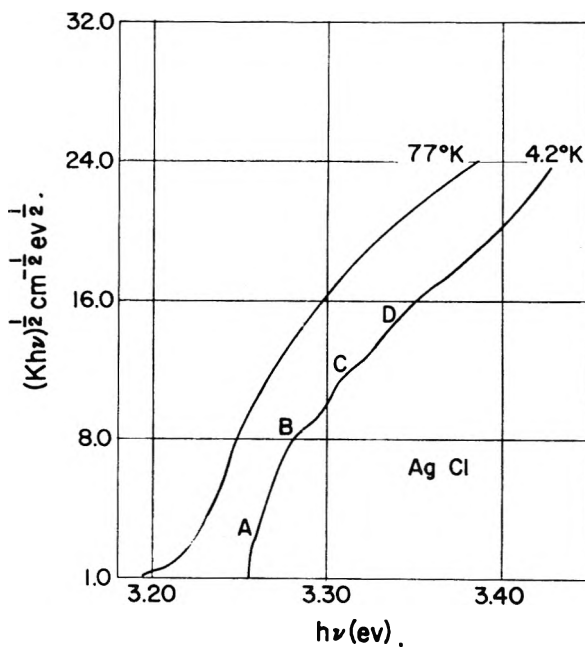


Fig. 9.—Data similar to Fig. 10 for AgCl at 4.2 and 77°K. From reference 29, courtesy of *J. Phys. Chem. Solids*.

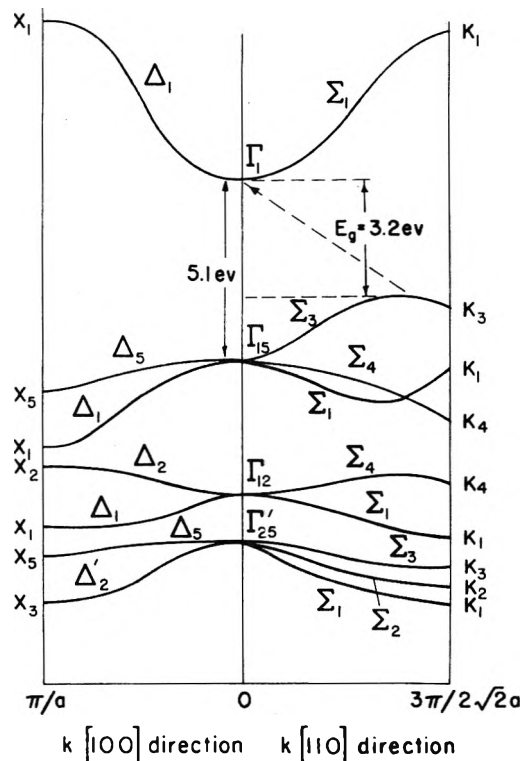


Fig. 10.—Hypothetical band structure of AgCl neglecting spin-orbit interaction. Two directions in k space are shown, the [100] and [110]. In the absence of a detailed calculation, we simply guess that the p states, Γ_{15} , associated with the Cl^- ion, lie above the d states of the Ag^+ ion, Γ_{25} and Γ_{12} at $k = 0$.

K in Fig. 10. If the maximum in the valence band actually occurs in the [110] direction it might be at points less than $k = \pi/a$, as found for KCl by Howland.²⁰ The beginning of indirect band to

(37) H. Cole, *J. Appl. Phys.*, **24**, 482 (1953).

(38) F. Bassani and R. S. Knox, private communication.

band transitions then would take place between valence and conduction band states connected by the diagonal dotted arrow in Fig. 10. The curvature of the conduction band at $k = 0$ is certainly fairly high, corresponding to a small electron effective mass,³⁹ but the curvature could be quite small at the maximum of the valence band as befits a somewhat higher hole mass. It should be emphasized that the band structure shown in Fig. 10 is hypothetical. A band calculation should be carried out to actually determine the relative positions of the Γ_{15} and Γ_{25} points. Spin orbit effects have to be taken into account and the character of the bands is expected to be considerably different from that shown in the figure, particularly as one proceeds out from $k = 0$.^{39a}

D. Efficiency of Excitation of Electrons and Holes.—A few remarks are in order on excitation efficiency first for optical excitation and second for the generation of electron-hole pairs by ionizing radiation.

Lehfeldt⁴⁰ and later Van Heyningen²³ showed that the quantum efficiency or number of conduction electrons produced per photon absorbed was high, of the order of 0.5–1.0, at 77°K. in AgCl. This statement applies not only in the beginning of absorption at long wave lengths but also in the direct exciton region in the ultraviolet. There may, however, be competing processes since a kind of structure in wave lengths was observed by Van Heyningen, who attributed at least a part of the dependence of yield on wave length to non-uniformity of electron range and imperfection of the crystal near the surface. Surface defective layers can cause the efficiency to decrease with increasing photon energy (increasing absorption constant).^{23, 41}

Similar effects of the surface can be seen from a study of photoconductivity at very low temperatures achieved by pumping over liquid helium. Figure 11 shows data obtained by Tippins²¹ for AgCl and AgBr at both 78 and 2°K. The data were taken using a vibrating reed electrometer to record a small amount of charge released by low intensity illumination from a monochromator. Care was taken to avoid polarization or space charge difficulties but the actual range or Schubweg of electrons was not determined. We can comment on the relative response at a given temperature for different wave lengths but not on the magnitude of quantum efficiency or the efficiency at 78°K. relative to 2°K.

The first thing to notice in connection with Fig. 11 is that even at 2°K. photo-response begins coincident with the absorption edge which was attributed to the onset of indirect transitions. The threshold absorption is thought to produce indirect excitons or bound states of the electron and hole.

These must have a reasonable probability for disassociation into free carriers. A second point to note is that a peaked response with decreasing yield toward shorter wave lengths is found in the cases of AgCl at both temperatures and AgBr at 2°K. This sort of behavior has been found to be dependent on preparation of the surface²³ and can be largely eliminated by careful etching. A third and important feature of the photo-response shown in Fig. 11 is the appearance of an abrupt increase, particularly at the lowest temperatures, at energies of about 0.2 e.v. beyond the threshold. This is most likely due to exciton structure and indicates the fact that the higher states, $n = 2$ and greater, are less strongly bound.

To summarize, we find that at the threshold of absorption indirect excitons are formed. They are, however, not strongly bound and can disassociate possibly at the surface with some probability into free carriers. This is also true of direct excitons produced at shorter wave lengths or higher energies. These higher energy direct excitons may actually auto-ionize or disassociate very readily, presumably because of the existence of the lower energy indirect energy gap. The surface plays an important role in these processes and can strongly influence the yield of free carriers into the bulk of the crystal.

It is appropriate at this time to point out the very high efficiency of the production of electron-hole pairs by ionizing radiation in AgCl and AgBr. An excellent estimate of the average energy to produce one electron-hole pair is had from crystal counter method.⁴² This energy turns out to be 7.5 ± 0.5 e.v. for 0.62 Mev. β -rays stopping in AgCl. A somewhat higher energy per pair was obtained in the case of α -particles incident on AgCl,⁴³ and for β -rays on AgBr.⁴⁴ These efficiencies are of the order of twice the band gap and might be explained by the fact that electron-electron scattering processes begin at about this energy. An estimate of the importance of excitons in connection with energy loss by fast particles is given in a recent note.⁴⁵ Energies to produce an electron-hole pair of about twice the band gap also are found for the elemental semiconductors.⁴⁶

The alkali halides seem to require a higher energy per pair.⁴⁷ An indirect estimate of 28 electron volts is obtained from the energy required to form one F-center in KCl containing negative ion vacancies at low temperature.⁴⁸ It would be a great help to have an adequate theoretical treatment of this energy loss problem in insulating crystals.

E. Luminescence in the Silver Halides.—It has been known for some time that AgCl and AgBr show an efficient characteristic visible luminescence at low temperature.^{49, 50} This emis-

(39) m/m_0 is of the order of 0.2 as determined by comparison of mobility data with theory [F. C. Brown and F. E. Dart, *Phys. Rev.*, **108**, 281 (1957)].

(39a) Note added in proof: Preliminary results of a valence band calculation for AgCl were presented by R. S. Knox, F. Baasani, and W. B. Fowler at a Symposium on Photographic Sensitivity, Tokyo, Sept. 14, 1962. The results are similar to Fig. 10 except that the highest lying point in the filled bands is at the zone boundary in the [111] direction.

(40) W. Lehfeldt, *Göttingen Nachr.*, [II] **1**, 171 (1935).

(41) A. M. Gordon, *Phys. Rev.*, **122**, 748 (1961).

(42) F. C. Brown, *ibid.*, **97**, 355 (1955).

(43) P. S. van Heerden, *Physica*, **16**, 505 (1950).

(44) K. A. Yamakawa, *Phys. Rev.*, **82**, 522 (1951).

(45) J. Lory, *Compt. rend.*, **250**, 3622 (1960).

(46) A. G. Chynoweth and K. G. McKay, *Phys. Rev.*, **102**, 369 (1956).

(47) H. Witt, *Z. Physik*, **128**, 442 (1950).

(48) H. Rabin and C. C. Klick, *Phys. Rev.*, **117**, 1005 (1960).

(49) G. C. Farnell, P. C. Burton, and R. Hallama, *Phil. Mag.*, **41**, 157 (1950); also **41**, 545 (1950).

(50) F. Moser and F. Urbach, *Phys. Rev.*, **106**, 852 (1957).

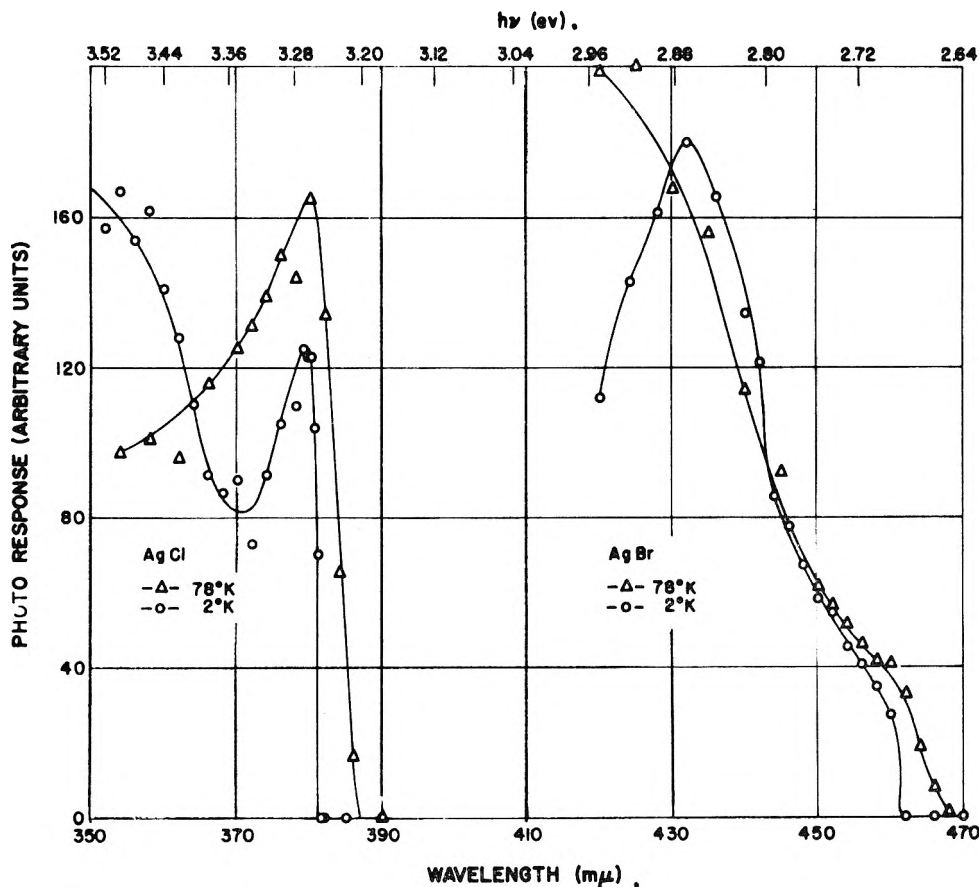


Fig. 11.—Transient photoconductivity vs. wavelength near the absorption edge for AgCl and AgBr. Photo-response is plotted vertically in arbitrary units. Each curve is drawn for a constant number of photons incident as a function of wave length. Scaling factors have been applied so that the curves for the two different materials and temperatures can be plotted on the same figure. For AgCl the photo-response at 2°K. is much lower than at 78°K., whereas it is about the same for AgBr at 2°K. as at 78°K. From reference 29, courtesy of *J. Phys. Chem. Solids*.

sion is quenched above 180°K. in AgCl and above 77°K. in AgBr. An excitation spectrum obtained on AgCl at liquid nitrogen temperature⁵¹ shows structure but the luminescence prevails for exciting wave lengths at least through the first direct exciton peak at 250 m μ . Wiegand⁵² has measured the time constant of luminescence down to liquid helium temperatures. The process seems to be associated with the transport of carriers and Wiegand suggests that holes are first trapped at positive ion vacancies which later serve as recombination centers for electrons. At least one impurity very effectively quenches the luminescence. This is the case for nickel,⁵³ which has been shown to be an effective electron trap.⁵⁴

The emission spectrum of the luminescence of AgCl has been studied at 77°K.⁵⁵ and more recently at 4.2°K. by Vacek and co-workers.⁵⁶ These investigators find an emission band which extends from 450 to 550 m μ and a red emission in the vicinity of 600 to 650 m μ . Fine structure

consisting of two different series is superimposed on the blue emission. They interpret this structure in terms of a localized exciton theory of Matyas.⁵⁷ One series involves an exciton on a positive ion vacancy, the other an exciton on a vacancy in the vicinity of a dislocation. The red emission is found to disappear at 4.2°K. and the line structure to shift to slightly longer wave lengths. Preliminary observations at the University of Illinois confirm the blue emission reported by Vacek but do not reveal the red band at 77°K. It may be the latter is associated with impurity or with photolytic silver as suggested by Farnell, Burton, and Hallama.⁴⁹

The luminescence of AgCl and AgBr is an exceedingly interesting and incompletely understood phenomenon. In some respects it resembles the edge luminescence of compound semiconductors.⁵⁸ It is possible, for instance, that the observed line structure in emission reflects the exciton structure seen in optical absorption together with a Stoke shift characteristic of the ionic crystal. Further work and careful measurements of efficiency are called for.

(51) R. S. Van Heyningen, "Transient Photoconductivity in AgCl at Low Temperature," Ph.D. Thesis, University of Illinois, 1958.

(52) A. P. Wiegand, *Phys. Rev.*, **113**, 52 (1959).

(53) R. S. Van Heyningen, private communication.

(54) A. E. Michel, *Phys. Rev.*, **121**, 968 (1961).

(55) K. Vacek, *J. Phys. Chem. Solids*, **16**, 337 (1960).

(56) K. Vacek and J. Ringeissen, *J. phys. radium*, **22**, 519 (1961); see also H. D. Koswig, *Z. Naturforsch.*, **16**, 1103 (1961).

(57) Z. Matyas, "Halbleiter und Phosphore. Vorträge de Int. Koll.," Vieweg Braunschweig S 426 (1958).

(58) R. E. Halsted, M. R. Lorenz, and B. Segall, *J. Phys. Chem. Solids*, **22**, 109 (1961).

III. Electron Mobility

Considerable experimental work has been carried out on both drift and Hall mobilities for photoelectrons in the silver halides. The main effort of this work has been to obtain an understanding of electron transport in ionic crystals in particular of the importance of various scattering processes. The polaron (electron in an ionic crystal plus associated lattice polarization) has received a good deal of theoretical attention and this serves as a compelling reason for experimental study of the electron mobility. We will not discuss the mobility measurements in detail here except to say that a general understanding of the scattering processes has been obtained for the temperature range below room temperature. There seems little doubt that the mobility of electrons in even only moderately pure AgCl and AgBr at room temperature is controlled by lattice scattering due to the longitudinal optical modes. Although the electron effective mass is quite small, the electron interaction with the optical mode reduces the room temperature mobility to values of the order of 40 cm.²/volt sec.

rather than several thousand as in elemental semiconductors.

Recent work has revealed the role which impurities play in determining mobility below 50°K. in AgCl and has demonstrated hot electron effects in the purest crystals. The results will be presented elsewhere.⁵⁹

In this paper we have discussed the results of experiments which bear on the energy band structure of AgCl and AgBr. Many details and interesting aspects of the problem have still to be cleared up. Nevertheless, we are beginning to understand the general features of the problem and one may look forward to rapid progress in the next few years.

Acknowledgment.—The author is indebted to his colleagues and students for many suggestions and for much of the work. In particular, he would like to cite the names of Drs. H. H. Tippins, Jr., G. Ascarelli, and T. Masumi. He is grateful for comments made by Professors A. Gold, R. S. Knox, and Dr. Garcia-Moliner.

(59) T. Masumi, to be published.

HALL MOBILITY OF HOLES IN SILVER BROMIDE¹

BY ROLAND C. HANSON

University of Illinois, Urbana, Illinois

Received June 20, 1962

Hall mobility measurements have been made on holes introduced into AgBr by a bromine atmosphere in the temperature range from room temperature to 150°. These measurements were made using conventional electrode geometry and sensitive high impedance a.c. techniques similar to those used by Macdonald and Robinson. The Hall mobility for holes varied from 2.0 ± 0.5 cm.²/v. sec. at room temperature (27°) to 0.5 ± 0.15 cm.²/v. sec. at 150°. The hole mobility is about $1/_{30}$ as large as the electron mobility determined by other workers at room temperature. The temperature dependence of the hole mobility is about T^{-4} . This is much steeper than the temperature dependence of the electron mobility in this region.

Introduction

The properties of holes (defect electrons) in the silver halides are of interest both because of their importance in the theory of the photographic process and because of a fundamental interest in the structure of the valence band. This paper presents the results of some Hall effect measurements on holes in silver bromide.

In the normal state, the silver halides are insulators from the electronic point of view, *i.e.*, they have a filled valence band, an empty conduction band, and a forbidden gap of several electron volts.

Electronic disorder can be produced in two ways in these crystals: (1) absorption of light quanta having energies equal to or greater than the forbidden gap produces electron-hole pairs; and (2) the absorption of excess halogen by the crystal produces free holes.

Experiments to detect the current produced by drift of the photoexcited holes have in general given no conclusive evidence for the motion of holes, although they show large currents due to the motion of electrons.¹⁻⁸

Rather indirect evidence for the motion of photo holes does come from a number of experiments which detect the hole motion by the bleaching of print out silver or latent image specks, or by the release of halogen from illuminated crystals.⁹⁻¹⁵

The effects of halogen atmospheres on silver halide crystals have been studied rather extensively.

(2) (a) K. Hecht, *Z. Physik*, **77**, 234 (1932); (b) W. Lehfeldt, *Nachr. Akad. Wiss. Göttingen, Math.-physik. Kl.*, **1**, 171 (1935).

(3) R. S. Van Heyningen and F. C. Brown, *Phys. Rev.*, **111**, 462 (1958).

(4) D. C. Burnham, F. C. Brown, and R. S. Knox, *ibid.*, **119**, 1560 (1960).

(5) F. C. Brown, *J. Phys. Chem. Solids*, **4**, 206 (1958).

(6) Quoted by L. P. Smith, "Semiconducting Materials," ed. by K. Henisch, Butterworths Scientific Publications, London, 1951, p. 114.

(7) M. S. Werman, ONR Technical Report, Department of Physics, Cornell University, Ithaca, New York, 1956.

(8) C. Yamanaka and T. Suita, *Tech. Repts. Osaka Univ.*, **5**, 47 (1955).

(9) J. F. Hamilton, F. Hamm, and L. E. Brady, *J. Appl. Phys.*, **27**, 874 (1956).

(10) J. F. Hamilton and L. E. Brady, *ibid.*, **30**, 1893, 1902 (1959).

(11) J. R. Haynes and J. W. Shockley, *Phys. Rev.*, **82**, 935 (1951).

(12) G. W. Luckey, *J. Chem. Phys.*, **23**, 882 (1955).

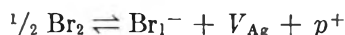
(13) C. A. Duboc, *Phys. Rev.*, **98**, 1557 (1955).

(14) F. Hamm, *J. Appl. Phys.*, **30**, 1468 (1959).

(15) H. Kanzaki in "Photographic Sensitivity," Tokyo Symposium, Vol. 2, ed. by S. Fujusawa, Maruzen Co., Ltd., Tokyo, 1958, p. 181.

(1) This work is based on a dissertation submitted in partial fulfillment of the requirements for the degree of Doctor of Philosophy at the University of Illinois, 1960. See also R. C. Hanson and F. C. Brown, *J. Appl. Phys.*, **31**, 210 (1960), for a preliminary report of this work.

The initial work of Wagner^{16,17} on the corrosion of silver by halogen gas led him to propose that the halogen atoms absorbed on the surface of the silver halide become halide ions by capture of an electron from the valence band, thus injecting a hole and also causing the injection of a silver ion vacancy to preserve neutrality in the ionic lattice. Writing a "chemical" reaction for this



where V_{Ag} is a silver ion vacancy and p^+ is a positive hole. From this, Wagner obtained the usual equilibrium relationship

$$[p] = K(T) \frac{P^{1/2}_{\text{Br}_2}}{[V_{\text{Ag}}]}$$

where $[p]$ is the concentration of positive holes, P_{Br_2} is the bromine pressure, $[V_{\text{Ag}}]$ is the concentration of silver ion vacancies, and $K(T)$ is the equilibrium constant. If the concentration of silver ion vacancies introduced is small compared with the concentration of silver ion vacancies already present (due either to divalent cation impurities or to intrinsic Frenkel disorder), the concentration of positive holes should be proportional to the square root of the halogen pressure and inversely proportional to the concentration of vacancies.

These predictions are borne out both by the data on the corrosion of silver by halogen^{17,18} and, especially by the data on the excess conductivity of silver halides in halogen atmospheres.¹⁹⁻²¹ The results of these excess conductivity measurements indicate that the excess (presumably hole) conductivity is always proportional to the square root of the halogen pressure, and at least approximately inversely proportional to the impurity concentration in the extrinsic region. Luckey's^{19,21} results also show that the time rate of conductivity increase is consistent with a diffusion limited mechanism.

In this work, experiments were performed to measure the Hall mobility of these halogen injected holes.

Experimental

A standard Hall experiment similar to that used by Macdonald and Robinson²² was performed. Alternating current was used to eliminate possible polarization and decomposition problems. Because of the high impedance of these crystals, it was necessary to use a preamplifier having a very low input capacitance as well as a high input resistance such as one of the augmented cathode followers designed by Macdonald.^{23,24}

The output of the preamplifier was amplified with a tunable narrow band amplifier and then was detected with a phase sensitive detector²⁵ and a chart recorder.

(16) C. Wagner, *Z. physik. Chem. (Leipzig)*, **B21**, 25 (1933).

(17) C. Wagner, *ibid.*, **B32**, 447 (1936).

(18) D. M. Smythe and M. Cutler, *J. Electrochem. Soc.*, **106**, 107 (1959).

(19) G. W. Luckey and W. West, *J. Chem. Phys.*, **24**, 879 (1956).

(20) L. M. Shamovskii, A. A. Dunina, and M. I. Gosteva, *Dokl. Akad. Nauk SSSR*, **106**, 830 (1956); *Soviet Phys. Doklady*, **1**, 124 (1956); *J. Ezptl. Theoret. Phys. (USSR)*, **30**, 640 (1956); *Soviet Phys. JETP*, **3**, 511 (1956).

(21) G. W. Luckey, *Discussions Faraday Soc.*, **28**, 113 (1959).

(22) J. R. Macdonald and J. E. Robinson, *Phys. Rev.*, **95**, 44 (1954).

(23) J. R. Macdonald, *Rev. Sci. Instr.*, **26**, 144 (1954).

(24) J. R. Macdonald, *Inst. Radio Engrs. Trans.*, **AU-5**, 65 (1957).

(25) N. A. Schuster, *Rev. Sci. Instr.*, **22**, 254 (1951).

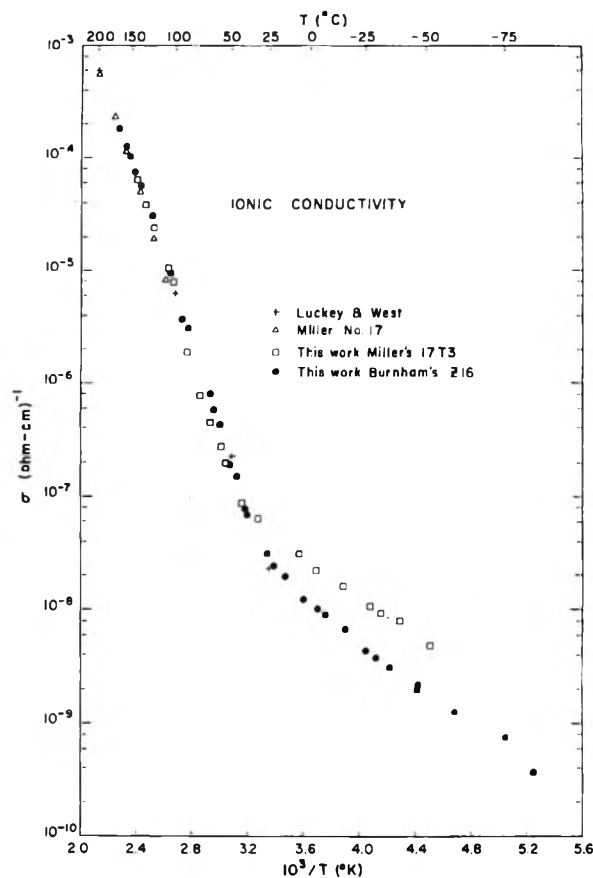


Fig. 1.—Ionic conductivity of silver bromide vs. temperature; also showing results from Miller^{26,27} and Luckey and West.¹⁹

Drift in the output due to irreversible changes in the crystal was the most serious difficulty in the experiment. The drift varied considerably between crystals. It was essentially independent of frequency and proportional to the applied electric field so no advantage could be gained by going to higher or lower frequencies or electric fields.

The crystal had painted graphite electrodes and was mounted between platinum foil. The flattened glass envelope which enclosed the crystal was surrounded by a small oven or a cold pipe which gave temperatures between -100 and 200° . These fitted between the poles of an electromagnet which gave a maximum magnetic field of 10^4 oersteds.

The envelope was connected to a manifold for evacuating and admitting the halogen. The bromine pressure was determined by the temperature of the liquid bromine in one of the side tubes of the manifold.

Two crystals were used for most of these experiments. Crystal 17T3 was grown by the Bridgeman technique from specially purified material by Miller.^{26,27} According to Miller's report, this crystal had 10 p.p.m. Fe and Cu. Crystal Z16 was from an ingot that was zone refined in vacuo by Burnham.^{28,29} According to spectrochemical analysis, this crystal had 0.25 p.p.m. Fe and 0.03 p.p.m. Cu.

Results

Ionic Conductivity.—Measurements of the ionic conductivity were made using a series resistor and an a.c. bridge method. The data are shown in

(26) A. S. Miller and R. J. Maurer, *J. Phys. Chem. Solids*, **4**, 196 (1958).

(27) A. S. Miller, Thesis, University of Illinois, Urbana, Illinois, 1957.

(28) D. C. Burnham, Thesis, University of Illinois, Urbana, Illinois, 1959.

(29) F. Moser, D. C. Burnham, and H. H. Tippins, *J. Appl. Phys.*, **32**, 48 (1961).

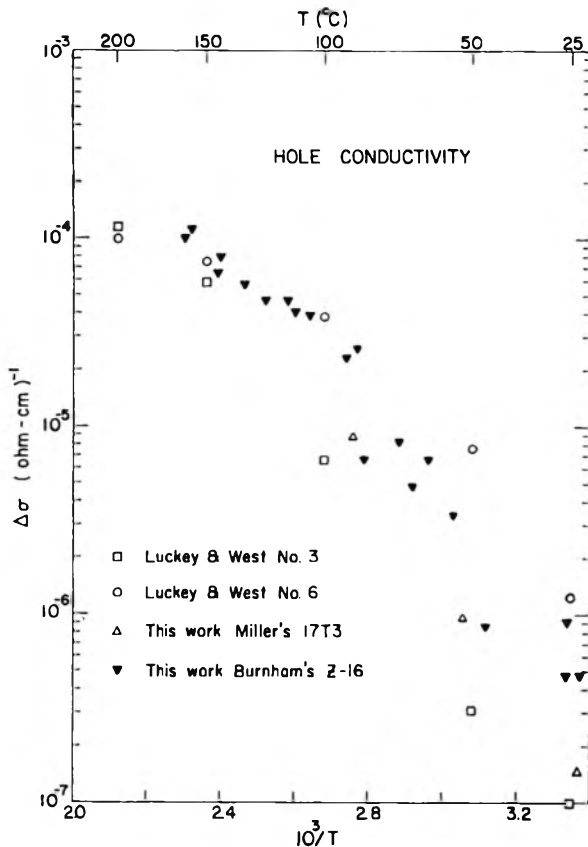


Fig. 2.—Excess or hole conductivity in silver bromide for a bromine pressure of 0.22 atm., also showing results of Luckey and West.¹⁹

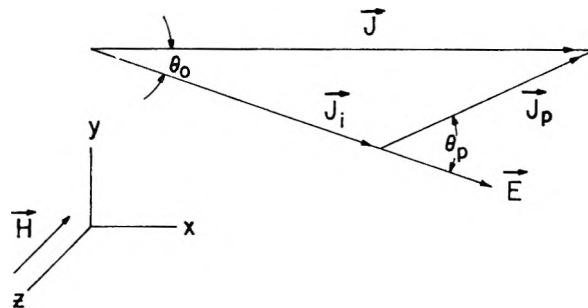


Fig. 3.—Ionic, hole, and total current density and electric field when crystal is in a magnetic field.

Fig. 1 along with representative values for quite pure crystals from the data of Miller²⁷ and Luckey and West.¹⁹

Hole Conductivity.—The excess conductivity upon the admission of bromine or chlorine was found to be independent of electric field from 0.1 to 100 v./cm. and of frequency from 50 to 5000 c.p.s. The excess conductivity was proportional to the square root of the halogen pressure in all cases.

The temperature dependence of the excess conductivity for the two crystals for a bromine pressure of 0.22 atm. is shown in Fig. 2. The excess conductivity is independent of crystal purity at the higher temperatures; however, at the lower temperatures the excess conductivity is greater in the purer Z16 than it is in 17T3.

It was observed on both crystals that the increase in conductivity upon the first exposure to bromine

at room temperature was significantly larger than on any subsequent exposure to bromine. This suggests that some permanent change was produced in the crystal by bromination.

The time constants for the conductivity increase were of the order of 1 hr. at room temperature and only somewhat faster at higher temperatures. These are much longer than the time constants reported by Luckey.^{19,21} The slow time constants probably are due to the reaction being limited by a layer of water and/or grease adsorbed on the surface of the crystal. In this experiment it was not possible to bake the crystal under vacuum as Luckey did. However, as seen in Fig. 2, the equilibrium excess conductivity in the intrinsic (high temperature range) agrees with the measurements of Luckey.¹⁹ Thus this adsorbed layer does not affect the equilibrium properties.

Hall Measurements.—It was not possible to detect a Hall effect for pure ionic conductivity (no halogen). Taking into consideration the noise generated in the crystal, the Hall mobility of the ionic carriers was less than 10^{-2} cm.²/v. sec.

With halogen atmospheres, the Hall measurements always gave results indicating the motion of positive current carriers. The measured Hall angles were independent of applied electric field from 0.1 to 100 v./cm. and of frequency from 50 to 2000 c.p.s. and were proportional to the magnetic field up to the maximum magnetic field of 10,000 gauss. Most of the measurements were made at 500 c.p.s., 1.0 v./cm., and the maximum magnetic field.

The presence of both ionic and electronic conductivity leads to an interesting dependence of the observed Hall angle upon the relative contributions of each carrier to the total conductivity. The effect is identical with the case of simultaneous electron and hole conduction in a semiconductor³⁰ except in this case the mobility of the ionic defects is negligible compared with the mobility of the holes.

In Fig. 3 E is the electric field, J_i is the ionic current density, J_p is the hole current density, and J is the resultant total current density. θ_0 is the observed Hall angle and θ_p is the Hall angle for holes. The Hall angle for the ionic current will be essentially zero. Then for small angles

$$\theta J = \theta_p J_p$$

$$\theta_p = \theta_0 \left[\frac{\sigma_0}{\Delta\sigma} + 1 \right] = \mu_p H / c$$

where σ_0 is the conductivity before bromination and $\Delta\sigma$ is the change in conductivity produced by bromination. The effect of this correction for several typical temperatures is shown in Table I.

Corrections also were made for the shorting effects of the current and Hall electrodes using the analysis of Wick³¹ and others^{32,33} and the analog method of Broudy.³⁴

(30) W. Shockley, "Electrons and Holes in Semiconductors," D. Van Nostrand Co., Inc., Princeton, N. J., 1950, p. 217.

(31) R. F. Wick, *J. Appl. Phys.*, **24**, 166 (1953).

(32) I. Isenberg, B. R. Russell, and R. F. Greene, *Rev. Sci. Instr.*, **19**, 685 (1948).

(33) J. Vogler, *Phys. Rev.*, **79**, 1023 (1950).

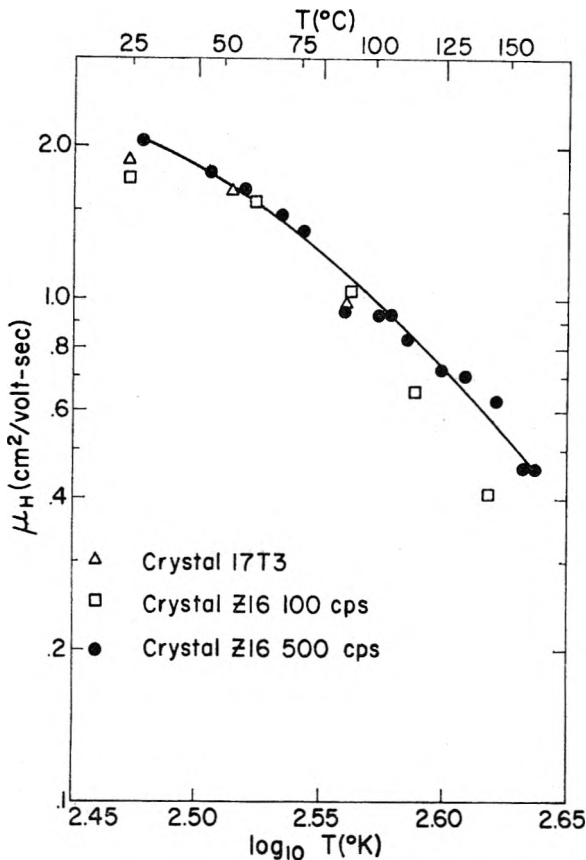


Fig. 4.—Hall mobility of holes in silver bromide vs. temperature.

TABLE I
TYPICAL DATA SHOWING DEPENDENCE OF OBSERVED HALL ANGLE ON HOLE CONDUCTIVITY AND CORRECTED HALL ANGLE FOR HOLES

T, °C.	H, k-coersted	Bromine pressure, mm.	σ_h , ohm ⁻¹ cm. ⁻¹ × 10 ⁷	$\Delta\sigma$, ohm ⁻¹ cm. ⁻¹ × 10 ⁷	1 + $\frac{\sigma_h}{\Delta\sigma}$	Observed	Corrected
						θ_p , radians × 10 ⁵	θ_p , radians × 10 ⁵
27	8.42	230	0.255	4.85	1.05	11.0	11.5
57	9.80	270	3.38	34.2	1.10	9.7	10.6
57	9.80	66	3.38	17.1	1.20	8.6	10.3
111	8.42	234	119	424	1.28	3.6	4.6
111	8.42	66	119	261	1.45	3.2	4.6
111	8.42	24	119	152	1.78	2.7	4.7

The Hall mobility of the holes as a function of temperature after these corrections have been made is shown in Fig. 4. Most of these data were taken on crystal Z16 because the noise and drift were less for this crystal. The probable error in the data on crystal Z16 ranged from ±15% at room temperature to ±25% at 150°.

The temperature range of these measurements was limited. The upper limit (about 160°) was set by the fact that the increase in conductivity upon bromination became so small that an immeasurable Hall angle was produced. The increase in conductivity was limited because the maximum pressure of bromine that could be used was the vapor pressure at room temperature. It might be

(34) R. M. Broudy, *J. Appl. Phys.*, **29**, 853 (1958).

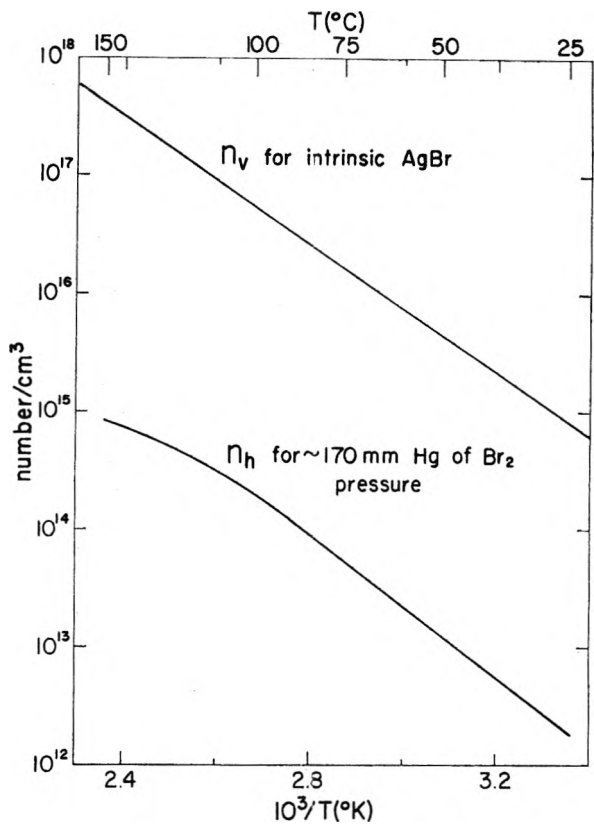


Fig. 5.—Concentration of holes in silver bromide vs. temperature for 0.22 atm. bromine pressure, and concentration of vacancies in intrinsic silver bromide from data of Teltow³⁵ and Miller.^{27,28}

possible to extend the range of these measurements by heating the whole system or by using chlorine, which would permit higher pressures. The measurements at the higher temperatures also were difficult because of the greater noise and drift. The low temperature limit was set by the high resistance of the crystal.

The concentration of free holes as a function of temperature for crystal Z16 with a Br₂ pressure of 0.22 atm. is shown in Fig. 5. This curve was calculated from $\Delta\sigma = p\epsilon\mu_p$ assuming that the conductivity mobility equals the Hall mobility. Because of the large scatter in the excess conductivity data, this curve should be regarded only as a rough indication of the hole concentration. The concentration of silver ion vacancies in intrinsic AgBr from the data of Teltow³⁵ and Miller^{27,28} also is shown in Fig. 5. This shows that the concentration of injected holes is much less than the concentration of vacancies, as was assumed earlier.

No attempt was made to detect trapped holes (V centers?) in these experiments. The presence or absence of holes trapped in shallow traps cannot be determined from experiments of this type. The recent data of Moser³⁶ on the optical absorption at approximately 1 μ induced by halogen in AgCl near the melting point may be an indication of trapped holes.

Discussion

The Hall mobility of the holes should be com-

(35) J. Teltow, *Ann. Physik*, **6**, 63, 71 (1949).

(36) F. Moser, *J. Appl. Phys.*, **33**, 343 (1962).

pared with the data for the mobility of electrons in the same temperature range. At room temperature the Hall mobility of holes of 2.0 cm.²/v. sec. compares with the drift mobility of electrons of 70 cm.²/v. sec. from the data of Yamanaka, *et al.*³⁷ The temperature dependence of the Hall mobility of the holes is approximately T^{-4} , while in the same temperature range the electron mobility will fit a $T^{-1.5}$ curve. Since these temperatures are well above the Debye temperature associated with the longitudinal optical modes (approximately 200°K. for AgBr), one would not necessarily expect the mobility to be proportional to $e^{-\theta_0/T}$ as predicted by Low and Pines³⁸ for lower temperatures. How-

(37) C. Yamanaka, N. Itoh, and T. Suita, see ref. 15, p. 175.

(38) F. Low and D. Pines, *Phys. Rev.*, **98**, 414 (1955).

ever, the very steep temperature dependence of the hole mobility is very strange, as one would expect the hole to interact with the lattice in much the same way as the electron. A temperature dependent effective mass would help to explain the steep temperature dependence. Attempts presently are being made to measure carefully the thermoelectric power of these holes in order to gain more information about the band structure.

Acknowledgments.—The author gratefully acknowledges the encouragement and guidance of Prof. F. C. Brown and Prof. R. J. Maurer during the course of this work. The fellowship provided by the Corning Glass Works Foundation for 1958–1959 and other support from the Air Force Office of Scientific Research are sincerely appreciated.

IONIC TRANSPORT PROCESSES IN THE SILVER HALIDES

BY ROBERT J. FRIAUF

University of Kansas, Lawrence, Kansas

Received June 20, 1962

The motion of ions in AgCl and AgBr has been studied by measurements of ionic conductivity and diffusion. The relationship between these phenomena is represented by the Einstein relation, and deviations from this relation can be interpreted in terms of correlation and displacement effects for diffusion. The presence of Frenkel defects is confirmed, and the occurrence of two kinds of *interstitialcy* jumps for interstitial silver ions is demonstrated. It is further estimated that the concentration of Schottky defects in AgBr cannot exceed 0.1% even at the melting point. The influence of the crystal structure and the nature of the ions on the defect structure is mentioned, and the significance of the results for the photographic process is discussed briefly.

I. Introduction

The silver halides are characterized by the presence of Frenkel defects: silver ion vacancies and interstitial silver ions. This feature of the defect structure has been recognized ever since the pioneer work of Koch and Wagner.¹ Subsequent measurements of ionic conductivity on samples doped with divalent ions have allowed the separate evaluation of the concentration of Frenkel defects and of the mobilities of vacancies and interstitials.^{2–4} The results described in this paper for AgCl and AgBr lend further confirmation to the existence of Frenkel defects and provide a more detailed description of the ionic jumps involved in the interstitial transport process.

The experiments have for the most part been carried out in the intrinsic defect region, that is, for pure crystals in the temperature range of several hundred degrees below the melting point. In this region the defect concentrations are determined by thermodynamic equilibrium, and the concentrations of vacancies and interstitials must be equal to maintain electric neutrality. At lower temperatures, below 100 to 200°, the defect concentrations usually will be determined by the presence of impurities, but the jump mechanisms for the defects that are present should be the same as at higher temperatures unless the defects are associated with impurities.

II. Conductivity and Diffusion

The presence of ionic defects is revealed most directly by measurements of ionic conductivity and of diffusion of radioactive tracers. Both of these phenomena occur by means of motion of defects through the crystalline lattice: diffusion represents a mixing of atoms by virtue of the random, thermally induced jumping of defects, whereas conductivity results from a slight drift velocity superimposed on the random motion by an applied electric field. The close relationship between the two phenomena is expressed quantitatively by the microscopic Einstein relation.⁵

$$d/\mu = kT/q \quad (1)$$

Here d is the microscopic diffusion coefficient, μ the mobility, and q the charge of the defect being considered.

In order to obtain a relationship between directly measurable quantities, it is necessary to introduce appropriate macroscopic quantities, namely, the conductivity, σ , and the macroscopic diffusion coefficient, D

$$\sigma = qn\mu, D = (n/N)d \quad (2)$$

where n is the concentration of defects and N is the concentration of atoms of one kind. By combining eq. 1 and 2 the normal form of the macroscopic Einstein relation is obtained.

(1) E. Koch and C. Wagner, *Z. physik. Chem.*, **B38**, 295 (1937).

(2) J. Teltow, *Ann. Physik*, **5**, 63, 71 (1949).

(3) S. W. Kurnick, *J. Chem. Phys.*, **20**, 218 (1952).

(4) I. Ebert and J. Teltow, *Ann. Physik*, **15**, 268 (1955).

(5) N. F. Mott and R. W. Gurney, "Electronic Processes in Ionic Crystals," 2nd Ed., Clarendon Press, Oxford, 1948, p. 63.

$$D_{\sigma} / \sigma = kT / Nq^2 \quad (3)$$

Since there usually are deviations from this relationship, for reasons described in section III, it is convenient to represent the experimental results in dimensionless form by introducing an experimental correlation factor

$$f_{\text{exp}} = D_{\text{exp}} / D_{\sigma} \quad (4)$$

where D_{exp} is the measured diffusion coefficient and D_{σ} is calculated from the conductivity by eq. 3.

III. Correlation and Displacement Effects

Deviations from the macroscopic Einstein relationship usually are traceable to a modification of the expression for the macroscopic diffusion coefficient in eq. 2. The existence of correlation effects for vacancy diffusion was first recognized by Bardeen and Herring.⁶ They pointed out that whereas a vacancy moves through the lattice in a genuine random walk sequence, the motion of a tracer atom has correlations between the directions of successive jumps. Suppose, for instance, that a vacancy has just caused a tracer atom to jump to the right; since the vacancy is now to the left of the tracer atom, a return jump is more likely than any other. Hence the diffusion coefficient measured by means of tracer atoms is somewhat less than would be expected from the conductivity.⁷

The various possible jump mechanisms for an interstitial ion in a silver halide are shown in Fig. 1. For the direct jump there is no correlation effect at all. For the remaining interstitialcy jumps, in which the interstitial ion knocks a neighboring silver ion out of a lattice site and then occupies the vacated site,^{2,8} there are displacement as well as correlation effects. For the collinear interstitialcy jump, for instance, the displacement of charge is twice as large as the displacement of either of the ions involved in the jump, and hence the relationship between conductivity and diffusion is affected. The experimental results indicate that both ν_1 and ν_2 jumps occur (ν_3 and ν_4 jumps presumably have too large an activation energy), and these will be designated simply as collinear (ν_1) and non-collinear (ν_2) in the following discussion. The actual path of an interstitial defect consists of a random mixture of the two kinds of jumps, with a frequency ratio depending on the temperature, and the correlation and displacement factors depend on this ratio. Values of correlation, displacement, and over-all combined correlation factors are given in Table I.

The theoretical evaluation of displacement factors is rather simple. The calculation of correlation factors is more complicated, but it can be reduced to a problem in diffusion of probability, and values have been obtained for all of the processes of in-

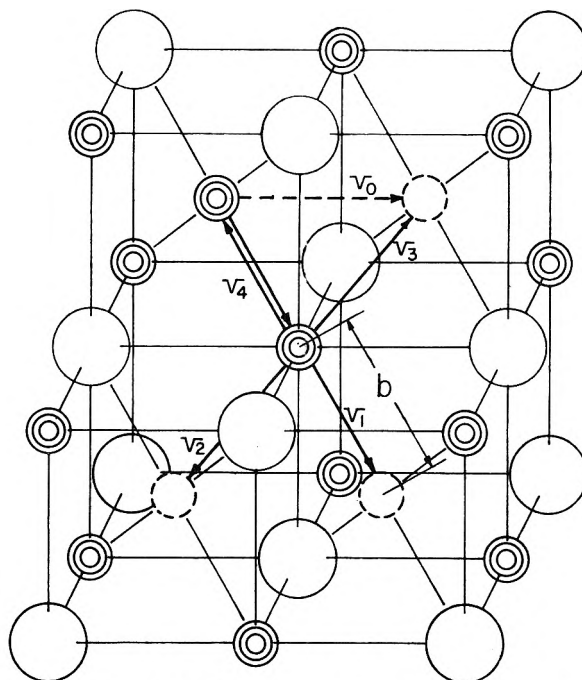


Fig. 1.—Interstitial jump mechanisms in AgCl and AgBr. Direct jump, ν_0 ; interstitialcy jumps: collinear, ν_1 ; non-collinear forward, ν_2 ; non-collinear backwards, ν_3 ; place exchange, ν_4 .

TABLE I
THEORETICAL CORRELATION AND DISPLACEMENT FACTORS FOR DIFFUSION IN THE SILVER HALIDES (NaCl TYPE STRUCTURE)^a

Mechanism	Correlation factor	Displacement factor	Over-all correlation factor
Vacancy	0.78146	1	0.78146
Direct interstitial (ν_0)	1	1	1
Collinear interstitialcy (ν_1)	$1/2$	$2/3$	0.3333
Non-collinear interstitialcy (ν_2)	$3/4$	$32/33$	0.7273
Mixed interstitialcy ($\nu_1 = \nu_2$)	$3/5$	0.8782	0.5269

^a Values are taken from ref. 9.

terest in the silver halides. The important feature for our present purposes is that these values are determined by the geometry of the structure and of the mechanism for defect motion. Hence by comparing experimentally determined correlation factors from eq. 4 to a table of theoretical values such as Table I, it is possible to identify the particular kind of defect motion in considerable detail.

IV. Interpretation of Experimental Results

The rather similar behavior of AgCl and AgBr is shown by the experimental results in Fig. 2 and 3. In each case the halogen diffusion is very small, indicating that any contribution by vacancy pair diffusion to the motion of silver ions is negligible;

(10) W. D. Compton, *Phys. Rev.*, **101**, 1209 (1956); W. D. Compton and R. J. Maurer, *J. Phys. Chem. Solids*, **1**, 191 (1956).

(11) R. J. Friauf, *Phys. Rev.*, **105**, 843 (1957).

(12) A. S. Miller and R. J. Maurer, *J. Phys. Chem. Solids*, **4**, 196 (1958).

(13) D. Tannhauser, *ibid.*, **5**, 224 (1958).

(6) J. Bardeen and C. Herring, in "Imperfections in Nearly Perfect Crystals," W. Shockley, Ed., John Wiley & Sons, Inc., New York, N. Y., 1952, p. 261.

(7) A more complete description, and a mathematical formulation, of correlation and displacement effects is given, for instance, in R. J. Friauf, *J. Appl. Phys.*, **33**, 492 (1962).

(8) F. Seitz, *Acta Cryst.*, **3**, 355 (1950).

(9) K. Compaan and Y. Haven, *Trans. Faraday Soc.*, **52**, 786 (1956); **54**, 1498 (1958).

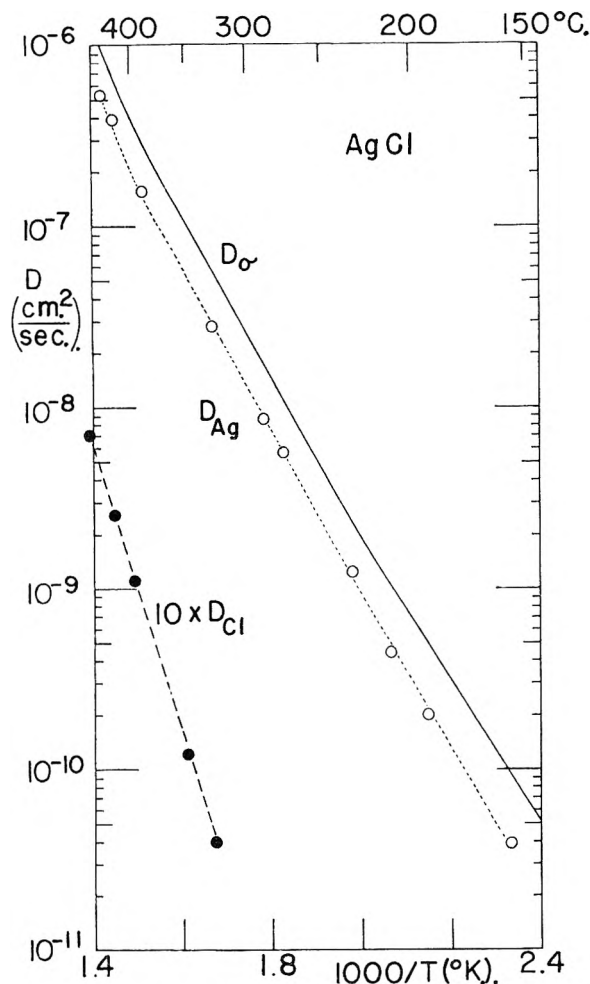


Fig. 2.—Diffusion coefficients for AgCl, from ref. 10. D_{σ} is calculated from the observed ionic conductivity by means of eq. 3.

this result is in agreement with transport experiments, which also show that the conductivity is due entirely to the motion of silver ions.^{3,14} Furthermore, both transport experiments and direct observations^{15,16} indicate that the electronic conductivity (in the dark) is several orders of magnitude smaller than the observed conductivity. Deviations from the normal Einstein relation caused by correlation and displacement effects are shown by the fact that D_{Ag} is noticeably smaller than D_{σ} .

The results for AgBr have been analyzed to determine the relative contributions of the two types of interstitialcy processes.¹¹ At each temperature the contribution of silver ion vacancies is subtracted by using the known transport numbers, and the ratio of jump frequencies (ν_1/ν_2) then is determined so as to make the theoretical interstitial correlation factor agree with the experimental value. Finally, the temperature dependence of the frequency ratio gives the activation energies in Table II.

(14) C. Tubandt and H. Reinhold, *Z. Elektrochem.*, **29**, 313 (1923); **31**, 84 (1925).

(15) J. Teltow, *Z. Physik. Chem.*, **195**, 213 (1950).

(16) K. V. Kiukkola and C. Wagner, *J. Electrochem. Soc.*, **104**, 304, 397 (1957); B. Ilachner, *J. Chem. Phys.*, **28**, 1109 (1958).

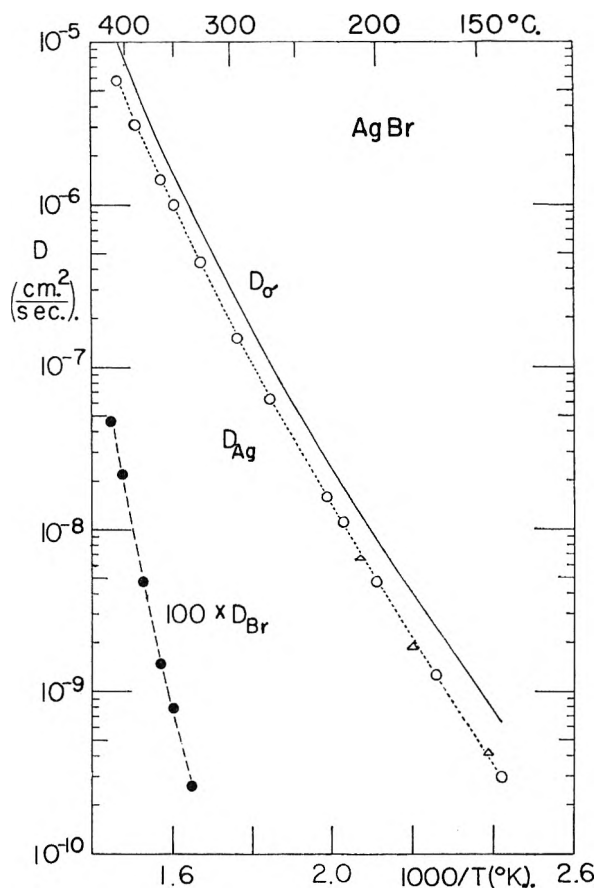


Fig. 3.—Diffusion coefficients for AgBr. Ionic conductivity and silver diffusion \circ are from ref. 11, silver diffusion Δ from ref. 12, and bromine diffusion from ref. 13.

Results for the diffusion of silver in AgBr at pressures up to 8000 atm. recently have been reported.¹⁷ The initial effect of pressure is to decrease the interstitial correlation factor f_i . This trend appears reasonable, for increasing pressure should tend to favor the collinear interstitialcy process, with its smaller free volume of activation, over the non-collinear process. At higher pressures, however, there is an upward trend of f_i , and in one case $f_i > 1$. The reason for these results is not clear; it may be that systematic experimental errors exist because of the sample preparation, uncertainties in temperature measurements, or lack of genuine hydrostatic pressure.

V. Discussion

The analysis of the results for AgBr definitely shows the presence of both collinear and non-collinear interstitialcy processes. Even though it is not feasible to carry through a detailed analysis for AgCl, the results are qualitatively very similar, and in particular it appears clear that the two kinds of interstitialcy processes must also be present in this substance. The comparison of the experimental and theoretical activation energies in Table II shows several interesting features, in particular the very low activation energy for collinear interstitialcy jumps. Also the large predicted energy

(17) A. N. Murin, B. G. Lur'e, and N. A. Lebedev, *Soviet Phys. Solid State*, **2**, 2324 (1961).

TABLE II

ACTIVATION ENERGIES FOR DEFECTS IN THE SILVER HALIDES

Process	Activation energies, e.v.		
	AgCl (exptl.)	AgCl (theory)	AgBr (exptl.)
Formation of Frenkel defects	1.69 ^b	1.76 ^c	1.27 ^a
Vacancy jump	0.33 ^b	<1.2 ^c	0.36 ^a
Interstitiality jump (average) ^a	0.15 ^b		0.15 ^a
Collinear interstitiality jump (ν_1)		-0.1 to 0.4 ^d	0.078 ^f
Non-collinear interstitiality jump (ν_2)		<0.8 ^d	0.23 ^f
Direct interstitiality jump (ν_0)		>3.0 ^d	

^a These values are obtained from electrical conductivity measurements, in which it is impossible to distinguish different kinds of interstitiality processes. ^b From ref. 4. ^c From ref. 18. ^d From ref. 18 and 19. ^e From ref. 2. ^f From ref. 11.

for the direct interstitial jumps is in good accord with the absence of these jumps in the experimental analysis.

The possibility of a negative activation energy for the collinear interstitiality jump merely indicates that an interstitial ion at the center of a small cube of the structure may not be in a stable position. The alternative arrangement may be called a dumbbell configuration: two silver ions share equally in the space around one lattice point.¹⁹ The dumbbell would diffuse through the crystal by oozing from one lattice site to another. If the orientation of the dumbbell does not change in this process, the over-all correlation factor is the same as for the collinear interstitiality process; if the dumbbell rotates while oozing, the result is the same as for the non-collinear interstitiality.²⁰ Hence even the analysis of the correlation effects cannot distinguish between these possibilities. In either case there is a remarkable similarity to the crowdion suggested a few years ago.²¹

Studies of diffusion in other ionic crystals demonstrate the profound influence of the crystal structure and the nature of the ions on the defect structure. In all of the alkali halides with the NaCl type structure, Schottky defects—equal numbers of cation and anion vacancies—are present, with cations considerably more mobile than anions. The rather different behavior of the silver halides, even though they have the same crystal structure, usually is

ascribed to the large polarizability of the silver ion with its newly filled d electron shell. For TlCl,^{7,22} CsBr,²³ and CsI,²³ however, all of which have the CsCl structure, it appears that Schottky defects predominate with the anion more mobile in all cases. Thus even the larger polarizability and smaller ionic radius of Tl⁺ compared to Cs⁺ do not seem to be sufficient to cause a change in the type of defects present in this structure.

One interesting feature of the results for AgBr is the indication that no large concentration of Schottky defects occurs at high temperatures, as has sometimes been suggested.^{3,24} If the concentration of Schottky defects were to become comparable to the concentration of Frenkel defects, the additional silver ion vacancies contributed by the Schottky defects would suppress the concentration of interstitial ions by a common ion effect, and with a greater fraction of the diffusion being caused by vacancies, the experimental correlation factor should become larger. Instead there is a decrease, for which only a very tentative explanation involving a general loosening of the lattice as a prelude to melting has been offered.¹¹ The unexpected downward trend near the melting point obscures the interpretation of the absence of Schottky defects to some extent, but it appears that an upper limit of about one tenth of the Frenkel defect concentration is reasonable. This would still allow a concentration of Schottky defects of about 0.1% at the melting point; such a value is apparently sufficient to account for conductivity²⁵ and dislocation climb²⁶ effects attributed to frozen-in Schottky defects in quenched samples.

It is evident that the ionic defects in the silver halides play an important role in the photographic process. In order for a latent image to be formed, it is necessary for a certain number of silver ions to come together at a single spot. The mass transport required for this coagulation is made possible by the large mobility of interstitial silver ions at room temperature, which in turn is due to the very low activation energy for the collinear interstitiality process. This feature, coupled with the fact that metallic silver forms a stable final image, is undoubtedly one of the primary reasons for the pre-eminent position of the silver halides among photographic materials.

(22) R. J. Friauf, *J. Phys. Chem. Solids*, **18**, 203 (1961).

(23) D. W. Lynch, *Phys. Rev.*, **118**, 468 (1960).

(24) O. Stasiw, *Z. Physik*, **127**, 522 (1950).

(25) H. Layer, M. G. Miller, and L. Slifkin, *J. Appl. Phys.*, **33**, 478 (1962). See also H. Layer and L. Slifkin, *J. Phys. Chem.*, **66**, 2396 (1962).

(26) J. W. Mitchell, *J. Appl. Phys.*, **33**, 406 (1962).

(18) J. E. Hove, Thesis, Cornell Univ., 1953.

(19) J. E. Hove, *Phys. Rev.*, **102**, 915 (1956).

(20) A. B. Lidiard, *Nuovo Cimento*, **7**, Suppl. No. 2, 620 (1958).

(21) H. R. Paneth, *Phys. Rev.*, **80**, 708 (1950).

THE ROLE OF MOBILE SILVER IONS IN LATENT-IMAGE FORMATION

BY J. F. HAMILTON AND L. E. BRADY

*Communication No. 2286 from the Kodak Research Laboratories, Eastman Kodak Company, Rochester, 5, N. Y.**Received June 20, 1962*

The effective dark conductance of the silver bromide grains of a photographic emulsion is higher by about two powers of ten than that of bulk silver bromide. The value increases with the surface-to-volume ratio of the grains and is markedly reduced by silver ion complexing agents adsorbed to the grain surface. These observations indicate that the surface is important in determining the dark electrical conductance of these grains. Reduction of the conductance by silver-complexing agents is accompanied by an increase in the high-intensity reciprocity law failure of the emulsion, showing that these mobile silver ions are also those involved in the ionic step during the growth of latent-image centers. A striking increase in electron lifetime caused by silver-complexing agents shows that these same mobile silver ions are instrumental in the initial trapping of photoelectrons in these grains.

The Principles of the Experiments

The absorption of a flash of light by the silver halide grains of a photographic emulsion causes the liberation within those grains of free electrons and holes. If, at the time of the flash, a strong electric field exists within the grains, the subsequent motion of the electrons and holes is influenced by the electrostatic force acting upon them. The electrons drift toward the positive electrode, become trapped preferentially on the sides of the grains nearest that electrode, and combine with silver ions to form aggregates of silver atoms. These act as developable latent-image centers, and are distributed with a preference for the positive sides of the grains.

The techniques for making such flash exposures on emulsions in high electric fields, and the techniques for determining the latent-image distributions thereafter, already have been described in detail.¹⁻³

The timing of the light flash with respect to the charging of the condenser is a critical factor for the displacement of the electrons. Each of these produces a rather short transient condition within the grain, and these two conditions are simultaneously necessary for the observed results. On the one hand, the grains are ionic dark conductors, and the electric field within the grains decays as conduction takes place; and on the other hand, the concentration of free photoelectrons decays to a negligible fraction within a short time, as they become localized at trapping sites.

It has been shown previously³ how controlled delays between the light and the electric field may be used to study the duration and form of either decay. If the condenser is charged before the light flash, then the technique of varying the delay interval can be used to determine the decay time of the field owing to ionic conduction; and if the light flash precedes the application of the field, then the dependence of latent-image displacement upon the delay interval reveals the length of time that the electrons remain free before final trapping.

In all experiments reported up to this time, the flash intensity was kept low, and each grain absorbed less than 10 quanta per flash. To obtain sufficient total exposures, the light was flashed repetitively as many as 1000 times, the condenser

being discharged between successive flashes and recharged at the specified time. In the present experiments, some exposures were made using only a single, high-intensity flash. The illuminating element from a high-pressure, mercury vapor lamp (General Electric H-2) was found to produce flashes of such high intensity that even unsensitized emulsions could be adequately exposed. The duration of the flash from this lamp, however, is slightly over 0.5 $\mu\text{sec.}$, so that quantitative measurements of field-decay times or electron lifetimes in this range have not yet been possible with single-flash exposures. In this range of times, only approximate upper limits can be set.

The use of multiple flashes with low intensity offers the advantage of assuring that the concentrations of photoelectronic carriers are always well below that at which any appreciable space charge could build up and limit their displacement. It has one feature which may constitute a disadvantage, at least in measuring dark ionic properties of the grains.

Consider the detailed sequence of one of the multiple exposures. First a field is applied. The ionic charges begin to move, causing a gradual decrease in the field strength. Then the light flash strikes the grain, freeing the photoelectrons and holes. These are displaced, to an extent which depends upon the residual field strength, and eventually are trapped. There follows an interval of a millisecond, during which time various events occur, or begin to occur, to re-establish a stable equilibrium. Silver ions presumably combine with the trapped electrons. Trapped holes probably also are neutralized, either by existing silver ion vacancies or by the liberation of new interstitial silver ions. Bromine may be liberated, single silver atoms may decompose thermally, the Frenkel equilibrium at least begins to be re-established, and so on. Now the field again is applied, and again decays. But the conductivity of the grains may be different, during the second decay, because of the photochemical changes which have occurred as a result of the first flash of exposure. As the exposure continues, these changes become progressively more significant, and by the last flash it is possible that the field decay may be entirely different from that in the unexposed grain.

In experiments of this kind, the over-all fraction of the electrons displaced is some sort of weighted average of the fractions displaced during each flash, and a measurement of field decay gives also

(1) J. H. Webb, *J. Appl. Phys.*, **26**, 1309 (1955).

(2) J. F. Hamilton, F. A. Hamm, and L. E. Brady, *ibid.*, **27**, 874 (1956).

(3) J. F. Hamilton and L. E. Brady, *ibid.*, **30**, 1893, 1902 (1959).

some average of the individual decays. The conductance, as determined from such a measurement, is characteristic of a grain, not in its unexposed state, but rather at some intermediate stage of exposure.

If an exposure is made, on the other hand, by a single, high-intensity flash, after a field pulse, then the field decay occurs only once, entirely before any exposure, and the conductance measured in this way is that of the unexposed grains.

In measuring electron lifetimes, in which case the light flash precedes the application of the field, the distinction between multiple- and single-flash exposures is of a different nature. First of all, there is a large intensity difference, which might in itself be responsible for a difference in the kinetics of electron-trapping. When the exposure is made with many low-intensity flashes, there are never more than a few electrons free at a time. If a grain contains a few electron traps with very large cross-section, these may be sufficient to effect the trapping of a small number of electrons. A high-intensity flash, however, frees a much larger number of electrons in a grain, perhaps much larger than the number of traps with large cross section. In this case only a few of the electrons can be trapped at those centers, and the additional ones must remain free until they are captured by less effective traps. Thus, a dependence of electron lifetime on intensity may result.

In addition, as the trapping continues, some of the filled traps may be reset, forming silver atoms or aggregates of silver atoms. These reset traps may well be more effective than those originally present in the grains. If this is the case, then the probability of trapping will increase as silver forms.

The consequences of a change in trapping probability are most easily visualized by examining a simplified extreme case. Suppose that a single, abrupt increase in trapping probability occurs when half of the photoproduct has been found. Figure 1a represents the effect of this change on a measurement made by applying a number u of low-intensity flashes. In each of these flashes, an average number n_0/u of electrons is freed in a grain. For the first half of the flashes, these are trapped with low probability, and the value of n , the number still free, decreases gradually, with a time constant τ_{e1} . In the last half of the flashes, the trapping probability increases drastically, and n decays much more quickly, with $\tau_{e2} < \tau_{e1}$. In the measurement, each of these individual decays contributes in such a way that the value determined for τ_e is neither τ_{e1} nor τ_{e2} , but is intermediate between the two. In Appendix I, the significance of such a measurement is considered in more detail.

Figure 1b represents schematically the situation encountered in a single-flash exposure. In this case, the entire number n_0 of electrons is freed by the single light flash at time zero. The first half of these are trapped with the initial low probability and n decays to a value of $n_0/2$ with the time constant τ_{e1} . As these traps are reset, the trapping probability increases, a break occurs in the curve, and it drops sharply, with the time constant

τ_{e2} .

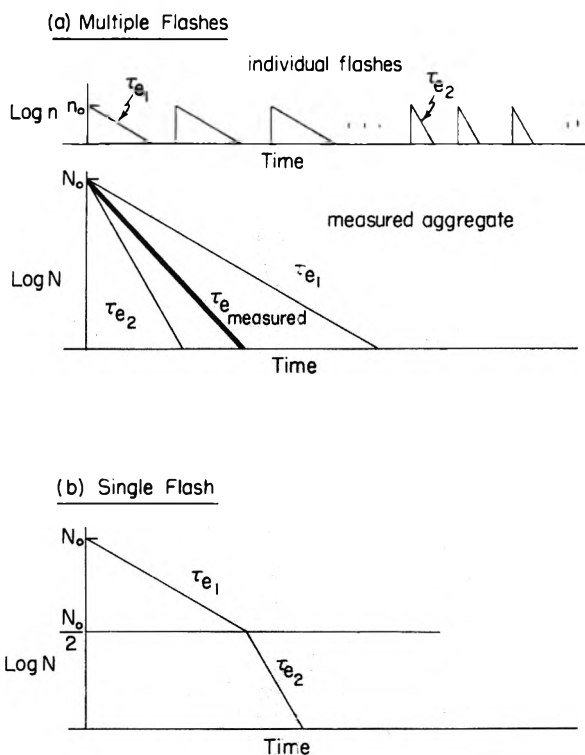


Fig. 1.—Schematic diagram illustrating the effect of an exposure-induced change in trapping probability on the results of (a) a multiple-flash and (b) a single-flash measurement of electron lifetimes.

If a change in trapping probability should occur, it would not, of course, appear as a single abrupt decrease, but rather as a gradual transition. The general effect is that shown in this simplified example, *viz.*, a multiple-flash measurement results in a lifetime value somewhere intermediate between the initial and final ones, whereas a single-flash measurement produces a curve which is concave downward, with its slope at any point being characteristic of the trapping probability at that stage of photoproduct formation.

Thus, for short delay times, single-flash measurements of electron lifetimes reflect the probability of trapping of an electron at a virgin site while multiple-flash measurements are more characteristic of the subsequent trapping of electrons at the same site; single-flash measurements are related to the *initiation or nucleation* of latent-image centers; multiple-flash, to their *growth*.

Results and Discussion

A. Ionic Conduction.—In experiments reported earlier,³ it was found that, in the unsensitized, large, silver bromide grains of an emulsion of the type described by Trivelli and Smith,⁴ the characteristic decay time of a field was just under a microsecond at room temperature. The electric field decay, as measured in this way, may be thought of as analogous to the decay of potential across a leaky condenser, and as such may be shown to be related to the electrical conductance σ of the grain by the approximate relation

(4) A. P. H. Trivelli and W. F. Smith, *Phot. J.*, **79**, 330 (1939).

$$\tau_i = RC \approx \frac{\epsilon}{4\pi\sigma} \quad (1)$$

where τ_i is the decay time, R and C are the effective resistance and capacitance of the grain, and ϵ is its dielectric constant. By this relation, a measured field decay time may be converted to an effective value of electrical conductance and compared with values measured on bulk silver halide samples.

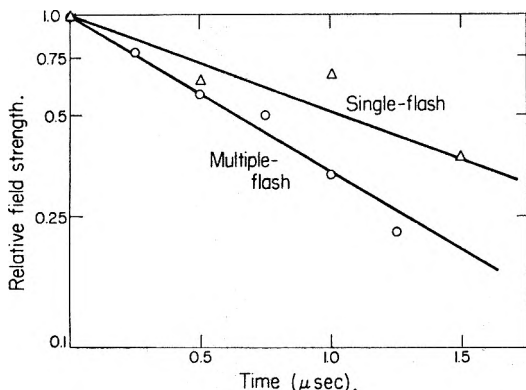


Fig. 2.—Electron field-decay curves for AgBr emulsion measured by multiple-flash (○) and single-flash (Δ) techniques.

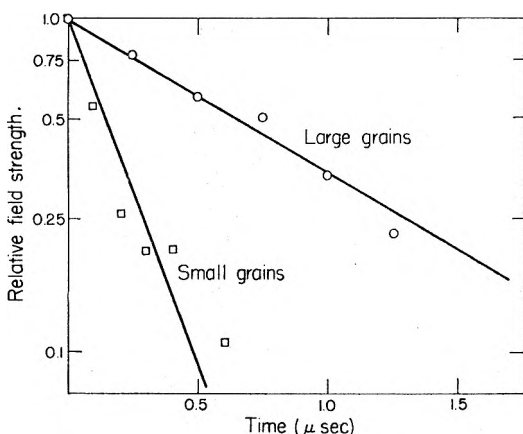


Fig. 3.—Electric field-decay curves for AgBr emulsions with different grain sizes: (○) larger grain, (□) smaller grains.

The field decay observed for these grains indicated that their effective ionic conductance was almost two powers of ten greater than intrinsic conductance in bulk silver halide. The determination was made using multiple-flash exposures, and was subject to the possible influence of an exposure-induced change in dark conductance. The decay unfortunately is too short to be measured precisely by single-flash techniques, but a semiquantitative confirmation of the rapid field decay has been made in this way. In Fig. 2 are shown the single-flash decay (triangles) and the multiple-flash decay (circles) of the field in the grains of the same emulsion used previously. Because of the long duration of the light flash, possibly combined with a space-charge effect, the maximum fraction of the image displaced by a single flash in this emulsion is only about one-half, and the precision of this curve is not high. Taken at face value, these

curves seem to indicate an increase in conduction with exposure, of perhaps 50%. This difference may well be within the limit of experimental error, and no significance can justifiably be attached to it at this time. The important feature of these curves is that there is no very large effect of exposure on field-decay time. Thus, the higher-than-intrinsic conductivity found previously is shown to be a property of the grains of this emulsion prior to exposure.

When this high dark conductivity was first observed, it was presumed to result from mobile ionic carriers associated in some unknown way with the grain surface. Evidence tending to confirm this idea is provided by the dependence of the field decay on the ratio of surface-to-volume of the grains of the emulsion. Figure 3 shows a comparison of the multiple-flash, field-decay curves of two primitive silver bromide emulsions alike in every respect except grain size. The larger-grained of these emulsions is the same as that represented by Fig. 2, and the grains of the other emulsion have a mean linear dimension (the cube root of the mean volume, as determined from shadowed electron micrographs) smaller by a factor of about four. The decay time indicated for the smaller-grained emulsion is about 0.2 μsec., less by a factor of 4.5 than that of the larger-grained emulsion. This ratio is remarkably close to that of the linear dimensions of the grains.

A decay of 0.2 μsec. is about the lower limit of the measuring technique, however, and the agreement cannot be taken as quantitative. In a qualitative way, the conductivity is shown to increase with the surface area, and the suggested importance of the surface is supported.

Further and still stronger evidence for the importance of the surface is provided by the fact that many substances added to the emulsion after precipitation and before coating (or after coating, by bathing treatments) very markedly influence the field decay. Figure 4 shows, on a very much compressed scale, the same data shown in Fig. 2 and 3 for the large-grained emulsion, compared with the results of single-flash, field-decay measurements on a similar emulsion, to which had been added, prior to coating, 0.1 g. of phenylmercaptotetrazole (PMT) per mole of silver bromide. This compound is tightly adsorbed to the surface of the silver bromide. Its addition to the emulsion may be seen to have increased the field-decay time in the grains by a factor of almost 50. These results show clearly that conditions at the grain surface exert a controlling influence on the dark conductivity of the grain.

They provide, in addition, another vital piece of information. It is known that PMT, for example, has a very strong affinity for silver ions, forming with them a highly insoluble complex. It is adsorbed at the silver bromide surface by means of the complex bond with surface silver ions. Hence, its effect on dark conductivity establishes the fact that the principal ionic current carrier is a silver ion, not a surface bromide ion nor a silver ion vacancy in the lattice.

A variety of surface-controlled electrical effects

are to be expected at interfaces such as that between a photographic grain and the gelatin binder. Excess conduction can result either from ions moving along the physical interface, or from interstitial ions and/or vacancies introduced at the surface, but moving through the crystal lattice. Although a distinction between these two types of effect is not essential to the main conclusions of this investigation, it is nevertheless a question of great interest and importance. Some attempts to clarify the mechanism of the enhanced conduction have been made, but so far they have been inconclusive. A further discussion of the apparent alternatives is given in Appendix II. For simplification in describing the remainder of the present investigation, it will be assumed that the conduction is a volume process, and that the mobile silver ions which have been shown to be the predominant current carriers are interstitial silver ions. Their concentration is determined by an equilibrium with the silver ions at the grain surface and, indirectly, with the excess silver ions in the gelatin. This equilibrium causes the concentration of interstitial silver ions to depend upon the surface-to-volume ratio. An agent such as PMT forms an undissociated complex with some of the surface ions, removing them from the reversible exchange with the interstitials. Thus, the equilibrium is upset, and the concentration of interstitials is reduced.

B. Reciprocity-Law Failure.—In the latent-image process, trapped electrons are believed to combine⁵ with mobile silver ions, presumably the same mobile silver ions which are responsible for electrical conduction in the grains. Using somewhat different electrical techniques, Klein and Matejec⁶ have been successful in demonstrating this identity experimentally. Thus, electrical measurements of this type are related directly to one step in the process of latent-image formation.

High-intensity, reciprocity-law failure is understood to result from the finite time for this ionic step. A silver ion must be added to a center between the trapping of two electrons at that site in order to neutralize the electrostatic repulsion between the two. If ionic conduction is high, this neutralization step occurs rapidly, and two electrons liberated within a short time of one another can be used efficiently at the same site. A correlation is to be expected, therefore, between high ionic conduction (and rapid electric field decay) and the reduction of high-intensity failure.

Evidence for such a correlation was given by Kartuzhanskii,⁷ who compared the two properties in silver chloride, silver chlorobromide, and silver bromide materials, by Fujisawa and Mizuki,⁸ who studied changes produced by cadmium and lead

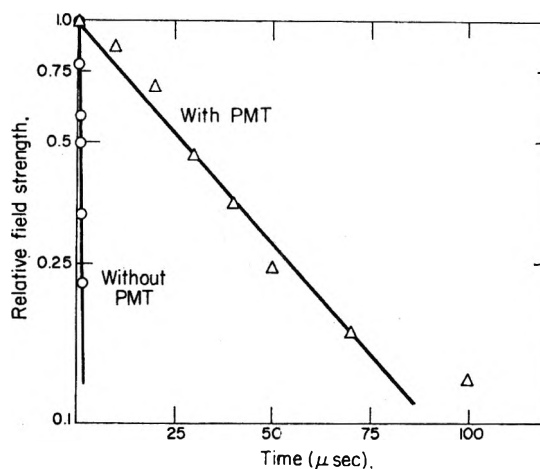


Fig. 4.—Electric field-decay curves for large-grained AgBr emulsions without (O) and with (Δ) the inclusion of 0.1 g. of phenylmercaptotetrazole per mole of AgBr.

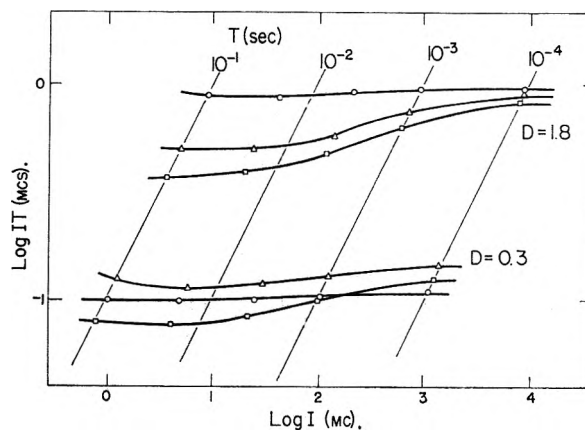


Fig. 5.—Reciprocity-law-failure curves for AgBr emulsions with no additions (O), with phenylmercaptotetrazole (Δ), and with hydroxymethyltetraazaindine (\square).

salts on the response of photographic emulsions, and by Wakabayashi and Kobayashi,⁹ whose investigations dealt with minute quantities of lead salts.

In Fig. 5 is shown the effect of the change in dark conductance introduced by silver ion complexing agents on the high-intensity sensitivity of an emulsion. These data were taken from a medium-grained, silver bromide, Trivelli-Smith emulsion, optimally sulfur-sensitized. The circular points represent the response of the emulsion with no additions. The curves are quite flat, showing that the law of reciprocity is followed quite closely throughout this range of exposure times, down to 10^{-4} sec.¹⁰ The triangles and squares are data taken from the same emulsion coated with additions

(8) S. Fujisawa and E. Mizuki, *Sci. Publ. Fuji Photo Film Co., Ltd.*, **2**, 35 (1954).

(9) Y. Wakabayashi and Y. Kotsayashi, *J. Soc. Sci. Phot. Japan*, **20**, 102 (1957).

(10) Thus, this silver bromide emulsion differs in its high-intensity characteristics from those investigated by Berg (W. F. Berg, *Proc. Roy. Soc. (London)*, **A174**, 559 (1940)) (which were probably silver bromide emulsions). The high-intensity response and the ionic conductance therefore are mutually compatible with an ionic neutralization process involving electrostatic attraction, contrary to the supposition advanced earlier.³ This possibility was anticipated by Kartuzhanskii (A. L. Kartuzhanskii, *Uspekhi Fiz. Nauk*, **73**, 471 (1961)).

(5) Throughout the discussions to follow, the ionic step which occurs between the arrival of each electron during the growth of a latent-image center is referred to as "ionic neutralization." The term neutralization is intended in a general sense to refer to the prevention of build-up of a large excess charge, over a number of electronic steps, and does not necessarily require the establishment of exact electrical neutrality at any particular stage in the process.

(6) E. Klein and R. Matejec, *Naturwiss.*, **46**, 1 (1959); *Z. Elektrochem.*, **63**, 883 (1959); R. Matejec, "International Kolloquium über Wiss. Phot.," Zurich, 1961, Paper No. IA9, in press.

(7) A. L. Kartuzhanskii, *Zh. Eksp. Teoret. Fiz.*, **26**, 763 (1954).

of phenylmercaptotetrazole and hydroxymethyl-tetraazaindine, respectively, both of which produce increases in field-decay times of between 50 and 100.

In these emulsions with lower ionic conductance, the sensitivity is not independent of intensity over the same range. Latent-image formation is shown to be less efficient at high intensities, in agreement with the expected influence of ionic conductance. These curves show an increase in contrast resulting from the addition of these compounds, such that for high densities the additions are seen to have an overall sensitizing effect. This sensitizing effect also may be explained as a direct result of the decrease in ionic conduction. However, the reasoning involved in this interpretation is rather complex, and, since the effect is somewhat incidental to the main observation, it will not be discussed further here. The important point in the present connection is that the introduction of these materials causes the sensitivity of the emulsion to be less for high-intensity exposure than for optimum intensity. This demonstrates once again the role of mobile silver ions in high-intensity, reciprocity-law failure, and the identity between these silver ions and the carriers responsible for the dark ionic conductance. There appears to be an indication of a "bend-over" in these curves at times of about 10^{-4} sec.; certainly they do not bend over at times much longer than this. The ionic neutralization time appears then to be in the range of 100 μ sec., or less.

C. Electron-Trapping. 1. Single-Flash Measurements.—One of the outstanding uncertainties in the present state of understanding of the elementary photographic process is the nature of the centers at which the initial electrons are trapped. Gurney and Mott,¹¹ in originally proposing their mechanism, assumed that there were no effective deep traps in an unsensitized grain, and that traps in the form of specks of silver sulfide were created during the sensitizing process. It is now known that latent-image centers can be formed, albeit with lower efficiency, in strictly primitive emulsion grains, in which it is certain that there are no silver sulfide specks.¹² Electrons obviously can become localized at some type of *primitive trap*, whose exact nature is unknown. The investigations of Mitchell and co-workers¹³ clearly reveal the importance of physical imperfections in the trapping of electrons. Seitz¹⁴ pointed out the fact that the ionic configuration at a surface kink site or a jog in a dislocation line is such that for long-range considerations, a feature of this type in an ionic crystal may be taken to have a charge of one-half electronic unit, either positive or negative, depending upon whether a cation or an anion is located at the discontinuity. Positively-

charged physical imperfections are very likely involved in trapping electrons, but Mitchell,¹⁵ in particular, has contended that the vacant electronic states provided by these physical imperfections have energy levels which are not far enough below the conduction band to hold electrons except for extremely short times at room temperature. Various schemes have been proposed by which mobile silver ions can act in combination with shallow traps to increase their depth.

Measurements of electron lifetimes by the use of electric-field techniques provide direct evidence for the role of mobile silver ions in the initial trapping of electrons. The data shown in Fig. 6 give the relative displacement of the latent-image centers by a field as a function of the delay interval between the flash exposure and the application of the field. This fractional displacement is a measure of the fraction of electrons produced by the flash which are still free at the time the field is applied. The two curves shown here are those for the same emulsion with and without the addition of PMT as a silver-complexing agent, measured by single-flash exposures. Without this addition, the electrons have a mean lifetime of about 3 μ sec.

The curve for the emulsion containing PMT shows several important features, but the most obvious effect is a very large increase in the mean lifetime of the electrons, to about 100 μ sec. This compound, which was found to decrease the concentration of mobile silver ions and extend field-decay times in this emulsion, is seen also to extend electron lifetimes, by a remarkably similar factor. It thus seems evident that these silver ions, which are responsible for the *dark conductance* of the grain, and which combine alternately with photoelectrons during the *growth* of the latent-image centers, also are instrumental in the *initial trapping* of electrons, as the first stage in latent-image formation.

Field-decay time also can be changed by temperature variations. The range of decay times which can be covered by moderate temperature changes combined with silver-complexing agents is greater than two decades. Throughout this range, an accompanying change in electron lifetimes also is produced. Figure 7 shows a logarithmic plot of the relation between these two values measured under similar conditions. The points shown represent changes produced both by complexing agents and by temperature variations. The line in this graph represents proportionality between the two parameters. None of the points is removed from this line by more than a factor of two. This graph reveals not only the proportionality between field-decay time and electron lifetime, but also a fairly close numerical similarity between these values. The line in this figure corresponds to electron lifetimes greater by only a factor of three than field-decay times.

It seems appropriate to explore the possibility that such a close numerical correlation is significant, rather than merely coincidental. Broadly, the possibility is suggested that the neutralization of an electron by a mobile silver ion is the process

(11) R. W. Gurney and N. F. Mott, *Proc. Roy. Soc. (London)*, **A164**, 151 (1938).

(12) W. G. Lowe, J. E. Jones, and H. E. Roberts, in "Fundamental Mechanisms of Photographic Sensitivity," J. W. Mitchell, Ed., Butterworths Sci. Publications Ltd., London, 1951, p. 112.

(13) J. M. Hedgcs and J. W. Mitchell, *Phil. Mag.*, **44**, 223, 357 (1953); J. W. Mitchell, *Z. Physik*, **138**, 381 (1954); *Discussions Paraday Soc.*, **28**, 242 (1959); J. T. Bartlett and J. W. Mitchell, *Phil. Mag.*, **5**, 445 (1960); **6**, 271 (1961).

(14) F. Seitz, *Phys. Rev.*, **80**, 239 (1950); *Rev. Mod. Phys.*, **23**, 328 (1951).

(15) J. W. Mitchell, *Rept. Progr. Phys.*, **22**, 433 (1957).

which limits the lifetime of the electron, as measured in these experiments. It will be shown that a rather straightforward extension of the detailed Gurney-Mott theory¹¹ accounts almost exactly for the relationship.

Let us assume that in a grain there are no permanent electron traps as such, but that physical imperfections provide a great many shallow traps. An electron trapped at one of these sites normally escapes again within a very short time, and barring recombination with a hole, continues to be repeatedly trapped and released. If, however, during the short interval of its localization in a shallow trap, it should be neutralized by a mobile silver ion, the energy with which it is bound to the center is appreciably increased, and the configuration is stabilized.

The diagram of Fig. 8 is a schematic representation of this process. At time $t = 0$, n_0 free electrons are liberated by a flash of light. These are trapped with a rate α in shallow traps, from which they escape with a rate β ; while in these shallow traps, they may be neutralized by mobile silver ions, with a rate γ . These rate constants have the following significance

$$\alpha = QXv \quad (2)$$

$$\beta = \nu e^{-E_Q/kT} \quad (3)$$

where Q is the concentration of traps with cross-section X and depth E_Q , v is the thermal velocity of a conduction electron, ν is a frequency factor, possibly of the order of the vibrational frequency of an electron in a trap, but probably smaller, k is the Boltzmann constant, and T is the absolute temperature. The constant γ is the rate of neutralization of trapped electrons by silver ions, and its exact significance depends upon the mechanism of this process. Notice that if electrons did not escape from traps, this process would result in a mean ionic neutralization time $\tau_n = 1/\gamma$. The rate equations of this system are

$$dn/dt = -\alpha n + \beta s \quad (4)$$

$$da/dt = \gamma s \quad (5)$$

$$n + s + a = n_0 \quad (6)$$

If the numbers of traps and of mobile silver ions are assumed to be large enough to be considered constants, the general solutions to these equations may be obtained in a straightforward manner. They are rather complex algebraic expressions, but may be made more informative by reasonable approximations.

Previous results³ have indicated a very low drift mobility of electrons in these grains, owing to the fact that less of their lifetime is spent free than in shallow traps. On this basis it may be concluded that $\alpha \gg \beta$. It is further assumed that an electron is, on the average, temporarily trapped and released many times before it is neutralized, or that $\alpha \gg \beta \gg \gamma$. With these assumptions, the solutions of the equations may be greatly simplified. The number of electrons not permanently trapped, which is the quantity measured in these experiments, is given by eq. 7.

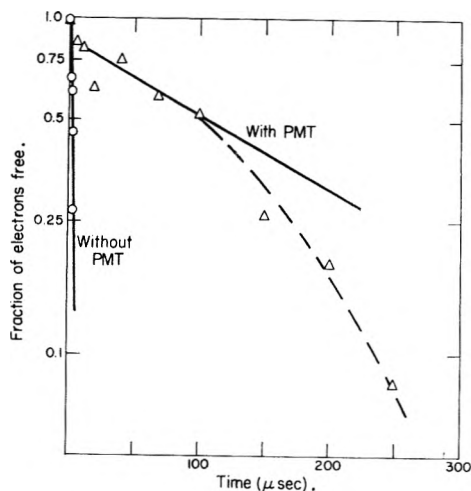


Fig. 6.—Curves showing decay of the concentration of free photoelectrons in a AgBr emulsion without (○) and with (Δ) 0.1 g. of phenylmercaptotetrazole per mole of AgBr.

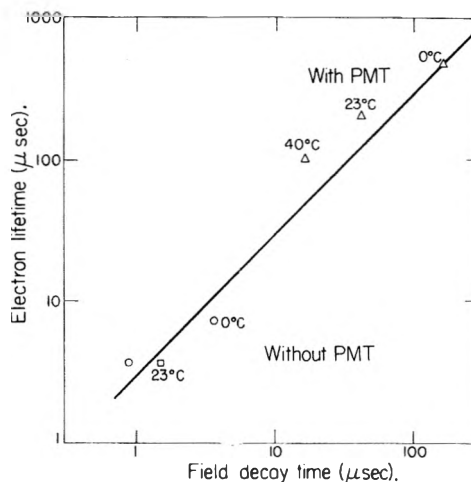


Fig. 7.—Relation between electric field-decay time and electron lifetime in AgBr emulsion with and without phenylmercaptotetrazole, and at three temperatures. Points ○ give field-decay time by multiple-flash measurement. All others are single-flash measurements.



Fig. 8.—Schematic diagram of the proposed trapping process.

$$\frac{N}{N_0} = \frac{n_0 - a}{n_0} = e^{-\gamma t} \quad (7)$$

Thus, the consequence of this process is that the mean lifetime of electrons is $\tau_e = 1/\gamma$, the same as the ionic neutralization time. In the absence of deep traps, the final trapping of electrons is accomplished by the neutralization act, and the lifetime is identical with the mean time of neutralization, independent of the fact that the electron repeatedly moves from trap to trap instead of remaining fixed at a single site.

The relation between neutralization time τ_n and ionic conductivity has been considered by Berg,¹⁰ who assumed that the motion of the silver

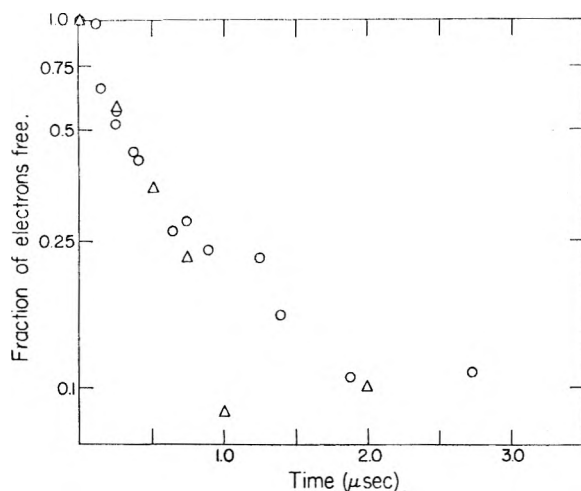


Fig. 9.—Decay of concentration of free photoelectrons in a AgBr emulsion without (○) and with (Δ) phenylmercaptotetrazole, measured with multiple-flash technique.

ion is controlled by the coulomb force between its own positive charge and the negative charge at the trap. For a single electron at an originally neutral trap, Berg's expression reduces to

$$\tau_n = \frac{\epsilon}{4\pi\sigma} \quad (8)$$

where ϵ is the dielectric constant and σ is the ionic conductance of the grain. Comparison between eq. 8 and eq. 1 shows that, with this model, the neutralization time should be the same as the field-decay time. If Berg's treatment is modified (as shown in Appendix III) to consider an electron trapped at the surface, rather than in the volume of a grain, and if the original electron trap is taken to be a kink site with a charge of $+1/2$, then the relationship between the electron lifetime, τ_e , the ionic neutralization time, τ_n , and the field-decay time, τ_i , as predicted from this simple model, is

$$\tau_e = \tau_n = 2.8\tau_i \quad (9)$$

accounting almost exactly for the threefold difference between τ_e and τ_i , seen in Fig. 7. The approximations used in the treatment probably are not good enough for this close numerical agreement to be taken as proof of such fine points as the charge of $+1/2$ on the original electron trap, even if the mechanism is correct. The agreement does show that it is reasonable to consider together the main features of this model in explaining the observed results. Specifically, these features are that, in these grains and under these exposure conditions, the trapping of an electron is accomplished by the act of neutralization by a mobile silver ion, while the electron is localized temporarily in a shallow trap. This neutralization comes about by virtue of the electrostatic force exerted on the silver ion by the negative charge at the site of the trapped electron. This imposes a limit on the original charge of the trap. It may be neutral, or even negatively charged, but if it is positively charged, then the magnitude of the charge must be less than one electronic unit.

According to the process just described, the trapping of an electron in itself forms an atom of silver and produces, with no delay, a permanent trap for a second electron. This accounts for an additional feature seen in the curve for the emulsion with PMT shown in Fig. 6. This curve is unmistakably concave downward, and no combination of processes with simple kinetics will result in such a shape. It indicates that the trapping probability increases in the course of events; in other words, that the trapping of electrons produces centers which have a very greatly increased trapping probability for subsequent electrons. The atoms of silver with charge $+1/2$ formed by the proposed mechanism would explain the increase.

This same curve also appears to show an initial sharp drop of 10 to 15% during the first few microseconds. This drop seems to be reproducible in curves taken at other temperatures (Fig. 11), and may indicate the presence in these grains of a few very effective traps, which become saturated after a small fraction of the electrons are trapped.

2. Multiple-Flash Measurements.—Electron lifetimes in this emulsion, when measured by multiple-flash exposures, are somewhat shorter than those determined from single-flash measurements, and are unaffected by the inclusion of silver-complexing agents.

The results of such multiple-flash determinations of electron lifetimes in the emulsion without additions have been given previously.³ It was shown that these results can be influenced by the displacement of holes as well as electrons, and that the form of the internal field pulse is instrumental in determining the apparent trapping curve. A field pulse embodying a reverse component, which resulted from polarization of the grain, was found most successful in separating electron-displacement effects from those of displacing holes. When the ionic conduction of the grains is reduced by silver-complexing agents, such internal polarization effects do not occur in comparable times. They may be simulated, however, by external means. A short voltage pulse was differentiated by a simple resistor-capacitor combination with a time constant of 0.9 $\mu\text{sec.}$, and this pulse was applied across the emulsion with PMT. The results of a multiple-flash lifetime determination under these conditions are given as the triangular points in Fig. 9. The circles on this plot are the similar data taken from the previous determination on the emulsion without PMT. The agreement is within the limit of experimental error, and in both emulsions the majority of the electrons are shown to be trapped in less than 0.5 $\mu\text{sec.}$ It must be concluded that under these conditions, mobile silver ions are not essential during the trapping process, and that the lifetime of electrons is determined by deep traps. These either are present in small numbers before exposure, or are produced as a consequence of the photographic process itself.

All these experimental results are consistently in almost exact agreement with the behavior expected from a simple, logical extension of the mechanism described by Gurney and Mott. There are, however, other proposed methods by which mobile

silver ions could enter into the electron-trapping process, and the main features, at least, of the experimental results are not in disagreement with some of these alternate proposals.

Matejec¹⁶ has suggested that the effective electron traps in a grain are nuclei of silver, silver sulfide, etc., to which silver ions are adsorbed in the dark, prior to exposure. The adsorbed silver ion is responsible for lowering the energy level of the trapping state, which would otherwise be too shallow to provide an effective permanent trap. When the electron becomes trapped at this site, an atom of silver is formed, and the center is made electrically neutral. In this state it is again ineffective as an electron trap. It must next adsorb another silver ion and be recharged positively, before trapping another electron. This silver ion which is adsorbed to the growing center must move to that site by diffusion, since there is no coulombic force between the two. The time for the ionic step, which resets the trap, would presumably be much longer, according to this mechanism, than by that proposed by Gurney and Mott (see Appendix IV).

In this process, as Matejec envisions it, the silver ions adsorbed at the trapping centers are presumably in equilibrium with mobile interstitial ions. The concentration of effective traps therefore would be proportional to the concentration of mobile silver ions, and factors which change this concentration would affect both the time of decay of an electric field and the lifetime of electrons, proportionally. The observed proportionality between these two quantities therefore would be expected, but the close numerical similarity between them would be merely a coincidence.

The mechanism of the photographic process as described by Mitchell¹⁵ cannot be applied in its entirety, at least to these grains, for the proposed absence of mobile silver ions prior to exposure is clearly inconsistent with these results. It is possible to consider his suggestions regarding the nature of electron traps, but assuming that a relatively large concentration of mobile silver ions are originally present. Mitchell's proposal is similar in some ways to that of Matejec, in that he considers a deep trap to be formed, prior to the arrival of an electron, by the combined effect of a silver ion and an otherwise-shallow potential well. The initial shallow trap he considers to be a surface kink site or a dislocation jog, having a silver ion at the displacement point so that its effective charge is $+1/2$. The additional mobile silver ion is not adsorbed, but chances to be in the vicinity of this site, near enough to interact and depress the energy level of the trap. At this deeper trap, the electron is localized, and the nearby silver ion joins it to form a silver atom, changing the net charge once again to $+1/2$. As in the model of Matejec, the trap must be reset before another electron can be trapped.

The relations between this mechanism and the experimental results are much the same as those described by Matejec. The proportionality between

electron lifetime and field-decay time is to be expected because of the equilibrium between mobile silver ions and deep traps. The numerical equivalence again is a happenstance, having no particular significance.

The significance of the non-exponential curve showing the decrease in concentration of free electrons (Fig. 6) was discussed earlier. Its explanation appears to rely upon the fact that the centers where electrons are trapped are reset, so they can act again as traps for additional electrons. The time at which this curve departs from an exponential shape is therefore another measure of the neutralization or resetting time. Moreover, these reset traps must not only be able to act again as traps, but their trapping efficiency must be quite appreciably increased, in order to influence markedly the overall trapping rate. If the original traps were initially only shallow temporary traps, this increased efficiency could amount to a lowering of the energy levels to convert them to permanent traps. If however, they already had become associated with silver ions and were deep enough to act as permanent traps for the first electrons to arrive, then this increased efficiency could result only from a much larger cross section for capture of the second electron than for the first. This large increase in cross section, which must be assumed in order to account for the present results according to the trapping mechanisms suggested by Matejec and by Mitchell, is in itself unlikely. That the resetting or neutralization process, as required in these models, would occur by diffusion within the times observed, which are of the order of the field-decay times, is perhaps even less likely. Without the electrostatic driving force, the neutralization times would be expected to be much longer than the field-decay times.

Except for this secondary trapping consideration, however, the mechanisms described by both Matejec and Mitchell are not inconsistent with the experimental results, although they do not provide as comprehensive an explanation for all the observations as does the Gurney-Mott extension presented earlier. The main distinguishing feature of this hypothesis is that silver ion *motion* is involved in providing the deep electron traps, thus accounting for the close numerical agreement between the electron lifetime, the ionic-neutralization time, and the field decay time. In the alternate schemes, the *concentration* of mobile silver ions is of importance, but not their *motion*, during the trapping process, to the latent-image site.

The dependence on temperature of the mean electron lifetime depends upon whether or not motion of silver ions is involved in the trapping process. This offers, in principle, a basis for evaluation of these two mechanisms.

If the electron lifetime is determined by the time for the electrostatic attraction of a mobile silver ion to an electron in a shallow trap, the temperature-dependence of the lifetime would reflect a contribution both from the activation energy of formation of an interstitial silver ion and from its energy of motion, and would be the same as the temperature-dependence of the field decay. If ionic

(16) R. Matejec, *Naturwiss.*, **55**, 533 (1956); *Z. Physik*, **148**, 454 (1957).

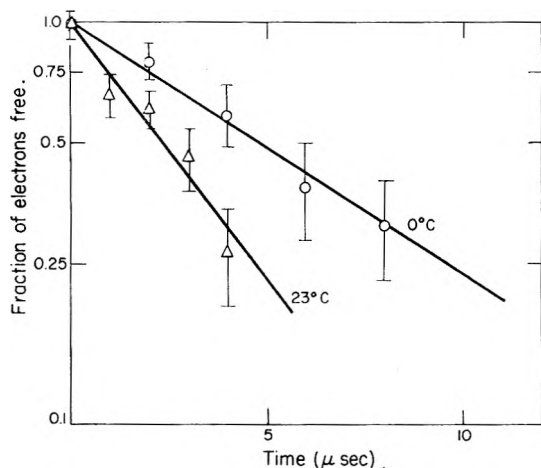


Fig. 10.—Decay of concentration of free photoelectrons in a AgBr emulsion without additions, at 23° (Δ) and 0° (\circ). Single-flash measurements.

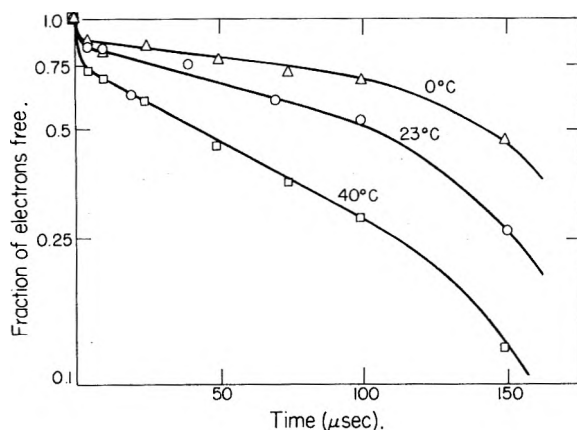


Fig. 11.—Decay of concentration of free photoelectrons in a AgBr emulsion with phenylmercaptotetrazole at 40° (\square), 23° (\circ), and 0° (Δ). Single-flash measurements.

motion is not involved, but the mere presence of the silver ion is the critical factor in permanent trapping, then the temperature-dependence of electron-trapping is determined by the energy of formation of permanent traps. This energy is, in turn, that of formation of an interstitial silver ion, less any adsorption or association energy at the trap. By this mechanism, then, the electron lifetime should be characterized by an activation energy less than that of the electric field-decay time by the sum of the energy of motion of a silver interstitial and the energy of association of such an interstitial with a potential trapping site. The energy of activation for motion of an interstitial silver ion is reported by Ebert and Teltow¹⁷ to be about 0.15 e.v.

The determination of activation energy with an accuracy of 0.15 e.v. requires either the exploration of a fairly wide temperature range or else the achievement of high precision and accuracy in the measurements. Unfortunately, neither of these conditions is conveniently possible in measurements of this type. Although temperature variations have been investigated in a preliminary way, it is not believed that the results obtained so far are

sufficiently accurate to make possible a conclusive decision between the possible mechanisms.

The reasons for this are evident from an examination of the data obtained in these experiments. In Fig. 10 are shown the points used for a determination of the mean lifetime of electrons in the emulsion without complexing agents, at temperatures of 0 and 23°, using single-flash exposures. As explained earlier, the maximum displacement of the image under these conditions is rather low: at 23° the maximum value is only about one-half. Low values of displacement are relatively less precise, because of the fact that they are obtained by means of the small difference between two large statistical quantities. As the limits of error on the graph indicate, the mean lifetimes from this determination are uncertain. Attempts to determine lifetimes at higher temperatures were completely unsuccessful.

In the emulsion with a silver-complexing agent, determination of the lifetime is also a questionable procedure, but partly for different reasons. The data used for determinations of lifetime on the emulsion containing PMT, taken from single-flash exposures at temperatures of 0, 23, and 40°, are shown in Fig. 11. Because these curves are non-linear at long times, the initial lifetime must be determined from the slope of the curves in the initial portions. These initial portions are complicated by the apparent rapid drop in the first few microseconds. Furthermore, the points at which these curves begin to be significantly influenced by the secondary trapping effect which causes their concave shape are uncertain. For this reason, values of lifetime must be determined from rather short portions of the curves, and are also quite imprecise. The longer-lifetime curve for the low-temperature case obviously is more seriously influenced by these complications and this value must be considered least reliable.

Figure 12 shows field-decay curves at these three temperatures as determined by single-flash exposures on the emulsion with PMT. The data are fitted quite well by exponential decay curves, and the $1/e$ decay times as determined from these probably are much more reliable.

In Fig. 13 values of electron lifetime (triangles) and field-decay times (circles) for the emulsion with (open points) and without PMT (solid points) are plotted logarithmically against the reciprocal of the absolute temperature. The slopes of the lines through the points give the activation energy of the process. The solid circles, giving the field-decay times for the emulsion without additions, are the same points reported previously, and are the only data on this graph taken by multiple-flash exposures. They lie on a straight line, whose slope indicates an activation energy of about 0.4 e.v. The data for the field decay with PMT also lie close to a straight line, with the same slope. Estimated limits of accuracy have been indicated for the values of electron lifetime. Lines with this same 0.4 e.v. slope can be fitted within these limits. However, the best values of lifetime judged from the present data seem to indicate a lower slope, and a lower energy of activation. If this

(17) I. Ebert and J. Teltow, *Ann. Physik*, **15**, 268 (1955).

indication proved to be valid, it would favor the interpretation that motion of silver ions is not involved in electron-trapping, and that the role of silver ions in this phase of the process is the conversion of shallow traps to deep ones, by association with these traps prior to the arrival of an electron. The present data cannot be considered conclusive. It may be possible to extend the measurements over a wider temperature range in the future, and to reduce the statistical uncertainty in the data, but the experimental obstacles are formidable, and a definite conclusion may never be possible on the basis of temperature-dependence.

For the present, it is reasonably certain that excess mobile silver ions are involved in the trapping of electrons, in some manner which is not yet clear. Two possible mechanisms are apparent: these are similar in some respects, yet they contain distinctive features, and may be taken at the present time as working hypotheses. The actual situation may well embody elements of both of these alternatives.

Appendix I

In this section is considered the effect of a change in trapping probability of electrons during the course of a measurement, made by a series of u repetitive flashes. During the i th flash, a number n_{0i} of electrons is released. Assume that a simple trapping mechanism is operative, resulting in an exponential decay of the number of free electrons, with a time constant τ_{ej} . As deep electron traps are created by the photochemical process, trapping occurs with increased probability, so that τ_{ej} decreases with increasing j . The fraction of electrons from the j th flash which are displaced by a pulse of field delayed by a time t after the flash is given by

$$\exp(-t/\tau_{ej}) \quad (10)$$

Over a series of u such flashes, during which a total of $N_0 = \sum n_{0j}$ electrons are liberated, the fraction displaced is

$$\frac{N}{N_0}(t) = \frac{\sum_{j=1}^u n_{0j} \exp\left(\frac{-t}{\tau_{ej}}\right)}{\sum_{j=1}^u n_{0j}} \quad (11)$$

This expression is the sum of a series of exponentials, having a distribution of time constants, and weighted by random quantum fluctuations. It is not difficult to imagine that τ_{ej} could change in such a way that this series is summed to give the approximate form of $1/(1 + \alpha t)$, which is the observed form for measurements made under these conditions.³ Thus it is possible to account for this shape by a progressive change in trap depth instead of requiring an initial distribution of trap depths as was suggested earlier.

Appendix II

The dark ionic conductivity of the grains used for the experiments described in this paper is a surface-controlled property. Surface-dependent electrical conduction appears not to be an uncommon effect in silver halide systems having large

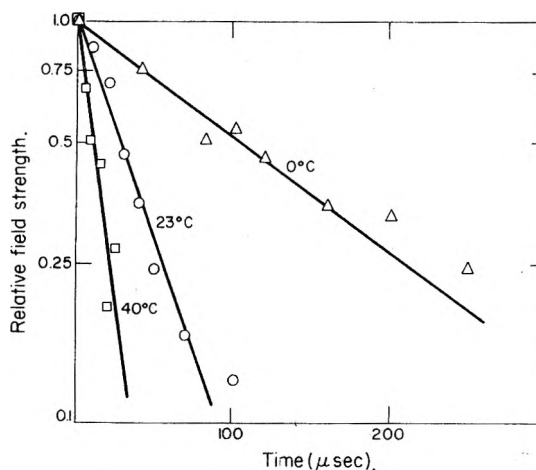


Fig. 12.—Electric-field decay in a AgBr emulsion with phenylmercaptotetrazole at 40° (□), 23° (○), and 0° (Δ). Single-flash measurements.

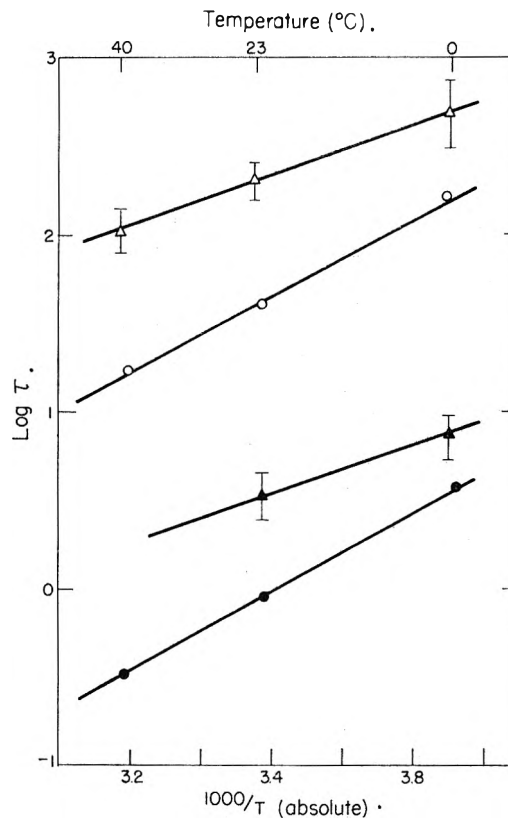


Fig. 13.—Log electric field-decay time (●, ○) or mean electron lifetime (▲, Δ) vs. $1000/T$ for AgBr emulsion without (●, ▲) and with (○, Δ) phenylmercaptotetrazole.

enough surface areas. Shapiro and Kolthoff¹⁸ observed such an effect in pressed powders of silver bromide. They found the conductance to be proportional to the specific surface, and to have an activation energy of 0.36 e.v. The photoconductive negative effect which has been studied by West,¹⁹ by Kirillov,²⁰ and by Yamada and Oka²¹

(18) I. Shapiro and I. M. Kolthoff, *J. Chem. Phys.*, **15**, 41 (1947); *J. Phys. Colloid Chem.*, **52**, 1319 (1948).

(19) W. West, *Phys. Rev.*, **84**, 1078 (1951); in "Fundamental Mechanisms of Photographic Sensitivity," J. W. Mitchell, Ed., Butterworths Sci. Publications, Ltd., London, 1951, p. 99.

(20) E. A. Kirillov, *Z. wiss. Phot.*, **26**, 235 (1928); **28**, 367 (1931).

(21) K. Yamada and S. Oka, *Naturwiss.*, **43**, 1 (1956).

appears to result from positively charged ionic carriers which can be controlled by changes at the surface. Matejec²² recently has measured conductivity in sheet crystals of silver bromide in contact with an electrolyte solution. He showed that the conductivity in the silver bromide could be modulated by means of the pAg of the electrolyte indicating an exchange between the crystal and the solution at the interface. He found a minimum in the conductivity of a pure crystal at a pAg value between 7 and 8, and showed that the position of the minimum was sensitive to the impurity content of the crystal.

Surface effects of two distinctly different types have been considered in relation to these electrical observations. The ions located at the surface of a crystal are sometimes presumed to be mobile along the surface and capable of contributing to the conduction. The structure of the surface of a photographic grain on the atomic scale is not well enough understood to warrant speculation regarding the detailed mechanism of surface migration of this type, except for the general observation that there are presumably a great many terraces on such a surface, and there are therefore a great many ions located at configurations such that motion to nearby sites with similar configurations should at least be possible.

In metals, surface migration of this type has been studied extensively in recent years, particularly with the field-emission electron microscope and the field ion microscope. The activation energy for surface motion in metals is found to be quite high as a rule, and apparently very little migration of this type occurs at room temperature. Since the melting point of silver bromide is relatively low, it is likely that less energy would be required for surface migration, but apparently no quantitative information is available.

The surface conductivity measured by Shapiro and Kolthoff has been presumed by some to be an effect of this type, apparently because of the fact that the observed activation energy was too low to account for other possible processes. The best estimates of activation energy of volume processes at the time do not now appear to have been correct, and there seems to be no valid basis for the conclusion. Aside from this possibility, no definite experimental evidence exists for interfacial conductivity in silver halides.

The mobile carriers involved in the photoconductive negative effect show features which associate them with both the surface and the volume of the crystal. The adsorption to the silver halide surface of gelatin or of silver-complexing agents, of the type used in the present investigation, has been shown to have a controlling effect on these mobile carriers, emphasizing the importance of the surface. Yet additional silver ion vacancies introduced with divalent cationic impurities are shown to reduce markedly the conduction of this type. Such vacancies exist in a mass-action equilibrium with interstitials in the crystal lattice, but would not be expected to have much effect on conductive processes at the interface.

(22) R. Matejec, "International Kolloquium über Wiss. Phot.," Zurich, 1961, Paper No. IA5, in press.

The experiments of Matejec clearly deal with a conductive effect of a similar type. The dark currents measured by Matejec are controlled by ionic conditions at the crystal surface, where equilibrium with ionic species in the electrolyte solution is established. Yet these currents are directed perpendicular to the contact surface. Migration along the interface therefore can be playing no part, and additional electrical carriers must exist in this case in the volume of the crystal, but in equilibrium with conditions at the surface.

The generation at the surface of excess volume ionic carriers has been treated from a theoretical viewpoint on the one hand by Frenkel²³ and by Lehovec,²⁴ who have considered a more or less inherent process, at a surface which is neutral with respect to the external environment, and on the other hand by Grimley and Mott²⁵ and later by Grimley,²⁶ who ignored such an "intrinsic" process and considered only the effects of the silver ion and bromide ion concentrations in the electrolyte. It has been found that an analysis of the present results requires a combination of the main features of both these mechanisms.

Consider first the electrolyte effect. It is well known that an ionic crystal in contact with a solution of its constituent ions becomes charged either positively or negatively if either the anion or the cation, respectively, is in excess in the solution. Grimley and Mott contend that the charge taken on by the solid resides not in the form of adsorbed ions at the interface, but as excess vacancies or interstitials in a space-charge layer within the crystal lattice, with a corresponding suppression of the defect with the opposite charge.

This space-charge layer resembles in many ways the diffuse layer in the electrolyte, which is largely responsible for the electrochemical properties of the solid. Within this region, local charge neutrality is not maintained, but a potential gradient exists. The concentration of excess charge decreases exponentially with increasing distance from the surface, but in crystals of the size of most photographic grains, the thickness of the layer may be an appreciable portion of a grain dimension.

The dependence of the excess charge concentration near the surface on the pAg of the solution was calculated by Grimley, and the external manifestations of this excess charge were reasonably well confirmed by the electrophoretic measurements of Davies and Holliday.²⁷ The space-charge layer is taken to be completely absent at the pAg corresponding to the external isoelectric point. Excess positive carriers, presumably interstitial silver ions, are introduced as the pAg is lowered, and excess silver ion vacancies as pAg is raised. Changes in charge concentration are small within the pAg range between about 3 and 9, but rise rapidly beyond these values, at either end of the range.

(23) J. Frenkel, "Kinetic Theory of Liquids," Oxford Univ. Press, New York, N. Y., 1956.

(24) K. Lehovec, *J. Chem. Phys.*, **21**, 1123 (1953).

(25) T. B. Grimley and N. F. Mott, *Discussions Faraday Soc.*, **1**, 3 (1947).

(26) T. B. Grimley, *Proc. Roy. Soc. (London)*, **A201**, 40 (1951).

(27) K. N. Davies and A. K. Holliday, *Trans. Faraday Soc.*, **48**, 1061, 1066 (1952).

In all normal photographic emulsions, the grains are held during the manufacturing process on the bromide ion excess side of the isoelectric point. According to the analysis of Grimley and Mott, a space-charge layer of excess silver ion vacancies would exist within such a grain, and if conduction within this layer were appreciable, silver ion vacancies would be the principal carriers of current. Yet the large decrease in conductivity introduced by silver ion complexing agents in this emulsion clearly indicates that the silver ion is the dominant carrier. In order to reconcile this experimental observation with the concept of conduction in a space-charge layer, the presence of excess interstitials at pAg values higher than the isoelectric point must be accounted for. The process described by Frenkel and more recently by Lehocan, in principle, do this.

In the volume of a pure crystal of silver bromide, interstitial ions and vacancies are formed in pairs. At the surface of such a crystal, however, either of these defects may be formed singly. The energy of surface formation of an interstitial silver ion is not expected to be the same as that of a silver ion vacancy, so that one or the other of these defects forms at the surface in greater numbers than the other. These excess, surface-generated, ionic defects diffuse into the crystal until a space charge is produced which compensates for the difference in formation energy. The equilibrium condition, therefore, even in the absence of electrolyte effects, is characterized by an internal electrical double layer of charge. The surface itself takes on a charge with respect to the interior of the crystal which is characteristic of the least easily formed defect, and the compensating charges are the defects with the lower formation energy, located in a diffuse layer extending into the crystal.

There is reason to believe that in silver bromide the interstitials are formed more easily than the vacancies, and that in the absence of an electrolyte effect, the excess carriers in the space-charge layer would normally be interstitial silver ions.

The effect of electrolyte concentration then would add to this inherent space-charge effect. At very low values of pAg, the concentration of interstitials would be increased to a still higher value, with a resulting increase in conductivity. At high pAg values the concentration of interstitials would be reduced, and the conduction would first decrease, as the excess carriers become less numerous, and then presumably increase again at very high pAg, owing to an excess vacancy concentration.

In a separate investigation, measurements were made of the dependence of field-decay time on the pAg of the emulsion, prior to coating. Results were in agreement with expected behavior, but were of little value in differentiating between interfacial and space-charge conduction, since the dependence is not specific to either model. Only minor changes in relaxation time are found between pAg values of 6 and 9, but a marked decrease in conductivity results in a much longer decay time at pAg 10. This result is not unreasonable, in view of the previous considerations.

There is no clear evidence showing whether the importance of the surface in the electrical conduction process in emulsion grains results from mobile interfacial ions, or from the role of the surface in generating ionic defect carriers which move within the volume of the crystal. Based mostly on evidence from different systems, the latter process has been assumed to be operative, and has been used in discussing the present results. Calculations have been simplified by considering the excess carriers to be distributed homogeneously through the volume. Presumably they are not, but rather are concentrated in a diffuse layer near the surface. This simplification introduces an approximation in the calculations, such that the exactness of the numerical agreement should not be overemphasized.

Appendix III

Consider now, following the general approach of Berg,¹⁰ the time of neutralization by a mobile silver ion of an electron trapped at a surface kink site having originally a charge of $+1/2$.

The mean distance, \bar{x} , from the electron, which is assumed to be trapped at a random site on the surface, to the nearest of the silver ions, which are taken to be homogeneously and randomly distributed, must in this case be found by a calculation slightly different from that of Berg. If λ is the concentration of silver ions per unit volume, then the probability that no silver ions lie within a hemispherical volume with radius ρ about the electron as a center is given by

$$\exp[-\lambda(2\pi\rho^3/3)] \quad (12)$$

and the probability that at least one is within this volume is

$$1 - \exp[-\lambda(2\pi\rho^3/3)] \quad (13)$$

The probability that the distance to the nearest ion lies between ρ and $\rho + d\rho$ is the first derivative of this expression, with respect to ρ , or

$$p(\rho) = 2\pi\lambda\rho^2 e^{-\lambda(2\pi\rho^3/3)} d\rho \quad (14)$$

The mean value of x is found by taking the integral of $\rho p(\rho)$ between zero and infinity

$$\bar{x} = \int_0^\infty 2\pi\lambda\rho^3 e^{-\lambda(2\pi\rho^3/3)} d\rho \quad (15)$$

This integral reduces to a gamma function of the form

$$\bar{x} = \left(\frac{3}{2\pi\lambda}\right)^{1/3} \Gamma\left(\frac{4}{3}\right) \quad (16)$$

Now the time τ_n for an ion to move this distance under the attractive influence of a net charge of $-e/2$ at the site where the electron is trapped is given by

$$\tau_n = \int_0^{\bar{x}} \frac{2\epsilon\rho}{\mu e} d\rho = \frac{2\epsilon\bar{x}^3}{3\mu e} \quad (17)$$

in which ϵ is the dielectric constant of the medium, μ is the ionic mobility, and e is the electronic charge.

Substituting for \bar{x} , from eq. 16, this becomes

$$\tau_n = \frac{\epsilon[\Gamma(4/3)]^3}{\pi\mu e\lambda} \quad (18)$$

But $\mu e\lambda = \sigma$, the conductance, and when $\Gamma(4/3)$ is evaluated, then

$$\tau_n = \frac{0.71\epsilon}{\pi\sigma} = 2.8\tau_i \quad (19)$$

Appendix IV

If an empty electron trap has a unit positive charge, so that upon trapping an electron the center becomes neutral, then the ionic neutralization step takes place by diffusion of an interstitial silver ion. Under these conditions the mean neutralization time can be expressed as

$$\tau_n = \frac{1}{\lambda X_i v_i} \quad (20)$$

where λ is the concentration of mobile silver ions per unit volume, X_i is the cross section for capture of one of these ions at the center, and v_i is the thermal velocity of a mobile ion. We may reasonably assume that there is no interaction between the interstitial ion and the neutral center except in the interstices immediately surrounding the center, so that X_i is approximately the square of the lattice constant, a^2 . The thermal velocity may be expressed as the jump frequency, ν_j , times the jump distance, again approximately a lattice spacing, or

$$v_i = \nu_j a \quad (21)$$

This equation may be combined with the relation between the diffusion coefficient, D , and the jump frequency²⁸

$$D = \nu_j a^2 \quad (22)$$

and the Einstein relation

$$D = \frac{\mu k T}{e} \quad (23)$$

to give

$$v_i = \frac{\mu k T}{ae} \quad (24)$$

Substituting (24) in (20) gives

$$\tau_n = \frac{e}{\lambda a \mu k T} \quad (25)$$

The product $\lambda\mu$ in the denominator is σ/e , where σ is the ionic conductance, and if the expression for the field-decay time given in eq. 1 is combined with this, a relation between τ_n and τ_i is obtained

$$\tau_n = \frac{e^2 4\pi}{aekT} \tau_i \quad (26)$$

Evaluation of the expression shows that the time of neutralization by diffusion of a silver ion to a neutral center would be greater than the time of decay of an electric field by a factor of about 6×10^3 . If the center had a negative charge, then the cross section would be much smaller, and the neutralization time correspondingly longer.

Acknowledgments.—The authors are pleased to express their thanks and appreciation to Dr. J. H. Webb for sustained interest in and support of the investigation. The inspiration and careful guidance of Dr. F. Urbach has contributed much to the progress of the research. Many helpful suggestions have been made by Dr. B. H. Carroll and Dr. A. H. Herz. In addition, grateful acknowledgment is made of assistance in many specific areas by other members of the staff of these Laboratories. The measurements for the reciprocity-failure curves were made in the Sensitometry Department, under the direction of F. C. Eisen. Contributions to the theoretical analyses were made by Dr. C. A. Duboc, Dr. E. W. Marchand, and B. E. Bayer. In addition, helpful discussions with many other persons of these Laboratories are gratefully acknowledged.

STUDIES OF POINT DEFECTS IN SILVER CHLORIDE¹

BY HOWARD LAYER AND LAWRENCE SLIFKIN

University of North Carolina, Chapel Hill, N. C.

Received June 20, 1962

Experiments on excess point defects introduced into single crystals of silver chloride by pulsed plastic extension or by rapid cooling from high temperature yield the following results. Point defects are created by plastic deformation much less efficiently in silver chloride than in other substances that have been studied. Interstitial silver ions so produced have a lifetime of the order of 10^8 jumps. Rapid cooling of very pure silver chloride quenches in approximately 0.1% Schottky defects. The silver and chloride vacancies are almost completely associated at room temperature. These divacancies have an activation energy for migration of 23 kcal./mole and a dissociation energy of 9.8 kcal./mole.

This paper surveys two experiments on point defects in single crystalline silver chloride, the results of which are being published in detail elsewhere. In both experiments the crystal is provided with an excess of point defects, either by pulsed plastic deformation or by rapid cooling from high

temperature. Perhaps the main significance of these results to the photographic process is that they provide information concerning Schottky defects, pairs of silver and chloride vacancies which may be either associated or dissociated.

First, however, it seems appropriate to the concern of this conference to quote two results obtained in our Laboratory by Dr. Max Miller. His observa-

(1) Supported in part by the U. S. Atomic Energy Commission and the Office of Scientific Research, USAF.

tions deal with the trapping of photoelectrons by dislocations in silver chloride. It has been proposed by Seitz² and discussed in detail by Mitchell³ that the sites at which dislocations trap photoelectrons are the positively charged jogs; *i.e.*, those steps on the dislocations where silver ions are exposed. Miller has decorated dislocations by driving photoelectrons into the crystal by means of a pulsed electric field.⁴ In such an experiment, each electron trap ultimately gives rise to a microscopically visible particle of silver.⁵ He has observed that (a) freshly deformed dislocations, which are believed to be severely jogged, decorate almost continuously in contrast to annealed dislocations which have only widely-spaced traps,⁶ and (b) doping the crystal with polyvalent cations, which should decrease the number of positive jogs by the mass action effect, eliminates the decorability of all dislocations.⁷ Thus, both of these observations lend support to the idea that dislocations trap photoelectrons primarily at positive jogs.

Pulsed Plasticity Experiment.—A number of laboratories have studied the enhancement of ionic conductivity produced by plastic deformation of alkali halides.⁸ These results usually have been interpreted in terms of the creation of excess point defects by intersecting dislocations.⁹ We have performed similar experiments on single crystalline silver chloride,¹⁰ which is available in very high purity and which differs from the alkali halides in that (a) the formation energy of interstitial cations is small, and (b) virtually any crystallographic plane containing the [110] slip direction can serve as a slip plane for dislocations.¹¹ Because point defects are much more mobile in silver halides than in alkali halides at room temperature, the experiment must be performed very rapidly, in times of the order of milliseconds.

Very pure (fractional impurity content about 3×10^{-7}) silver chloride (kindly provided by F. Moser, Kodak) was polished in the form of single crystalline slabs, approximately $2 \times 1 \times 0.2$ cm. Each crystal was extended along its long axis in pulses, consisting of 1% extension per each pulse of 5 msec. duration and monitored by a differential transformer. During and after extension, the dark (ionic) conductivity was measured across the flat faces by a capacitance bridge operating at 10 kc. A triggered dual-beam oscilloscope displayed both elongation and conductivity change as a function of time.

The first few extensions produced little or no effect on the ionic conductivity. After the crystal had been strained 5 to 10%, however, and intersecting slip systems had begun to appear, a transient increment which could be reproduced in the succeeding plastic pulses was observed. Figure 1, from a photograph of the oscilloscope display, shows a typical example. The conductance increase decays much too rapidly to be a dislocation short-circuiting effect, as studied in silver bromide by Johnston¹²; in these pure crystals it must be attributed to point defect formation. It is seen that the

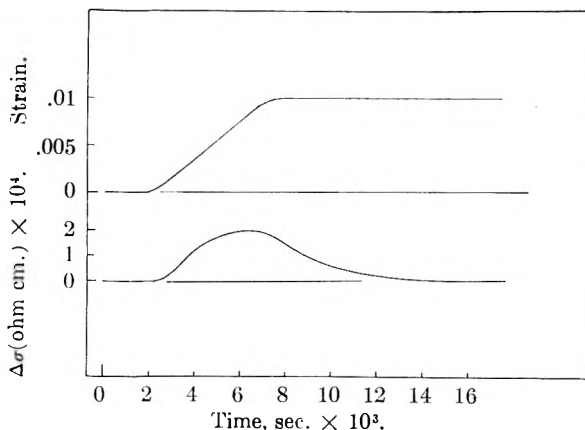


Fig. 1.—Conductivity increment produced by pulsed elongation. The upper curve gives the strain history and the lower curve gives the resulting change of ionic conductivity. The initial conductivity of 10^{-9} ohm⁻¹ cm.⁻¹ has been balanced out.

buildup of conductivity during the period of constant strain rate and the subsequent decay after cessation of straining resemble the charging and discharging of a capacitor, suggesting that creation of excess point defects is approximately proportional to strain and that the decay is by first-order kinetics. This first-order decay indicates that the defects are disappearing at traps, such as dislocations, rather than by recombination directly.

Of the various types of imperfections possible in silver chloride, the interstitial chloride presumably requires too large a formation energy to be produced in substantial numbers and the chloride vacancy is too immobile to contribute appreciably to the room temperature conductivity. It therefore appears that we are observing only silver defects. Of these, the interstitial is much more mobile than the vacancy¹³; since only one decay process is seen in Fig. 1, it thus must be associated with the more mobile defect, the interstitial silver ion. If we accept this interpretation, then several quantitative conclusions may be drawn. First, from the fact that the decay time is approximately 2 msec., and knowing that the interstitial jump frequency is between 10^{10} and 10^{11} /sec., we deduce that the extra interstitial silver ions make approximately 10^8 jumps before annihilation. This is a reasonable number, since it would result in a mean displacement of the order of several microns, which is approximately the spacing between dislocations in the deformed regions of the crystal. Second, from the known lifetime of the defects, the magnitude of the conductivity increment, and the strain rate, we may calculate the efficiency of the straining process for production of the excess point defects, obtaining 10^{-7} fractional concentration per unit strain. This is smaller by a factor of 1000 than the usually quoted estimates for other substances,⁹ and may be related to the observation that silver chloride shows very little work-hardening.

These experiments have been extended to doped crystals, containing of the order of 30 p.p.m. of polyvalent cation impurity. In these doped crystals additional processes are possible, involving atmospheres of impurities around static dislocations and impurity-vacancy complexes. If such an annealed crystal is subjected to a series of deformation pulses a very large conductivity increment, 10 times greater than that shown in Fig. 1, is obtained on the very first extension. This increase does not decay appreciably over times as long as many minutes. Successive extensions produce further, but progressively smaller, conductivity increments. If the crystal is left undisturbed for several hours (at room temperature), the conductivity will return to its original value and a further extension will now produce the same large increment observed in the initial strain pulse. These effects are not understood at present.

Quenching Experiment.—It has been found⁷ that if high purity silver chloride is cooled rapidly in a blast of cold air (0°) from temperatures a few degrees below the melting

- (2) F. Seitz, *Rev. Mod. Phys.*, **23**, 328 (1951).
- (3) J. W. Mitchell, *Rept. Progr. Phys.*, **20**, 443 (1957); see also *J. Phys. Chem.*, **66**, 2359 (1962).
- (4) C. Childs and L. Slifkin, *Phys. Rev. Letters*, **5**, 502 (1960).
- (5) J. R. Haynes and W. Shockley, *Phys. Rev.*, **82**, 935 (1951); F. A. Hamm, 141st National Meeting of the American Chemical Society, Washington, D. C., March, 1962, Symposium on Photographic Processes.
- (6) M. G. Miller, Ph.D. Thesis, Univ. of North Carolina, 1961; to be published.
- (7) H. Layer, M. G. Miller, and L. Slifkin, *J. Appl. Phys.*, **33**, 478 (1962).
- (8) See for example, V. Hovi, *et al.*, *ibid.*, **33**, 506 (1962); R. Davidge, C. Silverstone, and P. Pratt, *Phil. Mag.*, **4**, 985 (1959); A. Taylor and P. Pratt, *ibid.*, **3**, 1051 (1958); D. Fischbach and A. Nowick, *J. Phys. Chem. Solids*, **5**, 302 (1958).
- (9) F. Seitz, *Advan. Phys.*, **1**, 43 (1952).
- (10) H. Layer, M.S. Thesis, Univ. of North Carolina, 1962; to be published.
- (11) J. Nye, *Proc. Roy. Soc. (London)*, **A200**, 47 (1949).
- (12) W. Johnston, *Phys. Rev.*, **98**, 1777 (1955).

(13) See, for example, F. Brown and F. Seitz, "Photographic Sensitivity," a Symposium held at Tokyoc, Japan, 1957, Ed. by S. Fujisawa (Maruzen Company, Tokyo, 1958), Vol. 2, p. 5.

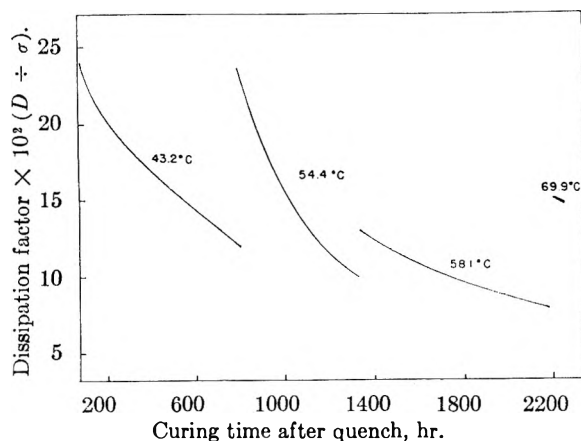


Fig. 2.—Annealing of excess conductivity after quenching. The conductivity, in $\text{ohm}^{-1} \text{cm.}^{-1}$, is 6×10^{-7} times the dissipation factor. The temperature was raised three times during the anneal.

point, the subsequent room temperature ionic conductivity is high relative to that of the slow-cooled crystal by a factor of about 50. It appears that the effect is due to a quenching-in of Schottky defects from high temperature, most of which are associated as vacancy pair "molecules," or divacancies, at room temperature. In equilibrium with these pairs is a "vapor pressure" of a few dissociated vacancies; the silver ion vacancies are mobile enough to contribute to the conductivity and the chloride ion vacancies serve to hold the silver vacancies in solution.

Figure 2 shows the decrease of this extra conductivity as a function of annealing time, the temperature being increased three times during the annealing run. From these curves,

we may obtain several useful data concerning the Schottky defects. First, from the increases in conductivity that occur when the temperature is raised, we deduce an effective activation energy of 13 kcal./mole. For equilibrium between divacancies and dissociated vacancies, and assuming a small degree of dissociation, then this activation energy must consist of the mobility activation energy of the silver vacancy (8.6 kcal./mole, from reference 13) plus one-half the dissociation or binding energy of the divacancy.⁷ We thereby deduce the binding energy of the divacancy to be 9.8 kcal./mole. From the temperature dependence of the rate of anneal (*i.e.*, from the changes in slope of the curves of Fig. 2 upon raising the temperature) it also was possible to obtain the activation energy for the migration of the divacancies. The value of this migration energy is 23 kcal./mole. Since we do not know whether the divacancy migrates as a unit or by dissociation and migration of the separate vacancies, we can conclude only that the 23 kcal./mole corresponds to the energy of migration of either the divacancy or the chloride vacancy, whichever is the more mobile.

We also can estimate the concentration of Schottky defects that have been quenched-in. The magnitude of the ionic conductivity just after quenching corresponds to a fractional concentration of free vacancies of 2.5×10^{-6} . Having determined the divacancy dissociation energy and estimating the structural contribution to the dissociation entropy to be of the order of 1 to 2 entropy units, then we obtain a fractional concentration of divacancies of 0.1%. This must be the concentration of Schottky defects present at high temperatures (*i.e.*, near the melting temperature). It is sufficiently small compared to the Frenkel defect concentration at high temperatures that it is not in conflict with the deductions of Friauf.¹⁴ It is also of the same order of magnitude as the vacancy concentrations found in metals¹⁶ and is just the value that was estimated for silver halides much earlier by Seitz.²

(14) R. J. Friauf, *J. Phys. Chem.*, **66**, 2380 (1962).

(15) R. Simmons and R. Balluffi, *Phys. Rev.*, **125**, 862 (1962).

SOME RECENT TRENDS IN THE THEORY OF SPECTRAL SENSITIZATION

By W. WEST

Research Laboratories, Eastman Kodak Company, Rochester 4, N. Y.

Received June 20, 1962

The present situation in the theory of spectral sensitization of the photographic process is reviewed. It seems probable that spectral sensitization involves the participation of energy-rich surface states of the silver halide at energies within the gap between the conventional valence and conduction bands. Conduction electrons are formed in the dye-sensitized process with properties similar to those excited by self-absorption by the silver halide. Positive holes derived from surface states, however, may be expected to be relatively immobile, and preliminary experiments showing the difficulty of observing displacement of positive holes by electric fields in dyed crystals exposed to light absorbed by the dye, without any corresponding difficulty when the same crystal is exposed to near-ultraviolet light, suggest that few mobile holes are formed in the sensitized process. Recent experimental data on the threshold wave lengths for the external photoelectric effect in sensitizing dyes show that the ground levels of crystalline dyes are situated some 1.5 to 2 e.v. above those for the corresponding isolated molecules, and, if it is assumed that the ground levels of cooperative adsorbed monolayers of sensitizing dyes are similar to those for the three-dimensional crystal, sensitization by electron transfer from the excited dye layer to the conduction band of the silver halide becomes energetically possible. It is doubtful, however, that electron transfer is energetically possible from isolated adsorbed molecules of sensitizer, which appear to sensitize at least as efficiently as cooperative monolayers. The selective loss of photographic sensitivity within the spectrally sensitized region at low temperature suggests the participation of some thermal activation process in sensitization, which, however, is not influenced essentially by the position of the absorption band of the dye. Comparative estimates of the fluorescence and phosphorescence yields of sensitizing dyes adsorbed to silver halides and to other substrates suggest that the excited singlet state rather than the triplet state of the sensitizer is involved in the sensitization.

This paper is intended to review some salient points in the theory of spectral sensitization as it appears to stand at present.

There can be little doubt that the primary process induced by the absorption of a photon by silver halide crystals is the creation of a mobile electron and of a mobile positive hole in the crystal. The photo-production of mobile charge-carriers in emulsions is signalled clearly by the observed photocon-

ductivity of emulsions, and experiments of the type introduced by Haynes and Shockley,¹⁻⁵ involving the displacement of print-out and of latent images in silver halide crystals placed in pulsed electric

(1) J. R. Haynes and W. Shockley, *Phys. Rev.*, [2] **82**, 935 (1951).

(2) J. H. Webb, *J. Appl. Phys.*, **26**, 1309 (1955).

(3) J. F. Hamilton, F. A. Hamm, and L. E. Brady, *ibid.*, **27**, 874 (1956).

(4) J. F. Hamilton and L. E. Brady, *ibid.*, **30**, 1893 (1959).

(5) P. Süptitz, *Z. Physik*, **153**, 174 (1958).

fields synchronized with light flashes, show that the latent image induced by the absorption of light by the crystals is formed through the intermediary of mobile electrons liberated by the light. Similar experiments in appropriately directed electric fields show the mobility of positive holes.^{4,6} In thin macroscopic crystals of silver bromide, the mobility of the positive holes was found to be $1.5 \text{ cm.}^2 \text{ v.}^{-1} \text{ sec.}^{-1}$, a few per cent of the value of $67 \text{ cm.}^2 \text{ v.}^{-1} \text{ sec.}^{-1}$ found for the mobility of electrons in the same material.⁷ Even in the absence of applied fields, exposure of thin macroscopic crystals forms latent-image centers in the interior, indicating the diffusion of photoelectrons from sites near the surface of incidence where they are liberated.^{8,9}

In the dye-sensitized photographic response to light of wave lengths absorbed only by the adsorbed layer of sensitizing dye at the surface of the silver halide crystallite, the photoelectrons also are free, as is indicated by a sensitized photoconductivity whose spectral sensitivity and response to supersensitizers and antisensitizers runs parallel to the corresponding characteristics of the photographic sensitivity.^{10,11} The formation of internal latent-image centers in emulsion grains, induced by light absorbed by sensitizing dyes, shows that electrons migrate into the interior from their points of origin at the crystal surface; in dyed macroscopic thin crystals, exposed to light absorbed by the dye, the appearance of internal latent-image centers 20 to 40μ from the dyed surface shows the diffusion of dye-induced free electrons over relatively great distances.

The mobility of the positive hole associated with the dye-sensitized photographic process is not so clearly established as that of the electrons. Some mechanisms of spectral sensitization to be discussed later suggest that the positive hole associated with the dye-sensitized photographic process should initially appear at a surface site which probably is localized. The observed bleaching of sensitizing dyes adsorbed to silver halides during exposure both to light absorbed by the halide and to light absorbed by the dye, and the inhibition of the bleaching on the addition of halogen acceptors to the system,¹² suggest attack of the dye, directly or indirectly, by bromine release during exposure to light both in the region of self-absorption and in the spectrally sensitized region, but do not in themselves show that the positive hole associated with the sensitized process can move through the crystal lattice. The motion of positive holes in thin sheet crystals of silver bromide, exposed to flashes of light absorbed by the crystal synchronized with an appropriately directed electric field, can be shown by the displacement in the field of the

bleaching effect of the holes on latent-image centers introduced before the flash.⁷ Recent experiments performed with V. I. Saunders and R. W. Tyler at the Research Laboratories of the Eastman Kodak Company show that when silver bromide sheets which have been dyed on the surface of incidence by a monolayer of sensitizing dye are exposed in this way to light absorbed by the silver halide, the motion of positive holes in the field is readily demonstrated, at the same exposure level as required to show the motion of electrons by the corresponding displacement of latent-image centers in an electric field of opposite polarity. When, however, the flash exposure is made to green and yellow light, absorbed by the dye, no such motion of positive holes is indicated. On the other hand, when the field is directed so as to displace electrons into the crystal, motion of the electrons excited by exposure of the dye crystal to green and yellow light is readily seen. There therefore seems to be strong evidence that the positive holes associated with the spectrally sensitized process lack the freedom of motion of those induced by self-absorption of the silver halide, consistent with trapping of the holes involved in spectral sensitization at localized surface sites.

A decade or so ago, a fundamental problem in discussions on spectral sensitization was the source of the energy which enabled the dye to induce the formation of latent image essentially similar to that formed in the unsensitized process by utilizing quanta of so much smaller energy. This problem appears to have been resolved by the recognition that the long wave length of appreciable absorption by the silver halide need not necessarily represent the minimum energy necessary to excite an electron into the conduction band of the crystal. Seitz has pointed out the possibility of radiationally forbidden transitions from levels in the valence band of the lattice above those from which radiational transitions of electrons to the conduction band can occur with appreciable intensity.^{13,14} In addition, on analogy with the better known surface states in homopolar crystals like germanium, it is expected that the silver bromide surface should possess occupied energy levels in the gap between the lattice valence band and the conduction band, associated with the surface as such, with crystalline imperfections and impurities and with adsorbed layers. From these levels, an electron can be excited into the conduction band with the expenditure of less energy than corresponds to the long-wave limit of strong absorption by the silver halide. Unfortunately very little is known, either theoretically or experimentally, about the nature of the levels in the energy gap of ionic crystals, and at present they are little more than a concept which secures conservation of energy in spectral sensitization on the assumption that the smaller quantum absorbed by the dye excites an electron to the same energy state as does the larger quantum absorbed by the crystal.

It is still uncertain whether the electron which appears in the conduction band of the silver halide

(6) F. A. Hamm, *J. Appl. Phys.*, **30**, 1468 (1959).

(7) V. I. Saunders, R. W. Tyler, and W. West, *J. Chem. Phys.*, **37**, 1126 (1962).

(8) P. W. McD. Clark and J. W. Mitchell, *J. Phot. Sci.*, **4**, 1 (1956).

(9) W. West and V. I. Saunders, *J. Phys. Chem.*, **63**, 45 (1959).

(10) W. West and B. H. Carroll, *J. Chem. Phys.*, **15**, 529 (1947).

(11) W. West, "Fundamental Mechanisms of Photographic Sensitivity," J. W. Mitchell, Ed., Butterworths Scientific Publications, Ltd., London, 1951, p. 99.

(12) S. E. Sheppard, R. H. Lambert, and R. D. Walker, *J. Chem. Phys.*, **7**, 426 (1939).

(13) F. Seitz, *Rev. Mod. Phys.*, **23**, 328 (1951).

(14) F. C. Brown and F. Seitz, "Photographic Sensitivity," Vol. 2, Tokyo Symposium, 1957, Maruzen Co., Ltd., Tokyo, 1958, p. 11.

as the result of the sensitization process is transferred from the dye, with the formation of a free radical ion in place of the dye molecule, or is excited from a site in the surface of the silver halide following some sort of resonance energy transfer between the excited dye molecule and a surface state. Both mechanisms require the participation of surface states to account for the low energy of activation experimentally observed for spectral sensitization. In the energy-transfer mechanism, the excited dye molecule must interact with a surface site from which an electron can be raised to the conduction band with the electronic energy available in the excited dye molecule.¹⁵ A positive hole, which may be initially localized, is left at the surface site, while the dye reverts to its ground state. Mitchell visualizes the transfer as the passage of an electron from an energy-rich surface bromide ion to the vacancy in the ground orbital of the excited dye molecule, with the simultaneous passage of an electron from the excited orbital of the dye to a surface silver ion, from which it is thermally ejected into the conduction band.¹⁶

If the sensitizing transfer is to be repeated, the surface state in the halide must again be occupied by an electron, or the dye must be able to find an equivalent filled state. Since the adsorbed dye molecule is in contact with several surface sites, it could possibly transfer energy several times before depleting the surface of states with which it can interact.

In the electron-transfer process, surface states may be invoked to regenerate the dye molecule from the free radical ion left after the passage of an electron from the dye into the conduction band.^{17,18} An electron can pass from a surface bromide ion site to the dye radical, regenerating the dye, and leaving a positive hole, probably initially localized, in the surface. The migration from the neighborhood of the site of a mobile surface silver ion as an interstitial ion in the lattice would discharge the hole as an adsorbed bromine atom, which might react with the dye, in a side reaction unconnected with the sensitizing transfer, in the absence of a more effective halogen acceptor. The charge of the photoelectron is now balanced by that of the interstitial silver ion.

In the energy transfer scheme, there are no restrictions on the energy levels of the dye relative to the conduction band of the silver halide—the energetic restriction is that the dye find a surface level from which an electron can be excited to the conduction band (or to a level sufficiently near the conduction band for the jump into the band to be accomplished by a small thermal activation) with the energy available in the excited dye molecule. Electron transfer, however, requires that the excited dye level be not much lower than the lowest level of the conduction band, about 3.5 e.v. below the vacuum level for silver bromide. The ground level of an adsorbed dye that sensitizes at wave length 6000 Å., equivalent to an excitation energy

of 2.15 e.v., must, therefore, be not much lower than about 5.6 e.v. below the vacuum level. The external photoelectric threshold frequency for the adsorbed dye must be equivalent to an ionization energy or work function not much above 5.6 e.v.

Measurements of the external photoelectric thresholds of layers of crystalline dyes by Fleischmann¹⁹ and more recently by Vilesov and Terenin²⁰⁻²² and by Nelson²³ indicate ionization energies of crystalline sensitizing dyes between 4.7 and 5.8 e.v. From these data it appears that the first excited singlet level of several crystalline dyes, including some photographic desensitizers like phenosafranin, lie above the bottom of the conduction band of silver bromide. The values of photoelectric thresholds of the vapors of some of these dyes, determined by Vilesov and Terenin,^{20,21} show that the ionization energy of the crystalline dye is about 1.5 to 2 e.v. less than that of the vapor. A similar relation has been found for condensed ring hydrocarbons.²⁴

In normal photographic practice, sensitizing dyes are adsorbed as incomplete coöperative monolayers on the surface of the emulsion grains. Coöperative layers constitute two-dimensional crystals, and if the ionization energy of these adsorbed layers approximates that of the corresponding normal crystal, spectral sensitization by electron transfer becomes energetically possible. The only data on the ionization energy of an adsorbed dye layer of a sensitizing dye refer to erythrosin on SnO₂,²² for which the value 6.7 e.v. was found. It is not certain whether this value applies to a coöperative layer or to a layer mostly consisting of approximately isolated dye molecules. Terenin and Akimov²² consider an energy transfer more probable than an electron transfer in the dye sensitization of photoconductivity of semiconductors, and in the absence of further data on the ionization energy of adsorbed layers, the question of the energetic possibility of the electron-transfer mechanism of spectral sensitization must be left open. In any case, spectral sensitization of the photographic process can occur with undiminished efficiency, and sometimes with increased efficiency compared with that of a coöperative layer, under conditions of very small coverage of the silver halide surface by dye when the dye appears to be adsorbed essentially as isolated molecules.²⁵ In this state, the ionization potential of the adsorbed dye probably would differ relatively little from that of the gas. Even if spectral sensitization of the photographic process by a coöperative layer of sensitizing dye by electron transfer is energetically possible, there is considerable doubt that all observed cases of dye sensitization can occur by this mechanism.

Contact potential differences between a relatively thick layer of a cyanine dye and silver

(19) R. Fleischmann, *Ann. Physik*, **5**, 73 (1930).

(20) F. I. Vilesov, *Dokl. Akad. Nauk SSSR*, **132**, 632 (1960).

(21) F. I. Vilesov and A. N. Terenin, *ibid.*, **133**, 1060 (1960); **134**, 71 (1960).

(22) For a comprehensive discussion, see A. N. Terenin and I. Akimov, *Z. physik. Chem. (Leipzig)*, **217**, 307 (1961).

(23) R. C. Nelson, *J. Opt. Soc. Am.*, **51**, 1186 (1961).

(24) L. E. Lyons and G. C. Morris, *J. Chem. Soc.*, 5192 (1960).

(25) W. West and B. H. Carroll, *J. Chem. Phys.*, **19**, 417 (1951).

(15) N. F. Mott, *Phot. J.*, **88B**, 119 (1948).

(16) J. W. Mitchell, *J. Phot. Sci.*, **6**, 57 (1958).

(17) N. F. Mott and R. W. Gurney, "Electronic Processes in Ionic Crystals," 2nd ed., Oxford Univ. Press, 1948, p. 242.

(18) J. Eggert, *Ann. Physik*, [7] **4**, 140 (1959).

For 1963 the page size of the following journals will be increased from 8 x 10½ inches to 8¼ x 11¼ inches. This change is made so as to take advantage of more efficient printing equipment with consequent savings.

JOURNAL OF THE AMERICAN CHEMICAL SOCIETY
JOURNAL OF ORGANIC CHEMISTRY
JOURNAL OF PHYSICAL CHEMISTRY
INORGANIC CHEMISTRY
JOURNAL OF MEDICINAL CHEMISTRY
BIOCHEMISTRY

bromide measured by Nelson²⁶ indicate that electrons may spontaneously flow from the dye layer to the silver bromide, but again, no such measurements have been made on the adsorbed monolayers of dyes which function in photographic practice.

It is of some interest to inquire how the excited level of the members of a vinylogous series of dyes is placed with respect to the conduction band of silver bromide with increasing chain length and concomitantly increasing wave length of the absorption band. Direct data on this question are not available, but for the series of condensed ring hydrocarbons naphthalene, anthracene, tetracene, in the crystalline state, the data on the photoelectric thresholds²⁴ show that the energy of the ground level measured from the vacuum level rises sufficiently to maintain the excited level at a nearly constant value. Indirect estimates of the variation of the ionization potential of the vinylogous series of thiocyanines with increasing chain length can be made from the oxidation-reduction potentials or the polarographic anodic and cathodic half-wave potentials. The half-wave potentials of the vinylogous series of thiocyanines in an organic solvent are linear in the frequency of the maximum of the absorption band of longest wave length,²⁷ and since for some classes of compounds there is a linear relation between the frequency of this absorption band and the ionization potential,²⁸ it seems likely that there may be a linear relation between the half-wave potentials of cyanine dyes and the ionization potentials. Stanienda's measurements show a regular fall of the half-wave potentials with increasing chain-length in the vinylogous series of 3,3'-diethylcyanines, and point to a correspondingly regular decrease of the ionization potential and a regular rise of the ground level of the dyes relative to the levels of silver bromide. Consideration of the data shows that the ground level rises with increasing chain-length just enough to maintain the first excited singlet level at an approximately constant value. Hence, if sensitization by electron transfer is energetically possible for a dye of short chain-length in the series, it also would be possible for members of longer chain-length, for which the electronic excitation energy is considerably less, always provided surface states of sufficiently high energy in the silver bromide are available. This conclusion is consistent with the observation of Scheibe and co-workers that the first excited singlet electronic state of many organic molecules is near the first excited level of the hydrogen atom, 3.39 e.v. below the vacuum level.²⁹

If intermediate levels in the energy gap of silver halides are associated with the sensitization process, it might be expected that grains prepared under different conditions would vary in the number and nature of intermediate levels and respond differently to dye sensitization. In a special emulsion containing silver bromide grains deposited by sedimentation, Eggert and Pestalozzi³⁰ observed a

preferential increase in the spectral sensitization conferred by a merocyanine dye after chemically sensitizing the emulsion by bathing in thiosulfate or after bathing in water before exposure, and attributed the effect to an increased probability of regeneration of the dye after a sensitizing transfer because of an increased number of surface states introduced by the bathing treatments. Latent-image formation in the sensitized spectral region therefore is facilitated.

On the other hand, Carroll, MacWilliam, and Henrickson,³¹ confirming earlier observations, found no significant change in the dye-induced sensitivity relative to the sensitivity to blue light after chemical sensitization of normal emulsions, and concluded that any intermediate levels introduced by chemical sensitization do not influence spectral sensitization. If intermediate levels intervene in the sensitizing transfer, they appear to be too numerous, in normal emulsions, for the additional levels introduced by chemical sensitization, which are all-important with respect to capture of electrons and positive holes, to cause a significant change in the spectral sensitization.

The temperature coefficient of spectral sensitization has drawn some recent attention. An inefficiency specific to spectral sensitization is shown by the considerably greater fall in sensitivity of dyed emulsion exposed at low temperatures, such as -196° , to light absorbed by the dye than to light absorbed by the silver halide, normal development at room temperature being used.³²⁻³⁴ It has been shown, however, that undyed emulsions exposed at -196° and developed normally at room temperature are underdeveloped, since the rate of development of image falls markedly when exposures are made at low temperature.³⁵ Nevertheless, although development of dyed emulsions is retarded for exposures made at all wave lengths at low temperatures, the differential loss in sensitivity in the spectrally sensitized region compared with that in the region of self-absorption persists for prolonged development,³⁶ and the conclusion remains valid that spectral sensitization is characterized by a specific loss in efficiency at low temperatures. The fall in spectral sensitivity at low temperature is not, in general, a result of decreased absorption of radiation by the dye, except at wave lengths on the long-wave-length edge of the absorption band.³⁴

A specially interesting observation by Frieser and co-workers is that the loss in spectral sensitivity at low temperature of a J-aggregated sensitizing dye in the presence of a supersensitizer is less than that for the J-aggregated sensitizer alone.³³

The observed temperature coefficient of spectral sensitization therefore suggests that the sensitization process is associated with some thermal activa-

(30) J. Eggert and H. Pestalozzi, *Z. Elektrochem.*, **65**, 50 (1961).

(31) B. H. Carroll, E. A. MacWilliam, and R. B. Henrickson, *Phot. Sci. Eng.*, **4**, 230 (1961).

(32) C. H. Evans, *J. Opt. Soc. Am.*, **32**, 214 (1942).

(33) H. Frieser, A. Graf, and D. Eschrich, *Z. Elektrochem.*, **65**, 870 (1961).

(34) W. West, *Phot. Sci. Eng.*, **6**, 92 (1962).

(35) T. H. James, W. Vanselow, and R. F. Quirk, *ibid.*, **5**, 219 (1961).

(36) W. Vanselow and T. H. James, *ibid.*, **6**, 104 (1962).

(26) R. C. Nelson, *J. Opt. Soc. Am.*, **46**, 13, 1016 (1956).

(27) A. Stanienda, *Naturwiss.*, **47**, 512 (1960).

(28) W. C. Price and A. D. Walsh, *Proc. Roy. Soc. (London)*, **A185**, 182 (1946).

(29) G. Scheibe, D. Brück, and F. Dörr, *Ber. deutsch. chem. Ges.*, **86**, 867 (1952).

tion. Although the variation of spectral sensitization with temperature is not accurately expressed by an equation of the Arrhenius type, it seems appropriate for orienting purposes to calculate an apparent energy of activation by assuming that the sensitivities at room temperature and at -196° are measures of the rate of sensitization at these temperatures and that the difference in sensitivity at the two temperatures is described by the Arrhenius equation. Apparent energies of activation so calculated do not exceed 0.05 e.v. and are probably larger than any true activation energy involved in the sensitization process.

In a vinylogous series of sensitizing dyes, there is a regular increase in the wave length of maximum absorption and sensitization of approximately 1000 Å. as the chain length is increased by 1 vinylene group. The electronic excitation energy available for sensitization falls steadily with increasing chain-length, but there is no related increase in the energy of activation—there is some tendency for the apparent energy of activation to increase with increasing chain-length, but this increase is trivial compared with the corresponding fall in excitation energy. The observed temperature coefficient of spectral sensitization therefore does not originate in an activation process which is concerned with thermally populating surface levels of the silver halide which can match the excitation energy available in the dye. If such levels exist, their population is not essentially temperature-dependent, between room temperature and -196° .

The activation process suggested by the temperature coefficient of spectral sensitization therefore is most likely connected with the transfer process itself. An energy barrier between the electronically excited dye molecule and the silver halide surface may be surmounted thermally. Dörr and Scheibe have shown that in the electron-transfer mechanism, a barrier rising as much as 2 e.v. above the excited level of the dye could be penetrated by tunneling at a rate well above the rate of radiational deactivation and permit efficient sensitization.³⁷ The effect of temperature on the rate of tunneling has not been explicitly examined in this case, but presumably would be consistent with the observed low apparent energy of activation.

Mitchell's scheme of sensitization,¹⁶ already referred to, represents another possible process in spectral sensitization that requires thermal activation—in this case a thermal jump of an electron into the conduction band from a level slightly below, to which it has been excited by the energy of the excited dye molecule.

As in other photochemical processes, the possible participation of the triplet state in spectral sensitization has been considered.³⁸⁻⁴¹ Cyanine dyes phosphoresce at low temperatures when dissolved in rigid glasses or when adsorbed to substrates like silica gel or lead bromide. On the usual identifica-

tion of the phosphorescent state with the triplet state, the excited triplet level of the dye is some 0.5 to 0.6 e.v. below the first excited singlet level.⁴¹ While, therefore, the long lifetime of the triplet state might ensure a relatively high concentration of excited dye molecules, certain mechanisms of sensitization, such as sensitization by electron transfer, energetically possible if the excited dye is in the first excited singlet state, become energetically improbable for the dye in the triplet state.

Sensitizing dyes adsorbed to silver bromide show a phosphorescence that is weak compared with that of the dyes adsorbed to silica gel or to lead bromide.⁴¹

The "heavy atom effect" whereby singlet-triplet transitions are facilitated by spin-orbital coupling in the neighborhood of atoms of high atomic number increases the quantum yield of phosphorescence of cyanine dyes when adsorbed on lead bromide over that for the dye adsorbed to silica gel,⁴⁰ and unless there is some competitive radiationless deactivation process when the dye is adsorbed to silver bromide, the phosphorescence yield also would be expected to exceed that on silica gel. The observed feeble phosphorescence of these dyes on silver bromide suggests that the photographic sensitizing transfer competes with phosphorescence, but does not show in itself whether it is the excited singlet or the excited triplet state that is deactivated in this way.

A comparison of the fluorescence intensity at room temperature of the strongly fluorescing cyanine dye, 1,1'-methylene-2,2'-cyanine chloride, adsorbed to silver halides and to other substrates, coupled with the low phosphorescence yield on silver halides, strongly suggests that it is the excited singlet state of the dye that participates in spectral sensitization.⁴¹ The fluorescence of the dye adsorbed to substrates such as SiO_2 , ZnO , Ag_2SO_4 , and PbBr_2 falls off regularly with increasing atomic weight of the cation in a manner qualitatively consistent with conversion to the triplet state by the heavy atom effect. The intensity of fluorescence of the dye adsorbed to silver halides and to cuprous halides is anomalously low compared with the fluorescence on photographically inert substrates of both lower and higher molecular weight. The fluorescence of the dye adsorbed to silver sulfate falls in the general series, and the anomalously feeble fluorescence on photographically active substrates, combined with the feeble phosphorescence on these substrates, strongly suggests that the sensitization process competes primarily with the fluorescence. The excited singlet state of the dye is therefore the active state in sensitization, and since the fluorescence yield of the dye adsorbed to silver bromide is low, the transfer must be accomplished in a time short compared with 10^{-9} sec.

The participation of the triplet states in supersensitization has been suggested.⁴² According to this suggestion, the triplet state of the supersensitizer is excited at the expense of the energy

(37) F. Dörr and G. Scheibe, *Z. wiss. Phot.*, **55**, 133 (1961).

(38) W. T. Simpson, *J. Chem. Phys.*, **15**, 414 (1947).

(39) S. Umano, *Bull. Soc. Sci. Phot. Japan*, No. 2, 7 (1957).

(40) E. Clemente and M. Kasha, *J. Chem. Phys.*, **26**, 956 (1957).

(41) W. West, *Proc. Intern. Congr. on Scientific Phot.*, Liège, 1959, in press.

(42) R. Brunner, A. E. Oberth, G. Pick, and G. Scheibe, *Z. Elektrochem.*, **62**, 132, 146 (1958); cf. C. E. K. Mees, "The Theory of the Photographic Process," revised ed., The Macmillan Co., New York, N. Y., 1954, p. 478.

of the excited singlet state of the sensitizer (a process in which spin is not conserved and which therefore is expected to be slow), and the triplet state of the supersensitizer reacts with the silver halide. This mechanism is based on experiments involving vinylogous series of supersensitizers with the same sensitizer, which seem to indicate that supersensitization occurred only when the triplet level of the supersensitizer was low enough to be excited by the excited singlet level of the sensitizer.

New physicochemical techniques promise to be useful in the study of spectral sensitization. For example, the production of free radicals in pre-

cipitates of silver bromide dyed with sensitizing dyes on illumination at -196° with light absorbed by the dye has been shown by electron paramagnetic resonance experiments.⁴³ Transient fading of sensitizing dyes adsorbed to emulsion grains has been recently observed by A. Buettner, of the Eastman Kodak Research Laboratories. These experiments are not sufficiently developed to merit further discussion at present, but it is at least clear that short-lived species are produced from sensitizing dyes under certain conditions of photographic exposure.

(43) W. C. Needler, R. L. Griffith, and W. West, *Nature*, **191**, 902 (1961).

INVESTIGATION OF SPECTRAL SENSITIZATION. I. SOME PROPERTIES OF SENSITIZING AND DESENSITIZING DYES

BY JAMES E. LUVALLE, ASA LEIFFER, P. H. DOUGHERTY, AND M. KORAL

Defense Products Division, Fairchild Camera and Instrument Corporation,¹ Syosset, L. I., N. Y.

Received June 20, 1962

The e.s.r. signal from crystalline cyanine and merocyanine dyes has been shown to arise from traces of impurities. It is not due to the crystallinity of the dye or to the extended structure. It also has been found that certain sensitizing and desensitizing dyes will initiate the photopolymerization of acrylonitrile when illuminated with light of wave length beyond 5000 Å. The data at present is ambiguous as to the mechanism; *i.e.*, electron transfer or energy transfer from dye to monomer.

Introduction

This paper is the first in a series on the investigation of spectral sensitization. The electron spin resonance (e.s.r.) signals arising from some crystalline sensitizing dyes and the ability of some of these dyes to initiate polymerization when exposed to light will constitute the subject matter of this paper.

During the past two years, several papers have appeared in which e.s.r. signals from crystalline sensitizing dyes and other dyes have been discussed.^{2,3} The authors of the first two papers^{2a,b} attributed the resonance to the crystal structure of the dye. They concluded that the resonance signal was characteristic of long unsaturated chains and that it also was related to the nature of the heterocyclic nuclei attached to the unsaturated chains. The third paper^{2c} did not attempt to explain the observed e.s.r. signal for some crystalline dyes. The fourth paper³ discussed some phenothiazine dyes and suggested the explanation given by Chernyakovskii, *et al.*^{2b}

During the past year, some thirty-odd sensitizing and desensitizing dyes have been synthesized and purified for the investigation of spectral sensitization. In view of the preceding papers, it was decided to investigate the source of the e.s.r. signal from crystalline dye samples.

(1) This work was supported in part by Contracts AF 33(616)-8167 and AF 33(616)-8249 with ASD and monitored by Wright Patterson Air Force Base.

(2) (a) Yu. Sh. Moshkovskii, *Dokl. Akad. Nauk SSSR*, **130**, 1277 (1960); (b) F. P. Chernyakovskii, F. P. Kalmanson, and L. A. Blyumenfeld, *Optika i Spektroskopiya*, **9**, 786 (1960); (c) W. C. Needler, R. L. Griffith, and W. West, *Nature*, **191**, 902 (1961).

(3) C. Layercrantz and M. Yhland, *Acta Chem. Scand.*, **15**, 1204 (1961).

Experimental

A simple set of experiments was devised. A sample of each dye that exhibited a radical signal (whose radical signal had been measured) was dissolved in chloroform and the e.s.r. signal of the solution measured. Then the dissolved dye was recrystallized and the e.s.r. signal of the crystallized dye obtained. The following assumptions were made in setting up this experiment: (1) if the signal were due to a stable radical, it would persist in the chloroform solution and in the recrystallized dye; (2) if the signal were due to the crystal structure of the dye, it would disappear when the dye was dissolved in chloroform and reappear when the dye was recrystallized; (3) if the signal were due to an unstable radical, stabilized while adsorbed to the surface of the dye crystal, it would disappear in the chloroform solution and not reappear in the recrystallized dye.

Another experiment on the ability of sensitizing dyes to initiate polymerization also was performed. At present, it appears that sensitizing dyes act by either exchanging energy with the substrate or passing electrons to the substrate.⁴ Recently, Needler, Griffith, and West^{2c} have reported an e.s.r. signal that appears when some sensitizing dyes are adsorbed on silver bromide and illuminated with light, which they attribute to free radicals derived from the dye molecules. This signal was observed at liquid nitrogen temperatures but not at room temperature.^{2c,5} If unstable free radicals were formed upon illumination, the sensitizing dyes might serve as polymerization initiators. Hence, a simple experiment was set up. A sensitizing dye was dissolved in deoxygenated acrylonitrile and exposed to light from a 100-watt tungsten ribbon filament lamp for 2 hr. at $\approx 13^\circ$ and at 55° . Controls were held at the same temperatures without illumination. The criterion for polymerization initiation was the appearance of a visible precipitate of polymer. Thus, any dye which caused only a minor amount of polymerization would not be classified as a polymerization initiator by these experiments. Obviously, if the dye forms a stable free radical, polymerization would not take place, but the build-up of a free radical should be detected. It may be argued that an adsorbed dye is in a different state

(4) B. H. Carroll, *Phot. Sci. Eng.*, **5**, 65 (1961).

(5) W. J. West, *J. chim. phys.*, **672** (1958).

TABLE I
CRYSTALLINE CYANINE AND MEROCYANINE DYES THAT WERE EXAMINED FOR DARK E.S.R. SIGNAL AND FOR ABILITY TO INITIATE POLYMERIZATION

Number	Dye
I	4-Bis-[1-ethylquinolyl]-pentamethine cyanine iodide
II	4-Bis-[1-ethylquinolyl]-heptamethine cyanine iodide
III	2-Bis-[3-ethylthiazolyl]-heptamethine cyanine iodide
IV	2-Bis-[1-ethyl-3,3-dimethyl indolyl]-heptamethine cyanine iodide
V	2-Bis-[triphenylphosphonium cyclopentadienyl]-pentamethine chloride
VI	2-Bis-[3-ethyl-4,5-diphenylthiazolyl]-pentamethine cyanine iodide
VII	2-Bis-[3-ethylbenzothiazolyl]-heptamethine cyanine iodide
VIII	2-Bis-[3-ethylbenzoselenazolyl]-pentamethine cyanine iodide
IX	2-Bis-[3-ethyl- β -naphthiazolyl]-pentamethine cyanine iodide
X	[2-(3-Ethylbenzothiazolyl)]-[4-(1-ethylquinolyl)]-pentamethine cyanine iodide
XI	[2-(3-Ethylbenzothiazolyl)]-[4-(1-ethylquinolyl)]-heptamethine cyanine iodide
XII	[2-(1-Ethylquinolyl)]-[4-(1-ethylquinolyl)]-pentamethine cyanine iodide
XIII	[2-(3-Ethylbenzothiazolyl)]-[4-(1-ethylquinolyl)]-trimethine cyanine iodide
XIV	[2-(3-Ethylbenzothiazolyl)]-[2-(3-ethylbenzoselenazolyl)]-pentamethine cyanine iodide
XV	[2-(3-Ethylbenzothiazolyl)]-[5-rhodanine]-hexamethine merocyanine
XVI	[2-(3-Ethylbenzothiazolyl)]-5-(3-phenyl rhodanine)-hexamethine merocyanine
XVII	[2-(3-Ethylbenzothiazolyl)]-[triphenylphosphonium-2-cyclopentadienyl]-hexamethine iodide
XVIII	[2-(3-Ethylbenzoxazolyl)]-[triphenylphosphonium-2-cyclopentadienyl]-hexamethine iodide
XIX	[4-(1-Ethylquinolyl)]-[triphenylphosphonium-2-cyclopentadienyl]-hexamethine iodide
XX	2-Bis-[1-ethylquinolyl]-trimethine cyanine iodide
XXI	2-Bis-[3-ethylbenzothiazolyl]-pentamethine cyanine iodide
XXII	2-Bis-[3-ethylbenzothiazolyl]-heptamethine cyanine iodide
XXIII	2-Bis-[3-ethylbenzothiazolyl]-9-methyltrimethine cyanine iodide
XXIV	[2-(3-Ethylbenzothiazolyl)]-[2-(1-ethylquinolyl)]-pentamethine cyanine iodide
XXV	2-Bis-[1-ethylquinolyl]-pentamethine cyanine iodide
XXVI	[2-(3-Ethylbenzothiazolyl)]-[5-rhodanine]-tetramethine merocyanine
XXVII	2-Bis-[3-ethylbenzothiazolyl]-9-[1,3-dimethyl-5-barbiturenolide]-pentamethine cyanine
XXVIII	2-Bis-[3-ethylbenzothiazolyl]-9-[1,3-diethyl-5-thiobarbiturenolide]-pentamethine cyanine
XXIX	4-Bis-[1-ethylquinolyl]-11-bromopentamethine cyanine iodide
XXX	2-Bis-[1-ethylquinolyl]-11-bromopentamethine cyanine iodide
XXXI	2-Bis-[3-ethylbenzothiazolyl]-10-bromopentamethine cyanine iodide
XXXII	2-[3-Ethylbenzothiazolyl]-[<i>p</i> -dimethylaminotolyl]-9-(1,3-diethyl-5-thiobarbituryl)-tetramethine cyanine
XXXIII	2-Bis-[3-ethylbenzothiazolyl]-9-dicyanomethylene pentamethine cyanine
XXXIV	2-Bis-[1-ethyl-3,3-dimethylindolyl]-trimethine cyanine iodide

than the dye dissolved in acrylonitrile and hence a negative result would not show that free radicals were not formed in the adsorbed state; on the other hand, a positive result would indicate either radical formation or energy transfer.

Experimental Results

The experiments described above were performed on some thirty-odd sensitizing and desensitizing dyes. In Table I, the names of some 34 cyanine and merocyanine dyes are listed. Note that nine symmetrical dyes were investigated, all being penta- or heptamethines. Ten unsymmetrical dyes also were investigated, with one exception all being pentamethines or higher. According to Moshkovskii, virtually all of these dyes should have given an e.s.r. signal in the crystalline state; however, not one exhibited an e.s.r. signal.

Needler, Griffith, and West^{2c} reported e.s.r. signals in the crystalline state for dyes XX, XXI, XXII, and XXIII. When these dyes were freshly prepared, none of them exhibited an e.s.r. signal. After three months, dyes XXI, XXII, and also dye II exhibited a small e.s.r. signal. The signals from these dyes are shown in Fig. 1. The width of all signals is about 25 gauss. The fraction of dye exhibiting the resonance signal was quite small in all cases. The signal from dye II indicates

fine structure. Attempts to recrystallize dye XXI resulted in decomposition.

Dyes XXIV, XXV, and XXVI exhibited e.s.r. signals in the dark. In all cases, the fraction of dye exhibiting the resonance signal was quite small. The resonance signal disappeared when each of these dyes was dissolved in chloroform. When each of these dyes was recrystallized, the resonance signal did not appear in the recrystallized dye.

Some additional experiments were performed on dye XXVI. Oxygen was bubbled through the crystalline dye. If the resonance signal were due to aerial oxidation of the surface of the crystal, the signal should increase with time. Figure 2 shows the spectra obtained from this dye at 1, 2.5, and 19 hr. It is obvious that oxygen had no effect upon the radical.

Some of dye XXVI was recrystallized; the recrystallized dye gave no e.s.r. signal. A sample of the recrystallized dye then was illuminated for 135 min. with the imaged light from a 300-watt zirconium arc lamp. No radical signal was detected at the end of this experiment. A sample of the recrystallized dye was illuminated at 55° for 135 min. No radical signal was detected at the end of this experiment. Thus, neither oxygen, light, heat, nor heat and light caused the radical

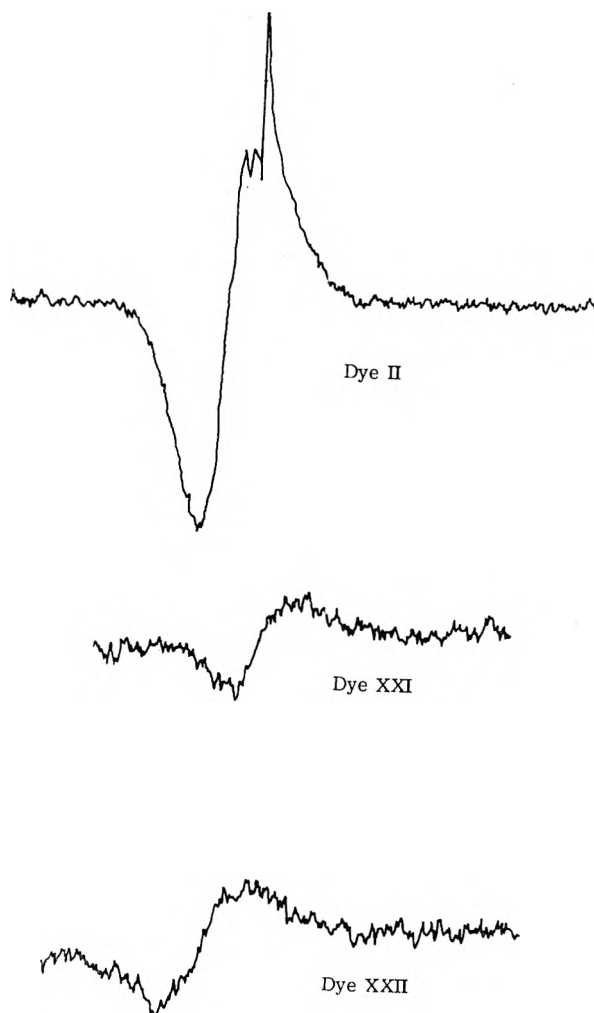


Fig. 1.—E.s.r. spectrum of dyes. All spectra are about 25 gauss wide. All spectra are centered around $g = 2$.

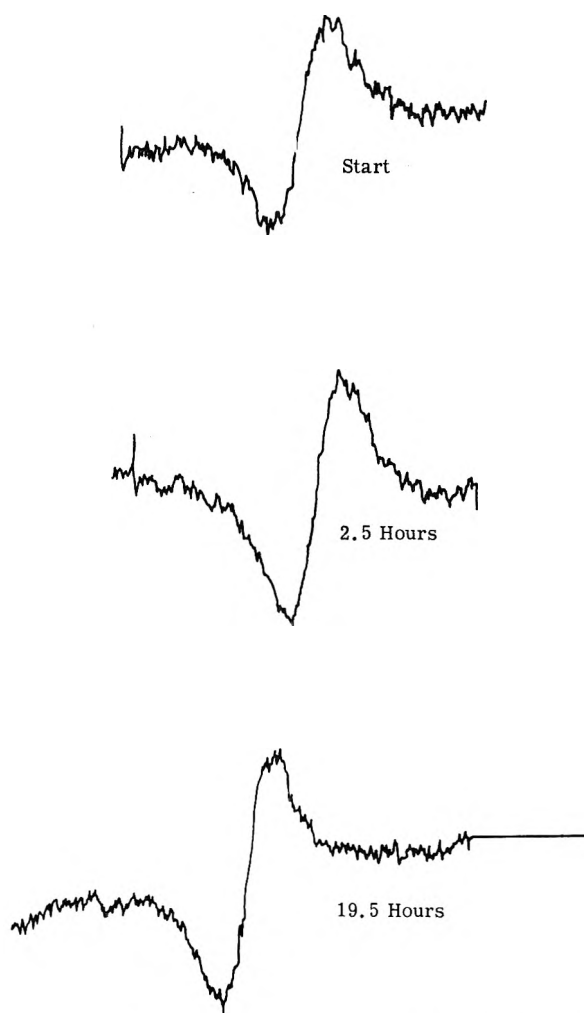


Fig. 2.—Signal from dye XXXI initially and after 2.5 and 19.5 hr. of treatment with oxygen.

signal to appear or in the case of oxygen to increase. However, long periods of time do cause the radical signal to appear.

Of a total of 34 cyanines and merocyanines tested, three exhibited resonance signals. In all cases, the resonance signal disappeared on solution or upon recrystallization. The signal appears to reside on the surface of the dye crystal. A sample of dye XXVI was shaken in tetrahydrofuran, in which the dye is only slightly soluble. Some traces of dye dissolved. The e.s.r. signal disappeared. This experiment strongly indicates that the signal arises from the surface of the dye. All of the data appear to confirm the conclusions that the signal is due to an impurity rather than the long-conjugated chains, the heterocyclic nuclei, or the crystal structure—unless the slow appearance of the signal with time is caused by a change in crystal structure of the surface molecules. These dyes were stored in brown bottles in a refrigerator. Hence, light has little chance to reach the dyes.

The signal may arise from peroxide formation; however, this has not been confirmed. It has been suggested that the signal may arise from cosmic ray bombardment. If so, the damage apparently migrates to the surface.

The low percentage of dyes which exhibited a resonance signal may have been due to the strict purification procedure. All dyes were prepared as pure as possible by the usual synthetic techniques. They then were chromatographed, and the hot solution was filtered and concentrated to obtain the dye. Finally, the dye was fractionally recrystallized. If the infrared spectrum of the dye changed appreciably during this final procedure, the procedure was repeated until the infrared spectrum of the crystalline material was unchanged.

Only two of the 34 cyanines and merocyanines tested, dyes XXVII and XXVIII, initiated polymerization with visible light. These dyes required both heat and light to initiate polymerization. Both of these dyes are trinuclear dyes and both are such that conjugation extends throughout all three nuclei. Table II gives the structure of these two dyes. Dyes XXIX, XXX, and XXXI, in which the third nucleus was a bromine atom, did not initiate polymerization. Dye XXXII, in which a benzothiazole group of dye XXVIII was replaced by a *p*-dimethylaminotolyl group, did not initiate polymerization. Dye XXXIII, in which the barbiturenolide group of dyes XXVII

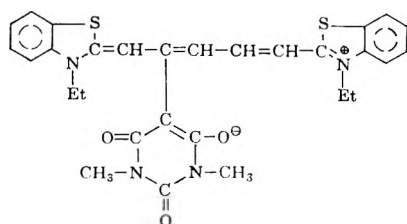
and XXVIII was replaced by $\text{C} \begin{array}{l} \text{CN} \\ \text{CN} \end{array}$, did not initiate

polymerization. Thus, the presence of a bis-ethylbenzothiazole pentamethine cyanine is not sufficient for the initiation of polymerization with visible light. The presence of the barbiturenolide nucleus is not sufficient for the dye to act as a photoinitiator. Apparently, the ability of a cyanine to act as a photoinitiator is a complex of properties. The structure of the end groups, the structure of the third nucleus, the number of atoms in the polymethine chain, and the location of the third nucleus along the chain all are involved. A group of tri- and tetranuclear dyes is being synthesized to evaluate these factors.

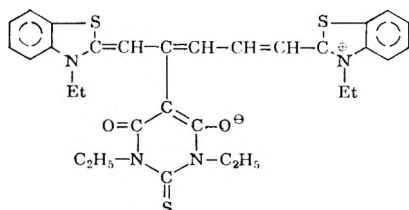
TABLE II

STRUCTURE OF CYANINE DYES WHICH INITIATED MASSIVE POLYMERIZATION

Dye XXVII 2-Bis-[3-ethylbenzothiazolyl]-9-(1,3-dimethyl-5-barbiturenolide)-pentamethine cyanine



Dye XXVIII 2-Bis-[3-ethylbenzothiazolyl]-9-(1,3-diethyl-5-thio-barbiturenolide)-pentamethine cyanine



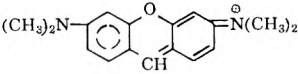
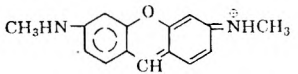
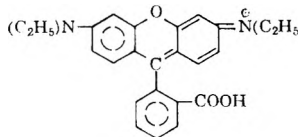
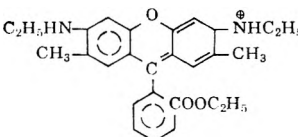
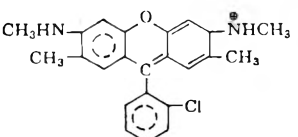
Several desensitizing dyes also were tested for their ability to initiate polymerization. All of the dyes in Table III initiated polymerization. These dyes all belong to the xanthene class. This group of dyes initiates polymerization with light longer than 5000 Å. and is much faster-acting than the trinuclear dyes which also utilize light beyond 5000 Å. The structures of the xanthene dyes do not indicate why these dyes act as polymerization initiators.

None of the dyes that failed to initiate polymerization exhibited a radical signal at the end of the illumination period. However, many of these dyes undergo a color change, not merely a dye fading, when illuminated for a period with a ribbon filament lamp.

Several of the xanthene dyes were dissolved in chloroform and illuminated in the e.s.r. cavity at room temperature. No radical signal was observed either at $g = 2$ or $g = 4$. Thus, at present, there is no positive evidence that the cyanine dyes

TABLE III

DESENSITIZING DYES THAT INITIATED POLYMERIZATION

Dye XXXV	Pyronin Y		Cl^\ominus
Dye XXXVI	Acridine red		Cl^\ominus
Dye XXXVII	Rhodamine B		Cl^\ominus
Dye XXXVIII	Rhodamine 6G		Cl^\ominus
Dye XXXIX	Rhodamine 5G		Cl^\ominus

or xanthene dyes that initiate polymerization utilize electron transfer or energy transfer.

The failure to observe e.s.r. signals from the illuminated cyanine dyes indicates that a stable free radical is not formed at room temperature in solution. The failure to observe polymerization initiation by the large majority of the illuminated cyanine and merocyanine dyes indicates that reactive free radicals are not formed by these dyes in solution. The observation that many of these dyes undergo somewhat drastic color changes upon illumination in solution indicates that a photochemical reaction takes place. As the dye is present in considerably smaller amounts than the acrylonitrile, each dye molecule probably is present in a cage of acrylonitrile molecules; hence, dissociation and recombination is not very probable.

Conclusions

The data in this paper clearly show that e.s.r. signals arising from crystalline sensitizing dyes in the dark are due to impurities and do not arise from the crystalline structure of the dye.

The data concerning photopolymerization initiation do not lead to a nice clean conclusion. The mechanism whereby some of the dyes initiate polymerization is not clear; considerable work must be done on this phase of the problem.

In subsequent papers, the results of investigations of these dyes in the adsorbed state and in solid solutions will be discussed.

THE THEORY OF THE PHOTOGRAPHIC SENSITIVITY

By E. KLEIN

*Agfa Research Laboratories, Leverkusen, Germany**Received June 20, 1962*

The absorption of a photon in a silver halide crystal is nothing but the formation of an electron in the conduction band and of a positive hole in the valence band. In order to avoid recombination both carriers of charge must be trapped at different places of the crystal. The trapped electron then forms silver atoms together with the movable silver ions. There are two processes leading to stable silver nuclei: (1) Small yet instable aggregates grow within their lifetime into small stable ones. (2) Stable ripening centers yet too small to be photographically active grow into active ones. These atomic processes are described in detail by solid state physics, particularly by a theory of dislocations. A theoretical analysis of the characteristic curve based on the experimental findings can complement the theory of the photographic sensitivity, merely derived from solid state physics. The theory of photographic sensitivity must answer the following basic questions: (1) How many quanta must be absorbed by a microcrystal to make it developable? (2) How many latent image specks are formed on a crystal by a given exposure? (3) How many ripening nuclei are to be found on a microcrystal? (4) What is the ultimate limit of the sensitivity? We try to answer these questions quantitatively by the proposed analysis of the H & D curve.

This paper is to give a survey of the present state of investigations; in the second part new results will be presented concerning the problem of the so-called sensitivity distribution; these studies were carried out in collaboration with Dr. Langner. The purpose of this paper is a discussion of the results obtained. Mathematical calculations are avoided.

The basis for a statistical theory of the characteristic curve is discussed by Burton in Mees' book,¹ and Freiser and Klein² published a detailed theory, based on Burton's work, two years ago. The following four factors must be taken into consideration.

(1) The thickness of the photographic coating influences the shape of the characteristic curve since the absorption in the single layers and therefore their contribution to the density varies with the depth of the layer. The so-called elementary characteristic curve is introduced which belongs to a layer so thin that absorption can be neglected.

In Fig. 1 the variation of the characteristic curve with increasing thickness of the layer is shown. The density is plotted vs. the logarithms of the number E_0 of quanta falling upon a unit area. The parameters are the concentrations of silver halide per area. In Fig. 2 the same curves are plotted but now related to the particular maximum densities.

An extrapolation to zero thickness yields the elementary characteristic curve $s(\log E_0)$ already introduced. Since the remission ρ and the transmission τ of an unexposed layer can be measured relatively easily, the mathematical connection between the characteristic curve of the thick layer and the elementary curve is given by the following quantities.

The exposure of the top layer ($z = 0$) amounts to $E_0(1 + \rho)$, and drops within the layer exponentially to $E_0\tau$ at the bottom. The pertaining results are compiled in Fig. 3.

Farnell showed that the effect of reflection on the boundary layer also can be taken into account.³ By this the limits of the integral in Fig. 3 are changed. (Approximately for ρ must be put 4ρ and for τ , 4τ .)

(1) C. E. K. Mees, "The Theory of the Photographic Process," the Macmillan Co., New York, N. Y., 1954.

(2) H. Freiser and E. Klein, *Phot. Sci. Eng.*, **4**, 264 (1960).

(3) G. C. Farnell, *J. Phot. Sci.*, **8**, 194 (1960).

(2) The size of the silver halide grains varies. There exists a distribution function. Both the absorption and the resulting density depend on the size of the single crystal. While absorption increases with the volume of the grain the density contribution increases with the cross section only.

(3) Even within a class of equal sized crystals, the absorption of the quanta occurs statistically. At least r^* quanta must be absorbed in order to render a single crystal developable; that means the fraction of the grains must be calculated which has at least absorbed r^* quanta if a grain has absorbed q quanta on the average.

(4) The quantity r^* may depend on the size of the individual crystals. However, it also may vary among crystals of equal size. Consequently there exists a distribution function for the different r^* -values. This distribution function is called *sensitivity-distribution*.

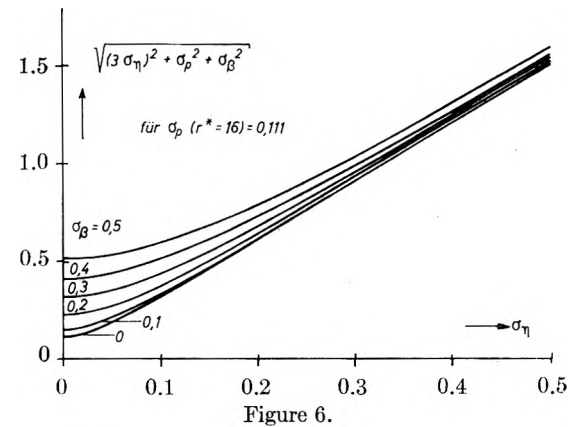
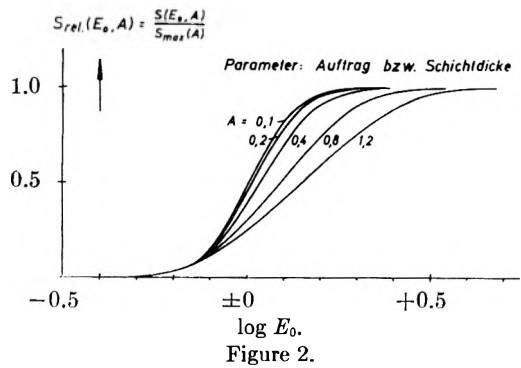
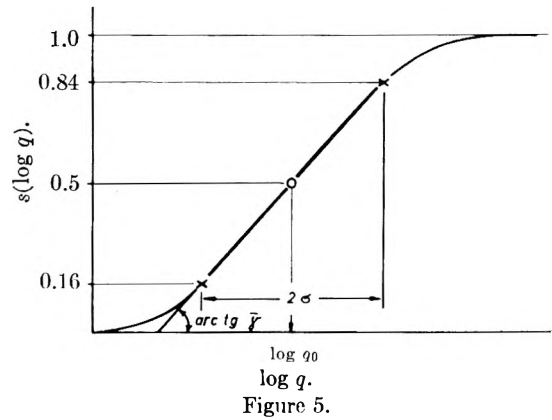
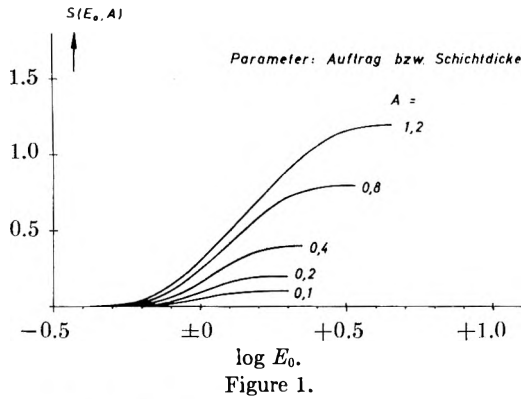
The four points are summarized in Fig. 4. The suffix i denotes the size class, η_i the size distribution function (log normal distribution), p is the distribution function for the statistical absorption of light quanta, derived from a Poisson distribution, and β denotes the sensitivity distribution (log normal distribution). The density again is related to the maximum density.

The function p can be approximated by the error function; moreover the three statistical distributions are mutually independent so that the root mean square of the total distribution σ is the geometrical sum of the individual root mean squares, which means

$$\sigma = \sqrt{(3\sigma_\eta)^2 + \sigma_p^2 + \sigma_\beta^2} \quad (1)$$

(The factor 3 results from the volume dependence of the absorption.)

Figure 5 indicates that the smaller the root mean square value σ , the higher is the gradation value of the H & D curve. The elementary characteristic curve is differentiated and the root mean square deviation of the resulting function is determined. Moreover the relation between σ and the gradation of the elementary characteristic curve is evident. Assuming practically occurring values for σ_β and σ_p we realize from Fig. 6 that the main variation of σ total is due to the variation σ_η of the size.



$$dS = \frac{S_{max}}{h} s(E(z)) dz$$

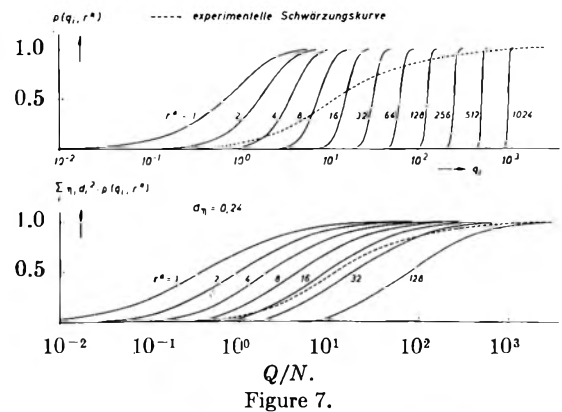
$$S(E_0) = \frac{S_{max}}{h} \int_{z=0}^h s(E(z)) dz$$

$$\log E(z) = \log E_0 (1 + g) - \frac{Dz}{h}, \quad D = \log \frac{1+g}{\tau}$$

$$\left[\log E(z) = \log E_0 - \frac{Dz}{h}, \quad D = \log \frac{E_0}{E(h)} = D(h) \right]$$

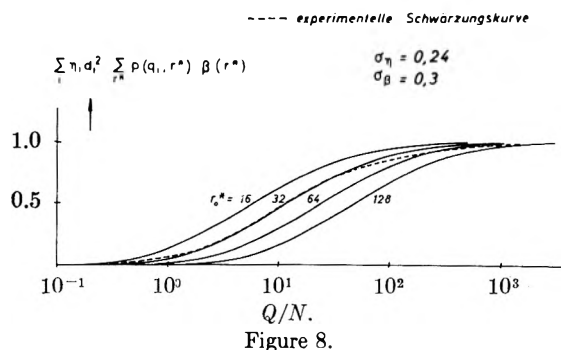
$$S(\log E_0) = \frac{S_{max}}{D} \int_{\log E_0 \tau}^{\log E_0 (1+g)} s(\log E) d \log E$$

Figure 3.



$$S = \frac{\sum_0^{\infty} \eta_i d_i^2 \sum_{r^*} p(q_i, r^*) \beta(i, r^*)}{\sum_0^{\infty} \eta_i d_i^2}$$

Figure 4.



Now we are going to apply the outlined theory step by step.

We are starting with the simplest curve, namely $\sigma_\eta = 0, \sigma_\beta = 0$.

The elementary characteristic curve which has been calculated from an experimental one is plotted as a broken line (Fig. 7, upper curves). Furthermore, the grain size distribution of this layer has been determined from electron micrographs (upper curves). Taking into account this size distribution, the theoretical elementary characteristic curves become flattened (Fig. 7) and thus more

similar to the experimental curves. But still there is no full agreement reached between theory and experiment. In order to achieve this, it was found necessary to introduce the sensitivity distribution (Fig. 8).

Figure 8 shows that a mean value of 32 for r^* makes the experimental and theoretical curves coincide; σ_β was chosen to be 0.3. It is of interest how the sensitivity distribution looks in order to explain the experimental H & D curve. Figure 9 shows the rather wide spread over more than one order of magnitude for a normal high speed emulsion.

Even grains with a quantum sensitivity as low as 4 evidently contribute to the characteristic curve. From Fig. 10 this point becomes clearer: 60% of the density of the toe (0.07) is produced by grains with the sensitivity of 4 quanta, whereas grains with a quantum sensitivity⁴ of some hundred quanta contribute to the higher density values (0.97).

Summarizing the facts, we recognize that (1) there is no doubt about the existence of a sensitivity distribution, and that (2) this distribution can be calculated from experimentally given H & D curves.

We now come to a more detailed description of the sensitivity distribution on the basis of recent publications. At first it was found that the mean quantum sensitivity⁴ of a high speed coarse grain emulsion has a value of about 60, while fine grain emulsions showed a value of about 20. It has to be pointed out, however, that the practical photographic sensitivity of a coarse grain emulsion is higher, as we all know, than that of a fine grain emulsion: the lower quantum sensitivity is overcompensated, namely, by the increase of absorption due to the larger grains.

By means of sedimentation Haase⁵ also was able to show experimentally that the quantum sensitivity indeed depends on the grain size.

Farnell and Chanter⁶ correlated grain size and quantum sensitivity in counting the developed grains under the microscope. Marriage⁷ carried out theoretical calculations pertaining to the experimental findings.

Figure 11 presents the mentioned results of Farnell and Chanter. The ordinate shows the mean number of quanta q_0 necessary to generate a photographic density of 0.5.

We have been able to derive from Farnell's and Chanter's results the dependence of the sensitivity on the grain volume shown in Fig. 12.

Hereby the sensitivity distribution is characterized by its root mean square value σ_β .

Now the question of what causes the sensitivity distribution must be discussed. The general knowledge about the formation of the latent image during exposure implies the concept that there are so-called ripening nuclei in the microcrystals, which, however, do not initiate the development of the grain (Ag or Au atoms). Only an increase in size of these ripening nuclei by photolytically formed Ag atoms leads to an efficient latent image speck.

In the following we denote the number of atoms of a ripening nucleus by r_0 . Adding r^* further

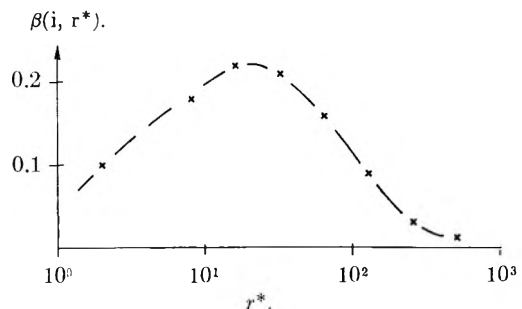


Figure 9.

$$\sigma_\eta = 0.098 \quad \sigma_\beta = 0.55$$

$$d_s = 3.4 \cdot 10^{-5} \text{ cm} \quad r_0^* = 16$$

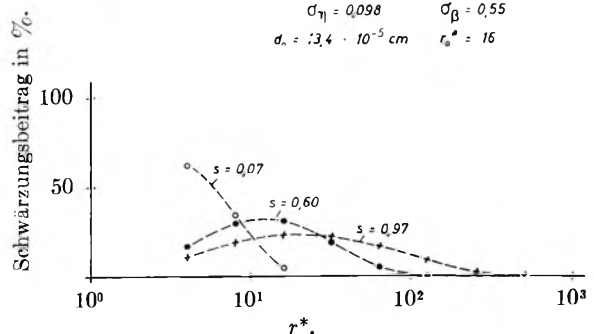


Figure 10.

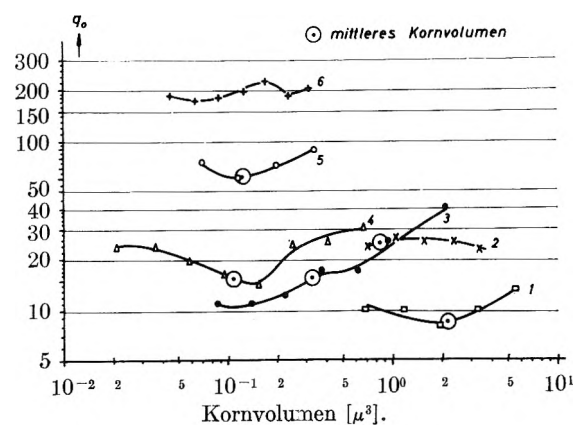


Figure 11.

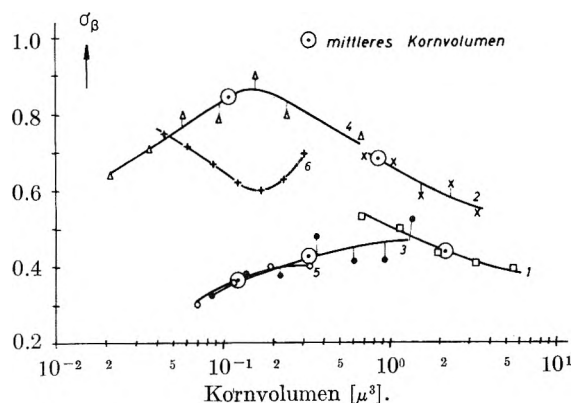


Figure 12.

atoms transforms this nucleus into a latent image speck with the critical number of atoms. A single grain may have Z nuclei. The sensitivity distribution then is caused by all possible deviations in r_0 or Z as well. A general treatment must consider

(4) "Quantum sensitivity" is expressed here by the number of quanta required to make one crystal developable.

(5) G. Haase, *Naturwiss.*, **47**, 320 (1960).

(6) G. C. Farnell and J. G. Chanter, *J. Phot. Sci.*, **9**, 73 (1961).

(7) A. J. Marriage, *ibid.*, **9**, 93 (1961).

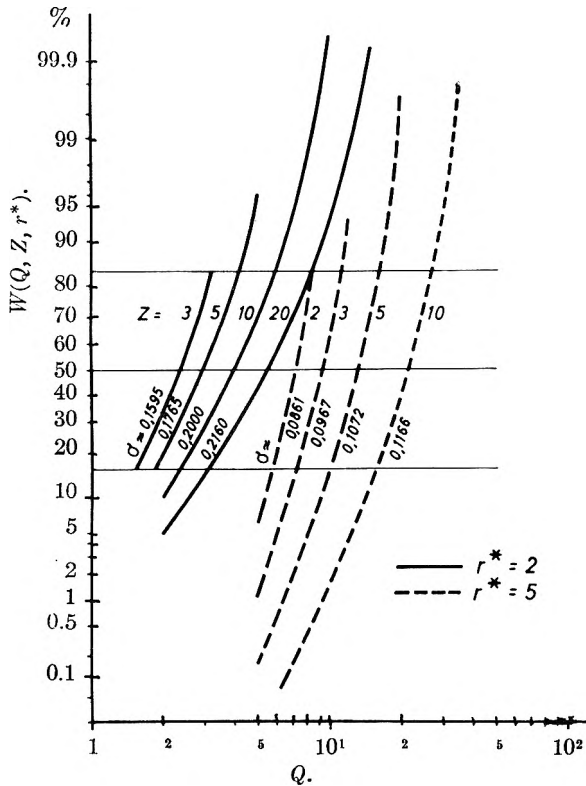


Figure 13.

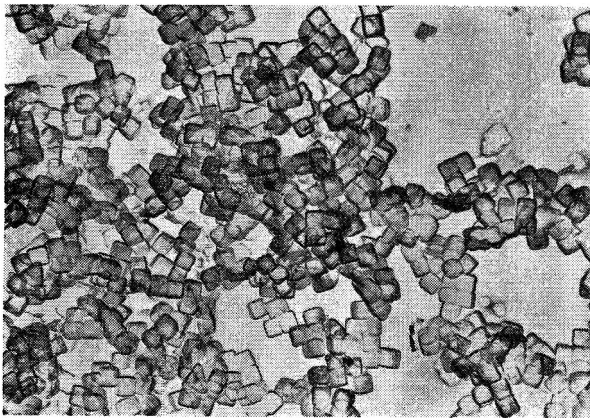


Figure 14.

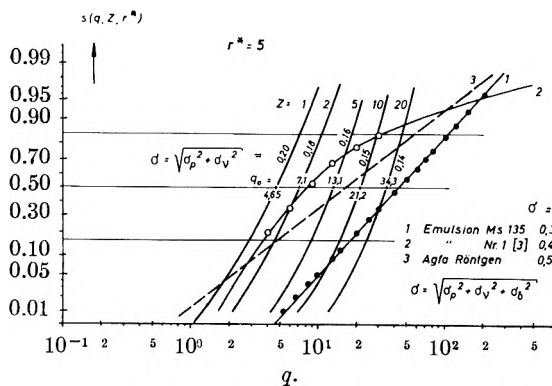


Figure 15.

the different capabilities of the nuclei to trap photoelectrons and thus to increase by photolytic Ag atoms. Formally this results in a change of r_0 . The fact that at least one of the Z nuclei may

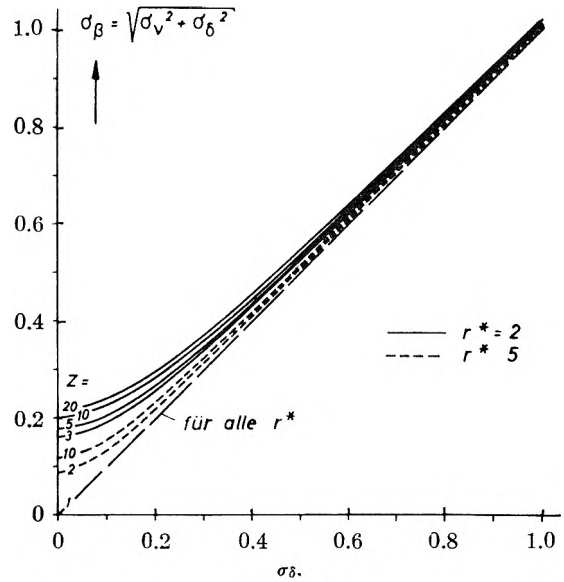


Figure 16.

grow or may not grow by at least the necessary r^* Ag atoms when the grain has absorbed Q quanta leads us to assume an intrinsic or natural sensitivity distribution, the root mean square value of which is called σ_v . In spite of equal Z and r_0 the necessary single speck can be formed by different exposures from grain to grain.

The total sensitivity distribution can generally be understood as composed of the variation in Z and r_0 and the natural distribution just introduced.

$$\sigma_\beta = \sqrt{\sigma_v^2 + \sigma_\delta^2}$$

Here σ_δ denotes the root mean square value of the variation in Z and r_0 . We now try to estimate both values σ_v and σ_δ .

The probability $W(Q, Z, r^*)$ that a microcrystal with the properties Z and r^* becomes developable after the absorption of Q quanta is shown in Fig. 13.

The curves for constant r^* shift with increasing Z toward higher quantum numbers; the same effect is obtained if Z is kept constant and r^* is increased. The complicated functions can be approximated by normal distributions within the range from 20 to 80%, so that it seems justified to take root mean square deviations from these curves. The root mean square, however, is small and depends only slightly on Z and r^* .

The main result is that σ_v is small compared with σ_β . If the function $W(Q, Z, r^*)$ is convoluted with the Poisson distribution taking into account the statistical distribution of the photons, elementary characteristic curves are obtained which still neglect the grain size distribution.

Now the grain size distribution can be taken into consideration. This was done by Farnell and Chanter.⁶ We also considered this for a commercial emulsion (Agfa X-ray). The theoretical elementary characteristic curves with a root mean square deviation $\sigma = \sqrt{\sigma_p^2 + \sigma_v^2}$ can be compared with the experimental values $\sigma = \sqrt{\sigma_p^2 + \sigma_\beta^2} = \sqrt{\sigma_p^2 + \sigma_v^2 + \sigma_\delta^2}$ (Fig. 15).

From these results, we must conclude that the

root mean square deviations of the experimental elementary characteristic curves are considerably greater than those computed theoretically when considering the influence of σ_v . Indeed, an important part of the sensitivity distribution is due to deviations in r^* or Z , respectively, characterized by σ_s .

Figure 16 demonstrates that the influence of σ_v on the total root mean square σ_β decreases rapidly with rising σ_s and finally becomes negligible. Since the deviations in r_0 can be only of the order of magnitude of r^* , which is rather small, these deviations cannot account for the wide distribution found experimentally. For their explanation only the deviations in Z can be responsible.

The formerly mentioned decrease of the quantum sensitivity with increasing grain volume may be explained readily: the larger the grain, the larger the probability that several ripening nuclei are formed per grain. The quantum sensitivity therefore decreases.

Further, it follows that the number of ripening nuclei must be small in high speed emulsions, probably one or two. In order to produce an emulsion with a narrow sensitivity distribution, the distribution of the number of structural dislocations per grain also must be kept narrow—this is a simple consequence of Mitchell's theory of photographic sensitivity—but as far as we know, no progress has been made in this respect.

ON THE MECHANISM OF THE ANTIFOGGING AND SENSITIZING ACTION OF NOBLE METAL SALTS ON PHOTOGRAPHIC EMULSION¹

BY P. A. FAELENs AND B. H. TAVERNIER

Research Laboratories, Gevaert Photo-Producten N.V., Mortsel, Belgium²

Received June 20, 1962

First a review is given on earlier results obtained with washed silver bromide suspensions which are sensitized with noble metal salts. It has now been found that fog inhibition does not only occur with the combined sensitizer: sodium thiosulfate and gold(I) thiocyanate, but also when, after the first ripening with sodium thiosulfate until fog, gold(I) thiocyanate was added. This result leads to the conclusion that the sensitivity specks and the fog centers (which are supposed to be silver sulfide) have been chemically transformed by adding gold salts. Chemical tests show that a silver sulfide suspension can be converted into gold sulfide by adding gold salts. The poor catalytic activity of the gold sulfide nuclei for silver deposition in physical development seems to be analogous to the fog inhibiting action of the gold sulfide sensitivity specks. By ripening with sodium thiosulfate or with gold(I) thiosulfate a gamma increase is obtained; by ripening, however, with gold(I) thiocyanate the gamma remains unchanged. This is ascribed to a better bromine acceptance of the sulfides compared to gold or gold(I) ions.

In view of the importance of noble metal sensitizers for obtaining high-sensitive materials we have tried in the past few years to gain further insight into this mechanism with special attention to gold salts.

According to Müller³ gold atoms should electrolytically condense from gold(I) thiocyanate solutions on silver nuclei formed during chemical or physical ripening. Furthermore, the excess of thiocyanate ions slightly etches the silver bromide grain so that more silver nuclei become superficial.

Many facts have supported this assumption: (1) The influence of gold salts on chemically unripened emulsions was found to be negligible, which implied that nuclei were necessary for the gold sensitization. (2) Emulsion layers exhibit latensification possibilities by adding gold salts. According to James,⁴ gold atoms are formed on the latent silver nuclei, which results in an increase of the sensitivity. (3) *In vacuo* evaporated gold can act as sensitivity centers for silver bromide crystals.⁵

On the other hand, the sensitizing gold atoms

would, according to Steigmann,⁶ be formed by the reducing action of gelatin. In recent articles,⁷ however, he pointed out that irradiated bromine ions, adsorbed on the silver bromide surface, reduce the gold salt to atomic gold.

Experimental

Our sensitization tests were mainly carried out on a fine grain silver bromide dispersion, which was obtained by adding such a quantity of a 10^{-2} molar solution of silver nitrate to a 10^{-2} molar solution of potassium bromide that a molar excess of potassium bromide equal to 1.3×10^{-2} was present.

The silver nitrate solution was poured at 25° within 5 sec. into the potassium bromide solution. The formed silver bromide crystals were allowed to grow slightly and to deposit on the bottom of the vessel. The non-deposited silver bromide was decanted after 48 hr. Too long a sedimentation time stimulates agglomeration and sintering of the grains. Then, distilled water is added to the deposit, whereupon it is gradually brought into suspension by slowly stirring.

In this way, a suspension containing about 50 g. of silver bromide per liter can be obtained with an average grain size of about 0.2 μ (Fig. 1). The pH of this suspension varies between 6.3 and 6.8 and the pAg between 8.4 and 8.7, values which normally occur in the photographic practice.

As binding agent, added either before or after the action of the chemical sensitizer, gelatin is used containing very small amounts of inhibiting substances and sulfur sensitizers (labile sulfur $\leq 2 \cdot 10^{-6}$ per gram of gelatin). In respect of the very large specific grain surface of these small silver halide grains, this gelatin may be considered as inert. Control tests show indeed that ripening at 45° for several hours yields but a small increase of sensitivity.

As noble metal sensitizers, solutions of hydrogen tetra-

(1) Presented at the Symposium on Photographic Processes at the 141st National Meeting of the American Chemical Society, Washington, D. C., March, 1962.

(2) Research made under the auspices of the "Institut pour l'Encouragement de la Recherche Scientifique dans l'Industrie et l'Agriculture" (I.R.S.I.A.).

(3) F. W. H. Müller, *J. Opt. Soc. Am.*, **39**, 494 (1949).

(4) T. H. James, *J. Colloid Sci.*, **3**, 447 (1948).

(5) J. M. Hedges and J. W. Mitchell, *Phil. Mag.*, [7] **44**, 357 (1953).

(6) A. Steigmann, *Brit. J. Phot.*, **96**, 223 (1949).

(7) A. Steigmann, *Sci. Ind. Phot.*, **26**, 289 (1955).

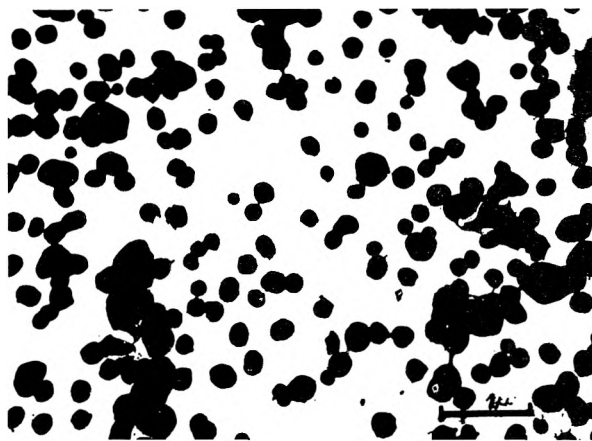


Fig. 1.—Electron micrograph of the silver bromide suspension.

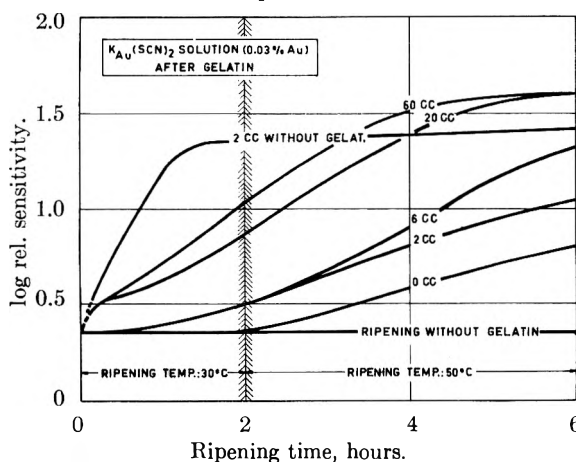


Fig. 2.—Influence of the gelatin on the ripening with gold salts.

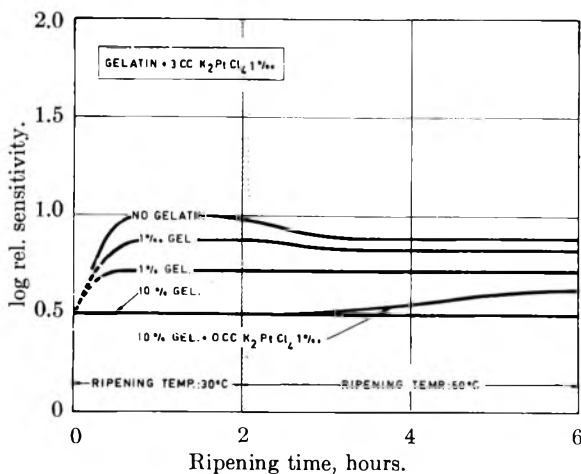


Fig. 3.—Influence of the gelatin on the ripening with platinum salts.

chloroaurate(III), potassium gold(I) thiocyanate in an excess of thiocyanate ions, potassium tetrachloroplatinate(II), and ammonium tetrachloropalladate(II) are used.

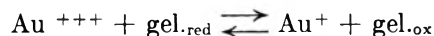
Earlier Results

Without gelatin the maximum sensitivity with noble metal salts is already obtained⁸: (1) at very reduced ripening temperatures (about 35°); (2)

in a much shorter time than in the presence of gelatin (almost immediately), and (3) with much lower amounts than needed in the presence of gelatin (Fig. 2).

In the absence of gelatin other noble metal salts such as platinum and palladium salts also showed sensitizing properties. In the presence of gelatin, however, these sensitizing properties are inversely proportional to the increase of the gelatin concentration (Fig. 3). The inefficient sensitizing action of these noble metal salts in the presence of gelatin may be due to a complex binding between gelatin and the noble metal ions. This complexing action is typical for the polypeptide chains of gelatin and does not occur to the same extent with other binding agents such as polyethylene oxide or polyvinyl alcohol.

The formation of a stable and practical non-migratory complex was shown in different ways. (1) The spectral absorption bands of aqueous solutions of noble metal salts disappear according to the amount of gelatin added⁸ (Fig. 4); (2) the gold(I or III) ions added to gelatin cannot be washed out and this applies also for palladium and platinum ions⁹; (3) oxidation-reduction titrations of the inert gelatin with a trivalent gold salt have shown¹⁰ that it is reduced by the gelatin to monovalent gold compounds according to the reaction



The ratio of the concentrations of monovalent and trivalent gold ions at the equilibrium can be represented by the equation

$$\log(\text{Au}^+) = 0.46 \log(\text{Au}^{+++}) - 2.25 \quad (\text{Fig. 5})$$

It has been found⁹ that sodium thiosulfate decreases the inhibiting action of the gelatin since a complex is formed with a stability higher than that of the complex between gold ions and inert gelatin. This new complex has been identified as gold(I) thiosulfate. Unlike the gold gelatin, this complex can migrate through the gelatin and adsorb on the surface of the silver bromide sol. In this way sodium thiosulfate, added to the wash-water, extracts the gold(I) ions from gelatin (Fig. 6). The special character of gold(I) thiosulfate sensitization is most striking in X-ray sensitivity, where the complex is much more effective than either gold or thiosulfate alone.

In the presence of gelatin and thiosulfate the same amount of gold(I) thiocyanate as in the absence of gelatin is needed for optimum sensitization.

In their potentiometric studies of the reactions between gold, platinum, and palladium salts with gelatin, Narath and Tiilikka¹¹ conclude that the noble metal salts can react with gelatin in two different ways: (1) with "microcomponents" in active gelatin (among others with labile sulfur, reduction sensitizers, or restrainers); (2) with the polypeptide chains of the gelatin to form complexes.

(9) P. Faelens, B. Tavernier, and F. Claes, *Phot. Korv.*, **98**, 3 (1962).

(10) B. Tavernier and P. Faelens, to be published in *Sci. Ind. Phot.*

(11) A. Narath and A. Tiilikka, *J. Phot. Sci.*, **9**, 303 (1961).

(8) P. Faelens, *Wiss. Phot. Intern. Konf. Köln*, 258 (1956), Verlag Dr. O. Helwich, Darmstadt.

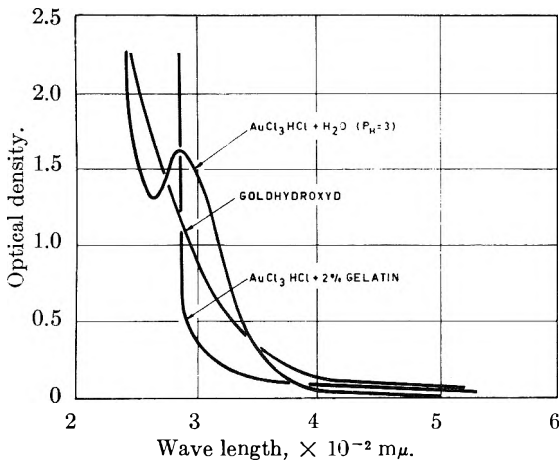


Fig. 4.—Influence of the gelatin on the absorption spectrum of hydrogen tetrachloroaurate(III) in water.

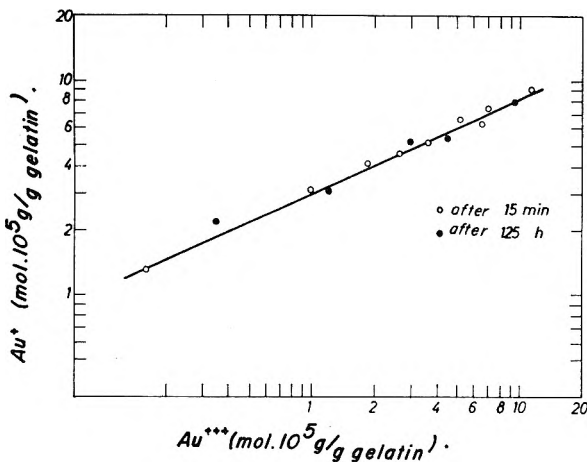


Fig. 5.—Relation between gold(I) and gold(III) ions in gelatinous medium.

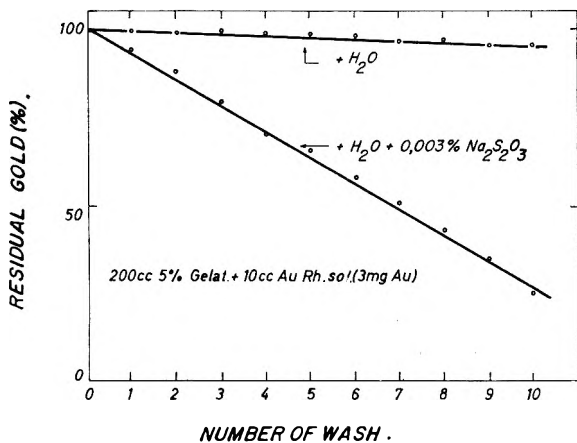


Fig. 6.—Extraction of gold(I) ions from a gelatin solution by adding sodium thiosulfate to the wash-water.

Ripening in the absence of gelatin, with the combined sensitizer sodium thiosulfate and gold(I) thiocyanate, we found a considerable fog decrease as compared to sodium thiosulfate ripening (Fig. 7). In gelatinous medium, however, the fog inhibiting action of the gold salts only becomes apparent after the optimum sensitivity is reached. Before this stage, ripening fog is more important than in the case of sulfur sensitization (Fig. 8).

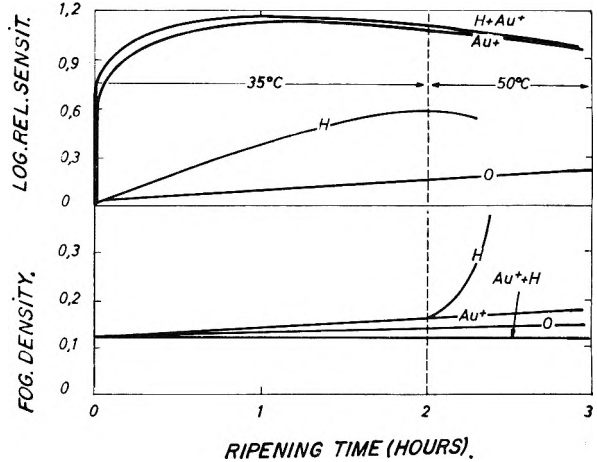


Fig. 7.—Ripening of silver bromide with sodium thiosulfate, gold thiocyanate, and the combination in the absence of gelatin.

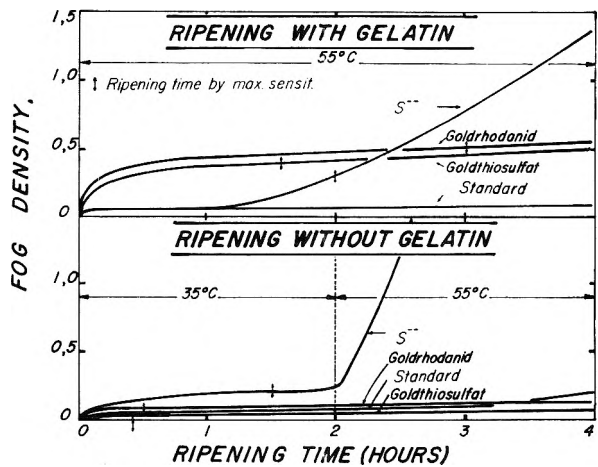


Fig. 8.—Difference in fog formation in the presence and the absence of gelatin after ripening with sodium thiosulfate and gold(I) thiocyanate.

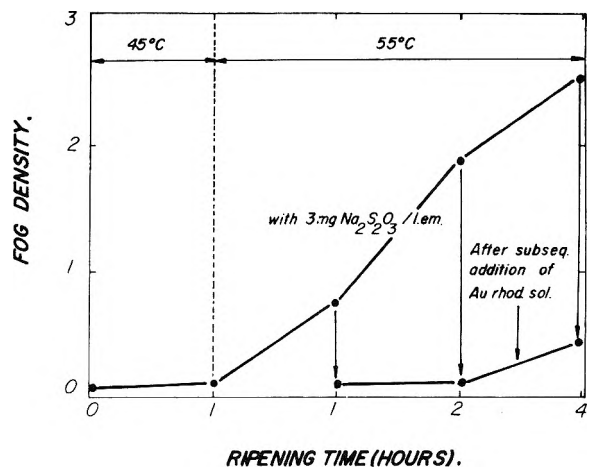


Fig. 9.—Fog decrease by adding gold salts to a silver bromide suspension.

Since this fog is not observed in the absence of gelatin it obviously is caused by interaction of gold ions with some microcomponents of gelatin.

Mechanism of the Antifogging Action of Noble Metal Salts.—The question arises whether the

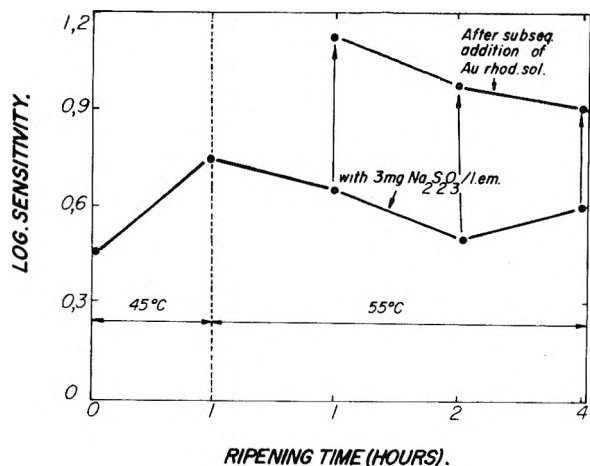


Fig. 10.—Addition of gold salts to a silver bromide suspension ripened with sodium thiosulfate.

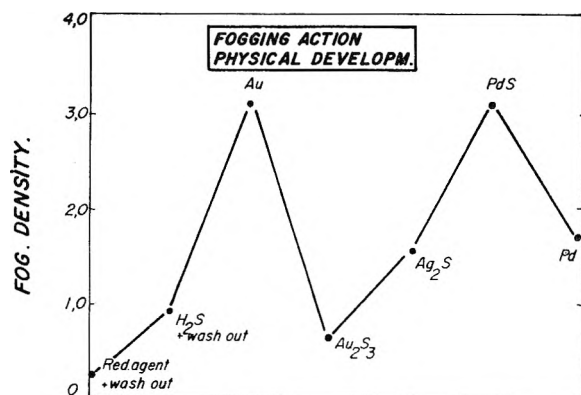


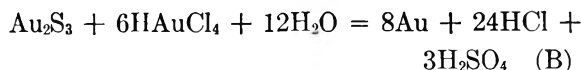
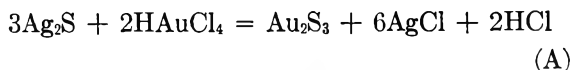
Fig. 11.—Catalytic activity in physical development for different nuclei.

decrease of fog, which is obtained by the ripening of silver bromide suspensions with sodium thiosulfate and gold(I) thiocyanate, also occurs when adding the gold salts only after ripening with sodium thiosulfate. Therefore, a washed gelatin-free silver bromide suspension was ripened with 3 mg. of sodium thiosulfate per 50 g. of silver bromide until a considerable fog was obtained. This fogged suspension was cooled and treated with 10 ml. of a solution of gold(I) thiocyanate or hydrogen tetrachloroaurate(III), equivalent to 3 mg. of gold per 50 g. of silver bromide (amount used in the combined sensitizer). It is seen from Fig. 9 and 10 that the addition of gold salts considerably decreases the fog density, while the sensitivity increases.

In order to obtain the same fog decrease in the presence of gelatin a larger amount of the gold(I) thiocyanate or hydrogen tetrachloroaurate(III) is required, undoubtedly because part of the gold salt reacts with the gelatin. This decrease of the fog level may suggest a chemical action of the noble metal salt on the fogging nuclei, usually supposed to be silver sulfide.

It was proved *in vitro*¹² that silver sulfide is really converted into gold sulfide by the action of gold(III) halides. The reaction products obtained are dependent on the amount of gold salt.

Below the stoichiometric quantity of hydrogen tetrachloroaurate(III), amorphous gold(III) sulfide is formed; an excess of gold(III) ions converts the initially formed gold(III) sulfide to crystalline gold according to reactions A and B.



Potassium tetrabromoaurate(III) reacts in a completely similar way.

When potassium gold(I) cyanide is added to a fogged emulsion, no fog decrease occurs, obviously because potassium gold(I) cyanide does not react with silver sulfide as shown *in vitro* tests. Tetrachloropalladates(II) do not show an antifogging action.

Another model experiment very similar to physical development was carried out. Glass supports were coated with colloidal dispersions of gold, gold(III) sulfide, silver sulfide, palladium(II) sulfide, and palladium, respectively, in gelatin and then immersed in a physical developer. It is remarkable that the colloidal amorphous gold(III) sulfide gives a much smaller density in comparison with the other particles used (Fig. 11).

Moreover, the amount of silver formed in physical development considerably decreased when the silver sulfide nuclei were previously treated with a solution of gold(I) thiocyanate or hydrogen tetrachloroaurate(III) before development.

It has further been observed that the formation of metallic silver in physical development is not decreased when the silver sulfide nuclei layer is treated in a potassium gold(I) cyanide solution.

These findings almost correspond with the very recent results of Ratner.¹³ In his experiments silver bromide emulsions were ripened until a heavy fog ($d = 1.2$) was obtained, whereupon different amounts of gold salts or other noble metal salts were added. In the presence of gelatin and an excess of bromine ions a certain increase of the fog level is noticed during the first ripening stage, followed by a decrease of the density. The same effect has been observed with gold(I) thiocyanate and other noble metal salts.

The author concludes that, at least in the presence of gelatin, two different processes take place in noble metal sensitization: (1) An oxidation process of the fog nuclei (supposed to be metallic silver) so that a decrease of the fog is obtained. This oxidation process is given by reaction C.



He further assumes that the fogging nuclei (silver) shall be oxidized more rapidly than the sensitizing nuclei so that no decrease of the sensitivity will occur.

(2) A reduction of gold(I) ions to metallic gold by the reductors of the gelatin, so that gold atoms can condense on the silver nuclei already present on the silver bromide surface. This

(12) B. Tavernier and P. Faelens, to be published in *Sci. Ind. Phot.*

(13) I. Ratner, *Trudy Nikfi* (Moscow), **42**, 44 (1961).

reduction is said to cause the increase of fog level as well as the increase of sensitivity.

Our experiments in gelatin-free medium have proved, however, that the reduction process caused by gelatin is not essential for the increase of sensitivity.

Where Ratner assumes that, for emulsions sensitized with thiosulfate ions and treated with gold(III) halides, the decrease of fog is due to an oxidation of silver, we admit (on experimental grounds) a conversion of silver sulfide.

Novikov and Gafroerova¹⁴ also carried out investigations in this field. They have observed that in the presence of gelatin a higher ripening fog is reached with amounts of gold salts smaller than those needed for obtaining maximum sensitivity. They suggest that the silver nuclei are converted into gold nuclei by oxidation. The active fogging nucleus is hereby said to consist of pure silver. By the addition of gold salts a mixed silver-gold nucleus is said to be formed whereby the ratio of gold to silver depends on the amount of gold salts added. A certain ratio of gold to silver in the gold-silver nucleus corresponds to a nucleus with optimum sensitizing action. A complete conversion of the fogging nucleus into a pure gold nucleus gives rise to desensitization.

We would like to argue that: (a) colloidal gold nuclei really can act as condensation nuclei for silver in physical development; (b) from our experiments with unripened silver bromide sols containing no binding agent and free from fog or ripening nuclei, we may conclude that the sensitization with gold is caused by pure gold or gold ions which by no means can be considered as desensitization nuclei.

Ratner¹⁵ assumes that this decrease of fog can be caused not only by the oxidation of the fogging nuclei of silver, but also by the fact that these fogging nuclei can change under the action of noble metal ions into crystalline and catalytically ineffective nuclei.

Photographic Action of the Sensitizers: Gold(I) Thiosulfate and Gold(I) Thiocyanate.—Since the same sensitivity and gradation can be obtained by ripening with gold(I) thiosulfate (gold(I) thiocyanate + sodium thiosulfate) as by adding gold(I) ions to a sol previously ripened with sodium thiosulfate (Fig. 12) we may conclude that the same sensitizing nuclei are formed. We notice that the same gradation increase is obtained: (1) after ripening with thiosulfate; (2) after the emulsion was ripened with the combination sodium thiosulfate + gold(I) thiocyanate; (3) after gold(I) thiocyanate was added to the emulsion, ripened with sodium thiosulfate.

The gradation obtained with gold(I) thiocyanate remains lower for any light intensity (Fig. 13). On the other hand the gradation of the primitive sol is practically not modified when the suspension is treated with gold(I) thiocyanate.

The increase of the sensitivity under the in-

(14) I. Novikov and N. Gafroerova, *Zh. Nauchn. Fot. Kin.*, **3**, 173 (1958).

(15) I. Ratner, *Trudy Nikfi* (Moscow), **42**, 60 (1961).

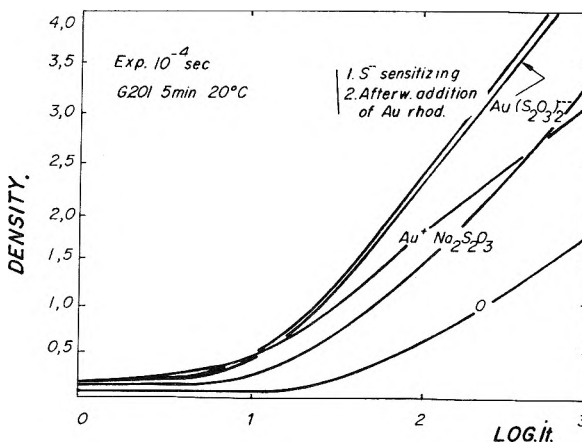


Fig. 12.—Density curves obtained with different chemical sensitizing methods (low intensity exposure).

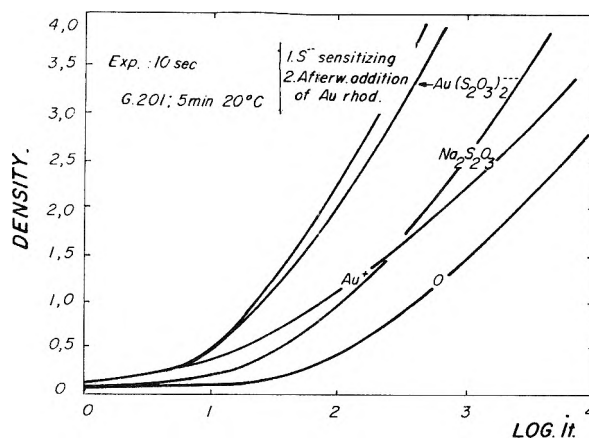


Fig. 13.—Density curves obtained with different chemical sensitizing methods (high intensity exposure).

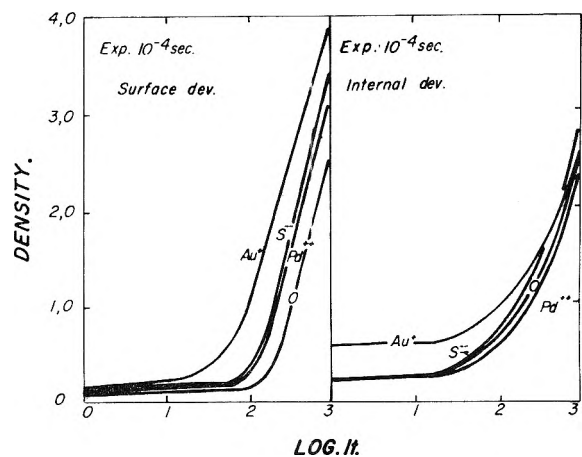


Fig. 14.—Sensitizing action of palladium(II) salts (low intensity exposure).

fluence of gold salts in the toe of the density curve (the gradation remaining unchanged) points to a uniform sensitization of the original silver bromide suspension over all grain sizes.

When ripening a silver bromide sol with sodium thiosulfate or gold(I) thiosulfate, the same increase of gradation is noticed.

Therefore we believe that silver sulfide as well as gold sulfide acts in two ways: (1) In the toe of the

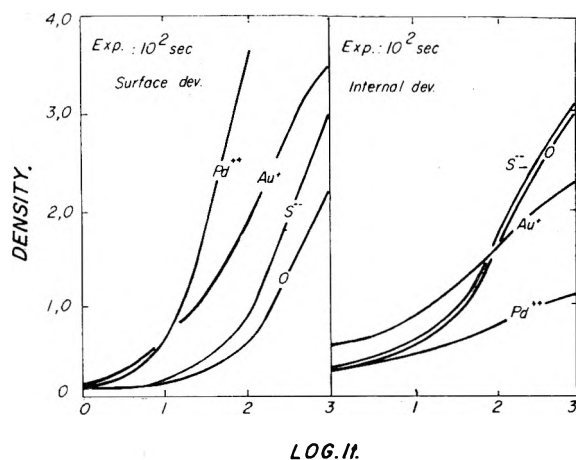


Fig. 15.—Sensitizing action of palladium(II) salts (high intensity exposure).

curve both sulfides act as electron traps. Sensitization with gold increases the efficiency of the trap. (2) In the upper part of the curve the bromine acceptor role of the sulfides becomes important and gives in this way an increase of gradation.

Sensitizing Action of Other Noble Metal Salts.—

It already was mentioned that besides gold salts other noble metal salts also can exert a sensitizing action. They are most effective in the absence of gelatin, or at least in the presence of binding agents which do not react with these noble metal salts.

Typical to the sensitization with palladium salts is the greater effectiveness at lower exposure intensity (Fig. 14 and 15). In this connection it is remarkable that the increase of the surface sensitivity at these low exposure intensities apparently is caused by a considerable decrease of the latent-image formation in the inner parts of the grains. It is indeed known¹⁶ that, when using sulfur sensi-

(16) A. Hautot, "Inventaire des travaux menés dans le champ de la photographie scientifique," Ed. Ceuterick, Louvain, 1958, p. 209.

tizers, the inner latent image can decrease at low intensities. When using palladium salts, this decrease is much more pronounced.

It also is typical that, in the absence of gelatin, palladium salts show no antifogging properties either when used alone or in combination with sodium thiosulfate. The sensitization mechanism of palladium salts is in our opinion fundamentally different from that of gold salts.

Conclusion

Experimental evidence is given for the suggestion of Hautot¹⁷ whereby the sensitizing nucleus which is obtained by ripening with the combination gold(I) thiocyanate-thiosulfate must be considered as gold sulfide. We wish to add that besides gold sulfide, gold also can act as a sensitivity germ.

The poor condensing power of colloidal gold sulfide, as compared to silver sulfide, also supports the thesis of a low fogging action of the gold sulfide speck.

The sensitization of silver bromide suspensions by means of the combination of gold(I) ions and thiosulfate ions not only causes an increase of the sensitivity, but gives the same gradation increase as obtained by ripening with sodium thiosulfate.

The increase of the sensitivity without gradation increase, when ripening with gold(I) thiocyanate, can be explained by more effective electron trapping.

The gradation increase obtained with sulfides such as silver or gold sulfides, contrary to gold or gold(I) ions, probably is due to the greater importance of the bromine accepting action at the higher exposure values.

Acknowledgment.—The authors are indebted to Prof. Dr. A. Van Dormael and Dr. P. Luyten for their interest in this work and for helpful discussions.

(17) A. Hautot, ref. 16, p. 261.

SOME VIEWS ON THE MECHANISM OF DEVELOPMENT

By T. H. JAMES

Research Laboratories, Eastman Kodak Company, Rochester, N. Y.

Received June 20, 1962

Some recent work on the mechanism of development is reviewed. Two types of development can be distinguished in conventional processes. One type, in its relatively pure form, produces compact, rounded, or hexagonal silver particles. Silver ions from the silver halide first pass into solution and then are catalytically reduced at silver surfaces supplied by the latent-image centers and the growing silver particles formed by their development. The process is essentially electrochemical, and may involve adsorption of silver ions, developing agent, or both by the silver surface. In the second type, rounded silver particles are formed initially, but subsequently grow primarily in one direction to form filaments. This type predominates when the developer has little solvent action on the silver halide. Adsorption effects involving the silver halide surface appear to be particularly important in the initiation stage of this type, where the silver centers may be too small to behave in all respects like massive silver. An opportunity to study this initiation stage of development is afforded by making the latent-image forming exposures at the temperature of liquid nitrogen, where the majority of the grains can acquire latent-image centers of near threshold size. Preliminary results are reported. After development has progressed to the point of filament formation, the mechanism may change. Fresh nuclei appear to be formed, however, by direct attack on silver halide surface that forms during development and is unprotected by adsorbed gelatin.

Postfixation Physical Development.—Development of the silver halide in a photographic emulsion can be accomplished in more than one way. The

simplest, from a theoretical viewpoint, is the process known as *postfixation physical development*. In this process, the silver halide in the emulsion is

dissolved out after the latent image is formed, and development subsequently is carried out with a solution that contains a soluble silver salt in addition to the developing agent and other addenda. A silver surface or latent-image center increases the rate of reduction of silver ions from such a solution, and hence more silver is reduced in a given time in the areas that contain latent-image centers. The reaction is self-propagating, in that the silver initially formed by reduction of silver ions at the latent-image centers will itself catalyze the reduction of more silver ions.

The mechanism of physical development has been the subject of several reviews,¹ and there appears to be no major point of dispute. The reduction occurs at the silver surface. The process is an essentially electrochemical one, with the silver serving as an electrode on which silver ions from the solution become adsorbed and to which the developing agent donates electrons. The silver electrode allows the ready transfer of electrons from the developing agent to the silver ions. The processes of oxidation of the developer and reduction of silver ions occur at the same surface, and hence the cathodic and anodic areas are the same. Adsorption of the developing agent by the silver appears to be important to the reaction of some developing agents, *e.g.*, *p*-phenylenediamines, but not to the reaction of others, *e.g.*, hydroquinone.^{1,2} Direct measurements of adsorption of developing agents by silver³ have supported the kinetic evidence by showing adsorption of the *p*-phenylenediamines but not hydroquinone. The over-all activation energy for physical development is low, at least for the developing agents that have been studied adequately. Values of 6.5 to 7.5 kcal./mole have been reported^{2,4,5} for agents belonging to the hydroquinone, *p*-aminophenol, and *p*-phenylenediamine classes. The silver formed in this process is compact, as shown by electron micrographs,^{6,7} and the particles formed under some conditions show well defined geometrical shapes.

Solution Physical Development.—The reduction of silver halide in ordinary development is more complex. The reduction can take place by a process that is essentially physical development. In this process, silver ions from the grains pass into the developer solution immediately surrounding the grains in the swollen gelatin layer. These silver ions, which usually will be in the form of a complex with solvent ions such as halide, thiocyanate, or sulfite, subsequently diffuse to latent-image sites or areas where silver already has been formed by development, and are there reduced to silver by the same mechanism as that which operates in postfixation physical development. The silver formed is

compact.⁷ This mechanism of reduction of silver halide grains has been termed *solution physical development*. Its occurrence has been recognized for many years, but methods of determining, on even a semiquantitative basis, to what extent it occurs during conventional development have been worked out only in recent years.

Results of investigations of solution physical development by James and Vanselow⁷⁻⁹ and by Klein^{10,11} are in good general agreement and show that, under most development conditions used in practice, some solution physical development occurs. The process can occur to an extent sufficient to influence the photographic properties of the developed image, and it is possible to adjust conditions so that development occurs exclusively by this process. The rate-determining step for active black-and-white developers is usually the rate at which the silver ions pass into solution, rather than the specific rate of reduction of the silver ions at the silver surface. Measurements of the activation energy of solution show a surprisingly small dependence on the particular halide. Some values are listed in Table I.^{5,8,12} These values are considerably higher than the 6.5 to 7.5 kcal./mole reported for the activation energy of the reduction of silver ions in physical development.

TABLE I
ACTIVATION ENERGIES OF SOLUTION OF SILVER HALIDES

Silver halide	Activation energies (kcal./mole)	
	No excess halide ion	0.01 M halide ion
AgCl	18	19
AgBr	18	20
AgI	22	21

Chemical or Direct Development.—When the developer has very little solvent action for silver halide, the major portion of development occurs, or is started, by another process. This has been termed *chemical* or *direct development* and commonly is assumed to occur at the interface between the silver nucleus and the silver halide. The silver formed in this process is filamentary, and the filaments formed in the development of silver chloride, silver bromide, and silver iodide are similar in appearance and dimensions.¹²

One or more of several stages may control the over-all rate of direct development: (1) diffusion of developer through the gelatin layer to the silver halide grain; (2) diffusion to the reaction site; (3) adsorption of the developer ion or molecule by the silver halide, the silver, or the silver-silver halide interface; (4) movement of silver ions; (5) electron transfer from the developer to the silver ion, either within an adsorption complex or through the silver nucleus; (6) desorption and diffusion away of the oxidation product of the developer; (7) desorption and diffusion away of the halide ion; (8) incorporation of the silver atom into the silver lattice. Some of these stages may involve more than one step.

(1) Cf. T. H. James, *Phot. Sci. Eng.*, **1**, 141 (1958), and references cited therein.

(2) T. H. James, *J. Am. Chem. Soc.*, **61**, 648 (1939).

(3) R. J. Newmiller and R. B. Pontius, *J. Phys. Chem.*, **64**, 584 (1960).

(4) R. B. Pontius, R. M. Cole, and R. J. Newmiller, *Phot. Sci. Eng.*, **4**, 23 (1960).

(5) T. H. James and W. Vanselow, *ibid.*, **5**, 21 (1961).

(6) C. E. K. Mees, "Theory of the Photographic Process," revised ed., the Macmillan Co., New York, N. Y., 1954, Chapter 13.

(7) T. H. James and W. Vanselow, *Phot. Sci. Eng.*, **1**, 104 (1958).

(8) T. H. James and W. Vanselow, *Phot. Sci. Tech.*, **2**, 135 (1955).

(9) T. H. James and W. Vanselow, *Phot. Eng.*, **7**, 90 (1956).

(10) E. Klein, *Z. Elektrochem.*, **62**, 993 (1958).

(11) E. Klein, *Z. wiss. Phot.*, **54**, 5 (1960).

(12) T. H. James, *Phot. Sci. Eng.*, **3**, 225 (1960).

The electron-transfer process has been considered from the electrochemical viewpoint by several workers.⁶ Keith and Mitchell¹³ and Baines⁶ demonstrated that reduction of silver halide by a developer can occur without direct contact of the silver halide and the developer solution. Gurney and Mott¹⁴ proposed an electrode mechanism which is an extension of their mechanism of latent-image formation and is dependent on the motion of interstitial silver ions through the crystal to the developing nucleus. Klein and Matejec¹⁵ and Levenson, West, and Saunders¹⁶ showed that movement of silver ions or ion vacancies through the crystal can occur in the development of macroscopic silver bromide sheets. However, the contribution of such ionic motion to the total development appears to be small for silver bromide¹⁶ and even smaller for silver chloride,¹⁵ whereas silver chloride grains in a photographic emulsion develop faster than silver bromide.¹²

Jaenicke and co-workers¹⁷⁻¹⁹ showed that important kinetic aspects of development of a simple photographic emulsion in a developer of simple composition can be duplicated in a model system in which the developer makes contact only with a silver electrode, although the correspondence is not complete.¹⁹ Jaenicke regards the mechanism of direct development as similar to the electrode process operative in physical development, except that the anodic and cathodic areas are now different, the anodic process being confined to the region between the silver nucleus and the grain, and the cathodic process to the area of contact between the silver and the developer. He assumes that the anodic reaction, the oxidation of the developer, is controlled by diffusion to or from the silver nucleus, and that the rate-controlling step of the cathodic reaction is either the neutralization of silver ions at the nucleus or the incorporation of silver atoms into the silver lattice.

The mechanism proposed by Mitchell²⁰ is a logical extension of his views on latent-image formation. He assumes that the latent sub-image speck consists of a pair of silver atoms adsorbed on the external or internal surface of the sensitivity center. This speck is unable to receive an electron from the reducing agent unless it first adsorbs a silver ion from the crystal. The positively charged combination of sub-center and adsorbed silver ion has only a very short lifetime at room temperature because of the small heat of adsorption of the silver ion and the very low concentration of free silver ions available during development, and if an electron is not transferred from the reducing agent near the speck during this lifetime, the group dissociates and the speck reverts to the uncharged state. The initiation of development of a sub-center, therefore, is slow. When the electron transfer to the positively

charged speck does occur, an uncharged group of three silver atoms is formed. This group can adsorb a silver ion from the surface of the crystal to form a stable positively charged group of four silver atoms in a tetrahedral arrangement. Once such a center is formed, either as described above or by sufficient exposure, further reduction proceeds rapidly as electrons are transferred from the developing agent to the group, and the positive charge is restored by adsorption of further silver ions from the crystal. Halide ions pass into solution from the surface of the crystal at its interface with the silver speck. Mitchell suggests, however, that a developer of high activity may charge the electrode negatively.

The electron transfer also has been considered as a reaction occurring at the triple interface: silver, silver halide, developer solution.^{1,6,21} Sheppard²² suggested that the importance of the silver nucleus is twofold: its interface with the silver halide provides the necessary ionic deformation for reactivity, and it provides a break in the adsorption layer, a platform for displacement processes. James²³ suggested that silver ions at the interface may be present in essentially an "adsorbed" condition, and that the activated complex of the reaction consists of the developing agent, the adsorbed silver ion, and the adsorption site.

Adsorption of the developing agent by the silver halide or at the silver-silver halide interface appears to be an important preliminary step to reaction.¹ The developer ion or molecule may form an adsorbed salt or complex with silver ions which, by itself, is comparatively stable in that it requires a high activation energy for decomposition into silver and oxidized developer. At the silver interface, the silver ion-developer complex is adsorbed by the silver and electron transfer is facilitated. Basically, this scheme does not differ significantly from the general electrode mechanism except that it localizes the cathodic and anodic processes to the same area and emphasizes the importance of adsorption of the developer. Evidence in support of this view is derived primarily from kinetic effects that suggest the importance of adsorption by silver halide but not by silver, and by the observation that a large increase in the available "cathodic" area between metal and developer solution, brought about by gold physical development of the latent image,²⁴ has relatively little effect upon the rate of subsequent direct development by hydroquinone. Adsorption effect can be invoked to explain cases of development inhibition, acceleration, and super-additivity²⁵⁻²⁸ that have not been completely explained by the generalized electrode mechanism.

The evidence is clear that reduction of the silver

- (13) H. D. Keith and J. W. Mitchell, *Phil. Mag.*, **42**, 887 (1953).
 (14) R. W. Gurney and N. F. Mott, *Proc. Roy. Soc. (London)*, **A164**, 151 (1938); N. F. Mott, *Rept. Progr. Phys.*, **6**, 186 (1939).
 (15) E. Klein and R. Matejec, *Z. Elektrochem.*, **61**, 1127 (1957).
 (16) G. I. P. Levenson, W. West, and V. Saunders, *Phot. Sci. Eng.*, **6**, 135 (1962).
 (17) W. Jaenicke and C. Schott, *Z. Elektrochem.*, **59**, 956 (1955).
 (18) W. Jaenicke and F. Sutter, *ibid.*, **63**, 722 (1959).
 (19) W. Jaenicke, *Phot. Sci. Eng.*, **6**, 185 (1962).
 (20) J. W. Mitchell, *Rept. Progr. Phys.*, **20**, 433 (1957).

- (21) S. E. Sheppard and G. Meyer, *J. Am. Chem. Soc.*, **42**, 689 (1920).
 (22) S. E. Sheppard, *Phot. J.*, **69**, 330 (1929).
 (23) T. H. James and G. Kornfeld, *Chem. Rev.*, **30**, 1 (1942); T. H. James, *J. Chem. Educ.*, **23**, 595 (1946).
 (24) T. H. James, *J. Colloid Sci.*, **3**, 447 (1948).
 (25) G. I. P. Levenson and T. H. James, *J. Phot. Sci.*, **2**, 169 (1954).
 (26) W. E. Lee and T. H. James, *Phot. Sci. Eng.*, **6**, 32 (1962).
 (27) J. F. Willems and G. F. VanVeele, *ibid.*, **6**, 39 (1962).
 (28) T. H. James and W. Vanselow, *J. Phys. Chem.*, **58**, 894 (1954); *Phot. Eng.*, **6**, 183 (1955).

halide can occur without direct contact of the reducing agent with the silver halide, *e.g.*, by the generalized electrode mechanism. The important and still unresolved question is whether this is the fastest way in which an exposed silver halide grain of a photographic emulsion can be reduced by the developer, or whether some other process, *e.g.*, the triple interface mechanism, may not occur faster in practice. It is not inconceivable that the triple interface mechanism may be the important one in the early stages of development, when the latent-image nucleus may be too small to act effectively as a massive silver electrode, and the more generalized electrode mechanism may be the more important during later stages of development.

We can differentiate, at least roughly, between two stages of development: a relatively slow stage of initiation and a more rapid stage of continuation. It is not certain that a qualitative difference exists in the mechanisms of the two stages, but quantitative differences do. The durations of the two stages are influenced to different degrees by some factors which affect the rate of development, and the adsorption effects that have been cited as evidence for the triple interface mechanism are much more pronounced in the early stages than in the later stages of development of the individual grain.

Meidinger²⁹ made an experimental differentiation between the initiation and the continuation stages on the basis of microscopic observations. He used very large grains and a highly restrained developer, and determined (1) the time that elapsed between the first contact of the developer with the grain and the first detection of a silver center in the grain, and (2) the additional time that elapsed before reduction of the grain was completed. A study of the type carried out by Meidinger is, in a sense, a study of a model, since the grains used for the microscopic observations were considerably larger than the grains of typical photographic emulsions and they were developed in an environment that is not typical. The rate of development of grains on a microscope slide, or even in a liquid emulsion, may be many times the rate of development in the coated emulsion, particularly in the later stage.

The electron microscope offers possibilities for a study of the initiation of development, since silver centers of much smaller size can be detected with this instrument than with the optical microscope. The arrested-development technique of Hamilton, Hamm, and Brady,³⁰ used thus far only as a tool in studies of latent-image formation, might be adapted to studies of the initiation of development in a coated emulsion. The study would of necessity be a statistical one and a tedious one, but it could be rewarding.

One distinction between the initiation stage and the continuation stage of development, based on electron-microscope observations, could depend on the form of the developed silver. The first detectable silver centers are compact and often

roughly spherical in form, as observed with the electron microscope. On continuation of development, the transition to filamentary silver is relatively rapid. For example, in the development of a fully exposed motion-picture-positive-type emulsion in a slow-acting developer consisting of 0.28 g. of Metol, 2.78 g. of *l*-ascorbic acid, and 1.0 g. of KBr per liter, buffered to pH 8.5 with borax, only spherical or somewhat elongated particles could be detected after development for 11 min. at 20°. By the end of 16 min., nearly all of the developed silver was filamentary. It does not necessarily follow, however, that the transition from compact to filamentary silver corresponds to a transition from one mechanism to another.

The initiation of development in a typical photographic emulsion has been studied by determining the time required to produce an analytically just detectable amount of developed silver, or a specific small amount that would represent only a small fraction of the total available silver halide. Sometimes this method gives results that can be readily interpreted in terms of the individual grain. For example, a high-level, moderate-intensity exposure produced in some emulsions a latent image of characteristics such that a simple, slow-acting developer reduced most of the grains in a roughly parallel fashion.³¹ After about 5% of the total available silver halide had been reduced, all or nearly all of the grains had started to develop, and further development resulted primarily in an increase in the degree of development of the individual grains. Under such conditions, an initiation period measured in terms of the time required to reduce 5% of the total available silver halide is a fair measure of the amount of time required to reduce 5% of a typical grain.

At lower levels of exposure, and this includes most of the photographically useful range, conditions are not so simple. The initiation period, or induction period of development of the individual grain, varies significantly from grain to grain. In the region of exposure corresponding to the toe of the characteristic curve, the variations in duration of induction periods appear to be much larger than the time required to reduce a grain once development reaches the rapid stage. The increase in amount of reduced silver with increasing time of development depends to a large extent on an increase in the number of developed grains, and the grains one sees under the microscope are rather fully developed.

The preceding statements are not generalizations applicable to all conditions. Other factors, such as diffusion, may dominate under some conditions. For example, the measured rate of increase of silver, under some conditions, is more a representation of the rate of diffusion of the developer into the emulsion layer than of the rate of either initiation or continuation of development of the individual grains. Silver halide solvent effects, unimportant in the early stages of development in a low-solvent solution, may become important as development proceeds if localized concentration of halide ion

(29) W. Meidinger, *Physik. Z.*, **36**, 312 (1935); *Phot. Ind.*, **34**, 1305 (1936).

(30) J. F. Hamilton, F. A. Hamm, and L. E. Brady, *J. Appl. Phys.*, **27**, 874 (1956).

(31) T. H. James, *J. Phys. Chem.*, **44**, 42 (1940); *J. Franklin Inst.*, **240**, 83, 229 (1945).

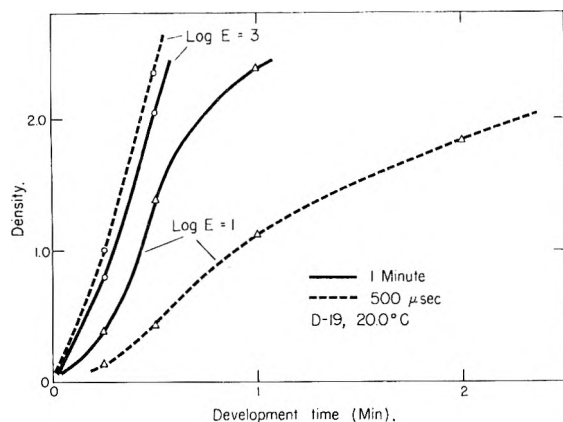


Fig. 1.—Effect of intensity of exposure on the rate of development of a motion-picture-positive-type emulsion. Developer, Kodak D-19 at 20.0°.

becomes sufficiently high. Hence, proper caution should be observed in interpreting kinetic data derived from measurements on coated emulsions.

Where a marked variation occurs in the induction periods of the individual grains, it is tempting to attribute this to a variation in the size of the latent-image nuclei. Meidinger found that the period of initiation of development of his large grains decreased with increasing exposure level, except in the region of solarization, and this is in general agreement with experience with normal emulsions. The dependence of the rate of initiation of development upon the intensity of the exposing light, first observed by Cabannes³² and later independently by Hofmann,³³ likewise falls in line with this view. The Cabannes-Hofmann effect is illustrated in Fig. 1. The broken curves represent 500- μ sec. and the solid curves 1-min. exposures that will give equal densities for prolonged development, but the latent image formed by the 1-min., low-intensity exposure develops about twice as fast as that formed by the 500- μ sec., high-intensity exposure for a moderate exposure level ($\log E = 1$). With this particular emulsion, which shows very little reciprocity failure for prolonged development, the two exposures involve nearly equal amounts of energy. The photolytic silver formed by the high-intensity exposure, however, is distributed over more latent-image centers and hence the average size of the center is smaller than for the low-intensity exposure.

The two curves for $\log E = 3$ show the inverse of the Cabannes-Hofmann effect. At this high-level exposure, which was several times that needed to make substantially all the grains developable in this emulsion, the latent image formed by the high-intensity exposure develops faster than that formed by the low-intensity exposure. In this case, even though the image formed by the high-intensity exposure is the more disperse of the two, the centers are large enough that the induction periods of most of the grains are relatively short, and the rate of increase of density is dependent primarily on the rate of continuation of development of the grains. The faster rate for the more disperse image can be

attributed to the larger number of centers from which development is spreading in the grains.

As the exposure level increases, the activation energy of initiation of development decreases.^{34,35} Sheberstov's data also show a dependence of the activation energy on the degree of chemical sensitization of the emulsion. If we make the reasonable assumption that the average size of the latent-image centers increases with increasing exposure, the data suggest that the activation energy decreases rather rapidly at first with increasing size (exposure) and subsequently tends to level off. The activation energy for a given exposure is lower in the chemically sensitized than in the non-sensitized emulsions. This also can be interpreted on the basis of size; larger centers form in the sensitized grains, either as a result of the concentration of photolytic silver at the sensitivity specks or of incorporation of the sensitizing material, e.g., silver or silver sulfide, in the latent-image centers.

One promising experimental approach to the study of the initiation of development by centers of near threshold size is to work with latent images formed by exposures at very low temperatures. A latent image formed as a result of exposure at liquid nitrogen temperatures (-196°) in many emulsions develops much more slowly than a latent image formed by an equivalent exposure made at room temperature,³⁶ even when the exposure level is many times that needed to make substantially all the grains developable. Figure 2 shows a comparison of the development of the image formed by an exposure at -196° with the images formed by exposures of various intensities at 20° for a motion-picture-positive emulsion. All exposures were adequate to make substantially all grains developable. The three exposures at 20° were of equal total energy. The low-temperature exposure was four times that of the 20° exposures, a factor corresponding to the difference in photographic speed for the two temperatures.

Not only the rate of development differs for the two temperatures, but the characteristics of development also differ. The covering power (the ratio of density to mass of silver), is substantially independent of development time for the low-temperature exposure, and the image tone is nearly neutral and likewise independent of development time. These properties of the developed image indicate³⁷ that it is made up primarily of completely or nearly completely developed grains at all times of development, except possibly for the first few minutes when not enough silver has been developed for accurate measurements. This conclusion is confirmed by electron micrographs. Hence, there is a wide distribution of induction period times among the developable grains. On the other hand, the grains exposed at 20° develop in roughly parallel fashion, and the increase in density represents primarily an increase in the degree of development of the grains. The covering

(34) T. H. James, *Phot. Sci. Tech.*, **2**, 81 (1955).

(35) V. I. Sheberstov, *Zh. Nauchn. i Prikl. Fotogr. i Kinematogr.*, **6**, 97 (1961).

(36) T. H. James, W. Vanselow, and R. F. Quirk, *Phot. Sci. Eng.*, **5**, 219 (1961).

(37) T. H. James and L. J. Fortmiller, *ibid.*, **5**, 297 (1961).

(32) J. Cabannes and Y. Rocard, "La diffusion moléculaire de la lumière," Les Presses Universitaires de France, Paris, 1929, p. 83.

(33) P. O. Hofmann, *Physik. Z.*, **36**, 650 (1935).

power decreases with increasing time of development and the absorption spectrum of the developed silver, which shows a much higher density at 400 $m\mu$ than at 700 $m\mu$ in the early stages of development, shifts toward neutrality as the time of development increases.

Figure 3 shows density-time of development curves for several temperatures of development of latent images formed by exposures at the two temperatures. The activation energy calculated from the rates of initiation of development, where these rates are expressed as the reciprocal of the time required to produce 0.5 mg. of silver per square decimeter, is approximately 15 kcal./mole for the 20° exposure. (Rates have been corrected for change in pH with temperature.³⁴) The activation energy for continuation of development, determined from the maximum rates, is only 12 kcal./mole. The situation is different for the low-temperature exposure. Here, the silver produced by development increases linearly with time of development until more than 50% of the total available silver halide has been reduced. The activation energy calculated for the initial stages of development is the same as that calculated for the maximum rate of development, and is approximately 22 kcal./mole.

It seems unlikely that the distribution of induction periods of the grains exposed at -196° is a consequence of a distribution in size of the latent-image centers. An improbably large variation would have to be assumed, and the constancy of the activation energy over such a large variation in size would be inconsistent with other considerations. More likely, the measured rate is that of some separate process which is acting to build up the size of latent sub-centers to the point where rapid development can commence, or in some way to make existing centers more accessible to the developer.

A wide distribution of induction periods would be consistent with Mitchell's description of the development of the sub-image, referred to earlier in this paper. Other possible mechanisms might involve (1) direct transfer of electrons from the developer to the conduction band and subsequent build-up of sub-centers by the same process as that operative in latent-image formation, or (2) an uncatalyzed reduction of silver ions by developer adsorbed on the silver halide surface, which could supply silver atoms that subsequently would directly or indirectly build up the size of latent-image sub-centers to that necessary to promote development.¹ The buildup as a result of the uncatalyzed reaction could occur as follows. The concentration of adsorption complex of silver ion and developing agent at the surface would be determined by a dynamic equilibrium with a constant supply of developing agent from the solution, and the rate of decomposition of the complex to form silver atoms might well follow a zero-order reaction equation. This would be consistent with the linear relation observed between the amount of developed silver and the time of development of the film exposed at -196°. Silver atoms formed at the sensitivity centers could join directly with existing

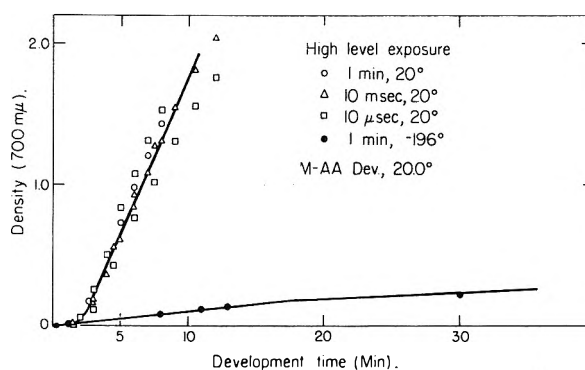


Fig. 2.—Effect of temperature of exposure on the rate of development of a motion-picture-positive-type emulsion. High-level exposure; developed at 20.0°. Developer: Metol, 1.4 g.; *l*-ascorbic acid, 3.3 g.; KBr, 1.0 g./l.; buffered to pH 8.5 with borax.

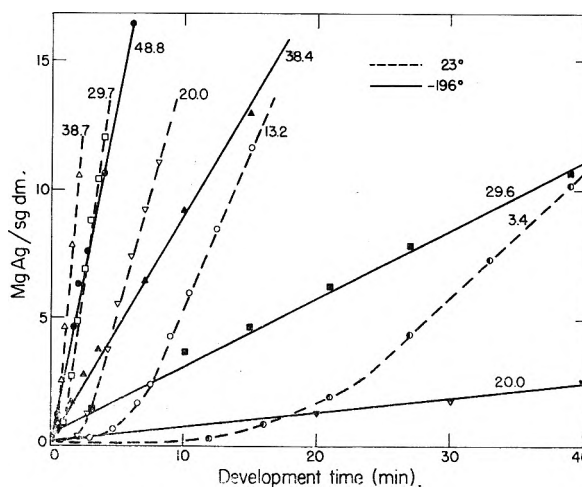


Fig. 3.—Effect of temperature of development upon the rate of development of latent image formed at 23° (broken curves) and -196° (solid curves). The numbers on the curves refer to development temperature. The same developer was used as for Fig. 2.

latent sub-centers to form full latent-image centers. Isolated silver atoms formed at a distance from such sub-centers would be thermally quite unstable and would lose electrons to the conduction band. These electrons then would act to build up the sub-centers in the same way as photoelectrons formed by exposure. Evidence in support of such a process has been obtained in work with ferro-EDTA developers,³⁸ where a correlation was found between the rate of development of low-level exposure areas and the rate of fog formation by the developer for a series of developers that developed a high-level exposure area at substantially equal rates. Moreover, the implication that the addition of a single silver atom to a very small center could markedly increase its ability to promote development is in keeping with current theory of the small size of the latent-image centers and with the evidence obtained from the Herschel effect that the removal of one silver atom from some centers substantially destroys the developability of those centers.³⁹

(38) T. H. James, *Phot. Sci. Eng.*, **4**, 271 (1960).

(39) G. Kornfeld and T. H. James, *J. Opt. Soc. Am.*, **33**, 615 (1943).

In the later stages of development of the individual grain, filamentary silver is formed rapidly in comparison with the rate of early growth of the silver nuclei. An increase in rate would be expected solely on the basis of the increase in the silver-silver halide interface or total silver surface as development of the grain proceeded, but other factors may be of importance in the increase in rate. Halide ions pass out into the solution and migration of silver atoms or recrystallization to form filaments also occurs. Fresh silver halide surface thus becomes exposed to the action of the developer and, if the restraining adsorbed gelatin layer is not constantly re-established, areas will form that are more susceptible to direct attack by the developer. New silver nuclei thus can arise, and grow catalytically in the same fashion as the original latent-image nuclei. Thus, a much larger number of growth centers for developing silver could arise than correspond to the number of latent-image centers.⁴⁰ The apparent multiplicity of silver filaments formed during development of larger grains may arise in this way.

When the developing agent is negatively charged in its active form, the rate of development of the individual grain in the early stage relative to that in the later stage decreases with increasing charge of the developer ion and the grain surface.^{23,41} This charge effect has been explained on the basis that the greater the charge the smaller will be the concentration of developer ions in the immediate vicinity of the grain surface and likewise the smaller will be the effective concentration of developer ions adsorbed by that surface. As development proceeds, it is assumed that the surface charge

decreases locally and hence the effective concentration of developer at the surface increases. Jaenicke¹⁹ regards this explanation as incompatible with the concept of reaction at the triple interface, the properties of which he assumes will remain approximately constant during development. It is possible that the properties of the interface do not remain constant, however. The adsorbed halide ions responsible for the net negative charge of the grain surface actually cover only a small portion of that surface in terms of monolayer coverage and probably are adsorbed primarily at the edges, corners, and regions of physical imperfections.⁴² Since the probable sites of latent-image center formation are the regions of physical imperfections, the charge effect in development may also be strongest in these regions. As development progresses and the silver-silver halide interface moves away from such regions, a marked drop in the localized surface charge may occur, leading to an increase in the effective concentration of developing agent adsorbed at the interface and hence an increase in the rate of the reaction.

As indicated previously, the reaction mechanism may actually change as development progresses from the early to the later stages. Apparent conflicts between experimental results and theory could be resolved if it were assumed that the initiation of development depended upon a reaction at the silver-silver halide interface and that the electrochemical mechanism became dominant in the later stages of development of the grain. There is, however, no compelling evidence for such a change in mechanism.

(42) E. J. W. Verwey, *Proc. Acad. Sci. Amsterdam*, **36**, 225 (1933); *Chem. Rev.*, **16**, 363 (1935); K. Astakhov and M. Suzal'tzev, *Zh. Fiz. Khim.*, **6**, 1348 (1935); A. H. Herz and J. O. Helling, *J. Colloid Sci.*, **17**, 293 (1962).

(40) T. H. James, *J. Chem. Phys.*, **11**, 338 (1943).

(41) T. H. James, *J. Phys. Chem.*, **43**, 701 (1939); **55**, 563 (1951); *J. Franklin Inst.*, **240**, 15 (1945).

THE PRESENCE OF TRANSIENT CHARGE-TRANSFER COMPLEXES IN HALOGEN ATOM RECOMBINATION AND PHOTOHALOGENATION PROCESSES

BY ROBERT L. STRONG

Department of Chemistry, Rensselaer Polytechnic Institute, Troy, N. Y.

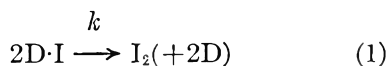
Received May 25, 1962

Transient halogen atom-aromatic complexes are formed after the flash photolysis of iodine in benzene, toluene, *o*- and *p*-xylene, mesitylene, and hexamethylbenzene, and of bromine in benzene. These complexes are detected by their very strong charge-transfer spectra in the visible region. The processes are completely reversible for iodine in benzene, toluene, and xylene, while very slight photoiodination occurs in the iodine-mesitylene and iodine-hexamethylbenzene systems. Disappearance of the complex following decay of the flash is second-order and diffusion-controlled. Rate constants based on dissociation quantum yields from a simple continuum solvent model are lower than those predicted by simple diffusion theory, and indicate that molecular complex formation can lead to lower primary quantum yields of dissociation through deactivation of the halogen molecule. Photobromination of the benzene occurs in the bromine-benzene system; the extent of reaction per flash is only slightly increased by oxygen, while the rate of disappearance of the bromine atom-benzene complex (which follows concurrent first- and second-order kinetics) is greatly decreased by oxygen. Presumably photobromination occurs in the primary process through an activated bromine molecule.

Introduction

The flash photolysis technique has been used extensively for the study of halogen atom recombination with various third bodies in the gas phase and in inert solvents. A relatively large fraction of the halogen molecules is dissociated by the flash resulting in a transitory decrease in the absorbance of the cell in the visible region; kinetics of the atom recombination process are determined by following spectrophotometrically as a function of time the subsequent increase in absorbance to its initial value. However, there is a transient increase in absorbance following the flash photolysis of iodine in various aromatic solvents in the visible region^{1,2} that has been attributed to the charge-transfer spectrum³ of a 1:1 complex between an iodine atom (acceptor) and the donor aromatic molecule, D. Similar transient spectra have been observed by Bridge⁴ and by Gover and Porter⁵ in a variety of solvents.

The formation of the complex is completely reversible for iodine in benzene, toluene, or xylene; disappearance of the complex after the flash has decayed to negligible intensity is second-order, as shown by linear time plots of the reciprocal of the change in absorbance, ΔA ($\approx -\Delta I/2.3I$ for small changes in transmittancy, where I is the transmitted light intensity) over at least a fivefold change in ΔA . This is consistent with the second-order recombination mechanism (1) if it is assumed that the



observed change of the absorbance is due entirely to change in the concentration of D·I—i.e., if one neglects the accompanying change in absorbance resulting from the concurrent formation of I_2 , either "free" or complexed with D. Disappearance of the mesitylene-iodine atom complex also follows second-order kinetics, although approximately

0.01–0.02% of the molecular iodine (initial concentration about $2 \times 10^{-6} M$) disappears per flash by photoiodination of the mesitylene.

The concentration of the complex is related to the change in absorbance at wave length λ by

$$\Delta A_\lambda = \epsilon_{c,\lambda} d [D \cdot I] \quad (2)$$

where $\epsilon_{c,\lambda}$ is the molar extinction coefficient of the complex and d is the absorbing light path. Integration of the second-order rate expression in terms of ΔA_λ leads to

$$\left(\frac{d}{dt}\right) \left(\frac{\epsilon_{c,\lambda}}{k}\right) \frac{1}{\Delta A_\lambda} = t + C \quad (3)$$

From slopes of the $(1/\Delta A)$ vs. t plots, values of the "relative extinction coefficients," $\epsilon_{c,\lambda}/k$, were calculated and plotted as a function of wave length for the pure solvents benzene, toluene, *o*-xylene, *p*-xylene, and mesitylene²; wave lengths of maximum absorption were 495, 515, 570, 520, and 590 $m\mu$, respectively. These shifts in λ_{max} , expressed in terms of differences in energy, $\Delta(h\nu_{max})$, relative to that of the benzene complex, were shown to be almost identical with those of comparable molecular halogen and interhalogen complexes, providing further confirmation of the charge-transfer nature of these spectra observed in the iodine atom systems.

The overlap of the D·I charge-transfer and I_2 spectra for each of these five aromatic donors prevents independent measurements of the rate of appearance of I_2 and the simultaneous rate of disappearance of D·I. With hexamethylbenzene as the donor species, however, the shift of λ_{max} toward the infrared has been shown⁶ to be so large that there is no absorption by D·I at 489 $m\mu$ over a hexamethylbenzene concentration range in carbon tetrachloride of from 0.062 to 0.434 M . By combining change in absorbance measurements at a given time after initiation of the flash at this wave length, ΔA^0 , with those at a wave length where absorption changes, ΔA_λ , are due largely to the complex (for example, 605 $m\mu$), it was further shown that

(6) R. L. Strong and J. P'errano, *J. Am. Chem. Soc.*, **83**, 2843 (1961).

(1) S. J. Rand and R. L. Strong, *J. Am. Chem. Soc.*, **82**, 5 (1960).

(2) R. L. Strong, S. J. Rand, and J. S. Britt, *ibid.*, **82**, 5053 (1960).

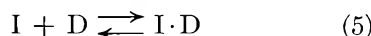
(3) R. S. Mulliken, *ibid.*, **74**, 811 (1952).

(4) N. K. Bridge, *J. Chem. Phys.*, **32**, 945 (1960).

(5) T. A. Gover and G. Porter, *Proc. Roy. Soc. (London)*, **A262**, 476 (1961).

$$\frac{2\Delta A^0[D]}{\epsilon_{I_2,\lambda}\Delta A^0 - \epsilon_{I_2^0}\Delta A_\lambda} = \frac{[D]}{\epsilon_{c,\lambda}} + \frac{1}{K_c\epsilon_{c,\lambda}} \quad (4)$$

where $\epsilon_{I_2,\lambda}$ and $\epsilon_{c,\lambda}$ are the molar extinction coefficients of I_2 and $D \cdot I$ at 605 $m\mu$, $\epsilon_{I_2^0}$ is the extinction coefficient of I_2 at 489 $m\mu$, and K_c is the equilibrium constant for the complex



Values for K_c of 2.7 l./mole and for $\epsilon_{c,\lambda}$ of 1600 l./mole cm. at 605 $m\mu$ and room temperature were obtained from the best straight line through the points plotted according to equation 4 as a function of hexamethylbenzene concentration ($[D]$) in carbon tetrachloride.

Linear plots were also obtained for this system when the reciprocals of ΔA^0 or ΔA_λ were plotted against time, again indicative of the second-order kinetic behavior of absorbance changes for the absorbing species. At 489 $m\mu$

$$-\frac{d[I]_{\text{total}}}{dt} = \frac{2d[I_2]}{dt} = 2k[I]_{\text{total}}^2 \quad (6)$$

where $[I]_{\text{total}}$ ($= -2\Delta[I_2]$) is the total iodine atom concentration—either as free iodine atoms or complexed with hexamethylbenzene; this assumes that the rate of formation of I_2 is the same regardless of the form of the iodine atoms. In terms of ΔA^0

$$\frac{d\Delta A^0}{dt} = \frac{4k}{\epsilon_{I_2^0}d} (\Delta A^0)^2 \quad (7)$$

At 605 $m\mu$

$$-\frac{d\Delta A_\lambda}{dt} = \frac{2k(K_c[D] + 1)}{d[K_c[D](\epsilon_{c,\lambda} - \frac{1}{2}\epsilon_{I_2,\lambda}) - \frac{1}{2}\epsilon_{I_2,\lambda}]} (\Delta A_\lambda)^2 \quad (8)$$

Values for k were calculated using equations 7 and 8 from slopes of $1/\Delta A$ vs. t plots at 489 and 605 $m\mu$, respectively, at room temperature, and are given in Table I.

TABLE I

SUMMARY OF RECOMBINATION RATE CONSTANTS, MEASURED AT 489 $m\mu$ AND 605 $m\mu$

[D] (moles/l.)	k (from eq. 7) (l./mole sec.)	k (from eq. 8) (l./mole sec.)
0.434	7.6×10^9	7.6×10^9
.434	7.0	6.4
.434	6.6	6.0
.372	6.2	7.1
.310	7.1	6.0
.310	9.0	8.0
.248	8.6	9.6
.186	10.1	7.3
.186	7.8	8.7
.124	10.4	7.9
.062	6.9	4.3
Average	7.9×10^9	7.2×10^9

The fact that there is no significant trend in k at either wave length over the concentration range

studied (where the ratio $[I]/[D \cdot I]$ varies from approximately unity to five) indicates that the rate of recombination is approximately the same for complexed and "free" iodine atoms, and is not a significant function of the encounter diameters. (This conclusion was also expressed by Gover and Porter.⁵) Further verification is found in the fact that the average value of k determined at either wave length is in fair agreement with the values obtained for the recombination of iodine in pure CCl_4 in earlier flash work^{7,8} and in work involving the combination of mean iodine atom lifetime and quantum yield measurements.⁹

Experimental

The apparatus was of conventional design for flash production and rapid spectrophotometric measurement of absorbance changes as a function of time at a single wave length,¹⁰ and has been described in detail in reference 1. The flash lamp consisted of four parallel quartz discharge tubes (each 18 mm. o.d. with aluminum electrodes 12 cm. apart) arranged in cylindrical form and surrounded by an aluminum reflector. The continuous analyzing beam from a 6.3-volt (battery-operated) automobile headlamp passed through the cylindrical reaction cell (10-cm. light path, 28 mm. o.d.) positioned along the cylindrical axis of the flash lamp, and rendered approximately monochromatic by the appropriate Bausch and Lomb interference filter. (Characteristics of the nine interference and necessary auxiliary filters are included in reference 2.) The output from a 931-A photomultiplier was fed through a capacitance-coupled cathode follower amplifier to a Tektronix Type 531 oscilloscope equipped with either a type 53B or D plug-in pre-amplifier, and the resulting oscillogram corresponding to a rapid change in transmittancy of the cell was photographically recorded. Four General Electric Pyranol capacitors (total capacitance 30 microfarads) were discharged through the flash lamp by a GL-5830 mercury thyratron tube controlled by the gate-out from the oscilloscope sweep circuit. Although rated at 10,000 volts, these capacitors were generally charged to 8,000 volts (960 joules); under these conditions the flash light intensity reached a maximum in less than 40 $\mu\text{sec.}$, and decayed with a half time of approximately 20 $\mu\text{sec.}$ Scattered flash light decayed to a negligible value by 150–200 $\mu\text{sec.}$ after initiation of the flash in most cases, although reliable measurements could be made after 70 $\mu\text{sec.}$ by applying a suitable scattered light correction.

Methods of solvent purification and drying are given in references 1 and 2. Highest purity hexamethylbenzene, bromine, and iodine were used without further purification, except that the iodine used in cells filled *in vacuo* was re-sublimed from a KI- I_2 mixture. Iodine-benzene and bromine-benzene cells were filled both in air and *in vacuo* (following rigorous outgassing consisting of trap-to-trap distillation and at least eight freezing, pumping, and thawing cycles). All other cells were filled in air but were tightly stoppered with ground-glass caps. The cells were wrapped with Eastman Kodak Co. gelatin Wratten filters to limit low-wave length absorption by the corresponding molecular halogen complexes; K2 and 2B filters were used for the iodine and bromine cells, respectively.

Discussion

Estimation of k and ϵ_c .—Although the extinction coefficient of the complex can be expressed in terms of ΔA_λ and d by equation 2, the concentration of the complex is not known and (as pointed out above) the overlap of the visible spectra prevents determination of k for the donors benzene, toluene, xylene, and mesitylene. If it is assumed, however, that recombination in each system is

(7) R. Marshall and N. Davidson, *J. Chem. Phys.*, **21**, 2086 (1953).

(8) R. L. Strong and J. E. Willard, *J. Am. Chem. Soc.*, **79**, 2098 (1957).

(9) H. Rosman and R. M. Noyes, *ibid.*, **80**, 2410 (1958).

(10) M. I. Christie, R. G. W. Norrish, and G. Porter, *Proc. Roy. Soc. (London)*, **A216**, 152 (1953).

diffusion-controlled and independent of the encounter diameters of the recombining species and that the diffusion process can be represented by a sphere moving through a continuous viscous medium, the rate constants at constant temperature should be inversely proportional to the coefficients of viscosity.⁹ Values for k were calculated using an average value of 7.5×10^9 l./mole sec. from Table I for the recombination process in carbon tetrachloride ($\eta = 0.97$ centipoise at 20°), and extinction coefficients at λ_{\max} were calculated from k/ϵ_c values given in reference 2 for air-filled cells. These are tabulated in Table II.

TABLE II

RATES OF RECOMBINATION AND EXTINCTION COEFFICIENTS ASSUMING DIFFUSION-CONTROLLED RECOMBINATION

Solvent	η (centi- poise) at 20°	k/ϵ_c at λ_{\max} (cm./sec.) (from ref. 2)	k (l./mole sec.)	ϵ_c (l./mole cm.)
Benzene	0.652	3.2×10^3	11.2×10^9	3500
Toluene	.590	3.6	12.3	3400
<i>o</i> -Xylene	.810	2.5	9.0	3600
<i>p</i> -Xylene	.648	3.8	11.2	2950
Mesitylene	.702	1.8	10.4	5800

The rate constants can be estimated in another manner. The complete rate expression for the photochemical formation of the complex (assumed to be instantaneous and therefore proportional to the light absorbed, I_a), and its disappearance is

$$d[\text{D}\cdot\text{I}]/dt = 2\phi I_a - 2k[\text{D}\cdot\text{I}]^2 \quad (9)$$

Or, in terms of ΔA_λ

$$\frac{d\Delta A_\lambda}{dt} = 2\phi \epsilon_{c,\lambda} dI_a - \left(\frac{2}{d}\right) \left(\frac{k}{\epsilon_{c,\lambda}}\right) (\Delta A_\lambda)^2 \quad (10)$$

where ϕ is the primary quantum yield of dissociation of the iodine molecule. A theory has been developed by Noyes,¹¹ based also on the model of the liquid being a continuous medium of viscosity η , that predicts

$$\phi = 1 -$$

$$\frac{1}{\left(1 + \frac{(m(h\nu - \epsilon))^{1/2}}{6\pi\eta a^2}\right) \left(1 + \frac{(mkT/24)^{1/2}}{\pi\eta a^2}\right)} \quad (11)$$

where m is the mass of the atom, a is its radius, and $(h\nu - \epsilon)$ is the excess kinetic energy of the atoms heading in opposite directions. Although this theory predicts a higher quantum yield (0.21) for iodine in carbon tetrachloride than is observed (0.13),^{8,9} it gives quite good agreement for low-viscosity hydrocarbons.¹² Equation 11 has been used to calculate ϕ for the five aromatic solvents assuming an average flash light wave length of 500 m μ , and equation 10 has been solved for the k/ϵ_c values given in Table II using an IBM-650 digital computer as previously described.¹ Resulting values of k and ϵ_c are listed in Table III.

(11) R. M. Noyes, *Z. Elektrochem.*, **64**, 153 (1960).

(12) D. Booth and R. M. Noyes, *J. Am. Chem. Soc.*, **82**, 1868 (1960).

TABLE III

RATES OF RECOMBINATION AND EXTINCTION COEFFICIENTS FROM EQUATION 10

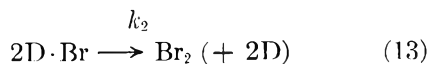
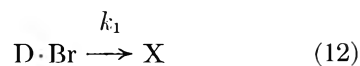
Solvent	ϕ (from eq. 11)	k (l./mole sec.)	ϵ_c (l./mole cm.)
Benzene	0.29	10.5×10^9	3300
Toluene	.31	6.6	1830
<i>o</i> -Xylene	.24	3.7	1480
<i>p</i> -Xylene	.29	4.4	1160
Mesitylene	.27	4.7	2600

Because of the extreme sensitivity of the computer integration to errors in I_a and ΔA_λ at a given time after the flash,¹ the absolute values for k and ϵ_c are qualitative only. However, the lower values for k relative to that of benzene, in contrast to those given in Table II, for the stronger molecular iodine charge-transfer complexes (lower donor ionization potentials) indicate that the primary quantum yields calculated from equation 11 are too high. Presumably charge-transfer interaction increases the probability of deactivation of the excited iodine molecule through a radiationless transition.

The Flash Photolysis of Bromine in Benzene.—

As in systems involving iodine, the flash photolysis of bromine in benzene is accompanied by a transitory increase in the visible-region absorbance, again indicative of the formation of the atom-benzene (D·Br) charge-transfer complex. There are, however, several important differences between this and the iodine-benzene system: (a) appreciable photobromination of the benzene occurs (ca. 0.04% of the bromine disappears per flash at an initial bromine concentration of 2×10^{-4} M); (b) the rate of disappearance of the complex—determined by following ΔA_λ as a function of time at wave lengths above the region of absorption by Br₂—is complex, apparently being neither first- nor second-order; and (c) the rate of disappearance of the complex in thoroughly outgassed cells is much faster, but the extent of reaction per flash only slightly less, than in air-filled cells with well dried benzene.

A possible mechanism for the disappearance of D·Br involving concurrent steps is



The expression for the rate of disappearance of D·Br is

$$-d[\text{D}\cdot\text{Br}]/dt = k_1[\text{D}\cdot\text{Br}] + 2k_2[\text{D}\cdot\text{Br}]^2 \quad (14)$$

At wave lengths above the absorption region of Br₂

$$\Delta A_\lambda = \epsilon_{c,\lambda} l [\text{D}\cdot\text{Br}] \quad (15)$$

and

$$-\frac{d\Delta A_\lambda}{dt} = k_1 \Delta A_\lambda + \frac{2k_2}{d\epsilon_{c,\lambda}} (\Delta A_\lambda)^2 \quad (16)$$

The integrated rate law then is

$$e^{k_1 t} = \frac{k_1 e^{k_1 C}}{\Delta A_\lambda} + \frac{2k_2}{d\epsilon_{c,\lambda}} e^{k_1 C} \quad (17)$$

where C is the constant of integration. The exponential term $e^{k_1 t}$ is plotted as a function of $1/\Delta A_\lambda$ for varying assumed values of k_1 until a straight line results, the constant $\epsilon_{c,\lambda}/k_2$ then being determinable from the slope/intercept ratio.

At wave lengths greater than 500 $m\mu$, k_1 is approximately constant for air-filled cells, independent of wave length, and equals *ca.* $1.8 \times 10^3 \text{ sec.}^{-1}$. In thoroughly outgassed cells it is approximately ten times larger, and almost completely masks the second-order contribution. The constant $\epsilon_{c,\lambda}/k_2$ is a function of wave length with a maximum value of $6 \times 10^{-7} \text{ cm./sec.}$ at approximately 560 $m\mu$ in air-filled cells; the spectrum is quite broad, however, extending over the complete visible region.

Initially it was assumed that the product of reaction 12 (X) eventually leads to bromination products. However, the fact that the extent of bromination per flash is (approximately) the same in outgassed and in air-filled cells, but that k_1 is an order of magnitude larger in the former, suggests that recombination to form molecular bromine must occur by reactions involving X in addition to reaction 13. Partial photobromination of the benzene presumably occurs through a primary process involving an activated bromine molecule, as suggested in earlier studies of benzene¹³ and bromo-

(13) E. Rabinowitsch, *Z. physik. Chem.*, **B19**, 190 (1932).

benzene¹⁴ photobrominations, rather than a complexed bromine atom. Reaction 12 might be a transition from the π -complex (D·Br) to a more localized σ -complex that can also react with another σ -complex, a D·Br, or a free Br atom to produce molecular bromine, although there is no experimental evidence for this second intermediate.

Products of the aromatic bromination have not as yet been completely identified, although the proton magnetic resonance spectrum of a residue from vacuum evaporation of the benzene indicates that tetrabromocyclohexene may be a major product. Neither bromobenzene nor hexabromocyclohexane was found to be a product, in contrast to earlier low-intensity benzene photobromination studies.^{13,15} It is possible that moisture and higher bromine concentrations can lead to acid-catalyzed ring substitution and complete addition reactions.¹⁶ Indeed, early runs in which the benzene was not rigorously dried gave greater amounts of bromine reacting per flash than in the runs reported here.

Acknowledgments.—Experimental details and further equilibrium results on these investigations of the bromine–benzene system will be reported in a later publication by Mrs. Jeanne S. Bartlett. This work was supported in part by National Science Foundation Grants NSF G-4181 and G-9988. We especially want to thank Professor M. J. S. Dewar for many helpful suggestions made during the Symposium.

(14) D. L. Hammick, J. M. Hutson, and G. I. Jenkins, *J. Chem. Soc.*, 1959 (1938).

(15) W. Meidinger, *Z. physik. Chem.*, **B5**, 29 (1929).

(16) R. Cornubert and A. Rio, *Bull. soc. chim. France*, 60 (1955).

KINETIC STUDIES OF PHOTOTROPIC REACTIONS. I. EVIDENCE FOR AN ION-PAIR INTERMEDIATE IN THE REACTION OF METHYL VIOLET WITH CYANIDE ION¹

BY GLENN H. BROWN, SETTY R. ADISESH, AND JAY E. TAYLOR

Department of Chemistry, Kent State University, Kent, Ohio

Received May 26, 1962

Methyl violet and cyanide ion react to form the leuconitrile, which reaction is reversed by the action of ultraviolet light. For the forward reaction in ethanol–water solutions, a decrease in the second order rate constant is observed as cyanide ion is increased over a wide range of concentration. The phenomenon is explained by ion-pair formation between the reactant ions. Assuming that a specific ion-pair is a reaction intermediate, a simple equation, $k_{\text{obsd}} = k^*K/(K[\text{CN}^-] + 1)$, where k_{obsd} and k^* are the observed and the corrected rate constants and K is the association constant for ion-pair formation, explains the kinetics of the reaction. As the dielectric constant of the solvent mixture is decreased, both the rate of reaction and ion-pair formation increase. The various rate constants at 25.0, 35.0, and 43.5° are given along with values for ΔF_{act} , ΔH_{act} , and ΔS_{act} . The values of the association constants are given at these same temperatures as well as the values for ΔF , ΔH , and ΔS for ion-pair formation.

Introduction

Marckwald² gave the name "phototropy" to the phenomenon in which a solid changes color when exposed to certain wave lengths of electromagnetic radiation but reverts to its original color on removal of the exciting radiation. This phenomenon now

goes under the name of phototropism or photochromism. The field has been reviewed recently by Brown and Shaw.³

Holmes⁴ has proposed that the triarylmethyl leuconitriles on excitation with ultraviolet radiation show phototropism by the formation of either a triarylmethyl radical or the corresponding dye,

(1) This work was supported by the Aerospace Medical Research Laboratories, Wright Air Development Center, Wright-Patterson Air Force Base, Ohio.

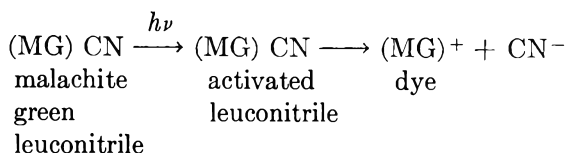
(2) W. Marckwald, *Z. physik. Chem.*, **30**, 140 (1899).

(3) G. H. Brown and W. G. Shaw, *Rev. Pure Appl. Chem.*, **11**, 1 (1961).

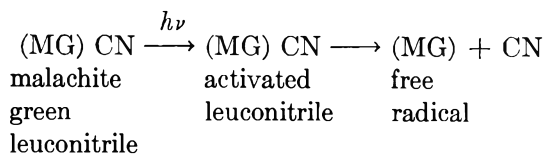
(4) E. O. Holmes, *J. Phys. Chem.*, **61**, 434 (1957).

depending upon the dipole moment and the dielectric constant of the solvent. This idea can be represented schematically as

Solvent of high dielectric constant

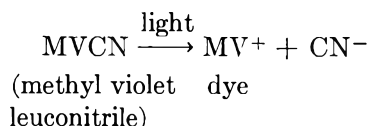


Solvent of low dielectric constant



Sporer⁵ has found that the triarylmethyl leuconitriles undergo two photoreactions, dye formation and cleavage of substituents on the amine nitrogens. The cleavage reaction was found to be most pronounced in solvents having a low dielectric constant; cleavage also was found in solvents of high dielectric constant but this process is masked by dye formation.

This paper is concerned with kinetics of the reaction of methyl violet with potassium cyanide in several solvent media, primarily the 87.6% ethanol-12.4% water (by weight) system. If there is the decomposition of the methyl violet leuconitrile to the dye as has been proposed by others



then, one should be able to follow the formation of the leuconitrile by mixing the dye and cyanide provided an equilibrium exists between the dye and the leuconitrile. The reaction between dye and cyanide ion proceeds smoothly and can be followed easily in a spectrophotometer by observing the change of absorbancy of the solution with change in concentration of dye. There does not appear to have been an approach, such as is described in this paper, to the investigation of the mechanism of the phototropism of leuconitriles. Previous studies have been of a qualitative nature^{6,7} and have used ultraviolet radiation to form the dye from the leuconitrile; then a study of the decay of the dye to the leuconitrile was made.

Experimental

Materials.—Methyl violet (Eastman Kodak Co.) was dissolved in absolute ethanol and filtered to remove any insoluble residue. The dye solution was cooled in an ice bath and diethyl ether was added to the solution to precipitate the dye. The dye was filtered and then dried in an oven at 105°.

A saturated solution of potassium cyanide of reagent grade quality was prepared at 60° in 1:3 water-ethanol mixture. The solution was filtered while warm and then cooled to room temperature. Absolute ethanol was added with stirring until crystallization ceased and then the solution was allowed to cool at room temperature for 2-3 hr. The potassium cyanide which crystallized was filtered and washed with absolute ethanol. The crystals were dried at 70-80° for 2-3 hr. and then at 105° for 2 hr. The composition of the cyanide was determined by the Liebig-Dénigès method and was found to have a purity of 99.8%.

A commercial grade of absolute ethanol was treated with magnesium ethoxide and refluxed with this reagent for about one-half hour. The alcohol was distilled and the middle fraction boiling at 78.4° under a standard atmosphere was collected for use. Ethanol prepared by this procedure was found to contain less than 0.1% by volume of water as determined by the Karl Fischer method. The alcohol was placed in a dark glass-stoppered bottle and stored in a desiccator over Drierite. The 95.6% ethanol, by weight, was prepared by distillation of commercial grade ethanol by collecting the middle fraction which boiled at 78.1° corrected to a standard atmosphere. The percentage of water was established by analysis with the Karl Fischer reagent. All ethanol-water systems were prepared by dilution of the absolute ethanol or the 95.6% ethanol.

Procedure.—The data in this study were taken on a Beckman DU spectrophotometer. The temperature was controlled by circulating water from a constant temperature bath through the thermospacer set in the cell compartment of the instrument; thus the temperature could be controlled to $\pm 0.1^\circ$. Calibration curves were established by the use of solutions of known concentrations of dye. The wave length used for the measurements was 580 m μ .

Stock solutions of methyl violet and potassium cyanide in each composition of ethanol and water were prepared by dissolving the proper amount of the purified dye or cyanide in a given volume of solvent. The quantitative rate measurements were made in a solvent composed of 12.4% water and 87.6% ethanol (by weight).

The solutions of cyanide and dye were each brought to temperature, mixed, and transferred to the absorption cell for measurement. The decrease in absorbancy with time was then followed on the spectrophotometer. In several observations the solvent composition, dye concentration, and temperature were fixed and the rate of the reaction as a function of concentration of cyanide was measured. The purpose of changing the composition of the solvent was to study its role on the rate of the reaction. The rate of the reaction as a function of temperature also was studied.

In addition to the 87.6% ethanol-12.4% water solvent system, several values were taken using the same reactants in another solvent system where the alcohol to water ratio was changed. Also, the methyl violet-cyanide reaction was observed in a few different compositions of a system of absolute ethanol and benzene. These latter observations are exploratory, but they support the mechanism proposed for the water-ethanol systems.

Discussion of Results

This discussion is concerned primarily with the ethanol-water systems. In all experiments described, the cyanide ion is in excess. The reaction is first order with respect to methyl violet at a given cyanide ion concentration. The water concentration in the ethanol also has an appreciable effect upon the rate of reaction. However, this aspect of the study is not emphasized in this paper. The absorption peak at 580 m μ does not shift with change in the ratio of water to ethanol or under any other experimental conditions as observed.

That there is no marked effect upon the activity of methyl violet due to the variation of cyanide concentration is clearly demonstrated since the logarithm of the methyl violet concentration plotted against time shows excellent linearity at all cyanide concentrations and at all temperatures. The linearity of these plots along with the observation

(5) A. H. Sporer, *Trans. Faraday Soc.*, **57**, 983 (1961).

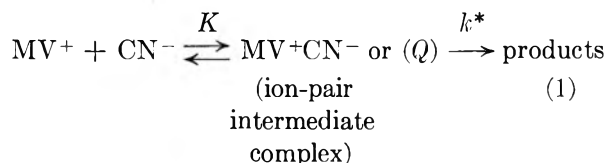
(6) E. O. Holmes, *J. Am. Chem. Soc.*, **44**, 1002 (1922).

(7) T. Ariga, *Bull. Chem. Soc. Japan*, **2**, 65 (1927).

that all curves originate at the same point supports very clearly that the concentration of cyanide has no significant effect upon the absorbancy of methyl violet. Further, it is definitely shown by such a plot that the rate of reaction is dependent upon the first power of methyl violet concentration and upon cyanide concentration, though the order with respect to cyanide is not indicated. In making a more detailed study of the effect of cyanide ion on the reaction, it is found that the reaction is not truly first order in cyanide with respect to widely varying cyanide ion concentrations. This is clearly demonstrated in Fig. 1, where the inverse values of the rate constant are plotted against cyanide ion concentration. If the reaction were truly second order, the graphs would be parallel to the abscissa.

There are at least two approaches which may be used to explain these rate data. One is to invoke the classical concept of the ionic strength effect based upon the Brönsted-Bjerrum-Christiansen treatment of the Debye-Hückel theory, and the other is to develop the explanation of the data on the basis of simple ion-pairing. In the case of the former concept, a non-specific ionic atmosphere is assumed and a plot of $\log k$ vs. the square root of ionic strength should give a straight line. This is found to be approximately true, although the data at 25°, when plotted in this manner, show a slight curvature.

If the concept of ion-pairing is invoked, then a different mathematical approach must be used. The basic supposition is that the cyanide ion reacts with the methyl violet ion reversibly to form a discrete ion-pair adduct. The mathematical derivation is quite simple.⁸



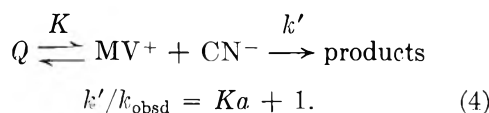
Then

$$K = [Q]/[\text{MV}^+][\text{CN}^-] \quad (2)$$

Let $a - x = [\text{CN}^-] + [Q]$ and $b - x = [\text{MV}^+] + [Q]$, where $a - x$ and $b - x$ are the total cyanide and methyl violet concentrations, respectively. Assuming that a is always much larger than Q , then

$$\begin{aligned} \text{Rate} &= k_{\text{obsd}}(a - x)(b - x) = k^*[Q] = \\ &= \frac{k^*K}{Ka + 1}(a - x)(b - x) \\ k^*/k_{\text{obsd}} &= \frac{Ka + 1}{K} \end{aligned} \quad (3)$$

If Q is not an intermediate, then



(8) J. E. Taylor, *J. Am. Chem. Soc.*, **75**, 3912 (1952).

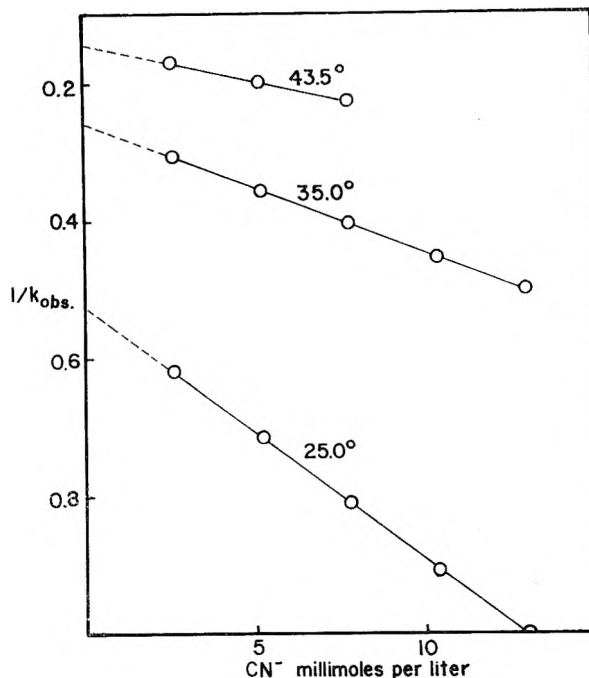


Fig. 1.—A plot from eq. 3 or 4 shown in support of the ion-pair theory.

A correlation of the rate data based upon eq. 3 or 4 is shown in Fig. 1. The graph of the variation of $1/k_{\text{obsd}}$ with cyanide concentration is satisfactorily linear. The slight curvature obtained for the plot of $\log k$ vs. $\sqrt{\mu}$ between the limits of 0.0026 and 0.013 M in cyanide ion is hardly sufficiently strong evidence to eliminate this explanation, but with the excellent linearity of the plot of $1/k_{\text{obsd}}$ vs. $[\text{CN}^-]$ a stronger case is made in favor of the ion-pair complex theory.

To determine if the curvature of the plot of $\log k$ vs. $\sqrt{\mu}$ is real, it is necessary to extend the curve to lower cyanide concentrations. Upon attempting to do this, a lack of constancy of k_{obsd} with time is observed. This is of such magnitude that it is not readily possible to distinguish between these two proposals. With either eq. 3 or 4 different limiting values of the rate constant are obtained when compared to the limiting value of the Brönsted equation. This presents an alternate method of distinguishing between these two equations, but again difficulty due to the drift of the rate constants at low cyanide concentrations is encountered. The averaged change between the values of k_{obsd} at cyanide concentrations of 0.00065 and 0.0013 M (Table I) is in accord with eq. 3 or 4 and not with the prediction from a plot of $\log K$ vs. $\sqrt{\mu}$.

Ion pairing does appear to be the more appropriate explanation and is emphasized in the remainder of the discussion. With either theory there must be ion-ion interactions, specific in the one case and non-specific in the other, which are responsible for the variation of the rate with cyanide concentration.

Based upon the proposed simple ion-pair concept it is possible to calculate the various kinetic and thermodynamic constants associated with the

TABLE I
 RATE DATA

Methyl violet: 1.269×10^{-5} mole/l.				
Solvent: 12.4% water, 87.6% ethanol (by weight)				
KCN mmoles/l.	KCl mmoles/l.	$k_{\text{obsd.}}$, l./mole sec.		
		25.0°	35.0°	43.5°
0.652		2.00 ^b		
1.303		2.51 ^c		
2.606		1.62 ^a	3.24	5.78
2.606	14.13	1.13 ^a		
5.212		1.40	2.81	5.00
7.818		1.23	2.45	4.40
10.42		1.10	2.20	
13.03		1.00	2.00	
Solvent: 4.4% water-95.6% ethanol (by weight)				
5.21		2.36		
7.82		2.01		
10.42		1.75		
13.03		1.56		

^a An averaged value. There is a decrease in the calculated rate constant of roughly 10% as experimentally determined. ^b An averaged value. The values vary from 2.27 at 117 sec. to 1.83 at 873 sec. ^c An averaged value. The values vary from 3.54 at 97 sec. to 2.16 at 862 sec.

equilibrium and rate expressions. These values have been calculated and are assembled in Table II. There is an unfavorable very small positive value for ΔH_{form} for the ion-pair whereas ΔS_{form} is more favorable and gives a negative ΔF_{form} . The ion-pair then exists in appreciable concentration. The positive ΔH_{form} probably is related to the extent of hydration of the ions. Presumably the ion-pair is formed only by displacement of water molecules about the positive and negative centers. This means that the heat of hydration for those water molecules displaced must be subtracted from the heat of ion-pair formation. It appears that the two quantities are about equal so that the resulting ΔH_{form} is approximately zero.

In order to define more clearly the nature of the ion-ion interaction, some studies with added potassium chloride were made. It is found that the effect of chloride ion to decrease the rate of reaction is somewhat less than that of cyanide ion (see Table I). With the added chloride there is a drift in the rate constants with time and this precludes an accurate evaluation of these data. The reason for this drift is discussed in a paragraph to follow. Based on the ion-pair theory, the effect of chloride ion is readily explained. Assuming $K_1 = Q_1/([MV^+]a)$ and $K_2 = Q_2/([MV^+][Cl^-])$ and that only Q_1 is intermediate, then

$$\frac{dx}{dt} = k^*Q_1 = \frac{k^*K_1(a-x)(b-x)}{1 + K_2[Cl^-] + K_1a}$$

This derivation may be applied to any salt since, in this system, specific ion pairing is assumed to be a general phenomenon. If the Debye-Hückel concept were to apply, there should be no difference depending upon the nature of the added ions. Since a difference does appear to exist even at these very low concentrations, additional support is given to the ion-pair theory as delineated in this paper. Attempts to study salt effects by calcium

TABLE II

	CALCULATED CONSTANTS				
	Rate constants in 12.4% water, 87.6% alcohol ^a				
	25.0°	25-35°	35.0°	35-43.5°	43.5°
k^* , l./mole sec.	0.0270		0.0536		0.0964
k'	1.92		3.81		6.87
ΔF^*_{act} , kcal./mole	10.3		10.8		11.3
$\Delta F'_{\text{act}}$	10.7		11.2		11.7
ΔH^*_{act}		12.5		13.5	
$\Delta H'_{\text{act}}$		12.6		13.5	
ΔS^*_{act} , cal./mole/deg.	7.3		7.1		6.9
$\Delta S'_{\text{act}}$	6.3		6.1		5.9
Equilibrium constants in 12.4% water, 87.6% alcohol					
K_{form} , l./mole	70.8		71.1		71.3
ΔF_{form} , kcal./mole	-2.54		-2.63		-2.70
ΔH_{form}		0.1		0.1	
ΔS_{form} , cal./mole deg.	8.8		8.8		8.7

Rate and equilibrium constants in 4.4% water, 95.6% alcohol

k^*	0.0360
k'	3.60
K_{form}	100

^a Assumes the complex is intermediate. All other values were calculated from k^* at the indicated temperatures using the Eyring rate equation. ^b Assumes the complex is inactive. All other calculations based on k' values.

chloride and potassium sulfate were unsuccessful due to solubility difficulties.

As noted in the subscripts to Table I, there is a drift in the rate constants with time for the lowest cyanide concentrations. This occurs even in the presence of high chloride ion concentrations. The best explanation appears to be that there are two competing reactions. Only when the concentration of cyanide ion is very high with respect to other substances present does a single reaction predominate. The nature of these competing reactions has not been determined. The second reaction may be a reaction with the hydroxyl ion resulting from hydrolysis of the cyanide ion.

The next consideration is the nature of the role of the ion-pair.⁹ Is it an intermediate which serves to tunnel the activation energy barrier, or does it deactivate in accord with eq. 4? As seen from eq. 3 and 4, either concept can explain the observed rate of reaction.

Several lines of evidence, mainly of an intuitive nature, favor at least the partial contribution of the mechanism associated with eq. 3.

1. The first concerns charge isolation within the methyl violet molecule. It is reasonable to assume that the maximum charge intensity is isolated within a small area on the surface of the molecule. If this is the case, then ion-pair formation should occur and it may be reasonably assumed that the ion-pair, because of a very low activation energy,

(9) The so-called ion-pair complex is not to be confused with the activated complex of the absolute reaction rate theory.

is formed previous to the leuconitrile, and eq. 3 is supported.

However, if the charge concentration were more diffuse, there would be a greater active area and both ion-pair and leuconitrile formation could occur either separately or successively. Both eq. 3 and 4 then could apply.

2. The low energy of formation of the ion-pair also favors its intermediacy since there is formed no energy sump upon contact of the reactants with each other. If such an energy sump were formed, partial or complete inactivation could occur depending upon the extent of formation of the complex and upon the relative degree of inactivation by complex formation.

3. The mechanism appears to change with the solvent in which the reaction takes place. Only limited data are available, but the trends are significant. In 4.4% water-95.6% ethanol solutions at 25° (as compared to the 12.4% water solutions) the value of k^* increases by a factor of 1.33, k' by a factor of 1.88, and K_{form} by a factor of 1.41. If the effect of varying cyanide upon the rate of reaction were only as indicated in eq. 3 or 4, then k' and K_{form} should change by equal factors since $k' = k^*K_{\text{form}}$; k' and K_{form} are both inversely

proportional to the concentrations of methyl violet and cyanide ions. Conversely, k^* is dependent solely upon Q and the effects of the ions are eliminated in the calculation of k^* . Since the experimentally determined k^* is not independent of these changes, a variation in the mechanism beyond that indicated by eq. 3 and 4 is suggested; however, clear evidence is not available. At high dielectric strengths, simple ionic interactions may occur to form the product and the Debye-Hückel theory would apply to explain the ion strength effects, while at lower dielectric strength ion-pairing occurs. The water concentrations used may represent intermediate conditions. Possibly the competing reactions mentioned earlier may also be a factor. This phenomenon is currently under investigation.

In some exploratory studies in benzene-alcohol solutions the rate is seen to increase with decreasing alcohol concentrations. For example, in benzene-alcohol solutions, as the alcohol concentration is increased from 5 to 10% the rate decreases roughly by a factor of 0.4. These observations using a different solvent system support further the above generalizations.

PHOTOCHEMICAL *cis-trans* ISOMERIZATION OF *p*-DIMETHYLAMINOCINNAMIC ACID NITRILE

BY E. LIPPERT AND W. LÜDER

Laboratorium für physikalische Chemie der TH Stuttgart, Stuttgart-N, Germany

Received May 25, 1962

As both the *cis* and *trans* isomers of $p\text{-(CH}_3)_2\text{N-C}_6\text{H}_4\text{-CH=CH-CN}$ are almost planar, their quartz ultraviolet absorption spectra are quite similar except for the intensities of the long axis polarized first and third transitions. Photochemical equilibrium is rapidly achieved by irradiating with the light of Hg 366 $m\mu$ ($27,400\text{ cm}^{-1}$), which is absorbed in the first absorption band ($\epsilon_{\text{max}} = 25,000$ and $36,000\text{ l./mole cm.}$, respectively). In ethyl alcohol at room temperature, the photochemical equilibrium mixture contains 37.5% *trans* form. The quantum efficiency for the *trans* \rightarrow *cis* isomerization is about 0.6 molecule/quantum and increases with decreasing solvent polarity. Due to the high dipole moments of the first excited singlet state [μ_e (*trans*) ≥ 14 Debye units] the *trans* form is more stabilized than the *cis* form by increasing electrostatic intermolecular interaction energy. The quantum efficiency for the *cis* \rightarrow *trans* isomerization is about 0.45 molecule/quantum. Both this reaction and its reverse are of first order. As the sum of the corresponding quantum efficiencies is unity within the limits of error, both processes might proceed through the same intermediate state, which presumably is the lowest triplet state. However, no effect could be observed when flushing out dissolved oxygen by nitrogen. Because of the competing *trans* \rightarrow *cis* isomerization, both the quantum yield and the decay time of the fluorescence of the *trans* form are small, 0.11 ± 0.04 and $\geq 6 \times 10^{-10}\text{ sec.}$, respectively, as compared with the high transition moment. Due to the Franck-Condon principle, the short lifetime of the first excited singlet state allows only for small reorientation of solvent molecules and a small anomalous Stokes red shift as compared with the corresponding stilbene, diphenyl, etc., derivatives. No fluorescence could be observed with the *cis* form. This probably is due to its lower activation energy for radiationless deactivation, which tends to shorten the lifetime of the excited state of the not-all-planar *cis* isomer. No thermal isomerization reaction occurs even up to 120°. Above this temperature decomposition of the isomers could be observed.

Introduction

In a preceding paper¹ we investigated the structures of the *cis* and *trans* forms and obtained these results:

(1) The two modifications with melting points at 65 and 163.5° are indeed the *cis* and *trans* isomers, respectively, as suggested by Coenen and Pestemer.² (The melting points mentioned by these authors are 62 and 63° for *cis*, and 158 and 163° for *trans*.)

(2) As both forms are almost planar in structure, resonance and maximum absorption wave numbers are nearly equal. Only the intensities of the long axis polarized bands are decreased since the oscillator length and strength are shortened by twisting the *trans* form into the *cis* form.

(3) The ultraviolet absorption spectra, however, are not congruent as has been assumed by previous authors.^{2,3} The apparent congruence obviously is the result of a rapidly achieved photo-

(1) E. Lippert and W. Lüder, *Z. phys. Chem. (Frankfurt)*, **33**, 60 (1962).

(2) M. Coenen and M. Pestemer, *Z. Elektrochem.*, **57**, 785 (1953).

(3) D. Lauerer, M. Coenen, M. Pestemer, and G. Scheibe, *Z. phys. Chem. (Frankfurt)*, **10**, 236 (1957).

chemical equilibrium which could be avoided by reduction of the amount of light absorbed.

(4) The cyano group acts as an -I as well as a -M substituent. In the *cis* configuration, there is a twisting vibration of about 180° amplitude for the cyanovinyl group around the $\text{C}-\text{C}$ single bond connecting to the ring.

(5) Both *cis* and *trans* bands show vibrational structure even in ethanol at room temperature.

In this paper the *cis/trans* isomerism is investigated in some detail by means of ultraviolet absorption and fluorescence spectroscopy.

Experimental

The origin and the purification of the solutes and solvents already have been described.¹ All work was carried out under red light and solutes and solutions were kept in the dark, since even daylight produces photoisomerization.

The absorption spectra at room temperature were measured with a Beckman DK 2 and at lower temperatures with a Carl Zeiss MQ II spectrophotometer; the fluorescence spectra were recorded with an oscilloscope-spectrometer system requiring only a few seconds for the scanning of a complete spectrum.⁴

The temperature cells have been described elsewhere.⁵ The kinetic measurements were carried out with an apparatus constructed by Zügel⁶ which records the time dependence of both the high pressure mercury lamp output at 366 m μ and the transmission of the solution by a calibrated photocell. The setups for the determination of the fluorescence quantum yields and their concentration dependence have been described by Hauser⁷ and Fischer.⁸

Results and Discussion

Absorption Spectra.—The absorption spectra of the solutions in ethyl alcohol and methycyclohexane with and without irradiation are shown in Fig. 1 and 2. The isosbestic points indicate that chemical reactions are not competing with the *cis/trans* isomerization. The photochemical equilibria achieved by irradiating solutions in ethyl alcohol and in methycyclohexane with Hg 366 m μ contain 37.5% and 24.8% of the *trans* form, respectively.

As the dipole moment of the *trans* form is higher than that of the *cis* form, the *trans* form is favored in polar solvents.⁹ No thermal equilibrium could be obtained for comparison. The *cis* form dissolved in well purified di-*n*-butyl-ether as well as in decalin gives no isomerization when heated at 100° for several hours, but decomposition does occur at 120°. This is in accordance with the *cis* \rightarrow *trans* activation energy of 46 kcal./mole of cinnamic acid nitrile in its vapor phase at 308–378°.¹⁰

Isomerization and Quantum Yield.—The isomerization is first order in light intensity as is shown for two different intensities in Fig. 3 and 4. Hence, the quantum yield $\eta_{i \rightarrow j}$ is given by

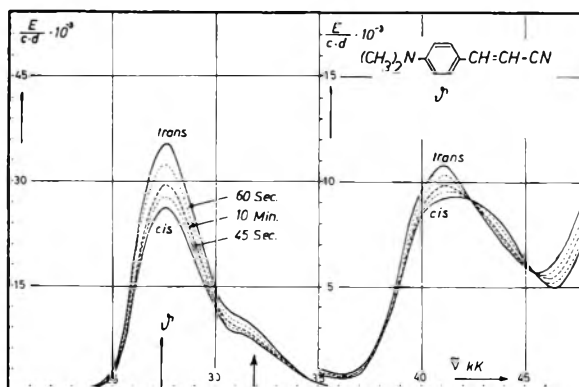


Fig. 1.—Absorption spectra in ethyl alcohol at 293°K. with (dotted line) and without (full line) irradiation with Hg 366 m μ ; wave number $\bar{\nu}$ in 1000 cm.⁻¹.

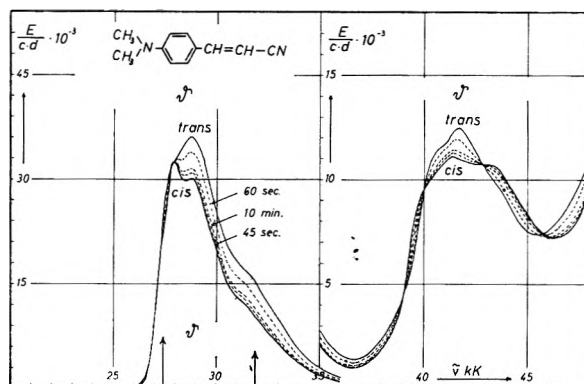


Fig. 2.—Absorption spectra in methycyclohexane at 296°K. under irradiation with Hg 366 m μ as in Fig. 1.

$$\frac{\eta_{i \rightarrow j}}{V} = - \left(\frac{dc_i}{dt} \right)_{t=0} / I_{\text{abs}}$$

where V is the cell volume, in liters, c_i is the concentration of species i , in moles/liter, and I_{abs} is the light intensity absorbed, in einstein units per time unit.

For solutions in ethyl alcohol, we obtain with the initial slopes in Fig. 5 and with the initial concentrations $c_0 = 1.505 \times 10^{-5}$ and 1.679×10^{-5} mole/l. for *cis* and *trans*, respectively

$$\eta_{\text{cis} \rightarrow \text{trans}} = 0.44 \text{ molecule/quantum}$$

$$\eta_{\text{trans} \rightarrow \text{cis}} = 0.65 \text{ molecule/quantum}$$

In less polar solvents the latter figure is even higher although precise measurements have not been possible because of the small changes in absorption spectra at room temperature.

The corresponding values for 4-dimethylamino-4'-nitrostilbene are 0.40 and 0.13, respectively.⁹ Its ratio $\eta_{\text{c} \rightarrow \text{t}} / \eta_{\text{t} \rightarrow \text{c}} \approx 3$ is relatively high since the *cis* form is not planar and its energy is somewhat higher than that of the *trans* form because of the voluminous additional phenyl group. The sum $\eta_{\text{c} \rightarrow \text{t}} + \eta_{\text{t} \rightarrow \text{c}} = 0.53$ of the latter compound is relatively small because of the heavier mass which moves less slowly. This more easily allows for competing effects.

For the compound under investigation, the sum $\eta_{\text{t} \rightarrow \text{c}} + \eta_{\text{c} \rightarrow \text{t}} = 1.09$ might be one within the limits

(4) E. Lippert, W. Nägele, I. Seibold-Blankenstein, U. Staiger, and W. Voss, *Z. anal. Chem.*, **170**, 1 (1959).

(5) E. Lippert, W. Lüder, and F. Moll, *Spectrochim. Acta*, **10**, 378 (1959).

(6) M. Zügel, Thesis, Stuttgart, 1961.

(7) M. Hauser, Diplomarbeit, Stuttgart, 1957.

(8) H. Fischer, Diplomarbeit, Stuttgart, 1959.

(9) D. Schulte-Frohlinde, *Ann. Chem.*, **615**, 114 (1958).

(10) G. B. Kistiakowski and W. R. Smith, *J. Am. Chem. Soc.*, **58**, 2428 (1936).

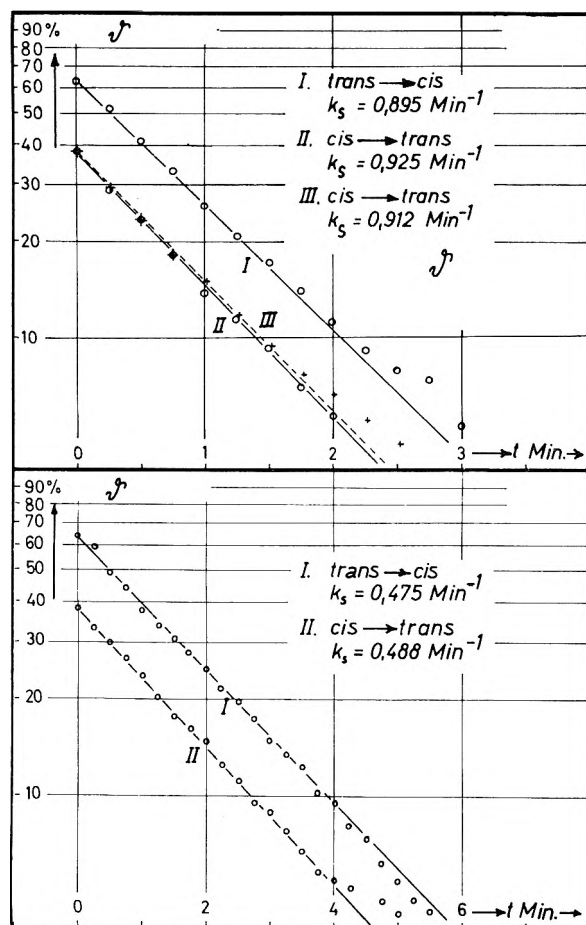


Fig. 3. (top) and Fig. 4 (bottom).—Difference between equilibrium concentration and effective concentration of the *trans* form and the *cis* form, respectively, in ethyl alcohol as a function of irradiation time at two different intensities; dotted line obtained after excluding oxygen by flushing for 1 hr. with nitrogen.

of error. This would mean that both reactions pass through the same intermediate state, which is assumed to be the triplet state.^{11,12} Contrary to the effect found for 4-dimethylamino-4'-nitrostilbene, no competing low temperature phosphorescence was observed. Also, for both compounds within the limits of error no oxygen effect could be observed. With a flash apparatus no singlet-triplet absorption could be measured. This evidence all points to a very short lifetime for the triplet intermediate state because of competing mechanisms. If it is shorter than the first relaxation time of ethyl alcohol, there would be two different transition states of the system depending on the orientation of the polar solvent molecules, and the fact that the value of $\eta_{c \rightarrow t} + \eta_{t \rightarrow c} = 1.09$ is greater than unity might have a real meaning.

Fluorescence Quantum Yield.—The fluorescence quantum yield of the *trans* form increases with solvent polarity (see above). In ethyl alcohol at room temperature it is $(10.8 \pm 4.0)\%$. No fluorescence of the *cis* form could be found even at lower temperatures. This is in accordance with the behavior of other aromatic 1,2-disubstituted

cis-ethylene compounds, the fluorescence of which is quenched by a competing transformation of the electronic excitation energy into heat by conversion into twisting (internal rotational) vibration energy. Such a transformation occurs more rapidly with the *cis* form, which needs less activation energy than the *trans* form. For *p*-dimethylamino- α -cyanocinnamic acid nitrile $((\text{CH}_3)_2\text{N} \cdot \text{C}_6\text{H}_4 \cdot \text{CH} : \text{C}(\text{CN})_2$, "dicyano" in Table I) a fluorescence has been observed. However, the quantum yield is less than 0.04. Here also decomposition may compete with the emission¹³ and hence the occurrence of fluorescence is surprising. The effect might be due to the dicyano group, which moves slowly, but a more thorough investigation of other quenching mechanisms is necessary. A *cis* solution cooled down to liquid air temperature and then irradiated with Hg 366 $m\mu$ soon starts to fluoresce. The same effect has been observed with stilbene.¹⁴ Hence *cis/trans* isomerization is possible at about 90° K., whereas reorientation (rotation) of molecules is not possible.¹⁵

TABLE I
EFFECT OF SOLVENT ON THE WAVE NUMBER (IN 1000 cm^{-1}) OF ABSORPTION AND FLUORESCENCE MAXIMA AT ROOM TEMPERATURE

No.	Solvent	— <i>trans</i> form—		—"Dicyano"—	
		$\bar{\nu}_A$	$\bar{\nu}_F$	$\bar{\nu}_A$	$\bar{\nu}_F$
1	Isopentane	28.95	25.85		
2	Heptane	28.8	25.85		
3	Cyclohexane	28.7	25.35		
4	Methylcyclohexane	28.48	25.42		
5	Benzene	27.68	24.88	23.35	21.15
6	Carbon tetrachloride	28.0	23.00		22.075
7	Methylene chloride	27.82	23.77		
8	Butyl chloride	27.92	24.2		
9	Chlorobenzene	27.2	24.35	23.00	20.35
10	Bromobenzene	27.1	24.35	22.9	21
11	<i>o</i> -Dichlorobenzene	27.1	24.0	22.8	20.7
12	Methanol	27.5	23.1	23.3	20.6
13	Ethanol	27.65	23.31	23.19	20.88
14	<i>n</i> -Propyl alcohol	27.5	23.8	23.25	21.2
15	Isopropyl alcohol			23.35	20.9
16	Isobutyl alcohol	27.52	24.09	23.3	21.05
17	Diethyl ether	28.25	24.7	23.85	21.6
18	Dibutyl ether	28.2	24.6		
19	Tetrahydrofuran	27.82	24.2	23.4	20.85
20	Dioxane	27.88	24.4	23.05	21.45
21	Acetone	27.7	23.35	23.3	20.5
22	Acetanhydride	27.6	23.15	23.1	20.45
23	Acetonitrile	27.65	23.1	23.2	20.3
24	Butyronitrile	27.65	23.35		

Stokes Red-Shift.—With increasing polarity of the solvent, the fluorescence maximum is shifted more to the red than the absorption maximum (Table I) and the so-called anomalous Stokes red shift increases. Doubtless, the first excited singlet state possesses a higher dipole moment than the ground state.¹³ Hence the energy difference between ground and excited states is lowered by increasing electrostatic solvent-solute interaction.

(11) Th. Förster, "Fluoreszenz organischer Verbindungen," Göttingen, 1951.

(12) G. M. Wyman, *Chem. Rev.*, 625 (1955).

(13) E. Lippert, *et al.*, *Angew. Chem.*, **73**, 695 (1961).

(14) G. N. Lewis, T. T. Magel, and D. Lipkin, *J. Am. Chem. Soc.*, **62**, 2973 (1940).

(15) G. N. Lewis and J. Bigeleisen, *ibid.*, **65**, 520 (1943).

Due to the Franck-Condon principle, the orientation of the molecules is fixed during the absorption process. If the lifetime of the excited state is larger than the first relaxation time of the solvent, re-orientation will take place in the stronger electric field of the excited dipole before fluorescence is emitted. Hence the fluorescence red shift is larger than the absorption red shift, and the dipole moment difference $\mu_e - \mu_g$ between ground and excited can be calculated from a plot of the Stokes red shift against a quantity Δf measuring the orientation

$$\bar{\nu}_A - \bar{\nu}_F = \text{const} +$$

$$\frac{(\mu_e - \mu_g)^2}{a^3 h c_0} \left(\frac{D - 1}{D + 1/2} - \frac{n_D^2 - 1}{n_D^2 + 1/2} \right) + \dots$$

a = interaction radius of solute

h = Planck's constant

c_0 = velocity of light

D = dielectric constant of solvent

n_D = refractive index of solvent

polarization of the solvent^{13,16} (Fig. 6).

However, the method is only applicable if the orientation equilibrium of the system is essentially achieved during the lifetime of the excited state. From a comparison of the maximum Stokes red shift of about 1700 cm^{-1} for the *trans* form and about 1000 cm^{-1} for the dicyano compound with the corresponding values 6000 and 13,000 cm^{-1} for *p*-dimethylamino-*p*'-cyanostilbene and *p*-cyano-N,N-dimethylaniline, respectively, it is obvious that this condition is not fulfilled with the compounds under investigation. Hence the value $\mu_e = 14$ D. for the dipole moment of the excited *trans* form obtained from the slope in Fig. 6 is only a lower limit, although it is the same value as has been calculated by electrooptical methods^{17,18} (private communications by Prof. Labhart and the late Dr. Czekalla, to whom we wish to express our thanks for these measurements). The lifetime of the excited state is shortened too much by the competing isomerization.

Fluorescence Decay Time.—The natural lifetime of the first excited singlet state of the *trans* form with an $\epsilon_{\text{max}} \approx 35000$ l./mole cm. might be of the order 10^{-8} – 10^{-9} sec. Because of the relatively small anomalous Stokes red shift mentioned above, the decay time should be of the order of the first relaxation time, which in most common organic solvents at room temperature, is of the order of 10^{-11} – 10^{-12} sec. Experimentally for 10^{-3} M solutions in methyl alcohol and in xylene at room temperature, 6×10^{-10} sec. has been found to be an upper limit for the decay time. (Private communication by Prof. A. Schmillen, to whom we wish to express our thanks for those measurements.) The limit mentioned presumably is only a function of the apparatus used as it does not depend on concentration or wave length of excitation

(16) E. Lippert, *Z. Naturforsch.*, **10a**, 541 (1955); *Z. Elektrochem.*, **61**, 962 (1957).

(17) J. Czekalla, *ibid.*, **65**, 733 (1961).

(18) H. Labhart, *Chimia*, **15**, 20 (1961); *Helv. Chim. Acta*, **44**, 457 (1961).

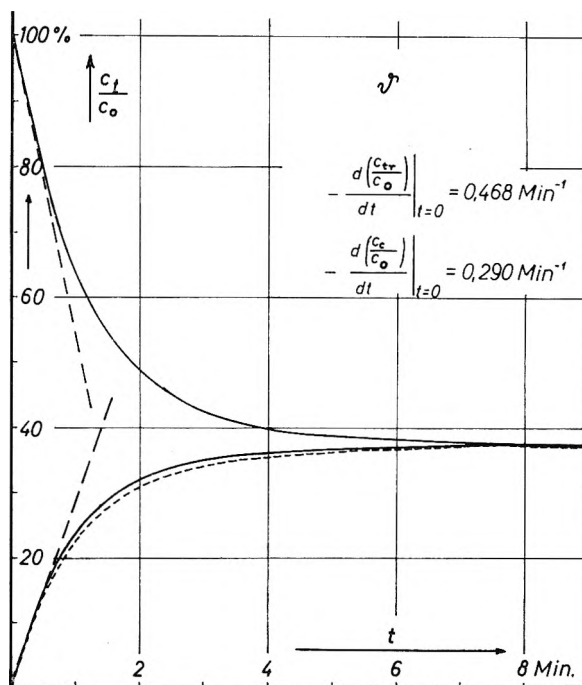


Fig. 5.—Relative concentration of the *trans* form as a function of the irradiation time; dotted line without oxygen.

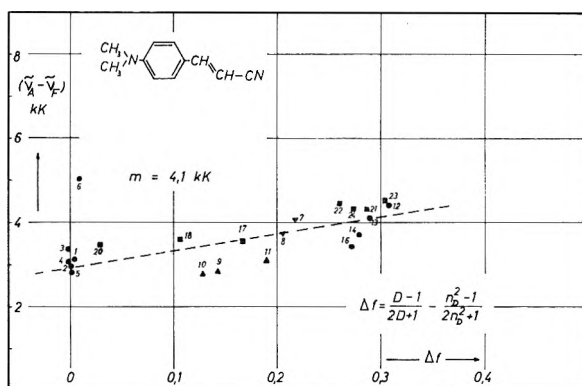


Fig. 6.—Anomalous Stokes red shift (in 1000 cm^{-1}) as a function of Δf , a quantity proportional to the solvent orientation polarization¹⁶; numbering refers to the solvents listed in Table I. D = dielectric constant and n_D = refractive index of the solvent.

so far observed. The powder decay time amounts to 4×10^{-9} sec. Because of the low fluorescence intensity, no decay time values have been obtained with the dicyano compound. On cooling the solution, one finds the Stokes red shift to be decreased, since the first relaxation time is increased. This is the case even in an isopentane/methylcyclohexane mixture. Hence it is not possible to determine the decay time from the maximum of the Stokes red shift (minimum of fluorescence wave number) which is supposed to occur at that temperature where the relaxation time of the solvent equals the decay time.¹⁹

Acknowledgment.—The authors are much indebted to Professor Th. Förster, whose obligingness enabled us to accomplish these investigations, as

(19) E. Lippert, W. Lüder, and F. Moll, *Spectrochim. Acta*, **10**, 858 (1959).

well as to the Deutsche Forschungsgemeinschaft, the Farbenfabriken Bayer, Leverkusen, for financial to the Verband der Chemischen Industrie, and to aids and sample gifts.

PHOTOTROPISM OF *ortho*-NITROBENZYL DERIVATIVES

BY J. D. MARGERUM,¹ L. J. MILLER,² E. SAITO,

Chemical Research Laboratories, Sundstrand Aviation-Denver, Pacoima, California

MELANCTHON S. BROWN, HARRY S. MOSHER,

Department of Chemistry, Stanford University, Stanford, California

AND R. HARDWICK

Department of Chemistry, University of California at Los Angeles, Los Angeles, California

Received May 25, 1962

In a study of the phototropic properties of various nitrobenzyl derivatives, no compound was found to be phototropic which did not have a nitro group *ortho* to a benzyl hydrogen. This structural requirement appears to be necessary but is not sufficient in itself to produce photochromic color under the conditions of our experiments. The results are consistent with the photochemical production of an excited species in which hydrogen is transferred from the methylene carbon to the oxygen of the *ortho* nitro group, producing a colored *aci* quinoid structure in equilibrium with its anion. The rate of fading of the colored photochemical product varies greatly with solvent, acidity, and temperature, as well as with the structure of the compounds.

Introduction

Studies by Chichibabin, *et al.*,³ on the phototropism of crystalline 2-(2',4'-dinitrobenzyl)-pyridine (α -DNBP) led to the proposal that a hydrogen transfer took place from the methylene bridge to the nitrogen of the pyridine ring. The more recent research on the solutions of this compound⁴ and its isomer, 4-(2',4'-dinitrobenzyl)-pyridine (γ -DNBP),⁵ suggested an alternate mechanism in which this hydrogen transfers to the oxygen of the nitro group. According to this mechanism, the pyridine ring need not be an essential structural feature for phototropic activity, and thus might be replaceable by other electrophilic groups. The present study of analogous compounds was undertaken to investigate this possibility.

Results and Discussion

Phototropic Activity.—Table I lists the compounds of this study, their properties, and references to their synthesis; Table II reports appropriate absorption maxima and colors produced with the phototropic compounds.

The compounds have in common a benzyl group substituted with one or more nitro groups. In this work a compound was considered to be non-phototropic if no color change was visible upon irradiation with unfiltered light from a 400-watt medium pressure mercury vapor lamp of a solution (95% ethanol) contained in a fused silica tube at temperatures down to that of liquid nitrogen.

Spectra were taken for each compound and the corresponding anion, which was prepared by adding

alcoholic potassium hydroxide to an alcoholic solution of the substance. When a compound was phototropic, its visible spectrum was taken in a low temperature cell. Because the concentrations of the colored species are not known, extinction coefficients are not reported.

As indicated in Table I the known compounds 2,4,2',4'-tetranitrodiphenylmethane and 2,4,4'-trinitrodiphenylmethane are strongly phototropic, a fact not previously reported. This result establishes that a pyridine ring is not essential for phototropic activity with this type of structure. Moreover, the N-oxides of α - and γ -DNBP, in which the nitrogen of the pyridine ring is no longer capable of binding a hydrogen, are also phototropic.

In general, of the compounds investigated, only those with a 2,4-dinitrophenyl group attached to a $-\text{CH}_2-$ or $-\text{CH}-$ group were found to be phototropic. Replacing the CH_2 with a CO group resulted in loss of activity, *e.g.*, 2-(2',4'-dinitrobenzoyl)-pyridine in the benzylpyridine series and 2,4,2',4'-tetranitrobenzophenone in the diphenylmethane series.

Two requisites for this type of phototropic activity seem to be: (a) a hydrogen on a benzyl carbon, sufficiently activated by *ortho* or *para* substituents and (b) a nitro substituent *ortho* to the benzyl carbon. The two isomers, 2,2'- and 2,4'-dinitrodiphenylmethane were not phototropic under the conditions of these experiments; evidently they do not meet requirement (a). Tris-(4-nitrophenyl)-methane, with three nitro substituents (none of which is in the *ortho* position) has a very active hydrogen on the bridge carbon, yet it is not phototropic, not meeting requirement (b). The 4,4'-dinitro isomer is sufficiently acidic to be thermochromic but is not phototropic. Tris-(2,4-dinitrophenyl)-methane and 2,4,4'-trinitrodiphenylmethane, on the other hand, are phototropic. It seems that three nitro groups (or their approximate electrophilic equivalent, as for instance the pyridine ring in α - and γ -DNBP)

(1) Hughes Research Laboratories, 3011 Malibu Canyon Road, Malibu, California.

(2) Hughes Aircraft Company, Aerospace Group, Culver City, California.

(3) A. E. Chichibabin, B. Kundshi, and S. V. Benewalenskaja, *Ber.*, **58**, 1580 (1925).

(4) R. Hardwick, H. S. Mosher, and P. Passailaigne, *Trans. Faraday Soc.*, **56**, 44 (1960).

(5) H. S. Mosher, C. Souers, and R. Hardwick, *J. Chem. Phys.*, **32**, 1888 (1960).

TABLE I
 LIST OF COMPOUNDS AND PROPERTIES

Name ^a	Melting points		Method of preparation	$\lambda_{\max.}^b$ m μ	$\epsilon \times 10^{-4}$
	Obsd., °C.	Lit., °C.			
2-(2'-Nitrobenzyl)-pyridine	<i>c</i>	<i>c</i>	<i>d, e</i>	262	1.3
2-(4'-Nitrobenzyl)-pyridine	78-80	81 ^f	<i>d, e</i>	269	1.6
4-(4'-Nitrobenzyl)-pyridine	67-69	72-73 ^g	<i>g, e</i>	264	1.4
*2-(2',4'-Dinitrobenzyl)-pyridine	93-94	92-93 ^d	<i>g</i>	248	1.6
*4-(2',4'-Dinitrobenzyl)-pyridine	80-81	80-81 ^g	<i>g</i>	244	1.8
*2-(2',4'-Dinitrobenzyl)-pyridine N-oxide	135-136	...	<i>h</i>	259	2.2
*4-(2',4'-Dinitrobenzyl)-pyridine N-oxide	157-158	...	<i>h</i>	268	2.3
2-(4'-Chloro-3'-nitrobenzyl)-pyridine	63-64	...	<i>h</i>	261	0.78
2-(4'-Chloro-3',5'-dinitrobenzyl)-pyridine	90-91	...	<i>h</i>	261	0.80
2-(2'-Nitro-4'-aminobenzyl)-pyridine	119-120	118.5 ⁱ	<i>g, e</i>	239	1.9
2-(2',4'-Dinitrobenzyl)-pyridine	146-147	148 ^f	<i>f</i>	238	2.3
2,2'-Dinitrodiphenylmethane	83-84	159 ^h	<i>h</i>	256	1.0
4,4'-Dinitrodiphenylmethane	181-183	183 ^j	<i>j</i>	277	2.3
2,4'-Dinitrodiphenylmethane	115-118	118 ^j	<i>j</i>	266	1.5
*2,4,2'-Trinitrodiphenylmethane	111-113	...	<i>h</i>	244	2.1
*2,4,4'-Trinitrodiphenylmethane	107-110	...	<i>h</i>	266	1.8
*2,4,2',4'-Tetranitrodiphenylmethane	170-172	173 ^k	<i>k</i>	242 ^l	2.8
4,4',4''-Trinitrotriphenylmethane	212-213	212.5 ^m	<i>m</i>	275	2.5
*2,4,2',4',2'',4'''-Hexanitrotriphenylmethane	256-258	260 ⁿ	<i>h</i>	253 ^o	4.4
*Ethyl bis-(2,4-dinitrophenyl)-acetate	152-154	154 ^p	<i>p</i>	241 ^o	3.1
2,4-Dinitrophenylacetic acid	185	185 ^q	..	242	...
*Ammonium 2,4-dinitrophenylacetate ^r	<i>h</i>	243	...

^a * Indicates that the compound has been observed to be phototropic. ^b Spectra in 95% ethanol except where noted otherwise because of low solubility. ^c This compound was an oil, b.p. found 200° (5 mm.); reported 160-170° (0.4 mm.). ^d K. Schofield, *J. Chem. Soc.*, 2408 (1949). ^e We wish to thank Mr. Clark Souers for the preparation of these compounds. ^f A. E. Chichibabin, B. Kuindshik, and S. V. Benevlenskaja, *Ber.*, 58, 1580 (1925). ^g A. J. Nunn, and K. Schofield, *J. Chem. Soc.*, 538 (1953). ^h See text for method of synthesis. ⁱ R. H. Wilson, *J. Chem. Soc.*, 1936 (1931). ^j W. Staedel, *Ann.*, 283, 151 (1894). ^k K. Matsumura, *J. Am. Chem. Soc.*, 51, 812 (1929). ^l Absolute ethanol solvent. ^m P. J. Montagne, *Rec. trav. chim.*, 24, 125 (1905). ⁿ A. Baeyer and V. Villiger, *Ber.*, 36, 2774 (1903). ^o Absolute methanol solvent. ^p Werner, *Ber.*, 39, 1290 (1906). ^q Eastman White Label. ^r The alkali metal salts of 2,4-dinitrophenylacetic acid were also phototropic.

 TABLE II
 COMPARISON OF THE PHOTOCHROMIC COLOR WITH THE COLORED ANION AND THE NEUTRALIZED SOLUTION

Compound	$\lambda_{\max.} \text{ m}\mu$		
	Photochromic ^a	Neutralized solution ^b	Colored anion ^c
2-(2',4'-Dinitrobenzyl)-pyridine	567.5 (purple)	...	650, 472 (green-yellow)
Same with some base present	... (green-yellow) ^d	...	
4-(2',4'-Dinitrobenzyl)-pyridine	575 (blue)	575 ^e	640, 480 (green-brown)
2-(2',4'-Dinitrobenzyl)-pyridine N-oxide	sh. 601, 501 ^f (pink)	...	sh. 600, 506 (pink)
4-(2',4'-Dinitrobenzyl)-pyridine N-oxide	sh. 650, 527 ^f (pink)	...	650, 525 (pink)
2,4,2'-Trinitrodiphenylmethane	... (faint rose)	...	645, 425 (green)
2,4,4'-Trinitrodiphenylmethane	580 (blue)	580 ^g	580 (blue)
2,4,2',4'-Tetranitrodiphenylmethane	712 ^h (blue)	712 ^{g,h}	700 ^h (blue)
2,4,2',4',2'',4'''-Hexanitrotriphenylmethane	715 ^{h,i} (blue)	...	715 ⁱ (blue)
Ethyl bis-(2,4-dinitrophenyl)-acetate	... (blue) ^k	...	650, 471 ^j (blue)
Ammonium 2,4-dinitrophenylacetate	... (green)	...	639, 425 (green)
2,4-Dinitrophenylacetic acid (plus base)	650, 425 (green) ^l	...	

^a Unless noted otherwise, refers to the observed color change on irradiation of an ethanolic soln. at approximately -100° in a fused silica cell by a high pressure mercury lamp. ^b Species formed by neutralization of the colored anion at a temperature low enough to prevent immediate fading to the colorless form. ^c Observed color change from addition of 0.1 N KOH to an ethanolic soln. at room temperature, unless noted otherwise. ^d Phototropic color formed with a slight excess of 0.1 N KOH added, but not enough to give anionic color. ^e -100°, R. Hardwick and H. S. Mosher, *J. Chem. Phys.*, 36, 1402 (1962). ^f -80°. ^g -125°, 0.03 ml. of 0.01 N KOH added to 3 ml. of 2×10^{-4} M soln., followed by 0.03 ml. of 0.01 N HCl. ^h In absolute ethanol. ⁱ -7°. ^j In absolute methanol. ^k In 50:50 methanol:acetonitrile. ^l -72°, with a slight excess of KOH after neutralization of the carboxylic acid.

ortho or *para* to the benzyl carbon are necessary for activation of the hydrogen to satisfy condition (a), in order to observe phototropism under the conditions of our experiments. The phototropic character of 2,4-dinitrophenyl acetate shows that it is not essential to have more than one aromatic ring attached to the benzyl carbon atom and that

the carboxylate group can play a role similar to a *p*-nitrophenyl group. Groups other than nitro should be able to replace the *ortho* substituent, but we have only preliminary data on such compounds. Yang and Rivas⁶ have reported on the photochemical enolization of *o*-benzylbenzophenone

(6) N. C. Yang and C. Rivas, *J. Am. Chem. Soc.*, 83, 2213 (1961).

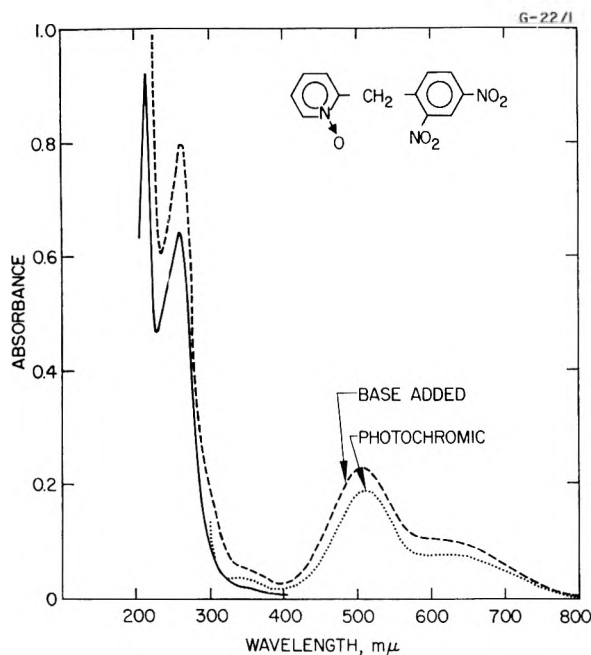


Fig. 1.—2-(2',4'-Dinitrobenzyl)-pyridine N-oxide, spectra of $2.91 \times 10^{-5} M$ solution in 95% ethanol, 1-cm. cell, 31° : broken line, addition of 0.06 ml. of 0.10 *N* KOH to 3.3 ml.; dotted line, irradiation of initial solution at -80° with tungsten lamp of the Cary 14 near infrared.

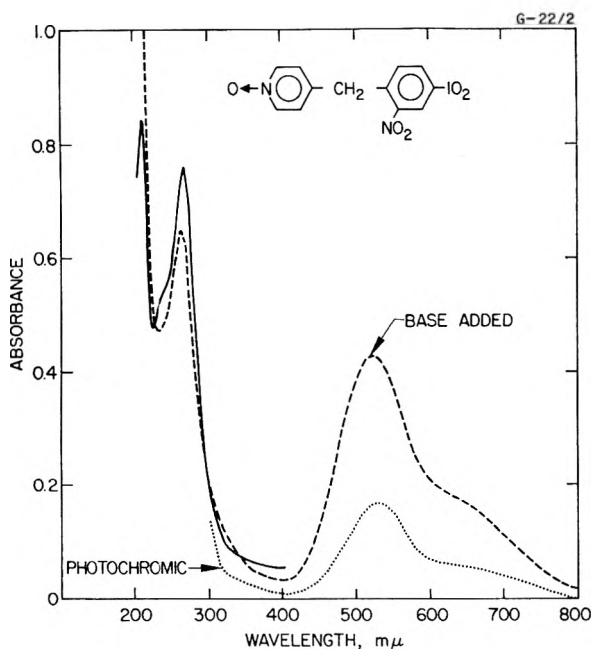


Fig. 2.—4-(2',4'-Dinitrobenzyl)-pyridine N-oxide, spectra of $3.02 \times 10^{-5} M$ solution in 95% ethanol, 1-cm. cell, 31° : broken line, addition of 0.03 ml. of 0.10 *N* KOH to 3.3 ml.; dotted line, irradiation of initial solution at -80° with tungsten lamp of the Cary 14 near infrared.

as detected by deuterium exchange experiments. We have observed the phototropism of this compound visually in ether-ethanol glass in which the yellow photochromic form is long-lived at -196° and presumably is the quinoidal intermediate postulated by Yang and Rivas. Also, there are several reports of photochemical (but not phototropic) reactions of *ortho* nitro derivatives⁷ such as 2,4,6-

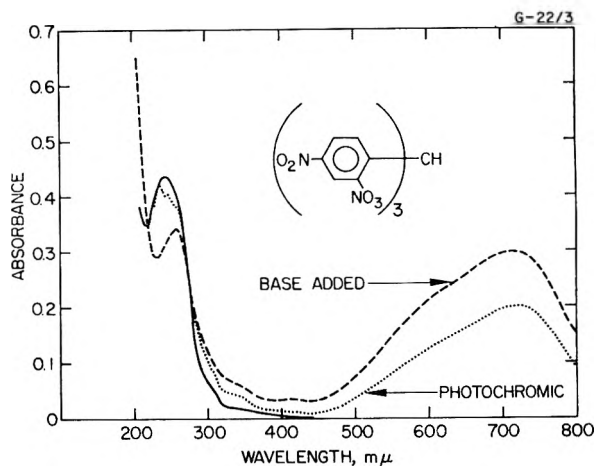


Fig. 3.—Hexanitrotriphenylmethane, spectra of $1.0 \times 10^{-5} M$ solution in absolute methanol, 1-cm. cell, 31° : broken line, addition of 0.03 ml. of 0.10 *N* KOH to 3.3 ml.; dotted line, after irradiation of initial solution at -16° with high pressure mercury lamp.

trinitrotoluene⁸ and *o*-nitrobenzaldehyde⁹ which indicate that these compounds may have the requisite structures, but for several experimental reasons (such as the concentration, extinction coefficient, absorption wave length, or lifetime of the unstable intermediate) no visual phototropic effect is observed.¹⁰ That the nitro groups act by a resonance effect and not solely through an inductive effect is illustrated by 2-(4'-chloro-3',5'-dinitrobenzyl)-pyridine, which was not phototropic. The sum of the Hammett constants for the phenyl substituents of α -DNBP (assuming that the electronic effect of the *ortho* group is approximately equal to that of the *para* nitro group) would be +1.56 and for the 2-(4'-chloro-3',5'-dinitrobenzyl)-pyridine +1.65, which indicates a similar polar effect in both cases. The latter compound, however, neither forms a colored anion on treatment with alcoholic potassium hydroxide nor displays phototropism. This behavior suggests that the same factors which contribute to the stabilization of the anion may also contribute to the phototropic reaction.

Figures 1, 2, and 3 show the spectral changes upon conversion of the colorless to the colored forms for three of the phototropic compounds. The close similarity of the anionic spectra with the photochromic spectra of these three compounds is clearly shown. The photochromic and the anionic spectra of 2,4,2',4'-tetranitrodiphenylmethane and of 2,4,4'-trinitrodiphenylmethane (see Table II) were also found to have broad absorption bands of the type shown by the hexanitro derivative in Fig. 3.

These results are entirely consistent with the hydrogen transfer photochemical mechanism^{4,5} producing the planar *aci* form in equilibrium with

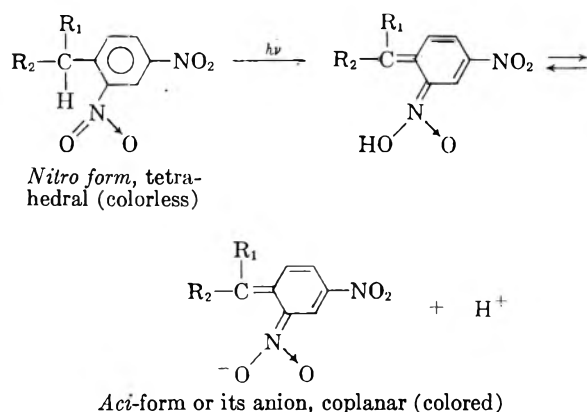
(7) P. De Mayo and S. T. Reid, *Quart. Rev. (London)*, **15**, 414 (1961).

(8) I. Tanasescu, *Bull. soc. chim. France*, [4] **39**, 1449 (1926).

(9) P. A. Leighton and F. A. Lucy, *J. Chem. Phys.*, **2**, 756, 760 (1934).

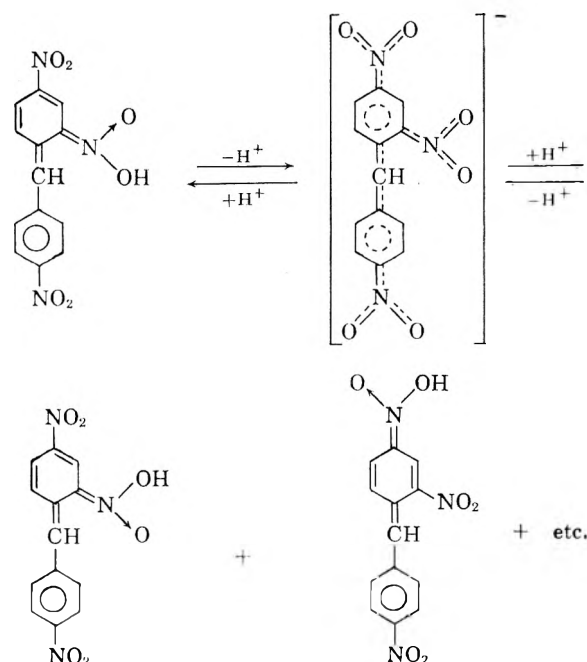
(10) Since the drafting of this paper, we have learned (private communication) that C. Wettermark has observed what is probably phototropism in the flash photolysis of *o*-nitrotoluene.

its anion. A more general form for this photochemical transformation can be written in which R_1 may be H, C_6H_5 , or presumably CH_3 , etc. R_2 may be a substituent that increases the ionizing ability of the central C-H bond without interfering with the light absorption of the 2,4-dinitrophenyl moiety and which becomes conjugated with quinoid structure of the *aci* form. It is apparent from Table II that several groups satisfy the requirements for R_2 ; there undoubtedly are many more.



The *ortho-aci* group initially formed photochemically is acidic and is thus in equilibrium with its anionic form and other *aci* structures. In 2,4,4'-trinitrodiphenylmethane for instance, there are three nitro groups and six possible *aci*-forms.

In the *o*-nitrobenzyl compounds the relative lifetimes of the photochromic forms increased as the acidity of the compounds increased. This probably is due to the increased dissociation of the *aci*-structure to the *aci*-anion and may also be related to the increased multiplicity of possible *aci*-forms with each additional *ortho*- or *para*-nitro group.



The photochromic spectra of the pyridine compounds are different from their anionic spectra, presumably because the basicity of the heterocyclic nitrogen causes a significant contribution of a N-H coplanar form in equilibrium with the *aci*-form and its anion.¹¹ However, in the presence of added base (just short of appreciable anion formation in the dark), irradiation of α -DNBP gave a phototropic reaction forming a colored species with the same color as the anion. This is taken as additional evidence that the photochromic intermediate is whatever would normally be formed from the *aci*-form, depending upon the acid-base equilibria in the solution.

Acid-Base Results.—The solutions obtained by the low temperature neutralization of the anions of 2,4,4'-trinitrodiphenylmethane and 2,4,2',4'-tetranitrodiphenylmethane showed the same absorption maxima as both the corresponding anions and the phototropic species within experimental error. Furthermore, the rate of fading of these neutralized anion solutions was the same (within experimental error) as that which the respective phototropic species produced in the same solution. Data for the tetranitrodiphenylmethane are shown in Table III.

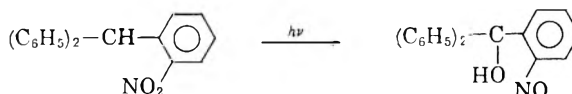
TABLE III

FADING RATE OF THE NEUTRALIZED ANION AND THE IRRADIATED SOLUTION OF 2,4,2',4'-TETRANITRODIPHENYLMETHANE

Temp., °C.	Rates of fading (sec. ⁻¹)	
	Neutralized anion solution ^a	Irradiated solution ^b
-91	3.3×10^3	2.5×10^3
-92	4.2×10^3	1.9×10^3
-93	3.7×10^3	1.7×10^3

^a 0.03 ml. of 0.01 *N* KOH added to 3 ml. of a 2×10^{-4} *M* solution of the tetranitrodiphenylmethane, with cooling to -100° and then adding of 0.03 ml. of cooled 0.01 *N* HCl. ^b From irradiation of the faded conjugate acid solution.

Photochemical and Thermochromic Results.—All of these phototropic nitro compounds also were observed to undergo an irreversible photochemical reaction which eventually interfered completely with the phototropic reaction. It is not known whether this is a photochemical reaction of the photochromic species or whether it is a concurrent side reaction. Although this photochemical decomposition reaction probably is similar to that reported by Tanasescu,⁸ it probably involves much more than this simple transformation.



We have observed also that the anions of some of these substances are sensitive to light. This was especially so for the anion of 2,4,2'-trinitrodiphenylmethane, which upon irradiation decreased in absorption at the 645 $m\mu$ band and increased at the 425 $m\mu$ band. It has been reported¹² that the

(11) E. R. Hardwick and H. S. Mosher, *J. Chem. Phys.*, in press.
 (12) O. Fischer and G. Schmidt, *Chem. Zentr.*, **76**, I, 460 (1904).

anion of tris-(4-nitrophenyl) methane decomposes upon reaction with oxygen bubbling through a solution to form tris-(4-nitrophenyl)-carbinol.

Thermochromic properties also were observed for those compounds in this study which had the more acidic hydrogens on the methylene bridge. Presumably this thermochromic effect is a shift of the equilibrium from the nitro form to the anion (or *aci*-nitro form). This phenomenon was most noticeable with tris-(2,4-dinitrophenyl)-methane, 4-(2',4'-dinitrobenzyl)-pyridine N-oxide, 2,4,2',4'-tetranitrodiphenylmethane, 4,4',4''-trinitrotriphenylmethane, 4,4'-dinitrodiphenylmethane, and ethyl bis-(2,4-dinitrophenyl)-acetate.

Materials

The references for the preparative methods are given in Table I. The new compounds and new methods of synthesis are given in this section.

2-(2',4'-Dinitrobenzyl)-pyridine N-Oxide.—2-(2',4'-Dinitrobenzyl)-pyridine (10.0 g., 0.039 *M*) was dissolved in 200 ml. of glacial acetic acid containing 25 ml. of 30% hydrogen peroxide and was heated on a steam bath for 6 hours. The solvent was removed at reduced pressure, and the residual yellow oil triturated with ether until it solidified. Filtration gave 9.0 g. of crude N-oxide. After recrystallization from acetone-water and benzene, the test sample was passed through a silicic acid column, using benzene-ether mixtures as the eluent, and was recrystallized from this solvent pair, m.p. 135–136.5°. *Anal.* Calcd. for $C_{12}H_9N_3O_5$: C, 52.37; H, 3.30; N, 15.27. Found: C, 52.58; H, 3.46; N, 15.15.

4-(2',4'-Dinitrobenzyl)-pyridine N-Oxide.—4-(2',4'-Dinitrobenzyl)-pyridine (7.04 g., 0.027 *M*) was dissolved in 140 ml. of glacial acetic acid containing 17.5 ml. of 30% hydrogen peroxide, and was heated at 70° for 5.5 hours. The solvent was removed at reduced pressure, and the residual oil was triturated with ether until crystallization occurred. Recrystallization from ethanol gave 5.4 g., m.p. 156–158°. The test sample was chromatographed on neutral alumina using ethanol as the eluent and then recrystallized from ethanol, m.p. 157.2–158°. *Anal.* Calcd. for $C_{12}H_9N_3O_5$: C, 52.37; H, 3.30; N, 15.27. Found: C, 52.49; H, 3.48; N, 15.05.

2-(4'-Chloro-3'-nitrobenzyl)-pyridine.—2-(4'-Chlorobenzyl)-pyridine (5.99 g., 0.029 *M*) was nitrated by slowly adding 2 ml. of yellow fuming nitric acid to a cooled solution in 22 ml. of concd. sulfuric acid. In a 2-hour period the mixture temperature was permitted to rise slowly to 40°, then it was poured onto ice and neutralized with ammonium hydroxide. Filtration gave a white product that turned purple in the dark. This material was allowed to crystallize from hexane by slow evaporation of the solvent for several weeks, forming three different crystalline products. A single large yellow crystal formed first; light yellow needles formed next on the bottom, and a band of purple material appeared on the sides of the container. The needles were separated mechanically, were treated in an isoctane solution with Darco G-60 carbon, and recrystallized from isoctane; 3.5 g., m.p. 60–61°. *Anal.* Calcd. for $C_{12}H_9N_2O_2Cl$: C, 57.96; H, 3.65; N, 11.27. Found: C, 57.88; H, 3.73; N, 11.44.

2-(4'-Chloro-3',5'-dinitrobenzyl)-pyridine.—2-(4'-Chlorobenzyl)-pyridine (7.5 g., 0.037 *M*) was added slowly to a mixed acid (7.5 ml. fuming nitric acid, d. 1.5, and 10.5 ml. concd. sulfuric acid) and stirred for 24 hours on a steam bath. The reaction mixture was poured onto ice, and 5.8 g. of crystals (sulfate salt, m.p. 137–139°) separated on standing. The salt was treated with ammonia to liberate the base which was recrystallized from ethanol, 3.2 g., m.p. 90–91°. *Anal.* Calcd. for $C_{12}H_8N_4O_4Cl$: C, 49.1; H, 2.73; N, 14.30. Found: C, 48.96; H, 2.79; N, 14.28.

This compound (and also the mononitro derivative) in ethanol solution shows no color when treated with ethanolic potassium hydroxide. This is taken as evidence that the nitro groups are not *ortho* to the methylene bridge.

2,2'-Dinitrodiphenylmethane.—4,4'-Diamino-2,2'-dinitrodiphenylmethane (18 g.), prepared according to Montagne and van Charante,¹³ m.p. 205°, was tetrazotized in 6 *N*

hydrochloric acid (100 cc.) by slow addition at –5° of a solution of sodium nitrite (10 g.) in water (25 cc.). To the clear orange solution, 50% hypophosphorous acid (50 cc.) was added slowly. Reduction occurs only on warming above 0°, and the mixture then becomes dark red. The reddish brown precipitate was washed well with water, extracted with 95% ethanol (250 cc.) and this extract chromatographed on Alcoa F-20 alumina with 50% benzene/50% *n*-hexane. The first fractions were recrystallized from *n*-hexane to give approximately 1 g. of material, m.p. 83.5–84.5°. *Anal.* Calcd. for $C_{12}H_{10}N_2O_4$: C, 60.46; H, 3.90. Found: C, 60.21; H, 3.77.

Schnitzpahn¹⁴ reports a melting point of 159° for this compound recrystallized from aqueous ethanol. The above material recrystallized from aqueous ethanol melts at 83–84°. On oxidation with chromium trioxide in acetic acid it gives a dinitrobenzophenone, m.p. 189–192°, reported¹⁵ for 2,2'-dinitrobenzophenone 188–189°. The infrared and ultraviolet spectra of the compound are compatible with a dinitrodiphenylmethane, and nitration gives 2,4,2',4'-dinitrodiphenylmethane, and thus the discrepancy in melting point is unexplained.

2,4,2'-Trinitrodiphenylmethane.—2,2'-Dinitrodiphenylmethane (0.656 g., 0.0025 *M*) was nitrated in concentrated sulfuric acid (7 cc.) at room temperature by the addition of a solution of sodium nitrate (0.216 g., 0.0026 *M*) in concentrated sulfuric acid (5 cc.). After heating at 70° for 1.5 hours, the nitration mixture was poured onto ice, the precipitate washed with water, dried and chromatographed on a basic alumina column (Alcoa F-20) using a 50:50 mixture of benzene and *n*-hexane at the start of the elution and progressing to a solvent richer in benzene as the separation proceeded. 2,2'-Dinitro-, 2,4,2'-trinitro-, and 2,4,2',4'-tetranitrodiphenylmethane were recovered in that order, the trinitro compound comprising about one-half of the total material. The trinitrodiphenylmethane was recrystallized from ethanol, m.p. 111–113°. *Anal.* Calcd. for $C_{12}H_9N_3O_6$: C, 51.49; H, 2.99; N, 13.86. Found: C, 51.67; H, 3.12; N, 13.95.

2,4,4'-Trinitrodiphenylmethane.—4,4'-Dinitrodiphenylmethane (3.88 g., 0.015 *M*) was nitrated in concentrated sulfuric acid (25 cc.) at room temperature by the addition of a solution of potassium nitrate (1.53 g., 0.016 *M*) in concentrated sulfuric acid (25 cc.). After heating at 70° for 1.5 hours, the nitration mixture was poured onto ice, and the precipitate was washed with water, dried and chromatographed on a basic alumina column (Alcoa F-20) using a 50:50 mixture of benzene and hexane at the start of the elution and progressing to a solvent richer in benzene as the separation proceeded. Approximately equal amounts of 4,4'-dinitro-, 2,4,4'-trinitro-, and 2,4,2',4'-tetranitrodiphenylmethane were recovered in that order. The trinitrodiphenylmethane was recrystallized from ethanol, m.p. 107–110°. *Anal.* Calcd. for $C_{12}H_9N_3O_6$: C, 51.49; H, 2.99. Found: C, 51.31; H, 2.93.

Staedel reported a melting point of 109–110° for an *x,x,x*-trinitrodiphenylmethane isolated from the nitration of diphenylmethane. The present synthesis from 4,4'-dinitrodiphenylmethane establishes the structure as that of the 2,4,4'-isomer.

2,4,2',4',2'',4''-Hexanitrotriphenylmethane.—Triphenylmethane (7.38 g., 0.030 *M*) was nitrated with a total of 17 ml. of fuming nitric acid in 90 ml. of concd. sulfuric acid. The nitric acid was added slowly, at first keeping the mixture below 20°, and then holding at 80° for 4 hr. The reaction mixture was poured onto ice, and the aqueous suspension was neutralized with ammonium hydroxide, filtered, and washed with methanol (yield, 12 g.). The test sample was recrystallized by adding water to a boiling acetonitrile solution, then recrystallized from acetonitrile and washed with ether, m.p. 256–258° dec. *Anal.* Calcd. for $C_{18}H_{10}N_6O_{12}$: C, 44.37; H, 1.96; N, 16.34. Found: C, 44.79; H, 2.09; N, 16.00.

Ammonium 2,4-Dinitrophenylacetate.—This salt was formed as a precipitate by passing dry ammonia gas through a methanol-ether solution of 2,4-dinitrophenylacetic acid (Eastman White Label).

(13) P. J. Montagne and J. M. van Charante, *Rec. trav. chim.*, **31**, 343 (1912).

(14) K. Schnitzpahn, *J. prakt. Chem.*, [2] **65**, 322 (1902).

(15) W. Staedel, *Ber.*, **23**, 2578 (1890).

OPTICAL PROPERTIES OF 2-(2',4'-DINITROBENZYL)-PYRIDINE IN THE ADSORBED STATE

BY G. KORTUM,¹ M. KORTUM-SEILER,¹ AND S. D. BAILEY

Contribution from the Pioneering Research Division,
Quartermaster Research and Engineering Center, Natick, Mass.

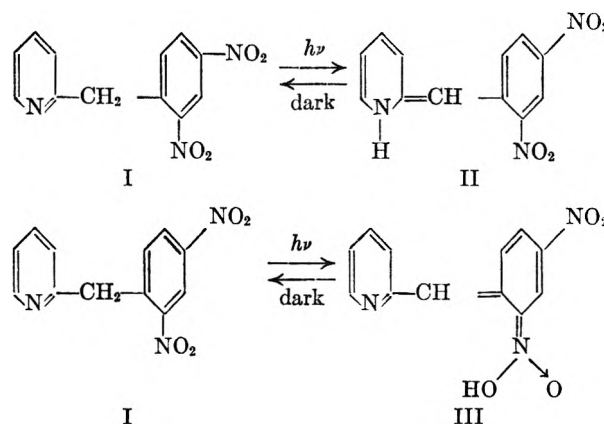
Received May 25, 1962

Diffuse reflectance spectroscopy has been used in an investigation of the reversible photochemical conversion of 2-(2',4'-dinitrobenzyl)-pyridine in the adsorbed state. The tautomeric shift associated with this conversion was studied in the phase boundary of those adsorbents which serve as electron acceptors. Two first order reactions were found which probably are due to the fading of a positive ion and of the neutral molecule, respectively. Activation energies have been estimated from the kinetic data.

The Kubelka-Munk theory,² describing the process of "diffuse reflectance" of finely powdered absorbing material, has not been extensively used because the invariably superimposed "regular reflectance" levels and broadens the derived spectra. To get the true absorption spectrum from reflectance measurements one therefore has to eliminate the regular part of the reflection. This can be done easily by triturating the sample together with a large excess of a non-absorbing standard of the same particle size.^{3,4} Since in this process all organic and many inorganic compounds are adsorbed on the surface of the standard, this method is especially suitable for the investigation of the optical behavior of adsorbed molecules.

Recent work, for instance on the reversible adsorption of different dyes on surfaces of appropriate adsorbents,^{5,6} has shown that frequently a chemisorption is taking place which is accompanied by a pronounced change of color. This can be attributed to an electron-donor-acceptor-process between adsorbed material and the adsorbent. Equally, irreversible photochemical reactions of adsorbed molecules have been investigated by this method.⁷ The method, therefore, appeared promising for the investigation of the reversible photochemical reaction of 2-(2',4'-dinitrobenzyl)-pyridine, which turns blue by illumination and fades again in the dark to its original colorless form. This reaction takes place in the crystalline form as well as in solution,⁸ but the rate of fading in solution is very rapid and can only be observed at low temperatures⁹ or by a special flash technique at room temperature.¹⁰

The reaction has been interpreted⁸ as a tautomeric shift which involves either the pyridine or the neighboring nitro group.



We have studied this reaction in the phase boundary of several adsorbents by measuring the reflectance spectra of mixtures, where the molar fraction of the nitro compound was 10^{-3} to 10^{-4} , against the pure adsorbent as standard. Adsorption was accomplished by grinding for several hours in a ball mill in the dark in a CO_2 atmosphere. The sample then was exposed to diffuse daylight for 30 minutes and measured again. The spectra on NaCl as adsorbent are shown in Fig. 1.

The logarithm of the Kubelka-Munk function

$$F(R_\infty) \equiv \frac{(1 - R_\infty)^2}{2R} = \frac{\epsilon c}{s}$$

is plotted against the wave number. $R_\infty \equiv I(\text{sample})/I(\text{standard})$ is the measured relative diffuse reflectivity, ϵ the molar extinction coefficient, c the molarity, and s the scattering coefficient, which is essentially independent of the wave length. The spectra are therefore identical with the true absorption spectra, except for a parallel shift in the values of $\log \epsilon$. Quite analogous spectra were obtained on silica and lithium fluoride as adsorbents. Prolonged irradiation changes the compound irreversibly both in the case of the pure substance and in the solutions.⁸

The adsorbed nitro compound when illuminated turns blue, like the pure crystalline compound ($\lambda_{\text{max}} \cong 600 \text{ m}\mu$), with the color fading slowly over a period of about 10 hours in the dark. The spectrum can be measured easily therefore at room temperature.

Since earlier studies had shown that the interaction between adsorbed molecules and the adsorbent can in some cases be prevented by adsorbed

(1) Visiting scientists from the Institute for Physical Chemistry, University of Tübingen, Tübingen, Germany.

(2) P. Kubelka and F. Munk, *Z. Techn. Phys.*, **12**, 513 (1931); P. Kubelka, *J. Opt. Soc. Am.*, **38**, 448, 1067 (1948).

(3) G. Kortum and G. Schreyer, *Angew. Chem.*, **67**, 694 (1955).

(4) G. Kortum and J. Vogel, *Z. Physik. Chem. (Frankfurt)*, **18**, 110, 230 (1958).

(5) G. Kortum, J. Vogel, and W. Braun, *Angew. Chem.*, **70**, 651 (1958).

(6) G. Kortum and J. Vogel, *Chem. Ber.*, **93**, 706 (1960).

(7) G. Kortum and W. Braun, *Ann. Chem.*, **632**, 104 (1960).

(8) R. Hardwick, H. S. Mosher, and P. Passailaigue, *Trans. Faraday Soc.*, **56**, 44 (1960); H. S. Mosher, C. Savers, and R. Hardwick, *J. Chem. Phys.*, **32**, 1888 (1960).

(9) J. Sousa and J. Weinstein, *J. Org. Chem.*, **27**, 3155 (1962).

(10) G. Wettermark, *J. Am. Chem. Soc.*, **84**, 3658 (1962).

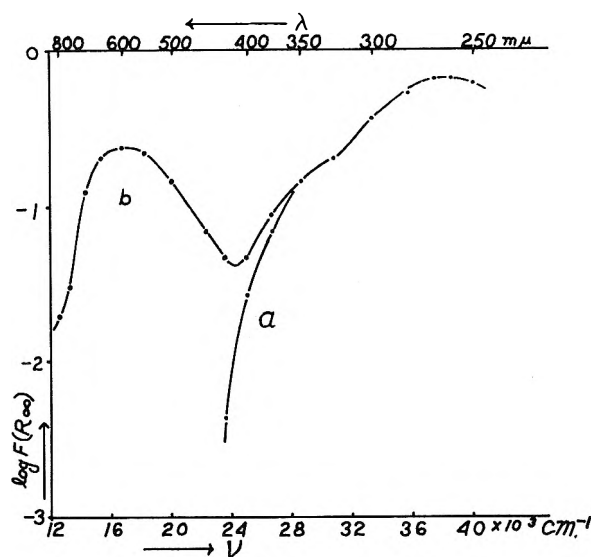


Fig. 1.—Reflectance spectra of 2-(2',4'-dinitrobenzyl)-pyridine adsorbed on NaCl before exposure to light (a) and after exposure to 30 minutes of diffuse sunlight (b).

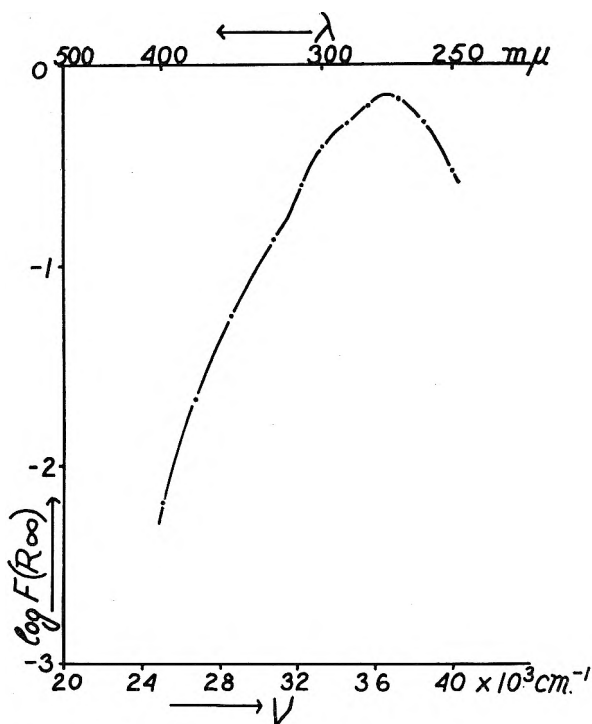
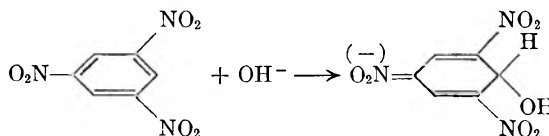


Fig. 2.—Reflectance spectrum of 2-(2',4'-dinitrobenzyl)-pyridine adsorbed on magnesium oxide.

water,^{5,6} we at first carried out all experiments in the absence of moisture by heating the adsorbents to 500° for several hours and sealing the sample cells with quartz plates in a glove-box in a dry carbon dioxide atmosphere. It was found, however, that the exposure of the adsorbed and converted compound to moist air did not change the intensity of absorption, so that later experiments were made with adsorbents which were air-dried only. The strong partial dipole moments of the nitro compound appear to be capable of displacing the water molecules from the surface of the adsorbent.

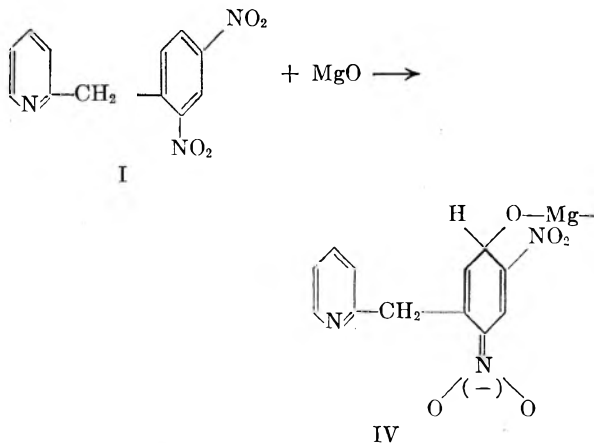
Quite unexpectedly the conversion to the blue form by illumination failed when the compound was adsorbed on MgO. Instead, an irreversible reaction in the dark took place, indicated by two maxima in the visible region at about 670 and 480 mμ, respectively, which did not change upon irradiation in the ultraviolet. This is shown in Fig. 2. This reaction, in contrast to the tautomeric shift, seems to be accelerated by water and can best be investigated on adsorbents which are only air-dried.

An indication of the reaction mechanism was given by earlier experiments⁵ on the reflectance spectra of *s*-trinitrobenzene adsorbed on MgO. Whereas *s*-trinitrobenzene adsorbed on SiO₂ or NaCl remains colorless, the adsorption on MgO produces a bright red compound, the spectrum of which is analogous to that of an alkaline solution of the same compound in water. This reaction has been explained according to polarographic investigations¹¹ as an addition of OH⁻ ions on the benzene nucleus:



We therefore trituated 2,4-dinitrotoluene with an excess of MgO and SiO₂, respectively, and found that it reacts with MgO in the same way whereas on silica it remains unchanged.

We may therefore conclude that an analogous reaction takes place between the dinitro compound and MgO at the phase boundary, the MgO acting as an electron donor



The quinoid structure of this compound explains the absorption in the visible and prevents the conversion I → III, but would not prevent the tautomeric reaction I → II. From the fact that the dinitro compound does not turn blue on MgO by illumination we conclude that the mechanism of this conversion consists more likely in an intramolecular shift I ⇌ III than in a shift I ⇌ II. This can be confirmed further by the optical behavior of the 2-(4'-nitrobenzyl)-pyridine, in which

(11) L. Holleck and G. Perret, *Z. Elektrochem.*, **59**, 114 (1955); **60**, 463 (1956).

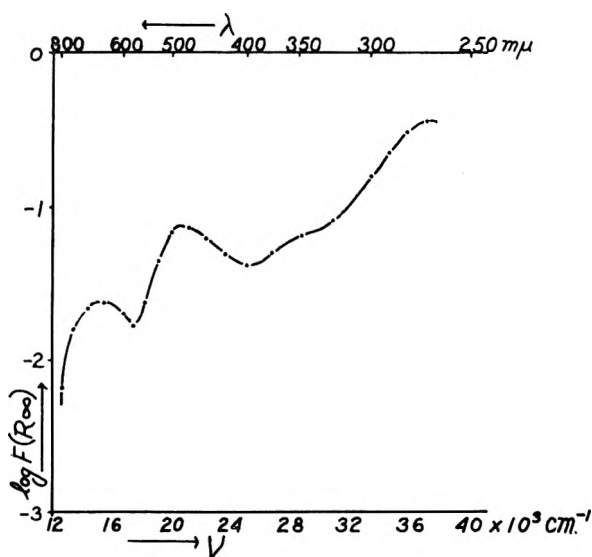


Fig. 3.—Reflectance spectrum of 2-(4'-nitrobenzyl)-pyridine adsorbed on silica.

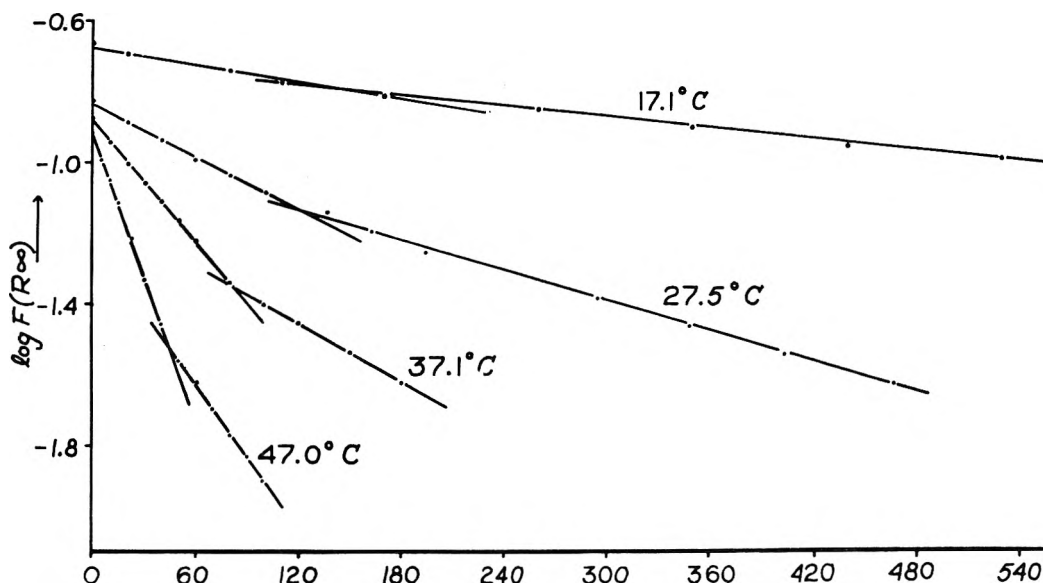
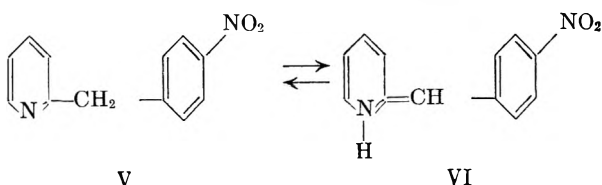


Fig. 4.—Fading reaction of 2-(2',4'-dinitrobenzyl)-pyridine as a function of temperature: plot of $\log F(R_\infty)$ vs. time in minutes at temperatures of 17.1, 27.5, 37.1 and 47.0°.

the analogous tautomeric shift to $I \rightleftharpoons II$ would be expected to take place

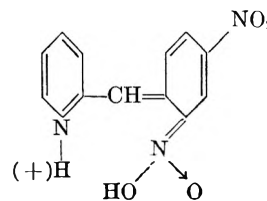


By this reaction a resonance system extending over the whole molecule should result, giving a shift of the absorption to longer wave lengths. The reflectance spectrum of the mononitro compound adsorbed on air-dry silica (Fig. 3) was measured and no shift in the absorption was found. This means that the reaction $V \rightarrow VI$ is very unlikely.

$MgCO_3$, CaO , and "alkaline" Al_2O_3 as adsorbents behave in the same manner as MgO in that the conversion to the blue form upon irradiation

does not occur. Neither does the irreversible reaction $I \rightarrow IV$ take place on $MgCO_3$ and Al_2O_3 . In the case of CaO it can be detected slightly. On very pure "neutral" Al_2O_3 the tautomeric shift $I \rightarrow III$ can be observed, but to a lesser degree than on SiO_2 , $NaCl$, or LiF , all other conditions being held constant.

In order to compare our results with those in solutions, we have made rate measurements of the fading reaction $III \rightarrow I$ as a function of temperature using silica as the adsorbent. For this purpose the samples were sealed in fused quartz cells which could be kept in a water thermostat and which were measured against the pure adsorbent as reference at 600 $m\mu$ as a function of time t . The logarithm of the Kubelka-Munk function $\log F(R_\infty)$ plotted against t at four different temperatures is shown in Fig. 4. Obviously there are two first order reactions with different rates which are analogous to reactions in solution at different pH's.¹⁰ This may be attributed to the fading of the cation



and of the neutral molecule (I), respectively, the proton being substituted by acid groups $-Si-OH$.

From the slopes of the straight lines the rate constants k of the two reactions can be calculated and are given in Table I.

The values of $\log k$ plotted against $1/T$ give approximately straight lines, the slopes of which give the activation energies E for the two fading reactions

$$-\frac{2.30R\Delta \log k}{\Delta(1/T)} = E$$

TABLE I

°C.	1/T	k_1 min. ⁻¹	log k_1	k_2 min. ⁻¹	log k_2
47.0	0.00312	0.0307	-1.513	0.0160	-1.796
37.1	0.00322	0.0128	-1.893	0.0061	-2.213
27.5	0.00333	0.0057	-2.240	0.0032	-2.492
17.1	0.00345	0.0017	-2.771	0.0011	-2.947

We find $E_1 \cong 17$ and $E_2 \cong 15$ kcal./mole, which is of the same order of magnitude and about three times larger than in solution,⁹ as is to be expected from the much smaller rates of fading in the adsorbed state. Since the activation energy E_1 of the faster reaction 1 is somewhat larger than that of the slower reaction 2, there must exist a difference in the frequency factor $f_1 > f_2$, which might be due to different interaction of the cation or the neutral molecule, respectively, with the surface.

PHOTOCHROMY AND THERMOCHROMY OF ANILS¹

BY M. D. COHEN AND G. M. J. SCHMIDT

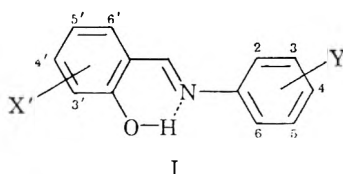
Department of X-Ray Crystallography, Weizmann Institute of Science, Rehovoth, Israel

Received May 26, 1962

In crystalline salicylidene anilines, photochromy and thermochromy are mutually exclusive properties. Thermochromy involves an *intramolecular* proton shift to the quinonoid tautomer; this shift occurs both in the ground state and excited state. In the photochromic process there is also an *intramolecular* proton shift in the excited state, but the nature of the colored product is not yet unambiguously defined. Photochromy is a property of the isolated anil molecule in an arbitrary rigid matrix; thermochromy, on the other hand, necessitates certain specific structural types.

Introduction

Some crystalline anils of salicylaldehyde (I) are



photochromic; on irradiation with near ultraviolet light their color deepens with the formation of an absorption band in the visible. This color-deepening can be reversed (eradicating) by irradiating with light absorbed in the latter band, or thermally in the dark.

Photochromy in this series is a topochemically determined phenomenon, *i.e.*, there seems to be no correlation of activity with substituents X' and Y, but the packing arrangement in the crystal is of importance. Thus, for example, of the chemically very similar 4-chloro- and 4-bromo-anils, the latter is photochromic but the former not. Further, several anils have two polymorphic modifications of which only one is photochromic.

Summary of Experimental Observations

We have reported previously that in rigid glassy solutions all anils derived from salicylaldehyde and substituted salicylaldehydes are photochromic, whether or not they are so in the crystal.² By varying the chemical structure of the anil molecule used in these experiments we were able, then, to determine what features of the molecule are essential for photo-colorability. We found that the anils of *ortho*-methoxy- and of *para*-hydroxy-benzaldehydes, and

of benzaldehyde itself, are not colorable; thus the *ortho*-hydroxyl group is essential to the process.

No cases of photochromy in the crystal have been found among the anils of hydroxy-naphthaldehydes. However, the anils of 2-hydroxy-1-naphthaldehyde (II) and of 1-hydroxy-2-naphthaldehyde (III) are photochromic in "high temperature" glassy solutions. Anils of II and III also have absorption bands in the visible when dissolved in hydroxylic solvents at room temperature, or in non-polar solvents at low temperatures.^{2a,3,4} This absorption is not observed in the absence of the hydroxyl group, nor is it found in solutions of anils of 2-hydroxy-3-naphthaldehyde.

In the crystal, the dark-fading of the photo-color is a typical rate process with activation energy of the order of 20 to 25 kcal. mole⁻¹. Above a certain temperature this process is so rapid that photochromy cannot be observed by conventional methods. This "upper temperature limit" is characteristic of the particular anil and crystal modification studied.

On the other hand, for many anils it has been observed that for irradiation carried out at successively lower temperatures the yield of photo-color drops off, and there is a "lower temperature limit" below which photochromy is not observed.

Because photochromy is, thus, found only between certain temperature limits it was necessary to study each compound over a range of temperatures. These experiments showed that many of the crystalline anils are thermochromic and that, in fact, thermochromy and photochromy are mutually exclusive properties; thus, each particular anil crystal modification is either photochromic or thermochromic, but not both. Neither photo-

(1) Further reports on these and other topochemical systems are to be submitted shortly to *J. Chem. Soc.*

(2) (a) M. D. Cohen, Y. Hirshberg, and G. M. J. Schmidt in "Hydrogen Bonding," D. Hadzi, Ed. Pergamon Press, London, 1959, p. 293; (b) M. D. Cohen and G. M. J. Schmidt in "Reactivity of Solids," J. H. de Boer, Ed., Elsevier, Amsterdam, 1961, p. 556.

(3) M. D. Cohen, Y. Hirshberg, and G. M. J. Schmidt, abstracts in *Bull. Res. Council Israel*, **6A**, 167 (1957); XIVth IUPAC Congress, Paris, 1957, Vol. II, p. 84.

(4) W. Vosz, "Elektronenspektren aromatischer Azomethin- und Azaverbindungen," Thesis, Technische Hochschule, Stuttgart, 1960.

chromy nor thermochromy (or the associated "chromo-isomerism") are observed in the absence of the *ortho*-hydroxyl group.

The spectral properties of a photochromic and of a thermochromic crystal are shown in Fig. 1 and 2. It will be noted that the long wave length bands of the two materials are very similar as regards the wave length of maximum absorption and the presence of a shoulder at about 4900 Å. On the other hand there is an appreciable difference in the range 5200–6000 Å.

There is evidence that both the forward and reverse photochemically-induced processes involve passage over a thermal barrier, probably in the excited state. Reference has been made to the drop in yields at low temperatures; on the other hand, a photochromic anil irradiated at a temperature at which the yield is high, and subsequently cooled, retains its full color. Similarly, it was found possible to achieve photoeradication of the colors formed in glassy solutions only for "high temperature solvents," *e.g.*, paraffin oil at -80° ; no photoeradication proved possible for solvents whose setting temperature is below -120° .

Confirmatory and more illuminating results have been obtained from preliminary fluorescence measurements. There is a clear-cut distinction between photochromic and thermochromic crystals in their fluorescence properties. Thermochromic crystals, on irradiation with 365 $m\mu$ light, luminesce an intense yellow-green; this luminescence, which is of half-life time less than 50 μ sec.,⁵ changes markedly with temperature. Of significance, however, is the observation that, at all temperatures, the short wave length cut-off of the fluorescence is at about 4900 Å. (Fig. 2). We have not been able to measure any light emission from photochromic crystals during irradiation with 365 $m\mu$ light, although to the eye they appear a dull red. However, at low temperature, where the yield of the photocolor drops, these crystals become strongly luminescent, the spectrum of the light emitted being as for the thermochromic materials.

Discussion of the Results

(i) The Nature of the Deeply Colored Species.—

There is overwhelming evidence for the importance of the *ortho*-hydroxyl group in these processes. Further, the results with the naphthylidene anils, and their analogy with the azonaphthols,^{6,7} argue strongly for the thermal color change being due to a quinoid–benzenoid tautomerism. Recent n.m.r. measurements⁸ provide more direct evidence for the quinoid nature of the colored species. We recall that Manchot⁹ showed that chromo-isomeric anils, dissolved and maintained at low temperatures, react at different rates with ferric chloride solution. Other reports on the tautomerism in solution have appeared in the literature.^{2–4,10}

(5) A. Tzalmona and A. Aharoni, private communication.

(6) A. Burawoy, A. G. Salem, and A. R. Thompson, *J. Chem. Soc.*, 4793 (1952).

(7) K. J. Morgan, *ibid.*, 2151 (1961).

(8) G. O. Dudek and R. H. Holm, *J. Am. Chem. Soc.*, **83**, 3914 (1961).

(9) W. Manchot, *Ann.*, **388**, 103 (1922).

(10) D. Heinert and A. E. Martell, Abstract A1-102 in XVIIIth IUPAC Congress, Montreal, 1961, p. 61.

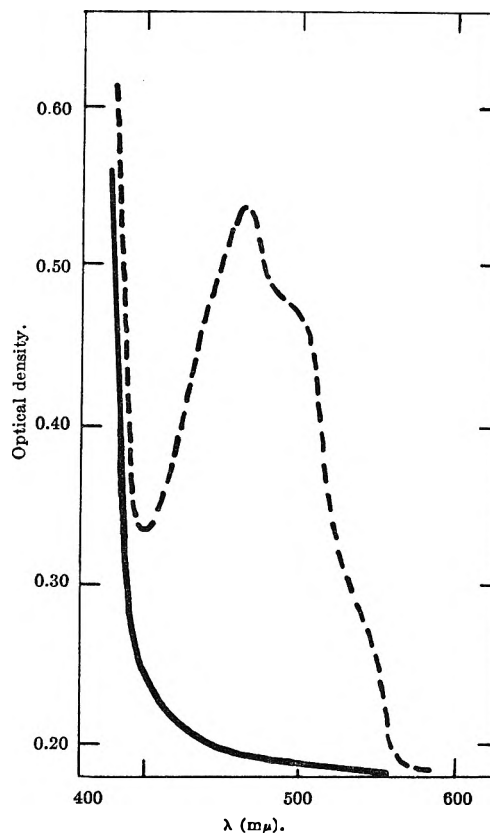
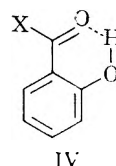


Fig. 1.—The absorption spectrum of a crystalline film of salicylidene 2-chloroaniline before (full curve) and after (broken curve) irradiation. (Temperature -131° ; irradiation 20 min. through Corning filter F5874, 250-watt high pressure mercury arc.)

There is no such direct information concerning the nature of the photo-formed deep color. Here the necessity for the *ortho*-hydroxyl group, and the similarity of the spectra to those of the thermochromic crystals, argue for the process being a tautomerization to a quinoid state. There are various possible explanations for the difference between the spectra of photochromic crystals in the long wave length region (*ca.* 5200–6000 Å.): it might be attributable to the difference in the strength of *inter*-molecular coupling in the two packing types¹¹; alternatively, the absorption in this region may be a partially submerged band due to a species found only in the photochromic crystals. These alternatives are being considered further.

(ii) **Mechanism.**—Weller has shown¹² that in compounds of the type IV a displacement of the



hydroxyl hydrogen to the carbonyl oxygen takes place in the excited state. This is evidenced by a large Stokes shift of the fluorescence.

(11) W. T. Simpson and D. L. Peterson, *J. Chem. Phys.*, **26**, 588 (1957).

(12) A. Weller, *Z. Elektrochem.*, **60**, 1144 (1956).

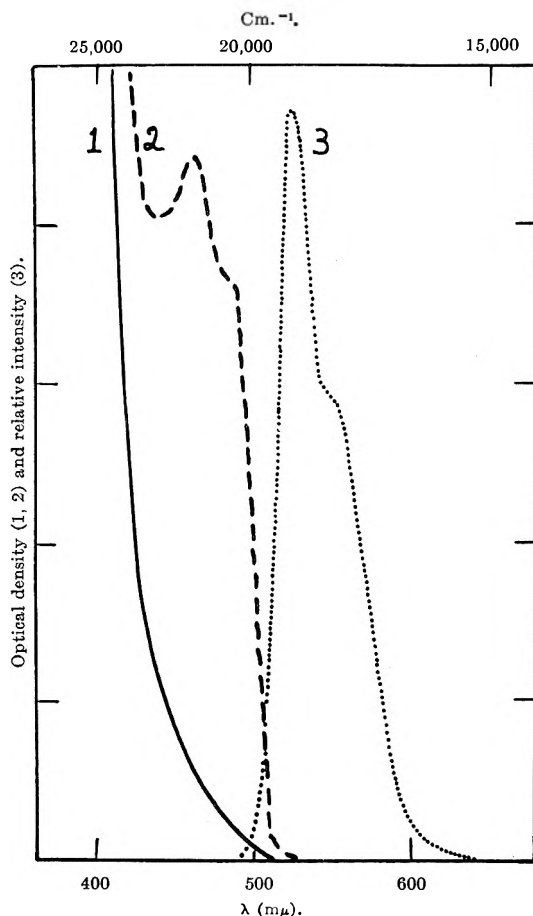


Fig. 2.—The absorption and fluorescence spectra of a crystalline film of the strongly thermochromic 5'-chlorosalicylidene aniline: 1 (full curve), absorption at -153° ; 2 (broken curve), absorption at -49° ; 3 (dotted), fluorescence at -153° on irradiation with $365\text{ m}\mu$ light. (The fluorescence results are not corrected for variation of the sensitivity of the measuring instrument with wave length.)

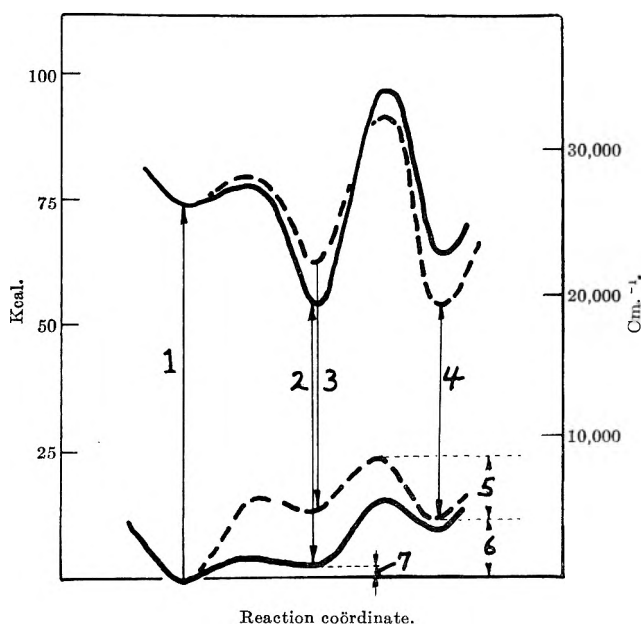


Fig. 3.—Schematic representation of energy surfaces of an anil molecule in a thermochromic (full curve) and photochromic (broken curve) crystal. The numbered arrows are defined in the text.

In the thermochromic anils we find a similar large displacement of the fluorescence to longer wave lengths relative to the low-temperature band which absorbs (1, Fig. 3) the $365\text{ m}\mu$ light used in the irradiation. In fact, the fluorescence approximately mirrors the high-temperature absorption band (2, Fig. 3).

Thermal measurements have shown that the difference in the energies of the ground states of the yellow and red forms of the thermochromic crystals (7, Fig. 3) is small. Thus the larger displacement of the fluorescence is due to a second minimum in the excited state energy surface; proton transfer in these crystals therefore occurs in both ground and excited states.

For the photochromic crystals, however, the results require us to postulate a triple-minimum potential energy surface for the excited state; at high temperatures the primary excitation (1, Fig. 3) is followed by a proton transfer, and then a process of appreciable activation energy leads to a state which undergoes radiationless deactivation (or luminescence in the red) (4, Fig. 3) to the colored ground state; at low temperatures also the primary excitation is followed by proton transfer, but then there is fluorescent deactivation (3, Fig. 3) to the phenolic ground state, or to a state related to the phenolic ground state by a path of low activation energy.

We have some indication that in the $5200\text{--}6000\text{ \AA.}$ range the thermochromic crystals have a very weak absorption band with λ_{max} at about 5600 \AA. ; further, that on application of heat to such crystals there is a time lag, of the order of milliseconds, in the appearance of this band, whereas the time lag in the appearance of the main thermochromic band had not been observed, but is certainly less than a few microseconds.⁵ These tentative results suggest the presence of a third minimum in the energy surface of thermochromic crystals, too. The difference between the two types of crystals would then lie in the relative energies of the three minima and in the activation energies for passage from one minimum to another (or the probabilities of intersystem crossing).

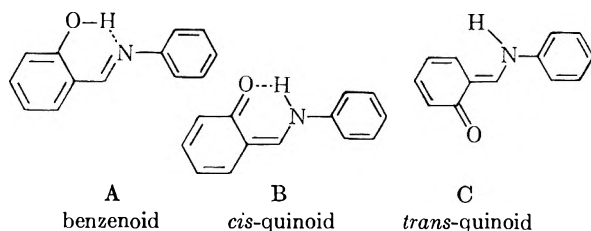
In Fig. 3 we illustrate diagrammatically the energy relationships we consider pertinent to the two classes of materials. In compiling these diagrams we have used the following additional considerations: (a) we have measured an energy difference of $1.76\text{ kcal. mole}^{-1}$ between the yellow and red forms of the thermochromic 5'-chloroanil (7, Fig. 3); (b) the activation energies for the interconversion of these forms are low, since their interconversion is rapid at all temperatures; (c) the energy difference between yellow and photo-formed red species (6, Fig. 3) is appreciable, as evidenced by the absence of thermal population of the latter state (cf., however, Lindemann's estimate¹³ of less than 4 kcal. mole^{-1} for the 3-methylanil); (d) the activation energy for the interconversion (fading) also is found to be much higher in the photochromic series (5, Fig. 3).

(13) G. Lindemann, *Z. wiss. Phot. Photophysik Photochem.*, **50**[11], 347 (1955).

TABLE I

System	A	B	C
Anils	Benzenoid	Quinoid " <i>cis</i> "	Quinoid " <i>trans</i> "
Spiropyrans	Benzenoid, ring	Quinoid, chain with C and O in close proximity	Quinoid, chain, with C and O well separated (several isomers)
Sydnones	Molecules	Sydnone ⁺ and e ⁻	Sydnone ⁺ + e ⁻ diffused an appreciable distance away
2,4-Dinitrobenzylpyridine	Benzenoid (nitro)	Quinoid (<i>aci</i>) " <i>cis</i> "	Quinoid (<i>aci</i>) " <i>trans</i> "
Tetrachloroketonaphthalene	Molecule	Aryloxy· and Cl·	Aryloxy· + Cl· diffused an appreciable distance away (possibly to another position in the molecule)

We have assigned the first two ground-state minima to the phenolic and quinoid molecular species; it remains for us to consider the third minimum. We have little evidence of direct bearing on the nature of the corresponding species; however, in keeping with all our data is the supposition that it is a geometric isomer of the quinoid molecule (*i.e.*, C below)



(the *cis* and *trans* labeling is based on relative positions of H and O).

We shall see that analogous states can be envisaged for other photochromic systems.

(iii) **Structural Information.**—The question next arises as to whether the energetics of these processes can be interpreted in terms of the crystal structures of the several anil types. The results obtained with rigid glasses suggest that photochromy is a property of the isolated anil molecule in an arbitrary rigid matrix; photochromic crystals are, then, a sub-group of this general case. On the other hand, in certain structure-types the intermolecular interactions are such as to lead to thermochromic behavior.

Our initial extension of these ideas was to suggest that the hydrogen-bond and hydrogen-transfer are *intramolecular* in the photochromic case, *intermolecular* in the thermochromic one.^{2a} This postulate proved to be incorrect; in both types of crystals the hydrogen bonds have been found to be *intramolecular*, with the distance from O of one molecule to N of an adjacent one being too great for *intermolecular* bonding.

The crystal-structure effect is twofold: it enables the photochemical *cis-trans* isomerization to occur in the photochromic but not in the thermochromic series; it also brings about a stabilization of the *cis*-quinoid species in the thermochromic lattices. Because thermochromy and photochromy are mutually exclusive properties it is probable the same aspects of the structures are responsible for both phenomena.

The most striking features of the crystal structures thus far solved are¹⁴: (i) In the thermochromic crystals the molecules are essentially planar and packed plane-to-plane at about 3.4-Å. spacing,

while displaced relative to one another along the long molecular direction; (ii) in the photochromic salicylidene *o*-chloroaniline the molecules are distinctly non-planar and there are no close plane-to-plane contacts as in (i).

We believe that such plane-to-plane packing is responsible for thermochromic properties, providing stabilization of the *cis*-quinone through dipole-dipole interaction; it is also responsible for lack of photochromic properties in such crystals by (sterically) preventing the *cis-trans* isomerization.

In photochromic crystals, on the other hand, the structure is sufficiently open to allow the isomerization, while packing is not of the right type for dipole-dipole interaction to lead to stabilization of the *cis*-quinone. Here we see the source of the analogous behavior of photochromic crystals and of rigid solutions of the anils.

Two modifying statements should be made: first, the molecules in photochromic crystals are not completely insulated from one another and some topochemical influences are to be expected; second, the cell dimensions and space groups of the thermochromic crystals show that there are a number of sub-groups between which there are marked differences in packing characteristics. The intensity of thermal color formation is more or less uniform within each sub-group, but differs markedly between sub-groups.

General Comments on Photochromy.—The energy surfaces which we have constructed for the anil systems appear to apply, with small modifications, to the other photochromic systems described in this symposium. (We speak here of "an energy surface" with the full realization that changes in multiplicity may be involved at some intermediate stages.) Some of these systems are non-fluorescent so that it is difficult to determine whether there are minima in the excited-state surface corresponding to those in the ground-state surface. There must, thus, remain open the possibility that internal conversion causes decay to a high vibrational level of the ground state, with further reaction occurring in this state.

For the ground state surface, however, the following species are clearly involved: (i) non-colored form (A); (ii) colored form (B), geometrically very similar to (A) but of higher energy and readily converted into it; (iii) colored form (C), geometrically different to (B) and requiring appreciable activation energy to allow conversion into (B).

(14) The structure analyses will be reported elsewhere; see J. Bregman, L. Leiserowitz, K. Osaki, and G. M. J. Schmidt, *J. Chem. Soc.*, in press.

This is a minimal set; there are in some cases a number of modifications of each of these species.

We note in Table I the possible natures of A, B, and C for various systems.

PHOTOCHROMIC BEHAVIOR OF SYDNONES

BY F. I. METZ, W. C. SERVOSS, AND F. E. WELSH

Midwest Research Institute, Kansas City, Missouri

Received May 25, 1962

Seven different sydnones (N-benzylsydnone; N-*p*-methylbenzylsydnone; N-3,4-dimethylbenzylsydnone; N-*p*-chlorobenzylsydnone; N,N'-ethylene-bis-sydnone; N,N'-tetramethylene-bis-sydnone; and N-3-pyridylsydnone) have been examined for photochromic behavior. Although all of the compound sydnones exhibited some degree of photochromism in the solid state, the response of the group of materials was inconsistent and could not be related to structural parameters. N-3-Pyridylsydnone (N3PS) was selected for more extensive study on the basis of the extent and spectral location of the photochromic change which it undergoes. The material was investigated in the solid state as well as in solution. A mechanism for the photochromic behavior of N3PS is suggested on the basis of experimental evidence presented.

I. Introduction

Increasing interest has been shown during the past few years in photochromism and photochromic materials.¹ Various applications such as devices for temperature control of satellites, computer memory elements, and optical filters with controllable, variable absorbancies have been proposed. Midwest Research Institute has been engaged in the study of photochromic materials and photochromism for several of these end uses.

A group of anhydro-compounds prepared by Earl and his collaborators^{2,3} at the University of Sydney have been termed "sydnones." These compounds have been shown to be neutral, highly crystalline, stable, and fairly soluble in most organic solvents including benzene. Baker, Ollis, and Poole⁴ have proposed a mesoionic hybrid structure of aromatic type.

The purpose of this paper is to report the results of solid state and solution studies of photochromism in sydnones, with particular emphasis on N-3-pyridylsydnone. The sydnones investigated are listed in Table I. The degree of photochromism (reversible color transformation in the visible region exhibited by solids or solutions upon exposure to exciting radiation) of each of these materials is presented in Table II. N-3-Pyridylsydnone was the most photochromic sydnone of the eight compounds investigated, and was therefore examined in greater detail.

II. Experimental Procedures and Results

A. Preparation of Materials.—Compounds I through VI (Table I) were made available for this study by the Cancer Chemotherapy National Service Center, National Institutes of Health, through the courtesy of Dr. C. C. Cheng, Head of the Cancer Chemotherapy Section, Midwest Research Institute. N-3-Pyridylsydnone (N3PS) was prepared by the methods of Tien and Hunsberger.⁵ Purification of all the compounds was by successive recrystallization.

B. Solution Studies.—In solution, the various sydnones were not photochromic, however, non-reversible color formation did occur in some instances. This type of change

TABLE I
SYDNONES EXAMINED FOR PHOTOCROMISM

Compound	Formula
(I) N-Benzylsydnone	
(II) N- <i>p</i> -Methylbenzylsydnone	
(III) N-3,4-Dimethylbenzylsydnone	
(IV) N- <i>p</i> -Chlorobenzylsydnone	
(V) N,N'-Ethylene-bis-sydnone	
(VI) N,N'-Tetramethylene-bis-sydnone	
(N3PS) N-3-Pyridylsydnone	

TABLE II
ULTRAVIOLET EXCITATION CHARACTERISTICS OF SYDNONE FILMS

Sydnone	Optical excitation characteristics		
	ΔT_{\max}^a (%)	ΔR^b (%)	Wave length (μ)
I	+3.3	+3.5	360
II	+1.9	+0.4	500
III	-3.0	+5.5	360
IV	-0.6	+4.8	360
V	-1.4	+0.2	400
VI	+1.2	+4.0	360
N3PS	-4.8	+5.0	600

^a Maximum change (plus or minus) in transmission, after 2-min. exposure to ultraviolet irradiation; ultraviolet source: GE H-100 FL-4 mercury projection bulb with a Corning D CVX RDL filter to screen the visible light. ^b Recovery-change in transmission after 5 min. exposure to infrared irradiation; infrared source: standard 250-watt infrared bulb; all values represent mean values obtained from several experiments.

(1) G. H. Brown and W. G. Shaw, *Rev. Pure Appl. Chem.*, **11**, 2 (1961).

(2) J. C. Earl and A. W. Mackey, *J. Chem. Soc.*, 899 (1935).

(3) R. A. Eade and J. C. Earl, *ibid.*, 591 (1946).

(4) W. Baker, W. D. Ollis, and V. D. Poole, *ibid.*, 307 (1949).

(5) J. M. Tien and I. M. Hunsberger, *J. Am. Chem. Soc.*, **77**, 6605 (1955); **83**, 181 (1961).

was studied in dilute (10 mM) solutions of N3PS. Water and propylene carbonate solutions slowly turned brown and exhibited a new absorption peak near 380 m μ . Benzene solutions turned brown and deposited a brown, water-soluble residue. A brown precipitate was also formed in cyclohexane. In water solution, the color formation was completed in a few days. The process was more rapid if nitrogen was bubbled through the solution. Oxygen did not cause a similar effect. In propylene carbonate, the color change required several weeks. Nitrogen caused an increase in color, as observed in the aqueous solutions. However, in this solvent, the absorption returned to the original value in 30 min. following the treatment with nitrogen.

Comparisons of the solution spectra of the various sydnones indicated that the absorptions at ca. 300 m μ are due to $n \rightarrow \pi^*$ transitions.⁶ N-Benzyl-, N-*p*-chlorobenzyl-, N-*p*-methylbenzyl-, and N-3-pyridylsydnone were examined as 0.25–0.35 mM solutions in cyclohexane and in water. The results are summarized in Table III. In each case, a blue shift of 10–20 m μ was observed in going from the former to the latter solvent. In addition, conductance measurements were made on solutions of N3PS in cyclohexane and water. No conductance (ca. 1 μ a. could have been detected) was observed when 0.5–1 v./cm. was applied to 1.5 mM solutions.

TABLE III

Sydnone	EXTINCTION COEFFICIENTS OF SYDNONE SOLUTIONS			
	Solvent			
	Cyclohexane		Water	
	λ (m μ)	log ϵ	λ (m μ)	log ϵ
N-Benzyl-	300	3.80	287	3.95
	307(sh)			
	320(sh)			
N- <i>p</i> -Chlorobenzyl-	253	3.60	ca. 215	ca. 4.
	300	3.04	287	3.94
	308(sh)			
	322(sh)			
N- <i>p</i> -Methylbenzyl-	300	3.75	289	3.93
	308(sh)			
	320(sh)			
N-(3-Pyridyl)-	238	3.67	232	4.04
	265	3.42
	325	3.15	305	3.74

C. Solid State Studies.—Thin films of each of the sydnones listed in Table I were prepared by vacuum vaporization, and their response to ultraviolet and infrared irradiation was determined in the spectral range 300 to 700 m μ . Compounds I, II, and VI exhibited an increase in transmission after exposure to ultraviolet irradiation, whereas the other sydnones showed a decrease in transmission.

The N3PS can be returned to its colorless state by irradiation with infrared light for periods of 1 to 5 min., or by storage in the dark for several days. A more rapid recovery of the films can be induced by the application of an e.m.f. for periods of 1 min. or less.

After prolonged or repeated ultraviolet exposure, thin films of N3PS showed fatigue or an inability to return to their original state. Although infrared irradiations or an applied e.m.f. were effective in hastening the recovery of sydnone films, four or five alternate exposures to ultraviolet and infrared radiation destroyed the photochromism of N3PS. The observed fatigue can be attributed to one or more factors: thermal decomposition of the N3PS film during infrared radiation or e.m.f. application; alteration of electronic configuration as a result of ultraviolet radiation; or a combination of several such factors which resulted in decomposition of the films. The first factor was eliminated by allowing the sydnone to recover in the dark. The second factor was examined by narrowing the range of wave lengths during ultraviolet radiation. If an optimum energy range for excitation-recovery exists, the excitation-recovery cycles for the selected energy ranges should differ, *i.e.*, possibly show a greater or lesser degree of fatigue. Table IV lists the filters used in these studies.

(6) G. S. Brealey and M. Kasha, *J. Am. Chem. Soc.*, **77**, 4462 (1955).

TABLE IV

WAVE LENGTHS USED IN FATIGUE STUDIES	Ultraviolet range (m μ)
Unfiltered ultraviolet lamp	200–400
Filtered ultraviolet lamp	300–400
Cerium oxide (thin film)	350–400

Several films were prepared and stored in the dark. The effect of ultraviolet irradiation was determined daily by comparing transmission spectra taken before and after each irradiation. Fatigue appeared after fewer irradiations when 5-min. periods were used than when irradiation lasted for only 1 min. In the latter series, the specimens recovered completely in all instances. The optimum (greatest change in per cent transmission) ultraviolet range for the shorter irradiation time appeared to be 300–400 m μ ; however, a smaller energy range (350–400 m μ) seemed to produce less fatigue over a greater number of cycles. These results indicate that fatigue of the sydnone film might be diminished by the use of a cerium oxide film as a filter.

D. Infrared Studies.—Infrared spectra were taken to determine if the effect of photochromic changes extended into the infrared region. A Beckman IR-4 spectrophotometer equipped with sodium chloride optics was used to obtain spectra in the region from 660 to 5000 cm.⁻¹. Spectra of N-benzylsydnone (I), N-*p*-methylbenzylsydnone (II), N-3,4-dimethylbenzylsydnone (III), N-*p*-chlorobenzylsydnone (IV), N,N'-ethylene-bis-sydnone (V), and N,N'-tetramethylene-bis-sydnone (VI) were obtained on thin films vacuum evaporated onto salt plates. Thin films and potassium bromide pellets of N3PS were studied.

The frequency of an infrared absorption is primarily determined by the mechanical motions in the molecule, while the intensity of an absorption is mainly dependent upon the electrical properties of the molecule. Thus, it would be expected that a structural alteration accompanying a photochromic change would appear as a difference in the position and intensity of certain absorptions in the spectrum. If a change occurred it would be most pronounced for N3PS, since this compound exhibits photochromism to a greater extent than do the other sydnones studied. Compounds I to IV were evaporated onto salt plates. Their infrared spectra were obtained and compared with the spectra taken after 2 min. irradiation with ultraviolet light. The two spectra of each compound were essentially identical, although a slight decrease in the intensity of the absorption bands of the irradiated material was noted. The similarity between the infrared spectra of compounds I to IV before and after ultraviolet irradiation is an indication that there are no structural alterations associated with photochromic changes under the conditions of our experiments.

The infrared spectrum of N3PS was obtained before and after irradiation with ultraviolet. The blue form of N3PS was caused to revert to the colorless form by irradiation with an infrared lamp before taking the next spectrum. The spectra differed only by slight changes in band intensity. The sample was then alternately irradiated with ultraviolet and infrared. After each exposure the spectrum was recorded in the region in which the greatest change in band intensity had occurred. A progressive slight decrease in band intensity was observed. This decrease in band intensity probably is due to a partial decomposition of the samples, rather than to structural changes.

All of the sydnones studied absorb in the 3100 to 3200 cm.⁻¹ range. Several authors⁷⁻⁹ have assigned peaks in this range to the sydnone ring C-H stretching mode. A spectrum of N-*p*-methylbenzyl-C-bromosydnone was taken in order to provide more conclusive evidence for assignment of these bands. A spectrum of this compound showed no absorption in the above mentioned region. In addition, the band at 3150 cm.⁻¹ in N3PS was not present after bromination. The common absorption of the sydnones in this range, plus the disappearance of the absorption in the brominated materials, make plausible the assignment of a

(7) C. Greco, "Synthesis of Some Substituted Pyridyl Sydnones," Doctoral Dissertation, Fordham University, New York, N. Y., 1960.

(8) J. M. Tien and I. M. Hunsberger, *J. Am. Chem. Soc.*, **77**, 6604 (1955).

(9) D. J. Voaden, Dissertation, Oxford University, England, 1957.

band in the 3100 to 3200 cm^{-1} region to the sydnone C-H stretching vibration. The assigned frequencies, accurate to within 20 cm^{-1} , are listed in Table V.

TABLE V
SYDNONE C-H STRETCHING FREQUENCIES

	Cm^{-1}
N-Benzylsydnone	3135
N- <i>p</i> -Methylbenzylsydnone	3120
N-3,4-Dimethylbenzylsydnone	3125
N- <i>p</i> -Chlorobenzylsydnone	3120
N,N'-Ethylene-bis-sydnone	3115
N,N'-Tetramethylene-bis-sydnone	3160
N3PS	3150

III. Discussion and Summary

Photochromism in solid organic materials has been explained by isomerism, free radical formation, molecular aggregation, and triplet state excitation. The slight photochromic response observed in the benzylsydnones indicates that the behavior may be a general property of the mesoionic ring. One might expect photochromism to be enhanced in the bis-sydnones, but such behavior has not been observed.

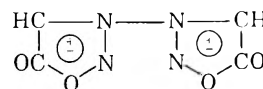
An analysis of the experimental evidence obtained does not permit an absolute elucidation of a mechanism for the photochromic behavior of N3PS. However, the observed fatigue and the diminution of several infrared absorption bands after ultraviolet excitation do support the formation of a metastable intermediate.

On the basis of the hybrid structure given by Baker, *et al.*,⁴ the substituted nitrogen atom in the sydnone ring would be expected to bear a large fractional positive charge, and the negative end of the sydnone dipole would be (diffusely) directed toward the carbonyl grouping. Stabilization of the sydnone ring requires the ring to be substituted; such substitution will, of course, influence the contributing resonance forms. The number of energy levels increases with the number of possible configurations, while the average separation between levels decreases. The increase in the number of possibilities of resonance for a molecule is associated with a displacement of the first absorption band toward longer wave lengths. The material thus can undergo a change of color, if the metastable state has more (or less) contributing forms than the ground state of the molecule. If resonance between such forms is restricted, as would be the case where two conjugated electron systems are separated by one or more $-\text{CH}_2-$ groups, the observed spectrum is only a superposition of the separate parts.

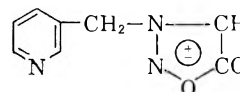
Steric inhibition of the resonance leads to band shifts toward shorter wave lengths. The molecular structure of several crystalline sydnones has been examined by Schmidt¹⁰ and Bärnighausen, *et al.*¹¹ Schmidt concluded that in N-phenyl- and N-*p*-tolylsydnone the benzene ring and the 5-membered sydnone ring system were approximately coplanar. However, Bärnighausen, *et al.*, indicate that the two ring planes in N-*p*-bromophenylsydnone contain a dihedral angle of 27°. No such studies on N3PS have been reported. Therefore, the effect of

crystal lattice forces on its inter-ring resonance cannot be estimated unambiguously.

The formation of a metastable sydnone intermediate by ultraviolet excitation can be postulated to decrease the number of contributing resonance forms in the case of compounds I, II, and VI; and to increase the number of contributing forms in compounds III, IV, V, and N3PS. In the case of N3PS, the most significant electronic difference is the lack of a $-\text{CH}_2-$ shielding group between the sydnone and pyridine rings. The entire molecule therefore contributes to the metastable intermediate, and the slight photochromic behavior of the benzylsydnones is understandable. Analytically, one would predict that bisydnyl



would be highly photochromic. On the other hand, decreased photochromism would be expected in 3-picolylsydnone



The metastable intermediate postulated as the blue form of N3PS may involve hydrogen bonding between the sydnone hydrogen of one molecule and the carbonyl oxygen of a second sydnone ring; however, the infrared data indicate only a slight diminution of the C-H band, not a shift as would be expected if hydrogen bonding existed.

The eventual stabilization of the intermediate (blue) form is not accomplished by repeated ultraviolet radiation. The "fatigued" material is thought to be the result of decomposition. Such decomposition may be enhanced by the presence of impurities. Nine preparations of N3PS of differing impurity content were examined. These preparations showed no major difference in response to ultraviolet irradiation, but recovery of the "impure" specimens was generally slow and fatigue quite rapid. Comparison of infrared spectra of these samples showed that the largest differences occurred in the 800-900 cm^{-1} region. The group of bands in this region is the same group which exhibits some variation in intensity during the photochromic change. Specific assignments for these bands are not yet available.

A recent study¹² of the photochromism and electron spin resonance absorption of N-3-pyridylsydnone has indicated that the photochromism results from color centers analogous to those of the alkali halides. This mode of energy storage had previously been suggested as one of several possibilities by Gutowsky, Rutledge, and Hunsberger.¹³ The mesoionic character of the sydnone ring lends support to a metastable state characterized by color center formation; however, further verification is required.

(12) T. Mill, A. Van Roggen, and C. F. Wakly, *J. Chem. Phys.*, **34**, 1139 (1961).

(13) H. S. Gutowsky, R. L. Rutledge, and I. M. Hunsberger, *ibid.*, **29**, 1183 (1958).

(10) G. M. J. Schmidt, *Bull. Res. Council Israel*, **1**, (1951-1952).

(11) H. Bärnighausen, F. Jellinek, and A. Vos, *Proc. Chem. Soc.*, **120**, (1961).

Acknowledgment.—This research was supported by NOas-59-6112-C, NOas-60-6105-C, and NOw-61-0587-d. in part by Bureau of Naval Weapons Contracts

THE PHOTOTROPY OF TETRACHLOROKETODIHYDRONAPHTHALENE AS A REVERSIBLE PHOTOCHEMICAL REACTION¹

BY G. SCHEIBE AND F. FEICHTMAYR

Institut für Physikalische Chemie der Technischen Hochschule, München, Germany

Received May 25, 1962

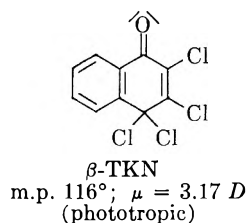
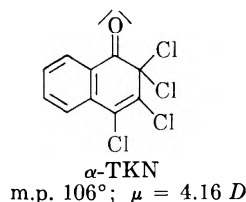
The phototropy of the crystals of β -tetrachloro-1-ketodihydronaphthalene, which has been observed in the past, is shown to be a dissociation of the excited molecule into a chlorine atom and an aroxyl radical. The reaction is induced by light absorption in the keto group. The same reversible reaction also can be observed in suitable solvents (a) at low temperature in a glass-like frozen state and (b) in carbon tetrachloride at room temperature. The rupture of the C-Cl bond is made possible by the gain in stabilization energy in the aroxyl radical. The anisotropy of light absorption observed by Weigert supports this theory.

A. Introduction

Many compounds are known which show a change in color when subjected to the action of light but revert to their original color in the dark. Marckwald² was the first to recognize that these light reactions are reversible. For this reaction, which he first observed in the crystals of β -tetrachloro-1-keto-dihydronaphthalene, he introduced the term "phototropy."

The colorless crystals of β -tetrachloro-1-ketodihydronaphthalene (β -TKN) become amethyst colored when exposed to light.³ When placed in the dark, the crystals lose their coloration within a few hours. This reversible reaction can be repeated practically as often as desired.

Hitherto it has not been possible to observe this photoreaction in solutions and melts of β -TKN. Nor do the crystals of the isomer α -TKN show this phenomenon. Incidentally, until quite recently, it was not definitely known which of the structures belongs to the α form and which belongs to the β form.



The opinion that the α and β forms are as shown in I and II originally was based on the results obtained by von Dobrogoiski in his spectroscopic

(1) Thesis of F. Feichtmayr, TH München, 1957; cf. F. Feichtmayr and G. Scheibe, *Z. Naturforsch.*, **13b**, 51 (1958); G. Scheibe, *Chem.-Ing.-Technik*, **31**, 321 (1959).

(2) W. Marckwald, *Z. physik. Chem.*, **30**, 140 (1899); this paper also contains a report on the phototropic behavior of quinoquinoline. Marckwald assumed that a *physical change* of the system was the cause of the phototropy.

(3) The color change of β -TKN when exposed to light had been observed by F. Zincke and O. Kegel when they first synthesized this compound, but they did not investigate it further (*Ber.*, **21**, 1027 (1888)). The term α - or β -TKN was first used by Zincke, who was able to isolate these two isomers, independent of the method of preparation. The two isomers differ from each other in the melting point and the behavior toward light, but they have much the same chemical behavior.

and chemical comparisons.⁴ The absorption spectra of both α - and β -TKN in ethanol and petroleum ether are shown in Fig. 1a and 1b.

More recently, results obtained by Hoppe and Rauch⁵ in their X-ray investigations into the structure of β -TKN by the "Faltmolekül" method and by the diffuse scattering method^{5,6} have shown that this opinion is correct. The dipole moments of α - and β -TKN, which have been determined recently in benzene solution,⁷ are also in conformity with this opinion.

B. General Observations on the Problem of Phototropy

Before we discuss our investigations with β -TKN, it may be useful to point out what explanations have been brought forward in the past to explain phototropy.

After Marckwald discovered phototropy in β -TKN, it was found that there are many other compounds⁸ which show this phenomenon in the solid, crystallized state. In some cases it was possible to explain the mechanism, and it was found that the new absorption was due to a system change which can be formulated chemically.⁸

In working with β -TKN, neither Marckwald¹ nor Stobbe⁸ were able to observe a chemical change of the system when exposed to light. It was assumed, therefore, that a *physical change* of the system was the cause of phototropy. This assumption was based on work carried out by Weigert.¹⁰ He subjected this compound in 1918 to an intensive crystallographic and spectroscopic investigation and came to the conclusion that the phototropy of this substance was bound up with the crystal form. He was not able to explain the mechanism, but he did observe that the crystals, which are rhombic in ultraviolet light of relatively short wave length, are phototropically excited by polarized light whose electric vector vibrates in

(4) Thesis of A. von. Dobrogoiski, TH München, 1954.

(5) W. Hoppe and R. Rauch, *Z. Krist.*, **115**, 141 (1961).

(6) Cf. W. Hoppe, *Angew. Chem.*, **69**, 659 (1957).

(7) F. Feichtmayr and F. Würstlin, unpublished results.

(8) Examples: anils, hydrazones, fulgides, stilben derivatives, etc. A survey is given by L. Chalkley, *Chem. Rev.*, **6**, 217 (1929); H. Stobbe, "Handw. Naturwissenschaften," 2nd ed., 1932, Vol. 7, p. 999.

(9) W. Marckwald, *Z. Elektrochem.*, **24**, 381 (1918).

(10) F. Weigert, *ibid.*, **24**, 222 (1918).

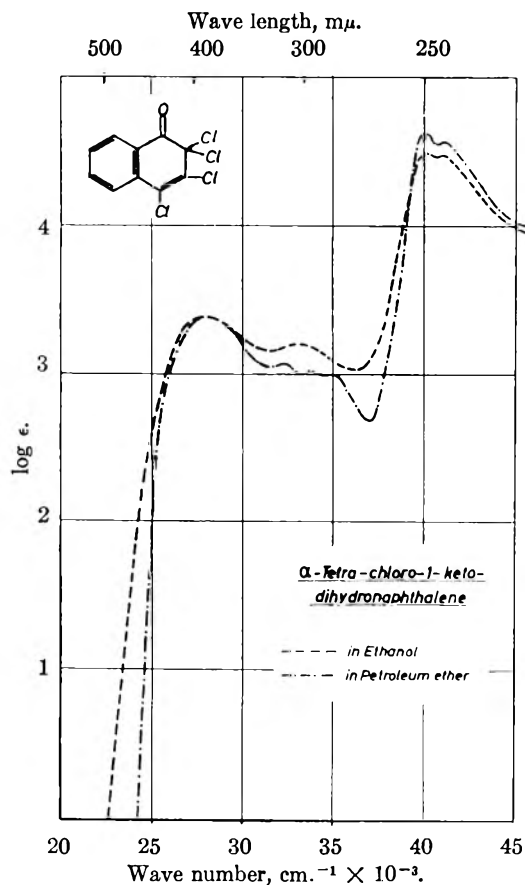


Fig. 1a. α -Tetrachloro-1-ketodihydronaphthalene: - - - in ethanol; - · - in petroleum ether.

the c axis. The absorption band which causes the red color (maximum about 525μ) absorbs only light which vibrates in the a - b plane. This pleochroism of the excited crystals already had been observed by Marckwald.²

This behavior is no longer surprising to us today, because Hertel¹¹ and also Hoppe and Rauch⁵ have shown that the aromatic rings all lie parallel in the a - b plane.

In aromatic systems, the transition moment for the $\pi \rightarrow \pi^*$ absorption lies in the ring plane,¹² and it would therefore appear logical to assume that the maximum excitation occurs in the a - b plane. The longest wave length band must, however, correspond to the $n \rightarrow \pi^*$ transition of the carbonyl group in view of the structure and intensity of this band and the dependence of its spectral position on the solvent¹³ (see Fig. 1). As the transition moment of this band is vertical to the C-O axis and thus vertical to the aromatic plane,¹⁴ it is not surprising that in long wave length ultraviolet light the excitation is particularly pronounced in the c axis. Incidentally, in α -TKN the $\pi \rightarrow \pi^*$ transition already covers the $n \rightarrow \pi^*$ transition (see Fig. 1).

(11) H. Hertel and K. Schneider, *Z. Elektrochem.*, **37**, 536 (1931).

(12) G. Scheibe, St. Hartwig, and R. Müller, *Z. Elektrochem.*, **49**, 372 (1943); F. Dörr and M. Held, *Angew. Chem.*, **72**, 287 (1960).

(13) G. Scheibe, *Ber.*, **59**, 2619 (1926); M. Kasha, *Discussions Faraday Soc.*, **9**, 14 (1950).

(14) Cf. J. W. Sidman, *Chem. Rev.*, **58**, 689 (1958): "Electronic Transitions due to Nonbonding Electrons in Carbonyl, Azo-Aromatic, and other Compounds."

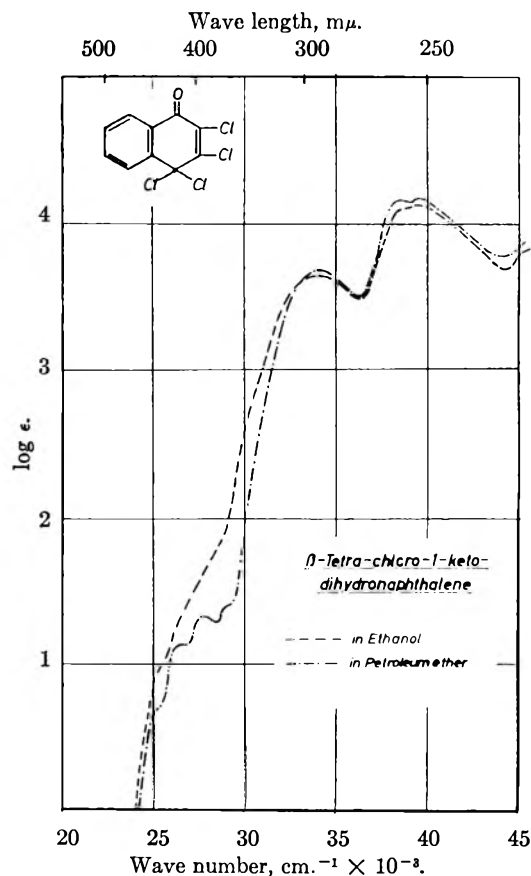


Fig. 1b.— β -Tetrachloro-1-ketodihydronaphthalene: - - - in ethanol; - · - in petroleum ether.

The question arose whether Weigert was right in claiming that a physical change¹⁵ occurs with β -TKN, or a chemical change which can be expressed as a formula is responsible for the phototropic behavior.

C. Investigation of the Phototropy of β -TKN

von Dobrogoiski recently has provided evidence⁴ in our Institute that the phototropy of β -TKN is not connected with the crystal form. When a diluted, glass-like frozen solution of the compound in alcohol is irradiated, it is possible to observe a color change which is comparable to the color change in the crystal and which disappears again when the solution thaws.

In Fig. 2 the absorption spectra of crystal and solution excited by light are compared with each other. The results show clearly that the phototropic condition is bound up with an individual molecule.

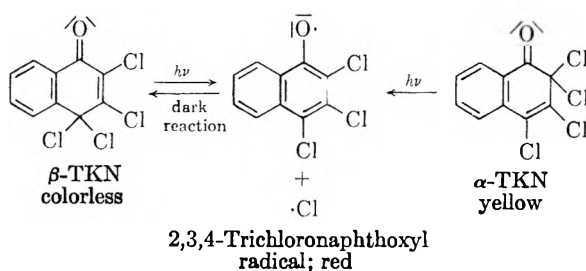
von Dobrogoiski also was able to show that the

(15) F. Weigert offered the following explanation of phototropy: when the crystal is exposed to light, intermolecular optical influences are developed in the crystal by neighboring carbonyl groups approaching one another, and these optical influences can be observed as coloration.

H. Hertel¹¹ assumed in view of the position of the molecules in the lattice that colored "quinhydron-like molecule compounds" are formed in the crystal under the action of light. It should also be pointed out that C. V. Gheorghiu in his paper (*Bull. école polytech. Jassy*, **1**, 141 (1947)) assumed that the "unexcited ground state" and the "light excited state" of β -TKN correspond to various resonance structures. This assumption was based on a mistaken conception of resonance.

isomeric α -TKN in glass-like frozen solution undergoes a phototropic coloration. He found that the absorption spectra of the phototropic states of α - and β -TKN are identical, although the two compounds absorb differently when they are not excited.

This observation was the first indication that the phototropic change in β -TKN may be due to a chemical change, *viz.*, a dissociation of the excited molecule into radicals. It was assumed as a hypothesis for working that a chlorine atom is split off from the tetrahedral carbon when α - and β -TKN are exposed to light. The resulting 2,3,4-trichloronaphthoxyl radical must be regarded as responsible for the red coloration. The dark reaction is then a recombination of chlorine atom and aroxyl.



This assumption made it possible to offer a plausible explanation for the paramagnetism of the excited crystals which had been measured by Dörr and Engelmann¹⁶ in 1952 with the magnetic balance. It must be mentioned, however, that subsequent investigations of the paramagnetic resonance absorption of the excited β -TKN^{1,4,17} gave negative results. An explanation for this has not yet been brought forward.

The results of flash spectroscopic investigations carried out for us by Porter and Morantz¹⁸ provided the first proof that our assumption is correct. In these investigations it was found that a transient intermediate product is formed in highly viscous paraffin oil even at room temperature during the photochemical decomposition of the β -TKN; this intermediate product is absorbed at approximately 500 μ , and in a 1.5×10^{-3} molar solution it has a half period of 3×10^{-3} second. This intermediate product also could be detected spectroscopically in the less viscous solvents hexane and alcohol. We shall deal in the next section with the photochemistry of β -TKN in solution.

D. Photochemistry of β -TKN in Solution

After phototropy was recognized to be a property of the individual molecules, and phototropy seemed to be based on a dissociation of β -TKN into a chlorine atom and a naphthoxyl radical, it was desirable to provide chemical proof for this hy-

(16) F. Dörr and F. Engelmann, *Naturwissenschaften*, **39**, 397 (1952). On the basis of the results obtained with fluorescein (G. N. Lewis, *et al.*, *J. Chem. Phys.*, **17**, 804 (1949)), the authors claim that the triplet form is responsible for the paramagnetism.

(17) H. S. Gutowsky, R. L. Rutledge, and J. H. Hunsberger, *J. Chem. Phys.*, **29**, 1183 (1958).

(18) Acknowledgments are due to Professor G. Porter and Dr. D. J. Morantz for carrying out the flash spectroscopic investigations and for their useful suggestions.

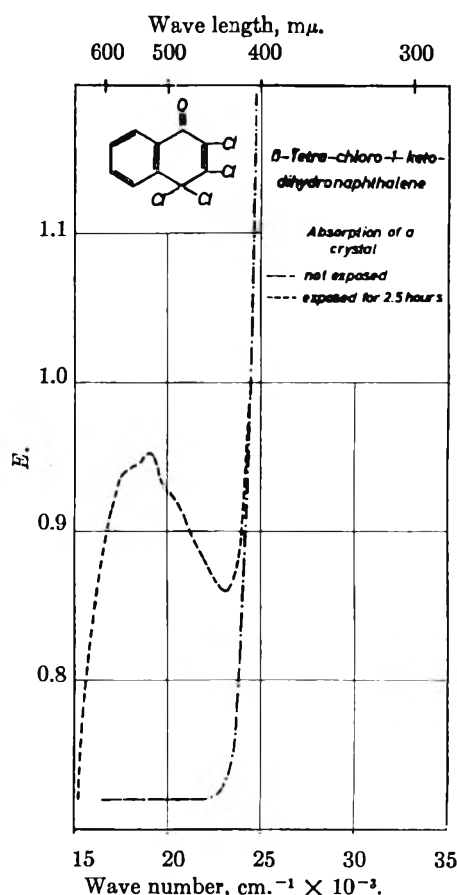


Fig. 2a.— β -Tetrachloro-1-ketodihydronaphthalene: absorption of a crystal, not exposed — — —; exposed for 2.5 hr. — — —.

pothesis. For this purpose it was necessary to investigate solutions which were not frozen.

Proof of the Dissociation of Excited β -TKN into Radicals.—When a benzene solution of β -TKN is irradiated at room temperature, no red coloration can be observed, but after some time the solution turns yellow and this change in color is irreversible. Flash spectroscopic investigations¹⁸ in hexane and alcohol also show distinctly that there is a decomposition reaction. It seemed likely that the yellow coloration is caused by compounds which are formed from the primary aroxyl radicals in subsequent reactions. We attempted to intercept these aroxyl radicals, which apparently have a short life, with other radicals. We succeeded in doing this with the yellow equilibrium solution of triphenylmethyl radicals in benzene containing β -TKN in dissolved form. In the dark no reaction occurs, but on exposure in the absorption range of β -TKN a complete decoloration occurs within approximately 10 sec. A benzene solution of triphenylmethyl radicals is also susceptible to light, but it takes at least 10 min. before any decoloration commences. There are indications that both the aroxyl radical¹⁹ and the chlorine atom²⁰ react with the triphenylmethyl.

(19) St. Goldschmidt and Ch. Steigerwald (*Ann.*, **438**, 202 (1924)). were able to show that the 9-chloro-1-phenanthroxyl radical reacts with triphenylmethyl instantly.

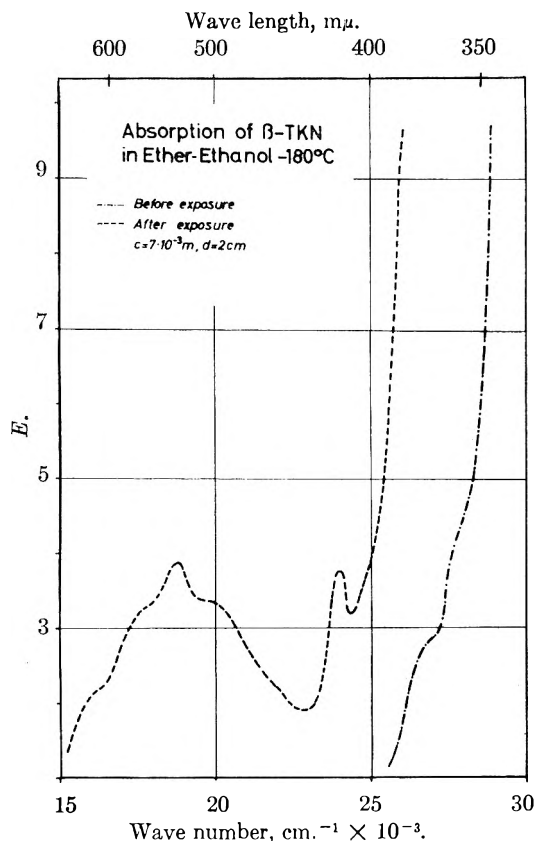
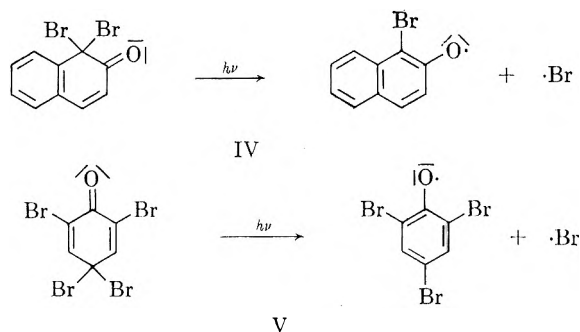


Fig. 2b.—Absorption of β -TKN in ether-ethanol at -180° , c is $7 \times 10^{-3} M$, d is 2 cm.: — before exposure; - - - after exposure.

The use of radicals as initiators in polymerization reactions can be regarded as the best method of detecting the presence of radicals. If a compound which can be polymerized by radicals is used as a solvent for the substance whose radical decomposition is to be investigated, the "cage" effect of the solvent, an effect which would favor a recombination of the radicals, is weak because the solvate sheath consists of the reactive molecules.

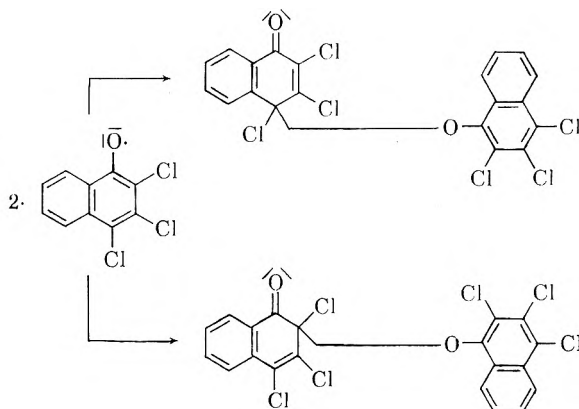
The polymerizable solvent used for β -TKN was vinyl acetate or acrylonitrile. In order to determine whether polymerization in vinyl acetate had been initiated, 0.2 cc. of the irradiated solution was taken with a pipet after 15, 30, and 60 minutes and dropped into 2 cc. of heptane. As the polymer is insoluble, the occurrence of turbidity indicates that polymerization is taking place. In acrylonitrile the photochemical polymerization is indicated by the instantaneous precipitation of the high polymer on exposure to light. This method was used to investigate the dissociation of the excited molecule into radicals of several substances, some of which gave a positive result, including α -TKN (I), β -TKN (II), 1,1-dibromo-2-ketodihydronaphthalene (IV), tribromophenolbromine (V).

(20) M. Gomberg (*Ber.*, **35**, 1822 (1902)) pointed out that the triphenylmethyl radical reacted very rapidly with halogen. Reactions of triphenylmethyl with simple radicals such as NO_2 , NO , H also proceed very rapidly (*cf.* J. E. Leffler, "The Reactive Intermediates of Organic Chemistry," Interscience Publishers, Inc., New York, N. Y., 1956).



The results hitherto obtained prove the dissociation of excited α - and β -TKN into radicals, but they give no indication regarding the structure of the molecule fractions. The experimental results to be discussed prove the decomposition of the excited β -TKN into aroxyl and Cl atom.

Phototropic Behavior of β -TKN in Solution.—The radicals which are formed on exposure to light exist in hexane, benzene, and alcohol only for a fraction of a second because there are numerous subsequent reactions which they can undergo (recombination, dimerization, reaction with the solvent, etc.). It is understandable, therefore, that it has not been possible hitherto to observe the phototropic behavior of β -TKN in solution. The use of carbon tetrachloride as solvent in photochemical reactions, however, made it possible to achieve such a high stationary radical concentration that the "phototropy" of β -TKN in solution could be observed. In this solvent, transfer reactions or other reactions of the radicals with the solvent hardly ever occur, so that the lifetime of the aroxyl radicals is increased markedly. The red color of the solution does not disappear until approximately 5 min. have elapsed. There is, however, a very light, bleaching, yellow dyeing which is just strong enough to be detected, and this indicates that a dimerization of the aroxyl radicals to quinol ether occurs in this system together with the recombination of aroxyl and Cl atom to β -TKN.



The colored solutions of the photochemically produced aroxyls in carbon tetrachloride now can be used for various tests to investigate the chemical behavior of the naphthoxyl radicals. These tests show that the disappearance of the red color is not influenced markedly by the presence of oxygen.

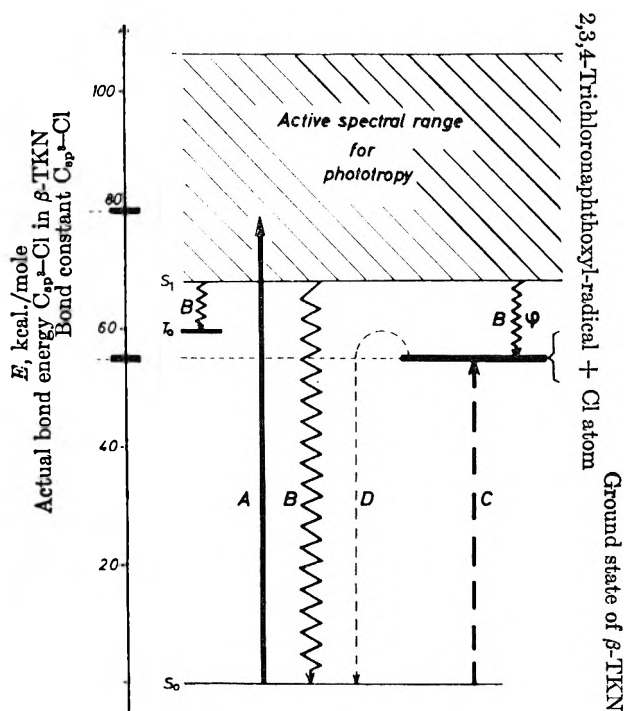


Fig. 3.—A, light excitation; B, radiationless transition; $\xi \leq 1$ is quantum efficiency; C is thermal excitation; D is dark reaction of the phototropy.

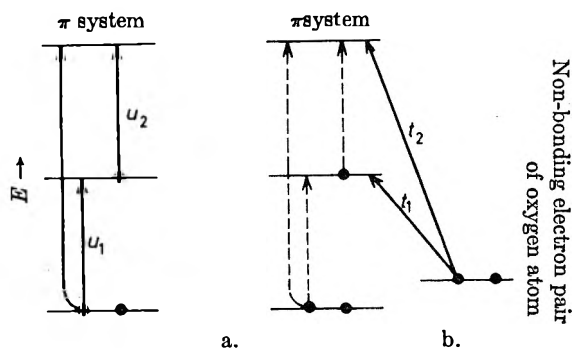


Fig. 4.—Configurational excitations: (a) in odd alternant hydrocarbons, u_1, u_2 are excitations of equivalent energy; (b) in aroxyl radicals, t_1, t_2 are additional $n \rightarrow \pi^*$ transitions.

taken up by the molecule is at least as high as the actual bond energy of the bond to be split. This actual bond energy E_B is the difference between the thermochemically derived bond constant E_C and the stabilization energy E_S .

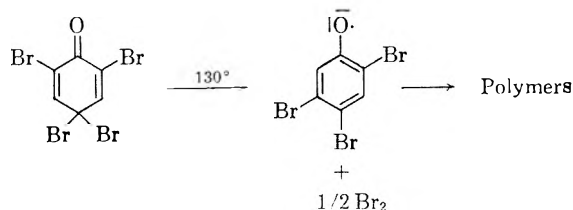
$$E_B = E_C - E_S$$

The bond constant E_C for a given C-X bond with given hybridization of the C atom²⁶ is thus regarded as a constant. The stabilization energy E_S is the sum of the energies which influence the bond constant by changing the hybridization of individual atoms, changing the strain, and by delocalization of the radical electrons in the individual molecule fractions during the (adiabatic) rupture of the bond.

In view of the low thermal stability of quinol ether and halogenized quinol derivatives we may assume that the actual bond energy of the C-X

(26) Cf. M. J. S. Dewar and H. N. Schmeising, *Tetrahedron*, **11**, 96 (1960).

bond (X = halogen, -O-R) in the tetrahedral carbon atom in this type of bond is very low. Tribromophenol-bromine decomposes very rapidly when heated to approximately 130° with liberation of bromine.²⁷ The residue must be regarded in view of its chemical composition as a dimer or polymer of the aroxyls which occur for a short time during the thermal decomposition.



β -TKN also decomposes with liberation of chlorine or hydrogen chloride when heated to approximately 150–160°. This indicates that the actual bond energy for the C_{sp^3} -Cl bond is here, too, far lower than the bond constant, which is approximately 80 kcal./mole.²⁸

On the basis of the known bond constants²⁸ and stabilization energies,²⁹ we have attempted to investigate the energy aspects of the “2,3,4-trichloronaphthoxyl radical + chlorine atom” system in relation to the ground state of β -TKN. These energies were used: (a) Energy to be consumed: stabilization energy of β -TKN = 50 kcal.,³⁰ bond constant of C-Cl bond = 80 kcal.,²⁸ π -bond constant of the carbonyl group = 80 kcal.,³¹ (b) Energy gained is: π -bond constant of the CC double bond = 65 kcal.,²⁸ stabilization energy of naphthalene = 60 kcal.²⁹

With these values it is possible to calculate the total energy for the resonance structure of the aroxyl, on which the lone electron in the oxygen atom is localized and has not yet interacted with the π -system of the naphthalene. We have assumed a value of 30 kcal. as delocalizing energy for this radical electron, using the gain in resonance energy in the case of naphthylmethyl radicals as a basis for our calculation.³² The actual bond energy for the C_{sp^3} -Cl bond in β -TKN thus amounts

(27) Cf. J. H. Kastle and A. S. Loevenhart, *Am. Chem. J.*, **27**, 32 (1905).

(28) Cf. T. L. Cottrell, “The Strength of Chemical Bonds,” Butterworths Scientific Publ., London, 1958.

(29) Cf. G. W. Wheland, “Resonance in Organic Chemistry,” John Wiley and Sons, Inc., New York, N. Y., 1955, p. 98.

(30) This value for the stabilizing energy of β -TKN has certainly been estimated too high, since the stabilizing energy for benzaldehyde, for instance, is only 35 kcal. (cf. G. W. Wheland, ref. 29). However, even when such unfavorable energy values are used, the actual bond energy for the C_{sp^3} -Cl bond in β -TKN is still smaller than the bond constant C_{sp^3} -Cl.

(31) Cf. D. Brück and G. Scheibe, *Z. Elektrochem.*, **61**, 901 (1957).

(32) The difference between the actual bond energy for the C_{sp^3} -H bond in α - or β -methylnaphthalene and the bond constant C_{sp^3} -H is 26 kcal. (cf. M. Szwarc, *Chem. Rev.*, **47**, 75 (1956)). It is approximately equivalent to the delocalization energy for the lone electron on the -CH₃ group in the naphthylmethyl radical (cf. G. W. Wheland, ref. 29). The electron configuration of the 2,3,4-trichloronaphthoxyl radical is comparable with that of the naphthylmethyl radical, so that at least the same delocalization energy may be expected. In view of the higher exchange energy between p-electrons on neighboring C and O atoms as compared with the p-electrons on neighboring C atoms, we feel that we are justified in assuming a somewhat higher value (30 kcal.) for the delocalization energy for the lone electron at the oxygen atom.

to 55 kcal. This value is, of course, only a very rough approximation as many energies could only be estimated very roughly or could not be taken into consideration at all; this applies, for instance, to the strain energy of the tetrahedral C atom in the ring system of the nine sp^2 -hybridized C atoms.

This estimation indicates that the actual bond energy for the C_{sp^2} -Cl bonds in β -TKN is far lower than the bond constant. It is, therefore, not surprising that this bond can be ruptured by a thermal influence.

How can we explain the dissociation of excited β -TKN into radicals against this background? Investigations carried out by von Dobrogojski have shown that this dissociation is initiated within the whole long wave length absorption range of β -TKN (420 μ to about 260 μ). As mentioned above the $n \rightarrow \pi^*$ and the $\pi \rightarrow \pi^*$ transitions of carbonyl chromophore and of the aromatic system lie within this spectral range. The C_{sp^2} -Cl σ -bond does not absorb in this spectral range, because it possesses no oscillator whose energy is comparable with the bond constant C-Cl. The longest wave length band in chloromethyl,³³ for instance, is 52000 cm^{-1} . It is assigned to a $n \rightarrow \sigma^*$ transition, which also causes a rupture of the C-Cl bond. This transition, however, is 157 kcal., which is far higher than the bond constant of the C-Cl bond (80 kcal.).

The dissociation of excited β -TKN into radicals is, therefore, quite clearly a pre-dissociation. In other words, it is only after the absorption of light in the molecule that radiationless transitions cause a potential surface³⁴ in which a rupture of the C-Cl bond becomes possible. As β -TKN shows neither fluorescence nor phosphorescence in the crystal, the light energy absorbed is converted into vibration energy of the lowest triplet T_0 or singlet S_0 term and dissipated as thermal energy.³⁵ It can be assumed with a fair degree of certainty that dur-

ing this radiationless de-activation so much energy becomes active in the C_{sp^2} -Cl bond that a rupture of this bond occurs (quantum yield ≤ 1). The dissociation of excited β -TKN into radicals can be regarded, therefore, as "light activation" of the splitting of the C_{sp^2} -Cl bond into radicals, which can also be effected thermally in view of the low actual bond energy of the C_{sp^2} -Cl bond. This is illustrated in the form of a term diagram in Fig. 3.

Light Absorption of Aroxylys.—A few general comments on the light absorption of aroxylys may conclude this paper.

The application of the "molecular-orbital" method to hydrocarbons containing an unpaired electron gives a non-bonding orbital π_n , which belongs only to certain C atoms.³⁶ Figure 4 shows the energy stages and the number of electrons in the orbitals in the ground state and in the excited configurations which are of interest in this connection.

An indication of the spectral position of these transitions is obtained when one considers the configuration interaction in the electron jumps (a) and (b), both of which have the same energy in the configuration excitation. A splitting then is obtained: the transitions out of the non-bonding orbital and into the non-bonding orbital no longer lie at the same spot.

When these considerations are applied to aroxy radical, one is forced to admit that there are more transition possibilities. Since the oxygen atoms contain non-bonding electron pairs, $n \rightarrow \pi^*$ transitions also have to be taken into consideration. Figure 4 illustrates the possible configuration excitations. It is still an open question whether the long wave length band, *e.g.*, in the naphthoxyl radical, is to be regarded as an $n \rightarrow \pi^*$ or a $\pi \rightarrow \pi^*$ transition. An argument speaking against the $n \rightarrow \pi^*$ is the observation made by Weigert¹⁰ that the new absorption of the radical lies in the plane of the aromatic system, whereas it would stand vertically on this plane if this were an $n \rightarrow \pi^*$ transition. Quantum mechanical investigations in this direction would be of interest for color theories.

(33) G. Herzberg and G. Scheibe, *Z. physik. Chem.*, **B7**, 390 (1930).

(34) A demonstrative model for the pre-dissociation of tri- (and poly-atomic molecules is to be found in J. Franck, H. Sponer, and E. Teller, *ibid.*, **B18**, 88 (1932).

(35) The high concentration of heavy Cl atoms makes the $S_0 \rightarrow T_1$ transition even more probable; *cf.* D. S. McClure, *J. Chem. Phys.*, **17**, 805 (1949).

(36) H. C. Longuet-Higgins and J. A. Pople, *Proc. Phys. Soc. (London)*, **68**, 591 (1955).

STRUCTURAL EFFECTS IN THE PHOTOCHEMICAL PROCESSES OF KETONES IN SOLUTION

By J. N. PITTS, JR., H. W. JOHNSON, JR., AND T. KUWANA¹

University of California, Riverside, California

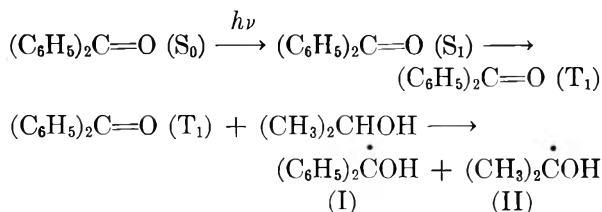
Received May 25, 1962

The behavior of a series of hydroxy, methoxy, amino, and chlorobenzophenones in the photopinacolization reaction has been studied using product isolation, ultraviolet spectral changes, electrochemical methods, phosphorescence and fluorescence techniques, and electron spin resonance spectroscopy. The results and correlations derived from these and published studies are discussed. Electron spin resonance evidence for long-lived triplets of certain *para*-substituted benzophenones is presented and correlated with their unusually long phosphorescent lifetimes and their unusually weak H atom abstracting power in the classic photopinacolization reaction. These phenomena are tentatively explained on the basis that in these ketones the lowest lying triplet state is π, π^* in nature rather than n, π^* as is the case for benzophenone. A preliminary report on a similar study in the anthraquinone system is included.

Introduction

The photochemical reduction of ketones to pinacols or benzohydrols was first reported by Ciamician and Silber.² In early work the reaction was studied to determine its synthetic usefulness and scope. Certain diaryl ketones, aryl alkyl ketones, and dialkyl ketones³ have been shown to give pinacols in varying yield. In certain cases the reaction proceeds in the reverse direction.⁴ The hydrogen source in the pinacol reaction usually has been an alcohol, but other sources have been employed.⁵⁻⁸ The reactions of photoactivated carbonyl compounds with other substrates have been reviewed.^{9,10}

There now seems to be substantial agreement that the first steps in the photopinacol reaction sequence are¹¹⁻¹⁴



(1) Presented at the Symposium on Reversible Photochemical Processes, Duke University, Durham, North Carolina, April, 1962.

(2) G. Ciamician and P. Silber, *Ber.*, **33**, 2911 (1900); **34**, 1541 (1901).

(3) C. Weizmann, F. Bergmann, and Y. Hirshberg, *J. Am. Chem. Soc.*, **60**, 1530 (1938); F. Bergmann and Y. Hirshberg, *ibid.*, **65**, 1429 (1943).

(4) A. Schonberg and A. Mustafa, *J. Chem. Soc.*, 67 (1944).

(5) G. S. Hammond, W. P. Baker, and W. R. Moore, *J. Am. Chem. Soc.*, **83**, 2795 (1961).

(6) A. Mustafa, *Nature*, **162**, 856 (1948).

(7) R. Pummerer, H. Hahn, F. Johne, and H. Kehlen, *Ber.*, **65B**, 867 (1942).

(8) E. J. Bowen and E. L. A. E. de la Praudiere, *J. Chem. Soc.*, 1503 (1934).

(9) A. Schonberg and A. Mustafa, *Chem. Rev.*, **40**, 181 (1947).

(10) C. R. Masson, V. Boekelheide, and W. A. Noyes, Jr., in A. Weissberger, Ed., "Techniques of Organic Chemistry," Vol. II, 2nd Ed., Interscience Publishers, Inc., New York, N. Y., 1956, p. 257 ff.

(11) H. L. J. Bäckström, *Z. physik. Chem.*, **25B**, 99 (1934).

(12) J. N. Pitts, Jr., R. L. Letsinger, R. P. Taylor, J. M. Patterson, G. Recktenwald, and R. B. Martin, *J. Am. Chem. Soc.*, **81**, 1068 (1959).

(13) (a) G. S. Hammond, and W. N. Moore, *ibid.*, **81**, 6334 (1959); (b) W. R. Moore, G. S. Hammond, and R. P. Foss, *ibid.*, **83**, 2789 (1961); (c) G. S. Hammond, W. P. Baker, and W. R. Moore, *ibid.*, **83**, 2795 (1961); (d) G. S. Hammond, N. J. Turro, and A. Fischer, *ibid.*, **83**, 4674 (1961).

(14) G. Porter and F. Wilkinson, *Trans. Faraday Soc.*, **57**, 1686 (1961).

In this scheme, S_0 indicates a ground state singlet, S_1 the first excited singlet, and T_1 the lowest excited triplet state. Species I has been called the ketyl radical.^{12,14}

The transfer of energy between photoexcited benzophenone triplets and naphthalene in the solid state was first noted by Terenin and Ermolaev.¹⁵ Energy transfer in solution between photoexcited benzophenone and biacetyl (and other molecules) was first reported by Bäckström and Sandros.¹⁶ Hammond, Turro, and Fischer¹³ utilized such solution phase energy transfer in an ingenious synthetic method while Moore and Ketchum determined the efficiency of the triplet-triplet transfer between benzophenone and naphthalene in benzene solution.¹⁷

Porter and Wilkinson¹⁴ studied the flash photolysis of benzophenone in alcohol both in the presence and in the absence of naphthalene. They confirmed the presence of a short-lived triplet of benzophenone which apparently absorbed at the same wave length as the ketyl radical (I), and showed that the triplet apparently is the chemically active species in the photopinacol reaction, since quenching of the triplet with naphthalene inhibited the pinacolization. The lifetime of the triplet measured by Porter and Wilkinson¹⁴ was in good agreement with that of Bäckström and Sandros.¹⁶ Hammond, *et al.*,¹³ arrived at the same conclusion by a study of the reaction of benzophenone with benzohydrol. Schenck,¹⁸ and Pitts, Letsinger, *et al.*,¹² independently found evidence for another species in the reaction chain and proposed possible structures. The work of Franzen¹⁹ should be mentioned here, as well as the observations of Bachmann on the color developed during the reduction of benzophenones to benzohydrols in alkaline solution.²⁰

(15) A. N. Terenin and V. I. Ermolaev, *Trans. Faraday Soc.*, **52**, 1042 (1956).

(16) H. L. J. Bäckström and K. Sandros, *Acta Chem. Scand.*, **14**, 48 (1960); *ibid.*, **12**, 823 (1958).

(17) W. M. Moore and M. Ketchum, *J. Am. Chem. Soc.*, **84**, 1368 (1962).

(18) G. O. Schenck, W. Meder, and M. Pape, *Proc. Intern. Conf. Peaceful Uses At. Energy*, Geneva, **29**, 352 (1958); Plenary Lecture, 5th International Symposium on Free Radicals, Uppsala, Sweden, 1961.

(19) V. Franzen, *Ann.*, **633**, 1 (1960).

(20) W. E. Bachmann, *J. Am. Chem. Soc.*, **55**, 391 (1933).

TABLE I
 PHOTOCHEMICAL BEHAVIOR OF SUBSTITUTED BENZOPHENONES

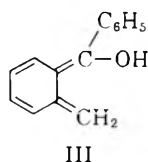
Compound	Pinacol formed	Phosphorescence mean lifetime, sec.	Remarks
Benzophenone	Yes ²	0.05-0.08	(C ₆ H ₅) ₂ COH· e.s.r. obs. ^{27,28}
Derivatives			
<i>ortho</i>			
Other groups			
OH	<i>p</i> -OH	No	
OH	<i>p</i> -OCH ₃	No	
OH	<i>p</i> -OCH ₃ ; <i>p'</i> -CH ₃	No	n.o. ^a
NH ₂		No	n.o.
NHCH ₃		Yes	No triplet or radical e.s.r. signal detected
CO ₂ H		Yes ^d	
<i>meta</i>			
NH ₂		Unusual behavior ^b	
<i>para</i>			
C ₆ H ₅		Yes	0.32 ± 0.01
NH ₂		No	.40, 0.3 ^c
N(CH ₃) ₂	<i>p'</i> -N(CH ₃) ₂	No ²⁰	.27 ± 0.02
N(CH ₃) ₂		Yes	.35 ± 0.03
OCH ₃	<i>p'</i> -OCH ₃	Yes ^{13,21}	.065 ± 0.007

^a n.o. = not observed, either not present or too short to measure. Phosphorescence lifetimes of less than 0.01 sec. could not be detected with the equipment used. ^b No change noted using Pyrex cell; in quartz cell with unfiltered mercury arc the absorbance at 2450 Å. (major peak) disappeared completely. ^c Mean lifetime of 0.3 sec. determined in rigid 2-propanol at 77°K.; in rigid EPA mean lifetime is of same order of magnitude; in benzene at 77°K. mean lifetime was about 0.09 sec. Phosphorescence maximum occurred at approximately 4800 Å. ^d Forms phthalide dimer.

Effect of Substituents: Pertinent Literature

Much qualitative information has been collected concerning the effect of substitution on the photoreduction of benzophenones, and it seems appropriate to summarize the literature reports found for certain simple benzophenones.

Alkylated Benzophenones.—Pinacols were obtained from *m*- and *p*-methylbenzophenones and *p,p*-dimethylbenzophenone.²¹ *o*-Methylbenzophenone gave rearrangement to III.²²



Halogenated Benzophenones.—These halogenated benzophenones gave photopinacols: *o*-, *m*-, and *p*-chlorobenzophenones; *o,o'*, *p,p'*-tetrachlorobenzophenone; *o,m* and *p,p'*-difluorobenzophenones.²¹

Nitrobenzophenones.—No reports of successful photopinacolization were found.

Aminobenzophenones.—No reports of successful photopinacolization found. *p,p'*-Bis-(dimethylamino)-benzophenone has been reported to be unreactive.²⁰

Hydroxybenzophenones.—*o*-Hydroxy-*p*-methoxybenzophenone does not photopinacolize, whereas the *o,p*-dimethoxy derivative does.²³ *o*-Hydroxy and *o,p*-dihydroxybenzophenone produced very low yields of pinacol with quantum yields of 7×10^{-3} and 2×10^{-2} mole/einstein, respec-

tively.²⁴ No other reports of successful photopinacolization were found.

Other Derivatives of Simple Benzophenones.—*p*-Methoxy and *p,p'*-dimethoxybenzophenones gave photopinacols^{13,21}; *p*-cyanobenzophenone photoreduced¹³; *o*-benzoylbenzoic acid photoreduced^{24,25}; *m*-phenylbenzophenone photoreduced²⁶; *o*-phenylbenzophenone failed to photoreduce.³ Conflicting reports were found with *p*-phenylbenzophenone^{3,20,21}; in the present work it was found to photoreduce slowly. Both monoacetyl naphthalenes and 1-benzoylnaphthalene failed to photoreduce in the presence of alcohols.^{3,13}

Results and Discussion

Benzophenones.—Tables I and II present data concerning the formation of isolated products, measurement of lifetimes of any observed phosphorescence, detection of intermediates by electron spin resonance (e.s.r.) techniques, and photopotential measurements in the photochemical reduction of some substituted benzophenones. Table III reports preliminary approximate quantum yields in the photopinacol reactions of some substituted benzophenones.

Changes in photopotential appear to correlate well with "go-no-go" photopinacolization properties of substituted benzophenones and anthraquinones. This is reasonable since the change in photopotential reflects the presence of a reduced species (with respect to the parent ketone), e.g., free radicals, as pointed out by Surash and Hercules, who first obtained reliable photopotentials in

(24) A. Beckett and G. Potter, Sheffield University, private communication.

(25) D. B. Lemaye, *J. Univ. Bombay*, **1**, part 2, 52 (1932); *Chem. Abstr.*, **27**, 2097 (1932).

(26) H. H. Hatt, A. Pilgrim, and E. F. M. Stephenson, *J. Chem. Soc.*, 478 (1911).

(21) B. Boeseken and E. Cohen, *Akad. Amsterdam Versl.*, **23**, 775 (1920).

(22) N. C. Yang and C. Rivas, *J. Am. Chem. Soc.*, **83**, 2213 (1961).

(23) J. N. Pitts, Jr., and R. Martin, Abstract, Report to Petroleum Research Fund, 278-B, 1959.

TABLE II
PHOTOPOTENTIAL MEASUREMENTS OF SOME BENZOPHENONES

Compound		Pinacol formed	Photopotential, ^a volts		
			MeOH	EtOH	IPA
Benzophenone		Yes	+	0.31	0.12
Derivatives					
<i>ortho</i>					
	<i>Other</i>				
OH	<i>p</i> -OH	No		—	
OH	<i>p</i> -OCH ₃ , <i>p</i> '-CH ₃	No	—	—	—
NH ₂		No	—	—	—
NHCH ₃		No			
<i>para</i>					
NH ₂		No	—	—	—
N(CH ₃) ₂	<i>p</i> '-N(CH ₃) ₂	No ^g	—	—	—
N(CH ₃) ₂		Yes			0.05
Cl	<i>p</i> '-Cl	Yes ²⁰	0.10	+	+
OCH ₃	<i>p</i> '-OCH ₃	Yes ^{21,13}	0.10	+	+
CH ₃	<i>p</i> '-CH ₃	Yes ^{20,21}	+ ²⁷		
Br		Yes ²¹	+ ²⁷		

^a (+) indicates a change in the photopotential after 5-min. irradiation greater than 10 mv., (—) indicates a change of 10 mv. or less. Numbers in the table give the magnitude of the change in volts. Without exception a negative photopotential (Pt electrode vs. s.c.e.) was obtained when a photochemical reaction occurred.

TABLE III

APPROXIMATE QUANTUM YIELDS FOR PINACOL REDUCTION OF SUBSTITUTED BENZOPHENONES^a

Substituent	Concentration of ketone	Φ acetone ^b	Φ ketone ^c
<i>p</i> -C ₆ H ₅	0.02 <i>M</i>	0.07	0.2
	0.02 <i>M</i> EtOH	0.07	0.2
<i>p</i> -NH ₂	10 ⁻³ <i>M</i>	No obs. change	
<i>p,p</i> '-diOCH ₃	10 ⁻² <i>M</i>		2.1
<i>p,p</i> '-di-(CH ₃) ₂ N	10 ⁻⁴ <i>M</i>	^d	3 × 10 ⁻³
<i>m</i> -NO ₂	10 ⁻² <i>M</i>	0.07 ^e	^f

^a Data of Dr. Graham Black. Quantum yields measured using Cary Model 14 spectrophotometer to follow benzophenone concentrations, vapor phase chromatography on calibrated columns to follow acetone concentrations. Used Xe/Hg arc operated at 460 w., filtered to allow only 3660 Å. radiation. Light intensity varied from 3.54 to 2.8 × 10¹⁷ quanta/min. from run to run. ^b Quantum yield for acetone formation. ^c Quantum yield for benzophenone disappearance. ^d Acetone appeared to be formed, but sensitivity of instrument did not permit quantitative measurement. ^e Very approximate value. ^f No apparent change in ketone concentration, but acetone did appear to be formed.

systems of this type.²⁷ Subsequent photopolarographic²⁸ and photochronopotentiometric²⁹ studies have verified the significance of photopotential changes in such ketone systems. In this paper the empirical changes in the photopotentials will be simply noted without further speculation on the

(27) J. J. Surash and D. M. Hercules, Abstracts of 138th National Meeting of American Chemical Society, New York, N. Y., September, 1960; J. J. Surash, "Studies on Photo-Induced Luminescence and Electrode Potentials," Ph.D. Thesis, Lehigh University, Bethlehem, Pa., 1960.

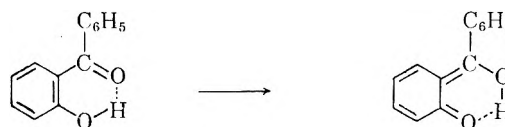
(28) H. Berg, *Z. Elektrochem.*, **64**, 1104 (1960); *Naturwiss.*, **47**, 320 (1960); H. Berg, *Collection Czech. Chem. Comm.*, **25**, 3404 (1960); H. Berg, *Naturwiss.*, **48**, 100 (1961); H. Berg and H. Schweiss, *Monatsh. (Berlin)*, **9**, 546 (1960); H. Berg and H. Schweiss, *Naturwiss.*, **47**, 513 (1960).

(29) T. Kuwana, J. N. Pitts, Jr., and A. Marchetti, Abstracts of Papers, 140th National Meeting of American Chemical Society, Chicago, 1960, p. 29-B, No. 78.

theoretical aspects of the electrochemical and photochemical processes in the irradiated solutions.

The prime purpose of this investigation was to check (by a variety of techniques) the effect of substituent groups and location of substitution on the photoreduction of a series of benzophenone derivatives. The following facts are evident from Table I.

ortho-Substitution by certain functional groups has a pronounced effect on the "go-no-go" photoproperties of benzophenone derivatives. It has been reported that *o*-hydroxybenzophenone did not fluoresce and was a "stabilizer" for the prevention of undesirable aging processes caused by ultraviolet light.³⁰ More recently it was shown in these Laboratories that while the *o*-hydroxy-*p*-methoxybenzophenone did not photopinacolize, *o,p*-dimethoxybenzophenone went readily.²⁴ Subsequently, Yang²² demonstrated that an intramolecular H atom transfer, "photoenolization," occurred in irradiation of *o*-methylbenzophenone. A similar photoenolization process may be responsible, at least in part, for the lack of reactivity found with *o*-amino and *o*-methylaminobenzophenones. Photoenolization is facilitated by the six membered ring available through internal hydrogen bonding, *i.e.*



Evidently, replacement of amino, hydroxy, or methyl by methoxy or carboxy restores the intermolecular hydrogen atom abstracting power of the benzophenone. These groups cannot form a stable photoenol of structure similar to III and intermolecular abstraction from the solvent becomes the predominant course of the reaction.

While this explanation originally seemed reasonable, there is evidence that effects other than steric (or intramolecular hydrogen bonding or photoenolization) can be important also. The compounds, *p*-aminobenzophenone and *p,p*'-bis-(dimethylamino)-benzophenone, have been studied. These derivatives do not photopinacolize (noted earlier²⁰ for the latter compound); neither do they show spectral or photopotential changes. However, *p*-dimethylaminobenzophenone gives a small yield of the photopinacol and a slight change in the photopotential.

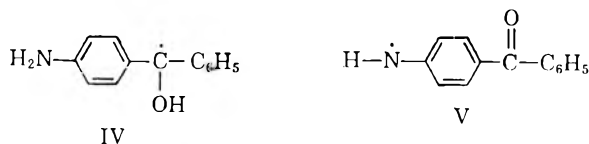
The *p*-aminobenzophenone has been studied the most thoroughly and, while certain of the results will be reported elsewhere,³¹ portions of the data will be summarized here.

Ten and twenty-four-hr. irradiations at room temperature of degassed 10⁻² *M* solutions of *p*-aminobenzophenone in isopropyl alcohol using a medium intensity mercury lamp (*ca.* 5 × 10⁻⁸ einstein/sec.) produced no significant permanent changes as ascertained by analysis of isolated

(30) J. H. Chaudet and J. W. Tamblin, Abstracts of Papers, 138th National Meeting of American Chemical Society, New York, N. Y., 1960, p. 19-T.

(31) L. Piette, J. Sharp, T. Kuwana, and J. N. Pitts, Jr., *J. Chem. Phys.*, **36**, 3094 (1962).

solid, gas-liquid chromatography of the liquid phase, and ultraviolet spectral and photopotential analyses of the reaction mixture. Low temperature (77°K.) electron spin resonance studies were conducted in conjunction with Dr. L. Piette of Varian Associates to see if radicals of the type IV or V could be detected (to determine whether a reversible hydrogen atom abstraction was the cause of the failure to photopinacolize). Upon irradiating this solid solution (10⁻² M *p*-aminobenzophenone in IPA) directly in the electron spin resonance cavity with light above 3000 Å. (Pyrex filter), no electron spin resonance (at *ca.* 3000 gauss) attributable to a *p*-aminobenzophenone free radical was detected. However, strong phosphores-



cence was noted during irradiation in the rigid medium at 77°K. and an electron spin resonance signal due to the triplet state of *p*-aminobenzophenone was observed at *ca.* 1500 gauss.³¹ This electron spin resonance is attributable to transitions between the highest and lowest sublevels and corresponds to $\Delta M_s = 2$.³² The mean life of the triplet state of *p*-aminobenzophenone in EPA measured by both electron spin resonance and phosphorescence decay (first order) was of the order of 0.3 sec.

Long-lived phosphorescence and electron spin resonance triplet signals were also observed for *p*-dimethylamino-, *p,p'*-bis-(dimethylamino)-, and *p*-phenylbenzophenones. The phosphorescence mean lifetimes of these compounds are listed in Table I.

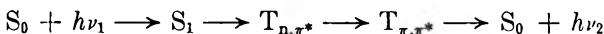
While the identification of a long-lived triplet state in these systems was of interest *per se*, an important correlation was that the long-lived triplets appeared to be observed with compounds which also gave low quantum yields (or no reaction at all) in the photopinacol reaction. Thus, a "normal" benzophenone such as *p,p'*-dimethoxybenzophenone has a quantum yield of 2.1 compared with 2.0 for benzophenone (presumably, the 2.1 is in error because of the approximate measurements) and has a triplet state with a mean lifetime of 0.06 sec. (Table I).

On the other hand, *p*-aminobenzophenone had a triplet whose mean lifetime (Table I) was 0.40 sec., and had a quantum yield which was too small to be observed in the photopinacol reaction. The data for *p,p'*-bis-dimethylaminobenzophenone were similar to those of *p*-aminobenzophenone: quantum yield in photopinacol 10⁻³; triplet lifetime 0.27 sec. With *p*-phenylbenzophenone a long-lived

triplet was observed (0.32 sec. mean lifetime), but Bachmann²⁰ had reported isolation of a photopinacol from this reaction. Others reported that the reaction failed. An approximate quantum yield measurement (Table III) indicated that the photopinacol reaction did proceed, but with a quantum yield of 0.2 mole/einstein, or 10% of the efficiency of the photopinacol reduction of benzophenone. Possibly the low quantum yield is responsible for the previous inconsistent observations.

These observations coupled with recent results of Ermolaev and Terenin^{15,35} for long-lived phosphorescence states suggest a possible explanation for the lack of H atom abstracting ability on the part of *para*-substituted benzophenones which do not pinacolize.

Ermolaev and Terenin³⁵ studied the absorption and phosphorescence spectrum of *p*-phenylbenzophenone (and other derivatives) in rigid solvents at 77°K. They pointed out that while its first absorption band was similar to that of unsubstituted benzophenone, and presumably resulted from an $n \rightarrow \pi^*$ transition, its phosphorescence spectrum resembled instead that of *p*-hydroxybiphenyl, which presumably is due to a transition from the lowest lying excited state, the π, π^* triplet, to the ground state. Thus, they suggest an *intramolecular* transfer of energy between triplet states of *p*-phenylbenzophenone. (Intermolecular triplet-singlet transfer of energy is well established.) The sequence of events being



where T_{n,π^*} and T_{π,π^*} are triplets with the latter lying at a *lower* level and reached by an internal conversion process from the T_{n,π^*} triplet (T_{n,π^*} is formed in the usual way by rapid intersystem crossing from the first excited singlet, S_1 .)

The failure of certain *p*-substituted benzophenones to photopinacolize now seems reasonable if it is assumed that the differences in the electronic structures of its two triplet states are reflected in their different chemical reactivities... that is, H atom abstraction is possible by the n, π^* triplet of benzophenone and its derivatives because of the localization of the excitation (a non-bonding electron on the O atom) but in the π, π^* triplet, the greater delocalization renders relatively ineffective the H atom abstracting "power" of the O atom in the carbonyl group.

While this is speculative, it is interesting to note that β -acetonephone behaves in a similar fashion, that is, its absorption appears to be $n \rightarrow \pi^*$ but its phosphorescence seems to originate from a π, π^* triplet state (both in mean lifetime and character of spectrum.³⁵ This correlates well with the results of independent photochemical studies of Hammond and Leermakers³⁶ for this compound. They found irradiation of β -acetonephone in optically active 2-octanol led to no racemization of the alcohol so that the failure of this compound is not due to reversal of the hydrogen transfer reaction. Instead they suggest that the "lowest

(32) Triplet resonance corresponding to $\Delta M_s = 2$ was first observed in rigid glass media by van der Waals and de Groot³³ by irradiating naphthalene in glycerol at liquid N₂ temperatures. More recently, Farmer, Gardner, and McDowell³⁴ have used similar techniques to study the exchange of energy between the triplet state of benzophenone and naphthalene in rigid EPA solution at 77°K.

(33) J. H. van der Waals and M. S. de Groot, *Mol. Phys.*, **2**, 233 (1959); *ibid.*, **3**, 190 (1960).

(34) J. B. Farmer, C. L. Gardner, and C. A. McDowell, *J. Chem. Phys.*, **34**, 1058 (1961).

(35) V. Ermolaev and A. Terenin, *J. chim. phys.*, 698 (1958).

(36) G. S. Hammond and P. A. Leermakers, *J. Am. Chem. Soc.*, **84**, 207 (1962).

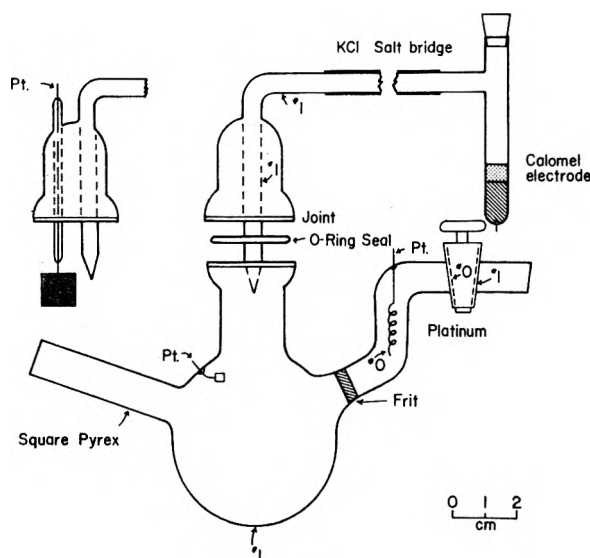


Figure 1.

triplet of reactive aldehydes and ketones have the n, π^* configuration, and those of the unreactive groups have the π, π^* configuration.”

With *o*-aminobenzophenone no electron spin resonance signal corresponding to a radical or a triplet state was observed. Thus the triplet \rightarrow triplet interconversion is not an attractive explanation for the failure of this benzophenone to pinacolyze. The photoenolization is the most probable explanation in these compounds.

Anthraquinones.—Table IV presents the results

TABLE IV
PHOTOCHEMICAL BEHAVIOR OF SOME SUBSTITUTED ANTHRAQUINONES

Compound	Photoreaction	Photopotential, ^a volts		
		MeOH	EtOH	IPA
Anthraquinone ^b	Yes ³⁹	0.6	+	0.28
Derivatives				
1,8-diOH	Little, if any	—	—	—
1,5-diOH	Little, if any	0.01	—	0.02
1,4-diOH	Little, if any	.01	—	0.02
1-Cl	+	.3	—	—
1,5-diCl	+	.3	—	—

^a Photopotentials have same significance as in Table II.

^b Radical e.s.r. signal noted in alkaline ethanol at room temperature when irradiated. In neutral alcohol the e.s.r. radical signal did not appear until the temperature was lowered to 77°K. during the irradiation. For previous work see references 37 and 38.

to date of studies in the anthraquinone series, both published and recent experimental data. Again the correspondence between the appearance of a significant photopotential and gross chemical reaction as detected by product isolation is to be noted. Anthraquinone also gave an electron spin resonance signal characteristic of a free radical when irradiated in alkaline ethanol or when irradiated in neutral ethanol at 77°K.^{37,38}

The effect of structure on reactivity in this series appears to follow closely that observed for the

(37) J. H. Sharp, T. Kuwana, A. Osborne, and J. N. Pitts, Jr., *Chem. Ind. (London)*, 508 (1962).

(38) K. Kuwata and K. Hirota, *Bull. Chem. Soc. Japan*, **34**, 458 (1961).

benzophenones. Substitution in the 1 or 5 position of the ring by a NH or OH group (see Table IV and references 39–41) inhibits photoreaction. The 2,6-dihydroxyanthraquinone has been reported^{39,41} to be non-photoreactive. Photoenolization may be important while in certain cases an intramolecular energy transfer process may occur to yield a π, π^* state which is photochemically unreactive. Abrahamson, *et al.*,⁴² have suggested the latter explanation to rationalize their results with anthraquinones substituted by (basic) groups capable of donating an electron pair (NH, OH, Cl, Br). However, apparently their results are not in agreement with ours in respect to the chloro derivatives (see Table IV).

Further work is necessary before a definitive statement can be made about substituents and their positional effects on the photoreactivity of anthraquinones. We have discussed this in detail with Dr. F. Wilkinson (Oxford University) who has studied the fluorescence spectra of some substituted anthraquinones. His results have been presented verbally⁴³ and will be published shortly.

Experimental

Macro scale photolysis for product isolation was conducted using irradiation from a Hanovia #73A-10 lamp. The irradiation cell used was constructed from 37 × 200 mm. Pyrex tubing with appropriate ground glass connections for vacuum degassing. All samples were carefully degassed (10^{-3} mm., oil diffusion pump vacuum system, liquid N₂ traps to prevent sample contamination) prior to photolysis. Products were isolated by crystallization, vacuum distillation, or column chromatography.

Infrared spectra were obtained using the Perkin-Elmer Model 221G infrared spectrometer. Vapor phase chromatograms were used to analyze for liquid phase photolysis products or to check solvent purity. The Cary Model 14 spectrophotometer was used for obtaining all ultraviolet-visible spectra. The electron spin resonance experiments were performed on the Varian Model V-4500 spectrometer.

Photopotentials and spectra of photolyzed solutions were obtained by utilizing a special cell shown in Fig. 1. The 5-cm. diameter cell has a depth of 3 cm. and has the provisions for measuring the solution ultraviolet-visible absorption by tipping the cell to fill the 1-cm.² Pyrex side-arm which fits the cell compartment of the Cary spectrophotometer. A newer cell with a 1-cm.² quartz side-arm has been constructed for lower wave length work. Photopotentials were measured using the 3-mm.² platinum indicator electrode and a probe-type calomel reference electrode. The latter electrode is secured to the cell through a clamped O-ring sealed joint. Contamination arising from stopcock grease is reduced by the use of this type of seal. The photopotentials were monitored using a Model 412A Hewlett-Packard VTVM (input impedance 200 megohm) whose output was fed to a 10-mv. Varian G-11 recorder. An auxiliary O-ring joint with a 1-cm.² platinum and calomel electrode attached can be used for conducting additional electrochemical experiments, such as chronopotentiometry, etc. To ensure against leakage, picein wax was used to outer seal the electrodes to the glass wall. This cell is particularly valuable for aiding the study of photochemical systems where product isolation and analysis are difficult

(39) N. K. Bridge and G. Porter, *Proc. Roy. Soc. (London)*, **244**, 259 (1958).

(40) J. L. Bolland and H. R. Cooper, *ibid.*, **A225**, 405 (1954); H. R. Cooper, unpublished results.

(41) G. O. Schenck and G. Koltzenburg, *Naturwiss.*, **41**, 452 (1954).

(42) E. W. Abrahamson, I. Panik, and K. V. Sarkanen, Proceedings of the Second Cellulose Conference, Cellulose Research Institute, Syracuse, New York, May, 1959.

(43) F. Wilkinson, Symposium on Reversible Photochemical Processes, Duke University, remarks presented from the floor, April, 1962.

(*e.g.*, soluble photolysis products that react rapidly when exposed to oxygen in the air).

The ketone-alcohol solutions (for photopotential, spectra, or electron spin resonance work) were photolyzed using either an Osram HBQ-200 or PEK-109 high pressure mercury arc lamp. The radiation was rendered approximately monochromatic in the 3130 or 3660 Å. region by appropriate Corning glass filters. Ferrioxalate procedure⁴⁴ was used for actinometry.

Phosphorescence measurements were made on vacuum degassed, sealed-tube samples in rigid ethanol (unless otherwise stated) at liquid N₂ temperatures. Irradiation from the PEK-109 lamp was filtered to allow transmission at 3150–4000 Å. which then passed through a rapid closing shutter system to the sample. At right angles to the excitation light, the phosphorescence was monitored by a photomultiplier tube (filtered to allow transmission only above 4400 Å.) which fed an input signal to an American Instrument Co. photomultiplier microphotometer whose output signal was recorded on a Sanborn Model 154-100 recorder (chart speed: 100 mm. per second).

Matheson, Coleman and Bell reagent grade alcohols were purified by the following procedure: to a 2-l. round-bottom flask containing ca. 200 ml. of alcohol were added 5 g. of granular magnesium metal and 0.5 g. of iodine crystals. The solution was refluxed for 1 hr., the remainder of the alcohol added (1 to 1.5 l.), refluxed for an additional 3–4 hr., and then distilled from a 60-cm. glass helices packed column. Only the middle fractions were collected and used.

(44) C. A. Parker and C. G. Harchard, *Proc. Roy. Soc. (London)*, **A220**, 104 (1953); *ibid.*, **A235**, 518 (1956); "Photochemistry in the Liquid and Solid States," John Wiley and Sons, Inc., New York, N. Y., 1960, p. 41.

The ketones used in this study were known compounds prepared by reported methods.^{45,46} They were purified by crystallization, sublimation, or column chromatography. The samples of the chloro- and hydroxy-substituted anthraquinones were kindly supplied by Dr. E. J. Bowen and Dr. D. Seaman, Oxford University.

Acknowledgment.—The authors wish to acknowledge the contributions of Mr. J. H. Sharp, Mr. T. C. Li, Mr. O. Paez, and Drs. P. West and G. Black to this paper. We are indebted to Drs. S. I. Chan and L. Piette for their helpful suggestions concerning the electron spin resonance aspects of the work, and to Dr. F. Wilkinson of the Physical Chemistry Laboratories, Oxford University, for interesting discussions of the problem. This research was supported in part by a grant from the Petroleum Research Fund administered by the American Chemical Society. Grateful acknowledgment is hereby made to the donors of this fund. The authors also gratefully acknowledge partial support of this work by grant No. AP-109 from the Public Health Service, Air Force Contract, AF 19(604)-8096, from the Geophysics Research Directorate of the Air Force Cambridge Research Laboratories, and a grant from the National Science Foundation.

(45) P. Grammaticakis, *Compt. rend.*, **235**, 546 (1952).

(46) J. P. Cordner and K. H. Pausacker, *J. Chem. Soc.*, 102 (1953).

BAND STRUCTURE AND TRANSPORT OF HOLES AND ELECTRONS IN HOMOLOGS OF ANTHRACENE¹

BY G. D. THAXTON, R. C. JARNAGIN,

Physics and Chemistry Departments, The University of North Carolina, Chapel Hill, North Carolina

AND M. SILVER

*Army Research Office (Durham), Durham, North Carolina, and
Physics Department, University of North Carolina, Chapel Hill, North Carolina*

Received May 25, 1962

Calculations of the band structure and of the mobility of excess holes and of excess electrons in homologs of anthracene have been completed. Following LeBlanc, the tight binding approximation was used and applied to naphthalene, tetracene, and pentacene. Calculated mobility tensors and band widths indicate the mobility properties of excess charge carriers in all four molecular crystals to be much alike. Experimental results for the crystals other than anthracene are not yet available.

Introduction

A theoretical treatment of the band structure and transport of excess holes and of excess electrons in anthracene has recently been reported by LeBlanc.² LeBlanc applied the tight binding approximation to construct crystal wave functions in order to describe the motion of *excess* charge carriers. The crystal wave functions are formed from linear combinations of molecular orbitals constructed within the Hückel approximations from Slater 2p_z atomic orbitals.³ Linear combinations of molecular orbitals for the highest bonding state describe the band for the excess hole, and linear combinations of the molecular orbitals for the lowest anti-bonding state describe the band for the excess

electron. Application of periodic boundary conditions enables one to obtain band widths and mobilities for both holes and electrons.

LeBlanc made computations only for anthracene. It is desirable to extend these type calculations to other members of the naphthalene-anthracene series (members which will probably be accessible to experiment) and see what major differences, if any, may be expected in the mobility properties.

In addition to calculations for naphthalene, tetracene, and pentacene, the computations for anthracene were repeated. LeBlanc⁴ has advised us of an error in his original work. The repeated computations were done to ensure computational consistency with LeBlanc's corrected results.

Molecular and Crystal Structure.—Naphthalene⁵

(1) Partially supported by the Army Research Office (Durham) and the National Science Foundation.

(2) O. H. LeBlanc, Jr., *J. Chem. Phys.*, **35**, 1275 (1961).

(3) J. C. Slater, *Phys. Rev.*, **36**, 57 (1930).

(4) Private communication, August, 1961.

(5) S. C. Abrahams, J. M. Robertson, and J. G. White, *Acta Cryst.*, **2**, 238 (1949).

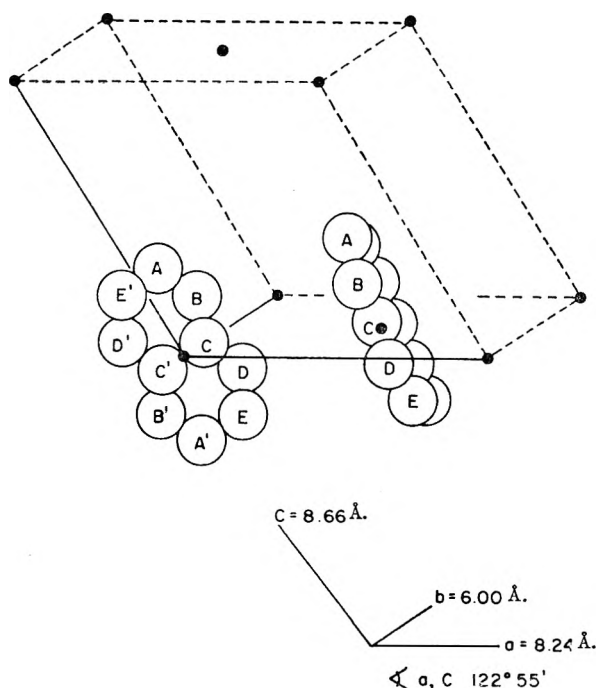


Fig. 1.—Unit cell geometry for naphthalene.

and anthracene⁶ are monoclinic with space group $P2_1/a$ (C_2h^6), while tetracene and pentacene^{7,8} are triclinic with space group $P\bar{1}$ (C_i^1). A structure typical for this series is that of naphthalene, which is shown in Fig. 1. Each substance has two molecules per unit cell and even though the space groups differ, the molecular arrangements of the four hydrocarbons closely resemble one another.

In the mobility calculations an orthogonal set of axes was chosen and is denoted by a' , b' , and c' . The \bar{b} crystallographic direction and the b' orthogonal direction are conveniently chosen colinear. In naphthalene and anthracene the crystallographic direction \bar{a} is perpendicular to \bar{b} , and hence is denoted by a' . In tetracene and pentacene \bar{a} and \bar{b} are not perpendicular and a' is defined so that it is perpendicular to \bar{b} and in the ab plane. The c' direction is then perpendicular to both \bar{a} and \bar{b} .

Following LeBlanc it is convenient to use a set of vectors which connect nearest neighbor molecules. The vectors are given by $\bar{\alpha} = \frac{1}{2}(\bar{a} + \bar{b})$, $\bar{\beta} = \frac{1}{2}(-\bar{a} + \bar{b})$, and \bar{c} . The vectors $\bar{\alpha}$, $\bar{\beta}$, and \bar{c} define what may be called a "pseudo unit cell," each containing one molecule.

The usual unit cell contains one molecule with its center at the origin and one with its center at the terminus of \bar{a} . The molecular and crystal symmetries of naphthalene and anthracene are such that the molecule at the \bar{a} site is obtained from the one at the origin by reflection in the ac plane followed by a translation of \bar{a} . In tetracene and pentacene the arrangement of the two molecules in

the unit cell closely resembles that for naphthalene and anthracene; however, the molecule at the \bar{a} site is no longer obtained by reflection and translation. The reflection is replaced by a rotation which causes the orientations of the molecules in these substances to differ slightly from that of naphthalene and anthracene.

Calculations

The calculations of the band structures and the mobility tensors for anthracene are given in detail by LeBlanc,² hence only an outline of the procedure is given here. These calculations are applicable to excess holes or electrons (one or the other but not both simultaneously) in concentrations of 10^{10} cm.⁻³ or smaller. Interactions between the carriers are thus probably negligible and one considers only one excess hole or electron in an unperturbed crystal in the ground state.

Taking advantage of the simple structure of these crystals and applying periodic boundary conditions (periodic under reflection or rotation followed by translation) one may use the tight binding approximation for constructing the hole or electron crystal wave functions. The crystal wave functions are linear combinations of molecular wave functions, $\varphi_n(\vec{r} - \vec{r}_n)$, which are identical except for spatial orientation. The vector \vec{r}_n is the position vector of the geometrical center of the n^{th} molecule. The orientation is such that the symmetries of the crystal are manifest in the crystal wave function, *i.e.*, $\varphi_n(\vec{r} - \vec{r}_n)$ transforms into $\varphi_{n+\alpha}(\vec{r} - \vec{r}_n - \bar{\alpha})$ or $\varphi_{n+\beta}(\vec{r} - \vec{r}_n - \bar{\beta})$ under reflection or rotation followed by a translation of α or β . The crystal wave function then is given by

$$\Psi_{\vec{k}}(\vec{r}) = \frac{1}{N^{1/2}} \sum_{n=1}^N \exp(i\vec{k} \cdot \vec{r}_n) \varphi_n(\vec{r} - \vec{r}_n) \quad (1)$$

in which N is the total number of molecules in the crystal.

The periodic boundary conditions used are

$$-\pi < \vec{k} \cdot \bar{\alpha}; \vec{k} \cdot \bar{\beta}; \vec{k} \cdot \bar{c} \leq \pi \quad (2)$$

The crystal potential used in the Hamiltonian for the excess hole or electron is a sum of molecular potentials, *i.e.*

$$V(\vec{r}) = \sum_{n=1}^N V_n(\vec{r} - \vec{r}_n) \quad (3)$$

with each molecular potential $V_n(\vec{r} - \vec{r}_n)$ given by a sum of Goepfert-Mayer and Sklar⁹ neutral carbon potentials centered on the atoms of the molecule, with the sum extending over the atoms of this one molecule. Then

$$V_n(\vec{r} - \vec{r}_n) = \sum_i V_i(r_i) \quad (4)$$

using Slater-type atomic orbitals one obtains

$$V_i = -e^2 r_i^{-1} \{4 + 6(\alpha r_i) + 4(\alpha r_i)^2 + \frac{4}{3}(\alpha r_i)^3\} \exp(-2\alpha r_i) \quad (5)$$

(6) V. C. Sinclair, J. M. Robertson, and A. M. Mathieson, *Acta Cryst.*, **3**, 251 (1950).

(7) R. B. Campbell, J. M. Robertson, and J. Trotter, *ibid.*, **14**, 705 (1961).

(8) J. M. Robertson, V. C. Sinclair, and J. Trotter, *ibid.*, **14**, 697 (1961).

(9) M. Goepfert-Mayer and A. L. Sklar, *J. Chem. Phys.*, **6**, 645 (1938).

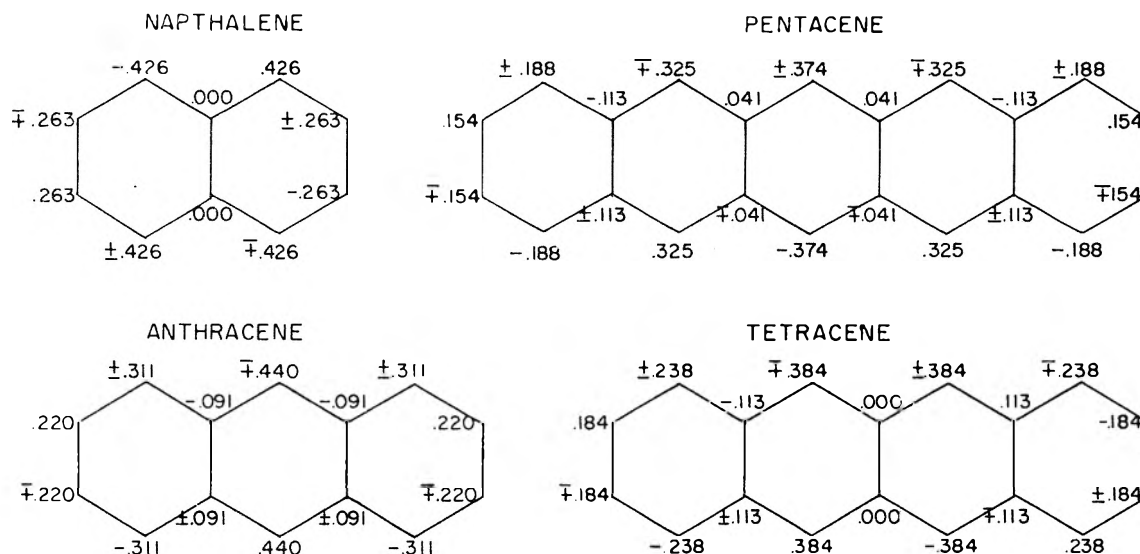


Fig. 2.—Values of coefficients for molecular wave functions. The magnitudes of these coefficients are the same for holes and electrons, and when they differ in phase, the upper sign is for the hole and the lower for the electron.

in which $\alpha = 1.64$ (a.u.) $^{-1} = 3.08 \times 10^8$ cm. $^{-1}$ is the parameter used by Slater³ and should not be confused with the magnitude of $\bar{\alpha}$.

Using appropriate simplifications one obtains expressions for the energies of both holes and electrons, each having the form¹⁰

$$E(\vec{k}) = \text{constant} + 2 \sum_s E_s \cos(\vec{k} \cdot \vec{r}_s) \quad (6)$$

in which

$$E_s = \int \varphi_{n+s} V_{n+s} \varphi_n d\tau \quad (7)$$

The constant in equation 6 is not evaluated; however, its value is immaterial to the determination of band widths and mobilities.

The molecular wave functions, φ_n , are linear combinations of Slater-type $2p_z$ atomic orbitals, *i.e.*

$$\varphi_n = \sum_i C_{ni} u_i \quad (8)$$

with

$$u_i = \left(\frac{\alpha^5}{\pi}\right)^{1/2} r_i \cos(\xi_i) \exp(-\alpha r_i) \quad (9)$$

The coefficients C_{ni} are determined from the secular equations using the approximation of Hückel.¹¹ The values of these coefficients are given in Fig. 2. In cases of multiple signs the lower sign is associated with the antibonding π orbital of lowest energy and the upper sign is associated with the bonding π orbital of highest energy.

The resonance integrals, E_s , of equation 6 are then written

$$\int \varphi_m V_m \varphi_n d\tau = \sum_{i,j} C_{mi} C_{nj} \int u_i V_i u_j d\tau = \sum_{i,j} C_{mi} C_{nj} I_{ij} \quad (10)$$

(10) F. Seitz, "Modern Theory of Solids," McGraw-Hill Book Company, Inc., New York, N.Y., 1940.

(11) R. Daudel, R. LeFebvre, and C. Moser, "Quantum Chemistry," Interscience Publishers, Inc., New York, N. Y., 1959.

with

$$I_{ij} = \int u_i V_i u_j d\tau \quad (11)$$

In obtaining equation 10 all three-center or higher interatomic integrals, I_{ij} , are neglected.

Let \bar{n}_i and \bar{n}_j be unit vectors such that equation 9 can be written

$$u_i = (\alpha^5/\pi)^{1/2} (\bar{r}_i \cdot \bar{n}_i) \exp(-\alpha r_i) \quad (12)$$

and let \bar{R}_{ij} be the vector from the i^{th} atom of the m^{th} molecule to the j^{th} atom of the n^{th} molecule; then I_{ij} is given by

$$I_{ij} = \frac{-\left(\frac{\alpha^5}{2\pi}\right) (\bar{n}_i \cdot \bar{R}_{ij}) (\bar{n}_j \cdot \bar{R}_{ij}) S_{ij}}{R_{ij}^2} + \left(\frac{\alpha^5}{2\pi}\right) \left\{ (\bar{n}_i \cdot \bar{n}_j) = \frac{(\bar{n}_i \cdot \bar{R}_{ij}) (\bar{n}_j \cdot \bar{R}_{ij})}{R_{ij}^2} \right\} C_{ij} \quad (13)$$

$$S_{ij} = \int \cos(\xi_i) \cos(\xi_j) r_i r_j V(r_i) \exp(-\alpha[r_i + r_j]) d\tau \quad (14)$$

and

$$C_{ij} = \int \sin(\xi_i) \sin(\xi_j) r_i r_j V(r_i) \exp(-\alpha[r_i + r_j]) d\tau \quad (15)$$

S_{ij} and C_{ij} have been reduced to polynomial form by LeBlanc.²

The resonance integrals are calculated and the results are given in Table I. All I_{ij} involving atoms separated by 5 Å. or more are neglected. The expression for the energy of the excess hole or electron is then given by

$$E(\vec{k}) = \text{constant} + 2E_b \cos(\vec{k} \cdot \vec{b}) + 2E_\alpha \cos(\vec{k} \cdot \vec{\alpha}) + 2E_\beta \cos(\vec{k} \cdot \vec{\beta}) + 2E_{c\alpha} \cos[\vec{k} \cdot (\vec{c} + \vec{\alpha})] + 2E_{c\beta} \cos[\vec{k} \cdot (\vec{c} - \vec{\beta})] + 2E_c \cos(\vec{k} \cdot \vec{c}) \quad (16)$$

TABLE I
INTERMOLECULAR RESONANCE INTEGRAL (10^{-16} ERG)

	Naphthalene		Anthracene		Tetracene		Pentacene	
	Electron	Hole	Electron	Hole	Electron	Hole	Electron	Hole
E_b	+ 6.93	-18.8	+19.1	-25.9	-26.2	+21.4	-24.5	+22.4
E_c	- 1.43	...	+ 0.283	...	- 1.25	- 0.401	+ 0.556	+ 0.181
E_α	-17.1	- 1.01	-31.6	-23.8	-45.9	-26.7	-37.5	-25.3
E_β	-17.1	- 1.01	-31.6	-23.8	+31.5	+34.3	+39.1	+34.1
$E_{c\alpha}$	- 0.778	- 4.74	+ 1.04	+ 4.96	...	- 1.13	...	+ 0.725
$E_{c\beta}$	- 0.778	- 4.74	+ 1.04	+ 4.96	- 0.189	...	+ 0.252	+ 0.374

The conditions for maxima and minima in $E(\vec{k})$ are found to be $\vec{k} \cdot \vec{c} = 0$ and $\vec{k} \cdot \vec{a} = \vec{k} \cdot \vec{b}$ for both naphthalene and anthracene. These conditions are used to obtain the band widths for these substances. The extremum conditions are not so simple in tetracene and pentacene and for simplicity only estimates are made for the band widths in these two substances. The band widths are given in Table II.

TABLE II
APPROXIMATE BAND WIDTHS IN UNITS OF kT AT ROOM TEMPERATURE

	Electron	Hole
Naphthalene	0.33	0.23
Anthracene	.58	.43
Tetracene	.53	.44
Pentacene	.61	.48

Mobility tensors have been calculated for two different cases (a) constant mean free time $\tau(\vec{k}) = \tau_0$ and (b) constant mean free path $\tau(\vec{k}) \times |\vec{v}(\vec{k})| = \lambda_0$. The first case permits the calculation of the mobility in closed form. For that reason (a) is assumed and the mobility components are given by

$$\mu_{ij} = e\tau_0 \frac{\langle v_i v_j \rangle}{kT} \quad (17)$$

in which $v_i(\vec{k})$ is the i^{th} component of the carrier velocity \vec{v} and is given by

$$\hbar v_i(\vec{k}) = \partial E(\vec{k}) / \partial k_i \quad (18)$$

The quantity $\langle v_i v_j \rangle$ is a statistical average over the appropriate band. By treating the density of states and the Boltzmann factor as constant over the extremely narrow bands, the integration is easily performed. The results are given in Table III.

Finally the mobility tensors (tensors with components $\langle v_i v_j \rangle$) have been diagonalized and the components along the principal axes are given in Table IV. In all four substances, for both holes and electrons, it is found that c' is a principal axis of the mobility tensor. In addition \vec{a} and \vec{b} are principal axes for both holes and electrons in naphthalene and anthracene. In tetracene and pentacene the principal axes are obtained by rotations of the orthogonal coordinate system about c' . In tetracene the rotation angle is 59.5° for holes and 51.5° for electrons and in pentacene the rotation angle is 63.7° for holes and 65.5° for elec-

trons. The angles are correct to approximately 1° .

Discussion and Conclusions

A significant result of these calculations is that in all cases the predicted mobility in the c' direction is found to be much smaller than the mobilities in the ab plane. This is due in part to the almost exact cancellation of the largest interatomic integrals in the sums for E_c , $E_{c\alpha}$, etc. However, in $E_{c\alpha}$ for holes in anthracene this cancellation does not occur and still the mobility is only about one-fifth of that in the ab plane. This is due to the fact that the average interatomic separation is larger between molecules in the \vec{c} or $\vec{c} + \vec{a}$ directions in addition to the hole and electron densities being smaller at the ends of the molecule than at positions nearer the center of the molecule.

Cancellation is also responsible for the small magnitudes of E_α and E_β for holes in naphthalene, and hence both E_α and E_β and the resulting small mobility in the \vec{a} crystallographic direction should be viewed with some skepticism. It would be interesting to have experimental data with which to compare this result.

Since a rigid lattice has been assumed in these calculations and is an obvious over-simplification, then one may argue that no significance can be attached to the large anisotropy of velocity components in naphthalene nor to the 180-fold asymmetry in electron and hole velocity components along the \vec{a} direction. However, these calculations clearly indicate the desirability of looking for these effects and suggest crystalline naphthalene to be the more promising material to examine, particularly at low temperatures where the rigid lattice assumption may be more closely attained.

With the exception of increased anisotropy in the ab plane for tetracene and pentacene, there does not appear to be any startling differences between the predicted mobilities in the substances investigated. In tetracene and pentacene the off-diagonal components of the mobility tensor are no longer negligible and the principal axes are near \vec{a} and \vec{b} rather than along \vec{a} and \vec{b} as in naphthalene and anthracene. Also, if τ_0 is comparable for holes and electrons, then there is a reversal of their relative mobility in the \vec{b} direction for tetracene and pentacene compared to their relative mobility in the same direction for naphthalene and anthracene.

On the basis of these calculations one would predict that the magnitude of the mobilities in all of these materials should be comparable but with significant differences in their anisotropy.

TABLE III
 VELOCITY COMPONENTS (10^{10} cm.²/sec.²)

	Naphthalene		Anthracene		Tetracene		Pentacene	
	Electron	Hole	Electron	Hole	Electron	Hole	Electron	Hole
$V_a'^2$	1.79	0.009	6.57	3.77	8.73	5.31	8.22	5.02
$V_b'^2$	1.26	2.38	5.67	6.35	9.90	6.01	8.83	6.13
$V_c'^2$	0.031	0.046	0.034	0.742	0.036	0.034	0.014	0.027
$V_a'V_c'$	0.000	0.000	-0.007	-0.168	-0.018	-0.004	-0.005	-0.004
$V_a'V_b'$	0.000	0.000	0.000	0.000	2.63	-0.648	0.360	-0.734
$V_b'V_c'$	0.000	0.000	0.000	0.000	-0.008	-0.003	-0.003	-0.003

 TABLE IV
 VELOCITY COMPONENTS IN PRINCIPAL AXES COÖRDINATE SYSTEM
 DENOTED BY a'' , b'' , AND c'' (10^{10} cm.²/sec.²)

	Naphthalene		Anthracene		Tetracene		Pentacene	
	Electron	Hole	Electron	Hole	Electron	Hole	Electron	Hole
$V_a''^2$	1.79	0.009	6.57	3.77	12.01	4.93	9.00	4.66
$V_b''^2$	1.26	2.38	5.67	6.35	6.62	6.40	8.05	6.50
$V_c''^2$	0.031	0.046	0.034	0.742	0.036	0.034	0.014	0.027

Acknowledgments.—The authors wish to thank Dr. O. H. LeBlanc, Jr., of the General Electric Company for several very helpful letters regarding

these calculations, and also Dr. J. Trotter for a letter containing revised crystal data for tetracene and pentacene.

PHOTOCHROMISM IN SPIROPYRANS. PART IV.¹ EVIDENCE FOR THE EXISTENCE OF SEVERAL FORMS OF THE COLORED MODIFICATION

BY RAHEL HEILIGMAN-RIM, YEHUDA HIRSHBERG, AND ERNST FISCHER

Laboratory of Photochemistry and Spectroscopy, The Weizmann Institute of Science, Rehovoth, Israel

Received May 25, 1962

Both the wave length and the relative intensity of bands in the absorption spectra of the colored modifications of photochromic spiropyrans strongly depend on the character of the solvent used. Moreover, cooling causes pronounced changes in the spectra of solutions in non-polar solvents, while the spectra of alcoholic solutions are not affected by variation of temperature. The effect of cooling ceases when a certain very low temperature (-150° , -160°) is reached. At this temperature all solvent mixtures used become highly viscous. When the colored modification is produced by ultraviolet irradiation at low temperature in such highly viscous glassy media, its spectrum is different from that of the colored modification produced by irradiation at a higher temperature and then cooled; the spectrum assumes the latter shape when the solution is warmed and then cooled again. The hypothesis of the existence of several stereoisomers of the dye molecule is forwarded, to account for these observations. Some of these stereoisomers are interconvertible thermally as long as the thermal energy of the molecules does not drop below a certain value and the viscosity of the medium does not exceed a certain limit. The various isomers differ both in their spectra and in their convertibility into the spiropyran by visible light.

Introduction

The general ideas about thermochromism and photochromism of spiropyrans, developed in previous publications, may be summarized as follows. Thermochromic "spiropyrans" exist in solution as an equilibrium mixture of two isomers—a colorless spiropyranic modification (A) and a colored merocyanine-like modification (B). The position of this equilibrium varies widely with the nature of the compound and the solvent, and with the temperature; high temperatures and polar solvents favoring the colored modification (B). The rate at which thermal equilibration takes place (starting from a non-equilibrium mixture) also depends on the same factors and is reduced to practically zero at sufficiently low temperatures. At such tem-

peratures any phototransformations which might take place can be investigated without the complication of thermal transformations between (A) and (B). The spiropyrans hitherto investigated can be classified as follows with regard to phototransformation: (1) Those in which the two modifications can be interconverted by the action of ultraviolet light, and (B) is converted into (A) by irradiation with visible light; (2) those in which ultraviolet light converts (A) into (B) and *vice versa* but visible light has no effect; (3) those in which the two modifications are not interconvertible by light, although both do exist. Compounds of classes (1) and (2) are called "photochromic."² The present report deals with compounds of class (1), as exemplified by I and IV; and of class (3), as exemplified by II and III. In compounds of class

(1) Part III: R. Heiligman-Rim, Y. Hirshberg, and E. Fischer, *J. Chem. Soc.*, 156 (1961).

(2) (a) Y. Hirshberg, *Compt. rend.*, **231**, 903 (1950); (b) Y. Hirshberg and E. Fischer, *J. Chem. Soc.*, 629 (1953).

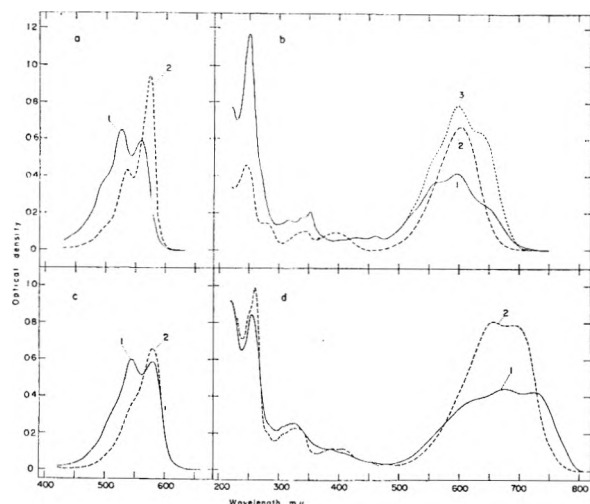
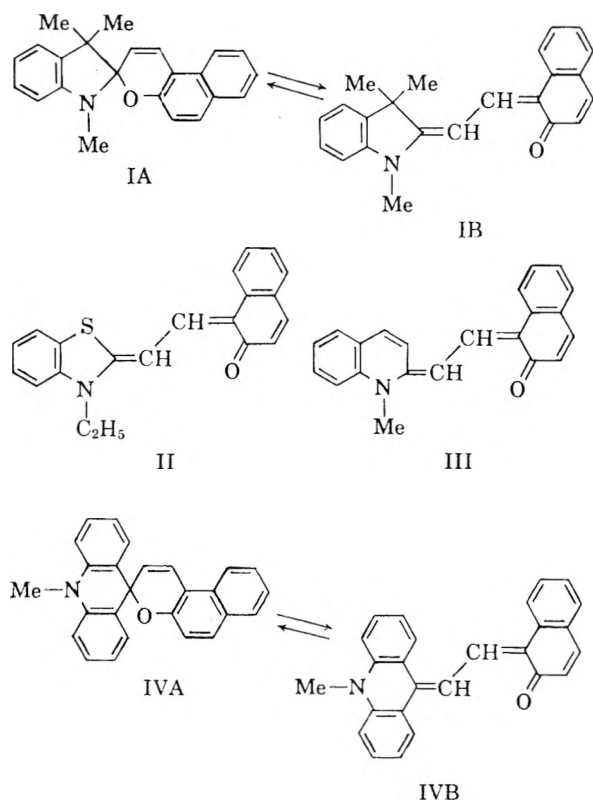


Fig. 1.—Solvent dependence of spectra of merocyanines: full curves, in non-polar solvents; broken curves, in alcohol. (a) Compound IB, 0.9×10^{-6} mole/l. at -100° : 1, in methylcyclohexane-petrol ether 1:1; 2, in ethanol-methanol 4:1, (b) compound III at room temperature: 1, in decalin, saturated solution; 3, in benzene; 2, in propanol, 1.6×10^{-6} mole/l.; (c) compound II, at room temperature: 1, in decalin, 2.3×10^{-4} mole/l.; 2, in propanol, 0.9×10^{-6} mole/l.; (d) compound IVB: 1, in methylcyclohexane-isohexane 1:1 at -150° , 2.2×10^{-6} mole/l.; 2, in propanol at -110° , 1.7×10^{-6} mole/l.



(1) irradiation with ultraviolet light, which is absorbed by both modifications, results in a photo-equilibrium mixture containing between about 70 and 100% (B), whereas irradiation with visible light which is absorbed only by (B) converts all of it into (A). Results will be reported for the influence of solvent and of temperature on the absorption spectrum of modification (B).

Results

The form of the spectra of the merocyanine-like compounds obtained by irradiation of photochromic spiropyran, such as I or IV, as well as that of the spectra of "merocyanines proper," such as II and III, depends to a great extent on the nature of the solvent used (*cf.* a similar observation regarding the thermochromic colored modification of the spiropyran).³ In non-polar solvents the spectra are, furthermore, strongly affected by the temperature. The effect of solvents and of the temperature on these spectra manifests itself both in frequency shifts and in variation of the ratio of the intensities of some absorption bands, these variations leading in extreme cases to complete disappearance of one or more bands.

Solvent Effects.—These are illustrated in Fig. 1. Figures 1a and 1d compare the spectra of compounds IB and IVB in a polar and in a non-polar solvent at low temperature. Figures 1b and 1c show a similar solvent dependence, at room temperature, in the spectra of the two merocyanines II and III, which resemble in structure the colored modification of I. The polar solvent is seen to suppress and even to obliterate some of the absorption bands.

Temperature Effects.—These are even more striking, as illustrated in Fig. 2. Figure 2a shows the effect of cooling on the spectrum of a solution of IB in a non-polar solvent. At -100° the intensities of the two main absorption bands in the visible, at about 530 and 560 $m\mu$, are approximately equal; as the solution is cooled the ratio of intensities changes in favor of the 530 $m\mu$ band until the value of this ratio reaches 2.3 at -160° . At the same time the peaks of both bands undergo a bathochromic shift from 525 to 532 $m\mu$ and from 559 to 577 $m\mu$, and a new absorption band appears at 610 $m\mu$. However, further cooling from -160 to -183° causes no further change in the shape of the absorption spectrum. The process to which the temperature-linked spectral changes are due thus appears to be "frozen" at about -160° .

Figure 2b shows the effect of cooling on a solution of IVB in a non-polar solvent. It is seen that the intensity of the 585 $m\mu$ absorption band diminishes while new absorption bands appear at 735 and 670 $m\mu$. In Fig. 2d a similar effect of cooling on a solution of the same compound in another non-polar solvent, of higher viscosity, is seen. In this solvent, a mixture of methylcyclohexane and decalin, the change of the shape of the spectrum with cooling ceases already at about -145° .

In a polar solvent cooling from -100 to -150° does not affect the form of the spectrum in any way. On the other hand, the emission spectrum of these compounds in a polar solvent changes with cooling, at least in some cases; thus the fluorescence of IB, which is orange-red at -100° , becomes yellow at -140° , whereas in a non-polar solvent it remains orange-red down to -180° .

Thermally-Irreversible Spectral Changes.—The spectral changes described hitherto are thermally reversible, *i.e.*, gradual cooling from -100 to -160° transforms the spectrum of IB as shown in

(3) (a) Part I, Y. Hirshberg and E. Fischer, *J. Chem. Soc.*, 297 (1954); (b) Part II, *ibid.*, 3129 (1954).

Fig. 2a, while gradual heating from -160 to -100° causes the same change in the reverse direction. This cycle can be repeated again and again, the reversibility indicating that a thermal equilibrium is established at each temperature. The spectrum corresponding to this thermal equilibrium also is obtained when a colorless solution of IA is irradiated with ultraviolet light at any temperature in the above range.

If, however, the colored form of I is formed at -180° by ultraviolet irradiation of IA at this temperature, its spectrum is different from that of the dye obtained by ultraviolet irradiation at -100° and subsequently cooled to -180° , as shown in Fig. 3a. In curve 1, the ratio between the intensities of the peaks at 530 and 560 $m\mu$ is even smaller than at -100° , and corresponds to the hypothetical ratio at some higher temperature. (This cannot be proved experimentally because above -100° thermal transformation into the colorless IA sets in.) When the dye produced by irradiation at -183° (Fig. 3a, curve 1) is gradually heated, it is transformed spontaneously, between about -160° and -150° , into the dye formed by irradiation at this temperature. Recooling to -183° causes only minor changes in the spectrum. Spectra 1 and 2 of Fig. 3a are seen to differ in their absorption not only in the visible but also in the ultraviolet. Ultraviolet irradiation of IA in a methylcyclohexane-isopentane rigid glass at -183° thus is seen to result in a spectrum corresponding to a non-equilibrium state which is frozen-in under these conditions. At temperatures above -160° this spectrum changes spontaneously into that corresponding to an equilibrium state. Cooling of this latter form to -183° results in its being frozen-in at the equilibrium corresponding to -160° . In a mixture of methylcyclohexane and decalin, which is more viscous and reaches rigidity already at somewhat higher temperatures, the non-equilibrium state seems to be frozen-in already at -150° , as shown in Fig. 3c. Similar phenomena were observed with solutions of compound IV, with the results shown in Fig. 3b and 3d. In all these cases the non-equilibrium form of the dye can be created only by ultraviolet irradiation of the solutions in rigid glasses at sufficiently low temperatures. As will be described in detail in Part V of this series, those colored forms of both I and IV which are obtained by irradiation at -183° (full curves in Fig. 3), and only they, can be made to revert into the corresponding colorless forms by irradiation with visible light at this temperature. This is another manifestation of the profound difference between these dyes and those corresponding to the broken curves of Fig. 3, which can be "erased" by visible light only very slowly and to a slight extent.

Discussion

The effect of solvent on the frequency of absorption bands has been studied extensively for dyes in general⁴⁻⁶ and for merocyanines in particular.⁷⁻¹⁵

- (4) N. S. Bayliss, *J. Chem. Phys.*, **18**, 292 (1950).
 (5) N. S. Bayliss and E. G. McRae, *J. Phys. Chem.*, **58**, 1002 (1954).
 (6) A. L. Le Rosen and C. E. Reid, *J. Chem. Phys.*, **20**, 232 (1953).

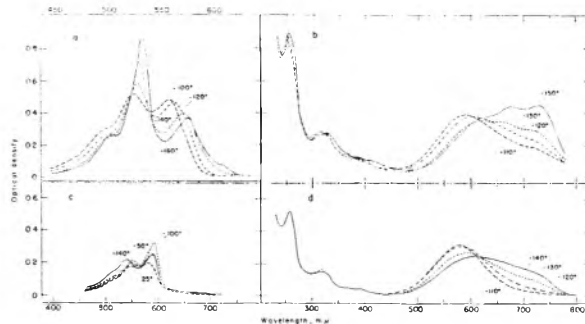


Fig. 2.—Reversible temperature dependence of spectra of merocyanines in non-polar solvents. (a) Compound IB in methylcyclohexane-petrol ether 1:1, 0.9×10^{-6} mole/l. (corrected for solvent contraction); (b) compound IVB in methylcyclohexane-isohexane 1:1, 2.2×10^{-5} mole/l.; (c) compound II in methylcyclohexane-toluene 1:1, 6.0×10^{-5} mole/l.; (d) compound IVB in methylcyclohexane-decalin 1:1, 1.1×10^{-6} mole/l.

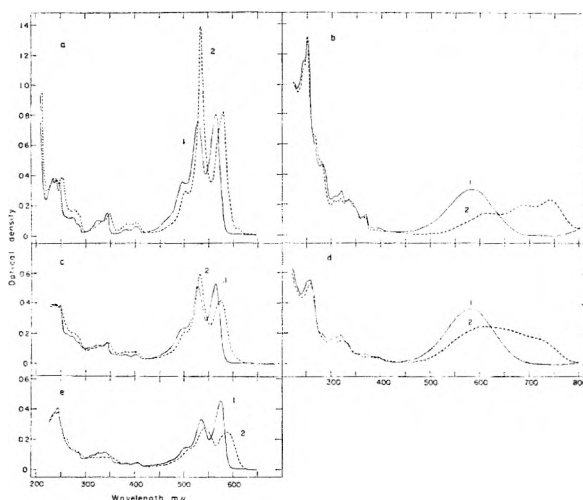


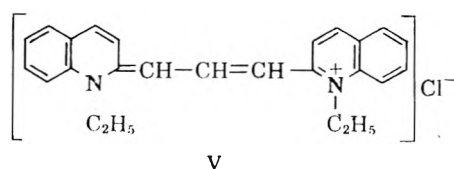
Fig. 3.—Spectra of merocyanines in non-polar solvents: full curves, formed by ultraviolet irradiation at low temperatures in rigid media; broken curves, warmed up and recooled. (a) Compound IB in methylcyclohexane-isohexane 1:1, 0.40×10^{-6} mole/l. (in a cell of 27 mm. light path): 1, formed by irradiation with 365 $m\mu$ at -183° ; 2, warmed to -120° and recooled to -183° ; (b) compound IVB in methylcyclohexane-isohexane 1:1, 2.2×10^{-5} mole/l.: 1, formed by irradiation with 365 $m\mu$ at -183° ; 2, warmed to -140° and recooled to -183° ; (c) compound IB in methylcyclohexane-decalin 1:1, 0.9×10^{-6} mole/l.; 1, irradiated with 365 + 313 + 303 $m\mu$ at -150° ; 2, warmed to -100° and recooled to -150° ; (d) compound IVB in methylcyclohexane-decalin 1:1, 1.1×10^{-6} mole/l.; 1, irradiated with 365 $m\mu$ at -150° ; 2, warmed to -110° and recooled to -150° ; (e) 5-methoxy-derivative of IB in methylcyclohexane-isohexane 2:1, 0.8×10^{-5} mole/l.: 1, irradiated with 365 + 313 + 303 $m\mu$ at -180° ; 2, warmed to -140° and recooled to -180° .

Observed shifts in frequency were correlated with solute-solvent interactions and their dependence

- (7) L. G. S. Brooker and R. H. Sprague, *J. Am. Chem. Soc.*, **63**, 3214 (1941).
 (8) L. G. S. Brooker and W. T. Simpson, *Ann. Rev. Phys. Chem.*, **2**, 121 (1951).
 (9) L. G. S. Brooker, *et al.*, *J. Am. Chem. Soc.*, **73**, 5332 (1951).
 (10) L. G. S. Brooker, G. H. Keyes, and D. W. Helseltine, *ibid.*, **73**, 5350 (1951).
 (11) E. B. Knott, *J. Chem. Soc.*, 3038 (1951).
 (12) J. R. Platt, *J. Chem. Phys.*, **25**, 80 (1956).
 (13) E. G. McRae, *Spectrochim. Acta*, **12**, 192 (1957).
 (14) E. G. McRae, *J. Phys. Chem.*, **61**, 562 (1957).
 (15) J. R. Platt, *J. Chem. Phys.*, **34**, 862 (1961).

on the dielectric constant and refractive index of the solvent, as well as with intermolecular hydrogen bonding. Similar considerations probably are valid for the spectra of the colored forms of the spiro-pyrans.

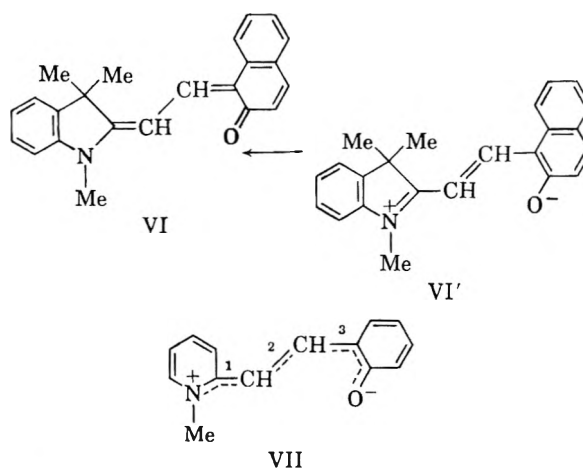
Before an attempt is made to interpret the effect of solvents on the shape of the absorption spectra, and in particular on the ratio between the intensities of various bands, the nature of such bands should be elucidated. The complex structure of absorption spectra, such as that of IB in the visible region (Fig. 1a), usually is interpreted as vibrational fine structure. The fact that spectra in polar solvents are often less complex than those in non-polar solvents was ascribed to obliteration of the vibrational structure, due to non-establishment of vibrational quantization during the lifetime of the "Franck-Condon excited state."^{5,16} However, it is difficult to explain in a similar way the solvent effects observed in spectra of compounds IB-IVB, Fig. 1, which involve wide variations in the relative height of the main absorption bands in the visible. The same holds with regard to the temperature dependence of the absorption spectra observed in non-polar solvents. Here, too, it is improbable that the variations in the population of the vibrational energy levels are responsible for the observed pronounced spectral changes. A more plausible explanation of both solvent and temperature effects seems to be offered by an assumption of the existence of several modifications of the colored form, the equilibrium among which is affected by temperature and by interaction with the solvent. Such an equilibrium may be either between monomers, dimers, and higher aggregates, or between various stereoisomers. The first explanation was forwarded by Scheibe,¹⁷ for similar variations observed in the spectra of aqueous solutions of ionic dyes, such as V, with increasing concentration or decreasing temperature. The cations



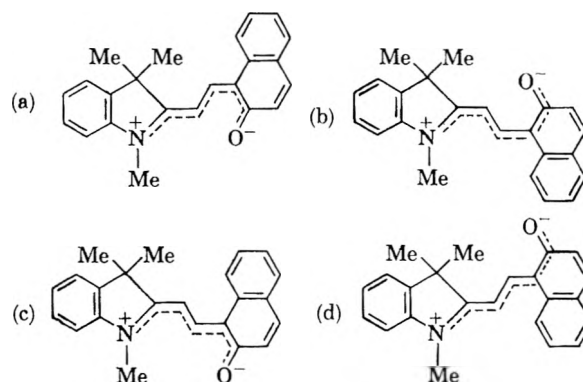
of these dyes are symmetrical structures, resembling the left-hand (heterocyclic) half of IB. Similar effects were reported by Rabinowitch and Epstein¹⁸ for solutions of thionine and of methylene blue in alcohol-ether mixtures, by Zanker^{19,20} for solutions of acridine orange, and by Bartels²¹ for aqueous solutions of "neutral red" (a phenazine dye).

Despite the similarity of the effect of temperature on the spectra in these cases and in the present experiments, the polymerization hypothesis does not appear to be applicable here, because no concentration dependence of the spectrum was observed in non-polar solvents in the concentration

range 5×10^{-6} to 5×10^{-4} mole/l. This may be compared with the results of Scheibe, who found strong effects with compound V in the same range of concentrations. The existence of equilibria between various stereoisomers has been postulated to explain environmental effects on the ratio between neighboring peaks of absorption spectra, in solutions of dyes, such as crystal violet (Lewis, *et al.*²²). As pointed out in an earlier publication³ and by Chaudé,²³ the methine bridge in IB, IVB, and similar compounds gives rise to several possible stereoisomers, as, owing to the mesomerism between the two extreme forms VI and VI', the order of the three bonds of this bridge is higher than unity.



Chaudé and Masse²⁴ calculated the bond indexes for the carbon-carbon π bonds 1, 2, and 3, of the related hypothetical compound VII to be 0.475, 0.783, and 0.468. For compound IB the following four isomers might exist without appreciable steric hindrance (since they are all *trans* with respect to the central bond 2)



In compound IIB only two such stereoisomers are possible because of the symmetrical structure of the left-hand, acridine, part of the molecule. A thermal equilibrium then would be expected to

(16) V. Zanker and F. Mader, *Chem. Ber.*, **93**, 850 (1960).

(17) G. Scheibe, *Kolloid Z.*, **82**, 1 (1938).

(18) E. Rabinowitch and L. Epstein, *J. Am. Chem. Soc.*, **63**, 69 (1941).

(19) V. Zanker, *Z. physik. Chem.*, **199**, 4 (1952).

(20) V. Zanker, *ibid.*, **200**, 250 (1952).

(21) P. Bartels, *Z. physik. Chem. (Frankfurt)*, **9**, 95 (1956).

(22) G. N. Lewis, T. T. Magel, and D. Lipkin, *J. Am. Chem. Soc.*, **64**, 1774 (1942).

(23) O. Chaudé, These, "Etude spectrophotométrique de l'isomérisation de divers spiranes thermochromes," Edition de la Revue d'Optique, 1954.

(24) O. Bloch-Chaudé and J. L. Masse, *Bull. soc. chim. France*, 625 (1955).

exist between these isomers, and perhaps also between some sterically hindered isomers which are in the *cis* form with respect to the central bond 2. The position of this equilibrium and its change with temperature depend on the difference in free energy and in enthalpy between the isomers.

In considering the relative stability of various isomers the electrostatic attraction between the opposite charges $N(\delta^+)$ and $O(\delta^-)$ also must be taken into account. In isomers a-d the steric hindrance is small,²³ and the stability of the compound therefore will increase with the decrease of the distance between (δ^+) and (δ^-) . If it is assumed²³ that all interatomic distances are 1.4 Å and all angles 120°, the distance between the nitrogen and the oxygen atom will be 4.2 Å. in (a), 4.9 Å. in (b) and (c), and 6.0 Å. in (d). According to this criterion isomer (a) should be the most stable one. In the "*cis*" isomers this distance is of course much smaller, and therefore the electrostatic attraction larger, but steric interference much more pronounced.

Assignment of spectra to the different isomers is not certain and therefore no quantitative interpretation of the variation of relative intensities of absorption bands is attempted. Thermal equilibrium among at least some of the possible isomers appears to be established down to very low temperatures, as shown in Fig. 2, where the spectra are seen to change continuously down to about -160° in methylcyclohexane-isopentane, and to about -145° in the more viscous methylcyclohexane-decalin mixture. At still lower temperatures the spectra do not change any more, indicating freezing-in of the equilibrium. This inhibition of equilibration between the stereoisomers probably is due also to the sharp increase in viscosity in these temperature regions, where both solvent mixtures form rigid glasses. The high viscosity may be expected to impede the motion of large groups within the molecule, which must occur during interconversion of isomers.

At the moment of formation of the dye by ultraviolet irradiation of the spiropyran, and the resulting rupture of the carbon-oxygen bond, the dye molecule is probably in an unstable form X, in which the oxygen atom and the original spiranic carbon atom are still close to each other. This sterically unstable isomer then undergoes a series of rearrangements involving the methine bridge, and leading eventually to an equilibrium mixture of some or all of the isomers (a)-(d), as well as X. As pointed out above, these rearrangements involve comparatively large movements of one-half of the molecule in relation to the other one. The combined effect of low temperature and very high viscosity of the medium therefore may be expected to slow down or even prevent this rearrangement, and thus freeze-in the unstable isomer X immediately following its formation.

These expectations are borne out by the experiments illustrated in Fig. 3, which show the result of ultraviolet irradiation of the spiropyran in rigid media, such as mixtures of methylcyclohexane and isohexane at -180°, or methylcyclohexane and decalin at -150°. Such irradiation results in the

formation of a colored modification whose absorption spectrum is quite different from that of the dye formed from the above after it had been heated to about -150° (or -120° in the m.c.h.-decalin mixture) and then recooled to the original low temperature. Such heating results in establishment of thermal equilibrium between the different stereoisomers, the equilibrium then being frozen-in by recooling.

Additional evidence in favor of the above conclusions is furnished by the observation (to be described in detail in Part V of this series) that the dye produced in the rigid glass is reconverted into the spiropyran by irradiation with visible light under the same conditions. This is not the case with the dye formed from the previous one on heating and recooling. Another feature of the spectrum of the dye formed on ultraviolet irradiation in the rigid glass is its similarity to the spectrum observed at the highest temperature at which the dyes are not yet converted spontaneously into the spiropyran (about -100°). This is seen from comparison of the "high temperature" curves in Fig. 2 with the "rigid glass" full curves in Fig. 3. Hence it can be assumed that the species formed by irradiation in a rigid medium is a high-energy isomer. One should, however, bear in mind that all the postulated stereoisomers probably have rather similar spectra, and the similarity of the above spectra does not necessarily prove the identity of the corresponding isomers.

The over-all picture emerging from the above discussion thus may be summarized as follows: Ultraviolet irradiation of the spiropyran results in formation of an unstable isomer, X, of the colored modification. In media whose viscosity is below a certain limit most of this isomer is immediately converted into other, more stable isomers, the equilibrium between the various isomers being established as long as the viscosity of the medium does not exceed that limit. However, in a rigid medium at low temperature the high viscosity of the medium and the low energy content of the dye molecule combine to prevent the spontaneous conversion of X into the other isomers. In fluid media a tiny fraction of the dye exists in the form of X, this fraction increasing with temperature because of the higher energy of X. Only this isomer is photoconvertible into the spiropyran by visible light. Photoconversion of all the dye thus will proceed as long as the thermal equilibration between X and the various other isomers of the colored modification takes place at a sufficiently high rate. When this equilibrium mixture is frozen by cooling to rigidity, visible light can transform into the spiropyran only that small fraction of the dye which is in the form of X. On the other hand, if the dye is formed from the spiropyran by ultraviolet irradiation in a rigid medium, most of it remains in the form of X, and therefore is photoconvertible by visible light.

In an alcoholic solution the contribution of the dipolar mesomeric structure is higher than in non-polar solvents, owing to interaction with the polar solvent. In addition one of the stereoisomers may be preferentially stabilized by solvation, the

resulting adduct being sensitive to visible light. This accounts for the absence of pronounced effects of cooling on the absorption spectra of the dyes and on the rate of their photoconversion into spiropyrans by visible light in alcoholic solution.

Experimental

Irradiations and spectrophotometric measurements were carried out in special dewar-type quartz cells, in a Cary

Model 14 recording spectrophotometer. Complete details are given in Part III of this series and in earlier publications. Experiments at the temperature of liquid air were carried out with the absorption cell placed in a specially constructed copper block cooled by liquid air. The copper block with the cell was placed in a silica dewar flask with optical windows.

Acknowledgments.—The authors wish to thank Mr. M. Kaganowitch for synthesizing the compounds investigated, and Mrs. N. Castel for technical assistance.

PHOTOCHROMISM IN SPIROPYRANS. PART V.¹ ON THE MECHANISM OF PHOTOTRANSFORMATION

BY RAHEL HEILIGMAN-RIM, YEHUDA HIRSHBERG, AND ERNST FISCHER

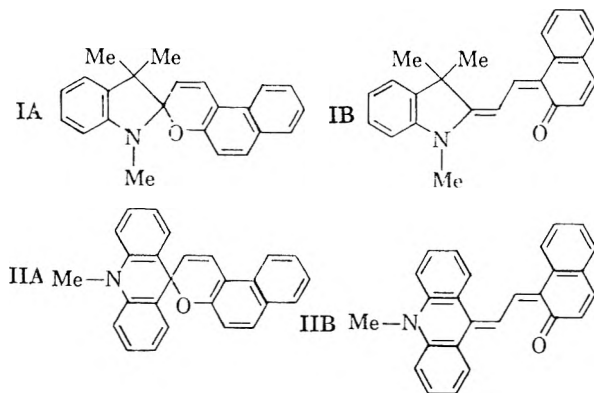
Laboratory of Photochemistry and Spectroscopy, The Weizmann Institute of Science, Rehovoth, Israel

Received May 25, 1962

Phototransformations spiropyran \rightarrow merocyanine and merocyanine \rightarrow spiropyran have been studied in some photochromic spiropyrans under varying environmental conditions. The dependence of the rates of these processes on the temperature and the chemical nature and viscosity of the solvent was observed. The relative and absolute quantum yields of both processes at different frequencies of the photoactive light were determined. The results indicate the occurrence of consecutive and concurrent phototransformations and thermal interconversions between stereoisomers of the colored modification, besides the "main" phototransformation spiropyran \rightleftharpoons merocyanine.

Introduction

The general ideas about thermochromism and photochromism have been summarized in previous publications,²⁻⁶ and in the introduction to the preceding paper (Part IV). The photochromic spiropyrans to be dealt with here are exemplified by compounds IA (1,3,3-trimethylindolinonaphthospiropyran), and IIA (N-methylacridinonaphthospiropyran), which are transformed by the action of ultraviolet light into strongly colored modifications usually represented by merocyanine-like formulas, such as IB and IIB



The B modifications can be converted into the A ones by irradiation with visible light. The number of π electrons in a merocyanine molecule exceeds by two their number in a spiropyran. The merocyanine molecule is planar, while the planes of the

two parts of the spiropyran molecule are approximately perpendicular to each other. The photoisomerization spiropyran \rightarrow merocyanine thus involves two aspects: (1) delocalization of two σ electrons, following excitation, and resulting in breaking of the C-O bond; (2) rearrangement of the methine chain and rotation of the two parts of the molecule in relation to each other so as to approach coplanarity. Such a process appears fairly plausible as soon as the energy required for delocalization of the C-O bond electrons is supplied either in the form of thermal energy or as radiation energy. The transformation in the reverse direction, B \rightarrow A ("ring closure"), involves the same two aspects, *i.e.*, two electrons have to be demoted and the molecule has to be induced to undergo the rearrangements in the methine chain and the relative rotation of the two parts of the molecule before a spiropyran molecule can be reformed. Processes A \rightarrow B and B \rightarrow A thus seem to be basically different, with B \rightarrow A being *a priori* less probable. This also is confirmed by the fact that radiative ring opening has been observed with all thermochromic and many non-thermochromic spiropyrans, whereas radiative ring closure by visible light was found hitherto only in spiropyrans derived from indoline, such as I, or from acridine, such as II.⁷ However, radiative ring closure by ultraviolet light does seem to take place, as shown by the incomplete conversion A \rightarrow B under the action of ultraviolet light, which probably is due to simultaneous occurrence of both A \rightarrow B and B \rightarrow A.

The experiments reported here on the temperature dependence of the rates of photoisomerization reactions in both directions and the determination of their quantum yields were undertaken in an at-

(1) Part IV, *J. Phys. Chem.*, **66**, 2465 (1962).
 (2) E. Fischer and Y. Hirshberg, *J. Chem. Soc.*, 4522 (1952).
 (3) (a) Part I, Y. Hirshberg and E. Fischer, *ibid.*, 297 (1954);
 (b) Part II, *ibid.*, 3129 (1954).
 (4) Y. Hirshberg, E. H. Frei, and E. Fischer, *ibid.*, 2184 (1953).
 (5) Y. Hirshberg, *J. Am. Chem. Soc.*, **78**, 2304 (1956).
 (6) Part III, R. Heiligman-Rim, Y. Hirshberg, and E. Fischer, *J. Chem. Soc.*, 156 (1961).

(7) However, recent experiments in this Laboratory showed that such ring closure with visible light does take place with certain bipyropyrans, containing only oxygen as hetero-atoms, under specific conditions.

TABLE I
HALF-LIFE TIMES, (MIN.) OF COLOR ERADICATION WITH "VISIBLE" LIGHT

Temp., °C.	-100	-110	-120	-130	-140	-150	-183
IB (MCH-IP)	6	100	200	∞	∞	∞	∞
IB (MCH-IH)	28	63	150	∞	∞	∞	∞ (132) ^a
IB (MCH-D)	13	25	...	80	100	∞ (24) ^a	∞
IIB (MCH-MCP)	160	(8) ^a
IIB (MCH-D)	..	43	43	53	68	260 (3) ^a	

^a Data in parentheses are explained in the following paragraph.

tempt to gain insight into the mechanism of these processes.

Results

1. Temperature Dependence of the Phototransformation A → B.—The rate of color formation by irradiation with ultraviolet light at either 365, 313, or 303 mμ was found to decrease slightly on cooling both in non-polar solvent mixtures (methylcyclohexane with either isopentane, isohexane, iso-octane, methylcyclopentane, or decalin) and in alcoholic solvents (ethanol with methanol, 1-propanol with 2-propanol). Thus for compound IA, with the same light source used throughout most of these experiments, half-life times of color formation were found to increase gradually from about 1.5 min. at -100° to 9 min. at -183° in methylcyclohexane-isohexane, and from 1.2 min. at -100° to 2.2 min. at -150° in methylcyclohexane-decalin. Similar results were obtained also in alcoholic solutions of this compound in the range -100 to -150°. With compound IIA retardation of color formation by cooling is more pronounced in both types of solvents. Thus, in methylcyclohexane-decalin the half-life times of color formation brought about by irradiation with the light of 365 + 313 + 303 mμ lines increase gradually from 2 sec. at -100° to 28 sec. at -150°. All the above solvent mixtures form rigid glasses at sufficiently low temperatures within the above-mentioned temperature range. It appears that this fact has no pronounced effect on the rate of merocyanine formation.

2. Temperature Dependence of the Phototransformation B → A.—As mentioned in the Introduction, the phototransformation B → A is of special interest, and the results therefore will be described at some length.

(a) **Temperature Dependence of the Process B → A with Visible Light.**—In all non-polar solvents the rate of this process is strongly reduced by lowering of the temperature. Table I summarizes the results obtained with compounds IB and IIB, in the form of half-life times of spiropyran formation. The concentration of the latter was followed at the characteristic sharp absorption peak in the ultraviolet.⁶ Irradiation was carried out with the light emitted by a mercury arc above 410 mμ, *i.e.*, in practice the three lines at 436, 546, and 578 mμ. (It was found that the ratio between the quantum yields of light at 546 and 436 mμ in non-polar solvents was not affected by change of temperature.) In all cases B was formed by ultraviolet irradiation at -100° for IB, at -110° for IIB and the solution then was cooled to the required temperature. Solvent mixtures used were methylcyclohexane (MCH) with either methylcyclopentane (MCP), isohexane (IH), or isopentane (IP) (all these mix-

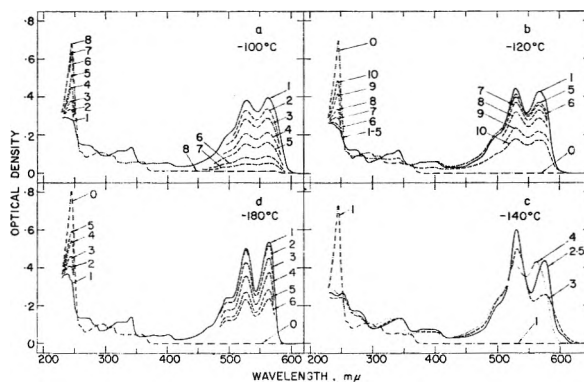


Fig. 1.—Compound I, 0.75×10^{-5} mole/l. in MCH-IH (2:1), irradiated with visible light at different temperatures; full lines, IB; broken lines, consecutive stages of irradiation; dash-dot lines, IA. (a), (b), and (d), irradiated with 578 + 546 + 436 mμ; (c), irradiated with 578 mμ (curve 3), heated to -110° (curve 4), and recooled to -140° (curve 5, identical with curve 2).

tures form rigid glasses at the temperature of liquid air), and methylcyclohexane with decalin (D) (this mixture forms a glass which tends to crack at temperatures below -160°). Actual absorption spectra in the course of irradiation are shown in Fig. 1a, 1d, and 3d, where the increase in the intensity of the ultraviolet and the decreases in the intensity of the visible bands are shown to run parallel. Deviations from this behavior are dealt with later on.

The data in Table I show that in all non-polar solvent mixtures the rate of B → A decreases on cooling, and approaches zero somewhere between -120° and -145°. The first two mixtures are fluid down to -135°, whereas the MCH-D mixture is highly viscous already at -100°. In solutions in alcohols the rate of formation of spiropyran from the corresponding merocyanine is little affected by variation of temperature when the process is brought about by irradiation with light at 546 and 578 mμ. Typical results for the process IB → IA in ethanol-methanol, effected by irradiation with light at 546 mμ, are given in Table II in the form of half-life times of color eradication at various temperatures.

TABLE II

HALF-LIFE TIMES, MIN.					
Temp., °C.	-95	-105	-120	-140	-155
Time, min.	6.5	6	5	7	12.5
					24

The rate of color eradication passes through a shallow maximum between -105 and -120° and then decreases slowly on further cooling. The same trend was observed with light at 578 mμ. However, when the process is brought about by

irradiation with light at 436 $m\mu$ the temperature dependence of its rate is different: after passing through a similar maximum at -115 to -120° its rate is sharply slowed down by further cooling and approaches zero already at -140° . In alcoholic solutions the formation of spiropyran runs strictly parallel to the disappearance of color during irradiation of B with visible light, throughout the temperature range investigated, -95 to -150° . It should be recalled here that in solutions in non-polar solvents the shape of the spectrum of the merocyanine is strongly temperature dependent while in alcoholic solutions it is altogether unaffected by variations of temperature.¹

(b) **Phototransformation $B \rightarrow A$ Effected by Visible Light in Rigid Media at Low Temperature.**

—In the experiments described in the preceding paragraph, B always was formed from A by ultraviolet irradiation at about -100° , at which temperature all solvent mixtures are fluid. However, as shown in the preceding publication, if the process $A \rightarrow B$ is carried out in a rigid medium at -183° , B created under these conditions is spectroscopically different from the B formed at -100° and then cooled to -183° . In solutions in a MCH-D mixture a similar behavior is observed already at about -155° (cf. Fig. 3 in the preceding paper). These colored modifications, denoted by X, proved to be photoconvertible into the corresponding spiropyrans by visible light. Figure 1d describes a typical experiment at -183° in which spiropyran formation and dye eradication are seen to run parallel, exactly as at -100° (Fig. 1a). Figure 3d shows a similar behavior in compound IIB irradiated with light at 546 $m\mu$ at -183° . Moreover, from the kinetics apparent from Fig. 2d, it seems that under these conditions at least a large part, if not all, of B is reconvertible into A. It is particularly striking to compare the comparatively rapid photoconversion $IB \rightarrow IA$ at -183° , at which temperature the medium forms a rigid glass, with the virtual absence of this reaction at -130° , where the medium is still fluid. $IIB \rightarrow IIA$ at -183 is still more rapid (half-life time 8 min. under irradiation with light at 546 $m\mu$). Some relevant results are given in Table I, in parentheses, and show that in compound IB the half-life time of color eradication under these conditions is about five times longer than at -100° , whereas in IIB it is even shorter than at -110° .

In solutions in a MCH-D mixture this phenomenon occurs already at -150° . It should be recalled here that if the X form is heated to about -165° (in MCH-IH), it is transformed spontaneously into the B modification, and cannot be re-formed by cooling.

(c) **Phototransformation $B \rightarrow A$ under the Action of Ultraviolet Light.**—There is no direct proof for the occurrence of the transformation $B \rightarrow A$ under the action of ultraviolet light on compounds IB and IIB as there is no way of isolating these compounds or of achieving complete transformation of IA and IIA into IB and IIB. In this case the existence of this process can only be deduced indirectly from the fact that the process $A \rightarrow B$ does not go to completion. In reversible

photoisomerizations photoequilibrium is established when the rates of the two opposing photoreactions $A \rightleftharpoons B$ under the action of the particular photoactive light used, are equal. Hence, in the ab-

sence of $B \xrightarrow{u.v.} A$ the reaction $A \xrightarrow{u.v.} B$ should go to completion and the conversion of A into B should be complete. Since this is not the case, $B \xrightarrow{u.v.} A$ must be inferred to occur. Moreover, if the ratio between the yields of the two processes $A \xrightarrow{u.v.} B$ and

$B \xrightarrow{u.v.} A$ would vary with temperature, this should affect the state of photoequilibrium. No pronounced temperature effect of this sort has been observed in I and II with light at 365 or 313 $m\mu$ in either solvent and it thus may be deduced that the rate of $B \xrightarrow{u.v.} A$ does not depend on temperature to any appreciable extent.⁸ Thus, in this respect the behavior of ultraviolet light, in a non-polar solvent, seems to differ from that of visible light described in section 2a.

(d) **Phototransformation of the Merocyanine Modification B Not Involving Formation of Spiropyrans ("Ring Closure").**

—As described in section 2a, the phototransformation of B into A by visible light in non-polar solvents is slowed down on cooling and virtually stops around -140° . However, at such temperature another effect is observed as a result of irradiation with visible light, as shown in Fig. 1c for compound IB. Irradiation at 578 $m\mu$ causes pronounced changes throughout the visible and near-ultraviolet region, but has no effect on the absorption in the region of the characteristic spiropyran band around 245 $m\mu$. It thus appears that a sort of "internal" photoisomerization within the

merocyanine, $B \xrightarrow{vis.} B'$, *i.e.*, photoisomerization between different stereoisomers of the colored form, takes place, proceeding with a much higher ef-

iciency than $B \xrightarrow{vis.} A$ and without retardation by cooling. Thus, the half-life of the change depicted in Fig. 1c is about 3 min. at -140° and practically also at -130 and -150° . This may be compared with a half-life of about 45 min. observed for $B \xrightarrow{vis.} A$ at -100° under otherwise similar conditions.

If a solution thus changed by visible irradiation at -140° is gradually warmed up, the above change reverts, the rate of this reversion increasing with temperature. For the case described in Fig. 1c this reversion is complete within a few minutes at -110° . As a result the original merocyanine spectrum is re-formed, and recooling to -140° results only in the usual temperature effect on the spectrum (cf. Part IV). A complete cycle is thus performed as follows: "color formation" by ultraviolet irradiation at -140° (curve 2), "color change" by visible irradiation at -140° (curve 3), heating to -110° (curve 4), and recooling to -140° (curve 5, identical with 2). All steps except the first one involve only the merocyanine.

(8) The occurrence both of the process $B \xrightarrow{u.v.} A$ and of the temperature dependence of the position of photoequilibrium has been proved in certain nitro derivatives of benzospiryran, which will be reported in the following part in this series.

Visible irradiation at temperatures above -140° causes two concurrent photoreactions, namely, $B \rightarrow A$ and $B \rightarrow B'$, as illustrated in Fig. 1b for -120° . An initial rapid change in the visible, without any change around $245 \text{ m}\mu$, is followed by a slower change in both regions. Exact and rapid measurements indicate a similar behavior even at -100° , though here $B \rightarrow B'$ is of course over-

shadowed by both $B \rightarrow A$ and $B' \rightarrow B$ (thermal reaction). Kinetic curves for all photoreactions described are shown in Fig. 2. Figures 3b and 3c show similar interconversions of the stereoisomers of IIB running concurrently with processes $IIB \rightarrow$

IIB $\xrightarrow{\text{u.v.}}$ IIA and $IIA \xrightarrow{\text{u.v.}}$ IIB.

3. Quantum Yields. (a) **Relative Quantum Yields of $A \rightarrow B$ and $B \rightarrow A$.**—In case of interconversion of two isomers A and B under the action of light, the photoequilibrium established by irradiation with light at any particular wave length, λ , depends only on the molar extinction coefficients ϵ of the two isomers at the particular λ , and on the quantum yields $\varphi_{A \rightarrow B}$ and $\varphi_{B \rightarrow A}$ of the photoconversion in both directions.⁹

Since at equilibrium the rates of reaction in both directions are equal

$$[A]\epsilon_A\varphi_A = [B]\epsilon_B\varphi_B$$

and therefore the equilibrium constant K is given by

$$K = \frac{[A]}{[B]} = \frac{\varphi_B\epsilon_B}{\varphi_A\epsilon_A}$$

and the ratio between the quantum yields in both directions is

$$\frac{\varphi_A}{\varphi_B} = \frac{[B]\epsilon_B}{[A]\epsilon_A}$$

Since both the merocyanine and the spirocyanine absorb in the ultraviolet, the irradiation of a spirocyanine with ultraviolet light results, at photoequilibrium, in incomplete conversion into the merocyanine.⁶ The ratio of the quantum yields of the reactions in the two opposite directions φ_A/φ_B can be calculated from the above equation. The values of

TABLE III

Compound	Solvent	φ_A/φ_B at -100°	φ_A/φ_B at -180°
(I) at $313 \text{ m}\mu$	MCH-IH	5	5
	alcohol	10	...
(I) at $365 \text{ m}\mu$	MCH-IH	2.5	2.5
	alcohol	6.5	...
(II) at $365 \text{ m}\mu$	MCH-D	10	10
	alcohol	3.5	...

φ_A/φ_B thus calculated from results obtained for I photoequilibrated by light at 365 and at $313 \text{ m}\mu$, and for II photoequilibrated by light of $313 \text{ m}\mu$, at -100° and -180° , are given in Table III. In all cases the efficiency of ultraviolet light in

(9) (a) G. Zimmerman, *et al.*, *J. Am. Chem. Soc.*, **80**, 3528 (1958); (b) E. Fischer, *ibid.*, **82**, 3249 (1960); (c) D. Schulte-Frohlinde, *Ann.*, **615**, 114 (1958).

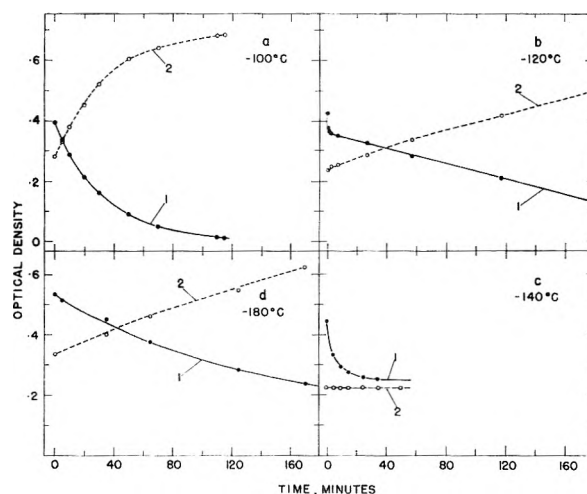


Fig. 2.—Temperature dependence of the kinetics of phototransformation of IB brought about by irradiation with visible light (cf. Fig. 1); full lines, variation of IB concentration, followed by optical density at $565 \text{ m}\mu$; broken lines, formation of spirocyanine IA followed by the changes in optical density at $245 \text{ m}\mu$. (a), (b), and (d), irradiated with $578 + 546 + 436 \text{ m}\mu$; (c), irradiated with $578 \text{ m}\mu$.

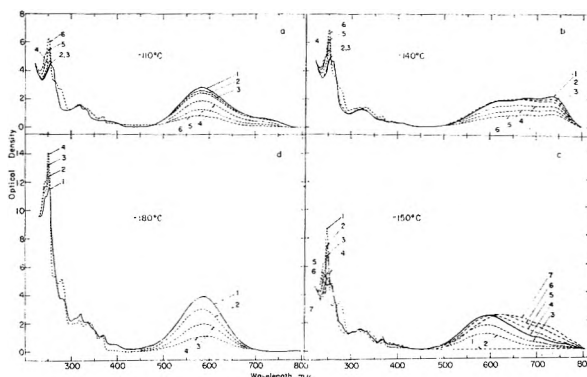


Fig. 3.—(a), (b), (d), compound IIB irradiated with visible light at different temperatures; full lines, before irradiation; broken lines, consecutive stages of irradiation. (a), (b), 1.1×10^{-5} mole/l. in MCH-D, irradiated with $578 + 546 + 436 \text{ m}\mu$; (d), 2.2×10^{-5} mole/l. in MCH-IH, irradiated with $546 \text{ m}\mu$; (c), IIA, 1.1×10^{-5} mole/l. in MCH-MCP, irradiated with $365 \text{ m}\mu$; curves, 5, 6, and 7 show interconversion of stereoisomers of IIB.

ring opening is seen to be higher than in ring closure.

The values given above are subject to the uncertainty in the equilibrium constant $[A]/[B]$ and in ϵ_B as described before.⁶ In compounds I and II the ratio φ_A/φ_B practically does not change with temperature.

(b) **Relative Quantum Yields of $B \rightarrow A$ at Different Wave Lengths.**—The spirocyanine A does not absorb in the visible region, $\epsilon_A = 0$, and φ_A obviously has no meaning. It is however of interest to compare the relative φ_B 's at various wave lengths in the visible region. Qualitative investigations reported earlier⁵ from this Laboratory were now repeated and analyzed quantitatively under well defined conditions, as described in the following section. The results may be summarized as follows: in non-polar solvents the yields at the four wave lengths investigated (the mercury emis-

sion lines at 405, 436, 546, and 578 $m\mu$) were identical within a factor of two, all of them decreasing on cooling; in alcoholic solutions in the presence of triethylamine (added as a weak base) the situation with respect to the ratio between the quantum yields at different wave lengths is similar; however, in the absence of a base, even in alcohol freshly distilled from potassium hydroxide, the efficiency of light at 436 $m\mu$ was 30–80 times higher than that of light at 546 or 578 $m\mu$, corroborating our earlier results.⁵ The range 30–80 is given here because values depend strongly on the alcohol used. Moreover, in such solutions the yield with light at 436 $m\mu$ falls sharply on cooling, and below about -130° approaches zero, whereas with light at 546 or 578 $m\mu$ the yield is substantially independent of temperature (cf. section 2a above).

(c) Calculation of the Relative Quantum Yields.

—The intensity I_λ of the incident monochromatic light of wave length λ (expressed as the number of light quanta per minute), the transmission T_λ of the solution at the same wave length, and the observed half-lives $\tau_{1/2}$ of the process

$B \xrightarrow{\text{vis.}} A$ were used as follows: under otherwise identical conditions the yields at various λ 's are inversely proportional to the numbers of light quanta Q_λ absorbed during $\tau_{1/2}(\lambda)$. During any infinitesimal time interval dt the number of quanta absorbed is $I_\lambda(1 - T_\lambda)dt$. During finite periods of irradiation the change of T_λ with time has to be taken into account by replacing $(1 - T)$ by

$$1 - (1/\tau_{1/2}) \int_0^{\tau_{1/2}} T dt$$

However, an exact evaluation shows that the error introduced by using the arithmetic mean of T_λ instead of the last expression is small in comparison with the experimental errors of the method. The final approximation for the number of quanta absorbed during the interval $\tau_{1/2}$ at any wave length λ is therefore $Q_\lambda \approx I_\lambda(1 - \bar{T}_\lambda)\tau_{1/2}$, where \bar{T}_λ is the average transmission of light at wave length λ during $\tau_{1/2}$. For the present purpose only relative values for I_λ at various wave lengths are needed. These were measured by Bowen's "fluorescent screen" method, as adapted to a somewhat similar purpose by Weber and Teale.¹⁰ This method is based on the observation that the fluorescence yield of rhodamine B is virtually independent of the wave length of the exciting light. The intensity of fluorescence, as measured by a photomultiplier, is therefore proportional to the rate at which quanta at wave length λ hit the solution, i.e., I_λ , and the photocurrent thus can serve as a measure of I_λ . Relative values of I_λ thus measured agree reasonably well with those calculated from the spectral energy distribution data of the mercury arc, given by the manufacturer, and the transmission of the filter combinations used.

(d) Absolute Quantum Yields of $A \xrightarrow{\text{u.v.}} B$ and

$B \xrightarrow{\text{vis.}} A$.—These were calculated from the basic equation given by Zimmerman.^{9a} The intensity of the incident monochromatic light was measured by

ferrioxalate actinometry¹¹ for light of wave lengths up to 436 $m\mu$. The absolute I_λ values for light at longer wave lengths were calculated from those at a shorter wave length and the relative I_λ values measured as described in section 3c above. The quantum yields thus calculated again depend on the accuracy with which ϵ_B and the photoequilibrium constants can be determined. These reservations should be kept in mind when evaluating the results summarized in Table IV for compound I at -100° .

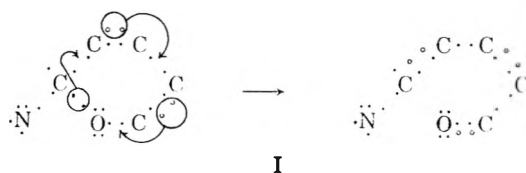
TABLE IV
ABSOLUTE QUANTUM YIELDS AT -100°

Photo-active light, $m\mu$	$\varphi_{A \rightarrow B}$	$\varphi_{B \rightarrow A}$	Solvent
313	5×10^{-2}	5×10^{-3}	Ethanol-methanol
	6×10^{-2}	1×10^{-2}	Non-polar
546	5×10^{-3}	Ethanol-methanol
	5×10^{-4}	Non-polar

Values for $\varphi_{B \rightarrow A}$ at higher temperatures cannot be measured because then thermal isomerization $B \rightarrow A$ sets in. In view of the sharp temperature dependence of $\varphi_{B \rightarrow A}$ in non-polar solvents, described in section 2a, the value of $\varphi_{B \rightarrow A}$ at 546 $m\mu$, given above, must be regarded as valid for -100° only. Higher values probably would be obtained if measurement at higher temperatures were possible.

Discussion

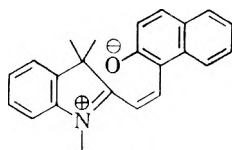
General Conclusions.—The radiative conversion of a spiropyran into a merocyanine involves two aspects: (a) redistribution of charge following electronic excitation and (b) change of molecular configuration. It can be inferred from the absorption spectrum of spiropyrans that the primary electronic excitation leading to $A \rightarrow B$ photoisomerization takes place in the aromatic, naphthopyran, part of the spiropyran molecule. The net result of the change of the electronic structure is the increase of the number of π electrons by two. This result may be represented by scheme I, whereby two σ electrons are transferred to the π electron system of the molecule and the C–O bond is broken



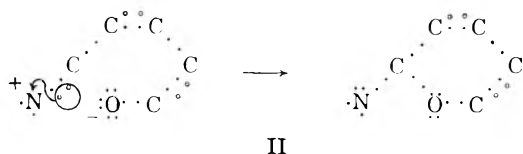
(σ and n electrons are denoted by points, π electrons by circles). The "ring opening" results in the formation of a high-energy isomer of the merocyanine in which the configuration of the spiropyran is still partly retained. In this isomer, designated "X," the distance between the oxygen and the "spiranic" carbon atoms is probably relatively small. This configuration could be related to the *cis* isomer with respect to the central bond in the methine chain, in which the strong steric repulsion

(11) C. G. Hatchard and C. A. Parker, *Proc. Roy. Soc. (London)*, **A236**, 518 (1956).

would be balanced by the electrostatic attraction between the negatively charged oxygen and the positively charged nitrogen or carbon atoms



The $B \xrightarrow{h\nu} A$, or "ring closure," process has hitherto been observed only in nitrogen-containing spiro-pyrans.¹² The net result of the charge redistribution in the course of this process might be represented either by scheme I, in the reverse direction, or alternatively, by scheme II, where the n electrons of the nitrogen atom are involved.



At this stage no attempt will be made to draw conclusions regarding the mechanism of these charge redistributions. The observations reported here pertain largely to the second aspect of the process of photoisomerization—the rearrangement of "X" into the "normal" equilibrium mixture of several stereoisomers of B, all of which are in the *trans* configuration with respect to the central bond of the methine chain.

In Fig. 4, A denotes the spiropyran, and B the equilibrium mixture of the stereoisomers B', B'', B''', and B'''. Reactions are numbered 1 to 20, and can be either thermal ones, denoted by italic numbers, or photochemical ones, denoted by starred numbers.

The following tentative postulates are forwarded to explain the results described above for solutions in non-polar solvents.

(1) At sufficiently low temperatures the rates of 1 and 2 are practically zero and do not have to be taken into account. These are the conditions of "thermal stability of the colored modifications."

(2) There is no direct conversion $A \rightarrow (B', B'', B''', B''')$ or $(B', B'', B''', B''') \rightarrow A$, either thermal or radiative. Steps "11" and "12" are actually superpositions of $1^* + 3$ or $4 + 2^*$, respectively. In other words, a spiropyran can be formed only from that isomer of the corresponding merocyanine which has the right configuration and is therefore "closable."

(3) Steps 4, 6, 8, 10 are slowed down sharply on cooling, to an extent depending somewhat on the nature of the non-polar solvent mixture used. The observed temperature dependence of "12" actually is due to 4, which becomes the rate determining step when $4 < 2^*$. This effect does not depend on the viscosity of the solutions, since it is observed both in fluid and in highly viscous media.

(4) Steps 3, 5, 7, 9 are slowed down by the combined effect of low temperature and high viscosity

(12) Cf., however, footnote 7.

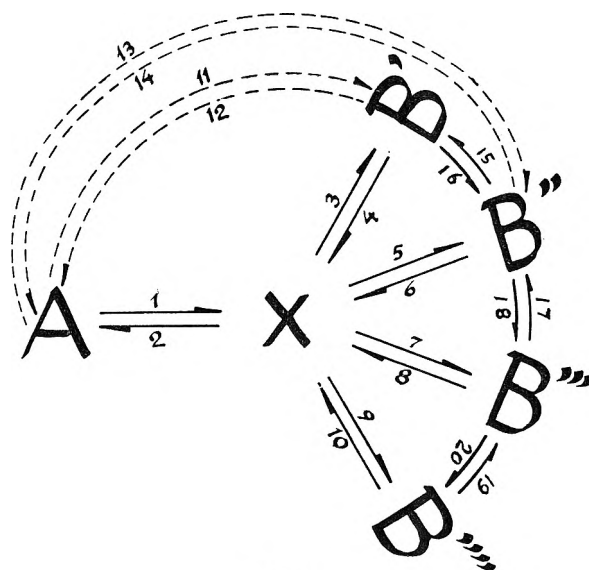


Figure 4.

and practically stop under conditions existing in a MCH-D mixture at around -150° , and in a MCH-IH mixture at around -180° . Ultraviolet irradiation of the spiropyran under such conditions results in the formation of "X" only, which can be reconverted into the spiropyran by visible light.

(5) Step 4* (and the analogous 6*, 8*, 10*) does not occur, as otherwise "12*" should proceed even with merocyanines formed at about -100° and then cooled to -180° . Step 3* probably also does not take place as shown by the fact that the colored modification formed at -180° is completely convertible into the spiropyran by visible irradiation.

(6) If, as stated in (3), step 4 virtually stops at around -140° , further cooling should freeze-in the equilibrium established at this temperature. On the other hand such a solution, when irradiated with visible light at -180° , changes very little. It therefore must be concluded that the fraction of X in the mixture is very low at around -140° , since any X present is photoconvertible into the spiropyran.

(7) The thermal equilibrations among the B's depend on the temperature and the viscosity to various extents. Some take place down to the temperature of high viscosity (-160° in MCH-IH, -140° in MCH-D) as evidenced by the continuous change of the absorption spectrum on cooling. Others already stop around -125° , as shown by the fact that the spectral changes caused in the merocyanine modification by visible irradiation at about -140° persist at this temperature are reversed by heating to above -125° . At least some, and perhaps all, of the reactions 15*-20* (and other photo-interconversions between B's not shown in the scheme for lack of space) are possible (Fig. 1c, 3c), and may be compared to the photoconversion of geometrical isomers. Since all isomers B'-B'''' absorb in the visible, irradiation should lead to a photoequilibrium mixture. Some of these photoisomerizations 15*-20* may be over-shadowed by "12*" (at temperatures where it also takes place), and also by thermal steps 15-20.

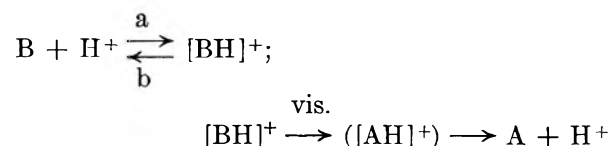
(8) It is evident from point (2) that the quantum yield measured for "12*" is meaningless. When k_4 is slow in comparison with 2^* , the over-all rate of "12*" will be given by that of k_4 , any X formed from B being immediately photoconverted into A; if k_4 is fast as compared with 2^* , the over-all rate will equal that of 2^* . It is by no means certain that at -100 and -110° , the highest temperatures at which photochromism of I and II, respectively, can be investigated, $k_4 \gg 2^*$. The quantum yield of "12*" under these conditions may therefore serve only as a lower limit for that of 2^* .

(9) The above postulates explain the observed dependence of the rate of "12*" on temperature, when brought about by visible light. With ultraviolet light the situation is less certain. In the compounds whose behavior has been described here φ_B for ultraviolet light seems to decrease only slightly on cooling. However, this is based on photoequilibria in which $[B]/[A] \geq 10$, and any small shift in these photoequilibria strongly affects the ratio φ_B/φ_A calculated from it. In the absence of additional evidence it is impossible to decide whether "12*" with ultraviolet light also decreases on cooling, or if ultraviolet light, as distinct from visible light, is capable of causing 4^* or even directly "12*".

(10) In this context it should be recalled that certain spiropyranes are converted into merocyanines by ultraviolet light, but visible light does not cause the reverse process.³ Nevertheless 1^* does not go to completion in these cases,⁶ indicating that a photoequilibrium is reached in which the rates of "11*" and "12*" are equal. A possible explanation would be that in these cases k_4 is too slow within the whole accessible temperature range, and therefore "12*" = $k_4 + 2^*$ cannot take place with visible light. Ultraviolet light is capable of acting as suggested at the end of point 9.

(11) The above results do not rule out the existence of a temperature dependence of the really photochemical part of process "12*", *i.e.*, 2^* . In fact, the observed temperature dependence of the process was originally¹³ regarded to be a consequence of a potential barrier between the excited states of X and A. (A similar explanation was forwarded for the observed temperature dependence of rates of photoisomerization in azocompounds and in stilbene.^{9b,14})

(12) The mechanism of photoconversion in alcoholic solution is apparently quite different and probably involves the complex solute-solvent, rather than the solute alone. With this complex "11*" and "12*" seem to take place directly and therefore depend only slightly on the temperature. In addition, light at $436 m\mu$ seems to act not on the merocyanine but on the cation formed from it with protons donated by the solvent alcohol



$[BH]^+$ of compound I has an absorption maximum at about $480 m\mu$ and absorbs appreciably at $436 m\mu$ (ϵ_{436} 18,000 at -100°), whereas the absorption of IB at this wave length is very low (ϵ_{436} 450 at -100°). As long as the thermal step *a* takes place, the whole of B eventually will be converted into A, even if the concentration of $(BH)^+$ is too low to be detected spectroscopically. As long as this is so, the absolute quantum yield at $436 m\mu$ should be calculated using the ϵ_{436} of $(BH)^+$, which is 40 times as high as that of B. The true yields at 436 and $546 m\mu$ thus calculated are of the same order of magnitude. At sufficiently low temperatures, process *a* is suppressed, and light at $436 m\mu$, like that at 546 or $578 m\mu$, acts only on B, the absorption of which at this wave length is negligible.

Viscosity Effects.—The above postulates involve the idea of a combined effect of low temperature and high viscosity to "clamp-in" a dye molecule in a certain configuration, assumed by the molecule immediately following its radiative formation. Effects of the viscosity or rigidity of the medium therefore should be discussed in a more general way. In doing so, it is necessary to differentiate between molecular rearrangements taking place by virtue of thermal equilibria being established (*i.e.*, where the energy stored in the molecule is the only source of energy), and between those brought about by irradiation (*i.e.*, where energy is added to the system from outside in the form of light).

With regard to the first case, the well known self-diffusion in crystals shows that even in the solid state molecular motion is not completely inhibited. Pimentel¹⁵ observed that NO_2 , H_2O , and NH_3 diffuse rapidly in solid argon at temperatures above $35^\circ K.$, while at $20^\circ K.$ the diffusion of even diatomic species in solid xenon, argon, and nitrogen is negligible.¹⁶ These experiments deal with small molecules trapped in lattices of atoms or small molecules. The present observations refer to large molecules or molecular groups in glasses also consisting of large molecules. It appears that under these conditions either low temperature or high viscosity alone do not suffice to prevent the thermal rearrangement of the high-energy form of the merocyanine, and also some of the internal rearrangements of the various "stable" merocyanines. Apparently the thermal energy of the molecules in viscous media suffices to overcome the resistance to motion offered by the medium, down to rather low temperatures. Other experimental results also show that high viscosity alone does not inhibit thermal isomerization at room temperature. Thus, the merocyanine modification of certain nitrospiropyranes dissolved in paraffin wax at room temperature reverted into spiropyran approximately at the same rate as in fluid solvents.¹⁷ On the other hand, the rate of this thermal isomerization was appreciably slowed down by cooling the paraffin wax solution to 0° . This view is confirmed by the experiments of Hardwick, Mosher, and Passailaigue,¹⁸ who reported that the colored

(15) G. C. Pimentel, *J. Am. Chem. Soc.*, **80**, 62 (1958).

(13) R. Heiligman-Rim, Y. Hirshberg, and E. Fischer, *Bull. Res. Council Israel*, **8A**, No. 3 (1959).

(16) E. D. Becker and G. C. Pimentel, *J. Chem. Phys.*, **25**, 224 (1956).

(14) S. Malkin and E. Fischer, *J. Phys. Chem.*, **66**, 2482 (1962).

(17) R. Heiligman-Rim, unpublished results.

modification of 2-(2',4'-dinitrobenzyl)-pyridine is not stable at room temperature even when the compound is dissolved in a rigid glass of sorbitol and fructose. On the other hand, this colored modification is rendered stable by cooling, even in a fluid medium. It thus may be concluded that in thermal transformations the mechanical effect of viscosity becomes a factor of importance only at low temperatures, when the energy content of the reactant molecules is very low. Still less important is the part that the viscosity of the medium plays in photochemical reactions. There the degradation of the light energy absorbed by molecules of the reactants may result in local heating and melting of the rigid glass or of the crystal lattice of the solvent in the vicinity of the molecules of the absorbing species. Thus DeMore and Davidson¹⁹ report that bimolecular photochemical reactions take place during photolysis of ozone in nitrogen matrices at 20°K. (or 4°K.). Lewis, Magel, and Lipkin²⁰ also consider that it hardly would be reasonable to expect that the rigidity of a solvent alone could hold an excited molecule in a fixed position, although it might inhibit *thermal* molecular motions (turning or diffusion) at low temperatures.²¹ From the widely differing results reported here for different compounds studied under similar conditions it may be concluded that the individual characteristics and energy relations of the molecules undergoing transformation play a far more important part in the determination of the rates and quantum yields of photochemical reactions than the mechanical properties of the medium.

In closing, it is appropriate to give some very crude data for the macroscopic viscosity-rigidity, at various temperatures, of the glass-forming solvent mixtures used. It is hoped to make more ac-

curate low-temperature measurements of macroscopic viscosity and of viscosity in molecular dimensions in the near future.

TABLE V
TEMPERATURE DEPENDENCE OF VISCOSITY OF SOLVENT MIXTURES

Solvent mixture	Onset of viscosity	Very viscous	Rigid	Lower limit of useful temp. range ^a
MCH-IH (2:1)	-132°	-135°	-138°	-185°
MCH-MCP (1:1)	-123°	-130°	-135°	-185°
MCH-decalin (1:1)	-80°	-90°	-100°	-160°
MCH-decalin (2:1)	-95°	-100°	-110°	-180°
Ethanol-methanol (4:1)	-100°	-125°	-140°	-170°
1-Propanol-2-propanol (3:2)	-65°	-80°	-90°	-160°

^aNo experiments were carried out at temperatures below that of liquid air.

Experimental

Spectrophotometry and Irradiation Techniques.—These were essentially as described in the preceding paper.¹

Relative and Absolute Light Intensities, Actinometry.—Relative intensities of the monochromatic light isolated from a mercury arc by suitable filters were measured with Bowen's method of "proportional quantum counting" as described in section 3c. With a Philips spectral lamp and either Corning glass filter combinations (365, 436, 546, 578 m μ), interference filters (405 m μ), or glass filter-solution combinations (313 m μ), the following relative numbers I_{λ} of quanta hitting the solutions were found

Wave length, m μ	313	365	405	436	546	578	>410
I_{λ}	28	100	57	52	318	128	810

Absolute actinometric measurements were made with Hatchard and Parker's micromethod under conditions identical with those under which the spiroyrans were irradiated. The absolute intensity at 365 m μ was about 4×10^{17} quanta per minute.

Acknowledgments.—The authors wish to thank Prof. G. Stein and Prof. H. Linschitz for most helpful discussions, Mr. M. Kaganowitch for synthesizing the compounds investigated, and Mrs. N. Castel for technical assistance. The efficient help of Mr. T. Bercovici is gratefully acknowledged.

(18) R. Hardwick, H. S. Mosher, and P. Passailaigue, *Trans. Faraday Soc.*, **56**, 44 (1960).

(19) W. B. DeMore and N. Davidson, *J. Am. Chem. Soc.*, **81**, 5869 (1959).

(20) G. N. Lewis, T. T. Magel, and D. Lipkin, *ibid.*, **62**, 2973 (1940).

(21) G. N. Lewis and J. Bigeleisen, *ibid.*, **65**, 520 (1943).

TAUTOMERISM AND GEOMETRICAL ISOMERISM IN ARYLAZOPHENOLS
AND NAPHTHOLS. PART II.^{1a} 2-PHENYLAZO-3-NAPHTHOL.
THE EFFECT OF INTERNAL HYDROGEN BONDS ON
PHOTOISOMERIZATION.^{1b} PART I

BY GAVRIELAH GABOR AND ERNST FISCHER

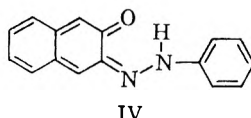
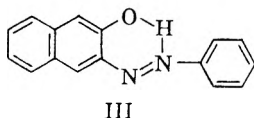
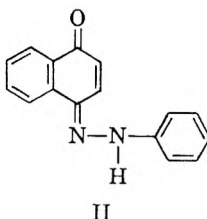
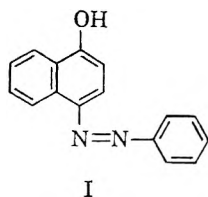
Laboratory of Photochemistry and Spectroscopy, The Weizmann Institute of Science, Rehovoth, Israel

Received May 25, 1962

The above compound is the only *ortho*-hydroxy azo-compound in which tautomerism with the corresponding phenylhydrazone is improbable. Geometrical isomerization may therefore be investigated without the complication of tautomerization. Comparison with the corresponding methoxy derivative thus shows the effect of the internal hydrogen bond on the isomerization. The *cis* isomers of the above compound and of its O-methyl ether were prepared, and the latter was isolated. Regarding the thermal *cis* → *trans* isomerization, the methoxy derivative behaves like the unsubstituted azo-compounds, ($E_A = 23$ kcal./mole), while for the hydroxy derivative $E_A = 12-14$ kcal./mole was observed. Regarding photoisomerization, the quantum yields for the *cis* → *trans* conversion were similar for both compounds, while those for the *trans* → *cis* conversion were smaller by 1-2 orders of magnitude for the hydroxy derivative. For both derivatives the quantum yields depend on temperature in the same manner as in the unsubstituted azo-compounds,^{2,3} i.e., the *cis* → *trans* yield is practically constant down to -180° , whereas the *trans* → *cis* yield decreases sharply on cooling. For the hydroxy compound there is an indication of a minimum limiting value for ϕ_t as the temperature is lowered to -160° to -180° .

Introduction

In Part I of this series^{1a} it was shown that in 4-phenylazo-1-naphthol (I) the thermal *cis* → *trans* isomerization proceeds not directly but through the hydrazone (II), i.e., *cis* → hydrazone → *trans*, in two consecutive reactions.



It was suggested that a similar mechanism may operate in *cis* → *trans* transformations of *ortho*-hydroxy azo-compounds, such as *o*- and *p*-phenylazophenol or 1-phenylazo-2-naphthol. This view is supported by the complex kinetics of these isomerizations,⁴ as compared with the first-order reactions observed in the corresponding methoxy derivatives. In order to differentiate between the effect of such tautomerization and that of hydrogen bonds in the *ortho*-hydroxy derivatives, 2-phenylazo-3-naphthol (III) was investigated. In accordance with the common view that 2,3-naphthoquinones are highly unstable or do not exist at all, it appears probable that its phenylhydrazone (IV) also does not exist, or at least does not appear as an intermediate, because of its high energy con-

tent. It then may be expected that any difference between the behavior of III and its O-methyl derivative is due to the internal hydrogen bond indicated. In addition it is of interest to study the effect of this hydrogen bond on the *cis* ⇌ *trans* photoisomerization and perhaps learn about the hydrogen bonds in the electronic excited states of the isomers. Finally, it was interesting to see whether the pronounced temperature dependence recently reported^{2,3} for azo-compounds also exists in III.

Experimental

Irradiations, spectrophotometric and actinometric determinations, procedures of photochemical kinetics, and calculation of quantum yields were all similar to those described elsewhere.³

Compound III and its O-methyl derivative were synthesized according to Fierz-David, *et al.*⁵ The *cis* isomer of the O-methyl derivative was prepared by ultraviolet irradiation of the *trans* isomer, followed by chromatographic separation on alumina, and served to measure its molar extinction coefficient. Its thermal stability is similar to that of azobenzene. *cis*-III is rapidly converted into the *trans* isomer at temperatures above -25° , and therefore cannot be separated under ordinary conditions. Its absorption spectrum was estimated, making a reasonable assumption regarding the absorption of the *cis* isomer in the region of the main absorption band of the *trans* isomer.^{2,6}

Results

Photoequilibria.—The photoequilibria attained by irradiation with light at various wave lengths are described in Fig. 1a for compound III and in Fig. 1c for O-methyl-III. The spectra of the *cis* isomers given in the same figures were calculated or measured directly as described above.

Thermal Isomerization.—The spontaneous *cis* → *trans* isomerization was measured for both compounds in isomer mixtures enriched in the *cis* isomer by irradiation at 365 m μ . Kinetic measurements were carried out over a range of temperatures in order to determine the activation energy of the thermal isomerization. At lower concentra-

(1) (a) Part I: E. Fischer and Y. F. Frei, *J. Chem. Soc.*, 3159 (1959); (b) a double title is given because the present paper is common to two series.

(2) E. Fischer, *J. Am. Chem. Soc.*, **82**, 3249 (1960).

(3) S. Malkin and E. Fischer, *J. Phys. Chem.*, **66**, 2482 (1962).

(4) E. Fischer and Y. F. Frei, unpublished results.

(5) H. E. Fierz-David, L. Blagney, and E. Merian, *Helv. Chim. Acta*, **34**, 846 (1951).

(6) W. R. Brode, J. H. Gould, and G. M. Wyman, *J. Am. Chem. Soc.*, **74**, 4641 (1952).

tions ($2 \times 10^{-5} M$) the isomerizations were first-order reactions for O-methyl-III and III up to at least 90% conversion, but only up to about 50% conversion for III at higher concentration ($5 \times 10^{-4} M$). The temperature dependence of this reaction in III was measured at two concentrations in methylcyclohexane, and also in propanol. The resulting values of E_A for III ($2 \times 10^{-5} M$) were: in methylcyclohexane, 12 kcal./mole; in alcohol, 14 kcal./mole. For the O-methyl derivative E_A was 23 kcal./mole in both solvents.

Spectra.—A comparison of the spectra of the two compounds, as given in Fig. 1a and 1c, shows the following differences between the two.

(1) **Frequency Shifts.**—In the "hydroxy" compound the $n-\pi^*$ band is blue-shifted to about 433 $m\mu$ from about 450 $m\mu$ in the "methoxy" compound. The $\pi \rightarrow \pi^*$ band is red-shifted from about 350 $m\mu$ in the "methoxy" to about 355 + 370 $m\mu$ in the "hydroxy," whereas the doublet at 270 + 280 $m\mu$ is shifted to 282 + 295 $m\mu$ in the "hydroxy" compound. The difference between the spectra of the *cis* isomers is more marked, despite the common view that the hydrogen bond can be formed only in the *trans* isomer. However, no conclusion may be drawn from this fact because the spectra of the two compounds compared were obtained in different ways as described above. Moreover, the steric interactions of the two *cis* isomers are probably different. The solvent has only a small effect, as seen from comparison of Fig. 1a and 1b or 1c and 1d.

(2) **Intensity Shifts.**—These are very pronounced, as proved by the relative heights of the various peaks in the spectra of the two compounds. Both frequency and intensity shifts may be due to hydrogen bonding.⁷⁻¹⁰

Temperature Dependence of Photoequilibria and Quantum Yields.—Photoequilibria were measured over a wide range of temperatures with light at 313, 365, 405, 436, and 546 $m\mu$. Some results are summarized in Tables I and II.

TABLE I

% *trans* ISOMER^a AT PHOTOEQUILIBRIUM ATTAINED AT VARIOUS TEMPERATURES BY IRRADIATION WITH LIGHT OF VARIOUS WAVE LENGTHS, IN A MIXTURE OF METHYLCYCLOHEXANE-ISOHEXANE

The concentrations of III and O-methyl-III are $2.58 \times 10^{-5} M$ and $3.66 \times 10^{-5} M$, respectively

Temp., °C.	313 $m\mu$		365 $m\mu$		405 $m\mu$		436 $m\mu$		546 $m\mu$	
	p_1^a	p_2^a	p_1^a	p_2^a	p_1^a	p_2^a	p_1^a	p_2^a	p_1^a	p_2^a
-25			43	5	85		89.5	75	38	
-50	90	41.5	50	10	86		90.5	80	38	
-75	98	57	60	15	88		92	84	40	
-100	97.5	65.5	70	24	96		94.5	96.5	48	
-120	97		91		96		97		52 (-110°)	
-125		77	91	35			98	93	51	
-140	98.5	80	94	42	98.5		98.5	97.5	71	
-150			95	55	100		100	100		
-160			97	50			100	100		
-180			98	77			100	100		

^a p_1 refers to III, p_2 to O-methyl-III.

(7) E. Lippert, "Hydrogen Bonding," ed. by D. Hadzi, Pergamon Press, New York, N. Y., 1959, pp. 217-257.

(8) H. Baba and S. Suzuki, *J. Chem. Phys.*, **35**, 1118 (1961).

(9) H. Baba, *Bull. Chem. Soc. Japan*, **31**, 169 (1958).

(10) G. C. Pimental, *J. Am. Chem. Soc.*, **79**, 3323 (1957).

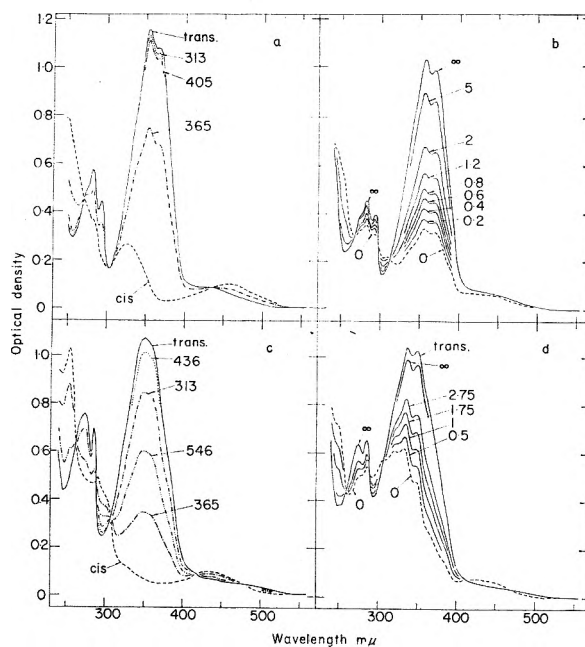


Fig. 1.—Absorption spectra: (a) Compound III in methylcyclohexane-isohehexane (1:1), $2.58 \times 10^{-5} M$, at -75° before and after photoequilibration with light at the indicated wave lengths. The "cis" curve is explained in the text. (c) Ditto, O-methyl-III, $3.7 \times 10^{-5} M$, in methylcyclohexane-isononane (1:1) at -125° . (b) Kinetics of photoisomerization *cis* \rightarrow *trans* of III, $2.2 \times 10^{-5} M$, in propanol-isopropyl alcohol (1:1) with light at 436 $m\mu$ at -150° . The irradiation times are indicated. (d) Ditto, O-methyl-III, $3.4 \times 10^{-5} M$, in propanol-isopropyl alcohol (1:1) at -120° .

TABLE II

% *trans* ISOMER OF III AT PHOTOEQUILIBRIUM IN NON-POLAR (np) AND HYDROXYLIC (p) SOLVENTS AT VARIOUS TEMPERATURES, ATTAINED BY IRRADIATION WITH LIGHT AT 365 $m\mu$ FROM A MERCURY ARC

Temp., °C.	np	p
-50	50	31
-75	60	41
-100	70	56
-120	91	78
-150	95	93

From the photoequilibrium composition and the molar extinction coefficients the ratio between the quantum yields ϕ_c and ϕ_t , for the *cis* \rightarrow *trans* and *trans* \rightarrow *cis* photoconversion, respectively, can be calculated, using the equation

$$\phi_c \epsilon_c X_c = \phi_t \epsilon_t X_t, \quad \phi_t / \phi_c = \epsilon_c X_c / \epsilon_t X_t$$

where X_c and X_t denote the mole fractions of the two isomers. Application of this equation to the data of Table I results in the values of ϕ_t / ϕ_c given in Table III. The most prominent feature of these results is the fact that ϕ_t / ϕ_c is much smaller in the "hydroxy" compound.

In order to determine the cause of this difference between the two compounds, absolute quantum yields were measured for the photoisomerization in both directions, again over a wide range of temperatures. In view of the greater complexity of such measurements, they were performed only with light at 365 and 436 $m\mu$; light at each of these wave lengths is absorbed in a different absorption

TABLE III

RELATIVE QUANTUM YIELDS ϕ_t/ϕ_c DENOTED BY k_1 AND k_2 FOR III AND O-METHYL-III, RESPECTIVELY, AT VARIOUS WAVE LENGTHS AND TEMPERATURES

Solvent: methylcyclohexane/isohehexane (1:1). Concentrations $C_1 = 2.15 \times 10^{-5} M$, $C_2 = 3.66 \times 10^{-5} M$

Temp., °C.	Wave length					
	313 m μ		365 m μ		436 m μ	
	k_1	k_2	k_1	k_2	k_1	k_2
- 50	0.07	0.6	0.06	0.7	0.08	0.26
- 75			.04	.4	.075	.23
-100	.025	.25	.024	.24	.065	.03
-125			.005	.14	.025	.02
-140	.015	.12	.0032	.07	.018	.04
-150			.003	.06	.013	.02
-160			.002	.06	.014	.02
-180			.001	.02	.015	.02

band. The results are shown in Fig. 2a and 2b for the two compounds, and are even more striking than those in Table III. While the ϕ_c 's are all of the same order of magnitude for both compounds, the ϕ_t 's of III are smaller than those of its O-methyl derivative by 1-2 orders of magnitude. In both compounds the general trend of change of ϕ_c and ϕ_t with temperature is seen to be similar to that described for unsubstituted azo-compounds and stilbene,³ *i.e.*, ϕ_t decreases sharply on cooling, whereas ϕ_c is more or less constant, or starts falling off only at the lowest temperatures investigated.

Discussion

The activation energy of the thermal isomerization *cis* \rightarrow *trans* of O-methyl-III is 23 kcal./mole, nearly the same as the activation energy of this reaction in other azo-compounds, as found for instance by Halpern, *et al.*¹¹ The activation energy of the same isomerization for III is much lower: 12 kcal./mole. There are two possible explanations for this lowering of the activation energy.

(a) **Existence of Hydrazonic Intermediates.**—Other *o*-phenylazonaphthols (1,2- and 2,1-) were found to exist in solutions,¹² as well as in the solid state,¹³ as tautomeric mixtures of the azoic and quinoidic, or hydrazone forms. It may be postulated that the mechanism of the thermal isomerization of III is similar to that suggested for these other hydroxyazo-compounds,¹ *i.e.*, it proceeds *via* a hydrazonic intermediate. This assumption could account for the lowering of the activation energy, but is rather unlikely because the corresponding quinone, 2,3-naphthoquinone, is unknown, and probably unstable.

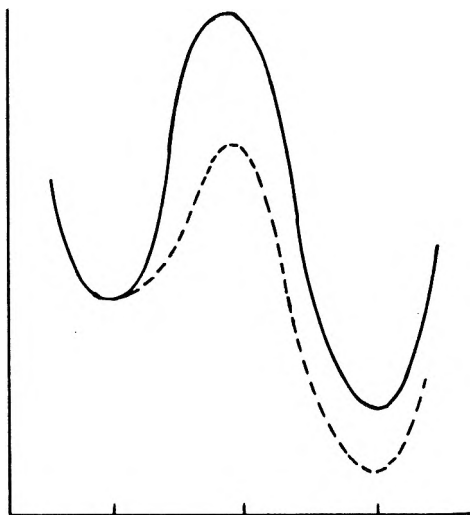
Also, the hydrazone should have a high energy content and its formation as an intermediate would therefore involve a high activation energy.

(b) **Direct Effect of Intramolecular Hydrogen Bonds.**—The kinetic transition state may be stabilized by hydrogen bonding, just like the ground state of the *trans* isomer, but not of the *cis* isomer. This is indicated in the scheme beyond, where the dashed curve denotes the molecule stabilized by internal hydrogen bonds.

(11) J. Halpern, G. W. Brady, and C. A. Winkler, *Can. J. Res.*, **28**, 140 (1950).

(12) A. Burawoy, A. G. Salem, and A. R. Thompson, *J. Chem. Soc.*, 4793 (1952).

(13) D. Hadzi, *ibid.*, 2143 (1956).



Thus the energy difference between the ground state of the *cis* isomer and the transition state is diminished by the hydrogen bond in the latter. The *trans* isomer of III fulfils the conditions for intramolecular hydrogen bonding, which are, according to Pauling¹⁴: (1) The hydrogen bond forming groups should be in conjugation with the aromatic system (planarity). (2) The formation of a hydrogen bond should give rise to a six-membered ring (counting the hydrogen atom). The *cis* isomer of III does not fulfil condition (1) because of steric hindrance and the resulting lack of planarity.

As shown in Fig. 2, ϕ_t is larger in a hydroxylic solvent (ethanol-methanol) than in a non-polar solvent, though it is still much smaller than that of O-methyl-III. This may be due to partial weakening of the intramolecular hydrogen bonds through formation of solute-solvent hydrogen bonds. This also may be the reason for the somewhat higher activation energy observed for the thermal *cis* \rightarrow *trans* conversion in alcoholic solvents.

One may now examine the spectroscopic evidence for the existence of the hydrogen bond. According to Pimentel¹⁰ the stabilization energy due to hydrogen bonding affects the electronic excited state. Baba⁹ showed that the electronic excited state is less stabilized by the hydrogen bond than the ground state. This is caused by weaker electron migration from the hydroxylic oxygen to the ring in the excited state, which diminishes the stability of the excited state and also the electronegativity of the oxygen, and therefore weakens the hydrogen bond in the excited state. This causes a blue-shift of the $n-\pi^*$ transition. This blue-shift was found in the $n-\pi^*$ band of III as compared with the same band of O-methyl-III. The red-shift of the $\pi-\pi^*$ band of III compared to that of O-methyl-III also indicates the existence of the hydrogen bond. Similar red-shifts of $\pi-\pi^*$ transition bands caused by hydrogen bonds were found for both intermolecular^{8,9,15} and intramolecular¹⁶ hydrogen bonding.

(14) L. C. Pauling, "The Nature of the Chemical Bond," Cornell Univ. Press, Ithaca, N. Y., 1960.

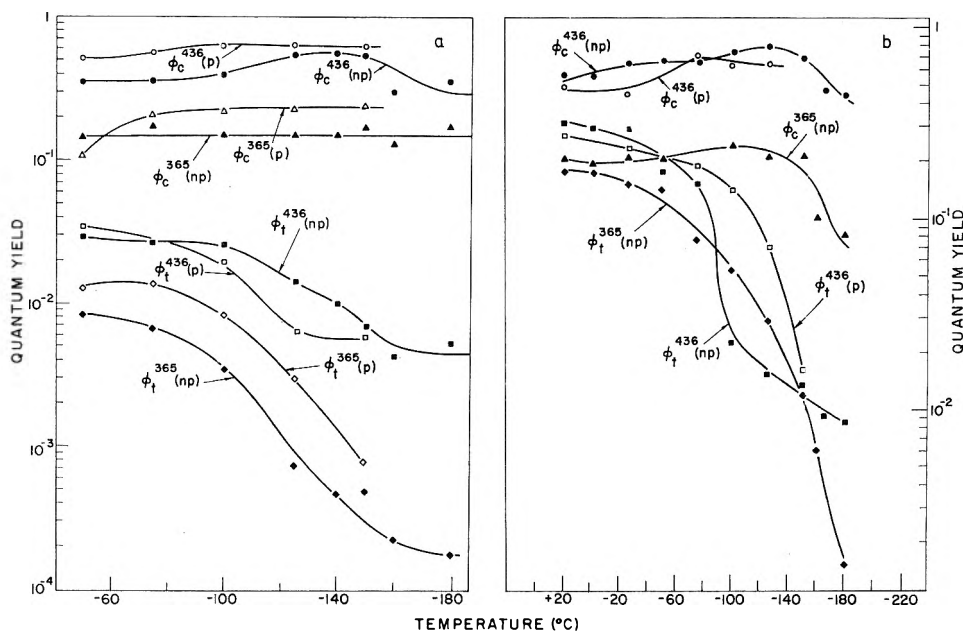
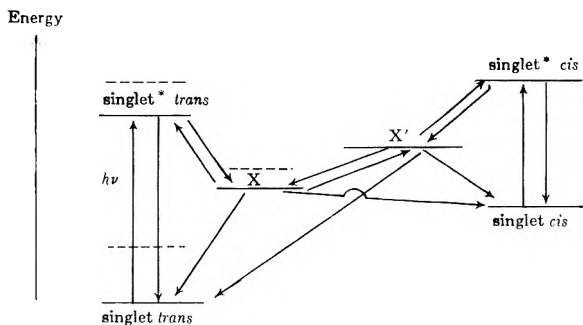


Fig. 2.—Temperature dependence of quantum yields ϕ_c and ϕ_t for light at 365 and 436 m μ in polar (p) and non-polar (np) solvents, as indicated. (a) Compound III: $2.15 \times 10^{-5} M$ in methylcyclohexane-isohexane (np); $2.2 \times 10^{-5} M$, in propanol-isopropyl alcohol (p). (b) Compound O-methyl-III: $3.7 \times 10^{-5} M$, in methylenecyclohexane-isohexane (np); $3.4 \times 10^{-5} M$, in propanol-isopropyl alcohol (p).

The influence of hydrogen bonding on the quantum yields ϕ_t of the photoisomerization may be interpreted as being due to hydrogen bonding stabilization in the ground and excited *trans* states. This is shown qualitatively in the energy diagram,



(15) G. J. Brealey and M. Kasha, *J. Am. Chem. Soc.*, **77**, 4467 (1955).

(16) H. Shingu, *Nature*, **143**, 1068 (1939).

which is similar to the one proposed³ for photoisomerization in the unsubstituted compounds.

The broken lines denote the energy levels of the *trans* molecule in the absence of hydrogen bonds. As seen from this oversimplified scheme, only the *trans* \rightarrow *cis*, but not the *cis* \rightarrow *trans* photoconversion might be expected to be attenuated by the existence of the hydrogen bond in the *trans* isomer. This appears to explain, albeit in a qualitative and naive way, the observation that the presence of an internal hydrogen bond affects primarily ϕ_t and not ϕ_c .

Similar effects in other *ortho*-hydroxy azo-compounds are being studied currently.

Acknowledgments.—The authors wish to thank Mr. M. Kaganowitch for synthesizing the compounds investigated, Mrs. N. Castel and Miss J. Horowitz for technical assistance, and Mr. A. Meitlis for drawing the figures. This investigation was supported in part by a grant from Giant Food Foundation, Inc., Washington, D. C.

TEMPERATURE DEPENDENCE OF PHOTOISOMERIZATION. PART II.¹ QUANTUM YIELDS OF *cis* \rightleftharpoons *trans* ISOMERIZATIONS IN AZO-COMPOUNDS

BY SHMUEL MALKIN AND ERNST FISCHER

Laboratory of Photochemistry and Spectroscopy, The Weizmann Institute of Science, Rehovoth, Israel

Received May 25, 1962

Quantum yields of the *cis* \rightleftharpoons *trans* photoisomerization of azobenzene and related compounds were measured in the temperature range of +20 to -183°. For each compound the yields in both directions were measured with light at two wave lengths, one within each of the two main absorption bands of the spectrum in the visible and near-ultraviolet regions, respectively. The yields for the *trans* \rightarrow *cis* transformation were found to decrease sharply on cooling, whereas those for the *cis* \rightarrow *trans* reaction change but little in this temperature range. These results corroborate conclusions from earlier results,¹ and indicate the existence of energy barriers somewhere between the electronically-excited singlet state of one isomer (formed by light absorption) and the ground state of the second isomer. Preliminary results with stilbene are basically similar, but in this case the yield for the reaction *cis* \rightarrow *trans* also is attenuated on cooling, though to a lesser extent.

Introduction

In Part I of this series¹ it was shown that the *cis* \rightleftharpoons *trans* photoequilibria attained on irradiation of azobenzene and related compounds all show a pronounced shift toward the *trans* isomer, if photo-equilibration is performed at low temperatures. In some cases irradiation at -180° with light at any wave length in the visible and ultraviolet region results in complete transformation into the *trans* isomer. Since the photoequilibrium constant is determined by the relative quantum yields in both directions, $\phi_{cis \rightarrow trans} / \phi_{trans \rightarrow cis}$, these results were interpreted as being due to the fact that $\phi_{c \rightarrow t}$ is little affected by cooling, whereas $\phi_{t \rightarrow c}$ approaches zero at sufficiently low temperatures. These conclusions were now checked by direct measurements of the quantum yields $\phi_{c \rightarrow t}$ and $\phi_{t \rightarrow c}$ at temperatures down to -183°, in an attempt to throw some light on the mechanism of photoisomerization in these cases.

Quantum yields of the reversible photoisomerization of azobenzene have been measured very accurately at room temperature and at various wave lengths by Zimmerman, *et al.*,² who found that the sum $\phi_{c \rightarrow t} + \phi_{t \rightarrow c}$ is significantly smaller than unity, proving non-existence of a common excited initial state of the two isomers. An earlier paper by Birnbaum and Style^{3a,3b} describes results obtained with a series of derivatives of azobenzene. Earlier results are cited in the above two papers.

Experimental

Spectrophotometry and Irradiation.—The low-temperature technique described previously⁴ was used, modified by using dewar vessels with three pairs of windows in experiments involving fluid solutions. This enabled irradiation at right angles to the measuring beam. All experiments were carried out in a Cary Model 14 recording spectrophotometer. A small magnetic stirrer was introduced into the measuring cells to ensure mixing, at least as long as the medium is not too viscous. At temperatures at which the medium forms a rigid glass, the system is essentially unmixed, since neither convectional nor diffusional mixing takes place. At intermediate temperatures the conditions are less defined and an effort usually was made to work under one of the two extreme conditions.

Solvents.—The present report deals only with non-polar solvents. The lowest melting one used was methylcyclo-

pentane (m.p. -144°) which, like other pure non-hydroxylic solvents, has the advantage of low viscosity down to its melting point. For lower temperatures mixtures of several solvents were used, such as methylcyclohexane with either methylcyclopentane, isohexane, or iso-octane. The viscosity of all these mixtures increases on cooling, and rigid glasses are formed at appropriate temperatures. All solvents were purified by passing them through columns filled with "Woelm" alumina,⁴ and the solvent was distilled from a K/Na alloy *in vacuo* onto the solute in the measuring cell, which then was fused off.⁴ This assured complete absence of air and hydroxylic contaminants.

Light Sources.—A Philips spectral lamp (125-watt) with a stabilized power supply was used throughout. The mercury emission lines were isolated either with Corning glass filter combinations (at 436 and 365 m μ) or with a combination of such filters and a solution of NiCl₂ at 313 m μ (*cf.* Part I where one of the filters was erroneously designated 0620 instead of 0160). Irradiations were carried out either at right angles to the measuring beam (in mixed fluid media) or in the direction of the measuring beam (in rigid media). In this case the dewar with the measuring cell was rotated through 90° during irradiation.

Light Intensity.—Hatchard and Parker's ferrioxalate actinometric method was used in the form modified to low intensities.⁵ Three ml. of actinometric solution is put into a spectrophotometer cell similar to the one used in photoisomerization, and irradiated for a certain time under conditions exactly identical with those pertaining during photoisomerization. One-half ml. of phenanthroline solution then is added, and the optical density of the resulting solution at 510 m μ is measured *in situ*. Calibrations were made according to Parker.⁵ At 436 m μ the absorption of ferrioxalate is rather small, and the actinometric results at this wave length of irradiation light therefore were checked by measuring the relative light intensities (in quanta/time unit) at 436 and 313 or 365 m μ , using Bowen's proportional quantum counting method, as modified by Weber and Teale.⁶ A solution of Rhodamine B in ethylene glycol served as "fluorescent screen." The intensity of the fluorescence excited in it with light at any wave length which is totally absorbed is proportional to the quantal intensity of the exciting light. The intensities of the monochromatic light incident on the solutions (expressed as quanta/minute) were about 1.2×10^{17} at 313 m μ , 2.5×10^{17} at 365 m μ , and 1.2×10^{17} at 436 m μ .

Compounds.—Azobenzene (I): A commercial product was purified chromatographically on alumina and recrystallized from hexane. 2,2'-Azonaphthalene (II): this was synthesized according to Friedlander as described before⁷ and recrystallized from iso-octane. 1-Phenylazonaphthalene (III): This was obtained by Martynoff's method⁸ and recrystallized from hexane.

(1) Part I: E. Fischer, *J. Am. Chem. Soc.*, **82**, 3249 (1960).

(2) G. Zimmerman, L. Chow, and U. Paik, *ibid.*, **80**, 3528 (1958).

(3) (a) P. P. Birnbaum and D. W. G. Style, *Trans. Faraday Soc.*, **50**, 1192 (1954); (b) P. P. Birnbaum, J. H. Linford, and D. W. G. Style, *ibid.*, **49**, 735 (1953).

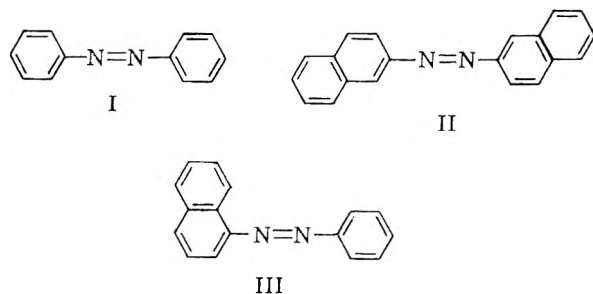
(4) Y. Hirschberg and E. Fischer, *Rev. Sci. Instr.*, **30**, 197 (1959).

(5) C. G. Hatchard and C. A. Parker, *Proc. Roy. Soc. (London)*, **A235**, 518 (1956).

(6) G. Weber and F. W. J. Teale, *Trans. Faraday Soc.*, **53**, 646 (1957).

(7) M. Frankel, R. Wolovsky, and E. Fischer, *J. Chem. Soc.*, 3441 (1955).

(8) M. Martynoff, *Bull. soc. chim. France*, **18**, 216 (1951).



The *cis* isomers were prepared by ultraviolet irradiation of solutions in petrol ether, followed by chromatography on alumina, elution, and evaporation to dryness. To prevent thermal and photochemical transformation into the *trans* isomer, all the above manipulations were carried out in a room at 0–4°, using only red light for illumination. Pure *cis* isomers were used only for the determination of their extinction coefficients.

Procedure for Determination of Photoisomerization Kinetics.—The isomeric composition was determined spectrophotometrically as a function of time of irradiation at each wave length of photoactive light. In each kinetic series the starting composition was chosen to be as different as possible from the final composition, *i.e.*, *trans* → *cis* isomerizations started with the pure *trans* isomer, and *cis* → *trans* conversions with a mixture containing as much *cis* isomer as is obtainable by irradiation at a suitable wave length and temperature. No photokinetic experiments were made with the pure *cis* isomers because of the latter's thermal instability. During the kinetic experiments full spectral curves were taken after each irradiation. Experiments were discarded if isobestic points were not obtained, or if prolonged irradiation did not cause an asymptotic approach to a final state. These two basic requirements were absent only in very few experiments, and could be blamed on technical reasons.

Calculation of Absolute Quantum Yields.—Using Zimmerman's basic rate equation² the experimental composition *vs.* time curves were analyzed either graphically or by an integration method, as detailed in the Appendix. Thermal isomerization could be disregarded at the temperatures of all kinetic experiments carried out.

Results

Absorption Spectra.—These have been analyzed in detail for azobenzene by Jaffe, Yeh, and Gardner,⁹ who distinguished between three main absorption bands of which the weakest one, in the visible region, is ascribed to the lone pair of electrons on the nitrogen atom, and therefore lacks in stilbene.¹⁰ As shown in Part I, the vibrational fine structure of all three *trans*-azonaphthalenes (1,1'; 1,2'; 2,2') is enhanced on cooling and is completely absent in the *cis* isomers. However, as seen in Fig. 1b, the *cis* isomer of compound III possesses such fine structure in its spectrum.

A comparison of the spectra of the two isomers (Fig. 1) shows in all cases that the main absorption bands differ only slightly in their position. It may be inferred that the electronic energy levels are spaced in a rather similar way in both isomers.

Quantum Yields.—The results are summarized in Fig. 2 for all four compounds investigated. In Part I we showed that the pronounced shift of the photoequilibrium in favor of the *trans* isomer on cooling also occurs in the two other azonaphthalenes and also in polar solvents (ethanol-methanol, tetrahydrofuran). It is therefore reasonable to

(9) H. H. Jaffe, Si-Jung Yeh, and R. W. Gardner, *J. Mol. Spectry.*, **2**, 120 (1958).

(10) *Cf.*, however, the recent paper by M. B. Robin and W. T. Simpson, published [*J. Chem. Phys.*, **36**, 580 (1962)] after the present communication was sent in.

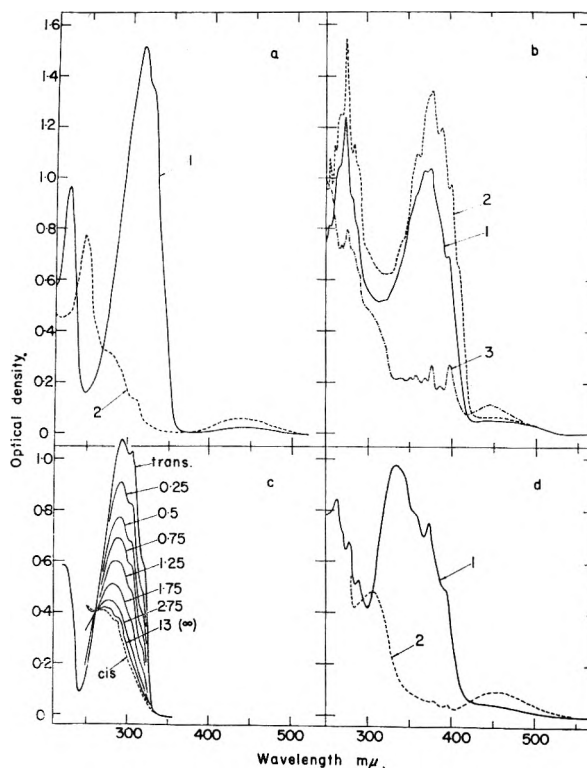


Fig. 1.—(a) Spectrum of azobenzene in isohexane, $0.7 \times 10^{-4} M$, at room temperature: 1, *trans*; 2, *cis*. (b) Spectrum of 1-phenylazobenzene in isohexane-methylcyclohexane (1:1), $0.75 \times 10^{-4} M$: 1, *trans* at 5°; 2, *trans* at -160°; 3, *cis* at 5°. (c) The progressive change of the spectrum of stilbene (in isohexane, $0.4 \times 10^{-4} M$) by irradiation with light at 313 $m\mu$. Numbers refer to time of irradiation (in minutes) at 25°. (d) Spectrum of a solution of 2,2'-azonaphthalene, $0.32 \times 10^{-4} M$, in isohexane-methylcyclohexane (1:1) at 10°: 1, *trans*; 2, *cis*.

expect that the temperature dependence of the quantum yields described in Fig. 2 characterizes at least all unsubstituted azo-compounds and does not depend on the solvent used. Furthermore the preliminary results with stilbene (Fig. 2c) indicate that this behavior may be of more general importance in *cis* ↔ *trans* photoisomerizations.

The results may be summarized thus: (a) In accordance with Zimmerman's results² at room temperature, the yields with ultraviolet light are lower than with visible light. (b) The yield of the process *trans* → *cis* in all cases decreases sharply on cooling, but in a way peculiar to each compound and wave length of photoactive light. (c) The yield of the process *cis* → *trans* changes much less with the temperature, and does so in a rather irregular way.

Discussion

The following ideas have been forwarded hitherto to explain the mechanism of photoisomerization.

(1) According to Lewis, *et al.*,¹¹ photoisomerization involves transformation of an electronically excited molecule into one at a high vibrational level of the ground electronic state. In the latter sufficient energy is available for those rotations which can bring about isomerization. Eventually

(11) G. N. Lewis, T. T. Magel, and D. Lipkin, *J. Am. Chem. Soc.*, **62**, 2973 (1940).

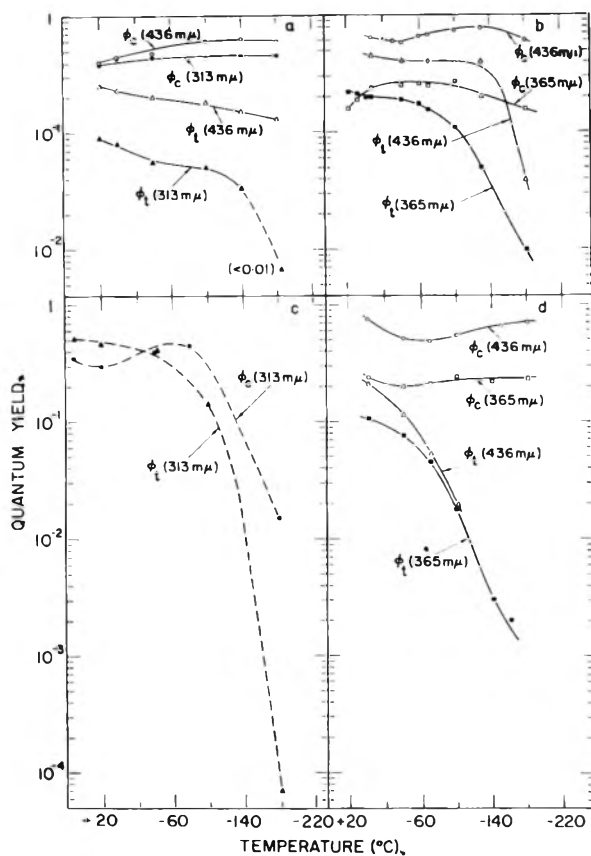


Fig. 2.—Quantum yields, ϕ_c and ϕ_t , for the *cis* \rightarrow *trans* and *trans* \rightarrow *cis* photoisomerization, respectively, as a function of temperature (in non-polar solvents): (a) azobenzene; (b) 1-phenylazonaphthalene; (c) stilbene; (d) 2,2'-azonaphthalene. (The results for stilbene are only preliminary and less accurate than the others. They are brought here only for the sake of comparison.)

the surplus energy is lost to the medium, and the molecule stays either in the *cis* or the *trans* form.

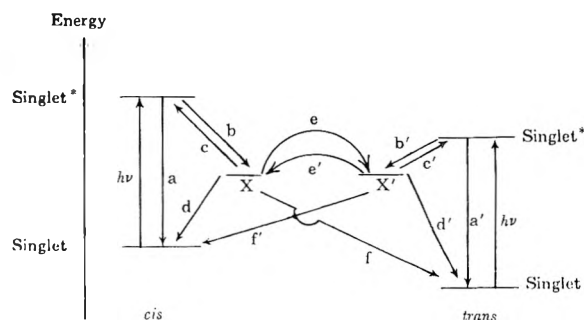
(2) According to Birnbaum and Style³ and other authors¹²⁻¹⁴ photoisomerization involves an intermediate state common to both *cis* and *trans* isomers. In this state there is no energy barrier between the two isomers.¹⁵

(3) According to Zimmerman² the above two hypotheses contradict the experimental results, and it therefore has to be assumed that "the isomerization takes place as an ordinary thermal reaction of an electronic excited state," *i.e.*, thermal interconversion of electronic excited *cis** and *trans** molecules across a (hypothetical) energy barrier. The latter must be low in order to enable such interconversion to occur within the short lifetime of the excited states ($<10^{-9}$ sec. in the absence of fluorescence). Furthermore, "the deviation from unity of the sum $\phi_c + \phi_t$ is significant . . . and in all cases a truly common kinetic state is excluded."²

Our previous¹ and present results support the idea of such energy barriers, which have to be postulated in order to explain the temperature dependence observed by us. However, at least the conversion *trans** \rightarrow *cis** is improbable for the fol-

lowing reason.¹⁶ Both in stilbene and in azo-compounds the absorption bands of the *cis* isomer are either similar to that of the *trans* isomer or even shifted toward higher frequencies. This shows that the distance between the *cis* and *trans* levels in the excited states is at least as big as that between the *cis* and *trans* levels in the ground state, which is about 10 kcal./mole. Accordingly the potential barrier for *cis** \leftarrow *trans** should be larger than 10 kcal./mole. For a reaction occurring within less than 10^{-9} sec. such a high activation energy seems improbable, and also would imply a much sharper temperature dependence than even the one observed here. Furthermore, in stilbene only the *trans* isomer is fluorescent,¹¹ showing that there is no *cis** \rightarrow *trans** conversion. In azo-compounds neither isomer is fluorescent, and the same argument can be applied only by analogy.

One therefore has to conclude that one or more intermediate excited states X of similar or lower energy than *cis** and *trans** are involved, and that the sequences are schematically *cis* $\xrightarrow{h\nu}$ *cis** \rightarrow X (\rightarrow X') \rightarrow *trans*, and *trans* $\xrightarrow{h\nu}$ *trans** \rightarrow X' (\rightarrow X) \rightarrow *cis*. The general reaction scheme thus would be



In the above scheme processes a-f and a'-f' all are thermal reactions whose relative importance for the over-all isomerization will determine the latter's temperature dependence. The present experimental data for the two quantum yields do not suffice to decide which of the above are responsible for the observed effects. Thus the decline of $\phi_{t \rightarrow c}$ on cooling may be due to any of the processes b', e', f', d being slowed down relative to the competing processes a', c', d', e, f.

It is of course tempting to assume that only c and e' are temperature-dependent, and to calculate the barrier between X' and X. If this assumption is made, X should be at a somewhat higher level than X', to explain that the barrier from X \rightarrow X' is lower (and often undetectable) than that from X' \rightarrow X.

Two points should be borne in mind: (a) It is impossible to draw any conclusions yet regarding the nature of the intermediate X states. One can postulate a different electronic state (*e.g.*, triplet), but since so far experimental work has not proved this with certainty, it will be safer to refer to them as unknown X states. (b) The above scheme does not exclude the possibility that the two X states may, in fact, be one common state. The

(12) D. Schulte-Frohlinde, *Ann.*, **615**, 114 (1958).

(13) Th. Forster, *Z. Elektrochem.*, **56**, 716 (1952).

(14) S. Yamashita, *Bull. Chem. Soc. Japan*, **34**, 490 (1961).

(15) R. S. Mulliken and C. C. Roothaun, *Chem. Rev.*, **41**, 219 (1947).

(16) The asterisk denotes excited singlet states.

fact that the sum $\phi_{c \rightarrow t} + \phi_{t \rightarrow c}$ fails to reach 1 may be attributed to the competing reactions a and a'.

In stilbene some additional information is available from fluorescence and phosphorescence measurements. Lewis and Kasha,¹⁷ as cited by Pariser,¹⁸ and by Rosenberg,¹⁹ report that *cis* stilbene is phosphorescent, while *trans* stilbene is not. In the above scheme this may be due to inhibition of b', but not b, at low temperatures. The same may hold for azo-compounds and azomethines, but as yet no phosphorescence has been observed with them. (This may be because emission is in the infrared,¹⁷ which has not yet been explored.)

Finally, there is the change of the quantum yields with the wave length of the exciting light. Even if, in analogy with normal fluorescence, higher excited electronic levels are deactivated thermally to the first excited level, one would expect the quantum yield to be independent of wave length, if not higher at shorter wave lengths. However, the ϕ_t 's actually observed in azo-compounds are lower for light absorbed within the two bands in the ultraviolet. A somewhat similar effect was observed by Weber and Teale²⁰ with regard to the quantum yield of fluorescence at different wave lengths of exciting light. They explained it, in certain cases, by competitive radiationless transitions from such higher levels to the ground state. A similar explanation may hold in the present case, although there is no proof for it.

It is interesting to note that even in the rigid glasses at -180° $\phi_{c \rightarrow t}$ is practically identical with that observed at higher temperatures in fluid media. The viscosity of the medium thus seems to have no effect on the photoisomerization.

In summarizing, it may be said that the determination of quantum yields and their change with temperature provide useful information about the energetics of the interconversion of electronic excited states, but that such information has to be supplemented by results obtained with other methods, capable of detecting triplet intermediates (*e.g.*, flash photolysis, phosphorescence in the infrared, triplet-triplet excitation spectra at very low temperatures, etc.).

Recent experiments in this Laboratory showed that photoisomerization of stilbene in both directions takes place in the presence of benzophenone, with light absorbed only by the latter. Details concerning this photosensitized isomerization and its quantum yield at various concentrations and temperatures will be published separately.

Acknowledgments.—The authors wish to thank Dr. E. Lippert for the privilege of discussing with him various aspects of this subject, and Dr. H. Stegemeyer for information about his pertinent results with stilbene²¹ which led him to ideas basically similar to those given here.

(17) G. N. Lewis and M. Kasha, *J. Am. Chem. Soc.*, **66**, 2100 (1944).

(18) R. Pariser, *J. Chem. Phys.*, **24**, 264 (1956).

(19) B. Rosenberg, *ibid.*, **31**, 238 (1959).

(20) G. Weber and F. W. Y. Teale, *Trans. Faraday Soc.*, **54**, 640 (1958).

(21) H. Stegemeyer, *Z. Naturforsch.*, **16a**, 634 (1961), and private communication.

Appendix 1

Fraction of the *trans* isomer in the photostationary state attained after irradiation at various temperatures with light at the indicated wave lengths.

Compound ^a	Wave length, m μ	Temperature ($^\circ$ C.)					
		+25	0	-40	-100	-140	-180
Azobenzene	313	0.18	0.23	0.29	0.34	0.60	0.95
	436	.88	.89	.9	.92	0.95	0.97
2,2'-Azonaphthalene	365	..	.12 ^b	.15 ^b	.46 ^b	0.85	0.98
	436	..	.85	.87	.97	1	1
1-Phenylazonaphthalene	365	.13	.19	.24	.39	0.61	0.98
	436	.79	.71	.74	.82	0.9	1
Stilbene	313	.07	.09	.11	.25	..	0.95

^a In methylcyclohexene-isohexane. ^b These results differ somewhat from those reported in Part I, owing to the present more precise determination of the molar extinction coefficients of the *cis* isomer.

Appendix 2

Calculation of the Quantum Yields from the Kinetic Data.—Formally the reaction may be

written as $A \xrightleftharpoons{h\nu} B$. The following symbols will

be used: C_1, C_2 —concentration of A, and B, respectively, expressed in moles/l.; C_1^0, C_2^0 —initial concentrations; C_1^∞, C_2^∞ —final concentrations in the photostationary state; $C_0 = C_1 + C_2 =$ total concentration (which remains constant during irradiation); D —optical density at the wave length of irradiation; ϵ_1, ϵ_2 —molar extinction coefficients of A and B, respectively, at the wave length of irradiation; ϕ_1, ϕ_2 —quantum yields for the reactions $A \xrightarrow{h\nu} B$ and $B \xrightarrow{h\nu} A$, respectively; V —the volume, (in liters); I —the light intensity, (in einsteins/unit time). Assuming that the quantum yields are independent of the concentration, that the rate of thermal reactions is negligible, and that the solution always is mixed, one arrives at the differential equation²

$$-V \frac{dC_1}{dt} = (\phi_1 \epsilon_1 C_1 - \phi_2 \epsilon_2 C_2) \left(\frac{1 - 10^{-D}}{D} \right) I \quad (1)$$

Using mole fractions $X = C/C_0$, defining $K = \phi_1 \epsilon_1 + \phi_2 \epsilon_2$, and rearranging, we have

$$\frac{dX_1}{dt} \cdot \frac{D}{1 - 10^{-D}} = \frac{I}{V} \left(KX_1 - \frac{\phi_2 \epsilon_2}{C_0} \right) \quad (2)$$

Equation 2 can be used directly by plotting the left-hand expression as a (linear) function of the isomeric composition X , and using the slope to evaluate K . (dX_1/dt is determined graphically from the slope of the experimental X_1 vs. time curve, at appropriate time intervals, while $D/(1 - 10^{-D})$ is read from tables for this function, using the D values at the same time intervals.)

Alternatively, we may define $f = \int_0^t (1 - 10^{-D}/D) dt$ and $R = \phi_2 \epsilon_2 / C_0$ and integrate eq. 2, thus arriving at

$$\ln \left(\frac{KX_1 - R}{KX_1^0 - R} \right) = f \frac{KI}{V} \quad (3)$$

At photoequilibrium $dX_1/dt = 0$ and therefore eq. 2 = 0, leading to

$$R = \frac{\phi_2 \epsilon_2}{C_0} = K X_1^\infty$$

$$\ln \left(\frac{K X_1 - K X_1^\infty}{K X_1^0 - K X_1^\infty} \right) = \ln \left(\frac{X_1 - X_1^\infty}{X_1^0 - X_1^\infty} \right) = f \frac{K I}{V} \quad (4)$$

K then may be calculated from the slope of the (linear) plot of $\ln(X_1 - X_1^\infty)$ against f , thus furnishing one equation for the two unknowns ϕ_1 and ϕ_2 . A second equation is furnished by the requirement that at photoequilibrium equation 1 equals zero and therefore

$$\phi_1 \epsilon_1 C_1^\infty = \phi_2 \epsilon_2 C_2^\infty, \text{ or } \phi_1 \epsilon_1 X_1^\infty = \phi_2 \epsilon_2 X_2^\infty \quad (5)$$

Together with $K = \phi_1 \epsilon_1 + \phi_2 \epsilon_2$ we finally arrive at

$$\phi_1 = K \frac{X_2^\infty}{\epsilon_1}, \phi_2 = K \frac{X_1^\infty}{\epsilon_2} \quad (6)$$

In using eq. 4 f is obtained by graphical integration, feeding the integrand with the experimental D 's (as a function of time). X_1 and X_2 are determined spectrophotometrically, from the absorption spectra of the pure isomers A and B and that of their mixtures.

In rigid media no mixing by diffusion or convection occurs. Equation 1 has to be modified, resulting in a rather complicated equation which can be solved only approximately. The first approximation in fact leads to eq. 4, V denoting the volume passed by the photoactive light.

PHOTOCHEMICAL *cis-trans*-ISOMERIZATION OF SUBSTITUTED STILBENES

BY DIETRICH SCHULTE-FROHLINDE, HARTWIG BLUME, AND HANS GÜSTEN

Kernforschungszentrum Karlsruhe, Strahlenchemisches Laboratorium, Karlsruhe, Germany

Received May 10, 1962

The quantum yields of *cis-trans*-isomerization of stilbenes have been measured as functions of substitution, solvent, temperature, concentration, and wave length of the exciting light. Six independent criteria indicate a markedly reduced lifetime of the excited *cis*-singlet-state (Table V). This short lifetime is responsible for the differences in photochemical behavior of stereoisomeric stilbenes. The results are discussed in the context of the triplet-theory in photochemical *cis-trans*-isomerization.

Introduction

According to Lewis and co-workers¹ the *cis-trans*-isomerization of stilbenes does not occur in the excited singlet state. Otherwise *cis*-stilbene also should give measurable fluorescence. Thus, two possibilities for the mechanism of isomerization remain. Either the rearrangement occurs in the triplet state or the electronic excitation energy after internal conversion, and present as point heat in the molecule, results in thermal rearrangement in the S_0 -ground state. Recent authors presume a transition in electronic excited states.²⁻⁵ Förster⁶ postulates a *cis-trans*-isomerization of the C=C double bond *via* the triplet state, both parts of the molecule being twisted by 90 degrees at the double bond. Earlier Hüchel⁶ and Mulliken⁷ considered twisted states in *cis-trans*-isomerization. The results of this work are discussed in the context of the triplet theory.

Experimental

Materials.—4-Nitro-4'-methoxystilbene, *cf.*⁴ 4,4'-Dinitrostilbene: preparation according to Walden and Kernbaum⁸; m.p. 298°, λ_{\max} 368 m μ , $\log \epsilon$ 4.577 (dimethylformamide). *cis*-Isomer: *trans*-4,4'-dinitrostilbene was

dissolved in benzene and irradiated using a high pressure quartz mercury arc lamp (Osram S 81). The irradiated solution was chromatographed on activated alumina (neutral) and the resulting *cis*-isomer was crystallized from benzene; m.p. 187°, λ_{\max} 320 m μ , $\log \epsilon$ 4.193 (dimethylformamide).

4-Nitro-3'-methoxystilbene: 3.4 g. of *m*-methoxybenzaldehyde, 4.5 g. of *p*-nitrophenylacetic acid, and 3 ml. of piperidine were heated for three hours to 180–190°; yellow crystals were recrystallized from ethanol; m.p. 87–88°, yield, 5.0 g. *cis*-Isomer: 1.8 g. of *trans*-4-nitro-3'-methoxystilbene was dissolved in 60 ml. of benzene and irradiated using a high pressure quartz mercury arc lamp (Osram S 81) for thirty hours. When placed on an activated alumina (neutral) chromatographic column the *cis*-isomer moved more rapidly as a zone of light yellow color. Repeatedly chromatographed, the *cis*-isomer was obtained as a pale yellow colored oil. After three days, the oil crystallized; m.p. 33–34°, λ_{\max} 320 m μ , $\log \epsilon$ 3.984 (benzene). *Anal.* Calcd. for $C_{15}H_{13}O_3N$ (255.3): C, 70.58; H, 5.13; N, 5.49. Found: C, 71.38; H, 5.23; N, 5.39.

trans-Isomer: elution from the column by means of acetone and recrystallization from acetone-alcohol; m.p. 87–88°, λ_{\max} 357 m μ , $\log \epsilon$ 4.403 (benzene). *Anal.* Calcd. for $C_{15}H_{13}O_2N$ (255.3): C, 70.58; H, 5.13; N, 5.49. Found: C, 70.94; H, 5.22; N, 5.22.

4-Nitro-4'-aminostilbene: the method of preparation of Calvin and Buckles⁹ (*trans*-isomer), and the *cis-trans*-separation according to Calvin and Alter,¹⁰ were used without alteration.

4-Nitro-4'-dimethylaminostilbene—*trans*-isomer: preparation according to Pfeiffer¹¹; m.p. 250–251°, λ_{\max} 432 m μ , $\log \epsilon$ 4.476 (benzene). *cis*-Isomer: 1.5 g. of *trans*-4-nitro-4'-dimethylaminostilbene in 750 ml. of benzene was irradiated for five hours in a high pressure mercury immersion arc lamp (Heraeus Q 81) at 40°. A sodium nitrite solution filter absorbed all light of shorter wave length than 366 m μ .

(1) G. N. Lewis, T. T. Magel, and D. Lipkin, *J. Am. Chem. Soc.*, **62**, 2973 (1940).

(2) P. P. Birnbaum and D. W. G. Style, *J. Chem. Soc.*, 1192 (1955).

(3) G. Zimmermann, L. Chow, and U. Paik, *J. Am. Chem. Soc.*, **80**, 3528 (1958).

(4) D. Schulte-Frohlinde, *Liebigs Ann. Chem.*, **612**, 138 (1958).

(5) Th. Förster, *Z. Elektrochem.*, **56**, 716 (1952).

(6) E. Hüchel, *Z. Physik*, **60**, 423 (1930).

(7) R. S. Mulliken, *Phys. Rev.*, **41**, 751 (1932).

(8) P. Walden and K. Kernbaum, *Ber.*, **23**, 1958 (1890).

(9) M. Calvin and R. E. Buckles, *J. Am. Chem. Soc.*, **62**, 3324 (1940).

(10) M. Calvin and H. W. Alter, *J. Chem. Phys.*, **19**, 765 (1951).

(11) P. Pfeiffer, *Ber.*, **48**, 1796 (1915).

The solution was placed on an inactivated basic alumina chromatographic column (2.5 × 100 cm.) and the pale pink colored *cis*-isomer zone eluted with ether. After evaporation, the residue was taken up in a few drops of benzene and crystallized in the cold to give red scaly crystals; m.p. 104–105°, yield 18 mg.; λ_{\max} 418 m μ , $\log \epsilon$ 3.944 (benzene). *Anal.* Calcd. for C₁₈H₁₆N₂O₂ (268.3): N, 10.44. Found: N, 10.98.

trans-Stilbene-4-diazonium Fluoroborate: A suspension of 400 mg. of pure *trans*-4-amino-stilbene in 50 ml. of 50% HCl was diazotized under stirring with a solution of 190 mg. of NaNO₂ in 1 ml. of H₂O at -5°. After one hour of stirring the precipitate was filtered off. The diazonium fluoroborate was precipitated from the filtrate with a few milliliters of HBF₄. The orange precipitate was drawn off, washed with a few milliliters of cold HBF₄, and an excess of ether, and crystallized as orange crystals from acetic acid: λ_{\max} 396 m μ , $\log \epsilon$ 4.468 (50% methanol-water). *Anal.* Calcd. for C₁₄H₁₁N₂BF₄ (294.1): C, 57.17; H, 3.77; N, 9.53; B, 3.68. Found: C, 56.18; H, 4.14; N, 9.65; B, 3.80.

cis-Stilbene-4-diazonium Fluoroborate: *cis*-4-aminostilbene hydrochloride was prepared according to Schmidt¹² by chromatographic *cis-trans*-separation of irradiated 4-nitrostilbene and subsequent reduction of the isolated *cis*-4-nitrostilbene. A suspension of 400 mg. of *cis*-4-aminostilbene hydrochloride was diazotized under stirring with 0.75 ml. of a 1 M solution of NaNO₂ in water at 20°. The oil and orange colored precipitate formed were filtered off. The diazonium fluoroborate was precipitated from the filtrate with 0.5 ml. of 40% HBF₄. The precipitate thus formed was *trans*-stilbene-4-diazonium salt. At +20° *cis*-stilbene-4-diazonium salt remained dissolved in the filtrate. At -20° the *cis*-diazonium salt crystallized. After drawing off, the salt was washed with ether. The bright yellow colored *cis*-stilbene-4-diazonium fluoroborate dissolved easily, thus making recrystallization or reprecipitation difficult; λ_{\max} 372 m μ , $\log \epsilon$ 4.008 (50% methanol-water). *Anal.* Calcd. for C₁₄H₁₁N₂BF₄ (294.1): C, 57.17; H, 3.77; N, 9.53. Found: C, 57.14; H, 3.90; N, 9.88.

Photochemistry and Spectrophotometry

The samples in 2 × 1 cm. quartz cells were irradiated with a stabilized high pressure mercury arc lamp (Osram HBO 200). Heat radiation was absorbed by a thermostated water filter (quartz windows, 7 cm. path length). The different mercury-lines were isolated by means of interference filters (Schott u. Gen., type IL). The purity of the radiation was examined by measuring the transmission spectra of the filters. Every filter has a single band of transmission greater than one per cent. Thus the percentage of light of the neighboring

Hg emission line, m μ	Transmission of the filter >1%, m μ
313	303–329
365	350–395
405	373–429
579	575–608

mercury emission lines is less than 0.1%. The change of isomeric composition was measured with a Zeiss-spectrophotometer PMQ II through the 2-cm. cell path length, and at 90 degrees to the irradiation over the 1-cm. path length. Thus, a decrease of the error introduced by the calculation formula,⁴ especially at higher optical densities, was effected. The optical density normally did not exceed 0.2. The systematic error usually ranged from 5 to 10%. An error calibration curve was used to eliminate this remaining error. The calculation of quantum yields from experimental data was carried out as published earlier.⁴

The intensity of the light incident upon the solution was measured with a calibrated thermopile (Pyro-Werk, Hannover). The thermo-current was measured in a compensating circuit. The absolute error in the determination of quantum yields is $\pm 10\%$; a relative error of not more than $\pm 5\%$ is calculated from the reproducibility of the measurements.

All spectra were taken with a Cary 14 recording spectrophotometer at room temperature. Spectra and quantum yields at high concentrations were measured in special cells.

Quartz plates of 5 mm. thickness and different metal foils were pressed together forming cells with 100 to 0.5 μ path length. The path length was determined by means of infrared interference.

Results

1. Effect of Solvent and Substituent. (a) Quantum Yields of *trans* → *cis*-Isomerization.—Different solvents do not affect the quantum yields of *trans* → *cis*-isomerization of unsubstituted stilbene⁴ and 4,4'-dinitrostilbene (Table I). How-

TABLE I
QUANTUM YIELDS FOR PHOTOCHEMICAL *cis* ⇌ *trans*-ISOMERIZATION OF SUBSTITUTED STILBENES IN DIFFERENT SOLVENTS (EXCITING WAVE LENGTH 366 m μ)

Solvent	Equilibrium % <i>cis</i>	$Q_{t \rightarrow c}$	$Q_{c \rightarrow t}$	Q_s
(a) 4,4'-Dinitrostilbene				
Benzene	80	0.27	0.34	0.61
Chloroform	83	0.29	0.34	0.63
Methanol	80.5	0.29	0.34	0.63
Dimethylformamide	82	0.31	0.33	0.64
(b) 4-Nitro-3'-methoxystilbene				
Cyclohexane	89.0	0.61	0.25	0.86
Benzene	85.5	0.38	0.40	0.78
<i>p</i> -Xylene	83.5	0.39	0.41	0.80
Methanol	82.5	0.28	0.40	0.68
Dimethylformamide	69.0	0.20	0.38	0.58
(c) 4-Nitro-4'-methoxystilbene ⁴				
Benzene	91	0.67	0.24	0.91
Benzene	73	0.40	0.43	0.83
Paraffin oil	74	0.34	0.26	0.60
Chloroform	56	0.17	0.37	0.54
Ethanol	60	0.13	0.40	0.53
Methanol	29	0.07	0.48	0.55
Dimethylformamide	17	0.035	0.42	0.45
(d) 4-Nitro-4'-aminostilbene				
Cyclohexane	75	0.44	0.36	0.80
Benzene	34	0.10	0.44	0.54
Ethanol	0	0	0.30	0.30
Dimethylformamide	0	0	0.20	0.20
(e) 4-Nitro-4'-dimethylaminostilbene				
Cyclohexane	52.5	0.20	0.40	0.60
Benzene	6.5	0.016	0.40	0.42
Ethanol	0	0	0.31	0.31
Dimethylformamide	0	0	0.15	0.15

ever substitution of one of the nitro groups by an electron donating group results in the dependence of the *trans* → *cis*-quantum yield upon the polarity of the solvent. This effect grows as the electron donating properties of the second substituent increase (Table I). In the 4,4'-position, the influence of the substituent on quantum yields is especially strong, while in the 4,3'-position a marked decrease in influence occurs. Consequently we have to consider the non-specific chemical effect of the substituents, as well as of the solvent.⁴

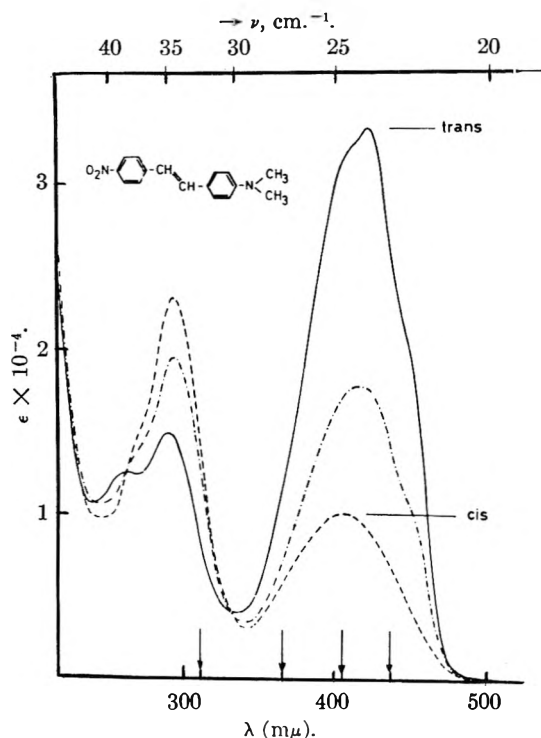


Fig. 1.—Ultraviolet absorption spectra of *trans*- and *cis*-4-nitro-4'-dimethylaminostilbene in cyclohexane: the monochromatic wave lengths used in irradiation are indicated by arrows. The spectrum was taken with a Cary 14 recording spectrophotometer at room temperature; $c = 7.22 \times 10^{-5}$ mole/l. (--- photochemical equilibrium for exciting light of 405 $m\mu$).

The influence of substitution and solvents on the quantum yields of *trans* \rightarrow *cis*-isomerization might be explained by solvation in the case of the excited singlet state. Interpreting the shift of fluorescence wave length caused by different solvents, Lippert^{13,14} has already postulated solvation of excited states by orientation polarization for the same molecules. The *trans* \rightarrow *cis*-isomerization probably is hindered by solvation.

(b) **Quantum Yields of *cis* \rightarrow *trans*-Isomerization.**—The quantum yields of *cis* \rightarrow *trans*-isomerization are in a first approximation independent of substitution and of solvents. Lewis, Magel, and Lipkin¹ concluded that the excited *cis*- S_1 -state was extremely short lived for two reasons: *cis*-stilbenes do not give measurable fluorescence and absorption spectra have no fine structure. If we assume that the $S_1 \rightarrow T$ -transition in *cis*-isomers occurs faster than the arrangement of orientation polarization of the solvent, no more influence upon the *cis* \rightarrow *trans*-quantum yield should be expected. Relaxation time in the solvents used is about 10^{-11} second.¹³ Therefore the excited *cis*- S_1 -state has a lifetime of less than 10^{-11} second. In those cases in which the quantum yield of the *cis* \rightarrow *trans*-isomerization also is affected by the solvent, it may be that the lifetime of the excited *cis*- S_1 -state is of the same order as the relaxation time of the solvents.

(13) E. Lippert. *Z. Elektrochem.*, **61**, 962 (1957); *Z. Naturforsch.*, **10a**, 541 (1955).

(14) E. Lippert with W. Lüder, F. Moll, W. Nägele, H. Boos, H. Prigge, and I. Seibold-Blankenstein, *Angew. Chem.*, **73**, 695 (1961).

2. Effect of Irradiating Wave Length on Quantum Yields.—The quantum yields of the *cis*-*trans*-isomerization of 4-nitro-4'-dimethylaminostilbene are independent of irradiating wave length, even if irradiated in different absorption bands (Fig. 1, Table II). This is another argument against *cis* \rightleftharpoons *trans*-isomerization in the excited singlet state. Normally $S \rightarrow T$ -transitions occur from the S_1 -state only. If this is valid for stilbenes and if the isomerization occurs *via* the triplet state, there should be no dependence of quantum yield upon the wave length of the exciting light. On the other hand, diazonium salts decompose in the excited singlet state. Quantum yields of this decomposition depend upon the energy of exciting light (Table III).¹⁵

TABLE II

QUANTUM YIELDS OF *cis*-*trans*-ISOMERIZATION OF 4-NITRO-4'-DIMETHYLAMINOSTILBENE AS A FUNCTION OF EXCITING WAVE LENGTH

$m\mu$	Equilibrium % <i>cis</i>	$Q_{t \rightarrow c}$	$Q_{c \rightarrow t}$	Q_0
(a) Solvent: Cyclohexane				
313	19.0	0.14	0.45	0.59
366	52.5	0.20	0.40	0.60
405	60.5	0.16	0.42	0.58
436	64.0	0.16	0.37	0.53
(b) Solvent: Benzene				
313	3.0	0.015	0.42	0.44
366	6.5	0.016	0.39	0.41
405	11.0	0.015	0.40	0.42
436	13.5	0.013	0.40	0.41

TABLE III

QUANTUM YIELDS OF THE PHOTODECOMPOSITION OF 2-METHYL-6-[N,N-DIMETHYLAMINO]-PHENAZINEDIAZONIUM FLUOROBORATE-(3) AS FUNCTION OF EXCITING WAVE LENGTH, SOLVENT 0.1 N HCl¹⁵

Wave length of exciting light, $m\mu$	313	366	405	579
Bands	I	II	II	III
Quantum yield	0.25	0.17	0.16	$<10^{-4}$

3. Effects of Temperature and Concentration on Quantum Yields.—*cis*-*trans*-Quantum yields and photochemical equilibrium of 4-nitro-4'-methoxystilbene (concn. 2×10^{-5} mole/l.) are independent of temperature in the range from +20 to +80° (exciting light 366 $m\mu$, solvent *m*-xylene). A thermal step having an activation energy of more than 5 kcal., which influences the quantum yield, does not participate in the isomerization.

The interesting temperature dependence of the *cis* \rightleftharpoons *trans*-isomerization of unsubstituted stilbene, recently found by Stegemeyer,¹⁶ cannot be explained as a thermal transition in the triplet state ($T_{cis} \rightleftharpoons T_{trans}$). Irradiating liquid *cis*-stilbene in a layer of 20 μ thickness at 25°, Stegemeyer obtained an equilibrium of 6% *cis*-isomer. In diluted hexane (10^{-3} mole/l.) solution, however, a photo-

(15) D. Schulte-Frohlind and H. Blume, in preparation.

(16) H. Stegemeyer, *Z. Naturforsch.*, **16a**, 634 (1961).

chemical equilibrium of more than 90% *cis*-isomer is obtained.¹⁷

The high concentration of *cis*-stilbene (~5 mole/l.) used by Stegemeyer would not give the kinetics involving single molecules. His results are influenced by interaction between excited and non-excited molecules. This effect is demonstrated from the dependence of quantum yields of the *trans*-*cis*-isomerization on concentration.

Quantum yields of *trans* → *cis*-isomerization of 4-nitro-3'-methoxystilbene decrease with increasing concentration (Table IV), while quantum yields of *cis* → *trans*-isomerization increase to some extent, causing a shift in photochemical equilibrium.¹⁸ No measurable side reaction has been observed at higher concentrations during the time of irradiation used.

TABLE IV

QUANTUM YIELDS OF *trans* → *cis*-ISOMERIZATION OF 4-NITRO-3'-METHOXYSTILBENE IN 1-METHYLNAPHTHALENE AT DIFFERENT CONCENTRATIONS (366 m μ) (RELATIVE ERROR CALCULATED FROM THE REPRODUCIBILITY $\pm 10\%$)

Concn., mole/l.	$Q_{t \rightarrow c}$	Equilibrium % <i>cis</i>
1.0×10^{-5}	0.32	80.5
1.0×10^{-4}	0.31	81.0
5.0×10^{-4}	0.30	77.5
5.0×10^{-3}	0.29	77.5
1.0×10^{-2}	0.25	75.5
5.0×10^{-2}	0.22	58.5
1.0×10^{-1}	0.18	41.0
5.0×10^{-1}	0.13	22.0
7.5×10^{-1}	0.04	4.0
1.0×10^0	0.00	0.0

These results require a new outlook in preparative photochemistry. In certain cases irradiation at concentrations $> 10^{-2}$ mole/l. should be avoided, otherwise markedly decreased yields might be obtained.

4. Photochemical Reactions of *cis*- and *trans*-Stilbene-4-diazonium Fluoroborate.—Irradiation of *trans*-stilbene-4-diazonium fluoroborate in 0.1 *N* HCl results in the formation of nitrogen, 10% *cis*-, and 90% *trans*-4-hydroxystilbene. The short wave length absorbing *trans*-4-hydroxystilbene did not absorb the incident light. The kinetics of the decomposition are of the first order (Fig. 3). The thermal decomposition of *trans*-stilbene-4-diazonium fluoroborate results in the formation of pure *trans*-4-hydroxystilbene.

In contrast to the *trans*-form, the irradiation of *cis*-stilbene-4-diazonium fluoroborate results in complicated kinetics (Fig. 3), caused by superposition of the photochemical *cis* → *trans*-isomerization and the subsequent photodecomposition of the *trans*-isomer formed; 75% *trans*-4-hydroxystilbene is obtained from the photodecomposition.

From the corresponding thermal decomposition of *cis*-stilbene-4-diazonium fluoroborate, pure *cis*-4-hydroxystilbene is obtained. This result shows that the thermal separation of nitrogen from the diazonium ion does not cause *cis* → *trans*-isomerization.

(17) A. Smakula, *Z. physik. Chem.*, **B25**, 90 (1934).

(18) D. Schulte-Frohlinde and H. G \ddot{u} sten, *Z. physik. Chem.* (Frankfurt), in preparation.

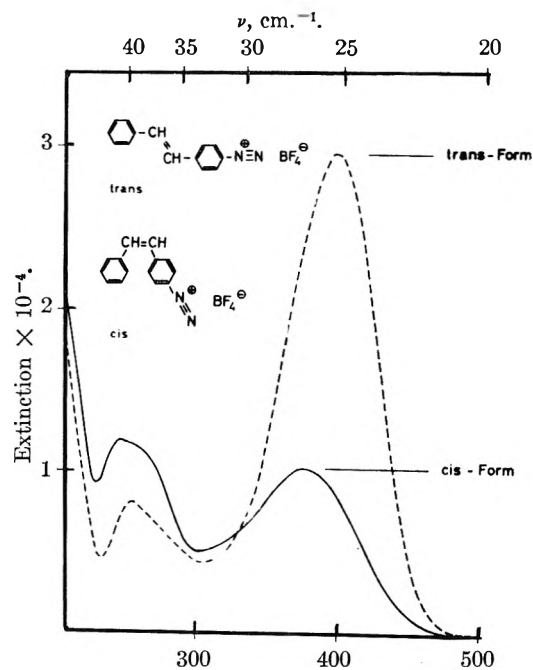


Fig. 2.—Absorption spectra of *trans*- and *cis*-stilbene-4-diazonium fluoroborate in 50% methanol/water. The spectra were taken with a Cary 14 recording spectrophotometer at room temperature; $c_{trans} = 2.51 \times 10^{-5}$ mole/l., $c_{cis} = 7.12 \times 10^{-6}$ mole/l.

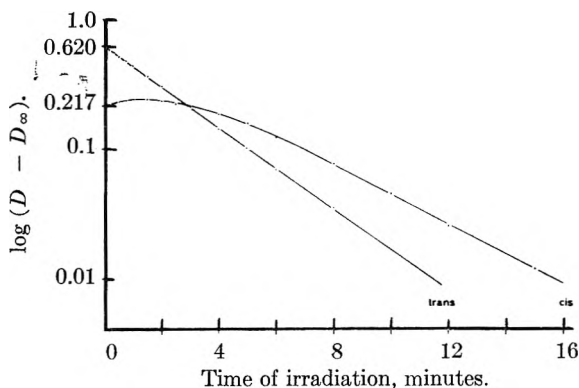


Fig. 3.—Kinetics of photodecomposition of *cis*- and *trans*-stilbene-4-diazonium fluoroborate in 0.1 *N* HCl.

These results may be explained by the rapid $S_1 \rightarrow T$ -transition in *cis*-stilbenes. In the normal-lived *trans* singlet state dissociation is faster than isomerization. In the short-lived *cis* singlet state, however, isomerization is faster than dissociation. Obviously deactivation of the *cis*- S_1 -state occurs so fast that dissociation of the C-N bond cannot compete. Therefore we conclude that *cis*-*trans*-isomerization and dissociation occur from different electronic states.

We know that the photodecomposition of diazonium salts occurs *via* excited singlet states.^{15,19} Therefore we assume that the *cis*-*trans*-isomerization occurs in the triplet state.

Discussion

The results favoring the short lifetime of the excited *cis*-singlet state are compiled in Table V.

(19) Two facts support this mechanism: first, diazonium salts do not fluoresce and second, quantum yields of the decomposition of diazonium salts depend on the wave length of exciting light.

TABLE V

PROPERTIES OF SUBSTITUTED <i>cis</i> - AND <i>trans</i> -STILBENES			
		<i>trans</i>	<i>cis</i>
1	Fluorescence	yes	no
2	Fine structure of ultraviolet absorption spectrum	yes	no
3	Dependence of quantum yields on concentration	yes	no
4	Dependence of quantum yields on solvents	yes	no
5	<i>cis-trans</i> -Isomerization of stilbene-4-diazonium salt	no	yes
6	Dependence of quantum yields on temperature ²⁰	large	small

The short lifetime of exciting singlet states in *cis*-isomers is caused by steric hindrance.⁴ *trans*-Stilbenes are in nearly planar configuration. However, in *cis*-stilbenes the phenyl rings are twisted in relation to each other by about 30°. ²¹ Thus, the steric structure of the triplet state is preconditioned by this twist in *cis*-isomers and it seems possible that by this means the radiationless S₁ → T-transition is activated.

Förster²² considered an activation of the S₁ → T-transition by molecular twisting. The lack of fluorescence or the relatively small fluorescence of large organic molecules and dyes, which are sterically hindered by twisting, probably is caused also by an activated S₁ → T-transition. One example is the lack of fluorescence in the first sterically hindered species of several series of cyanine dyes.²³ Further examples are given by Förster.²⁴

Mechanism of the Photochemical *cis-trans*-Isomerization.—At present two of the proposed mechanisms of photochemical *cis-trans*-isomerization are still under discussion: first, thermal isomerization of an excited singlet state; second, photoisomerization of stilbenes *via* a triplet state.

I. Thermal Isomerization of an Excited Singlet State.—The average lifetimes of the first excited singlet states of substituted *trans*-stilbenes are 1.5–3.3 × 10⁻⁹ sec. as calculated from fluorescence measurements.²⁵ *cis*-Stilbenes do not emit fluorescence. The fluorescence of *trans*-stilbenes is only possible if we assume that in the first excited singlet state the *trans*- and the *cis*-form are separated by a barrier of potential energy. This potential barrier hinders the rotation.

From the dependence of quantum yield of the photochemical *cis-trans*-isomerization on temperature, Fischer¹⁹ calculated a value of about 2 kcal./mole. If we assume these 2 kcal. as being the activation energy of the thermal *cis-trans*-isomerization in the first excited singlet state, then the Arrhenius equation gives such short lifetimes for the *trans*-singlet state that no fluorescence

should be observed. Therefore we have to consider a higher barrier of potential energy.

Recently McClure²⁶ calculated the height of the potential barrier in the excited singlet state of stilbene from spectroscopic data. He obtained a value of 40 kcal./mole. This result is inconsistent with the photochemical *cis-trans*-isomerization at moderate temperatures. Therefore a thermal isomerization in the first excited singlet state seems to be improbable. In agreement with Förster,⁵ we assume that the photochemical *cis-trans*-isomerization of stilbenes occurs in the triplet state. From similar considerations Fischer²⁰ comes to the same conclusion, as well as McClure.²⁶

II. Photoisomerization of Stilbenes *via* a Triplet State.—These arguments favor photoisomerization of stilbenes *via* triplet states: (1) *cis-trans*-Isomerization can be obtained by direct excitation of singlet-triplet transitions from the singlet ground state.²⁷ (2) Triplet-triplet energy transfer induces *cis-trans*-isomerization.^{28,29} (3) The results of the photodecomposition of isomeric stilbene-4-diazonium salts support the theory.

The question of whether the diagram of potential energy *versus* twisting angle of the triplet state shows a minimum or a maximum at 90° is not yet answered. In the case of stilbenes Förster⁵ assumes a minimum. If this is correct the triplet state of stilbenes should be very short-lived. According to Evans³⁰ the energy of the 0-0-S₀ → T-transition of untwisted stilbene is 51 kcal./mole. The activation energy of the thermal *cis* → *trans*-isomerization in solution is 36.7 kcal./mole.³¹ Then the barrier of potential energy of twisting from the *trans*-ground state is the sum of this value and the energy difference of the *cis*- and the *trans*-isomer of 5.66 kcal./mole.²⁶ Thus, for the twisted singlet-ground state a potential energy of 42.4 kcal./mole results. If we consider finally that the potential energy of the triplet state of 51 kcal./mole is lowered by twisting, we can assume that in stilbenes the potential surfaces of the triplet state and of the singlet-ground state contact or even overlap each other. Under these conditions the lifetime of the triplet state is shortened. These criteria favor these assumptions: (1) Hitherto no phosphorescence has been obtained in rigid media at liquid nitrogen temperatures for *cis*- and *trans*-stilbenes.³² Furthermore in compounds containing a C=C double bond phosphorescence has not been established. The report of phosphorescence of *cis*-stilbene and halogen substituted ethylenes published earlier by Lewis and Kasha³³ has in the meantime been retracted by Kasha.³⁴ (2) No normal long-lived triplet states

(20) S. Malkin and E. Fischer, *J. Phys. Chem.*, **66**, 2482 (1962).

(21) H. Suzuki, *Bull. Chem. Soc. Japan*, **33**, 379 (1960); *Chem. Abstr.*, **54**, 20471 (1960); F. J. Adrian, *J. Chem. Phys.*, **28**, 608 (1958).

(22) Th. Förster, "Fluoreszenz organischer Verbindungen," Vandenhoeck and Ruprecht, 1951, p. 122.

(23) L. J. E. Hofer, R. J. Grabenstetter, and E. O. Wiig, *J. Am. Chem. Soc.*, **72**, 703 (1950).

(24) Reference 22, p. 110.

(25) P. P. Shorygin and T. M. Ivanova, *Soviet Phys. "Doklady,"* **3**, 764 (1958).

(26) R. H. Dyck and D. S. McClure, *J. Chem. Phys.*, **36**, 2326 (1962).

(27) D. F. Evans, *J. Chem. Soc.*, 1735 (1960).

(28) G. S. Hammond, N. J. Turro, and P. A. Leermakers, *J. Phys. Chem.*, **66**, 1144 (1962).

(29) W. Berends and J. Posthuma, *ibid.*, **66**, 2547 (1962).

(30) D. F. Evans, *J. Chem. Soc. (London)*, 1351 (1957).

(31) F. W. J. Taylor and A. R. Murray, *ibid.*, 2078 (1938).

(32) D. Schulte-Frohlinde, 1957, unpublished.

(33) G. N. Lewis and M. Kasha, *J. Am. Chem. Soc.*, **66**, 2100 (1944).

(34) M. Kasha, *Ann. Rev. Phys. Chem.*, **7**, 403 (1956).

have been found by means of photoflash techniques in stilbenes.^{35,36}

A maximum of potential energy at a twisting angle of 90° is inconsistent with the experimental result that *cis* ⇌ *trans*-isomerization occurs even in rigid media at low temperature.^{1,17,20,37} These

(35) G. Porter, private communication.

(36) K. Breitschwerdt and A. Weller, *Z. physik. Chem.* (Frankfurt), **20**, 353 (1959).

(37) E. Lippert and W. Lüder, *J. Phys. Chem.*, **66**, 2430 (1962).

results can be understood if a torsion force is assumed effective in the triplet state. This torsion force exists if the triplet state has a minimum potential energy at 90 degrees twisting angle. Accordingly we consider the activation energy of 2-3 kcal./mole found by Fischer²⁰ for the *trans* → *cis*-isomerization of stilbene as being the activation energy of the transition from the first excited singlet to the triplet state in the *trans*-isomer.

HYDROGEN BONDING OF EXCITED STATES

By E. J. BOWEN, N. J. HOLDER, AND G. B. WOODGER

Physical Chemistry Laboratory, Oxford University, Oxford, England

Received May 25, 1962

Measurements have been made of the quantum yields of fluorescence of acridine dissolved in mixtures of water (alkaline) and certain organic solvents. The results are interpreted on the assumption that hydrogen bonding with the solvent, and particularly with water, takes place rapidly after the molecule is excited by absorbing a light quantum, and that such complexes represent the fluorescent entity; thermal breaking of the hydrogen bonds leading to degradation of electronic excitation energy. The acridinium ion shows a different behavior; its fluorescence changes little in solvent mixtures of different composition and is much less dependent on temperature.

Acridine is classed as a "π-electron deficient" heterocyclic¹ and as such would be expected to show poor fluorescence properties. It is in fact non-fluorescent in the crystalline state, or when dissolved in organic solvents such as benzene or ethyl acetate, but it fluoresces blue in solution in water or aqueous alcohol. The acridinium ion fluoresces a green color in whatever solvent it may be formed. For example, the addition of proton-donors such as the chloroacetic acids to benzene solutions of acridine causes the development of the characteristic green fluorescence.² Acridine is a weak base, and the molecule in water changes over to the ion at about pH 5.45, as shown by change of absorption spectrum. The fluorescence change-over from blue to green, however, occurs at about pH 10.35. The explanation of this effect has been given by Förster³ and Weller.⁴ The electronic excitation of acridine makes it a much stronger base, and between the pH limits given above light is absorbed by the molecule, and this in its excited state very rapidly acquires a proton, so that the green fluorescence emission occurs from the excited ionic form. The blue fluorescence of aqueous acridine solutions observed at pH values greater than 10.35 is the chief subject of this paper. Bowen and Sahu described measurements of the variation of the fluorescence of acridine in water-alcohol mixtures.⁵ Their results, however, require some revision since, as pointed out, in neutral solutions the solute fluoresces partly as the molecule and partly as the ion. In the work now presented 1.3 *N* ammonia or 0.02 *N* sodium hydroxide solutions were used instead of neutral water for making up mixtures, to ensure that the acridine was kept

(1) A. Albert, "Heterocyclic Chemistry," Chap. 3, Univ. of London, 1959.

(2) N. Mataga and S. Tsuno, *Bull. Chem. Soc. Japan*, **30**, 368 (1957).

(3) Th. Förster, *Z. Elektrochem.*, **54**, 42 (1950).

(4) A. Weller, *ibid.*, **61**, 956 (1957).

(5) E. J. Bowen and J. Sahu, *J. Chem. Soc.*, 3716 (1958).

TABLE I

Volume % of water	Quantum yield of fluorescence <i>F</i>			
	Ethanol	Formamide	Dioxane	Dimethyl- formamide
100	0.37	0.37	0.37	0.37
90	.34	.33	.32	.31
80	.28	.29	.23	.24
70	.18	.24	.13	.18
60	.11	.19	.086	.12
50	.079	.15	.055	.084
40	.062	.10	.035	.053
30	.048	.073	.019	.022
20	.036	.047	.012	.000
10	.034	.023	.006	.000
0	.032	.012	.000	.000

TABLE II

DIOXANE-WATER MIXTURES

Temp., °K.	Water % by volume					
	90		70		50	
	<i>E</i> = 6190 log <i>K</i> = 4.96		<i>E</i> = 5900 log <i>K</i> = 5.21		<i>E</i> = 5750 log <i>K</i> = 5.51	
	<i>F</i>		<i>F</i>		<i>F</i>	
	Exptl.	Calcd.	Exptl.	Calcd.	Exptl.	Calcd.
283	0.38	0.385	0.17	0.173	0.07	0.075
293	.30	.299	.13	.128	.05	.054
303	.24	.230	.10	.094	.04	.039
313	.18	.179	.07	.071	.03	.029
323	.14	.137	.05	.054	.02	.022
333	.11	.107	.04	.04	.02	.017
343	.08	.083

almost entirely in the molecular form even in its excited state. Acridine concentrations of about 10⁻⁴ *M* were used. The solutions were contained in a small transparent dewar vessel and the temperature adjusted by the insertion of hot or cold glass "fingers." The fluorescence was excited by 3660 Å. radiation, and a calibrated photomultiplier-spectrograph combination, corrected for instrumental wave length sensitivity differences,

TABLE III
 ETHANOL-WATER MIXTURES

Temp., °K.	Water % by volume									
	90		80		70		60		50	
	$E = 6590$ $\log K = 5.16$		$E = 6410$ $\log K = 5.16$		$E = 6050$ $\log K = 5.16$		$E = 5090$ $\log K = 4.69$		$E = 4750$ $\log K = 4.60$	
	F		F		F		F		F	
	Exptl.	Calcd.	Exptl.	Calcd.	Exptl.	Calcd.	Exptl.	Calcd.	Exptl.	Calcd.
273	0.49	0.51	0.42	0.45	0.30	0.31	0.17	0.19	0.12	0.13
283	.40	.44	.34	.36	.23	.23	.14	.14	.10	.10
293	.33	.35	.27	.27	.17	.17	.11	.11	.08	.08
303	.26	.27	.21	.21	.13	.13	.09	.08	.06	.06
313	.21	.21	.16	.16	.10	.10	.07	.07	.05	.05
323	.16	.16	.12	.12	.08	.08	.05	.05	.04	.04
333	.12	.12	.09	.09	.06	.06	.04	.04	.03	.03
343	.09	.09	.07	.07	.04	.05	.03	.04	.02	.02

collected and dispersed into a spectrum the fluorescence emerging at right angles. Absolute fluorescence quantum yields F were determined by comparing the area of the corrected fluorescence spectra with that from a solution of quinine sulfate in 0.1 *N* sulfuric acid made up to an equal optical density, taking F for this standard at 18° as 0.55.⁶

Table I gives the values of quantum yields of fluorescence F at 18° for mixtures of (alkaline) water with four organic liquids.

Tables II and III give values of F at different temperatures for water-dioxane and water-ethanol mixtures of different compositions.

If a degradatory process requiring an energy of activation E is assumed to compete with fluorescence emission, it follows that

$$\log(1/F - 1) = \log k - \frac{E}{2.3RT}$$

The experimental F values in Tables II and III are compared with the calculated values. Values of E range from 6600 to 4750 cal./mole, diminishing as the water content is decreased, but more so for ethanol than for dioxane mixtures. Table I shows that values of F reach zero for pure dioxane or dimethylformamide but are non-zero for ethanol or formamide. These facts point strongly to the interpretation that the blue fluorescent entity of acridine is a state hydrogen-bonded to the solvent, and that the E value represents the heat of such bonding. However, the absorption spectra of acridine in water, alcohol, or benzene are remarkably similar, and the solubility of acridine in water is very low ($\approx 2 \times 10^{-4}$ mole/l.), indicating negligible hydrogen bonding of the ground state. It would seem that light is absorbed by the molecule (in

alkaline solutions) and that the excited state, which is much more strongly basic, rapidly hydrogen-bonds with the solvent, particularly with water, and that these entities either fluoresce or dissociate with energy degradation. The frequency factor of this latter process is given by the product of k -values of Tables II and III and the reciprocal of the mean radiational lifetime of the excited state ($\approx 6.7 \times 10^7$ sec.⁻¹ from absorption band area⁷), and reaches the high value of about 10^{13} . If the excited state is hydrogen bonded to the solvent and its thermally activated state is released from this bonding the high value of the frequency factor of the degradation reaction may be explained in terms of an entropy of activation.⁸

The green fluorescence of the acridinium ion shows a different behavior in solvent mixtures. Table IV gives fluorescence yields for various water-ethanol compositions at 18°, the water being acidified to 0.02 *N* with sulfuric acid. The yields fall off very little as the alcohol concentration is increased, and the effect of temperature is also small, E being about 950 cal./mole. These results indicate that there is no large difference in the degree of hydrogen bonding between the ground and excited states of the acridinium ion.

TABLE IV

Volume % of aqueous N H ₂ SO ₄	Quantum yield of fluorescence	Volume % of aqueous N H ₂ SO ₄	Quantum yield of fluorescence
100	0.54	50	0.52
90	.54	40	.51
80	.54	30	.50
70	.54	20	.49
60	.53	10	.49

(7) Th. Förster, "Fluoreszenz Organischer Verbindungen," Vandenhoeck and Ruprecht, Göttingen, 1951, p. 158.

(8) C. Steel and K. J. Laidler, *J. Chem. Phys.*, **34**, 1827 (1961).

(6) C. A. Parker and W. T. Rees, *Analyst*, **85**, 596 (1960); **87**, 83 (1962); C. A. Parker, *Anal. Chem.*, **34**, 502 (1962).

SPECTROSCOPIC STUDIES OF RARE EARTH CHELATES

BY G. A. CROSBY, R. E. WHAN, AND J. J. FREEMAN

Department of Chemistry, University of New Mexico, Albuquerque, New Mexico

Received May 26, 1962

Intramolecular energy transfer in rare earth chelates is discussed and the role of the triplet states of the complexes in this type of energy migration is reviewed briefly. A spectroscopic study of the chelates of La^{3+} , Pr^{3+} , Sm^{3+} , Eu^{3+} , and Gd^{3+} with *o*-hydroxybenzophenone is reported. Luminescence spectra (at 77°K.) of these compounds are presented and the triplet state energies of the chelates and their dissociation products have been determined utilizing energy transfer as an aid in interpreting the complicated luminescences observed. Very weak "line" emission from the coordinated Pr^{3+} ion is reported and selective excitation of the $^1\text{D}_2$, $^3\text{P}_0$, and $^3\text{P}_1$ resonance levels of this ion *via* intramolecular energy transfer is demonstrated.

Introduction

Luminescence spectra of rare earth chelates yield useful information about energy migration in complex molecules and furnish additional data on the ions themselves.

The trivalent ions of the rare earth elements, lanthanum through lutetium, exhibit remarkable similarities in chemical properties. These ions with the exception of Ce^{3+} all form stable complexes, and a series of chelates of them derived from a specific complexing agent can be prepared by the same chemical method. Such a series of chelates possesses similar properties (solubility, melting point, solvate formation, etc.). The similarities are reflected also in the nearly identical absorption spectra of a given series. For example, the reported near ultraviolet absorption spectra of all the trisbenzoylacetone chelates ($\sim 10^{-5} M$) of the trivalent rare earths (no data on Ce^{3+} and Pm^{3+}) are identical within experimental error; the same is true for the trisdibenzoylmethide chelates.¹ Such similarities do not obtain in the luminescence spectra.

Excitation of rare earth chelates to low excited singlet states results in complex luminescence spectra consisting of varying yields of molecular fluorescence and phosphorescence and of "line" emissions characteristic of the lanthanide ions. The quantum yields of total luminescence also vary widely, ranging from values approaching unity to values of less than 10^{-4} . The diversity in these observations must be explained in terms of competing radiative and radiationless processes for molecular de-excitation. The dependence of the luminescences of a series of chelates upon the central coordinated ions affords a sensitive means of studying these processes.

Experimental

Details for the preparation and analyses of the rare earth chelates of dibenzoylmethane and benzoylacetone are reported elsewhere.¹ The rare earth chelates of *o*-hydroxybenzophenone were prepared in the following manner. Stoichiometric quantities of the rare earth chloride and *o*-hydroxybenzophenone were dissolved in absolute ethanol, and anhydrous ammonia gas was bubbled into this solution until no more precipitation occurred. Distilled water was added with stirring to the reaction mixture to complete the precipitation of the chelate, which was quite soluble in absolute ethanol. The product was filtered, washed with distilled water, and dried under vacuum at room temperature for 8 hr. The analyses for metal were performed by ignition in air, and the results were consistent with the expected theoretical values.

Rare earth oxides (99.9%) were obtained from Research Chemicals, Burbank, California, and were converted to the chlorides by treatment with hydrochloric acid and evaporation to dryness. The *o*-hydroxybenzophenone was obtained from K and K Laboratories, Jamaica 33, New York, and was purified by distillation under vacuum.

For luminescence studies all chelates were studied at 77°K. at concentrations of $\sim 10^{-5} M$ in the following solvents which form rigid glasses at this temperature: (a) pure 3-methylpentane, (b) one part diethyl ether and one part 3-methylpentane by volume (EP), and (c) two parts diethyl ether, two parts 3-methylpentane, and one part ethanol by volume (EPA).

The 3-methylpentane (Phillips pure grade) was passed through a column of silica gel and then distilled from sodium ribbon. The absolute ethanol (USI Co. absolute pure ethanol, reagent grade) was distilled from $\text{Mg}(\text{OEt})_2$. The diethyl ether (Mallinckrodt anhydrous grade) was distilled from sodium ribbon.

The apparatus and experimental details for the spectroscopic studies are given in reference 1. Filter combinations for all chelates excepting those of *o*-hydroxybenzophenone are reported in reference 2. A combination of two Corning glass 9863 filters and a 5 cm. path of $\text{CuSO}_4 \cdot 5\text{H}_2\text{O}$ (100 g./l.) which transmitted light from ~ 3000 to 4000 \AA . was used for excitation of the *o*-hydroxybenzophenone chelates.

Energy Migration in Chelates.—In order to delineate the possible paths of energy migration within a rare earth chelate molecule it is convenient to refer to an energy level diagram (Fig. 1). After excitation of a chelate to a vibrational level of the first excited singlet state ($S_0 \rightarrow S_1$), the molecule undergoes rapid internal conversion to lower vibrational levels through interaction with the solvent matrix. The excited singlet state may be deactivated by combining radiatively with the ground state ($S_0 \leftarrow S_1$), resulting in molecular fluorescence, or the molecule may undergo non-radiative intersystem crossing from the singlet to the triplet system. Again by internal conversion the molecule may reach the lowest triplet state, T_1 . From this state it can then combine radiatively with the ground state by means of a spin-forbidden transition ($S_0 \leftarrow T_1$) giving rise to a typical long-lived molecular phosphorescence. Alternatively, the molecule may undergo a non-radiative transition from the triplet system to a low-lying rare earth ion state.² The latter states are derived from the 4f electronic configuration of the coordinated trivalent rare earth ion. After this indirect excitation by energy transfer, the metal ion may undergo a radiative transition to a lower ion state resulting in characteristic line emission, or it may be deactivated *via* radiationless processes. Direct transfer of energy from the excited singlet state to the low-lying rare earth ion states has been shown to

(1) R. E. Whan and G. A. Crosby, *J. Mol. Spectry.*, **8**, 315 (1962).(2) G. A. Crosby, R. E. Whan, and R. M. Alire, *J. Chem. Phys.*, **34**, 743 (1961).

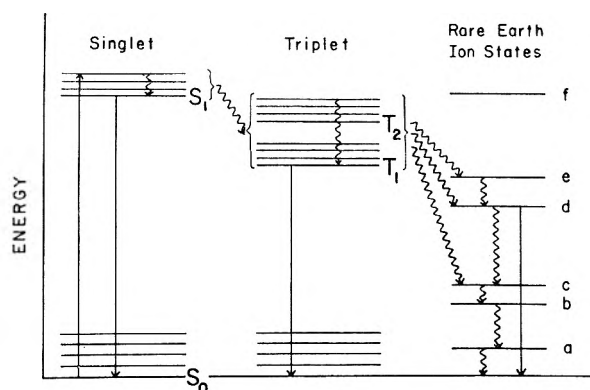


Fig. 1.—Schematic energy level diagram for a rare earth chelate possessing low-lying $4f$ electronic states: \rightarrow , radiative transitions; \rightsquigarrow , radiationless transitions. Reproduced with permission from ref. 1.

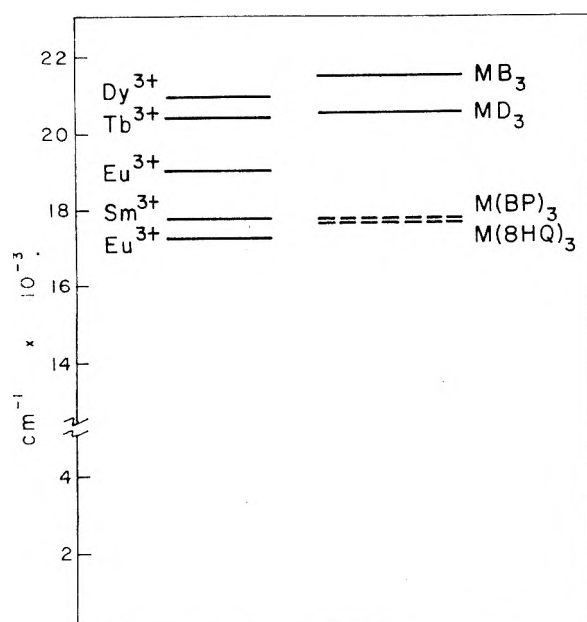


Fig. 2.—Principal resonance levels of those rare earth ions exhibiting especially bright line emission and the triplet state energies of some typical rare earth chelates. Chelates derived from benzoylacetone (MB_3), dibenzoylmethane (MD_3), *o*-hydroxybenzophenone ($M(BP)_3$), and 8-hydroxyquinoline ($M(8HQ)_3$).

be unimportant.² Likewise it has been shown that direct excitation of the ion is unimportant.

Previous work on rare earth inorganic salts has shown that line emission characteristic of the ion originates from only a few specific states termed resonance levels. If the ion is excited to a non-emitting level, either directly or indirectly, the excitation energy is degraded *via* radiationless processes to lower states until a resonance level is reached. Radiative transitions then become competitive and characteristic ion emission is observed. These processes are indicated in Fig. 1 with d representing the resonance level.

In order to obtain the characteristic emission from a rare earth ion, it is necessary to excite a resonance level. For excitation of a rare earth ion by transfer of energy from an excited chelate molecule to the central coordinated metal ion, *resulting in line emission* from the ion, it is necessary that

the lowest triplet state energy level of the complex be nearly equal to or lie above a resonance level of the ion. Otherwise sufficient energy is not available to excite the ion indirectly to its emitting level, and no line emission is observed. Thus the luminescence observed from a specific chelated rare earth ion is a sensitive function of the position of the lowest triplet energy level of the complex relative to a resonance level of the ion. Consequently, it is possible to control the emission from a given ion by varying the ligand and therefore the position of the triplet state of the complex. In other words the emission from an ion may be turned on or off by an appropriate choice of complexing agent. For example, the luminescence observed from dysprosium trisdibenzoylmethide consists of molecular fluorescence and phosphorescence, whereas dysprosium trisbenzoylacetone exhibits primarily bright line emission characteristic of Dy^{3+} . Here only a relatively minor change in the structure of the ligand results in a striking difference in the luminescences observed from the two compounds, when they are irradiated with near ultraviolet light.³

Another example of the phenomenon and an indication of the selectivity of this method of indirect ion excitation is illustrated by chelates of trivalent europium. This ion, which usually emits brightly from two well established resonance levels, can be limited to emit radiation only from the lower level by choosing appropriate complexing agents.²

If the triplet state energies of the complexes are known with certainty, one can use energy transfer to simplify the emission spectrum of a given ion by selectively exciting resonance levels. This technique has been used to aid in the assignment of a new group of lines in the emission spectrum of Tm^{3+} .⁴

Bracketing Triplet State Energies.—Conversely, whenever the luminescence spectra observed from a series of lanthanide chelates are too weak or too complex to ensure accurate measurements of the phosphorescing (triplet) states, one can employ energy transfer as an aid in bracketing the energies of these states.

In Fig. 2 we have plotted the principal resonance levels of those rare earth ions exhibiting especially bright line emission and the triplet state energies of some typical rare earth chelates. Both resonance levels of trivalent europium have been included. This manifold of resonance levels spans an energy range of ~ 3700 cm^{-1} . The energies of the lowest triplet states of most of the rare earth complexes studied thus far fall within the same region. This happy circumstance has enabled us to determine the positions of the triplet state energies within certain limits whenever direct measurements of the phosphorescences led to uncertain results.

Benzoylacetone chelates of the ions indicated in Fig. 2 all yield bright line emission, thus locating the lowest triplet level above $20,958$ cm^{-1} (Dy^{3+} resonance level). For the corresponding dibenzoylmethide chelates, line emission originating from

(3) G. A. Crosby and R. E. Whan, *J. Chem. Phys.*, **32**, 614 (1960).

(4) G. A. Crosby and R. E. Whan, *ibid.*, **36**, 863 (1962).

all these trivalent ions is observed with the single exception of Dy^{3+} . This brackets the triplet levels of these complexes between 20,430 and 20,958 cm^{-1} .² For many of the benzoylacetone and dibenzoylmethide chelates (trivalent La, Sm, Gd, Dy, Tm, Yb, Lu) the phosphorescences were sufficiently intense so that measurements of the highest energy phosphorescence bands were readily obtained. The averages of these measurements place the triplet state energies of the benzoylacetone and dibenzoylmethide chelates at 21,480 and 20,520 cm^{-1} , respectively. These measured values of the triplet state energies fall within the limits determined by the line emission properties of the chelates as given above.

For the rare earth chelates derived from 8-hydroxyquinoline the problem is more complicated. The phosphorescences from these complexes are very weak and the measurements of the weak emissions observed are subject to much uncertainty. The difficulty is compounded further by the fact that dissociation and photodecomposition of the complexes occur, which casts considerable doubt concerning the origins of the emissions photographed experimentally. A very weak and diffuse band is found at $\sim 17,760 \pm 100 \text{ cm}^{-1}$ for the gadolinium complex. That this is indeed the emission from the triplet state of the chelate is rendered more certain by the fact that europium forms the only rare earth complex derived from 8-hydroxyquinoline that exhibits bright line emission, and this emission originates only from the lower resonance level (17,250 cm^{-1}). This brackets the triplet energy level of the rare earth complexes derived from 8-hydroxyquinoline between 17,250 and 17,800 cm^{-1} , lending credence to the previously measured value of 17,760 cm^{-1} . The utility of employing intramolecular energy transfer as an aid for assigning triplet state energies is well illustrated by this series of compounds.

An even more complicated set of luminescence spectra is obtained from the series of chelates derived from *o*-hydroxybenzophenone. A solution of $Gd(BP)_3$ in pure 3-methylpentane exhibits an intense but diffuse phosphorescence with the first band maximum appearing at 17,400 cm^{-1} (Fig. 3a). In an EP glass⁵ this compound also phosphoresces brightly, but the phosphorescence extends to somewhat shorter wave lengths with an additional prominent peak appearing at $\sim 18,200 \text{ cm}^{-1}$. In a hydroxylic EPA glass at least two phosphorescences are observed; an intense but diffuse band in the range of 5000–7000 Å. and a less intense but well defined phosphorescence between 4000 and 5000 Å. There is no observable fluorescence in any of the solvents. Analogous behavior is exhibited by the corresponding La^{3+} complex in EP and EPA (Fig. 3b). The change of the observed luminescences with solvent change and the appearance of more than one molecular phosphorescence suggest that appreciable dissociation is occurring. Increased dissociation of the complex upon addition of a hydroxylic component is expected on the basis of increased polarity and the possibility of solvation through hydrogen bonding.

(5) See Experimental section.

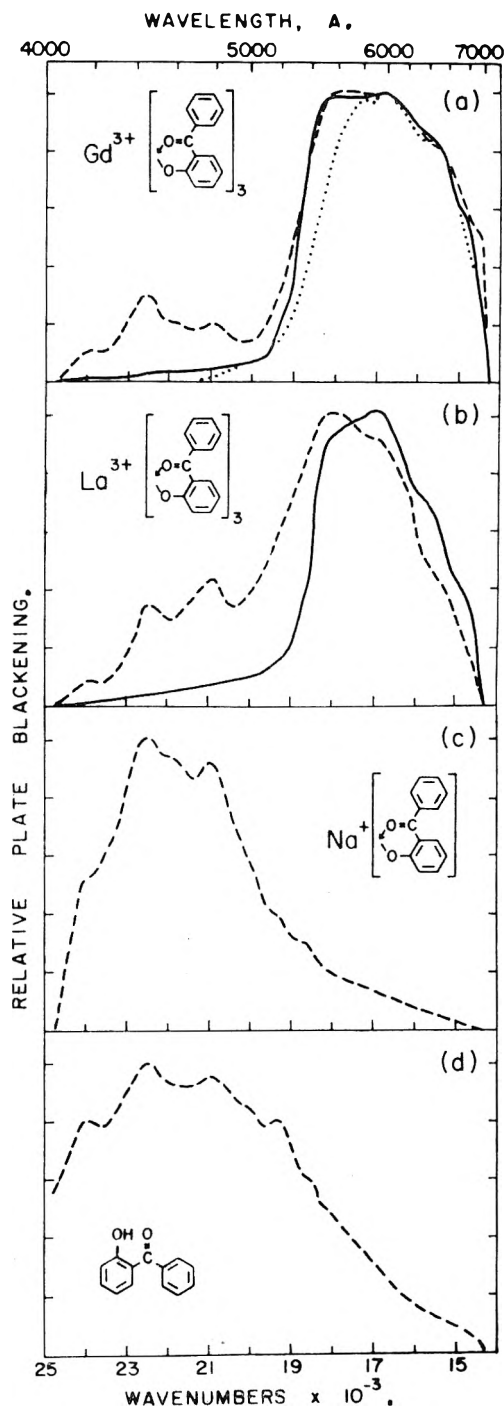


Fig. 3.—Total emission spectra: (a) $Gd(BP)_3$; (b) $La(BP)_3$; (c) $Na(BP)$; (d) *o*-hydroxybenzophenone; —, EP glass at 77°K.; ---, EPA glass at 77°K.; ·····, 3-methylpentane glass at 77°K.

Further evidence for dissociation is presented in Fig. 3c and 3d. The total emission spectra of *o*-hydroxybenzophenone and its sodium salt should be compared with the spectra of the rare earth complexes in EPA. The well defined 4000–5000 Å. phosphorescences in the latter spectra correlate in detail with the prominent emissions observed from the chelating agent and its sodium salt. A conspicuous $\sim 1550 \text{ cm}^{-1}$ progression is common to them all. The addition of trichloroacetic acid

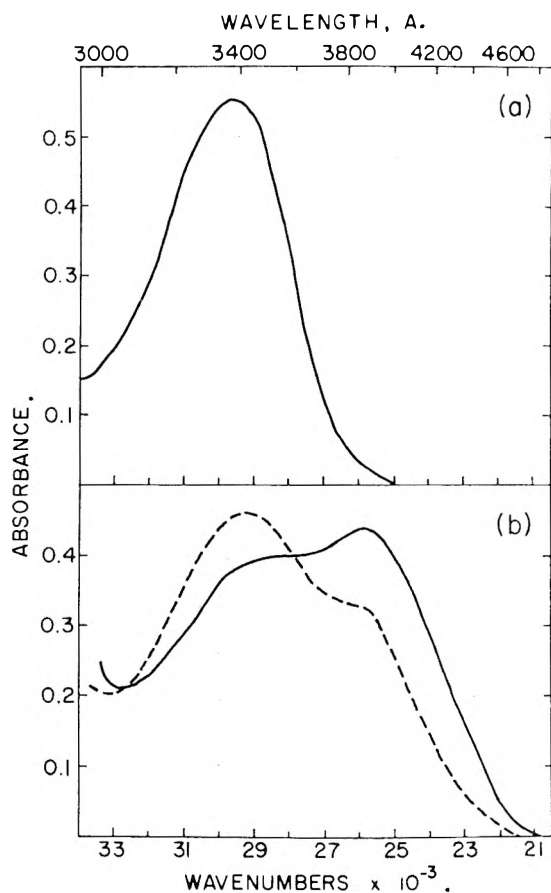


Fig. 4.—(a) Absorption spectrum of *o*-hydroxybenzophenone at $1.4 \times 10^{-4} M$ in EPA or EP at 25° in 1 cm. path. (b) Absorption spectra of the trivalent lanthanum chelate of *o*-hydroxybenzophenone at $5.5 \times 10^{-5} M$ at 25° : —, EP; ----, EPA.

to the EPA solution of the $Gd(BP)_3$ complex, which dissociates extensively in an acidic medium, results in a solution which exhibits *only* this blue phosphorescence. From this we conclude that the dissociation product giving rise to this phosphorescence is the parent chelating agent.

Material balance requires the existence of other species such as complexes of a rare earth ion with two or possibly only one ligand. Emission from these species is expected to be at longer wave lengths than the emission from the parent chelating agent but at shorter wave lengths than the phosphorescence from the fully chelated species. The appearance of the additional peak at $18,200 \text{ cm}^{-1}$ in the phosphorescence of $Gd(BP)_3$ in EP and EPA glasses, where dissociation does occur, suggests that this peak originates from the partially chelated species. The addition of excess $GdCl_3$ to an EPA solution of $Gd(BP)_3$ results in an increase in the intensity of this $18,200 \text{ cm}^{-1}$ peak. Reasoning from chemical equilibrium this addition is expected to increase the concentration of partially chelated species and to diminish that of the fully chelated one.

Absorption spectra of the compounds also support these conclusions. The absorption spectrum of *o*-hydroxybenzophenone in either EP or EPA possesses a broad band in the near ultraviolet with $\lambda_{\text{max}} 3375 \text{ \AA}$. ($\epsilon_{\text{max}} 4300$) (Fig. 4a). Solutions of

the corresponding rare earth complexes in 3-methylpentane, where little or no dissociation is expected, show two broad peaks in this region; one with $\lambda_{\text{max}} 3425 \text{ \AA}$., and another with $\lambda_{\text{max}} 3850 \text{ \AA}$.. Both these bands must be attributed to transitions within the fully chelated rare earth complexes. The absorption spectra in EP are very similar to those obtained in 3-methylpentane with the long wave length band having a greater absorbance than the short wave length one (Fig. 4b). In EPA, where more extensive dissociation is expected, however, the relative absorbances are reversed.

The absorption spectrum of the sodium salt of *o*-hydroxybenzophenone also shows solvent effects. This compound exhibits two absorption maxima at about the same wave lengths as those present in the rare earth complex (no figure included). These two bands have about equal intensities when the sodium salt is dissolved in EPA but the long wave length band almost disappears when the solvent is changed to water. (The compound is not soluble in carefully dried EP.) Since the absorbance of the 3400 \AA . band of the sodium salt and the rare earth complexes always increases on going to more hydroxylic solvents, then part of the absorbance must be attributed to a dissociation product, probably the parent chelating agent. The corresponding decrease in the intensity of the 3850 \AA . peak accompanying the same changes in solvent identifies it as belonging to the complexes. Thus the absorption spectra of these compounds establish the presence of a dissociation species possessing an electronic transition similar to that of the parent chelating agent, supporting our previous assignment of the blue phosphorescence ($4000\text{--}5000 \text{ \AA}$.) to the parent chelating agent.

The low energy and long life ($> 10^{-4} \text{ sec.}$) of the $5000\text{--}7000 \text{ \AA}$. band appearing prominently in the luminescences of the chelates establish it to be triplet-singlet emission. The enhancement of the intensity of this band upon changing the coordinated metal ion from Pr^{3+} to Gd^{3+} shows that the emitting species in these cases contain the metal ions. This enhancement is in accord with the general observation that for a series of chelates the Gd^{3+} compound has the highest yield of luminescence.¹ The lack of any well defined structure on this long wave length phosphorescence band and its intensity changes upon addition of metal chloride to a solution of chelate suggest that it originates from more than one species containing a metal ion.

That the $5000\text{--}7000 \text{ \AA}$. phosphorescence band does originate from more than one species is clearly demonstrated by the emission properties of solutions of the samarium chelate of *o*-hydroxybenzophenone. When the samarium complex is dissolved in 3-methylpentane and excited by ultraviolet light, only extremely weak lines are observed from the complexed Sm^{3+} ion. In an EP solvent the lines are slightly enhanced. Addition of ethanol to the solution results in a definite increase of intensity of these lines. A marked enhancement of them is observed upon addition of excess $SmCl_3$ to the chelate solution (see Fig. 5). $SmCl_3$ alone, at this concentration, yields negligible luminescence. Since addition of alcohol favors

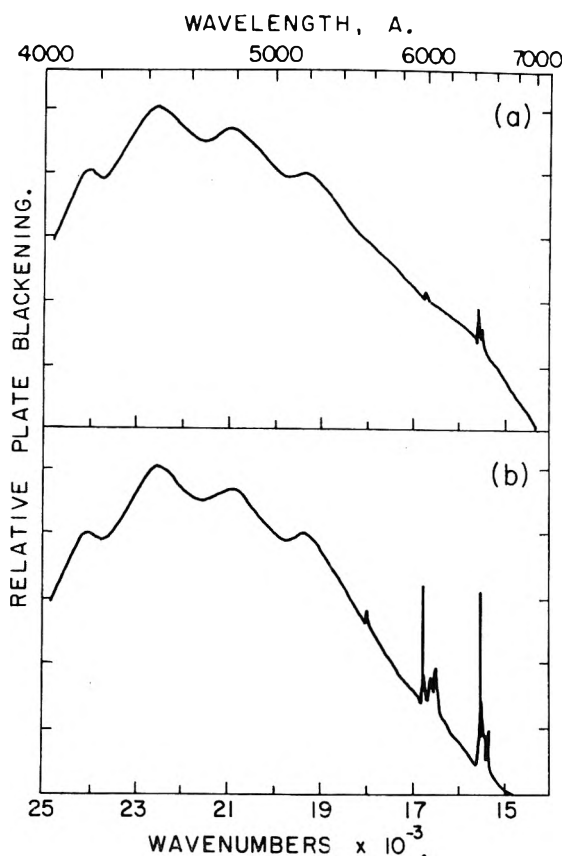


Fig. 5.—Total emission spectra of solutions of $\text{Sm}(\text{BP})_3$ ($1 \times 10^{-5} M$): (a) EPA glass at 77°K .; (b) plus $5 \times 10^{-5} M \text{SmCl}_3$ in EPA glass at 77°K .

more dissociation of the trichelated species and the subsequent addition of excess SmCl_3 also promotes an increase in concentration of the mono- and dichelated Sm^{3+} ion, we conclude that the species giving rise to the Sm^{3+} lines is either the $\text{Sm}(\text{BP})_2^{1+}$ or $\text{Sm}(\text{BP})_1^{2+}$ but is certainly not $\text{Sm}(\text{BP})_3$. (An attempt to suppress the dissociation of the $\text{Sm}(\text{BP})_3$ by addition of the corresponding sodium salt failed because of precipitation at low temperatures.) Further evidence in support of this conclusion is the unexpected low intensity of the Sm^{3+} line emission observed from this chelate in 3-methylpentane and EP; for when line emission from chelates of Sm^{3+} is observed, it is generally much stronger (by a factor of 10^3). We interpret these results to mean that the dissociation products giving rise to the sensitized line emission of Sm^{3+} are present only at low concentrations.

Even though accurate measurements of the triplet energy levels of the various dissociation products present in solutions of these rare earth complexes are precluded by the complexity of the phosphorescences measured from an equilibrium mixture, it is still possible to bracket the energy levels within narrow limits by a study of the luminescence spectra obtained from the Sm^{3+} and Eu^{3+} complexes. Europium trisdibenzoylmethide exhibits bright line emission originating from both the Eu^{3+} resonance levels (Fig. 6a) but the europium complex of *o*-hydroxybenzophenone exhibits bright line emission originating *only* from the lower resonance level of the ion ($17,250 \text{ cm}^{-1}$) (Fig. 6b), in-

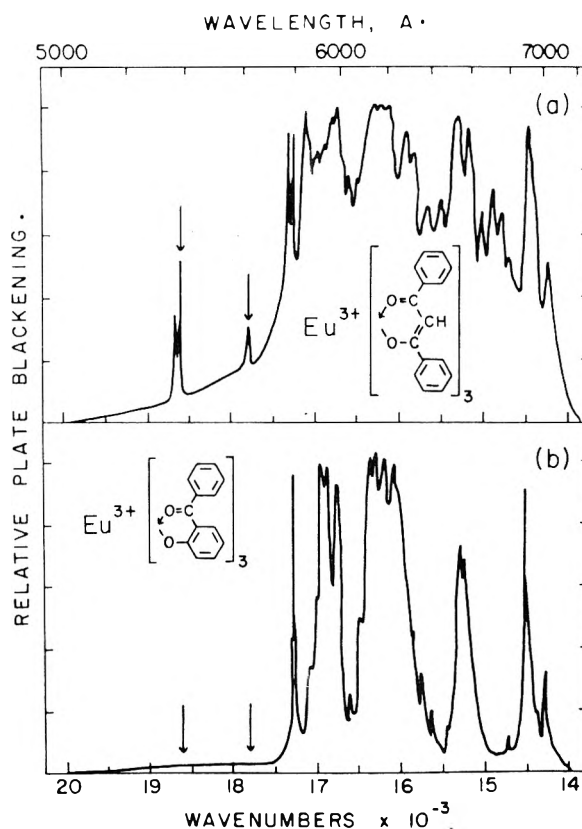


Fig. 6.— Eu^{3+} line emission from: (a) chelate of dibenzoylmethane in EPA glass at 77°K .; (b) chelate of *o*-hydroxybenzophenone in EPA glass at 77°K . The arrows in (a) indicate prominent lines originating from the upper resonance level of the europium ion; these lines do not appear in (b).

dicating that all the species in solution containing coordinated Eu^{3+} have triplet levels below $19,020 \text{ cm}^{-1}$ and that the fully chelated species has a triplet level between $17,250$ and $19,020 \text{ cm}^{-1}$ (the two Eu^{3+} resonance levels; see Fig. 2). For solutions of the chelate of samarium with *o*-hydroxybenzophenone the weak line emission observed does not originate from the fully chelated ion, placing the triplet of this species below $17,800 \text{ cm}^{-1}$ (samarium resonance level) but above $17,250 \text{ cm}^{-1}$ (the lower Eu^{3+} level). The value of $17,400 \text{ cm}^{-1}$ measured from $\text{Gd}(\text{BP})_3$ in 3-methylpentane falls within this range. Since Sm^{3+} line emission is observed from a dissociation product, this locates the triplet level of the product above $17,800 \text{ cm}^{-1}$ but below $19,020 \text{ cm}^{-1}$. The $18,200 \text{ cm}^{-1}$ peak (mentioned above), which was attributed to a partially chelated species, lies in an energy region consistent with this analysis.

It is assumed for the above arguments that the absence of fluorescence from the second resonance level of Eu^{3+} is proof that the triplet level of the complex lies below this level. It might be argued that interactions with the ligand are quenching this higher level so efficiently that no fluorescence can be observed from it. Because the local environment of the metal ion does not differ appreciably from one chelate to the other, one would not expect the quenching to differ much either. For chelates of Eu^{3+} with benzoylacetone and dibenzoyl-

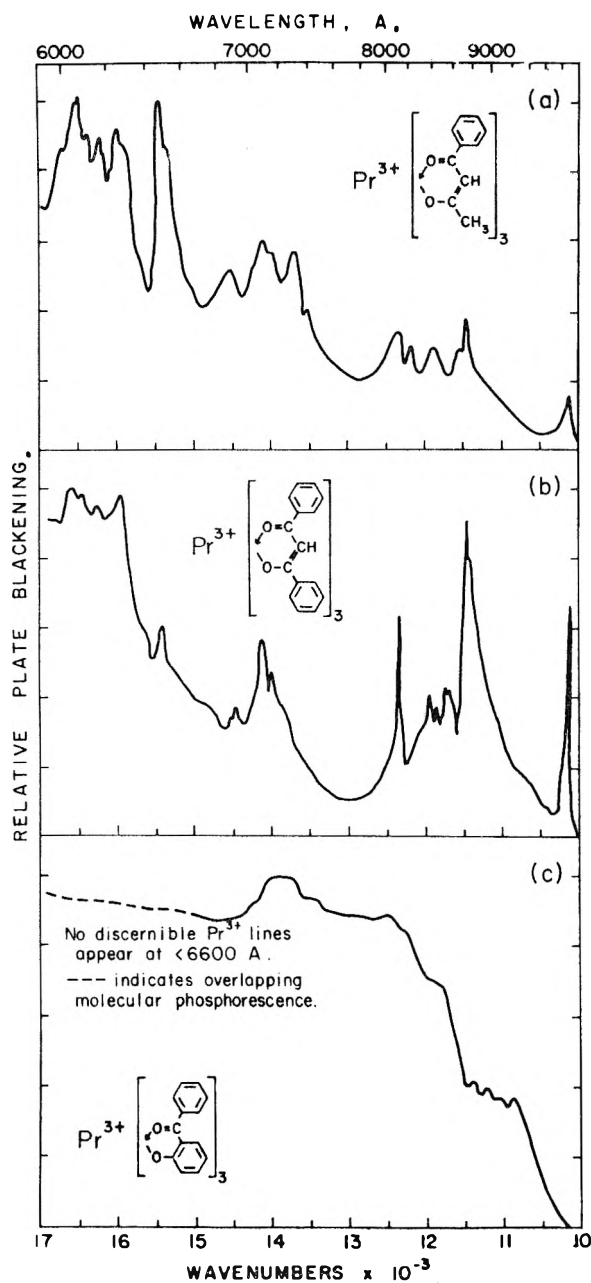


Fig. 7.—The line emission spectra of Pr^{3+} chelates of: (a) benzoylacetone ($10^{-5} M$) in EPA glass at 77°K .; (b) dibenzoylmethane ($10^{-5} M$) in EPA glass at 77°K .; (c) *o*-hydroxybenzophenone ($10^{-5} M$) in EP glass at 77°K .

methane, the upper resonance level is not quenched out (see Fig. 6). This lends strong support to our thesis that the position of the triplet level of the complex is the variable which is responsible for the presence or absence of luminescence from ion resonance levels.

Another interesting feature of the emission spectra of the rare earth chelates of *o*-hydroxybenzophenone is the virtual disappearance of the composite 5000–7000 Å. phosphorescence band upon changing the coordinated metal ion from La^{3+} or Gd^{3+} to Sm^{3+} , Pr^{3+} , or Eu^{3+} . This behavior is in agreement with the evidence from other series of rare earth chelates that low-lying 4f electronic energy levels provide an efficient path for the

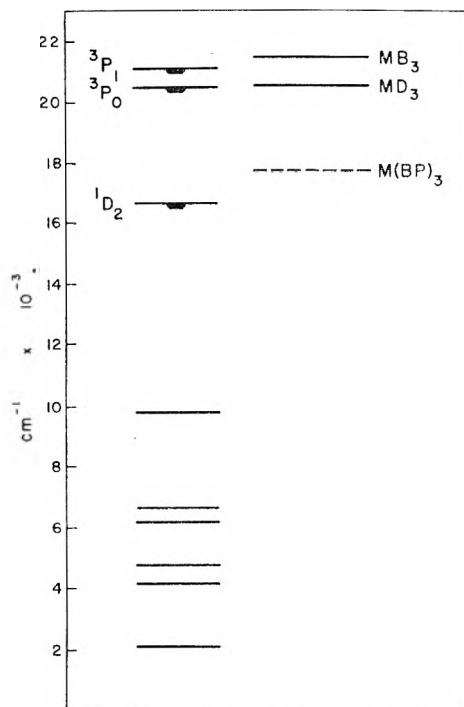


Fig. 8.—Energy level diagram showing the energy levels of Pr^{3+} (after Dieke and Sarup, ref. 6) and triplet state energies of Pr^{3+} chelates. For abbreviations see Fig. 2. — indicates resonance level.

quenching of the phosphorescence state of the complex molecules.¹

In summary, it has been shown that (a) rare earth chelates of *o*-hydroxybenzophenone dissociate appreciably in EPA; (b) the triplet state energy of the fully chelated metal ion complex lies definitely between 17,250 and 17,800 cm^{-1} with a measured value of approximately 17,400 cm^{-1} ; (c) at least one dissociation product containing the metal ion has a triplet state energy above 17,800 cm^{-1} but below 19,000 cm^{-1} , with a measured value of approximately 18,200 cm^{-1} ; (d) intramolecular energy transfer to the metal ion is an efficient process even in partially dissociated complexes; and (e) low-lying 4f electronic levels of the rare earth ions provide an efficient means for quenching the phosphorescence of the complex molecules.

Selective Excitation of Coordinated Pr^{3+} .—Having established the triplet state energies of the lanthanide chelates of benzoylacetone, dibenzoylmethane, and *o*-hydroxybenzophenone, this information can be used to study the luminescences of other rare earth ions whose spectra are more difficult to interpret. These data are useful in the study of the emission spectrum of the coordinated trivalent praseodymium ion. This ion is reported to fluoresce brightly from the anhydrous chloride under direct excitation and the prominent resonance levels have been established.⁶ No emission from the coordinated ion has been reported. By using energy transfer in the above chelates to excite this ion indirectly, we have succeeded in photographing the emission of the coordinated Pr^{3+} ion.

For all the complexes the luminescences consist

(6) G. H. Dieke and R. Sarup, *J. Chem. Phys.*, **29**, 741 (1958).

of molecular fluorescence and phosphorescence and groups of very weak lines characteristic of the Pr^{3+} ion. The latter are diffuse and ill-defined and are obtained only under prolonged exposures. For the benzoylacetate chelate, four groups of lines are observed in the region of 6000–10,000 Å. (see Fig. 7). The Pr^{3+} emission from the dibenzoylmethide chelate also consists of four groups of lines, but some prominent components present in the spectrum of the benzoylacetate chelate are missing. The line emission from the *o*-hydroxybenzophenone chelate of Pr^{3+} is simpler still, with the highest energy group of lines disappearing entirely.

In Fig. 8 we have plotted the known resonance levels of the Pr^{3+} ion and triplet state energies of the three chelates used in this study. The progressive simplification of the line spectra discussed above can be correlated to the positions of the resonance levels of the ion relative to the triplet state energies of the complexes. In praseodymium tris-benzoylacetate, all three resonance levels can be excited by energy transfer. In the dibenzoylmethide chelate, just the lower two levels can be excited, adequately accounting for the non-appearance of some of the Pr^{3+} lines in the spectrum of this compound. For the chelate derived from *o*-hydroxybenzophenone only the lowest resonance

level of the Pr^{3+} ion can be excited by intramolecular energy transfer, resulting in the simplest ion spectrum observed from the three compounds.

We wish to emphasize that the emission spectra observed from chelates of the Pr^{3+} ion are extremely weak and require many hours of exposure. Total luminescence yields from the compounds are low, indicating that the closely packed energy levels of the Pr^{3+} ion provide an extremely efficient path for energy degradation. This fact along with the diffuseness of the observed lines shows that the Pr^{3+} ion is coupled strongly to the ligands. Strong coupling for this ion also is reported for hydrated inorganic salts.

Rare earth chelates comprise a class of compounds especially valuable for studying energy migration in complex molecules. Because of the intrinsic optical properties of these ions, they assume a unique role as internal indicators for these radiationless processes. In addition, the phenomenon of intramolecular energy transfer permits selective excitation of rare earth ions and provides useful information for locating the lowest triplet states of the complexes themselves.

Acknowledgments.—The research presented in this communication was sponsored by Sandia Corporation under P.O. No. 51-0244 and by the National Science Foundation.

THE EXTERNAL HEAVY-ATOM SPIN-ORBITAL COUPLING EFFECT. III. PHOSPHORESCENCE SPECTRA AND LIFETIMES OF EXTERNALLY PERTURBED NAPHTHALENES^{1,2}

BY S. P. MCGLYNN, M. J. REYNOLDS, G. W. DAIGRE, AND N. D. CHRISTODOYLEAS

Coates Chemical Laboratories, Louisiana State University, Baton Rouge 3, Louisiana

Received May 25, 1962

The phosphorescence spectra and decay times of naphthalene and all of its 1-monohalogenated derivatives have been measured at -190° in EPA,¹⁸ and in cracked glasses which consisted of the various combinations of halonaphthalene and propyl halide in 2:5 mole ratio. The lifetimes were found to decrease as the spin-orbital coupling factor of either the internal or external halogen increased. It is concluded that weak complexes of a charge-transfer nature form and that there is a genuine heavy-atom effect. The phosphorescence decays, as expected, were found in all cases to be non-exponential, and to be reproducible analytically only as the sum of a large number of first order decays of different rate constants. It is concluded from this behavior that complex geometry can vary considerably about some most probable conformation.

It is found that the product $\tau_p(\zeta_I + \zeta_E)^2$ is roughly constant, deviations from constancy being interpretable as due to increasing phosphorescence quenching and radial contributions to the perturbation integral $H'_{T,SP}$. The results obtained at $+30^\circ$ from absorption data and at -195.8° from phosphorescence data are shown to be identical, and to validate the spin-orbital coupling and complexing premises.

Shifts in the 0,0 position of the T \rightarrow S emission have been observed for the one emitter in various matrices. These shifts are of the order of 0.25–0.5 kcal./mole and are of the same relative behavior as the ratios of lifetimes in the various media. Shifts in various fundamental vibrational frequencies also have been noted, and a geometric specificity of interaction is derived therefrom. An analysis of the T \rightarrow S emission of naphthalene is possible in terms of four a_g vibrational frequencies, in accord with the $B_{2u} \rightarrow A_{1g}$ nature of this transition.

Introduction

It was observed by Kasha³ in 1952 that a binary solution of two colorless components: 1-chloronaphthalene and ethyl iodide, was of a yellow color.

(1) This research was supported by a National Science Foundation Grant to The Louisiana State University, and by a Grant-in-aid from the American Instrument Company of Silver Spring, Maryland.

(2) Other papers in the present series are: (I) S. P. McGlynn, R. Sunseri, and N. Christodoyles, *J. Chem. Phys.*, submitted for publication; and (II) J. Nag-Chaudhuri, L. Stoessel, and S. P. McGlynn, *J. Mol. Spectroscopy*, submitted for publication.

(3) M. Kasha, *J. Chem. Phys.*, **20**, 71 (1952).

The effect was attributed to an increase of spin-orbit coupling in the halonaphthalene. The supposition that just such a relaxation of spin-forbiddenness might occur preceded the observation,⁴ and this supposition apparently derived from an intuitive association of the known effectiveness of ethyl iodide as a fluorescence quencher⁵ with the demonstration of *intramolecular* heavy-atom spin-

(4) M. Kasha, private discussion.

(5) P. Pringsheim, "Fluorescence and Phosphorescence," Interscience Publishers, New York, N. Y., 1949.

orbital coupling by McClure.⁶ It was thought that the ethyl iodide was functioning as a fluorescence quencher in liquid solution by promoting inter-system crossing from the fluorescent singlet level to the triplet manifold of levels.

The generality of this intermolecular heavy-atom enhancement of $T \leftarrow S$ transition probabilities now has been reasonably well established.^{2,7,8} However, all investigations, with a few exceptions have been confined to measurement of absorption spectra. No significant attention has been given to the equally relevant measurements of phosphorescence lifetimes or the relative phosphorescence to fluorescence quantum yields of externally perturbed emitters. And yet these types of measurements would seem to afford a very direct means of establishing whether the observed spin-orbital coupling increases were brought about by energetic collisions as suggested by Kasha or by a weak complexation as suggested by McGlynn.⁹ The reasons for this differentiation might be stated as follows: since emission experiments will be carried out at -190° in the conventional manner in some sort of solid matrix, "energetic collision" will be impossible, and an observed decrease of phosphorescence lifetime, τ_p , or of the ratio fluorescence/phosphorescence, Φ_f/Φ_p , will be compatible only, to a good level of approximation, with the idea of a complex between the emitter and the perturber. It is true that high local pressures resulting from strains, defects, etc., in the solid matrix might produce the same effect as an "energetic collision." However, in view of the results of the high pressure experiments of Robertson and (R. E.) Reynolds¹⁰ on the 1-chloronaphthalene-ethyl iodide liquid system, where significant changes of pressure produced only small changes in optical density, major decrease of τ_p or of Φ_f/Φ_p due to local pressures (or "frozen collisional conformations") in glasses would not seem likely.

The reasons behind the suggestion of a weak complex between emitter (absorber) and perturber also must be elaborated. The interpenetration of the π -electrons of, let us say, 1-chloronaphthalene into the vicinity of the large field gradient of iodine which is necessitated by the results of Kasha³ obviously implies charge transfer from the 1-chloronaphthalene to the ethyl iodide. The question then becomes one of degree: is the charge transfer caused by complexing, contacting,¹¹ or collision? It seems appropriate to consider the concept of "contact." A "contact" implies that at a distance of separation of a donor-acceptor pair equal to the sum of their van der Waals radii, there is some donor-acceptor orbital mixing. It implies^{11a} that mixing of wave functions can occur

(6) D. S. McClure, *J. Chem. Phys.*, **17**, 905 (1949).

(7) S. P. McGlynn and M. Kasha, "Symposium on Molecular Structure and Spectra," Ohio State University, Columbus, Ohio, June, 1954, to be published shortly: fluorine, chlorine, bromine, and iodine substituted in saturated hydrocarbons, and sulfur in carbon disulfide.

(8) R. S. Becker, private discussion: lead in tetraalkyllead derivatives.

(9) S. P. McGlynn, *Chem. Rev.*, **58**, 1113 (1958).

(10) W. W. Robertson and R. E. Reynolds, *J. Chem. Phys.*, **29**, 138 (1958).

(11) R. S. Mulliken, *Rec. trav. chim.*, **75**, 845 (1956).

(11a) J. N. Murrell, *Mol. Phys.*, **3**, 319 (1960).

without any resulting significant stabilization or destabilization of the donor-acceptor pair. In practice, however, it denotes the situation where effects not attributable to energetic collisions are observed, but where definite complexing cannot be detected either. If some effect due to contacts (and not to complexes or collisions) were isolable then presumably such an effect would be temperature independent. No such "clean" effect has thus far been unearthed, and in its absence the present authors prefer to consider a contact as a complex, the stabilization energy of which is less than ambient thermal energy kT . This latter viewpoint is, of course, pragmatic in that it makes logical for us the situation in which at room temperature one can measure for a binary solution by Benesi-Hildebrand procedures¹² an equilibrium constant $K \sim 0$ and an extinction coefficient $\epsilon \sim \infty$,¹³ and for which at -190° , where collisions must be considered unimportant, one can detect large decreases of τ_p for one of the components attributable to the presence of the second constituent.

Recent work by Tsubomora and Mulliken¹⁴ on the oxygen enhancement of $T \leftarrow S$ transition probabilities indicates that this relaxation of spin-forbiddenness is not connected with the magnetic moment of oxygen. Rather, it would seem to indicate that the charge-transfer state functions by mediating the mixing of singlet and triplet states of the donor, and that the phenomenon should be quite general (at least for weak complexes) and independent of acceptor species (*i.e.*, oxygen or ethyl iodide). There exists evidence that such is true in some well defined complexes: it is known¹⁵ that in the complex of anthracene with *sym*-trinitrobenzene, τ_p decreases and Φ_p increases relative to uncomplexed anthracene, and Czekalla¹⁶ has shown that in a wide variety of complexes of non-paramagnetic non-heavy-atom-containing components, decreases of τ_p by an order of magnitude are not uncommon. An increase of the ratio Φ_p/Φ_f has been observed¹⁷ for some of the same complexes. Similar decreases of τ_p of solutes dissolved in media with which no interactions of significance have ever been detected also have been observed (*vide infra*). At least this latter case accords with the predictions of Tsubomora and Mulliken,¹⁴ and undoubtedly the case of strong interaction could be similarly interpreted, although probably with lesser validity.

Now that the situation to which the present work has reference has been sketched it is well to say what this work is and what it hopes to do. Briefly, the lifetimes (τ_p) and phosphorescence spectra of naphthalene, 1-fluoronaphthalene, 1-chloronaphthalene, 1-bromonaphthalene, and 1-iodonaphthalene have been measured separately in

(12) H. A. Benesi and J. H. Hildebrand, *J. Am. Chem. Soc.*, **71**, 2703 (1949).

(13) S. P. McGlynn and R. Sunseri, to be published; system 1-chloronaphthalene and ethyl iodide.

(14) H. Tsubomora and R. S. Mulliken, *J. Am. Chem. Soc.*, **82**, 5966 (1960), and references contained therein.

(15) S. P. McGlynn, J. D. Boggus, and E. Elder, *J. Chem. Phys.*, **32**, 357 (1960).

(16) J. Czekalla, G. Briegleb, W. Herre, and H. J. Vahlensieck, *Z. Elektrochem.*, **63**, 715 (1959).

(17) N. Christodoules and S. P. McGlynn, to be published.

each of the four solvent media: EPA,¹⁸ propyl chloride, propyl bromide, and propyl iodide. It is thought that the results will show that the heavy atom enhancement effect of $T \leftrightarrow S$ transition probabilities is not collisional, and that there is a valid heavy-atom effect, in contradistinction to the apparently insignificant paramagnetic field effects of oxygen, nitric oxide, and various transition metal ions. This latter finding would require some modification of the Mulliken-Tsubomora theory at least for these systems. However, such is not the purpose of this note, and it will be deferred until presentation of the available experimental evidence^{7,13,17} is complete.

It is to be noted that some of these stated aims previously have been achieved by others. It has been observed¹⁹ that the phosphorescent lifetimes various substituted phthalimides measured in some twenty-one different solvent media were lowest, or among the lowest, in cracked glasses (?) of propyl bromide. Large decreases of τ_p were, however, also observed by these authors in non-heavy-atom-containing media. The benzene triplet lifetime at liquid nitrogen temperatures is in EPA,²⁰ 7 sec.; dioxane,²⁰ 5 sec.; alcohol,²¹ 3.3 sec.; water,²¹ 0.95 sec.; and carbon tetrachloride, 0.66 sec. Graham-Bryce and Corkhill²² undertook an investigation of the phosphorescence of coumarin, acid fluorescein, N,N-dimethylaniline, and eight isomeric dinitronaphthalenes in glassy solutions containing one part in twenty-one (by volume) of ethyl iodide; in all cases the effect of the ethyl iodide was to increase the intensity of phosphorescence and decrease τ_p . The experimental work of these latter authors was superior to the present in at least one respect: the use of a glassy medium at liquid nitrogen temperatures. However, the effect of ethyl iodide probably was somewhat obscured, in view of the results of Sveshnikov and Petrov,²¹ by the large proportion of alcohols in the glass used; in addition since only one heavy atom-containing solvent was used it is impossible to state unambiguously that a heavy atom effect is operative. Apart from these comments, the motives and results of these authors²² accord with those of the present work.

Experimental

Chemicals.—Diethyl ether, ethyl alcohol, and isopentane were purified in the previously described manner.¹⁵ The other chemicals were all Eastman White Label grades. 1-Fluoronaphthalene, 1-chloronaphthalene, and 1-bromonaphthalene were fractionated under vacuum. The fractions used were: 1-chloronaphthalene 142–144° (30 mm.), 1-bromonaphthalene 95–96.5° (3 mm.), and 1-fluoronaphthalene 57–59° (3 mm.). The 1-bromonaphthalene was run through a column of activated alumina prior to use. Naphthalene and propyl chloride were used without further purification. Samples of naphthalene which had been extensively zone-purified and chromatogrammed were available and it was verified that direct use of the Eastman product

did not adversely affect any of the work reported herein. 1-Iodonaphthalene, propyl bromide, and propyl iodide were run through a 15-cm. column of activated alumina prior to use.

Apparatus and Methods.—(a) **Lifetimes:** The phosphorescence emission was excited by either a d.c. operated Hanovia high pressure mercury-xenon lamp or a d.c. General Electric AH-6 mercury lamp. The phosphorescence emission was purified mechanically by a Becquerel phosphoscope driven by a Zeromax motor continuously variable from 0–1200 r.p.m. The phosphorescence decay was picked up by a 1P21 photomultiplier, displayed on the screen of a Tektronix 545A oscilloscope, photographed, and analyzed on a microfilm reader.

The photomultiplier voltage was supplied by an Atomic Instrument Co. super-stable high voltage source to a standard voltage dividing network of resistors which held the successive stages 100 v. apart. The 1 megohm input impedance of the oscilloscope was used as the anode load resistor. The entrance slit to the photomultiplier was adjusted so that the anode load current was always less than 10 μ a. for a display on the oscilloscope screen and was thus within operational limits for maximum linearity recommended by the manufacturer.

The oscilloscope was operated on d.c. coupled internal trigger with signal inverted. The sharp pulse given by the initial burst of light as each slot of the phosphoscope opened was used as the trigger for the horizontal sweep. Single sweep pictures were taken only of the first two half-lives. However, some visual observations were made on later lifetimes using the sweep delay feature of the Tektronix 545A. This was effected by the simultaneous use of two time bases, A and B. Time base B was used to provide an accurate time delay while time base A presented a normal horizontal sweep at the end of the delay period. After determination of the magnitude of the first observable half-life, this value was used on B as the delay. The value of τ_p measured for each successive half-life was added to the delay time. The entrance slit on the phototube was adjusted each time to give full scale display at the beginning of the delayed sweep. In this manner as many as eleven consecutive half-lives were measured.

All measurements were made at 77°K. in quartz sample holders immersed in quartz liquid nitrogen dewar vessels. The experimental arrangement was such that selective filters, neutral density filters, or monochromators could be interposed in the exciting beam or the purified phosphorescent beam. A variety of high intensity flash sources with flash times from 5×10^{-7} sec. to 10^{-3} sec. were available, and were used, particularly, in conjunction with manual shuttering. In addition the Aminco-Keirs spectrophosphorimeter became available toward the end of this project, and most of the lifetimes quoted were measured or checked with this instrument.

(b) **Phosphorescence Spectra:** Essentially the same physical set-up was used as for the lifetime measurements except that an a.c. operated AH-6 lamp was used, and that a Steinheil spectrograph replaced the multiplier-oscilloscope assembly. The linear reciprocal dispersion at the employed spectrograph setting was 80 Å./mm. at 5800 Å. and 20 Å./mm. at 4250 Å. Kodak spectroscopic plates, Type 103a-F (3) were used throughout, and were traced on a Leeds and Northrup recording microphotometer.

(c) **Glass Matrix:** It was found that a mixture of a propyl halide and 1-halonaphthalene in a 5:2 mole ratio would form rigid cracked glasses at 77°K. if extreme care were taken in preparation and cooling. Indeed glasses sometimes could be obtained but these cracked upon the slightest provocation (*i.e.*, exposure to the exciting light). However, the transmittancy of these "cracked glasses" was quite high and since significant crystallization seemed not to have occurred it is these glasses which were used in all cases of mixtures investigated.

Resort to these cracked glasses was had for a number of reasons. *First*, amounts of propyl halide which are capable of producing changes in τ_p of the 1-halonaphthalene may not be added to the solution of 1-halonaphthalene in EPA without the occurrence of considerable cracking and crystallization upon cooling the resulting mixture; in other words one must have high concentrations of perturber. *Second*, even though heavy-atom-containing glasses are available (*e.g.*, replacement of alcohol of the EPA by ethyl iodide), these

(18) 5 parts ether, 5 parts isopentane, and 2 parts alcohol, by volume.

(19) E. N. Viktorova, I. A. Zhmyreva, V. P. Kolobkov, and A. A. Saganenko, *Optika i Spekt.*, **9**, 349 (1960).

(20) Y. Kanda and R. Shimada, *Spectrochim. Acta*, **17**, 7 (1961).

(21) B. Y. Sveshnikov and A. A. Petrov, *Doklady Akad. Nauk SSSR*, **71**, 46 (1950).

(22) I. J. Graham-Bryce and J. M. Corkhill, *Nature*, **186**, 965 (1960).

glasses do not cover a representative range of heavy atoms. *Third*, it was considered important to investigate all samples under as closely identical conditions as possible, and thus a series of cracked glasses was to be preferred to a series in which some were cracked and some were not. *Fourth*, it is significantly easier to work with propyl halides than with ethyl halides.

Results

Phosphorescence Lifetimes.—The first lifetimes (actually "first observable mean lifetimes," *vide infra*) of the pure halonaphthalenes in EPA, as well as those of the halonaphthalene-propyl halide cracked glasses, are given in Table I. Marked changes of τ_p have occurred, and cover a total range of 2.6 to 0.0009₅ sec. The remarkable fact emerges immediately that the decrease in τ_p occasioned by an external I-atom is greater than that caused by an *internal* Cl-atom, and roughly comparable to that due to an *internal* Br; an *internal* Cl is less effective than an *external* Br, and roughly equal to an *external* Cl.

TABLE I

FIRST OBSERVABLE MEAN LIFETIMES (IN SECONDS) OF NAPHTHALENE AND ITS HALOGEN DERIVATIVES IN SEVERAL SOLVENTS

Emitter	Solvent			
	EPA	Propyl chloride	Propyl bromide	Propyl iodide
Naphthalene	2.6	0.52	0.14	0.076
α -Fluoronaphthalene	1.4	0.17	0.10	0.029
α -Chloronaphthalene	0.23	0.075	0.059	0.023
α -Bromonaphthalene	0.014	0.0073	0.0069	0.0063
α -Iodonaphthalene	0.0023	0.0014	0.0012	0.0009 ₅

It is further to be noted that the heavier the halogen of the propyl halide the smaller is τ_p . A sufficiently representative series of solutions have been studied to conclude that there is indeed a valid heavy-atom effect. This immediately implies extension of the Mulliken-Tsubomora model,¹⁴ since in its present form it does not encompass these results. McClure studied the effect on lifetimes of changing like atoms in a substitutional series, as for example in going from 1-fluoronaphthalene to 1-chloronaphthalene, etc. The product $\tau_p \zeta_I^2$, where ζ_I is the atomic spin-orbital coupling factor of the internal halogen, was found to be a reasonable constant. If the perturbation by an external halogen is considered to be also of spin-orbital coupling origin, and to be independent of the internal perturbation, then one may conclude that $\tau_p(\zeta_I + \zeta_E)^2$, where ζ_E is the atomic spin-orbital coupling factor of the *external* halogen, should be a constant. Such a tabulation is given in Table II, wherein it is seen that the constancy of the tabulated numbers is better by a factor of 10² than the numbers of Table I, and is sufficiently impressive to conclude the approximate truth of the assumptions made. The ζ_I considered characteristic of naphthalene was that for the H-atom, and ζ_E of EPA was considered to be that for the OH-group. It would seem that these assumptions, however naïve, are justified by the numbers of Table II.

TABLE II

MEAN LIFETIME TIMES THE SUM OF INTERNAL AND EXTERNAL SPIN-ORBITAL COUPLING FACTORS SQUARED (IN SECONDS CM.⁻² $\times 10^{-4}$)

Emitter	Solvent			
	EPA	Propyl chloride	Propyl bromide	Propyl iodide
Naphthalene	50.2	39	104	219
α -Fluoronaphthalene	27.4	12.6	74.5	82.5
α -Chloronaphthalene	12.6	10.3	55.3	73.7
α -Bromonaphthalene	9.4	6.8	16.7	35.8
α -Iodonaphthalene	6.2	4.16	6.85	11.4

The inconstancies in Table II are quite regular: a decrease occurs in going down any column, and when the EPA and propyl chloride columns are inverted an increase occurs on traversing any row from left to right. Two explanations may be provided for these results: (1) An increase of ζ_I is known to increase Φ_{ISC} , the quantum yield of radiationless intersystem crossing from the lowest excited singlet state to the triplet state; by the same token it also must be expected to increase Φ_{QP} , the quantum yield of the radiationless intersystem crossing from the lowest triplet state to the singlet ground state (*i.e.*, increased quenching of phosphorescence is expected). In other words, $\tau_p = 1/(k_p + k_{QP})$, and the effect of *internal* spin-orbital coupling is to increase k_{QP} at a rate comparable to if not greater than the rate of increase of k_p . Some evidence may be adduced in favor of these assertions.¹⁷ The trends within a given row may be rationalized by assuming that ζ_E increases k_p at a rate significantly faster than the rate of increase of k_{QP} . Again, some experimental quantum yield data favor this conclusion.

(2) Use of the expression $\tau_p(\zeta_I + \zeta_E)^2 = \text{constant}$ implies neglect of, or assumes constancy of, overlap factors in the integral $(\Phi_0^T/\mathcal{H}'/\Phi_0^{SP})$, where Φ_0^T is the zeroth order triplet wave function, Φ_0^{SP} is the zeroth order perturbing singlet wave function, and \mathcal{H}' is the spin-orbital coupling Hamiltonian. The perturbation of spin-orbital coupling in π -electron systems depends on two main factors: (a) the degree of penetration of the π -electrons into the field gradient of the nucleus of the perturbing atom, and (b) the magnitude of the field gradient. An overlap integral of the form (π -electron orbital of emitter/halogen orbital) will be a limiting parameter for (a), and ζ will be a limiting parameter for (b). It is thus to be appreciated that Table II neglects contribution (a). In the case of the external heavy atom effect we may say² that the donor-acceptor overlap integral,¹⁴ S_{DA} , is the quantity of importance, in which case we conclude from Table II that propyl chloride is a better acceptor species than propyl iodide, a result already deduced² from room temperature absorption data.

It seems reasonable that the trends of Table II will find explanation in terms of a combination of (1) and (2) above, or by introduction of exchange coupling constants into the external and internal heavy nuclei.

TABLE III

A COMPARISON OF THE PERTURBATION INDUCED BY PROPYL IODIDE IN HALONAPHTHALENES AT 33 AND -195.8°

Naphthalenic species	Δf^a	f^b	$\Delta f/f$	Δk_p^c	k_p^d	$\Delta k_p/k_p$
Naphthalene	12.815	0.385	33.3
1-Fluoronaphthalene	22.81	0.42	54.31	33.7	0.73	46.4
1-Chloronaphthalene	30.21	2.86	11.27	39.15	4.35	9.0
1-Bromonaphthalene	53.08	42.11	1.261	95	73	1.3
1-Iodonaphthalene	172.30	386.60	0.44	525	435	1.21

^a Increase in the integrated extinction of $T \leftarrow S$ absorption of the halonaphthalene when in binary solution with propyl iodide. ^b Integrated extinction, $\int \epsilon d\nu$, of $T \leftarrow S$ transition of pure liquid halonaphthalene. ^c $\Delta k_p \equiv 1/\tau_p' - 1/\tau_p$, where τ_p' is the phosphorescence lifetime of the binary cracked-glass system of naphthalenic species and propyl iodide and τ_p is the phosphorescence lifetime of the naphthalenic species in EPA. ^d $k_p \equiv 1/\tau_p$.

TABLE IV

COMPARISON OF MEASURED PHOSPHORESCENT LIFETIMES IN EPA WITH PREVIOUSLY REPORTED VALUES (IN SEC.)

Emitter	This research	DeGroot and van der Waals ^a				
		McClure ^b	Hutchison ^c	Ermolaev ^d	Czekalla ^e	
Naphthalene	2.6	30	2.6	2.1	2.3	2.5
α -Fluoronaphthalene	1.4	..	1.5
α -Chloronaphthalene	0.23	..	0.30	..	0.29	..
α -Bromonaphthalene	0.014	..	0.018
α -Iodonaphthalene	0.0023	..	0.0025	..	0.002	..

^a M. S. DeGroot and J. H. van der Waals, *Mol. Phys.*, **3**, 190 (1960). ^b See ref. 6 of text. ^c C. A. Hutchison, Jr., and B. W. Mangum, *J. Chem. Phys.*, **29**, 952 (1958). ^d V. L. Ermolaev, *Optika i Spektroskopiya*, **6**, 417 (translation) (1959). ^e See ref. 16 of text.

A Comparison With Room-Temperature Absorption Data.—The ratio for external to internal perturbation effects as measured by absorption at room temperature in binary liquid solutions and by τ_p at 77°K . in cracked glasses are compared in Table III, the external perturber being propyl iodide in all cases. It is seen that as ζ_I increases the external effect increases much as could be expected because of the occurrence of a cross-term $\zeta_I\zeta_E$ in the product $(\zeta_I + \zeta_E)^2$. It is seen that as ζ_I increases the ratio of external effect to internal effect decreases, again as expected, since this ratio is given by $(\zeta_E/\zeta_I)^2 + 2\zeta_E/\zeta_I$. It is further seen that a remarkable parallelism exists between the relative perturbations $\Delta f/f$ and $\Delta k_p/k_p$ at 33° and -195.8° , respectively. The one case where significant discrepancy exists is 1-iodonaphthalene where Δk_p , which actually equals $\Delta(k_p + k_{QD})$, is increased by a large increase¹⁷ of the quenching rate constant, k_{QD} .

The data of Table III are of importance in two regards. First the two sets of data mutually validate each other, and second it is implied that whatever the origin of the effect at room temperature, it is the same at low temperature. It is to be realized in this regard that the observation of a decreased lifetime at low temperatures is indicative of a certain preponderance of perturber-perturbed pairs, but that the value of this lifetime is itself independent of the concentration of such pairs once a certain minimal value of their concentration is exceeded. Such is the case in the present instance, and the good correlation of the two sets of data at 33° and -195.8° is hardly in accord with a collisional mechanism which should exhibit a $T^{1/2}$ dependence in fluid media.

The precision in these measurements was calculated to be 2% in measuring a given frozen sample repeatedly. When a cracked glass sample was

allowed to warm up and then refrozen between runs reproducibility was of the order of 20%. This was not true of EPA glassy solutions. Some idea of the errors involved in these latter measurements may be gained from Table IV. In the worst comparison there is a 23% difference between the present τ_p and that of McClure,⁶ and in the best, 0%. However, it is interesting to note that the results of this study were equal to or consistently lower than those of McClure (*vide infra*).

The Decay of Phosphorescence.—The phosphorescence of naphthalene in EPA was found to be exponential over a time interval of seven half-lives. Indeed, the extent of exponentiality exhibited by a given material is an extremely good criterion of purity. None of the binary cracked glass systems investigated in this work had exponential decays of phosphorescence; this non-exponentiality is to be expected. Let us suppose, for instance, that there exist only complexed emitter species and uncomplexed emitter species, and that all the species within one of the two types specified are identical; in this case we find

$$I = I^0 e^{-k_T^c t} + I^0 e^{-k_T t}$$

where I is the phosphorescence intensity, n_T^c is the number of complexed species in the triplet state and k_T^c their decay constant, and n_T is the number of uncomplexed species in the triplet state and k_T their decay constant. The decay will be non-exponential, but will be resolvable into two exponential processes. Indeed it is possible that such decay curves may be used to determine equilibrium constants; such is presently being investigated, and will be reported¹⁷ elsewhere.

The use of the term "lifetime" in conjunction with a non-exponential process might seem odd. However, in the sense used here the first half-life is the time required for the phosphorescence intensity to

TABLE V
 THE PHOSPHORESCENCE SPECTRA OF NAPHTHALENE IN VARIOUS MATRICES AT 77°K.

Ether-isopentane glass			Propyl chloride		Propyl bromide		Propyl iodide	
ν cm. ⁻¹	$\Delta\nu$	Interpretation	ν cm. ⁻¹	$\Delta\nu$	ν cm. ⁻¹	$\Delta\nu$	ν cm. ⁻¹	$\Delta\nu$
21335	0	...	21280	0	21180	0	21010	0
20825	510	512	20770	510	20700	500	20510	500
20550	785?	763
20290	1045	2(512) = 1024	20290	990
20170	1165	1146	20120	1160	20020	1160	19910	1100
19935	1400	1380	19880	1400	19740	1400
19745	1590	1575	19780	1500	19650	1530	19550	1460
19435	1900	512 + 1380 = 1892	19380	1900	19330	1850
19260	2075	512 + 1575 = 2087	19260	2020	19100	2010
18960	2375	2(512) + 1380 = 2404
18780	2555	2(512) + 1575 = 2597
18535	2800	2(1380) = 2760	18500	2780	18210	2800
18465	2970	1380 + 1575 = 2955	18390	2890	18330	2850	18100	2910
18100	3235	2(1380) + 512 = 3272 or 2(1575) = 3150	18140	3140
17780	3555	1380 + 1575 + 512 = 3467	17860	3420
17610	3725	2(512) + 2(1380) = 3784	17620	3660
17350	3985	1575 + 1380 + 2(512) = 3979	17300	3980
17130	4205	3(1380) = 4140	17180	4100
17000	4355	2(1380) + 1575 = 4335	17010	4270	16850	4330	16900	4310
16825	4510	1575 + 1380 + 3(512) = 4491 or 2(1575) + 1380 = 4530
16550	4685	3(1380) + 512 = 4652
16310	5025	2(1575) + 1380 + 512 = 5042
15980	5355	2(1380) + 1575 + 2(512) = 5359
15790	5545	4(1380) = 5520	15720	5560
15470	5865	2(1380) + 2(1575) = 5910	15410	5870	15320	5860	15180	5830
15040	5995	4(1380) + 512 = 6032	15200	6080
14600	6735	3(1380) + 2(1575) = 6715

drop to one half its original intensity at zero time after cut-off of excitation, the second half-life is the time required to drop from one half to one fourth its original intensity, etc. All the lifetimes of Table I are *first observable lifetimes*; it is necessary to make this distinction because there is a finite time required for the phosphoroscope to cut off the exciting light and open the photomultiplier to the phosphorescent light. Thus, with slow phosphoroscope speeds the measured lifetime was too long due to the deviation of the decay curve from exponential. It was found that the measured apparent lifetime decreased as phosphoroscope motor speed increased, but become constant above some minimal rate of revolution. With motor speeds above this point one was investigating an approximate exponential region of decay (first two or three half-lives), and constancy of τ_p was to be expected. Still there might be a small difference between the first observable lifetime and the first lifetime. For this reason the phosphoroscope was run as fast as possible while still maintaining a display of one or two half-lives on the oscilloscope screen. A good approximation to the first lifetime should be obtained by plotting $\log(\text{intensity})$ versus time and using the limiting slope at zero time to determine the *limiting slope lifetime*. All such limiting slope lifetimes measured corresponded within experimental error to the first observable lifetime measured at rotor speeds above the previous noted minimal r.p.m.; either one or both of these life-

times may then be assumed to correspond to the first lifetime, and it is such mean-lives that are reported in Table I. It is thought that this is also the reason for the consistently smaller values of τ_p than those of McClure⁶ obtained in the present work.

Phosphorescence Spectra.—The phosphorescence spectra of naphthalene in various media are analyzed vibrationally in Table V. As is evident, there is no significant self-absorption of the luminescence, and the widespread similarity of the spectra in Table V indicates that the measured lifetimes are indeed those of the naphthalene. A similar conclusion is appropriate to all halonaphthalene spectra. For example, despite the considerable self-absorption of the cracked glasses of 1-iodonaphthalene shown in Fig. 1, it is still readily apparent that the phosphorescence spectra are identical. This identity was further confirmed by front-face illumination experiments wherein the self-absorbed high energy bands of the phosphorescences of Fig. 1 were recovered. It is not generally realized that self-absorption of phosphorescence may be important in emission experiments; for example, in the work of Czekalla and co-workers¹⁶ it was noted that large shifts of the phosphorescence spectra of many aromatics occurred (~ 3000 cm.⁻¹) when they were studied as *crystalline* complexes with tetrachlorophthalic anhydride. A comparison of these authors' Fig. 1, curve 3, with Fig. 1 of the present work will indicate that at least for the com-

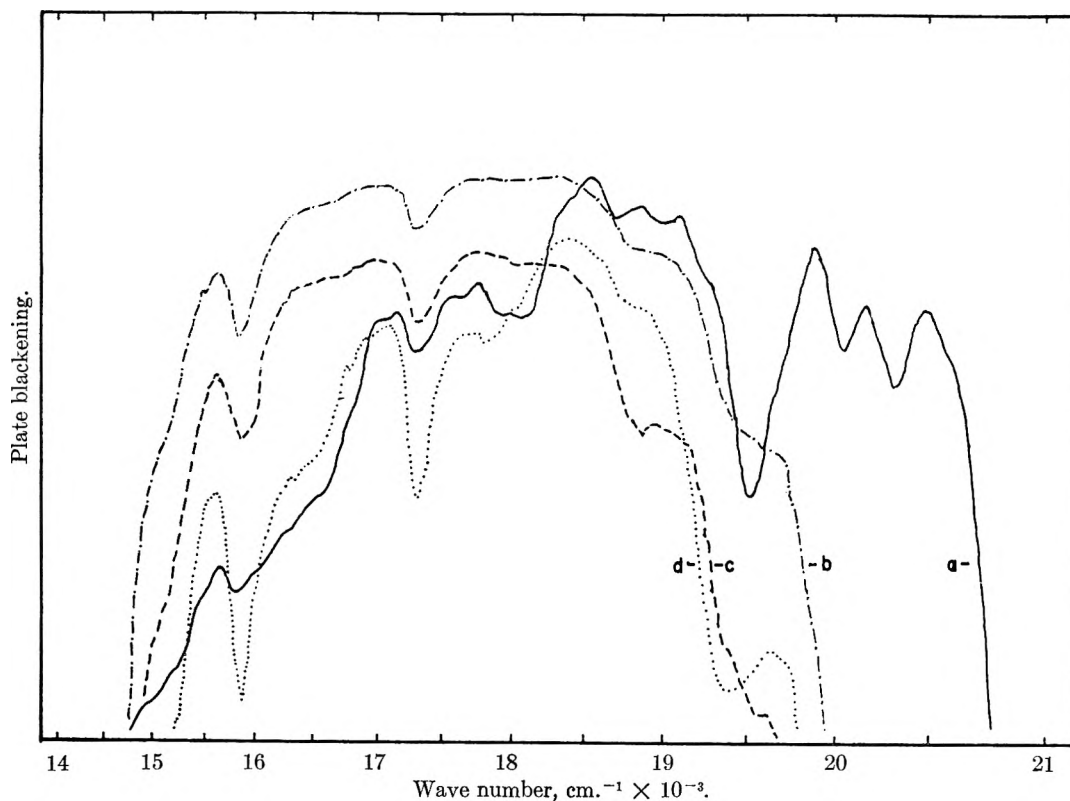


Fig. 1.—The phosphorescence emissions of 1-iodonaphthalene in several solvents at 77°K: (a) in EPA glass; (b) in propyl bromide cracked glass; (c) in propyl chloride cracked glass; and (d) in propyl iodide cracked glass.

plex tetrachlorophthalic anhydride-naphthalene these shifts were spurious (*i.e.*, they are not shifts of the 0,0 vibrational band) and entirely due to self-absorption. A similar conclusion seems relevant to the other crystalline complexes studied by Czekała, *et al.*¹⁶

The order of accuracy in Table V is $\pm 10 \text{ cm.}^{-1}$. Consequently, a number of conclusions are pertinent. The triplet state experiences a red-shift relative to the ground singlet state as the spin-orbital coupling nature of the matrix is increased. This is entirely to be expected if the perturbing singlet which mixes with the triplet of the aromatic lies higher in energy than the triplet states. This accords with the Tsubomora-Mulliken idea that this singlet is the charge-transfer singlet state, although as far as the present results are concerned it could be any higher energy singlet. The 0,0 shift in going from propyl bromide to propyl iodide matrices is approximately twice as large as that experienced in going from propyl chloride to propyl bromide. This indicates that there are factors other than spin-orbital coupling operative, since if this coupling were solely responsible a reverse order of shift would be expected. These conclusions accord exactly with those from the lifetime data. It is also to be noted that decreases

of some vibrational frequencies (the 1575 and 512 a_g modes) have occurred, indicative of a geometric specificity of interaction.

The lowest triplet state of naphthalene is of ${}^3B_{2u}(D_{2h})$ species. The analysis of Table V agrees with this assignment since the only active vibrations are the 512, 1146, 1380, and 1575 cm.^{-1} frequencies, and these are all of a_g species.²³ This agrees with the analysis of Ferguson, Iredale, and Taylor,²⁴ except that the difficulties these authors experienced with the 1146 and 1575 cm.^{-1} fundamentals which were thought to be of b_{1g} species are no longer relevant. Furthermore the present analysis covers a phosphorescence spectral width of 6735 cm.^{-1} as compared to a width of 2987 in the work of Ferguson, *et al.*, because of the limitations of photomultiplier detection.²⁴

Acknowledgment.—The authors acknowledge their indebtedness to the National Science Foundation and The American Instrument Company for having sponsored this work. They are also grateful to the Misses D. Chapman and K. Calnan who photographed many of the emission spectra run in conjunction with this research.

(23) E. W. Schmid, *Z. Elektrochem.*, **62**, 1005 (1958).

(24) J. Ferguson, T. Iredale, and J. A. Taylor, *J. Chem. Soc.*, 3160 (1954).

TRIPLET-SINGLET EMISSION IN FLUID SOLUTION

By C. A. PARKER AND C. G. HATCHARD

Royal Naval Scientific Service, Admiralty Materials Laboratory, Holton Heath, Poole, Dorset, England

Received May 25, 1962

Using a photoelectric spectrophosphorimeter of novel design, the long-lived luminescence from solutions of two dyestuffs and two aromatic hydrocarbons has been investigated. Solutions of eosin and proflavine hydrochloride in ethanol or glycerol give rise to two bands of long-lived luminescence which are attributed, respectively, to the triplet-singlet radiative transition and to delayed fluorescence arising from triplet-upper singlet thermal activation. A study of the band intensities as a function of temperature and solvent can provide information about the probabilities of the three intersystem crossing processes. Triplet-singlet emission has been observed from phenanthrene in ethanol at room temperature. At lower temperature weak delayed fluorescence also is emitted. Phenanthrene solutions containing trace quantities of anthracene give sensitized anthracene delayed fluorescence. Solutions of pure anthracene also give anthracene delayed fluorescence. The observations of delayed fluorescence from the hydrocarbons are discussed only briefly. They are described in detail elsewhere.

Introduction

The investigation of molecules in the triplet state in solution is normally made by the method of flash photolysis. By using an intense flash of sufficiently short duration a relatively high concentration of triplet molecules can be produced, their absorption spectrum can be measured, and the kinetics of the subsequent changes which they undergo can be followed in detail. The effect of medium and temperature upon the rate of the intersystem crossing process from triplet to lower singlet can thus (in principle at least) be investigated. Unfortunately, it is difficult to obtain by this method similar information about the equally important transition from excited singlet state to triplet state because it is difficult to determine precise quantum efficiencies for triplet formation. Information about the latter has so far been obtained mainly by measurements of the triplet-singlet phosphorescence of solutes in rigid media where triplet quenching is often small and high phosphorescence efficiencies can be observed. The pioneering work of Lewis and co-workers¹ in this field also showed that thermal excitation from triplet to upper singlet can occur and can be detected by measuring the "delayed fluorescence" which results from it.

The same method can in principle be applied to the investigation of upper singlet-triplet conversion and triplet-upper singlet activation in solution. In practice, however, the phosphorescence intensity is often very low owing to the long radiative lifetime of most molecules in the triplet state and the comparatively high rate of the triplet-lower singlet radiationless transition. (The experimental difficulties are of course accentuated by the susceptibility of the triplet molecules to quenching by trace impurities in the solution—particularly oxygen.) A phosphorimeter therefore is required capable of measuring phosphorescence and delayed fluorescence intensities which may be one thousandth or less of the normal fluorescence intensity from the same solution. To facilitate the measurement of such a weak phosphorescence spectrum and to measure the ratio of its intensity to that of the much more intense fluorescence, we have set up a photoelectric spectrophosphorimeter capable of measuring phosphorescence/fluorescence ratios down to values of 10^{-5} in favorable cases.

Some measurements of the phosphorescence of eosin solution made with this instrument have been reported previously.² It is our purpose here to review these results and to describe some preliminary results obtained with other compounds.

The Spectrophosphorimeter.—The instrument was built round two Hilger D247 quartz prism monochromators, one for isolation of the appropriate frequency of exciting light (from either a 1 kw. high pressure mercury lamp or a 375 w. xenon lamp) and the second for analysis of the fluorescence or phosphorescence emission from the specimen. The detector was an E.M.I. 9558 photomultiplier, the output from which, after amplification, was fed to one arm of a ratio recorder, the other arm of which was fed from a fluorescent screen monitor³ situated in the beam of exciting light. The recorded output thus was automatically compensated for fluctuations in light intensity.

The principle of the Becquerel phosphoroscope was used to distinguish between fluorescence and delayed luminescence, but the inconvenience of having mechanically coupled sectors in the beams of exciting light and luminescence light was avoided by arranging for each of the sector disks to be driven by a synchronous motor. The disks could then be put in, or out of, phase by simply turning one of the motors. With the disks in phase, the detector recorded the sum of the fluorescence and delayed emission spectra. With the disks out of phase, only the delayed luminescence was observed. In the latter position the fluorescence light leakage past the sectors was less than 1 part in 10^5 .

The rate of chopping by the sectors was 800 c./sec. The size of the slots in the first sector were adjusted so that the specimen was irradiated for $1/4$ of a complete cycle. The luminescence was viewed through the second sector for $1/3$ of a complete cycle. Thus, with the sectors in phase, the whole of the fluorescence emission was received by the detector, and with the sectors out of phase $1/3$ of the long-lived luminescence was received, assuming that the lifetime of the latter was long compared with the chopping time ($1/800$ sec.). For lifetimes comparable with the chopping time, the long-lived luminescence decayed appreciably before observation. The relationship between the intensity of luminescence observed and its lifetime is given by the expression

$$\frac{P_D}{P} = \frac{\tau}{t_1} \left(\frac{1 - e^{-t_1/\tau}}{1 - e^{-t_0/\tau}} \right) \left(e^{-(t_2 - t_1)/2\tau} - e^{-(t_2 + t_1)/2\tau} \right)$$

where

- P_D = luminescence received in the out-of-phase position
- P = total luminescence emitted per cycle
- τ = lifetime of luminescence
- t_1 = period of illumination
- t_2 = period of darkness
- t_3 = period of viewing through second sector
- t_0 = period of cycle = $(t_1 + t_2) = 1/800$ sec.

(1) G. N. Lewis, D. Lipkin, and T. T. Magel, *J. Am. Chem. Soc.*, **63**, 3005 (1941).

(2) C. A. Parker and C. G. Hatchard, *Trans. Faraday Soc.*, **57**, 1894 (1961).

(3) C. A. Parker, *Nature*, **182**, 1002 (1958).

For $t_1 = tc/4$ and $t_3 = tc/3$, the following relationship between τ and P_D/P is obtained

τ (msec.)	>5	1	0.5	0.25
P_D/P	0.333	0.316	0.271	0.165
τ (msec.)	0.15	0.10	0.07	
P_D/P	0.070	0.022	0.005	

The "resolution time" of the instrument (*i.e.*, the lifetime for which the observed intensity is reduced to one-half of the value corresponding to infinite lifetime) is 0.25 msec., and for the lifetimes shorter than this, the observed intensity decreases very rapidly.

It is feasible to reduce t_c by a factor of 5. The corresponding resolution time would then be 0.05 msec. and the scope of the instrument would be greatly increased, although a greater "fluorescence leakage" past the choppers probably would have to be accepted.

Long luminescence lifetimes (*e.g.*, those observed with many solutes at liquid nitrogen temperature) could readily be determined by recording the decay of luminescence (with sectors out of phase) when the exciting light was cut off. For measuring shorter lifetimes down to 0.5 msec. the 800 c./sec. sectors were replaced by 100 c./sec. sectors. The photomultiplier output was fed to an oscilloscope so that, with the sectors out of phase, the luminescence was viewed for a period of about 5 msec. during the "dark" periods. The lifetimes then were estimated by visual or photographic observation of the oscilloscope traces. To obtain sufficient intensity, wider slits had to be used on the spectrometer than was necessary for recording the luminescence spectra.

Phosphorescence of Eosin.—Typical spectra measured in glycerol and ethanol at various temperatures have been reported previously.² Two bands are present, the relative intensities of which are strongly temperature-dependent. The visible band ($\sim 1.8 \mu^{-1}$) has a contour identical with the fluorescence band in the same solution. (This is the visible "phosphorescence" originally observed by Boudin⁴ in glycerol solutions, and has an intensity about $1/400$ th of the fluorescence at room temperature.) To interpret our results we assume that this band is the result of thermal activation from the triplet to the upper singlet level followed by radiative transition from there to the ground state, and we therefore call this the delayed fluorescence band. We assume that the far red band ($\sim 1.4 \mu^{-1}$) corresponds to a direct transition from the triplet level to the ground state and we call this the phosphorescence band. If it is further assumed that the dyestuff is present as only one species and that no dissociation or association occurs in either of the excited states, then it can be simply shown² that

$$\frac{\phi_e}{\phi_p} = \frac{k_e \phi_t}{k_p} \quad (1)$$

where ϕ_t , ϕ_e , and ϕ_p are the quantum efficiencies of normal fluorescence, delayed fluorescence, and phosphorescence, k_e is the rate constant for thermal activation from the triplet to the upper singlet level, and k_p is the reciprocal of the radiative lifetime (τ_0) of the triplet state.

The ratio of the intensities of the two delayed emission bands thus should be completely independent of triplet formation efficiency (ϕ_t) and of all triplet quenching processes. Since k_e represents a thermal activation

$$\frac{\phi_e}{\phi_p} = \tau_0 \phi_t A \exp\left(-\frac{\Delta E}{RT}\right) \quad (2)$$

where A is a frequency factor and ΔE is the activation energy, which should be equal to the energy difference between the triplet and the upper singlet levels as determined by the frequency difference between the fluorescence and phosphorescence bands. Plots of $\ln(\phi_e/\phi_p)$ against $1/T$ were found to be linear and the derived value of ΔE (10 kcal.) agreed within experimental error with that determined from the spectroscopic data.²

The values obtained for A were $1.0 \times 10^9 \text{ sec.}^{-1}$ for glycerol and $7.2 \times 10^7 \text{ sec.}^{-1}$ for ethanol. The process k_e consists of a thermal activation to an upper vibrational level of the triplet state (rate = $k_1 \exp(-\Delta E/RT)$) followed by an intersystem crossing (rate = k_2). If we make the reasonable assumption that energy is equilibrated on every collision with solvent molecules, then k_1 will be equal to $2 \times 10^{12} \text{ sec.}^{-1}$ at room temperature. Of those molecules which acquire sufficient energy, some return to the lower level (rate = k_4) and some cross over to the upper singlet (rate = k_2). If all the activated molecules crossed over, A would be equal to k_1 . In fact A is less than one thousandth of this (for glycerol) and hence $k_2/k_4 \sim 10^{-3}$. The rate k_4 of degradation of vibrational energy in the triplet state is uncertain. Intermolecular vibrations occur at a rate of $10^{13} \cong 10^{14} \text{ sec.}^{-1}$ but a complex molecule such as eosin probably would have to execute a large number of vibrations before losing its excess of vibrational energy. Assuming $k_4 = 10^{12} \text{ sec.}^{-1}$, values of the intersystem crossing rate (k_2) can be calculated (see Table I). The rate in glycerol is more than ten times that in ethanol, in spite of the lower viscosity of the latter.

TABLE I
APPROXIMATE RATES OF INTERSYSTEM CROSSING FOR
EOSIN DISODIUM SALT

Process	In glycerol	In ethanol
$k_3(S^* \rightarrow t)$	$4 \times 10^7 \text{ sec.}^{-1}$	$1 \times 10^7 \text{ sec.}^{-1}$
$k_2(t \rightarrow S^*)$	5×10^8	4×10^7
$k_4(t \rightarrow S)$	$2.4 \times 10^2 (-20^\circ)$	$2.5 \times 10^2 (-20^\circ)$

Comparison of the rates for the reverse intersystem crossing (from upper singlet to triplet) can be obtained by calculating ϕ_e from the absolute values of ϕ_p together with the corresponding phosphorescence lifetimes at various temperatures.² The relevant data are shown in Table II. It is of particular interest that the yield of triplet in one solvent remains fairly constant when the temperature and viscosity vary over a wide range. In changing from glycerol to the more fluid ethanol, however, a reduction in the yield of triplet is observed. This is reflected in the difference between the rates of intersystem crossing from upper singlet to triplet (Table I).

At -20° the lifetime in both solvents was approximately the same, as was the lifetime at 77°K. (assumed to be the natural radiative lifetime τ_0). In view of the high viscosity of glycerol at -20° it is reasonable to assume that impurity quenching is negligible, and the same therefore must have been

(4) S. Boudin, *J. chim. phys.*, **27**, 285²(1930).

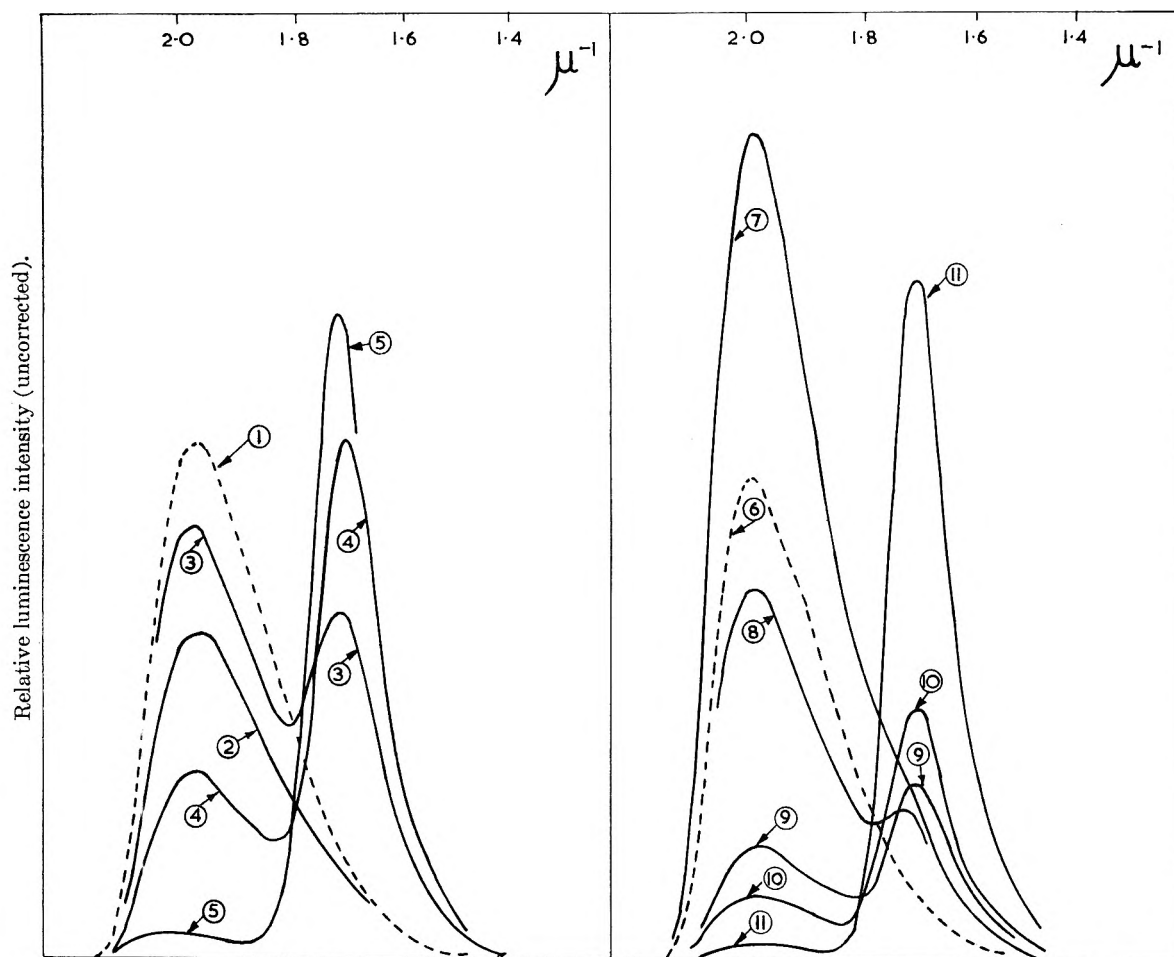


Fig. 1.—Delayed emission spectra of $10^{-4} M$ proflavine hydrochloride in glycerol (left) and ethanol (right) (excitation at $2.73 \mu^{-1}$ ($366 m\mu$)): (1) fluorescence emission spectrum at 20° ; (2) delayed emission spectrum (DES) at 20° ; (3) DES at -18° ; (4) DES at -38° ; (5) DES at -76° . Delayed emission spectra at a sensitivity approximately 80 times greater than that for the fluorescence emission spectrum. (6) Fluorescence emission spectrum at 20° ; (7) DES at 20° ; (8) DES at 0° ; (9) DES at -21° ; (10) DES at -39° ; (11) DES at -74° . Delayed emission spectra at a sensitivity approximately 10,000 times greater than that for the fluorescence emission spectrum.

TABLE II
QUANTUM EFFICIENCIES OF TRIPLET FORMATION AT
SELECTED TEMPERATURES

Note: The first result of each pair refers to an eosin concentration of $7 \times 10^{-5} M$, the second to $1.5 \times 10^{-5} M$

°C.	Glycerol solutions			Ethanol solutions		
	τ , msec.	ϕ_p	ϕ_t	τ , msec.	ϕ_p	ϕ_t
-196	10.7	0.0643	0.065	8.9	0.0237	0.024
	10.8	.0553	.055	9.3	.0224	.022
-70	5.5	.0328	.064	3.9	.0099	.023
	6.0	.0312	.056	3.5	.0099	.026
-20	3.0	.0160	.058	2.6	.0070	.024
	3.0	.0120	.043	2.9	.0070	.022
+25	2.6	.0124	.052	1.4	.0039	.025
	2.7	.0091	.036	1.7	.0039	.021
+70	0.9	.0047	.056	0.7	.0015	.020
	1.0	.0039	.042	0.6	.0015	.023

true for ethanol at this temperature. Comparison of τ at -20° with τ_0 thus gives the value of the rate of intersystem crossing (k_h) from triplet to ground state (see Table II) which is apparently independent of viscosity at this temperature (a result which also has been suggested recently by Livingston and co-workers⁵ for anthracene). At

lower temperatures, the quenching rate in glycerol falls sharply and this may be due to a rapid increase in the rigidity of the glycerol.

Possibility of Excited Dimer Formation in Dye-stuff Solutions.—It has been suggested⁶ that the weak phosphorescence observed by Kautsky⁷ in many dyestuff solutions is due to the formation of long-lived excited dimers, and the question therefore arises whether the phosphorescence of eosin is produced by the same mechanism. The evidence presented here and previously² seems to be conclusive that it is not. Thus the delayed fluorescence clearly arises through thermal activation from the energy level responsible for the far red emission band, and the latter is most intense in rigid media at $77^\circ K.$, where the formation of excited dimer by a collisional process is ruled out. We have commenced an investigation of some other dyestuffs and we present below some preliminary results obtained with solutions of proflavine hydrochloride which show that the mechanism of delayed luminescence with this dyestuff

(5) G. Jackson, R. Livingston, and A. C. Pugh, *Trans. Faraday Soc.*, **56**, 1635 (1960).

(6) B. Stevens, *Nature*, **192**, 725 (1961).

(7) H. Kautsky, *Ber.*, **68**, 152 (1935).

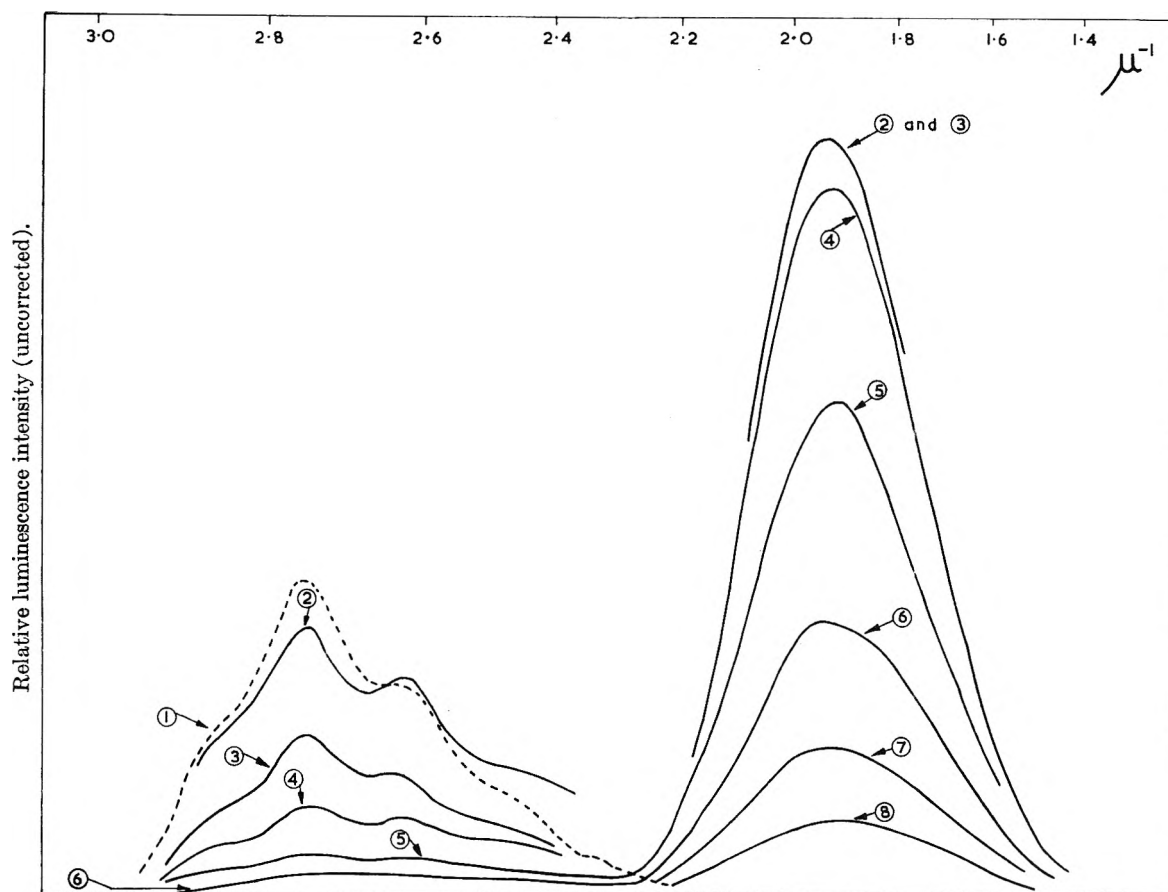


Fig. 2.—Delayed emission spectra of $10^{-3} M$ phenanthrene in ethanol. The left hand sections of the spectra (delayed fluorescence) all were recorded at a sensitivity approximately 1000 times greater than that used for curve (1) (normal fluorescence). The right hand sections of the curves (phosphorescence) were recorded at the following sensitivities: (2) -107° at $\times 60$; (3) -80° at $\times 300$; (4) -70° at $\times 600$; (5) -48° at $\times 1000$; (6) -32° at $\times 1000$; (7) -14° at $\times 1000$; (8) $+13^\circ$ at $\times 1000$.

(at the concentrations so far investigated) is analogous to that of eosin. Our results do not of course eliminate the possibility of excited dimer formation but show that the majority of the luminescence does not arise by this mechanism.

Phosphorescence of Proflavine Hydrochloride.—Proflavine in its monoprotonated form is interesting for two reasons. First, it is one of the amino acridines which most easily undergo photoreduction in aqueous solution and the kinetics of the process at pH 4 have been investigated.⁸ Second, its triplet state has a long radiative lifetime (3.4 sec.) compared with that of eosin (10 msec.). It might be expected therefore that at room temperature in fluid solution its triplet state would be particularly susceptible to quenching and that phosphorescence would be weak. In fact this is not so. Quite intense delayed fluorescence is observed in glycerol solution at room temperature, having a lifetime of about 70 msec. (see Fig. 1) and even in ethanol at room temperature the intensity of delayed fluorescence has the same order of magnitude as that observed for eosin. Proflavine thus must be particularly resistant to solvent quenching processes and warrants more detailed investigation than we have yet been able to give.

The preliminary results (Fig. 1) are qualitatively similar to those obtained with eosin. The de-

layed emission spectra consist of a "delayed fluorescence" band and a "phosphorescence" band, the ratio of the band intensities being highly temperature-dependent. The log ratio of the band intensities is (within experimental error) a linear function of $1/T$ and the activation energy derived from the slope of this plot (~ 8 kcal.) is close to that corresponding to the frequency difference between the two bands. The "delayed fluorescence" therefore arises by thermal activation from the level responsible for the low frequency band and since the latter persists at $77^\circ K.$ in EPA it corresponds to a metastable level of a species already present in the ground state and not to a dimer formed by a collisional process in the excited state.

Our present data are not sufficiently accurate nor extensive to justify detailed calculations. It may, however, be noted that the frequency factor in glycerol is $\sim 10^7$ sec.⁻¹, i.e., about one hundredth that for eosin in the same solvent. This would imply that the probability of intersystem crossing ($t \rightarrow S^*$) is lower than for eosin.

It should be emphasized that the interpretation of our results in terms of triplet-singlet and singlet-triplet transitions depends on the assumption that the dyestuffs were present in solution as only one species (the monomer) and that no protolytic reactions occurred on excitation. The results do not entirely rule out the possibility of excitation of a

(8) F. Millich and G. Oster, *J. Am. Chem. Soc.*, **81**, 1357 (1959).

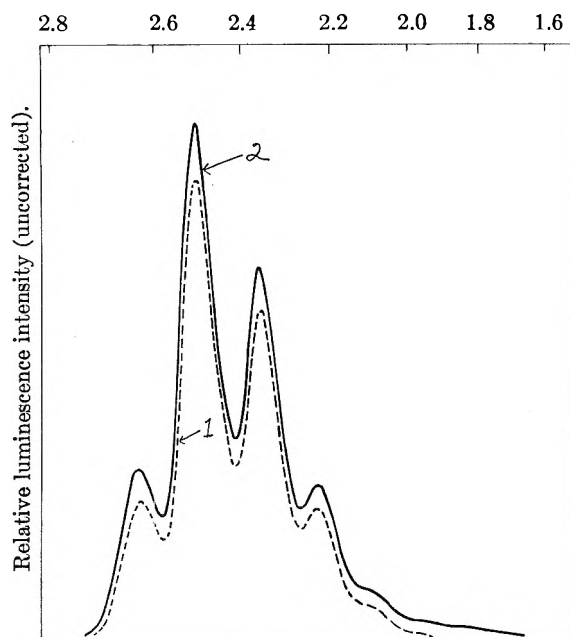


Fig. 3.—Delayed fluorescence from $5 \times 10^{-4} M$ anthracene in ethanol. Intensity of exciting light was approximately 1.4×10^{-8} einstein $\text{cm}^{-2} \text{sec}^{-1}$ at $2.73 \mu^{-1}$ ($366 m\mu$). Half-band width of analyzing monochromator was $0.05 \mu^{-1}$ at $2.5 \mu^{-1}$. (1) Normal fluorescence spectrum, (2) delayed fluorescence spectrum at 380 times greater sensitivity (spectra are distorted by self-absorption).

dimer already present in the ground state although in the case of eosin the comparatively small dependence of ϕ_p/ϕ_f on concentration suggests that this is unlikely. A full interpretation of the effects requires an investigation of the dependence of both luminescence and absorption spectra on pH, concentration, solvent, and temperature. For example, the position of the peak absorption of proflavine monohydrochloride in ethanol ($458 m\mu$) is shifted from that in water ($443 m\mu$); the fluorescence band shifts in the opposite direction. Again, Millich and Oster⁸ observed an increased quantum yield of photoreduction, and strong self-quenching of fluorescence on increasing the concentration of proflavine in aqueous solution. They interpreted their results in terms of a transition of the excited singlet species to a long-lived state induced by the dye itself. If the same is true in ethanol, it would imply an increased delayed luminescence as the concentration is increased. Preliminary measurements in ethanol suggest that there is little change in ϕ_o/ϕ_f or in τ , for concentrations in the range 10^{-4} – $10^{-6} M$.

Delayed Emission from Solutions of Aromatic Hydrocarbons.—The observation of long-lived luminescence from vapors of aromatic hydrocarbons (e.g., phenanthrene and anthracene)⁹ has been attributed to excited dimers formed from an excited singlet molecule and a normal molecule. The blue structureless band emitted by concentrated solutions of pyrene also has been shown to be due to an excited dimer,¹⁰ although in this case the majority of the luminescence has a short lifetime.¹¹ Long-lived emission so far has not been

reported from fluid solutions of other hydrocarbons at room temperature and the results shown in Fig. 2 which refer to a deaerated solution of phenanthrene in ethanol are therefore of particular interest.

At 77°K . in EPA phenanthrene shows a strong phosphorescence band in the region of $2.0 \mu^{-1}$ with well resolved fine structure, for which ϕ_p/ϕ_f was found to be about unity.¹² At -107° this band still appears at high intensity (about one quarter of that observed in liquid nitrogen). The intensity decreases rapidly as the temperature is raised but the phosphorescence can still be observed at room temperature ($+13^\circ$) where its intensity is about $1/1000$ th of that observed at liquid nitrogen temperature. Unfortunately, to record the low values of phosphorescence shown by some of the curves in Fig. 2, wide slits had to be used and vibrational structure in both the fluorescence and phosphorescence bands is largely lost. However, there is little doubt that this band is due to the triplet-lower singlet radiative transition and this is the first time, so far as is known, that such an emission has been observed from an aromatic hydrocarbon in fluid solution at room temperature.

The point of special interest in Fig. 2 is the appearance, as the temperature is lowered, of delayed fluorescence emission, although admittedly at low intensity. To test whether this could be due to thermal activation from the triplet level, the log ratio of the band intensities was plotted against $1/T$. The plot was not linear, but from the maximum slope an activation energy of 2–3 kcal. was derived. This is so much less than the energy difference between the two bands (~ 20 – 25 kcal.) that activation from the triplet level is ruled out.

We have observed a more intense delayed fluorescence from carefully deoxygenated solutions of anthracene in ethanol. Typical results for $5 \times 10^{-4} M$ anthracene are shown in Fig. 3, where the quantum efficiency of delayed fluorescence was almost 1% of that of the normal fluorescence. We also have observed quite intense delayed emission from solutions of phenanthrene containing very small amounts of anthracene. The spectral distribution of this emission was characteristic of normal anthracene fluorescence and it therefore must have been produced by sensitization of the anthracene by a long-lived phenanthrene species. The detailed results of our investigation of anthracene and phenanthrene solutions are presented elsewhere¹³ but it may be mentioned that the delayed fluorescence efficiency is in both cases proportional to the intensity of the exciting light and it cannot be explained in terms of an excited dimer similar to that postulated to explain the delayed fluorescence observed in the vapor phase.^{6,9,14} The results can, however, be explained by a mechanism in which triplet-triplet quenching produces a molecular species carrying the energy from two triplet molecules. We have some evidence that a similar process can occur with solutions of pro-

(9) R. Williams, *J. Chem. Phys.*, **28**, 577 (1958).

(10) Th. Förster and K. Kasper, *Z. Elektrochem.*, **59**, 977 (1955).

(11) C. A. Parker and C. G. Hatchard, *Nature*, **190**, 165 (1961).

(12) C. A. Parker and C. G. Hatchard, *Analyst*, **87**, 664 (1962).

(13) C. A. Parker and C. G. Hatchard, *Proc. Chem. Soc.*, **147** (1962); *Proc. Roy. Soc. (London)*, **A269**, 574 (1962).

(14) B. Stevens, E. Hutton, and G. Porter, *Nature*, **185**, 917 (1960).

flavine hydrochloride at high light intensities, although at the light intensities used to obtain the results shown in Fig. 1 the delayed fluorescence produced by this mechanism was small compared

with that produced by thermal activation from the triplet level.

This paper is published with the permission of the Superintendent, Admiralty Materials Laboratory.

STEPWISE PHOTOREVERSIBLE DYE SYSTEMS^{1,2}

BY GISELA KALLMANN OSTER, GERALD OSTER, AND CECILY DOBIN

Department of Chemistry, Polytechnic Institute of Brooklyn, Brooklyn, N. Y.

Received May 25, 1962

In oxygen-free solution phenosafranin bound to polymethacrylic acid is photoreduced by green light when EDTA is present as the electron donor for the light excited dye. The leuco species is converted by ultraviolet light to a fluorescent yellow species. This intermediate is insensitive to light and is insensitive to oxygen. The yellow species can be thermally decomposed to give predominantly leuco dye. Leuco dye in the presence of oxygen is readily converted to the normal red dye. Arguments are given against the yellow intermediate being a semiquinone.

Introduction

One problem which arises in the photoreduction of dyes is whether the reduction is a two-step or a one-step process. Certainly the leuco form of the dye bears two more electrons than the original dye and is identical with the leuco dye produced by reaction in the dark with powerful reducing agents. If the photochemical reduction proceeds by the two-step process proposed by Michaelis³ for purely chemical reductions then one might be able to detect semiquinone intermediates during the photochemical reaction. With this in mind we have made a search for colored intermediates in photoreducing systems. One dye which seemed to show promise is phenosafranin. In the presence of an electron donor for the light excited dye the red dye is photoreduced to its leuco form. If the reaction is carried out slowly or if the dye is bound to a high polymer and if a polychromatic light source is used, a yellow intermediate is observed. We should like to demonstrate that this intermediate does not occur, however, in the photoreduction step but arises from the leuco species.

Experimental

Materials.—Phenosafranin (3,8-diamino-12-phenylphenazinium chloride) was Histological Grade, obtained from Fisher Scientific Co. The chelating agent, disodium ethylenediaminetetraacetic acid (EDTA), Analytical Grade, was obtained from the same source. Acrylamide was obtained from American Cyanamide Co. and was purified by repeated crystallization from methanol. Polymethacrylic acid was made by Bofors Co., Sweden, and, for the sample used, had a molecular weight as found by diffusion and ultracentrifugation measurements (carried out by Mr. B. Palm of Uppsala University) of 5×10^4 . Purified nitrogen (Airco) was purified further by passing through a freshly prepared solution of chromous chloride. This removes traces of oxygen which may be present.

Procedure and Apparatus.—All the dye solutions were made up in 0.1 M acetate buffer at pH 5.3. Prior to illumination the solutions were deaerated by passing bubbling nitrogen through the solution for 30 min.

(1) Supported by the United States Air Force through the Air Force Cambridge Research Laboratories under Contract No. AF 19(604)-8056 and by the United States Atomic Energy Commission under Contract No. AT(30-1)-2206.

(2) Taken in part from Master of Science thesis of Cecily Dobin, Polytechnic Institute of Brooklyn, 1962.

(3) For reviews, see for example, L. Michaelis and M. P. Schubert, *Chem. Rev.*, **22**, 437 (1938), and L. Michaelis, *Ann. N. Y. Acad. Sci.*, **40**, 39 (1940).

Sample cells containing a gas inlet and outlet were illuminated with white light from a 500-watt tungsten lamp slide projector with a pale yellow filter to cut off light below 400 m μ . To follow the disappearance of a particular colored species an apparatus was employed⁴ using a Bausch and Lomb monochromator in conjunction with a photomultiplier whose output was recorded continuously.

Near ultraviolet light of predominantly 365 m μ was obtained with an AH-4 mercury lamp fitted with a Wood's glass filter.

Absorption spectra were obtained with a Cary Model 11 recording spectrophotometer. For temperatures above room temperature a cell housing was employed whereby heating liquid from a temperature bath could be circulated.

Paper electrophoresis was carried out in a Model E-800-2B Research Specialties Company apparatus. The solutions (in 0.1 M acetate buffer at pH 5.3) were applied to strips of Whatman No. 1 paper and a potential of 250 volts was applied.

Equilibrium dialysis was carried out using Visking seamless sausage casings closed at both ends. The dialysis sacks containing 20 ml. of solution (dye and polymer) were placed in 100 ml. of buffer and allowed to equilibrate for three days. The amount of dye bound was calculated from the concentration of dye, determined colorimetrically, which dialyzed out of the sack. In all cases the amount of dye bound to the dialysis sack (determined when no polymer was present) was taken into account.

Results

There are a number of criteria to demonstrate that phenosafranin is bound to polymethacrylic acid at pH 5.3. When polymer is in excess so that all the dye is bound the maximum in absorption of the dye at 518 m μ is shifted to 530 m μ . In Table I are given the spectral data on bound and free phenosafranin. Incidentally, there is an absorption maximum for phenosafranin also at 273 m μ but this is unchanged on addition of polymer. Binding of the dye also is accompanied by an increase of orange fluorescence. No spectral shifts are observed above pH 6 although the polymer is fully charged. This is in contrast to nucleic acids (both RNA⁵ and DNA⁶) as substrates where binding of phenosafranin occurs even in basic media (up to pH 11.9). Also the spectral shift is somewhat greater for the nucleic acids; to 540 m μ when the dye is fully bound. For polymeth-

(4) N. Wotherspoon and G. Oster, *J. Am. Chem. Soc.*, **79**, 3992 (1957).

(5) L. Michaelis, *Cold Spring Harbor Symp. Quant. Biol.*, **12**, 131 (1947).

(6) G. Oster and H. Grimsson, *Arch. Biochem.*, **24**, 119 (1949).

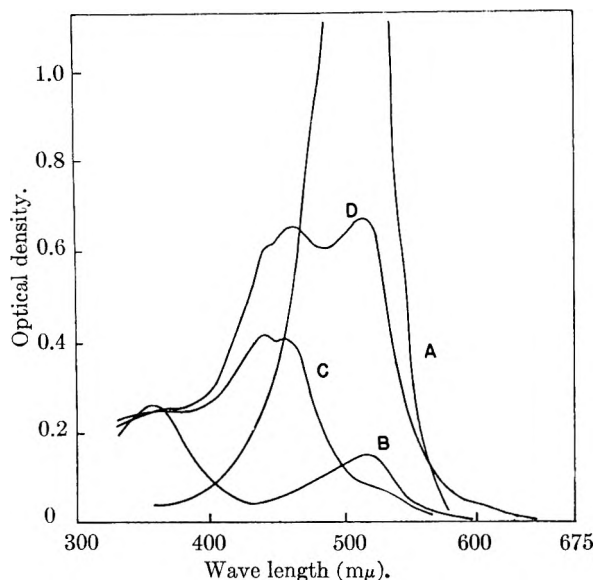


Fig. 1.—Optical density (for 5 cm. path length) of free phenosafranin ($8.8 \times 10^{-4} M$) in the presence of EDTA ($10^{-3} M$): A, original dye; B, visible light faded solution; C, illumination of solution B with near ultraviolet ($363 m\mu$) for 30 min.; D, after solution C had been allowed to stand for 18 hr. under nitrogen.

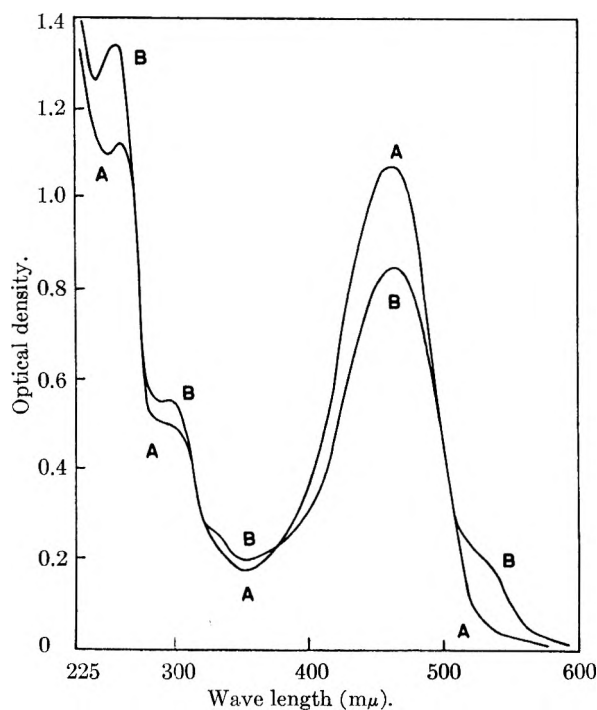


Fig. 2.—Decay of bound yellow intermediate: A, original yellow species formed from ultraviolet irradiation of bound leuco dye; B, solution A after standing in the dark for 1 hr. Spectra taken in 5 cm. path length cell. Dye concentration $10^{-5} M$, EDTA $10^{-3} M$, and polymethacrylic acid $8 \times 10^{-5} M$.

acrylic acid the dye was considered fully bound when the molar ratio of polymer to dye was 1:1.25, since further addition of polymer caused no further shift in spectra. Dialysis experiments starting with various ratios of dye and polymer revealed that the binding followed closely a Langmuir isotherm. If r is the ratio of dye bound per polymer molecule (average molecular weight 5×10^4)

and c is the equilibrium dye concentration then the binding follows the expression $r = nc/K + c$, where the number of binding sites n per polymer chain is 200 and the intrinsic dissociation constant K of the dye-substrate complex is 2.5×10^{-6} .

TABLE I
SPECTRAL CHARACTERISTICS OF PHENOSAFRANIN AND ITS
PHOTOCHEMICAL PRODUCTS

	Free		Bound	
	λ_{\max} ($m\mu$)	ϵ ($\times 10^{-3}$)	λ_{\max} ($m\mu$)	ϵ ($\times 10^{-3}$)
Phenosafranin	518	39.0	530	41.0
Phenosafranin	273	39.0	273	40.0
Yellow intermediate	450	21.2	465	22.0
Leuco dye	360	7.5	365	7.9
Leuco dye	249	53.5	254	55.0

Further evidence of binding is revealed from paper electrophoresis. The dye alone migrates to the negative electrode. On the addition of small amounts of polymer two spots appear, each moving in opposite directions. When the molar ratio of polymer to dye exceeds 1:1.25 only one spot appears and this dye-polymer complex moves toward the positive electrode. This ratio of polymer to dye was utilized in all subsequent experiments involving bound dye.

In oxygen-free solution phenosafranin is photo-reduced to the leuco species when EDTA is present as the electron donor for the light excited dye. Table I gives the spectral data of the leuco species. These values are based on the assumption that all the original dye is transformed only to the leuco species. On introduction of oxygen immediately after fading the red species is completely recovered. The rate of fading is proportional to EDTA concentration (at least for concentrations up to $10^{-3} M$) and to incident light intensity. In the bound state the dye fades at a rate roughly 40% that of the free dye. This is in contrast to triphenylmethane dyes where binding to polymethacrylic acid at pH 5 actually enhances photoreduction, in fact, such dyes do not undergo photoreduction in the free state.^{7,8}

In the rigorous absence of oxygen the free leuco species slowly, over a period of hours, is converted into a yellow species whose spectral characteristics are given in Table I. Since the process is slow, oxygen inadvertently leaks into the system so that the formation of yellow species is accompanied by the formation of the red dye. The yellow species is insensitive to visible light and to oxygen. Hence if illumination with white (or green) light is maintained, the red form is continuously photoreduced and the build-up of yellow species from leuco dye proceeds. If the unfiltered mercury lamp is used, the rate of formation of the yellow species is not affected appreciably but the spectral character is changed (Fig. 1). In particular two yellow species are produced in addition to the normal dye and a small tail absorbing beyond $600 m\mu$ is observed. This tail accounts for

(7) G. Oster and J. Bellin, *J. Am. Chem. Soc.*, **79**, 294 (1957).

(8) G. Oster and G. K. Oster, "Proc. Int. Conf. Luminescence", John Wiley and Sons, New York, N. Y., 1962.

the green color observed in the ultraviolet illumination of leuco phenosafranin in glucose glasses.⁹

Bound leuco dye also is converted slowly to a yellow species. Here, however, the conversion is enormously accelerated by near ultraviolet light. Using the 365 $m\mu$ line of the mercury lamp the bound leuco dye is completely converted in three minutes to a strongly fluorescent yellow species. The production of yellow species is accompanied by a proportional loss of the leuco species.

The yellow intermediate is insensitive to visible light and to oxygen. The bound yellow species decays in the dark to give predominantly bound leuco dye (Fig. 2). Since it is difficult to eliminate oxygen from the absorption cell for long periods some red always is formed which presumably arises from oxidation of leuco dye formed from the yellow species. The conversion of yellow to leuco species is first order in yellow species. The rate is accelerated by roughly a factor of six at 65° over that at 25°.

The phenosafranin-EDTA system is a photosensitizer for polymerization of vinyl monomers. One notices that for acrylamide polymerization the reaction proceeds after an induction period during which the red dye is not decolorized. The onset of polymerization appears to take place at the moment that yellow species appears. For a 50% monomer solution the resultant highly viscous solution is yellow and strongly fluorescent. Unlike other dye systems which also act as sensitizers,¹⁰ here there is no restoration of original dye as oxygen diffuses slowly into the polymer mass.

Discussion

Phenosafranin, like a number of other water-soluble dyes, undergoes photoreduction to the leuco form in the presence of secondary and tertiary amines.¹¹ Most of these amines are not reducing agents in the ordinary sense and are, in fact, normally quite resistant to oxidation. The light excited dye in its triplet state^{12,13} is a powerful electron abstractor and destroys the amine¹³ to give an

oxidized product.¹⁴ The leuco dye appears to be identical with that produced in the dark by the action of strong reducing agents.

During the course of investigations on the properties of chemically produced leuco phenosafranin it was noticed that a yellow species was produced when the system was kept deaerated for several hours.¹⁵ The yellow (unbound) dye reported in the present paper is probably the same species. On the other hand, the pale yellow semiquinone obtained from phenosafranin in strongly acid solution¹⁶ is different in that first its absorption maximum is in the near ultraviolet and second, it is readily oxidized by oxygen to give regenerated dye.

The photochemistry of the bound dye-EDTA system bears a formal resemblance to that of thiazine dyes in glucose glass.¹⁷ There it was found that the blue dye was photoreduced (glucose acting as the electron donor) to the leuco species. This latter species when illuminated with near ultraviolet light gave a red intermediate. This intermediate was strongly fluorescent and yet was light stable. On softening the glass, the red species reverted to the leuco form of the thiazine dye.

The yellow phenosafranin intermediate cannot be simply a semiquinone or a dimer of a semiquinone since its spontaneous decomposition to leuco dye in the dark takes place in the absence of a reducing agent. It is difficult to understand what other reaction of a semiquinone could take place to give leuco dye without the concurrent production of red dye (*i.e.*, dismutation).

It is conceivable that the yellow species is a photodimer of the leuco dye. Thermal decomposition of the yellow species would give the monomeric leuco species. It seems unlikely, however, that in the case of thiazine dyes in rigid glucose¹⁷ photodimers could form, since the viscosity of the medium is so extremely great.

The fact that bound leuco dye is photosensitive whereas free leuco dye is practically insensitive may be due to the rigidity which the polymer imparts to the poorly resonating leuco species.

(9) B. Broyde, Ph.D. thesis, Polytechnic Institute of Brooklyn, 1960, p. 89.

(10) G. Oster, *Nature*, **173**, 300 (1954).

(11) For review see G. Oster, *J. chim. phys.*, **55**, 899 (1958).

(12) G. Oster and A. H. Adelman, *J. Am. Chem. Soc.*, **78**, 913 (1956).

(13) G. Oster and N. Wotherspoon, *ibid.*, **79**, 4836 (1957).

(14) D. Mauzerall, *ibid.*, **82**, 1832 (1960).

(15) R. D. Stiehler, T. T. Chen, and W. M. Clark, *ibid.*, **55**, 891 (1933).

(16) L. Michaelis, *ibid.*, **58**, 1816 (1936).

(17) B. Broyde and G. Oster, *ibid.*, **81**, 5099 (1959).

EXTREMELY LONG-LIVED INTERMEDIATES IN PHOTOCHEMICAL REACTIONS OF DYES IN NON-VISCOUS MEDIA^{1,2}

BY GERALD OSTER, GISELA KALLMANN OSTER, AND GERHART KARG³

Department of Chemistry, Polytechnic Institute of Brooklyn, Brooklyn, N. Y.

Received May 25, 1962

Halogenated fluorescein dyes in the presence of tertiary amines are photochemically dehalogenated by visible light. With longer wave lengths of illumination iodine atoms may be removed but chlorines remain. Dechlorination takes place with shorter wave lengths. Selective dehalogenation also can take place using white light when properly chosen amines are present. In all cases an unstable yellow intermediate with a lifetime of the order of seconds is formed. It is postulated that the intermediate is a semiquinone which decomposes spontaneously to yield dark-stable partially dehalogenated species.

Introduction

Previous work in our Laboratory^{4,5} has demonstrated that fluorescein and its halogenated derivatives undergo photofading in the presence of a mild reducing agent such as allyl thiourea. We have extended this work recently using various secondary and, particularly, tertiary amines as electron donors for the light excited dyes. It has been found previously with thiazine dyes that these amines participate in photochemical reactions to give the leuco thiazine.⁶ With the halogenated fluoresceins, however, certain of the amines also cause a photodehalogenation. These reactions are selective as to which halogen atoms are removed from the light-excited dye molecules. In the course of these studies we further noted that in the early stages of the photodehalogenation there is some reversibility in the dark and that the reaction involves the formation of yellow intermediates having a lifetime of the order of seconds.

It is the purpose of the present paper to describe the process of photodehalogenation, to identify the stable products produced, and to try to establish the identity of the intermediate.

Experimental

Materials.—The dyes (fluorescein, 2',7'-dichlorofluorescein, 4',5'-dibromofluorescein, 4',5'-diiodofluorescein, 2',4',5',7'-tetrabromofluorescein, 2',4',5',7'-tetraiodofluorescein, 2',4',5',7'-tetrabromo-3,4,5,6-tetrachlorofluorescein, 2',4',5',7'-tetraiodo-3,4,5,6-tetrachlorofluorescein) were obtained either from Eastman Kodak Co. Organic Chemicals or from Allied Chemical and Dye Corporation. Hereafter, these dyes are referred to as FI, FI₂, FI₂Br₂, FI₂I₂, FI₂Br₂Cl₂, FI₂Br₂Cl₂, and FI₂I₂Cl₂, respectively. The dyes were employed as the sodium salts. Those dyes obtained from Eastman (reagent grade FI₂Cl₂ and FI₂I₂, practical FI and FI₂) were available only in the acid form so that in these cases the sodium salt was prepared. The remaining dyes from Allied were histological grade.

Triethanolamine and nitrilotriacetic acid were Eastman Reagent grade. Ethylenediaminetetraacetic acid, disodium salt, was Dow Chemical Co. reagent grade. Anhydrous N,N,N',N'-tetramethylethylenediamine was obtained from Ames Laboratories, South Norwalk, Conn.

Oxygen, helium, and prepurified nitrogen were obtained from Airco. The nitrogen was purified further by passing it

through a chromous chloride solution. Nitric oxide (Matheson Co.) was purified with sulfuric acid and potassium hydroxide solutions according to the method of Moser.⁷

Procedures.—Photochemical conversion of the dyes was accomplished by illuminating with visible light from a slide projector containing a 500-watt tungsten lamp (General Electric CZX) and a glass filter (Corning 3-73) which removes light of wave lengths shorter than about 400 m μ . Provision was made to both deaerate and stir the solutions by passing nitrogen through the samples. To obtain oxygen-free conditions, the solutions were flushed with nitrogen for 15 min. prior to and during the irradiation.

When a continuous recording of transmittance *versus* time was required, the light passing through the sample was filtered with appropriate glass and interference filters and the output of the detector (Type 2A-L6 Hoffman Electronics Corp. silicon photovoltaic cell) registered on a Varian Associates Type G-10 recorder.

Transient phenomena were studied with two different sets of apparatus. For studies at 550 m μ with rose bengal (FI₂Cl₂), the dye chosen for most of these studies, the continuously recording apparatus described above was employed. This apparatus also included sliding mechanisms for quickly interposing or removing filters placed before or after the sample. After a brief (3 sec. or less) strong illumination with white light the analyzing filters (*i.e.*, filters between the sample and the detector) were removed and an identical set of filters was interposed between the light source and the sample. In this way the dark recovery of the species produced during the strong illumination could be recorded. The other apparatus, a single-beam recording monochromator, consisting of a Bausch and Lomb grating monochromator with an RCA 1P21 multiplier phototube as the detector and a Leeds and Northrup Speedomax recorder, has been described elsewhere.⁸ Here the transient species was measured at a variety of wave lengths. The procedure was to interpose, after a brief strong illumination, neutral density filters between the light source and the sample, and to record at each wave length the time-course of the decay of the transient species. The same arrangement was employed to measure the dark recovery at various wave lengths.

All light sources and recorders were operated through voltage stabilizers (Sola Electric Co. transformers). The spectra of stable species were determined in a Cary Model 11 recording spectrophotometer with 1 cm. path length cells.

The pK values of the dyes were obtained by the usual technique of plotting the optical density of the dyes at appropriate wave lengths as a function of pH and reading the pK from the inflection point of the resulting sigmoidal curve.

Chromatographic *R_f* values were obtained by a descending method using Whatman No. 1 paper with 88% ammonia, ethanol, and water in the proportion of 5:10:85 by volume.⁹

Electrophoretic mobilities were determined on a Research Specialties Model E-800-2B paper electrophoresis apparatus. Whatman No. 1 paper was employed and the determination was carried out in 0.1 M phosphate buffer at pH 8.0 with an applied potential of 250 volts.

Results

The values of absorption maxima, pK's, *R_f* numbers, and electrophoretic mobilities of the

(7) L. Moser, *Z. anal. Chem.*, **50**, 401 (1911).

(8) N. Wotherspoon and G. Oster, *J. Am. Chem. Soc.*, **79**, 3992 (1957).

(9) K. Taylor, *Nature*, **185**, 243 (1960).

(1) Supported by the United States Air Force through the Air Force Cambridge Research Laboratories under Contract No. AF 19(604)-8056.

(2) Taken in part from the dissertation of Gerhart Karg to be submitted to the Faculty of the Polytechnic Institute of Brooklyn in partial fulfillment of the requirements for the degree of Doctor of Philosophy.

(3) National Science Foundation Predoctoral Fellow, 1958-1961.

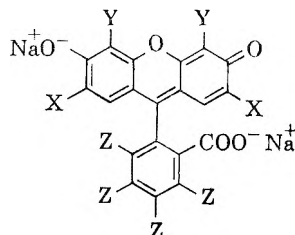
(4) G. Oster and A. H. Adelman, *J. Am. Chem. Soc.*, **78**, 913 (1956).

(5) A. H. Adelman and G. Oster, *ibid.*, **78**, 3977 (1956).

(6) G. Oster and N. Wotherspoon, *ibid.*, **79**, 4836 (1957).

dyes employed are given in Table I. These quantities were determined in order to identify the stable photoproducts of the reaction. It should be noted that there is a correlation between the R_f values and the electrophoretic mobilities of the various dyes.

TABLE I



pK values in parentheses are uncertain.

Dye	X	Y	Z	Abs. max. ($m\mu$)	pK	R_f	Electrophoretic mobility (10^4 cm. ² /sec./volt)
Fl	H	H	H	490	6.7 4.4 2.2	0.58	0.46
FlCl ₂	Cl	H	H	500	5.1 3.9 (0.6)	.46	.37
FlBr ₂	H	Br	H	506	5.3 3.9 (0.5)	.26	.23
FlI ₂	H	I	H	510	5.2 4.2 (0.6)	.19	.08
FlBr ₄	Br	Br	H	518	3.6	.12	.05
FlI ₄	I	I	H	528	4.3	.07	.03
FlBr ₄ Cl ₄	Br	Br	Cl	540	3.7	.34	.16
FlI ₄ Cl ₄	I	I	Cl	550	4.3	.24	.09

In Fig. 1 are illustrated the spectra of erythrosin (FlI₄) before and after illumination with white light, triethanolamine being present. The colored photoproduct formed has a spectrum identical with fluorescein. Furthermore, the values of the pKs, R_f number, and electrophoretic mobility of the photoproduct are identical with those for fluorescein. With rose bengal, on the other hand, an intermediate colored species is produced in addition to fluorescein (Fig. 2). The conversion to fluorescein can be carried out in a stepwise fashion. Rose bengal (spectral curve A of Fig. 2) in the presence of triethanolamine gives, on illumination with green light, a stable species which absorbs maximally at 510 $m\mu$ (curve B of Fig. 2). On illumination of the new species with blue-green light (or white light) fluorescein is obtained (curve C of Fig. 2). Alternatively, fluorescein is obtained directly from rose bengal by extended illumination with white light. The intermediate species has the same R_f number (namely, 0.77⁹) as 3,4,5,6-tetrachlorofluorescein. Illumination of phloxine (FlBr₄Cl₄) with green light yields the same intermediate.

Ethylenediaminetetraacetic acid and nitrilotriacetic acid are ineffectual for the photochemical conversion to fluorescein of rose bengal, phloxine, and 2',7'-dichlorofluorescein. The other dyes, however, are convertible to fluorescein in the presence of either of these two chelating agents.

Fluorescein is relatively light stable in the presence of all of the chelating agents excepting tetramethylethylenediamine, where photoreduction to a leuco species proceeds rapidly. For rose bengal at pH 10 with triethanolamine or tetramethylethylenediamine, a greater spectral shift is obtained than with ethylenediaminetetraacetic acid or

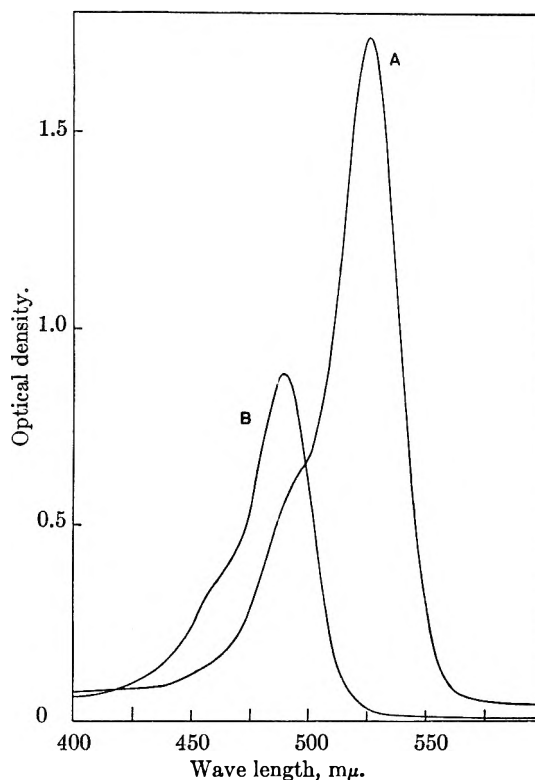


Fig. 1.—Spectra of erythrosin before (A) and after (B) 2 min. of illumination with white light; dye concentration $1.8 \times 10^{-5} M$ in the presence of triethanolamine (0.1 M).

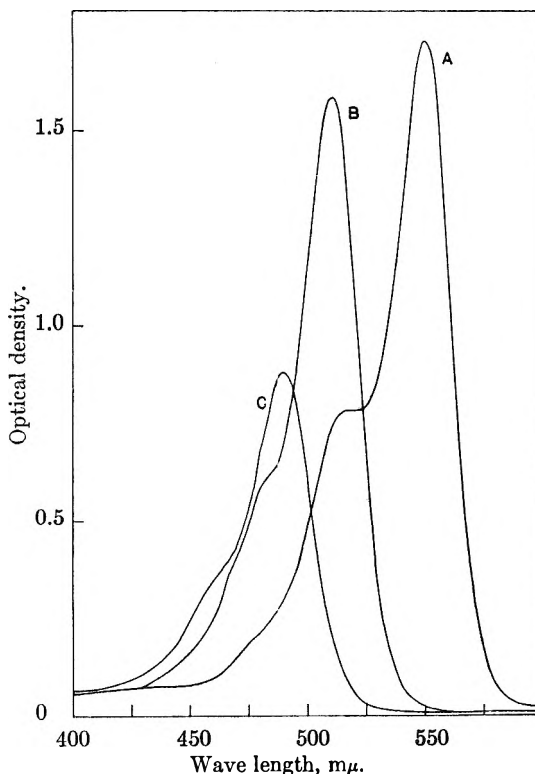


Fig. 2.—Spectra of rose bengal: (A) before illumination; (B) after illumination with green light; (C) after illumination with blue-green light (or with white light); concentrations as in Fig. 1.

nitrilotriacetic acid for the same period of illumination. Not all of the rose bengal is converted to

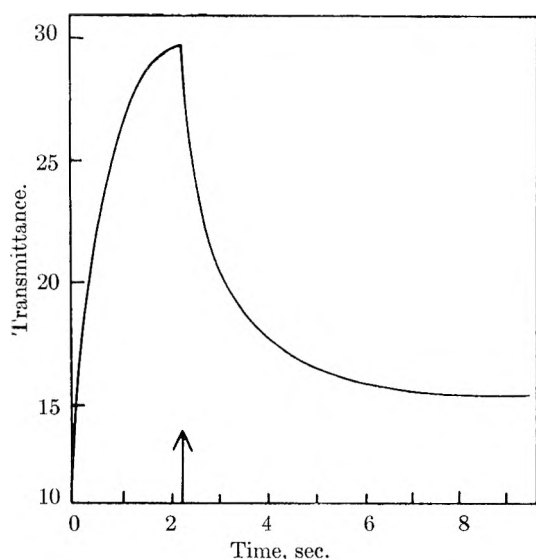


Fig. 3.—Fading and dark recovery of rose bengal: white light illumination ceased after time indicated by the arrow; dye concentration $10^{-4} M$; triethanolamine concentration $10^{-3} M$.

colored species. A large fraction is converted irreversibly to colorless species. This is especially true if tetramethylethylenediamine is used.

In Fig. 3 is illustrated the fading and dark recovery of rose bengal in the presence of triethanolamine. If T_{∞} is the final transmittance in the dark, T_0 its value at the beginning of the dark period, and T_t its value at any time t , then the results can be represented as $\ln(T_t/T_{\infty})/\ln(T_0/T_{\infty}) = e^{-t/\tau}$, where τ is the lifetime. Since the dye obeys Beer's law, the ratio of the logarithmic functions is merely the ratio of the concentration at time t to that at the beginning of the dark period. The lifetime of the decay is 1.6 sec. independent of the dye concentration (at least for 10^{-5} to $10^{-4} M$ in dye). For tetramethylethylenediamine the lifetime decreases slightly with increasing chelating agent concentration (1.7 sec. for $3 \times 10^{-5} M$ and 1.0 sec. for 30 times this concentration).

When oxygen or nitric oxide is introduced suddenly at the end of the illumination period the recovery is more rapid. The spectra of the photoproducts are unaffected by the presence of these gases.

Using the spectrophotometric techniques we find that the rate of recovery of rose bengal is greatest at $540 m\mu$. During irradiation there is produced a strongly colored yellow species which absorbs maximally at about $422 m\mu$. This species decays in the dark at a rate close to the rate of the production of the $540 m\mu$ absorbing species. The other halogen-containing dyes also show intermediates absorbing close to the values for the rose bengal intermediate but the intermediate is less pronounced the less the degree of halogenation of the original dye. No colored intermediate could be detected for fluorescein.

Discussion

The amines employed in the present work all cause a photoreduction of thiazine dyes to give the leuco species.⁶ Certainly some photoreduction

occurs for the fluorescein dyes as well, since metal ions are reduced when any one of these dyes, in the presence of chelating agents, is used as the photosensitizer.¹⁰ The tertiary amine causes a photodehalogenation as well, however. By using controlled wave lengths when illuminating rose bengal, selective dehalogenation can take place. Thus, green light causes the removal of the iodine atoms, allowing the chlorine atoms to remain. The chlorine atoms are removed when shorter wave length light (blue-green) is employed. Selective removal of halogen atoms also can be achieved with the proper choice of tertiary amine. Thus, when ethylenediaminetetraacetic acid is present, illumination of rose bengal with white light causes removal of the iodine atoms only.

Amines which serve as electron donors for light-excited dye molecules are destroyed in the reaction.⁶ There are indications that the amine is oxidized at the alpha carbon atom.¹¹ In one case, at least, that of acridine orange, the photoreaction involves the addition of the chelating agent to the dye.¹² It should be noted that the two amines which are ineffectual in the removal of chlorines from the fluorescein dyes bear the same sign of charge as the dye molecules.

It is likely that the intermediate species absorbing around $422 m\mu$ is a semiquinone ion. It would be expected that a semiquinone is formed through the quinoid oxygen on the dye. The spectra of such semiquinones would not be expected to be appreciably affected by substituent halogens. Their stability, on the other hand, would be strongly dependent on substituents. It is significant in this connection that the intermediates found with the fluorescein dyes all had nearly the same spectra but were produced in greater amount the greater was the extent of substitution and degree of polarizability of the substituent halogen atoms. The electron-rich semiquinone should permit easy release of the halogen.

Somewhat stable intermediates have been found in the visible light excitation of eosin (FlBr₃) in the presence of ascorbic acid, pure pyridine being the solvent.¹³ Electron paramagnetic resonance spectra indicate that a semiquinone is produced and that there is interaction between an unpaired electron and two protons. The absorption spectra of species, presumed to be semiquinones, which are formed during the photoreduction of rose bengal, erythrosin, and eosin in pyridine-ascorbic acid, and for eosin in ethanol-butyraldehyde, at -35° , have been determined.¹⁴ The spectrum reported for rose bengal under these conditions is quite similar to that obtained in the present work in water at room temperature. The photochemical reaction of chlorophyll in pyridine with ascorbic acid (the "Krasnovsky reaction"¹⁵) leads to an unstable red intermediate, the nature of which is

(10) G. K. Oster and G. Oster, *J. Am. Chem. Soc.*, **81**, 5543 (1959).

(11) D. Mauzerall, *ibid.*, **82**, 1832 (1960).

(12) A. Kellmann and G. Oster, *J. chim. phys.*, **58**, 355 (1961).

(13) N. N. Bubnov, V. F. Tsepalov, and V. Ya. Shlyapintokh, *Izv. Akad. Nauk SSSR, Ser. Fiz.*, **23**, 1265 (1959).

(14) V. F. Tsepalov and V. Ya. Shlyapintokh, *Izv. Akad. Nauk SSSR, Otd. Khim. Nauk*, 637 (1959).

(15) A. A. Krasnovsky, *Dokl. Akad. Nauk SSSR*, **60**, 421 (1948).

imperfectly understood. Water-soluble chlorophyll (potassium chlorophyllin) undergoes the Krasnovsky reaction in water with ascorbic acid when pyridine is present only to the extent of 10%.¹⁶ This reaction does not proceed, however, if the ascorbic acid is replaced by a secondary or tertiary amine. Hence we cannot at this time simply associate our yellow intermediate with the intermediate found by the Russian workers¹³ for eosin.

The intermediate apparently is not that observed for eosin by means of flash spectroscopy.^{17,18} The lifetimes of such intermediates are of the order of one millisecond or less while ours has a lifetime some thousand times greater. Although a yellow intermediate absorbing at 405 m μ has been observed for eosin by flash spectroscopy,¹⁸ this species was obtained only in the presence of phenol. In common with species produced by high intensity flash our intermediate exhibits a shortened lifetime when oxygen is introduced. Furthermore, nitric oxide also decreases the lifetime of our intermediate without producing any over-all chemical change, thus indicating the paramagnetic nature of this intermediate.

(16) G. Oster and S. B. Brody, *Nature*, **192**, 132 (1961).

(17) S. Kato, T. Watanabe, S. Nagaki, and M. Koizumi, *Bull. Chem. Soc. Japan*, **33**, 262 (1960).

(18) L. Grossweiner and E. Zwicker, *J. Chem. Phys.*, **34**, 1411 (1961).

The transient species decomposes to give what appears to be, in the case of rose bengal, a mono-iodinated species. The maximum in its absorption spectrum, namely, 540 m μ , lies between that of the tetraiodinated species and the location where the diiodinated species should absorb. Due to overlapping spectra with the original dye the absorption at 550 m μ of this species appears as an apparent recovery of the original rose bengal. Continued irradiation of this triiodinated species leads to complete removal of the iodine atoms.

Recently we have found that the yellow intermediate can be stabilized by carrying out the reaction in glycerol at low temperatures where the systems form rigid glasses. Future experiments of this kind which have yielded intermediates in the photofading of visual purple¹⁹ and of thiobenzophenone²⁰ are contemplated to obtain more detailed spectra of the intermediates. We feel that this intermediate may play a role in dye-sensitized photopolymerization²¹ since our dye-tertiary amine mixtures are photosensitizers for the initiation of polymerization of vinyl monomers.

(19) G. Wald, J. Durell, and R. C. C. St. George, *Science*, **111**, 179 (1950).

(20) G. Oster, *Ann. N. Y. Acad. Sci.*, **74**, 305 (1958).

(21) G. Oster, *Nature*, **173**, 300 (1954); G. K. Oster, G. Oster, and G. Prati, *J. Am. Chem. Soc.*, **79**, 595 (1957).

THE EFFECT OF LIGHT ON OXIDATION AND REDUCTION REACTIONS INVOLVING PHTHALOCYANINE AND ETIOPORPHYRIN I MANGANESE COMPLEXES

BY G. ENGELSMA,¹ AKIO YAMAMOTO,² E. MARKHAM,³ AND MELVIN CALVIN

*Department of Chemistry and Lawrence Radiation Laboratory,⁴
University of California, Berkeley 4, California*

Received May 25, 1962

A detailed study of the chemistry and photochemistry of phthalocyanine manganese and a few metal derivatives of porphyrins has been made. It has been shown that the stable oxidation level of manganese may be shifted among the II, III, and IV oxidation states, depending on the nature of the fifth and sixth coordinating groups. Furthermore, photochemical oxidation as well as photochemical reduction of the phthalocyanine manganese(III) has been observed, and photochemical reduction of the manganese(IV) compound demonstrated. Mn(III), Fe(III) and Co(III), etioporphyrins also are photoreduced to the II state. The possible participation of such photochemical transformations in the oxygen evolution sequence of photosynthesis is indicated.

Introduction

Recent investigations have shown that manganese plays an important role in photosynthesis.⁵⁻¹¹

(1) The Philips' Research Laboratory, Eindhoven, The Netherlands, NATO Fellow, 1960-1961.

(2) On leave from the Research Laboratory of Resources Utilization, Tokyo Institute of Technology, Tokyo, Japan.

(3) University Chemical Laboratory, Lensfield Road, Cambridge, England.

(4) This work was supported, in part, by the U. S. Atomic Energy Commission.

(5) E. Kessler, *Planta*, **49**, 435 (1957).

(6) E. Kessler, W. Arthur, and J. E. Brugger, *Arch. Biochem. Biophys.*, **71**, 326 (1957).

(7) T. E. Brown, H. C. Eyster, and H. A. Tanner, "Trace Elements," Academic Press, Inc., New York, N. Y., 1958, p. 135.

(8) T. E. Brown, H. C. Eyster, and E. A. Tanner, *ibid.*, p. 157.

(9) H. A. Tanner, T. E. Brown, H. C. Eyster, and R. W. Treharne, *Ohio J. Sci.*, **60**, 231 (1960).

In particular, manganese seems to be essential in the oxygen evolving systems.⁶ Recently it was reported that a manganese chelate related to the porphyrins, namely, phthalocyaninemanganese, apparently formed a peroxide reversibly which, in turn, seemed to be capable of dissociating the oxygen-oxygen bond in a reversible fashion.¹² This observation was so unusual that it attracted our attention immediately. It seemed possible to incorporate such stages in the oxygen evolution scheme of photosynthesis with great ease.

In order to determine the feasibility of using

(10) R. W. Treharne, T. E. Brown, H. C. Eyster, and H. A. Tanner, *Biochem. Biophys. Res. Comm.*, **3**, 119 (1960).

(11) H. A. Tanner, T. E. Brown, H. C. Eyster, and R. W. Treharne, *ibid.*, **3**, 205 (1960).

(12) J. A. Elvidge and A. B. P. Lever, *Proc. Chem. Soc.*, 195 (1959).

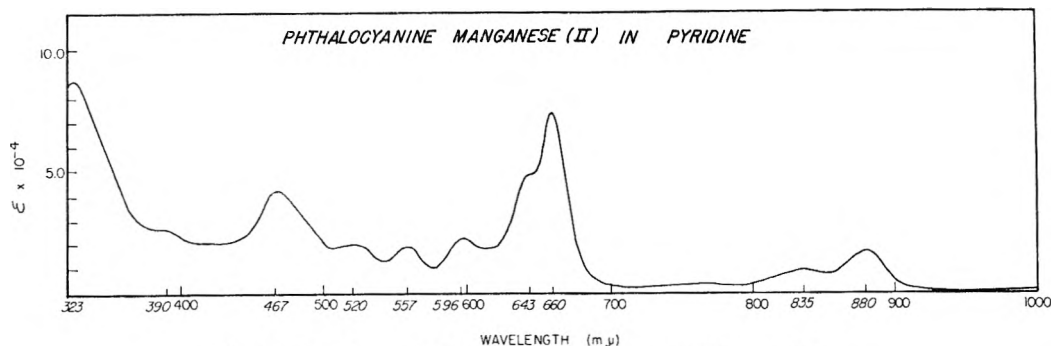


Fig. 1.—Spectrum of phthalocyaninemanganese(II) in pyridine.

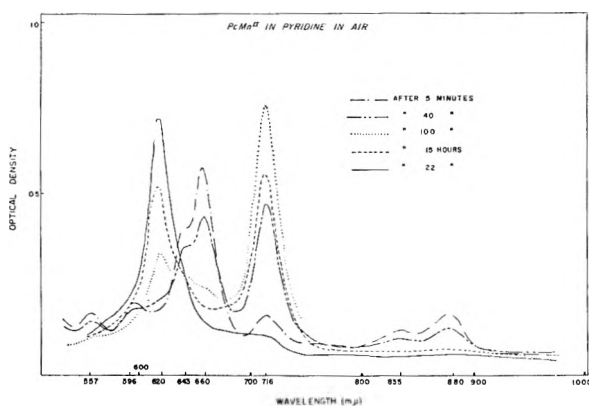


Fig. 2.—Oxidation by air of a $8.5 \times 10^{-6} M$ solution of phthalocyaninemanganese(II) in pyridine with cell thickness 1 cm.

phthalocyaninemanganese complexes as model compounds, a study was undertaken of the oxidation and reduction reactions of these complexes. The influence of light on these reactions was especially investigated.

The basic compound of this series, phthalocyaninemanganese(II) (I) is prepared from phthalonitrile and manganese dioxide¹³ or manganese acetate.¹⁴ Elvidge and Lever¹² have reported that phthalocyaninemanganese(II) in a pyridine solution has an absorption band at 712.5 $m\mu$, whereas Rutter and McQueen¹⁴ stated that its main absorption band in the visible region is at 620 $m\mu$. We have found that these spectra belong to oxidized phthalocyaninemanganese compounds. A solution of phthalocyaninemanganese(II) prepared in the absence of air has absorption peaks at 830, 835, 660, 643, and 467 $m\mu$ (Fig. 1). On introduction of air, these bands decreased and a new band at 716 $m\mu$ was observed. This band probably corresponds to Elvidge and Lever's band at 712.5 $m\mu$. It gradually built up to a maximum and then decreased again, a band at 620 $m\mu$ finally being formed (Fig. 2).

On evaporation of a solution of phthalocyaninemanganese(II) (I), prepared in the absence of air (660 $m\mu$), a green compound was obtained which changed in contact with the air. It probably is phthalocyaninedipyridinemanganese(II) (II). From the completely oxidized solution (620 $m\mu$,

$\log \epsilon 4.94$) a purple compound was obtained for which the elementary analysis was in approximate agreement with the formula given by Elvidge and Lever¹²: phthalocyanine-oxo-pyridinemanganese(IV) (III).^{14a} Magnetic susceptibility measurement of this crystalline compound at room temperature showed that it is almost diamagnetic with a molar susceptibility of -270×10^{-6} c.g.s., which, when adjusted by diamagnetic correction of phthalocyanine, pyridine, and oxygen, gives a slightly paramagnetic magnetic moment of 0.71 Bohr magneton. This would require some kind of electron pairing in the crystal, either by dimerization through two oxygen atoms (the peroxide which apparently is not present) or by metal-oxygen-metal interaction, or metal-metal interaction. Solubility limitations have so far prevented any reliable magnetic susceptibility measurement or molecular weight measurement in solution, and we tentatively assume the monomeric structure phthalocyanine-oxo-pyridinemanganese(IV) for this species (absorption maximum, 620 $m\mu$) in pyridine solution.

In the absence of air the transient oxidation product (716 $m\mu$) is broken down under the influence of light to form phthalocyaninedipyridinemanganese(II) and phthalocyanine-oxo-pyridinemanganese(IV). This appeared to indicate that the 716 $m\mu$ species might be the presumed reversible peroxide of phthalocyaninemanganese suggested by Elvidge and Lever.¹² They assume that the oxidation of phthalocyaninemanganese(II) to phthalocyanine-oxo-pyridinemanganese(IV) and the reverse reaction, reduction to phthalocyaninemanganese(II) by boiling a solution of phthalocyanine-oxo-pyridinemanganese(IV) in pyridine, have, as a common intermediate, a bis-(phthalocyanine pyridinemanganese) peroxide $(PcMn-Py)_2O_2$. The first part of this work is centered around the question of whether our photosensitive intermediate corresponds to a dimanganese peroxy complex, and if so, whether oxygen is released on its decomposition.

Isolation of Intermediate Oxidation Level Compounds

A direct isolation of the intermediate from the

(14a) The crystals as they originally come out of the pyridine solution at room temperature seem to have two molecules of pyridine per manganese atom. Removal of the pyridine by vacuum heating, reabsorption of pyridine, and removal of excess or lightly bound pyridine leave behind crystals with only one molecule of pyridine per manganese atom.

(13) P. A. Barrett, C. E. Dent, and R. P. Linstead, *J. Chem. Soc.*, 1719 (1936).

(14) H. A. Rutter, Jr., and J. D. McQueen, *J. Inorg. Nucl. Chem.*, **12**, 362 (1960).

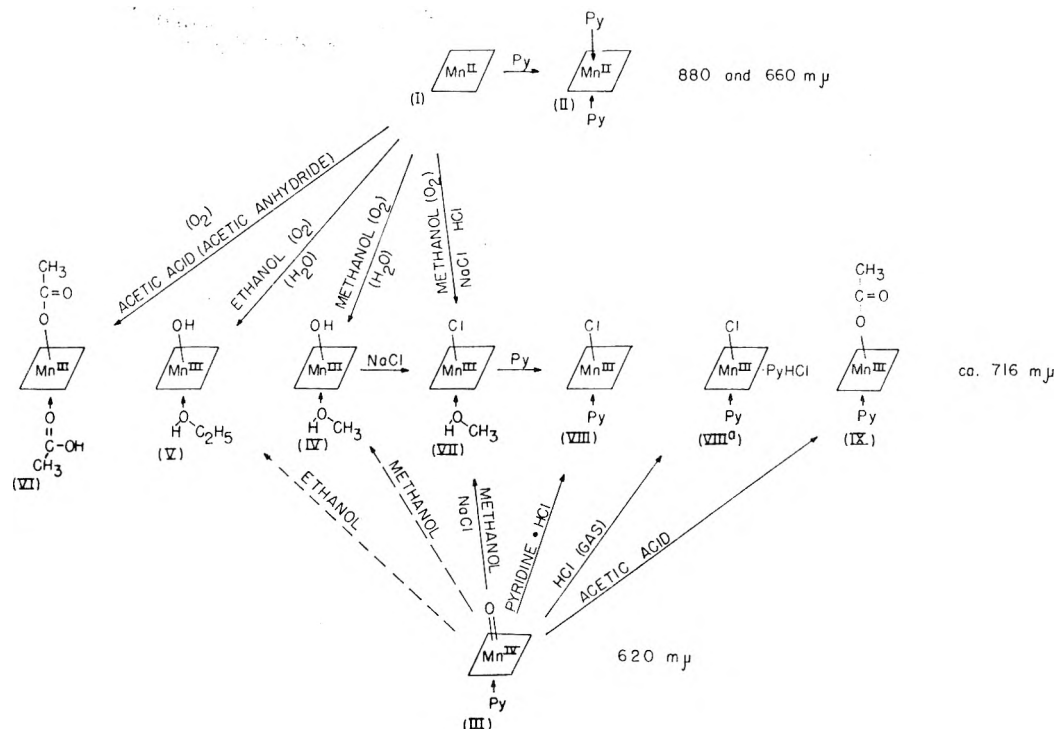


Fig. 3.—Interrelationship of phthalocyaninemanganese complexes. The rhombs and Pc represent the square planar tetradentate bivalent phthalocyanine ligand, $C_{32}H_{16}N_8$; Py for pyridine.

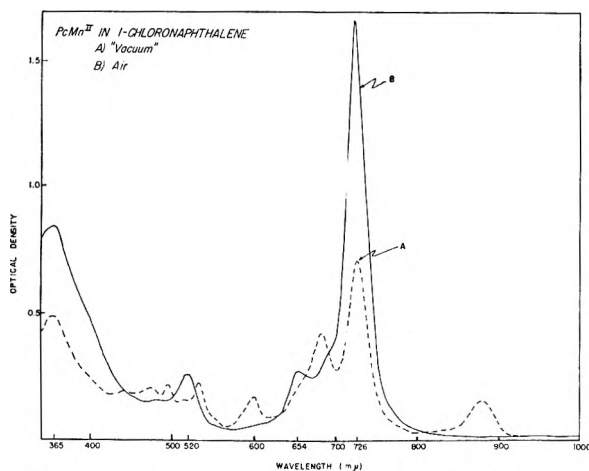


Fig. 4.—(a) Spectrum of a solution of phthalocyaninemanganese(II), in 1-chloronaphthalene, prepared in the "absence" of air. (b) Spectrum of the same solution one hour after air had been admitted. The optical densities of the two curves are not necessarily comparable, since all of the compound may not have been dissolved in (a).

solution in pyridine is not feasible because of its equilibrium with the manganese(II) and manganese(IV) compounds. A solution in which only the species absorbing at $716\text{ m}\mu$ is present can be obtained by dissolving phthalocyaninemanganese(II) in a mixture of equal amounts of pyridine and water (in the presence of air). On evaporation of this solution *in vacuo* a green compound precipitates. However, attempts to identify this compound failed, since in contact with the air it is converted rapidly to a violet compound which appeared to be identical with phthalocyanine-oxopyridinemanganese(IV) (III). A chart exhibiting the interrelationships to be described is shown in Fig. 3.

Solutions of phthalocyaninemanganese(II) in 1-chloronaphthalene, methanol, ethanol, chloroform, ethyl acetate, chlorobenzene, dimethylformamide, nitromethane, and acetic acid, prepared in the presence of air, have spectra which are very similar to the spectrum of the intermediate oxidation product in pyridine ($716\text{ m}\mu$). They have high absorption bands between 710 and $726\text{ m}\mu$. In the case of 1-chloronaphthalene it was shown that this spectrum belongs to an oxidized phthalocyaninemanganese. A solution prepared with exclusion of air as far as possible had a spectrum with peaks at 878 , 726 , 682 , 654 , 598 , 532 , 494 , 473 , and $440\text{ m}\mu$. Except for the peak at $726\text{ m}\mu$ this spectrum is very similar to the spectrum of phthalocyaninemanganese(II) in pyridine. On introduction of air, the peak at $726\text{ m}\mu$ increased rapidly whereas all the other absorption bands decreased, indicating that the $726\text{ m}\mu$ band belongs to oxidized phthalocyanine manganese (Fig. 4).

From the solutions in methanol and ethanol we isolated complexes to which, based on elementary analysis, we assigned the formulas phthalocyanine-hydroxo-methanolmanganese(III) (IV) and phthalocyanine-hydroxo-ethanolmanganese(III) (V), respectively. The magnetic moment of the compound (IV) was 4.87 Bohr magnetons (θ , $+17^\circ\text{ K}$.) corresponding to four spin-free unpaired electrons of manganese(III).

A complex which according to the elementary analysis is phthalocyanine-chloro-methanolmanganese(III) (VII) was obtained by extracting phthalocyaninemanganese(II) with methanol saturated with sodium chloride and a trace of HCl. On evaporating a solution of this complex in pyridine, dark green crystals of phthalocyanine-chloropyridinemanganese(III) (VIII) appeared. Phthal-

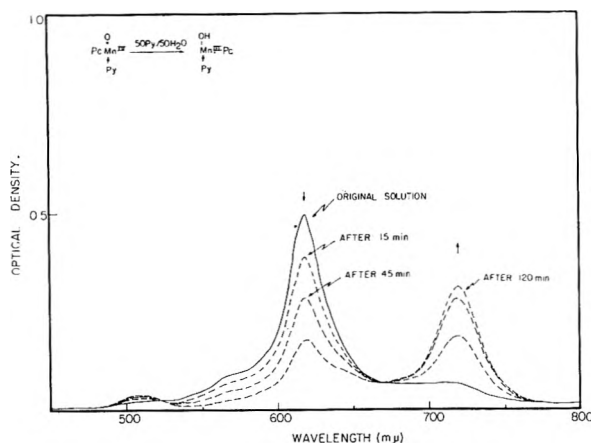


Fig. 5.—Reduction of phthalocyanine-oxo-pyridine-manganese(IV) in a pyridine-water 1:1 mixture: —, freshly prepared solution; ---, spectra after 15, 45, and 120 min., respectively.

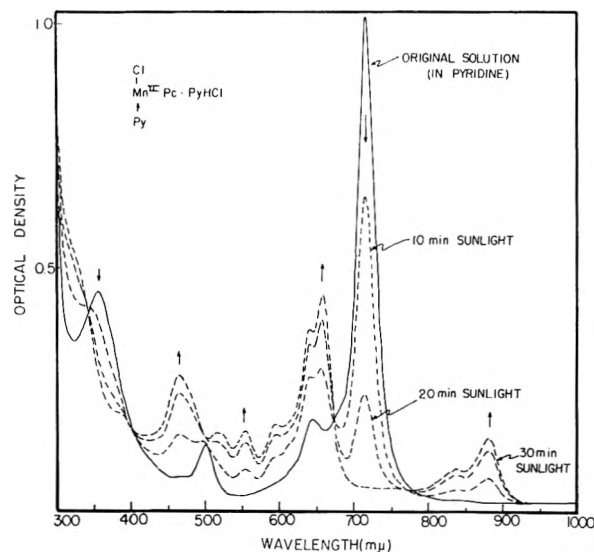


Fig. 6.—Photo-reduction of phthalocyanine-chloro-pyridinemanganese(III) in pyridine in the absence of air: —, original solution; ---, after illumination in the sun for 10, 20, and 30 min., respectively.

ocyanine-chloro-methanolemanganese also could be prepared by adding sodium chloride to a methanolic solution of IV.

Extracting phthalocyaninemanganese(II) with glacial acetic acid containing 5% acetic anhydride resulted in a complex for which the elementary analysis was in agreement with phthalocyanine-acetato-(acetic acid)-manganese(III) (VI).

Also starting with phthalocyanine-oxo-pyridine-manganese(IV) (III), it is possible to obtain complexes with absorption spectra which are very similar to the spectrum of the intermediate oxidation product seen in pyridine.

When crystals of phthalocyanine-oxo-pyridine-manganese(IV) are dissolved in methanol, ethanol, or 1-chloronaphthalene the band at 620 $m\mu$ is observed first, but it soon disappears and exactly the same spectra are obtained as those that appear when phthalocyaninemanganese(II) is dissolved in the same solvents in the presence of air. Also on addition of methanol to a solution of phthalocyanine-oxo-pyridinemanganese(IV) in pyridine,

the band at 620 $m\mu$ decreases slowly with an increase of the 716 $m\mu$ band at the same time. Adding sodium chloride to such a solution in which the 620 $m\mu$ band had disappeared completely resulted in a precipitate of phthalocyanine-chloro-methanolemanganese(III) (VII).

A similar spectral change corresponding to Mn(IV) reduction can be induced by adding water to a pyridine solution of manganese(IV). In Fig. 5 the decrease of the peak at 620 $m\mu$ and the increase of the peak at 716 $m\mu$ can be followed for a pyridine solution of phthalocyanine-oxo-pyridinemanganese(IV) to which an equal volume of water had been added. Considerable bleaching of the solution takes place, possibly due to oxidation of the phthalocyanine ring. The reduction of the Mn(IV) complex is greatly accelerated by acids. On introduction of dry HCl gas to the pyridine solution, the color changes from blue to green, and a dark green complex precipitates which according to the elementary analysis is phthalocyaninedipyridinemanganese(III) dichloride or phthalocyanine-chloro-pyridinemanganese(III) pyridine hydrochloride (VIIIa). When a small amount of pyridine hydrochloride is added to a solution of phthalocyanine-oxo-pyridinemanganese(IV) in pyridine, a complex slowly crystallizes for which the analysis corresponds to phthalocyanine-chloro-pyridinemanganese(III) (VIII). Both complexes have an identical absorption spectrum in pyridine with a maximum at 716 $m\mu$. We therefore assume that the complex first isolated is phthalocyanine-chloro-pyridinemanganese(III) pyridine hydrochloride (VIIIa).

When a limited amount of glacial acetic acid is added to a pyridine solution of (III) the color changes from blue (620 $m\mu$) to green (713 $m\mu$) and green crystals slowly appear. They show analysis for phthalocyanine-acetato-pyridinemanganese(III) (IX). The magnetic moment of this compound was 4.76 Bohr magnetons (θ , -40° K.) corresponding to four spin-free unpaired electrons of manganese(III).

Thermal- and Photochemistry of Intermediate Oxidation Level Manganese Compounds.—Solutions in pyridine, prepared in the absence of air, of all these intermediate complexes obtained either from phthalocyaninemanganese(II) or from phthalocyanine-oxo-pyridinemanganese(IV), have very similar spectra with a main absorption band around 716 $m\mu$. When these solutions, in the absence of air, are illuminated (GE Photospot RSP2 (DXB) at about 30 cm., or sunlight) a reduction to phthalocyaninedipyridinemanganese(II) (660 $m\mu$) takes place as shown in Fig. 6 for a solution of phthalocyanine-chloro-pyridinemanganese(III) pyridine hydrochloride (VIIIa).

On the other hand, when air is admitted, oxidation to phthalocyanine-oxo-pyridinemanganese(IV) (620 $m\mu$) takes place. This reaction is fast in the case of the hydroxo complexes and relatively slow in the case of the chloro complexes. Light also accelerates the oxidation in the presence of oxygen.

When pyridine is added to a solution of a manganese(III) complex in ethanol, methanol, or 1-chloronaphthalene, this oxidation in air to a

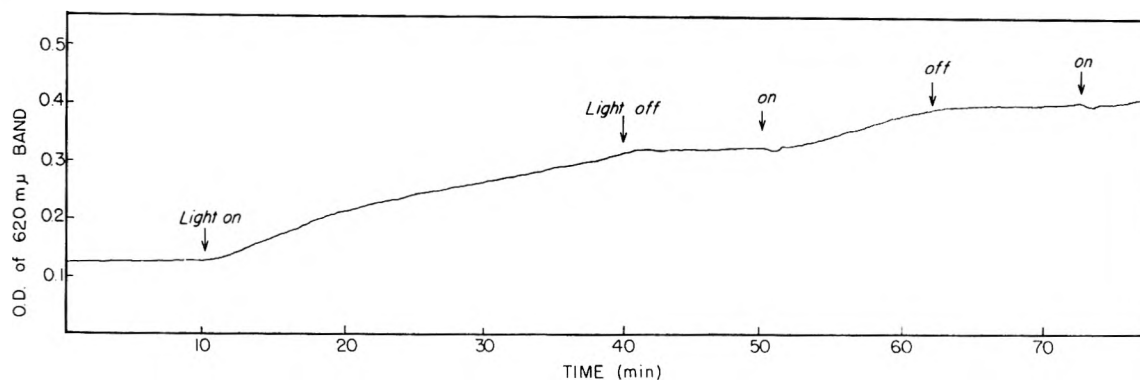


Fig. 7.—Effect of light of a specific wave length ($720\text{ m}\mu$) in the oxidation of a phthalocyanine-hydroxo-manganese (III) complex to a phthalocyanine-oxo-manganese(IV) complex in a mixture of 1-chloronaphthalene and pyridine 2:1 (by volume).

manganese(IV) complex also can be observed. Figure 7 shows the effect of light of a specific wave length ($720\text{ m}\mu$) on the growth of the $620\text{ m}\mu$ band for a solution of manganese(III) complex in 2.0 ml. of 1-chloronaphthalene to which 1.0 ml. of pyridine has been added (original spectrum has only the $723\text{ m}\mu$ band). Illumination with light of $620\text{ m}\mu$ had no effect on the rate of disappearance of the $723\text{ m}\mu$ band.

When a pyridine solution of phthalocyanine-manganese(III) complex, in the absence of air, is kept in the dark at room temperature, a slow disproportionation into manganese(II) and manganese(IV) complexes takes place. This is shown in Fig. 8, where a solution of phthalocyanine-acetato-(acetic acid)-manganese(III) (VI) in pyridine in the presence of air is compared with a solution of the same concentration from which the air has been carefully evacuated. Both solutions were kept in the dark for 12 hours.

The spectrum of the first solution (exposed to air) shows that the manganese(III) complex after 12 hours is largely oxidized to the Mn(IV) complex ($620\text{ m}\mu$). During the same time in the second solution (evacuated) both Mn(IV) ($620\text{ m}\mu$) and Mn(II) complexes (660 and $880\text{ m}\mu$) have been formed. The rate of this disproportionation is increased by heating.

Also, illumination of a manganese(III) complex other than the chloride in pyridine appears to accelerate this disproportionation. Here it is accompanied by a direct photoreduction of the manganese(III) complex so that more manganese(II) than manganese(IV) complex is formed. The further increase of both the 620 and $660\text{ m}\mu$ bands when the second sample (evacuated) was kept in the light is shown in Fig. 9. With continued illumination the $620\text{ m}\mu$ peak decreased, the final spectrum being the spectrum of phthalocyanine-dipyridinemanganese(II).

This experiment shows that not only phthalocyanine manganese(III) complexes but also a phthalocyaninemanganese(IV) complex in pyridine is "photosensitive." In Fig. 10 it is shown that a solution of phthalocyanine-oxo-pyridinemanganese(IV) in pyridine, in the absence of air, is reduced rapidly to phthalocyaninedipyridinemanganese(II) in the sunlight. An intermediate Mn(III) complex ($716\text{ m}\mu$) is not observed in this case.

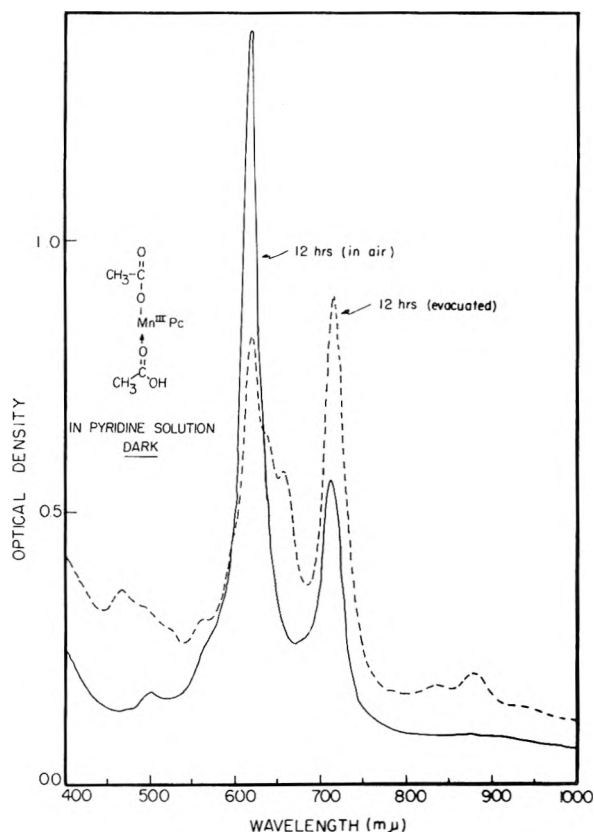


Fig. 8.—Disproportionation in the dark of phthalocyanine-acetato-(acetic acid)-manganese(III) in pyridine in the absence of air. The original solution showed only a very high peak at $716\text{ m}\mu$: —, after 12 hours in contact with the air; - -, after 12 hours in the absence of air.

Elvidge and Lever¹² have reported that a solution of phthalocyanine-oxo-pyridinemanganese(IV) in pyridine was reduced when the solution was boiled. From their publication it is not clear whether they obtained phthalocyaninemanganese(II) or (III). We found that a solution of phthalocyanine-oxo-pyridinemanganese(IV) in "dry" pyridine, from which the air had been carefully removed, kept in the dark at 75° for three days was reduced completely to phthalocyaninemanganese(II). The rate of this reduction is much faster when the pyridine contains a small amount of water. More careful "drying" has inhibited not only the thermal

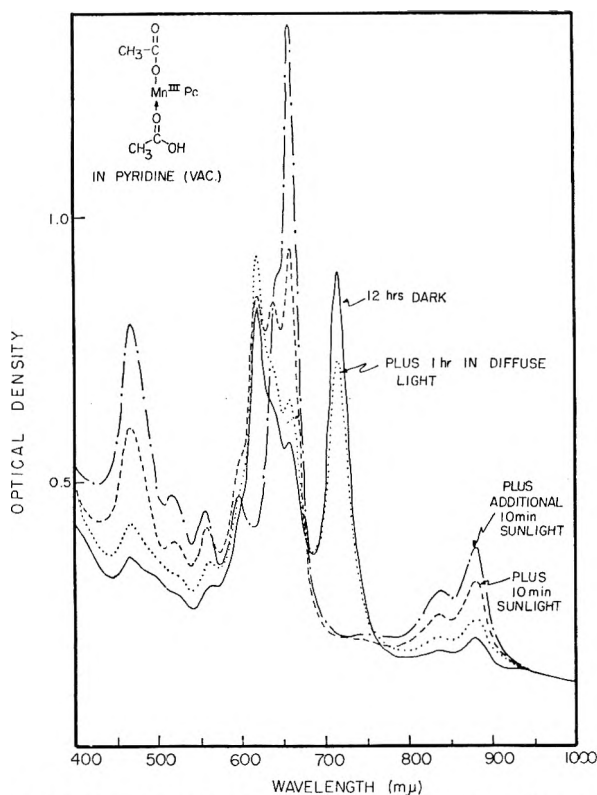


Fig. 9.—Disproportionation and photoreduction of phthalocyanine-acetato-(acetic acid)-manganese(III) in pyridine in the absence of air. The sample was kept in the dark for 12 hours (—), then exposed to diffuse light for one hour (.....), and finally illuminated in the sun for a total of 20 min.: (--- after 10 min., — · — after 20 min.).

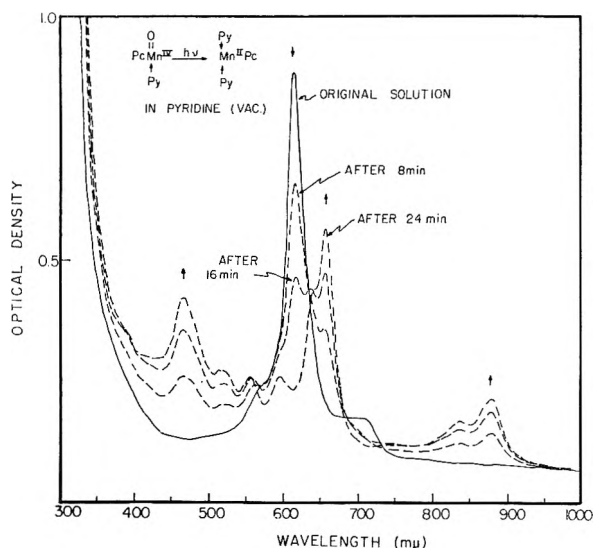


Fig. 10.—Photoreduction of phthalocyanine-oxo-pyridine-manganese(IV) in pyridine in the absence of air: —, original solution; ---, after illumination in the sun for 8, 16, and 24 min., respectively.

reduction of the phthalocyanine-oxo-pyridine-manganese(IV) but the photoreduction as well.

The Intermediate Oxidation Level Manganese Complex in Pyridine.—As we have seen, the stable complex in weakly donating solvents (methanol, ethanol, chloroform, 1-chloronaphthalene) is a phthalocyanine-hydroxo-manganese(III) com-

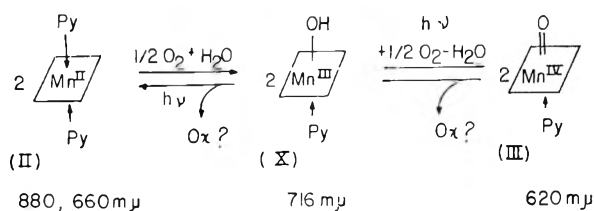


Fig. 11.—Scheme of oxidation and reduction of phthalocyanine-manganese complexes in pyridine.

plex. This is obtained on dissolving in the presence of air either a phthalocyanine-manganese(II) or a manganese(IV) complex, in such a solvent. In a strongly donating solvent or solvent system, such as pyridine, diethylamine, quinoline, or ammonia in methanol, the stable oxidation level in the presence of oxygen is manganese(IV). However, when excess chloride or acetate is present, the stable complex in pyridine is a chloro- or acetato-pyridine-manganese(III) complex even in the presence of air.

Based on these observations we are now able to suggest a structure for the intermediate oxidation product which was called a peroxide by Elvidge and Lever.¹² By analogy with the complexes isolated, we assign to the intermediate the formula phthalocyanine-hydroxo-pyridine-manganese(III) (X). This makes our scheme of oxidation and reduction in pyridine as shown in Fig. 11.

The chemistry of the intermediate dissolved in pyridine can be summarized as follows: In the presence of oxygen it is oxidized slowly to phthalocyanine-oxo-pyridine-manganese(IV). This oxidation is accelerated by light. In the absence of oxygen a disproportionation into phthalocyanine-dipyridine-manganese(II) and phthalocyanine-oxo-pyridine-manganese(IV) takes place. On illumination the rate of this disproportionation is increased and at the same time a rapid reduction of the manganese(III) complex to the manganese(II) complex takes place.

It should be mentioned here that there are evidences that the 716 $m\mu$ band is a composite one, indicating the possibility of another intermediate manganese(III) complex. In the course of the decrease of the 716 $m\mu$ band on illumination of the hydroxomanganese(III) complex in pyridine in the absence of air, a slight shift from 716 $m\mu$ to longer wave length takes place (reaching to about 730 $m\mu$). When air is introduced to a solution of phthalocyanine-dipyridine-manganese(II) in pyridine (660 $m\mu$) the 716 $m\mu$ band builds up in a reverse order. A peak at 730 $m\mu$ appears first; on further increase of the band intensity its peak shifts to 716 $m\mu$.

Photoreductions in Solvents Other Than Pyridine.—In order to determine whether pyridine is essential for the photoreductions, we dissolved phthalocyanine-manganese(II) in methanol, ethanol, or 1-chloronaphthalene and obtained manganese(III) compounds absorbing in the 716 $m\mu$ region. The air was removed from the solutions and they were illuminated for a prolonged time. No changes in the spectra could be observed. Only when pyridine was present (20% by volume of the solution) did the reduction to phthalocyanine-

manganese(II) take place on illumination of these solutions. Apparently the amount of pyridine needed is much smaller. A solution of phthalocyanine-chloro-pyridinemanganese(III) pyridine hydrochloride in ethanol is reduced slowly in the sunlight in the absence of air, as can be seen in Fig. 12.

Cyano Complexes.—A potent donor group which might be expected to affect the oxidation-reduction relationships among the manganese levels is CN^- . Figure 13 shows the interrelationships of the cyanomanganese complexes with other phthalocyaninemanganese complexes which will be discussed in this section.

Manganese(II) Complexes.—The spectrum of a freshly prepared solution of phthalocyanine-manganese(II) (I) in ethanol saturated with sodium cyanide shows absorption maxima at 824, 660, 598, 533, 464, and 373 $m\mu$ (Fig. 14). On evaporation of the solvent we obtained green crystals for which the elementary analysis corresponded to phthalocyanine-cyano-ethanolmanganese(II) sodium (XI). A solution prepared by dissolving this complex in pyridine, in the absence of air, showed the spectrum of phthalocyanine-dipyridinemanganese(II). This proves that the cyano complex is a manganese(II) complex.

When sodium cyanide is added to a solution of phthalocyaninemanganese(II) in pyridine containing 5% water, the spectrum is very similar to the spectrum of phthalocyanine-cyano-ethanolmanganese(II) sodium (XI) in ethanol (Fig. 15). This solution of what is probably phthalocyanine-cyano-pyridinemanganese(II) sodium (XII) is very stable in air. Only after long standing does a small peak at 620 $m\mu$ (Mn(IV)) sometimes appear.

Manganese(III) Complexes.—In air, phthalocyanine-cyano-ethanolmanganese(II) sodium (XI) dissolved in ethanol, containing excess sodium cyanide, is slowly oxidized, as can be seen in Fig. 16. The final spectrum has maxima at (892), 752, 669, 636, 614, 557, and 385 $m\mu$. On evaporation of the ethanol, a complex crystallized which according to the elementary analysis is phthalocyaninedicyanomanganese(III) sodium (XIII). On addition of a methanol solution of sodium cyanide to a solution of phthalocyanine-hydroxo-methanolmanganese(III) (IV) in methanol, the same complex is formed. Figure 17 shows that with a small amount of sodium cyanide a complex which has a main absorption band at 701 $m\mu$ is formed. With more sodium cyanide, the spectrum ascribed to phthalocyaninedicyanomanganese(III) sodium (as in Fig. 16) is obtained. Attempts to isolate the intermediate absorbing at 701 $m\mu$ have failed so far.

Phthalocyaninedicyanomanganese(III) sodium (XII) also can be prepared from phthalocyanine-oxo-pyridinemanganese(IV) (III). In the previous section it was mentioned that on dissolving phthalocyanine-oxo-pyridinemanganese(IV) in ethanol it is reduced very rapidly to what is probably a phthalocyanine-hydroxo-manganese(III) complex (716 $m\mu$). A solution prepared by dissolving phthalocyanine-oxo-pyridinemanganese(IV) in ethanol saturated with sodium cyanide is more stable (620 $m\mu$). It is not known whether the complex in

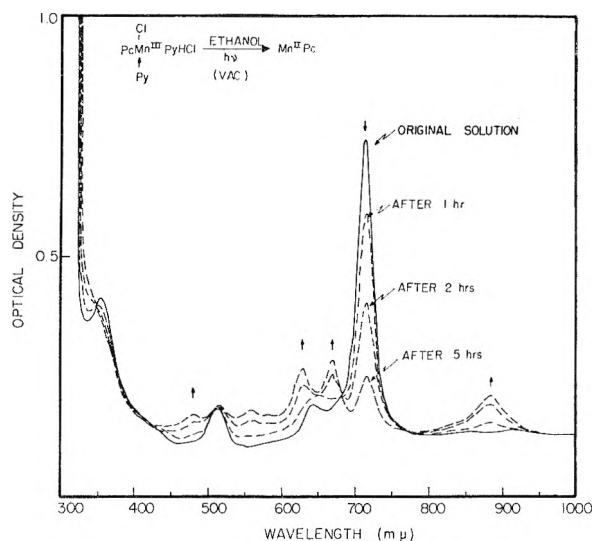


Fig. 12.—Photoreduction of phthalocyanine-chloro-pyridinemanganese(III) pyridine hydrochloride in ethanol in the absence of air: —, original solution; - -, after 1, 2, and 5 hours in the sunlight, respectively.

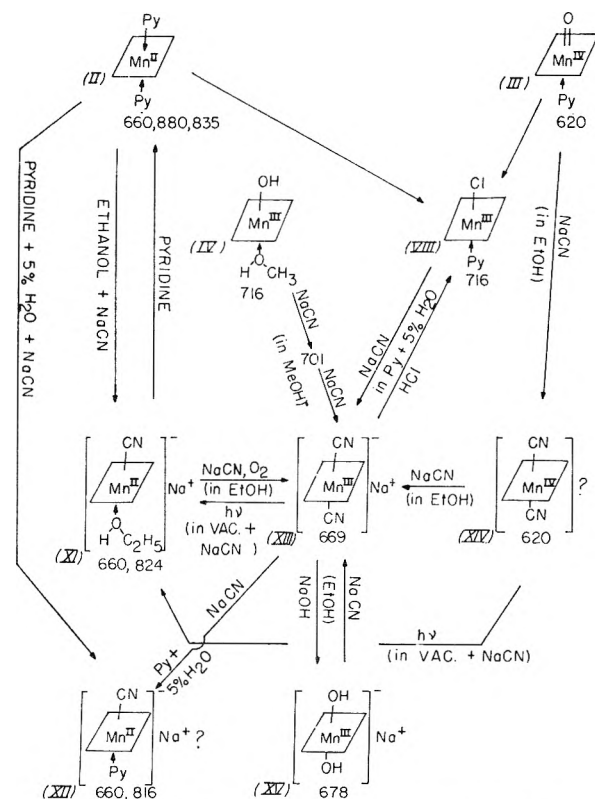


Fig. 13.—Phthalocyanine-cyano-manganese complexes.

solution is phthalocyaninedicyanomanganese(IV) (XIV). On standing, the manganese(IV) complex is slowly reduced to the dicyanomanganese(III) complex (669 $m\mu$), as can be seen in Fig. 18. Also, by addition of sodium cyanide to a solution of phthalocyanine-chloro-pyridinemanganese(III) (VIII) in pyridine containing 5% water, phthalocyaninedicyanomanganese(III) sodium (XIII) is formed, as can be seen from the spectral change of the solution. The reaction is reversed by addition of hydrogen chloride. With this solvent system the

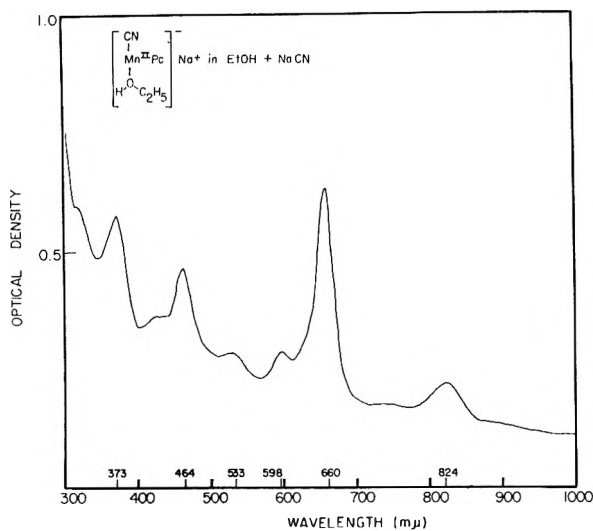


Fig. 14.—Spectrum of phthalocyanine-cyano-ethanolmanganese(IV) sodium in ethanol containing sodium cyanide.

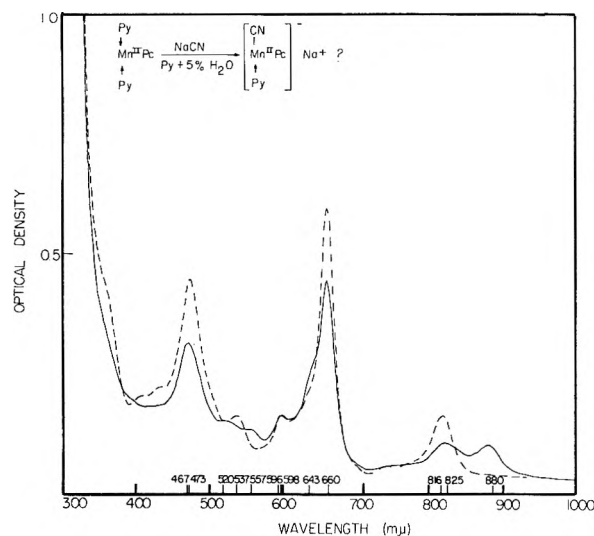


Fig. 15.— —, spectrum of phthalocyaninedipyridine-manganese(II) in pyridine with 5% water; - -, spectrum after addition of sodium cyanide (*in vacuo*).

intermediate absorbing at 701 $m\mu$ is not observed. At room temperature in the dark in contact with air, phthalocyaninedicyanomanganese(III) sodium (XIII) dissolved in pyridine with 5% water saturated with sodium cyanide is reduced slowly to the cyanomanganese(II) (XII) complex absorbing at 660, 816 $m\mu$ (Fig. 19). The solution obtained by dissolving phthalocyaninedicyanomanganese(III) sodium (XIII) in pyridine, in the absence of air, has a main absorption peak at 716 $m\mu$, indicating that one or both cyano groups have been replaced. The complex thus obtained undergoes the same reactions as the manganese(III) complexes described in the previous section: disproportionation on standing in the dark, complete reduction on keeping the sample in the dark at an elevated temperature, and a disproportionation followed by reduction on illumination of the sample at room temperature.

No change in the spectrum can be observed when a solution obtained by dissolving phthalocyaninedicyanomanganese(III) sodium (XIII) in ethanol (713 $m\mu$), from which the air has been removed, is illuminated in the sun. However, when excess sodium cyanide is added so that the phthalocyaninemanganese(III) is present as the dicyano complex (669 $m\mu$) in the solution, a reduction to phthalocyanine-cyano-ethanolmanganese(II) sodium (XI) takes place in the evacuated system on illumination (Fig. 20). We also found that the manganese(IV) complex (620 $m\mu$) obtained by dissolving phthalocyanine-oxo-pyridinemanganese(IV) in the absence of air in ethanol saturated with sodium cyanide is reduced to a manganese(II) complex in the sunlight, as can be seen in Fig. 21. The final solution obtained shows the spectrum of phthalocyanine-cyano-ethanolmanganese(II) sodium (XI) (824, 660 $m\mu$).

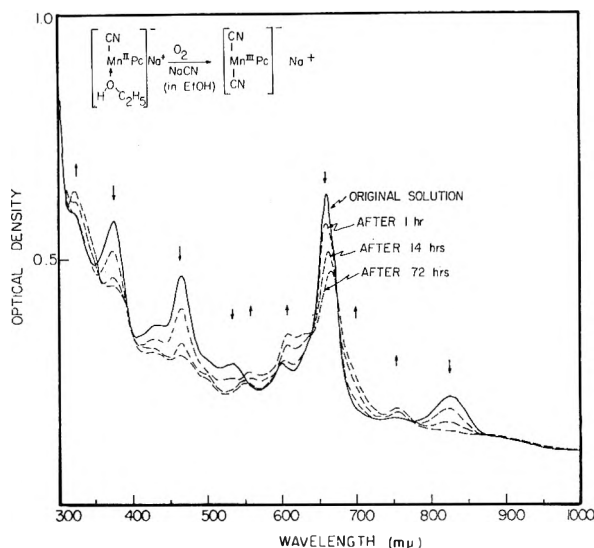


Fig. 16.—Oxidation of phthalocyanine-cyano-ethanolmanganese(II) sodium to phthalocyaninedicyanomanganese(III) sodium at room temperature in the dark: —, solution freshly prepared by dissolving phthalocyaninemanganese(II) in ethanol saturated with sodium cyanide; - -, after standing in contact with the air for 1, 14, and 72 hours, respectively.

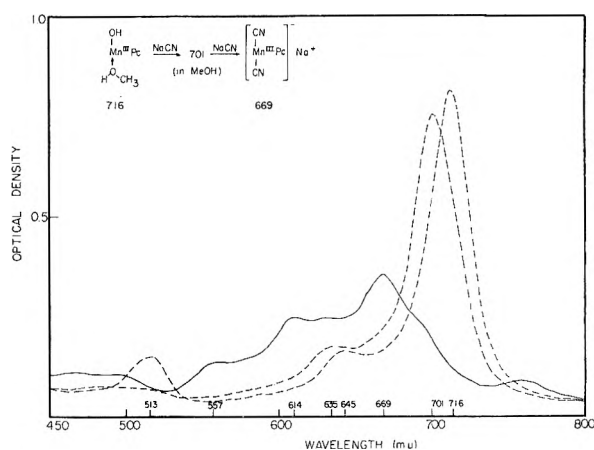


Fig. 17.—Spectral changes on addition of sodium cyanide to a solution of phthalocyanine-hydroxo-methanolmanganese(III) in methanol. The final curve is the spectrum ascribed to phthalocyaninedicyanomanganese(III) sodium.

phthalocyaninedicyanomanganese(III) sodium (XIII) in ethanol (713 $m\mu$), from which the air has been removed, is illuminated in the sun. However, when excess sodium cyanide is added so that the phthalocyaninemanganese(III) is present as the dicyano complex (669 $m\mu$) in the solution, a reduction to phthalocyanine-cyano-ethanolmanganese(II) sodium (XI) takes place in the evacuated system on illumination (Fig. 20). We also found that the manganese(IV) complex (620 $m\mu$) obtained by dissolving phthalocyanine-oxo-pyridinemanganese(IV) in the absence of air in ethanol saturated with sodium cyanide is reduced to a manganese(II) complex in the sunlight, as can be seen in Fig. 21. The final solution obtained shows the spectrum of phthalocyanine-cyano-ethanolmanganese(II) sodium (XI) (824, 660 $m\mu$).

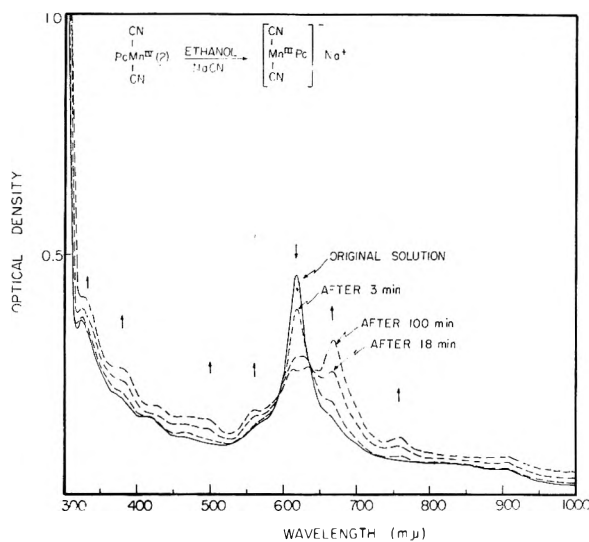


Fig. 18.—Reduction of phthalocyaninedicyanomanganese(IV) (XIV) to phthalocyaninedicyanomanganese(III) sodium in ethanol saturated with sodium cyanide: —, phthalocyanine-oxo-pyridinemanganese(IV) dissolved in ethanol saturated with sodium cyanide; - -, after standing in the dark for 3, 18, and 100 min., respectively.

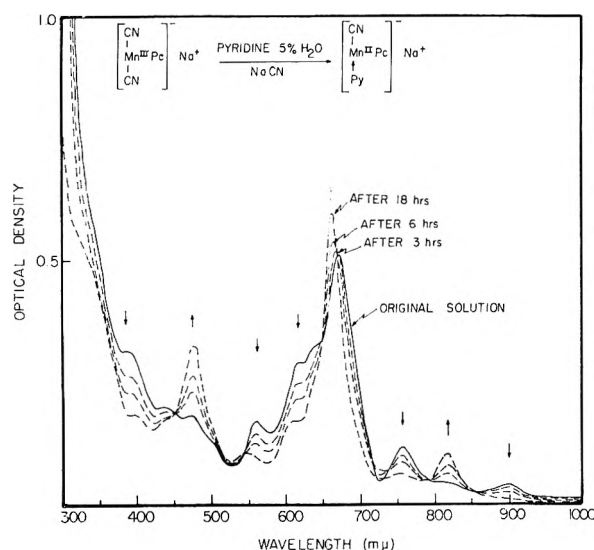


Fig. 19.—Reduction of phthalocyaninedicyanomanganese(III) sodium in pyridine with 5% water, saturated with sodium cyanide: —, directly after addition of sodium cyanide to a solution of phthalocyanine-hydroxo-methanolmanganese(III) in pyridine with 5% water; - -, after 3, 6, and 18 hours, respectively, in the dark.

Preliminary Experiments with Phthalocyanine Hydroxo Manganese Complexes

Manganese(III) Complex.—When an aqueous methanol solution of phthalocyanine-hydroxo-methanolmanganese(III) (IV) is titrated with a dilute sodium hydroxide solution, the bands at 716 and 513 $m\mu$ disappear and a new band at 702 $m\mu$ appears at pH 10.0. Above pH 11.3 this band decreases and a spectrum with a high band at 678 $m\mu$ and a smaller band at 625 $m\mu$ is now obtained (Fig. 22). These changes are reversible.

The solution which is obtained when phthalocyaninemanganese(II) is extracted in air with methanol containing sodium hydroxide has the same spectrum (678 $m\mu$). On evaporating the solvent,

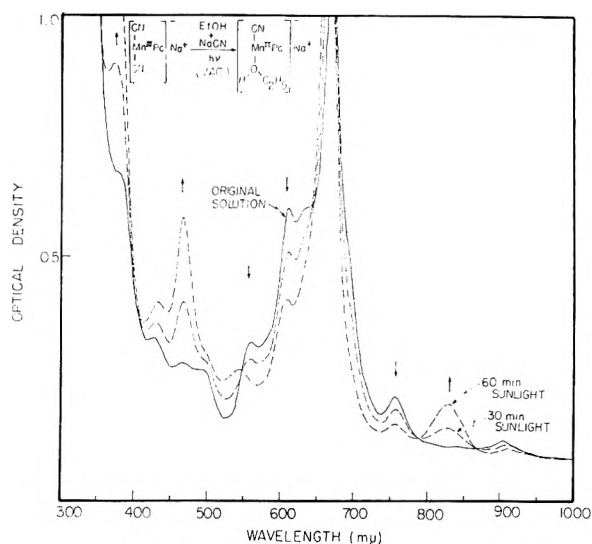


Fig. 20.—Photoreduction of phthalocyaninedicyanomanganese(III) sodium to phthalocyanine-cyano-ethanolmanganese(II) sodium in ethanol saturated with sodium cyanide in the absence of air: —, original solution; - -, after illumination in the sun for 30 and 60 min., respectively.

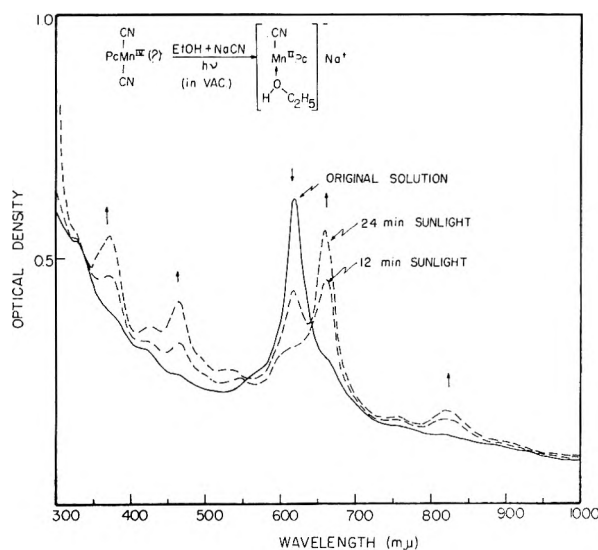


Fig. 21.—Photoreduction of phthalocyaninedicyanomanganese(IV) (XIV) to phthalocyanine-cyano-ethanolmanganese(II) sodium in ethanol saturated with sodium cyanide: —, original solution obtained by dissolving phthalocyanine-oxo-pyridinemanganese(IV) in ethanol saturated with sodium cyanide in the absence of air; - -, after illumination in the sun for 12 and 24 min., respectively.

a blue-green compound crystallizes. The elementary analysis for this complex varies. After prolonged washing with water it comes close to what is calculated for phthalocyaninedihydroxymanganese(III) sodium (XV). Partial formation of a di- or trisodium salt may be the reason for the varying composition of this complex. In the absence of air this complex gives a green solution in pyridine with a main absorption peak at 716 $m\mu$, indicating that it is a manganese(III) complex.

The rate of oxidation of phthalocyanine-hydroxopyridinemanganese(III) (716 $m\mu$) to phthalocyanine-oxo-pyridinemanganese(IV) (620 $m\mu$) in pyridine with 10% water is much increased by the addition of a small amount of sodium hydroxide.

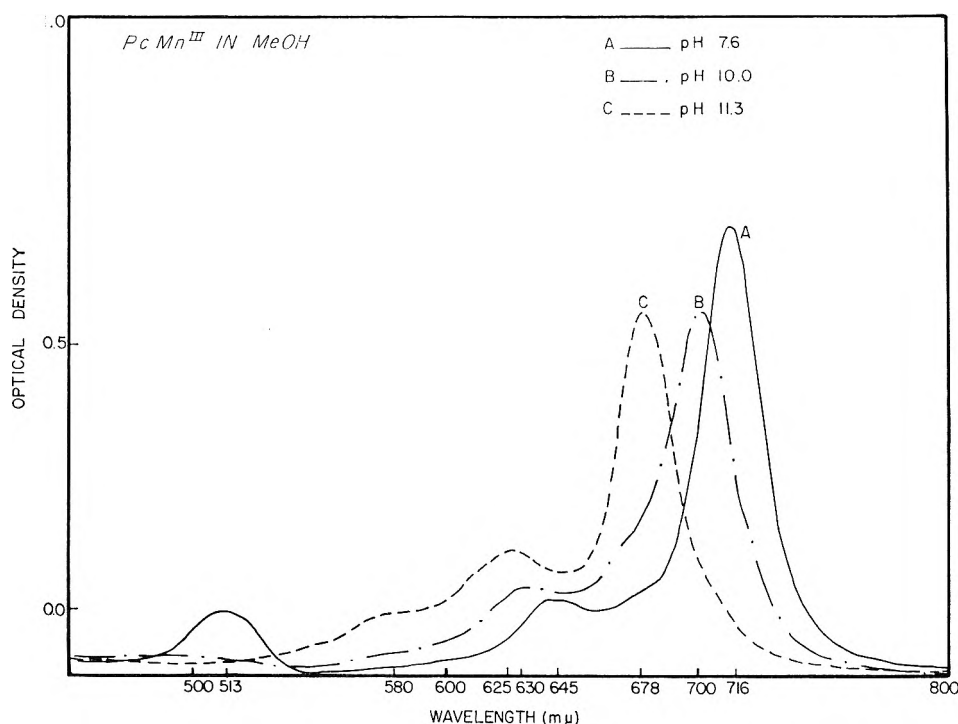


Fig. 22.—Phthalocyaninemanganese(III) complexes in methanol containing sodium hydroxide at pH 7.6, 10.0, and 11.3, respectively.

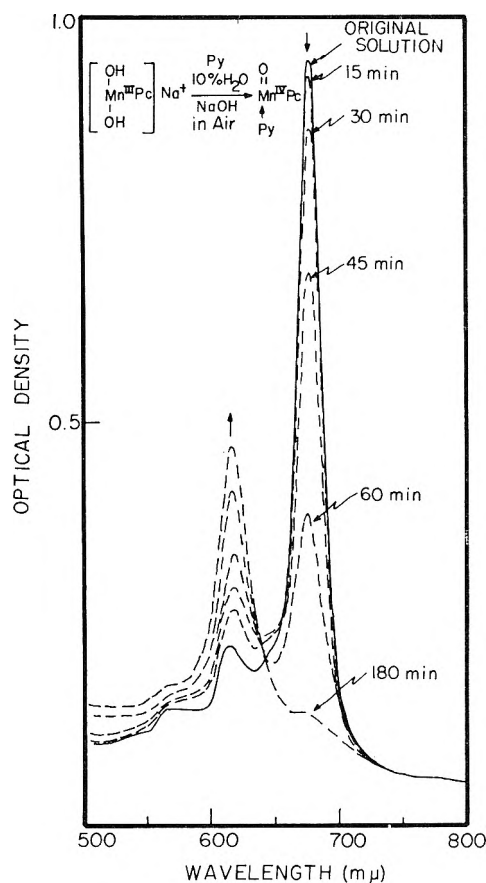


Fig. 23.—Oxidation in air of phthalocyaninedihydroxomanganese(III) sodium to phthalocyanine-oxo-pyridine-manganese(IV) in pyridine (10% water) saturated with sodium hydroxide: —, freshly prepared solution; - - -, after standing in the dark in contact with the air for 15, 30, 45, 60, and 180 min., respectively.

However, when excess sodium hydroxide is added rapidly, the complex absorbing at 678 $m\mu$ is formed, which on standing in contact with the air is oxidized slowly to a Mn(IV) complex (620 $m\mu$), as can be seen in Fig. 23. In the absence of air, in the dark, disproportionation, then complete reduction, takes place at room temperature (Fig. 24). We have tried to obtain a photoreduction similar to that obtained with the cyano complexes. Although photoinduced spectral changes can be observed in the evacuated ethanolic solutions, the identity of the products is as yet undetermined.

Studies with Etioporphyrin Complexes

The translation of the results of the phthalocyanine studies into porphyrin complexes more closely related to natural products has only just begun. But a few observations of considerable relevance can already be reported.

The etioporphyrin I complexes of the metallic ions Mn(III), Fe(III), and Co(II) have been prepared. We have observed the photoreduction of the higher oxidation level and the reoxidation by O_2 of the lower oxidation level in each case.

Figure 25 shows the change in absorption spectrum on illumination in the sun of an etioporphyrin I manganese(III) complex, prepared by dissolving etioporphyrin I acetato-(acetic acid)-manganese(III) in pyridine in the absence of air. The final spectrum with absorption bands at 550 and 584 $m\mu$ is similar to the spectra in pyridine of the copper(II), nickel(II), and zinc(II) complexes of etioporphyrin I, indicating that a manganese(II) complex has been formed. The reoxidation to the original manganese(III) complex on introduction of air is very fast (Fig. 26).

The cyano complex of etioporphyrin I manganese(III) prepared by dissolving etioporphyrin I

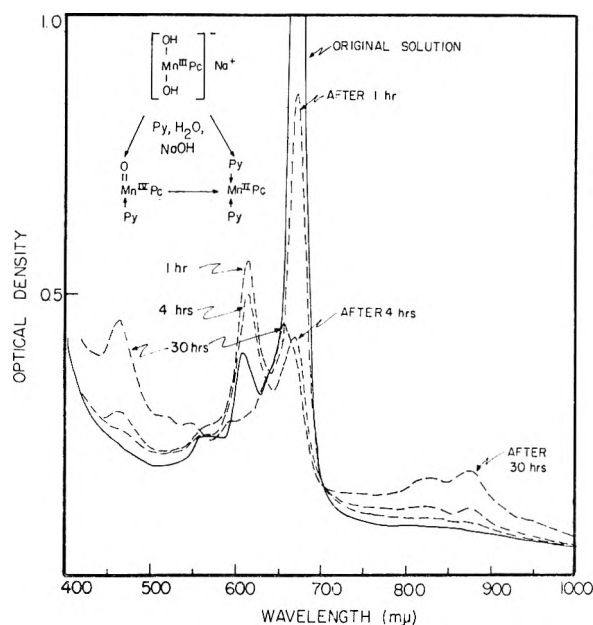


Fig. 24.—Disproportionation and reduction in the dark at room temperature of phthalocyaninedihydroxomanganese(III) sodium in pyridine with 5% water, saturated with sodium hydroxide: —, original solution prepared in the absence of air; - -, after 1, 4, and 30 hours in the dark, respectively.

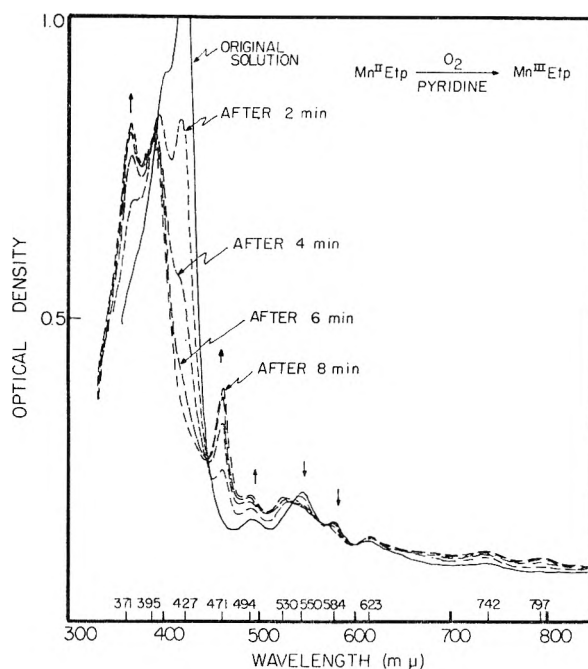


Fig. 26.—Oxidation with oxygen (2 mm.) of photo-reduced etioporphyrin I acetato-(acetic acid)-manganese(III) in pyridine: —, before admission of oxygen; - -, 2, 4, 6, and 8 min., respectively, after admission of oxygen.

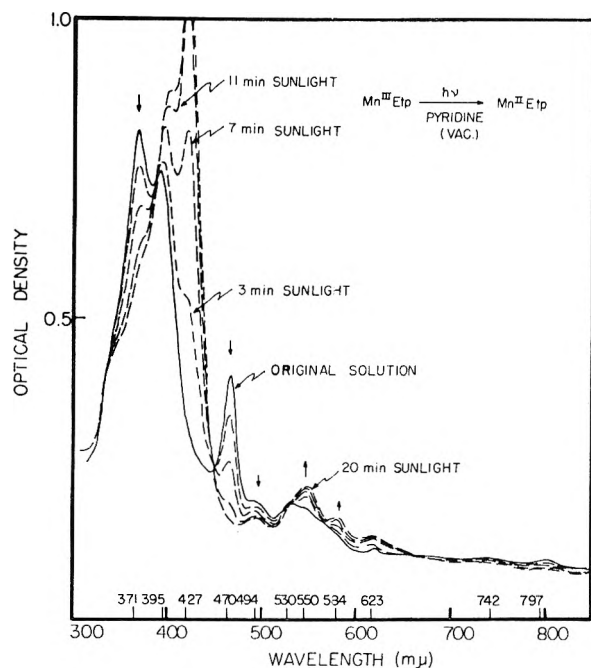


Fig. 25.—Photoreduction of etioporphyrin I acetato-(acetic acid)-manganese(III) in pyridine in the absence of air: —, original solution; - -, after illumination in the sun for 3, 7, 11, and 20 min., respectively.

acetato-(acetic acid)-manganese(III) in ethanol saturated with sodium cyanide, in the absence of air, is also reduced in the sunlight. On introduction of air, reoxidation to the original complex takes place.

Figure 27 shows the oxidation of etioporphyrin I cobalt(II) dissolved in pyridine in the presence of air. After eight hours in the dark the spectrum no longer changed. The air was now removed and

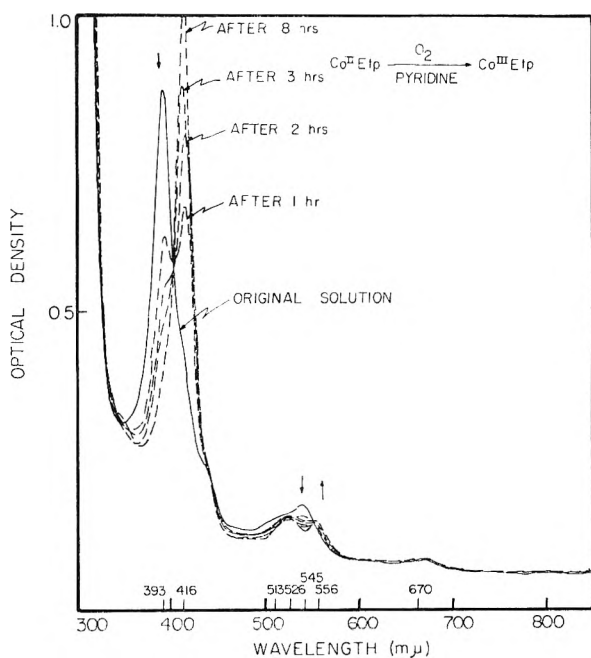


Fig. 27.—Oxidation in air of etioporphyrin I cobalt(II) dissolved in pyridine: —, original solution prepared in the absence of air; - -, 1, 2, 3, and 8 hours, respectively, after the air has been admitted.

the sample was placed in the sunlight. In 15 minutes the original spectrum of etioporphyrin I cobalt(II) was obtained again (Fig. 28).

Figure 29 shows that a solution of etioporphyrin I chloroiron(III) in pyridine has a rather diffuse band at 500 to 560 μ . On illumination of the evacuated sample in sunlight, two sharp bands at 518 and 547 μ appear. This resembles very much the spectral change observed on reduction of

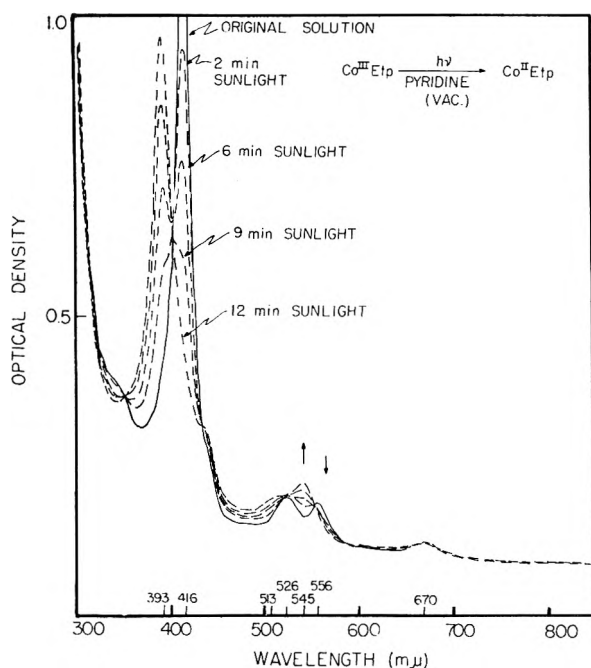


Fig. 28.—Photoreduction of oxidized etioporphyrin I cobalt(II) in pyridine in the absence of air: —, original solution; - - -, after 3, 6, 9, and 12 min., respectively, in the sun.

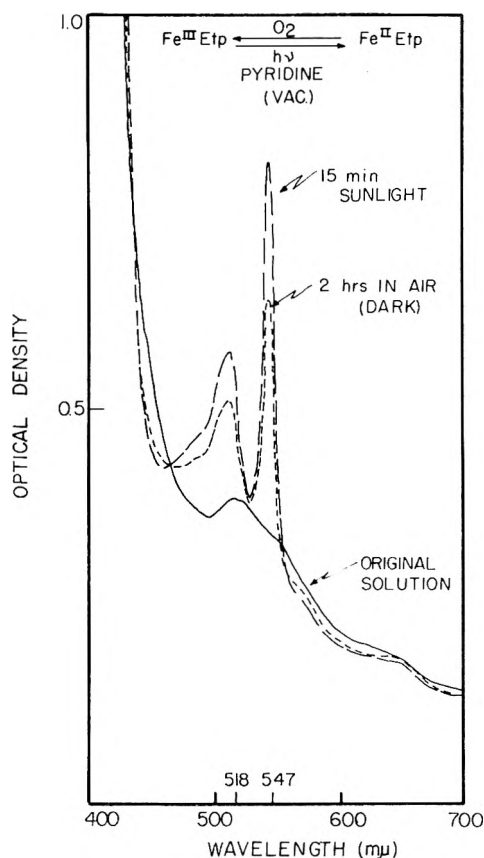


Fig. 29.—Photoreduction of etioporphyrin I chloroiron(II) in pyridine in the absence of air and reoxidation with air in the dark: —, original solution in the absence of air; - - -, after 15 min. in the sun; - - -, 2 hours after air has been admitted (in the dark).

cytochrome-c. After introduction of oxygen the 518 and 547 $m\mu$ bands slowly decrease.

The Oxidized Products

Reduction of manganese complexes is observed on changing the medium, on heating, and on illumination. We have tried to establish the nature of the oxidation products which these reactions produce. The photoreduction of a number of transition element complexes has been reported.¹⁵ When the complex involves cyanide, it has been presumed that cyanogen is formed; when the complex is hydroxy or aquo, it is presumed that peroxide is formed. In neither case were these oxidized products firmly established, and in all these cases the light used to perform the reduction was in the near ultraviolet or ultraviolet, the so-called charge-transfer absorption.

In order to determine whether oxygen is formed on reduction of a phthalocyanine-hydroxy or oxo-manganese complex, the following experiments were carried out:

A concentrated solution of phthalocyanine-oxo-pyridinemanganese(IV) from which the air had been evacuated carefully was heated until the reduction to phthalocyaninemanganese(II) was completed. The liquid phase was frozen in a Dry Ice-acetone bath and the gas phase was analyzed with a mass spectrometer. No oxygen could be detected. Infrared examination of the residue obtained upon cold evaporation of the solvent showed the material to be largely phthalocyaninemanganese(II).

In another experiment a mixture of phthalocyanine-hydroxy-pyridinemanganese(III) and phthalocyanine-oxo-pyridinemanganese(IV) in pyridine with 1% water containing O^{18} (30.2% O^{18}) in a closed system containing a small amount of oxygen gas (2 mm.) was illuminated in the sun under continuous stirring. After illumination for three hours the oxygen isotope ratio of the gaseous oxygen was determined. No enrichment was found. In a similar experiment with a pyridine solution of an etioporphyrin I manganese(III) complex we found that all the oxygen had been used up during the illumination, with a concomitant destruction of the etioporphyrin ring.

When, after a photoreduction, a phthalocyaninemanganese complex is reoxidized with oxygen, the extinction of the resulting absorption bands is in many cases slightly lower than before the photoreduction. A solution of phthalocyanine-oxo-pyridinemanganese(IV) is bleached slowly in the sunlight in the presence of oxygen. Also in some cases, where by a change in the medium a reduction was forced upon a phthalocyaninemanganese complex, considerable bleaching could be observed.

All this indicates that the phthalocyanine ring system is oxidized. A preliminary attempt to find oxidation products has been made. The aqueous pyridine solution of phthalocyaninemanganese in any initial oxidation level was boiled (open to air) until most of the phthalocyanine was bleached. Infrared examination of the residue upon evaporation

(15) F. Basolo and R. J. Pearson, "Mechanisms of Inorganic Reactions: A Study of Metal Complexes in Solution," John Wiley and Sons, Inc., New York, N. Y., 1958, p. 374.

of the solvent shows that the phthalocyanine has been largely converted into phthalimide. This should not be construed as evidence of the source of the electrons required in the cold vacuum photo-reduction of manganese(III) or manganese(IV) to manganese(II).

Experimental

Spectra in the visible region were measured with a Cary recording spectrophotometer, Model 14, and a Beckman Model DK-2 spectrophotometer. All the quantitative data were obtained with the Cary. Infrared spectra were measured with a Beckman IR-7 spectrophotometer. For the mass spectra we used a Consolidated Electro Dynamics Corp. Model 21-130 mass spectrometer. Magnetic susceptibility measurements were carried out by a Faraday method, using an apparatus developed by Cunningham.¹⁶ The measurements were carried out at room temperature, liquid Freon temperature (230° K.), and liquid nitrogen temperature (77° K.). The diamagnetic corrections applied were as follows: pyridine, -49×10^{-6} c.g.s.; phthalocyanine, -422×10^{-6} c.g.s. (obtained by averaging the values for the three crystal axes determined by Lonsdale¹⁷). Diamagnetic corrections for other groups were obtained from tables of Pascal's constants.

These solvents were used for the spectrophotometric measurements: pyridine distilled from barium oxide, 1-chloronaphthalene distilled under reduced pressure, chloroform, methanol, and absolute ethanol, all redistilled under normal pressure.

In order to study reactions in the absence of air spectrophotometrically, a special cell was constructed (Fig. 30). The cell consists of a small flask of about 15 to 20 ml. capacity connected by a side arm, which can be closed with a stopcock, to a 1 cm. optical cell (Fyrex). The flask can be connected at the top to a vacuum line.

A Typical Illumination Experiment.—A small amount of the solid compound to be studied was put into the optical cell. The cell was connected with a high vacuum line and evacuated to 10^{-6} mm. The stopcock in the side arm was then closed, and 10 to 15 ml. of solvent was introduced into the flask. The vacuum cell was again connected with the vacuum line and the solvent was frozen with liquid nitrogen. After evacuation of the system, the stopcock connecting the reaction vessel with the vacuum line was closed and the solvent allowed to thaw and degas. The system then was evacuated again with the solvent frozen in liquid nitrogen. This process was repeated at least five times until the final pressure (with the solvent frozen) was less than 10^{-6} mm. After disconnecting the closed vacuum cell from the vacuum line, the solvent was poured over into the optical cell and the compound was allowed to dissolve.

The light reactions were carried out in the sunlight or with one or two GE Photospot RSP2 lamps at a distance of 30 cm. When lamps were used, an infrared absorbing screen which was cooled with water was placed between the lamp and the sample.

For most dark reactions in the absence of air, we used the same vacuum cells, wrapped in aluminum foil. For experiments lasting longer than two days, the optical cell containing the solution was glass-sealed off from the rest of the system in order to avoid any possibility of air leakage.

Oxygen Exchange Experiment.—Phthalocyaninemanganese(II) (25 mg.) was dissolved in 50 ml. of pyridine to which 0.5 ml. of H₂O (30.2% O¹⁸) had been added. After allowing the solution to stand in contact with the air for 15 minutes, so that both Mn(III) and Mn(IV) complexes were formed, the system was evacuated as above. After the air had been removed, oxygen gas was introduced slowly to a pressure of 2 mm. The system was glass-sealed off and under continuous stirring with a magnetic stirrer it was illuminated in the sun for 3 hours. The liquid phase then was frozen in liquid nitrogen and the isotope distribution of the oxygen was measured with the mass spectrometer:

Before illumination: $O_2^{34}/O_2^{32} \times 100 = 0.395$

After illumination: $O_2^{34}/O_2^{32} \times 100 = 0.397$

Experiments to Identify the Oxidation Product.—Phthalocyanine-oxo-pyridinemanganese(IV) (10–20 mg.) was placed

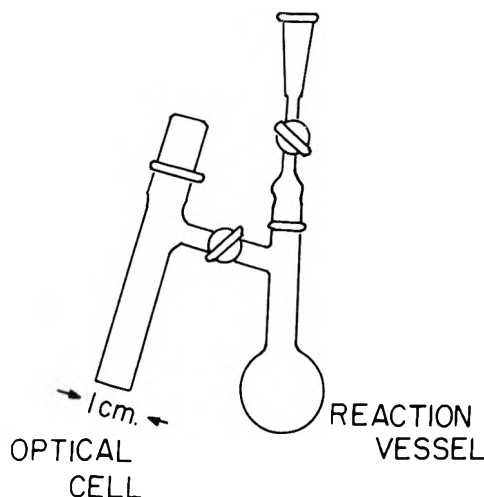


Fig. 30.—Vacuum cell used for experiments in the absence of air.

in a cell with a breakable tip and the cell was evacuated to 10^{-6} mm. Pyridine (10–20 ml.) was distilled into the cell *in vacuo*, and the cell was sealed off. The solution was illuminated by sunlight or heated at 70° in the dark to reduce Mn(IV) to Mn(II). The reduction was faster when the pyridine contained a small amount of water.

After the reduction was complete, all the volatile materials condensable at the temperature of liquid nitrogen *in vacuo* were collected in a side arm with a breakable tip and sealed off. This cell was attached to the mass spectrometer. After the solution was frozen with a Dry Ice–acetone bath, a mass spectrum of the gas phase was taken. This showed that no oxygen was present.

The residue was examined with the infrared spectrophotometer. The spectrum was similar to that of phthalocyaninemanganese(II) except that sometimes a band at 1740 cm^{-1} appeared. This band is considered to be due to the C=O stretching vibration and probably belongs to some oxidation product of the phthalocyanine ring. When phthalocyanine-oxo-pyridinemanganese(IV) was refluxed in pyridine containing 20% water in contact with air, the blue color readily disappeared. After prolonged boiling, the formation of phthalimide having the strong C=O band around 1750 cm^{-1} could be shown by comparing the infrared spectrum of the residue with the infrared spectrum of an authentic sample of phthalimide.

Synthesis: a. Phthalocyaninemanganese(II) (I).—This compound was prepared according to the method of Rutter and McQueen¹⁴ from manganese acetate and phthalonitrile. The product (yield; 52%) was purified by vacuum sublimation at 420° (10^{-5} mm.). It also was prepared by the method of Barrett, Dent, and Linstead¹³ by fusing manganese dioxide and phthalonitrile together. The chloronaphthalene extraction was omitted. The crude material was sublimed as above and long, fibrous black needles were obtained. The visible and infrared spectra for both samples were identical. The magnetic moment of this compound was 4.33 Bohr magnetons (θ , +20° K.) corresponding to about 3 unpaired electrons with some orbital contributions.

Anal. Calcd. for C₃₂H₁₆N₈Mn: C, 67.73; H, 2.84; N, 19.75. Found: C, 67.7; H, 2.99; N, 19.7.

b. Attempts to Prepare Phthalocyaninedipyridinemanganese(II) (II).—Sublimed phthalocyaninemanganese(II) was dissolved in the absence of air in pyridine which had been freshly distilled from barium oxide. The pyridine was distilled off in a vacuum rotating evaporator. In contact with the air the green precipitate slowly became brown. A solution in pyridine prepared in the absence of air showed 716 and 620 $m\mu$ bands, indicating that oxidation had taken place.

c. Phthalocyanine-oxo-pyridinemanganese(IV) (III).—Sublimed phthalocyaninemanganese(II) (~50 mg.) was dissolved in pyridine (~100 ml.) at room temperature. The solution was allowed to stand for a few days exposed to the air and concentrated (cold). The product crystallized as large purple rhombs with a metallic luster. After washing three times with pyridine and once with water they were dried in a vacuum desiccator. The complex gives off pyri-

(16) B. B. Cunningham, *Microchem. J.*, Symposium, 79 (1961).

(17) K. Lonsdale, *J. Chem. Soc.*, 364 (1938).

dine on heating *in vacuo* at 190° as detected with a mass spectrometer. On heating the crystals at 420° *in vacuo*, phthalocyaninemanganese(II) was obtained as sublimate and CO₂ gas was formed. The spectrum in pyridine has a maximum at 620 m μ with a log of 4.94.

Anal. Calcd. for C₃₇H₂₁N₉OMn: C, 67.07; H, 3.19; N, 19.03. Found: C, 67.34; H, 3.38; N, 18.92.

d. Phthalocyanine-hydroxo-methanolmanganese(III) (IV).—Phthalocyaninemanganese(II) was extracted in a Soxhlet extractor with methanol. The complex crystallized as dark needles in the boiler. They were filtered off, washed with methanol, and dried in a vacuum desiccator. The complex gives off the methanol on heating *in vacuo* at 70° as could be shown with the mass spectrometer. At 190° *in vacuo*, the formation of CO₂ also was observed. On heating the crystals to about 400° *in vacuo*, we obtained a sublimate for which the solid spectrum was identical with the solid spectrum of phthalocyaninemanganese(II).

Anal. Calcd. for C₃₃H₂₁N₉O₂Mn: C, 64.29; H, 3.43; N, 18.18; Mn, 8.91. Found: C, 64.30; H, 3.39; N, 18.44; Mn, 8.94 (calcd. for residue).

e. Phthalocyanine-hydroxo-ethanolmanganese(III) (V).—Phthalocyaninemanganese(II) was extracted in a Soxhlet apparatus with ethanol. The dark green crystals were washed with ethanol and ether and dried in a vacuum desiccator.

Anal. Calcd. for C₃₄H₂₃N₉O₂Mn: C, 64.69; H, 3.67; N, 17.85. Found: C, 64.75; H, 3.58; N, 17.87.

f. Phthalocyanine-acetato-(acetic acid)-manganese(III) (VI).—Phthalocyaninemanganese(II) (I) was extracted in a Soxhlet extractor with glacial acetic acid containing 5% acetic anhydride. The dark green crystals were washed with acetic acid and ether and dried in a desiccator.

Anal. Calcd. for C₃₆H₂₃N₉O₄Mn: C, 63.01; H, 3.23; N, 16.42. Found: C, 63.24; H, 3.45; N, 16.51.

g. Phthalocyanine-chloro-methanolmanganese(III) (VII).—Methanol was saturated in the cold with sodium chloride and a trace of hydrochloric acid was added. With this solution, phthalocyaninemanganese(II) was extracted in a Soxhlet apparatus. The dark green crystals were washed with methanol and ether and dried in a desiccator.

Anal. Calcd. for C₃₃H₂₀N₉OMnCl: C, 62.46; H, 3.02; N, 17.75; Cl, 5.59. Found: C, 62.74; H, 3.09; N, 17.72; Cl, 5.83.

This complex was also prepared from phthalocyanine-oxopyridinemanganese(IV) (III). Three volumes of methanol were added to one volume of a solution of phthalocyanine-oxo-pyridinemanganese(IV) in pyridine. After one hour the solution was saturated with sodium chloride. The dark green precipitate was filtered off after 12 hours, washed three times with water, and then with acetone. It was dried in a desiccator.

Anal. Found: C, 62.63; H, 2.74; N, 17.64; Cl, 5.43.

h. Phthalocyanine-chloro-pyridinemanganese(III) (VIII).—A solution of phthalocyanine-oxo-pyridinemanganese(IV) was prepared by dissolving 50 mg. of sublimed phthalocyaninemanganese(II) in 200 ml. of pyridine and allowing the solution to stand in contact with the air for 24 hours. Fifty mg. of pyridine hydrochloride then was added. The blue solution gradually turned to green and fine crystals separated out. After two days the crystals were filtered off, washed with pyridine and anhydrous diethyl ether, and dried in a vacuum desiccator over potassium hydroxide.

Anal. Calcd. for C₃₇H₂₁N₉MnCl: C, 65.16; H, 3.10; Mn, 8.05; Cl, 5.20. Found: C, 64.49; H, 3.30; Mn, 7.92; Cl, 6.00.

The same complex was obtained on dissolving phthalocyanine-chloro-methanolmanganese(III) (VII) in pyridine in the cold and concentrating the solution *in vacuo*.

i. Phthalocyanine-chloro-pyridinemanganese(III) Pyridine Hydrochloride (XIIIa).—Dry HCl gas was passed into a solution of phthalocyanine-oxo-pyridinemanganese(IV) in pyridine, prepared as above, until the color changed to green. After one hour the dark green precipitate of the manganese(III) complex was separated from the solution by centrifugation. It was washed with pyridine and ether, and dried in a vacuum desiccator.

Anal. Calcd. for C₄₂H₂₇N₁₀MnCl₂: C, 63.29; H, 3.29; N, 17.67; Cl, 8.90. Found: C, 63.01; H, 3.27; N, 17.90; Cl, 8.74.

j. Phthalocyanine-acetato-pyridinemanganese(III) (IX).—One ml. of glacial acetic acid was added to 100 ml. of a pyridine solution of phthalocyanine-oxo-pyridinemanganese-

(IV) prepared from 80 mg. of phthalocyaninemanganese(II). The blue solution turned gradually to green and fine crystals were formed slowly. They were filtered off after two days, washed with pyridine and diethyl ether, and dried in a vacuum desiccator over potassium hydroxide.

Anal. Calcd. for C₃₈H₂₁N₉O₂Mn: C, 66.09; H, 3.07; N, 18.26; Mn, 7.95. Found: C, 66.40; H, 3.41; N, 18.29; Mn, 7.85.

k. Attempted Preparation of Phthalocyanine-hydroxopyridinemanganese(III) (X).—Phthalocyaninemanganese(II) was dissolved in a mixture of equal amounts of pyridine and water. The solution was filtered and then evaporated to dryness in a vacuum type rotating evaporator. The green residue became violet on contact with the air. A solution in pyridine, prepared in the absence of air, showed the 620 m μ (Mn(IV)) band.

l. Phthalocyanine-cyano-ethanolmanganese(II) Sodium (XI).—Phthalocyaninemanganese(II) (I) was dissolved in the cold in ethanol saturated with sodium cyanide. During this process the solution was swept with nitrogen. The solution was filtered, after which the solvent was distilled off *in vacuo*. The green residue was washed three times with water to remove the excess sodium cyanide. After washing with acetone, the compound was dried in a desiccator.

Anal. Calcd. for C₃₆H₂₂N₉OMnNa: C, 63.44; H, 3.35; N, 19.04. Found: C, 63.14; H, 3.22; N, 19.32.

m. Phthalocyaninedicyanomanganese(III) Sodium (XIII).—Phthalocyaninemanganese(II) (I) was dissolved in boiling ethanol which was saturated in the cold with sodium cyanide. After refluxing for two hours, all the manganese(II) complex was oxidized as could be seen from the disappearance of the 827 m μ band in the spectrum. On cooling, the manganese(III) complex crystallized as green needles. After washing three times with water and once with acetone, they were dried in a desiccator.

Anal. Calcd. for C₃₇H₁₆N₁₀MnNa: C, 63.52; H, 2.51; N, 21.79. Found: C, 63.52; H, 2.66; N, 21.31.

n. Phthalocyaninedihydroxomanganese(III) Sodium (XV).—Phthalocyaninemanganese(II) was extracted in the cold with a strong solution of sodium hydroxide in ethanol. After filtration, the extract was evaporated to a small volume *in vacuo*. After standing for one night, the blue-green precipitate was filtered off and extracted three times with water. It then was washed with acetone and dried in a desiccator.

Anal. Calcd. for C₃₂H₁₈N₉O₂MnNa: C, 61.59; H, 2.91; N, 17.95. Found: C, 62.13; H, 3.74; N, 17.83.

o. Etioporphyrin I.—Twenty g. of 5-bromo-4,3'-dimethyl-5'-bromomethyl-3,4'-diethylpyrromethane hydrobromide (made by bromination of cryptopyrrole according to Fischer and Orth)¹⁸ was heated in 80 g. of succinic acid at 190–200° for one hour. After cooling, the hard cake was powdered and the succinic acid was extracted with a 10% NaOH solution. The residue then was treated with chloroform to dissolve the etioporphyrin I. This solution was purified by chromatography over an aluminum oxide (Merck) column. The chloroform solution then was concentrated *in vacuo* and methanol was added to crystallize the etioporphyrin I.

The spectrum in pyridine shows maxima at 376 m μ (log ϵ 4.90), 399 m μ (log ϵ 5.15), 471 m μ (a shoulder, log ϵ 3.43), 498 m μ (log ϵ 4.10), 503 m μ (a shoulder, log ϵ 4.06), 532 m μ (log ϵ 3.95), 558 m μ (a shoulder, log ϵ 3.31), 568 m μ (log ϵ 3.77), 576 m μ (a shoulder, log ϵ 3.66), 596 m μ (log ϵ 3.09), 611 m μ (a shoulder, log ϵ 3.16), 622 m μ (log ϵ 3.69), and 652 m μ (log ϵ 3.38).

Anal. Calcd. for C₃₂H₃₈N₄: C, 80.3; H, 8.0; N, 11.7. Found: C, 80.2; H, 7.8; N, 11.9.

p. Etioporphyrin I Acetato-(acetic acid)-manganese(III).—Five hundred mg. of etioporphyrin I was extracted from an extraction thimble into 100 ml. of glacial acetic acid containing 500 mg. of manganese chloride and 500 mg. of sodium acetate. The solution was concentrated to 25 ml. and the product which separated was washed with water and dried. To purify the product it was sublimed under high vacuum at 350°.

Anal. Calcd. for C₃₆H₄₃N₄O₄Mn: C, 66.4; H, 6.7; N, 8.6. Found: C, 67.5; H, 6.5; N, 8.5.

The absorption curve in pyridine has maxima at: 371 m μ (log ϵ 4.75), 395 m μ (a shoulder, log ϵ 4.51), 471 m μ (log ϵ 4.51), 547 m μ (log ϵ 4.02), 580 m μ (a shoulder, log ϵ 3.72),

(18) H. Fischer and H. Orth, "Die Chemie des Pyrrols," Band II, 1. Hälfte, 106 (1937).

653 $m\mu$ ($\log \epsilon$ 3.44), 675 $m\mu$ ($\log \epsilon$ 3.45), 742 $m\mu$ ($\log \epsilon$ 3.49), and 797 $m\mu$ ($\log \epsilon$ 3.26).

q. **Etioporphyrin I Cobalt(II)**.—This and the iron complex were prepared according to Fischer and Orth.¹⁹ Five hundred mg. of etioporphyrin I was extracted from a thimble into 100 ml. of glacial acetic acid containing 600 mg. of $\text{CoCl}_2 \cdot 6\text{H}_2\text{O}$ and 600 mg. of sodium acetate. The product was purified by vacuum sublimation at 350°.

(19) H. Fischer and H. Orth, "Die Chemie des Pyrrols," Band II, 1. Hälfte, 193 (1937).

Anal. Calcd. for $\text{C}_{22}\text{H}_{18}\text{N}_4\text{Co}$: C, 71.7; H, 6.8; N, 10.5. Found: C, 71.5; H, 6.8; N, 10.8.

r. **Etioporphyrin I Chloroiron(III)**.—Five hundred mg. of etioporphyrin I was extracted from a thimble into 100 ml. of glacial acetic acid containing 500 mg. of ferric chloride and 500 mg. of sodium acetate. The precipitate was filtered off and extracted with water. After washing with methanol the product was dried in a desiccator.

Anal. Calcd. for $\text{C}_{22}\text{H}_{18}\text{N}_4\text{FeCl}$: Cl, 6.24. Found: Cl, 6.87.

THE PHOTOREDUCTION OF UROPORPHYRIN: EFFECT OF pH ON THE REACTION WITH EDTA

BY D. MAUZERALL

The Rockefeller Institute, New York 21, N. Y.

Received May 26, 1962

The quantum yield of the photoreduction of uroporphyrin to the dihydroporphyrin in 0.1 *M* EDTA reaches a maximum of 0.4 at pH 5.7, and is independent of the wave length of the exciting light and of temperature between 3 and 56°. The data are consistent with the reaction of the free amine with the protonated, excited porphyrin.

Introduction

The photoreduction of porphyrins leads to dihydro- and tetrahydroporphyrins in which the hydrogens are added to the methine bridges. A variety of evidence for these structures has been obtained.¹ Bis-tertiary amines were very useful as mild reducing agents in this work. However, the pH dependence of the reaction of porphyrins with ethylenediaminetetraacetic acid (EDTA) was different from that found with most other dyes. Since these differences may give direct evidence concerning the reactive photo-excited state of the porphyrin, they were investigated in detail.

Experimental

Uroporphyrin isomer III was isolated from feathers of the Turaco bird. The porphyrin and other materials and most of the experimental methods have been described previously.¹ A brass block with suitable windows served both to define the area of the photochemical light beam and to act as a thermostat in the cell compartment of the spectrophotometer. Heating or cooling fluid was circulated through channels in the block. For experiments at very low temperatures the whole block was suspended in a dewar flask with three windows.

Oxygen was removed by either freeze-thawing the solution *in vacuo* (0.01 mm.) with intermittent flushing with prepurified nitrogen and sealing off the cell, or by bubbling helium through the solution. Diffusion of oxygen through the Teflon capillary tubing was greatly reduced by using concentric tubes, with helium flowing through both. The inner tubing used for deoxygenation was thus in an atmosphere of almost pure helium. The amount of residual oxygen in the solution was estimated by measuring both the (very slow) rate and the extent of reoxidation of the reduced porphyrin or other dye. With allowance for the disproportionation of the dihydroporphyrin¹ the average oxygen concentration was about 5×10^{-7} *M*.

Monochromatic light was obtained from a 500-w. tungsten projection lamp and interference filters of average half-band width of 5 $m\mu$, and suitable blocking filters. Over the range of wave lengths absorbed by the porphyrin in the Pyrex cell, 300 to 650 $m\mu$, these filters transmitted less than 0.1% of light of wave lengths outside the band pass. The energy of this light beam was measured with a thermopile (Eppley) and a microvoltmeter (Keithley 150 A). The accuracy was $\pm 3\%$. The intensity of the 398 $m\mu$

light also was determined with the ferric oxalate actinometer,² and agreement within 10% was obtained. The average light intensities ranged from 0.16 to 5.0×10^{-9} einstein $\text{sec}^{-1} \text{cm}^{-2}$ at 398 and 605 $m\mu$, respectively. The fraction of light absorbed by the solution varied from complete absorption at the Soret band, 398 $m\mu$, to 10% at 605 $m\mu$ at the usual concentration, 2×10^{-5} *M*. The number of molecules converted per short, usually 10-sec., illumination period was calculated from changes in the absorption of the dihydroporphyrin at 440 or 735 $m\mu$ and the known extinction coefficients of the porphyrin and phlorin and the volume of the solution. These changes were at least 20 times the photometric error, $\pm 0.001 \text{ \AA}$. The quanta absorbed were calculated from the measured absorption spectra of the porphyrin under these conditions and the percentage of reaction which had occurred. An average of only 3% reaction per illumination period allowed linear corrections for changes in light absorption, back reflection, and screening to be made with small error. The illuminating wave length was changed after measuring the photoreaction rate over a range of two to sixteen in light intensity by the use of neutral density filters. An average of six measurements at each wave length was made. When a sealed cell was used for the experiments at various temperatures, the solution was not stirred, and the illumination was confined to wave lengths where low (10%) absorption of light occurred. The helium bubbling technique allowed stirring during and/or after illumination. There was good agreement between the results obtained by the two methods (Table I, sealed tubes, and Fig. 1, helium). The over-all accuracy of the quantum yield determinations is $\pm 10\%$.

TABLE I

EFFECT OF TEMPERATURE ON THE QUANTUM YIELD OF FORMATION OF UROPHLORIN FROM UROPORPHYRIN (2×10^{-6} *M*) IN EDTA (0.1 *M*, pH 5.9, 25°)

Temp., °C.	Quantum yield	
	605 $m\mu$	502 $m\mu$
2.8	0.41	0.37
25.5	.38	.37
56.4	.36	.40
86.0	.20	.15

Results

The quantum yield of the photoreduction of uroporphyrin III to the dihydroporphyrin, uro-

(1) D. Mauzerall, *J. Am. Chem. Soc.*, **84**, 2437 (1962).

(2) C. G. Hatchard and C. A. Parker, *Proc. Roy. Soc. (London)*, **A235**, 518 (1956).

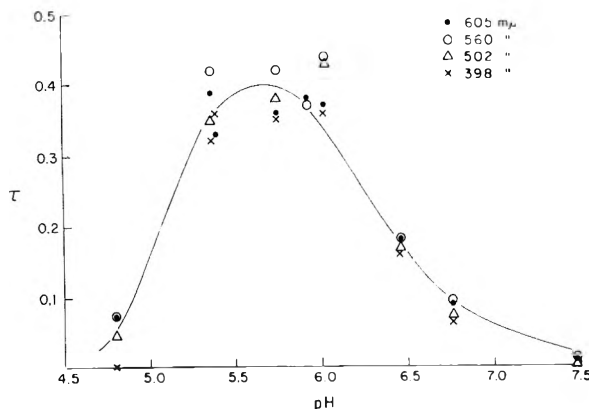


Fig. 1.—The quantum yield of formation of uroporphyrin from uroporphyrin III at $2.6 \times 10^{-5} M$ in $0.1 M$ EDTA at 25° is plotted against the pH of the solution.

phlorin, by EDTA is independent of temperature from 3 to 56° (Table I). The decrease in quantum yield at 86° may be caused by a shift away from the pH optimum since the pK values of both the EDTA and of the porphyrin change with temperature.

The photoreduction of uroporphyrin to the dihydroporphyrin by EDTA is sharply dependent on pH. No reaction occurs in strongly alkaline or acid solution. The variation in the quantum yield of the reduction near the optimum pH is shown in Fig. 1. The quantum yields were calculated on the basis of the light absorbed by the porphyrin at the pH under study. On the alkaline side of the pH optimum, the quantum yield is independent of wave length. Irradiation in either of the two visible band systems or in the Soret band gave the same value. At more acid pH, however, the quantum yield shows definite dependence on wave length. Light absorbed in the Soret band, at pH 4.8, is only about one-tenth as effective as that absorbed in the visible region of the spectrum. In this pH region aggregation of the porphyrin occurs as shown by the spectrum and by the fact that Beer's law does not hold. The variation in quantum yield with wave length may be caused by internal screening: the aggregated or diprotonated forms of the porphyrin absorb the light, but are photochemically less reactive. Three facts argue against the existence of photoreactive polymeric forms of uroporphyrin at pH 6 in $0.1 M$ EDTA. (1) At pH 6, solutions of uroporphyrin follow Beer's law over a 1000-fold dilution, 2×10^{-5} to $2 \times 10^{-8} M$, with a maximum deviation of 4% and an average deviation of 1.5%. (2) The quantum yield is constant to $\pm 10\%$ over the range of 4×10^{-5} to $4 \times 10^{-6} M$ uroporphyrin. (3) The quantum yield of the photoreduction of coproporphyrin, which is aggregated at this pH, is less than one-tenth that of uroporphyrin. More highly aggregated porphyrins, *e.g.*, mesoporphyrin, are even less photoreactive. The rate of photoreduction of uroporphyrin was linearly related to the light intensity near the optimum pH. The average deviation of 23 determinations over a two to sixteenfold variation in light intensity was 12%. A lag period sometimes was observed at the

beginning of the irradiation period, but this always could be attributed to excess oxygen in the system.

The dependence of the quantum yield on the concentration of the reducing agent is more complex. The pK values of EDTA and of uroporphyrin are sensitive to changes in ionic strength. At pH 6.4 in the presence of $0.2 M$ NaCl, which has no effect on the quantum yield in $0.1 M$ EDTA, no definite saturation of the photochemical rate between 0.01 and $0.1 M$ EDTA was observed. Increasing the EDTA concentration from 0.1 to $0.35 M$ did not alter significantly the ratio (0.2) of the quantum yield at pH 6.8 to that at pH 5.9.

Discussion

There is both kinetic³ and structural^{4,5} evidence that the free, unprotonated amine is oxidized by photoexcited dyes such as methylene blue during the photoreduction of these dyes by tertiary amines. 1,4-Diazabicyclo-(2,2,2)-octane does not react under conditions where N,N'-dimethylpiperazine serves as a photoreductant,⁵ indicating that the oxidation occurs on the α carbon of the tertiary amine.

The most likely explanation for the observed increase in quantum yield with decreasing pH which occurs during the photoreduction of uroporphyrin by EDTA is that the protonated porphyrin in the excited state reacts with the free amine. It is unlikely that a non-zwitterionic form of EDTA, which has an apparent pK at 6.1, is the only reactive species, since the quantum yield of photoreduction of methylene blue in dilute ($10^{-3} M$) EDTA solution increased with increasing pH.³ Our measurements show that the quantum yield of photoreduction of thionin in $0.1 M$ EDTA is the same (0.3) at both pH 6 and pH 10. Experiments with crude tetramethyl ester of EDTA indicate it is less than one-tenth as effective as is EDTA itself at pH 5.8. The data of Fig. 1 thus indicate that the photoreactive state of the porphyrin must be protonated and that the protonation occurs near pH 6. The exact shape of the curve relating quantum yield to pH will depend on the relative reaction constants of the photoexcited states, on their pH dependence, and on the variation of the rate of reaction with EDTA concentration. Clearly, many more experiments will be required to define these parameters. However, the fact that the observed protonation of the excited porphyrin occurs near that of the ground state of uroporphyrin⁶ suggests that it is the triplet state of the porphyrin that is photoreactive. The measurements made on the excited states of various molecules show that whereas the pK values of the triplet state are close to those of the ground state,⁷ those of the singlet state are far different, often 6 pK units more acidic. Some other evidence also suggests that the photoreactive state is a triplet. The photoreduction of uroporphyrin by

(3) G. Oster and N. Wotherspoon, *J. Am. Chem. Soc.*, **79**, 4836 (1957).

(4) F. Millich and G. Oster, *ibid.*, **81**, 1357 (1959).

(5) D. Mauzerall, *ibid.*, **82**, 1832 (1960).

(6) A. Neuberger and J. J. Scott, *Proc. Roy. Soc. (London)*, **A213**, 307 (1952).

(7) G. Jackson, *Discussions Faraday Soc.*, **27**, 103 (1959).

EDTA is strongly inhibited by low concentrations (10^{-5} M) of tetrachloro-*p*-hydroquinone. This implies that the photoreactive state has a half-life much longer than that of the singlet fluorescent state. On visual examination, the fluorescence of the porphyrin is not appreciably quenched by high concentrations of EDTA. If this identifi-

cation is correct, the internal conversion to the triplet state must be very efficient in the porphyrin.

Acknowledgment.—This research was supported by a grant from the Division of Research Grants and Fellowships of the National Institutes of Health, United States Public Health Service, R. G. No. 4922.

A FURTHER STUDY OF THE PHOTOTROPY OF CHLOROPHYLL IN SOLUTION¹

BY ROBERT LIVINGSTON AND DAVID STOCKMAN

Division of Physical Chemistry, Institute of Technology, University of Minnesota, Minneapolis, Minn.

Received June 6, 1962

The reversible photobleaching of chlorophyll and related compounds has been studied in anaerobic ethyl acetate, methanol, pyridine, cyclohexanol, and castor oil. The extent of the steady state bleaching appears to be independent of the viscosity of the solvent, and under our experimental conditions varies between the limits of 0.31% in cyclohexanol and 0.65% in pyridine. The absorption spectrum of the bleached form of chlorophyll resembles but differs from that of the Krasnovsky pink pigment. The principal absorption maximum (for chlorophyll *b* in pyridine) is at 545 m μ and has an extinction coefficient of about 7×10^4 m⁻¹ cm.⁻¹. Pheophytin and metal-free porphyrins exhibit little if any bleaching, but the bleaching of the metal-complexed pigments (including copper chlorophyll) resembles that of ordinary chlorophyll. A mechanism is suggested, which involves a charge transfer between the pigment and a molecule of solvent, or some other reductant, complexed with it.

Introduction

The reversible photobleaching, or phototropy, of chlorophyll in air-free methanolic solutions has been investigated² intermittently for about 25 years. Although certain of its features (such as the proportionality of the bleaching to the square root of the light intensity) appear to be definitely established, progress in the study of this process has been retarded by the difficulty of obtaining quantitatively reproducible results. Experience which has been gained in the study of the triplet state of chlorophyll suggested that the use of similar experimental techniques in the preparation of the solutions might greatly reduce the scatter in the measurements of the phototropic response. Accordingly, we constructed a sensitive, differential, recording spectrophotometer and used it to reexamine the phototropy of chlorophyll solutions.

Experimental Methods

Materials.—Chlorophylls *a* and *b* were prepared by a modification of the method of Zscheile and Comar.³ The chromatographic developer was low-boiling petroleum ether (which had been freed from high-boiling fractions by careful distillation) containing 2% isopropyl alcohol. Pheophytin *a* was prepared by treating an ethereal solution of chlorophyll *a* with anhydrous HCl dissolved in methanol. It was purified chromatographically on a sugar column. Copper chlorophyll *a* was prepared by treating pheophytin *a* with copper acetate. The purity of these materials was checked spectrographically with the aid of a Cary spectrophotometer. We are indebted to Dr. S. Schwartz, of the Medical School of the University of Minnesota, for purified samples of protoporphyrin, mesoporphyrin, copper protoporphyrin, and hemin (ferric protoporphyrin chloride), and to the Du-

Pont Corp. for a purified sample of magnesium phthalocyanine. These pigments were used without further purification. The ascorbic acid and phenylhydrazine were commercial A.R. preparations and were used without additional purification. The β -carotene and butter yellow were recrystallized before use. The castor oil was U.S.P. grade and was used without additional purification. The other solvents were high grade commercial materials. Metallic sodium or CaH₂ was used to dry the solvents, which were distilled from these reagents, out of contact with air, in baked-out all-glass apparatus.

Preparation of Solutions.—The chlorophyll was introduced into the cell as a known volume of a standardized solution in ether. The ether then was pumped off. The solvent was placed in a vessel, joined to the cuvette through a manifold, which was attached to the vacuum line by a ground glass joint. The solvent was degassed by successively freezing it with liquid nitrogen, pumping until a "black vacuum" (about 10^{-6} mm.) was obtained, closing it off from the vacuum line, allowing it to warm to room temperature, and boiling off some of the solvent. This procedure was repeated from six to eight times, after which the desired volume of solvent was poured into the cell by tilting the manifold, and the cell was sealed off under vacuum. In those experiments in which reagents were to be added to the solution, a weighed quantity of the reagent was sealed off in an evacuated, thin-walled capillary which was placed, with a heavy glass breaker, in a side tube attached to the cell.

The Differential Photometer.—The differential photometer was essentially similar to the apparatus described by McBrady and Livingston.^{2b} Scanning light from a battery-operated tungsten filament lamp was split into two parallel collimated beams and passed through two identical 15-cm. cuvettes containing the pigment solution being investigated. The beams then were brought together and focused on the slit of a Bausch and Lomb grating monochromator. A chopper of special design⁴ alternately interrupted each beam 150 times a second before it entered the cuvette, producing a sinusoidal variation in intensity. When the solutions in the cells were identical and the two beams properly balanced, the intensity of the combined beam which entered the monochromator was constant. However, if the solution in one cuvette was illuminated at right angles with relatively intense light, the resulting "bleaching" unbalanced the two beams and a sinusoidal difference signal fell on the photocell, which was situated

(1) This investigation was supported in part by a Research Grant (A-2733) from the Division of Arthritis and Metabolic Diseases of the United States Public Health Service.

(2) (a) D. Porret and E. Rabinowitch, *Nature*, **140**, 321 (1937); (b) J. McBrady and R. Livingston, *J. Phys. Chem.*, **50**, 177 (1946); (c) J. Knight and R. Livingston, *ibid.*, **54**, 703 (1950); (d) R. Livingston and V. Ryan, *J. Am. Chem. Soc.*, **75**, 2176 (1953).

(3) F. Zscheile and C. Comar, *Botan. Gaz.*, **102**, 463 (1941).

(4) D. Stockman, Doctoral Thesis, Univ. of Minnesota, 1961.

at the exit slit of the monochromator. The output of the phototube was fed through a high-gain sharply tuned (150-cycle) amplifier to a rectifier and then to a Varian recorder. An AH-6 Hg arc produced the actinic light, from which the ultraviolet and infrared light were removed by glass optics and 2 cm. of 5% CuSO₄ solution. During most of the measurements, the gain was adjusted to give full scale deflection for a change in intensity of 1%. Under these conditions, the time of response was 1.5 sec. and the response was linear. The uncertainty of a reading was not greater than 5% of full scale in the wave length range 4800 to 6700 Å., but was two- or threefold larger for shorter wave lengths. Absolute calibrations of the observed deflections in terms of the changes in concentration of chlorophyll were made by using small auxiliary cells, which had plane parallel windows 1.3 mm. apart. With both cuvettes in place and filled with 2×10^{-6} M chlorophyll, solvent-filled auxiliary cells were introduced into both beams. The deflection, produced by replacing one of the solvent-filled cells with an identical cell containing (*e.g.*) 1.0×10^{-6} M chlorophyll, corresponded to an increase of $(1.0 \times 10^{-6} / 2.0 \times 10^{-6})(1.3/150)100 = 0.43\%$ in the chlorophyll concentration. A detailed description of the spectrophotometer is given elsewhere.⁴

Experimental Results

As a test of reproducibility of the observed extent of bleaching, eight experiments were performed at room temperature with 2.0×10^{-6} M chlorophyll *b* in various samples of methanol. The intensity of the actinic light and the wave length (6530 Å.) of the scanning light were kept constant. The results of these measurements are listed in Table I.

TABLE I
TEST OF REPRODUCIBILITY OF PHOTBLEACHING

Sample of methanol	Extent of reversible bleaching (moles/l.) $\times 10^6$
Mallinckrodt A.R.	7.1, 7.8
Mallinckrodt A.R., dried	8.2, 7.4
Merck A.R.	8.0, 7.3
Merck A.R., dried	7.1
Technical	5.4

All of these solutions were exhaustively degassed. The solvents marked "dried" were treated with an amount of metallic sodium in excess of that required to react with 0.2% of water, were refluxed with dimethyl phthalate, and were distilled through a packed column which was protected from air. The other samples were taken directly from the reagent bottles. Irreversible bleaching was detectable only when technical grade methanol was the solvent. Excluding this measurement, the relative standard deviation of a single measurement is 6%. This marked improvement in reproducibility, relative to the published results,² probably is due to improvement in the technique of deoxygenation and in the purification of chlorophyll.

Since it has been established that the extent of bleaching in methanol is proportional to the square root of the intensity of the absorbed light, the back reaction must be second order. Therefore, its rate should decrease with increasing viscosity and produce an increase in the extent of the steady state bleaching, unless compensated by a similar change in the quantum yield for the formation of the bleached state. To test this prediction, the reversible bleaching was measured in several sol-

vents. The results of these measurements are given in Table II.

TABLE II
STEADY STATE BLEACHING IN VARIOUS SOLVENTS

Solvent	Viscosity, cp.	Extent of reversible bleaching (moles/l.) $\times 10^6$
Ethyl acetate	0.44	6.8
Methanol (dry)	.55	7.6
Methanol (1% H ₂ O)	.55	7.6
Pyridine (dry)	.97	13.0
Cyclohexanol	70	6.2
Castor oil	950	9.0

Contrary to expectations, the extent of bleaching appears to be independent of the viscosity of the solvent. It also is noteworthy that, in all cases, the back reaction was complete within 1.5 sec., the response time of the apparatus. Similar short-lived, reversible spectral changes were observed by Linschitz and Rennert⁵ when they subjected chlorophyll *a* to intense illumination in EPA at liquid nitrogen temperatures.

These results suggest that, in viscous media, the back reaction is first order rather than second order. As a test of this possibility, the reversible bleaching of chlorophyll *a* in castor oil was measured at 19°, using actinic illumination at relative intensities of 1.00, 0.49, and 0.29. The corresponding relative values for the steady-state bleaching were 1.00, 0.62, and 0.43. These values are proportional to neither the first nor one-half power of the intensity, but conform to the relation

$$J = A \times \Delta + B \times \Delta^2$$

where *J* is the relative intensity of the absorbed light and Δ is the relative extent of photobleaching. *A* and *B* are constants, whose values are, respectively, 0.48 and 0.52. Measurements made at 62°, but otherwise under unchanged conditions, yielded values of 0.40 and 0.60. It is doubtful if the difference is significant. In contrast to these results, measurements made with methanolic solutions agree with the published square root relation; at intensities of 1.00, 0.49, and 0.29, the values of $\Delta/I^{1/2}$ were 1.00, 1.03, and 0.93, respectively.

For 2×10^{-6} M chlorophyll *b* in methanol, the relative values of the extent of bleaching, observed at 7, 22, and 52°, were 1.00, 1.05, and 0.89, respectively. These values, as well as those obtained by Knight and Livingston²⁰ for a 1.0×10^{-6} M solution of chlorophyll *a* in methanol, are plotted in Fig. 1. Assuming that the effect of temperature is the same for both solutions, an increase of 40° results in a 20% decrease in the extent of bleaching. The corresponding difference in the energies of activation of the opposing reactions is -0.9 ± 0.5 kcal.

Since it has been suggested²⁰ that the triplet state is intermediate in the formation of the bleached form of chlorophyll, the effect of an efficient triplet-state quencher, β -carotene, was investigated, using 2×10^{-6} M chlorophyll *b* in dry pyridine. To eliminate any possible effect of absorption of light

(5) H. Linschitz and J. Rennert, *Nature*, **169**, 193 (1952).

by the carotene, a dark yellow glass filter was placed between the actinic-light source and the cuvette. Upon the introduction (by breaking an evacuated capillary) of sufficient β -carotene to make its concentration $2 \times 10^{-6} M$, the extent of reversible bleaching was reduced by the factor 0.44. This effect is similar in magnitude to the quenching by oxygen.^{2c}

For reasons which are presented in the Discussion, a series of critical experiments were performed in purified, dried benzene and in benzene to which known small amounts of reagents were added. All solutions were carefully deaerated and contained $2 \times 10^{-6} M$ chlorophyll *b*. The results are presented in Table III.

TABLE III
REVERSIBLE PHOTBLEACHING IN BENZENE

Solution	Steady state bleaching (moles/l. $\times 10^3$)
Benzene (dry)	0.0
Benzene + 0.1% methanol	3
Benzene + 0.1% methanol + 1.0% H ₂ O	1
Benzene + 0.01 <i>m</i> phenylhydrazine	14.5
Benzene + 0.01 <i>m</i> phenylhydrazine + 0.5% H ₂ O	3.4

The extinction coefficients of the bleached form of chlorophyll were determined, at a series of wave lengths, by comparing the deflection, r , produced by the illumination of the chlorophyll solution to the deflection, r_0 , caused by the insertion of a clean glass plate in the water bath, so that one of the light beams passed through the plate perpendicular to its surface. Using the Fresnel law for reflection, ΔOD_0 , the effective optical density of the glass plate, was calculated to be 0.00363 at 6000 Å. and to vary by about 5% over the range from 4000 to 7000 Å. The extinction coefficient, ϵ_R , of the bleached form of chlorophyll can be calculated from the equation

$$\epsilon_R = \epsilon_{GH} + \frac{r}{r_0} \times \frac{\Delta OD_0}{\Delta [GH]l}$$

where l is the length of the cell and ϵ_{GH} is the extinction coefficient of chlorophyll. An approximate value of $\Delta [GH]$, the concentration of the "bleached" chlorophyll, was obtained by assuming that ϵ_R is equal to zero at the wave length of the red maximum of ϵ_{GH} . However, this assumption leads to negative values of ϵ_R for wave lengths near 6200 Å. Accordingly, the value of (the constant) $\Delta [GH]$ was increased sufficiently to render the minimum value of ϵ_R equal to zero. Since the true value of ϵ_R at 6200 Å. is very probably greater than zero, these limiting values of ϵ_R should be increased, at each wave length, by a term which is proportional to $r \times \Delta OD_0 / r_0$, or approximately to r . This correction would not change the wave lengths corresponding to the maxima nor increase the values of ϵ_R by more than $5 \times 10^3 M^{-1} \text{cm.}^{-1}$ at 6200 Å. and at 5450 Å. (for chlorophyll *a* in pyridine).

The absorption spectra, obtained in this way, for the bleached state of chlorophylls *a* and *b* in pyridine are shown in Fig. 2 and 3. It is questionable whether the differences in the spectra observed

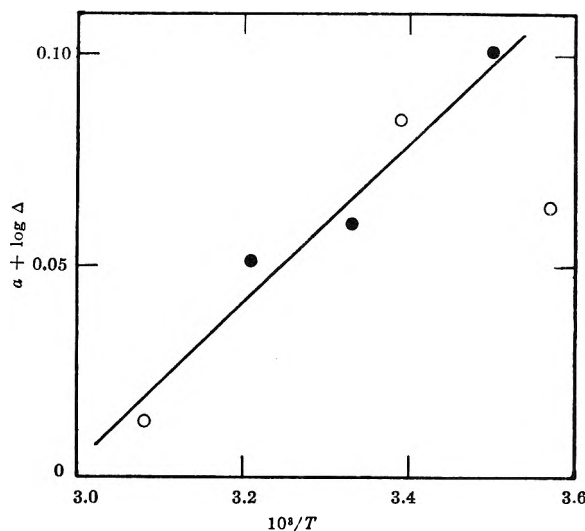


Fig. 1.—The extent of bleaching as a function of temperature (solvent methanol): ●, $1 \times 10^{-6} M$ chlorophyll *a*; ○, $2 \times 10^{-6} M$ chlorophyll *b*.

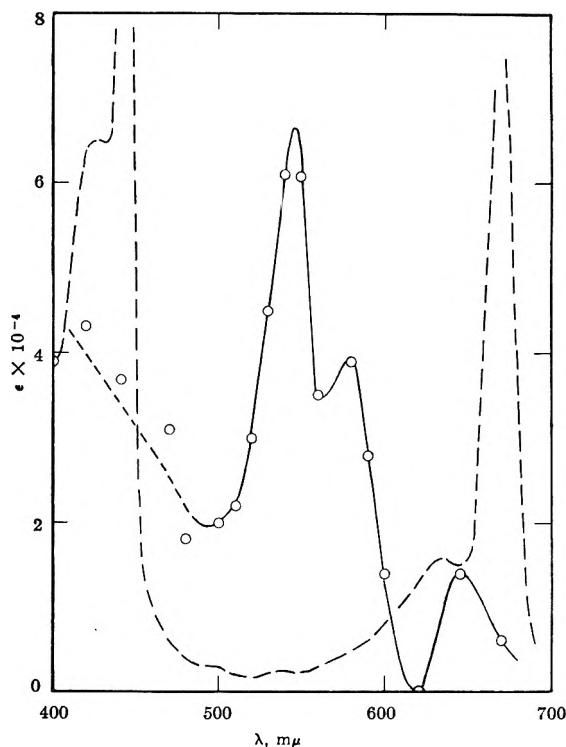


Fig. 2.—The absorption spectra of chlorophyll *a* in its ground state and its "bleached" state.

in dry and wet pyridine (Fig. 3) are significant. The corresponding spectra for methanolic solutions exhibit somewhat broadened maxima. These data are in crude qualitative agreement with the preliminary values of Livingston and Ryan.^{2d} Table IV lists the positions and heights of the principal maxima, in methanol and in dry pyridine.

The spectra observed in these experiments are generally similar to those of other labile photochemical intermediates of chlorophyll inasmuch as they all show marked decrease of absorption corresponding to the red and blue bands of normal chlorophyll and an increase at intermediate wave lengths. However, as illustrated by Fig. 4, the

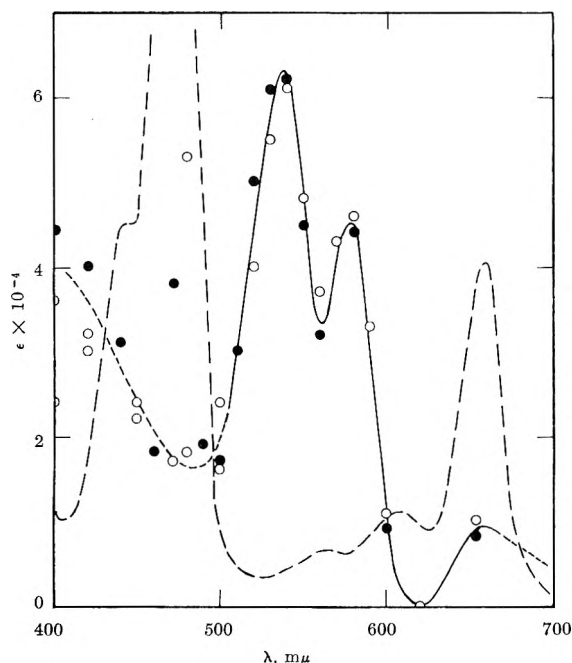


Fig. 3.—The absorption spectra of chlorophyll *b* in its ground singlet and its "bleached" state: ●, in pyridine; ○, in pyridine containing 5% water.

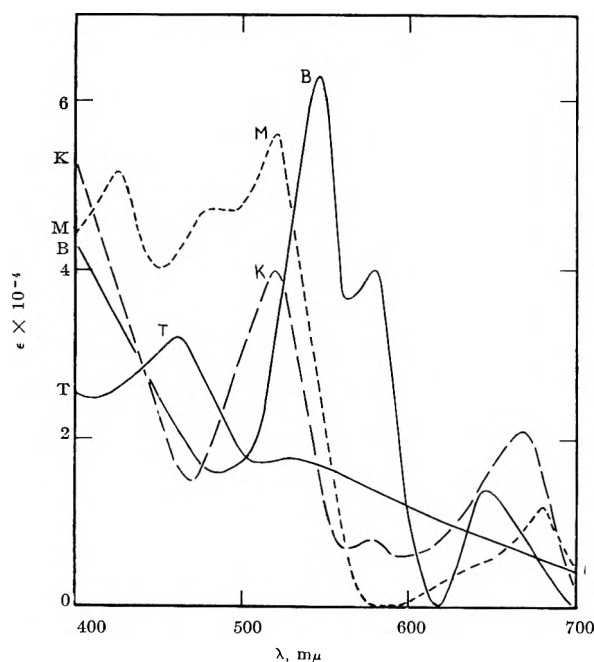


Fig. 4.—The absorption spectra of several labile states of chlorophyll *b* in solution: T, the triplet state in pyridine; K, the Krasnovskii pink pigment in toluene; M, the Molisch brown phase in pyridine; B, the "bleached" state in pyridine.

TABLE IV

ABSORPTION MAXIMA OF THE BLEACHED STATE OF CHLOROPHYLL

Solvent	Pigment	λ in Å. and $\epsilon_R \times 10^{-4}$ in l./mole ⁻¹ cm. ⁻¹
Methanol	Chlorophyll <i>a</i>	5320, 5.0; 5800, 3.2; 6600, 1.0
Pyridine	Chlorophyll <i>a</i>	5450, 6.8; 5800, 4.0; 6450, 1.5
Methanol	Chlorophyll <i>b</i>	5250, 5.0; 5800, 3.0; 6550, 0.6
Pyridine	Chlorophyll <i>b</i>	5360, 7.0; 5800, 4.0; 6450, 0.5

spectra of no two of these intermediates are identical. The spectra for the bleached state, the Molisch phase intermediate, and the triplet state were measured for chlorophyll *a* in pyridine. The data for the Krasnovskii pink pigment are taken from Bannister's⁶ measurement, using phenylhydrazine in toluene; however, similar results⁷ were obtained with ascorbic acid in pyridine.

Recent flash photolytic studies⁸ of chlorophyll *a* dissolved in pyridine containing ascorbic acid show that there is a relatively short-lived transient having an absorption maximum near 480 m μ and negligible absorption between 540 and 580 m μ . It follows that this species, presumably the electrode-active intermediate of Evstigneev, *et al.*,⁹ is not identical with the "bleached form" observed in the present experiments.

In addition to the chlorophylls, anaerobic solutions of pheophytin *a*, magnesium phthalocyanine, and several porphyrins were examined for reversible photobleaching. In all cases, the intensity of the incident light was the same, the solvent was (dry) pyridine, the concentration of the pigment was $1.0 \times 10^{-6} M$, and the wave length of the scanning light corresponded to the principal (visible) maximum of the normal absorption spectrum. Pheophytin and two metal-free porphyrins showed relatively little photobleaching, it being about 0.1% for pheophytin *a* and undetectable (*i.e.*, <0.1%) for protoporphyrin and mesoporphyrin. The extent of bleaching for magnesium phthalocyanine was about 1%, slightly greater than the 0.7% which was observed for chlorophyll *a*. Unexpectedly, cupric pheophytin *a*, cupric protoporphyrin, and hemin (ferric protoporphyrin chloride) exhibited marked photobleaching, the per cent of bleaching being 0.6, 1, and 4%, respectively.

The absorption spectrum of the bleached form of copper chlorophyll *a* was measured roughly and was found to be closely similar to that of (magnesium-containing) chlorophyll *a*. Unlike the other pigments, magnesium phthalocyanine exhibits no new visible absorption bands accompanying the reversible bleaching of its normal spectra.

Discussion

Any mechanism postulated in explanation of the reversible photobleaching of chlorophyll should be compatible with the following observations. In fluid media, the steady state concentration, Δ , of the bleached form is proportional to the square root of the intensity, I_0 , of the incident light, but in the viscous solvent, castor oil, the bleaching conforms to the following equation, where A and B are constants of comparable magnitude.

$$I_0 = A \times \Delta + B \times \Delta^2$$

At constant I_0 , Δ appears to be independent of the concentration of the pigment, although, under the experimental conditions, the intensity of the ab-

(6) T. Bannister, Doctoral Thesis, Univ. of Illinois, 1957.

(7) E. Rabinowitch, "Photosynthesis," Vol. II, Interscience Publishers, Inc., New York, N. Y., 1956, p. 1502.

(8) (a) G. Ziegler and H. Witt, *Z. physik. Chem. (Frankfurt)*, **28**, 286 (1961); (b) R. Livingston and A. Pugh, *Nature*, **185**, 4729 (1960).

(9) V. Evstigneev, V. Gavrilova, and A. Krasnovsky, *Dokl. Akad. Nauk SSSR*, **74**, 315 (1950).

sorbed light must be approximately proportional to this concentration.¹⁰ The back reaction is fast and, under all conditions studied, seems to be complete within 1 sec.¹¹ The effect of temperature is small; either the bleaching is constant over a 45° range, or it decreases slightly with increasing temperature. The presence of O₂ or β -carotene, at concentrations (about 10⁻⁶ *m*) too small to quench appreciably the fluorescence of chlorophyll, practically eliminates reversible photobleaching. No reversible bleaching occurs in benzene (either dry or saturated with water), but it is restored if about 1% of methanol is added to the dry hydrocarbon solvent. The bleaching of metal-free pigments (*e.g.*, *pheophytin*) is scarcely detectable, but copper chlorophyll undergoes normal bleaching, both in respect to its extent and to the spectrum of the labile form.

The effect of O₂, and of β -carotene, indicates that the triplet state of chlorophyll is an intermediate in the reaction, as was postulated by Knight and Livingston.^{2c} However, some of the results presented here necessitate modification of the mechanism, which was outlined by these authors. In particular, it appears necessary to assume that only pigment molecules which are complexed with organic bases can be reversibly bleached. This leads to the plausible postulate that the primary reaction is an intramolecular, charge-transfer process, followed by dissociation into a pair of radicals. In castor oil, the solvent cage largely prevents the radicals from diffusing apart and their recombination is a first order reaction. One of the difficulties with the former mechanism is the assumption that the decay of the triplet is a self-quenched rather than a unimolecular process. This assumption is inconsistent with direct measurements of the decay

(10) In this respect, the present work confirms the findings of Knight and Livingston^{2c} but is in disagreement with the earlier results of McBrady and Livingston.^{2b} Although the reason for this discrepancy is unknown, we shall assume that the newer results are essentially correct.

(11) Traces of I₂, etc., alter the character of the back reaction, rendering it relatively slow and first order.^{2c}

of the triplet in pyridine¹² and in methanol.¹³ The new measurements in benzene solutions to which small amounts of water and organic bases had been added introduce an additional difficulty. Qualitatively, they are consistent with the postulate that water and (*e.g.*) methanol compete for the possibility of complexing chlorophyll and that it is only the pigment which is complexed with the methanol that can react. However, the equilibrium constants for the formation of the several addition compounds are known,¹⁴ and when these values are used, the difference between the calculated and observed yields is much greater than the uncertainties of the measurements.

These two inconsistencies can be eliminated by introducing the arbitrary assumption that disolvates^{14b,15} and dimers of the monosolvates are formed and that only the disolvate undergoes reversible bleaching.

A mechanism based upon this postulate was outlined in the Preprints of Papers, Symposium on Reversible Photochemical Processes, Durham, N. C., 1962.

The present results, although they may raise more questions than they answer, emphasize the important role which thermally stable addition complexes play in some photochemical reactions. They also suggest that "reversible bleaching" of chlorophyll may be closely related to the formation of Evstigneev's precursor to the Krasnovskii pink pigment. It is by no means established that the reversible photobleaching of hemin is a process similar to the reversible bleaching of chlorophyll. The hemin reaction is intrinsically interesting and is worthy of further study.

(12) (a) H. Linschitz and K. Sarkanen, *J. Am. Chem. Soc.*, **80**, 4826, (1958); (b) E. Fujimori and R. Livingston, *Nature*, **180**, 1036 (1957).

(13) P. McCartin, unpublished work, Univ. of Minnesota.

(14) (a) R. Livingston, W. Watson, and J. McArdle, *J. Am. Chem. Soc.*, **71**, 1542 (1949); (b) R. Livingston, "Handbuch der Pflanzenphysiologie," Vol. V, Springer-Verlag, Heidelberg, 1960, pp. 835-837.

(15) S. Freed and K. Sancier, *J. Am. Chem. Soc.*, **76**, 198 (1954).

REVERSIBLE PHOTOCHEMICAL REACTIONS OF CHLOROPHYLL IN PHOTOSYNTHESIS

By EUGENE RABINOWITZ

University of Illinois, Urbana, Illinois

Received May 24, 1962

The chemical participation of chlorophyll in the primary process of photosynthesis is considered with particular emphasis on evidence provided by "difference spectra." Witt's conclusions are compared with unpublished observations by Rubinstein in our Laboratory. The latter support the hypothesis that two forms of chlorophyll *c in vivo* have different photochemical functions, and indicate that the light-induced absorption band at 520 m μ (or, at least, its component which appears in weak light and under anaerobic conditions) is produced mainly by light absorption in the long-wave component of chlorophyll *a*. This band does appear only in green algae and higher plants. This is more consistent with its attribution to a carotenoid than to a chlorophyll.

1. Introduction

Photosynthesis involves reversible photochemical reactions of two types. One is associated with light saturation. In the saturated state, the absorption of all "excess" quanta, above the number utilized for the net reaction, must lead to cyclical processes.

Probably not one but several "shunts" contribute to the closing of the cycle. Other reactions, reversible only in respect to the sensitizing pigment (or other catalytic components of the system), can be involved in the normal sequence of forward reactions of photosynthesis.

Observations of the intensity of chlorophyll *a* fluorescence at the beginning of illumination have first revealed the occurrence of reversible changes in the chlorophyll molecule (or its immediate surroundings), associated with photosynthesis. Comparisons of the absorption of light by cells in the dark and in light ("difference spectroscopy") also indicate reversible changes, both in chlorophyll and in other components of the catalytic mechanism.

We anticipate these changes to be mainly oxidation-reductions, since photosynthesis, in its net result, is an oxidation-reduction reaction against the gradient of chemical potential.

It is widely presumed that in photosynthesis excited chlorophyll molecules accept electrons (or H-atoms)—directly or indirectly—from water, and pass them—indirectly—to carbon dioxide. The immediate electron donor could be the OH⁻ ion; but obvious involvement of an enzyme in the oxygen-liberating state of photosynthesis and of the Hill reaction suggests the existence of an intermediate oxidation-reduction system between chlorophyll and the OH⁻/O₂ couple. It is often postulated that this intermediate is a "cytochrome," *i.e.*, an iron-bearing porphyrin-protein complex. However, in order to be able to mediate the oxidation of water, the postulated "cytochrome" must have an oxidation potential > +0.8 volt; while commonly known cytochromes have potentials between 0.0 and +0.4 volt. The potential of non-complexed Fe⁺³ ions is +0.75 volt; complexing usually stabilizes the higher-charged form of a ion more strongly than its lower-charged form, and thus reduces the oxidation potential; consequently, the existence of iron complexes with potentials of +0.75 volt is unlikely. Perhaps the "cytochrome" in photosynthesis contains a metal atom other than iron!

As to the immediate acceptor, to which chlorophyll transfers the electrons (or hydrogen atoms) acquired from water, it is widely presumed that it is a pyridine nucleotide, perhaps, TPN⁺, and that reduced TPNH then reduces a carboxyl group formed by addition of CO₂ to an organic acceptor (RH + CO₂ → RCOOH). RCOOH has a reduction potential (about -0.5 v.) markedly lower than that of TPNH (about -0.35 volt); but we know that TPNH can reduce carboxyls, by coupling this reduction with energy-liberating dephosphorylation. Reduction of glyceric acid to glyceraldehyde, made possible by such coupling, is postulated in Calvin's scheme of photosynthesis.

It is, however, not impossible that the photochemical electron acceptor in photosynthesis is not TPN⁺, but a compound with a more negative potential, able to achieve the reduction of a carboxyl group without the aid of ATP.

The hypothesis of chlorophyll serving in light as transmitter of H-atoms or electrons between a donor and an acceptor permits three formulations: light excitation may be required only for the oxidation of the donor, or only for the reduction of the acceptor, or for both steps. Since four electrons (or H-atoms) must be transferred to reduce CO₂ to the CH₂O level, the last hypothesis implies a

minimum quantum requirement of 8, while the first two could operate with a minimum of 4 quanta. Additional quanta may be needed, however, for "auxiliary" photophosphorylations, such as are postulated in Calvin's scheme.

2. The Two Chlorophyll *a* Components

Emerson's observations of the "red drop" in the action spectrum of photosynthesis, and of its elimination by supplementary shorter-wave light, lead to the conclusion that photosynthesis may involve two primary photochemical reactions, sensitized by different pigments. Emerson¹ thought that the one pigment is chlorophyll *a*, and the other, one of the "accessory" pigments (chlorophyll *b*, phycoerythrin, fucoxanthol, etc.). Subsequent experiments by Govindjee and Rabinowitch² suggested that the two pigments may be both forms of chlorophyll *a*, one with an absorption band at about 670 mμ and the other with an absorption band at 680-690 mμ. Figure 1 shows the action spectrum of the "Emerson effect" in *Chlorella* and *Navicula* obtained by Govindjee.² This provides clear evidence of the existence and a specific photochemical function of a form of chlorophyll *a* (Chl *a* 670). This function is not shared by the long wave form of chlorophyll *a* (Chl *a* 680/690). Because of resonance energy transfer from pigments absorbing at shorter to such absorbing at longer waves, excitation of both chlorophyll *a* components is achieved whenever light is absorbed by any pigment other than Chl *a* 680/690 itself. Therefore, only in the spectral region where absorbed light goes mainly to Chl *a* 680/690, simultaneous excitation of one of the other pigments is needed for effective photosynthesis.

If the two photochemical primary reactions, sensitized by Chl *a* 670 and Chl *a* 680/690, respectively, are both oxidation-reduction reactions, one of them could involve the reduction of a carboxyl and the other that of a carbonyl. Alternatively, one may involve the photooxidation, and the other the photoreduction of a form of chlorophyll. These two reactions would leave one chlorophyll (*e.g.*, Chl *a* 670) reduced, and the other (*e.g.*, Chl *a* 680/690) oxidized, and the cycle would have to be completed by a reaction between these two products.

One could also imagine one chlorophyll sensitizing an energy-storing oxidation-reduction, and the other an oxidation-reduction which is immediately reversed, with some energy of the back reaction stored in "high energy phosphate."

Be this as it may, all these schemes require Chl *a* to be reversibly changed in photosynthesis. The capacity of Chl *a* for reversible photochemical transformations is confirmed, *in vitro*, by such reactions as its "phototropic" transformation (perhaps, dismutation?) in methanol (Rabinowitch and Porret,³ later studied by Livingston and co-

(1) R. Emerson and R. V. Chalmers, *Phycological Society News Bull.*, **11**, 51 (1958); *cf.* also R. Emerson and E. Rabinowitch, *Plant Physiol.*, **35**, 477 (1960).

(2) R. Govindjee and E. Rabinowitch, *Biophys. J.*, **1**, 377 (1960); E. Rabinowitch and R. Govindjee, "Light and Life," John Hopkins University Press, Baltimore, Md., 1961, p. 378.

(3) E. Porret and E. Rabinowitch, *Nature*, **140**, 32 (1937).

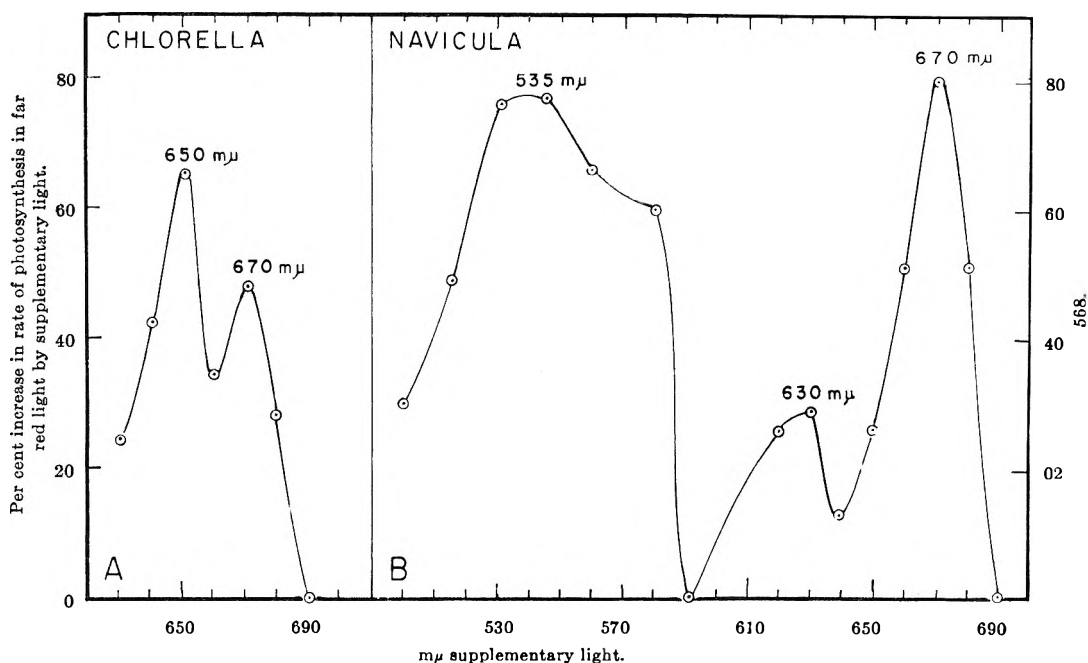


Fig. 1.—Action spectrum of Emerson's enhancement effect showing activity of chlorophyll *a* 670 (in addition to those of chlorophyll *b* at 650 $m\mu$, of fucoxanthol at 535 $m\mu$, and of chlorophyll *c* at 630 $m\mu$ (after Govindjee, *et al.*).

workers,⁴ its reversible change (probably, oxidation) in methanol in the presence of ferric salts (Rabinowitch and Weiss⁵), and its reversible reduction in aqueous pyridine by ascorbate (or in ether, by phenylhydrazine) (Krasnovsky and co-workers,⁶ and Bannister⁷).

In assessing the relevancy of these observations to the role of chlorophyll in photosynthesis, it should not be forgotten that many organic dyes have the capacity for reversible oxidation-reduction reactions. Therefore, only evidence of reversible changes of the chlorophylls (or other pigments) *in vivo*, actually accompanying photosynthesis, can be fully convincing.

3. Difference Spectra

Two methods have been used in the study of difference spectra in cells. One consists in measuring absorption changes after a flash of light (Witt⁸ and Kok⁹); the other in measuring absorption

spectrum changes in the steady state of illumination and darkness (Duysens,¹⁰ Coleman, *et al.*¹¹).

Witt⁸ has studied the time course of absorption changes in the 400–500 $m\mu$ region, when *Chlorella* cells or fragmented plastids were exposed to the flash of red light. Through measurements at different temperatures (–200 to +70°), with cells and plastide fragments, intact or extracted with different solvents, Witt arrived at the conclusion that absorption changes caused by such exposure consist of several components (1, 2a, 2b, and 3) which decay with different rate constants.

From these experiments Witt derived an interesting, even if highly speculative, scheme of the photochemical part of photosynthesis. It is an "eight quanta" scheme, suggesting two successive photochemical oxidation-reduction steps, one sensitized by Chl *a* 670, and one by Chl *a* 680/690. Such schemes are not new¹²; original in Witt's scheme is, however, the inclusion of (at least) two oxidation-reduction systems *between* the two chlorophylls (instead of making photoreduced chlorophyll *a* of one type reduce the photooxidized chlorophyll *a* of the other type, as suggested in section 2). One of these intermediate catalysts—a "cytochrome"—is ascribed a normal potential of +0.37 v. (that of cytochrome *f*!); while the other (designated as X/OX) is assigned a potential of ~ 0 v. Under

(4) R. Livingston, *et al.*, *J. Phys. Colloid Chem.*, **45**, 1312 (1941); **52**, 662 (1948); **54**, 703 (1950); *J. Am. Chem. Soc.*, **75**, 1776 (1953); *Nature*, **173**, 485 (1954).

(5) E. Rabinowitch and J. Weiss, *Proc. Roy. Soc. (London)*, **A162**, 2511 (1937); *cf.* also W. Watson, *J. Am. Chem. Soc.*, **75**, 2522 (1953).

(6) A. A. Krasnovsky, V. B. Evstigneev, *et al.*, *Doklady Akad. Sci., USSR*, **60**, 421; **61**, 91; **63**, 163 (1948); **66**, 663; **67**, 325; **69**, 393 (1949); **73**, 1239; **74**, 315, 781 (1950); **81**, 879, 1105 (1951); **82**, 947; **87**, 109 (1952); **89**, 523; **91**, 899; **92**, 381 (1953); **95**, 841; **96**, 1201, 1209 (1954); **103**, 97, 283; **104**, 440, 882 (1955); **112**, 911 (1957); *Biofizika*, **1**, 120, 328 (1956); **4**, 3, 124, 289, 521 (1959); **5**, 599 (1960); **6**, 30, 392 (1961); *Uspekhi Khimii*, **29**, 736 (1960); *Zh. Fiz. Khim.*, **30**, 968 (1956); *Biokhimiya*, **20**, 123 (1955); **21**, 126 (1956); *J. chim. phys.*, **968** (1958). Papers up to 1955 available in translation, AEC-tr 2156.

(7) T. T. Bannister, *Plant Physiol.*, **34**, 246 (1959).

(8) H. T. Witt, *et al.*, *Nature*, **42**, 72 (1955); *Z. Elektrochem.*, **59**, 981 (1955); **60**, 1148 (1956); **64**, 181 (1960); *Z. physik. Chem.*, **4**, 120 (1955); **12**, 393; **13**, 113, 119 (1957); **20**, 193, 253; **21**, 1 (1959); **28**, 273, 286; **29**, 13, 25 (1961); *Biochem. Biophys. Acta*, **43**, 134 (1960); "Research in Photosynthesis," Interscience Publishers, Inc., New York, N. Y., 1957, p. 75; *Nature*, **189**, 944; **191**, 194 (1961); **194**, 854 (1962); also *cf.* R. Hill and F. Bendall, *ibid.*, **186**, 136 (1960).

(9) B. Kok, *et al.*, *Biochem. Biophys. Acta*, **22**, 299 (1956); *Acta Botanica Neerl.*, **6**, 316 (1957); *Plant Physiol.*, **34**, 189 (1959); **35**, 802 (1960); *Nature*, **179**, 583 (1957); "Light and Life," ref. 2, p. 397.

(10) L. N. M. Duysens, *et al.*, Thesis, Univ. Utrecht, 1952; *Science*, **120**, 353 (1954); *Nature*, **173**, 692 (1954); Progress in Photobiology, Proc. of 3rd Intern. Conf. on Photobiology (Christenson and Buchmann, 1960); *Nature*, **190**, 511 (1961).

(11) J. W. Coleman, A. S. Hoyt, and E. Rabinowitch, "Research in Photosynthesis," Interscience Publishers, Inc., New York, N. Y., 1957, p. 68; J. W. Coleman and E. Rabinowitch, *J. Phys. Chem.*, **63**, 30 (1959).

(12) E. Rabinowitch, "Photosynthesis and Related Phenomena," Interscience Publishers, New York, N. Y., 1945, Vol. I, Chapter 7.

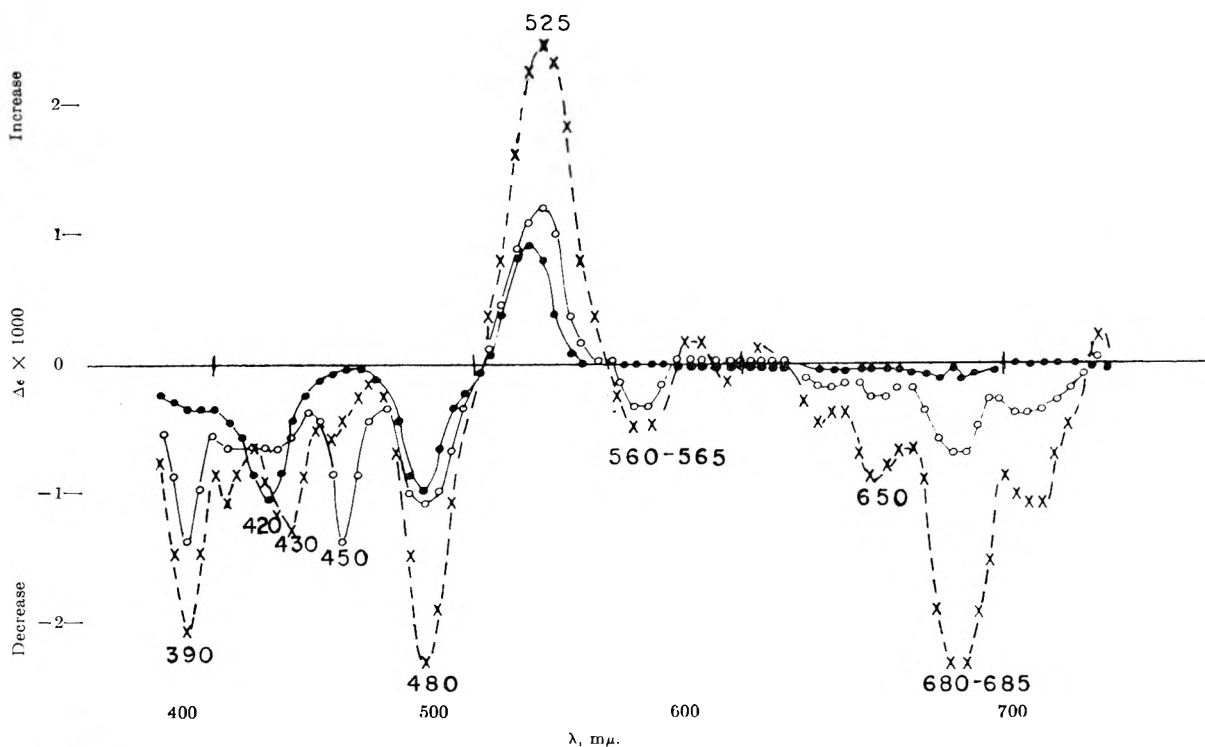


Fig. 2.—Difference spectra of exposed *Chlorella* to constant white light: four incident light intensities, dots—3.4, circles—12, and crosses—31 $\times 10^{14}$ quanta per cm^2 per sec. (after Coleman).

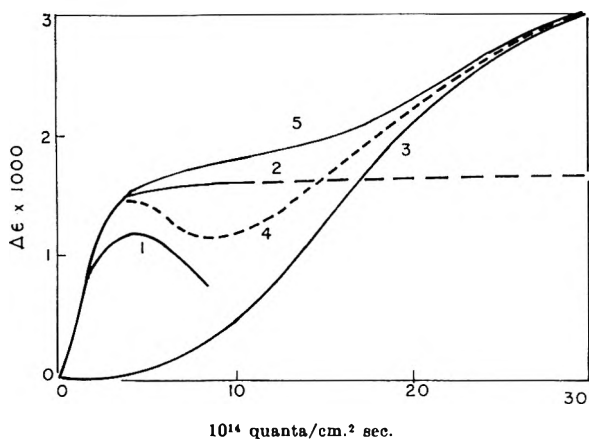


Fig. 3.—Difference spectrum in *Chlorella* as function of the intensity of incident light (after Coleman): curve 1, 420 $\text{m}\mu$; curve 2, hypothetical; curve 3, 680 $\text{m}\mu$; curve 4, 480 $\text{m}\mu$ (1 + 2); curve 5, 520 $\text{m}\mu$ (2 + 3).

these conditions, about 0.8 v. (18 cal./mole) is stored in each of the two photochemical steps, while 0.37 v. (8.5 cal./mole) is lost in the back reaction between oxidized "cytochrome" and reduced X, which closes the cycle. Some of this energy could be salvaged as ATP energy, thus avoiding the need for additional quanta (above 8) for the production of ATP! A reducing potential of -0.4 v. is ascribed to Chl *a* 680/690 and an oxidizing potential of $+0.8$ v. to Chl *a* 670.

Witt did not support his conclusions by data on correlated changes in the red part of the spectrum, which must accompany oxidation or reduction of chlorophyll; also, he did not report action spectra for the production of the spectrum changes of different types, except for an observation that the

spectrum attributed by him to photooxidation of chlorophyll was preserved, while the spectrum attributed by him to photoreduction of chlorophyll was weakened, when excitation occurred at 710 $\text{m}\mu$.

Kok⁹ found a variety of effects in the red part of the difference spectrum in flashing light. He put a particular emphasis on one: The loss of absorption at 705 $\text{m}\mu$, which he attributed to a minor chlorophyll *a* component with a particularly low excitation level. This component could serve as the ultimate excitation energy "sink" and immediate sensitizer of the photochemical reaction in photosynthesis.

A scheme similar to that of Witt was proposed by Duysens.¹⁰ Duysens observed the difference bands at 410 and 420 $\text{m}\mu$, in the red alga *Porphyridium*, attributed to the oxidation-reduction of a cytochrome. Oxidation (growth of the 420 band at the expense of the 410 band) was caused by light absorption in the phycoerythrin band, and reduction (inverse effect) by absorption in the chlorophyll band (at 680 $\text{m}\mu$). Duysens concluded that auxiliary pigments (*e.g.*, the phycobilins, according to Govindjee, *et al.*,² also Chl *a* 670) sensitize a photooxidation, and Chl *a* 680/690 sensitizes a photoreduction; a cytochrome was suggested to be the intermediate between the oxidized "photooxidizing" pigment, and the reduced "photoreducing" pigment.

Arnon, *et al.*,¹³ obtained similar conclusions from biochemical experiments, in which the activities of the two postulated pigment systems were separated (in chloroplast preparations) by specific poi-

(13) M. Losada, F. R. Whatley, and D. I. Arnon, *Nature*, **190**, 619 (1961); D. I. Arnon, M. Losada, F. R. Whatley, H. Y. Tsujimoto, O. O. Hall, and A. A. Horton, *Proc. Natl. Acad. Sci. U. S.*, **47**, 1314 (1961).

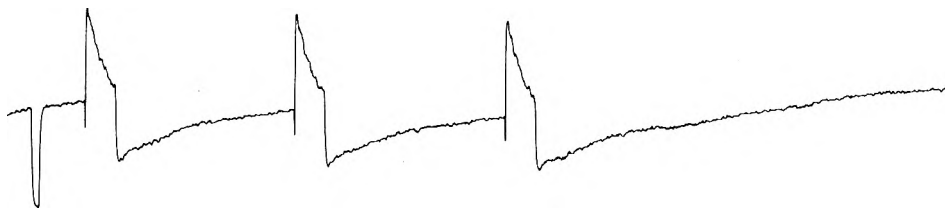


Fig. 4.—Recording of absorption changes in *Chlorella* at 520 $m\mu$ upon exposure to red light: -1% calibration mark on the left; 0.5 min. light and 2.5 min. dark periods; downward spikes signal the beginning of illumination (after Rubinstein).

soning. One system (the photooxidizing one) was able, by itself, to liberate oxygen in light, if supplied with a dye known to act as a Hill oxidant; the other, to reduce in light the reduced form of the same dye.

Figure 2 shows, in the short-wave range, all the bands described by Witt, and a few more, in particular, a strong negative band at 390 $m\mu$. It also suggests—as had been pointed out before¹⁴—that the positive band at 520 $m\mu$ may consist of two bands with slightly displaced peaks, which may correspond to bands attributed by Witt to his spectra "1" and "2b," respectively.

An equally complex difference spectrum appears in the red region, with bands at 630, 650, 680, and 710 $m\mu$. The last one may correspond to the 705 $m\mu$ peak of Kok. The 680 $m\mu$ peak must be due to Chl *a* (or one of its components); the 650 $m\mu$ peak could be due to Chl *b*.

It is tempting to ascribe the many changes observed in the absorption spectrum of photosynthesizing plants in light to reversible transformations of the pigments. Spectral changes in the main red absorption bands clearly point to a reversible transformation of chlorophyll; they should be accompanied by changes in the "Soret bands" in the blue-violet region. One is inclined to seek in these difference spectra evidences of reversible oxidation or reduction of the various forms of chlorophyll; but the fact that absorption changes in the short-wave part of the spectrum appear long before those in the red absorption band (Fig. 3) suggests that the difference spectrum involves also components of the photosynthetic complex other than chlorophyll.

One difference band—that at 420 $m\mu$ —has been attributed by Duysens¹⁰ to the oxidation of cytochrome *f*; but the origin of the most striking features of the difference spectrum of *Chlorella*—the negative band at 480 $m\mu$ and the positive band at 520 $m\mu$ —is still uncertain. It has been suggested by Chance and Strehler¹⁵ and Rabinowitch¹⁶ that it may be due to the transformation of a carotenoid; but typical carotenoid spectra show two (or three) bands in the blue. Also, there is no strict correlation of the spectral changes at 470–480 with those at 515–520 $m\mu$ in their dependence on light intensity and other factors. This may be due to the above-suggested doublet nature of the

(14) D. Rubinstein, paper presented at the meeting of American Biophysical Society in Washington, March, 1962.

(15) B. Chance and B. Strehler, *Plant Physiol.*, **32**, 536 (1957).

(16) E. Rabinowitch, "Photosynthesis and Related Phenomena," Interscience Publishers, New York, N. Y., 1956, Vol. II, Chapter 33B, p. 34.

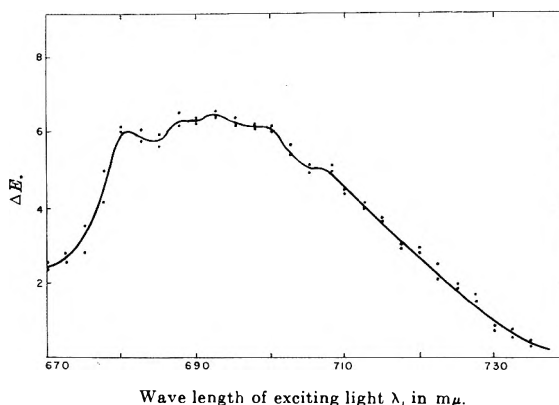


Fig. 5.—Low intensity action spectrum of the "fast" 520 $m\mu$ light effect in *Chlorella* (relative effect, $\Delta I/I$ for equal number of incident quanta) (after Rubinstein).

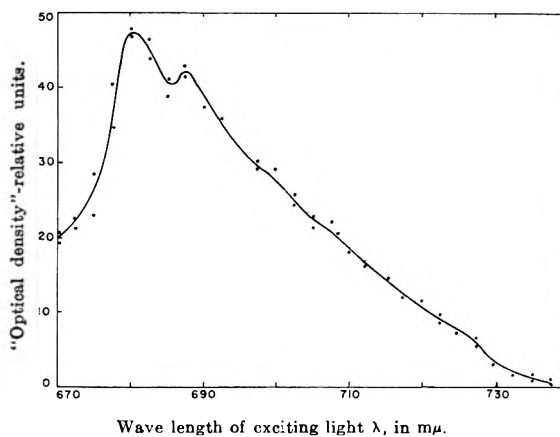


Fig. 6.—"Optical density" of the active pigment component calculated from Fig. 7 by multiplication with A (total absorption at the given wave length) and dividing by OD (total optical density of the system) (after Rubinstein).

520 $m\mu$ band, which may be only partly related to the negative band at 470–480 $m\mu$, and partly—in stronger light—to the decrease of absorption in the red region (*i.e.*, perhaps partly to a carotenoid and partly to a chlorophyll).

Experiments in constant light show, in addition to rapid (and rapidly reversible) effects—probably related to those noted by Witt and Kok in flashing light—also reversible changes which require illumination periods of the order of a minute for their development and dark periods of several minutes for their reversal. Figure 4 shows this on the example of absorption changes at 520 $m\mu$, produced by illuminating *Chlorella* with steady red light of low intensity, under conditions described as

"anaerobic" by Chance and Sager.¹⁷ The mark corresponds to 1 per cent change. A sequence of three illumination cycles of three minutes each is shown. The fast increase in absorption (which is equally rapidly reversed upon the cessation of illumination) is superimposed on a slow change in the opposite direction, which is not quite completed at the end of the illumination period, and requires about three minutes in darkness to be completely reversed. The spectrum of the slow negative change is different from that of the fast positive one, and so is the action spectrum for its development.

While the time scale of the "rapid" effect is similar to that of the rapid induction period in fluorescence (Kautsky, *et al.*,¹⁸ and Franck and co-workers¹⁹), the time scale of the "slow" effect is similar to that of the well known "long" induction period of photosynthesis (also shown by fluorescence curves). It is known that the "long" induction does not occur in the Hill reaction; it remains to be seen whether, in a medium free of CO₂, but containing a Hill oxidant, it will disappear also on absorption and fluorescence curves. Occurrence of the "long" induction period in fluorescence and absorption suggests that chemical reactions involved in the reduction of CO₂ are not as far re-

moved from the primary photochemical complex as has been often assumed.

The several bands in the difference spectrum have different action spectra, suggesting that they are sensitized by different components of the pigment system (Rubinstein¹⁴). This is shown by Fig. 5 and 6. The curve in Fig. 6 shows the magnitude of the "fast" effect, produced by a constant number of quanta absorbed at different wave lengths, multiplied by the total absorption at the same wave lengths. This product should be proportional to the optical density of the pigment responsible for the effect. This curve has a peak at 680 m μ , and drops rather slowly toward the far red. It suggests that it is the long-wave component of the Chl *a* system that is primarily responsible for the effect (in some contradiction to the conclusions of Witt).

Obviously, all the above described experiments provide only a first glimpse of a complex picture. They must be developed into a systematic study, under a variety of conditions and using a variety of objects, and correlated with simultaneous observations of changes in fluorescence and in the rate of photosynthesis or Hill reaction. These studies constitute the most hopeful approach to the understanding of the primary photophysical and photochemical stages of photosynthesis—the aspect which is particularly important because of its uniqueness, and often given short shift in the treatment of photosynthesis as a biochemical phenomenon.

(17) B. Chance and R. Sager, *Plant Physiol.*, **32**, 548 (1957).

(18) H. Kautsky and U. Franck, *Nature*, **35**, 43, 74 (1948); H. Kautsky, W. Appel, and H. Amann, *Biochem. Z.*, **332**, 277 (1960).

(19) J. Franck, *et al.*, *J. Phys. Chem.*, **45**, 1268 (1941); *Arch. Biochem.*, **14**, 253 (1947); "Photosynthesis in Plants," Iowa State Univ. Press, Ames, Iowa, 1949, p. 293.

POPULATION AND DECAY OF THE LOWEST TRIPLET STATE IN POLYENES WITH CONJUGATED HETEROATOMS: RETINENE

BY WILLIAM DAWSON AND E. W. ABRAHAMSON

Department of Chemistry, Case Institute of Technology, Cleveland 6, Ohio

Received May 25, 1962

The population of the lowest triplet state of the linear conjugated polyene, retinene, by flash illumination appears to take place through two successive radiationless transitions; first from the π, π^* excited singlet state reached by primary excitation to an intermediate n, π^* singlet and thence to the lowest π, π^* triplet. The quantum yield of triplet population is about 11% in hydrocarbon solvents and decreases with increasing polarity of the solvent. Triplet yields measured in mixed hydrocarbon-alcohol and alcohol-water solvents indicate that hydrogen bonded complexes of retinene and alcohol (or water) are formed in which the triplet state cannot be measurably populated. The formation constant for the hydrogen bonded methanol complex of retinene based on triplet yield data agrees closely with that of the ethanol complex measured directly by infrared spectrophotometry. The decay rate of the lowest triplet of retinene appears to have a slight viscosity dependence in hydrocarbon solvents which may not be due to impurity quenching. Increasing solvent polarity decreases the triplet decay rate, the effect being most pronounced in hydrogen bonding solvents. Triplet decay kinetics in mixed solvents point to the existence of an equilibrium between a normal triplet and its hydrogen bonded complex, the latter decaying at a slower rate than the former. There also appears to be a red shift in the triplet-triplet absorption spectrum associated with hydrogen bonding of the triplet retinene

Introduction

It has been shown¹ that the lowest triplet state of the polyene aldehyde, retinene, (which is the chromophore of the visual pigment, rhodopsin) can be populated in good yield by flash illumination in oxygen-free hydrocarbon and ether solutions. However, the corresponding alcohol, vitamin A, and protonated Schiff's base complexes of retinene showed no triplet population on flash illumination.

(1) E. W. Abrahamson, R. Adams, and V. J. Wulff, *J. Phys. Chem.*, **63**, 441 (1959).

To explain the difference in behavior with respect to triplet population, it was suggested¹ that in retinene there was an n, π^* singlet state whose energy was intermediate between the upper π, π^* singlet reached by primary excitation and the lowest π, π^* triplet. Rapid internal conversion from the π, π^* singlet to the n, π^* singlet state followed by intersystem crossing to the π, π^* triplet then would compete successfully with internal conversion to the ground state from both the π, π^* and n, π^* excited singlet states. When

there is no intermediate n, π^* singlet state, as is the case with vitamin A and the protonated Schiff's base complex, population of the lowest π, π^* triplet state from the π, π^* excited singlet state can only be accomplished by a slow intersystem crossing (10^{-7} sec.). This process is a very poor competitor to internal conversion of the excited π, π^* singlet to the ground state, which appears to have a lifetime of about 10^{-11} sec. in fluid solvents at room temperature.

In the present paper we have extended these earlier observations on retinene with the purpose of ascertaining the factors that govern the population and decay of the lowest triplet of the general class of linear polyene molecules with conjugated heteroatoms.

Experimental

Materials and Preparations.—All hydrocarbon solvents were Phillips "pure grade" which were further purified by distillation from sodium followed by passage through a silica gel (200 mesh) column. The constancy of the ultraviolet spectrum was considered an adequate criterion of purity. Tetrahydrofuran (Distillation Products) was distilled (fractionally) from sodium and its spectrum was checked. Methanol and absolute ethanol (Fisher spectro-analyzed grade) were distilled in small amounts from large quantities dried over sodium. Carbon tetrachloride (Fisher) was passed through a silica gel column. *trans*-Retinene (Distillation Products) was checked for purity by chromatography in petroleum ether on Aridzone A (Arizona Minerals Corp.) and stored in evacuated ampoules at -20° when not in use.

Stock solutions of retinene in hydrocarbons were kept refrigerated in the dark and used within 3 days. Spectral checks for deterioration were made before use. In order to inhibit hemiacetal formation² all alcoholic solutions were prepared in containers and cells which were prerinsed with dilute sodium hydroxide. Oxygen-free solutions of retinene were prepared on a high vacuum system in 5-cm. cylindrical Pyrex cells attached to a special adapter which permitted repeated cycles of trap-to-trap distillation followed by freezing and pumping until a constant pressure of approximately 10^{-6} mm. was obtained on a McLeod gage.

Apparatus and Procedure.—A Cary Model 11 spectrophotometer was used to measure visible and ultraviolet absorption spectra, while infrared spectra were determined with a Beckman IR-7.

The apparatus used for flash illumination was the type usually employed for kinetics studies, with provision for simultaneous display of light absorption changes at two different wave lengths, which made possible the correction of errors due to variations in triplet population from sample to sample. This was accomplished by splitting the polychromatic scanning beam after it had emerged from the photolysis cell; passing each beam through two separate monochromators, a Bausch and Lomb 250-mm. grating instrument and 436-mm. maximum transmission interference filter.

Light transmission changes in each monochromatic beam were followed with reasonably matched multiplier phototubes (RCA-6217) operated from the same dynode supply and the responses of both tubes were displayed simultaneously on a dual beam oscilloscope (Tektronix 555).

The flash chamber was a large aluminum cylinder (8-in. diam.) coated with high reflectivity white paint (DuPont 29-915). Two flash tubes were mounted symmetrically with respect to the photolysis cell and were connected in series across a low inductance capacitance (Wego-2xl mfd.) operated at 10,000 v.

The flash tubes were made of heavy wall (1.4 mm.) quartz tubing (7 mm. i.d.) with standard taper 12/30 ground quartz outer joints sealed to both ends. For electrodes $1/8$ -in. tungsten rod was force fitted to brass inserts which were machined to fit the outer joints to which they were sealed in with Apiezon W wax. A hole was drilled

through one of the brass inserts to which was silver soldered a Kovar-Pyrex seal for connection to a high vacuum system. The tubes were outgassed, filled with xenon and prefired about 20 times, and re-evacuated before final filling with xenon at 130 mm. In normal operation the tubes fired reproducibly for about 1000 flashes with a half-life of 2 μ sec. The long tail usually observed at long wave lengths on the flash profile was less than 2% after 15 μ sec.

For a spectral scanning light, a d.c. xenon arc (Osram HBO-162) was used. Rapid fluctuations in intensity were minimized considerably by using a specially designed d.c. power supply with a large dropping resistor. Slow "wandering" of the arc was corrected easily by a simple lateral adjustment.

The procedure for taking rate data and the calculation of the decay kinetics already has been described.¹ In order to calculate total triplet yield per flash, it was assumed that no more triplet is formed after 10 μ sec. On this basis the total triplet produced, C_T can be expressed by

$$C_T = \frac{1}{E_T l} (D_{10} + kA_0^{10}) \quad (1)$$

where E_T and l are the extinction coefficients of the triplet and the optical path length, respectively, D_{10} is the absorbance of the triplet at 10 μ sec. after the start of the flash, k is the first order rate constant for triplet decay, and A_0^{10} is the area under the absorbance vs. time curve between the limits of zero and 10 μ sec.

The absolute quantum yield of triplet population was determined by ferrioxalate actinometry.³ Bathophenanthroline in 10% by volume aqueous ethanol was used in place of 1,10-orthophenanthroline to gain added precision. Actual measurements in the flash chamber were made using aqueous solutions of cobalt and copper sulfates as a filter in a jacket surrounding the cell. The concentrations were adjusted so as to achieve an optimum match of the transmission spectrum of the filter with the absorption spectrum of the retinene without appreciably attenuating the actinic light. Assuming the actinic light to be normal to the optic axis of the cell and of constant intensity over the pass band of the filter, less than 20% of the actinic light was transmitted on the first pass with essentially quantitative absorption after three passes. The ferrioxalate solution was used under conditions of total absorption on the first pass using the same filter solution.

The two largest sources of error in the quantum yield were the uncertainties in the difference in the amount of actinic light absorbed by the ferrioxalate and retinene solutions and in the estimation of the fraction of actinic light absorbed by triplet retinene. To estimate this latter quantity, an initial quantum yield of triplet, assuming no participation of the triplet in actinic light absorption, was calculated from the total triplet yield divided by the number of einsteins absorbed by the actinometer solution. Taking one-half of this fraction as the average population of the triplet during the duration of the flash, the fraction of actinic light absorbed by the triplet was calculated from the areas of absorption spectral curves of the singlet and triplet plotted on a per cent absorption basis at their respective concentrations and corrected for the transmittance of the filter. By such successive approximations a final quantum yield was obtained.

Results

From a series of flash oscillograms taken over the spectral region 340 to 550 $m\mu$, the total amount of triplet retinene formed by the flash as well as the first-order rate constants for triplet decay were computed. The quantum yield of triplet population is reported in Table I as per cent triplet formed from excited singlet. This was measured only for retinene in methylcyclohexane and it was assumed to be constant over the wave length range passed by the filter (300 to 440 $m\mu$). Quantum yields in the other solvents reported in Table I were obtained from the total triplet population using the same ratio of

(2) K. Grellmann, R. Memming, and R. Livingston, *J. Am. Chem. Soc.*, **84**, 546 (1962).

(3) C. G. Hatchard and C. A. Parker, *Proc. Roy. Soc. (London)*, **A235**, 518 (1956).

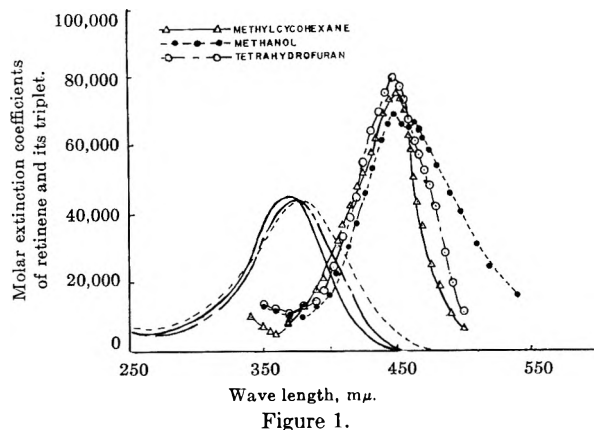


Figure 1.

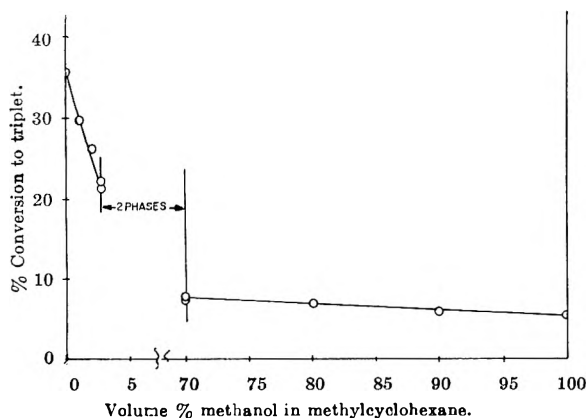


Figure 2.

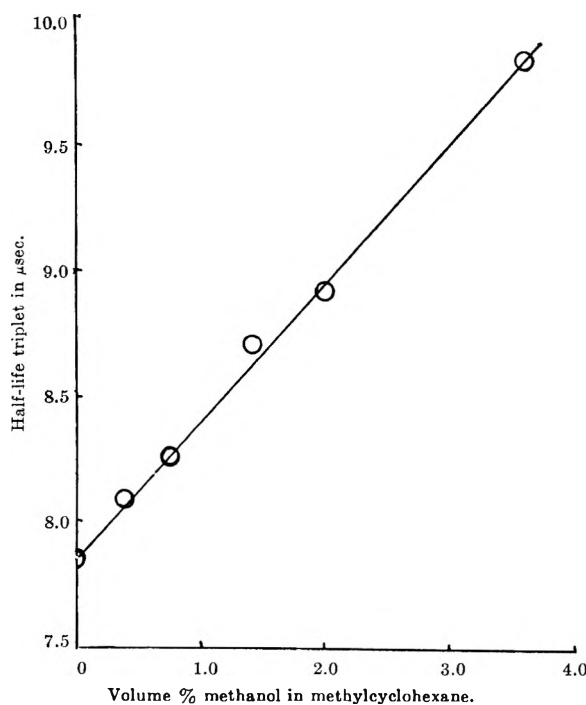


Figure 3.

quantum yield to total triplet population obtained for retinene in methylcyclohexane with adjustments for slightly different fractions of the actinic light absorbed by the triplet. Actually the quantum yields were almost one-third the total triplet

yield per flash, indicating that a single flash excited each molecule three times.

TABLE I

Solvent	$10^6 \times$ moles/l. retinene concentration	% triplet formed from excited singlet	Rate constant at 20° for triplet decay k (sec.) $^{-1}$ $\times 10^{-4}$
Methylcyclohexane	2.18	11.0 ± 1.6	8.83
Isooctane	2.35	...	9.24
<i>n</i> -Pentane	2.60	...	9.63
Undecane	1.50	...	9.00
Carbon tetrachloride	1.0	...	8.20
Tetrahydrofuran	2.28	4.5 ± 0.5	7.30
Methanol	2.30	1.7 ± 0.2	5.80
Ethanol	2.30	2.3 ± 0.3	5.55
2-Propanol	2.30	2.7 ± 0.3	5.55

TABLE II

Solvent	Half-widths in $m\mu$		Absorbance max. ($m\mu$)		Max. extinction coefficient $\times 10^{-4}$	
	Singlet	Triplet	Singlet	Triplet	Singlet	Triplet
Methylcyclohexane	65	59	370	450	4.55	7.58
Methanol	90	90	380	450	4.33	6.89
Tetrahydrofuran	70	65	375	448	4.40	7.86

The absorption spectra for the singlet ground state as well as the lowest triplet state are shown in Fig. 1. Table II tabulates the extinction coefficient and half-width data.

Figure 2 shows how the relative triplet yield of retinene varies with increasing concentration of methanol in methylcyclohexane solution while Fig. 3 shows the corresponding triplet half-life variation. The triplet yield as a function of solution composition in water-methanol and water-ethanol solutions is shown in Fig. 4. Corresponding triplet half-life data for these two cases show slight increases in half-life with increasing water concentration approaching an extrapolated value of approximately $13 \mu\text{sec.}$ in pure water.

Discussion

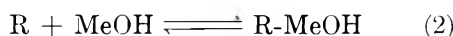
It appears from Table I that an increase in solvent polarity decreases both the triplet yield as well as the decay rate. In non-hydrogen bonding solvents like tetrahydrofuran, the decrease in triplet population over that in hydrocarbon solvents appears to be related to a variation in the crossing parameters of the potential energy surfaces of the excited π, π^* and n, π^* singlet states. There is, of course, the possibility that a variation in the crossing of the potential surfaces of the n, π^* singlet and the ground state also may account in some measure for the decreased triplet yield. A similar argument involving the lowest triplet and the ground state could account for the decrease in the triplet decay rate.

In previous studies of the decay of triplet states in aromatic molecules,⁴ a decrease in the first-order rate constant with increasing viscosity was ob-

(4) G. Porter and M. Windsor, *Discussions Faraday Soc.*, **17**, 178 (1954).

served. Recent work, however, has shown this effect to be a consequence of the inhibition of bimolecular quenching of the triplet state by traces of solvent impurities, particularly oxygen.⁵⁻⁸ However, in the case of retinene there is a 7% decrease in rate constant over a fourfold increase in viscosity (compare rate constants for pentane and undecane in Table I). This may not be due to inhibition of impurity quenching, as these solutions were rigorously purified and degassed. Furthermore, the rate constant for the decay of the retinene triplet is threefold larger than that of 9,10-dibromoanthracene, which showed no variation in the first-order rate constant triplet decay over a 170-fold change in viscosity.⁸ Therefore it would seem that the small viscosity effect in retinene may be a first-order effect most likely traced to a viscosity dependence of the crossing parameters. The rate data for the retinene triplet decay agree quite well with the recent data from Livingston's laboratory² for those solvents studied in common.

Hydrogen bonding solvents such as alcohol and water appear to exert a unique effect, independent of the polarity effect, on both the population and decay of the lowest triplet of retinene. The sharp decrease in triplet population with increasing methanol concentration in the mixed methanol-hydrocarbon solvent suggested that a hydrogen bonded complex is formed between retinene and methanol. The controlling equilibrium, even after excitation, is assumed to be that involving retinene in its ground state. However, at high methanol concentrations equilibrium of the complex involving retinene in its lowest π, π^* singlet state may be established. In any event this should have the effect of raising the energy of the n, π^* singlet above the π, π^* , thus removing the only feasible radiationless path to the triplet. Consequently there should be a correlation between the triplet yield and the concentration of uncomplexed retinene. If the assumed equilibrium is



then the formation constant K_{MeOH} is given by

$$(\text{MeOH})K_{\text{MeOH}} = \frac{(R\text{-MeOH})}{(R)} = \frac{T_0 - T}{T} \quad (3)$$

where (R-MeOH) is the mole fraction of the hydrogen bonded complex, and (R) and (MeOH) are the mole fractions of uncomplexed retinene and methanol, respectively. T_0 is the triplet yield in pure methylcyclohexane and T is the triplet yield in methanol-methylcyclohexane solution. The linearity of the plot of $(T_0 - T)/T$ vs. (MeOH) at low concentrations of methanol shown in Fig. 5 lends strong support to the notion of a hydrogen bonded complex between retinene and methanol. The formation constant of 7.3 is about twice that

(5) G. Jackson, R. Livingston, and A. Pugh, *Trans. Faraday Soc.*, **56**, 1635 (1960).

(6) H. Linschitz and L. Pekkarinen, *J. Am. Chem. Soc.*, **82**, 2411 (1960).

(7) G. Jackson and R. Livingston, *J. Chem. Phys.*, **35**, 2182 (1961).

(8) M. Hoffman and G. Porter, Abstracts, American Chemical Society National Meeting, Washington, D. C., March, 1962.

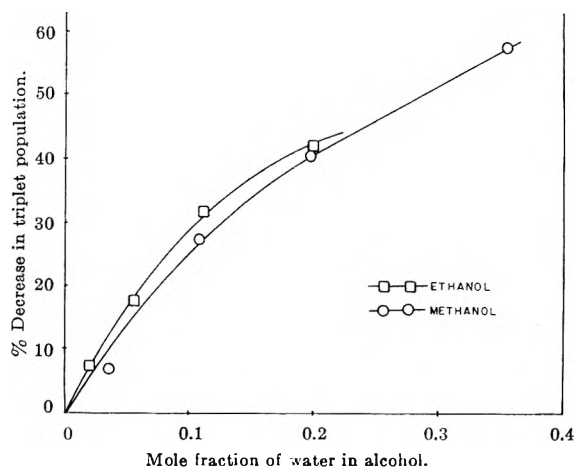


Figure 4.

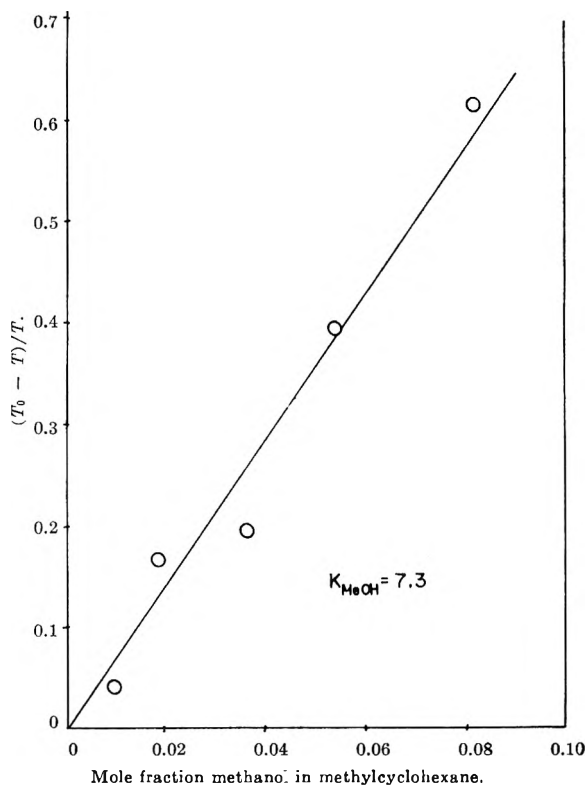


Figure 5.

measured directly by Brealey and Kasha⁹ for the benzophenone complex with ethanol.

One might expect slight differences in the absorption spectra of the uncomplexed and methanol complexed retinene and although no resolution of absorption maxima is evident in Fig. 1, the red shift in the absorption maximum coupled with the much increased band half-width relative to the spectra in methylcyclohexane and tetrahydrofuran suggests two close lying absorption bands.

The gradual shift in the absorption maxima at 370 $m\mu$ toward larger wave lengths along with increased broadening and decreased extinction of the absorption band also were apparent as increasing small amounts of methanol (less than 5%) were added to retinene in methylcyclohexane. Al-

(9) G. Brealey and M. Kasha, *J. Am. Chem. Soc.*, **77**, 4467 (1955).

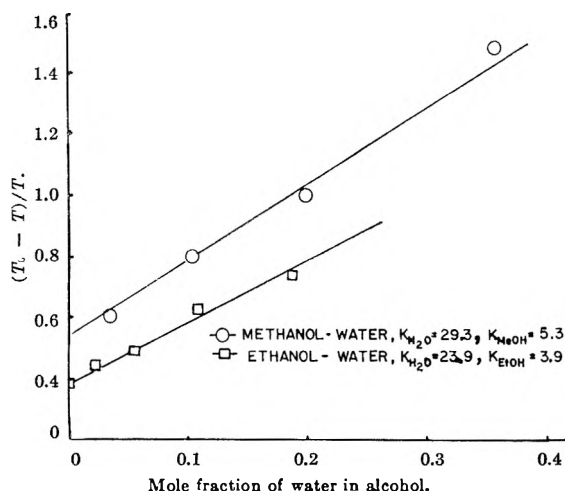


Figure 6.

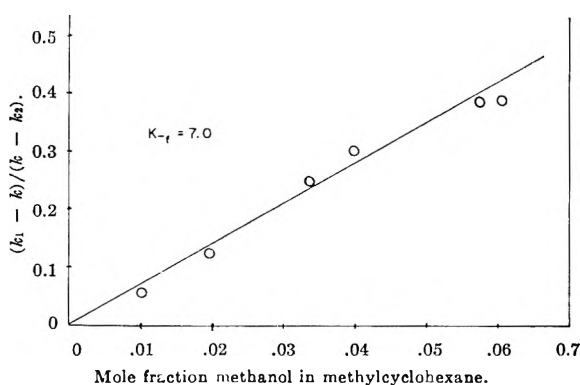


Figure 7.

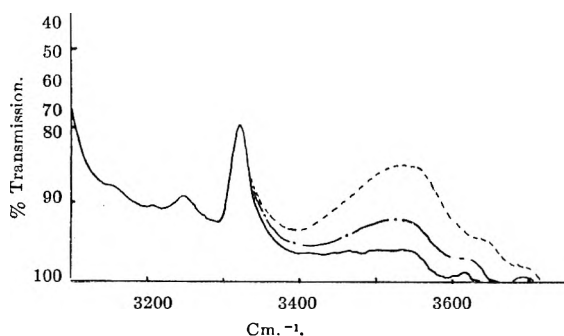
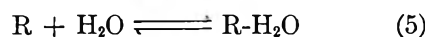
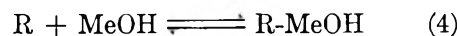


Fig. 8.—Infrared absorption spectrum of $1.084 \times 10^{-2} M$ *trans*-retinene in carbon tetrachloride-ethanol solutions. —, pure carbon tetrachloride; ---, $3.42 \times 10^{-2} M$ ethanol; - · - ·, $8.56 \times 10^{-3} M$ ethanol. Taken in 1-cm. sodium chloride cells and compensated for ethanol.

though this was indicative of complex formation, an isobestic point could not be resolved and attempts to calculate a complex formation constant by this method were abandoned. However, an ethanol-retinene complex was clearly apparent when ethanolic solutions of retinene in carbon tetrachloride were examined in the infrared region. Figure 8 clearly shows the appearance of a new broad band at 3540 cm^{-1} characteristic of hydrogen bonding.⁹ Since the ethanol concentrations in this case were too small for appreciable polymer formation and furthermore were compensated for by using identical concentrations of ethanol in the blank cell, this new band clearly indicates hydrogen

bonding of ethanol to the carbonyl oxygen of retinene. From the data, a formation constant of 6.5 was calculated, which is not too different from the value of 7.3 derived from the triplet yield data of retinene in methanol-methylcyclohexane solutions.

The triplet yield data in methanol-water solutions (Fig. 4) suggest that two hydrogen bonded species of retinene are present. If the following equilibria are assumed in methanol-water solutions

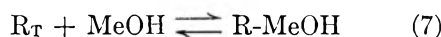


it can be shown that

$$\frac{T_0 - T}{T} = K_{\text{MeOH}} + 1 + (\text{H}_2\text{O})(K_{\text{H}_2\text{O}} - K_{\text{MeOH}}) \quad (6)$$

where (H_2O) is the mole fraction of water and $K_{\text{H}_2\text{O}}$ is the formation constant of the water-retinene complex. In Fig. 6 a linear plot of $(T_0 - T)/T$ against (H_2O) indicates the existence of the two hydrogen bonded retinene complexes. The calculated K_{MeOH} for methanol-water is of course, less than the methylcyclohexane value, which no doubt reflects the reduced activity coefficient for methanol in high concentration in aqueous solution. As expected, water shows a five- to sixfold increase in hydrogen bonding power over methanol.

The marked increase in triplet half-life with increasing alcohol concentration (Fig. 3) suggests a hydrogen bonded complex between the retinene triplet and methanol. A slower decay rate can reasonably be assumed for the hydrogen bonded triplet and an extrapolated value of $13 \mu\text{sec.}$ in pure water is arbitrarily taken as the half-life of the complex. Assuming that the equilibrium is rapidly established between the retinene triplet and its methanol complex



and k_1 and k_2 represent the first-order rate constants for decay of the retinene triplet and its methanol complex, respectively, and k is the observed first-order rate constant for triplet decay in the methanol-methylcyclohexane solvent, then it can be shown that

$$\frac{k_1 - k}{k - k_2} = (\text{MeOH})K_{Tf} \quad (8)$$

The linearity of the curve in Fig. 7 verifies the relations assumed in eq. 7 and 8. The corresponding formation constant K_{Tf} of the hydrogen bonded triplet is 7.0 and agrees very well with that of 7.3 obtained for the ground state complex. This is consistent with the observations of Jackson and Porter¹⁰ that the acidity constants of a number of aromatic triplets are comparable with those for the corresponding ground state singlets. The close agreement of these two values also lends strong support to the assignment of the lowest triplet as

(10) G. Jackson and G. Porter, *Proc. Roy. Soc. (London)*, **A260**, 13 (1961).

π, π^* , which probably is populated by direct inter-system crossing from the n, π^* singlet state.¹¹

If one examines the triplet-triplet absorption spectrum for retinene in pure methanol (Fig. 1), two peaks are quite evident. These possibly represent the spectra of the two forms, complexed and uncomplexed, of triplet retinene. From the wave number separation there seems to be an additional stabilization energy of 2000 cal. in the excited triplet state of the retinene complex over that in the lowest triplet. This is certainly greater than the stabilization energy in the excited singlet over that of the ground state for the retinene-methanol complex.

An important consequence of the hydrogen

(11) M. A. El-Sayed, *J. Chem. Phys.*, **36**, 573 (1962).

bonded triplet of retinene is that the large activation energy (2.4 ± 0.8 kcal.) observed² for the decay of the retinene triplet in glycerol logically can be assigned to a variation in K_{Tf} with temperature for the retinene triplet-glycerol complex.

Acknowledgments.—This work was supported by The Institute of Neurological Diseases and Blindness of the National Institutes of Health, Grant No. B2340, and The Atomic Energy Commission, Contract No. AT(11-1)-904. The authors are indebted to Miss Kim Vo and Dr. Joseph Gresser, who did much of the associated spectrophotometric work, and to Mr. Joseph Marquisee, Dr. Eric Thomas, Mr. Robert Vollmer, and Dr. Seymour West, who were in part responsible for the construction of the flash photolysis apparatus.

ENERGY TRANSFER IN AQUEOUS SOLUTION

BY W. BERENDS AND J. POSTHUMA

Technological University of Delft, Delft, The Netherlands

Received May 25, 1962

Energy transfer in aqueous solution may be of great importance in biochemical processes. The photodecomposition of the polyene fungicide pimarinol sensitized by riboflavin and lumichrome in aqueous solution has been found. The inhibiting effect of added substances including paramagnetic ions on this destruction runs completely parallel to their quenching effect on the phosphorescence of the sensitizers. A triplet-triplet transfer therefore is proposed as a mechanism for this destruction. This mechanism probably also is involved in the photosensitized *cis-trans* and *trans-cis* rearrangements of stilbene compounds in aqueous solutions.

During work on the mechanism of action of the fungicide pimarinol on yeast cells it was observed that visible light destroys the pimarinol if riboflavin is present.¹ This effect is remarkable because pimarinol does not show any absorption in the visible region. Since the presence of riboflavin is obligatory for the destruction of the pimarinol, it appears that the riboflavin absorbs the light and brings about the destruction of pimarinol. Pimarinol belongs to a group of polyene antibiotics.²⁻⁴ Though the structure of the molecule is rather complicated, the part of the molecule which is responsible for the ultraviolet spectrum is practically limited to a tetraen grouping. Compounds with a reactive system of conjugated double bonds are usually very sensitive to free radicals, which could have their origin in the decomposition of riboflavin by light.¹

Though the molecule of pimarinol is very complex, we have initially continued to use this compound since a change under the influence of light can be detected easily spectrophotometrically. It is obvious that a more simple tetraen would be better suited for our study, but these compounds are rare, are generally very labile, and usually are too insoluble in water. Pimarinol, on the other hand, has several advantages: it is commercially available, it is relatively stable, and the solubility is sufficient for the experimental conditions.

Pimarinol has maxima at 281, 292, 304, and 319 $m\mu$. The spectrum of riboflavin is more complicated, with maxima at 223, 268, 373, and 445 $m\mu$ (Fig. 1).

Several photodynamic destructions in which riboflavin is involved have been described in the literature, *e.g.*, aerobic photooxidation of phenols, ascorbic acid, 3-indoleacetic acid, and histidine^{5,6}; usually an oxidation of the substrate or a free radical mechanism is supposed to occur.⁷⁻¹⁰

From earlier experiments and those to be described in this paper it will appear that neither is acceptable as an explanation for our observations of the photodynamic behavior of an aqueous solution of the system riboflavin-pimarinol.¹¹

As a source of irradiation we used a Kromayer high-pressure mercury lamp. This lamp was placed at a distance of 3 cm. from the aqueous solution. By using an interference filter light with a wave length of about 443 $m\mu$ was obtained. The destruction of pimarinol could be followed by measuring the absorbancies at 304 and 319 $m\mu$ by means of a Unicam spectrophotometer SP 500. About 23% of the pimarinol was destroyed after 5 min. of irradiation. The absorption spectrum of riboflavin remained unchanged under these conditions and no pimarinol destruction could be observed by irradiating pimarinol alone.

(5) P. A. Kolensnikow, *Biokhimiya*, **22**, 434 (1958).

(6) A. W. Galston, *Science*, **111**, 619 (1950).

(7) H. R. Merkel and W. J. Nickerson, *Biochim. Biophys. Acta*, **24**, 115 (1957).

(8) W. J. Rutter, *Acta Chem. Scand.*, **12**, 438 (1958).

(9) L. P. Vernon and E. D. Ihnen, *Biochim. Biophys. Acta*, **24**, 115 (1957).

(10) L. P. Vernon, *ibid.*, **36**, 117 (1959).

(11) E. Zondag, J. Posthuma, and W. Berends, *ibid.*, **39**, 178 (1960); J. Posthuma and W. Berends, *ibid.*, **41**, 538 (1960); **51**, 392 (1961).

(1) B. Hendriks and W. Berends, *Rec. trav. chim.*, **77**, 145 (1958).

(2) A. P. Struyk, I. Hoette, C. Drost, J. M. Waisvisz, Th. van Eek, and J. C. Hoogerheide, *Antibiot. Ann.*, 878 (1957, 1958).

(3) J. B. Patrick, R. P. Williams, C. F. de Wolf, and J. S. Webb, *J. Am. Chem. Soc.*, **80**, 6688 (1958).

(4) J. B. Patrick, R. P. Williams, and J. S. Webb, *ibid.*, **80**, 6639 (1958).

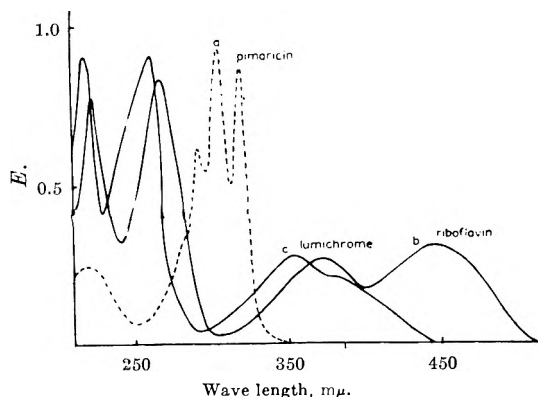


Fig. 1.—Absorption spectrum of pimaricin, riboflavin, and lumichrome in water: (a) pimaricin ($1.44 \times 10^{-5} M$); (b) riboflavin ($2.66 \times 10^{-5} M$); (c) lumichrome ($2.24 \times 10^{-5} M$); light path, 1 cm.

Though riboflavin is decomposed by prolonged irradiation, yielding lumichrome, a free radical mechanism is not likely to occur in the reaction just described because lumichrome alone is also able to bring about this pimaricin destruction. (Lumichrome is stable to the light used in these experiments (338 and 395 $m\mu$) and even to ultraviolet light of shorter wave lengths.¹²) Moreover, the photolysis of riboflavin in alcohol is much stronger than in water and nevertheless no destruction of pimaricin takes place in alcohol.

Vernon^{9,10} has suggested a free radical mechanism in which excited riboflavin decomposes water; the $\text{OH}\cdot$ -radicals thus formed oxidize the substrate, or give rise to H_2O_2 in the absence of a substrate. We have strong evidence, however, that no H_2O_2 is formed in irradiated aqueous solutions of lumichrome.

Lumichrome is completely stable to ultraviolet radiation,¹² but addition of a very small amount of H_2O_2 ($10^{-6} M$) brings about a very rapid destruction of lumichrome. Consequently any H_2O_2 formed under the experimental conditions would easily be detected. As apparently no H_2O_2 arises the formation of $\text{OH}\cdot$ -radicals is also not very probable.

If oxidation of pimaricin, accompanied by the simultaneous reduction of riboflavin, were the primary cause of the reaction between riboflavin and pimaricin it could be expected that oxygen would accelerate the photodynamic reaction. However, enhancement of the oxygen concentration in solution diminished the destruction of pimaricin.

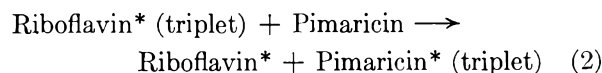
Bubbling through N_2 , prior to illumination, on the other hand strongly accelerates the pimaricin destruction. The remarkable inhibiting effect of oxygen on the photodynamic destruction in the systems riboflavin-pimaricin and lumichrome-pimaricin suggests a direct transfer of excitation energy and makes it unlikely that free radicals are involved. It is not probable that this transfer proceeds *via* a riboflavin-pimaricin or lumichrome-pimaricin complex because we were not able to detect such complexes by absorption and fluorescence measurements. Szent-Györgyi¹³ has re-

cently given some examples of charge-transfer complexes, but the concentrations used in his experiments ($10^{-3} M$) were much higher than in ours ($<10^{-5} M$). However, we cannot exclude completely intermediate complex formation.

Further observations of the reaction mentioned have brought us to the conclusion that the sensitizers riboflavin and lumichrome react in their triplet states. These triplet states have a rather long lifetime compared with the corresponding singlets and their importance in many photosensitized reactions in non-aqueous solutions has been recognized in the last decade.^{14,15} These long-lived excited states can be demonstrated by phosphorescence of the frozen solutions.

In our reactions the average time for collisions between riboflavin and pimaricin in a $10^{-5} M$ solution will be about 10^{-4} – 10^{-5} sec.¹⁶ From the lifetime of the singlet state, about 10^{-8} sec., it is evident that only relatively long-lived excited states like triplets have a reasonable chance to transfer their energy.

We therefore propose the following reaction sequence as an explanation of the photodynamic destruction of pimaricin



In reaction 1 riboflavin is first excited by a 445 $m\mu$ light quantum to its singlet state and next a singlet-triplet transition takes place (conversion of the spin moment). From this state an energy transfer to a pimaricin is possible if the triplet of pimaricin is lower than the similar state of riboflavin. Reaction 2 is allowed by spin-conservation rules.¹⁷ A few examples of such transfers have been described recently.^{15,18}

The over-all result of this triplet-triplet transfer would be an excited pimaricin molecule. It is conceivable that a very sensitive compound like pimaricin with its reactive tetraen structure decomposes if it is excited. The lability of pimaricin is demonstrated by its sensitivity to ultraviolet light.

This reaction mechanism is supported by the effect of several substances upon the system riboflavin-pimaricin. A compound that quenches the phosphorescence of riboflavin is supposed to act in this way by facilitating the radiationless dissipation of excitation energy by collisions with molecules of the solvent. Consequently, the lifetime of the triplet state is shorter. This means the triplet-triplet transfer is less probable.

It appears that the phosphorescence quenching effect of the compounds tested ran completely

(14) C. Reid, "Excited States in Chemistry and Biology," Butterworths Scientific Publications, London, 1957.

(15) G. Porter, *Proc. Chem. Soc. (London)*, 291 (1959).

(16) G. Oster and A. H. Adelman, *J. Am. Chem. Soc.*, **78**, 913 (1956).

(17) G. Porter and M. R. Wright, "Symposia Faraday Soc. Nottingham," 1959.

(18) A. Terenin and V. Ermolaev, *Trans. Faraday Soc.*, **52**, 1042 (1956).

(12) General Electric Germicidal lamp (4-watt).

(13)(a) I. Isenberg and A. Szent-Györgyi, *Proc. Natl. Acad. Sci. U. S.*, **44**, 857 (1958); 1231 (1959); (b) G. Karreman, I. Isenberg, and A. Szent-Györgyi, *Science*, **130**, 1191 (1959).

TABLE I

EFFECT OF VARIOUS SUBSTANCES ON PHOTODYNAMIC DESTRUCTION OF PIMARICIN, AND ON RIBOFLAVIN PHOSPHORESCENCE

Added substance	Photodynamic destruction of pimaricin		Riboflavin phosphorescence	
	Concn., <i>M</i>	% loss pimaricin	Concn., <i>M</i>	Color of frozen part of the soln.
.....	...	23	...	Orange
Cystine	10 ⁻³	35	10 ⁻³	Orange
Cysteine	10 ⁻³	33	10 ⁻³	Orange
Methionine	10 ⁻³	21	10 ⁻³	Orange
Thioglycolic acid	10 ⁻³	79	10 ⁻³	Yellow
Glutathione	10 ⁻³	58	10 ⁻³	Yellow
Na ₂ SO ₃	10 ⁻³	93	10 ⁻³	Orange
Ethyl iodide	10 ⁻³	22	10 ⁻³	Orange
Monoiodoacetic acid	10 ⁻³	23	10 ⁻³	Orange
KI	10 ⁻³	2	10 ⁻³	No color
KI	10 ⁻⁴	5	10 ⁻⁴	No color
Potassium rhodanide	10 ⁻³	5	10 ⁻³	No color
Thiourea	10 ⁻³	5	10 ⁻³	No color
Thiouracil	10 ⁻⁴	8	10 ⁻⁴	No color
Ascorbic acid	5 × 10 ⁻⁶	Inhibition	5 × 10 ⁻⁶	No color
Hydroquinone	5 × 10 ⁻⁶		5 × 10 ⁻⁶	No color
Methanol	75 vol. %	2	5 vol. %	Yellow
Ethanol	96 vol. %	0	5 vol. %	Yellow
Pimaricin ^a	2 × 10 ⁻⁶	Weakly orange

^a Because of the low solubility of the pimaricin a 2 × 10⁻⁶ *M* solution of riboflavin was used to observe the phosphorescence quenching.

TABLE II

Salt added	Aerobic conditions, light acceptor riboflavin (1.9 × 10 ⁻⁶ <i>M</i>)			Anaerobic conditions, light acceptor lumichrome (2 × 10 ⁻⁶ <i>M</i>)		
	Concn. of the salt (m <i>M</i>)	% decrease of extinction of pimaricin	Color of the frozen soln.	Concn. of the salt (m <i>M</i>)	% decrease of extinction of pimaricin	Color of the frozen soln.
Paramagnetic	54	Orange phosphor.	22	Yellow phosphor.
	NiCl ₂ 2.5	42	Colorless	0.5	17	Colorless
	CuCl ₂ 2.5	24	Colorless	.5	11	Colorless
Paramagnetic	MnCl ₂ 2.5	45	Colorless	.5	20	Colorless
	CoCl ₃ 2.5	43	Colorless	.5	15	Colorless
	CrCl ₃ 2.5	43	Colorless	.5	18	Colorless
Diamagnetic	MgCl ₂ 2.5	53	Orange phosphor.	.5	21	Yellow phosphor.
	ZnCl ₂ 2.5	51	Orange phosphor.	.5	21	Yellow phosphor.
	CaCl ₂ 2.5	52	Orange phosphor.	.5	20	Yellow phosphor.
	CdCl ₂ 2.5	52	Orange phosphor.	.5	21	Yellow phosphor.
	KCl 2.5	52	Orange phosphor.	.5	21	Yellow phosphor.
NaCl 2.5	52	Orange phosphor.	.5	21	Yellow phosphor.	

parallel to their degree of inhibition of the photodynamic destruction of pimaricin in the combination riboflavin-pimaricin.

On the other hand, compounds without visible observable quenching effect show no inhibition but in many cases even accelerate the pimaricin destruction.

The quenching effect of compounds on the phosphorescence of riboflavin was tested by adding them to a 2 × 10⁻⁵ *M* aqueous solution of riboflavin and visually observing the phosphorescence in ultraviolet light after freezing.¹⁹

In order to keep the solutions at constant pH a phosphate buffer (0.06 *M*, pH 6.8) was used. The concentration of riboflavin was 2 × 10⁻⁵ *M*, that of pimaricin 9 × 10⁻⁶ *M*.

The ultraviolet light was obtained from a Philips lamp H.P.W. 125. The results are given in Table I.

Besides the compounds mentioned in this table,

(19) A. Szent-Györgyi, "Bioenergetics," Academic Press, New York, N. Y., 1957.

the paramagnetic metal ions are particularly active as quenchers of phosphorescence, which means that these ions shorten the triplet lifetime. For this reason we have tested a number of para- and diamagnetic ions in the same manner as we did the compounds of Table I.

To aqueous solutions containing 9 × 10⁻⁶ *M* pimaricin and 0.01 *M* sodium acetate-acetic acid (pH 4.3) were added riboflavin or lumichrome and the salts recorded in Table II. The solutions were exposed to light in glass tubes (inner diameter 2.2 cm.) for 5 min. Again the light was obtained from the Kromayer lamp and the desired wave length was isolated by means of a Schott interference filter. For the system riboflavin-pimaricin light of 443 mμ was used. In the case of lumichrome-pimaricin a wave length of 395 mμ was chosen. In the anaerobic experiments the air was removed by bubbling through nitrogen during 20 min. prior to illumination. Riboflavin could not be used under anaerobic conditions because an appreciable destruction of this compound occurs in the time of irradiation.

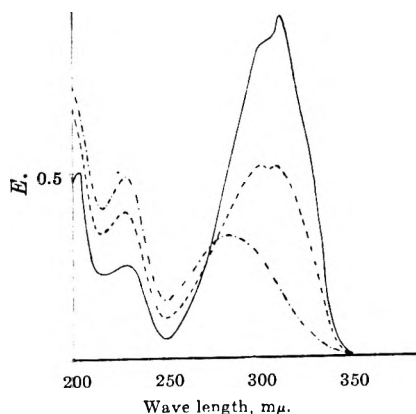


Fig. 2.—Irradiation of aqueous solutions of $2.4 \times 10^{-6} M$ *cis*- and *trans*-stilbene carboxylic acid-4 in the presence of $3.7 \times 10^{-6} M$ lumichrome: - - - - , *cis*-stilbene carboxylic acid-4; ———, *trans*-stilbene carboxylic acid-4; - - - - , after irradiation sensitized by lumichrome.

Table II shows that all paramagnetic ions tested diminish the photodynamic pimaricin decomposition and that the phosphorescence of riboflavin and lumichrome also is quenched by these ions. Diamagnetic ions have no effect at all. These observations apparently are in complete agreement with the paramagnetic quenching of the triplet state. These ions affect only the triplet state of the sensitizer, for the direct destruction of pimaricin by ultraviolet light is not influenced by the paramagnetic compounds.

For the study of the triplet states of riboflavin and lumichrome, pimaricin was not quite satisfactory because it has a very complicated structure and consequently it is not known exactly what kind of conversion is responsible for the decrease of extinction. We therefore looked for a more simple compound and we found the possibility of replacing pimaricin by stilbene derivatives.

The first compounds tested were *cis*- and *trans*-stilbene carboxylic acid-4. The *cis* compound shows absorption maxima at 230 and 288 $m\mu$;

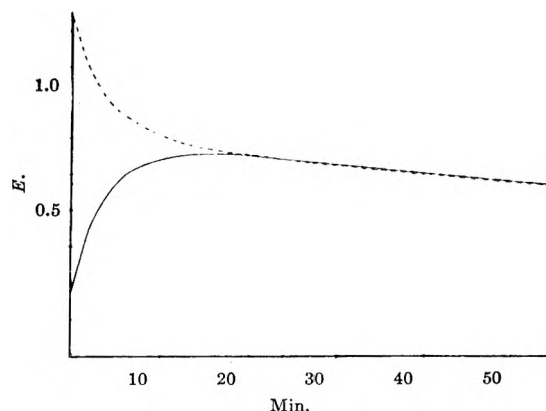


Fig. 3.—Change of the extinction at 317 $m\mu$ (maximum of the *trans* compound) during the irradiation in the presence of lumichrome: ———, *cis*-stilbene carboxylic acid-4; - - - - , *trans*-stilbene carboxylic acid-4.

those of the *trans* compound are found at 230 and 317 $m\mu$ with a shoulder at 308 $m\mu$ (Fig. 2).

Irradiation of either the *cis* or the *trans* form in the presence of lumichrome rapidly leads to a spectrum which in the region above 250 $m\mu$ agrees with a mixture of about 40% *cis* and 50% *trans* of the original concentration (Fig. 2). This equilibrium mixture slowly decomposes on further irradiation (Fig. 3).

A similar equilibrium mixture is obtained by irradiation in the absence of the sensitizer with light of 253.7 $m\mu$. Apparently a *cis-trans* and a *trans-cis* rearrangement are involved. Preliminary experiments have shown that the lumichrome-sensitized isomerizations also are inhibited by neutral quenchers like O_2 , KI, and KCNS, just as is the destruction of pimaricin in the system lumichrome phosphorescence, so we may assume that in these photosensitized rearrangements a triplet-triplet transfer is involved.

Investigations with stilbene sulfonic acids instead of the carboxylic acids are in progress. The quantum efficiencies of the reactions also are being studied at present.

A REVERSIBLE PHOTOREACTION REGULATING PLANT GROWTH¹

BY STERLING B. HENDRICKS, WARREN L. BUTLER, AND H. W. SIEGELMAN

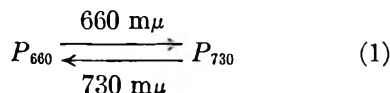
Mineral Nutrition Laboratory and Plant Physiology Laboratory, Agricultural Research Service, and Instrumentation Research Laboratory, Agricultural Marketing Service, U. S. Department of Agriculture, Beltsville, Maryland

Received May 25, 1962

Results of action spectra indicated that many aspects of plant growth are controlled by a reversible change of a blue protein, phytochrome. The manner in which the photoreversibility is used for detection and assay is described. Measurements of absorptive and fluorescent properties of phytochrome are presented. Observations on dark reversion of the far-red- (P_{730}) to the red- (P_{660}) absorbing forms are given.

Introduction

A reversible photoreaction in which 660 and 730



$m\mu$ are the respective absorption maxima of two

forms of a chromoprotein, phytochrome (P), has been shown to control many aspects of growth and development of higher plants.² The controlled re-

(1) Prepared for presentation at the International Symposium on "Reversible Photochemical Processes," sponsored by the U. S. Army Research Office, Duke University, Durham, North Carolina, April 16-18, 1962.

(2) H. A. Borthwick, S. B. Hendricks, M. W. Parker, E. H. Toole, and V. K. Toole, *Proc. Natl. Acad. Sci. U. S. A.*, **38**, 662 (1952).

sponses include flowering, stem elongation (etiolation), leaf movement and expansion, plastid formation, seed germination, anthocyanin production, and bud dormancies. In darkness P_{730} changes to P_{660} .³ Many seasonal responses of plants, including growth, flowering, and the autumnal color changes, depend primarily upon this reversion. These responses, which are termed photoperiodic, control the induction of reproduction and dormancy and are important for the preservation of the species in unfavorable seasons.

The pigment change can be followed both by physiological responses, such as flowering, etiolation, or seed germination, and by spectrophotometric measurement. A mass of pertinent results has been presented in about 120 papers by H. A. Borthwick and his associates, chiefly in journals devoted to plant sciences.⁴ Some of the aspects of this work with particular bearing on the molecular biology are presented here, but the original papers should be read for the biological control and important experimental conditions and nuances. The necessity of interweaving physiological and physical approaches and the contrasting logic of the several approaches might be borne in mind.

Detection of Phytochrome by Physiological Methods.—Initial development of the subject was based on discoveries of light-sensitive phenomena chiefly in etiolation, seed germination, and flowering. This culminated in the discovery of the day length dependence of flowering in many plants by Garner and Allard in 1918.⁵ Insight into the relationship between these varied phenomena resulted from the measurement of the action spectra for etiolation, flowering, and seed germination. These action spectra expressed as the incident energies in various spectral regions required to produce a given response, such as 50% seed germination or 50% flowering, are illustrated in Fig. 1. The action spectra for the effects of light in the 560 to 700 $m\mu$ region on the enhancement of lettuce seed germination, the elongation of pea leaves, the induction of flowering of barley (a long-day plant), and the inhibition of flowering of cocklebur (a short-day plant) are shown in Fig. 1a. The action spectra for the effects of longer wave length radiation (700 to 800 $m\mu$) on reversing the effects of red light on lettuce seed germination and cocklebur flowering are shown in Fig. 1b. Actions for wave lengths shorter than 560 $m\mu$ are present but low, both for the forward and reverse reaction.

On the basis of these action spectra the reversible photoreaction of equation 1 was proposed⁶ as the controlling mechanism for all these light-sensitive responses. Since then, more aspects of plant growth and development have been shown to be controlled by the action of light on phytochrome.

Detection of Phytochrome by Differential Spectrophotometry.—A physical method for detection

(3) H. A. Borthwick, S. B. Hendricks, E. H. Toole, and V. E. Toole, *Bot. Gaz.*, **115**, 205 (1954).

(4) H. A. Borthwick and S. B. Hendricks, "Hand. der Pflanzenphysiol.," Vol. 26, p. 299, ed. by W. Ruhland, Springer-Verlag, Berlin, 1961.

(5) W. W. Garner and H. A. Allard, *J. Agr. Res.*, **18**, 553 (1920).

(6) S. B. Hendricks and H. A. Borthwick, in "Aspects of Synthesis and Order of Growth," ed. by Dorothea Rudnick, Princeton University Press, Princeton, N. J., 1955, pp. 149-168.

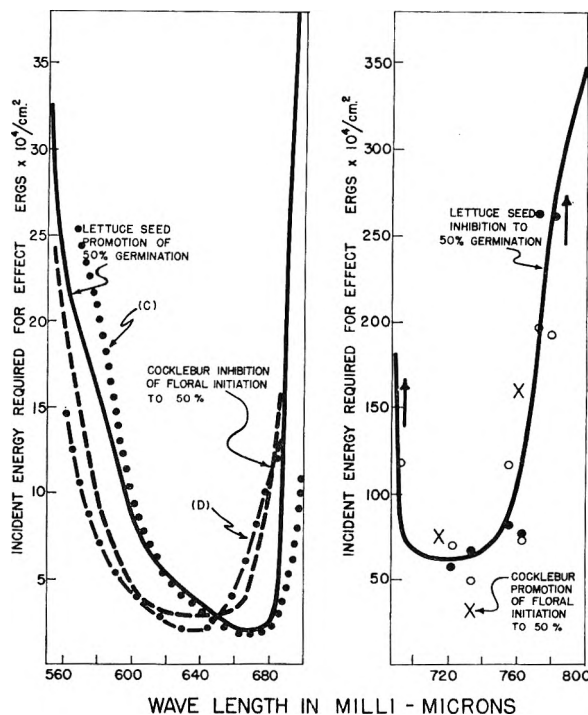


Fig. 1.—Action spectra: (a) Energy required to promote germination of imbibed lettuce seed to 50%, solid curve; to enhance elongation of a pea leaf by 45%, dotted curve; to induce flowering of barley to 50%, dot-dash curve; and to inhibit floral initiation of cocklebur to 50%, dotted curve. (b) Effect of far-red radiation given immediately after a saturating exposure to red light: energy required to inhibit germination of lettuce seed to 50% (control showed 96% germination), solid curve through open and closed circles; to induce floral initiation of cocklebur to 50% (control shown as floral initiation), crosses.

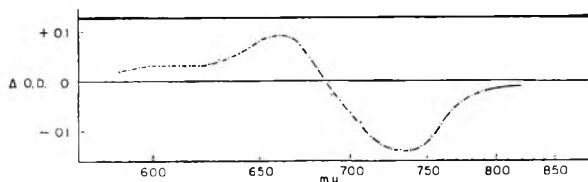


Fig. 2.—Far-red-irradiated minus red-irradiated difference spectrum of dark-grown maize seedlings.

of phytochrome was based on the difference between absorption spectra of responsive dark-grown tissue with the pigment in first one form and then the other.⁷ Measurements were made on intact plant tissue with spectrophotometers designed to accommodate optically dense, highly scattering samples. Figure 2 is an example of the differential results obtained. The absorption spectrum was first run after irradiation of the 1-cm. thick sample of dark-grown maize seedlings with a high intensity auxiliary source of red light to put the phytochrome in the P_{730} far-red-absorbing form. A second spectrum was run after far-red irradiation of the sample. The observed density changes were repeatedly reversible and the maxima of the two forms were at 660 and 730 $m\mu$, respectively, in agreement with the physiological measurements of Fig. 1.

Rapid assay for phytochrome is made with a

(7) W. L. Butler, K. H. Norris, H. W. Siegelman, and S. B. Hendricks, *Proc. Natl. Acad. Sci. U. S. A.*, **45**, 1703 (1959).

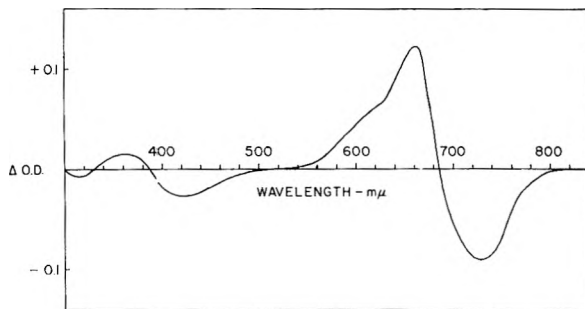


Fig. 3.—Far-red-irradiated minus red-irradiated difference spectrum of a partially purified solution of phytochrome extracted from maize seedlings (1-cm. cuvettes).

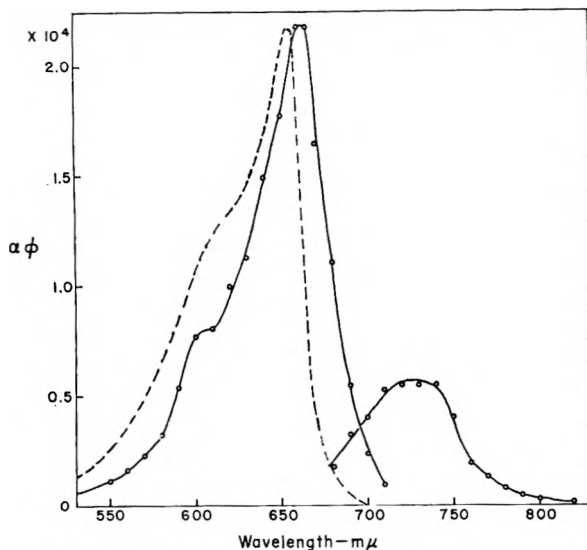


Fig. 4.—Action spectra for the photochemical conversions of P_{660} and P_{730} plotted as the product (liter/mole/cm.) ϕ (moles/einstein) vs. wave length. The dashed curve is the absorption spectrum of allophycocyanin (C. OhEocha, *Arch. Biochem. Biophys.*, 54, 102 (1955); 73, 207 (1958)).

difference spectrophotometer, which measures directly the optical-density difference of a sample between two fixed wave lengths. The optical density difference between 660 and 730 $m\mu$ ($\Delta O.D._{660}^{660}$) is measured with phytochrome in each of its two forms. The difference in the two readings, $\Delta(\Delta O.D.) = (\Delta O.D._{730}^{660})$ red irradiated $- (\Delta O.D._{730}^{660})$ far-red irradiated, is an assay for the total amount of phytochrome.

Separation and Enrichment.—Phytochrome is readily detected as a component of soluble protein extracted from etiolated plant material ($\Delta(\Delta O.D.)$ values of 0.032/cm. in the original solution) and is presumably a cytoplasmic rather than a particulate protein. A survey of etiolated materials indicated that the content was highest in young gramineous plants, of which maize and barley were selected for most of the extractions. Bonner,⁸ at Yale University, used etiolated peas. Enrichments have been effected to the point of making the pigment reversal readily visible to the eye.

Greatest success with separations depends on selective denaturation with resulting lowered solubility of phytochrome. Phytochrome from barley undergoes this denaturation upon standing in

solution at 2° for periods of 24 hours or less. This modified material separating from solutions of high protein concentration obtained by osmotic withdrawal of water with polyethylene glycol can be partially redissolved in neutral solutions having low salt contents.

Phytochrome in maize is apparently more stable against protein change. It has proven refractory, without serious loss, to enrichment by methods of salting out and absorption. Some purification has been effected by use of molecular sieves formed in gel columns. Solutions enriched from the several sources are adequate for following some of the properties of phytochrome *in vitro*.

Properties of Phytochrome.—The difference spectrum of a solution of phytochrome partially purified from maize (Fig. 3) shows the same reversible absorption bands as the *in vivo* difference spectrum (Fig. 2). The action spectra for the photochemical transformations have been determined by measuring photometrically the degree of pigment conversion resulting from the irradiation of a thin, optically clear solution of phytochrome with monochromatic light of known intensity. Both photochemical conversions of equation 1 have been shown to be first order.⁹ The solution of the differential-rate equation for P_{660}

$$dP_{660}/dt = -E_{\lambda}\epsilon_{\lambda 660}\phi_{660}P_{660} + E_{\lambda}\epsilon_{\lambda 730}\phi_{730}P_{730} \quad (2)$$

is

$$\log(P_{660} - P_{660\infty}) = -0.43 \frac{E_{\lambda}\epsilon_{\lambda 660}\phi_{660}}{P_{730\infty}}t + c \quad (3)$$

where

$$P_{660} = \text{mole fraction at time } t; P_{660} = 1 - P_{730}$$

$$P_{660\infty} = \text{mole fraction } P_{660} \text{ at } t = \infty$$

$$E_{\lambda} = \text{incident energy (einsteins/cm.}^2\text{/sec.)}$$

$$\epsilon_{660\lambda} = \text{extinction coefficient of } P_{660} \text{ at } \lambda \text{ (cm.}^2\text{/mole, base } e)$$

$$\phi_{660} = \text{quantum yield of } P_{660} \rightarrow P_{730} \text{ reaction (moles/einstein)}$$

$$c = \text{a constant of integration}$$

E_{λ} and $P_{730\infty}$ can be measured and the first-order reaction constant, K , is determined by the slope of the semilogarithmic plot of $(P_{660} - P_{660\infty})$ vs. t . The product $\epsilon\phi$ can be calculated from these parameters even though the concentration or molecular weight of the pigment is unknown.

$$\epsilon_{660\lambda}\phi_{660} = 2.3K(P_{730\infty}/E_{\lambda})$$

A similar treatment for P_{730} gives

$$\epsilon_{730\lambda}\phi_{730} = -2.3K(P_{660\infty}/E_{\lambda})$$

In Fig. 4 the action spectra for both photochemical transformations are plotted as $\alpha\phi$ versus λ where α is the molecular extinction coefficient expressed as liter/mole/cm. to the base 10. $\alpha = 0.43 (\epsilon/1000)$.

The difference spectra of Fig. 2 and 3 show that

(9) W. L. Butler, in "Progress in Photobiology," ed. by B. Christensen and B. Buchmann, Elsevier, Amsterdam, 1961, p. 569.

(8) B. A. Bonner, *Plant Physiol. Suppl.*, 36, xliii (1961).

the extinction coefficients of P_{660} and P_{730} are approximately equal at their absorption maxima. The difference in the magnitude of $\alpha\phi$ for the two forms at their maxima must be attributed, therefore, to a difference of the ϕ values: $\phi_{660} \simeq 4\phi_{730}$. If $\phi_{660} = 1$, which is the maximum value it can have

$$\alpha_{660} \simeq \alpha_{730} \simeq 2 \times 10^4 \text{ liter/mole/cm.}$$

which is a high value for a molecular extinction coefficient. If ϕ_{660} is less than unity, the extinction coefficients must be correspondingly higher.

The measurement of the extinction coefficient does not require extracts. The reversibility of the physiological responses permitted minimum values of the extinction coefficients for both P_{660} and P_{730} to be determined from seed germination and internode elongation.¹⁰ Values of 2×10^4 liter/mole/cm. for P_{660} of lettuce seed and 0.8×10^4 for P_{730} of *Lepidium* seed are in good agreement with those obtained *in vitro*.

An altered far-red absorbing form is obtained from phytochrome solutions extracted from barley. P_{730} , having normal extinction, is present in the plant, but in the partially purified extracts the extinction of a far-red-absorbing form progressively decreases. This change is accompanied by a decrease in solubility indicative of an early stage of protein denaturation. The difference spectrum (Fig. 5) indicates that the absorption in the region of the red absorption maximum remains near its initial value while that in the region of 710 to 740 $m\mu$ decreases to less than 10% of the initial value. A similar change has been reported by Bonner for phytochrome enriched from pea plants. Reversibility is retained in this change of protein configuration but is lost by denaturation of the protein by heat or low pH.

Reversibility is independent of temperature down to -20° but is gradually lost below that temperature. No photoreaction occurs at -196° , but reversibility is regained on warming. The temperature effects suggest a photochemical transformation which can be prevented by a sufficiently rigid medium.

Fluorescence from P_{660} has been observed both *in vivo* and *in vitro* with marked enhancement upon cooling to -196° . Fluorescence from P_{730} has not been detected. The emission maximum from P_{660} is near 690 $m\mu$ and the excitation maximum for this fluorescence appears near 670 $m\mu$. The presence of phytochrome in a dark-grown bean leaf is shown in the fluorescent-excitation spectrum at -196° in Fig. 6. The leaves were grown in complete darkness because a small amount of chlorophyll would mask the fluorescence of phytochrome. Fluorescence emission from the leaf was excited by light from a scanning monochromator and was measured through a cut-off filter, which limited the measurement to wave lengths longer than 730 $m\mu$.¹¹ Protochlorophyll is evident from its absorption and fluorescence-excitation band at 650 $m\mu$. An excitation band appears at 670 $m\mu$, which is not detected in the absorption spectrum.

(10) S. B. Hendricks, H. A. Borthwick, and R. J. Downs, *Proc. Natl. Acad. Sci. U. S. A.*, **42**, 19 (1957).

(11) W. L. Butler, *Arch. Biochem. Biophys.*, **93**, 413 (1961).

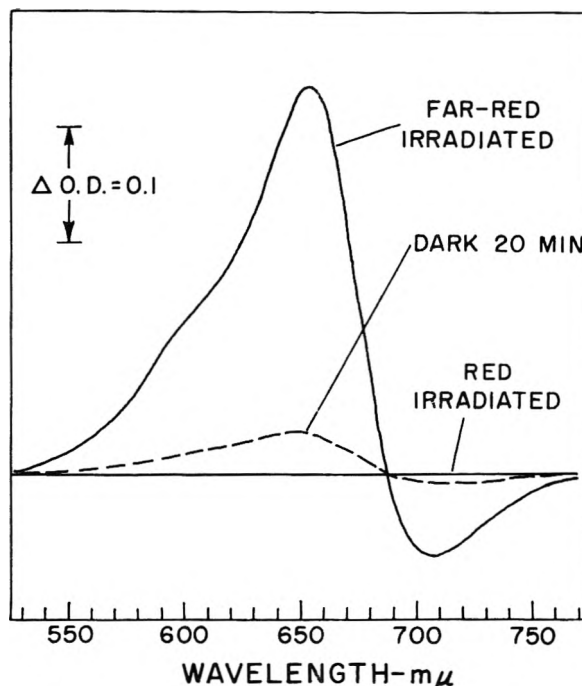


Fig. 5.—Difference spectra of a centrifuged pellet obtained from partially purified solution of barley phytochrome which has been concentrated by dialysis against polyethylene glycol. This pellet represents the material which came out of solution during the concentration. The absorption spectrum of the red-irradiated sample was arbitrarily selected as the base line.

The fluorescence-excitation spectrum is selectively more sensitive to the longer wave length component because a greater proportion of its fluorescence emission extends beyond 730 $m\mu$. This excitation band at 670 $m\mu$ can be attributed to phytochrome because phytochrome has been shown to be present in dark-grown bean leaves by differential spectrophotometry and solutions of phytochrome in the P_{660} form show this same excitation band.

The Dark Reaction.—Phytochrome is always found in the P_{660} form in a dark-grown plant. If any P_{730} is formed, it is converted to P_{660} in the dark. The dark reaction $P_{730} \rightarrow P_{660}$ in intact, dark-grown maize seedlings is shown in Fig. 7. A box of dark-grown maize seedlings was irradiated briefly with red light to convert the phytochrome to P_{730} and returned to darkness. At various times thereafter a sample of seedlings was harvested and relative amounts of P_{730} and total phytochrome, P_{730} plus P_{660} , were determined spectrophotometrically. The difference between these two values gives the relative amount of P_{660} present at the time of the harvest. Figure 7 shows that the P_{730} reverts back to P_{660} during the course of several hours. There is also a net loss of reversibility.

The dark reaction is much slower at 3° than at 27° and it does not occur in the absence of oxygen. Material extracted from maize seedlings does not change form upon standing in darkness. Material extracted from barley, however, reverts from the modified form P_{730} to P_{660} in darkness.

The dark reversion of P_{730} was first detected by physiological observations on seed germination and flowering. The effects of brief illumination in the

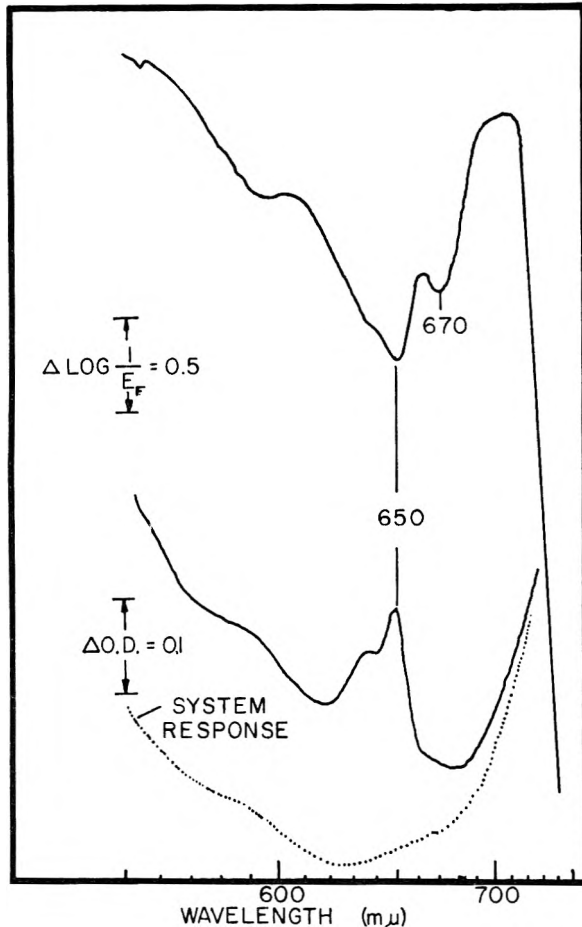


Fig. 6.—Absorption spectrum and excitation spectrum of fluorescence of wave length longer than 730 $m\mu$ of a dark-grown bean leaf at -196° . The system response curve represents the base line for the absorption spectrum. The fluorescence excitation spectrum is not corrected for the monotonous increase in the energy of the exciting light with increasing wave length.

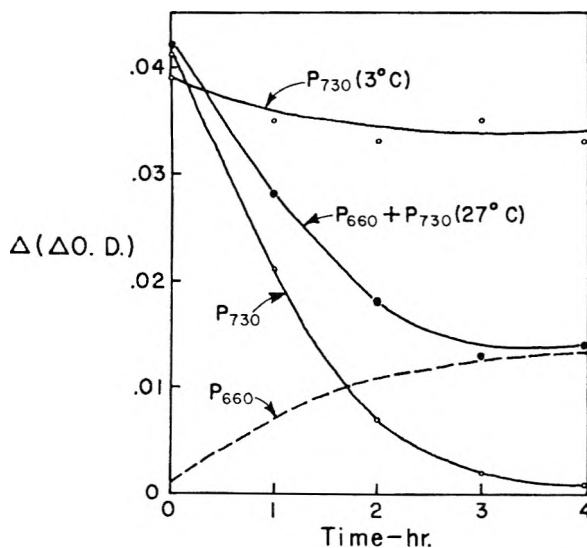


Fig. 7.—Changes in the relative amounts of phytochrome present in dark-grown maize seedlings immediately following a single irradiation with red light: $P_{730} = \Delta O.D._{730}^{660}$ (initial) $- \Delta O.D._{730}^{660}$ (far-red irradiated); $P_{660} + P_{730} = \Delta O.D._{730}^{660}$ (red irradiated) $- \Delta O.D._{730}^{660}$ (far-red irradiated).

night on the photoperiodic responses of flowering and dormancy showed that this dark reaction is an essential part of the timing mechanism by which the plant reckons the length of the night. The experiments by Borthwick and Cathey¹² on the effects of cyclic night-time lighting on the flowering of the short-day plants show that the plant can measure dark periods to within 15 minutes by this dark reaction.

The Enzymatic Action of Phytochrome.—While the exact action of phytochrome is still unknown, physiological observations indicate that P_{730} is an enzyme, which is in keeping with its sensitivity to protein configuration. A light-sensitive seed remains dormant in the dark because phytochrome is maintained as P_{660} in darkness. A weak irradiation with light which converts P_{660} to P_{730} triggers germination. Phytochrome is active in many plant tissues in concentrations less than 10^{-7} molar. While most of the displays of phytochrome, such as flowering and stem lengthening, have not been reduced to chemical terms, anthocyanin synthesis may afford a system in which the point of phytochrome action can be localized.

Anthocyanin synthesis in many plants requires high radiant energies. A product of the high-energy photoreaction requires a number of reactions over a period of about 12 hours at 20° before it appears in anthocyanin. In sorghum and red cabbage seedlings,¹³ as well as many others, P_{730} must be present after about 4 hours of the dark period has passed if anthocyanin is to form. The control has the usual reversibility as shown by action spectra. P_{730} appears to be acting as a specific enzyme in the reaction sequence leading to anthocyanin.

A general argument based on the wide diversity of phenomena regulated by phytochrome indicates that the enzymatic action must be at a metabolic crossing point, which is common to many biochemical pathways. The oxidation and reduction of pyridine nucleotides and the acyl activation by coenzyme A are examples of reactions which have sufficient generality to be considered as the site of control. Both of these reactions are likely to be involved in the reaction series of anthocyanin formation as well as the other physiological displays of phytochrome.

The Prosthetic Group of the Pigment.—Phytochrome has not been sufficiently purified to permit the identification of its prosthetic group by chemical means. The comparison of the absorption spectrum of P_{660} with that of allophycocyanin¹⁴ in Fig. 4 suggests a similarity of structure. The low absorption of both forms of phytochrome in the blue region is evidence against a cyclic tetrapyrrole of the chlorophyll or hemin type. Allophycocyanin is considered to be a bilidiene such as biliviolin. A possible bilatriene or other open chain tetrapyrrole would also have to be considered for the prosthetic group at this stage. The phyco-

(12) H. A. Borthwick and H. M. Cathey, *Bot. Gaz.*, in press (1962).

(13) H. W. Siegelman and S. B. Hendricks, *Plant Physiol.*, **32**, 393 (1957).

(14) C. Ó'hEocha, *Arch. Biochem. Biophys.*, **54**, 102 (1955); **73**, 207 (1958).

cyanins have only been found in blue-green and red algae, in mollusk feeding upon these sources, and possibly among feather pigments. Enzymes involving them are not known.

The open-chain tetrapyrroles can undergo several types of isomerization. They can form *cis* or

trans isomers at the methene bridges and the terminal rings can be lactams or lactims. The four pyrrole rings can be folded back to approximate the close ringed tetrapyrroles and this structure might be stabilized by hydrogen-bond formation to a native protein.

ON THE MECHANISM OF PHOTOCHEMICAL *cis* \rightleftharpoons *trans* ISOMERIZATION

By HORST STEGEMEYER

Lehrstuhl für Erdölchemie der Technischen Hochschule, Hannover, Germany

Received May 25, 1962

In connection with earlier considerations¹⁻³ a simple model of *cis* \rightleftharpoons *trans* photoisomerization had been developed supposing two forms of different energies in the intermediate state involved during isomerization. Calculations lead to equations of quantum yields which mainly depend only on the rate of thermal conversion in the intermediate and on the rate of deactivation to the ground state. Another model involving only one common intermediate state also had been discussed in view of the experimental results of Fischer.³ In a first proof the temperature dependence of quantum yields of stilbene was shown to be satisfied best by the former model.

Introduction

In previous investigations concerning the photochemistry of stilbene¹ we had re-investigated the quantum yields of photoisomerization of this compound for the *trans* \rightarrow *cis* (q_t) and *cis* \rightarrow *trans* (q_c) direction, respectively (cf. Table I). Values of quantum yields measured before by Smakula,⁴ Lewis and co-workers,⁵ Hausser,⁶ and Yamashita⁷ seem to be erroneous for the following reasons. At first, the quantum yields will be effected by the

TABLE I

PHOTOISOMERIZATION OF STILBENE IN *n*-HEXANE (10^{-5} M), 25°. QUANTUM YIELDS (q) AND MOLE FRACTION OF EQUILIBRIUM (x)

Wave length, Å.	x_t	q_t	q_c	Σq
2537	0.424	0.67	0.28	0.95
3130	0.070	0.59	0.32	0.91

side reaction forming phenanthrene. In an earlier work⁸ it had been shown that this process of dehydrocyclization occurs *via* an excited singlet state of the *cis* isomer of stilbene only. Subtracting the quantity of phenanthrene being formed during photoisomerization the mole fractions of stilbene isomers were corrected by the relations $x_t(\text{cor}) = x_t/(x_t + x_c)$ or $x_c(\text{cor}) = x_c/(x_t + x_c)$. Using these corrected values the side reaction will be eliminated in the calculation of quantum yields. Further, it was shown that the calculation method of quantum yields given by Zimmerman and co-workers⁹ only leads to exact values. The equation reported by Schulte-Frohlinde¹⁰ cannot be used without empirical correction factors.

(1) H. Stegemeyer, Dissertation, Hannover, 1961.

(2) E. Fischer, *J. Am. Chem. Soc.*, **82**, 3249 (1960).

(3) S. Malkin and E. Fischer, *J. Phys. Chem.*, **66**, 2482 (1962).

(4) A. Smakula, *Z. physik. Chem.*, **B25**, 90 (1934).

(5) G. N. Lewis, T. T. Magel, and D. Lipkin, *J. Am. Chem. Soc.*, **62**, 2973 (1940).

(6) I. Hausser, *Naturwissenschaften*, **36**, 315 (1949).

(7) S. Yamashita, *Bull. Chem. Soc. Japan*, **34**, 490 (1961).

(8) H. Stegemeyer, *Z. Naturforsch.*, **17b**, 153 (1962).

(9) G. Zimmerman, L. Chow, and E. Paik, *J. Am. Chem. Soc.*, **80**, 3528 (1958).

(10) D. Schulte-Frohlinde, *Liebigs Ann. Chem.*, **615**, 114 (1958).

As may be seen from Table I, the sum of quantum yields for both directions approaches unity at room temperature. From this it might be derived that the isomerization occurs *via* an intermediate state common both to *cis* and *trans* isomers. However, Fischer^{2,3} observed a temperature dependence of photoisomerization in dilute solutions, as we had found in liquid *cis*-stilbene.¹¹

These results lead to the conclusion that there must be a thermal activated step in photoisomerization. According to the results of Malkin and Fischer³ the relation $\Sigma q \rightarrow 1$ no longer holds at low temperatures. Therefore we have to assume that there is no common intermediate but a small energy barrier between two different forms in the excited intermediate state involved during isomerization. The first ideas leading in this direction were given by Förster¹² and Zimmerman.⁹ Förster pointed out that the photoisomerization of stilbene might occur *via* a metastable excited state even if there would be two different forms divided by a small energy barrier. In more detail, Zimmerman first suggested an ordinary thermal isomerization in an electronic excited state in the case of azobenzenes.

Contrasting this perception, there is another model proposed by Schulte-Frohlinde¹³ and, rather similarly, by Dyck and McClure.¹⁴ This model only involves one common intermediate explaining the temperature dependence by a thermal activated transition from the excited singlets to the intermediate.

The purpose of this paper is to develop relations between quantum yields and the rates of the partial processes and to prove which type of mechanism satisfies the experimental results.

Derivation of Kinetic Relations

Model A Involving an Energy Barrier in the Intermediate.—This type of mechanism is outlined by processes 1-5 and 1'-5' at rates k_1, k_2, \dots and $k'_1,$

(11) H. Stegemeyer, *Z. Naturforsch.*, **16a**, 634 (1961).

(12) T. Förster, *Z. Elektrochem.*, **56**, 716 (1952).

(13) D. Schulte-Frohlinde, private discussion.

(14) H. Dyck and D. S. McClure, *J. Chem. Phys.*, **36**, 2326 (1962).

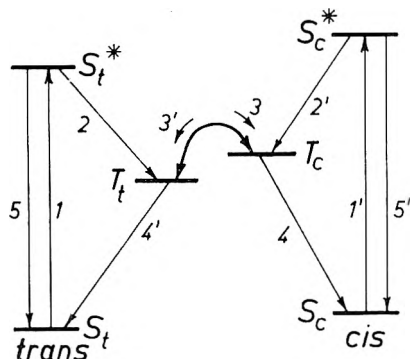
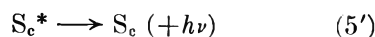
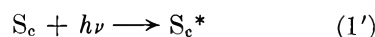
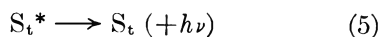
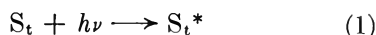


Fig. 1.—Supposed reaction scheme of photoisomerization, model A (explanations *cf.* text).

k_2', \dots , respectively. S_t represents the singlet ground state, S_t^* the first excited singlet state of a *trans* isomer. T_t means an intermediate state (perhaps a triplet) of a sterical configuration equal or similar to the *trans* form. The corresponding states of a *cis* isomer are denoted by S_c, S_c^* , and T_c , respectively (*cf.* Fig. 1).



In a first approximation, only processes 3 and 3' may be taken as dependent on temperature

$$k_3 = A \exp(-\Delta U_t/RT) \quad k_3' = A' \exp(-\Delta U_c/RT)$$

where A and A' denote the frequency factors and ΔU_t and ΔU_c the activation energies of processes 3 and 3', respectively.

The change of concentration in the ground state is given by

$$\frac{d}{dt} [S_t] = -k_1[S_t] + k_5[S_c] \quad (I)$$

The aim of the derivation is to represent the rate constant k_t of the *trans* \rightarrow *cis* isomerization in terms of k_1, k_2, \dots and to bring out a relation between k_t and q_t , on the other hand. The same holds for the *cis* \rightarrow *trans* direction.

Concerning the partial steps of model A (*cf.* Fig. 1) eq. I may be written as

$$\frac{d}{dt} [S_t] = -k_1[S_t] + k_5[S_t^*] + k_4'[T_t] \quad (Ia)$$

Similar equations can be obtained for the excited states of model A. In the photostationary state, each of these equations equals zero. Under this condition the concentrations in the excited states

during photoequilibrium may be represented in terms of $[S_t]$ and $[S_c]$, respectively.

Substituting the relations for $[S_t^*]$ and $[T_t]$ into Ia we obtain the following relations of the rates of isomerization in both directions

$$k_t = \frac{k_1 k_2 k_3 k_4}{(k_2 + k_5)[(k_3 + k_4')(k_3' + k_4) - k_3 k_3']} \quad (IIa)$$

$$k_c = \frac{k_1' k_2' k_3' k_4'}{(k_2' + k_5')[k_3 + k_4](k_3' + k_4) - k_3 k_3'} \quad (IIb)$$

Considering the definition of quantum yield there may be found a relation between k_t and q_t

$$q_t = \frac{d(N_t)/dt}{I_t^a} = \frac{V \frac{d}{dt} [S_t]}{I_t^a} = \frac{V k_t [S_t]}{I_t^a}$$

where $d(N_t)/dt$ means the number of *trans* molecules being converted into *cis* per unit of time. I_t^a , the number of quanta absorbed per unit of time by *trans* molecules in the volume V equals the number of *trans* molecules being raised from S_t to S_t^* per unit of time

$$I_t^a = \left(\frac{d}{dt} (N_t) \right)_{S_t \rightarrow S_t^*} = V \left(\frac{d}{dt} [S_t] \right)_{S_t \rightarrow S_t^*} = V k_1 [S_t]$$

Thus we can write

$$q_t = \frac{k_t}{k_1}$$

and a symmetrical expression for q_c .

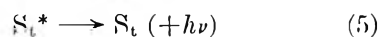
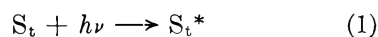
From IIa and IIb we get the equations for the quantum yields

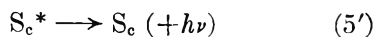
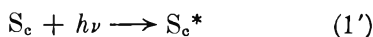
$$q_t = \frac{k_2}{k_2 + k_5} \times \frac{k_3 k_4}{k_3 k_4 + k_3' k_4' + k_4 k_4'} \quad (III)$$

$$q_c = \frac{k_2'}{k_2' + k_5'} \times \frac{k_3' k_4'}{k_3 k_4 + k_3' k_4' + k_4 k_4'} \quad (IV)$$

Model B Involving Only One Common Intermediate.—The reaction scheme of this model as proposed by Schulte-Frohlinde¹³ is shown by Fig. 2. $S_t^{*'}$ represents an energy level of the first excited singlet state in which a *trans* molecule possesses a small surplus energy (of vibration or rotation) equal to the activation energy ΔU_t of the thermal activated singlet \rightarrow triplet transition. A similar definition is given for $S_c^{*'}$. T means the common intermediate state. The other states are designed according to model A.

The following processes are involved in this model





Processes 1, 5, 1', and 5' are equal to those of model A. Only processes 3 and 3' are taken as thermal activated steps depending on temperature.

Concerning this model, eq. Ia had to be written as

$$\frac{d}{dt} [S_t] = -k_1[S_t] + k_5[S_t^*] + k_4'[T] \quad (\text{Va})$$

The relations for $[S_t^*]$ and $[T]$ may be obtained in a similar way as described for model A.

Considering $q_t = k_t/k_1$, we get the following equations of quantum yields

$$q_t = \frac{k_3}{k_3 + k_5} \times \frac{k_4}{k_4 + k_4'} \quad (\text{VI})$$

$$q_c = \frac{k_3'}{k_3' + k_5'} \times \frac{k_4'}{k_4 + k_4'} \quad (\text{VII})$$

Numerical Calculations and Discussion

The aim of this section is to prove which type of equation for quantum yield, either of model A or model B, satisfies the experimental curves of stilbene as a function of temperature as found by Malkin and Fischer.³

Model A.—The theoretical quantum yields in this model are given by two factors (*cf.* eq. III and IV). The first factor $F = k_2/(k_2 + k_5)$ or $F' = k_2'/(k_2' + k_5')$, respectively, concerns the efficiency of singlet → triplet transitions taken as independent of temperature.

As for *trans* → *cis* conversion, some conclusions about the absolute value of F may be derived from the absolute quantum yield $q_F = k_5/(k_2 + k_5)$ and decay constant $k_D = k_2 + k_5$ of fluorescence. Unfortunately, these values had not yet been measured for stilbene. In the case of *p*-dimethylaminocinnamonnitrile, Lippert and Lüder¹⁵ had found $q_F = 0.11 \pm 0.04$ and $k_D > 10^{10} \text{ sec.}^{-1}$ at photoequilibrium. From this they concluded another radiationless process to compete with the fluorescence emission. One possible type of competing reaction is the *trans* → *cis* conversion of the nitrile. From the values measured we can derive that $k_2 > k_5$. Therefore F will approximate unity at room temperature. Under these conditions F would not depend on temperature. However, there is also the radiationless $S_t^* \rightarrow S_t$ transition, which is caused by collisions with solvent molecules, to be taken into account. The evidence for this process may be seen from the relative quantum yield of fluorescence of stilbene depending on solvent¹ and on temperature.¹⁴ Considering this process too, F would increase with decreasing temperature, approaching unity at lower temperatures.

As the quantum yield of *trans* → *cis* isomerization usually is very high and the sum of q_t and q_c

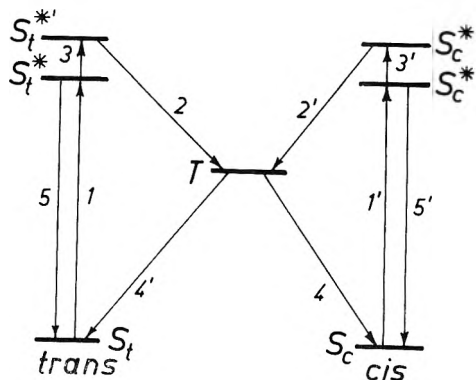


Fig. 2.—Supposed reaction scheme of photoisomerization, model B (explanations *cf.* text).

is near unity in stilbenes (*cf.* Table I and ref. 15) the strong decrease of q_F in *p*-dimethylaminocinnamonnitrile mainly seems to be due to $S_t^* \rightarrow T_t$ transition and less to collision processes. Thus F would not deviate far from unity even at room temperature.

As for *cis* → *trans* isomerization, no fluorescence had ever been observed in *cis*-stilbene. Due to the very short lifetime of S_c^* reported by Schulte-Frohlinde¹⁶ any deactivation by collision can be excluded. Thus, no reaction described by process 5' occurs ($k_5' = 0$) and F' equals unity.

Setting $F \rightarrow 1$ and $F' = 1$, eq. III and IV reduce to

$$q_t = \frac{k_3 k_4}{k_3 k_4 + k_3' k_4' + k_4 k_4'} \quad (\text{IIIa})$$

$$q_c = \frac{k_3' k_4'}{k_3 k_4 + k_3' k_4' + k_4 k_4'} \quad (\text{IVa})$$

where $k_3 = A \exp(-\Delta U_t/RT)$ and $k_3' = A' \exp(-\Delta U_c/RT)$.

At high temperatures, the rate of step 3 exceeds that of 4. Thus quenching to ground state (4) determines the rate of *trans* → *cis* isomerization. At low temperatures, $k_3 \ll k_4$, therefore thermal reaction 3 gets the rate-determining step. A similar consideration holds for *cis* → *trans* isomerization. If $k_3 \ll k_4$ and $k_3' \ll k_4'$ eq. IIIa and IVa reduce to

$$q_t = \frac{k_3}{k_4'} = \frac{A}{k_4'} e^{-\Delta U_t/RT} \quad (\text{IIIb})$$

$$q_c = \frac{k_3'}{k_4} = \frac{A'}{k_4} e^{-\Delta U_c/RT} \quad (\text{IVb})$$

Thus, from an Arrhenius plot of the quantum yields of stilbene as found by Malkin and Fischer,³ activation energies ΔU_t or ΔU_c can be estimated from the slope of the curves at low temperatures. Extrapolating the low temperature slope of the curves, from the ordinate intercept we may obtain the ratio A/k_4' or A'/k_4 , respectively (*cf.* eq. IIIb and IVb). However, the number of values measured at low temperatures are very few until now, so that this extrapolation method would be too erroneous. Setting $A = A'$ the ratios between fre-

(15) E. Lippert and W. Lüder, *J. Phys. Chem.*, **66**, 2430 (1962).

(16) D. Schulte-Frohlinde, *ibid.*, **66**, 2486 (1962).

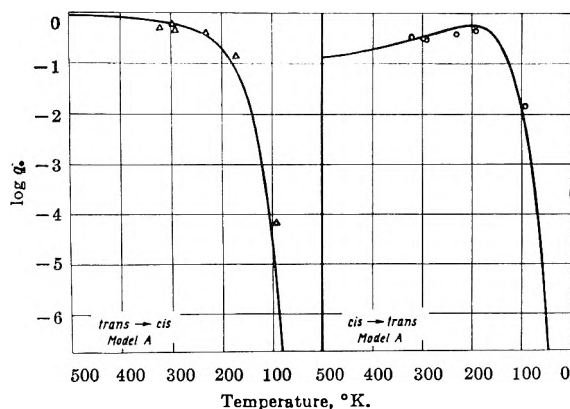


Fig. 3.—Logarithmic plot of quantum yields of stilbene vs. temperature. Theoretical curves by model A. Triangles, quantum yield *trans* → *cis*; circles, quantum yield *cis* → *trans* (values by Malkin and Fischer³).

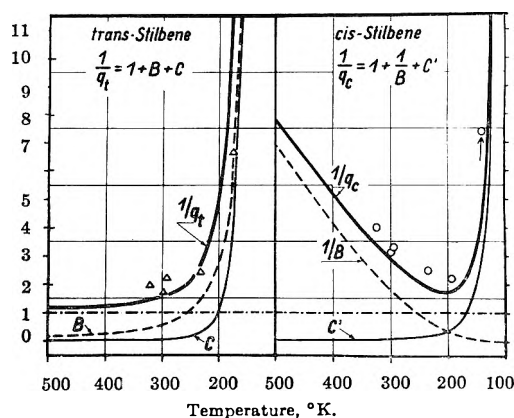


Fig. 4.—Reciprocal quantum yields of stilbene vs. temperature (explanation cf. text and eq. IIIc and IVc).

quency factors and decay constants and between k_4 and k_4' were chosen to give the best approximation of the experimental curves (cf. Table II). Notice that the absolute values of frequency factors and decay constants are arbitrary. Only the ratios of these values result from the experimental curves.

TABLE II

ACTIVATION ENERGIES, FREQUENCY FACTORS, AND TRIPLET DECAY CONSTANTS OF MODEL A

<i>trans</i> → <i>cis</i>	$\Delta U_t = 4$ kcal./mole
	$A = 2 \times 10^8$ sec. ⁻¹
	$k_4 = 5 \times 10^6$ sec. ⁻¹
<i>cis</i> → <i>trans</i>	$\Delta U_c = 2$ kcal./mole
	$A' = 2 \times 10^8$ sec. ⁻¹
	$k_4' = 1 \times 10^4$ sec. ⁻¹

Supposing the values given in Table II we get the theoretical curves from IIIa and IVa as shown by Fig. 3. It may be seen that the experimental values were satisfied by the theoretical curves. Even the maximum in the curve of q_c found by Malkin and Fischer³ is brought out by the theory.

The reason for this maximum can be understood better by looking at the curves of reciprocal quantum yields (cf. Fig. 4). From IIIa and IVa it follows that $1/q$ results from three terms (cf. IIIc and IVc).

$$\frac{1}{q_t} = 1 + \frac{k_3'k_4'}{k_3k_4} + \frac{k_4'}{k_3} = 1 + B + C \quad (\text{IIIc})$$

$$\frac{1}{q_c} = 1 + \frac{k_3k_4}{k_3'k_4'} + \frac{k_4}{k_3'} = 1 + \frac{1}{B} + C' \quad (\text{IVc})$$

The first term is unity in both cases. In the case of "*cis*" the second term is reciprocal as compared with "*trans*." The third one shows a similar slope for both cases. The curves for the second ($1/B$) and the third term (C') of "*cis*" cross each other, which brings about a minimum in the reciprocal of quantum yield and thus results in a maximum for the quantum yield itself.

In non-polar solvents, providing low concentrations, the sum of quantum yields in both directions has been found near unity at room temperature (cf. Table I). This fact follows from model A, for adding IIIa and IVa gives

$$q_t + q_c = \frac{k_3k_4 + k_3'k_4'}{k_3k_4 + k_3'k_4' + k_4k_4'} \quad (\text{VIII})$$

At higher temperatures, if $k_3 \gg k_4$ and $k_3' \gg k_4'$, the third term in the denominator of VIII can be neglected. Therefore, VIII becomes unity. From this it may be derived that there is no evidence for a common state to exist as long as the sum of quantum yields approaches unity only at high temperatures.

Schulte-Frohlinde¹⁶ had found the quantum yields of 4-nitro-4'-methoxystilbene in dilute solution to be independent of temperature in the range of 20 to 80°. As may be seen from Fig. 3 this result is in agreement with model A.

The temperature dependence of photoisomerization in liquid *cis*-stilbene¹¹ which we had measured in the range 25 to 100° does not contradict the conception given above. An increase of the triplet decay constants k_4 and k_4' with increasing concentration may be taken as a reasonable assumption. Thus, at high temperatures the third term C or C' in IIIc or IVc, respectively, would increase at higher temperatures as compared with dilute solutions. As the absolute values of C and C' also increase, the resulting curves for $1/q_t$ and $1/q_c$ will be determined mainly by the third terms, which brings about a shift to higher temperatures. This explains the possibility of finding a temperature dependence in liquid stilbene at temperatures above 25°. We cannot accept the explanation of our results given by Schulte-Frohlinde¹⁶ for the following reasons: An interaction between excited and non-excited molecules ought to decrease quantum yields with increasing temperatures. As to the short lifetime of S_c^* , a temperature dependence of *cis* → *trans* isomerization should not occur. Both assumptions contradict the experimental results. However, the activation energies measured in liquid phase¹¹ are higher than those estimated from the quantum yields found in dilute solution.³ As to association processes we had better consider single molecules in dilute solution.

Model B.—The equations of quantum yields derived from this model (cf. VI and VII) consist of two terms. The first one $k_3/(k_3 + k_3')$ or $k_3'/(k_3' +$

k_6') gives the efficiency of the singlet \rightarrow triplet transition taken as a thermal activated process.^{13,14} The second factor $w = k_4/(k_4 + k_4')$ or $w' = k_4'/(k_4 + k_4')$ describes the probability of a molecule falling from the triplet to the *cis* or *trans* form of the ground state, respectively. The sum $w + w'$ must be unity. Therefore, at high temperatures if $k_3 \gg k_5$ and $k_3' \gg k_6'$ the sum of quantum yields is expected to approach unity too. From the quantum yields of stilbene at 25°, $\lambda = 3130 \text{ \AA}$. (cf. Table I), we obtain by normalization $\Sigma q = 1$ the values of w and w' given in Table III.

As the common intermediate state is supposed by Schulte-Frohlinde^{13,16} to be a "triplet state both part of molecule twisted by 90 degrees" the values of w and w' will depend on the slope of the potential curve of the ground state near a distortion angle of 90°. The difference of energies between *cis*- and *trans*-stilbene in the ground state is very small as compared with the activation energy of thermal isomerization in the ground state.¹⁷ Thus, w and w' may be taken as independent of temperature. No absolute values of triplet decay constants k_4 and k_4' are required by this model. The activation energies of photoisomerization can be estimated from the experimental values in the same way as described for model A. Supposing the values of frequency factor A for process 3 and singlet decay constant k_6 as given by Dyck and McClure¹⁴ for *trans*-stilbene (cf. Table III, I), the calculated curve for $\log q_t$ (Fig. 5, I) does not satisfy the experimental values. We have to choose a higher value of A to get better agreement (see curve II, Fig. 5).

TABLE III

ACTIVATION ENERGIES, FREQUENCY FACTORS, AND SINGLET DECAY CONSTANTS OF MODEL B

<i>trans</i> \rightarrow <i>cis</i>	$\Delta U_t = 4 \text{ kcal./mole}$
	I ¹⁴ $A = 1 \times 10^{12} \text{ sec.}^{-1}$; $k_6 = 4 \times 10^8 \text{ sec.}^{-1}$
	II $A = 1 \times 10^{13} \text{ sec.}^{-1}$; $k_3 = 4 \times 10^8 \text{ sec.}^{-1}$
	$w = k_4/(k_4 + k_4') = 0.65$
<i>cis</i> \rightarrow <i>trans</i>	$\Delta U_c = 2 \text{ kcal./mole}$
	$A' = 1 \times 10^{12} \text{ sec.}^{-1}$; $k_6' = 1 \times 10^9 \text{ sec.}^{-1}$
	$w' = k_4'/(k_4 + k_4') = 0.35$

The values of A' and k_6' are chosen arbitrarily to yield a curve which satisfies the experimental values of quantum yields best.

From the theoretical curves given by model B (cf. Fig. 5) the following features may be concluded.

***trans* \rightarrow *cis* Conversion.**—The experimental values found by Malkin and Fischer³ would only be satisfied by model B providing a very large value of frequency factor A for the thermal singlet \rightarrow

(17) From calculations of normalized energies of formation in the gaseous state we get an energy difference between *cis*- and *trans*-stilbene in the ground state of 3.9 kcal./mole.¹ About the same value (3 kcal./mole) had been estimated by Kistiakowski and Smith¹⁸ from the temperature dependence of the equilibrium constant in the gaseous phase. The authors also determined an activation energy of 42.8 kcal./mole.

(18) G. B. Kistiakowski and W. R. Smith, *J. Am. Chem. Soc.*, **56**, 638 (1934).

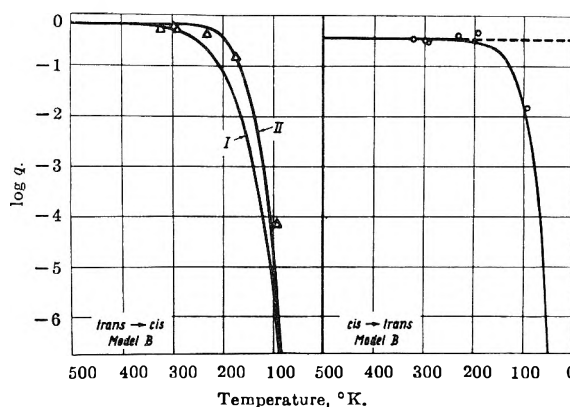


Fig. 5.—Logarithmic plot of quantum yields of stilbene vs. temperature. Theoretical curves by model B (*trans* \rightarrow *cis*: I and II result from different values of frequency factor A , cf. Table III). Design of experimental values: see Fig. 3.

triplet transition. From the molecular velocity at room temperature and from the dimensions of a stilbene molecule as well as from the number of solvent molecules per cm.³ we calculated a number of collisions of $10^{15} \text{ sec.}^{-1}$ for dilute solutions, which means an upper limit. Concerning a reasonable lifetime of 10^{-8} sec. in the S_1^* state, an upper limit of 10^7 collisions per second will be expected in the excited singlet state of *trans*-stilbene. According to the conception of model B the activation energies of the thermal activated singlet \rightarrow triplet transition can only be provided by thermal collisions of an S_1^* molecule with neighboring molecules. The frequency factor of such a process, however, is not allowed to exceed 10^7 sec.^{-1} for the reasons given above, but to satisfy the experimental values by model B we have to assume a frequency factor of $10^{13} \text{ sec.}^{-1}$. Though the estimations of collision numbers given above are only approximate, the difference of six orders of magnitude seems to be too large a discrepancy.

Notice that in the thermal $T_t \rightarrow T_c$ isomerization of model A a frequency factor of 10^7 sec.^{-1} or less can be brought into agreement with the experimental curves. Also such a value can be explained using the theory because of the longer lifetime of the intermediate state.

***cis* \rightarrow *trans* Conversion.**—Even if the theoretical curve for q_c satisfies the experimental values at high temperatures as well as at low ones there is no possibility of explaining the maximum in the curve $\log q_c = f(T)$ found by Malkin and Fischer³ (cf. Fig. 5). This also follows from equation VII. However, the calculation of the curve $\log q_c = f(T)$ from the arbitrary values of A' and k_6' is quite unreasonable because Schulte-Frohlinde¹⁶ had found considerable evidence for the S_0^* being very short-lived. It cannot be understood how a molecule might get any of the activation energy required by a thermal activated $S \rightarrow T$ transition during this short lifetime. Therefore, in view of model B, $\log q_c$ ought to be independent of temperature as shown by the dashed line in Fig. 5.

As to the *trans* \rightarrow *cis* isomerization, Dyck and McClure¹⁴ had derived some interesting conclusions from the temperature dependence of fluorescence efficiency of *trans*-stilbene which led them to a con-

ception similar to that of model B. Note that the measurements of relative fluorescence efficiency had been carried out under non-photostationary conditions. The conclusions given in our paper, however, concern the photoequilibrium of isomers where $d[S_t^*]/dt = 0$. Further, there might occur a thermal quenching $S_t^* \rightarrow S_t$ by solvent molecules competing with fluorescence emission which had not been taken into account by Dyck and McClure. The evidence for this process may be seen from the dependence of fluorescence efficiency on solvents.¹ We feel that only measurements of the absolute quantum yield of fluorescence as a function of temperature performed at photoequilibrium would help to decide if any thermally activated $S \rightarrow T$ transition takes place in photoisomerization. As to model B, quantum yields should increase at low temperatures with decreasing wave length of irradiating light but this effect never has been found.³

Conclusions

The experimental results on photochemical *cis* \rightleftharpoons *trans* isomerization of stilbene available hitherto seem to be satisfied better by model A than by model B. Even the results of Malkin and Fischer³ on azo compounds are in agreement with the mechanism of model A, as may be seen, for example, in 1-phenylazonaphthalene.³ In azo compounds, the activation energy for $T_c \rightarrow T_t$ conversion seems to be very small.

No special conception is necessary in model A

about the type of electronic excited intermediate state. Note that Zimmerman and co-workers⁹ suggesting a thermal isomerization in an excited singlet state already had pointed out qualitatively the main features involved in model A.

However, in order to decide exactly which type of mechanism is involved in photoisomerization, a conclusive proof might be obtained only from more extensive information about the triplet state. Possibly, measurements of the phosphorescent lifetime of *cis*-stilbene¹⁹ may indicate the order of magnitude of k_{11} .

Acknowledgments.—The author gratefully acknowledges the support of the U. S. Army Research Office (Durham) for his participation in the International Symposium on "Reversible Photochemical Processes" held at Duke University, Durham, N.C., April 16–18, 1962. The helpful criticism of Professor Dr. E. Kuss also is greatly appreciated, as well as the interesting discussions of Dr. E. Fischer and Professor Dr. G. Zimmerman.

(19) The phosphorescence of *cis*-stilbene reported by Lewis and Kasha²⁰ and, in more detail, by Nauman²¹ really is due to phenanthrene.²² Recently, we observed a strong blue luminescence of *cis*-stilbene in rigid solvents at -194° mainly in the region of about 4700 Å. This effect is not exactly due to phenanthrene or other impurities as shown by special measurements. As the emission vanishes in fluid solvents even at -78° a phosphorescence emission is supposed.

(20) G. N. Lewis and M. Kasha, *J. Am. Chem. Soc.*, **66**, 2100 (1944).

(21) R. V. Nauman, Dissertation, University of California, 1947.

(22) The author wishes to thank Dr. Zander, Castrop-Rauxel, for referring him to the paper of Nauman.²¹

LIGHT-INDUCED ISOMERIZATION OF *o*-NITROTOLUENE IN WATER SOLUTION

BY GUNNAR WETTERMARK¹

Pioneering Research Division, Quartermaster Research and Engineering Center, Natick, Mass.

Received May 25, 1962

If *o*-nitrotoluene in water is exposed to ultraviolet light, a short-lived species is formed which has a strong absorption band in the blue and near ultraviolet regions of the spectrum. Two different absorption spectra of the species are given, interpreted as the absorption spectrum of the acid form and the anionic form of the species, respectively. The decay follows that of a first-order reaction with a rate constant of $0.76 \times 10^2 \text{ sec.}^{-1}$ for the acid and 1.0 sec.^{-1} for the anion.

Introduction

It recently was found in this Laboratory that *o*-nitrotoluene in solution on exposure to light undergoes a transformation to a short-lived colored state.² The decay of this colored state was found to follow the kinetics of a first-order reaction. In ethanol at room temperature ($24 \pm 1^\circ$) the half-life time was evaluated to be 5 msec.

Photochromism has been detected in compounds which are derivatives of *o*-nitrotoluene. Tschitschibabin and co-workers³ discovered that crystals of 2-(2',4'-dinitrobenzyl)-pyridine turn blue when

exposed to light and revert to the original colorless state in the dark. The solid has been extensively investigated over the last two decades^{4–7} but it has been found only recently by employing low temperatures that the color change can be brought about in solution.⁸ Also by employing low temperatures it has been found that other compounds closely related structurally, namely, 4-(2',4'-dinitrobenzyl)-pyridine⁹ and 2-(2'-nitro-4'-cyano-

(4) (a) K. Schofield, *J. Chem. Soc.*, 2408 (1949); (b) A. J. Nunn and K. Schofield, *ibid.*, 583 (1952).

(5) W. C. Clark and G. F. Lothian, *Trans. Faraday Soc.*, **54**, 1790 (1958).

(6) H. S. Gutowsky and R. L. Rutledge, *J. Chem. Phys.*, **29**, 1183 (1958).

(7) B. M. Kuindshi, L. A. Igonin, Z. P. Gribova, and A. N. Shabadash, *Optics and Spectroscopy*, **12**, No. 2 (1962).

(8) R. Hardwick, H. S. Mosher, and P. Passalunghi, *Trans. Faraday Soc.*, **56**, 44 (1960).

(1) National Academy of Sciences–National Research Council Visiting Scientists Research Associate and Guest of the Massachusetts Institute of Technology associated with Prof. L. J. Heidt of the Department of Chemistry.

(2) G. Wettermark, *Nature*, **194**, 677 (1962).

(3) A. E. Tschitschibabin, B. M. Kuindshi, and S. W. Benewolenskaja, *Ber.*, **58**, 1580 (1925).

benzyl)-pyridine¹⁰ are phototropic in solution as well.

Preliminary experiments in this Laboratory using flash photolysis have indicated that a variety of compounds, all being derivatives of *o*-nitrotoluene, are photochromic.² A closer study of the color change of *o*-nitrotoluene therefore has been undertaken and is reported in this article.

Experimental

Flash Apparatus.—A description of the flash apparatus will be given shortly by L. Lindqvist, Institute of Physical Chemistry, Uppsala University. Only some data pertinent to the actual experiments are given here. Briefly an electrical energy of 1800 joules (9 μ f., 20 kv.) was discharged through four straight quartz lamps symmetrically arranged around a cylindrical reaction vessel giving a flash duration of 5 μ sec. ($1/e$ time). The reaction vessel had an optical path length of 20 cm. and was provided with an outer filter jacket which contained a 0.5 cm. layer of 50% aqueous acetic acid. This filter absorbed all light of wave lengths shorter than approximately 250 $m\mu$.

The light absorption changes in the system were recorded by means of a single beam absorption spectrophotometer. The monitoring lamp was a zirconium lamp (Sylvania K 100 Q) powered by a large bank of storage batteries. Other essential parts of the spectrophotometer consisted of a Bausch & Lomb small grating monochromator, an E.M.I. 9552B photomultiplier tube, and a Tektronix 535A oscilloscope. The slit width of the monochromator was kept constant (0.5 mm.), corresponding to a spectral band width of 3 $m\mu$. Various Corning color filters were used to cut off the secondary pass band from the grating of the monochromator. The anode current from the photomultiplier was amplified in a cathode follower mounted directly on the photomultiplier tube. The over-all circuit had a time resolution of about 5 μ sec. in the present experiments.

All experiments were carried out at room temperature ($24 \pm 1^\circ$).

Solutions.—*o*-Nitrotoluene (Matheson Coleman & Bell) was recrystallized from absolute ethanol seven times. A simple apparatus¹¹ for low temperature recrystallization was used with Dry Ice and alcohol in the cooling bath. Further purification was obtained by passing an ethanol solution of the sample through a 60 cm. long column filled with aluminum oxide and collecting the middle fraction.

The concentration of *o*-nitrotoluene in the test solutions was 2×10^{-4} *M*. *o*-Nitrotoluene was mixed with absolute ethanol and diluted with aqueous 0.1 *N* NaOH and 1 *N* HCl, respectively. The final alcohol concentration amounted to 0.5% by volume.

Deaerating of Solutions.—Before each experiment the solution was carefully deaerated. The technique employed was to freeze, evacuate, and melt three times and to shake the solution in the presence of argon (Aircro for aluminum welding), then to freeze, evacuate, and melt three more times. The flask used for the deaeration was connected to the reaction vessel through a ground standard taper joint in such a way that the solution could be transferred without coming in contact with the stopcock grease.

Results and Discussion

Flashing a solution of *o*-nitrotoluene revealed that short-lived species (A^*) are formed which absorb strongly in the blue and near ultraviolet regions of the spectrum. A stable photo product (B) also is formed, as could be seen by a permanent change in the optical transmission of the solution. Scanning the spectrum over the region 300 to 600 $m\mu$ showed that the photo product (B) had an absorption band in the same region as A^* . Over the wave length region investigated the permanent (irreversible) increase in optical density on exposure

(9) H. S. Mosher, C. Souers, and R. Hardwick, *J. Chem. Phys.*, **32**, 1888 (1960).

(10) J. A. Sousa and J. Weinstein, *J. Org. Chem.*, **27**, 3155 (1962).

(11) A. L. Bluhm, *J. Chem. Educ.*, **35**, 200 (1958).

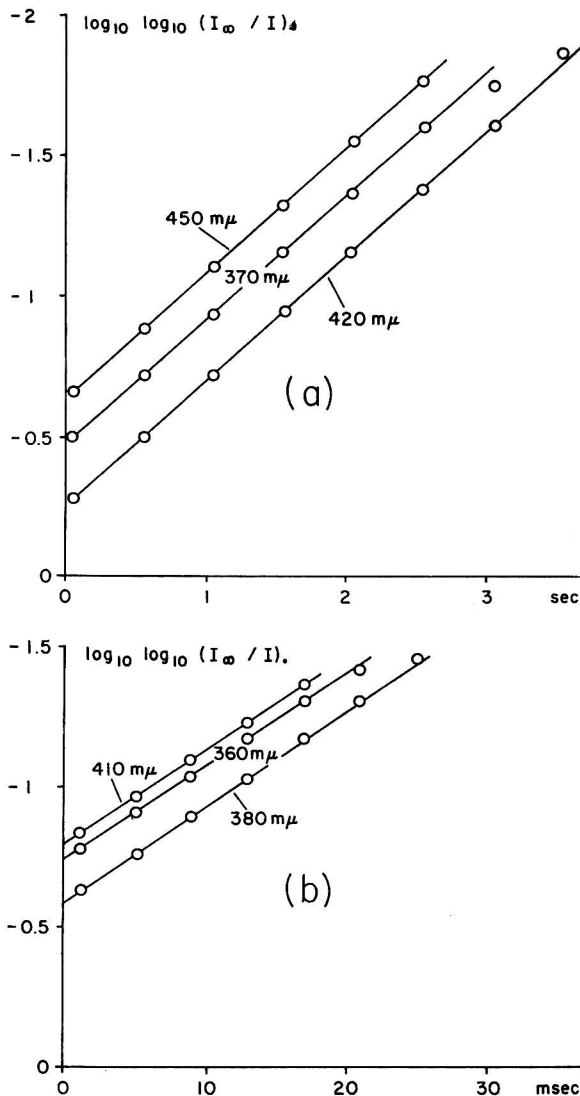


Fig. 1.—Plots of $\log \log (I_\infty / I)$ as a function of time for various wave lengths. (I is the intensity of the light transmitted through the solution during the fading of the short-lived species and I_∞ the intensity after completion of the reaction.) (a) *o*-Nitrotoluene in 0.1 *N* NaOH; (b) *o*-nitrotoluene in 1 *N* HCl.

to a flash was less than 4% of the reversible change. When the same solution was flashed several times the response gradually weakened due to the accumulation of photo product. No effect on the rate of decay of A^* was observed even after extensive flashing (20–30 flashes). After about 20 flashes the degree of conversion of *o*-nitrotoluene into A^* was about half of that which was observed at the first flash. The portion of *o*-nitrotoluene converted to A^* in a flash could not be determined from these experiments.

The question arises whether the decay reaction of A^* constitutes the transformation of A^* into the new species B or the decay back to the original *o*-nitrotoluene (A) (or both).

As the photo product (B) has an absorption band in the same region as A^* it was impossible to measure the rate of formation of B by isolating a wave length where only B absorbed the light.

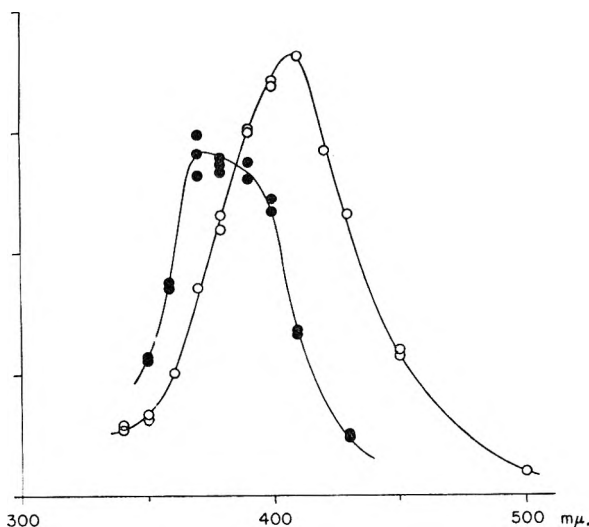


Fig. 2.—Absorption for *o*-nitrotoluene in 0.1 *N* NaOH (○) and 1 *N* HCl (●) after exposure to ultraviolet light. The ordinate is proportional to optical density with different proportionality constants for the two solutions.

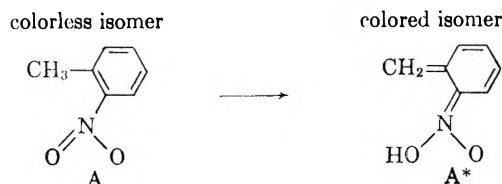
The available information on the system might support the assumption that A^* decays predominantly to A , that is, the over-all process is essentially reversible.

If A^* decays back to A in a first-order reaction a straight line should be obtained if $\log \log (I_\infty/I)$ is plotted as a function of time. (I symbolizes the intensity of the light transmitted through the solution during the decay of A^* and I_∞ the intensity after completion of the reaction.) In fact when such plots are made straight lines are obtained. All plots were made from the first or the second flashing of a fresh solution. Figure 1 gives some of these plots for different monitoring wave lengths.

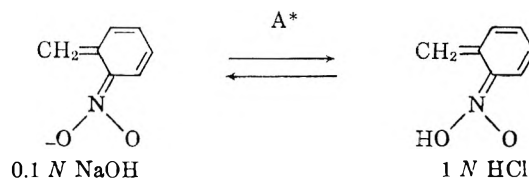
From the plots of $\log \log (I_\infty/I)$ vs. time at different wave lengths the absorption spectra of A^* in 0.1 *N* NaOH and in 1 *N* HCl could be calculated and are given in Fig. 2. It has been visualized³⁻¹² that the photochromism of 2-(2',4'-dinitrobenzyl)-pyridine is due to a proton transfer from the

(12) G. Wettermark, *J. Am. Chem. Soc.*, **84**, 3658 (1962).

$-\text{CH}_2-$ group to the 2'-nitro group together with a change in the structure of the aromatic ring to a quinoid configuration. It seems reasonable, therefore, to propose that the formation of A^* in *o*-nitrotoluene is described by the reaction



The colored isomer is probably a relatively strong acid. It is, however, reasonable to believe that in 1 *N* HCl mostly the acid is present. In 0.1 *N* NaOH the colored isomer should exist mostly as the anion.



One might thus conclude that the two spectra given in Fig. 2 are the spectrum of the anion (○) and the spectrum of the acid (●).

Table I gives the rate constants for the fading of A^* in 0.1 *N* NaOH and in 1 *N* HCl visualized as the fading of the anion and the acid, respectively. The data represent mean values obtained from all the plots of $\log \log (I_\infty/I)$ as a function of time for the different wave lengths (compare Fig. 1).

TABLE I
RATE CONSTANT FOR THE FIRST-ORDER FADING REACTION OF A^* AT ROOM TEMPERATURE ($24 \pm 1^\circ$)

Solution	Rate constant (sec. ⁻¹)
<i>o</i> -Nitrotoluene in 0.1 <i>N</i> NaOH (anion)	1.0
<i>o</i> -Nitrotoluene in 1 <i>N</i> HCl (acid)	0.76×10^2

Acknowledgment.—The author wishes to express his sincere thanks to Dr. S. D. Bailey, Chief of this Laboratory, who helped make this work possible.

THIONINE-SENSITIZED PHOTOPOLYMERIZATION OF ACRYLAMIDE¹

BY A. SHEPP, S. CHABEREK, AND R. MACNEIL

Technical Operations Research, Burlington, Massachusetts

Received May 25, 1962

Visible light excitation in the 5900 Å. band of thionine induces the free radical polymerization of acrylamide in aqueous solution at pH 8.4. In oxygen-free solution (oxygen reduced to 0.005 p.p.m. by a lengthy dye-scrubbed helium purge) there is no induction period before the onset of polymerization and the simultaneous fading of the dye. Similar behavior was observed using methylene blue and proflavin. If the solution is made more acidic than pH 8.4, polymerization does not occur. If oxygen is added to the solution in the range 1.5 to 6 p.p.m., there is a lengthy induction period during which there is no dye fading and no polymerization. At the conclusion of the induction period, both dye fading and polymerization proceed, but at inhibited rate compared to the oxygen-free rates. If H₂O₂ is added to the oxygen-free reactant solution at a 1:1 ratio to thionine, the polymerization and dye fading proceed at inhibited rate after a short induction period. At higher concentrations of H₂O₂ (4:1 of thionine) the induction period is removed, and at great excess of H₂O₂, the inhibition of rates is removed. Although it is now recognized that the excited thionine species is probably the triplet, we give evidence to show that the triplet does not appear to be the polymerization-initiating radical. The possibility of radical formation by hydrogen abstraction from monomer appears unlikely on energetic grounds. We postulate that the radical initiator is the semiquinone form of thionine (ST) formed by the reductive couple $\text{OH}^- \rightarrow \text{OH}\cdot + e$, whose E^0 at this pH is comparable to E^0 for the couple $\text{T}^* \rightarrow \text{ST} + e$. A kinetic mechanism is postulated which explains the broad rate behavior of thionine fading and polymer formation in oxygen-free solution.

Introduction

In our study of visible light-induced polymerization, we have found that the absorption of light by thionine in oxygen-free solutions at alkaline pH can lead directly to highly efficient vinyl polymerization. Previous literature on visible light-induced polymerization covers three areas. In one, there are reports of visible light-induced polymerization at very low yields. Koizumi, Watanabe, and Kuroda² noted the augmentation of styrene polymerization at 60° by light-excited pinacyanol iodide. Uri³ found that light-excited chlorophyll apparently photopolymerized methyl methacrylate at very low efficiency. At about the same time, Krasnovski and Umkrihina⁴ reported that light-excited chlorophyll would induce the polymerization of ascorbic and dihydroxymaleic acids.

In a second area of research, there are reports of the ultraviolet excitation of anthracene to the triplet state by flash photolysis⁵ which induces polymerization of styrene. Presumably, it is the triplet radical which is the chain initiator. This is not to be confused with the use of ultraviolet light to excite thermal sensitizers, such as AIBN, or peroxides, to form radicals which induce polymerization.

In a third area, Oster and co-workers⁶⁻⁸ have demonstrated that visible light excitation of dye-electron donor systems can induce vinyl polymerization. In particular, Oster, Oster, and Prati⁸ gave a very detailed study of an efficient visible light-induced polymerization of acrylamide by riboflavin. In this work it has been emphasized that an electron donor (a weak reducing agent, EDTA,

etc.) must be present to cause dye reduction and that some trace of oxygen also is needed. In more recent work on dye reduction,⁹ the need for electron donors in visible light-induced polymerization has been re-emphasized. In all of this work there is an induction period before the onset of polymerization associated with removal of oxygen from the system.

The work described in this paper shows that the visible light excitation of thionine in oxygen-free aqueous solution at alkaline pH causes the highly efficient polymerization of acrylamide directly without any induction period. The addition of oxygen does cause an induction period and then inhibition of the reaction. These experiments have been done with very pure thionine and are anaerobic to the level of ≈ 0.005 p.p.m. of oxygen. Three possible mechanisms for the initiation of the photopolymerization are the direct initiation by the excited triplet-state radical, the formation of a dye radical by hydrogen abstraction from the monomer, and the interaction of dye plus hydroxide ion to form the thionine semiquinone and hydroxyl radical. The last possibility appears most likely, on the basis of our experimental evidence.

Experimental

Thionine.—Thionine samples which are certified by the Biological Stain Commission are highly impure. Chromatography of this material on alumina allows the separation of five major components of which thionine represents only about 60% of the total dye. We have purified thionine by two recrystallizations from water followed by chromatography on alumina using chloroform as eluting agent. Material prepared in this way shows no impurities upon subsequent repetition of the chromatographic step. The molecular coefficient of this purified thionine at 5900 Å. is 6.2×10^4 l. per mole. This is the grade of thionine with which our experimental work was done.

Acrylamide.—Acrylamide supplied by the American Cyanamid Company was used without further purification. In most experiments the concentration of monomer used was 5% (0.74 M). To analyze for polymer during the reaction, 5-ml. aliquots of the reactant solution were removed and injected into 100 ml. of methanol. The precipitated polymer was filtered, dried, and weighed. The average molecular weight of selected polymer samples was determined

(1) This work was supported by a contract from the Aeronautical Systems Division, Wright-Patterson Air Force Base, USAF, Contract No. AF 33(616)-7092, J. Pecqueux, initiator.

(2) M. Koizumi, A. Watanabe, and Z. Kuroda, *Nature*, **175**, 770 (1955).

(3) N. Uri, *J. Am. Chem. Soc.*, **74**, 5808 (1952).

(4) A. Krasnovski and A. Umkrihina, *Dokl. Akad. Nauk SSSR*, **104**, 882 (1955).

(5) (a) V. Sten-Andersen and R. Norrish, *Proc. Roy. Soc. (London)*, **A251**, 1 (1959); (b) R. Norrish and J. Simons, *ibid.*, **A251**, 4 (1959).

(6) G. Oster, *Nature*, **173**, 300 (1954).

(7) G. Oster, *Phot. Eng.*, **4**, 173 (1953).

(8) G. K. Oster, G. Oster, and G. Prati, *J. Am. Chem. Soc.*, **79**, 595 (1957).

(9) B. Holmström and G. Oster, *ibid.*, **83**, 1867 (1961).

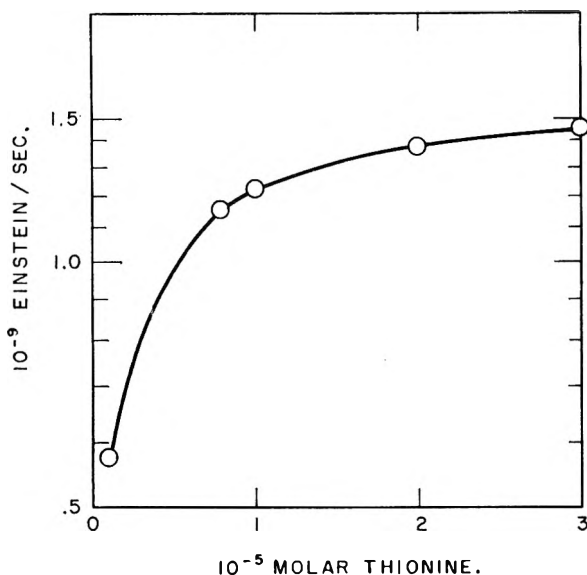
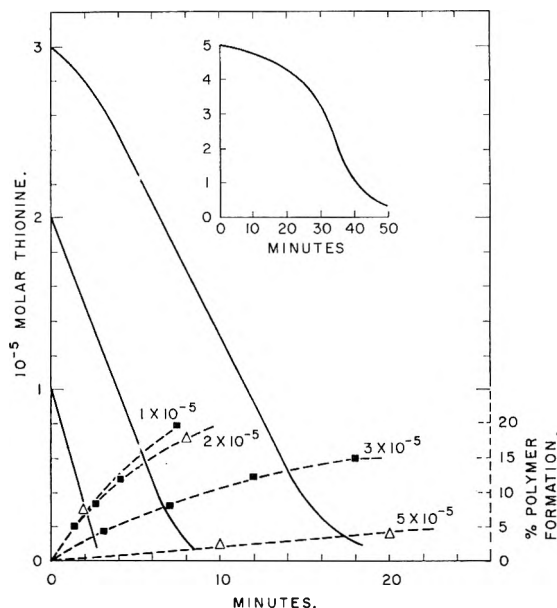


Fig. 1.—Energy absorption calibration curve.

Fig. 2.—Photoreaction of thionine in 5% acrylamide at pH 8.4, O_2 10^{-7} M.

by viscosity measurements¹⁰ and in all cases was found to be within 10% of 10^6 .

Oxygen Determination.—Because of the sampling and purging procedures needed in our optical cell, we were not able to effect oxygen removal from our solutions by pumping and freezing cycles. Therefore, a gas purge was used, and consequently an accurate method for oxygen analysis was required. Standard colorimetric tests were used to determine low oxygen concentrations. The recent test described by Buchoff and Ingber,¹¹ using carmine indigo in alkaline solution, was the most effective. The range of oxygen concentrations covered by this test is from 0.005 to 0.16 p.p.m. (1.5×10^{-7} to 0.5×10^{-6} M). We have found that the oxygen concentration of 100 ml. of water is reduced to the order of 0.005 p.p.m. after purging with a rapid flow of helium for 2 hr. Best results were obtained when the helium gas was prescrubbed through a leuco thionine solution, before being bubbled into the reaction cell. This 2-hr. purge

procedure was used to prepare all "oxygen-free" solutions. To prepare standard oxygen solutions, water was saturated with oxygen and the Scott¹² values for the concentrations were used. Dilute oxygen solutions were prepared by the addition of stock solution to oxygen-free water.

Experimental Details.—The light source was a 300-watt stabilized projection lamp run at 80 volts. The reaction cell was an optical glass rectangular cell, 5.5 cm. per side, fitted with a tight lucite cover through which purge and syringe injection tubes were fitted. The initial volume of reactant solutions was held constant at 100 ml. The thionine concentration was measured photometrically as a function of time during the reaction, using a Beckman Quartz DU-monochromator set at the thionine absorption band of 5900 Å. The transmitted light was measured using an RCA 6199 photomultiplier whose output was displayed on a Brown recorder.

In a conventional kinetic study in solution photochemistry, one tries to irradiate dilute dye solutions uniformly over the face of a cell which has a short path length. In this way uniformity of excited species is obtained throughout the solution, and stirring of the solution is not necessary. In our experiments the key problem was detection of small quantities of polymer. For viscosity reasons, 5% monomer solution was the most concentrated with which we could work. With fairly intense illumination it was found that dye concentrations in the range $1-3 \times 10^{-5}$ M were needed to produce polymer conversions of 5-20% within a reasonable time. Even so, using 5-ml. aliquot samples from the 100-ml. reaction solution, these conversions would produce only 12.5 to 50 mg. of polymer. The need for 100 ml. of solution led us to use a cell with a 5.5-cm. light path even though 90% of the incident light was absorbed within 1 cm. of path length at the initial dye concentrations used. This required continual fast stirring of the reaction solution during the experiment, which was done with a "Teflon" covered bar magnet. Consequently, the detection beam of light used to determine thionine concentration had to be transmitted across the top of the cell to avoid disturbance from the stirrer. Thionine in the range $1-3 \times 10^{-5}$ M shows some dimerization,¹³ and consequently some deviation from Beer's law at these concentrations. Furthermore, since we desired to determine the extent of dye fading as a function of polymer formation, the reaction was run to high percentages of thionine conversion. All of these effects were detrimental to a careful kinetic analysis but were found necessary in order to determine the over-all parameters of the reaction.

All experiments were done at room temperature in 0.1 M phosphate buffer (pH 8.4). Our experimental procedure was to calibrate our recording instrument against four thionine concentrations immediately prior to an experiment. To start an oxygen-free run, buffered water in the cell was purged with helium for 2 hr., the oxygen-free thionine stock solution was injected, the stirrer was started, and, at time zero, the illumination was started. The thionine concentration was recorded on the chart as a function of time, and sample removal for polymer analysis was made periodically during the run.

The output of the lamp and the light absorption by the thionine solution were measured with a selenium photocell which had been calibrated in meter candles/cm.² against a standard NBS 500-watt candle power lamp. One meter candle is equal to (146./0.75) milliwatts per cm.² at 5900 Å. and from this, conversion to einsteins per second per cm.² at 5900 Å. is straightforward. Figure 1 shows a calibration of einsteins absorbed per second by the entire reaction solution as a function of thionine concentration. Therefore, the molar rates of thionine fading presented below can be converted to einsteins absorbed by the use of Fig. 1.

Results

Polymerization in Oxygen-Free Solutions.—Figure 2 shows the results of photopolymerization of 5% acrylamide at pH 8.4 at oxygen levels about 10^{-7} M (oxygen-free), using four different initial concentrations of thionine: 1, 2, 3, and 5×10^{-5}

(10) "Chemistry of Acrylamide," Am. Cyanamid Co., Petrochem Dept., New York, N. Y., 1957.

(11) L. S. Buchoff and N. M. Ingber, U. S. Patent 2,967,092, Jan. 3, 1961.

(12) "Scott's Standard Method of Chemical Analysis," N. H. Furman, Ed., D. Van Nostrand Co., Inc., New York, N. Y., 1950, 5th Ed.

(13) E. Rabinowitch and L. Epstein, *J. Am. Chem. Soc.*, **63**, 69 (1941).

M . In all cases, polymer proceeds to yields in the 5–20% range in a matter of minutes without any measurable induction period and with the simultaneous rapid fading of thionine. The rates of thionine fading and of polymer formation vary inversely with the thionine concentration. In general, the rates of polymerization are linear, and from the light intensity calibration, the quantum yield can be calculated. Let this quantum yield for polymerization, ϕ_p , be defined by $\phi_p = \bar{M}_p/E_a$, where \bar{M}_p is the average number of moles of polymer formed, and E_a is the einsteins absorbed. One can compute \bar{M}_p from the per cent polymer formation by the equation

$$\bar{M}_p = (\% \text{ polymer formation})(5/100)/10^6$$

where 10^6 is taken as the average polymer molecular weight. The quantum yield of polymer formation calculated in this manner is plotted in Fig. 3 and is seen to vary from 0.27 at $1 \times 10^{-5} M$ thionine to 0.02 at $5 \times 10^{-5} M$ thionine. One can relate the quantum yield of monomer removal ϕ_m to ϕ_p , by the equation $\phi_m = \phi_p \times 10^6/71$, from which ϕ_m is seen to vary from about 30 to 4000 over the range studied. The rates of thionine fading go through an initial linear portion and then fall to a lower steady-state value. Complications due to high dye concentration, long path length, and stirring effects may contribute to this behavior. The quantum yield for the initial rate of thionine fading, $\phi_{th}(i)$, may be defined as $\phi_{th}(i) = (\Delta M_{th}/E_a)$, where ΔM_{th} is the actual number of moles of thionine faded over a time increment in which E_a is measured. Values for $\phi_{th}(i)$ also are plotted in Fig. 3 and are seen to be in the range of 0.5 at $1 \times 10^{-5} M$ thionine to 0.05 at $5 \times 10^{-5} M$ thionine.

In Fig. 4, we show the rates of polymerization and thionine fading at two other initial monomer concentrations: 2.5% (0.35 M) and 1.25% (0.18 M) each run in oxygen-free solution at $3 \times 10^{-5} M$ thionine at pH 8.4. The comparable curves at 5% monomer taken from Fig. 2 are included in Fig. 4 for comparison. One observes a decrease in the rate of polymerization at 2.5%; the quantum yield ϕ_p falls from 0.08 at 5% monomer to 0.01 at 2.5% monomer. At 1.25% monomer concentrations, no polymer formation was detected throughout the run. Assuming the detectability of 1.0 mg. of polymer in a 5-ml. aliquot, the maximum percentage of polymer formation which may have occurred would have been about 1.6%. The rate of fading of thionine is seen to vary inversely with the monomer concentration.

In Fig. 5, we show the results of photopolymerization of 5% monomer solutions at 1×10^{-5} and $2 \times 10^{-5} M$ thionine in which the light intensity was attenuated to $0.3I_0$ (where I_0 is the light intensity of Fig. 2 and 4) by placing a 0.5 neutral density filter in the light path. The comparable curves at intensity I_0 taken from Fig. 2 are included in Fig. 5 for reference. It is seen that the initial rates of dye fading are roughly proportional to the light intensity, while the rates of polymerization appear to vary less strongly, more as the square root of the light intensity.

At the conclusion of these irradiation experi-

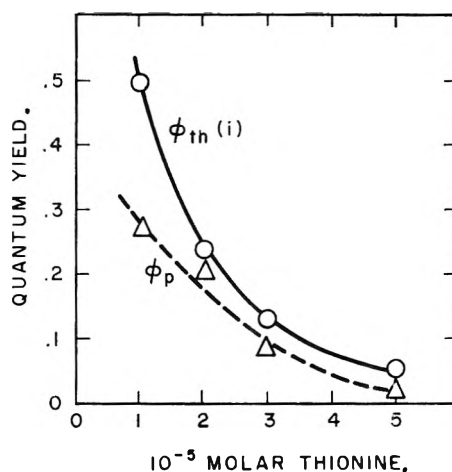


Fig. 3.—Quantum yields for initial thionine fading $\phi_{th}(i)$, and polymer formation ϕ_p , oxygen-free solutions at pH 8.4.

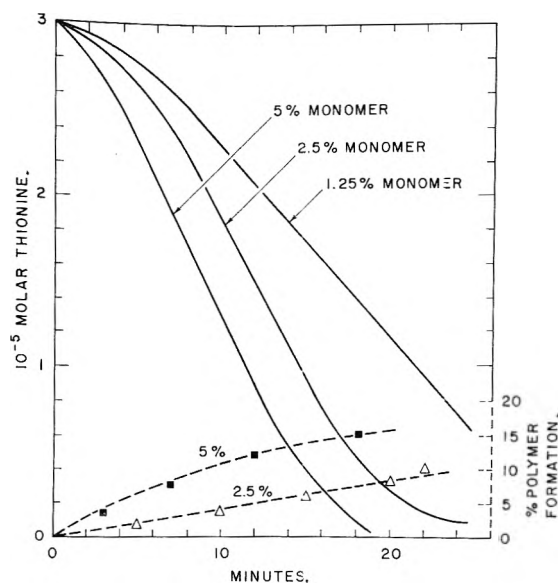


Fig. 4.—Polymerization and thionine fading as a function of monomer concentration, O_2 -free, pH 8.4.

ments, oxygen was bubbled into the reaction solution and, in general, a regeneration of up to 50% of the original thionine color would appear. Since the reaction had by this time been carried to a high degree of completion, quantitative data were not taken on this observation.

To determine the effect of pH on this reaction, a solution of 5% monomer at $2 \times 10^{-5} M$ thionine was adjusted to pH 6.4 and then irradiated. It was found that the rate of thionine fading was greatly retarded; the thionine faded to $1 \times 10^{-5} M$ in 25 min. and faded to $1 \times 10^{-6} M$ in 40 min. (compared to 4 and 7 min., respectively, at pH 8.4) without the formation of any detectable polymer. Another solution under the same concentration conditions was adjusted to pH 4.5 and irradiated. In this case, no dye fading and no polymerization occurred after 60 min. We believe this behavior is related to the pH dependence of the oxidation-reduction potentials involved.

Two other dyes, methylene blue and proflavin, were tested for photopolymerization activity in 5%

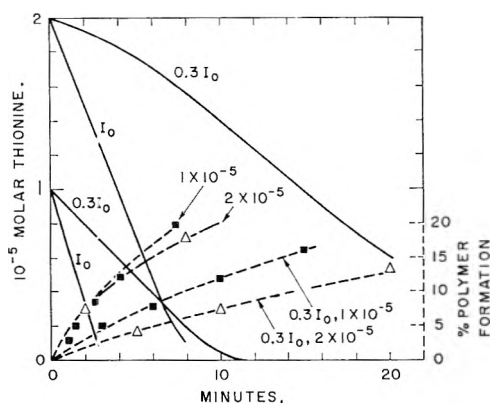


Fig. 5.—Polymerization and thionine fading as a function of light intensity (I_0), O_2 -free, pH 8.4.

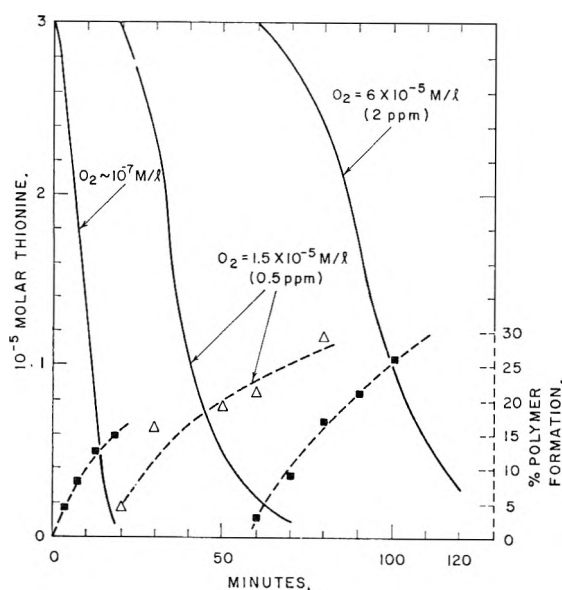


Fig. 6.—Oxygen inhibition of polymerization and of dye fading at pH 8.4.

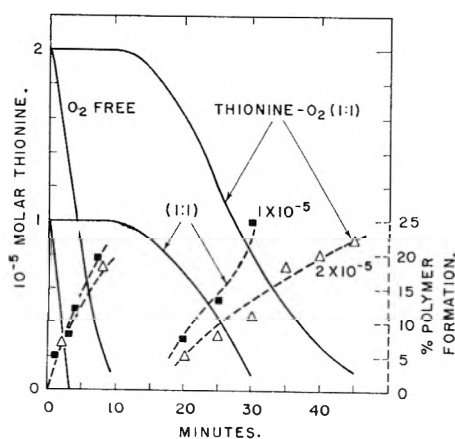


Fig. 7.—Oxygen inhibition at (1:1) thionine to oxygen ratio at pH 8.4.

acrylamide at pH 8.4 under anaerobic conditions. Both of these dyes caused polymerization, but neither of them underwent dye fading. More extensive data of this type are now being taken.

Oxygen-Inhibited Experiments.—Figure 6 shows the effect of $1.5 \times 10^{-5} M$ and $6 \times 10^{-5} M$ oxygen

concentrations on the photopolymerization of 5% acrylamide in $3 \times 10^{-5} M$ thionine at pH 8.5. The comparable oxygen-free run taken from Fig. 2 is included in Fig. 6 for reference. Four observations are to be made about these experiments. First, the presence of oxygen causes an induction period before the onset of polymerization. Second, there is no dye fading during the induction period, but dye fading commences with the onset of polymerization. Third, the rates of both polymerization and dye fading are inhibited with reference to the oxygen-free experiments. Fourth, extremely high yields of polymerization were obtained in these experiments after dye fading had been completed. Figure 7 shows these results confirmed when oxygen is added in 1:1 ratio to thionine, at 1×10^{-5} and $2 \times 10^{-5} M$ thionine in 5% acrylamide at pH 8.4. An estimate of the reduction of both ϕ_p and ϕ_{th} due to oxygen inhibition relative to oxygen-free conditions can be made from Fig. 6 and 7 by taking the ratio of reaction times needed to produce the same degree of polymerization or of dye fading in the comparable oxygen-free runs of experiment 2. It is seen that the induction period reduced both ϕ_p and ϕ_m by a factor of about 10.

The normal oxygen concentration in an air-saturated water solution is 8.5 p.p.m. ($2.5 \times 10^{-4} M$) at which concentration photopolymerization under these conditions is completely quenched.

The Effect of H_2O_2 Addition.—The indication that H_2O_2 is an end product of oxygen inhibition led us to study the effect of H_2O_2 inhibition of photopolymerization. Reagent grade hydrogen peroxide was diluted with boiled water to make up stock solutions and was injected into a 100-ml. sample of purged reaction solution in quantities no greater than 3-ml. Since the oxygen content of H_2O_2 solutions is difficult to determine, we cannot speak with certainty as to the oxygen levels of these H_2O_2 addition experiments.

Figure 8 shows the effects of H_2O_2 at concentrations of 3×10^{-5} , 1.2×10^{-4} , and $2 \times 10^{-3} M$ on the photopolymerization reaction run under the same conditions of the oxygen-inhibited experiments of Fig. 6. In Fig. 8 these H_2O_2 concentrations are noted as the ratio of thionine to H_2O_2 , i.e., (1:1), (1:4), and (1:66), respectively. The comparable oxygen-free run of Fig. 2 is included for comparison. We notice that at the 1:1 ratio of H_2O_2 to thionine, the induction period and inhibition introduced are comparable to that observed in the oxygen experiments of Fig. 6 and 7. When the ratio of H_2O_2 to thionine is increased to 4:1, the duration of the induction period decreases, but the degree of inhibition remains comparable to those of Fig. 6 and 7. At 66:1 excess of H_2O_2 to thionine, the induction and inhibition periods are removed. Here again very high polymer yields were obtained after dye fading had been completed, comparable to those obtained in the oxygen inhibition runs.

We may conclude that the inhibited rates of polymerization and dye fading at the conclusion of the induction period in oxygen-inhibited experiments may be due to the formation of H_2O_2 as oxygen is removed. The high polymer yields

obtained in oxygen-inhibited runs may be due to the formation of H_2O_2 and may be related to the well known activity of peroxides as polymer initiators.

Experiments with EDTA.—Two experiments were run with 5% acrylamide and $3 \times 10^{-5} M$ thionine at pH 8.4 in oxygen-free solutions with the addition of $2 \times 10^{-4} M$ EDTA and $8 \times 10^{-4} M$ EDTA. In the former case, thionine faded to $1 \times 10^{-6} M$ within 10 min., and in the latter it faded to $1 \times 10^{-6} M$ within 5 min. In neither case did polymerization occur. This confirms the observation of Oster^{8,9} that a dye-electron donor system will not polymerize the absence of oxygen. Addition of traces of oxygen to the system then did bring about photopolymerization.

Discussion

A mechanistic discussion of our results must explain these observations: (i) the initiation of polymerization by irradiated thionine alone in oxygen-free solutions; (ii) the induction period introduced by oxygen during which there is no dye fading, and the inhibition of dye fading and polymerization rates at the conclusion of the oxygen induction period; (iii) the inhibition effects of hydrogen peroxide at low concentrations; (iv) the dye fading without polymerization when an electron donor or weak reducing agent is added to the oxygen-free reaction; (v) the inverse dependence of polymerization rates and thionine fading rates on thionine concentration and monomer concentration; (vi) the pH dependence of the reaction.

There is now convincing evidence from flash photolysis work that the reactive light-excited state of thionine, T^* , is the triplet.^{14,15} From this it might be inferred that the radical initiator species in the polymerization is the triplet biradical, especially since this is the mechanism proposed in the anthracene-excited polymerization of styrene.⁵ There are two difficulties with this proposal. First, oxygen quenching of the triplet by collision could explain the induction period without dye fading, but would not explain the ultimate removal of oxygen which allows polymerization and dye fading to occur at the conclusion of the induction period. If one proposes that oxygen is removed as a thionine-oxygen complex, then one cannot explain the removal of a 2:1 excess of oxygen to thionine as shown in Fig. 6, which is still followed by polymerization and dye fading at the end of the induction period.

It is more likely that the reactive radical species which initiates polymerization is the singly-reduced semiquinone form of thionine (ST). This species has been proposed as the reactive intermediate in recent thionine photochemistry^{14,16-18} and semiquinones have been proposed as the initiators in dye-electron donor reactions by Oster.^{8,9} Let us assume for now that the semi-dye radical is the polymerization initiator and attempt

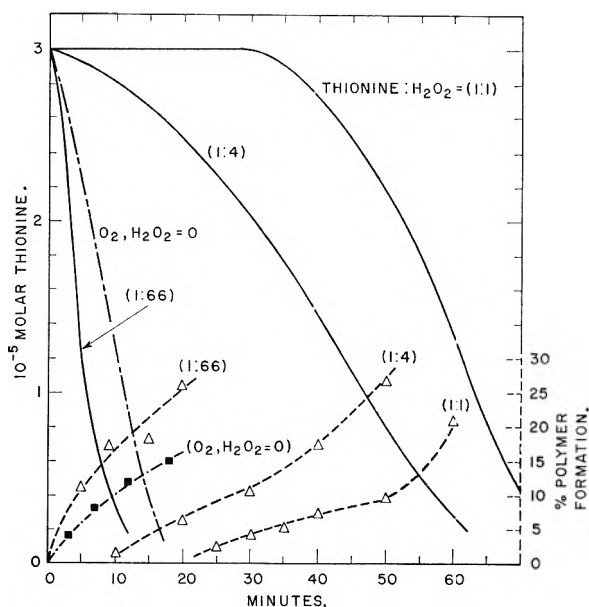
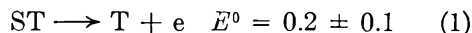
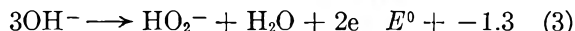


Fig. 8.—Effects of H_2O_2 addition on polymerization and dye fading in O_2 -free solution at pH 8.4.

to explain observations (ii) and (iii) on this assumption. The standard E^0 for thionine-leucothionine (T-LT) has been reported over the entire pH range¹⁹ and the potentials for the half couples, T-ST, and ST-LT, have been calculated by Rabinowitch²⁰ in the pH 1-4 range. By extrapolation, the standard potential for the T-ST couple at pH 8.4 is given by

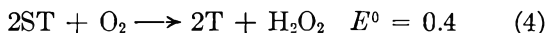


Values of E^0 for the water- H_2O_2 and the H_2O_2 - O_2 couples are known over the entire pH range.²¹ At pH 8.4, they are

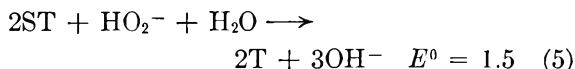


where hydrogen peroxide is written in the alkaline form in reaction 3.

From these potentials it is clear that the oxygen induction period can be explained by the reaction



which can quantitatively remove oxygen and suppress the polymerization reaction of ST with monomer. The further inhibition effect after the removal of oxygen can be explained by the formation of H_2O_2 in reaction 4, which may then undergo reaction 5



Reaction 5 may not be as effective in removing ST as is reaction 4 and so may allow some polymerization to occur. Another possibility is that the H_2O_2 formed in reaction 4, or introduced in the H_2O_2

(14) C. G. Hatchard and C. A. Parker, *Trans. Faraday Soc.*, **57**, 1093 (1961).

(15) C. A. Parker, *J. Phys. Chem.*, **63**, 26 (1959).

(16) J. Schlag, *Z. physik. Chem. (Frankfurt)*, **20**, 53 (1959).

(17) S. Ainsworth, *Z. Elektrochem.*, **64**, 93 (1960).

(18) R. Hardwick, *J. Phys. Chem.*, **66**, 349 (1962).

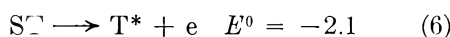
(19) W. M. Clark, "Oxidation Reduction Potentials of Organic Systems," Williams and Wilkins Company, Baltimore, Md., 1960, p. 132.

(20) E. Rabinowitch, *J. Chem. Phys.*, **8**, 551 (1940).

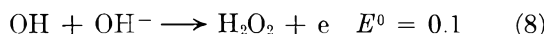
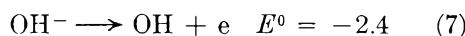
(21) W. M. Latimer, "Oxidation Potentials," Prentice-Hall, Inc., New York, N. Y., 1952, Chapter 4.

addition experiments, may undergo catalytic decomposition²¹ to O₂ and H₂O, whereupon a degree of oxygen inhibition occurs. The detection of H₂O₂ in dye photoreduction²² and in dye oxidation-reduction photopolymerization²³ has been reported. Detection is a problem because quantitative removal of all the oxygen in our most concentrated oxygen experiment ($6 \times 10^{-5} M$) would produce only 2 p.p.m. of H₂O₂. The postulates of reactions 4 and 8 therefore explain observations (ii) and (iii) above.

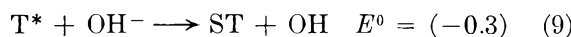
The key question then becomes the mechanism of formation of ST from excited thionine, T*, in the absence of an added reducing agent. Two possibilities present themselves: (i) the photoreduction of OH⁻ to the radical OH and ultimately to H₂O₂ as suggested by Parker¹⁵ in the flash photolysis of methylene blue and also by Strauss and Nickerson^{22,24} in the photoreduction of riboflavin; (ii) the formation of ST by hydrogen abstraction from the monomer as proposed by Holmström and Oster⁹ in the riboflavin photoreduction. The energetics of hydroxyl ion oxidation do not appear unfavorable when one considers that the absorption of light in the 5500 to 5900 Å. band by thionine makes thionine an oxidizing agent with a potential of 2.0 to 2.2 volts (about 46 kcal./mole) at pH 8.4



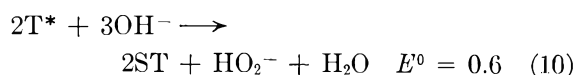
At pH 8.4, the pertinent hydroxyl ion couples²¹ are



where the sum of couples (7) and (8) is given by reaction 3 above. It would seem that reaction 6 is not sufficiently energetic to drive reaction 7

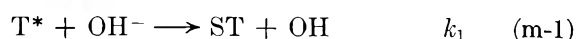


However, E^c is a calculated value which may be in error (the 1950 edition of Latimer²¹ reported E^0 for (7) to be only -1.8 at pH 8.4), and the hydration effects involving thionine may raise E^0 to bring (9) to a positive value. Moreover, stabilization of reaction 9 by reaction 8 results in reaction 10, which is energetically favorable.



The pH dependence of couples (6), (7), and (8) indicates that reactions 9 and 10 are favored at high pH and are not favored at low pH, which tends to explain observation (vi), the pH dependence of the reaction.

A mechanism based on reactions 9 and 10 can be used to explain observation (v), the functional dependence of the reaction rates on M and T.



(22) W. J. Nickerson and G. Strauss, *J. Am. Chem. Soc.*, **82**, 5007 (1960).

(23) G. Delzenne, S. Toppet, and G. Smets, *J. Polymer Sci.*, **48**, 347 (1960).

(24) G. Strauss and W. J. Nickerson, *J. Am. Chem. Soc.*, **83**, 3187 (1961).

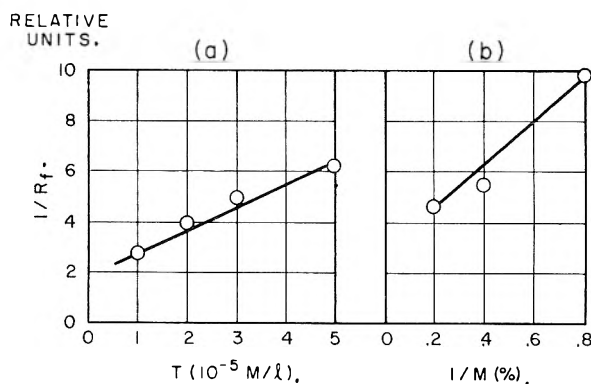
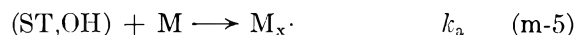
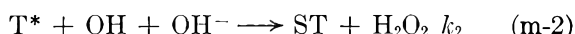


Fig. 9.—Functional dependence of $(1/R_f)$ on $(1/M)$ and on T.



In this mechanism M represents monomer, $M_x \cdot$ represents the propagating polymerization radical, T, T*, ST, OH, OH⁻ are as defined above, and the rate constants have their usual meaning. We have discussed the rationale of reactions m-0, m-1, and m-2 above. Reaction m-3, the inverse of m-1, represents competition with the polymerization reaction (m-5) and leads to a monomer dependence for the rate of thionine fading. Reaction m-4 represents the collisional self-quenching of thionine and is introduced to account for the dependence of the rate of fading on thionine concentration. Reaction m-5 represents the generation of the polymerizing radical, $M_x \cdot$, which undergoes free radical polymerization with monomer. It contains the simplifying assumption that k_a for both OH and ST is the same. Solving for the steady-state values of T* and of ST, one obtains for the rate of thionine for fading, R_f

$$R_f = (k_1 + k_2OH)T^* - k_3(ST)(OH) = k_aM(ST)$$

$$R_f = k_aM(k_1 + k_2OH)I_0 / (k_3OH + k_aM) (k_1 + k_2OH + k_qT) \quad (m-6)$$

Equation m-6 is left in terms of the transient species, OH, which cannot be solved without the appearance of quadratics. If we were to assume that $k_3OH \ll k_aM$, i.e., that OH from (m-1) is immediately removed by (m-2) to peroxide, then there would be no dependence of R_f on M, a result contrary to experiment. We therefore assumed that reaction m-2 is in competition with m-5 and that $k_3OH \leq k_aM$ and $k_2OH < k_1$. If we then assume that terms in OH do not vary strongly with I_0 , M, and T compared to the terms to which they are added, the expression for R_f becomes

$$R_f = \frac{c_1MI_0}{(c_2 + c_3M)(c_4 + c_5T)} \quad (m-7)$$

where c_1 through c_5 are constants. The predicted linear dependence of R_f on I_0 has been demonstrated in Fig. 5. The linear dependence of $(1/R_f)$ vs. T at constant monomer concentration is shown in Fig. 9a, using the steady-state values of R_f taken from

Fig. 2. Equation m-7 also predicts a linear plot of $(1/R_f)$ vs. $(1/M)$ at constant thionine concentration. This plot is shown in Fig. 9b using the steady-state rate data in Fig. 5. We note that it is necessary to use the steady rates of fading in (m-7) to obtain satisfactory plots, but the data are not strong enough to draw conclusions from this.

An estimate of the dependence of the rate of polymerization R_p can be made from the mechanism. The rate of appearance of the radical $M_x\cdot$ is given by

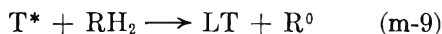
$$dM_x\cdot/dt = k_a(ST)M + k_a(OH)M \doteq 2R_f$$

Using the usual procedure in polymer kinetics, one assumes that the rate of removal of $M_x\cdot$ is bimolecular in $M_x\cdot$ with rate constant k_t and that the rate of polymerization is given by eq. m-8.

$$R_p = k_p M(M_x\cdot) = k_p M(2R_f/k_t)^{1/2} \quad (\text{m-8})$$

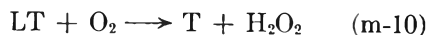
From eq. m-8, R_p should follow a $(I_0)^{1/2}$ law, should depend on M as $M^{3/2}/(c_1 + c_2M^{1/2})$, and should depend on T as $1/(c_1 + c_2T)^{1/2}$. Figure 4 shows that the $(I_0)^{1/2}$ is approximately followed, and a plot of data from Fig. 4 shows R_p to be roughly linear with $M^{3/2}$. The thionine-rate data of Fig. 2, however, do not show a linear dependence of T vs. $1/R_p^2$. We find, therefore, that the functional dependence of R_p given by eq. m-8 is not as well verified as the functional dependence of R_f given by eq. m-7.

Assumption of this mechanism allows one to use the well known explanation⁸ of the effects of added electron donor RH_2 in the absence of oxygen: the successive two-electron reduction of T^* to LT which suppresses reactions m-1 and m-2



when R^0 is the oxidized form of RH_2 . If oxygen is

added to the thionine-acrylamide-EDTA system at concentrations less than those of LT , then T will be regenerated



and an H_2O_2 -suppressed photopolymerization will occur. If an excess of O_2 over LT is added to the system, then we believe that after reactions m-9 and m-10 have occurred, an O_2 -inhibition photopolymerization will follow.

The possibility that the mechanism of formation of ST is by hydrogen abstraction from monomer⁹ appears improbable from the energetic point of view. Available bond energy data²⁵ for C-H bonds indicate that they are in the range of 70 to 100 kcal./mole, which is beyond the 46-kcal./mole range of light-excited thionine. Data are not available on the strength of the N-II bond in the amide group of acrylamide, but it is possible that in alkaline solution it might be in the 46-kcal. range. To check this we have photopolymerized acrylic acid in oxygen-free aqueous solution at pH 8.4 with $3 \times 10^{-5} M$ thionine. In this case thionine fading was not observed, but copious polymerization resulted. Hydrogen abstraction from acrylic acid would seem to be impossible because hydrogen is bound only as C-H bonds in this molecule. It must be pointed out, however, that if one assumes semi-dye formation by hydrogen abstraction, one can write a mechanism very similar to that written above. The dependence of R_f and R_p from such a mechanism is virtually the same as that derived in eq. m-7 and m-8. Consequently, further experimentation with different dyes, monomers, and solvents is needed to resolve further the nature of the polymerization-initiator species.

(25) E. W. R. Stacie, "Atomic and Free Radical Reactions," Second Ed., Reinhold Publ. Corp., New York, N. Y. 1954, p. 97.

TRANSFER OF TRIPLET STATE ENERGY AND THE CHEMISTRY OF EXCITED STATES

By F. WILKINSON¹

Physical Chemistry Laboratory, South Parks Road, Oxford, England

Received May 25, 1962

The general principles of the way in which triplet energy transfer can be used to obtain information concerning photoreactive states in solution is outlined. Aromatic hydrocarbons are recommended as good inert acceptors while aromatic ketones and aldehydes often make good donors. Results on two systems where these principles have been applied are presented. The first example concerns the photoreactions of a number of substituted anthraquinones with isopropyl alcohol. Some derivatives, "good sensitizers," give acetone with a quantum yield of unity in the presence or absence of oxygen. In the absence of oxygen they also produce anthraquinol with a quantum yield of unity. Other derivatives, "poor sensitizers," give these same reactions with quantum yields < 0.1 . The photoreactive state of anthraquinone, itself a good sensitizer, is shown to be its triplet state. Thus the presence of compounds with lower triplet states inhibits drastically its photoreactions while those with higher triplet levels have no effect. The rate constant for the reaction of triplet anthraquinone with isopropyl alcohol is estimated to be 3×10^6 l. mole⁻¹ sec.⁻¹. The lifetime of triplet anthraquinone in a 4:1 mixture of benzene:isopropyl alcohol therefore is 1.3×10^{-7} sec. The second example concerns the photodecomposition of 1-iodonaphthalene to give iodine (quantum yield at 3130 Å. = 0.09). Many compounds with higher triplet levels than 1-iodonaphthalene sensitize its decomposition (quantum yield of sensitized production of iodine with 3660 Å. irradiation = 0.04-0.05). Triplet 1-iodonaphthalene therefore undergoes some but not complete decomposition. Although 2-acetonaphthone does not photoreact with isopropyl alcohol, it does photosensitize the decomposition of 1-iodonaphthalene. This is interpreted as showing that the triplet state of 2-acetonaphthone is present in solution but it does not react as it is $\pi-\pi^*$ and not $n-\pi^*$ in character.

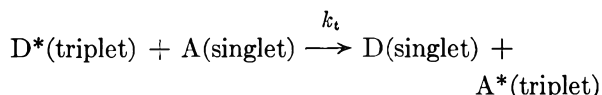
Information concerning photoreactive states is not easily obtained and although the triplet state

often has been proposed as the photoreactive state in a variety of systems due to its longer lifetime and greater biradical character than excited singlet states, its role in such reactions has been estab-

(1) Albright and Wilson Research Fellow, Pembroke College, Oxford.

lished for only a few cases. It is important to have criteria for the participation of triplet states in reactions other than the effect of added oxygen, as this effect may be difficult to interpret due to the extremely reactive nature of oxygen. Oxygen not only quenches both singlet and triplet states, but it also reacts with any easily oxidized state, radical, intermediate, or product.

For many systems, a number of chemically inert compounds can be found which are non-absorbing in a region where the reactive molecule absorbs and which are selective in quenching only triplet states. Such compounds quench triplet states by a process of electronic energy transfer which may be represented by the equation



where D denotes the donor, A, the acceptor, and the asterisk, an electronically excited state. This process, which leads to the sensitized phosphorescence of acceptor compounds in rigid media,² recently has been found to occur with high efficiency in normal solution.^{3a,b} For many donor and acceptor pairs values of $\sim 10^{10}$ l. mole⁻¹ sec.⁻¹ in hexane and benzene and $\sim 3 \times 10^8$ l. mole⁻¹ sec.⁻¹ in ethylene glycol have been found for k_t . These values are very similar to those obtained for oxygen quenching of triplet states⁴ and are what would be expected for a process which depends only on the rate of diffusion of the reactants together, *i.e.*, one which occurs at every collision. In rigid media the rate constants are very low, $\sim 10^2$ l. mole⁻¹ sec.⁻¹ or less, but this corresponds to transfer distances equivalent to normal collision diameters.⁵ No evidence for long range transfer and no dependence of the transfer efficiency upon the strength of the $S_g \rightarrow T_1$ transition probability in either the donor or the acceptor has been found.^{3b,5}

Porter and Wilkinson^{3b} have made the following general observations from flash photolysis studies of 20 donor and acceptor pairs. When the energy of the donor triplet was considerably higher than that of the acceptor, *i.e.*, greater than *ca.* 1000 cm.⁻¹, the transfer was diffusion controlled. As the triplet energies became comparable, the efficiency decreased and no quenching by molecules with triplet levels higher than that of the donor was observed.

Use of Triplet Energy Transfer in Distinguishing between Reactions of Excited Singlet and Triplet States.—Since triplet energy transfer occurs with such high efficiency, it should be possible to make use of it to learn more about triplet states. A number of applications already have been made⁶⁻⁸

(2) A. Terenin and V. Ermolaev, *Trans. Faraday Soc.*, **52**, 1042 (1956).

(3) (a) H. L. J. Bäckström and K. Sandros, *Acta Chem. Scand.*, **12**, 823 (1958); (b) G. Porter and F. Wilkinson, *Proc. Roy. Soc. (London)*, **A264**, 1 (1961).

(4) G. Jackson, R. Livingston, and A. C. Pugh, *Trans. Faraday Soc.*, **56**, 1635 (1960).

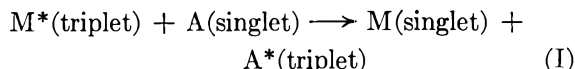
(5) V. Ermolaev and A. Terenin, *J. chim. phys.*, **55**, 698 (1958).

(6) H. L. J. Bäckström and K. Sandros, *Acta Chem. Scand.*, **14**, 48 (1960).

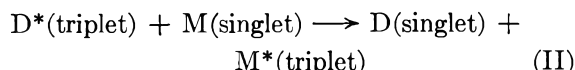
(7) G. S. Hammond, P. A. Leermakers, and N. J. Turro, *J. Am. Chem. Soc.*, **83**, 2395, 2396 (1961).

and there seems no reason why these should not be greatly extended. The general principles of the applications of this process, many of which are illustrated later in this paper, are outlined briefly here.

Consider a photoreactive molecule M. It may be used as either a donor



or as an acceptor



In each case partners should be chosen which allow the relative energy levels of each pair to be as shown in Fig. 1. A filter can be used which allows only the donor to absorb light. A very concentrated solution of the acceptor often makes an excellent filter for this purpose. Under such circumstances energy transfer from the excited singlet state of the donor to that of the acceptor is energetically impossible. Transfer from excited singlet donors to the triplet state of the acceptors, although energetically possible, is unlikely due to the lack of spin conservation. Furthermore, this process has been shown to be absent for quite a number of systems under conditions where efficient triplet transfer was occurring.^{1,3b,6}

If process (I) above occurs with high efficiency, it should be possible to add a high enough concentration of the acceptor so that the decay of the triplet M is all due to energy transfer. Under these conditions any remaining reactions would be due to the singlet state and these reactions could therefore be studied in the absence of reactions due to triplet states. On the other hand, reactions which have been inhibited by the presence of the acceptor may reasonably be attributed to triplet states. The presence, lifetime, and heights of triplet states which decay too rapidly to be detected by flash photolysis or other techniques or which do not phosphoresce in rigid media may be established using process (I), provided always that it can be shown that the role of the quencher is simply to accept energy by the physical process of energy transfer. Other types of quenching often are possible and therefore it is important to take care in choosing quenchers for this kind of study.

Aromatic hydrocarbons constitute a good class of quenchers because (a) much is known about their energy states, (b) they are generally chemically inert, and (c) the sensitized production of their triplet states can be illustrated by detecting their triplet-triplet absorption spectra, which have been well characterized, using flash photolysis techniques.^{3b}

Process (II) leads to the photosensitized production of the triplet state of M by-passing excited singlet states. This allows a study to be made of the chemistry of the triplet state of M. By choosing donors which give high quantum yields of triplet production (many aromatic aldehydes and

(8) G. Porter and F. Wilkinson, *Trans. Faraday Soc.*, **57**, 1686 (1961).

ketones are ideal for this purpose) and by increasing the concentration of M until virtually all the triplet donor is disappearing by process (I), the triplet state of M can be produced in high yields with the possibility of higher quantum yields for certain reactions of M than are normally found when M itself is irradiated. This is because photochemical and photophysical reactions of the singlet state of M which normally compete for each quantum absorbed are not present.

There also is the possibility of populating by process (II) triplet states of compounds which upon self irradiation do not normally undergo internal conversion to form triplets.

Another point of interest is that photochemical reactions due to triplet states often can be effected with longer wave lengths, due to the sensitized production of triplet states, than those necessary using self absorption, with obvious advantages for some systems. Some of these possibilities have been raised and illustrated by Hammond and co-workers,⁹ and some other examples are given later in this paper.

Results and Discussion

This work represents an attempt by the author to apply the principles outlined in the previous section to some photochemical reactions of general interest. Some of these results are of a preliminary nature while others are at present being prepared for publication elsewhere in a more detailed form. The discussion here will be confined, wherever possible, to the application of triplet energy transfer.

Photochemical Reactions of Quinones.—Much previous work has been done on the photochemistry of quinones. A selection of references is given below.¹⁰⁻¹⁵ The photosensitized oxidation of various alcohols by quinones especially has attracted attention and much is known about the reaction mechanism (see ref. 10 and 11). However, until now the photoreactive state has been determined for only one system. Using flash photolysis techniques, Bridge and Porter¹⁶ have shown that the poor sensitizer duroquinone reacts *via* its singlet and not its triplet state to give durosemiquinone. The question arises—do other quinones, especially those which react with high quantum yields, also react *via* their singlet states?

It was decided to attempt to answer this question by making use of triplet energy transfer. Anthraquinone and a number of its derivatives were selected for this purpose and isopropyl alcohol was chosen as substrate.

Solutions of various anthraquinones were irradiated with 3660-Å. irradiation in the presence and absence of oxygen. The results obtained are

(9) G. S. Hammond, N. J. Turro, and P. A. Leermakers, *J. Phys. Chem.*, **66**, 1144 (1962).

(10) J. L. Bolland and H. R. Cooper, *Proc. Roy. Soc. (London)*, **A225**, 405 (1954).

(11) C. F. Wells, *Trans. Faraday Soc.*, **57**, 1703 (1961).

(12) B. Atkinson and M. Di, *ibid.*, **54**, 1331 (1958).

(13) A. Berthoud and D. Porret, *Helv. chim. Acta*, **17**, 694 (1934).

(14) G. O. Schenk and G. Koltzenberg, *Naturwiss.*, **41**, 452 (1954).

(15) P. A. Leighton and G. S. Forbes, *J. Am. Chem. Soc.*, **51**, 3549 (1929).

(16) N. K. Bridge and G. Porter, *Proc. Roy. Soc. (London)*, **A244**, 259, 276 (1958).

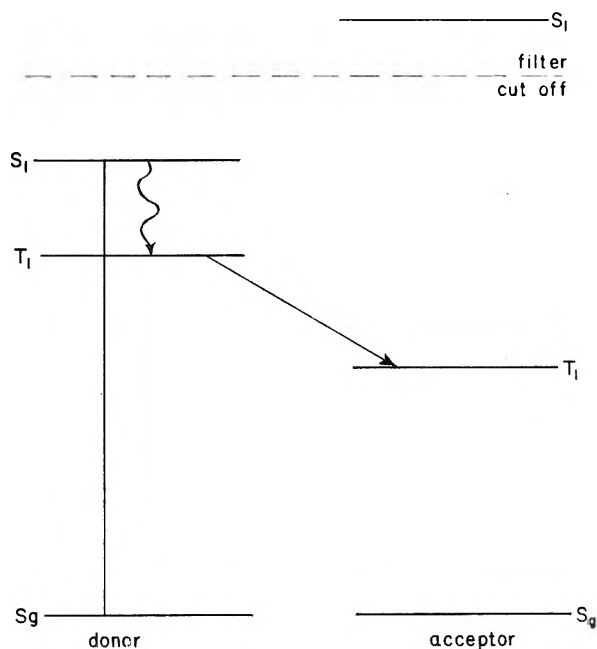


Fig. 1.—Energy levels of donor and acceptor.

summarized in Table I. In neutral degassed solutions, the disappearance of the anthraquinones and the production of the anthraquinols were followed by absorption measurements. Unless otherwise stated, each anthraquinone (AQ) gave quantitative conversion to its anthraquinol (AQH₂) and complete recovery of the AQ was effected by admitting oxygen. We shall note in passing that those systems which show reversible quantitative conversion in neutral and acid solutions to give AQH₂ give reversible and quantitative production of the semiquinone radical ion AQ^{•-} in alkaline solution.

The absolute values of the quantum yields given in Table I would be expected to be subject to errors not greater than 10%. Where quantum yield measurements are not available at present, the words high and low are used to indicate the efficiency of the reaction as judged by comparison with those systems where the yields have been measured and which have been studied under almost identical conditions. The estimates of quantum yields are high about unity, and low <0.1.

All measurements in the presence of oxygen were comparative. Wells¹¹ has shown that the quantum yield of photosensitized oxidation of isopropyl alcohol by sodium anthraquinone-2-sulfonate (2-SO₃Na-AQ) in water-isopropyl alcohol mixtures ([isopropyl alcohol] = 4 M) with 3660-Å. irradiation is unity. The amount of acetone formed or the oxygen uptake of each quinone was compared to that of 2-SO₃Na-AQ and any which gave comparable effects under the same conditions, indicating quantum yields of 0.8-1.0, were classed as good sensitizers, while those which indicated quantum yields < 0.1 were classed as poor sensitizers.

Structural effects on photochemical reactions have been discussed at this symposium by Pitts and co-workers.²⁰ These authors also have studied the photochemical reactions of anthraquinones and where overlap occurs their results are in general agreement with those given in Table I.²¹

TABLE I
PHOTOREACTIONS OF SOLUTIONS OF ANTHRAQUINONE DERIVATIVES DUE TO 3660-Å. IRRADIATION¹⁷

Derivatives ^a	In presence of oxygen	Quantum yields of production of anthraquinols in the absence of oxygen	
(1) Anthraquinone	Good sensitizer (i) ^b	0.91	(iii)
(2) 2-SO ₃ Na	Good sensitizer (ii)	1.06	(ii)
(3) 2,6-diSO ₃ Na	Good sensitizer (ii)	1.07	(ii)
(4) 2,7-diSO ₃ Na	Good sensitizer (ii)	1.14	(ii)
(5) 2-Me	Good sensitizer (i)	High	(i)
(6) 1-Cl	Good sensitizer (i)	High but with some irreversible reactions	(i)
(7) 1,5-diCl	Good sensitizer (i)		(i)
(8) 3,4,7,8-tetraCl	Good sensitizer (i)		(i)
(9) 1-SO ₃ Na	Poor sensitizer (ii)	0.050	(ii)
(10) 1,5-diSO ₃ Na	Poor sensitizer (ii)	0.015	(ii)
(11) 1-NH ₂	Poor sensitizer (i)	Low	(i)
(12) 1,4-diOH	Poor sensitizer (i)	Low	(i)
(13) 1,5-diOH	Poor sensitizer (i)	Low	(i)
(14) 1,8-diOH	Poor sensitizer (i)	Low	(i)

^a Concentrations were in the range 10^{-2} – 10^{-4} M. ^b The letters in brackets indicate the solvents used. These were (i) isopropyl alcohol; (ii) 1:1 water:isopropyl alcohol (by volume); and (iii) 4:1 benzene:isopropyl alcohol (by volume).

The effect of change of structure on photoreactivity cannot be discussed here in detail. However the pronounced difference between the reactivity of 1-substituted and 2-substituted sulfonates is worthy of note, since the unreactivity of the 1-substituted sulfonates cannot be due to the presence of internal hydrogen bonds within a six-membered ring (see ref. 20) as can the unreactivity of all the other unreactive anthraquinones given in Table I. The sulfonate group in position 1 may simply inhibit reaction at the quinone oxygen due to steric hindrance. Further work on this problem is now in progress.

It can be seen from Table I that anthraquinone itself is a typical good sensitizer. The effect of adding possible acceptors of triplet energy therefore was investigated. A 2.75×10^{-3} M solution of anthraquinone in a 4:1 benzene:isopropyl alcohol mixture was irradiated with light from a tungsten lamp which had passed through 2 cm. of an almost saturated solution of anthracene in benzene. Thus, using anthracene, which has a higher excited singlet but lower triplet state than anthraquinone, as an acceptor the conditions were as shown in Fig. 1. The rate of production of anthraquinol was found to be 14 times greater in the absence than in the presence of 10^{-2} M anthracene. The triplet levels of anthraquinone and anthracene are given as 20,400 cm.^{-1} and 14,700 cm.^{-1} , respectively, by Lewis and Kasha.²²

This result indicated that triplet anthraquinone was photoreactive and its reactions could be in-

hibited by the competing process of triplet energy transfer. To confirm this, 10^{-2} M naphthalene was added to the anthraquinone solution and, as triplet naphthalene lies at 21,300 cm.^{-1} ,²² no effect was expected. However, naphthalene gave strong quenching, reducing the rate of anthraquinol production down to one-fourth of what it was for anthraquinone alone. Another hydrocarbon, diphenyl, was added with an even higher triplet, 22,800 cm.^{-1} .²² This time 1.2×10^{-2} M diphenyl had no effect. The photosensitized oxidation of isopropyl alcohol also was inhibited by anthracene and naphthalene, but not by diphenyl.

The most probable explanation of this seemed to be that triplet anthraquinone was indeed the photoreactive state, but that its triplet height was not 20,400 cm.^{-1} but lay somewhere between 21,300 and 22,800 cm.^{-1} . The lower efficiency of quenching by naphthalene than by anthracene thus could be interpreted as another example of a reduction in the efficiency of triplet energy transfer as the triplet levels of donor and acceptor became comparable.²⁶

A search through the literature revealed that this explanation was correct at least concerning the triplet level of anthraquinone, as a value of 22,000 cm.^{-1} for the triplet state of anthraquinone may be read directly from the spectrum of anthraquinone phosphorescence published by Kasha in 1960.²³

In agreement with this later value for triplet anthraquinone, we have been able to show in our Laboratories that anthraquinone sensitizes the phosphorescence of naphthalene but not that of diphenyl in rigid media.²⁴

To show that anthraquinone does indeed sensitize triplet states of the acceptor molecules in normal solution, flash photolysis measurements have been made in our Laboratories and a sensitized absorption due to triplet anthracene is easily detectable.¹⁸

Anthraquinone forms ground state complexes with anthracene, naphthalene, and diphenyl, which

(17) The present author has found the quantum yield of production of anthraquinol from anthraquinone in 1:1 water:isopropyl alcohol to be unity within experimental error at 2537, 3130, and 3660 Å.¹⁸ This contradicts the large wave length dependence found by Bridge¹⁹ in his flash photolysis studies of anthraquinones. This will be discussed elsewhere.¹⁸

(18) F. Wilkinson, to be published.

(19) N. K. Bridge, *Trans. Faraday Soc.*, **56**, 1001 (1960).

(20) J. N. Pitts, Jr., H. W. Johnson, and T. Kuwana, *J. Phys. Chem.*, **66**, 2456 (1962).

(21) The author would like to thank Professor J. N. Pitts, Jr., and his co-workers for their cooperation since the original discovery that independent work on anthraquinones was being pursued in both Riverside, California, and Oxford, England. They have made available to him results prior to publication and he is extremely grateful for this.

(22) G. N. Lewis and M. Kasha, *J. Am. Chem. Soc.*, **66**, 2100 (1944).

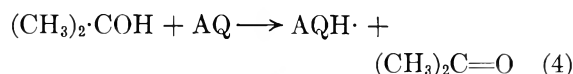
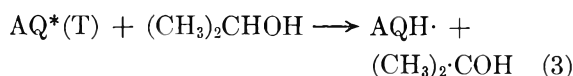
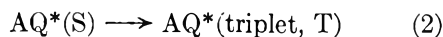
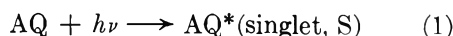
(23) M. Kasha, *Radiation Res. Suppl.*, **2**, 243 (1960).

(24) E. B. Smith and F. Wilkinson, unpublished results.

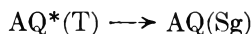
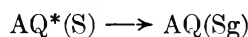
are presumably "charge transfer" complexes. The equilibrium constants for complex formation are ca. 10^{-1} at room temperature.²⁵ In the presence of 10^{-2} M of acceptor, therefore, less than 1% of the anthraquinone irradiated in these experiments is present as complexes. Such a small percentage of complexes could not possibly account for the extensive inhibition of the photochemical reactions of anthraquinone.

Thus for the good sensitizer, anthraquinone, the triplet state is the photoreactive state and not the singlet state as in the case of the poor sensitizer, duroquinone.¹⁶ Preliminary results with the other good sensitizers given in Table I indicate that they also react *via* their triplet states.

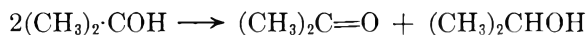
The following mechanism for photoreaction is consistent with the experimental facts so far discussed for good sensitizers.



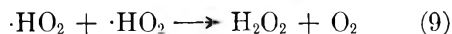
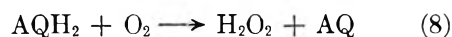
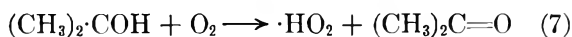
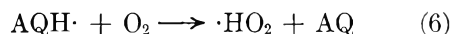
Reactions such as



and



can be eliminated since the quantum yield of production of AQH_2 is within experimental error, 1.0, for all the good sensitizers. In the presence of oxygen, the following reactions



combined with reactions 1-5 taken in any sequence account for the photosensitized oxidation of alcohols with a quantum yield of unity for oxygen uptake and for the production of hydrogen peroxide and of acetone as found by Wells¹¹ for 2-SO₃Na-AQ and by comparison as found in this work for all the good sensitizers in Table I.

Reactions 6-9 may be an over-simplification of the actual mechanism for oxygen reaction. Peroxy radicals may act as intermediates but the over-all reactions are as shown.

In the presence of an acceptor, A, of triplet energy the following reaction occurs.



(25) F. Wilkinson, unpublished results.

The lifetime of the photoreactive triplet state in this 4:1 benzene:isopropyl alcohol mixture, τ , in the absence of any quenching is given by

$$\tau = \frac{1}{k_3[(\text{CH}_3)_2\text{CHOH}]}$$

In the presence of 10^{-3} M anthracene, only $1/14$ of the $\text{AQ}^*(\text{T})$ present reacts *via* reaction 3. The rest undergoes triplet energy transfer.

$$\therefore 13k_3[(\text{CH}_3)_2\text{CHOH}] = k_{10}[\text{A}]$$

If k_{10} is assumed to be $\sim 10^{10}$ l. mole⁻¹ sec.⁻¹, *i.e.*, diffusion controlled, then as $[\text{A}] = 10^{-2}$ M

$$\tau \approx 1.3 \times 10^{-7} \text{ sec.}$$

and as $[(\text{CH}_3)_2\text{CHOH}] = 2.6$ M

$$k_3 \approx 3 \times 10^6 \text{ l. mole}^{-1} \text{ sec.}^{-1}$$

Photosensitized Decomposition of 1-Iodonaphthalene.—Benzene solutions of 1-iodonaphthalene undergo photodecomposition to give detectable amounts of iodine. The quantum yield of iodine production using 3130-Å. irradiation was found to be 0.085, corresponding to a quantum yield of decomposition of 1-iodonaphthalene of at least 0.16. With 3660-Å. irradiation, degassed solutions of 1-iodonaphthalene showed almost no decomposition, as 1-iodonaphthalene has only weak absorption at this wave length due to its $\text{S}_g \rightarrow \text{T}_1$. However, it was possible to photosensitize the decomposition of 1-iodonaphthalene by transferring energy to form its triplet state which lies at 20,500 cm.⁻¹.⁵ The results obtained for a number of sensitizers in degassed benzene solutions, all 10^{-2} M in 1-iodonaphthalene, are given in Table II.

TABLE II
PHOTOSENSITIZED DECOMPOSITION OF 1-IODONAPHTHALENE
WITH 3660-Å. IRRADIATION

Sensitizer ^a	Triplet level of sensitizer in cm. ⁻¹	Quantum yield of production of iodine
Acetophenone	25,850	0.055
Benzophenone	24,400	.054
Anthraquinone	22,000	.044
2-Acetonaphthone	20,775	.039
Anthracene	14,700	No reaction
o-OH-acetophenone	?	No reaction

^a Sensitizer concentration 10^{-2} - 10^{-1} M.

A complete discussion of the results in Table II must await further experiments, but the following points may be made. With benzophenone and anthraquinone as sensitizers there can be no doubt that the triplet state of 1-iodonaphthalene is being formed with a quantum yield of at least 0.9. Yet the quantum yield of photosensitized production of iodine is only about one-half that of the value obtained when 1-iodonaphthalene itself is irradiated. It follows, therefore, that the triplet state of 1-iodonaphthalene is capable of dissociation but it does not always do so. In fact, the energy supplied to the molecule may be more important than the particular state excited.

Neither *o*-OH-acetophenone nor 2-acetonaphthone photoreact with alcohols as do other ketones such as acetophenone, etc. From the fact that 2-acetonaphthone photosensitizes the decomposition of 1-iodonaphthalene, we can conclude that the triplet state of 2-acetonaphthone is present in solution. The explanation for its unreactive nature surely is, therefore, that it has a lower $\pi-\pi^*$ and not a lower $n-\pi^*$ triplet state.⁵ This supports the recent work of Hammond and Leermakers on compounds of this type.²⁶

No conclusions can be arrived at concerning the triplet state of *o*-hydroxyacetophenone. The reasons for the photochemical behavior of compounds containing the *o*-hydroxybenzoyl group have been discussed elsewhere and the reader is referred to these discussions.^{9,20}

Experimental

It is intended to publish a more detailed account of much of this work and full experimental details therefore will be given elsewhere.¹⁸

The materials used were of the highest purity commercially available and often were subjected to further purification by standard methods. As solvents, B.D.H. isopropyl alcohol (special for spectroscopy), further purified "Analar"

(26) G. S. Hammond and P. A. Leermakers, *J. Am. Chem. Soc.*, **84**, 207 (1962).

benzene, and doubly distilled water were used throughout. The degassing procedure was identical with that used in ref. 8. Absorption measurements were made using a Perkin-Elmer 4000A recording spectrophotometer. Anthraquinol, acetone,²⁷ and iodine were estimated spectrophotometrically.

Oxygen uptake was estimated by measuring the reduction in oxygen pressure above solutions due to irradiation. These solutions were shaken continuously during irradiation.

A high pressure mercury lamp enclosed in a Chance OX 1 filter was used for 3660-Å. irradiation. For 3130-Å. irradiation, filter solutions were used as recommended by Bowen.²⁸

Quantum yields were measured using potassium ferrioxalate as actinometer in the recommended way.²⁹

Acknowledgments.—It is a pleasure to acknowledge the help given by Dr. E. J. Bowen, who has made supplies of materials and equipment readily available to the author. The author wishes to thank Dr. D. Seaman for making some preliminary measurements on anthraquinones. He also is grateful to Professors G. Porter and J. N. Pitts, Jr., for interesting discussions on various aspects of this subject.

(27) See J. N. Pitts, Jr., R. L. Letsinger, R. P. Taylor, J. M. Patterson, G. Recktenwald, and R. B. Martin, *ibid.*, **81**, 1068 (1959).

(28) E. J. Bowen, "The Chemical Aspects of Light," Oxford University Press, 1946, p. 278.

(29) C. G. Hatchard and C. A. Parker, *Proc. Roy. Soc. (London)*, **A235**, 518 (1956).

THE UNCATALYZED DECAY OF ANTHRACENE AND PORPHYRIN TRIPLETS IN FLUID SOLVENTS¹

BY HENRY LINSCHITZ, COLIN STEEL, AND JERRY A. BELL

Department of Chemistry, Brandeis University, Waltham, Mass.

Received May 31, 1962

The decay kinetics of anthracene and porphyrin triplets have been measured, using flash-excitation technique. In purified and thoroughly deoxygenated pyridine or hexane, the first-order rate constant is less than 150 sec.⁻¹. In tetrahydrofuran, chemically deoxygenated by liquid NaK alloy, the first-order decay constant is less than 40 sec.⁻¹. Correspondingly low values are found also for porphyrins. The anomalously large viscosity dependence of this rate constant is assigned to pseudo first-order processes rather than to an intrinsic effect. The bearing of this on radiationless energy degradation in excited molecules is discussed.

The nature of radiationless transitions in complex molecules still remains one of the major problems in photochemistry. Interactions with the medium evidently must be involved, if only to remove vibrational energy. However, more specific properties of the solvent also may play a role, as for example, the viscosity. In the case of triplet-singlet transitions, much discussion has been devoted to the seeming paradox of a strong viscosity dependence for the radiationless $T \rightarrow S$ (triplet to ground state) transition, compared with a weak viscosity dependence of the analogous $S' \rightarrow T$ (excited singlet to triplet) transition.²⁻⁴ Thus, the appearance of phosphorescence in passing from a fluid to a rigid medium requires that the $S' \rightarrow T$ transition rate remain high to compete with $S' \rightarrow S$

transitions, whereas the radiationless $T \rightarrow S$ transition rate must greatly decrease, to permit the long-lived emission to occur. However, it has been appreciated for some time that it is extremely difficult to measure the "true" first-order rate constant for the radiationless $T \rightarrow S$ transition in fluid solvents because of competing pseudo first-order quenching reactions of the triplet with traces of impurity, particularly oxygen, and perhaps solvent peroxides.³⁻⁷

The extremely long radiative lifetime of the triplet makes it especially susceptible to such quenching, and the apparent strong viscosity dependence of the "unimolecular" $T \rightarrow S$ transition may, in fact, be most reasonably interpreted in this way.⁵⁻⁷ In this paper we present further direct measurements of the decay kinetics of anthracene and porphyrin triplets in fluid solvents which set new lower limits to the intrinsic first-order decay rate.

(1) This work was assisted by a grant from the U. S. Atomic Energy Commission to Brandeis University (No. AT (30-1)-2003).

(2) G. N. Lewis, D. Lipkin, and T. T. Magel, *J. Am. Chem. Soc.*, **63**, 3005 (1941).

(3) G. Porter and M. R. Wright, *Discussions Faraday Soc.*, **27**, 18 (1959).

(4) G. Porter and M. R. Wright, *ibid.*, **27**, 94 (1959).

(5) H. Linschitz and L. Pekkarinen, *J. Am. Chem. Soc.*, **82**, 2411 (1960).

(6) G. Jackson, R. Livingston, and A. Pugh, *Trans. Faraday Soc.*, **56**, 1635 (1960).

(7) G. Jackson and R. Livingston, *J. Chem. Phys.*, **35**, 2182 (1961).

Experimental

Materials.—Reagent-grade pyridine was twice purified over KOH and distilled through an efficient column. Freshly-opened "spectro-grade" hexane was used directly, after distillation was found to have no effect on the decay rate of anthracene in this solvent. Fisher reagent tetrahydrofuran (THF) was distilled from lithium aluminum hydride and then treated with liquid NaK eutectic (see below). Anthracene was either E.K. "fluorescent grade" or a highly purified scintillation grade sample from Pilot Chemical Co. (Waltham). Both materials gave the same results, in pyridine or hexane, within experimental error. Measurements in THF were confined to the Pilot sample. Porphyrins were purified as described previously.⁸

Degassing Procedure.—In previous studies,⁵ solvent degassing was done by repeated trap-to-trap distillation in order to carry all materials through the vapor phase. This is a rather slow operation, subject to unavoidable leaks in the vacuum system and possible re-adsorption of oxygen on successive layers of frozen solvent during the transfer, while the traps are closed off from the pump. In this work, pyridine and hexane were degassed by subjecting the solutions to repeated cycles of freezing, pumping, and thawing, with vigorous agitation of the liquid by an enclosed magnetic stirrer. Solutions were sealed off only after at least three consecutive cycles gave "stick-vacuum." In sealing off, care was taken to allow gas released from the heated glass to be pumped away before completing the closure. Glassware was thoroughly cleaned and rinsed to remove possible traces of heavy-metal contamination.

After initial drying and distillation, tetrahydrofuran was degassed by freezing, pumping, and thawing, and then further deoxygenated chemically, by allowing the solvent to stand for several weeks over liquid NaK alloy in a Pyrex ampoule fitted with a greaseless Hoke Hi-vacuum valve, with occasional agitation by an enclosed magnetic stirrer. The completion of the "getter" action is visibly indicated by the appearance of a blue color characteristic of alkali metal solutions in ethers.^{9,10} This blue color generally appeared shortly after contact of the THF with NaK, and deepened somewhat after prolonged standing. In preparing solutions for study, the cleaned flash-cell and side arm assembly was pumped and flamed, removed from the line, solute added, the cell immediately re-evacuated on the line, purified THF quickly distilled from its storage bulb, and the sample finally sealed off. To study concentration effects, various test solutions were prepared from a single sealed-off preparation, by adjusting the solute distribution between the flash-cell and side arm. Concentrations were determined on a Cary Model 14 spectrophotometer.

Apparatus and Measurement Procedure.—The apparatus and general measuring procedure have been described previously.^{5,7,11} A slight modification of technique was made to improve the precision of measuring small absorbance changes (less than 0.2). Monochromator slit width and photometer gain were adjusted so that the initial light transmission of the sample gave full-scale deflection on the oscilloscope screen. The oscilloscope gain then was increased by a known factor, and the vertical control re-adjusted to bring the deflected sweep back on scale. The relatively small change in absorption due to the flash then could be measured at higher gain. The change in optical density, ΔD , due to the flash, then is given by $\Delta D = \log [f r_0 / (f r_0 + \Delta r)]$, where r_0 is the transmission of the original solution, in oscilloscope scale units, Δr is the observed (algebraic) change in reading due to the flash, and f is the ratio by which the gain is increased. The signal to noise level of the photometer and the stability of the measuring light source permitted "f" values as high as 4 or 5 to be used. This technique is most helpful, since the points at low ΔD are especially significant in the extrapolation by which the first-order component of the decay curve is obtained. The precision of the experimental

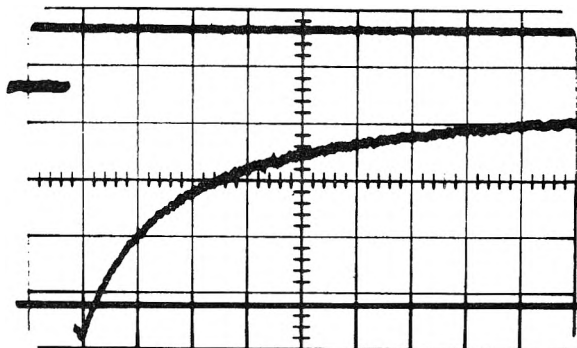


Fig. 1.—Typical oscillogram showing multiple gain technique; anthracene in THF; concn. = $16.5 \times 10^{-6} M$; $\lambda = 4240 \text{ \AA}$; slit = 35 \AA ; sweep = 2 msec., full scale; lower trace, base line; upper trace, initial transmission, 0.2 volt/cm.; central trace, effect of flash, 0.1 volt/cm.

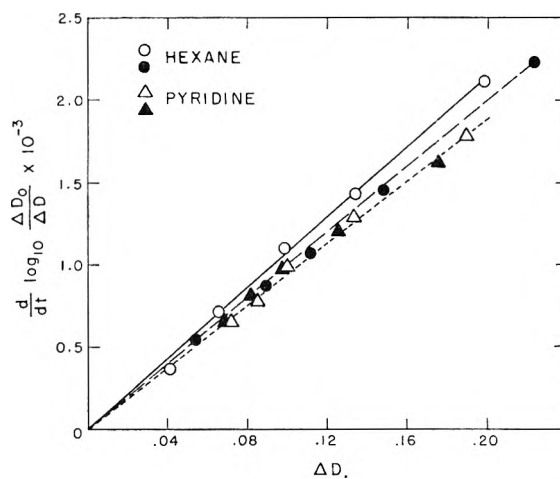


Fig. 2.—Decay kinetics of anthracene in pyridine ($6 \times 10^{-5} M$) and hexane ($4 \times 10^{-5} M$): slit = 20 \AA , $\lambda = 4240 \text{ \AA}$.

data may be judged from a typical oscillogram, shown in Fig. 1.

The data were treated as in our earlier work,^{5,11} taking the rate law to be

$$-\frac{dC^*}{dt} = k_1 C^* + k_2 (C^*)^2 + k_3 C^* C_g + \sum_i (k_4)_i (M_i) C^*$$

in which k_1 is the total (radiative and radiationless) unimolecular rate constant and k_2 , k_3 , and k_4 correspond, respectively, to quenching by other triplets, ground state molecules, and foreign substances. A plot of $d/dt [\ln(\Delta D_0/\Delta D)]$ vs. ΔD has an intercept A given by

$$A = k_1 + k_2 C_0 + \sum_i (k_4)_i (M_i)$$

in which C_0 is the total solute concentration.⁵

Results and Discussion

1. Kinetics in Hexane and Pyridine.—Figure 2 presents typical decay data for anthracene in hexane and pyridine, from which the uncertainty in the extrapolation may be judged. For pyridine, the least squares plot (shown in Fig. 2) had an intercept of 55 and standard error of $\pm 62 \text{ sec}^{-1}$. In hexane, a typical result was $56 \pm 76 \text{ sec}^{-1}$. Although it is difficult to evaluate systematic errors, a conservative upper limit for A , in both solvents, is about 150 sec^{-1} . Accordingly, the value for A

(8) L. Pekkarinen and H. Linschitz, *J. Am. Chem. Soc.*, **82**, 2407 (1960).

(9) J. L. Downs, J. Lewis, B. Moore, and G. Wilkinson, *J. Chem. Soc.*, 3767 (1959).

(10) We wish to thank Mr. R. Felton for assistance in this preparation.

(11) H. Linschitz and K. Sarkanen, *J. Am. Chem. Soc.*, **80**, 4826 (1958).

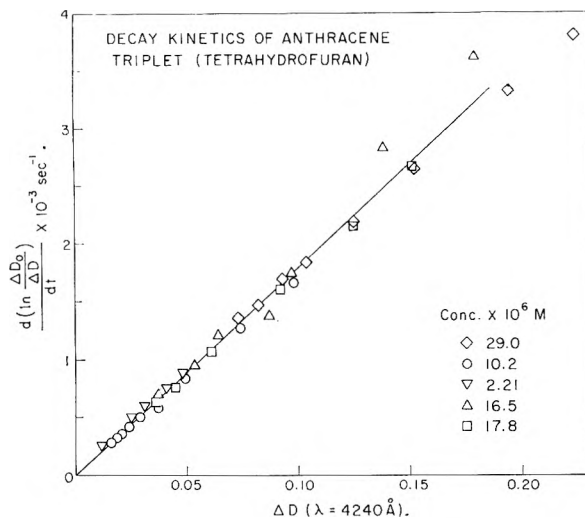


Fig. 3.—Decay kinetics of anthracene in THF at various concentrations: slit = 35 Å., $\lambda = 4240 \text{ \AA}$.

is taken to be about $75 \pm 75 \text{ sec.}^{-1}$. This upper limit of A , and therefore k_1 , is appreciably less than that found in our previous work (580 sec.^{-1} in hexane) or in other direct measurements (340 sec.^{-1}).⁶ To check that the differences found in our work are due to modifications of technique, first-order decay rates were redetermined for tetraphenylporphine and zinc tetraphenylporphine in pyridine, a new value of A of 150 sec.^{-1} being obtained instead of $700\text{--}800 \text{ sec.}^{-1}$.⁸ The decrease is comparable to that observed for anthracene. The second-order slopes (Fig. 2) agree closely with our previous results.⁸

2. Kinetics in Tetrahydrofuran.—Since the chemical deoxygenation of THF appeared to be effective, particularly detailed studies were made in this solvent. The anthracene data are summarized in Fig. 3, in which only a few typical runs can be shown. The straight line is a least-squares plot, using 150 points in the ΔD range from 0.01 to 0.10, derived from several oscillograms taken at each of 9 different concentrations. No drift in A , nor any irreversibility, was detected throughout the entire series of measurements. The points at ΔD 's higher than 0.10 scattered somewhat, possibly due to tailing of the flash, and were not used.

The intercept is actually very slightly negative (-6 sec.^{-1}). Ninety per cent of the points lay below a line drawn parallel to that of Fig. 3 and with intercept 50 sec.^{-1} . The estimated error of $\pm 40 \text{ sec.}^{-1}$ is taken as an upper limit for k_1 in THF. Within our error, this is evidently indistinguishable from the radiative rate constant of anthracene (between 10 and 100 sec.^{-1})¹² or the limiting rate in highly viscous media (27 sec.^{-1}).⁷

It is noteworthy that, over the concentration range studied (2.2×10^{-6} to $29 \times 10^{-6} M$) no trend toward increasing intercept with concentration was discernible. Thus, $k_3 C_0 < 40 \text{ sec.}^{-1}$ and k_3 must be less than about $10^6 M^{-1} \text{ sec.}^{-1}$. Values of k_3 near $10^7 M^{-1} \text{ sec.}^{-1}$ reported for chlorophyll triplets may possibly be in error due to impurities introduced with the solute at high concentrations.¹¹

(12) S. McGlynn, M. Padhye, and M. Kasha, *J. Chem. Phys.*, **23**, 593 (1955).

Jackson and Livingston have attempted to eliminate the bimolecular viscosity-dependent contributions to the first-order decay by plotting A against k_2 for a given solution at a series of temperatures, and finding the limiting value of A corresponding to $k_2 = 0$. This limit then is taken to be the intrinsic k_1 , on the assumption that k_1 is temperature independent. The values thus obtained for anthracene are 110 sec.^{-1} in THF and 160 sec.^{-1} in hexane. This THF rate is higher than the directly measured value reported here. The difference in k_1 's in hexane seems to be within the experimental error of both methods.

Measurements also were carried out on zinc tetraphenylporphine in THF ($2.75 \times 10^{-7} M$). Data taken at two wave lengths corresponding, respectively, to dye bleaching (4220 \AA) or triplet absorption (4500 \AA) fell on lines, with intercept 50 sec.^{-1} and estimated error $\pm 50 \text{ sec.}^{-1}$, again considerably lower than our previous measurements.⁵ The bimolecular triplet quenching constant, k_2 , for ZnTPP was $5.5 \times 10^9 M^{-1} \text{ sec.}^{-1}$.

3. Remarks on Radiationless Transitions.

In the light of this and other work⁵⁻⁷ there can be no doubt that the apparent (and puzzling) large difference in viscosity dependence between the $S' \rightarrow T$ and $T \rightarrow S$ radiationless transitions is an artifact. At least for the cases considered, the "intrinsic" $T \rightarrow S$ transition is evidently much slower than the $S' \rightarrow T$ process, even in fluid solvents. Thus, the triplet-singlet transitions fall in with the familiar generalization that radiationless transitions among the upper excited states are much faster than the final transition from the lowest excited state to the ground state. This finds its simplest explanation in the Franck-Condon Principle¹³ and in the intuitively helpful notion of an intramolecular sensitized transition.¹⁴ In considering the pattern of energy degradation in electronically excited molecules, the intercombination transitions may be treated similarly to their spin-conserving counterparts, except of course for the special spin restriction. For molecules with inherently high triplet yields, as for example, those with low-lying $n-\pi$ levels,¹⁵ bimolecular quenching processes, particularly by ubiquitous oxygen, must play a major role in energy degradation. The mechanism of reversible quenching thus assumes new importance for our understanding of such dissipative processes.

The question is still open whether viscosity can indeed affect the rate of a "unimolecular" process in solution,^{16,17} or whether temperature alone is the essential rate-determining variable for radiationless decay processes in thermally equilibrated excited states. The trend of " A " over the past years suggests that the latter is indeed the case, except perhaps in the situation where slow torsional vibrations of large molecular segments are coupled to the electronic transitions.

(13) G. W. Robinson and R. P. Frosch, International Symposium on Reversible Photochemical Processes, Durham, N. C., April, 1962, and references therein.

(14) J. Franck and H. Spöner, *J. Chem. Phys.*, **25**, 172 (1956).

(15) E. Clementi and M. Kasha, *J. Molec. Spectry.*, **2**, 297 (1958).

(16) G. N. Lewis and M. Calvin, *Chem. Rev.*, **25**, 273 (1939).

(17) J. Franck and R. Livingston, *J. Chem. Phys.*, **9**, 184 (1941).

THE CATALYSIS OF ANTHRACENE TRIPLET DECAY BY COPPER COMPLEXES¹

BY COLIN STEEL AND HENRY LINSCHITZ

Department of Chemistry, Brandeis University, Waltham, Mass.

Received May 31, 1962

The catalysis of anthracene triplet decay by cupric ion depends on the state of complexing of the metal. In pyridine solution, the order of increasing catalytic effect is ethylenediamine < pyridine < *o*-phenanthroline. The results are consistent with a postulated charge-transfer interaction for the catalysis.

Transition metal ions catalyze the conversion of aromatic triplet states to the ground state.²⁻⁴ Strong experimental evidence has been given in previous work on this subject²⁻⁴ that this catalysis is not simply a "physical" effect of the magnetic field of the metal ion, leading to enhancement of triplet-singlet transition probabilities *via* "mixing" of the states.^{5,6} For example, the catalytic effect⁷ bears no direct correlation with the magnetic moment of the ion.²⁻⁴ Moreover, the notably weak effect of Mn²⁺, relative to the other transition metals, is found for excited singlets (fluorescence quenching) as well as for triplets,³ indicating that the effect is not directly limited to breakdown of spin selection rules. Finally, in non-aqueous complexing solvents, hydration of the metal ion markedly decreases quenching efficiency, a result difficult to reconcile with a simple magnetic catalysis mechanism. To account for these and other observations, we have therefore assumed that a more specific ("chemical") mechanism applies, and have postulated formation of a charge-transfer complex between the excited molecule and metal ion.³ Theoretical studies in agreement with this view have been published by Tsubomura and Mulliken.⁸ The complex then is presumed to undergo rapid radiationless⁷ transition to the ground state.

There evidently remain many questions to be clarified, which may have quite general chemical as well as spectroscopic interest. Accordingly, a systematic study is being made of excited molecule-metal interactions, as a function of the complexing environment of the ion and nature and multiplicity of the excited state. We present in this paper measurements of the catalysis of triplet-singlet conversion in anthracene by copper complexes, in pyridine solution.

Experimental

Materials.—Pyridine and anthracene were the same materials described in the previous paper.⁹ Eastman ethyl-

enediamine ("98%"), Fisher reagent *o*-phenanthroline, and reagent grade CuCl₂·2H₂O were used. Tests with anhydrous CuCl₂ gave identical results, as expected under the conditions of strong complexing in these experiments.³

Method.—Spectrophotometric titrations and Job variation experiments were performed using a Cary Model 14 spectrophotometer. The flash apparatus and procedure has been described previously^{2,3,9} and the degassing technique was similar to that given in the previous paper.⁹ In experiments involving organic solvents and transition metal salts the possibility exists of peroxide contamination by metal-catalyzed oxidation.³ Therefore, stock salt solution was measured into a small side arm on the cell-ampoule assembly and evaporated by a current of air before placing the anthracene solution in the ampoule. Mixing of the salt and anthracene solution was done after the assembly had been degassed and sealed off. The data were analyzed as in previous studies, by plotting the quantity $d/dt [\log (\Delta D_0 / \Delta D)]$ against ΔD , in which ΔD_0 is the measured change in optical density (corresponding to triplet state formation) at a conveniently chosen zero time, and ΔD is the change at time, t , thereafter. The increase of the intercept of the resulting straight line with increasing quencher concentration then gives the bimolecular quenching constant, k_4 .

Results and Discussion

1. Ethylenediamine-Copper Complex in Pyridine.—Spectrophotometric titration and Job variation experiments were carried out to establish the nature of the copper-en complex in pyridine. The variation measurements gave excellent maxima, corresponding to a 1:1 Cu-en complex, which, in pyridine, presumably contains also the two chlorides. Figure 1 gives typical spectrophotometric results, and Fig. 2 the fitting of these data by a 1:1 complex equilibrium, assuming a formation constant of 2×10^5 . Addition of diamine in excess causes complete precipitation of copper as a dark blue-violet compound, analyzing correctly for Cu(en)₂Cl₂.

2. Effect of Complexing on Copper-Catalyzed Anthracene Triplet Decay.—The experiments are summarized in Fig. 3, which shows the effect on anthracene triplet decay of adding varying amounts of ethylenediamine or *o*-phenanthroline to a CuCl₂-anthracene solution. It is evident that the original copper-ion catalysis *decreases* toward a new limiting value, as ethylenediamine is added, up to the point where precipitation of the higher complex begins. On the other hand, the catalysis *increases* toward another limiting value as *o*-phenanthroline is added. These two limiting rates must represent the change in catalytic effect due to replacing two pyridines by en or *o*-phenanthroline, respectively. Blank runs containing only added ethylenediamine or *o*-phenanthroline but no copper gave negligible catalytic effects. The values obtained for the

(1) This work was assisted by a grant from the U. S. Atomic Energy Commission to Brandeis University (Contract No. AT(30-1)-2003).

(2) H. Linschitz and K. Sarkanen, *J. Am. Chem. Soc.*, **80**, 4826 (1958).

(3) H. Linschitz and L. Pekkarinen, *ibid.*, **82**, 2411 (1960).

(4) G. Porter and M. R. Wright, *Discussions Faraday Soc.*, **27**, 18 (1959).

(5) E. Wigner, *Z. physik. Chem.*, **B43**, 28 (1933).

(6) R. A. Harman and H. Eyring, *J. Chem. Phys.*, **10**, 559 (1942).

(7) The term "catalytic" is used here rather than "quenching," since it is not entirely certain that the enhanced rate of triplet-singlet transition in anthracene is due to an increase in radiationless rather than radiative processes. This has been established for eosin in recent studies in this Laboratory.

(8) H. Tsubomura and R. S. Mulliken, *J. Am. Chem. Soc.*, **82**, 5966 (1960).

(9) H. Linschitz, C. Steel, and J. A. Bell, *J. Phys. Chem.*, **66**, 2574 (1962).

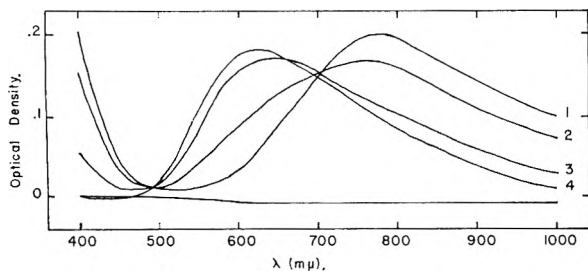


Fig. 1.—Absorption spectra of CuCl_2 ($1.5 \times 10^{-4} M$) in pyridine (10-cm. cell), with added ethylenediamine; en/ CuCl_2 : curve 1 = 0; curve 2 = 0.406; curve 3 = 1.23; curve 4 = 4.06.

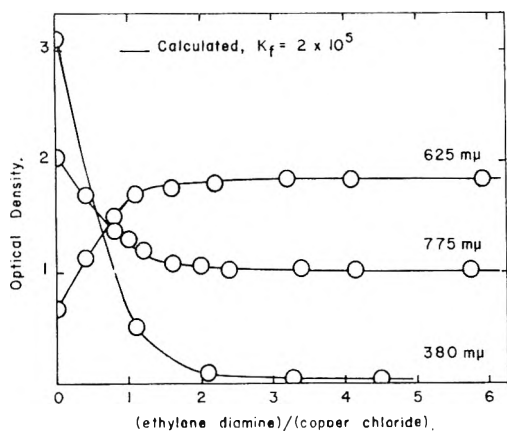


Fig. 2.—Formation constant of $\text{Cu}(\text{en})\text{Cl}_2$ in pyridine; absorbance vs. en/ CuCl_2 ; circles, observed points; lines, calcd. for $K_f = 2 \times 10^5$.

respective k_4 's are given in Table I. The present measurement for $\text{CuCl}_2(\text{py})_2$ agrees well with our previous determination.³

TABLE I
RATE CONSTANTS FOR COPPER-CATALYZED ANTHRACENE
TRIPLET DECAY

Complex (in pyridine soln.)	Catalytic constant $k_4 \times 10^{-6} (M^{-1} \text{sec.}^{-1})$
$\text{Cu}(\text{en})\text{Cl}_2$	2.2
$\text{Cu}(\text{py})_2\text{Cl}_2$	4.6
$\text{Cu}(\text{phen})\text{Cl}_2$	13.0

These data may be tested in another way, by calculating from the over-all observed catalysis the distribution of copper among its various complexes, for ligand concentrations too low to bind completely the available metal. It is assumed that each complex will contribute to the total catalysis independently, and that the over-all catalytic constant may be written as

$$k_4[\text{Cu}_{\text{total}}] = \sum k_i \text{Cu}_i$$

where k_i and Cu_i are, respectively, the rate constants and concentrations of the i 'th complex. The results of such a calculation are given in Fig. 4 for the ethylenediamine system, in which the amount of uncomplexed copper is obtained from both spectrophotometric and kinetic data. Good agreement is found.

The rate constants of Table I may be discussed in the light of the reversible charge-transfer mechanism mentioned above. Taube has studied the

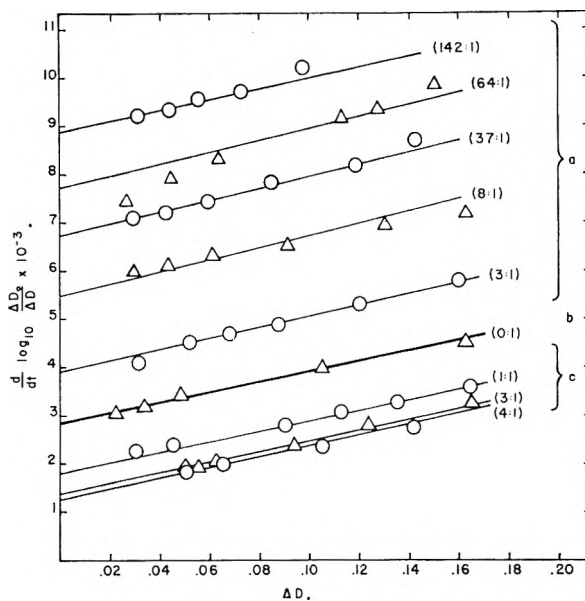


Fig. 3.—Decay kinetics of anthracene in pyridine, in the presence of (b) CuCl_2 ; (a) CuCl_2 + *o*-phenanthroline; (c) CuCl_2 + ethylenediamine. Numbers indicate concentration ratio (ligand/ Cu). CuCl_2 concn., $1.30 \times 10^{-6} M$.

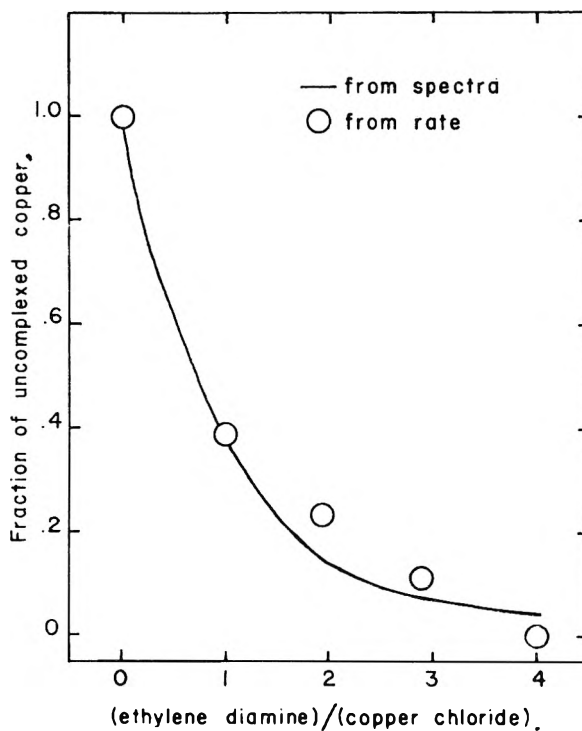


Fig. 4.—Fraction of uncomplexed CuCl_2 vs. ethylene diamine; line, calcd. from spectroscopic data; circles calcd. from catalyzed triplet decay data (Fig. 3).

effect of complexing of Cr^{+2} on the rate of its reduction of Co^{+3} . When $\text{Cr}(\text{en})_3^{+2}$ is replaced by $\text{Cr}(\text{phen})(\text{en})_2^{+2}$, the rate is increased twentyfold.¹⁰ Our previous data on the marked effect of metal ion hydration, in decreasing triplet-singlet catalysis,³ also may be compared with the rate of reaction of $\text{Cr}(\text{H}_2\text{O})_6^{+2}$ and $\text{Cr}(\text{dipyridyl})_3^{+2}$ with $\text{Co}(\text{NH}_3)_6^{+3}$. The dipyridyl complex reduces $\text{Co}(\text{III})$ about 10^8

(10) H. Taube, *J. Am. Chem. Soc.*, **77**, 4481 (1955).

times faster than does the aquo complex.¹¹ Thus, the effects of metal complexing on triplet-singlet catalysis seem to be similar to the effects on charge-

(11) A. M. Zwickel and H. Taube, *Discussions Faraday Soc.*, **29**, 42 (1960).

transfer reactions. The notion that conjugated systems are better "electron-conductors" than unconjugated ones, combined with a charge-transfer quenching mechanism, offers a simple explanation of these data.

PHOSPHINE OXIDE, SULFIDE, AND SELENIDE COMPLEXES WITH HALOGENS: VISIBLE AND ULTRAVIOLET STUDIES

BY RALPH A. ZINGARO, RAYMOND E. MCGLOTHLIN, AND EDWARD A. MEYERS

Department of Chemistry of the Agricultural and Mechanical College of Texas, College Station, Texas

Received July 31, 1961

The interaction of iodine, iodine monobromide, or iodine monochloride with various phosphine oxides, and phosphine chalcogenides, has been studied spectrophotometrically. In those cases where 1:1 complexes are the principal ones formed, and when the substituents on the phosphorus atom are identical, there is a considerable increase in the value of the formation constant, which follows the sequence $\text{Se} > \text{S} > \text{O}$. The formation of higher complexes, in which several moles of either donor or acceptor may be involved, has been observed, especially in the case of the phosphine oxides, when phenyl substituents are present, or when an interhalogen is the acceptor. Triphenylphosphine oxide has been found to undergo a photochemical decomposition which is iodine-catalyzed.

Introduction

The donor properties of the phosphine oxides have been demonstrated primarily by way of the numerous metal complexes¹⁻³ which they have been shown to form. This property has been utilized in a number of analytical methods which involve the separation of metals by solvent extraction.⁴ Tsubomura and Kliegman⁵ have studied the iodine-tri-*n*-butyl phosphite interaction and have speculated on the relative donor properties of the P-O groups as compared with R-O groups in the alkyl phosphonates. Recent studies⁶ dealing with the effect of halogen complexing on the P-O and P-S stretching frequencies in phosphine oxides and phosphine sulfides clearly demonstrate that, in the absence of phenyl substituents, molecular complex formation occurs *via* the phosphoryl or thio-phosphoryl linkage. In the present paper, the effect, upon halogen complexing, brought about by varying the group VI substituent or the organic groups on the phosphorus atom has been studied.

Experimental

Phosphine Oxides and Chalcogenides.—The source, method of purification, and the physical properties of all of these compounds are described in related publications.^{6,7} All of the compounds used possessed a very high degree of purity.

Other Materials.—J. T. Baker resublimed iodine was sublimed again in a dry, nitrogen atmosphere and stored over P_2O_5 . The bromine, "Analytical Reagent" grade, was distilled in a dry, inert atmosphere from concentrated sulfuric acid to remove any moisture. The preparation and purification of the interhalogens is described in a previous

publication.⁸ Chloroform and carbon tetrachloride were Mallinckrodt "Analytical Reagent" grade and were dried over calcium chloride and distilled in a dry atmosphere before use.

Methods.—A Beckman Model DK-1 recording quartz spectrophotometer was used for measuring absorption spectra. The temperature of the absorption compartment was maintained at $25.0 \pm 0.3^\circ$ by means of a water bath. Stopped quartz cells were used for all measurements. Although precautions were taken to minimize the effect of hydration, it was found that reproducible results could be obtained without exercising excessive precautions. It was necessary to weigh out and mix solutions of hygroscopic materials such as tri-*n*-butylphosphine oxide in a completely dry atmosphere. Once prepared, however, these solutions were found to be quite stable.

Due to the extreme insolubility of the chalcogenides, especially of the selenides, in hydrocarbons, the latter were not used as solvents and for this reason studies were carried out in chloroform when iodine was the halogen, or in carbon tetrachloride in the case of the interhalogens since the latter are unstable in chloroform. At the very low concentrations used, no precipitation or decolorization occurred during the time of execution of the experiments.

Results and Calculations

The experimental observations revealed that in many cases the tacit assumption of the sole existence of a 1:1 association equilibrium was much too naïve. The formation of higher complexes involving several moles of either donor or acceptor was found to take place in the case of the phosphine oxides and the interhalogens. Whereas the sulfides and selenides formed predominantly 1:1 complexes, few of the oxides showed such behavior. The experiments were set up in such a manner that a single equilibrium predominated, and the experimental data then were treated accordingly.

Case 1.—This represents those systems in which the formation of a 1:1 complex was indicated by the presence of a true isosbestic point and corroborated by Job's method of continuous variations. Such a case is illustrated by Fig. 1 where the typical "blue shift" is accompanied by a large increase in absorbancy in the higher frequency region, indicat-

(1) (a) R. H. Pickard and J. Kenyon, *J. Chem. Soc.*, 262 (1906); (b) J. C. Sheldon and S. Y. Tyree, *J. Am. Chem. Soc.*, **80**, 4775 (1958).

(2) F. A. Cotton, R. D. Barnes, and E. Bannister, *J. Chem. Soc.*, 2199 (1960).

(3) K. Issleib and B. Mitscherling, *Z. anorg. allgem. Chem.*, **304**, 73 (1960).

(4) J. C. White, *Anal. Chem.*, **30**, 989 (1958); C. A. Horton and J. C. White, *ibid.*, **30**, 1779 (1958); J. P. Young and J. C. White, *ibid.*, **31**, 393 (1959).

(5) H. Tsubomura and J. Kliegman, *J. Am. Chem. Soc.*, **82**, 1314 (1960).

(6) R. A. Zingaro and R. M. Hedges, *J. Phys. Chem.*, **65**, 1132 (1961).

(7) C. G. Screttas and A. F. Isbell, *J. Org. Chem.*, **27**, 2573 (1962).

(8) R. A. Zingaro and W. B. Witmer, *J. Phys. Chem.*, **64**, 1705 (1960).

TABLE I
EQUILIBRIUM FORMATION CONSTANTS FOR 1:1 IODINE-PHOSPHINE CHALCOGENIDE COMPLEXES IN CHLOROFORM

Donor	λ_{\max} (m μ) of complex band ^c	$\Delta\bar{\nu}_{1/2}$, cm. ⁻¹ ^d	ϵ^e	K
Tris-(<i>n</i> -octyl)-phosphine oxide ^a (TOPO)	437 (ϵ 930)	4500	506 (401)	588
Tris-(cyclohexyl)-phosphine oxide	370 ^b	4340	3,800	39
Tris-(cyclohexyl)-phosphine sulfide	421 (ϵ 2700)	2830	2,500 (402)	1,820
Tris-(cyclohexyl)-phosphine selenide	319	4940	89,000	46,600
Triphenylphosphine sulfide (TPPS)	430 (ϵ 3190)	2880	3,070 (417)	106
Triphenylphosphine selenide (TPPSe)	324	5570	44,000	3,370
Trimethylphosphine sulfide	425	4470	1,980	604
Tris-(<i>n</i> -butyl)-phosphine sulfide (TBPS)	421 (ϵ 3050)	4670	2,590 (395)	59

^a This run carried out in heptane. ^b A second band, of slightly greater intensity, was observed at 297 m μ in this case. The possibility that triiodide formation must be considered has been suggested by one of the reviewers as this would be an unusually large "blue shift." ^c The existence of two bands ("charge-transfer," or "blue-shift"), and their origin is given in the Discussion. ^d The half-intensity widths are calculated at the wave lengths given in the preceding column. ^e Where so indicated, ϵ is calculated at the wave length indicated in parentheses. This was done in order to minimize any contribution arising from overlap with the iodine absorption band.

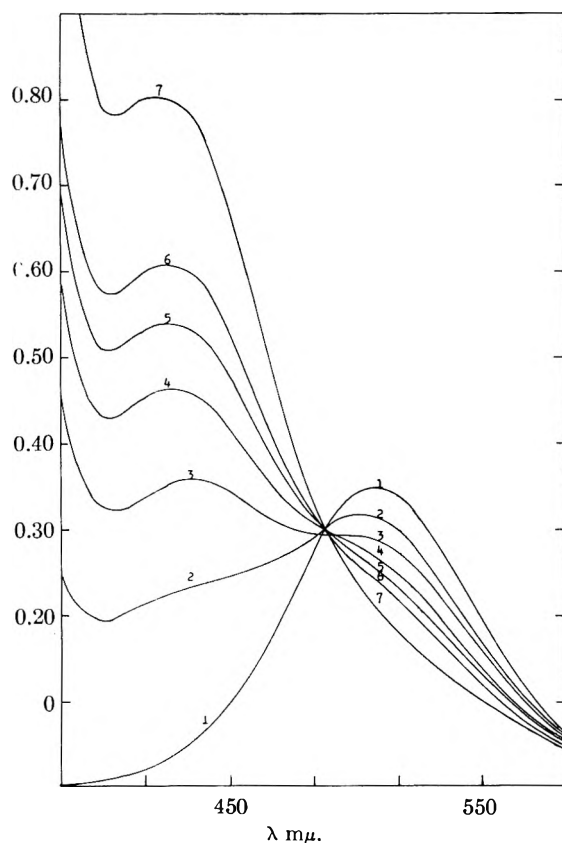


Fig. 1.—Absorption spectra for the system triphenylphosphine sulfide-iodine in chloroform. The initial concentration of iodine is $3.99 \times 10^{-4} M$ in each case. Initial concentrations of TPPS are: (1) 0; (2) $1.84 \times 10^{-3} M$; (3) $3.69 \times 10^{-3} M$; (4) $5.53 \times 10^{-3} M$; (5) $7.38 \times 10^{-3} M$; (6) $9.22 \times 10^{-3} M$; (7) $1.84 \times 10^{-2} M$.

ing the presence of a "charge transfer" band. The data obtained for these systems could be readily treated by the method of Rose and Drago⁹ which involves a graphical method of solution for both the equilibrium constant and the extinction coefficient. A typical example of the application of the equation of Rose and Drago to the data obtained for the system triphenylphosphine sulfide-iodine is shown in Fig. 2. In Table I are summarized the results obtained for the systems typical of case 1. The values in the last two columns are reliable to

(9) N. J. Rose and R. S. Drago, *J. Am. Chem. Soc.*, **81**, 6141 (1959).

within $\pm 10\%$. The values of half-intensity band widths are subject to greater error because of the overlap with adjacent bands.

Case 2.—For these systems the linear equation of Rose and Drago was inapplicable and they were treated on an individual basis with limited success.

As shown in Fig. 3, the system, IBr-triphenylphosphine sulfide (TPPS), at [IBr]/[TPPS] ratios from 0.25–3, illustrates the typical "blue shift" and tremendous increase in absorption beyond 350 m μ . Calculations based on the usual assumption that the band at 390 m μ is due to the formation of a 1:1 complex failed to give any acceptable consistency in either the values of the formation constant or of the extinction coefficient. When the ratio of IBr to TPPS was increased, the band at 390 m μ attributed to the "blue shift" disappeared (curves a–e), and, if the concentration of TPPS was maintained at sufficiently low levels, a peak at 283 m μ was clearly observed. That this absorption was due to a complex involving more than one mole of IBr to one of TPPS was established by calculating the amount of IBr consumed from the difference in the IBr peak at 492 m μ , before and after complexing. It was found that the amount of IBr used up at the higher [IBr]/[TPPS] ratios exceeded the total initial amount of TPPS used in the experiment. The possibility of formation of polyhalide ions such as IBr_2^- , Br_3^- ,¹⁰ etc., is considered in the Discussion. From the results of a series of 20 experiments in which the [IBr]/[TPPS] ratio was gradually increased from 5 to 100, while maintaining the [TPPS] at a constant value, the extinction coefficient of the complex was calculated as follows. The total absorbance, A_t , of the solution at 285 m μ is given by

$$A_t = \epsilon_a C_a + \epsilon_c C_c + \epsilon_d C_d \quad (1)$$

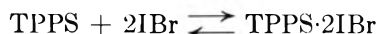
Where the ϵ 's and C 's refer to the extinction coefficients and concentrations, respectively, and the subscripts refer to the acceptor, a; complex, c; and donor, d. The extinction coefficient of the donor and acceptor were readily obtained from curves run on the pure materials. One mole of the complex absorbing at 285 m μ then was assumed to be formed from two moles of IBr reacting with one

(10) (a) A. E. Gillam, *Trans. Faraday Soc.*, **29**, 1131 (1933); (b) A. I. Popov, K. C. Brinker, L. Campanaro, and R. W. Rinehart, *J. Am. Chem. Soc.*, **73**, 514 (1951); (c) A. I. Popov and R. T. Pflaum, *ibid.*, **79**, 570 (1957), and numerous references therein.

of acceptor. The extinction coefficient of the complex then was calculated by subtracting $\epsilon_{\text{IBr}}C_{\text{IBr}}$ from A_t until A_c became constant, indicating that all of the donor was complexed.¹¹ Beyond $[\text{IBr}]/[\text{TPPS}]$ ratios of 6:1, ϵ_c reached a constant value, and remained unchanged within 1.5% up to the final concentration ratio used of 100:1. Hence ϵ_c could be used with a high level of confidence. Algebraic manipulation of eq. 1 leads to the following expression (2) for calculating C_c , the equilibrium concentration of complex

$$C_c = \frac{A_t - A_{\text{IBr}} - \epsilon_d C_{d_i}}{\epsilon_c - \epsilon_d} \quad (2)$$

In (2), C_{d_i} is the initial donor concentration. Thus, direct calculations were made of the concentrations of the various species present at equilibrium. Results calculated from ten independent experiments for the equilibrium



gave a value of $3.38 \pm 0.39 \times 10^7$ for the formation constant and a value of $4.05 \pm 0.45 \times 10^4$ for the extinction coefficient of the complex.

For the phosphine oxides as a group, complications arise. The triphenylphosphine oxide (TPPO)-iodine system was studied carefully over a wide range of concentrations and no consistency in the results was noted. It finally was established that TPPO undergoes a photochemical decomposition which is halogen catalyzed. It is not certain whether the complex behavior of the other phosphine oxides was due also, at least in part, to photochemical instability. In some experiments with phosphine oxides other than TPPO it was possible to calculate fairly consistent values for equilibrium constants for a 1:1 complex. In these cases, 1:1 complex formation was assumed and the amount of halogen complex formed was calculated by the changes in absorption of the characteristic halogen band as the donor concentration was varied. The results of these calculations are given in the footnote below.¹²

Discussion

The ability of the phosphine oxides and chalcogenides to complex with halogens has been demonstrated beyond any doubt. That the interaction occurs *via* the P=O group has been clearly shown in infrared studies,⁶ where a reversible shift in the fundamental P=O stretching frequency before and after halogen complexing has been found.

A comparison of the relative complexing ability of the molecule as a function of the group VI substituent on the phosphorus atom is complicated by the formation of complexes possessing different stoichiometries. The tris-(cyclohexyl) series, Table I, shows a progressive increase in the formation

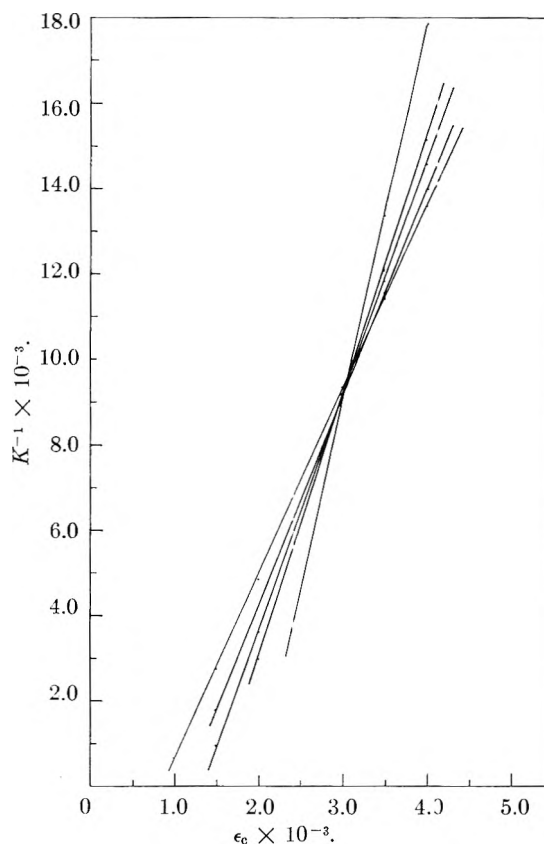


Fig. 2.—Graphical solution for the formation constant, K , and the extinction coefficient of the complex, ϵ_c , by the method of Drago and Rose⁹ for the system TPPS-I₂, using the data of Fig. 1.

constant as one proceeds from O to S to Se. However, no other sequence can be compared, although this trend is further apparent if pairs of otherwise identical molecules are examined. For instance (Table I and footnote 12) the formation constant of the complex formed with the molecule bearing the more electropositive group VI substituent always is greater, *e.g.*, TBPS > TBPO; TPPSe > TPPS. No exception to this regularity is noted, but a generalization must be deferred pending a more exhaustive study of this series of molecules. The effect of π - π interaction involving the $p\pi$ halogen electrons and the availability of empty 3d orbitals in sulfur and of 4d orbitals in selenium has been discussed⁶ in a previous publication.

In view of the foregoing it is interesting to note that the triphenylphosphorus derivatives bearing S or Se atoms form stable 1:1 complexes, whereas two moles of donor are involved in what seems to be the stable TPPO-halogen complex. Infrared studies⁶ clearly demonstrate that TPPO is the only one of the phosphine oxides which shows a reverse trend in the direction of the shift of the P=O fundamental on halogen complexing. Although the experimental evidence is not conclusive, it does suggest that complexing *via* the phenyl groups is involved. This further substantiates the stronger donor ability of the thio- or selenophosphoryl group as compared with the phosphoryl group.

The lack of correlation between the nature of the substituent organic groups and the formation con-

(11) This procedure is described in more detail elsewhere, see A. I. Popov and R. H. Rygg, *J. Am. Chem. Soc.*, **79**, 4622 (1957).

(12) (a) Tris-(2-ethylhexyl)-phosphine oxide-I₂: λ_{max} 361 m μ ; $\epsilon_c \approx 1700$; $K \approx 5.8$; (b) Tris-(*n*-butyl)-phosphine oxide-I₂: λ_{max} 364 m μ ; $\epsilon_c \approx 5100$; $K \approx 10.6$; (c) Dicyclohexylphenylphosphine oxide-I₂: no λ_{max} since there occurred a continual rise in absorption; ϵ_c (433 m μ) 1500; $K \approx 17$; (d) TOPP-IBr; λ_{max} 400 m μ ; $K \approx 4.9 \times 10^3$, based entirely on IBr absorption. Because of the experimental difficulties described, estimates of the uncertainties in these values are not given.

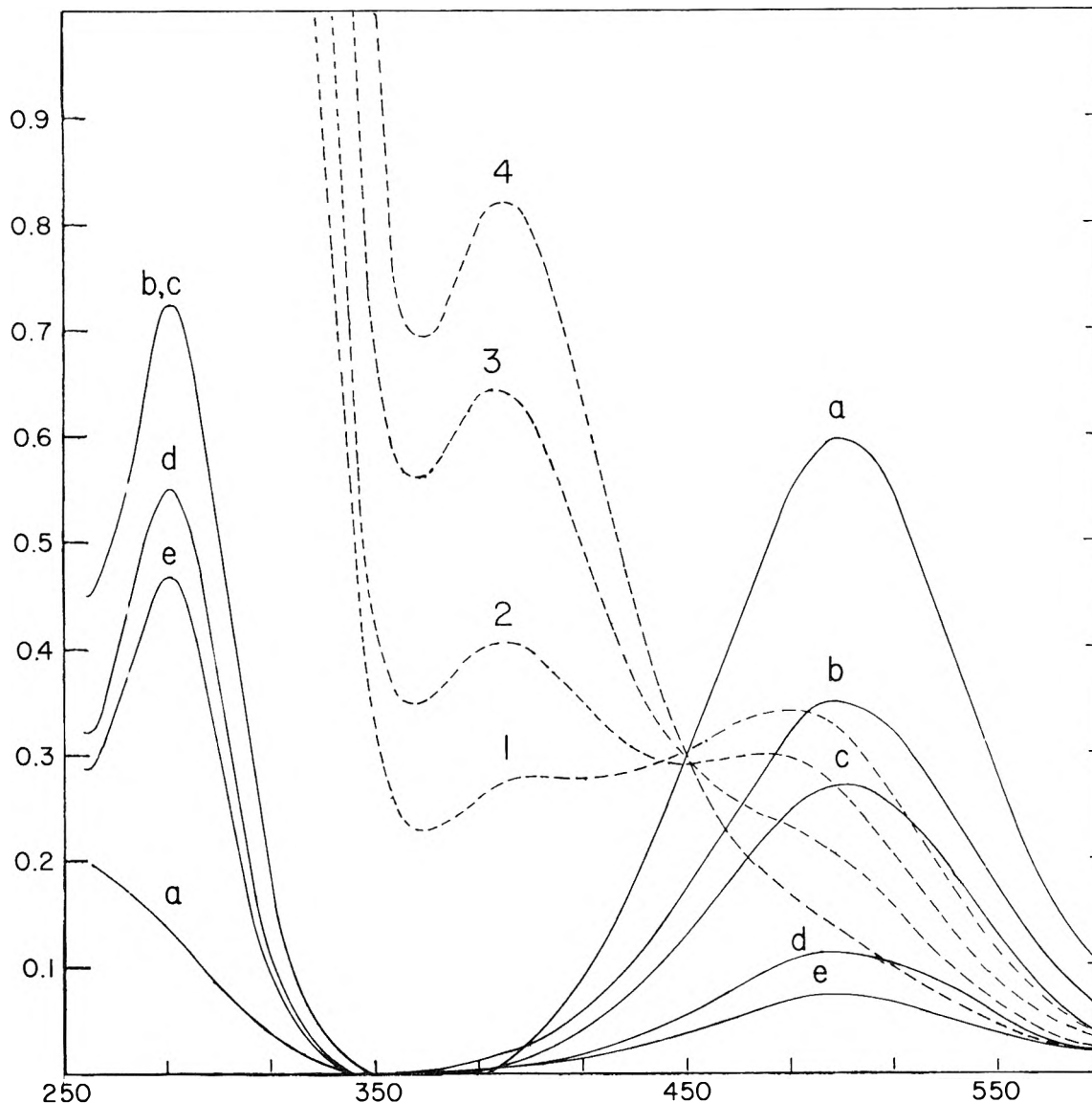


Fig. 3.—Absorption spectra for the system IBr-TPPS in carbon tetrachloride at 25°. The initial concentration of IBr for the dashed curves is $9.22 \times 10^{-4} M$ in each case and the TPPS concentrations and [TPPS]/[IBr] ratios are, respectively, (1) $1.84 \times 10^{-4} M$, 0.20; (2) $3.69 \times 10^{-4} M$, 0.40; (3) $7.38 \times 10^{-4} M$, 0.80; (4) $1.48 \times 10^{-3} M$, 1.60. For the solid curves the initial concentrations of IBr, TPPS, and the [TPPS]/[IBr] ratios are, respectively, (a) $1.41 \times 10^{-3} M$, 0, —; (b) $8.46 \times 10^{-4} M$, $1.84 \times 10^{-6} M$, 45.8; (c) $6.77 \times 10^{-4} M$, same as (b), 36.6; (d) $2.32 \times 10^{-4} M$, same as (b), 15.3; (e) $1.62 \times 10^{-4} M$, same as (b), 8.8.

stant, is quite obvious. The formation constant for the TOPO-I₂ complex is 60 times greater than that of the TBPO complex, but it seems unlikely that sufficient difference exists between the donor strength of an *n*-butyl and an octyl group to account for the variation. There is no apparent reason for the sequence tricyclohexyl > trimethyl > tri-*n*-butyl observed in the formation constants of the respective phosphine sulfide complexes. This apparent lack of correlation may be attributable to a number of factors including the geometry of the complexes, but this type of solution study reveals nothing about such factors. One conclusion which may be drawn is that the group VI atom attached to the phosphorus is much more important than the nature of the organic substituents in determining the magnitude of the formation constant.

The effect on the interaction of increasing the

polarity of the interhalogen would be interesting to evaluate, but no conclusions were drawn from this work for several reasons. As has been shown in the preceding section, IBr tends to form complexes involving several moles of interhalogen to one of the donor. This makes a direct comparison with iodine, for instance, difficult. Furthermore, experiments involving ICl gave data which did not yield to any of the conventional approaches insofar as establishing the stoichiometry of any species formed. In addition, no reproducibility was found in the values for the formation constants calculated as was done for other systems. The system TOPO-ICl, for example, gave an eightfold spread in calculated values of *K*. In another case, TPPS-ICl, a rapid formation of iodine was observed on mixing, so that pertinent equilibria could not be examined.

In Table I, the location of the bands and the

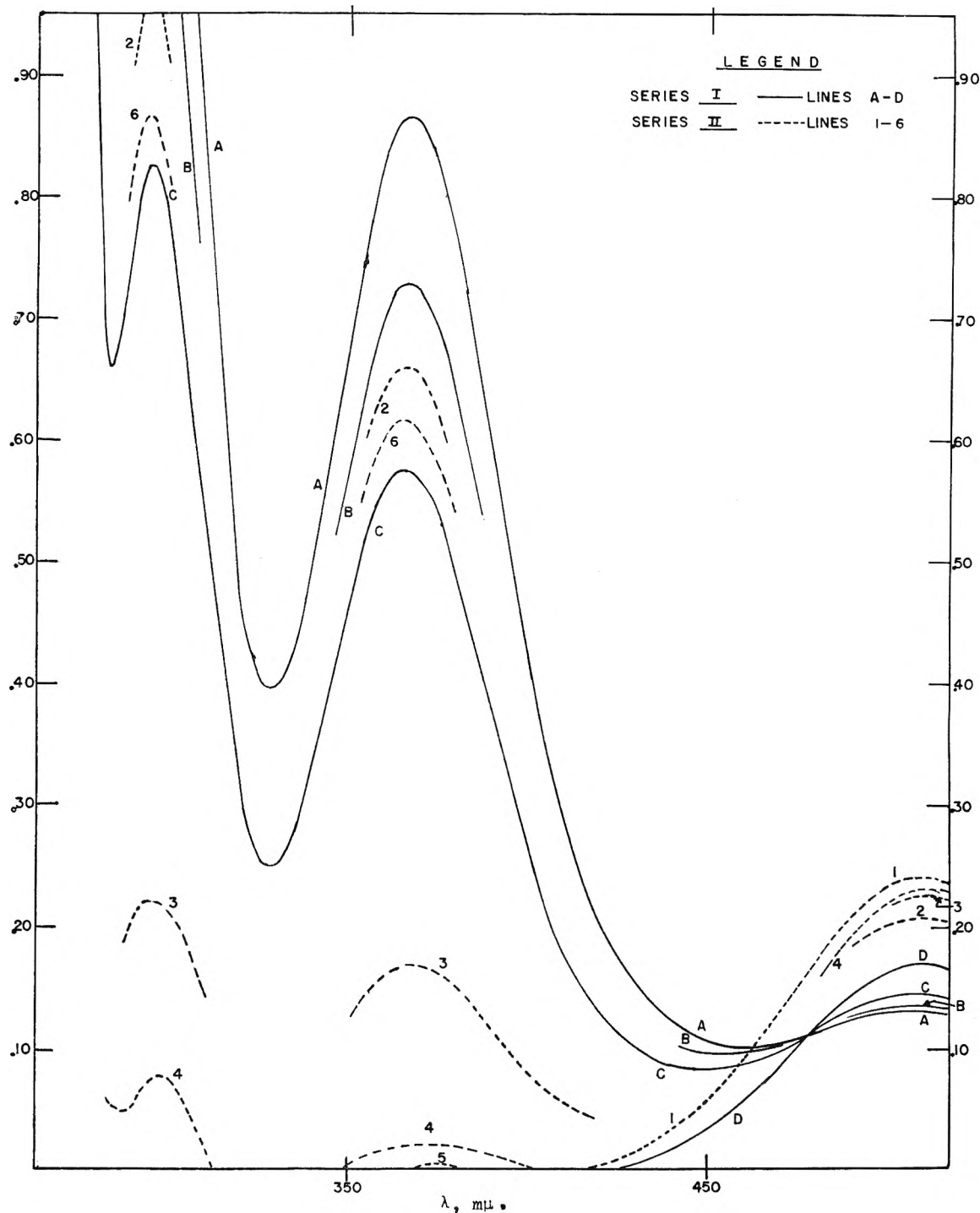


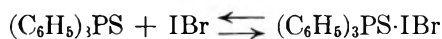
Fig. 4.—Effect of light and time on spectra of TPPO-I₂ solutions. In series I, stock solutions in chloroform, of iodine, $9.8 \times 10^{-4} M$ (A), and of TPPO, $4.61 \times 10^{-2} M$, one of the latter stored in a clear glass flask (L) and the other stored in a flask coated with opaque black tape (D), were used. All solutions in series I were mixed *immediately prior to measurement*, from 5 ml. of A and 5 ml. of either L or D, diluted to 25 ml. Curve A represents fresh solutions made up from either L or D. Curves B and C are each 72 hr. old, but curve C represents a solution made up from L and curve B from D. Series II shows the spectra of solutions containing iodine, $2.84 \times 10^{-4} M$, and TPPO, $7.18 \times 10^{-3} M$, so that both components are present at all times. Solutions 2-5 were stored in a clear flask exposed to daylight. Curve 2 was measured as soon as possible after mixing, curve 3 after 45 min., curve 4 after 104 min., and curve 5 after 165 min. Curve 6 is a solution of the same composition after 20 hr., but stored in a flask coated with black tape. Curve 1 is for pure iodine of the same concentration. Curve 5 is superimposed upon curve 1 at the longer wave length. The restoration of the iodine peak is to be noted.

values of the corresponding extinction coefficients indicate that they may be classified into one of two well known categories. Those whose maxima lie above $350 m\mu$ are illustrative of the "blue-shift"

which is the shift of the visible iodine absorption to a shorter wave length as a result of donor perturbation. With the exception of tri-(cyclohexyl)-phosphine oxide, it will be noted that all of the "blue-shifted"

bands fall in the region 421–437 $m\mu$. In those two cases where the bands at 319 $m\mu$ have been utilized for the purpose of making calculations, these probably are "charge-transfer" bands. Although it is likely that both bands are present in all of these systems, the search for these was complicated by the extraordinary stability and high absorbancy of these complexes, which limited the range of experimental concentrations. In the case of the tris-(cyclohexyl)-phosphine oxide-iodine complex, the 370 $m\mu$ band probably arises from the "blue-shift" as indicated by the order of magnitude of its extinction coefficient and the presence of a higher frequency absorption band of greater intensity. The latter may well be the charge-transfer band.¹³

Both the location (283 $m\mu$) and the magnitude of the extinction coefficient (40,500) of the absorption band observed for the TPPS-IBr complex, as well as its stoichiometry, suggest the possibility of polyhalide formation. The limiting value reached in the absorptivity of the peak at constant TPPS concentration, even at large $[IBr]/[TPPS]$ ratios, clearly indicates that an equilibrium involving TPPS is involved. A polyhalide equilibrium involving the interhalogen itself is ruled out by the limiting value of the peak height attained under the conditions just described. Based upon published values¹⁴ of the extinction coefficients and absorption maxima for various polyhalides, I_3^- and I_2Br^- formation does not seem likely since characteristic absorption bands of sufficient intensity at 360 or 351 $m\mu$, respectively, should be observed concurrently with the ultraviolet bands in the concentration ranges utilized. Reference to Fig. 3 shows the absence of such bands. However, for IBr_2^- in ethylene dichloride, absorption bands at 370 $m\mu$ (ϵ 660) and 256 $m\mu$ (ϵ 54000) are reported,^{10,14} while for Br_3^- a single band at 269 $m\mu$ (ϵ 55000) is reported and under the experimental conditions utilized in the present studies, only a single band would be observable. The location and intensity of the band observed in this study, allowing for errors in calibration and solvent effects, suggests that the formation of one of these ions is a possibility. Tribromide ion could only form by decomposition of IBr, and this does not appear to happen. It is not unlikely, however, that an "inner complex" may be formed which would give rise to IBr_2^- or an IBr_2^- like structure of the type $[(C_6H_5)_3PSI]^+[IBr_2]^-$ in two steps



This would be very similar to the situation observed in the case of pyridine-iodine solutions.¹⁵

(13) See footnote b, Table I.

(14) A. I. Popov and R. F. Swensen, *J. Am. Chem. Soc.*, **77**, 3724 (1955).

(15) C. Reid and R. S. Mulliken, *ibid.*, **76**, 3869 (1954).

The phosphine oxides, with the exception of TOPO, exhibited complicated, difficultly reproducible behavior. The triphenylphosphine oxide (TPPO)-iodine system was studied in most detail. As is shown in Fig. 4, this system is characterized by absorption bands at 293 and at 363 $m\mu$. This strongly suggests the formation of triiodide ion. Examination of Fig. 4 reveals the following important facts. A photochemical reaction of TPPO itself occurs. This reaction does *not* involve consumption of iodine since the iodine concentration reverts to its initial value following the irreversible decomposition of TPPO. The absorption bands observed in TPPO- I_2 systems must be due to the formation of a complex between these two species since these bands disappear upon exposure to light. If they arose from interaction of iodine with the decomposition products, they should *increase* in intensity and the band due to free iodine should not be restored.

The obviously more rapid photodecomposition of solutions containing iodine throughout light exposure as compared with those of the same age and conditions of exposure, but in which the iodine is added just prior to measurement (Fig. 4), indicates very strongly that the iodine is acting as a catalyst. A series of measurements was carried out in which the rate of disappearance of the absorption peaks was measured as a function of iodine concentration. The rate of decomposition was the same in all cases, indicating a zero-order dependency on the iodine concentration.

While it is obvious that the photochemical reaction is one of the factors involved in complicating measurements of equilibria in the TPPO- I_2 system, it cannot be generalized that this type of behavior is characteristic of all the phosphine oxides.

In the case of the TPPO- I_2 complex, the formation of an "inner complex" of the type already discussed is strongly suspected. That triiodide formation takes place was indicated by measurements made on pure tetramethylammonium triiodide¹⁶ in $CHCl_3$. We tentatively suggest for this complex a stoichiometry of the type $(TPPOI) + I_3^-$.

A number of pure, crystalline addition compounds have been found to form between the halogens, or interhalogens, and the phosphine chalcogenides. These are currently being investigated and their preparations and properties will be reported in a forthcoming publication.

Acknowledgment.—We should like to express our appreciation to the United States Atomic Energy Commission for financial support under Contract AT-(40-1)-2733. We are indebted to the referees for their very helpful and constructive criticism.

(16) Solutions of $Me_4N^+I_3^-$ in chloroform showed absorption peaks at exactly 365 and 295 $m\mu$, but the extinction coefficients varied widely as a function of concentration. For example, at concentrations of 2.2 and $2.6 \times 10^{-3}M$ the respective extinction coefficients are: at 365 $m\mu$, 11,950 and 14,200; and at 295 $m\mu$, 16,300 and 20,800. We are extending these measurements to other pure polyhalides.

ON THE INTERACTION OF DYES AND POLYSACCHARIDES^{1,2}

BY BENJAMIN CARROLL AND HERBERT C. CHEUNG

*Chemistry Department of Rutgers, The State University, Newark 2, New Jersey**Received September 26, 1961*

Quantitative studies were made on the binding of cationic methylene blue and anionic congo red by soluble polysaccharides, using a spectral technique. The interaction of methylene blue and carboxylated starches was found to be predominantly electrostatic. The dye appeared to be absorbed in the dimeric form. At infinite dilution of the dye the binding data, when extrapolated to zero ionic strength, yielded a 1-1 correspondence between the dye and the carboxylate group of the starch. The competitive effect of the buffer ions was evaluated. The binding constants for the competing cation were found to be two orders of magnitude smaller than those for methylene blue. The binding of congo red by linear polysaccharides was found to be independent of chain length of the substrate over a wide range from about 17 to 860 glucose units. The effect of chain length was studied using corn amylose, hydrolysates of the amylose, and amyloextrins isolated by column chromatography. Branching of the substrate was found to decrease markedly the extent of binding of congo red. Because the dye interaction was independent of chain length over a wider range than that for iodine, it appeared advantageous to use congo red for the determination of the degree of branching in starch. This technique may have general applicability for high polymers. Binding by carboxylated starches was observed for congo red at pH 8. The extent of binding was about the same as that for neutral starches, indicating the small effect of charge of the substrate on the binding affinity for this dye. A mechanism based on the concept of configurational adaptability is suggested for the binding of congo red.

Introduction

Although the study of reversible binding of small ions by proteins has been reported in the literature for some time, there appears to be little work done with soluble polysaccharides. The well known interaction of iodine and starch certainly falls into the category of binding of small ions. This interaction, however, is restricted to larger linear molecules, and is thermodynamically irreversible. Further, in the description of starch splitting enzymes, amylolytic activity measurements have been restricted to the use of iodine. The use of other indicators could possibly extend the range of substrates which presently are too small in size to sorb iodine. It appeared desirable, therefore, to search for other types of small ions which could overcome these limitations.

Previous communications³⁻⁶ from these Laboratories indicated the possibility of using both cationic and anionic dyes for the binding study of starch. In the present paper some aspects of the nature of the binding of an anionic dye, congo red, and a cationic dye, methylene blue, by soluble polysaccharides are reported. Data have been obtained regarding the effects of charge, chain length, and the degree of branching of the polymer on the binding affinity.

In considering the possible methods for determining adsorption, the use of equilibrium dialysis was ruled out because of the retrogradation of amylose during the time required for equilibration. The applicability of spectral changes has been shown for congo red. Equilibrium is achieved in a matter of seconds, and the dye follows Beer's law.⁴ While equilibrium values are attained instantly with methylene blue, some explanation is required regarding the adherence to Beer's law. Over a concentration range from 10^{-6} to

10^{-4} M, methylene blue goes from a solution of mainly monomers to a solution of dimers, and Beer's law is not obeyed. However, it was found that over the restricted range (7 to 20×10^{-5} M), where adsorption was studied, Beer's law was followed probably because more than 95% of the dye was in a single (dimeric) form. Beer's law also was followed by the adsorbed form of the dye. Thus, the requirements were met for using spectral changes for quantitatively determining the adsorption of a so-called metachromatic dye.

Experimental

1. **Materials.**—Stock solutions of methylene blue (Fisher Scientific Co.) and congo red (National Aniline Division, Allied Chemical and Dye Corp.) were prepared from highest grade materials. Both dyes were used directly without further purification; appropriate corrections for the purity of the dye were made using the spectral values reported in the literature.^{4,7} The methylene blue solution was stored in a paraffined amber bottle, and kept in the dark.

All inorganic chemicals were of reagent grade. Buffers were prepared from sodium acetate and glacial acetic acid for pH 5.3, and from monopotassium phosphate and sodium hydroxide for pH 8.

The β -amylase was obtained from Wallerstein Co., Inc., New York, N. Y., and was free of the α -amylase activity.

The carboxylated starches prepared by the hypochlorite oxidation process were obtained from Dr. T. J. Schoch. The carboxyl content had been determined by titration with NaOH. In this method, the carboxyl groups were converted into the free acid form and the starch was leached with dilute acid to remove soluble materials which were titratable. Titration was then carried out in the gelatinized sample. The degree of carboxylation was expressed on a weight basis. The high linear corn and wrinkled pea starches were obtained from Corn Products Co. The corn starch was a product of National Starch and Chemical Corp., New York, N. Y., and was defatted subsequently during the course of this work. From Dr. R. J. Dimler of the Northern Utilization Research and Development Division, U. S. Department of Agriculture, Peoria, Ill., were obtained the corn amylose 14SSP and corn amylopectin 14SSP. These substances had been fractionated in the latter laboratory using a procedure based on the Schoch method.⁸ With the exception of the defatted starch and the amylose, all starches were used without further purification. The amylose was treated with methanol four times and dried at 60° for 3 hr. under a reduced pressure. Moisture content was determined by heating separate portions of the substances at 110° for 2 hr.

2. **Binding of the Dyes.** Binding was studied by a spec-

(1) Abstracted from the Ph.D. dissertation of Herbert C. Cheung, Rutgers, The State University of New Jersey, 1960.

(2) This investigation was supported by a grant from the Corn Industries Research Foundation, Inc.

(3) B. Carroll and J. W. Van Dyk, *Science*, **116**, 168 (1952).

(4) B. Carroll and J. W. Van Dyk, *J. Am. Chem. Soc.*, **76**, 2506 (1954).

(5) B. Carroll and H. C. Cheung, *J. Agr. Food Chem.*, **8**, 76 (1960).

(6) H. C. Cheung, B. Carroll, and C. E. Weill, *Anal. Chem.*, **32**, 818 (1960).

(7) A. Levine and M. Schubert, *J. Am. Chem. Soc.*, **74**, 91 (1952).

(8) T. J. Schoch, *Cereal Chem.*, **18**, 121 (1941).

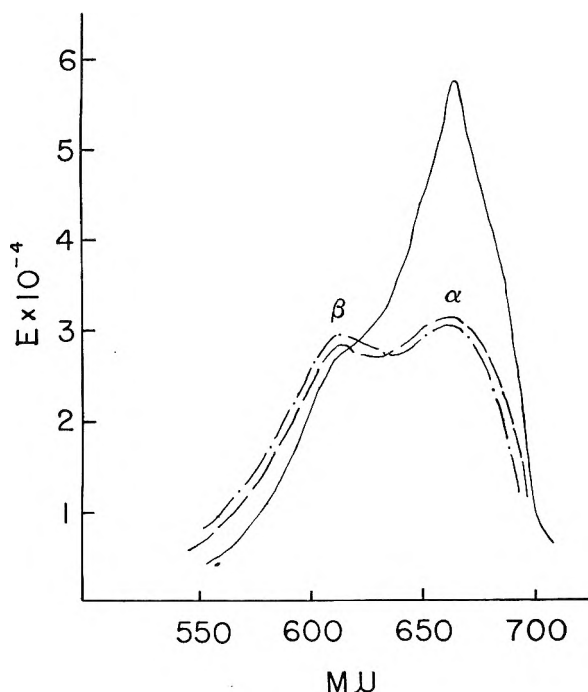


Fig. 1.—Effect of concentration and carboxylated starch on the spectral curve of methylene blue at pH 8: ——— dye alone at $1 \times 10^{-5} M$; - - - dye alone at $1 \times 10^{-4} M$; - · - · - dye at $1 \times 10^{-4} M$ plus 0.2% carboxylated starch (1.67% carboxyl).

tral technique. The extent of binding was determined directly in the dye-substrate mixture. Spectral measurements were made on a Beckman DU spectrophotometer, equipped with cells of 1-cm. path length. Cooling blocks were installed to permit control of temperature to within $\pm 0.1^\circ$. A Beckman Model G pH meter was used for pH measurements.

A. Methylene Blue.—The general procedure for the binding of methylene blue and carboxylated starches has been reported.⁶ The total dye concentration was about $10^{-4} M$. The extinction coefficient of the dye was obtained by a differential method. For the effect of ionic strength on the degree of binding, a series of spectral measurements was made for each concentration of starch. Keeping the concentration of the dye fixed, the ionic strength was varied using different amounts of buffer. A dye solution of the same ionic strength was used as a blank. The extinction coefficient of the dye-starch mixture in the absence of salts then was obtained from an extrapolation of the spectral data to zero ionic strength.

B. Congo Red.—The present procedure for the binding of congo red by polysaccharides has been described.⁵ For the dependence of binding affinity on chain length, samples of the substrate were prepared from corn amylose 14SSP which was first hydrolyzed in 6.2 *N* HCl. This was done by first dispersing the amylose in 1 *N* NaOH. The ratio of starch to alkaline solution was 1:20. To every 10 ml. of the amylose solution, 55 ml. of chilled concentrated HCl was added. Then sufficient water was added to yield a final volume of 100 ml. At given time intervals, 5 ml. of the hydrolyzed mixture was removed and neutralized with an equivalence of 1 *N* NaOH in a 50-ml. volumetric flask. Five milliliters of pH 5.3 buffer and 5 ml. of $1 \times 10^{-4} M$ congo red then were added, followed by dilution to volume. Spectral measurements were made at 500 *mμ* immediately thereafter.

A portion of the hydrolyzing mixture was removed after 45 min. After neutralizing with NaHCO_3 to methyl orange, the hydrolysate was separated into several amyloextrins in a charcoal-Celite column. The general procedure was that of Whistler and Tu.⁹

The average chain length of the isolated amyloextrins as well as the original amylose was obtained from their reducing values. The latter was determined from oxidation of the aldehydic groups by alkaline potassium ferricyanide, using the colorimetric procedure of Nussenbaum and Hassid.¹⁰

3. The Iodine Reaction.—The iodine sorption values were obtained from potentiometric titration using a Beckman Model G pH meter. A bright platinum electrode was used against a calomel half-cell.¹¹ The colorimetric measurements were made at 615 *mμ*. The final solutions contained 0.003% I_2 , 0.003% substrate, and 0.03% KI.

4. Viscosity.—A No. 50 Cannon-Fenske viscometer was used. The efflux time for water was about 100 sec. The kinetic energy correction was assumed to be negligible. All measurements were made at $25 \pm 0.1^\circ$.

5. Analysis of Maltose Content.—A sample of starch was hydrolyzed with β -amylase. The resulting maltose upon complete hydrolysis was determined by an iodine-thiosulfate method.¹²

Results

A. The Binding of Methylene Blue by Carboxylated Starches.—The effect of carboxylated starch on the spectral curve of methylene blue at $10^{-4} M$ is shown in Fig. 1. Also included for comparison is the absorption spectrum of the free dye at low concentration ($10^{-5} M$). These curves were obtained at pH 8. Addition of the substrate caused an enhancement of the β -band (615 *mμ*) and a depression of the α -band (665 *mμ*). The spectral changes may be taken as evidence of binding. Similar changes were observed for the free dye when the aqueous concentration increased from 10^{-5} to $10^{-4} M$.

No appreciable binding of methylene blue was detected when the concentration of the dye was in the vicinity of $10^{-5} M$ and below. Also, no binding was observed when the pH was below 5. Therefore, all spectral measurements were made at pH 8 and in the neighborhood of $10^{-4} M$.

The binding data may be treated quantitatively in terms of multiple equilibria. This procedure¹³ is based on the assumption of statistical binding, and it neglects any possible lateral interaction among the bound ions. The binding data may be represented by the following two equations

$$1/r = 1/\{nk[A]\} + 1/n \quad (1)$$

and

$$r/[A] = kn - kr \quad (2)$$

where r is the number of moles of bound dye per mole of substrate, $[A]$ is the free dye concentration, n is the number of binding sites on the polymer, and k is the intrinsic binding constant.

According to eq. 1, a plot of $1/r$ against $1/[A]$ should yield a straight line. This is shown in Fig. 2. The value of r_0 here is the ratio of moles of bound (dimeric) dye to mole of carboxylate group of the starch. The intercept on the $1/r_0$ axis is $1/n$, the reciprocal of the number of binding sites per carboxylate group. The upper two lines (full and half-filled circles) were obtained at an ionic strength of 0.01 for two samples of different carboxyl content. It is seen that $1/n$ is about 2.2

(10) S. Nussenbaum and W. Z. Hassid, *Anal. Chem.*, **24**, 501 (1952).

(11) F. L. Bates, D. French, and R. E. Rundle, *J. Am. Chem. Soc.*, **65**, 142 (1943).

(12) M. MacLeod and R. Robinson, *Biochem. J.*, **23**, 517 (1929).

(13) I. M. Klotz, *J. Am. Chem. Soc.*, **68**, 1486, 2299 (1946).

(9) R. L. Whistler and C. C. Tu, *J. Am. Chem. Soc.*, **74**, 3069 (1952).

for both materials. The open circles represent data obtained at zero ionic strength. Every point of this latter line was obtained by extrapolating the binding data to zero ionic strength. The value of $1/n$ for zero ionic strength is seen to be 0.98.

A 97% decrease in optical density was observed for the dye-substrate system when the ionic strength increased from 0.004 to 0.05. It is to be noted that in the absence of substrate the addition of electrolyte of this concentration had little effect upon the spectral properties of methylene blue. A quantitative estimate of the competitive effect of the buffer ions was evaluated by extrapolating the binding to zero ionic strength. The extrapolation was possible because the binding was not affected by the small change in pH [7-9] which was caused by the variation in concentration of electrolytes. From the binding constants of the dye at finite and zero ionic strengths, the binding constants of the carboxylated starch for the buffer ions were calculated at 27 and 40°. This was done using a relation derived by Klotz.¹³ The results are shown in Table I. The binding constants of the dye were obtained from linear plots of $r/[A]$ vs. $[A]$ according to eq. 2. The intercept on the $r/[A]$ axis is the first binding constant, k_1

$$\lim_{[A] \rightarrow 0} [r/[A]] = kn = k_1$$

Included in Table I are the values of the first binding constant per mole of carboxylate group, for the dye at zero ionic strength, and 27 and 40°, and the corresponding values of ΔS^0 and ΔH^0 for both the dye and the buffer ions (Na^+ and K^+). These values were calculated using the standard thermodynamic relations.

B. The Binding of Congo Red by Polysaccharides.—The relative effect of chain length of linear polysaccharides on the binding affinity of congo red was studied using corn amylose 14SSP, and hydrolysates of the amylose. Figure 3 shows the relative adsorptivity of congo red for linear polysaccharides of various chain lengths. Included for comparison is the iodine adsorptivity obtained from colorimetric measurements. The relative adsorptivity of an amylopectin has been taken as the ratio of the spectral change for a fixed weight of substrate to that of the same weight of original (unhydrolyzed) amylose. Thus, the relative adsorptivity is given by the quantity

$$\frac{(\text{O.D.})_s - (\text{O.D.})_{ap}}{(\text{O.D.})_{am} - (\text{O.D.})_{ap}}$$

where $[\text{O.D.}]_s$, $[\text{O.D.}]_{ap}$, and $[\text{O.D.}]_{am}$ are the optical densities of the sample, amylopectin, and amylose, respectively (see ref. 6). Both curves were drawn through the points obtained from the hydrolysates (open points). The filled points represent data obtained from the amylopectins isolated by column chromatography. It is to be noted that the adsorptivity of congo red begins to level off at about 17 glucose units in chain length. On the other hand, the binding of iodine appears

TABLE I
THERMODYNAMICS OF THE BINDING OF METHYLENE BLUE AT ZERO IONIC STRENGTH, AND OF BUFFER IONS (Na^+ , K^+) AT 0.01 IONIC STRENGTH BY CARBOXYLATED STARCH (0.84% CARBOXYL)

	Dye ^a	Buffer ions
k_1 at 27°	1.74×10^4	1.74×10^2
k_1 at 40°	2.70×10^4	4.45×10^2
ΔH^0 , kcal./mole	+6.32	+13.5
ΔS^0 , e.u. (cal./mole/deg.) ^b	+40	+55

^a The binding constants, k_1 , are for the uptake of one dye ion by one mole of carboxylate group of the substance.

^b These values are based on one mole of carboxyl group.

to increase indefinitely with increase in chain length, until a chain length of about 100 to 150 glucose units is attained.

The effect of chain length may be expressed quantitatively in terms of the binding constant. Using eq. 2, the values of k_1 , the first binding constant per glucose unit, may be calculated. The results are summarized in Table II for several samples ranging in chain length from 860 to about 8 glucose units. The binding constants are for the first congo red ion complexed with the linear substrate.

TABLE II
BINDING^a OF CONGO RED BY AMYLOSE AND AMYLODEXTRINS AT pH 5.3 AND 23.0.1°

Sample	Average chain length	$k_1 \times 10^{-3}$
14SSP	860 glucose units	13.2
G ₁₇	17	13.0
G ₁₂	12	9.61
G ₉	8.6	8.70
G ₈	7.8	7.73

^a The binding constants, k_1 , are for the uptake of one dye ion by one glucose unit of substrate.

From the data obtained at 23 and 31°, it is possible to calculate the molar changes in entropy and enthalpy for the binding of congo red by linear polysaccharides. The values are listed in Table III. Both ΔH^0 and ΔS^0 are positive.

The degree of branching of the substrate was found to decrease markedly the binding affinity of congo red. Contained in Table IV are the first binding constants for several native starches and amylopectin. The iodine sorption values and the per cent of amylose determined from the colorimetric iodine procedure are also included in Table IV.

The effect of heating of granular amylose at 110° in air on the binding of congo red was investigated. At given time intervals, a portion of the heated sample was cooled to room temperature and its binding for congo red and iodine was determined. Another portion of the heated material was hydrolyzed with β -amylase, and the resulting maltose content upon complete hydrolysis was determined. Figure 4 contains the data for these heat treated samples. Here the relative adsorptivity is plotted against the maltose content, and the time of heating of the original amylose is included. The data of the dye appear to fall on a straight line, while no linear relation appears to exist for the iodine data.

TABLE III

THERMODYNAMICS^a OF THE BINDING OF CONGO RED AND LINEAR POLYSACCHARIDES AT pH 5.3

Chair length	k_1 at 23°	k_1 at 31°	ΔH^0	ΔS^0
860 glucose units	1.32×10^4	2.09×10^4	+10.3 kcal./mole	+21. e.u.
17	1.30×10^4	2.03×10^4	+10.0	+31

^a The binding constants, k_1 , are for one glucose unit of substrate, whereas the values for ΔH^0 and ΔS^0 are molar quantities.

TABLE IV

BINDING OF POLYSACCHARIDES FOR CONGO RED AND IODINE AT 23°

Sample	Congo red, ^a $k_1 \times 10^{-3}$	Iodine	
		Sorption ^b	% Amylose ^c
Amylopectin	1.78	0.50	0.0 ^d
Defatted cornstarch	3.70	5.20	24.5
High linear cornstarch	5.25	12.0	46.5
Wrinkled pea starch	6.90	15.0	76.5
Amylose	13.2	19.4	100.0 ^d

^a The binding constants, k_1 , were determined at pH 8 for glucose unit weight of starch. ^b Milligrams of iodine taken up per 100 mg. of polysaccharide. ^c From colorimetric measurement. ^d Basis of calibration.

Carboxylated starches were used to study the effect of charge. Addition of carboxylated starch to congo red caused an increase in the extinction coefficient at the spectral peak of the dye, 500 m μ . This effect was similar to that caused by the addition of neutral starches. This spectral change was taken as evidence of binding. The binding values of three carboxylated starches are shown in Table V.

TABLE V

BINDING^a OF CONGO RED BY CARBOXYLATED CORNSTARCH AT pH 8 AND 25°

Sample	% carboxyl	$k_1 \times 10^{-3}$
OC1	0.36	1.69
OC2	0.84	4.36
OC3	1.67	3.12

^a The values of k_1 are for glucose unit weight of starch.

The effect of binding of congo red on the viscosity of corn amylose was studied at pH 5.3 and 0.2 *N* NaCl. The results indicate a decrease in intrinsic viscosity from 50.0 ml./g. for the starch to 36.7 ml./g. for the dye-starch complex.

Discussion

The Binding of Methylene Blue. A. The Structural Form of the Adsorbed Dye.—The α -band at 665 m μ of the absorption curve of methylene blue (Fig. 1) is considered to be caused by the monomers of the dye. The subsidiary β -band is indicative of the presence of dimers. The effect of the addition of carboxylated starch to aqueous methylene blue at 10^{-4} *M* and pH 8 is similar to that caused by increasing the aqueous concentration of the free dye (Fig. 1). The same phenomenon is observed¹⁴ by adding ammonium sulfate to a very dilute solution of the dye in water (10^{-6} *M*). Since binding was detected in the present work only at higher concentration of the dye, *viz.* 10^{-4} *M*, it appears that the dye was adsorbed in the dimeric form. The absence of subsidiary peaks other than the β -band suggests the absence of aggregates higher than dimers.

The ratio of monomers to dimers may be estimated for the free dye from the spectral curves of the dye at 10^{-6} *M* in alcohol, and at 10^{-4} *M* in water. This involves the assumption that the dye exists exclusively in the monomeric form in alcohol. The extinction coefficient of the α -band is 90,400 in alcohol and is 30,000 at 10^{-4} *M* in water. In the presence of large excess of carboxylated starch, the extinction was found to be 29,000 at 10^{-4} *M*. It is seen that the absolute quantity of the monomeric materials is inappreciably changed upon adsorption. Thus, the correction due to change in the monomeric form of the dye may be neglected without introducing appreciable error.

B. Binding at Finite and Zero Ionic Strength.—

Figure 2 indicates two carboxylate groups per dye ion at 0.01 ionic strength ($1/n \approx 2.2$). Since the binding was found to be dependent upon ionic strength, this value is not entirely unexpected. When the data are extrapolated to zero ionic strength, the value of $1/n$ becomes 1.0 within experimental error. Figure 2 clearly shows the 1-1 correspondence between the dimeric dye ion and the carboxylate group of the starch.

It is interesting to note that the significance of the value of $1/n$ from the Klotz equation (1) has been considered by other investigators in the case of protein interactions. For the case of binding of inorganic cations and albumin,^{15,16} it has been assumed that the main sites of interaction are the carboxylate groups of the protein. Yet there does not appear to be any simple correlation between the number of bound cations and the number of anionic residues of the protein. In the case of carboxylated polysaccharides at zero ionic strength, the present work indicates that it is possible to attach physical significance to the values of $1/n$ because of the absolute method of determining carboxyl groups by titration. It appears that previous failure of other investigators to obtain reasonable agreement for the value of $1/n$ may be due in part to the effect of buffer ions. Since the binding of proteins is sensitive toward variation in pH, it would be difficult to obtain reliable data at low ionic strength, and hence to extrapolate the data to zero ionic strength. No such difficulty appears to be encountered in the case of starch.

C. The Thermodynamic Functions for the Binding Process.—Correction has been made for any competitive effects in calculating the binding values of methylene blue listed in Table I. A decrease of two orders of magnitude is found for the first binding constants, k_1 , going from methylene blue to the small monovalent cations, Na⁺ and K⁺. The binding constants, k_1 , are not the stoichiometric binding constants. To obtain the

(15) E. Brand, *Ann. N. Y. Acad. Sci.*, **47**, 187 (1946).

(16) I. M. Klotz, and H. G. Curme, *J. Am. Chem. Soc.*, **70**, 939 (1948).

(14) L. Michaelis, *J. Phys. Colloid Chem.*, **54**, 1 (1950).

latter, r must be expressed in terms of bound dye per mole of substrate. However, k_1 may be considered to be proportional to the stoichiometric constant, and hence taken to be a measure of the binding affinity.

It is possible to calculate the molar change in enthalpy from temperature measurements, without knowing the stoichiometric constants. The only assumption to be made here is that n is independent of temperature. Upon differentiation, the proportionality constant between k_1 and the stoichiometric constant drops out. The thermodynamic values are listed in Table I. Unlike the value for the change in enthalpy, the entropy change will depend upon the units chosen for the substrate. The entropy values listed in Table I have been calculated on the basis of one mole of carboxyl group.

The increase in entropy for both the dye and buffer ions may be ascribed to the release of water molecules from the hydrated substrate and small ions. Such an increase appears to be characteristic of many interactions between small ions and macromolecules. A change in configuration may also contribute to the observed increase in entropy. In the absence of complexing ions, the charged carboxylated starch probably assumes a more or less extended form. Upon binding with cations, the electrostatic effect is removed so that the complex assumes a more random configuration, contributing to the observed ΔS^0 .

The strong dependence of the binding affinity on ionic strength suggests that the binding is of coulombic origin. The fact that no binding was observed below pH 5 may be taken as additional evidence substantiating this idea. It would seem desirable to compare the observed energetics with those calculated for electrostatic interaction. Direct calculation of the electrostatic free energy requires certain assumptions which may not be realistic. Instead of making a direct calculation, one may follow Klotz's approach¹⁷ by assuming that the observed binding is entirely electrostatic. Using the observed binding constants at different temperatures, one may calculate the corresponding changes in enthalpy and entropy. This procedure leads to a value of +2.8 kcal. for ΔH^0 and +26 e.u. for ΔS^0 . These values are to be compared with the observed quantities of +6.32 kcal. and +40 e.u. (Table I). Such a calculation does not depend explicitly on the radius of the substrate molecule.

It is seen that the calculated values compare favorably with the observed values. Both the entropy and enthalpy agree in sign and in order of magnitude. This comparison should be considered qualitatively because of the precision involved in the determination of the temperature coefficient.

The present results suggest that a carboxylated polysaccharide may be taken as a substance to test an adsorption isotherm, as for example, the Klotz equation, since the number of binding sites is well defined and can be determined analytically. When the degree of carboxylation is of a few per cent or less, the substance conforms to the simple model

(17) I. M. Klotz and H. A. Fiess, *J. Phys. Colloid Chem.*, **55**, 101 (1951).

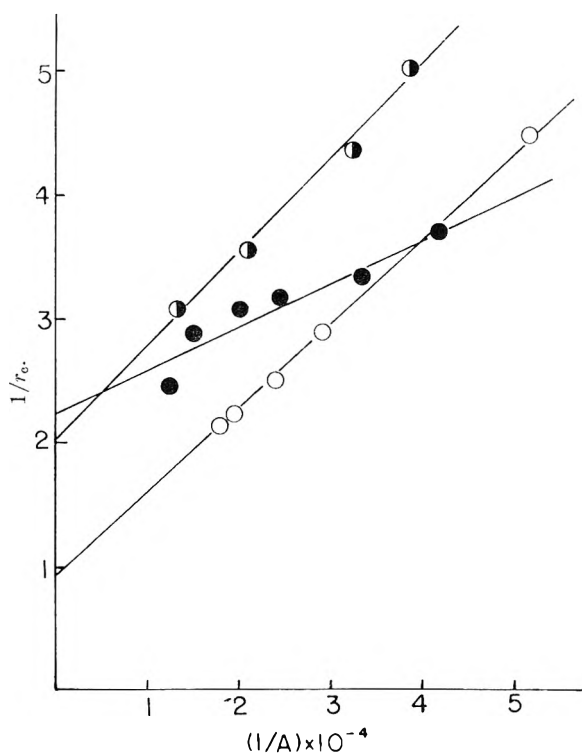


Fig. 2.—Extrapolation to determine the number of binding sites per carboxylate group for the binding of methylene blue and carboxylated starches at pH 8 and 27°. The upper two lines are for an ionic strength of 0.01: half-filled circle for OC3 (1.67% carboxyl); full circle for OC2 (0.84% carboxyl); open circle for zero ionic strength (OC2); $[A]$, molar concentration of free dye; r_e , specific adsorption per carboxylate group; total dye $ca. 1 \times 10^{-4} M$.

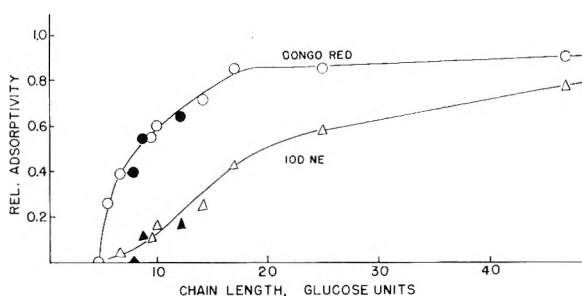


Fig. 3.—Relative adsorptivity vs. chain length for the binding of congo red and iodine by amylose and amylo-dextrins. Upper curve for congo red, lower curve for iodine. Both curves are drawn through data obtained from the binding of hydrolyzed amylose (unfilled points). Included are three points which were obtained from fractionated amylo-dextrins (filled points). Conditions for spectral analysis: congo red: dye $1 \times 10^{-5} M$, substrate 0.005%, NaCl 0.062 N, pH 5.3; iodine: I_2 0.003%, KI 0.03%, NaCl 0.025%, substrate 0.002%.

used in those adsorption equations where one assumes the absence of lateral interaction of the adsorbate molecules.

The Binding of Congo Red. A. Linear Polysaccharides.—The binding of congo red by linear polysaccharides is fairly independent of chain length for substrates larger than 17 glucose units in size (Fig. 3). For the iodine interaction, however, there is a steady increase in the relative adsorptivity. The latter effect is well known. The adsorptivity of congo red for the fractionated materials falls on the same curve as that for the un-

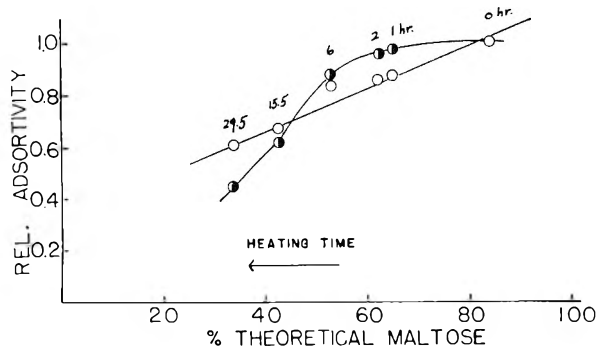


Fig. 4.—Effect of heating of solid amylose on the binding of congo red and iodine. Relative adsorptivity vs. per cent of theoretical content of maltose obtained upon complete hydrolysis of the heat-treated solid amylose with β -amylase. The numbers immediately above the points indicate the time of heating of the solid starch. Conditions for the binding studies identical with those in Fig. 3. Open circle, congo red; half-filled circle, iodine

fractionated hydrolysates. The iodine data indicate a lower affinity for the fractionated amyloextrins. This is not unexpected since the hydrolysates have a random distribution of molecular fragments and iodine is quite sensitive to the larger fragments. With the fractionated materials, there is an absence of the larger molecules, resulting in the lower adsorptivity for iodine. Because the dye binding is relatively insensitive toward the larger molecules, one would expect the fractionated materials to behave similarly to the unfractionated hydrolysates.

The values of k_1 in Table II, as in the case of methylene blue interaction, may be taken as a measure of the relative binding affinity. Thus, the binding affinity is approximately constant for long chain materials, the chain length studied ranging from 860 to 17. Below G_{17} (17 glucose units), there is a steady decrease in the values of k_1 with decrease in the size of the substrate molecule. Although the decrease is small, the trend is apparent.

No attempt is made to obtain the intrinsic binding constant k and the value of n . Unlike the interaction of methylene blue and carboxylated starch, for which $1/n$ is expected to approach unity, the uncertainty involved in the extrapolation of eq. 1 to obtain $1/n$ is very large. This is the case because $1/n$ here is expected to be different from unity. In this connection, Scatchard¹⁸ has suggested a plot of $r/[A]$ vs. r (eq. 2). In this case even if eq. 2 is used, n is still burdened with a large error since its determination involves an extrapolation in the region of large r , and hence large $[A]$, a region in which experimental data are poor.

The binding of azo dyes has been reported for polyvinylpyrrolidone and polyvinyl alcohol by Scholtan.¹⁹ Hydrogen bonding was believed to be responsible for the binding. However, Frank and co-workers²⁰ have expressed doubt on hydrogen bonding for the polyvinylpyrrolidone complex. In the present system of congo red and polysaccharides, hydrogen bonding appears to be unfavorable because of the positive value of ΔH^0 (Table

III). The positive entropy effect²¹ may be attributed to the release of hydrated water molecules from both the dye and the substrate upon binding. It is of interest to note that the observed energetics listed in Table III are consistent with those characteristic for the formation of a hydrophobic bond.²² However, it is difficult to conceive that this is the driving force in the binding of polysaccharides because of the predominant hydrophilic nature of the substrate.

B. Branched Polysaccharides.—Native starch contains both the linear component amylose, and the branched component amylopectin. As indicated by the iodine values (Table IV), the binding of congo red increases with increasing amylose content, or with decrease in the degree of branching. A 700% increase in the binding constant over that for amylopectin is observed for amylose. The binding constants for the defatted and high linear corn starches are in fair agreement with the weight averages of the binding constants of the individual components. The agreement for the wrinkled pea starch is somewhat poor, being about 15% higher than the estimated value.

It is well known that there are two major effects in the heating of granular amylose. One is reduction of chain length and the other is branching. Consider the data in Fig. 4, where the relative change in optical density of congo red and iodine is plotted against the maltose generated from the heated corn amylose. The amylose originally had a chain length of 860 glucose units. Reduction in chain length by a factor of 2 or 3 would not appreciably affect the adsorptivity of either indicator, as can be seen from the data in Fig. 3. Thus, the changes in optical density in the early stages of the heat treatment may be ascribed largely to branching. Since the maltose content may be taken as a measure of branching (increased branching yielding a lower amount of maltose), a linear relationship would be expected if the adsorptivity of congo red were determined primarily by the degree of branching. This is indeed the case. Apparently, the size of the starch fragments at the end of the longest heating was still sufficiently large so as to make the behavior of the dye reflect changes in branching only. Iodine was found to respond differently. In the beginning of the heating, the adsorptivity of iodine changed slightly compared to that for congo red. This would be due to the relative insensitivity of iodine toward branching. With amylose subjected to prolonged heat treatment, iodine passed into a region of greater sensitivity because the extended fragmentation of the amylose in addition to branching has caused a marked drop in the iodine adsorption.

It is not certain at this stage as to how much information one may obtain from the binding data concerning the degree of branching of the substrate molecule. The interaction of the dye is not specific for starch, but is a general phenomenon with many substances. It would appear that the adsorption procedure may prove useful in determining the

(18) G. Scatchard, *Ann. N. Y. Acad. Sci.*, **51**, 660 (1949).

(19) W. Scholtan, *Makromol. Chem.*, **11**, 131 (1953).

(20) H. P. Franz, S. Barkin, and F. R. Eirich, *J. Phys. Chem.*, **61**, 1375 (1957).

(21) The entropy values here have been calculated on the molar basis of the substrate.

(22) W. Kauzmann, American Chemical Society National Meeting, Atlantic City, N. J., September, 1959.

degree of branching in high polymers. This has been shown to be the case for starch.⁵

C. Carboxylated Polysaccharides.—The observation of the binding of congo red by carboxylated starch is in contrast with the staining of oxidized granular starch.²³ No staining has been observed with anionic starches and anionic dyes. Also little or no staining has been detected with anionic dyes and neutral starches, such as cornstarch.

While no information is available on the molecular weights and chain length of the carboxylated starches, it would seem reasonable to assume that chemical modification of the starch does not reduce the molecular weight much beyond an order of magnitude. The conclusion appears to have support due to the fact that the average value of the binding constants (Table V) for the carboxylated starches is reasonably close to that for native cornstarch (Table IV). At pH 8 the carboxylate groups are expected to be completely ionized. The data, therefore, suggest that the binding is not influenced to any appreciable extent by the presence of the carboxylate groups. This is contrary to prevailing opinion that an anionic dye will not bind an anionic substrate. The data also suggest that previous failure to detect staining of negative starches by negative dyes in the solid state may not be entirely an electrostatic effect, as has been suggested.²³ Perhaps a contributing factor in the binding of dyes

(23) T. J. Schoch and E. C. Maywald, *Anal. Chem.*, **28**, 382 (1956).

by starches is the internal flexibility of the polysaccharide chain. The binding in solution may be considered to be a consequence of the loss of rigidity of the starch molecules. An implication of this suggestion is that the reduction of the binding of amylopectin may be due in part to the rigid frame of the substrate. This is in accordance with the concept of configurational adaptability advanced by Karush.²⁴

It is conceivable that the configurational changes are favored by complexing with certain small ions. Thus there is established on the surface of the substrate a measure of complementarity with the surface of some small ions approaching it. An important feature of this concept is that complementarity need not imply specificity. As has been pointed out by Kauzmann,²⁵ there exists the probability, in some instances, that the specific complementarity structure may be developed only in the presence of certain small ions. This appears to be the case for the amylose-iodine helix.

D. Interpretation of Viscosity Data.—The lowering in intrinsic viscosity (from 50.0 to 36.7) indicates a reduction in the hydrodynamic volume of the starch-dye complex over the starch. The complex is more compact than the substrate since $[\eta] \propto [\bar{r}^2]^{3/2}$, where \bar{r} is the radius of gyration of the macromolecule.

(24) F. Karush, *J. Am. Chem. Soc.*, **72**, 2705 (1950).

(25) W. Kauzmann, *Rev. Mod. Phys.*, **31**, 546 (1959).

EFFECTS OF NEUTRON AND ULTRAVIOLET IRRADIATION ON THE CATALYTIC ACTIVITY OF MAGNESIUM OXIDE

BY JACK H. LUNSFORD AND THOMAS W. LELAND, JR.

Department of Chemical Engineering, Rice University, Houston 1, Texas

Received December 11, 1961

This work further develops a technique for changing the electronic and defect structure of magnesium oxide catalysts. Relatively small doses of ultraviolet and neutron irradiation have been found to enhance the catalytic activity of MgO for the reaction $H_2 + D_2 \rightleftharpoons 2HD$. The enhancement by radiation depends on the extent of degassing of the catalyst prior to irradiation; the less active samples are more sensitive to irradiation. For samples activated at 291°, ultraviolet-irradiated MgO reaches a precise saturation value of catalytic activity, while neutron-irradiated samples continue to increase in activity upon further irradiation. Both types of irradiation produce a large initial increase in activity. Changes in activation energy depend on the thermal activation and type of irradiation. The activation energy either increases or remains unchanged for neutron irradiation, while ultraviolet irradiation does not cause a change. For this system, a simple model based upon Fe^{+3} as the irradiation-induced site has been developed. Other possibilities are discussed. It has been shown that most of the activity change must be attributed to changes in the electronic structure of the crystal rather than in the number of lattice imperfections.

Introduction

The purposes of this investigation were to observe how low neutron fluxes and ultraviolet irradiation affect catalytic activity, and to relate changes in the solid state to the catalytic activity by proposing a model for irradiation-induced activity. The model proposed is not set forth as the unique mechanism for the effect of irradiation on catalytic activity, but it should serve as a proposition toward which other research efforts can be directed. The model is produced by comparing radiation effects on the bulk solid with the effects on catalysis.

Experiments involving the irradiation of catalysts have several interesting advantages. They

can be conducted on a single sample of a catalyst, with no complications from sample variability, and without the introduction of extraneous changes, as by alloying. The effects are largely local, and some of the properties suggested as important in active centers (paramagnetism, local strain, abnormal atomic spacing) can be associated with the point defects. Furthermore, by making comparisons between radiation effects on the bulk solid and effects of similar radiation on the catalytic activity, it is possible to gain some insight into catalytic mechanisms.

It appears that the magnitude of the effect of irradiation on catalysts is inversely proportional to

the number of current carriers in the catalysts; hence, irradiation has a more pronounced effect on insulators than on metals or semiconductors. A number of irradiations carried out by various workers have indicated this correlation; yet, there have been no two investigations using the same gas phase reactions and comparable dosages which could be used for comparison.¹⁻⁴ While this paper deals primarily with MgO, other work from this Laboratory on the irradiation of ZnO under similar conditions showed that comparable dosages produced changes in the catalytic activity of ZnO amounting to less than 5%.⁵ Neutron irradiation of MgO at the flux level used in this work produces no radioactivity in the irradiated samples.

Experimental

Apparatus and Materials.—The MgO catalyst used was "Baker Analyzed" powder. One batch was used throughout the experimental work. Impurity concentrations as reported on the label are 0.005% Cl, 0.01% SiO₂, <0.005% NO₃, 0.003% Ba, 0.01% Ca, 0.0002% Mn, 0.002% heavy metals (Pb), and 0.0002% Fe. Because of an interest in the transition elements, the powder was further analyzed by emission spectroscopy. The per cent impurities by weight are: <0.0003 Co, 0.0002 Cr, 0.0007 Fe, 0.001 Ni, and <0.0003 V.

High purity gases were used. The purification method is described by Lunsford.⁵

All work was carried out in a glass system capable of vacuums in the 10⁻⁶–10⁻⁷ mm. range. Mercury from manometers and a mercury diffusion pump was suitably removed by cold traps. The vacuum was continuously monitored by means of a Veeco ionization and thermocouple gage. Apiezon "N" stopcock grease was used throughout the system.

The reaction vessels were normally made from fused quartz to prevent poisoning the nuclear reactor with B¹⁰ or adsorption of short wave length ultraviolet light. All reactors ranged from 25 to 40 cc. in volume.

Neutron irradiation experiments were made in the center of an A.G.N. 211 nuclear reactor. Maximum power was 15 w., which corresponded to a peak thermal flux of 5.4×10^3 n./cm.²/sec. and a fast flux of about 6.7×10^8 n./cm.²/sec. The γ -intensity at 15 w. was about 5×10^3 r./hr.

Ultraviolet light was obtained primarily from a "Mineralight" source of 9 w. (electrical power) with a predominant wave length of 3660 Å. A 100-w. mercury vapor light and a 2537 Å. "Mineralight" also were used.

The gas samples were analyzed for per cent HD by means of gas chromatography, using the method of Moore and Ward.⁶

Experimental Procedure.—Rate measurements on the catalysts were made by expanding an equimolar mixture of H₂-D₂ into a catalytic reactor. The pressure of the reacting mixture varied from 100 to 700 mm. throughout the experiment. After a known length of time, the gas in the reactor was expanded into a chromatographic unit for analysis. The catalyst chamber was then thoroughly evacuated before the next charge was admitted.

After determining the catalytic activity of the catalyst in the absence of radiation, the catalyst and its container were removed from the vacuum system with the valve closed to prevent air from contacting the catalyst. The quartz container was then lowered into a 1-in. i.d. aluminum tube going into the center of the core of the nuclear reactor. Upon completion of the neutron irradiation, the catalytic reactor was placed back on the vacuum system for further activity measurements.

The term "neutron irradiation" is used to denote irradiations taking place in the nuclear reactor. There exists in the reactor a background of gammas, betas, and fission frag-

ments; however, relatively few gammas are absorbed in the catalyst and the beta and fission fragment flux will be reduced greatly by the aluminum, air, quartz, and self shielding in the fuel elements.

A special stopcock⁵ made it possible to admit the reactants to the catalyst while the quartz chemical reactor was being irradiated. The system was capable of maintaining a vacuum in the 10⁻⁶ mm. range.

During ultraviolet irradiation, the light source was placed a few cm. from the chemical reactor. Both the light source and the reactor were mounted horizontally so that the powder could be spread over a greater area. An aluminum foil reflector was used to better utilize the available light.

Experimental Results

A. Activation of Catalysts by Heating *in vacuo*.—For the MgO powder to exhibit any catalytic activity it was necessary to degas it *in vacuo* at elevated temperatures. The activity attained was a function primarily of the temperature; however, the amount of catalyst and time of heating had some effect. The thermally activated catalysts studied here can be divided into three groups: (a) catalysts activated at 291°, (b) catalysts activated at 374°, and (c) catalysts activated at about 520°. The catalysts were normally activated for a period of 2 hr. The rate of evolution of adsorbed gases was indicated by an ionization gage. A more quantitative measure of the rate was obtained gravimetrically with a quartz spring. Large evolution rates were obtained at 100° and for temperatures ranging from 200 to 300°. Other investigations have shown that much of this gas is water vapor.⁷ After thermal activation of the catalyst by heating *in vacuo*, reactions were run for various lengths of time. The data closely fitted a first-order, pressure independent rate equation similar to the results of Holm and Blue.⁸ Because of the sensitivity of the rate constant to the activity of the catalyst, the independence of the rate constant with pressure, and the fairly long contact times used, it is certain that the reaction is not diffusion controlled. At temperatures from 300 to 194°K., the reaction rate for catalysts activated in this manner is fairly stable prior to irradiation, indicating no poisoning or enhancement by the gases used. The rate constants obtained are characteristic of a clean catalytic surface in the sense that prior to irradiation the surface does not become poisoned or enhanced with use. This is not true, however, for catalysts which have been irradiated.

The effect of temperature on the rate constant follows the Arrhenius equation, $k = Ae^{-E/kt}$. As the temperature for thermal activation is increased, the activation energy decreases. This activation energy was so small for the catalysts activated at 520° that the reaction could be carried out conveniently at liquid nitrogen temperatures. The activation energies for MgO powders activated for 2 hr. at 520, 374, and 291° are, respectively, 1.0, 1.6, and 4.6 kcal./g. mole.

The effect of neutron irradiation on MgO is strongly dependent on the preceding thermal activation. The activity of the less active samples increased almost two orders of magnitude after

(1) H. B. Bragg, F. Morritz, R. Holtzman, P. Feng, and F. Pizzarello, Armour Research Foundation, WADC Tech. Rept. 59-286.

(2) H. W. Kohn and E. H. Taylor, *J. Phys. Chem.*, **63**, 500 (1959).

(3) H. W. Kohn and E. H. Taylor, *ibid.*, **63**, 966 (1959).

(4) E. H. Taylor and J. Wethington, *J. Am. Chem. Soc.*, **76**, 971 (1954).

(5) J. H. Lunsford, Ph.D. Thesis, Rice University.

(6) R. M. Moore and H. Ward, *J. Phys. Chem.*, **64**, 832 (1960).

(7) S. G. Hindin and S. Weller, "Advances in Catalysis," Vol. IX Academic Press, Inc., New York, N. Y., 1957.

(8) V. C. F. Holm and R. Blue, *Ind. Eng. Chem.*, **44**, 107 (1952).

exposure to integrated thermal neutron fluxes of about 6×10^{12} n./cm.². The samples of intermediate activity which were thermally activated at 374° increased only slightly and the more active samples activated at 520° decreased in activity at temperatures lower than room temperature. These effects are summarized in Table I. The activity induced by radiation in the less active samples was much more permanent than the radiation induced activity in the 374° activated samples.

B. Effect of Neutron Irradiation on Catalysts Activated at 291°.—Figure 1 shows the result of neutron irradiation on three samples of MgO initially activated at 291°. All of the data points were observed within 30 min. after removal from the reactor. The lower curve is taken from Day's work⁹ in which he measured the photoconductivity of MgO single crystals after exposure to similar integrated neutron fluxes. It should be observed that the activity rises rapidly at first but then attains a much slower rate of increase, though it appears that no saturation is imminent. This result agrees with electrical and optical measurements made by other investigators.⁹⁻¹¹

A series of experiments was conducted to investigate the stability of the catalytic activity induced by neutron irradiation. On all the catalysts studied, the neutron-enhanced reaction rate constant shows an initial period in which its value decreases rapidly followed by a second stage in which it decreases more slowly. In this second stage the logarithm of the rate constant decreases approximately linearly with time. For the 291° activated catalysts, the rate constant at 23° showed a very brief period of rapid decline and an extremely slow decrease during the second period in which about 50 hr. was required for the rate constant to fall to half its value.

To study the rapid decrease of the rate constant in the early period, measurements of reaction rates were made while the catalyst was being irradiated at various fluxes. Curve A in Fig. 2 represents rate constants measured at 23° during exposure to a thermal neutron flux of 2.4×10^{12} n./cm.²/hr. on a clean catalyst activated at 291°. The sharp break in curve A occurred when the flux was suddenly lowered by a factor of 15. The flux was kept at this reduced level for about 1 hr. and then stopped entirely. The rate constant decreased sharply as soon as the flux level was reduced and dropped to about 1/3 of its high flux value in a period of roughly 20 min. After this initial rapid rate of decline, the rate constant leveled off and decreased only with the very slow 50-hr. half-life characteristic of the catalysts in the slow logarithmic decay period.

This logarithmic decay period is much more rapid in catalysts initially poisoned with adsorbed water. Curve B in Fig. 2 represents the rate constant measured while radiation is in progress under the same conditions as curve A except that the catalyst has been poisoned initially, presumably with H₂O, by a 2-min. exposure to the atmo-

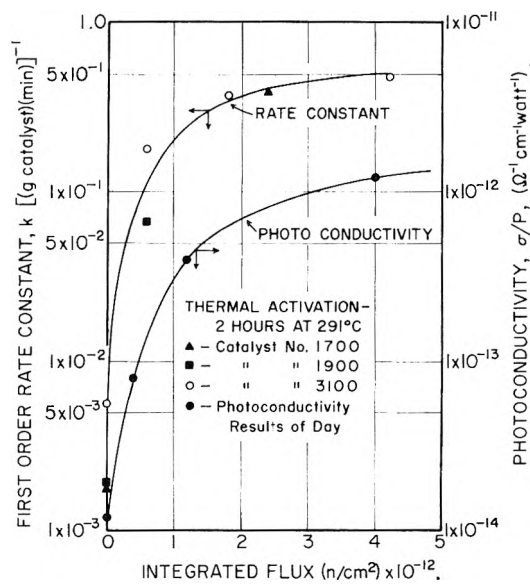


Fig. 1.—Effects of neutron irradiation on the catalytic activity of MgO.

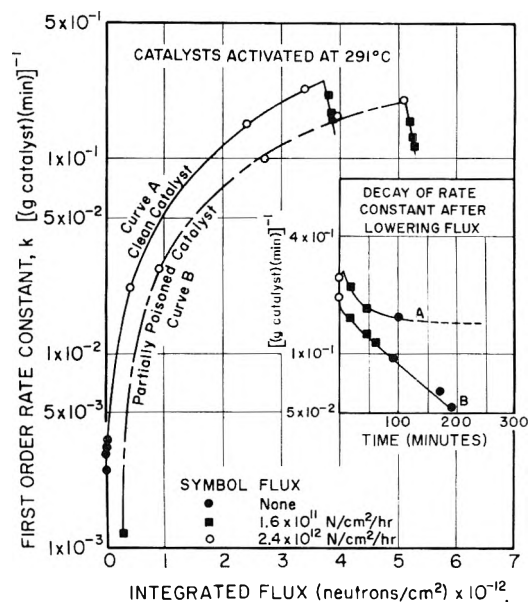


Fig. 2.—Effects of neutron irradiation on catalytic activity of MgO during irradiation.

sphere before evacuating and admitting the reactants. On reducing the flux and eventually stopping it as in the previous case, the rate constant goes through a similar brief period of very rapid decrease, but the following linear logarithmic decay is much more rapid than for the cleaner catalyst. The half-life of the rate constant is now only 2 hr. instead of 50 hr. for the cleaner catalyst. The initial period of rapid decline in rate constant followed by the region of very slow decline for both the clean and poisoned catalyst at 23° is shown by the inset in Fig. 2.

Arrhenius plots of the rate constants for the 291° activated catalysts show an increase in both the activation energy and in the pre-exponential term following neutron irradiation.

Heating an irradiated catalyst to various tem-

(9) H. R. Day, *Phys. Rev.*, **91**, 822 (1953).

(10) R. P. Clarks, *Phil. Mag.*, **2**, 607 (1957).

(11) C. M. Nelson and P. Pringsheim, Argonne Nat. Lab. Rept., ANL-4232 (1948).

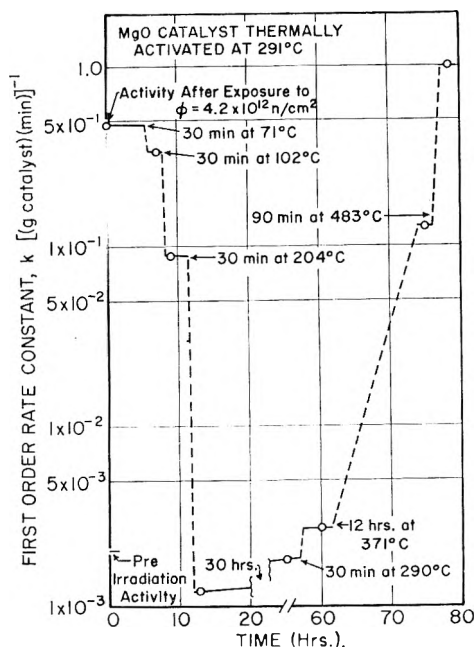


Fig. 3.—Effect of annealing followed by thermal activation.

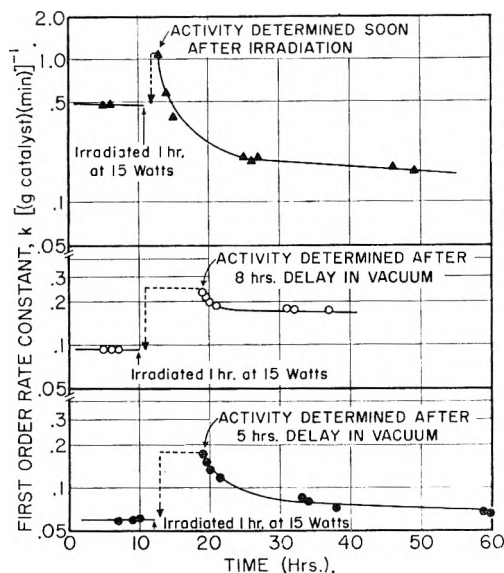


Fig. 4.—Effects of time of exposure to reactants on irradiated catalysts activated thermally at about 375°.

peratures, followed by cooling to 23° for reaction rate measurement, tends to remove the induced activity effects at moderate heating followed by thermal activation at higher temperatures. The effect of the annealing, as shown in Fig. 3, was to increase the rate of decay of activity. The activity fell to slightly below its pre-irradiation level, after which thermal treatment at temperatures above 290° once more increased the catalytic activity. The rapid decay at about 100° is in accord with the photoconductivity work of Day⁹ and the luminescence work of Yamaka.¹²

C. Effect of Neutron Irradiation on Catalysts Activated at 374°.—Catalysts which have been thermally activated at 374° show a much smaller increase in activity due to irradiation, and part of

the increase observed is quite unstable. Figure 4 shows the result of an integrated neutron flux of 2.4×10^{12} neutrons/cm². As observed for the catalysts activated at 291°, there is a sharp decay of the activity followed by a much slower decay in each case. The rapid decay seems to take place on contact with H₂-D₂ regardless of time after irradiation.

Activity energies do not change by a noticeable amount due to irradiation, in contrast to the situation for 291° activated catalysts.

D. Effect of Neutron Irradiation on a Catalyst Activated at 521°.—Neutron irradiation following 521° thermal activation has a tendency to decrease the activity of the catalyst slightly at a reaction temperature below 23°. An Arrhenius plot shows that this is primarily the result of an activation energy increase from 1.0 to 1.36 kcal./g.-mole. The change appears to be fairly stable and illustrates the necessity for measuring catalytic activities over a wide range of temperatures in order to obtain a true shift. For example, if the activity had been measured at room temperature only, no change would have been observed, while at 77°K. there is a substantial decrease in activity.

E. Ultraviolet Irradiation of Catalysts.—Low activity catalysts were irradiated with ultraviolet light to determine the effect of electromagnetic radiation on the activity. The photon energy of such radiation is too low to cause lattice displacements. It was observed that much the same phenomena occurred as in neutron irradiation but with several important differences. These differences are: (a) the rate constant reaches a definite saturation value, whereas the activity induced by neutron irradiation continues to show a slow increase at long exposures; (b) the activation energy does not change upon irradiation; and (c) the rate of decay after irradiation is faster and the logarithm of the first-order rate constant decreases linearly with time as soon as the irradiation ceases. The fastest loss in activity occurs in catalysts which were irradiated for the shortest period.

Figure 5 shows the results of a sample activated for 2 hr. at 291° and irradiated at 29° with predominantly 3660 Å. wave length light. The curve shows a saturation after 4 hr. of irradiation. Catalytic measurements were made while the sample was being irradiated. Arrhenius plots showed no change in activation energy produced by the irradiation.

F. Surface Area Measurements.—The surface area of the MgO catalyst was measured by the B.E.T. method using N₂ at 77°K. The amount adsorbed was measured with a quartz spring having a spring constant of 0.2825 ± 0.006 mm./mg. at room temperature. Expansion of the spring was measured by a Griffin and George cathetometer capable of measuring to ± 0.01 mm. Results indicate that the surface area, 16.7 m²/g., did not change within experimental error upon irradiation or heat treatment.

G. Summary of Results.—Table I is a qualitative summary of the work done on magnesium oxide.

TABLE I
A SUMMARY OF CATALYTIC CHANGES OF MgO

Thermal activation	Type of irradiation	Change in activation energy	Change in pre-exponential factor
Increasing thermal activation temp.	...	Decreases	Little change or decrease
2 hr. at 291°	Neutron	Increases	Large increase
2 hr. at 291°	Ultraviolet	No change	Large increase
2 hr. at 372°	Neutron	No change	Small increase or decrease
2 hr. at 520°	Neutron	Increases	Little change

Discussion of Results

The value of radiation effect studies on catalysts lies in the fact that comparisons can be made between the effect of a given type of radiation on the reaction rate and the observed effect of this type of radiation on the properties of the solid. Important assistance in understanding the catalysis investigated here can be obtained by comparing the results of the work with the optical absorption and electron paramagnetic resonance (e.p.r.) studies of other investigators on irradiated magnesium oxide.

Wertz and co-authors^{13,14} have shown, for example, that the number of negative ion vacancies in magnesium oxide usually is very small and that ultraviolet or X-irradiation cannot produce F centers. On the other hand, neutron irradiation can produce them at the rate of one F center for every 5.7 incident neutrons, and these centers are stable up to 400°. F centers then could not be responsible for the irradiation induced activity since (1) the activity could be enhanced by ultraviolet irradiation, and (2) the induced active site began to anneal out rather rapidly at 100°.

Optical absorption measurements on irradiated MgO single crystals have been reported by Clarks,¹⁰ Nelson and Pringsheim,¹¹ and Boyd.¹⁵

A striking similarity is apparent between the behavior of the optical center responsible for 2.4 e.v. absorption and the site responsible for catalytic activity. Absorption peaks occur at 2.4, 4.3, 4.8, and 5.6 e.v.^{10,11,15} The 2.4 e.v. peak decays out in 30 min. at 100°, while the 4.3, 3.8, and 5.6 e.v. peaks are stable to 600°. It was further observed that the 2.4 e.v. and other peaks saturate after exposure to neutron fluxes of 10¹⁴ n./cm.², while the 4.8 e.v. peak continues to grow. These optical absorption measurements also show that lower neutron dosages give rise to the same peaks as X-ray and ultraviolet irradiations; however, the neutron induced peaks are much more stable. This was also found to be true of catalytic activity.

E.p.r. work has revealed that radiation causes an electron transfer among the transition element impurities in MgO. Upon irradiation Cr⁺³ goes to Cr⁺² and Fe⁺² changes to Fe⁺³ and Fe⁺¹. The stability of Fe⁺³ thus produced is intimately

(13) J. E. Wertz, P. Auzins, R. Weeks, and R. Silsbee, *Phys. Rev.*, **107**, 1535 (1957).

(14) J. E. Wertz, unpublished data.

(15) C. A. Boyd, D. Rich, and E. Avery, A.E.C. Report, MDDC-1508 (1947).

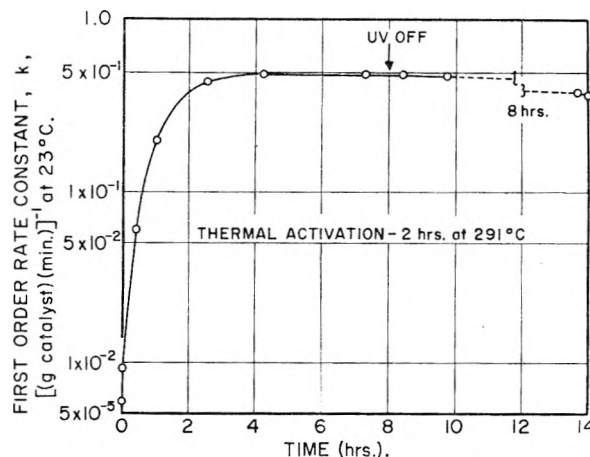
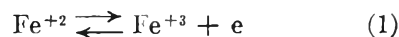


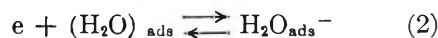
Fig. 5.—Effects of ultraviolet radiation on the catalytic activity of MgO.

related to the concentration of positive ion vacancies which afford a charge compensation in the crystal. Changes in other transition elements also have been observed but have not been studied in as much detail. This redistribution of filled and empty levels associated with transition element impurities apparently causes an increase in optical absorption and photoconductivity.¹⁶⁻¹⁸ This post-irradiation system represents an unstable state with a rather long relaxation time, similar to what has been observed catalytically.

Based upon the work outlined above, there could be at least two catalytic sites. One, possibly Cr⁺³, is present at the surface in limited amounts and could be responsible for the activity before irradiation. Another, such as Fe⁺³, is produced by irradiation. Trivalent iron is positive with respect to the surrounding surface and should be attractive to a hydrogen molecule. With relatively small amounts of irradiation, the trivalent iron sites may outnumber the other active sites. Upon formation of Fe⁺³ an electron is set free, but for the Fe⁺³ to exist, the electron must be trapped quickly by some other specie. Adsorbed water can act as the principal electron trap for those Fe⁺³ ions formed at the surface. Furthermore, without the water there probably are not enough other traps to increase the Fe⁺³ concentration significantly. This mechanism for the formation of Fe⁺³ and removal of an electron may be described by



and



The possibility of an adsorbed molecule trapping an electron has been discussed by Wolkenstein.¹⁹

Figure 3 shows that neutron irradiated catalysts show a slight but continuous rise in activity with

(16) J. E. Wertz, P. Auzins, J. Griffiths, and J. Orton, *Trans. Faraday Soc.*, **26**, 66 (1958).

(17) R. W. Soshea, A. J. Dekker, and J. P. Sturtz, *J. Phys. Chem. Solids*, **5**, 23 (1958).

(18) W. T. Peria, *Phys. Rev.*, **112**, 423 (1958).

(19) Th. Wolkenstein, "Advances in Catalysis," Vol. XII, Academic Press, New York, N. Y., 1960, p. 189.

continuing irradiation, while the ultraviolet irradiated samples come to a definite steady state value, as shown in Fig. 5. The neutron effect can be explained by a continued formation of positive-ion vacancies which would increase the Fe^{+3} stability. The decay in activity after irradiation on contact with the reactants may be due to removal of these Fe^{+3} ions or their stabilizers by charge transfer mechanisms.

These concepts of growth in activity upon irradiation and saturation may be summarized in differential form by

$$\frac{dN_{\text{Fe}^{+3}}}{dt} = (\phi_p \sigma_p + \phi_s \sigma_s) N_{\text{Fe}^{+2}} - (\phi_p \sigma_p + \phi_s \sigma_s) N_{\text{Fe}^{+3}} - k N_e N_{\text{Fe}^{+3}} \quad (3)$$

where ϕ_p and ϕ_s are the primary and secondary fluxes of ionizing irradiation, σ is the appropriate interaction cross section of the ion, and k is a reaction rate constant for the removal of Fe^{+3} ions by electron capture. This rate constant may be expressed as some function of the cation vacancy concentration. $N_{\text{Fe}^{+2}}$, $N_{\text{Fe}^{+3}}$, and N_e are, respectively, the concentrations of divalent iron atoms, trivalent iron atoms, and electrons which have either not been trapped or have been released by traps.

Thermal activation at 520° has been shown to remove most of the water which was adsorbed on the catalyst. Because there is little water to act as the primary sink for electrons, the radiation induced Fe^{+3} immediately reverts back to its divalent state and there is little effect catalytically. Actually, a few Fe^{+3} ions could be stabilized by other traps such as Cr^{+3} . Perhaps this increase in number of Fe^{+3} ions is offset by the irradiation induced decrease in Cr^{+3} ions, so that the number of active sites does not change. The slight increase in activation energy may be due to the influence of a few stable Fe^{+3} sites.

To show that there is enough iron impurity present for this model to be feasible, an estimate of the number of active sites necessary may be obtained by assuming that the first order rate constant of one ideal site, k_i , is given by

$$k_i = \sigma n \bar{c} \exp(-E/RT)/4nV \quad (4)$$

where σ = area of a unit site (assumed to $16 \times 10^{-16} \text{ cm}^2$), n = number of molecules in the gas, \bar{c} = average molecular velocity (assumed to be $1.5 \times 10^5 \text{ cm./sec.}$ for H_2 - D_2 at 25°), E = activation energy (assumed to be 6 kcal./mole), and V = volume of gas above catalyst (cm^3). From this equation k_i is of the order of $3 \times 10^{-15} \text{ site}^{-1} \text{ min.}^{-1}$. The corresponding experimentally determined rate constant was $k = 0.5 \text{ (g. catalyst)}^{-1} \text{ (min.)}^{-1}$.

$$\frac{k}{k_i} = \frac{0.5 \text{ g.}^{-1} \text{ min.}^{-1}}{3 \times 10^{-15} \text{ min.}^{-1} \text{ site}^{-1}} = 1.7 \times 10^{14} \text{ sites/g.} \quad (5)$$

Since the surface area of the catalyst is $16 \times 10^4 \text{ cm}^2/\text{g.}$, the required number of sites per unit area is about $1 \times 10^9 \text{ sites/cm}^2$. The lattice spacing for MgO is 4.20 Å.; hence, the number of

atoms per unit area is $5.7 \times 10^{14} \text{ atoms/cm}^2$. At an iron concentration of 7 p.p.m. there then are $4.0 \times 10^9 \text{ iron atoms/cm}^2$. Approximately four times more iron atoms/ cm^2 exist on the surface than are necessary according to this model. It should be mentioned that the "diving molecule" theory of reaction rates, as expressed by eq. 4, does not hold for certain catalysts.²⁰ Its validity for MgO has not been tested. As additional support for the small number of active sites, it has been found that the amount of hydrogen adsorbed on MgO is immeasurably small²¹; indicating that the surface, as a whole, is not greatly attractive to hydrogen.

Because of the importance of the free electron in the current theories of semiconductor catalysis, it seems important to consider this entity as a possible active site. At room temperature magnesium oxide exhibits a very low electrical conductivity. Day⁹ found a photoconductivity of about $10^{-15} \text{ ohm}^{-1} \text{ cm.}^{-1} \text{ watt}^{-1}$ at 39 μwatts of light, so the conductivity may be as low as $10^{-20} \text{ ohm}^{-1} \text{ cm.}^{-1}$. Lempicki²² found that before heat treatment an unstable conductivity of $10^{-9} \text{ ohm}^{-1} \text{ cm.}^{-1}$ could be obtained at room temperature, but heating the crystal to 1450°K. reduced the conductivity at room temperature below his limits of detection ($10^{-11} \text{ ohm}^{-1} \text{ cm.}^{-1}$). Yamaka²³ has shown that the main current carriers at room temperature are electron holes. The number of holes may be related to the conductivity by

$$n = \frac{\sigma}{\mu e} \quad (6)$$

where σ is the conductivity (assumed to be $1 \times 10^{-9} \text{ ohm}^{-1} \text{ cm.}^{-1}$), μ is the mobility ($\text{cm}^2/\text{v. sec.}$), n is the hole concentration ($1/\text{cm}^3$), and e is the electron charge. Using a theoretical value of 210 $\text{cm}^2/\text{v. sec.}$ for the mobility,²⁴ one obtains a hole concentration of

$$n = 3 \times 10^7 \text{ holes/cm}^3$$

Assuming that all of the holes are at the surface leads to the conclusion that there are about 50 holes per cm^2 of surface area. Equation 5 indicates that at least $1 \times 10^9 \text{ sites/cm}^2$ are needed to bring about the catalytic reaction.

Finally, one needs to consider the possibility of adsorbed water molecules acting as poisons for active sites. Is the effect of irradiation simply to remove water as thermal activation does? Catalysts in most cases were carefully evacuated before irradiation, then sealed off by means of the stopcock, and irradiated. When opened to the vacuum system, the pressure rose slightly, but no more than if the catalyst had been left off the vacuum system without irradiation. The rise in pressure certainly was not enough to account for

(20) G. Parravano, H. Friedrich, and M. Boudart, *J. Phys. Chem.*, **63**, 1144 (1959).

(21) A. Wheeler, "Structure and Properties of Solid Surfaces," Univ. of Chicago Press, Chicago, 1953, p. 440.

(22) A. Lempicki, *Proc. Roy. Soc. (London)*, **B66**, 281 (1953).

(23) E. Yamaka and K. Sawamoto, *Phys. Rev.*, **101**, 565 (1956).

(24) N. B. Hanay, "Semiconductors," Reinhold Publ. Corp., New York, N. Y., 1959.

the 2.1% weight loss due to heating from 290 to 520°. Also, the effects of irradiation and thermal activation on the activation energy were quite different. While thermal activation lowered the activation energy a significant amount, irradiation either raised the activation energy or left it unchanged. The mechanism of activation by irradiation therefore could not be the same as that of thermal activation.

Conclusions.—(1) Under proper conditions both neutron and ultraviolet radiation have a marked effect on the catalytic activity of MgO. The radiation effects depend on the extent of the previous degassing of the surface.

(2) By comparing radiation effects on catalytic properties with those effects on the solid properties,

a model for the catalytic activity can be developed based on Fe^{+3} impurity ions as the irradiation induced active sites. This model was shown to fit qualitatively the experimental data.

(3) Results of ultraviolet irradiation have shown that the bulk of the activity change must be attributed to changes in the electronic structure of the crystal rather than to changes in the number of lattice imperfections.

Acknowledgment.—The authors wish to express their appreciation to the National Aeronautics and Space Administration for a grant to carry out this research. They also wish to thank Dr. W. Fulkerson and Mr. C. L. Hearn for assistance in the experimental portion of this study.

INFRARED AND VOLUMETRIC DATA ON THE ADSORPTION OF AMMONIA, WATER, AND OTHER GASES ON ACTIVATED IRON(III) OXIDE¹

BY GEORGE BLYHOLDER AND EDWIN A. RICHARDSON

Department of Chemistry, University of Arkansas, Fayetteville, Arkansas

Received March 15, 1962

Infrared spectra in the 2 to 13 μ range have been obtained of NH_3 , H_2O , H_2S , EtOH , and Et_2O chemisorbed on $\alpha\text{-Fe}_2\text{O}_3$. N_2 , O_2 , H_2 , CO , SO_2 , Cl_2 , C_2H_6 , and C_2H_4 do not chemisorb at 25° on $\alpha\text{-Fe}_2\text{O}_3$. H_2O chemisorbs by dissociating to form a OH^- ion and a proton which reacts with a surface O^{2-} ion to produce another OH^- ion. NH_3 upon chemisorption occupies the same surface sites as H_2O and does not dissociate. Ion-dipole interaction between NH_3 and Fe^{+3} ions together with hydrogen bonding furnishes the heat of chemisorption which was measured by equilibrium pressure data from 200 to 350° to be 11.5 kcal. per mole. NH_4^+ formation occurred only when physically adsorbed H_2O and NH_3 were present and not when only NH_3 and surface hydroxyl groups from chemisorbed water were present. The infrared bands of physically and chemically adsorbed NH_3 showed no evidence of rotational structure superimposed on the vibrational bands. The adsorption of the other gases is discussed briefly.

Introduction

A major improvement in the tools available for adsorption studies has occurred in the past few years. The application of infrared techniques has been reported by several investigators.²⁻⁴ The utility of infrared methods in studies involving structural assignments for surface species is apparent. Mapes and Eischens³ obtained the infrared spectra of NH_3 adsorbed on a silica-alumina cracking catalyst. On the basis of the spectra indicating that most of the chemisorbed NH_3 still had a NH_3 structure as opposed to a NH_4^+ structure, they concluded that the catalyst behaved largely as a Lewis acid. However, their spectra indicated some NH_4^+ was present, which they attributed to the fact that they could never get rid of all hydroxyl groups on the surface. While the above system is sufficient to indicate the type of acidity involved in the catalyst, it is not well suited to a detailed study of the structure of the

surface complex; the silica-alumina cracking catalyst is essentially opaque beyond 7.5 μ . Since two of the fundamentals of ammonia complexed with metals⁵ occur beyond 7 μ , it is of interest to obtain the spectra on a metal oxide in which this range is accessible.

It has been found that $\alpha\text{-Fe}_2\text{O}_3$ not only meets the criterion of sufficient infrared transmission but it also can be completely dehydrated.

A number of volumetric studies have been carried out involving the adsorption of various gases on iron(III) oxide. Isotherms of NH_3 on Al_2O_3 , Fe_2O_3 , and Cr_2O_3 in the 10 to 700 mm. pressure range have been described.⁶ Cremer and Gruner⁷ observed no adsorption of NH_3 beyond a simple monolayer at 20° on Fe_2O_3 . A Freundlich isotherm was obtained at high coverages and the first portion of NH_3 allowed to contact the activated $\alpha\text{-Fe}_2\text{O}_3$ was taken up non-reversibly. No measure of this quantity was reported. These investigators evidently were unaware of the difficulty in removing the surface hydroxyl groups, and hence chemisorption was noted to take place only in minor amounts since OH groups probably were covering most of the active chemisorption sites on the adsorbent.

(1) (a) This work was supported in part by a grant from the American Oil Company and in part by a grant from the Monsanto Chemical Company. Acknowledgment is made to the donors of the Petroleum Research Fund, administered by the American Chemical Society, for partial support of this research. (b) Abstracted in part from a thesis presented by E. A. Richardson to the University of Arkansas in partial fulfillment of the requirements for the degree of Doctor of Philosophy, 1962.

(2) R. P. Eischens and W. A. Pliskin, "Advances in Catalysis," Academic Press, Inc., New York, N. Y., 1958.

(3) J. E. Mapes and R. P. Eischens, *J. Phys. Chem.*, **58**, 1059 (1954).

(4) E. M. Eyring and M. F. Wadsworth, *Mining Eng.*, **5**, 531 (1956).

(5) J. P. Faust and J. V. Quagliano, *J. Am. Chem. Soc.*, **76**, 5346 (1954).

(6) Von N. Niktin, *Z. anorg. allgem. Chem.*, **155**, 358 (1926).

(7) E. Cremer and R. Gruner, *Z. physik. Chem.*, **196**, 319 (1951).

It therefore was necessary to redetermine the isotherms of Cremer and Gruner using activated (OH-free) Fe_2O_3 . In this manner the ratio of the number of moles of NH_3 required to complete the chemisorbed layer (or fill all chemisorption sites) to the number of moles of NH_3 required to complete the monolayer of chemisorbed and physically adsorbed NH_3 can be determined for a given weight of activated Fe_2O_3 .

The principal purpose of this article is to describe the adsorption of ammonia, water, and other gases on iron(III) oxide and to ascertain the structure of the surface complexes. Another article in preparation deals with the absorption spectrum of the solid Fe_2O_3 .

Experimental

Apparatus.—A Perkin-Elmer Model 21 infrared recording spectrometer was employed. To expand the low transmission range of the instrument, the reference beam was partially blocked off with screen wires. The sample disk was mounted in a modified gas cell as described by Blyholder and Neff.⁸ The effective range of the system was 2 to 13 μ .

A conventional vacuum apparatus capable of maintaining 0.001 μ pressure was employed in degassing the disk.

Materials.—Certified reagent grade iron(III) oxide obtained from Fisher Scientific Company was employed without further treatment. Particle sizes were in the 5 μ range and the material had a surface area of about 15 m.²/g. The far infrared spectrum of this material is essentially that of $\alpha\text{-Fe}_2\text{O}_3$ ⁹ and so the material is considered to be $\alpha\text{-Fe}_2\text{O}_3$.

Anhydrous ammonia obtained from the Matheson Company was used without further purification.

Commercial grade welding oxygen obtained from the National Cylinder Gen. Division of Chemetron Corp., Chicago, Illinois, was used after passing through a 2-ft. column of anhydrous magnesium perchlorate to remove any moisture.

The vapor from distilled water, degassed at room temperature, was employed.

Commercial tank CO was used after heating to 350° to decompose iron carbonyl and passage over activated charcoal at liquid air temperatures to remove any other impurities.

Commercial tank SO_2 obtained from the Matheson Company was employed without further purification.

Hydrogen sulfide was used after degassing and distillation. Commercial tank gas was employed after passing through a 2-ft. column of anhydrous magnesium perchlorate to remove moisture.

Absolute ethyl alcohol and ethyl ether were used after distillation and degassing.

Preparation of Disks.—About 0.3 g. of $\alpha\text{-Fe}_2\text{O}_3$ was transferred to a 1 in. diameter die and pressed at 8000 p.s.i. The die was heated before pressing in an oven at 140° to prevent sticking of the disk to the die face. By careful handling, the disk could be removed from the die without breaking and transferred to the cell.

Activation of $\alpha\text{-Fe}_2\text{O}_3$ Disks.—The disks prepared above contained considerable water and thus were not active in chemisorption. The activation process consisted of degassing the disk at room temperature for several hours or until a vacuum in the order of 0.05 μ could be maintained. This disk then was heated to 375° in an atmosphere of O_2 and maintained for several hours. This oxidized any impurities (such as magnetite) which might cause subsequent reduction. The cell then was evacuated and the temperature raised to 475° for the final activation step, which was complete after about 16 hr. when the absorption spectrum of the disk no longer indicated the presence of hydroxyl groups.

Chemisorption.—A controlled amount (usually 100 μ) of adsorbate was allowed to contact the disk. If the pressure in the system (about 300 ml. volume) dropped immediately to less than 1 μ pressure, the adsorbate was assumed to be chemisorbed. The adsorption spectrum thus

could be obtained before and after each such addition and changes caused by the adsorbate readily detected. Any material which remained on the disk after evacuation for 1 hr. at 25° was taken as chemisorbed.

Isotherms and Surface Area.—Isotherms for NH_3 at 25° were obtained in the usual manner by adding increments of NH_3 and measuring the equilibrium pressure. The total surface area for activated $\alpha\text{-Fe}_2\text{O}_3$ was calculated from this isotherm. The physically adsorbed ammonia then was desorbed by evacuating the system at room temperature overnight and another isotherm obtained. This is essentially the method of Cremer and Gruner⁷ and yields the amount of material on a physically adsorbed monolayer from which the area involved can be calculated. Subtracting this from the value for the total gives the area involved in chemisorption. This subsequently will be referred to as method 1 for determining the amount of chemisorption.

It was found possible to measure the amount of material adsorbed before a measurable equilibrium pressure persisted in the system and this was taken to represent chemisorption. The surface area involved was calculated directly. This will be referred to as method 2. The amount of ammonia physically adsorbed at low pressures is negligible compared to the chemisorbed monolayer. These methods give somewhat different amounts of chemisorption.

To obtain isotherms at several hundred degrees centigrade where the chemisorbed NH_3 is in equilibrium with the gas phase, a small bulb was filled with about 10 g. of Fe_2O_3 and sealed to the manifold of the vacuum system with a 6 in. capillary tube. A furnace was placed around the bulb. The volume of the bulb is negligible compared to the volume of the manifold so that the amount of gas desorbed by heating a sample in the bulb can be determined from the pressure in the manifold.

Results

A small known amount of each adsorbate was added to an adsorption cell containing an activated disk of Fe_2O_3 . Since each chemisorbed gas gave easily detected infrared bands, the occurrence of chemisorption could be verified by ascertaining that the intensities of these bands were constant upon prolonged evacuation of the cell. From these measurements H_2O , NH_3 , H_2S , EtOH , and Et_2O were found to chemisorb at 25° on activated $\alpha\text{-Fe}_2\text{O}_3$. Similarly N_2 , O_2 , H_2 , CO , SO_2 , Cl_2 , C_2H_6 , and C_2H_4 were found not to chemisorb.

For two powder samples tested (Fisher Fe_2O_3) and one disk sample, the total surface area of a monolayer including chemisorbed and physically adsorbed material was found to be 12.1, 15.9, and 14.1 m.²/g., respectively. This indicates that the disk pressing procedure does not seriously diminish the surface area and the differences found are well within the precision expected of the method. Adsorption isotherms were obtained for pressures from less than 1 to 650 mm. Since these appear just like Cremer's,⁷ they are not reproduced here. The isotherms leveled out past about 400 mm., so the amount adsorbed at 450 mm. pressure was assumed to represent a monolayer. The area covered per NH_3 molecule was taken as 12.9 \AA^2 . It should be pointed out that these calculations are based upon the assumption that NH_3 does not physically adsorb on top of the chemisorbed ammonia. This appears valid since multilayers of physically adsorbed NH_3 do not form under these conditions⁷ and a chemisorbed NH_3 molecule is assumed to present a surface for interaction with other NH_3 molecules just like a physically adsorbed NH_3 molecule.

The results of using the two methods of determining the surface area for chemical adsorption of

(8) G. Blyholder and L. D. Neff, *J. Phys. Chem.*, **66**, 1464 (1962).

(9) Private communication, Shell Oil Company, Houston, Texas.

NH₃ on α -Fe₂O₃ in both powder and disk form at 20° compared to the total area determined, as described in the preceding paragraph, are given in Table I.

TABLE I

THE RATIO OF CHEMISORBED TO TOTAL ADSORBED NH₃ ON Fe₂O₃

Method	% Total surface covered with chemisorbed NH ₃		Disk
	Powder		
	Sample 1	Sample 2	
1	48 ± 3	49 ± 3	62 ± 3
2	32 ± 7	37 ± 5	37 ± 10

From volumetric measurements at 25° the amount of H₂O and NH₃ required to yield a chemisorbed monolayer was determined by adding increments until a measurable equilibrium pressure (5 μ) persisted. After desorption, a small amount of H₂O was added to the activated surface followed by sufficient NH₃ to complete the monolayer. This was repeated each time, adding various amounts of H₂O and NH₃ until the completed monolayer was obtained. Approximately the same results were obtained if NH₃ was first chemisorbed and H₂O then added. The data are summarized in Table II. The data in Table II were obtained on one 0.3-g. disk, completely degassed between each run. It is interesting to note that water will not chemisorb on a surface covered with NH₃ and *vice versa*. From the data in Table II, it can be seen that the total volume of gas required to form a chemisorbed monolayer is approximately the same regardless of whether H₂O or NH₃ is used as the adsorbate. Further, if the chemisorbed monolayer is composed of a mixture of those two gases, the same total volume of gas is required to form a chemisorbed monolayer.

TABLE II

AMOUNT OF NH₃ AND H₂O IN A CHEMISORBED MONOLAYER

Volume of gas chemisorbed ^a		Total volume of gas chemisorbed in monolayer
H ₂ O	NH ₃	
0	400	400
85	338	423
285	200	485
455	0	455
0	455	455

^a Volume measured in units equivalent to the amount of gas in 1 cc. at 1 mm. pressure and 298°K.

An isotherm for chemisorbed ammonia at 235° is shown in Fig. 1. The solid line is drawn from the equation for a Langmuir isotherm.

With the surface completely covered with chemisorbed ammonia (no physically adsorbed ammonia present), a sample in the high temperature bulb was heated slowly and the desorbed gas collected in the closed manifold of the vacuum system. Above 150° sufficient gas was desorbed to give a pressure reading on a mercury manometer. The reaction equilibrated rapidly so that the equilibrium pressure was obtained as soon as the temperature became constant. A plot of the equilibrium pressure as a function of temperature is shown in Fig. 2. The fact that the same pressure was obtained whether

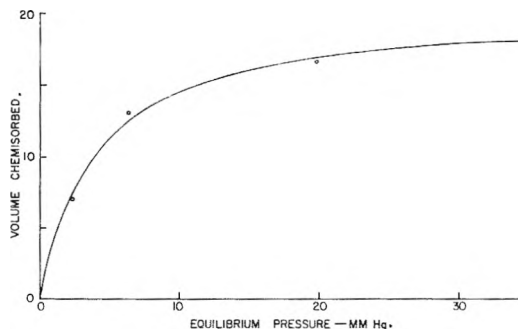


Fig. 1.—Isotherm of NH₃ chemisorbed on α -Fe₂O₃ at 235°. The solid curve is a Langmuir isotherm.

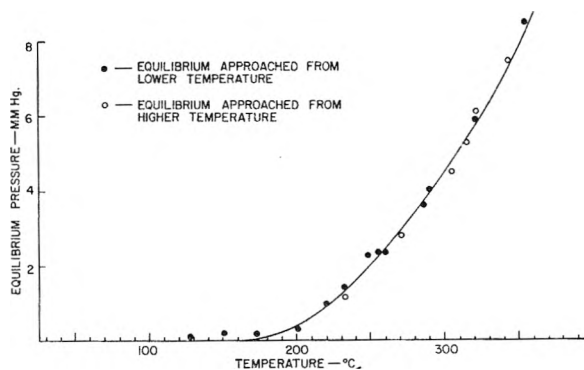


Fig. 2.—Equilibrium pressure of NH₃ vs. temperature for NH₃ chemisorbed on α -Fe₂O₃.

the temperature was approached from below or above indicates that equilibrium existed and that no appreciable decomposition of NH₃ occurred.

These data were used to calculate values of an equilibrium constant for the reaction



The equilibrium constant is defined as

$$K^1 = N_{\text{SE}} P_{\text{NH}_3} / N_{\text{SO}}$$

where N_{SE} = concn. of empty surface sites

N_{SO} = concn. of occupied surface sites

P_{NH_3} = pressure of NH₃

Since the data in Fig. 2 were obtained starting with the chemisorption sites all occupied and zero gas pressure, the value of N_{SE} is proportional to P_{NH_3} and the value of N_{SO} in appropriate units is equal to the amount of NH₃ originally chemisorbed (A) minus P_{NH_3} . The equilibrium constant then is given by

$$K = P_{\text{NH}_3}^2 / (A - P_{\text{NH}_3})$$

The value of log K , so determined, plotted *vs.* $1/T$ is shown in Fig. 3. The slope of this straight line gives the heat of chemisorption as 11.5 kcal. per mole. This method of determining the heat of adsorption depends on the Langmuir isotherm being obeyed at all temperatures covered.

As shown in Fig. 4, a freshly pressed disk has a very large and broad OH band at 2.7–3.3 μ . Also present is a substantial band at 6.2 μ , which indicates the presence of water having the usual HOH structure. The 6.2 μ band can be removed com-

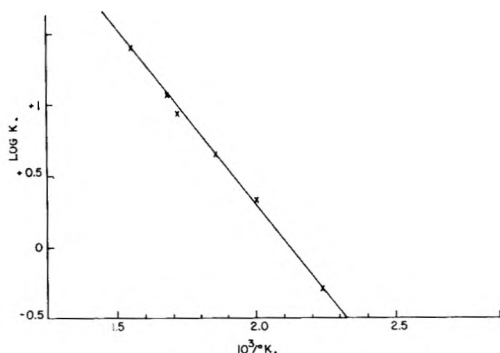


Fig. 3.—Log K vs. $1/T$ for NH_3 chemisorbed on $\alpha\text{-Fe}_2\text{O}_3$.

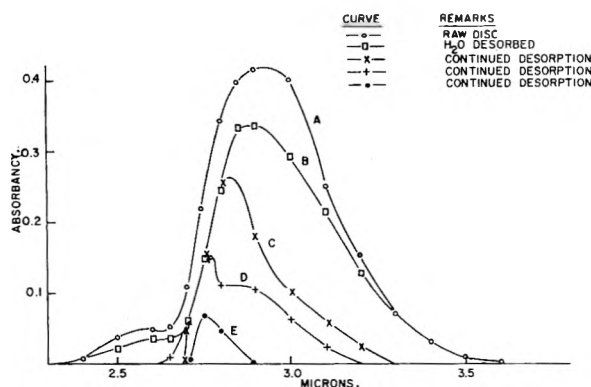


Fig. 4.—Variation of absorbancy in the 2 to 4 μ region upon desorption of hydroxyl groups from a freshly pressed $\alpha\text{-Fe}_2\text{O}_3$ disk as the temperature is increased from 25 to 475° over an 8-hr. period while pumping on the sample.

pletely by prolonged evacuation at room temperature, although the usual procedure is to heat the disk to about 150° to hasten the process. This indicates that adsorbed H_2O , which still has the structure H_2O , is held rather loosely and should be classified as physically adsorbed water.

During the process of removing the 6.2 μ band, the OH band is narrowed considerably, having lost some absorption on the long wave length side. It is apparent from Fig. 4 that associated hydroxide, *i.e.*, hydrogen bonded hydroxide which absorbs mostly from 2.8 to 3.2 μ , is the principal constituent removed at this point. Further desorption (by heating *in vacuo*) continues to remove associated OH predominantly but some free OH probably is removed also. After considerable desorption, the surface is left with essentially free OH, *i.e.*, non-hydrogen bonded OH, as shown by a single sharp peak at 2.75 μ (curve E). Continued heating and evacuation slowly removes the last trace of the OH band in the spectrum.

In Fig. 5 is found a plot of absorbancy at 2.8 and 6.2 μ vs. the amount of water adsorbed on an activated, OH-free disk. It can be seen that the first increments of H_2O chemisorb in a manner giving rise only to O-H vibrations. No HOH bending mode is observed at this point. This suggests that the activation process is simply reversed. Further, when the number of chemisorption sites becomes sufficiently reduced, physically adsorbed water appears on the disk, producing the typical 6.2 μ absorption band in the spectrum. The gas phase pressure of water in the cell was less than 5 μ

for the first 5 points on Fig. 5, while for the last 2 points the pressure was 48 μ and 150 μ , respectively.

The infrared spectra of a bare activated disk and the disk with NH_3 chemisorbed are shown in Fig. 6. The bands at 3.1 and 6.3 μ are characteristic of chemisorbed ammonia. The changes in the spectra beyond 7 μ are produced by all chemisorbed gases and cannot be ascribed to the chemisorbed NH_3 species itself. No other bands are observed for the chemisorbed NH_3 species. The ratio of the integrated intensities of the 3.1 μ band to the 6.3 μ band for chemically adsorbed NH_3 is 4 to 1 as determined from spectra with only chemisorbed NH_3 present, while the same ratio for physically adsorbed NH_3 , determined by subtracting the spectra for chemisorbed NH_3 from that for both physically plus chemisorbed NH_3 , is 2 to 1.

The formation of NH_4^+ with bands at 3.4 and 6.9 μ occurs only when physically adsorbed water and ammonia are present. This reaction can be carried out by contacting a wet disk with NH_3 or by adding H_2O to a disk already containing physically adsorbed ammonia. The NH_4^+ formed by either method can be removed by degassing of the disk at room temperature. If only chemisorbed NH_3 and H_2O (surface OH groups only) are present, no NH_4^+ forms.

The infrared bands observed for chemisorbed H_2O , EtOH , and Et_2O are shown in Table III. The chemisorption of H_2S produces an OH band with about $1/2$ the intensity of the OH band produced by chemisorbed water.

TABLE III
INFRARED BANDS FOR EtOH , H_2S , AND Et_2O CHEMISORBED ON $\alpha\text{-Fe}_2\text{O}_3$

Adsorbate	Spectral bands observed
Ethyl alcohol	3.0 (weak)
	3.4 (weak)
	6.9 (very weak)
	7.2 (strong)
	9.0 (strong)
H_2S	9.4 (strong)
	3.0 (medium)
Ethyl ether	6.2 (very weak)
	3.5 (strong)
	7.2 (weak)

Discussion

The infrared spectra reveal that when H_2O chemisorbs it reacts with a surface oxide ion to produce two hydroxide ions. In this work chemisorbed species are defined as those which cannot be removed by evacuation at room temperature. All adsorbed H_2O which retains the HOH configuration so as to give a band at 6.2 μ can be removed by evacuation at room temperature. Since removal of the physically adsorbed water decreases the OH stretching band mostly in the region around 3 μ , hydrogen bonding is presumed to play a large role in holding the physically adsorbed water on the surface.

The crystal lattice of $\alpha\text{-Fe}_2\text{O}_3$ consists essentially of oxide ions in a distorted hexagonal close packed system with Fe^{+3} ions occupying interstitial posi-

tions and distorting the lattice because of their size. The iron ions are surrounded by six oxide ions in an approximate octahedral arrangement. The hydroxide ions formed by water chemisorption are presumed to occupy surface lattice positions, which are in the first coordination shell of a Fe^{+3} ion. Any position on the surface, lattice point or not, which is not in the first coordination shell of a Fe^{+3} ion is assumed to be a satisfactory physical adsorption site.

The data in Table II show that the total number of moles of NH_3 and H_2O chemisorbed is approximately constant regardless of whether all chemisorption sites are filled with NH_3 or H_2O or a mixture of the two gases put on the surface in any ratio or order of addition to the surface. From this it is concluded that NH_3 and H_2O occupy the same sites on the surface.

The data indicate that NH_3 does not dissociate as water does upon chemisorption. The fact that the equilibrium data in Fig. 2 can be obtained with increasing and decreasing temperatures indicates that the NH_3 does not dissociate to form other gaseous products which would change the pressure or to change the surface which would change the value of the equilibrium constant unless all changes are rapidly reversible. The most likely dissociation would be to split a proton off an NH_3 molecule to form a surface hydroxide ion. The infrared spectra of chemisorbed NH_3 show no band which can be interpreted as an OH stretch. Chemisorbed water produces a band centered at 2.8μ like curve E of Fig. 4, while chemisorbed NH_3 produces a band centered at 3.1μ . When both H_2O and NH_3 are chemisorbed, the bands overlap but still produce distinct maxima at 2.8 and 3.1μ . It also is noted that NH_3 does not react with surface hydroxide ions to form NH_4^+ on the surface. Therefore NH_3 is believed to retain its identity as an NH_3 unit upon chemisorption.

If NH_3 retains its configuration, the question arises as to just what is the nature of its interaction with the surface. It has been shown that the NH_3 molecules occupy the same sites, presumably around Fe^{+3} ions, as do OH^- ions formed upon H_2O chemisorption. This leads to the consideration of the possibility of coordinate bond formation involving the lone pair of electrons on the nitrogen atom and the vacant d orbitals of the Fe^{+3} ions. Comparison of the infrared spectra of metal complexes¹⁰ with our spectra of chemisorbed NH_3 does not encourage this idea. The metal complexes give a band at 12.0μ , corresponding to ν_2 of gaseous NH_3 , and split ν_4 into two bands at 6.3 and 7.5μ . If these bands had approximately the same intensities relative to the 6.3 and 3.1μ bands for the chemisorbed species as exists in the complexes, they would have been readily detectable in our spectra. Since bands at 12.0 and 7.5μ were not detected for the chemisorbed species, coordinate bonding is assumed to not be the predominate surface interaction.

A combination of ion-dipole interaction and hydrogen bonding is sufficient to account for the

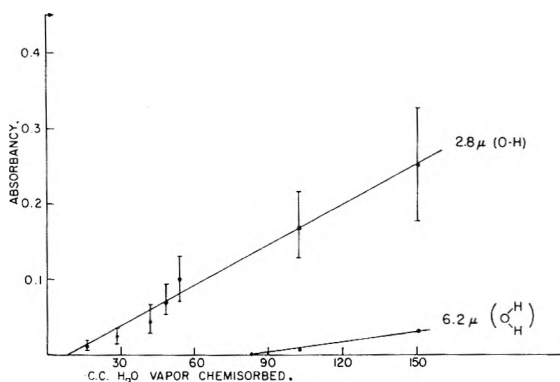


Fig. 5.—Absorbance of water at 2.8 and 6.2μ as a function of the amount of water adsorbed on an $\alpha\text{-Fe}_2\text{O}_3$ disk measured in units equivalent to the amount of gas in one cc. at 1 mm. pressure and 293° .

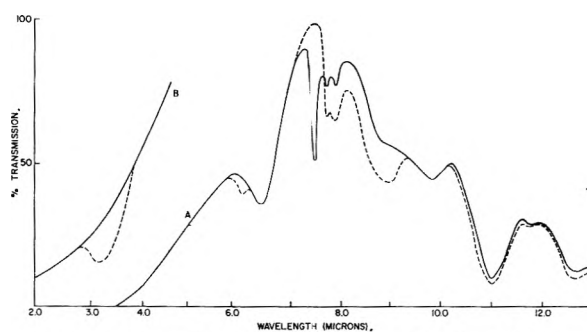


Fig. 6.—Adsorption of NH_3 on $\alpha\text{-Fe}_2\text{O}_3$: the solid line is the spectrum of an activated $\alpha\text{-Fe}_2\text{O}_3$ disk; the dashed line is the spectrum with NH_3 chemisorbed on the disk; curve A goes with the % transmission scale given while curve B is expanded by the insertion of screens in the reference beam.

observed heat of chemisorption of 11.5 kcal. per mole. Calculations of ion-dipole interactions for the dipole of NH_3 and the Fe^{+3} taking account of repulsion of oxide ions give an interaction energy of 5 to 10 kcal. per mole if the NH_3 approaches to within about the sum of the van der Waals radii of the interacting pair. The exact energy is quite sensitive to the distance apart of the reactants and to the assumed surface configuration of the surrounding oxide ions. Thus ion-dipole interaction plus 4 to 6 kcal. per mole expected from hydrogen bonding is adequate to account for the observed 11.5 kcal. per mole heat of chemisorption. The energy for physical adsorption is assumed to be largely supplied by hydrogen bonding. The difference between physical adsorption and chemisorption in this case aside from perhaps a difference in the average number of hydrogen bonds per molecule is that the chemisorbed species occupy lattice positions in the first coordination shell of Fe^{+3} , thereby gaining ion-dipole interaction energy, whereas physically adsorbed NH_3 does not occupy this energetically favored position and so has mostly only hydrogen bonding interactions.

The relative intensities of the bands at 3.1 and 6.3μ support the idea of hydrogen bonding. Hydrogen bonding is known¹¹ to increase markedly the ratio of the intensity of the 3.1 to 6.3μ bands. In gaseous NH_3 this ratio is much less than one

(10) J. Lewis and R. G. Wilkins, "Modern Coördination Chemistry," Interscience Publishers, New York, N. Y., 1960.

(11) G. C. Pimentel and A. L. McClellan, "The Hydrogen Bond," W. H. Freeman and Co., San Francisco, Calif., 1960.

whereas in metal complexes it is about one, for physically adsorbed NH_3 here it is about two and for chemisorbed NH_3 it is about four. The lack of a band corresponding to ν_2 of gaseous NH_3 in the region of 10 to 12 μ is assumed to be due to extensive hydrogen bonding interfering with this mode.

For ammonia gas, rotational effects are readily noted in combination with the vibrational bands present in the spectrum. These are not observed for chemisorbed or physically adsorbed ammonia and this indicates that some, if not all, of the rotational degrees of freedom are lost by the NH_3 molecule upon adsorption on Fe_2O_3 .

This work illustrates the difficulty and futility in trying to draw a sharp distinction between physical and chemical adsorption. Certainly no one would argue against calling the material herein referred to as chemisorbed water chemisorbed because of its obviously having undergone a chemical reaction, *i.e.*, bonds broken and made. One might, however, object to calling it water. Our justification for this is that when we get it back from the surface it is still or again water. The case for NH_3 is rather different. Our definition of chemisorbed material as that which is not removed by evacuation at room temperature in a "reasonable" length of time is entirely arbitrary. All of the forces invoked to explain the energy of adsorption are classically physical forces. The definite structure of the chemisorption site and the clear existence of two types of adsorbed NH_3 and H_2O justifies, to us at least, our terminology. If others wish to refer to all of our NH_3 as physically adsorbed because of the relatively low heat of adsorption and the lack of "chemical bond" formation, we will not argue. The data of Table I show the wide divergence in the amount of chemisorption here depending on the type of measurement.

We now turn our attention to the other gases

which were not studied as thoroughly as NH_3 and H_2O . The principal feature of the spectrum of chemisorbed H_2S is the formation of a hydroxyl band. The fact that the intensity of this band is about one-half that of a chemisorbed water layer may be accounted for by assuming that H_2S interacts with the surface to produce one hydroxide ion and one SH^- ion upon chemisorption. The intensity of the SH stretching band is such that it would not be observed for the number of chemisorbed species in the infrared beam.

Ethyl ether forms a very strongly held, though few in number, chemisorbed species. The spectrum is too weak to permit detailed evaluation. This compound is different from the other chemisorbates in that no protons are attached to the electronegative atom.

Ethyl alcohol might be expected to adsorb in a manner analogous to water and the above data appear to be consistent with this idea. The shift in the hydroxyl from 2.7 (in the gas phase) to 3.0 μ in the chemisorbed species is typical of hydrogen bonding or associated hydroxide groups.

Surveying the molecules which chemisorb it is noted that all have appreciable dipole moments and all contain protons capable of forming hydrogen bonds except ethyl ether, which only chemisorbs to a limited extent. At least two of the five molecules which chemisorb undergo decomposition by splitting off protons. Of the gases which do not chemisorb at room temperature, N_2 , O_2 , H_2 , CO , SO_2 , Cl_2 , ethane, and ethylene, only one, SO_2 , has an appreciable dipole moment. None of these molecules is capable of forming hydrogen bonds. Trapnell¹² suggests gases like CO , CO_2 , SO_2 , and H_2 chemisorb on some oxide surfaces to form CO_3^{-2} , SO_4^{-2} , and OH^- ions. Apparently these processes do not occur at 25° on $\alpha\text{-Fe}_2\text{O}_3$.

(12) B. M. Trapnell, "Chemisorption," Butterworths Scientific Publications, London, 1955.

FORMATION AND DECAY OF ATOMS AND SMALL FREE RADICALS AT LOW TEMPERATURES¹

BY DANIEL W. BROWN, ROLAND E. FLORIN, AND LEO A. WALL

National Bureau of Standards, Washington 25, D. C.

Received April 2, 1962

The maximum numbers of atoms that can be produced by exposing solid H_2 , D_2 , N_2 , and CH_4 to γ -radiation at 4.2°K. were investigated using the electron spin resonance method. The limiting values expressed in mole % were estimated to be 0.1% N atoms in N_2 ; 0.2% each of H atoms and CH_3 radicals in CH_4 ; less than 0.008% D atoms in D_2 ; and 0.0001% H atoms in H_2 . The lifetimes of the atoms were found to be highly dependent on the nature of their surrounding media. The decay behavior suggests complex mechanisms involving several types of processes including autoignition types. Certain spectral changes were observed upon decay or annealing of the irradiated materials. Besides obtaining sharper and more resolved spectra, additional lines, usually of weak intensity, were seen. The possible interactions or species responsible for these lines are discussed.

Introduction

This paper summarizes results of several investigations in which electron spin resonance

(*e.s.r.*) was used to measure radical concentrations. Certain spectra not mentioned in the literature were observed.

Theoretical studies suggest that the maximum percentages of atoms and small radicals that can be stabilized in low melting materials at 4.2°K.

(1) Based on work supported by the Free Radical Research Program of the Department of the Army and also by the Aeronautical Research Laboratory, Wright-Patterson Air Force Base, Ohio.

will be a few tenths of one mole per cent.² Experimental results^{3,4} on the deposition of nitrogen atoms from an electric discharge support this view. These maxima have not been demonstrated in systems subject to ionizing radiation at 4.2°K. In previous radiation work 0.06 mole % N atoms in N₂ and 0.15% each of H atoms and of CH₃ radicals in methane were obtained without indication of decreased *G*-value, radicals produced per 100 e.v. absorbed, for accumulation; the percentages of atoms in H₂ and D₂ were much less, but the numbers obtained were uncertain because the spectra were extremely distorted.⁵ Irradiations now have been carried to doses roughly five times as great as before and the results are reported herein.

The stability of given concentrations of atoms at different temperatures is of interest. Long storage experiments were carried out at 4.2°K. Samples also were immersed in liquid H₂ and spectra were obtained several hours later.

Under certain conditions the spectra of methyl radicals at 4.2°K. have more than four lines. Similarly, more than seven lines sometimes are seen in the spectrum of nitrogen atoms. These spectra are presented, although we are not certain of the explanation of the added lines.

Experimental

The techniques are identical with those previously described except as outlined below.⁵ The samples all were pre-irradiated in accordance with results from previous work. Doses were accumulated from one measurement to the next. Samples containing N₂ and CH₄ (see Table I) were handled in one group, and the samples of D₂ and H₂ were handled in another.

All spectra were obtained at two power levels, and approximate corrections for saturation were applied by extrapolating to zero microwave power a plot of the integral absorption ratio of sample and a reference material free from power saturation, vs. integral absorption of the reference material. A Varian low-power bridge was used to obtain spectra of atoms in hydrogen and deuterium in order to have undistorted spectra. Some difficulty was encountered in getting reproducible quantitative results with it. All other spectra were obtained with an ordinary Varian bridge operating at about 0.3 to 1 mw. A sample of commercial ultramarine, an inorganic sulfur-containing pigment, was permanently mounted in the cavity. The resonance from it is displaced from $g = 2.0$ and so was recorded with each spectrum and used to determine relative power levels.

Results

1. Atomic Content at Different Doses.—Results for samples that contained N₂ are shown in Fig. 1 and 2, and those for CH₄, D₂, and H₂ in Fig. 3, 4, and 5, respectively. In each figure the mole per cent of atoms or radicals ($100 \times$ (number of atoms/number of molecules)) is plotted as a function of dose. In the samples that contain neon and xenon, the percentage of atoms is based on the N₂ in the mixture because e.s.r. spectra suggest that the atoms are in a matrix of N₂.⁵

The initial *G*-value, number of atoms stored per 100 e.v. absorbed, is 0.3 for atomic N in N₂, 0.9

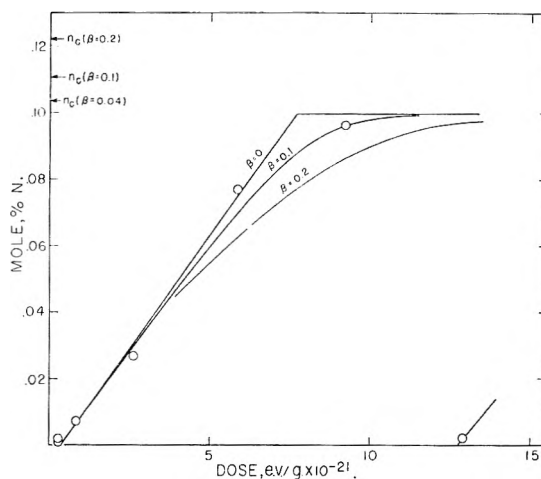


Fig. 1.—Mole % of N atoms in N₂ vs. dose. Curves, according to Jackson,² for $n_a = 0.1$ mole %, $\beta = 0, 0.1, 0.2$; n_c critical levels assuming indicated β and $n_a = 0.1$ mole %.

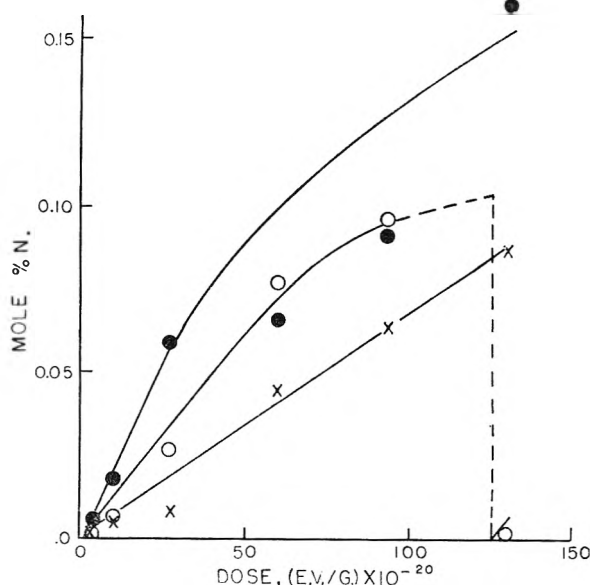


Fig. 2.—Mole % of N atoms in N₂ vs. dose: O, undiluted N₂; ● (Xe:N₂) = 4:1; × (Ne:N₂) = 16:1.

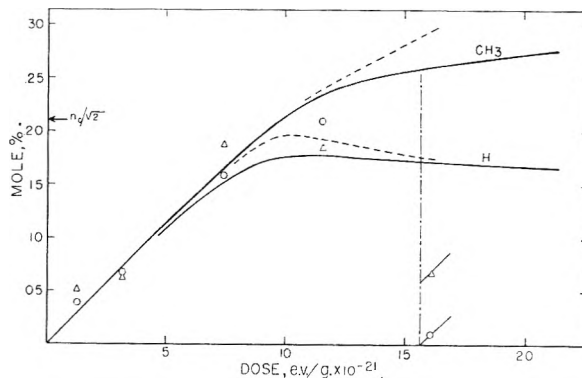


Fig. 3.—Mole % of H atoms and of CH₃ radicals in CH₄ vs. dose: O, H atoms; Δ, methyl radicals. Curves, theoretical (see Appendix); dashed line, $\beta = 0.04$; full line, $\beta = 0.1$; $n_c/\sqrt{2}$, critical level for (H) = (CH₃).

each for H and CH₃ in CH₄, and 2.4 for D in D₂. For N in N₂ + Xe, 1:4 mole ratio, it is 0.032, and

(2) (a) J. L. Jackson, *J. Chem. Phys.*, **31**, 154 (1959); (b) **31**, 722 (1959).

(3) B. J. Fontana, *J. Appl. Phys.*, **29**, 1668 (1958).

(4) B. J. Fontana, *J. Chem. Phys.*, **31**, 148 (1959).

(5) L. A. Wall, D. W. Brown, and R. E. Florin, *J. Phys. Chem.*, **63**, 1762 (1959).

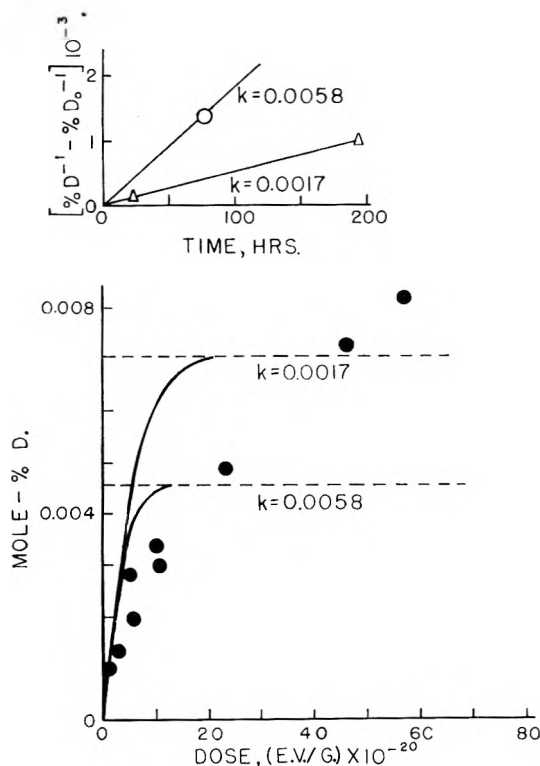


Fig. 4.—Lower section: mole % D atoms in D_2 vs. dose; ●, experimental points, k = second-order decay constant calculated from data in the upper section. Upper section: results of decay of deuterium atoms: $[(\% D \text{ after storage})^{-1} - (\text{initial } \% D)^{-1}] \times 10^{-3}$ vs. time at $4.2^\circ K$; Δ , initial % D = 0.002; \circ , initial % D = 0.003.

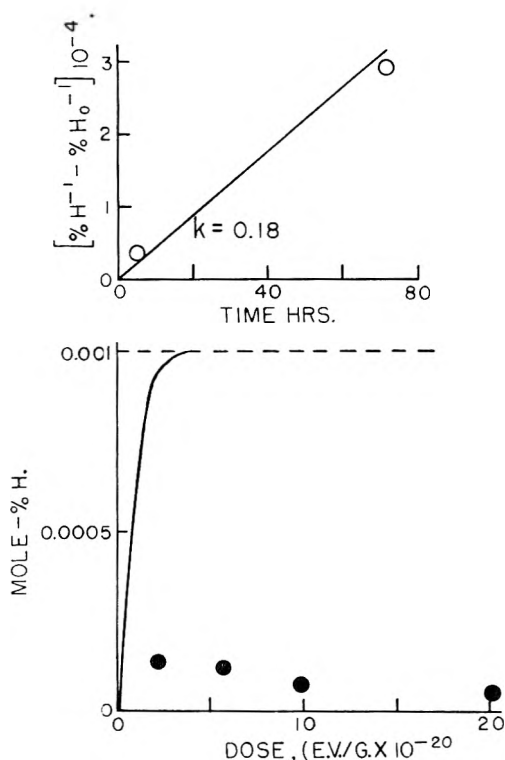


Fig. 5.—Lower section: mole % of H atoms in H_2 vs. dose; ●, experimental points. Upper section: results of decay of hydrogen atoms: $[(\% H \text{ after storage})^{-1} - (\text{initial } \% H)^{-1}] \times 10^{-4}$ vs. time at $4.2^\circ K$.

for N in $N_2 + Ne$, 1:16 mole ratio, it is .006; the latter two values are equivalent to 0.4 and 0.1, respectively, if one considers only the energy absorbed in the N_2 component, arbitrarily distributed according to electron fraction. In the absence of diluent, these values are uncertain in an absolute sense by about 50%. In the mixtures, the error can be greater because of possible uneven distribution of the N_2 component in the e.s.r. cavity. The converted values, referred to N_2 component of the mixture, are of interest because of their order of magnitude, but because of electronic non-equilibrium and other energy transfer effects in mixtures, they must be regarded as mere ratios resulting from the indicated calculation.

In Fig. 1 and 2, it is seen that the concentration of atoms in the mixtures rises continually with dose. In undiluted N_2 , the atom concentration first rises and then falls to a low value. The region of increasing slope at low atom concentrations probably is an error resulting from insufficient correction for power saturation in this region. At the highest doses, it is assumed that the concentration of atoms in this sample went to zero and then increased again at the original rate. The dashed line illustrates this behavior. A similar decrease was observed with CH_4 (see Fig. 3), although the difference between the final concentrations of H and CH_3 suggests that only the concentration of H atoms could have decreased to zero.

Theory predicts that the concentration of atoms will increase with dose until some steady value is reached.² Since the sample of CH_4 and those that contained N_2 were irradiated at the same time, a reasonable explanation of the observations is as follows. Presumably, a slight temperature rise occurred which permitted autoaccelerated recombination of atoms through self-heating in the samples of methane and undiluted N_2 but not in the others, because only in the former were the radicals close to their limiting concentrations. In the latter the limiting concentrations probably are higher because the surface area through which heat is transferred is relatively large if small crystals of N_2 are dispersed in an inert matrix. The theory of thermal explosions indicates that the explosion temperature increases as the surface-to-volume ratio of the system increases.⁶

The slopes of the lines for radicals in undiluted N_2 and CH_4 decreased in the radiation period that preceded the one in which the concentrations decreased. This suggests that the limiting concentrations are not much higher than the maximum values observed, 0.1% N in undiluted N_2 and 0.2% each of H and CH_3 in CH_4 . The former value agrees with the value calculated by Jackson for a large sample of undiluted N_2 .² No indication of an approach to a limiting concentration of atoms is suggested by the data for the samples which contain neon and xenon.

In Fig. 4 results of experiments are shown which involve D_2 at $4.2^\circ K$. Concentrations of D atoms after irradiation are shown in the lower section.

(6) N. N. Semenov, "Some Problems in Chemical Kinetics and Reactivity," Vol. II, Princeton University Press, Princeton, N. J., 1959, p. 95.

Values are much lower than in N_2 or CH_4 . Downward curvature is observed at low doses, but the limiting concentration of atoms was not reached.

Similar plots for irradiated H_2 are shown in Fig. 5. In the lower section the concentration of atoms appears to decrease somewhat with increasing dose. At present we regard these results as indicating that the concentration is constant at about 0.0001% at all doses. This value is so small that the atoms could possibly be on the wall of the container. Since the concentration of H atoms is independent of dose in the experimental range, the rate of formation was calculated by assuming that the G -value for production of H atoms equals that for the production of D atoms. This probably is conservative because H atoms should diffuse more rapidly than D atoms. The initial rate of formation based on this assumption is 0.45×10^{-7} mole/l. sec. The full interpretation of Fig. 4 and 5 requires consideration of thermal decay rates, which were appreciable.

2. Storage and Heating Experiments.—At 4.2°K., atoms are stable for long periods of time in CH_4 and N_2 . Data illustrating this are given in Table I, which lists the mole percentage of atoms before and after storage at 4.2°K. Results from a mixture of N_2 and argon are included. Mole % of N atoms in this mixture only is based on the total number of moles, instead of just the N_2 , because the e.s.r. spectra of N atoms in the sample suggest that the atoms are in an argon matrix.⁵ Apparently, any changes are small, even after 525 hr. storage, compared with the precision of the measurements. This is estimated to be $\pm 25\%$ from the apparent increases in radical concentration during the storage. If decay is second order, it proceeds with a rate constant that is less than 5×10^{-5} l./mole sec.

The effect of immersing samples that contain N atoms, H atoms, or CH_3 radicals in liquid hydrogen (b.p. 20.4°K.) is shown in Table II. Irradiation and initial measurements of the atom concentrations were performed at 4.2°K. Subsequent measurements were made with the sample in liquid hydrogen. Decay upon immersion is rapid but there are not enough data after immersion to calculate rate constants at 20.4°K. The fact that atoms remain in undiluted N_2 after 7 hr. suggests that decay is slow if the atom concentration is low. However, over-all final concentrations below 0.001% give weak spectra at 20°K., and values reported in this range are only approximate.

The temperature may have exceeded 20.4°K. initially because energy is released by the recombining atoms. The heat released in the second experiment with CH_4 could have raised the temperature by about 5°. Temperature increases that result from combination are superimposed in an unknown way on the normal temperature increase incidental to the immersion. Discussion of the effects of immersion in liquid hydrogen is complicated by these factors.

In samples that contain N atoms, smaller relative decreases in the concentrations of atoms occur if the initial concentration is very small. This suggests that the order of the combination is greater

than unity or that self-heating, which is greater when more atoms combine, may influence this result. However, in xenon the two highest initial concentrations of N atoms differed by a factor of 9, and these both decreased by about a factor of 4 to 5 on immersion in liquid hydrogen. This factor also is about equal to that found for the loss of atoms in the first of the results listed for the mixture that contained neon. Intercomparison of the results for these mixtures should be approximately valid if both mixtures consist of crystals of N_2 in different matrices. The relatively constant ratio obtained suggests that first-order processes occur. This implication of the data conflicts with the previous one.

Initial local concentrations of atoms of 0.005–0.006% decrease much more on immersion in liquid hydrogen if the medium is undiluted N_2 than if it is argon. Within a fairly large experimental uncertainty, decreases do not occur when the diluent is neon or xenon. An argon matrix would be expected to be more restrictive than would one of N_2 because the melting point and density of the former are greater. The lack of any decay in the other matrices may result from better cooling of the small crystals of N_2 that are thought to be present. Possibly, considering the concentration level involved, there is only one atom per crystal of N_2 , and diffusion between crystals does not occur.

The pair of experiments with methane is interesting because the initial ratio of CH_3 to H was high in one case and about equal to unity in the other case. Since the concentration of the CH_3 radical decreased in the absence of a substantial concentration of H atoms, combination between CH_3 radicals is appreciable. Presumably, three types of radical combination occur in the second experiment. The final concentrations indicate that processes that use up H atoms are more rapid than those involving combination of methyl radicals.

Results of storage experiments upon irradiated D_2 at 4.2°K. are shown in the upper section of Fig. 4. The apparent concentration decreased from 0.003 to 0.0006% in 77 hr. in one experiment and from 0.002 to 0.0007% in 192 hr. in another experiment. Obviously, no simple kinetic relation fits these results, but the precision of the measurements is such that the difference between the final concentrations could be greater and also in the reverse direction. The data are presented as second-order plots in the upper section of Fig. 6. The most extreme of the slopes were used to calculate the rate constants, k , which are entered on the plots in conventional units, l./mole sec. Values of these constants are such that an activation energy of 300 cal. reduces a pre-exponential factor of 10^{12} to the magnitude observed.

The initial points in the lower section of the figure were used to calculate a rate of formation of D atoms equal to 0.33×10^{-7} mole/l. sec. It was assumed that the rate of accumulation of D atoms equaled $0.33 \times 10^{-7} - 2k(D)^2$ moles/l. sec. The values of k were taken from the upper section and used to calculate the lines in the lower section. The actual accumulation of atoms is slower initially,

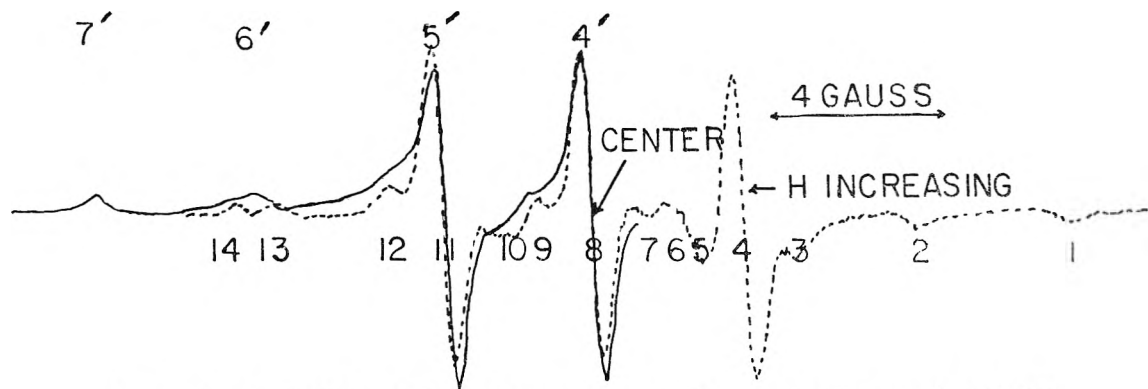


Fig. 6.—Spectra of N atoms in N_2 : full line, sample at $4.2^\circ K$.; dashed line, sample at $20.4^\circ K$.

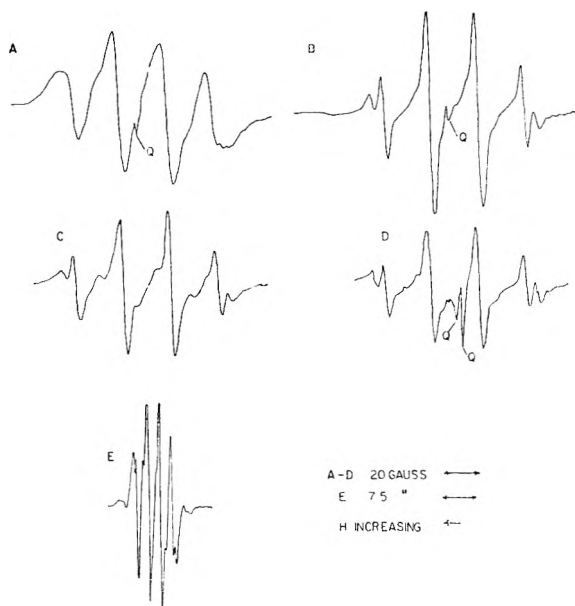


Fig. 7.—Spectra of radicals in CH_4 : (A) normal for CH_4 at $4.2^\circ K$.; (B) after concentration decrease indicated in Fig. 3; (C) repeat of B after changing position of sample in cavity (whole spectrum pieced from partial scans in the opposite direction); (D) sample at $20.4^\circ K$.; spectrum was like A before temperature was raised; (E) obtained on another occasion when the concentration of atoms was lower than expected; (Q) line from quartz container.

but eventually the concentration exceeds the limit set by either k . This observation may indicate that several trapping sites exist and that after long irradiation a greater fraction of the observed atoms are in the deeper traps because more of those in shallow traps will have combined. The rate constants for decay were calculated after doses of less than 11×10^{20} e.v./g.; the initial concentrations differed by only 30%. Therefore, these values of k may not apply after long irradiation.

Similar plots of results of experiments with irradiated H_2 are shown in Fig. 5. Here the decay rate is 30 times as rapid as that of D atoms in D_2 . The data do not scatter as badly as in Fig. 7 but only one starting concentration was used. The line in the lower section was constructed using the second-order decay constant shown, and a formation rate of 0.45×10^{-7} mole/l. sec. estimated from D_2 irradiations. In H_2 the observed limiting concentration of atoms is much less than that cal-

culated. Since the observed limiting concentration depends inversely on the square root of the recombination constant, a much more rapid recombination rate than observed seems indicated. Possibly during irradiation the concentration of trapped atoms is so low that combination with hot atoms diffusing from the spurs is important. This process would be first order in trapped atoms but would not show up in the decay studies.

3. E.s.r. Spectra.—The e.s.r. spectra of N atoms in undiluted N_2 between doses of 3.7×10^{20} and 93×10^{20} e.v./g. are very similar to one another and also to that which we published previously.⁵ The saturation of the spectra at 1 mw. power decreases as the concentration of atoms increases, becoming substantially negligible at about 0.06 mole % atoms. At 130×10^{20} e.v./g., i.e., after the decay, the spectrum is unlike the others in that additional lines are present and the old lines are narrower than before. Subsequently, it was found that similar spectra were obtained in experiments in which atom concentrations were substantially less than values consistent with those in Fig. 1. They also were obtained from samples in liquid hydrogen which had given the normal spectrum when in liquid helium. In Fig. 6 the normal and narrow-line spectra at high resolution are shown; the latter was taken with the sample in liquid hydrogen. Only about half of the normal spectrum was taken in order to conserve helium, but it is symmetrical about the center.

It was found also that spectra from irradiated methane were narrower and had extra lines if the samples contained abnormally few methyl radicals or had been immersed in hydrogen. Variations of such spectra are shown in Fig 7. Lines marked Q are thought to be due to quartz. Shoulders exist in the normal spectrum and the recording fails to return to the base line in the interval scanned. These observations suggest that the same sources of absorption are present in both types of spectra but that normally the lines are too broad to be resolved.

We cannot account for all the lines in these spectra; their number varies, and some changes in slope indicate that additional lines are present but not resolved.

If samples which give the many-lined spectra are subjected to more irradiation without being annealed, the extra lines are retained, although they

are broadened somewhat; the intensities of all lines increase. If such samples are melted and re-irradiated, the normal spectra are obtained. The correction for power saturation of the spectra of CH_3 and H decreases with dose like the correction in undiluted N_2 . It never becomes negligible, however, and line widths are constant at all concentrations of atoms.

The e.s.r. spectra of D atoms in D_2 and H atoms in H_2 are three and two widely spaced lines, respectively⁷; with the low-power bridge, relatively undistorted spectra are obtained but the signal-to-noise ratio is low.⁸ Observed line widths between points of maximum slope are 0.5 gauss for H atoms and 1.5 gauss for D atoms. These widths were not significantly different at different doses.

Discussion

1. **Stability of Trapped Radicals.**—The growth curves for atoms and radicals in irradiated pure nitrogen (Fig. 1 and 2) and methane (Fig. 3) are in reasonable accord with Jackson's development² of the theory of chain reactions as applied to irradiated solids at low temperature. Radicals or atoms are considered to exist mainly in traps in the crystal lattice, characterized by a single temperature T_f above which the radicals are thermally liberated. A reaction between two radicals liberates all trapped radicals in a characteristic volume V_f derived from T_f and the heat of reaction and heat capacity. Whether these radicals react with existing radicals or become trapped again depends only upon the ratio of suitable lattice sites, the time spent in diffusion being short enough to neglect. At the low concentrations prevailing, the probability of reacting is given by $\zeta n/M$, where n is the number of trapped radicals per unit volume, M is the total number of trapping sites per unit volume, and ζ is a numerical parameter which does not need an explicit physical definition for further development of the theory. However, it is useful to consider ζ to be the number of lattice sites sufficiently near one trapped radical to permit reaction. The probability of being trapped, *i.e.*, not reacting, is then $1 - \zeta n/M$. The liberation of radicals and their further reaction constitute a branched chain reaction, and hence the mixture can become explosively unstable when the ratio of radical released to those consumed exceeds unity. Where γ -radiation is producing new radicals at a rate κ , reaction chains of shorter length act to reduce the realized yield of radicals. On this basis, the critical concentration for instability is $n_c = (M/\zeta V_f)^{1/2}$, and the growth equation is given by

$$\frac{dn}{dt} = \kappa \left[1 - \frac{2\zeta n/M}{1 - (n/n_c)^2} \right]$$

The form of the growth curve depends upon the value of parameter $\beta = (\zeta/MV_f)^{1/2} = n_c\zeta/M$. Low values of β indicate great chain lengths, and the corresponding growth curves are approximately

linear up to high concentrations, where they suddenly level off to a steady-state concentration n_s just slightly below the critical n_c (Fig. 2). For high values of β , the growth curves approach a familiar first-order type and level off at concentrations far below n_c . In small particles, the value of n_c depends inversely upon particle size; this conclusion, familiar in explosion theory,⁶ results from a more complicated treatment with diffusion appearing explicitly.

The results upon irradiated pure nitrogen, taking in conjunction both the form of the growth curve and the instability manifested by the sudden drop in concentration near 10×10^{21} e.v./g. in Fig. 2, strongly support the theory outlined above, with a low value of β , *i.e.*, a large chain length. A growth curve alone, with many experimental points of high precision below and above the leveling-off region, would be sufficient to establish this conclusion; however, with the limited precision of e.s.r. measurements and the presence of only one experimental point above the leveling-off region, it becomes necessary to rely heavily upon the instability as well. The sudden fall in concentration does not occur automatically in irradiations at constant temperature according to theory, but can be brought about by a very slight temperature excursion, provided the value of β is sufficiently low. Such a temperature excursion could occur experimentally, for example, during a refilling with liquid helium, or from a small piece of frozen air or ice dropping into the helium dewar. That the excursion was only slight is evident from the fact that the catastrophe in nitrogen did not affect the atom and radical concentrations in irradiated methane in the same dewar; and the later event in methane did not affect any other samples. Assuming $T_f = 20^\circ\text{K}$., and noting $n_c \propto V_f^{1/2} \propto (T_f - T)^{-1/2}$, an arbitrary temperature rise of 1° would decrease n_c by 6%. The parameter β would be decreased by the same amount. From the relations between n_c , β , and the steady-state level n_s given by Jackson,² a few of the possible n_c values for various β are sketched in Fig. 2, under the assumption that n_s is approximately equal to the highest nitrogen atom level reached, 0.1 mole %. The 1° temperature rise causes the existing n_s at 4°K . to exceed the 5°K . value of n_c when the $4^\circ\beta$ is 0.06 or lower. Higher assumed temperature rises, or lower T_f , permit the explosive condition for a wide range of β . For reasonable values of T_f , the level reached is near n_c , and β is necessarily rather low.

The evidence of the growth curve alone is less decisive, as the experimental points could be fitted loosely by many combinations of chain parameter β and steady-state level n_s . As all reasonable growth curves are linear initially, great reliance must be placed upon the one experimental point which deviates strongly from linearity. The formation rate κ is rather closely established at 1.37×10^{-23} mole % per e.v./g. dose, aside from systematic errors. In Fig. 1 the experimental points are compared with theoretical growth curves for $n_s = 0.1$ mole %, $\beta = 0.2$, and for $n_s = 0.1$ mole %, $\beta = 0.1$. The linear portion of the experimental data extrapolates to zero concentration at

(7) C. K. Jen, S. N. Foner, E. L. Cochran, and V. A. Bowers, *Phys. Rev.*, **104**, 846 (1956).

(8) L. H. Piette, R. C. Rempel, H. E. Weaver, and J. M. Flournoy, *J. Chem. Phys.*, **30**, 1623 (1959).

0.36×10^{21} e.v./g. dose, indicating probably some residual inhibition of the type mentioned in ref. 5, and therefore the theoretical curves have been shifted to the right by this amount. The best values of β and n_s can be sought systematically with the aid of a set of curves such as Jackson's,^{2b} showing $y = n/n_s$ as a function of $\tau = \kappa t/n_s$. The method is not restricted to small β . One must assume a rather small error, say 10%, in the relative value of n/n_s for any dose, and a much smaller error in the slope of the linear portion of the curve, which is derived from many experimental points. Designating the slope of the linear portion by m and the dose D , one chooses preferably the experimental point 1, the highest point at which the deviation from linearity B_1 is within the assumed error, e.g., $0.10 \leq B_1 = 1 - n_1/mD_1$, and another point 2, at which the deviation $B_2 = 1 - n_2/mD_2$ is large. One draws on the set of y, τ curves the line L of slope $1 - B_1$, the region between L_1 and the line $y = \tau$ satisfying the conditions of point 1; and the line L_2 of slope $1 - B_2$ which satisfies the conditions of point 2. The intersections of L_2 with the curves represent values of (y, β, τ) satisfying the experimental point 2. For each (β_i, τ_{2i}) obtained, one draws the vertical line $\tau_{1i} = \tau_{2i}(D_1/D_2)$ and examines its intersections with curve β_1 . If an intersection lies between the lines L_1 and $y = \tau$, the corresponding β_i satisfies both points 1 and 2. For any β thus found, the corresponding n_s is obtained from $y_2 = n_2/n_s$. Assuming a relative error in point 1 of 10%, this procedure places β at 0.04 or less, n_s at 0.09 to 0.1 mole %, and n_c at 0.1 to 0.11 mole %, in substantial agreement with Jackson's estimates from other data, and probably with greater precision. The low level of N atoms found at 12.6×10^{21} e.v./g. in Fig. 2 is presumed to result from a fall to zero concentration and renewed buildup at the linear rate, as illustrated by the curve.

Detailed comparison of experimental results with theory is not possible for the mixtures of N_2 with diluents. As it is not known whether the system is structurally a solid solution, a mixture of microcrystals, or a more complicated arrangement, the meaning of N atom concentrations becomes ambiguous. If the N atoms are located at random in a solid solution, mole % N atoms in the total mixture is an appropriate basis for expression, while if they are located entirely within N_2 crystals, a better basis is mole % referred to the N_2 content only, which for the present Ne- N_2 and Xe- N_2 mixtures is 17 times and 5 times the over-all concentration, respectively. The ambiguity cannot easily be resolved without X-ray diffraction studies; however, it is likely from relative molecular dimensions that N_2 will not form concentrated solid solutions with Ne or Xe, although it may do so with Ar. Also, the e.s.r. spectra of the mixtures are less saturated than those of undiluted N_2 at equivalent over-all concentrations of atoms. This suggests that the local concentrations of atoms in the mixtures are higher than the over-all value. It is assumed, therefore, that the Ne and Xe mixtures consist of separate crystals, and the N atom concentrations are stated in mole % referred to N_2 content.

In films deposited rapidly from dilute vapor upon a surface at 4°K.,⁹ these crystallographic considerations do not apply, and such products can be highly disperse mixtures. The over-all concentrations achieved in the present experiments with Ne- N_2 and Xe- N_2 are quite low, but concentrations referred to N_2 content are roughly comparable to those in pure N_2 (Fig. 1), Ne- N_2 falling below and Xe- N_2 above pure N_2 . The rates of accumulation of N atoms in mixtures cannot be compared readily, since the dose received in the N_2 component is affected by electronic non-equilibrium and is not known. The mixtures did not level off in concentration and survived unchanged the slight temperature excursions which made pure irradiated N_2 unstable. In Xe- N_2 the N atom concentration had not leveled off nor approached instability at a concentration, referred to the N_2 component, of 0.16 mole %, which is 60% over the maximum attainable in pure N_2 . In a solid solution, the result would not be surprising because the over-all concentration is in any event low. If the atoms are located in N_2 crystals, the result illustrates the stabilizing effect of small particle size.^{2,6} If one takes at face value Jackson's estimate of $l_0 = 2 \times 10^4$ lattice layers for the diffusion parameter, in his equation 32

$$l_c = \frac{\pi l_0}{[(n/n_c)^2 - 1]^{1/2}}$$

One finds, for example, that in microcrystals of conceivable size (infinite slabs 10 Å. thick) the atom concentration might exceed the usual n_c by 3-fold without dynamic instability. The surrounding medium must be a good trapping agent for N atoms, a requirement which may be approached by Xe. If this is so, however, many of the N atoms observed reside in the Xe crystalline matrix. In a diluent of poor trapping character, perhaps approached by Ne, the loss of mobile atoms from one crystal of N_2 could be compensated by gains from other crystals, and the critical concentration of N in the N_2 portion should be little greater than in pure N_2 , although (Fig. 1) it is evidently more slowly approached. One might hope to describe the N_2 -Ar system as an idealized solid solution in which differences in trapping sites, specific heats, and energy transfer phenomena are neglected. In this ideal case, the analysis should follow that for pure N_2 , using over-all mole fraction concentrations. The critical and steady-state concentrations should be the same, with κ reduced by the factor X_{N_2} = mole fraction N_2 and the time scale of the diagram extended by $1/X_{N_2}$. The complicated concentration dependence in the data of ref. 5, Table I, column 6, invalidate this model, perhaps because of energy transfer effects, but in addition, the dose dependence suggests that even n_c and n_s cannot be the same as in pure N_2 . The data were all at relatively low dose, and no attempt was made to approach n_s .

Irradiated methane contains two free-radical species, CH_3 and H. In the Appendix, Jackson's

(9) S. N. Foner, C. K. Jen, E. L. Cochran, and V. A. Bowers, *J. Chem. Phys.*, **29**, 351 (1958).

analysis has been extended to this case. The value of T_f for methyl radicals presumably is higher than T_f for hydrogen atoms, as the CH_3 concentration following the temperature-excursion catastrophe remains rather high. As simplified extreme cases one may consider (1) CH_3 and H identical in all properties and (2) $V_f = 0$ for CH_3 . Either case, with low β , gives a fair agreement with data as far as they go, and in either case the value of β must be rather low. Case 1 offers no novelties. Figure 3 compares the experimental data with a curve for case 2, with κ and ζ alike for the two species, $V_f = 0$ for CH_3 , $n_c' = \{(\text{H})(\text{CH}_3 + \text{H})\}^{1/2} = 0.3$, and $\beta = 0.04$ and 0.1 . If case 2 applies, the concentrations of H and CH_3 cannot in general remain equal; after the sudden arrest in growth rate, (H) will decline slowly to zero and (CH_3) will rise slowly to an ultimate high level of n_c/β . When V_f for CH_3 is finite, the two concentrations should level off at intermediate values.

In both methane and nitrogen, the long linear region with sudden leveling off which is incompatible with large β automatically rules out any scheme of simultaneous growth and first- or second-order decay, unless there is a large random error in concentration levels. Since no decay is observed in long storage, such schemes would furthermore require special values of the decay constant, valid only during irradiation.

The formation rates κ and the initial G -values in all the systems probably are the result of a balance between opposing rates of dissociation and of back reaction within the cage of the crystal matrix. Recent observations of methyl iodide photolyzed in hydrocarbons at 20°K .¹⁰ suggest that as much as 80% of the observed reactions occur within the cage, and before much loss of kinetic energy. In the present series, the weakest cage for which reliable data exist, D_2 , had the highest initial G -value for atoms, 2.4. This may be a consequence of the easier escape of dissociation products from the cage. In irradiated methane, one of the products, H, may escape the dissociation cage efficiently, accounting for the fairly high G -values of 0.9 each for H and CH_3 .

The available results on irradiated hydrogen and deuterium cannot be discussed in the light of Jackson's chain reaction theory, for several reasons: (1) Experimental growth curves are incomplete. In hydrogen, the steady-state concentration of atoms was reached at the lowest dose investigated, 2×10^{20} e.v./g. In deuterium, a steady-state concentration was not attained at 60×10^{20} e.v./g. (2) The precision of e.s.r. measurements is especially poor, because of the low concentrations involved and the lengthy extrapolations to correct for power saturation. (3) The existence of a spontaneous thermal decay rate violates a basic postulate of the theory, that liberation of radicals is negligible at temperatures below T_f and complete above it. It is not impossible that both the leveling-off and the thermal decay have considerable chain-reaction character. One could, with some inconsistency, modify the theory by introducing a

small first-order rate of liberation from traps, with rate constant k . The equation for growth during irradiation would then become

$$\frac{dn}{dt} \kappa \left[1 - \frac{2(\zeta/M)n}{1 - (n/n_c)^2} \right] - \frac{2k(\zeta/M)n^2}{1 - (n/n_c)^2}$$

and the equation for spontaneous thermal decay

$$\frac{dn}{dt} = - \frac{2k(\zeta/M)n^2}{1 - (n/n_c)^2}$$

The equation for thermal decay would be second order at low atom concentrations, $n \ll n_c$, and of variable high order at higher concentrations. For large k and large β , the growth curve would be simply one with second-order decay; in any case, the curve would level off at lower concentrations than in the absence of the last term.

A serious difficulty is that, for deuterium atoms, the concentrations actually attained are greater than allowed by the measured decay rate. This is shown (Fig. 4) for zero-order growth and second-order decay; the disagreement will be still greater for the chain-reaction treatment. The only reasonable explanation is that based on a variety of trapping sites of differing energies. Qualitatively, the growth curve could resemble the sum of H and CH_3 in Fig. 3, the D atoms at high dose being predominantly the species in the deeper traps. The decay rates measured at lower dose would not apply to this more stable species.

TABLE I
EFFECT OF STORAGE AT 4.2°K . ON RADICAL CONCENTRATIONS

Sample ^a	Product	Amount of product, mole %			
		Initial	144 hr.	356 hr.	456 hr.
N_2	N	0.0012	0.0012	0.0012	
		.0014			0.0008
		.0075	.0075		
		.032	.024		
$\text{Ne} + \text{N}_2$ (16:1 molar ratio)	N	0.0013	.0012		
		.0054	.0054		
		.016	.019		
		.087			.074
$\text{Xe} + \text{N}_2$ (4:1 molar ratio)	N	.0045	.0049	.0054	
		.018	.018		
		.055	.063		
		.16			.13
$\text{Ar} + \text{N}_2$ (16:1 molar ratio)	N	.0047			.0052
CH_4	CH_3	.058	.065		
	H	.047	.047		
CH_4	CH_3	.062	.066		
	H	.067	.085		

^a In the mixtures that contain Xe or Ne, the percentages of N atoms are based on the content of N_2 .

Like the results of storage of deuterium at 4°K ., the complicated results of heating irradiated nitrogen, nitrogen mixtures, and methane to 20°K ., Table II, probably reveal a weakness of the theory in assuming a single liberation temperature T_f for all trapped atoms in the sample. The drastic

results of a slight temperature increase, Fig. 1, are most easily explained with a T_f lower than 20°K., while some atoms in fact survive. The apparent high order of recombination in most of the cases is qualitatively consistent with the chain reaction theory; the apparent low order in N_2 -Xe could be accommodated by the suggestion already advanced for deuterium growth curves, that there are several species of traps, with the more stable variety predominating in samples initially at high concentration and high dose. In $N_2 + Ne$, Ne m.p. 24.5°K., the survival of any atoms so near the melting point of the diluent suggests that the neon plays only a minor part in the trapping of atoms.

TABLE II
EFFECT OF TEMPERATURE INCREASE TO 20.4°K. ON RADICAL CONCENTRATIONS

Sample ^a	Product	Amount of product, mole %			
		Initial	Time after immersion in liquid H_2		
			1 hr.	2 hr.	7 hr.
N_2	N	0.0063	0.0005	0.0004	
		.0017	.0014		
		.0008	.0006		0.0006
Ne + N_2 (16:1 molar ratio)	N	.074		.013	
		.005		.008	
Xe + N_2 (4:1 molar ratio)	N	.13		.033	
		.017		.0035	
		.005	.006		
Ar + N_2 (16:1 molar ratio)	N	.0047		.0021	
CH_4	CH_3	.070		.038	
	H	.001		.0006	
CH_4	CH_3	.053		.014	
	H	.039		.001	

^a In the mixtures that contain Xe or Ne, the percentages of N atoms are based on the content of N_2 .

E.s.r. Spectra—Line Breadth and Power Saturation.—Some of the e.s.r. spectra are shown in Fig. 3 with power-saturation correction at 1 mw. indicated by the number in the lower right corner. At high dose, the spectral lines in N_2 mixtures are broader than in pure N_2 . One likely cause of this broadening is spin-spin interaction of neighboring atoms at high concentration. This also is a relaxation mechanism which should act to reduce power saturation. Since over-all atom concentrations in mixtures are low, this suggests that local concentrations are high, which agrees with the model of atoms confined to N_2 crystals. Even at low doses where line broadening is imperceptible, the power saturation in mixtures is less pronounced than in pure N_2 . This may imply that the atom concentrations plotted for Ne + N_2 , Fig. 2, are too low, a possible error if during preparation the sample deposited most of its N_2 in the less sensitive regions of its tube. An unexplained discordant observation is that at high dose, the mixtures exhibit not less but more power saturation than does pure N_2 , while line breadth and corrected absorption both indicate a higher local concentration of atoms.

E.s.r. Spectra—Additional Lines.—The spectra obtained after warming to 20° usually show weak

lines in addition to the narrowed main lines. No satisfactory explanation for these lines has been found. Figure 6 shows the normal and narrow-line spectra for N in N_2 . Possible explanations are based on (1) instrumental difficulties, (2) forbidden transitions, (3) impurities, (4) different trapping sites, (5) crystal field splitting, and (6) a radical species N_3 in small amounts.

Satellite lines originating from frequency relationships in the instrument often are encountered in nuclear resonance, but in e.s.r., with the present arrangement, no such satellites have been found with hydrogen and other narrow lines. Satellite lines due to forbidden transitions ($\Delta m_s = \pm 1$, $\Delta m_I = \pm 1, \pm 2$) have been reported by other workers, for example on hydrogen lines in certain matrices⁹; however, the requisite field differences would be too small to observe in nitrogen. The lines 6 and 14, Fig. 6, do not have symmetrically located partners, and very probably are due to the quartz container. They will not be considered further. Of the likely impurities in nitrogen itself, NO_2 has a broad triplet spacing of the order of 50 gauss⁹ and NO has not given observable resonances at low temperatures, and its paramagnetic $2\pi_{3/2}$ state, if excited by γ -radiation, is unlikely to have sufficiently long life. In any event, these impurities could only account for three lines.

The sets 5-9-12 and 3-7-10 have the common hyperfine spacing for nitrogen, about 3.8 gauss, and could be due to N atoms in trapping sites of different g -value. The largest reported displacements in g -value by differences in matrix environment, however, would amount to only 0.2 gauss here,⁹ as against the 1.4 gauss difference between 3 and 4, and moreover are accompanied by much larger changes in hyperfine spacing, up to 1.2 gauss.

The crystal field splitting of the $-3/2 \rightarrow -1/2$ and $+1/2 \rightarrow +3/2$ transitions is commonly accepted as the cause of lines 1, 2, 13, and another not shown, beyond 14.¹¹ It appeared at first that 3 and 12 might be the crystal-field splitting lines normally hidden under 4 and 9, but the spacing interval is wrong, as the separation 2-3 is only 3.0 gauss instead of the 3.8 or 4.0 gauss interval of 1-2 and other hyperfine sets.

Peiser has observed that deposits of N_2 containing N atoms have greater crystalline order than deposits without atoms, and considers that the difference is due to annealing by the heat of combination of part of the atoms.¹² As a special case of crystal-field splitting, one might suppose that orientation effects during freezing or annealing, the former often being observed in small cylindrical containers, produced a second favored orientation in addition to the usual statistically favored $\theta = 90^\circ$ in a randomly oriented polycrystalline assembly. If so, the sets (3-7-10) and (5-9-12) correspond to (1-2-hidden 4) and (hidden 9-13-beyond 14) for the special orientation. The special orientation, if it exists, is either $\theta = 51^\circ$ or $\theta = 58^\circ$, and must be rather sharply defined.

Finally, there is the possibility of a species N_3 ,

- (11) T. Cole and H. M. McConnell, *J. Chem. Phys.*, **29**, 451 (1958).
(12) A. M. Bass and H. P. Broida, "Formation and Trapping of Free Radicals," Academic Press, New York, N. Y., 1960, p. 320.

or N loosely coordinated to N₂, for which some disputed spectroscopic evidence has been advanced.¹³ In the radical considered, the odd electron must have a strong hyperfine interaction with one nitrogen (equal to that in a nitrogen atom), a weak interaction with the second (about 30% of the first), and negligible interaction with the third. This might be plausible for an unsymmetrical linear N₃ complex although not for the linear N₃ discussed by Griffing.¹⁴ According to unsymmetrical N₃ model, each of the hyperfine lines 4, 8, 11 is split by the second nucleus to a triplet (3,4,5), (7,8,9), (10,11,12). If this species exists, it is only in small concentrations in addition to N atoms, perhaps 5% of the latter as judged from peak heights.

In irradiated methane, Fig. 7, the general causes for extra lines roughly parallel those in nitrogen. Crystal-field splitting is excluded as the electron spin transition is only $-1/2 \leftrightarrow +1/2$; however, anisotropic hyperfine interaction will have superficially similar effects. The first line of spectrum C, Fig. 7, suggests at first the theoretical line shape for the case $B/A = -1.0$,¹⁵ where B is the anisotropic and A the isotropic hyperfine parameter, but the line shapes here, where three protons contribute, should be more complicated than is found. In a methyl group rotating rapidly about a fixed axis perpendicular to the plane of the molecule, the three protons would be geometrically equivalent, and for a given proton spin combination, *e.g.*, $\Sigma m_I = -3/2$, a random assembly of orientations then could give a simple line shape of the type mentioned, but the dimensions of different lines of the spectrum would differ. From the figure, the dimensions (intervals between satellite peaks) seem approximately equal for all lines; therefore, this rotational hypothesis, while perhaps accounting for the general narrowing of lines, does not seem to explain the satellites. The possibility that the satellites are due to further splitting, of the isotropic kind, by another proton is offset by the generally asymmetrical appearance of a line with its satellites or humps, *e.g.*, the extreme left line of Fig. 7C. Such protons could be intramolecular, as in CH₄⁺ or CH₅⁺, or extramolecular, in adjacent methane molecules. The shape of the group (line and satellites) is better fitted by supposing that the three peaks in the above example are a superposition of a broad and a narrow line, with the center of the broad line farther to the left, so that the left-hand derivative peaks of the two nearly coincide, while the right-hand peaks are better separated. This line arrangement could come from methyl groups in two sites, those in the second kind of site having a 5 to 10% larger splitting parameter A and also a greater line breadth.

Spectrum E, Fig. 7, has additional pairs of peaks about 30 gauss beyond the first and last normal peaks. They may be the extreme members of a system of six peaks due to another radical having five nearly equivalent protons. An obvious possibility is the radical $\sim\text{CH}_2\dot{\text{C}}\text{HCH}_2\sim$, which could be formed from secondary chemical products

on prolonged radiolysis. To furnish a sufficient amount of secondary products, the radiolysis of methane at low temperatures would have to yield unsuspectedly large amounts of longer-chain hydrocarbons.

Summary

The γ -irradiation of N₂, N₂ + 4Xe, N₂ + 16Ne, CH₄, H₂, and D₂ has been carried out to doses up to 16×10^{21} e.v./g. The concentrations of atoms and radicals in pure N₂ and CH₄ appear to level off and the materials manifest great instability; the growth curves are in fair agreement with Jackson's chain reaction theory and an extension of it to two species.

Initial G -values and limiting concentrations in mole per cent (computed per electron fraction N₂ in N₂ mixtures) are: for N in N₂, 0.3, 0.1%; for N in N₂ + 4Xe, 0.4, unknown; for N in N₂ + 16Ne, 0.1, unknown; for CH₃ in CH₄, 0.9, 0.2%; for H in CH₄, the same; for H in H₂, $>>0.1$, 0.0001%; for D in D₂, 2.4, 0.008%. The absolute values are uncertain by 50%, although relative values within a growth curve are much better. Most of the atoms and radicals disappear very slowly if at all at 4°K., but rapidly at 20°K. In H₂ and D₂, however, the atoms disappear at appreciable rates at 4°K.

Appendix

Extension of Jackson's Dynamic Stability Theory to Two Radical Species.—Assume equal heats of reaction for H + H, H + CH₃, and CH₃ + CH₃. Assume all trapping sites for H characterized by liberation temperature T_1 and that a reaction of any kind liberates all H in a volume V_1 ; likewise for CH₃, T_2 , and V_2 .

Let the number of trapping sites for H per unit volume be M_1 and for CH₃, M_2 . About a stationary H atom, there will be a number of H sites, ξ_{11} , such that H atoms arriving at the site will react with the stationary atom and a number of CH₃ sites, ζ_{21} , such that an arriving CH₃ will react. Similarly, for H and CH₃ arriving about CH₃, define ξ_{12} and ξ_{22} , and let $z_{11} = \xi_{11}/M_1$, $z_{21} = \zeta_{21}/M_2$, $z_{12} = \xi_{12}/M_1$, $z_{22} = \zeta_{22}/M_2$. Then the probability that an atom of H comes to rest near a site occupied by H is $z_{11}n_1$, where n_1 is the number per unit volume of H atoms; likewise

for CH₃ near H $z_{21}n$

for H near CH₃ . . . $z_{12}n_2$

for CH₃ near CH₃ . . . $z_{22}n_2$

The average number of all second-stage recombinations resulting from one initial reaction of either kind is

$$V_1 n_1 (z_{11} n_1 + z_{12} n_2) + V_2 n_2 (z_{21} n_1 + z_{22} n_2) = 1$$

and if this is greater than unity, the mixture will explode. There no longer is a unique critical concentration n_c ; instead, the joint critical concentrations of the two species are the number pairs represented by the points of an ellipse in n_1 and n_2 .

$$V_1 n_1 (z_{11} n_1 + z_{12} n_2) + V_2 n_2 (z_{21} n_1 + z_{22} n_2) = 1$$

(13) D. E. Milligan, H. W. Brown, and G. C. Pimentel, *J. Chem. Phys.*, **25**, 1080L (1956).

(14) V. Griffing, private communication.

(15) S. M. Blinder, *J. Chem. Phys.*, **33**, 751 (1960).

The average chain length r' is defined (differently from Jackson) as the number of reactions resulting from an initial reaction. One then proceeds according to the scheme

1st stage, reactions: 1

1st stage, radicals: H: $V_1/n_1 \equiv v$
 R: $V_2n_2 \equiv w$

2nd stage, reactions: $V_1n_1(z_{11}n_1 + z_{12}n_2) + V_2n_2(z_{21}n_1 + z_{22}n_2) \equiv v\sigma + w\rho$

2nd stage, radicals: H: $v(v\sigma + w\rho)$
 R: $w(v\sigma + w\rho)$

3rd stage, reactions: $v\sigma(v\sigma + w\rho) + w\rho(v\sigma + w\rho) = (v\sigma + w\rho)^2$

n th stage, reactions: $(v\sigma + w\rho)^{n-1}$

$$\text{Total: } \bar{r}' = \sum_{n=1}^{\infty} (v\sigma + w\rho)^{n-1} = \frac{1}{1 - (v\sigma + w\rho)} = \frac{1}{1 - D}$$

where

$$D = v\sigma + w\rho = V_1/n_1(z_{11}n_1 + z_{12}n_2) + V_2n_2(z_{21}n_1 + z_{22}n_2)$$

The n_1 and n_2 in individual volume elements can vary according to a Poisson distribution without changing the argument, as by the independence of events each H or R released reacts separately, and one seeks only the sum $\sum_0^{\infty} m\rho(m)$. The number of reactions due to H in a subsequent stage, for example is $\sum_0^{\infty} \frac{m(n_1V_1)^m}{m!} e^{-n_1V_1(z_{11}n_1 + z_{12}n_2)}$, which is simply $n_1V_1(z_{11}n_1 + z_{12}n_2)$ as in the naïve argument. A reaction of any kind at any stage produces in the next stage V_1n_1 H atoms and V_2n_2 CH_3 radicals and results in the following consumption of various species

Reaction type	Occurrence	H consumed	R consumed
H + H	$V_1n_1(z_{11}n_1)$	$2.V_1n_1(z_{11}n_1)$	0
H + R	$V_1n_1(z_{12}n_2)$	$1.V_1n_1(z_{12}n_2)$	$1.V_1n_1(z_{12}n_2)$
R + H	$V_2n_2(z_{21}n_1)$	$1.V_2n_2(z_{21}n_1)$	$1.V_2n_2(z_{21}n_1)$
R + R	$V_2n_2(z_{22}n_2)$	0	$2.V_2n_2(z_{22}n_2)$

Thus the average reaction, excluding the first, consumes $(2V_1z_{11}n_1^2 + (V_1z_{12} + V_2z_{21})n_1n_2)/D$ H atoms per reaction and $[(V_1z_{12} + V_2z_{21})n_1n_2 + 2V_2z_{22}n_2^2]/D$ CH_3 radicals per reaction, where $D = V_1n_1(z_{11}n_1 + z_{12}n_2) + V_2n_2(z_{21}n_1 + z_{22}n_2)$.

If H and CH_3 are produced by γ -radiation, in the mobile condition, at rates κ_1 and κ_2 , respectively, they induce a first reaction with probabilities $z_{11}n_1, z_{12}n_2, z_{21}n_1,$ and $z_{22}n_2$ for the types H + H, H + CH_3 , CH_3 + H, and CH_3 + CH_3 and thus at rates $\kappa_1z_{11}n_1, \dots, \kappa_2z_{22}n_2$. The resultant rates of accumulation for the two species are

$$\frac{dn_1}{dt} = \kappa_1 - 2\kappa_1z_{11}n_1 - \kappa_1z_{12}n_2 - \kappa_2z_{21}n_1 - \kappa_1(z_{11}n_1 + z_{12}n_2) + \kappa_2(z_{21}n_1 + z_{22}n_2) \times [2V_1z_{11}n_1^2 + (V_1z_{12} + V_2z_{21})n_1n_2]/(1 - D)$$

$$\frac{dn_2}{dt} = \kappa_2 - \kappa_1z_{12}n_2 - \kappa_2z_{21}n_1 - 2\kappa_2z_{22}n_2 - \kappa_1(z_{11}n_1 + z_{12}n_2) + \kappa_2(z_{21}n_1 + z_{22}n_2) \times [(V_1z_{12} + V_2z_{21})n_1n_2 + 2V_2z_{22}n_2^2]/(1 - D)$$

Use was made of $\bar{r}' - 1 = D/(1 - D)$. Errors in r' arise from neglecting the fact that one of the H atoms in V_1 may be consumed, not liberated. For $V_1n_1, V_2n_2 \gg 1$, these are not serious. For given values of the $\kappa, V,$ and z parameters, one can form the derivative dn_1/dn_2 , which is a quotient of polynomials in n_1 and n_2 , and solve numerically by the Kutta-Runge method, then evaluate t by graphical integration of dt/dn_1 .

In the choice of parameters, the equal initial rates of accumulation require $\kappa_1 = \kappa_2$, and the results of heating experiments suggest $T_2 > T_1, V_2 < V_1$. The choice of z values is difficult without detailed assumptions about the lattice and trapping sites. In the absence of better knowledge, $z_{11} = z_{12} = z_{21} = z_{22}$ is not too unrealistic, since the greater space available around a CH_3 would be compensated by orientation requirements.

For the extreme case $V_2 = 0$ and $z_{11} = z_{12} = z_{21} = z_{22}$, the equations become

$$\frac{dx}{d\tau} = 1 - \frac{\beta(2x + y)}{1 - x(x + y)}$$

$$\frac{dy}{d\tau} = 1 - \frac{\beta y}{1 - x(x + y)}$$

where the special distribution in the first step is neglected, and where

$$n_c' = \left(\frac{1}{V_1z}\right)^{1/2} = [n_1(n_1 + n_2)]^{1/2}, x = n_1/n_c',$$

$$y = n_2/n_c', \tau = \kappa t/n_c', \text{ and } \beta = 2n_c'z = 2(z/V_1)^{1/2}$$

The growth curves for $\beta = 0.04$ and $\beta = 0.1$ are shown in Fig. 3.

THE EFFECT OF ELECTRON IRRADIATION PRIOR TO REACTION ON THE ACTIVITY OF A SEMICONDUCTOR CATALYST

BY NICHOLAS J. STEVENS, JR., EDWARD A. MASON, AND ROBERT C. REID

Massachusetts Institute of Technology, Cambridge 39, Massachusetts

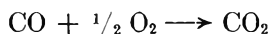
Received April 5, 1962

Pre-irradiation of solid catalysts has not been studied extensively. Moreover, the relationship between catalyst activity and solid state defect properties is not well understood. The principal objective of the paper is to examine the effect of electron irradiation on the catalytic properties of cuprous oxide for the oxidation of carbon monoxide. Measurements of the rate of reaction on cuprous oxide were carried out before and after irradiation. In addition, measurements were made of the bulk electrical properties and surface area of both irradiated and unirradiated cuprous oxide. The description of these studies is divided into two parts; the first examines the kinetics of the reaction and a plausible reaction mechanism is suggested; the second concerns the effect of electron irradiation on the catalyst activity of cuprous oxide and attempts to relate changes in the defect nature of this oxide semiconductor to its catalytic and electrical properties.

Kinetics of the Carbon Monoxide Oxidation on Cuprous Oxide.—The catalytic oxidation of carbon monoxide on cuprous oxide has been investigated at room temperature and 0.1 mm. pressure by Garner, *et al.*,^{1,2} and at slightly higher temperatures and pressures by Winter.² At room temperature, the kinetics were found to be first order with respect to oxygen. Between 50 and 86° and at 1 to 9 cm. pressure, the rate was found to depend on both the oxygen and the carbon monoxide concentration with the order of the reaction a function of the temperature. No kinetic data have been reported at temperatures above 86°.

Experimental

Reaction Conditions.—The rate experiments were conducted in a constant volume reactor immersed in a temperature bath. Since the reaction



proceeds with a decrease in the system pressure, the extent of the reaction could be followed manometrically. All runs were made at an initial pressure of one atmosphere, but temperatures were varied between 135 and 160° and initial mole fractions of carbon monoxide between 0.2 and 0.6. Since no diluent was used, oxygen was the only other component initially present.

Reactants.—Carbon monoxide (C.P. grade) was supplied by the Matheson Company and oxygen by the Air Reduction Company. The purity of the gases exceeded 99.5%. Before use, however, all gases were filtered through glass wool, dried with calcium sulfate, and freed of carbon dioxide with Ascarite.

Catalysts.—Sets of 25 copper disks (2 in. in diameter and 0.002 in. thick) were used as the catalyst. Oxygen-free high conductivity copper was supplied by the J. L. Anthony Company, Providence, Rhode Island, and analyzed to be better than 99.9% copper. A thin layer (1,000–3,500 Å.) of cuprous oxide was formed on the outside surface of the disks by an oxidation technique developed by Garner.^{1a}

The oxide films on similarly prepared catalyst disks were electrolytically reduced in 0.1 *N* KCl using Ag–AgCl electrodes and a voltage of about 0.8 volt was measured. This voltage compares favorably with values reported by Campbell and Thomas³ for the electrolytic reduction of cuprous oxide.

Four different sets of catalyst disks were used during the investigation. The geometrical surface area of each set of 25 disks was 0.10 m.². Based on the results of surface area measurements on similarly prepared groups of disks, the roughness factor (true surface area/geometrical surface

area) ranged from 1.5 to 3.0. Because of their extreme sensitivity to poisoning, the catalysts were carefully protected from exposure to mercury, water, and hydrocarbons.

Apparatus.—A flow diagram of the system is shown in Fig. 1. The reaction vessel was a 330-cc. stainless steel cylinder in which the catalyst disks were stacked vertically on a stainless steel rod. A Conax thermocouple was provided to measure the gas temperature inside the vessel. The reactor was fitted with a thin (0.012-in.) aluminum window at the top for use in subsequent catalyst irradiation studies. Suitable gas connections and a pressure tap were provided and the vessel immersed in a constant temperature bath.

Procedure.—The reactants were metered in the desired proportion using capillary flowmeters and passed through the reactor for a period of 100 sec. before the beginning of an experimental run. The reactor gas inlet valves then were closed, and the reaction followed by noting pressure changes with a manometer. The runs were generally of 1,000 sec. duration, although longer times were used at the lower range of temperature investigated. Pressure readings were recorded at 100-sec. intervals throughout the run. Immediately after the completion of a run, the reactor was evacuated to a pressure of 0.5 mm. for a period of 5 min. prior to starting the next run.

Blank runs, *i.e.*, runs carried out without the catalyst present, indicated that no pressure change occurred under these conditions. Thus, none of the pressure decrease during reaction could be attributed to wall catalytic effects, homogeneous reactions, or to adsorption phenomena on non-catalyst surfaces.

Results

The pressure change, ΔP , for the oxidation of carbon monoxide is related to the extent of reaction by the simple expression

$$\frac{\Delta P}{P_0} = -\frac{x/2}{(a+b)} \quad (1)$$

In this expression ΔP is the measured change in pressure, P_0 the initial total pressure, a the original moles of CO present, b the original moles of O₂ present, and x the moles of CO reacted.

That is

$$dx = -dN_{\text{CO}} = -2dN_{\text{O}_2} = dN_{\text{CO}_2} \quad (2)$$

or,

$$x = N_{\text{CO}_2} = N_{\text{CO}_0} - N_{\text{CO}} = 2(N_{\text{O}_20} - N_{\text{O}_2}) \quad (3)$$

N is the number of moles present and the subscript 0 indicates initial quantities.

The experimental data consisted of values of ΔP as a function of time for many runs at different temperatures and initial mole ratios of CO to O₂. A typical plot of experimental data is shown in

(1) (a) W. E. Garner, T. J. Gray, and F. S. Stone, *Proc. Roy. Soc. (London)*, **A197**, 294 (1949); (b) W. E. Garner, F. S. Stone, and P. F. Tiley, *ibid.*, **A211**, 472 (1952).

(2) E. R. S. Winter, *J. Chem. Soc.*, 2726 (1955).

(3) W. F. Campbell and U. B. Thomas, *Trans. Electrochem. Soc.*, **76**, 303 (1939).

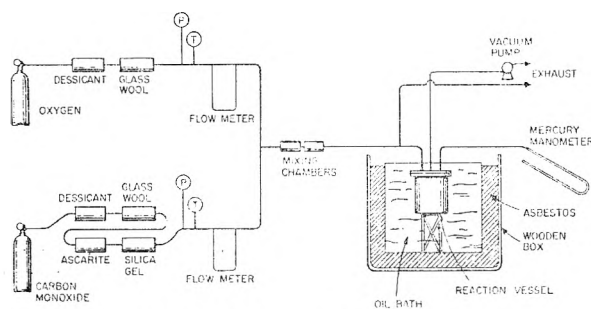


Fig. 1.—Flow diagram of reaction system.

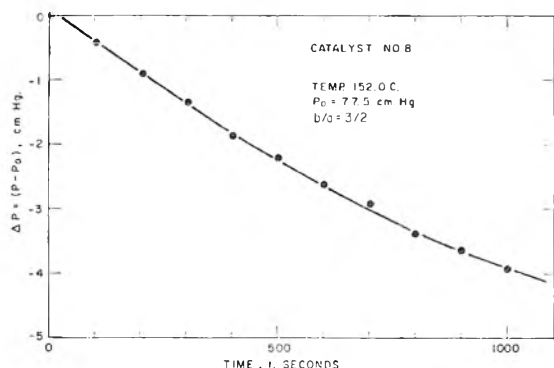


Fig. 2.—Pressure drop-time curve for a typical run.

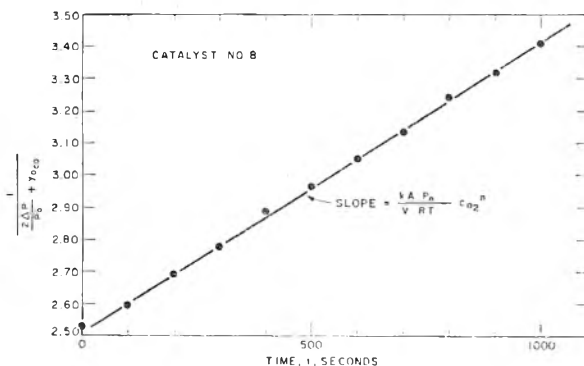


Fig. 3.—Plot of integrated pseudo-second order expression.

Fig. 2. Here ΔP is plotted as a function of time for a temperature of 152.0° and initial concentrations of CO and O₂ of 1.17×10^{-2} and 1.75×10^{-2} g.-mole/l., respectively; these concentrations correspond to a and b values of 3.86×10^{-3} g. mole and 5.78×10^{-3} g. mole since the reactor volume is 330 cc.

Rate Expression.—A number of different rate expressions were investigated, but it was found that eq. 4 best fit the experimental data

$$r = \frac{dx}{A dt} = \frac{dN_{\text{CO}_2}}{A dt} = \frac{-2Vd(\Delta P)}{ART dt} = kc_{\text{CO}}^m c_{\text{O}_2}^n \quad (4)$$

The order of the reaction for each component, *i.e.*, m and n , was determined in the following way. First, a series of runs was made at various temperatures keeping the initial mole ratio of oxygen-to-carbon monoxide constant at $b/a = 3/2$. For such an oxygen-rich mixture, the concentration of oxygen does not change greatly for reasonable

values of x and may be assumed constant. As an illustration, for a value of x/a of 0.5, the oxygen concentration would have decreased only 17%, whereas the carbon monoxide concentration decreased by 50%.

Assuming that the concentration of oxygen is constant during this set of experiments, eq. 4 may be easily integrated for various values of the order of the reaction with respect to carbon monoxide, m . Each of the integrated expressions can be arranged in linear form and the exponent determined if a straight line is obtained from a plot of the data. Such a plot is shown in Fig. 3 for a value of $m = 2$. Although this value of two for the order with respect to carbon monoxide was obtained with the assumption of constant oxygen concentration, the validity of the assumption is shown below.

To determine the order of the reaction with respect to oxygen, a number of experiments were conducted in which the initial mole fractions of oxygen were varied from 0.40 to 0.80. By employing these various initial oxygen concentrations, the rate dependence upon oxygen could be ascertained with accuracy because the oxygen concentration in any given oxidation experiment varied only slightly. To determine n with these new data, eq. 4 with $m = 2$ was expressed as

$$\ln(r/c_{\text{CO}}^2) = \ln k + n \ln c_{\text{O}_2} \quad (5)$$

Plots of $\ln(r/c_{\text{CO}}^2)$ against $\ln c_{\text{O}_2}$ for various temperatures are shown in Fig. 4.

Values of r were calculated using eq. 4 with $d(\Delta P)/dt$ determined from a graphical differentiation of curves such as shown in Fig. 2. At any value of r , the concentrations c_{CO} and c_{O_2} were calculated from the observed ΔP and the initial b/a ratio by a material balance.

Three different series of runs are plotted. Each of the three series was carried out at a different temperature and at a different level of activity, *i.e.*, at a different pre-exponential factor of the reaction rate constant. The effect of these two factors influences the value obtained for the reaction rate constant, k . Thus, according to eq. 5, the intercept value, $\ln k$, might be expected to be different for the three groups of data, as is observed. However, the slope rather than the position of the straight lines in Fig. 4 is of importance in determining the order of the reaction with respect to oxygen. The slope of the different lines indicates that n is also 2.0.

It is important to note that the size of each data point depicted in Fig. 4 covers a range of values taken during a single experiment. The changes in the partial pressure of carbon monoxide and oxygen during each of the experimental runs are small compared to the variation resulting from the changes in the initial reactant concentrations from one set of reactant conditions to another. Thus, for the scale used in Fig. 4, each point on the plot represents several points obtained for an individual batch run.

The final rate equation then is expressed as

$$r = \frac{dx}{A dt} = \frac{dN_{\text{CO}_2}}{A dt} = kc_{\text{CO}}^2 c_{\text{O}_2}^2 \quad (6)$$

or in the integrated form in terms of the pressure drop, the initial total pressure, and initial mole fraction of CO, $Y_{0\text{CO}}$, as

$$\frac{4}{2 - 3Y_{0\text{CO}}} \left[\frac{P_0}{P_0 Y_{0\text{CO}} + 2\Delta P} - \frac{1}{2 - 3Y_{0\text{CO}}} \times \ln \left\{ \frac{P_0(1 - Y_{0\text{CO}}) + \Delta P}{P_0 Y_{0\text{CO}} + 2\Delta P} \right\} \right] - \frac{P_0^2}{[P_0 Y_{0\text{CO}} + 2\Delta P][P_0(1 - Y_{0\text{CO}}) + \Delta P]} = \frac{kA \left(\frac{P_0}{RT} \right)^3 (2 - 3Y_{0\text{CO}})t + \frac{4}{2 - 3Y_{0\text{CO}}} \times \left[\frac{1}{Y_{0\text{CO}}} - \frac{1}{2 - 3Y_{0\text{CO}}} \ln \left\{ \frac{1 - Y_{0\text{CO}}}{Y_{0\text{CO}}} \right\} \right] - \frac{1}{Y_{0\text{CO}}(1 - Y_{0\text{CO}})} \quad (7)$$

By the use of eq. 7, the reaction rate constant can be determined from the linear representation of the data. Least square values were obtained for each of the experimental runs employing an IBM 709 computer. The deviation of k for different concentration levels at a given temperature rarely exceeded 5%.

Because of the unusually high over-all order of the reaction, a large number of other reaction rate expressions were examined in attempting to describe the data. Langmuir-type expressions with reactant or product inhibition terms in the denominator appeared most likely to be applicable. However, none of the expressions with a denominator different from unity adequately fit the experimental data. Since eq. 6 best represented the data, it was chosen for the range of conditions investigated.

Activation Energy.—The logarithm of the reaction rate constant, k , for the four catalysts used is a linear function of reciprocal temperature as shown in Fig. 5. In analytical form

$$k = k_0 \exp(-\Delta E/RT) \quad (8)$$

where k_0 is the so-called pre-exponential factor, R the gas constant, and ΔE the activation energy.

Table I indicates the values of ΔE and k_0 obtained. The confidence limits on the activation energy were determined at the 95% level.

TABLE I
COMPARISON OF RATE CONSTANTS

Catalyst no.	k_0 , (l./g.-mole) ³ × $\frac{1}{\text{sec.-m.}^2}$	ΔE , kcal./g.-mole
8	6.00×10^{23}	41.1 ± 2.3
9	5.17×10^{19}	32.8 ± 1.4
11	1.62×10^{13}	75.6 ± 4.1
12	6.89×10^{38}	69.1 ± 7.4

Several points are of particular interest in Fig. 5 and Table I. First, the large activation energies show that the reaction rate is quite sensitive to temperature. Second, a wide variation in ΔE was observed for the four catalysts used. Third, lower

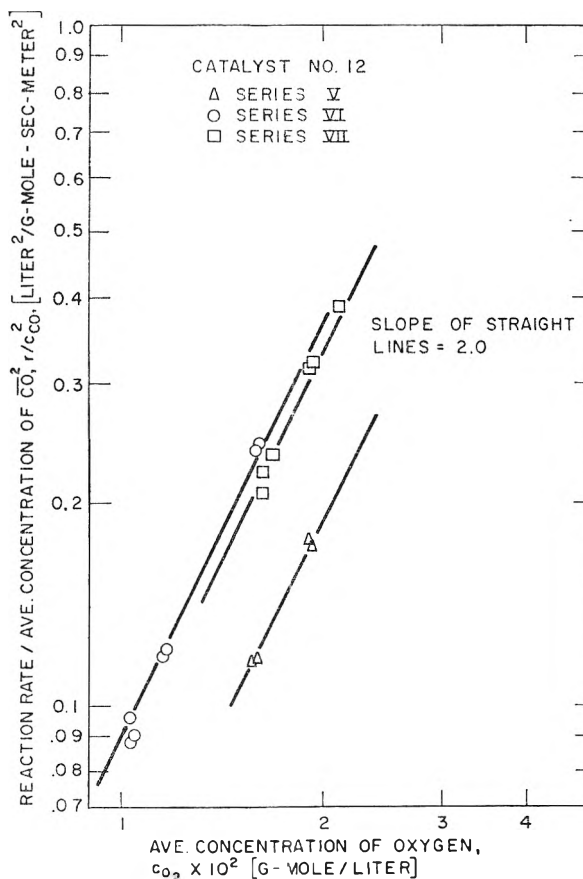


Fig. 4.—Determination of reaction order with respect to oxygen.

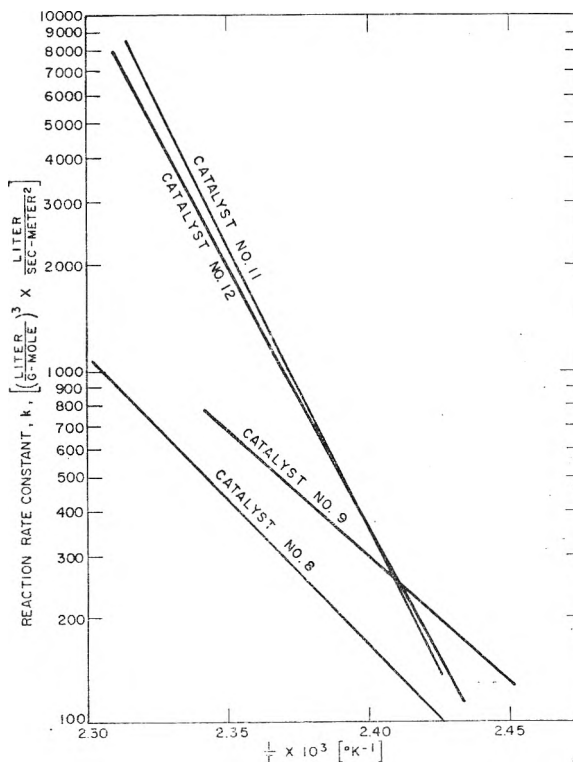
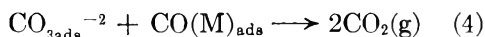
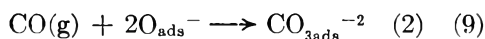
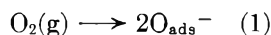


Fig. 5.—Comparison of catalyst activity.

values of k_0 were found to correspond to the lower activation energies and k_0 increased with ΔE . The third phenomenon has been noted by others⁴ and called the "Theta-Rule." There has been no adequate explanation given for this effect.

Returning to the second point of interest, the apparent activation energies are seen to vary from 32.8 ± 1.4 kcal./g.-mole on catalyst no. 9 to 75.6 ± 4.1 kcal./g.-mole on catalyst no. 11. The reason for the differences in activation energy is unknown, although variations in the method of catalyst preparation may account for the changes. Catalyst specimens no. 8 and 9 were prepared by a different experimenter than were no. 11 and 12. The apparent activation energies were nearly similar for those catalysts prepared by any one individual. As far as can be determined, however, the same procedure was followed in the preparation of all four samples. The catalysts no. 1-7 and no. 10 were damaged during the investigation, and no kinetic data were obtained on these specimens.

Reaction Mechanism.—In order to explain the first-order rate expression in oxygen found by Garner at room temperature and 0.1 mm., a four-step mechanism was proposed.^{1b} The steps in the mechanism are

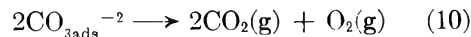


The first two steps in the mechanism involve the surface entities of adsorbed oxygen ions, O_{ads}^- , and adsorbed "carbonate-type complexes," $\text{CO}_{3\text{ads}}^{-2}$. The final step producing carbon dioxide involves the reaction between carbon monoxide adsorbed as the "carbonate complex" and that adsorbed on a copper ion. The adsorption of oxygen was found to be the slowest step in the reaction. Although carbon monoxide is adsorbed reversibly on the metal ions of the catalyst (step 3) at temperatures of even up to 100° , there is evidence that at 150° essentially all the chemisorbed carbon monoxide is in the "carbonate complex" form.⁵

While the mechanism describes the kinetics obtained by Garner at 20° , all the steps do not hold in the region considered in the present investigation. Therefore, it was necessary to propose a different mechanism to explain the fourth-order rate dependency obtained from the data in the studies at 150° and one atmosphere pressure. A simple three-step mechanism in which the first two steps are identical with steps 1 and 2 of the Garner mechanism results in the fourth-order expression. Steps 1 and 2 are rapid and proceed to an equilibrium state. The final step in the proposed reaction mechanism is postulated to be rate controlling and to involve the combination of adjacent carbonate complexes to yield carbon dioxide and oxygen.

(4) M. Boudart, *Chem. Eng. Progr.*, **57**, No. 8, 33 (1961).

(5) W. E. Garner, T. J. Gray, and F. S. Stone, *Discussions Faraday Soc.*, **8**, 257 (1959).



Either by applying the law of mass action to the steps at equilibrium or by using stationary-state approximations for the concentration of adsorbed species, eq. 6 can be derived from this mechanism. The over-all fourth-order rate expression results from the fact that the two "carbonate-type complexes" in the rate-controlling step each depend on the concentration of both carbon monoxide and oxygen.

Using electrical conductivity measurements to follow the reaction, the carbon monoxide oxidation has been carried out near 200° by Garner, Gray, and Stone.⁶ Only a limited number of measurements were carried out, but from their description of the changes in conductivity with time, the three-step mechanism presented above satisfies the observed trends.

Electron Irradiation Studies.—The concept of irradiating solid catalysts to affect permanent changes in the activity or specificity is not new, but only recently has this approach produced positive results.⁷⁻¹¹ Semiconductor catalysts are particularly interesting, since irradiation produces solid state defects, the nature and number of which are believed to be intimately related to the catalytic activity. For example, Bragg, *et al.*,¹² reported an increase in the activity of zinc oxide for the hydrogenation of ethylene when the reaction was carried out during neutron bombardment, but a decrease was observed when the bombardment was terminated. The increase during irradiation was attributed to the large amount of ionization in the solid, while the decrease noted after irradiation was thought to be related to new imperfections created in the atomic lattice. For the decomposition of methanol, Teller, Poska, and Davies¹³ found an increase in the activity of zinc oxide and a decrease in the activity of chromium oxide as a result of γ -radiation. In these cases the activity was measured during the irradiations and changes were attributed to electron displacement. Another interesting study was conducted by Saito, Yoneda, and Makishima¹⁴ in which the effect of neutrons on the activity of metal oxide catalysts used for the decomposition of nitrous oxide was observed. On NiO (a p-type semiconductor), Al_2O_3 (an insulator), and SnO_2 (an n-type semiconductor) containing small amounts of added chemical impurities, the change in activity produced by irradiation was more pronounced as the p-typeness of the catalyst increased.

The present investigation was undertaken to determine the effect of electron irradiation on the

(6) W. E. Garner, T. J. Gray, and F. S. Stone, *ibid.*, **8**, 246 (1959).

(7) R. W. Clarke and E. J. Gibson, *Nature*, **180**, 140 (1957).

(8) C. C. Roberts, A. Spilners, and R. Smoluehowski, *Bull. Am. Phys. Soc.*, [2] **3**, 116 (1958).

(9) H. M. C. Sosnovsky, G. J. Ogilvie, and E. Gillam, *ibid.*, **182**, 523 (1958).

(10) E. H. Taylor and H. W. Kohn, *J. Am. Chem. Soc.*, **79**, 252 (1957).

(11) P. B. Weisz and E. W. Swigler, *J. Chem. Phys.*, **23**, 1567 (1955).

(12) R. H. Bragg, F. L. Morrirtz, R. Holtzman, P. Y. Feng, and F. Pizzarello, WADC Technical Report 59-286.

(13) A. J. Teller, F. L. Poska, and H. A. Davies, Preprint 44, A.I. Che.E. 42nd National Meeting, Atlanta, Georgia, 1960.

(14) Y. Saito, Y. Yoneda, and S. Makishima, *Nature*, **183**, 388 (1959).

activity of cuprous oxide for the oxidation of carbon monoxide and upon the reaction mechanism discussed earlier. In addition, the effect of irradiation on several important electrical properties of the catalyst was determined in an attempt to interpret the catalytic changes in terms of the defect structure of the oxide. The effect of irradiation on the surface area also was measured.

Experimental

Irradiation Studies. Radiation Source.—A Van de Graaf generator located at the Massachusetts Institute of Technology High Voltage Research Laboratory was used as the source of monoenergetic electrons.

Irradiation Procedure.—The same procedure was used for all the experiments in the determination of the effects of radiation on the activity, surface area, and electrical properties of cuprous oxide. Measurements were carried out before and after electron bombardment and the results compared.

Irradiation Conditions.—3.5 Mev. electrons were employed at a flux of $0.5 \mu\text{a./cm.}^2$ (3.12×10^{12} electrons/cm.² sec.) for total periods of 150, 300, and 600 sec. at room temperature. The irradiations were carried out in 30-sec. intervals to limit the temperature rise of the samples. In some experiments, a vacuum of about 0.5 mm. was maintained over the specimen during irradiation while, in others, helium gas at one atmosphere was continuously passed through the sample container; no difference in results was found using the two techniques.

Kinetics Studies. Reactants and Catalysts.—The source and purity of the reactants employed is discussed earlier. Two of the four catalysts, no. 8 and 12, used in determining the reaction rate expression, were subjected to electron irradiation.

Apparatus and Procedure.—The reaction system and procedure mentioned earlier were used for the kinetic experiments. The catalyst samples were irradiated in the reaction vessel without being removed at any time. The electrons penetrated the reaction vessel through a thin (0.012 in.) 2-in. diameter aluminum window which was exposed after the removal of the stainless steel top plate of the reactor. (Catalyst no. 8 was irradiated under vacuum while no. 12 was cooled by helium gas during bombardment.)

B.E.T. Measurements.—Method and Apparatus.—The conventional B.E.T. Method using krypton as the adsorbate as described by Brown¹⁵ was employed. The catalyst sets of 25 disks were contained in an all-Pyrex vessel designed for use in both the surface area determinations and the irradiation studies without the removal of the disks. During the irradiation a vacuum of 0.5 mm. was maintained in the Pyrex container.

Catalysts.—The cuprous oxide on copper catalysts used were specimens prepared by the same procedure as that described earlier.

Electron Micrographs.—An R.C.A.-type EMB-4 electron microscope was used to obtain an image of the catalyst surface. Pictures at 3,000 magnification were taken of a collodion film shadow casted with chromium vapor which was removed from the surface. The pictures were enlarged photographically to 14,000 \times and 38,000 \times . For the irradiation of the catalyst disks to be photographed, a special brass container was constructed and covered with a 0.012-in. sheet of aluminum. The disks were placed inside, and one-half of each disk was covered with a 0.5-in. thick aluminum plate to absorb the electrons. By this technique the same disk would yield photographs of both an irradiated and unirradiated surface.

Electrical Measurements. Materials.—Polycrystalline samples of cuprous oxide with a room temperature resistivity of 1,200 to 1,400 ohm-cm. were obtained through the courtesy of W. H. Brattain of the Bell Telephone Laboratories. The samples were made from completely oxidized sheets of Chilean copper by a technique which included an air oxidation at 1,000° followed by a 3-min. annealing at 600° and air quenching. The main body of the final samples as prepared for use in this work were 2 cm. long, 0.3 cm.

wide, and 0.042 cm. thick; electrical connections were made with soldered contacts.

Apparatus and Procedure.—A simple d.c. circuit consisting of a 6-volt battery and a number of resistors in series with the cuprous oxide specimen was used for the electrical measurements. A Varian V-4004 4-in. electromagnet provided the magnetic field for the Hall effect measurements. A Rubicon Type B-1 potentiometer was used to measure the various voltages.

A cuprous oxide sample was mounted on a copper holder located in a cryostat placed between the poles of the electromagnet. The specimen was electrically insulated from the copper by a thin film of mica which permitted adequate conduction of heat between the holder and the sample. For measurements below room temperature, an acetone-Dry Ice mixture was used in the cylindrical reservoir located directly above the mounted sample. Above room temperature, silicone oil was heated by a resistance coil and the temperature regulated by controlling the power supply with a Variac.

The electrical conductivity and Hall effect were measured at intervals of 5 or 10° over a range of temperatures from -70 to 150° as the sample was slowly heated or cooled. The measurements were carried out under a pressure of 50 to 70 μ .

The current flow through the sample was obtained from the voltage drop across a standard resistor in series with the cuprous oxide specimen. By measuring the voltage drop between two points on the sample and knowing the current from the previous measurement, the electrical conductivity was obtained.

The Hall effect occurs when a magnetic field is applied perpendicular to the flow of current through the specimen producing a force perpendicular to both the magnetic field and the current. The force is balanced by an electrical force set up in the specimen producing a transverse voltage. The difference in the voltage between two points across the width of the sample in the presence and absence of a magnetic field yielded the Hall voltage. The Hall voltage is inversely proportional to the concentration of positive holes in the sample.

The container for the cuprous oxide specimens used in the irradiation experiments was a cylindrical carbon steel vessel equipped with an aluminum window. Helium gas passed through the vessel during the entire period of bombardment.

Experimental Results and Discussion

Kinetic Studies.—After irradiation the two cuprous oxide catalysts were tested for activity in the carbon monoxide oxidation as described earlier. One of the most important results noted is the fact that the form of the rate expression was not affected. For the irradiated catalysts the rate equation was found to be

$$r = \frac{dx}{A dt} = \frac{dN_{\text{CO}_2}}{A dt} = k' c_{\text{CO}}^2 c_{\text{O}_2}^2 \quad (11)$$

where the symbols have identical meanings to those used in eq. 4, except for the reaction rate constant, where k' indicates the value after irradiation. The value of the rate constant decreased after irradiation, *e.g.*, a decrease of approximately 50% was noted in each case after 300 sec. of electron bombardment. This 50% change held for both catalyst sets used, no. 8 and no. 12, even though the pre-irradiated values of the activation energy and pre-exponential factor of the two specimens differed greatly.

The rate of reaction also was measured on catalyst no. 8 after 150 sec. of exposure to electrons. At this time, a decrease of 30% from the unirradiated level of activity was observed over the entire temperature range investigated. The final 150 sec. of irradiation of catalyst no. 8 produced an additional drop in the remaining activity of about

(15) J. H. Brown, "Experimental Procedure for Specific Surface Determination by Krypton Gas Adsorption Method," Dept. of Metallurgy, Mass. Institute of Technology.

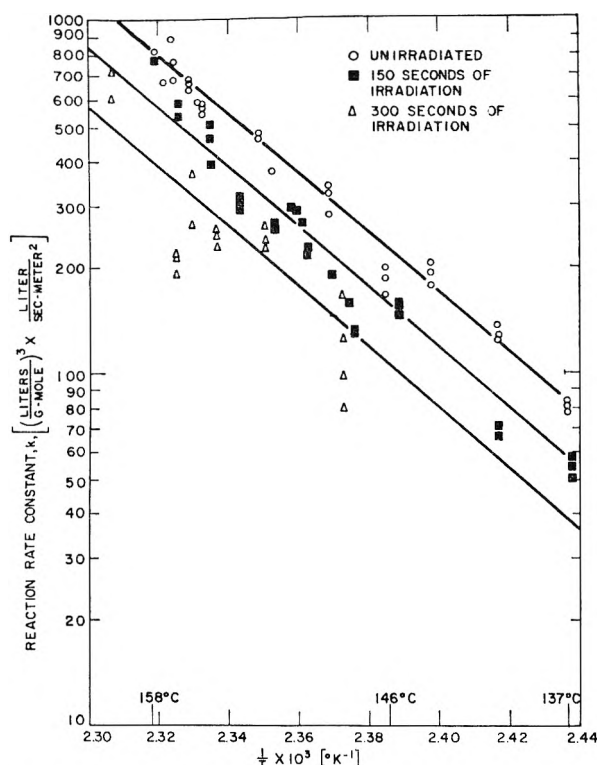


Fig. 6.—Effect of electron irradiation on catalyst activity—catalyst no. 8.

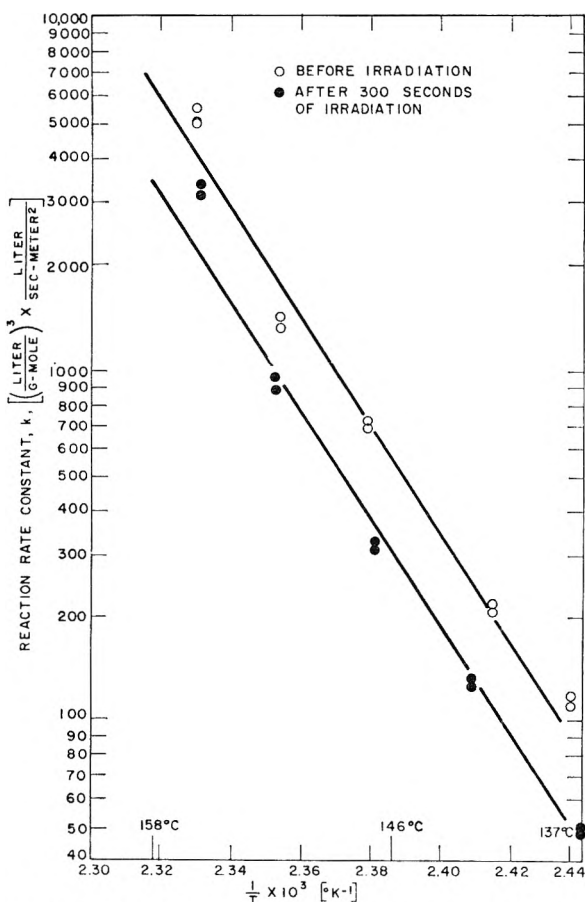


Fig. 7.—Effect of electron irradiation on catalyst activity—catalyst no. 12.

30% to yield an over-all decrease of 50% after 300 sec. For the small doses of catalyst irradiation used, the percentage decreases in activity are proportional to the radiation dose.

Figures 6 and 7 show plots of k and k' as a function of reciprocal temperature. From the figures it can be seen that the activation energy is not affected by irradiation, and the entire effect of the bombardment is reflected by a decrease in the pre-exponential factor. The measured values of k_0 , k_0' , and ΔE are presented in Table II. For catalyst no. 8 a blank run was made prior to irradiation to test for the effect of handling and transporting the catalyst and reactor to and from the Van de Graaf generator. During the experiment, all the steps required to irradiate the catalyst except the irradiation itself were performed. Several kinetic runs were conducted after the blank run, and the catalyst activity was found to be unchanged. These results indicate that the decreases in activity are produced by the electron bombardment.

TABLE II

EFFECT OF IRRADIATION ON REACTION RATE CONSTANT

Pre-exponential factor k_0 or k_0' $\left(\frac{\text{l.}}{\text{g.-mole}}\right)^2 \times \frac{\text{l.}}{\text{sec.-meter}^2}$	Before irradiation	After 150 sec. of irradiation	After 300 sec. of irradiation
Catalyst no. 8	6.00×10^{23}	4.18×10^{23}	2.79×10^{23}
Catalyst no. 12	6.89×10^{24}	3.72×10^{24}
Activation energy ΔE , kcal./g.-mole			
Catalyst no. 8	41.1 ± 2.3	43.1 ± 3.7	41–43
Catalyst no. 12	69.1 ± 7.4	75.7 ± 7.8

B. E. T. Measurements.—Increases of 30 to 40% in the measured surface area were noted on two different catalyst specimens after 300 sec. of irradiation. An additional increase of 26% was observed on one of the specimens as a result of a second 300 sec. of bombardment. Thus, for the relatively small doses used, the percentage changes in surface area are roughly proportional to the amount of irradiation dose. The percentage changes were calculated from the average value of several determinations made prior to and after irradiation (Table III). For the sample on which a 40% increase was observed, a few of the values measured before irradiation, although included for the determination of the average, are believed to be somewhat low. If these low values are not included, the percentage increase in measured surface area after 300 sec. amounts to about 30% as in the other instances.

Electron Micrographs.—Photomicrographs of the catalyst surface indicate that the increase in area results from an increase in the roughness of the surface layer. The pictures show the irradiated surface to be marked by a greater degree of unevenness and by more pronounced irregularities. Rounded areas of the order of 1000 Å. in diameter cover the surface after irradiation where little or none existed previously. A number of pictures were taken before and after irradiation, and a comparison is presented in Fig. 8. From a consid-

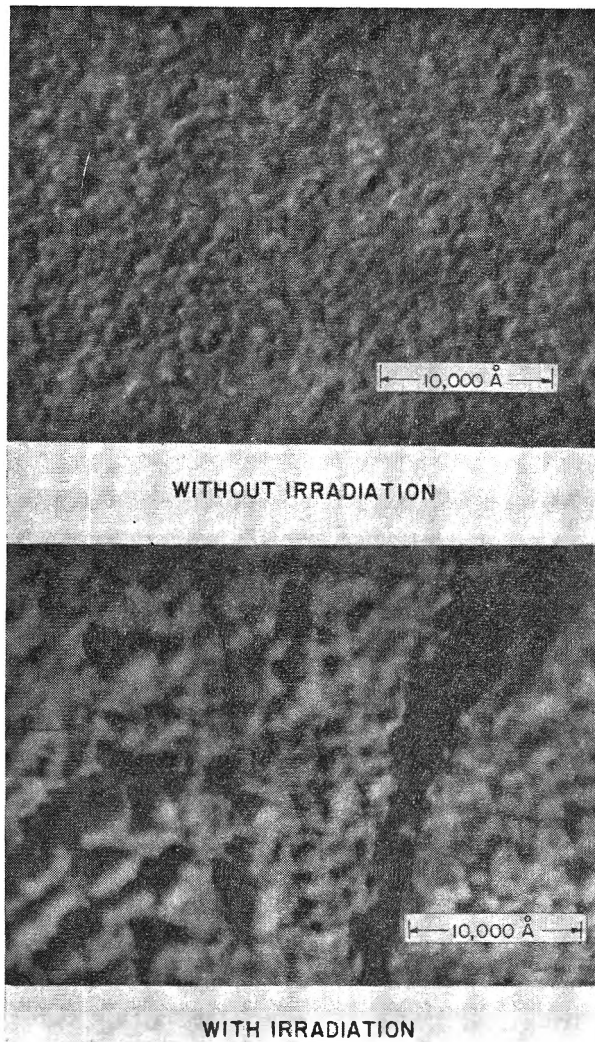


Fig. 8.—Electron micrographs of cuprous oxide catalyst disks at 38,000X.

TABLE III
THE EFFECT OF IRRADIATION ON SURFACE AREA

Surface area before irradiation (m. ²)	Surface area after 300 sec. of irradiation (m. ²)	Surface area after 600 sec. of irradiation (m. ²)
Sample A		
0.230	0.380	0.428
.277	.325	.457
.271	.377	
.258		
.220		
.210		
.283		
Av. value 0.25	0.35	0.44
% increase over unirradiated value	40	76
Sample B		
0.112	0.163	...
.173	.167	...
.150	.199	...
.114
Av. value 0.14	.18	...
% increase over unirradiated value	29	...

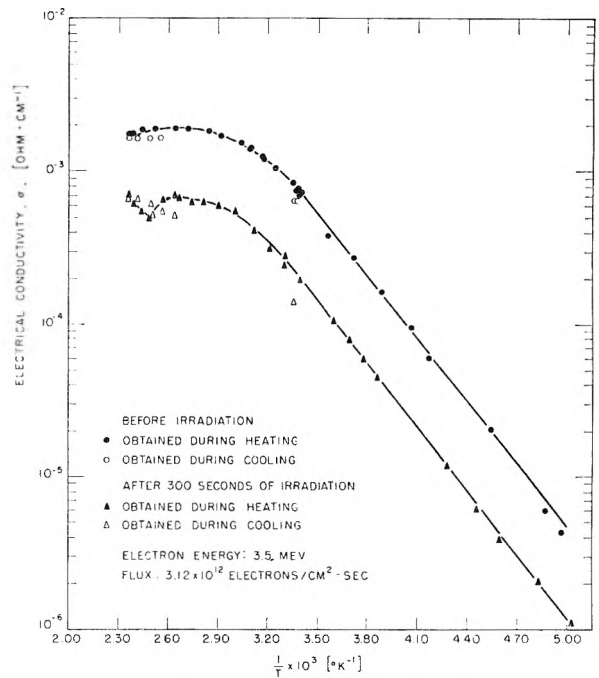


Fig. 9.—Effect of electron irradiation on the conductivity of cuprous oxide.

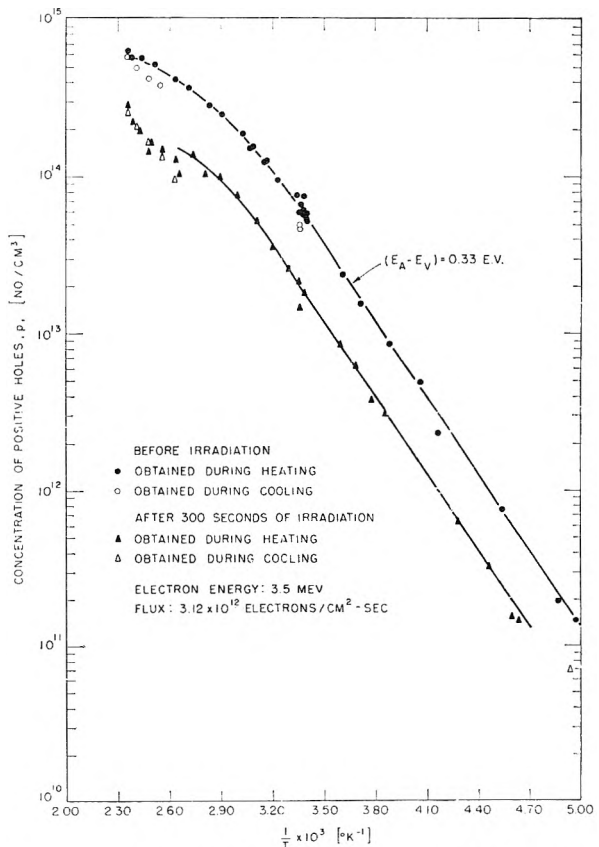


Fig. 10.—Effect of electron irradiation on the positive hole concentration of cuprous oxide.

eration of all the photographs, the irradiated surface also was characterized by a greater number of surface fissures than were present without bombardment.

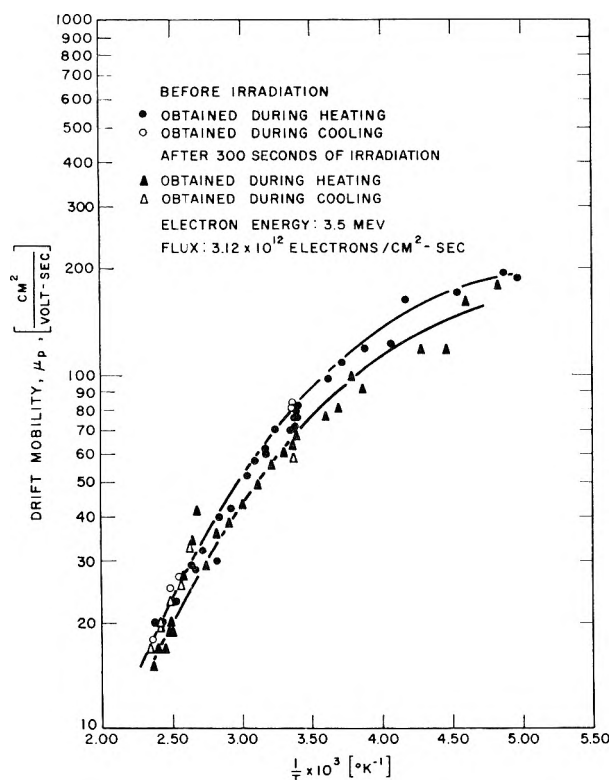


Fig. 11.—Effect of electron irradiation on the mobility of cuprous oxide.

The causes of the roughened surface are not clear. Simple atomic displacements by the electrons are not sufficient to produce the gross damage observed. A more likely possibility is that thermal stresses resulting from a heat-up of the catalyst during irradiation produce a wrinkling of the surface oxide layer. It is estimated that an adiabatic temperature rise of the catalyst of as much as 100° may occur in each of the 30-sec. intervals used for bombardment. Even with smaller temperature variations, surface roughening might very readily result from the heating and subsequent cooling of the catalyst disks.

Electrical Properties.—The electrical conductivity and Hall effect were recorded for cuprous oxide before and after irradiation from -70 to 150° for one sample and from -70° to room temperature for a second sample. From these measurements, the conductivity, positive hole concentration, and mobility were found to be lowered as a result of 3.5 Mev. electron bombardment. The effects are shown in Fig. 9–11 for one sample. The other sample yielded similar results.

As observed in the catalyst activity and surface area experiments, a given dose of electron irradiation produced roughly equal percentage changes in the bulk electrical properties of different samples of cuprous oxide. As well, the relative damage created is proportional to the radiation dose.

Electron irradiation introduces atomic displacements resulting in vacancies and accompanying interstitials. For the system studied here, the changes in electrical properties may be interpreted in terms of a model in which additional numbers of copper and oxygen vacancies are created. (The

actual effect of electron radiation on such a semiconductor may be more complicated, as suggested, for example, by Billington and Crawford.¹⁶) The concentrations of these vacancies control the positive hole concentration and the electrical conductivity of cuprous oxide. As may be seen in Fig. 10, up to a temperature of about 60° , the positive hole concentration fits the relationship^{17,18}

$$p = 2 \left[\frac{2\pi mkT}{h^2} \right]^{3/2} \left[\frac{N_A}{N_D} - 1 \right] \exp \left[- \frac{E_A - E_V}{kT} \right] \quad (12)$$

where p is the positive hole concentration, m is the effective mass of the hole, k is the Boltzmann constant, h is the Planck constant, T is the absolute temperature, and $(E_A - E_V)$ is the ionization energy. According to eq. 12, the positive hole concentration is essentially proportional to the ratio of copper acceptor vacancies, N_A , to oxygen donor vacancies, N_D , present since $N_A/N_D \gg 1$.

The concentrations of copper and oxygen vacancies in cuprous oxide after irradiation may be deduced using eq. 12 at a given temperature. The terms m , k , T , and h are the same before and after irradiation; the ionization energy $(E_A - E_V)$ also is unaffected, since the slope of the plot of the logarithm of the positive hole concentration vs. reciprocal temperature (Fig. 10) is unchanged by bombardment. Thus the ratio of the positive hole concentration before and after irradiation is

$$\frac{p}{p'} = \frac{(N_A/N_D - 1)}{(N_A'/N_D' - 1)} \quad (13)$$

where the primes indicate conditions after irradiation. Calculations using the plots of Oen and Holmes¹⁹ indicate that as a result of irradiation, 50% more copper vacancies are created than oxygen vacancies. Letting Δ equal the additional concentration of oxygen vacancies created and using this calculated result

$$N_D' = N_D + \Delta$$

$$N_A' = N_A + 1.5\Delta$$

To solve for Δ , the initial values of the copper and oxygen vacancies present, N_A and N_D , are necessary. Using eq. 12 and the upper curve of Fig. 10, N_A/N_D is determined to equal about 10. However, to calculate N_A and N_D individually, the equation $p_{SAT} = N_A - N_D$ must be used, corresponding to the positive hole concentration at saturation. An extrapolated value (from Fig. 10) indicates p_{SAT} to be about $10^{15}/\text{cm}^3$. Thus with

$$N_A - N_D = 10^{15}$$

$$N_A/N_D = 10$$

$$N_A = 1.1 \times 10^{15}/\text{cm}^3$$

(16) D. S. Billington and J. H. Crawford, "Radiation Damage in Solids," Princeton Univ. Press, Princeton, N. J., 1961, pp. 312–313.

(17) W. H. Brattain, *Rev. Mod. Phys.*, **23**, 203 (1951).

(18) W. Shockley, "Electrons and Holes in Semiconductors," D. Van Nostrand Co., Inc., New York, N. Y., 1950, pp. 471–472.

(19) O. S. Oen and D. K. Holmes, *J. Appl. Phys.*, **30**, 1289 (1959).

$$N_D = 1.1 \times 10^{14}/\text{cm.}^3$$

From a value of the ratio of the positive hole concentration before and after irradiation determined from the electrical measurements and the values of N_A and N_D , Δ then may be estimated. For the 70% drop in positive hole concentration that occurred on sample no. 2, 4.8×10^{14} additional copper vacancies and 3.2×10^{14} additional oxygen vacancies are produced per cubic centimeter. These calculated values for the additional vacancies created are seen to be of the same order of magnitude as the defect concentration present before irradiation. They also compare favorably to the value calculated from theory for the concentration of atomic displacements produced by electron irradiation of roughly $10^{15}/\text{cm.}^3$.

Since the conductivity is proportional to the product of the positive hole concentration and the hole mobility, a decrease in the positive hole concentration tends to lower the electrical conductivity. This reduction is further accentuated by the decrease in the mobility produced by irradiation. The mobility is reduced by the presence of increased amounts of solid state defects after irradiation which retard the motion of the positive holes in the cuprous oxide lattice. The introduction of vacancies and interstitials as a result of irradiation increases the contribution of impurity lattice scattering which probably produces the decrease in mobility observed.

For sample no. 2 a range of values is listed in Table IV for the percentage change produced by 300 sec. of electron bombardment. The higher end of the range represents the values obtained from lines drawn through the major portion of the data. However, immediately before irradiation, a number of experiments were conducted at temperatures up to 150° . During the measurements at the higher temperature, "aging" of the sample occurred, resulting in a permanent irreversible lowering of the conductivity and positive hole concentration. The aging reputedly is caused by the loss of excess oxygen from the cuprous oxide lattice.²⁰ The loss produces an increase in the concentration of oxygen vacancies, N_D , and as seen from eq. 12, a decrease in the carrier concentration. The decrease amounts to a 20–25% change in the positive hole concentration. Therefore, the actual changes produced by electron irradiation are less than might at first be apparent.

TABLE IV

EFFECT OF IRRADIATION ON THE ELECTRICAL PROPERTIES OF CUPROUS OXIDE^a

	% change from unirradiated value at room temp.
Conductivity, (ohm-cm.) ⁻¹	–65 to –75
Carrier concn., number/cm. ³	–55 to –70
Mobility, cm. ² /v.-sec.	–20

^a Sample no. 2, 300 sec. of irradiation.

General Discussion

Based on the effect of high-energy electron bombardment on the catalyst activity and electrical conductivity of cuprous oxide, the solid-state defect

constitution is found to influence strongly semiconductor properties. The parallel changes produced in these properties as a result of irradiation indicate the importance of the amount and kind of defects present. By increasing the concentration of the copper and oxygen vacancies in cuprous oxide, the catalytic activity and the electrical properties of conductivity and carrier concentration are decreased. In addition, it is interesting to note that the percentage decrease in the catalytic activity and positive hole concentration as a result of irradiation were very nearly equal.

The amount of atomic displacements created in the lattice is extremely small compared to the concentration of atoms present in the metal oxide. Of the order of 10^{15} defects per cubic centimeter were produced by electron irradiation compared to the 10^{22} atoms of copper and oxygen per cubic centimeter. However, the additional concentration of vacancies introduced was about the same as the amount of defects which existed before bombardment. Since the defect concentration of cuprous oxide was increased significantly, the properties that depend on the defect level also were affected.

In terms of the energy absorbed by the catalyst, the amount of irradiation required to produce the 10^{15} defects per cubic centimeter is equal to approximately 10^{10} ergs/g. From a survey of previous investigations, this value has been found to form a lower limit for the amount of energy needed to alter appreciably catalyst activity.

The experimental results point to the fact that for cuprous oxide, the more p-type the semiconductor, the greater the catalytic activity for the oxidation of carbon monoxide. Electron irradiation produced a decrease in the electrical properties making the semiconductor less p-type. A corresponding decrease in the catalytic activity of cuprous oxide as a result of irradiation also was observed. These trends are consistent with the finding that the activity of metal oxide semiconductors for the oxidation of carbon monoxide increases in the order, insulators–n-type–p-type.²¹

The reduction in the catalyst activity of cuprous oxide as a result of irradiation cannot be caused by the increases in surface area. On the other hand, the roughening of the surface which produced the increases in surface area also may have caused some deactivation of the catalyst. The manner in which the roughening of the surface influences the activity is unknown. However, in view of the correlations obtained in this study between the catalyst activity, electrical properties, and the amount of defects as a result of irradiation, the changes in semiconductor defect nature of cuprous oxide appear to be the important factor in altering the catalyst activity.

Acknowledgment.—This work was sponsored by the United States Atomic Energy Commission, Division of Isotopes Development, under Contract No. AT(30-1)–2329 Task-I. This work was done in part at the Computation Center at the Massachusetts Institute of Technology, Cambridge, Massachusetts. Special acknowledgment is due

(20) S. J. Angello, *Phys. Rev.*, **62**, 371 (1942).

(21) F. S. Stone, "Chemistry of the Solid State," ed. by W. F. Garner, Butterworths Scientific Publications, 1955, pp. 397–398.

to Mr. S.-L. Hsu for performing a considerable part of the kinetic experiments and to Mr. H. Alcalay for his work in studying the effect of irradiation on the surface area of cuprous oxide catalysts.

Nomenclature

a	original moles of carbon monoxide present
A	geometrical surface area of catalyst disks
b	original moles of oxygen present
c	concentration of reactant
$E_A - E_V$	ionization energy
ΔE	apparent activation energy
h	Planck's constant
k	specific reaction rate constant or Foltzmann's constant
k_0	apparent pre-exponential factor
m	unknown order of reaction with respect to CO or effective mass of a hole
n	unknown order of reaction with respect to O ₂
N	number of moles
N_A	acceptor impurity concentration (copper vacancies)

N_D	donor impurity concentration (oxygen vacancies)
p	positive hole concentration
p_{SAT}	positive hole concentration at saturation
P	total pressure at time t
p_0	initial total pressure
ΔP	pressure difference, $(P - P_0)$
r	reaction rate
R	gas constant
t	time
T	temperature
V	volume of reactor
x	extent of reaction
Y_{CO}	initial mole fraction of carbon monoxide
Greek letters	
Δ	oxygen vacancy concn. produced by electron irradiation
μ_p	drift mobility
σ	electrical conductivity
Subscript	
0	initial value

THE REACTIONS OF RECOIL TRITIUM ATOMS WITH CYCLOPROPANE PLATINOUS CHLORIDE¹

BY EDWARD K. C. LEE AND F. S. ROWLAND

Department of Chemistry, University of Kansas, Lawrence, Kansas

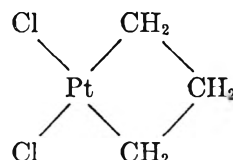
Received April 5, 1962

Recoil tritium atoms react with cyclopropane platinous chloride to produce labeled cyclopropane and propylene in the ratio of approximately 1 to 3. The yield of propylene is higher than for reactions with the free molecule in the gas phase and indicates an influence on the reaction course from the strong binding of the cyclopropane molecule in the complex.

Introduction

Gas phase investigations with many volatile hydrocarbons have established the mechanisms of reaction of recoil tritium atoms with both saturated and unsaturated molecules,^{2,3} and some liquid and solid phase investigations have shown that the general pattern of reaction is quite similar in the condensed phases.⁴⁻⁶ In all cases, these studies have involved essentially the reaction of the tritium atom with an isolated molecule, and the primary effects of condensed phases are more rapid collisional de-excitation of excited molecules and radicals, and enhanced third body recombination processes.⁶ Our interest in the present experiments has been to investigate the nature of recoil tritium reactions with a hydrocarbon molecule while it is influenced by strong bonding to an external system and should no longer be considered as an isolated molecule. The target molecule in these investigations has been cyclopropane platinous chloride, symbolized hereafter by C₃H₆PtCl₂. The cyclo-

propane molecule in this compound is considerably perturbed from the normal molecule as shown by the alterations in the infrared absorption bands for C-H stretching, etc. Chatt, *et al.*, describe the structure of cyclopropane platinous chloride as a chlorine-bridged polymer built from dichloro-(trimethylene)-platinum (IV), as⁷



Recoil tritium atoms have been introduced into C₃H₆PtCl₂ by irradiation of the powder mixed with LiF, utilizing the 2.7 Mev. kinetic energy of recoil from the Li⁶(n,α)H³ reaction to transport the tritium atom from the crystals of LiF into the neighboring platinum complex.

Experimental

Preparation of Cyclopropane Platinous Chloride.—The light, brown C₃H₆PtCl₂ solid was prepared by bubbling gaseous cyclopropane through a dilute solution of chloroplatinic acid in acetic anhydride.⁸ The original crystals were purified by repeated thorough soakings in 1:1 acetone-ether solution. The samples were pulverized in this solution and allowed to stand for 7 to 10 days each time. After sufficient purification, regeneration of the hydrocarbon from this compound by the addition of cold, concentrated aqueous KCN

(1) Research supported by A.E.C. Contract No. AT-(1-1)-407.
 (2) J. K. Lee, B. Musgrave, and F. S. Rowland, *J. Am. Chem. Soc.*, **82**, 3545 (1960); *Can. J. Chem.*, **38**, 1756 (1960); F. S. Rowland, J. K. Lee, B. Musgrave, and R. M. White, "Chemical Effects of Nuclear Transformations," I.A.E.A., Vol. 2, Vienna, 1961, p. 67.
 (3) D. Ureh and R. Wolfgang, *J. Am. Chem. Soc.*, **83**, 2982 (1961); "Chemical Effects of Nuclear Transformations," I.A.E.A., Vol. 2, Vienna, 1961, p. 83.
 (4) W. J. Hoff, Jr., and F. S. Rowland, *J. Am. Chem. Soc.*, **79**, 4987 (1957).
 (5) A. M. Elatrash, R. H. Johnsen, and R. Wolfgang, *J. Phys. Chem.*, **64**, 785 (1960).
 (6) E. K. C. Lee and F. S. Rowland, *J. Am. Chem. Soc.*, **84**, 3085 (1962).

(7) D. M. Adams, J. Chatt, R. G. Guy, and N. Sheppard, *Proc. Chem. Soc.*, 179 (1960); *J. Chem. Soc.*, 738 (1961).
 (8) C. F. J. Tipper, *ibid.*, 2045 (1955).

TABLE I
 RADIOACTIVE PRODUCTS FROM RECOIL TRITIUM REACTIONS WITH CYCLOPROPANE PLATINOUS CHLORIDE

	Sample								
	B-5	B-15	21	22	24	26	27	28	25 ^b
LiF, mg.	2.01	9.72	5.89	7.68	7.58	7.84	7.91	7.86	9.72
C ₃ H ₅ PtCl ₂ , mg.	10.0	9.66	6.51	8.35	8.02	8.19	8.19	8.19	8.19
Irradiation, hr.	3.5	3.5	~1.5	~1.5	3	3	12	12	3
Flux	10 ¹¹	10 ¹¹	10 ¹²	10 ¹²	10 ¹²	10 ¹²	10 ¹²	10 ¹⁴	10 ¹²
Total activity									
50-ft. DMS	1900	6500	19,400	21,300	21,800	60,200	1.9 × 10 ⁵	1.7 × 10 ⁵	51,900
	Activity relative to C—C=C as 100								
HT	} 5	} 11	} 15	} 10	} 11	2	2	} 10	2
CH ₃ T									
C—C	} 2	} 4	1	1	1	1	3	3	1
C=C			4	6	5	5	7	7	5
C—C—C	1	6	8	8	6	8	10	15	6
C—C=C	100	100	100	100	100	100	100	100	100
Δ	42	39	28	28	27	30	17	15	24
	% Macroscopic composition of regenerated gas								
C—C=C	3.2 ^a	4.8 ^a	5.1	4.9	7.4	6.3	~45	~33	7.4
C—C—C			0.1	0.1	0.1	0.1	0.7	1.4	0.1
C=C			0.3	0.3	0.6	0.4	1.7	2.1	0.5
C—C			<0.01	<0.01	<0.02	0.03	0.3	0.3	<0.02
C C—Cl								~3	
C C—C—C—Cl							...	~6	

^a Not all from radiation damage; some present initially. ^b Break-off tip opened and sample pumped on prior to solution in aqueous KCN.

solution gives cyclopropane as the only important hydrocarbon detected by gas chromatography. Small percentages of propylene were observed from early aliquots during the purification, but the final material showed $\leq 1\%$ propylene upon regeneration of the hydrocarbon. The infrared spectrum of the purified compound corresponds to that published by Chatt, *et al.*⁷

Irradiation.—Each sample consisted of an intimate mixture of approximately 10 mg. of C₃H₅PtCl₂ and 10 mg. of LiF powder in an evacuated 1720 Pyrex glass ampoule equipped with a break-tip. The neutron fluxes and times of irradiation were varied as shown in Table I, always with an ambient temperature during irradiation of 25–30°.

After irradiation, the ampoule was placed in a vacuum system, degassed, and broken open to release the contents. Cold aqueous KCN solution (0.5 g. of KCN in 0.5 ml. of water) then was introduced, and the regeneration of gas was complete in approximately 5 min.

Aliquots were taken for gas chromatography from the gas reservoir above the aqueous KCN solution. Since the gas reservoir system also contained the aqueous solution and undissolved solid LiF, several experiments were performed to determine whether this heterogeneity affected the nature of the sample taken for gas chromatography. Two aliquots from sample no. 27, taken 2 hr. apart and each analyzed on a silica gel column, showed a 100% increase in the HT yield, and an apparent 13% decrease in the amount of CH₃CHT with lengthening time of contact between the gas and the condensed phases. The variation in HT may have involved diffusion of active tritium from the undissolved LiF crystals, which contained more than half of the total tritium formed in the system. Such relative yield fluctuations for two aliquots were avoided in most cases by simultaneous filling of two sample loops for gas chromatography. This filling was performed as soon as possible after regeneration of the gas, and usually was complete within 20 min. In any event, the fluctuations represented only a very small percentage of the total gaseous tritium activity.

The break-off tip of sample no. 25 was deliberately broken before evacuation and the irradiated powders then were pumped to remove any gaseous compounds not still trapped

in the cyclopropane platinumous chloride. Distinct loss of tritium-labeled alkanes was observed, especially for CH₃T. The olefinic radioactive products apparently are strongly held in the crystal, perhaps actually complexed, while the CH₃T remains free to diffuse through the lattice, and eventually into the gas space above the crystals. The HT yield apparently was unaffected by the degassing of the irradiated crystals.

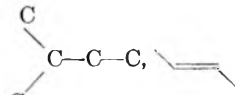

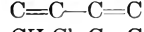
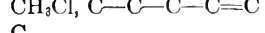
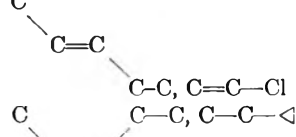
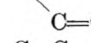
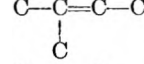
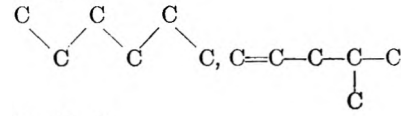
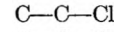
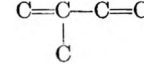
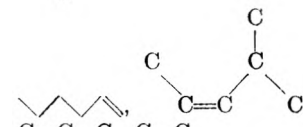
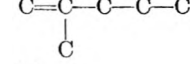
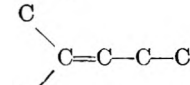
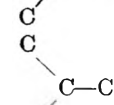
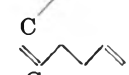
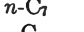
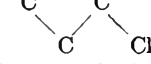
Separation and Analysis.—The separation and measurement of the radioactivity in various volatile molecules was accomplished through gas chromatography, followed by gas proportional counting of the effluent stream.⁹ The basic separations have been carried out on 50- and 15-ft. dimethylsulfolane columns at 24°. Labeled methane and HT were separated on silica gel. The macroscopic mass peaks were measured in the flowing helium stream prior to its mixture with propane for counting purposes. Only about 35–40% of the tritium radioactivity stopped in the C₃H₅PtCl₂ appeared in volatile compounds, while the rest was present as labile tritium activity from reaction with platinum or chlorine. The experimental distributions of radioactivity and the macroscopic sample compositions are given in Table I. Typical complete radiochemical analyses of higher boiling products are shown in Table II.

Non-gaseous Tritium Activity.—Non-volatile tritium activity was assayed for sample B-5 through measurement of aliquots of the cyanide regeneration solution, after the undissolved LiF had first been removed from it. The total activity of this solution was approximately 1.6 times as much as appeared in the gas chromatographic measurements from that sample.

The total amount of tritium activity formed in the samples was measured by separate irradiation and assay of a pure LiF sample in a similar irradiation tube. This yield in the solid powder was only 15% of the amount that would be calculated from the conditions of Table I, while an additional 2.2% was imbedded in the glass. All of these assays were performed by combustion at 700° of the sample in the presence of zinc, nickelic oxide, and paraffin.⁹ The glass

(9) J. K. Lee, *et al.*, *Anal. Chem.*, **34**, 741 (1962).

TABLE II
COMPLETE RADIOCHEMICAL ANALYSIS OF SOME SAMPLES OF CYCLOPROPANE PLATINOUS CHLORIDE

Retention time (min.) ^a	Possible peak identifications	Run 21	Run 22	Run 28
		Activity in C—C=C peak, counts 6600	5500	66,000
		Radioactive yields; (C—C=C) = 100		
4.8			0.7	0.50
5.5				0.47
7.3				0.38
8.1		0.7	0.7	2.80
9.4		1.1		0.20
10.1				0.14
11.5		3.0	5.3	0.90
13.2				1.00
16.4		1.8	0.8	0.96
18.9				~2/5
20.0		2.1	1.0	2.4
21.0				~1/5
23.5				0.50
25.3		4.6	3.7	9.4
28.4				1.9
32.5				0.76
41.2		6.2	2.0	7.0

^a The retention times are obtained with 15 ft. dimethylsulfolane⁻ at 24°, 8 lb. He pressure (0.95 ml./sec.).

tube was broken into very small pieces, from which diffusion could more readily take place. A second combustion of the same sample yielded a negligible amount of additional tritium activity.

This total yield of 17% is quite reasonable because of neutron absorption in the boron of the Pyrex 1720 glass, and of our use of depleted LiF, with a Li⁶ isotopic content of approximately 2%.

The LiF is 1.72 times as efficient per mg. in slowing down the recoil tritium and α -particles as is C₃H₆PtCl₂,¹⁰ and hence should contain about 63% of the total tritium in powdered mixtures with equal weights of the two components. This tritium was not released for assay in these experiments. The sum of the observed gaseous activity and labile activity from sample B-5 is in good agreement with

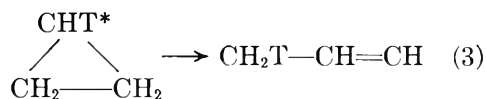
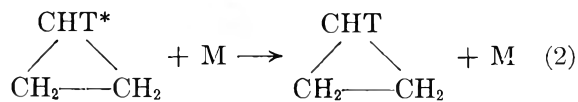
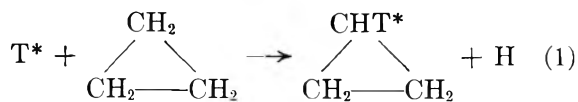
the amount of activity expected in the C₃H₆PtCl₂ component.

Discussion

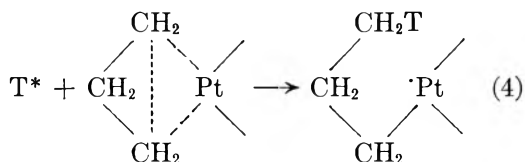
The most important observation among the recoil tritium reactions with cyclopropane platinumous chloride is the relative yield of labeled cyclopropane and propylene, which falls in the range of 0.3 to 0.4 for samples with moderate radiation damage. These ratios are in contrast to the gas and liquid phase observations of energetic tritium reactions with cyclopropane, for which the same ratio has values > 1.^{2,11} The gas phase reactions with the isolated hydrocarbon form these two labeled molecules in comparable amounts by reactions 1 to 3.

(10) Calculated from the stopping power formula of G. Friedlander and J. Kennedy, "Nuclear and Radiochemistry," John Wiley and Sons, New York, N. Y., 1955.

(11) E. K. C. Lee and F. S. Rowland, unpublished results.



Higher pressures favor the formation of cyclopropane, and the liquid phase results show a cyclopropane/propylene ratio of approximately three.¹¹ The much higher yield of labeled propylene from recoil reaction with $\text{C}_3\text{H}_6\text{PtCl}_2$ can be explained readily if the energetic reaction of tritium with the platinum-bonded methylene groups proceeds as in (4)



The subsequent reaction of this species could lead to $\text{CH}_2\text{T}-\text{CH}_2-\text{CH}_2\cdot$ or $\text{CH}_2\text{T}\cdot$ radicals, but would not go back to the cyclic structure which regenerates cyclopropane under KCN treatment. The labeled *n*-propyl radical from the decomposition of the product in (4) also could go to propylene through the loss of H to the Pt atom.

Energetic reaction with the methylene group not bonded to platinum probably is the source of the tritium-labeled cyclopropane found upon regeneration. In this case, the interactions should be similar to the reactions with the molecule as found in the liquid and gaseous states. The nearby neighbors can remove the excess energy rapidly through reaction 2, leaving the ring system intact except for the replacement of one hydrogen atom by tritium.

The over-all cyclopropane/propylene ratio is consistent with the occurrence of energetic reactions leading to tritiated cyclopropane at only one carbon atom, and propylene-forming substitutions at the other two carbon atoms. The physico-chemical reason for preferential rupture of the carbon-platinum bond is not known, but other energetic tritium reactions in the solid phase have been shown to proceed with preferential bond-rupture. The preference is especially strong when the bond to carbon is a weak one as in carbon-iodine bonds.¹²

(12) R. M. White and F. S. Rowland, *J. Am. Chem. Soc.*, **82**, 4713 (1960).

Other noteworthy features in the pattern of radioactive products are the comparative absence of HT and the presence of chlorine-containing radioactive molecules. The latter can be formed through the reactions of labeled free radicals from the decomposition of the complex radical of eq. 4. The low yield of HT, which is formed in amounts comparable to labeled parent when cyclopropane is irradiated in the liquid or gas phase, is unexpected. It may perhaps be removed by chemical reaction to give labile activity, subsequent to formation in higher yield in the initial energetic reaction.

Radiation Damage to Cyclopropane Platinous Chloride.—The bulk of the ionizing energy deposited in these systems came from the recoiling tritium atom and its alpha recoil partner. This energy, as with the tritium itself, is distributed between the LiF and the $\text{C}_3\text{H}_6\text{PtCl}_2$ components. Since the range of both recoil particles is very much longer than the average particle size in the powders, this energy is deposited approximately in proportion to the stopping powers of the two compounds.

Approximate *G*-values for decomposition of cyclopropane have been calculated from the observed decomposition (e.g., ~8% for number 24) and the total energy deposition, assuming 17% of nominal as the actual tritium production rate. Typical values are about $G(\text{-cyclopropane}) \cong 3$ on the basis of energy loss in $\text{C}_3\text{H}_6\text{PtCl}_2$, or $\cong 9$ for the energy deposited in the C_3H_6 part of the molecular complex (about 30%). The latter value is about the same as the *G*-values obtained for the radiolysis of gaseous cyclopropane,² thus indicating that the cyclopropane is neither greatly sensitized nor protected by the changed molecular surroundings.

The macroscopic hydrocarbon peaks are markedly different from those observed with similar irradiations of liquid cyclopropane. Mass peaks for ethylene and propylene are nearly equal from the liquid cyclopropane, with the ethylene presumably arising from ion-molecule reactions, as it does from gaseous cyclopropane.^{2,11,13} The physical structure of the complex, of course, makes C_3H_6^+ plus C_3H_6 a much less probable reaction than with the pure hydrocarbon.

Radiation damage interactions involving chlorine atoms are shown by the prominent mass peaks for *n*-propyl and isopropyl chlorides.

Acknowledgments.—Our use of the Omaha Veterans Administration Hospital Reactor for some of the irradiations is gratefully acknowledged. The Li^6 content of the LiF was kindly assayed by Dr. S. Amiel of the Israel Atomic Energy Commission.

(13) H. Umezawa and F. S. Rowland, *ibid.*, **84**, 3077 (1962).

ON THE LOW-FREQUENCY DIELECTRIC DISPERSION OF COLLOIDAL PARTICLES IN ELECTROLYTE SOLUTION¹

BY H. P. SCHWAN, G. SCHWARZ, J. MACZUK, AND H. PAULY

Electromedical Division, Moore School of Electrical Engineering, University of Pennsylvania, Philadelphia 4, Pa.

Received April 12, 1962

Determinations of the dielectric properties of suspension of spherical colloidal particles are reported over the frequency range from 20 c.p.s. to several hundred kilocycles. Very large dielectric constants are observed at low frequencies. Since the experimental data approach constant values at very low and high frequencies, they can be described by a fairly well defined spectrum of relaxation times. Simple relationships exist between particle size, low frequency dielectric increment, and average relaxation time. Several physical processes, such as relaxation due to Maxwell-Wagner effects, to electrophoretic particle acceleration, or to the presence of a frequency-independent surface conductance, are shown not to account for the observed data. Surface conductance and capacitance data are determined, the conductance having one frequency-independent and one frequency-dependent part.

Introduction

Very high dielectric constants often have been observed with colloidal and biological-cell suspensions at low frequencies (see for example Schwan).² The dielectric constant ϵ always decreases as the frequency increases. Although the frequency dependence of ϵ has been characterized by a power function f^{-m} ,³ details of this phenomenon and its origin have not been treated satisfactorily.

Refinements in technique have enabled us to determine that the dielectric behavior of fat-particle suspensions and polystyrene latex at very low frequencies is clearly a relaxation process characterized by a fairly well defined spectrum of time constants.⁴ Preliminary data have been given by us elsewhere.^{2,5} This article summarizes our results in greater detail.

In an effort to explain the observed dielectric phenomenon, relaxation of the Maxwell-Wagner type, relaxation associated with electrophoretic movement, and relaxation due to the existence of a frequency-independent surface conductance or admittance are considered and rejected. Therefore, this dielectric phenomenon must reflect linear and frequency-dependent properties of alternating-current boundary potentials. A frequency-dependent surface conductance and capacitance can be introduced to account for the observed data.

Equations for the determination of surface conductance and capacitance from experimental data are developed. The total surface conductance is found to consist of two parts. One part, which changes with the conductance κ_a of the suspending medium, is frequency-independent. The other part, less dependent on κ_a , is frequency-dependent. Therefore, as the theory will show, the surface capacitance term also must be frequency-dependent and thereby must be responsible for the high dielectric constants experimentally observed.

Measurement Technique.—Measurements were carried out between 10 c.p.s. and 200 kc. with a bridge, Fig. 1, built for the precise determination of dielectric constants

and conductivities of highly conductive materials. Sometimes, additional measurements from 500 kc. to several Mc. were conducted, using the Boonton RX-meter, to establish more clearly the limit values approached at high frequencies. The bridge is of the Wheatstone type, using General Radio variable precision capacitors. The reactive components of the conductance box and internal bridge connections have been determined with an accuracy which reflects the high resolution of the bridge.

Measurements are made by substitution. The sample cell is always in parallel with the calibrated conductance box. The conductance box is set to its initial value of 0.1 mmho with the cell filled with the sample fluid. It is reset to a higher conductance value after removal of the sample in order to re-establish balance without a change in the setting of the other bridge arm. Balance of the reactive components is achieved with the variable capacitors. For further details about the bridge and the calibration procedure see Schwan and Sittel.⁵

Very high resolution is required to obtain significant results. Most impedance techniques rely ultimately on the observation of one scalar quantity, for example the minimal deflection of an instrument. They cannot differentiate between meter deflections due to unbalance in capacitance C or conductance G . Suppose the admittance $Y = G + j\omega C$ is determined with an error $\Delta Y = \Delta G + j\omega\Delta C$. The area of uncertainty, which reflects limits of resolutions, then is given by a circle as indicated in Fig. 2.

$$\Delta G = \omega\Delta C \quad (1)$$

This may be rearranged.

$$\frac{\Delta G}{G} = \frac{\Delta C}{C} \frac{1}{\tan \delta} \quad (2)$$

where $\tan \delta$ characterizes the dielectric loss factor and equals $G/\omega C$. If the input impedance of the null detector is larger than the bridge impedances, then the input voltage V and output ΔV of the Wheatstone bridge are related as

$$\Delta V = \frac{V}{4} \sqrt{\frac{(\Delta G)^2 + (\omega\Delta C)^2}{G^2 + (\omega C)^2}} \quad (3)$$

Thus, in case of a perfect balance in G ($\Delta G = 0$)

$$\frac{\Delta V}{V} = \frac{1}{4} \frac{\Delta C}{C} \frac{1}{\sqrt{1 + \tan^2 \delta}} \quad (4)$$

and in the case of a perfect balance in C ($\Delta C = 0$)

$$\frac{\Delta V}{V} = \frac{1}{4} \frac{\Delta G}{G} \frac{1}{\sqrt{1 + 1/\tan^2 \delta}} \quad (5)$$

At low frequencies the conductive currents of our samples are larger than the capacitive ones ($\tan \delta > 1$). The

(1) This investigation was supported by National Institute of Health Grant H 1253 (C9).

(2) H. P. Schwan, *Advan. Biol. Med. Phys.*, **5**, 147 (1957).

(3) H. Fricke and H. J. Curtis, *J. Phys. Chem.*, **41**, 729 (1937).

(4) H. P. Schwan, in "Physical Techniques in Biological Research," W. L. Nastuk, Ed. 1, Vol. VI, Academic Press, New York, N. Y., in press.

(5) H. P. Schwan and J. Maczuk, *Proc. Natl. Biophys. Conf.*, **1st**, Columbus, Ohio, 348 (1959).

(6) H. P. Schwan and K. Sittel, *Trans. Am. Inst. Elec. Engrs. (Communications and Electronics)*, **72**, 114 (1953).

resolution $\Delta G/G$ is then largely frequency independent and equal to $4\Delta V/V$. The accuracy in C is inversely related with frequency (eq. 4), requiring increasingly better resolution in G in order to obtain good results in C as the frequency decreases.

A Hewlett Packard wave analyzer is used as a filter up to 16 kc. and a radio receiver RAK 8 as a filter up to 500 kc. Additionally, use of a low-noise-level preamplifier establishes a threshold signal level of $0.03 \mu\text{v.}$ over most of the frequency range. This very low noise level and an input signal of about 0.1 v. permit resistance balance settings with a resolution of 1 part in a million. Input voltages larger than 0.1 v. are avoided since they can cause temperature drifts with consequent changes in G . The resolution of our bridge permits us to determine high dielectric constants of conducting solutions at frequencies even below 100 c.p.s. For example, a dielectric constant of 1000 can be measured with an accuracy of 10% at a frequency of 20 c.p.s. in the presence of a conductivity of 1 mmho/cm.

The change of conductivity with frequency is usually fairly small, so that minor temperature drift can affect it. Compensation for such temperature drift is made by returning after each reading to a standard frequency (say 1 kc.). Plots of the 1-kc. values vs. time usually establish smooth curves which permit the application of an interpolated time-correction to conductivity values at other frequencies. The validity of this technique is based on the experimentally-verified assumption that the drift equally affects values at all frequencies.

The cylindrical sample cell, shown in Fig. 3, is kept at a constant temperature of 25° . The platinum electrodes are heavily covered with platinum black in order to reduce electrode polarization. Readings at various distances are taken and converted into impedance values which subsequently are subtracted from each other.^{3,4,7,8} This technique satisfactorily eliminates polarization effects if constancy of electrode polarization with time is checked by taking a repeat reading at the original electrode distance. But inaccuracies result if the impedance differences are small in comparison with the impedances measured at various distances, i.e., if the electrode impedance becomes large as the frequency decreases.

In order further to minimize electrode polarization effects, the sample impedance must be large in comparison with the electrode impedance, i.e., large electrode separation is required. In this case the electrical field is no longer confined to the sample. However, the error which the resulting stray field components causes can be evaluated for the cylindrical geometry employed.⁹ In most cases dielectric constants were high enough so that stray field errors were small.

It was decided to choose suspensions with particles of uniform size. The particles consist of polystyrene and are kept independently in suspension by a stabilizing surface coating.¹⁰ Particle size is extremely uniform as ascertained by various electron microscopic studies.¹¹ Particle concentration values also were obtained from the manufacturer. In some instances concentrations were checked either by using a high-speed centrifuge or by carrying out a dry weight determination. The ionic strength of the medium surrounding the polystyrene spheres may be estimated from its electrical conductivity κ_a . This latter value is obtained from the low frequency conductivity κ_0 of the sample of interest and the known particle volume fraction p , using an equation given first by Maxwell.¹² For particles whose conductivity is small compared to κ_a , this equation reduces to

$$\kappa_0 = \kappa_a \frac{1 - p}{1 + p/2} \quad (6)$$

In some cases the polystyrene spheres were resuspended in a medium of low and known conductivity. Then a measure-

(7) K. S. Cole and H. J. Curtis, *Rev. Sci. Instr.*, **8**, 333 (1937).

(8) H. P. Schwan, *Z. Naturforsch.*, **6b**, 121 (1951).

(9) H. P. Schwan and J. Maczuk, *Rev. Sci. Instr.*, **31**, 59 (1960).

(10) We are indebted to Dr. Vanderhoff, Dow Chemical Co., for making polystyrene latex material available to us.

(11) E. B. Bradford and J. W. Vanderhoff, *J. Appl. Phys.*, **26**, 864 (1955).

(12) J. C. Maxwell, "A Treatise on Electricity and Magnetism," Oxford Univ. Press, 1873, article 314.

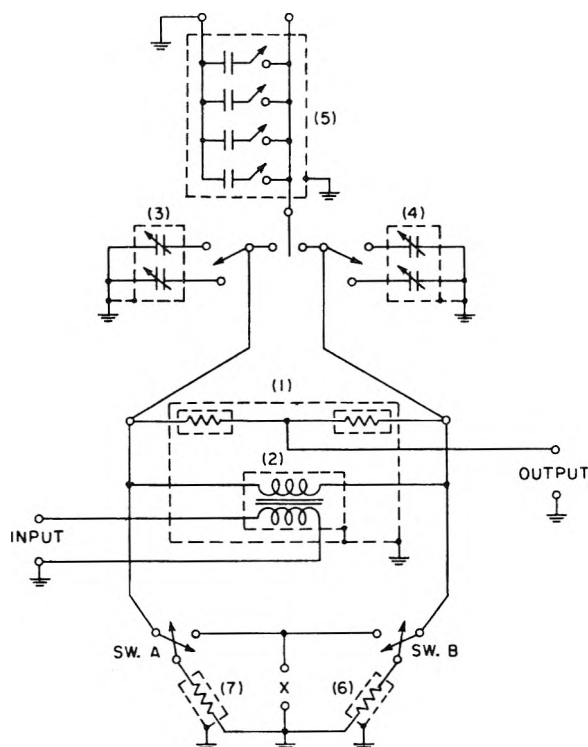


Fig. 1.—Wiring diagram of Wheatstone bridge: (1) shielded ratio box with shielded input transformer (2); (3) and (4) variable precision capacitors; (5) decade capacitor; (6) shielded resistance box (variable resistance decades in series); (7) shielded conductance box (variable conductance decades in parallel). The switches SW permit balance of the unknown X against either resistance or conductance box or the use of substitution techniques (see text). A combination of a conductance box with six dials and a resistance box of six dials in opposite bridge arms is desirable if dial adjustment to one part in a million is needed over a large range of resistances.

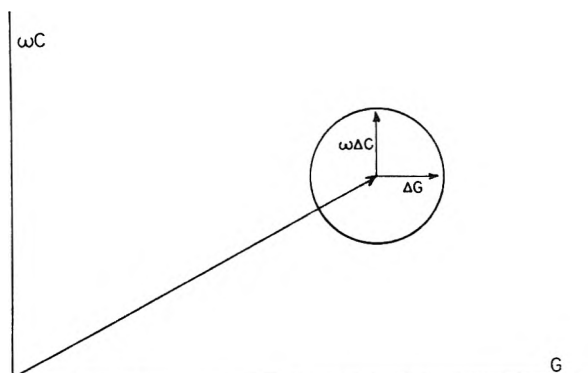


Fig. 2.—Errors in capacitance and conductance (see text).

ment of κ_a did not compare very well with the value calculated from eq. 6, even though ionic leakage from the stabilizer coat was minimized by repeated washing. This discrepancy was due to the surface conductance of the particles, as will be discussed later.

Analysis of Data.—Conductance and capacitance readings, taken with the sample cell filled and empty, are corrected for stray field components⁹ and for the lead inductance to the sample cells.^{4,13} This process is performed at two electrode distances, and electrode polarization is eliminated as explained above. Final conductance G and capacitance C

(13) H. Pauly, L. Packer, and H. P. Schwan, *J. Biophys. Biochem. Cytol.*, **7**, 589 (1960).

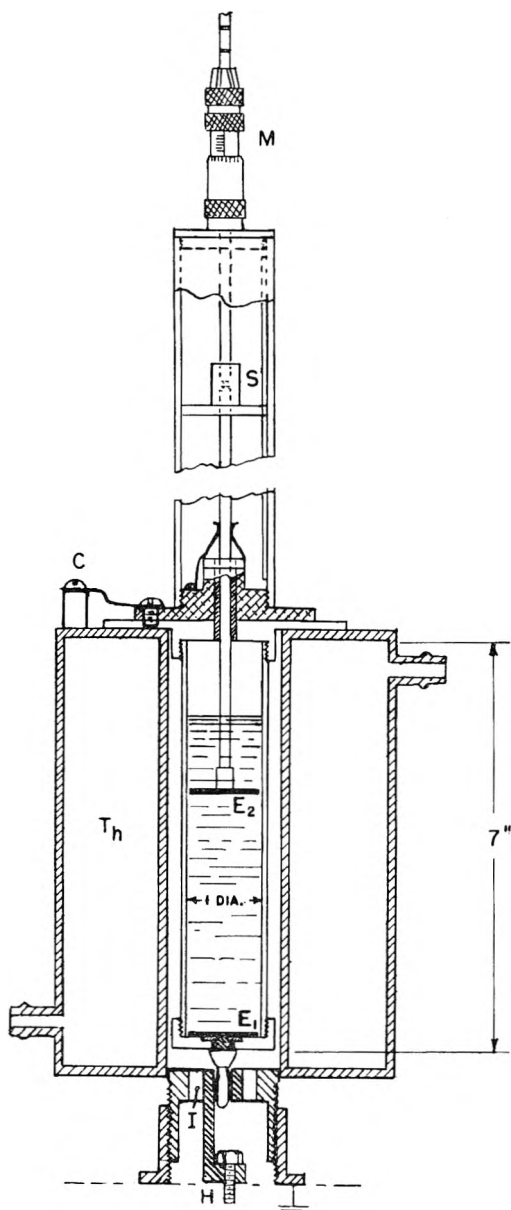


Fig. 3.—Electrolytic cell. Electrode E_2 is movable and grounded. The washer I separates the "hot" terminal H from ground; C connects E_2 to ground; M , micrometer; S transmits the movement of the micrometer shaft to E_2 ; T_h , thermostatic shield for temperature control and definition of electrical field (see text).

are reduced to dielectric constant and conductivity values. The required cell constants, calculated from the dimensions of the sample cell, are checked experimentally, using electrolytes of established conductivity. The total procedure was verified with electrolytes of known conductivity and dielectric constant.⁹

Several techniques have been used to extract significant information from the dielectric data collected. Dielectric constants and conductivity values approach constant values at sufficiently high and low frequencies. In the presence of only one relaxation time the frequency dependence can be expressed by the dispersion equations (7 and 8).

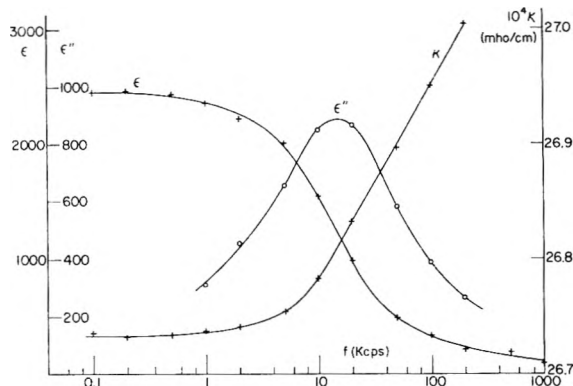


Fig. 4.—Real dielectric constant ϵ , imaginary dielectric constant ϵ'' , and conductivity κ of a suspension of polystyrene particles as a function of frequency: particle diameter 0.188μ , particle concentration 30%, 23° .

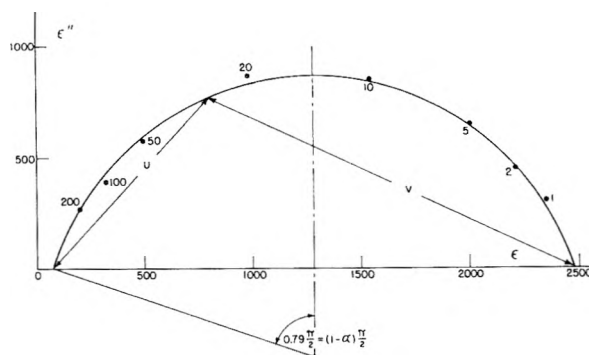


Fig. 5.—Cole-Cole circle. The same data as presented in Fig. 4 are used.

$$\epsilon = \epsilon_\infty + \frac{\epsilon_0 - \epsilon_\infty}{1 + (\omega T)^2} \quad (7)$$

$$\kappa = \kappa_0 + (\kappa_\infty - \kappa_0) \frac{(\omega T)^2}{1 + (\omega T)^2} \quad (8)$$

where the terms ϵ_0 , ϵ_∞ , κ_0 , κ_∞ are limit values of ϵ and κ observed at frequencies which are very small and large, respectively, in comparison to the characteristic frequency $f_0 = 1/2\pi T$. At the characteristic frequency, ϵ and κ are averages, $(\epsilon_0 + \epsilon_\infty)/2$ and $(\kappa_0 + \kappa_\infty)/2$, and the dielectric loss $\epsilon'' = (\kappa - \kappa_0)/\omega$ reaches a peak value. The changes $(\epsilon_0 - \epsilon_\infty)$ and $(\kappa_\infty - \kappa_0)$ are interrelated by the equation

$$\epsilon_0 - \epsilon_\infty = T (\kappa_\infty - \kappa_0) \quad (9)$$

The equations are identical with the well known Debye expression except for the addition of the term κ_0 . It is added to account for finite low frequency conductance of ionic origin and is not related to the relaxation process characterized by the relaxation time constant T .

For large particles the approach to constant values of ϵ at low frequencies is somewhat difficult to observe, while the approach to constant values of both κ and ϵ is readily observed at high frequencies. For smaller particles, however, the limit values are well defined at low frequencies, but κ has not yet approached κ_∞ at 200 kc. Usually limit values ϵ_0 , ϵ_∞ , κ_0 , and κ_∞ can be obtained by extrapolation. Different values of the time con-

stant are obtained from the two curves for ϵ and κ , the value from the κ -curve usually being lower (see Fig. 4). This behavior is in contradiction to eq. 7 and 8, which demand that the means for ϵ and κ should occur at the same frequency $1/2\pi T$. This and the fact that the experimental curves are flatter than those calculated from eq. 7 and 8 indicate that a spectrum of time constants replaces a single one. The plot of ϵ'' vs. frequency reaches a peak at a frequency which is virtually equal to the one where ϵ has undergone half its dispersion. It is much lower than the frequency where κ is identical with the mean of κ_0 and κ_∞ .

Figure 5 shows a typical Cole-Cole plot, *i.e.*, a plot of $(\kappa - \kappa_0)/\omega = \epsilon''$ vs. ϵ' , where ϵ'' is the imaginary part of the complex dielectric constant $\epsilon^* = \epsilon - j\epsilon''$. This plot yields a circle in the complex dielectric plane if the distribution function of time constants is given by a Cole-Cole distribution function.¹⁴ However, the plot is also near-circular for other distribution functions which are symmetrical if plotted against $\ln T$ (see Fig. 6 in a previous article²). The extrapolated values of ϵ_0 and ϵ_∞ , taken from Cole-Cole plots, agree fairly well with those obtained from plots of ϵ against frequency (Table I).

The distribution of the frequency parameter u/v along the Cole-Cole circle is evaluated in Fig. 6. This curve should be a straight line of slope α in a logarithmic presentation and fits well with the depression of the circle characterized by an angle $(1 - \alpha)\pi/2$ as indicated in Fig. 5. This is to be expected for symmetrical distribution functions $f(T)$ vs. $\ln T$, as discussed by us previously (ref. 2, pp. 155-157). Thus the data clearly indicate the presence of a symmetrical spectrum of

TABLE I

ESTIMATES OF ZERO-FREQUENCY DIELECTRIC CONSTANT, ϵ_0 , OBTAINED FROM DISPERSION CURVES (D) AND COLE-COLE CIRCLE PLOTS (C) AS FUNCTION OF PARTICLE DIAMETER

Polystyrene sphere suspensions. Volume concentration values close to 30%. The increasing accuracy with decrease in particle size is due to better definition of the low frequency limit value ϵ_0 as a result of the rapid increase in characteristic frequency.

μ	ϵ_0 (D)	ϵ_0 (C)	Accuracy
1.17	10000	8500	± 1000
0.566	3000	2500	+500
.188	2450	2480	+50
.0878	540	525	+25

relaxation times if plotted against $\ln T$. Slight and perhaps systematic deviations from the straight line in Fig. 6 are indicative that a Cole-Cole distribution function may not be exactly adequate. However the deviations are too small to serve for a determination of the exact character of the distribution function.

Finally, Fig. 7 displays ϵ as a function of κ , following a suggestion of Cole.¹⁵ If only one relaxation time were involved, a straight line would be obtained with a slope of $-T$ and intercepts to $\epsilon_\infty + T\kappa_\infty$ and $\kappa_\infty + \epsilon_0/T$. The presence

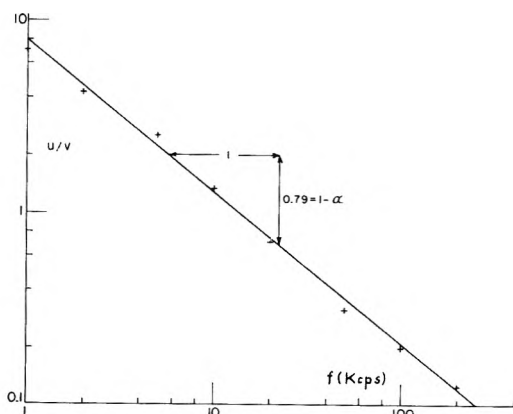


Fig. 6.—The ratio u/v as obtained from the data of Fig. 5 as function of frequency. The results given in Fig. 5 and 6 mean that the dielectric data can be presented in terms of a Cole-Cole distribution function of relaxation times. The results given in the figures are typical for all polystyrene particle suspensions investigated.

of a changing slope reflects the existence of several T -values.

The results displayed in Fig. 4, 5, and 6 are typical for all experimental data and are indicative of a fairly small distribution of time constants T . The Cole-Cole parameter α , defined by Fig. 5 and 6, is a measure of the width of the assumed Cole-Cole distribution function. For example, in Fig. 5 the $1 - \alpha$ value of 0.79 corresponds to a relative half width of the T -distribution function, taken at half the peak, of 2.5. This means that about one-third of all time constants are contained within a T -range of 1:6. This corresponds to a $\ln T$ spectrum extending over a range of about 1:2. Two-thirds of all $\ln T$ values are contained within a range of about 1:3. These estimates are fairly independent of the detailed character of the distribution curve as may be seen from a pertinent evaluation (see Fig. 5 in ref. 2).

All of the above-mentioned techniques have been applied in an effort to extract the parameters ϵ_0 , ϵ_∞ , κ_0 , κ_∞ , and T . The Robert Cole plots (Fig. 7) usually turn out to be fairly unsatisfactory, due to significant deviations from straight lines. However, we observe that the slope of a properly chosen tangent yields a time constant which agrees with other estimates if it is taken at a frequency which coincides with the characteristic frequency $f_0 = 1/2\pi T$. Good agreement in time constant is obtained furthermore from the circle data and from the ϵ'' -curve (see Table II), which both reach their maximum at the characteristic frequency. Low-frequency dielectric constants in good agreement are determined from dispersion curves and Cole-Cole circles (see Table II). The low frequency conductivity κ_0 is always clearly indicated by the dispersion curves. But κ_∞ is uncertain for small particle size, reflecting the more-limited resolution of the RX-meter, which is used for measurements above 0.5 Mc. It is somewhat larger than the value given in Table II for a frequency of 200 kc. ϵ_∞ values have been obtained in some cases. As expected they are found between the dielectric constant of the particle (about 2.5 for polystyrene) and that of the electrolyte (about

(14) K. S. Cole and R. H. Cole, *J. Chem. Phys.*, **9**, 341 (1941).

(15) R. H. Cole, *ibid.*, **23**, 493 (1955).

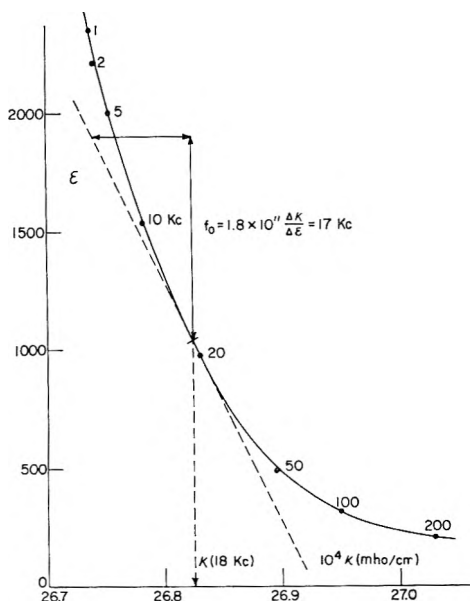


Fig. 7.—Plot of ϵ against κ . This plot should be a straight line if the frequency dependence were due to the presence of only one relaxation time.

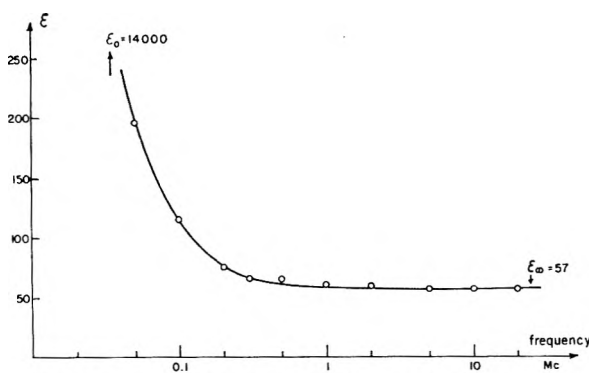


Fig. 8.—Dielectric constant of a polystyrene sphere suspension at high frequencies. Special sample: diameter of spheres $2R = 0.557 \mu$, volume concentration $p = 19.5\%$, conductivity of the electrolyte $\kappa_a = 1.25$ mmhos/cm.

78), according to the Maxwell-Wagner dispersion theory (eq. 12). For the special sample shown in Fig. 8, the experimental result of $\epsilon_\infty = 57$ is exactly as given by that theory.

TABLE II

ELECTRICAL PROPERTIES OF FOUR SUSPENSIONS OF POLYSTYRENE PARTICLES OF DIFFERENT SIZE

Volume fraction close to 30%; diameter in μ ; accuracy in f_0 values about 10%. The κ values taken at 200 kc. are somewhat lower than κ_∞ for the smaller sizes. Absolute accuracy in κ about 3%, accuracy between κ_0 and κ (200 kc.) significant to the last digit quoted. Accuracy for ϵ_0 , see Table I; accuracy for ϵ_∞ , about 5%. The κ values are given in mmho/cm.

	1.17 μ	0.566 μ	0.188 μ	0.088 μ
ϵ_0	10000	3000	2450	540
ϵ_∞	44	46
κ_0	2.2814	2.8177	2.6735	6.4803
κ (200 kc.)	2.2872	2.8254	2.7030	6.4897
f_0 (ϵ'')	0.6	1.8	15	80
f_0 (circle)	0.48	2.0	14	80

Results

The following materials have been investigated: (1) Polystyrene latex containing spherical particles of the following diameters: 1.17, 0.566, 0.188, and 0.0878 μ . Altogether eight samples were investigated. The relative volume fraction was near 30%. (2) Two polystyrene suspensions with 1.17 and 0.557 μ particles, resuspended in KCl using dialysis. Suspensions with volume concentrations between 4 and 30% and electrolyte conductivities between 0.5 and 2.0 mmhos/cm. were measured. (3) Polystyrene suspensions in media of different and known ionic strengths. Original samples were dialyzed for 40 hr. against solutions containing ion exchangers. Then, defined amounts of KCl were added and the samples well stirred for 0.5 hr. in order to reduce the tendency of particles to clump. Periodically, samples were examined under the microscope for clump formation. (4) A variety of fat particle emulsions. Particle size was not sharply defined and varied between 1 and 3 μ diameter. (5) Biological cell suspensions. The results have been summarized elsewhere.²

In all cases dispersion curves have been clearly established. The results with fat particle suspensions are quite similar to those obtained with the polystyrene latex. They do not contribute further essential information and, hence, are omitted. For a typical dispersion curve see Schwan and Maczuk.⁵ While working with the fat emulsions and biological cells, it became apparent that the characteristic frequency is a strong function of size (see for example Table IV in ref. 2). Hence the fat emulsions, whose particles vary in diameter between 1 and 3 μ , involve a fairly broad spectrum of time constants. However, the polystyrene data, obtained with particles of well defined and uniform size, only had a partially reduced spectrum of time constants, indicating that mechanisms other than size also contribute to the spread of time constants.

Characteristic data obtained with the polystyrene latex material (item 1 above) are summarized in Table II. Dispersion curves, Cole-Cole, and R. Cole plots are shown in Fig. 4 to 7 for one particle size. Results for other particle sizes are similar, except for variations in magnitude of dispersion and characteristic frequency, as stated in Table II. The characteristic frequency, shown as a function of particle size in Fig. 9, simply changes inversely with the square of the particle size. This relation has been found virtually to be independent of the nature and the concentration of the electrolyte as well as of the concentration of the particles.

In Fig. 10 is plotted the static dielectric increment $\Delta\epsilon_0 = \epsilon_0 - \epsilon_\infty$ vs. the volume concentration of the polystyrene for two particle sizes and two electrolyte concentrations (item 2 above). It increases linearly with particle concentration. The initial slope of the lines decreases, and at higher particle concentrations the lines become curved, for a KCl conductivity of 1.4 mmhos/cm. and the same particle diameters.

Figure 10 demonstrates also that bigger particles yield higher dielectric increments. This is shown more clearly in Fig. 11, where $\Delta\epsilon_0/p$ is plotted vs.

TABLE III

CONDUCTIVITY IN MMHO/CM. AS FUNCTION OF FREQUENCY FOR 0.557 μ DIAMETER POLYSTYRENE SPHERE SUSPENSIONS IN KCl OF CONDUCTIVITY κ_a

p is the volume fraction taken by the spheres.

$f(\text{kc.})$	κ (I)	κ (II)	κ (III)
0.02	0.08515	0.41623	1.35848
0.05	.08512	.41617	1.35847
0.1	.08515	.41625	1.35853
0.2	.08521	.41633	1.35864
0.5	.08532	.41656	1.35888
1	.08549	.41685	1.35926
2	.08584	.41756	1.36015
5	.08699	.42018	1.3629
10	.08859	.42471	1.3665
20	.09101	.42921	1.3700
50	.09433	.43516	1.3733
100	.09645	.43764	1.3746
200	.09824	.43892	1.3755
300	.09925	.43911	1.3757
κ_a	0.09772	0.5314	1.82
p (%)	17.2	20.7	23.3

the diameter for the two primarily investigated particle sizes. Although drawn as a straight line, the exact dependence may be somewhat stronger than linear.

The maximum of the dielectric loss $\Delta\epsilon''_{\text{max}}$ should be equal to $\Delta\epsilon_0/2$ in the simple case of a single relaxation step. Since the experimental evidence indicates a relaxation spectrum, smaller values must be expected. In fact, the ratio $2\Delta\epsilon''_{\text{max}}/\Delta\epsilon_0$ turned out to be about 0.8.

The influence of the ionic composition of the suspending medium (item 3 above) has been the subject of our interest, particularly with regard to the conductivity. Pertinent results are summarized in Table III. It will be noted from these data that the dispersion of the conductivity term is not very strongly affected by the conductivity of the suspending medium throughout the range from 0.1 to 2 mmhos/cm.

Discussion

Several mechanisms can be rejected as being responsible for the observed data. They will be discussed in sequence. The concept of a frequency-dependent surface admittance will be used to account for the observed effects.

1. **Maxwell-Wagner Dispersion Phenomena.**—We consider a suspension of spheres of complex dielectric constant ϵ_i^* in a medium of complex dielectric constant ϵ_a^* . Such a system displays a dielectric relaxation effect which is due to the time-dependent polarization of the interfaces between particle and surrounding medium. This may be seen from an alternating current expansion of an equation first given by Maxwell.¹² The pertinent equations have been given by Wagner for the case of low volume fractions of suspended particles,¹⁶ and for higher volume concentrations by Pauly and Schwan¹⁷ (eq. 53 to 57 in their article).

(16) K. W. Wagner, *Arch. Elektrotech.*, **3**, 83 (1914).

(17) H. Pauly and H. P. Schwan, *Z. Naturforsch.*, **146**, 125 (1959).

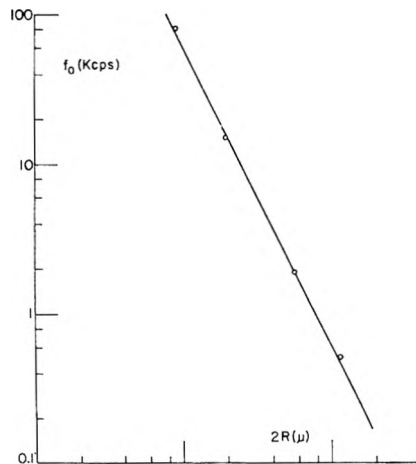


Fig. 9.—The characteristic frequency is plotted against particle size and is proportional to $1/R^2$.

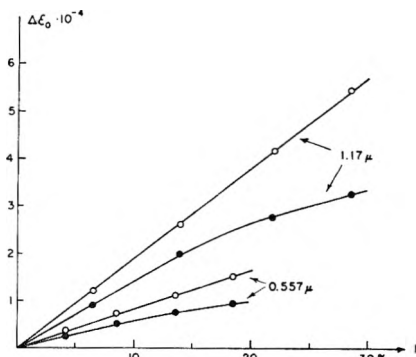


Fig. 10.—The low-frequency limit of the dielectric increment $\Delta\epsilon_0$ vs. volume concentration of spheres for two particle sizes and two electrolyte conductivities $\kappa_a = 0.7$ mmho/cm. (O) and 1.4 mmho/cm. (●).

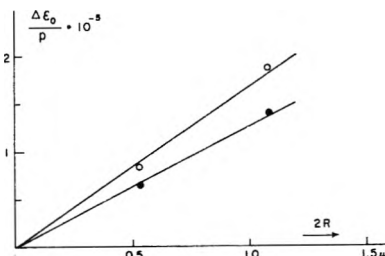


Fig. 11.—Dependence of the initial slope $\Delta\epsilon_0/p$ upon particle diameter for $\kappa_a = 0.7$ mmho/cm. (O) and 1.4 mmho/cm. (●).

$$T = \frac{\epsilon_i + 2\epsilon_a - p(\epsilon_i - \epsilon_a)}{\kappa_i + 2\kappa_a - p(\kappa_i - \kappa_a)} \epsilon_r \quad (10)$$

$$\kappa_0 = \kappa_a \frac{(\kappa_i + 2\kappa_a) + 2p(\kappa_i - \kappa_a)}{(\kappa_i + 2\kappa_a) - p(\kappa_i - \kappa_a)} \quad (11)$$

$$\epsilon_\infty = \epsilon_a \frac{(\epsilon_i + 2\epsilon_a) + 2p(\epsilon_i - \epsilon_a)}{(\epsilon_i + 2\epsilon_a) - p(\epsilon_i - \epsilon_a)} \quad (12)$$

$$\kappa_\infty = \kappa_0 + 9p(1-p) \times \frac{(\epsilon_a \kappa_i - \kappa_a \epsilon_i)^2}{[(\epsilon_i + 2\epsilon_a) - p(\epsilon_i - \epsilon_a)]^2 [(\kappa_i + 2\kappa_a) - p(\kappa_i - \kappa_a)]} \quad (13)$$

$$\epsilon_0 = \epsilon_\infty + 9p(1-p) \times \frac{(\epsilon_a \kappa_i - \kappa_a \epsilon_i)^2}{[(\epsilon_i + 2\epsilon_a) - p(\epsilon_i - \epsilon_a)][(\kappa_i + 2\kappa_a) - p(\kappa_i - \kappa_a)]^2} \quad (14)$$

$\epsilon_r = 8.85 \times 10^{-14}$ farad./cm. is the dielectric constant of vacuum, ϵ_i and ϵ_a are dielectric constants relative to vacuum, and p is the volume fraction taken by the particles. In our case the following parameters apply: $\epsilon_i = 2.5$; $\epsilon_a = 78$; $\kappa_i = 0$; $\kappa_a = 0.1$ to 10 mmho/cm.; $p = 0.3$. The characteristic frequency $f_0 = 1/2\pi T$ is calculated from eq. 10 to be between 2 and 200 Mc., *i.e.*, higher by orders of magnitude than that observed. The change of the dielectric constant, eq. 14, is about 0.01, *i.e.*, by far too small. The Maxwell-Wagner type of interface polarization therefore is not responsible for the observed data.

2. Electrophoretic Movements.¹⁸—Colloidal particles usually carry an electrical charge. In the case of polystyrene particles, it probably is due to the surface coating used for stabilizing purposes. The particle charge is only in part compensated by counterions close to the particle, so that the particle will move if exposed to an electric field. We now consider how such a movement affects the dielectric properties of a suspension of charged particles.

The movement of a charged particle in an electrical field $E = E_0 e^{j\omega t}$ is characterized by the differential equation

$$m\dot{v} + rv = qE \quad (15)$$

m is the mass of the particle, v its velocity, \dot{v} the time derivative of v , q the particle charge, and r the frictional constant. Under alternating current steady state conditions $v = v_0 e^{j\omega t}$. Then eq. 15 reduces to

$$v_0 = \frac{qE_0}{r} \frac{1}{1 + j\omega T} \quad (16)$$

where $T = m/r$. The electrophoretic current which results from the movement of charged particles with the field is given by the equation

$$i = Nqv; i_0 = Nqv_0 \quad (17)$$

where i_0 is the peak value of i and N is the number of particles per volume unit (cm.³). Since the complex conductivity $K = \kappa + j\omega\epsilon\epsilon_r$ is related to i_0 and E_0

$$i_0 = KE_c \quad (18)$$

we can combine (16) and (17)

$$K = \frac{Nq^2}{r} \frac{1}{1 + j\omega T} \quad (19)$$

This separates into

$$\kappa = \kappa_\infty + \frac{Nq^2}{r} \frac{1}{1 + (\omega T)^2} \quad (20)$$

(18) We appreciate Dr. K. S. Cole's suggestion that we investigate this effect.

$$\epsilon = \epsilon_\infty - \frac{Nq^2}{r\epsilon_r} \frac{T}{1 + (\omega T)^2} \quad (21)$$

where κ_∞ and ϵ_∞ have been added to account for contributions due to mechanisms other than that discussed here.

Colloidal particles have a surface charge of less than 0.1 elementary charge per Å.² surface. Thus q is smaller than $2 \times 10^{-3} R^2$ if the radius R is expressed in cm. and q in coulombs. Stokes law applies for spherical particles

$$r = 6\pi\eta R \quad (22)$$

where the viscosity η of the suspending medium is near 0.01 poise for electrolytes. We may further restrict our discussions to the case that the particle density is near unity, a case which is closely approximated by biological cells and polystyrene particles. Equations 20 and 21 then reduce to

$$\kappa = \kappa_\infty + 5 \times 10^{-6} p \frac{1}{1 + (\omega T)^2} \text{ (mho/cm.)} \quad (23)$$

$$\epsilon = \epsilon_\infty - 12.7 \times 10^8 R^2 p \frac{1}{1 + (\omega T)^2} \quad (24)$$

with

$$T = 22.2R^2; f_0 = 1/140R^2 \quad (25)$$

where N has been replaced by the volume fraction p taken by the particles.

Thus for a particle of 1 μ radius, the characteristic frequency is near 700 kc. $\epsilon_\infty - \epsilon_0$ is smaller than 4 for $p = 0.3$, and the conductivity difference $\kappa_0 - \kappa_\infty$ is less than 2 μ mhos/cm.

We conclude that the electrophoretic dispersion effect is located at higher frequencies than those of interest here, that the magnitude of the change in ϵ is much too small, and that the direction of the dispersion is opposite to the one experimentally observed. Hence electrophoretic movement in an alternating field cannot explain our data.

3. Surface Conductance.—The existence of a frequency-independent and consequently time-independent tangential surface conductance has been proposed as being responsible for dielectric dispersion phenomena in colloidal suspensions at low and at radiofrequencies.^{19,20} As a prerequisite to our present discussion and to that in the next section, the admittance of a suspension of particles surrounded by shells will be considered. This most conveniently starts from equations given by Maxwell¹² (articles 312–314 of reference). The alternating current extension of Maxwell's equation can be written as follows (see for example Cole²¹ or Daenzer²²)

$$\frac{K - K_a}{K + 2K_a} = p \frac{Y - K_a}{Y + 2K_a} \quad (26)$$

(19) C. T. O'Konski, *J. Chem. Phys.*, **23**, 1559 (1955).

(20) C. T. O'Konski, *J. Phys. Chem.*, **64**, 605 (1960).

(21) K. S. Cole, *J. Gen. Physiol.*, **12**, 29 (1928).

(22) H. Daenzer, *Ann. Phys.*, [V] **20**, 463; [V] **21**, 783 (1934).

where $K = \kappa + j\omega\epsilon_r$ stands for the complex conductivity. Y is the specific admittance of a homogeneous particle which can replace the shell-surrounded particle without changing its field perturbation in the suspending medium. Y is determined by the particle properties as

$$\frac{Y - K_s}{Y + 2K_s} = \left(\frac{R - d}{R}\right)^3 \frac{K_i - K_s}{K_i + 2K_s} \quad (27)$$

where the symbols are defined in Fig. 12. The 3-phase system expressed by eq. 26 and 27 has a frequency dependence which reflects the presence of two time constants (Pauly and Schwan¹⁷). We will restrict our further discussions to cases which fulfil the following requirements: (1) The particle conductivity κ_i is small compared to that of the surface layer, and (2) the thickness of the surface layer d is much smaller than the radius R . These two assumptions are well fulfilled in the present study. Equation 27 then reduces to

$$Y = K_i + 2 \frac{d}{R} K_s \quad (28)$$

In this case the frequency dependence reduces to that of a single relaxation process, characterized by eq. 7, 8, and 9. The parameters T , κ_0 , κ_∞ , ϵ_0 , ϵ_∞ are given by eq. 10 to 14 if we add to κ_i and ϵ_i the quantities $2(d/R)\kappa_s$ and $2(d/R)\epsilon_s$.

$$\kappa_i \longrightarrow \kappa_i + 2 \frac{d}{R} \kappa_s; \quad \epsilon_i \longrightarrow \epsilon_i + 2 \frac{d}{R} \epsilon_s \quad (29)$$

The magnitude of the dispersion $\epsilon_0 - \epsilon_\infty$ is identical with the expression given by Schwan² (eq. 27 of reference), for the case of small particle concentration. The time constant expression reduces to the one previously given by Miles and Robertson²³ for the same model, provided p is very small. The time constant would further reduce to the value given by O'Konski¹⁹ if the outside medium were practically non-conducting and the surface layer were purely conductive, but the first assumption is not applicable in our case.

We now consider the possibility that a frequency-independent purely-conductive surface layer may explain the desired relaxation behavior. In this case the term ϵ_s can be neglected. Furthermore, it is appropriate to neglect κ_i in comparison with $2(d/R)\kappa_s$, since polystyrene is an excellent dielectric. Then

$$T = \frac{\epsilon_i + 2\epsilon_a - p(\epsilon_i - \epsilon_a)}{2 \frac{d}{R} \kappa_s + 2\kappa_a - p\left(2 \frac{d}{R} \kappa_s - \kappa_a\right)} \epsilon_r \quad (30)$$

$$\epsilon_0 - \epsilon_\infty = 9p(1 - p) \times \frac{\epsilon_i + 2\epsilon_a - p(\epsilon_i - \epsilon_a)}{\left[(\epsilon_i + 2\epsilon_a) - p(\epsilon_i - \epsilon_a)\right] \left[\left(2 \frac{d}{R} \kappa_s + 2\kappa_a\right) - p\left(2 \frac{d}{R} \kappa_s - \kappa_a\right)\right]^2} \quad (31)$$

(23) J. B. Miles and H. P. Robertson, *Phys. Rev.*, **40**, 583 (1932).

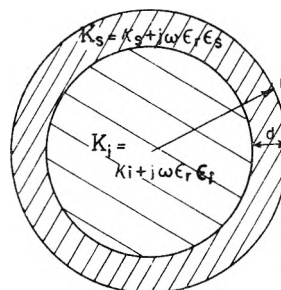


Fig. 12.—See text.

The surface conductance $G_s = d\kappa_s$ usually is found to be between 10^{-9} and 10^{-8} mho. Thus, for typical κ_a values in the mmho/cm. range and for particle sizes in the μ -range, $d\kappa_s < R\kappa_a$. For fat particles and polystyrene particles in aqueous media, ϵ_i is near 3 and ϵ_a near 80. Then the equations for T and ϵ_0 reduce to

$$T = \frac{\epsilon_a}{\kappa_a} \epsilon_r \quad (32)$$

$$\epsilon_0 - \epsilon_\infty = 9p \frac{1 - p}{(2 + p)^3} \frac{\epsilon_i^2}{\epsilon_a} \quad (33)$$

These equations are independent of κ_s and are identical with (10) and (14) under the assumptions made. Thus the characteristic frequency is in the upper Mc. range, and the difference $\epsilon_0 - \epsilon_\infty$ is a small fraction of a dielectric unit. Therefore a frequency-independent surface conductance cannot explain the dielectric phenomenon of interest to us.

4. Surface Admittance.—That the experimental data can be explained by a surface admittance, composed of both a surface conductance and capacitance term, already was apparent from the study conducted by Fricke and Curtis.³ Since $\kappa_i = 0$ the specific admittance of an equivalent homogeneous particle (eq. 28, 29) reduces to

$$Y = 2 \frac{d}{R} \kappa_s + j\omega \left(\epsilon_i + 2 \frac{d}{R} \epsilon_s \right) \epsilon_r \quad (34)$$

For low p -values the dispersion has the time constant (see eq. 10, 29)

$$T = \frac{\frac{d}{R} \epsilon_s + \epsilon_a}{\frac{d}{R} \kappa_s + \kappa_a} \epsilon_r \quad (35)$$

The dispersion has a magnitude (eq. 14, 29)

$$\epsilon_0 - \epsilon_\infty = 9p \frac{\left(\frac{d}{R} \epsilon_s + \epsilon_a \right)^2}{\left(2\epsilon_a + 2 \frac{d}{R} \epsilon_s \right) \left(\kappa_a + \frac{d}{R} \kappa_s \right)^2} \quad (36)$$

since we may neglect ϵ_i in comparison to $2\epsilon_a$.

Since $\frac{d}{R} \kappa_s \ll \kappa_a$, then T reduces to

$$T = \frac{\epsilon_a}{\kappa_a} \epsilon_r + \frac{d\epsilon_s/R}{\kappa_a} \epsilon_r \quad (37)$$

If this time constant is to correspond to a dispersion in the low frequency range, then the second term must predominate over the very small first term. So it must be concluded that $\epsilon_a \ll d\epsilon_s/R$.

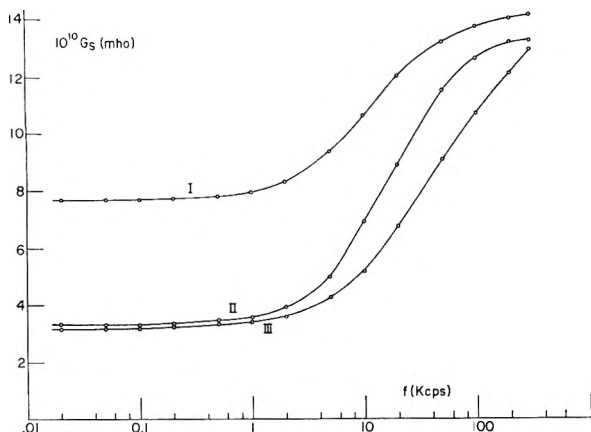


Fig. 13.—Surface conductance as function of frequency. Particle size diameter 0.557μ in all cases. The three curves pertain to different conductivities of the suspending medium and are calculated from the data given in Table III. In order to conveniently accommodate all data, the G_s values have been reduced by frequency independent values. Curve I is $G_s - 3 \times 10^{-9}$ mho, II is $G_s - 10^{-9}$ mho, III is $G_s - 2 \times 10^{-10}$ mho.

But with $\epsilon_a \ll d\epsilon_s/R$ and $2d\kappa_s R \ll \kappa_a$, the dispersion magnitude (eq. 36) reduces to

$$\epsilon_0 - \epsilon_\infty = \frac{9}{2} \frac{d}{pR} \epsilon_s = \frac{9}{2} p \kappa_a T \quad (38)$$

For an $\epsilon_0 - \epsilon_\infty$ near 10^4 and κ_a near 10^{-3} mho/cm; this expression requires that $T \sim 10^7$, *i.e.*, a dispersion in the Mc. range. Thus the additional inclusion of a frequency-independent surface capacitance term leads to an inconsistency and fails, therefore, to explain the observed data.

We have seen that the dispersion phenomenon which reflects the mere presence of a surface admittance (eq. 10–14, modification 29) is always located in the high Mc. range. This fact enables us to state that in the frequency range of interest here all our experimental data are to be considered ϵ_0 and κ_0 values for which eq. 11 and 14 apply with the modification (29)

$$\kappa_0 = \kappa_a \frac{\left(\frac{d}{R} \kappa_s + \kappa_a\right) + \left(\frac{d}{R} \kappa_s - \kappa_a\right)}{\left(\frac{d}{R} \kappa_s + \kappa_a\right) - \frac{p}{2} \left(\frac{d}{R} \kappa_s - \kappa_a\right)} \quad (39)$$

where the very low particle conductivity κ_i has been neglected. For $(d/R) \kappa_s < \kappa_a$, to a good approximation

$$\kappa_0 = \kappa_a \frac{1-p}{1+\frac{p}{2}} + \frac{d}{R} \kappa_s \frac{4.5p}{\left(1+\frac{p}{2}\right)^2} \quad (40)$$

The surface conductance term $G_s = d\kappa_s$ is some-

where between 10^{-9} and 10^{-8} mho according to various investigators (White, *et al.*²⁴; McBain and Forster²⁵; Fricke and Curtis^{2,26}; Rutgers and de'Smet²⁷) and in accordance with our data (Fig. 13). The surface capacitance $C_s = d\epsilon_s \epsilon_r$ is $0.01 \mu\text{mf}$. in order of magnitude, according to values given by Fricke and Curtis and our values in Table IV. On the other hand, the terms $R\epsilon_i \epsilon_r$ and $R\epsilon_a \epsilon_r$ are smaller than $7R \mu\text{mf}$. Since the radius R is in our case between 10^{-5} and 10^{-4} cm., we conclude that

$$\frac{d}{R} \epsilon_s \gg \epsilon_i, \epsilon_a \quad (41)$$

In view of this and $(d/R)\kappa_s \ll \kappa_a$ and $\kappa_i = 0$, the low frequency dielectric constant equation

$$\epsilon_0 - \epsilon_\infty = 9p(1-p) \times \frac{\left[2\epsilon_a \frac{d}{R} \kappa_s - \left(\frac{d}{R} \epsilon_s + \epsilon_i\right) \kappa_a\right]^2}{\left[2\frac{d}{R} \epsilon_s + \epsilon_i + 2\epsilon_a - p\left(\frac{d}{R} \epsilon_s + \epsilon_i - \epsilon_a\right)\right] \left[2\frac{d}{R} \kappa_s + 2\kappa_a - p\left(\frac{d}{R} \kappa_s - \kappa_a\right)\right]^2} \quad (42)$$

as derived from eq. 14 and 29, reduces to

$$\epsilon_0 = \epsilon_\infty + \frac{4.5p}{\left(1+\frac{p}{2}\right)^2} \times \frac{d}{R} \epsilon_s \quad (43)$$

Equations 40 and 43 state that the changes in ϵ and κ observed at low frequencies must reflect proportionate changes in ϵ_s and κ_s . That is, the frequency dependence of ϵ and κ simply reflects a corresponding frequency dependence of surface conductance and capacitance. In conclusion we can state that the introduction of a surface admittance concept, involving both resistive and capacitive components, is not much aid in explaining the relaxation phenomenon discussed here. However, we can describe the observed relaxation effects in terms of a frequency-dependent surface admittance component, and we can readily compute this surface admittance by use of the simple eq. 40 and 43.

In Fig. 13 and Table IV are listed surface conductance and capacitance values. It is demonstrated: (a) The surface admittance quantities depend on particle size. (b) They change with frequency and their relaxation occurs at a frequency which changes strongly with the particle size even though the surface admittance data are given per unit surface area. (c) The surface conductance term is composed of two parts, one being independent of and the other dependent on frequency. The

(24) H. L. White, E. Monaghan, and F. Urban, *J. Phys. Chem.*, **40**, 207 (1936).

(25) J. W. McBain and J. F. Forster, *ibid.*, **39**, 331 (1935).

(26) H. Fricke and H. J. Curtis, *ibid.*, **40**, 715 (1936).

(27) A. J. Rutgers and M. de'Smet, *Trans. Faraday Soc.*, **43**, 102 (1947).

TABLE IV

SURFACE CAPACITANCE VALUES C_s IN $\mu\text{mf. PER CM.}^2$ SURFACE AREA AS FUNCTION OF FREQUENCY AND FOR DIFFERENT PARTICLE SIZES

Polystyrene latex material; p volume fraction taken by the polystyrene particles; arrows indicate approximate mid-point of the dispersion of C_s and its dependence on particle size. The C_s values approached at low frequency also depend strongly on particle size. Temperature near 23°.

f	$2R$	1.17μ	0.566μ	0.188μ	0.0878μ
	p (%)	30.5	29	30.5	32.3
	κ_c (mmho/cm.)	2.3	2.8	2.7	6.5
$f = 0.1$ kc.p.s.		44.3×10^{-3}	7.3×10^{-3}	1.94×10^{-3}
0.2		33.3	5.9	1.94
		←			
0.5		20.3	4.4	1.92	0.178×10^{-3}
1		11.8	3.65	1.85	0.175
			←		
2		6.3	2.82	1.74	0.167
5		2.6	1.74	1.57	0.158
10		1.22	1.01	1.20	0.146
				←	
20		0.56	0.57	0.75	0.128
50		0.24	0.22	0.36	0.117
100		0.17	0.11	0.20	0.096
					←
200		0.14	0.05	0.12	0.079

frequency-independent component of the surface conductance changes approximately in proportion with the conductivity of the suspending medium, while the magnitude of the conductivity dispersion is almost independent of the ionic strength of the suspending medium.

Conclusions

Several mechanisms have been ruled out as responsible for the relaxation effect observed in colloidal suspensions at low frequencies. They include a simple Maxwell-Wagner relaxation, existence of frequency-independent surface conductance or admittance, and electrophoretic movement of the charged suspended particles. The concept of a frequency-dependent surface admittance must be introduced. Its components, surface capacitance and conductance, change with frequency according to relaxation equations which involve a fairly small spectrum of time constants. The surface conductance is composed of two parts, one frequency independent and the other changing with frequency. The magnitude of these two components is comparable (Fig. 13). The introduction of a frequency dependent surface admittance explains the high dielectric constants which colloidal suspensions display at low frequencies. However it does not provide an insight as to the physical mechanism which gives rise to its existence. The dependence of the surface admittance data on particle size rules out the possibility that material properties of the suspended particles are responsible.

One other effect has not been considered. It is the counterpart of the above-considered electrophoretic effect and concerns the movement, under the influence of an applied field, of counterions which surround charged particles. This movement has been suggested previously as likely to be responsible for the observed phenomenon² (pp.

182-185 of reference). A detailed analysis of this effect is given by Schwarz.²⁸

Summary

The dielectric properties of colloidal suspensions have been investigated from 10 c.p.s. to several Mc. This article presents material in support of the following conclusions:

(1) At low frequencies colloidal suspensions display very high, frequency-dependent dielectric constants. The dielectric properties are described analytically by a fairly well defined spectrum of relaxation times. Hence, dielectric constant and conductivity become frequency-independent at sufficiently low frequencies.

(2) The Maxwell-Wagner type of relaxation phenomenon exhibited by inhomogeneous dielectrics is not responsible for the reported dielectric effects.

(3) Relaxation effects result from the electrophoretic movement of charged particles in an alternating electrical field. This effect is shown to cause a "negative" dispersion, where the high frequency dielectric constant is larger than the one observed at low frequencies. This difference is of small magnitude and is also not responsible for the observed dielectric data.

(4) The concept of a frequency-independent surface conductance or surface admittance cannot explain the observed data. The surface admittance data change with frequency in accordance with equations which assume a spectrum of relaxation times.

(5) Surface conductance and capacitance change with particle size and ionic strength of the suspending medium. The total surface conductance includes a frequency-independent component, which is comparable to the frequency-dependent part observed at high frequencies.

(28) G. Schwarz, *J. Phys. Chem.*, **66**, 2636 (1962).

A THEORY OF THE LOW-FREQUENCY DIELECTRIC DISPERSION OF COLLOIDAL PARTICLES IN ELECTROLYTE SOLUTION^{1,2}

BY GERHARD SCHWARZ

Electromedical Division, Moore School of Electrical Engineering, University of Pennsylvania, Philadelphia 4, Pa.

Received April 12, 1962

It is proposed that the low-frequency dielectric dispersion observed with colloidal particles suspended in electrolytes is due to the polarization of the counterion atmosphere around the particles by an external electric field. A simplified theory of this effect is developed for particles of spherical shape. The displacement of counterions in the double layer is shown to be equivalent to the existence of a surface capacitance displaying a diffusion-controlled relaxation. This effect can be expressed by an additional "apparent" dielectric constant of the suspended particles, exceeding their actual dielectric constant at low frequencies by many orders of magnitude. The theory is applied to the special case of particles suspended in a fairly well conducting electrolyte. Such colloidal systems display a particularly well pronounced low frequency dispersion effect. The results of previous experimental investigations with suspensions of uniformly sized polystyrene spheres are used in order to test the theory. Assuming reasonable values for the density and the mobility of the counterions in the double layer, the theory agrees very well with the static dielectric increment and the characteristic frequency of the dispersion as experimentally observed. A distribution of activation energies of the counterion motion on the particle surface is introduced to account for the relaxation spectrum of the dispersion curves.

Introduction

Suspensions of colloidal particles in aqueous electrolyte solutions generally display unusually high dielectric constants at low frequencies.³ Thus, for sphere-like particles about 1μ in diameter, the dielectric constant may rise well above 10^4 below 1 kc.^{3,4} However, the experimental difficulties are considerable. Due to the appreciable electrolytic conductivity and the low frequencies used, it was possible only recently to achieve sufficient accuracy in the dielectric measurements and in the control of electrode polarization to take complete curves of the low frequency dielectric dispersion. For example, while investigating the dielectric behavior of biological material down to about 10 c.p.s., Schwan and co-workers found a well pronounced dispersion in the low frequency range.⁵ This so-called α -dispersion perhaps is the same effect which occurs in the case of non-biological colloids. In fact, similar dispersion curves for fat particles and polystyrene spheres suspended in electrolyte solution have been measured by Schwan, *et al.*^{3,5,6}

It has been suggested that displacements of electrical charges within the interface between the particle and the electrolyte may be responsible for the α -dispersion (*e.g.*, Murphy and Lowry⁷ and Schwan⁵). Colloidal particles are electrically charged by fixed or adsorbed ions and are surrounded by counterions, forming an electric double layer or ionic atmosphere. A shift of ions within this layer by an external electrical field would result in a dielectric dispersion. Yet merely introducing an ohmic surface conductance around the particle into the Maxwell-Wagner theory of

heterogeneous dielectrics,⁸ as done by Miles and Robertson⁹ and more recently by O'Konski,¹⁰ cannot account for the experimental facts.³ As has been demonstrated by Fricke and Curtis⁴ and Schwan, *et al.*³, only a frequency-dependent capacitive part of the surface admittance can explain the measured high dielectric constants. Unfortunately there has been no detailed justification of such a term so far.

Apparently it is possible to explain the effect only by a consideration of the microphysical structure of the double layer and the behavior of an individual charge carrier. Kirkwood and Shumaker¹¹ have considered this effect in the special case of the proton fluctuation around protein molecules by employing a statistical method. They demonstrated that the dielectric properties of protein solutions at radiofrequencies may be explained in this way just as well as by orientation of permanent dipoles, the latter being the commonly adopted interpretation.¹² In the general case of non-polar, spherical, and dielectrically-isotropic particles, an orientation mechanism is out of the question.¹³ But a deformation of the ionic atmosphere due to an applied field can be anticipated and must be reflected in a corresponding dielectric relaxation. Whether this model explains the above-quoted dielectric phenomenon will be the subject of this paper.

Counterions on the surface of the highly-charged colloidal particle are strongly bound by electrostatic attraction. In order to escape from the surface into the free solution, they have to overcome a high potential barrier. Along the surface, however, they can be moved much more easily. Thus

(1) Presented before the Division of Physical Chemistry of the American Chemical Society, 140th National Meeting, Chicago, Illinois, Sept., 1961.

(2) This investigation was supported by National Institute of Health Grant H 1253 (C9).

(3) H. P. Schwan, G. Schwarz, J. Maczuk, and H. Pauly, *J. Phys. Chem.*, **66**, 2626 (1962).

(4) H. Fricke and H. J. Curtis, *ibid.*, **41**, 729 (1937). Further reference of older papers will be found here.

(5) H. P. Schwan, *Advan. Biol. Med. Phys.*, **5**, 147 (1957).

(6) H. P. Schwan and J. Maczuk, *Proc. Natl. Biophys. Conf., 1st, Columbus, Ohio*, 348 (1959).

(7) E. J. Murphy and H. H. Lowry, *J. Phys. Chem.*, **34**, 598 (1930).

(8) K. W. Wagner, *Arch. Elektrotech.*, **3**, 83 (1914).

(9) J. B. Miles, Jr., and H. P. Robertson, *Phys. Rev.*, **40**, 583 (1932).

(10) C. T. O'Konski, *J. Phys. Chem.*, **64**, 605 (1960).

(11) J. G. Kirkwood and J. B. Shumaker, *Proc. Natl. Acad. Sci. U. S.*, **38**, 855 (1952).

(12) J. L. Oncley, in Cohn and Edsall, "Proteins, Amino Acids and Peptides," Reinhold Publ. Corp., New York, N. Y., 1943.

(13) Moreover, an orientation mechanism would not account for the dielectric dispersion in question. The characteristic frequency of such an effect is inversely proportional to the third power of the diameter, according to Debye's well known equation of the relaxation time of oriented, spherical dipoles. This is in contrast to the experimental evidence discussed by Schwan, *et al.*³ Furthermore, the quantitative value of such a characteristic frequency is found to be far below those of interest here.

they will be moved tangentially by an external field, polarizing the ion atmosphere and inducing an electric dipole moment of the particle. This concept has proved to be successful for rod-like particles in recent investigations on the orientation field effect of polyelectrolytes.¹⁴⁻¹⁷ In place of a rigorous and difficult theory of the polarization of the counterion atmosphere, a fairly simplified model of the colloidal system is used in the calculations. Despite this rather crude model, the theoretical results yield a surprisingly good qualitative and quantitative representation of the experimental facts previously reported.³

Theory

Effect of an Electric Field on a Sphere with a Counterion Layer.—The colloidal particle will be introduced as a sphere of radius R and complex conductivity (in the presence of an alternating field of angular frequency ω)

$$K_i = \kappa_i + i\omega\epsilon_r\epsilon_i \quad (1)$$

suspended in an electrolyte solution of complex conductivity

$$K_a = \kappa_a + i\omega\epsilon_r\epsilon_a \quad (2)$$

where κ_i , κ_a and ϵ_i , ϵ_a are the conductivities and the (relative) dielectric constants of the particle and the electrolyte, respectively. $\epsilon_r = 8.854 \times 10^{-12}$ f./m. is the absolute dielectric constant of free space. The sphere is electrically charged by fixed or adsorbed ions and is surrounded by counterions of electric charge e_0 and mechanical mobility u (i.e., velocity per unit force), which can be moved only along the surface but not perpendicular to it. The electric double layer is assumed to be infinitely thin (in comparison with the radius of the particle) with a total net charge equal to zero. When the colloidal particle is not affected by external forces, the counterions are randomly distributed, so that the surface density σ (ions per unit area) is a constant σ_0 . An applied external electric field E will result in a shift of the counterions along the surface, thus disturbing the random distribution. The counterion surface density may generally be denoted

$$\sigma = \sigma_0 + \bar{\sigma} \quad (3)$$

where $\bar{\sigma}$ represents the counterion surface density in excess of the constant value σ_0 .

It is suitable now to introduce spherical coordinates r and θ with $r = 0$ at the center of the sphere and $\theta = 0$ in the direction of E . If ψ_s is the electric potential on the surface of the sphere, the corresponding electric field

$$E_s = -\frac{1}{R} \times \frac{\partial \psi_s}{\partial \theta} \quad (4)$$

causes a surface flux of counterions

$$j_E = -\frac{e_0\sigma u}{R} \times \frac{\partial \psi_s}{\partial \theta} \quad (5)$$

In addition to the flux induced by the impressed electric field there is a counteracting diffusion flux which tends to re-establish the random distribution

$$j_D = -\frac{ukT}{R} \frac{\partial \sigma}{\partial \theta} \quad (6)$$

Since the counterions can move only tangentially to the surface, any change of the counterion density must be due to those fluxes. Consequently the equation of continuity can be written as

$$\frac{\partial \sigma}{\partial t} - \text{div} (j_E + j_D) = 0 \quad (7)$$

This is a partial differential equation for σ , namely

$$\frac{\partial \sigma}{\partial t} = \frac{ukT}{R^2} \times \frac{1}{\sin \theta} \times \frac{\partial}{\partial \theta} \left\{ \sin \theta \frac{\partial \sigma}{\partial \theta} + \frac{e_0}{kT} \frac{\partial \psi_s}{\partial \theta} \sigma \sin \theta \right\} \quad (8)$$

To compare the possible energy gain of a counterion responding to the external field with the energy due to thermal movement, the quantity

$$\gamma = \frac{e_0RE}{kT} \quad (9)$$

may be introduced. For all cases discussed here

$$\gamma \ll 1 \quad (10)$$

It stands to reason that the electric field along the surface is of the same order of magnitude as the external field or even smaller, therefore the factor of $\sigma \sin \theta$ in eq. 8 is also small compared with unity

$$\left| \frac{e_0}{kT} \times \frac{\partial \psi_s}{\partial \theta} \right| = \frac{e_0R}{kT} \cdot |E_s| \approx \gamma \ll 1 \quad (11)$$

This indicates that the counterion density will deviate only little from the random distribution, that is

$$\sigma - \sigma_0 = \bar{\sigma} \ll \sigma_0 \quad (12)$$

Because of relations 11 and 12, σ_0 can be substituted for σ in the second term on the right-hand side of eq. 8. Further simplification is possible if the external field is assumed to be alternating with the angular frequency ω , so that

$$E = E_0 e^{i\omega t} \quad (13)$$

Under these circumstances one may write

$$\frac{\partial \sigma}{\partial t} = \frac{\partial \bar{\sigma}}{\partial t} = i\omega \bar{\sigma} \quad (14)$$

Using this result the equation for σ (8) takes the form

$$i\omega \bar{\sigma} = \frac{ukT}{R^2} \frac{1}{\sin \theta} \frac{d}{d\theta} \left\{ \sin \theta \frac{d\bar{\sigma}}{d\theta} + \frac{e_0\sigma_0}{kT} \sin \theta \frac{d\psi_s}{d\theta} \right\} \quad (15)$$

(14) G. Schwarz, *Z. Physik*, **145**, 563 (1956).

(15) M. Eigen and G. Schwarz, *J. Colloid Sci.*, **12**, 181 (1957).

(16) C. T. O'Konski and A. J. Haltner, *J. Am. Chem. Soc.*, **79**, 5634 (1957).

(17) G. Schwarz, *Z. physik. Chem. (Frankfurt)*, **19**, 286 (1959).

The potential ψ_s must be derived from the over-all distribution of the electric potential. The potential in the electrolyte ψ_a as well as the potential inside the sphere ψ_i has to satisfy the Laplace equation

$$\Delta\psi_a = 0 \quad (r > R) \quad (16)$$

$$\Delta\psi_i = 0 \quad (r < R) \quad (17)$$

The boundary conditions are

$$1. \quad \lim_{r \rightarrow R} \psi_a = \lim_{r \rightarrow R} \psi_i = \psi_s \quad (18)$$

$$2. \quad \psi_a \rightarrow -Er \cos \theta \text{ for } r \rightarrow \infty \quad (19)$$

$$3. \quad \psi_i \text{ must remain finite for } r \rightarrow 0 \quad (20)$$

$$4. \quad K_a \frac{\partial \psi_a}{\partial r} - K_i \frac{\partial \psi_i}{\partial r} = -i\omega \epsilon_0 \bar{\sigma} \text{ for } r \rightarrow R \quad (21)$$

The last condition results from the fact that the temporal change of the total surface density of charge depends completely upon the net influx of electrical charges perpendicular and parallel to the surface. The parallel flux is provided by the counterion motion, while the conductivities of the electrolyte and the particle are responsible for the flux in the perpendicular direction.

Now the three equations 15, 16, and 17 can be solved by standard methods. Using a representation of $\bar{\sigma}$ and ψ_s by means of Legendre polynomials $P_n(\cos \theta)$

$$\bar{\sigma} = \sum \alpha_n P_n(\cos \theta) \quad (22)$$

$$\psi_s = \sum \beta_n P_n(\cos \theta) \quad (23)$$

eq. 15 yields the following relation between the coefficients α_n and β_n of these series

$$\alpha_n = - \frac{1}{1 + i\omega \frac{R^2}{n(n+1)ukT}} \times \frac{\epsilon_0 \sigma_0}{kT} \times \beta_n \quad (24)$$

As is well known the solutions of eq. 16 and 17 can be represented as

$$\psi_a = \sum \{A_{1n} r^n + B_{1n} r^{-n-1}\} P_n(\cos \theta) \quad (25)$$

and

$$\psi_i = \sum \{A_{2n} r^n + B_{2n} r^{-n-1}\} P_n(\cos \theta) \quad (26)$$

Taking into account the above-mentioned boundary conditions as well as eq. 22, 23, and 24 we find that all but the terms with $n = 1$ vanish. Under these circumstances eq. 24 is equivalent to

$$\bar{\sigma} = - \frac{1}{1 + i\omega \tau} \times \frac{\epsilon_0 \sigma_0}{kT} \times \psi_s \quad (27)$$

where

$$\tau = \frac{R^2}{2ukT} \quad (28)$$

Thus we obtain a simple relaxation of the change in the counterion surface density. Obviously the relaxation time τ is determined by the rate of diffusion of the counterions along the particle. With

respect to the actual electric potential ψ_s on the particle surface, the relaxation of the counterion layer is always diffusion-controlled. The same is not necessarily true with regard to the applied field, since there is in general a frequency-dependent phase shift between E_s and E .

According to eq. 5 and 6 the surface current density is

$$i_s = e_0(j_E + j_D) = - \frac{e_0^2 u \sigma}{R} \frac{\partial \psi_i}{\partial \theta} - \frac{e_0 u k T}{R} \times \frac{\partial \sigma}{\partial \theta} \quad (29)$$

In the first term σ_0 may be substituted for σ and in the second term $\bar{\sigma}$ for σ . Taking advantage of eq. 27

$$i_s = - \frac{i\omega \tau}{1 + i\omega \tau} \times \lambda_0 \frac{\partial \psi_s}{R \partial \theta} = \frac{i\omega \tau}{1 + i\omega \tau} \lambda_0 E_s \quad (30)$$

The quantity

$$\lambda_0 = e_0^2 \sigma_0 u \quad (31)$$

has been called surface conductivity by O'Konski,¹⁰ who used the relation $i_s = \lambda_0 E_s$. As can be seen from eq. 30, this relation is indicated only at very very high frequencies or in cases where the diffusion effect can be neglected. In general the diffusion effect results in a phase shift between current and field on the surface. Thus λ_0 can be replaced by a complex surface conductivity

$$\lambda = \frac{i\omega \tau}{1 + i\omega \tau} \lambda_0 \quad (32)$$

It appears to be more suitable, however, to represent the current-field correlation by a surface dielectric constant ϵ_s^* instead of a surface conductivity, so that

$$\epsilon_s^* = \frac{1}{1 + i\omega \tau} \times \frac{\lambda_0 \tau}{\epsilon_r} \quad (33)$$

The electric potentials ψ_a and ψ_i , as evaluated from the above-mentioned system of equations, can now be written

$$\psi_a = -Er \cos \theta + \frac{\bar{K}_i - K_a}{\bar{K}_i + 2K_a} R^3 E \frac{\cos \theta}{r^2} \quad (r \geq R) \quad (34)$$

$$\psi_i = - \frac{3K_a}{2K_a + \bar{K}_i} Er \cos \theta \quad (r \leq R) \quad (35)$$

where

$$\bar{K}_i = K_i + i\omega \epsilon_r \frac{2\epsilon_s^*}{R} \quad (36)$$

ψ_i becomes ψ_s by merely substituting R for r . Evidently the dielectric behavior of the sphere with the counterion layer is identical with that of a sphere without such a layer but an apparent dielectric constant

$$\bar{\epsilon}_i = \epsilon_i + \frac{2\epsilon_s^*}{R} \quad (37)$$

The additional dielectric constant

$$\Delta\epsilon_i = \frac{2\epsilon_s^*}{R} = \frac{1}{1 + i\omega\tau} \frac{e_0^2 R \sigma_0}{\epsilon_r k T} \quad (38)$$

may rise far above the actual dielectric constant ϵ_i .

The Dielectric Behavior of a Suspension of Spheres with a Counterion Layer.—If p is the volume concentration of spheres with a complex conductivity \bar{K}_i suspended in material of complex conductivity K_a , the complex conductivity K of the system can be evaluated from the relation^{3,18}

$$\frac{K - K_a}{K + 2K_a} = p \frac{\bar{K}_i - K_a}{\bar{K}_i + 2K_a} \quad (39)$$

This equation was essentially derived by Maxwell¹⁹ for small values of p but has been found useful even for a fairly high volume concentration. The theoretical determination of K by means of eq. 39 can be eased if we assume a fairly well conducting electrolyte with

$$\kappa_a \gg \frac{\lambda_0}{R} \quad (40)$$

Since ϵ_i and κ_i are much smaller than ϵ_a and κ_a , respectively, this relation is equivalent to

$$|\bar{K}_i| \ll |K_a| \quad (41)$$

Under these circumstances K follows from eq. 39 as

$$K = \frac{1-p}{1+\frac{p}{2}} K_a + \frac{9}{4} \frac{p}{\left(1+\frac{p}{2}\right)^2} \bar{K}_i \quad (42)$$

This expression deviates from the complex conductivity K_∞ due to the simple Maxwell-Wagner effect only by the term \bar{K}_i in place of K_i . Thus

$$K - K_\infty = \frac{9}{4} \frac{p}{\left(1+\frac{p}{2}\right)^2} (\bar{K}_i - K_i) \quad (43)$$

is the additional complex conductivity resulting from the polarization of the counterion layer. It is suitable, however, to transform this relation into the corresponding equation for complex dielectric constants

$$\epsilon^* = \epsilon' - i\epsilon'' \quad (44)$$

where ϵ' is the real dielectric constant ϵ , and ϵ'' is the dielectric loss $\kappa/\epsilon_r\omega$, κ being the ohmic conductivity. Taking into account eq. 36 and 38, we obtain for the complex dielectric increment

$$\epsilon^* - \epsilon_\infty^* = \Delta\epsilon^* = \frac{\Delta\epsilon_0}{1 + i\omega\tau} \quad (45)$$

with the static dielectric increment

$$\Delta\epsilon_0 = \frac{9}{4} \frac{p}{\left(1+\frac{p}{2}\right)^2} \frac{e_0^2 R \sigma_0}{\epsilon_r k T} \quad (46)$$

$\Delta\epsilon^*$ displays a simple Debye-type dispersion and the characteristic frequency

$$f = \frac{1}{2\pi\tau} = \frac{ukT}{\pi R^2} \quad (47)$$

The counterion surface mobility u should be smaller than the mobility u_0 in free solution. In general the counterion motion along the surface is subject to an additional activation energy α , so that

$$u = u_0 e^{-\alpha/kT} \quad (48)$$

This activation energy α is of electrostatic origin. Since the fixed charges on the surface of the sphere are discretely distributed, the electric potential is changing periodically parallel to the surface. A counterion within the double layer must overcome potential barriers in order to follow an applied electric field. The height of the potential wall multiplied by the charge of a counterion yields the additional activation energy α . Generally the minimum distance δ between an individual counterion and its counter charge on the surface can be assumed to be at least several times smaller than the distance between the surface charges. In this case

$$\alpha \approx \frac{e_0^2}{\epsilon_a \delta} \quad (49)$$

For a δ of a few Angstrom units this equation yields an activation energy α of the order of magnitude of 1 kcal./mole.

Activation Energy Distribution and the Relaxation Spectrum.—On account of eq. 48, we can write the relaxation time τ (eq. 28 and 47) as

$$\tau = \tau_0 e^{\alpha/kT} \quad (50)$$

with

$$\tau_0 = \frac{R^2}{2u_0 k T} \quad (51)$$

If the suspended particles are not of uniform size, a relaxation spectrum according to the particle size distribution will occur. The resulting dispersion curves are flatter than those corresponding to a single relaxation time. However, as shown by experimental evidence, a relaxation spectrum may exist even in the case of particles of uniform size where all counterions are of the same kind. This discrepancy between our model theory and the experimental data simply may be due to the mathematical simplification of the problem. A more rigorous theoretical treatment of the diffusion-controlled relaxation of the counterion atmosphere possibly may result in a relaxation spectrum. Such an idea is suggested in view of the relaxation

(18) K. S. Cole, *J. Gen. Physiol.*, **12**, 29 (1928).

(19) J. C. Maxwell, "A Treatise on Electricity and Magnetism (1873)," Oxford Univ. Press, article 314.

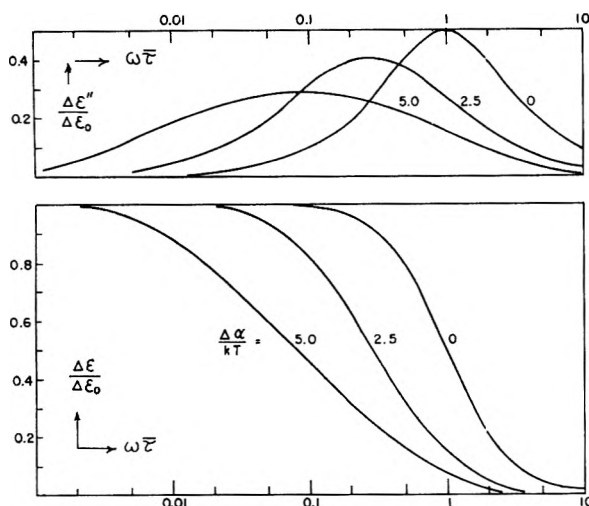


Fig. 1.—Effect of a statistical distribution of activation energies over a range $\Delta\alpha$ on the dispersion curves ($\bar{\tau}$ = relaxation time corresponding to the minimum activation energy $\bar{\alpha}$).

spectrum found for the ionic cloud of simple ions.^{20,21} But the mechanism which is responsible for the relaxation spectrum will not be discussed here. Only a formal extension of the theory outlined above will be given in order to describe the experimental dispersion curves. This extension can only be done by a superposition of independent relaxation steps due to counterions with different activation energies, as is obvious from eq. 50 and 51. We define a distribution function $\rho(\alpha)$, so that there are in the mean

$$d\sigma_0 = \sigma_0 \rho(\alpha) d\alpha \quad (52)$$

counterions per unit area which are subject to an activation energy between α and $\alpha + d\alpha$. Then the relation

$$\int_0^\infty \rho(\alpha) d\alpha = 1 \quad (53)$$

must hold. Now the total complex dielectric increment is derived simply from eq. 45 by integrating over the distribution of activation energies

$$\Delta\epsilon^* = \Delta\epsilon_0 \int_0^\infty \frac{\rho(\alpha) d\alpha}{1 + i\omega\tau_0 e^{\alpha/kT}} \quad (54)$$

Since the static dielectric increment $\Delta\epsilon_0$ is not affected by the activation energy, it is unchanged (eq. 46). Naturally the function must be known in order to evaluate eq. 54 rigorously. However, the shape of the distribution curve is not very crucial with regard to the result of the integration. For example, it has been shown by Schwann⁵ that several distribution functions which are symmetrical when plotted *vs.* $\ln \tau$ (which is proportional to α in our case) yield almost identical dispersion curves. Hence for practical purposes we use a function $\rho(\alpha)$ which is a constant in an activation energy range from $\bar{\alpha}$ up to a maximum $\bar{\alpha} + \Delta\alpha$, but is zero otherwise. Because of eq. 53 the constant has to be $1/\Delta\alpha$. Then if

(20) P. Debye and H. Falkenhagen, *Z. Elektrochem.*, **54**, 562 (1928).
 (21) M. Eigen, *Discussions Faraday Soc.*, **24**, 24 (1957).

$$\xi = \epsilon^{-(\alpha-\bar{\alpha})/kT}, \quad \xi_0 = e^{-\Delta\alpha/kT} \quad (55)$$

and

$$\bar{\tau} = \tau_0 e^{\bar{\alpha}/kT} \quad (56)$$

eq. 54 gives

$$\Delta\epsilon^* = \frac{\Delta\epsilon_0}{\ln \xi_0^{-1}} \int_{\xi_0}^1 \frac{d\xi}{\xi + i\omega\bar{\tau}} = \frac{\Delta\epsilon_0}{\ln \xi_0^{-1}} \ln \frac{1 + i\omega\bar{\tau}}{\xi_0 + i\omega\bar{\tau}} \quad (57)$$

Separating the real and the imaginary part of this expression, we obtain for the dielectric increment

$$\Delta\epsilon = \frac{\Delta\epsilon_0}{2 \ln \xi_0^{-1}} \ln \frac{1 + \omega^2\bar{\tau}^2}{\xi_0^2 + \omega^2\bar{\tau}^2} \quad (58)$$

and for the increment of the dielectric loss

$$\Delta\epsilon'' = \frac{\Delta\epsilon_0}{\ln \xi_0^{-1}} \tan^{-1} \frac{(1 - \xi_0)\omega\bar{\tau}}{\xi_0 + \omega^2\bar{\tau}^2} \quad (59)$$

Dispersion curves of this kind are shown in Fig. 1 for several values of $\Delta\alpha/kT$. With increasing width $\Delta\alpha$ of the activation energy range, they flatten out and differ more and more from the Debye-type curves ($\Delta\alpha = 0$). Simultaneously there is a decrease of the characteristic frequency f defined as the frequency for which $\Delta\epsilon = 1/2\Delta\epsilon_0$. This behavior also is shown by the relation

$$f = \frac{1}{2\pi\bar{\tau}} \sqrt{\xi_0} = \frac{1}{2\pi\bar{\tau}} e^{-\Delta\alpha/2kT} \quad (60)$$

as evaluated from eq. 58.

The maximum of the dielectric loss $\Delta\epsilon''$ always is found at the characteristic frequency, but its absolute magnitude declines for increasing values of $\Delta\alpha$ while the shape of the curve becomes broader. The quantitative relation

$$\frac{\Delta\epsilon''}{\Delta\epsilon_0} = \frac{2 \tan^{-1} \frac{1 - \xi_0}{\sqrt{\xi_0}}}{\ln \xi_0^{-1}} \quad (61)$$

as derived from eq. 58 and 59 is presented in Fig. 2 as a function of $\ln \xi_0^{-1} = \Delta\alpha/kT$. This curve can be used to determine $\Delta\alpha$ from measurements of $\Delta\epsilon$ and $\Delta\epsilon''$.

The quantity $\Delta\alpha$, which characterizes the width of the relaxation spectrum, can be determined even if only one of the dispersion curves (either that for $\Delta\epsilon$ or that for $\Delta\epsilon''$) has been measured. Since the degree of flattening depends on $\Delta\alpha$, one has to find out which value of ξ_0 in eq. 58 or 59, respectively, best fits the measured curve. For this purpose it is suitable to express $\bar{\tau}$, according to eq. 60, by a mean relaxation time

$$\tau_m = \frac{1}{2\pi f} = \frac{\bar{\tau}}{\sqrt{\xi_0}} \quad (62)$$

because f and therefore τ_m can be obtained experimentally from either curve in a very simple way. Equations 58 and 59 then are written

$$\Delta\epsilon = \frac{\Delta\epsilon_0}{2 \ln \xi_0^{-1}} \ln \frac{\xi_0^{-1} + \omega^2 \tau_m^2}{\xi_0 + \omega^2 \tau_m^2} \quad (63)$$

$$\Delta\epsilon'' = \frac{\Delta\epsilon_0}{\ln \xi_0^{-1}} \tan^{-1} \frac{1 - \xi_0}{\sqrt{\xi_0}} \frac{\omega \tau_m}{1 + \omega^2 \tau_m^2} \quad (64)$$

Discussion

The theory presented in this paper has been developed on the basis of a model which is to a certain extent rather crude. Nevertheless the experimental data can be interpreted surprisingly well in the light of this theory. On the assumption of reasonable values for the basic parameters, *i.e.*, the counterion surface density σ_0 and the activation energy α , the theoretical results agree more than satisfactorily with the measurements.

Sufficient experimental data for a qualitative and quantitative test of the theoretical results can be found in the article of Schwan, *et al.*³ The suspensions of polystyrene spheres used by these authors are most suitable for our purpose because the colloidal particles are non-polar spheres of extremely uniform and well known size. We shall discuss in particular the measurements carried out with polystyrene spheres in KCl solution. The diameters were either 1.17 or 0.557 μ . Experimental results for various concentrations of the polystyrene and the electrolyte, respectively, are shown in Fig. 8, 9, 10, and 11 of the mentioned article.

In order to apply the theory to a colloidal system, the electrolyte has to be fairly well conducting in accordance with relation 40. In fact, this inequality is generally satisfied in the case of the suspensions which are to be discussed. The quantity λ_0 can be determined from the conductivity of the system at higher frequencies (where $\lambda \rightarrow \lambda_0$ according to eq. 32). With regard to the previous investigation,³ λ_0 has to be interpreted as the high frequency limit of the frequency-dependent part of the surface conductance (see footnote 23). It always has been found in the order of magnitude of 10^{-9} mho.^{3,4} Moreover we can estimate λ_0 by means of eq. 31, using a result of Sieglaff and Mazur.²² From electrophoretic measurements these authors determined the density of charge units on the surface of polystyrene spheres in a comparable system to be 1.9×10^{13} cm.⁻². Thus we may reasonably assume a σ_0 in the order of magnitude of 10^{13} cm.⁻². With potassium ions as the counterions, the calculation likewise yields a λ_0 around 10^{-9} mho. Hence for the particle sizes of interest, λ_0/R has to be expected to be in the order of magnitude of 10^{-5} mho/cm. This value is indeed well below the conductivity of the electrolyte solution in virtually all the suspensions in consideration.

Now we may compare the experimental results with the theoretical equations. Below about $p = 15\%$ the measured values of the static dielectric increment $\Delta\epsilon_0$ for the 1.17 μ sample, as shown in Fig. 10 of ref. 3, are in good agreement with eq. 46 if the counterion surface density is set as $\sigma_0 = 2.0 \times 10^{13}$ cm.⁻² for $\kappa_a = 0.7$ mmho/cm. and $\sigma_0 = 1.5 \times 10^{13}$ cm.⁻² for $\kappa_a = 1.4$ mmhos/cm. In view of the above remarks on λ_0 and σ_0 , these

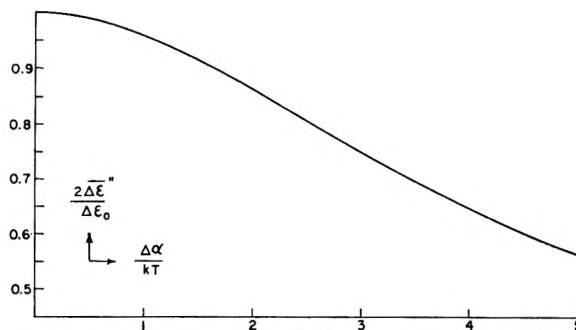


Fig. 2.—Effect of the activation energy distribution on the ratio of the maximum increment of the dielectric loss and the low-frequency limit of the dielectric increment.

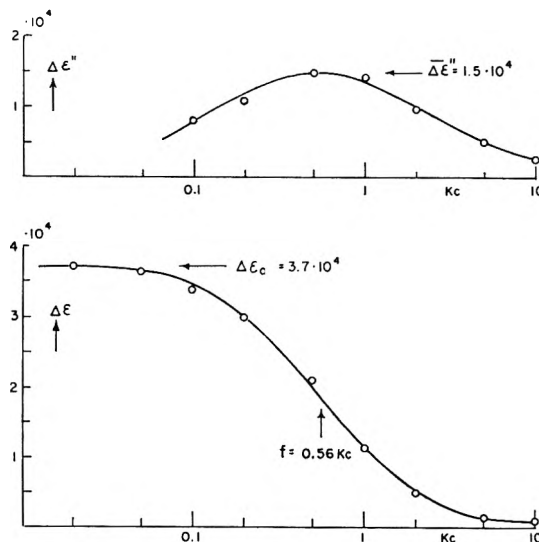


Fig. 3.—Low-frequency dielectric dispersion of $\Delta\epsilon$ and $\Delta\epsilon''$ as measured with a special sample: $2R = 1.17 \mu$, $p = 22\%$, $K_a = 0.81$ mmho/cm. (KCl). The curves are computed theoretically with $\bar{\alpha} = 0$, $\Delta\alpha = 2.6 kT$.

σ_0 values obviously are very reasonable. At higher volume concentrations the measured dielectric increments exceed those computed from eq. 46 with the same σ_0 as before. However, since the basic eq. 39 has been proven only for small values of p , a disagreement between experiment and theory in this range of p is not surprising. Moreover, the quantity σ_0 may become a function of p here; thus the deviations between measurement and theory could be due also to an increase of σ_0 with increasing volume concentration. Such an interaction effect is not unlikely in view of the fact that other parameters of the suspension evidently affect the surface density of the counterions. This is shown with regard to the electrolyte concentration (conductivity) by the fact that it was necessary to use different values of σ_0 for different electrolyte conductivities. There are also indications of a slight dependence of σ_0 on the particle diameter, since according to Fig. 11 of ref. 3 the initial slope $\Delta\epsilon_0/p$ is not an exact linear function of R as it should be for a σ_0 independent of the diameter. Strictly speaking the counterion density σ_0 which appears in the theory represents only the ions bound to the particle surface, that is the "undissociated" counterions in contrast to the "dissociated" ones in free solution.²³ The degree

of "dissociation" and thereby σ_0 may well depend on the parameters κ_a , p , and R . Fortunately the previous assumption of a zero net charge of the double layer is not crucial here, so it may be dropped in compliance with this picture. An adequate extension of the basic theory will be discussed in a future paper.

An especially good agreement between our theory and the experiments is encountered in the case of the characteristic frequency f . Even the simple eq. 47 yields a proportionality to the inverse square of the radius of the particles, exactly as found experimentally (Fig. 9 of ref. 3). Furthermore it yields the quantitative results of the measurements by employing a counterion mobility $u = 1.35 \times 10^8$ c.g.s. units. Since the u_0 -value for a potassium ion in water at 25° is 5×10^8 c.g.s. units, an activation energy $\alpha = 1.3 kT = 0.8$ kcal./mole has to be assumed. This agrees very well with the estimation in the discussion of eq. 49. The successful interpretation of the characteristic frequency is not affected if an activation energy distribution is introduced in order to account for the shape of the dispersion curves. Then we have to use eq. 60 for the characteristic frequency f . The activation energy range $\Delta\alpha$ can be obtained from the measured ratio $2\Delta\epsilon''/\Delta\epsilon_0 \approx 0.8$. According to Fig. 2 that results in $\Delta\alpha = 2.6 kT$. With an $\bar{\alpha} = 0$, that is $\bar{\tau} = \tau_0$, eq. 60 results in the same quantitative relation as eq. 47. Dispersion curves computed on the assumption of such an activation energy distribution fit the experimental data very well as demonstrated by a set of measured curves in Fig. 3. According to eq. 49 the upper limit of the activation energy $\Delta\alpha = 2.6 kT \approx 1.5$ kcal./mole corresponds to a minimum distance between opposite charges of $\delta = 3.0 \times 10^{-8}$ cm., obviously a very reasonable value.

In view of the very encouraging results obtained

(23) According to Cole,²⁴ Fricke and Curtis,⁴ and Schwan, *et al.*,³ the surface conductance of a colloidal particle is composed of two parts; one is frequency independent while the other one depends upon the frequency. The latter one apparently is due to the counterions which are "undissociated." The frequency independent part of the surface conductance causes virtually no dielectric dispersion in the cases of interest here³ and is not discussed in this paper.

(24) K. S. Cole, *Cold Spring Harbor Symp. Quant. Biol.*, **1**, 1 (1933).

in comparing the experimental data with the theory, we may well conclude that the basic model of the colloidal particle used in this paper is essentially true. That means a diffusion-controlled polarization of a counterion layer around the colloidal particles is responsible for the low frequency dielectric dispersion under consideration. Particularly striking evidence for this conclusion is furnished by the following facts: (1) The characteristic frequency can be excellently expressed by the diffusion time of a counterion around the particle. (2) A very reasonable value of the counterion density on the surface of the particle results in a quantitative explanation of the increment of the dielectric dispersion.

Outlook

The theory as presented in this paper has been applied only to a special type of colloidal system. However, there can be no doubt that the basic effect of the polarization of the counterion layer is of significance for all kinds of systems including those in the biological field, where ion layers on interfaces are involved. Obviously there are no essential difficulties in extending the theory to the more general case of suspensions of spherical particles with no restrictions concerning the electrical properties of the spheres and the surrounding medium. Furthermore, the theoretical considerations are suitable to be adapted to more complicated colloidal particles which may be shaped like ellipsoids or carrying a non-conductive shell. Particles of the latter kind are of special biological interest, since they represent the living cell with its cell wall. Investigations dealing with all these generalizations for the fundamental theory, as well as with the question of how the density σ_0 and the mobility u of the counterions in the double layer depend on the structure of the system, are in progress. They are to be discussed in future articles.

Acknowledgment.—The author wishes to thank Dr. H. P. Schwan for many interesting and valuable discussions concerning the subject of this paper.

HYDROGEN BONDING IN β -NITRO ALCOHOLS. II. ASSOCIATION IN SOLUTION^{1,2}

BY H. E. UNGNADE, E. D. LOUGHRAN, AND L. W. KISSINGER

University of California, Los Alamos Scientific Laboratory, Los Alamos, New Mexico

Received April 28, 1962

Infrared absorption spectra of β -nitro alcohols $R_2C(NO_2)CH_2OH$ (where $R = CH_3$ and NO_2) show them to be largely monomeric in dichloromethane but partially associated in carbon tetrachloride. The nitro group exerts a strong influence on the association, changing the association number from three in neopentyl alcohol to a value near two in the nitro alcohols. The association constants of the nitro alcohols in carbon tetrachloride increase with the number of nitro groups, indicating that the tendency for hydrogen bonding in these compounds is related to the electron deficiency on the hydroxyl carbon.

Introduction

It has been established recently¹ that β -nitro alcohols and diols have predominantly monomeric hydroxyl absorption in dichloromethane and carbon tetrachloride. The diols particularly, however, are so insoluble in the latter solvent that it has not been possible to investigate more concentrated solutions where bonded species might be expected.³ For this reason the more soluble monohydric β -nitro alcohols $R_2C(NO_2)CH_2OH$ have been re-examined in dichloromethane and carbon tetrachloride in more concentrated solutions and compared with the structurally related neopentyl alcohol.

Experimental⁴

Materials.—2-Methyl-2-nitropropanol was prepared from 2-nitropropane and paraformaldehyde⁵ and melted at 91–92° (lit. m.p. 82°).⁵

Anal. Calcd. for $C_4H_9NO_2$: C, 40.34; H, 7.61; N, 11.76. Found: C, 40.66, 40.60; H, 8.41, 7.69; N, 11.74.

Commercial neopentyl alcohol melted at 52–53° and was sufficiently pure for the spectral measurements.

Anal. Calcd. for $C_5H_{12}O$: C, 68.15; H, 13.71. Found: C, 67.96; H, 13.82.

The other compounds have been described previously.¹

Measurements.—Infrared absorption spectra were determined at 25° with a Model 21 Perkin-Elmer infrared spectrophotometer with a sodium chloride prism in matched sodium chloride liquid sealed cells of 0.1 and 0.05 cm. length and quartz cells of 1 cm. length against pure solvent in the reference beam. The spectrophotometer was operated at slit schedule 984, response 1, gain 4.5, speed 2, and suppression 0 and the curves were recorded on the scale $1 \mu = 5 \text{ cm.}$ from 2–15 μ .

Solutions were made up from weighed amounts of alcohols and pure solvents in 10-ml. volumetric flasks and diluted by pipetting 5 ml. into 10-ml. flasks and filling to the mark with solvent. The solutions were stable and the readings reproducible.

Absorbance values were determined by the base line technique⁶ and limited to instrumental readings between 0.08 and 0.8. In view of instrumental limitations the ϵ values should be regarded as "apparent" molar absorptivities.

Results

The β -nitro alcohols have little tendency to associate in dichloromethane, probably due to interaction with the solvent. 2,2-Dinitropropanol,

for instance, has a single strong band at 2.78 μ . This band as well as the as-nitro band at 6.36 μ remains unchanged when the solution contains one equivalent of concentrated sulfuric acid (Fig. 1).⁷

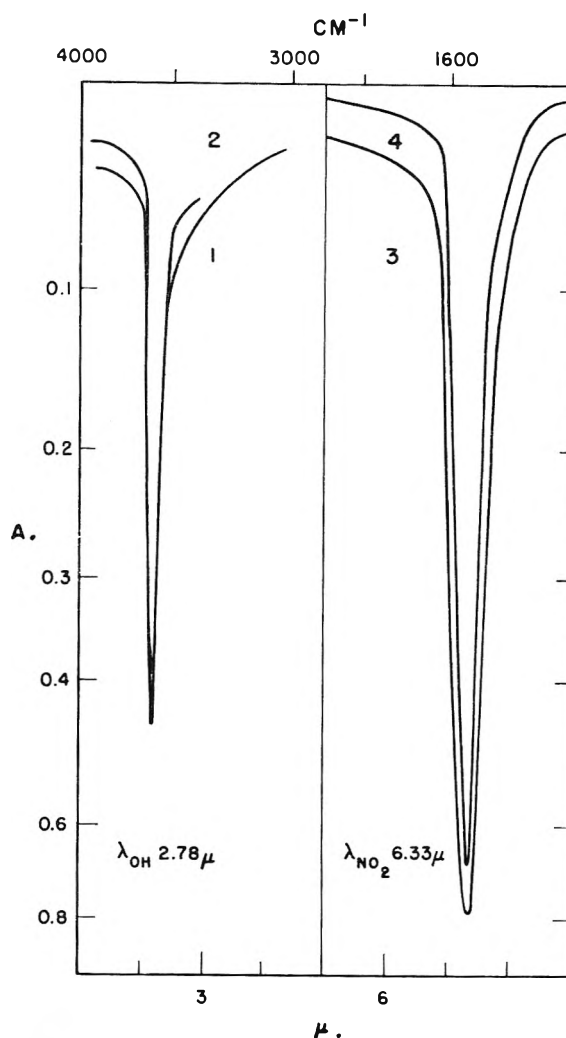


Fig. 1.—Infrared absorption bands for 2,2-dinitropropanol in dichloromethane: (1) 0.1 *N* alcohol; (2) 0.1 *N* alcohol and 0.1 *N* sulfuric acid; (3) 0.025 *N* alcohol; (4) 0.025 *N* alcohol and 0.025 *N* sulfuric acid, all in 0.05-cm. cells.

(1) Paper I, H. E. Ungnade and L. W. Kissinger, *Tetrahedron*, in press.

(2) This work was performed under the auspices of the U. S. Atomic Energy Commission.

(3) Z. Eckstein, P. Gluzinsky, W. Sobotka, and T. Urbanski, *J. Chem. Soc.*, 1370 (1961).

(4) Microanalyses by M. Naranjo. All temperatures are corrected.

(5) L. Henry, *Bull. soc. chim. France*, [3] 13, 1002 (1895).

(6) J. J. Heigl, M. F. Bell, and J. U. White, *Anal. Chem.*, 19, 293 (1947).

(7) It has been proposed by A. Nielsen and H. Feuer (Symposium on Nitro Aliphatic Chemistry at West Lafayette, Ind., May 26, 1961) that certain β -nitro alcohols can form internally hydrogen-bonded protonated species in solutions. The present evidence would indicate that such bonding does not occur in 2,2-dinitropropanol in 0.1 *N* solutions.

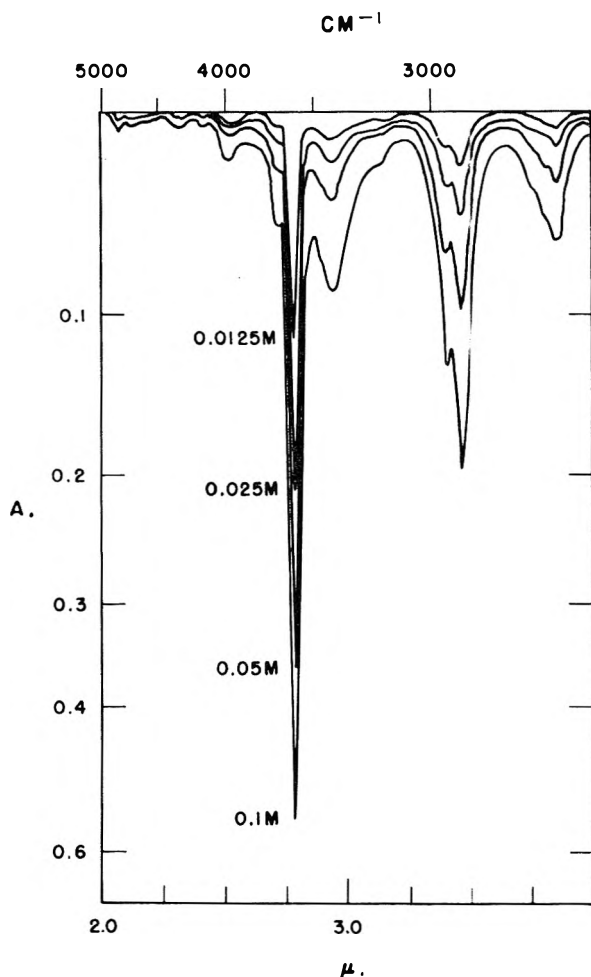


Fig. 2.—Infrared absorption bands of trinitroethanol in carbon tetrachloride (0.1-cm. cells).

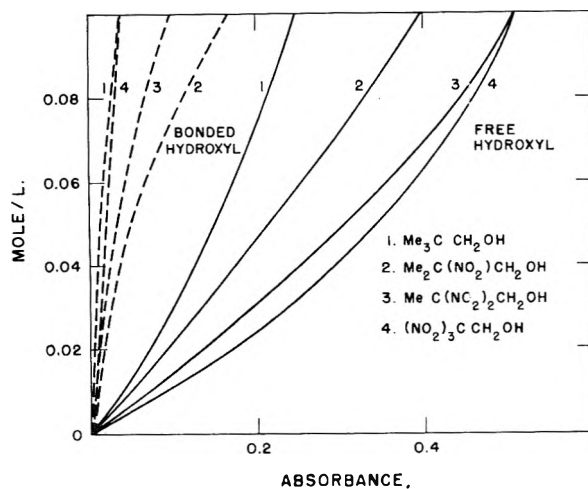


Fig. 3.—Absorbance of hydroxyl bands of alcohols in carbon tetrachloride (0.1-cm. cells).

Only trinitroethanol has a small band for bonded hydroxyl at 2.97μ in more concentrated solutions ($\geq 0.1 M$). In dilute solutions Beer's law holds for hydroxyl as well as nitro bands and it therefore is possible to calculate molar absorptivities (Table I). The structurally related neopentyl alcohol, on the other hand, has both monomer and

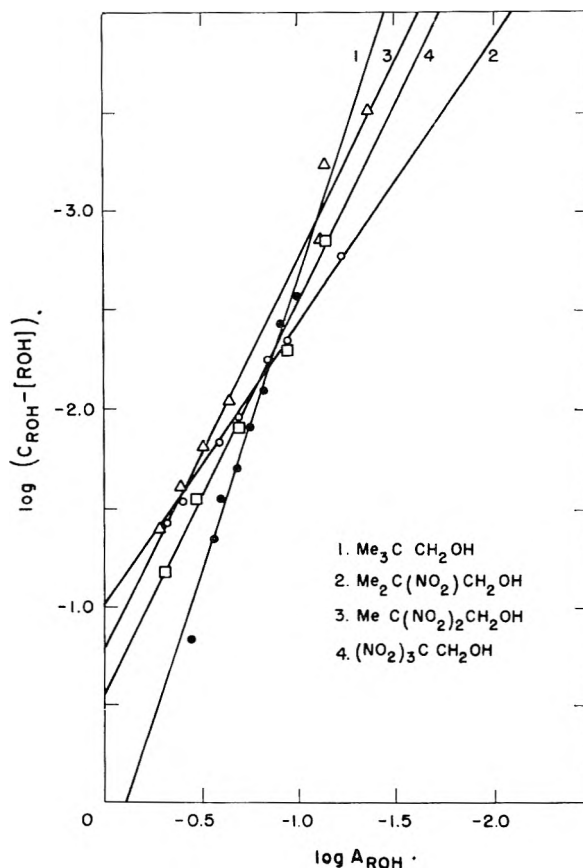


Fig. 4.—Plot of log of analytical concentration of alcohol minus monomeric alcohol concentration against log absorbance of monomeric hydroxyl for the four alcohols.

bonded hydroxyl in $0.1 M$ solution and is monomeric only in higher dilution. To account for this difference in the behavior of the nitro alcohols it is assumed that one or two nitro groups can inhibit association, as was observed previously.¹ The magnitude of the absorption intensity for *as*-nitro groups is in agreement with published values for related compounds.³

TABLE I

INFRARED ABSORPTION BANDS OF ALCOHOLS IN DICHLOROMETHANE^a

Alcohol	λ_{OH}	ϵ	λ_{as-NO_2}	ϵ	λ_{s-NO_2}	ϵ
CMe_3CH_2OH	2.77^b	52
$CMe_2(NO_2)CH_2OH$	2.77	65	6.46	335	7.41	93
$CMe(NO_2)_2CH_2OH$	2.78	90	6.36	840	7.54	160
$C(NO_2)_3CH_2OH$	2.78^c	125	6.23	1060	7.67^d	300

^a Determined in 0.1-cm. cells except as noted. ^b Bonded hydroxyl absorption occurs in concentrated solutions at 2.86μ . ^c Weak bonded hydroxyl absorption can be observed in $0.1 M$ solution at 2.97μ . ^d Because of solvent absorption the intensity of this band was determined in thinner cells.

Carbon tetrachloride solutions of neopentyl alcohol exhibit the characteristic bands of primary alcohols in the OH-stretching region at 2.74 , 2.84 , and 2.96μ , which have been assigned to monomer, trimer (or tetramer), and polymeric hydroxyl

(8) C. E. Grabiell, D. E. Bisgrove, and L. B. Clapp, *J. Am. Chem. Soc.*, **77**, 1293 (1955).

TABLE II
INFRARED ABSORPTION BANDS OF ALCOHOLS IN CARBON TETRACHLORIDE

Alcohol	λ_{OH}	ϵ^a	λ_{OH}	ϵ^b	λ_{as-NO_2}	ϵ	λ_{s-NO_2}	ϵ
$CM_e_3CH_2OH$	2.77	37.9	2.84	46.1
$CM_e_2(NO_2)CH_2OH$	2.77	57.6	2.87	94	6.46 ^c	280	7.42	90
$CM_e(NO_2)_2CH_2OH$	2.78	93.2	2.90	45.6	6.34 ^c	835	7.54	190
$C(NO_2)_3CH_2OH$	2.78	165.7	2.95	16.5	6.24	1030	7.67	316

^a Absorbance values were determined in 0.1-cm. cells except as noted. The molar absorptivities ϵ for monomeric hydroxyl were obtained from absorbance, cell length, and the concentration of monomeric alcohols, $\epsilon = A_{ROH}/[ROH]l$, which in turn was determined from the association equilibrium, the analytical concentration of the alcohol, and the association constant in the expression $K = (C_{ROH} - [ROH])/n[ROH]^n$, from which $nK[ROH]^n + [ROH] - C_{ROH} = 0$. For a rough approximation the association constant could be determined from absorbance and concentration of the most dilute solution. In the case of dimers $[ROH] = -1 \pm \sqrt{1 + 8KC_{ROH}/4K}$, while the equation for trimers was solved by trial and error iteration for various C_{ROH} values. The numerical ϵ values represent averages over the concentration range of 0.01–0.1 M. ^b The concentration of alcohol polymers was obtained from the monomer concentration, $[(ROH)_n] = C_{ROH} - [ROH]/n$, and also from the equilibrium equation $K = [(ROH)_n]/(C_{ROH} - n[(ROH)_n])^n$. The two methods were in good agreement. ^c Because of solvent absorption the intensity of this band was determined in thinner cells.

groups.⁹ In contrast the β -nitro alcohols have only two bands in this region (Fig. 2) in the concentrations investigated. The more intense band occurs at 2.77 μ in the region of monomeric hydroxyl and increases in relative intensity with dilution. The weaker band at 2.87–2.95 μ (Table II) decreases in relative intensity with dilution and is assigned to bonded hydroxyl (Fig. 3).

The degree of association of these alcohols has been determined from the plot of $\log(C_{ROH} - [ROH])$ against $\log A_{ROH}$ using the assumptions made previously (Fig. 4).¹⁰ The results (Table III) are regarded as fairly reliable since only the most precise measurements, *i.e.*, C_{ROH} and A_{ROH} , were used. Since the method assumes, however, that only cyclic polymers are present, this assumption has been further examined by determining a necessary condition for cyclic polymers: $A_{(ROH)_n}/(A_{ROH})^n = K'$. Over a limited range of concentrations the values for this expression were reasonably constant for neopentyl alcohol, 2,2-dinitropropanol, and trinitroethanol but showed large deviations for 2-methyl-2-nitropropanol (Table III). One would conclude that in the latter case the cyclic dimers probably are accompanied by dimers with terminal hydroxyl groups.

Association constants have been determined for the four alcohols from the intercepts of the linear

(9) W. C. Coburn and E. Grunwald, *J. Am. Chem. Soc.*, **80**, 1318 (1958).

(10) A. Ens and F. E. Murray, *Can. J. Chem.*, **35**, 161 (1957); R. Mecke, *Discussions Faraday Soc.*, **9**, 161 (1950). In the present investigation ROH signifies monomeric alcohol, C the analytical concentration, and $(ROH)_n$ polymeric alcohol. The spectroscopic nomenclature corresponds to the recommendations of the Hughes Committee, H. K. Hughes, *et al.*, *Anal. Chem.*, **24**, 1349 (1952).

TABLE III

ASSOCIATION CONSTANTS OF ALCOHOLS IN CARBON TETRACHLORIDE

Alcohol	$\lambda_{(ROH)_n}$	n^a	$A_{(ROH)_n}/(A_{ROH})^n$	K^c
$CM_e_3CH_2OH$	2.84	3.0	2.97 ± 0.7	30.0
$CM_e_2(NO_2)CH_2OH$	2.87	1.5	0.57 ± 0.4^d	0.9
$CM_e(NO_2)_2CH_2OH$	2.90	2.0	$.40 \pm .07$	5.9
$C(NO_2)_3CH_2OH$	2.95	2.0	$.21 \pm .07$	33.5

^a Association number = slope of linear plot of $\log(C_{ROH} - [ROH])$ vs. $\log A_{ROH}$. ^b Average value from seven solutions including the concentration range of 0.02 to 0.1 M. ^c The intercept from the linear plot of $\log(C_{ROH} - [ROH])$ against $\log A_{ROH}$ is $\log nK - n \log \epsilon_{ROH}$. ^d The large deviations from the constant indicate that terminal hydroxyl probably is present also. Since $A_{(ROH)_n}/(A_{ROH})^2 = 1.03 \pm 0.08$ the main species may be dimers.

plots of $\log(C_{ROH} - [ROH])$ against $\log A_{ROH}$.¹⁰ The value for 2-methyl-2-nitropropanol (Table III) should be regarded as approximate because the monomer hydroxyl band probably measures not only monomeric alcohol as in the other cases but also terminal hydroxyl polymers. The order of magnitude for the constant probably is correct.

The replacement of one methyl in neopentyl alcohol by a nitro group has a remarkable effect. It reduces the association number and thus changes the type of bonded species. Simultaneously it causes a large decrease in the value of the association constant, *i.e.*, it affects also the degree of association, which is regained only by further introduction of nitro groups. The formation of cyclic alcohol dimers evidently is promoted by an electron deficiency on the hydroxyl carbon.

THERMAL INITIATION OF EXPLOSIVES¹

BY JOHN ZINN AND R. N. ROGERS

*University of California, Los Alamos Scientific Laboratory, Los Alamos, New Mexico**Received May 3, 1962*

Theoretical calculations are described which pertain to the behavior of explosives when heated under known conditions of confinement. Effects of depletion and pressure buildup are explicitly considered. The results are capable of generalization to a large class of reactive materials of which explosives are a special case. Experiments are described wherein confined samples of several common explosives have been heated and their times to explosion recorded. The measurements are compared with two previously published sets of data, and the results are shown to be consistent if geometry effects are properly considered. All three groups of data are in agreement with the calculations. Explosion time data are used (in Appendix A) to derive reaction rate parameters for TNT.

Introduction

Previously published data on the thermal initiation of explosives²⁻⁴ have pointed out a strong dependence of induction times on experimental geometry, and it has been shown that such a dependence is to be expected on theoretical grounds.² The data reported herein are found to correlate with the previous data in the expected manner. However, an important purpose of the present experiments has been to study the temperature dependence of explosion times at relatively low temperatures, and here the results have not been entirely as anticipated. In order to interpret the data it has been necessary to extend the theoretical model to take account of the pressure in the sample and also to account for the depletion of reactants as a reaction proceeds.

If a reactive material is heated or cooled, and if it simultaneously decomposes by a single first-order rate process, then variations of temperature and concentration within the sample will be described by the equations

$$\frac{\partial T}{\partial t} = k\nabla^2 T + \frac{QZ}{C} w e^{-E/RT} \quad (1)$$

$$\frac{\partial w}{\partial t} = -Z w e^{-E/RT} \quad (2)$$

Here T is the temperature at time t , w is the mass fraction of undecomposed reactant at any point, k is the thermal diffusivity in cm^2/sec ., Q is the heat of reaction per gram, C is the specific heat, Z is the "collision number," and E/R is the activation temperature. It will be assumed that the quantities k , Q/C , Z , and E/R are constant.

For configurations having one-dimensional, cylindrical, or spherical symmetry, the Laplacian operator, ∇^2 , takes the form

$$\frac{\partial^2}{\partial x^2} + \frac{m}{x} \frac{\partial}{\partial x}$$

where $m = 0$ for the one-dimensional system, 1 for cylinders, and 2 for spheres. We assume that initially the temperature is everywhere equal to a constant, T_0 , and w is everywhere equal to 1. The boundary condition will be taken to be $T = T_1$

= a constant at the surface or surfaces defined by $|x| = a$. This is intended to represent a physical process such as the sudden immersion of a sample whose temperature is T_0 initially into a Wood's metal bath at the temperature T_1 .

For pure explosives the quantity Q/C is frequently of the order of 10^3 degrees, and in many cases, therefore, a large temperature increase can result from a very small amount of chemical reaction. Under these circumstances the thermal behavior of the system prior to explosion can be described adequately by the first equation alone, with w set equal to unity; *i.e.*, a zero-order reaction can be assumed. In a previous paper,² certain numerical solutions to eq. 1 were described for $w = 1$, and these were shown to be consistent with experimental data then available. The simple zero-order reaction model is nevertheless limited in its applicability, and this paper will attempt to identify conditions under which it may or may not be a useful approximation.

The zero-order reaction model permits two useful quantities to be defined, *viz.*, a "critical temperature" and an "explosion time." The "critical temperature," T_m , is defined as a limiting value of T_1 which, if exceeded, leads to runaway exothermic reactions (thermal explosions), and, if not exceeded, leads to temperature distributions which approach, instead, certain well defined steady states.⁵ The steady-state problem has been treated by Frank-Kamenetskii⁶ and Chambre,⁷ and through their analyses the critical temperature is given by

$$T_m = \frac{E/R}{\ln \frac{\tau Q Z E}{C R T_m^2 \delta}} \quad (3)$$

Here $\tau = a^2/k$, a being the radius or half-thickness of the explosive sample. δ is a dimensionless parameter equal to 3.32 for spheres, 2.00 for cylinders, and 0.88 for slabs.

In the event that T_1 exceeds T_m , an explosion takes place after a certain induction time, t_{exp} . Since in the zero-order reaction model w is assumed to be constant, T and dT/dt can increase without limit, and t_{exp} can be precisely defined as the time when this occurs. It was found² that the induc-

(1) Based on work performed under the auspices of the U. S. Atomic Energy Commission.

(2) J. Zinn and C. L. Mader, *J. Appl. Phys.*, **31**, 323 (1960).

(3) J. Wenograc, *Trans. Faraday Soc.*, **57**, 1612 (1961).

(4) H. Henkin and R. McGill, *Ind. Eng. Chem.*, **44**, 1391 (1952).

(5) We exclude from consideration those cases in which the initial temperature, T_0 , is higher than T_1 .

(6) D. A. Frank-Kamenetskii, *Acta Physicochem. URSS*, **10**, 365 (1939).

(7) P. L. Chambre, *J. Chem. Phys.*, **20**, 1795 (1952).

tion times, t_{exp} , conformed to the functional relationship

$$t_{\text{exp}}/\tau = \text{function of } (E/T_m - E/T_1) \quad (4)$$

That is, for a fixed sample geometry and fixed T_0 , the quantity t_{exp}/τ is, to a very good approximation, a function of the single variable $(E/T_m - E/T_1)$. The computed relationship between t_{exp}/τ and $(E/T_m - E/T_1)$ is as plotted in Fig. 3 of reference 2. It can be shown rigorously that t_{exp}/τ depends on only three variables, such as E , T_m , and T_1 ; however, we are unable to provide an existence proof for eq. 4.

In a real physical situation, the amount of undecomposed explosive at any point decreases as reaction proceeds. It is commonly found that the decomposition is first order, so that the depletion process follows eq. 2. But if w is a continuously decreasing function of time, a true stationary state cannot exist, and the critical temperature is not easily defined; moreover, an "explosion" must now be carefully defined.

An explosion is most often associated with some pressure effect, such as the sudden rupture of a sample container. Therefore, before a realistic comparison between experimental and computed explosion times can be made, it is necessary to examine the relationship between the thermal processes described by eq. 1 and 2 and the buildup of pressure in the container.

Suppose that the sample has a crystal density of ρ and the sealed container is loaded to a density of D g./cc., and suppose that N moles of gaseous products are produced per gram of explosive decomposed. If the products are assumed to obey the Abel-type equation of state, $V = NRT/P + 1/\rho$, where V represents specific volume, then at an instant when a fraction $F = (1 - \bar{w})$ of the total sample has reacted, the pressure in the container will be approximately

$$P = \frac{FNRTD\rho}{\rho - D} = \frac{NRTD\rho}{\rho - D} (1 - \bar{w}) \quad (5)$$

Here \bar{w} represents the volume average of w . The container presumably will rupture at some fixed value of P , which we shall designate by P^* . Then the experimentally determined explosion time will be the time at which the pressure reaches P^* . Under many circumstances, the explosion times determined by this criterion will be in close agreement with those defined by the occurrence of a runaway exotherm. However, this is not always the case. Large differences can occur, especially at low temperatures below T_m .

It may be noted that the process causing the pressure buildup is not necessarily related in any way to a thermal explosion. It will be useful to consider the case of a material which decomposes to gaseous products without liberating or absorbing heat. The decomposition reaction will be assumed to follow eq. 2. If a sample of this material were heated, its internal temperature distributions would not be influenced by the chemical reaction, and the variations in temperature in the sample could be described by familiar heat transfer relations. The

reaction rate at each point would follow the temperature without influencing it. According to eq. 5 the sample container would "explode" when the extent of reaction, F , reached a certain value, F^* .

At low temperatures such that explosion times are much longer than τ , the chemical reaction can be regarded as approximately isothermal. Under these circumstances, eq. 2 can be integrated, and leads to the expression

$$t = \frac{-\ln \bar{w}}{Z \exp(-E/RT)} \quad (6)$$

Accordingly, the explosion time is given by

$$t_{\text{exp}} = \frac{-\ln(1 - F^*)}{Z \exp(-E/RT)} \quad (7)$$

At higher temperatures, the isothermal approximation would not apply, and the explosion times invariably would be longer than those given by eq. 7. At much higher temperatures, heat conduction would become the rate-limiting process, and chemical reaction would proceed in layerwise fashion from the surface inward.

At early times when only the surface region has been heated, the temperature distribution is approximated⁸ by

$$T = T_0 + (T_1 - T_0) \times \left[1 - \frac{2}{\sqrt{\pi}} \int_0^{(a-x)/2\sqrt{kt}} e^{-\lambda^2} d\lambda \right] \quad (8)$$

where λ is the thermal conductivity (cal. deg.⁻¹ cm.⁻¹ sec.⁻¹). If eq. 2 is approximated by

$$\frac{\partial w}{\partial t} = -Z e^{-E/RT} \quad (2')$$

and T is that given by eq. 8, then it can be shown that for a symmetric cylindrical system

$$t_{\text{exp}} = \left[\frac{3E(T_1 - T_0)F^*}{4\sqrt{\pi}RT_1^2 Z \tau \exp(-E/RT_1)} \right]^{2/3} \quad (9)$$

This formula is derived in Appendix B. For small values of F^* and high values of T , it gives a good approximation to explosion times obtained by numerical computations.

Explosion times for a wide range of temperature have been computed for one such hypothetical $Q = 0$ system, using the numerical procedure to be described in the last section. The results are plotted in Fig. 1 (curve A), along with the limiting times given by eq. 7 and 9 (curves A'₁ and A'₂).

In cases where the chemical reaction is exothermic, self-heating effects can operate, tending to increase the over-all reaction rate. Then, if other things are equal, the explosion times to be expected for a system with $Q > 0$ (exothermic) invariably are shorter than for the corresponding $Q = 0$ system. The differences, however, are in many cases small. Curve B of Fig. 1 is derived from computations of explosion times for a system that

(8) R. V. Churchill, "Modern Operational Mathematics in Engineering," McGraw-Hill Book Co., New York, N. Y., 1944.

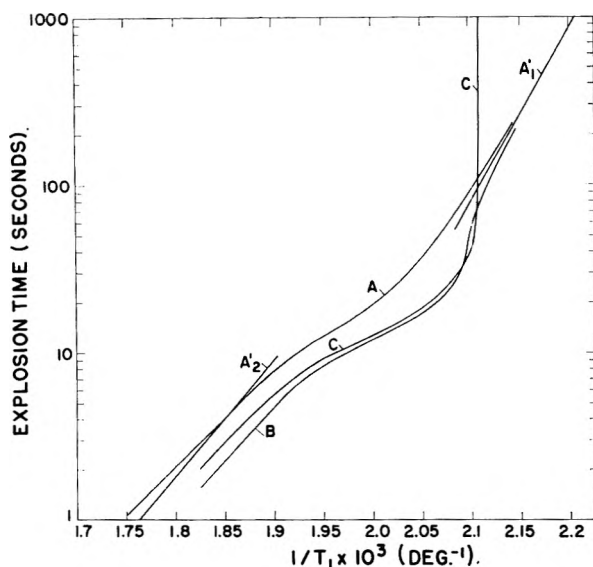


Fig. 1.—Computed explosion times for cylindrical samples with $Z = 10^{18.6} \text{ sec.}^{-1}$, $E = 47.5 \text{ kcal./mole}$, $\tau = 22.5$, and $T_0 = 298^\circ\text{K}$: curve A, first-order reaction with $Q = 0$ and $t_{\text{exp}} = \text{time when } F = 0.04$; curve A_1 , times for $F = 0.04$ for isothermal reaction; curve A_2 , times for $F = 0.04$ for zero-order reaction (high temperature limit); curve B, first-order reaction with $Q/C = 2000^\circ$ and $t_{\text{exp}} = \text{time when } F = 0.04$; curve C, zero-order reaction with $Q/C = 2000^\circ$ and $t_{\text{exp}} = \text{time of thermal explosion}$.

is identical with that of curve A except that $Q/C = 2000^\circ$ instead of 0° . For curves A, A_1 , A_2 , and B, an "explosion" is assumed to occur when $F = 0.04$.

Curve C of Fig. 1 is the explosion time curve for a system equivalent to that of curve B, except that it has a zero-order reaction ($w = \text{constant} = 1$), and an explosion is identified with a runaway exotherm. This curve was generated from the reduced explosion time curve for cylinders shown in Fig. 3, ref. 2.

Over a range of approximately 100°K ., curves A, B, and C of Fig. 1 are remarkably similar in shape and position. Therefore, within this range, self-heating and depletion effects do not play a dominant role in determining explosion times. Over much of the range, curve B is almost coincident with curve C, the zero-order reaction curve. This shows that thermal explosions are generally well under way by the time $F = 0.04$. Although at higher temperatures curve B most closely resembles curve C, below T_m the resemblance ceases, and B then approaches the $Q = 0$ curve (curve A). Below T_m , thermal explosions are impossible, and with further lowering of T_1 the influence of self heating continuously decreases. Far below T_m , the explosion time curve merges with the isothermal line, A_1 .

Geometry Effects

When the zero-order reaction model is applicable, eq. 3 and 4 provide a means of reducing to a common basis explosion time data for different explosives and different sizes of sample. According to eq. 4, if the data for all cylindrical explosive samples are plotted at t_{exp}/τ vs. $(E/T_m - E/T_1)$, the points all should fall on the theoretical curve for cylinders given in Fig. 3, ref. 2, regardless of the

size of the cylinder or the identity of the explosive. Equivalent statements apply to samples of other shapes.

The time constant, τ , is equal to a^2/k , and k is, to a satisfactory approximation, the same for all the explosives studied in this paper, having a value of about $0.00066 \text{ cm.}^2/\text{sec}$. Values of E frequently are to be found in the literature, and also can be obtained from the explosion time data in the manner shown in Appendix A. The values of T_m for a given explosive in two different geometries are related by the expression

$$\frac{1}{T_{m(2)}} = \frac{1}{T_{m(1)}} + \frac{R}{E} \left[\ln \frac{a_{(2)}^2 \delta_{(1)}}{a_{(1)}^2 \delta_{(2)}} + 2 \ln \frac{T_{m(1)}}{T_{m(2)}} \right] \quad (10)$$

where the subscripts (1) and (2) refer to the two geometries. This equation follows directly from eq. 3. There remains only to find one value of T_m for each explosive. T_m can be calculated from eq. 3 if QZ/C and E are known; however, for present purposes, we propose to obtain T_m directly from the data. The following is a convenient procedure.

If, for an explosive in a given geometry, explosion time data are available at temperatures such that $t_{\text{exp}} \approx \tau$, the value of T_1 for which $t_{\text{exp}} = \tau$ can be obtained by interpolation. According to Fig. 3, ref. 2, when $t_{\text{exp}} = \tau$, the corresponding value of $(E/T_m - E/T_1)$ (for cylinders) is 1.6. Since the appropriate T_1 is an experimental quantity and an approximate E is presumed to be known, T_m follows. The T_m for other geometries then can be obtained from eq. 10.

Experimental

Apparatus.—The experimental arrangement is similar to that of Henkin and McGill,⁴ with the important difference that the sample is tightly confined.

Procedure.—Weigh the desired sample, usually 40 mg., into a new, empty, no. 8 blasting cap shell (6.5 mm. i.d., 0.2 mm. wall thickness, copper). Insert the shell into a suitable die, and ram one 6.5 mm. gascheck (a small metal cup used to protect the base of a lead alloy bullet in reloading ammunition) part way into the shell. Place one 00 cork into the shell and ram both to the level of the sample. Place a second gascheck over the cork, and press the assembled shell to an applied force of 300 lb. (approximately 6000 p.s.i.). Eject the shell from the die, and, using a dull tubing cutter, crimp the walls of the shell just above the upper and lower gaschecks. The resulting sample depth is 0.75 to 1.0 mm., depending upon sample density and crystal habit.

As in the original method of Henkin and McGill, times to explosion are determined by dropping the samples into a Wood's-metal bath at fixed temperatures and measuring the time required for the sample cell to rupture. The temperature of the bath should be controlled to $\pm 0.25^\circ$.

Measurements of the mechanical force necessary to unseat the gas checks lead to an estimate of 15,000 p.s.i. for the failure limit of the container.

Loading densities of the samples are estimated to be approximately 90% of crystal densities.

Experimentally determined explosion times are reported herein for six pure explosives: TNT (2,4,6-trinitrotoluene), RDX (hexahydro-1,3,5-trinitro-s-triazine), HMX (octahydro-1,3,5,7-tetranitro-1,3,5,7-tetrazocine, 99.5% purity), tetryl (N-methyl-N,2,4,6-tetranitroaniline), PETN (pentaerythritol tetranitrate), and ammonium nitrate. The raw data are plotted in Fig. 2. Additional data on mixed explosives will be reported elsewhere.⁹

(9) R. N. Rogers, *Ind. Eng. Chem., Prod. Res. Dev.*, **1**, 169 (1962).

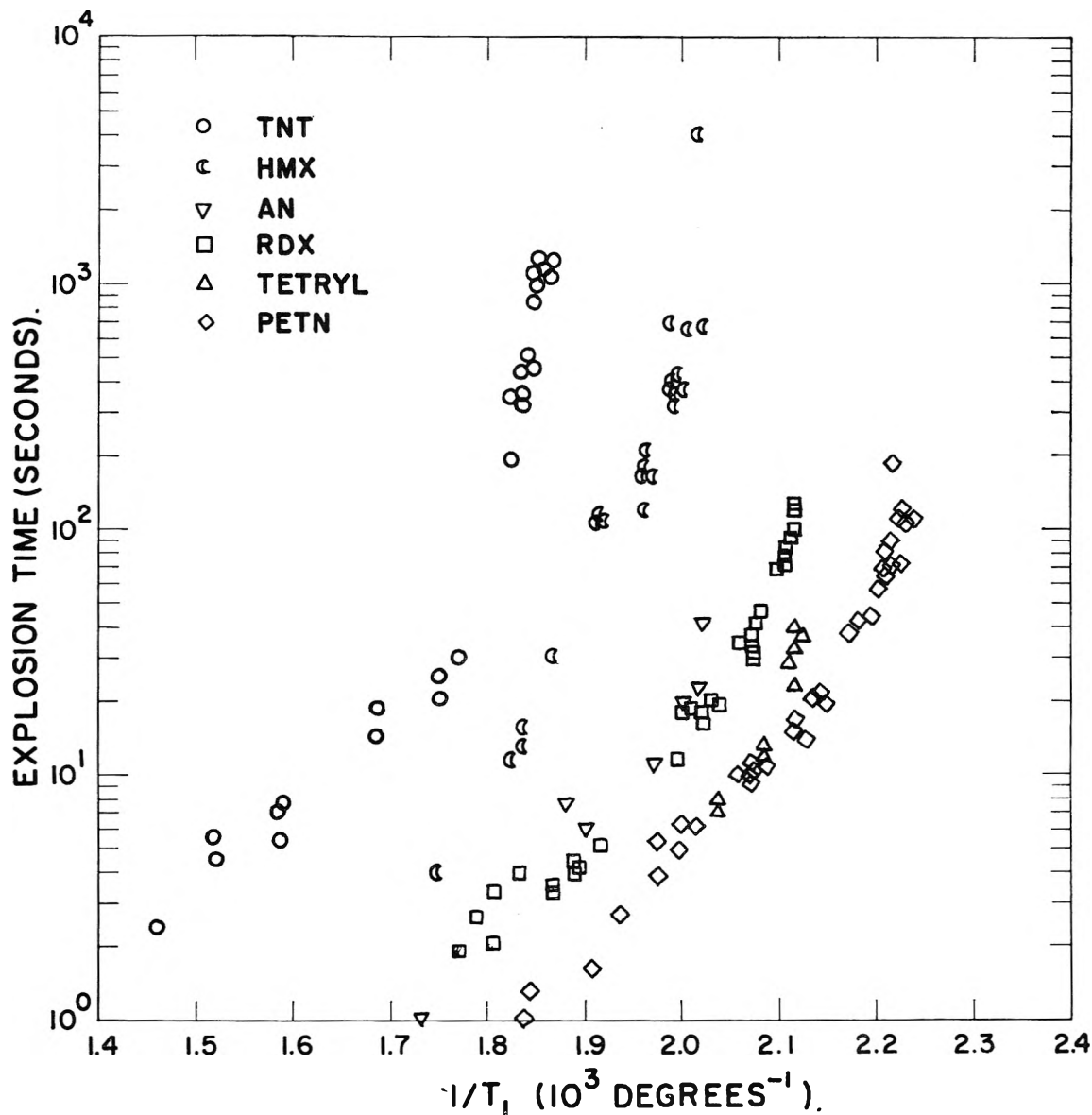


Fig. 2.—Explosion time data for various explosives.

Discussion of the Data

Assuming that the cell ruptures at a pressure of 15,000 p.s.i. and that the loading density $D = 0.9\rho$, then it is possible to estimate the maximum extent of decomposition that can take place before the cell ruptures. Taking $\rho = 1.8$ g./cc., $T = 500^\circ\text{K}$., and $N = 0.04$ mole/g., we obtain $F^* = 0.04$. That is, the cell will rupture when 4% of the sample is decomposed. The value to be taken for N depends on the decomposition process which occurs, and this is in most cases unknown. For many explosives, the thermal decomposition products will be species of higher molecular weight, and the corresponding value of N should be less than 0.04. Accordingly, F^* then would be greater than 0.04.

It is probable that TNT constitutes a case where F^* is comparatively large. The decomposition of TNT has been studied extensively by Wiseman,¹⁰

(10) L. A. Wiseman, Bristol Research Report No. 51, A.C. 2670, Ministry of Supply, Great Britain, 1942.

who reports that the initial reaction step produces no gas, but leads to the formation of an insoluble black substance which was isolated but not identified. Since this reaction produces no gas, it will not contribute to the slow pressure buildup which is evidenced with the other explosives; however, if it is exothermic, it can still lead to thermal explosions. According to Wiseman, the black substance is itself capable of further decomposition.

For the purposes of reducing the data, we have proceeded as follows: For each of the explosives studied, a value of T_m has been calculated from the data, using the procedure to be described in the next section. In each case, k is assumed to be 0.00066 cm.²/sec., so that $\tau = 34$ sec. The values assumed for E are listed in Table I. Using the best average curve through the experimental points in the vicinity of $t_{\text{exp}} = \tau = 34$ sec., we arrive at the value of T_1 for which $t_{\text{exp}}/\tau = 1$. From Fig. 3, ref. 2, the corresponding value of $(E/T_m - E/T_1) = 1.6$. Then $1/T_m = 1/T_1 + 1.6/E$.

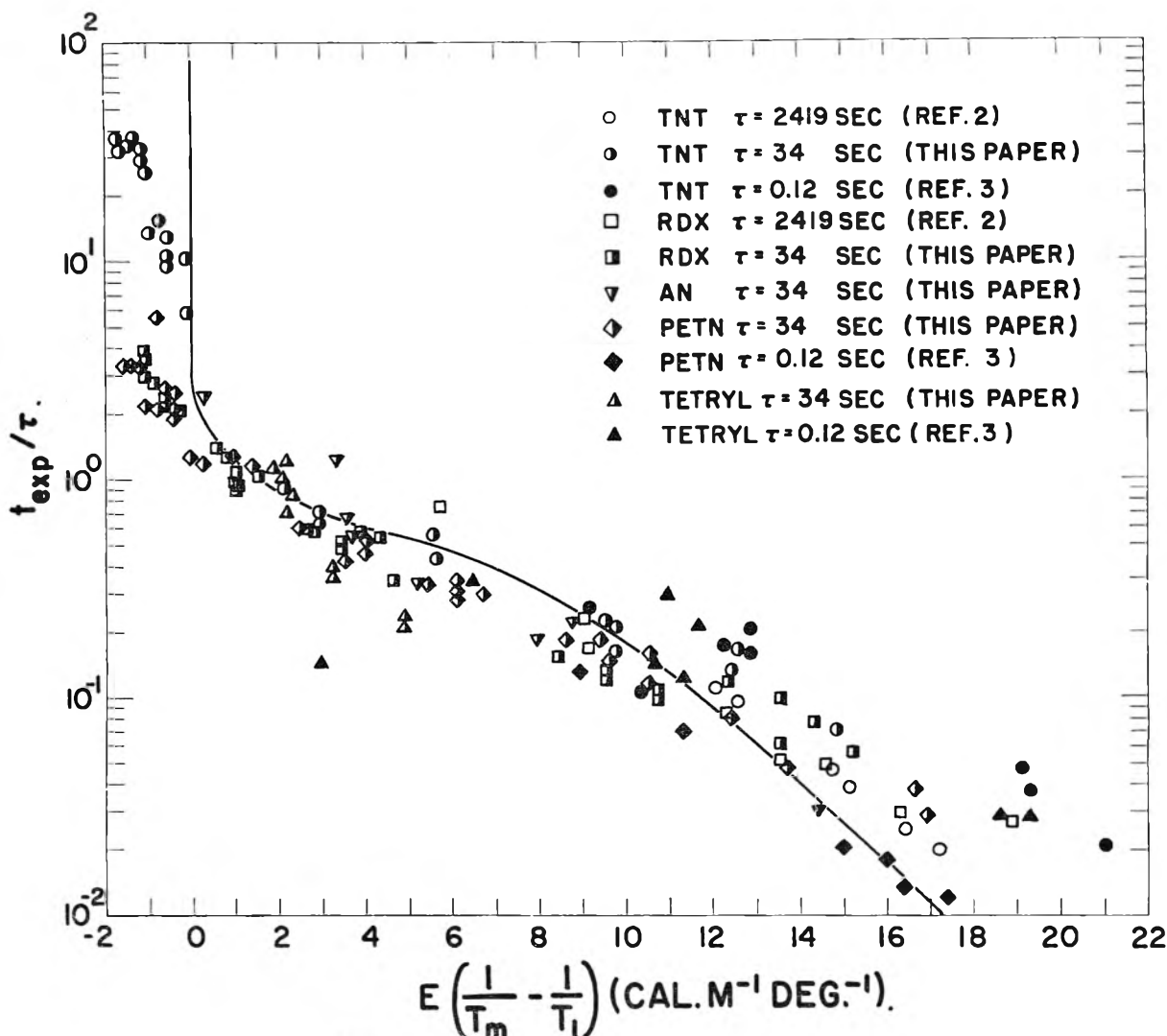


Fig. 3.—Combined plot of t_{exp}/τ vs. $E(1/T_m - 1/T_1)$ for various explosives in three different geometries.

The values of T_m so derived are listed in Table I.

It will be noted from Fig. 3 that explosions were recorded for TNT, PETN, RDX, and HMX, at temperatures below the T_m listed in Table I, and that in all cases except that of HMX these are believed to be of the non-thermal type described in the Introduction. In the case of RDX, the value of t_{exp} in this region corresponds fairly closely to the expected value of $F^* \approx 0.04$. The t_{exp} measured for TNT in the same region corresponds more nearly to $F^* = 0.3$. If E and Z are known, an approximate value of F^* can be obtained from measured explosion times by the use of eq. 7. The experimental t_{exp} data used for this purpose should be 5τ or longer. The results of three such calculations are listed in Table II, where F^* has been obtained for RDX, PETN, and TNT. The behavior of HMX is believed to be essentially different from the rest of the explosives studied, and will be discussed separately.

It will be of interest to compare the present experimental results with earlier data reported in ref. 2 and 3. The measurements in ref. 2 were made in cylindrical containers of 1.27 cm. inner radius; those of ref. 3 used a cylindrical geometry of 0.0089

TABLE I

VALUES OF T_m FOR THREE EXPERIMENTAL GEOMETRIES

Explosive	Measured T_1 for $t_{\text{exp}} = \tau$ ($\tau = 34$ sec.)	E (kcal./mole)	T_m ($^{\circ}\text{K.}$) for $\tau =$		
			2419 sec.	34 sec.	0.12 sec.
TNT	561 $^{\circ}\text{K.}$	41.1 (this paper)	491	549	653
RDX	486	47.5 (ref. 11)	439	478	
PETN	462	47.0 (ref. 12)		455	513
NH_4NO_3	484	38.3 (ref. 13)		475	
Tetryl	470	34.9 (ref. 14)		460	545

TABLE II

CALCULATIONS OF F^*

Explosive	t_{exp} (sec.)	T_1 ($^{\circ}\text{K.}$)	E (kcal./mole)	Z (sec. $^{-1}$)	F^*
RDX	120	473	47.5	$10^{18.5}$	0.04
PETN	110	449	47.0	$10^{19.8}$	0.09
TNT	1130	538	41.1	$10^{13.2}$	0.3

- (11) A. J. B. Robertson, *Trans. Faraday Soc.*, **45**, 85 (1949).
 (12) A. J. B. Robertson, *J. Soc. Chem. Ind. (London)*, **61**, 221 (1948).
 (13) M. A. Cook and M. T. Abegg, *Ind. Eng. Chem.*, **48**, 1090 (1956).
 (14) E. K. Rideal and A. J. B. Robertson, *Proc. Roy. Soc. (London)*, **A195**, 135 (1948).

cm. radius. If $k = 0.000666$ cm.²/sec., then the time constants, τ , for these two systems are 0.12 and 2419 sec., respectively, as compared to 34 sec. for the present system. Values of T_m for various explosives in the present geometry having been obtained, the corresponding T_m for the other two systems can be calculated by eq. 10. The results are listed in Table I. Having estimates of τ and T_m for each set of experiments, and assuming the values of E given in Table I, one can calculate the quantities t_{exp}/τ and $(E/T_m - E/T_1)$ for each measurement of t_{exp} and T_1 . According to eq. 4, if all the data from the three sets of experiments are plotted as t_{exp}/τ vs. $(E/T_m - E/T_1)$, the points all should fall on the same curve. Such a plot is shown in Fig. 3, which contains the aggregate of points for TNT in all three geometries, PETN and tetryl in the 34 sec. and 0.12 sec. geometries, RDX in the 2419 and 34 sec. geometries, and ammonium nitrate in the 34 sec. geometry. Also shown is the theoretical zero-order reaction curve for cylinders, as given in Fig. 3 of ref. 2. The width of the band of points is not appreciably greater than the scatter within any single set of measurements; moreover, the theoretical curve is in good agreement with the data over the entire range of positive values of $(E/T_m - E/T_1)$. In view of the fact that the several groups of data are scattered over a range of seven powers of ten in explosion time and a temperature range of 550°, this degree of agreement is felt to be quite remarkable.

The data for HMX have not been included in Fig. 3, and must be considered separately. It can be noted from the raw data of Fig. 2 that the t_{exp} vs. $1/T_1$ curve for this explosive is steeper than equivalent curves for the other materials. HMX is the only one of the organic explosives studied which is still a solid in the experimental temperature range, and much of its unusual behavior is attributable to this fact. The rate of decomposition of the pure crystalline solid is believed to be considerably slower than that of the melt, or of the mixed phase formed between the explosive and its decomposition products. It therefore would be expected that a small amount of decomposition in a confined sample would tend to catalyze further decomposition. If autocatalysis of this sort does indeed take place, it could account for the extraordinary steepness of the t_{exp} vs. $1/T_1$ curve and the extremely long explosion times recorded below T_m . A few auxiliary facts can be noted in this connection. It is found that thermal initiation of HMX is greatly accelerated by the admixture of other explosives or the presence of minor impurities. The t_{exp} vs. $1/T_1$ curve for standard production HMX containing 5% RDX is displaced downward in temperature by 11° from the curve for 99.5% HMX shown in Fig. 2. The curve for octol, a 75:25 mixture of HMX with TNT, is displaced downward by 17°. No parallel effect can be noted with mixtures of RDX with TNT; the curve for cyclotol, a 75:25 mixture of RDX and TNT, is coincident within experimental error with the curve for RDX alone.

Numerical Computations.—Except within the limited range where the isothermal approximation

can be used, solutions of eq. 1 and 2 must be obtained numerically. The differential equations are conveniently integrated by means of the finite difference approximations

$$T_j^{n+1} = \delta T_{j-1}^n + (1 - 2\delta)T_j^n + \delta T_{j+1}^n + \frac{m\delta h}{2x_j} (T_{j+1}^n - T_{j-1}^n) + \frac{Q}{C} (w_j^n - w_j^{n+1}) \quad (11)$$

and

$$w_j^{n+1} = w_j^n [1 - Z\Delta t \exp(-E/RT_j^n)] \quad (12)$$

Here superscript n is the time index, and subscript j , the space index. h is the (constant) mesh interval, so that $x = jh$; Δt is the time interval, so that $t = n\Delta t$. $\delta = k\Delta t/h^2$, Δt being so chosen that δ is in the vicinity of 0.16. This system is stable as long as $\delta < 0.5$.

The region $0 \leq x \leq a$ is divided into J equal intervals of width h , where J has been given values between 10 and 200, depending on the problem. The physical magnitude of h is given by $h = a/J$.

The initial conditions are described by $T_j^0 = T_0 = \text{constant}$, and $w_j^0 = 1$. The boundary condition is $T_0^n = T_1^n = \text{constant}$. The condition $\partial T/\partial x$ at $x = 0$ is maintained by setting $T_0^n = T_1^n$.

The computations were performed with an IBM 704 digital computer. The present method of computation differs from that described in ref. 2, and is in most cases faster. Experimental runs designed to compare the two methods showed them to be in good agreement. The appropriate mesh spacing to be used for a given problem was determined by trial and error. Progressively smaller mesh intervals were necessary as T_1 was increased. This computational method was used to obtain curves A and B of Fig. 1.

Conclusions

It is concluded that at least the gross features of the temperature dependence of explosion times can be understood on the basis of the simple model expressed by eq. 1 and 2, and that for certain ranges of conditions this model can be further simplified. Earlier calculations based on the assumption of a zero-order reaction lead to quite accurate predictions of explosion times within the range $0.1\tau < t_{\text{exp}} < \tau$. At temperatures appreciably lower than the hypothetical critical temperature, the isothermal assumption can be used. The agreement between the predicted and observed behavior is sufficient to permit reasonable extrapolations of the data to larger or smaller geometries.

Appendix A

Determination of Rate Parameters for TNT.—The present type of experiment is potentially useful for the determination of rate parameters. It offers definite advantages in the case of volatile materials, where techniques based on gas evolution are complicated by the effects of vaporization, and it also is advantageous for studies of reaction rates at high temperatures. Since the theoretical treatment of the data will take explicit account of effects due to temperature gradients and self heating, these will not be a source of confusion.

Whereas "isothermal" experiments are restricted to situations where the times involved are much longer than τ , the present method is not so restricted.

A case in which the present method has distinct advantages is that of TNT, where the existing published data^{13,15} are in poor agreement. The previous measurements apparently were complicated by both vaporization and self heating effects.

Given two data points (t_{exp} , T_1), and the pertinent sample dimensions, the corresponding values of $(E/T_m - E/T_1)$ can be obtained from Fig. 3 of ref. 2. If these are denoted by $A_{(1)}$ and $A_{(2)}$, and the corresponding values of T_1 are denoted by $T_{1(1)}$ and $T_{1(2)}$, it then follows from eq. 10 that

$$E = \frac{A_{(1)} - A_{(2)} + R \ln (a^{(2)}\delta_{(1)}/a^{(1)}\delta_{(2)}) + 2R \ln (T_{m(1)}/T_{m(2)})}{1/T_{1(2)} - 1/T_{1(1)}} \quad (\text{A1})$$

The experimental values of t_{exp} used for this purpose should preferably be between 0.1 and 1.0 τ . It also is advantageous, as in any determination of E , for the two data points to be taken at widely different temperatures. These two requirements, to be compatible, entail the further requirement that the two measurements be made with very different sizes of sample.

For the case of TNT, the two data points which have been chosen are

$$t_{\text{exp}} = 250 \text{ sec.}, \tau = 2419 \text{ sec.}, \delta = 2.00, T_1 = 571^\circ\text{K. (ref. 2)}$$

$$t_{\text{exp}} = 0.030 \text{ sec.}, \tau = 0.12 \text{ sec.}, \delta = 2.00, T_1 = 763^\circ\text{K. (ref. 3)}$$

Then by eq. A1 we obtain $E = 41.1$ kcal./mole. Substituting this value of E in eq. 3, we obtain $QZ/C = 10^{16.2}$ deg./sec.

The above value of E is intermediate between the values quoted in ref. 15 and 13. The two data points used are separated in temperature by 192°, and thereby provide a large amount of leverage for determination of E .

The slope of a $\ln t_{\text{exp}}$ vs. $1/T$ plot should not be used as a measure of E/R . It will be noted from Fig. 1 (curve B) that this slope is almost always less than E/R .

Appendix B

An Approximate Expression for Explosion Times at High Temperatures.—The early stages in the heating of a sample with $Q = 0$ can be described approximately by the equations

$$T = T_0 + (T_1 - T_0) \times \left[1 - \frac{2}{\sqrt{\pi}} \int_0^{\frac{a-x}{2\sqrt{kt}}} e^{-\lambda^2} d\lambda \right] \quad (8)$$

and

$$\frac{\partial w}{\partial t} = -Z e^{-E/RT} \quad (2')$$

It will be convenient to substitute the variables $\theta = t/\tau = kt/a^2$, $\xi = x/a$, and $\phi = E(T - T_1)/RT_1^2$. Then eq. 8 becomes

$$\phi = \frac{2\phi_0}{\sqrt{\pi}} \int_0^{\frac{1-\xi}{2\sqrt{\theta}}} e^{-\lambda^2} d\lambda \quad (\text{B1})$$

The Arrhenius expression, $\exp(-E/RT)$, can be approximated by $\exp(-E/RT_1)\exp \phi$, so that eq. 2' becomes

$$\frac{\partial w}{\partial \theta} = -(Z\tau e^{-E/RT_1})e\phi \quad (\text{B2})$$

For cylindrical samples the volume average of w is given by

$$\bar{w} = 2 \int_0^1 \xi w d\xi$$

But since $w = 1$ everywhere except where ξ is nearly equal to 1, this becomes

$$\bar{w} = 1 - 2 \int_0^1 \xi(1-w) d\xi \cong 1 - 2 \int_0^1 (1-w) d\xi = 2 \int_0^1 w d\xi - 1 \quad (\text{B3})$$

Now

$$w = 1 - (Z\tau e^{-E/RT_1}) \int_0^\theta e^\phi d\theta$$

Therefore

$$\bar{w} = 2 \int_0^1 \left[1 - (Z\tau e^{-E/RT_1}) \int_0^\theta e^\phi d\theta \right] d\xi - 1 = 1 - (2Z\tau e^{-E/RT_1}) \int_0^1 \int_0^1 e^\phi d\xi d\theta \quad (\text{B4})$$

We define the new variable $z = (1 - \xi)/2\sqrt{\theta}$, so that

$$\phi = \frac{2\phi_0}{\sqrt{\pi}} \int_0^z e^{-\lambda^2} d\lambda \quad \text{and} \quad \int_0^1 e^\phi d\xi = 2\sqrt{\theta} \int_0^{1/2\sqrt{\theta}} e^\phi dz$$

The values of $2\phi_0\sqrt{\pi}$ which are of interest are generally of the order of -20 ; therefore $\exp(\phi)$ decreases rapidly with increasing z , and the integral $\int_0^z e^\phi dz$ has effectively a constant value for values of z greater than about 0.2. Within the range $0 \leq z \leq 0.2$, ϕ is approximated closely by $\phi = 2\phi_0 z/\sqrt{\pi}$. It follows that, for values of θ less than 1

$$\int_0^{1/2\sqrt{\theta}} e^\phi dz \cong -\frac{\sqrt{\pi}}{2\phi_0}$$

Therefore

$$\int_0^1 e^\phi d\xi \cong -\frac{\sqrt{\pi\theta}}{\phi_0} \quad (\text{B5})$$

Referring to eq. B4, the value of \bar{w} then is given by

$$\bar{w} = 1 + (2Z\tau e^{-E/RT_1} \sqrt{\pi/\phi_0}) \int_0^\theta \sqrt{\theta} d\theta = 1 + \frac{4\sqrt{\pi}}{3\phi_0} (Z\tau e^{-E/RT_1})\theta^{3/2} \quad (\text{B6})$$

By the definitions of θ and ϕ it then follows that

$$t = \tau \left[\frac{3E(T_1 - T_0)(1 - \bar{w})}{4\sqrt{\pi}RT_1^2 Z\tau \exp(-E/RT_1)} \right]^{2/3} \quad (\text{B7})$$

Analogous expressions can be obtained for spherical systems and for slabs. For a sphere, the factor $3/4$ in eq. B7 is replaced by $1/2$. For a slab, the factor becomes $3/2$.

Equation B7 gives the time corresponding to any given value of \bar{w} . If an "explosion" occurs at a known value of \bar{w} , then eq. B7 gives the explosion time.

DIRECTED SOLUTE-SOLVENT INTERACTIONS IN BENZENE SOLUTIONS¹

BY W. G. SCHNEIDER

Division of Pure Chemistry, National Research Council, Ottawa, Canada

Received May 6, 1962

By means of proton magnetic resonance techniques it has been possible to demonstrate directed molecular interactions between polar solute molecules and benzene solvent molecules. The pronounced sensitivity of the proton resonance method for this purpose is due to the large magnetic anisotropy of the benzene solvent, which greatly magnifies the solute proton shifts arising from non-randomization in the solution. For polar alkyl-X and vinyl-X solutes the interaction with benzene is interpreted in terms of a dipole-induced dipole interaction, which leads to preferred mutual orientations of the solute and solvent molecules. The magnitude of the interaction appears to depend on the magnitude of the molecular dipole moment of the solute, as well as its molecular volume; molecular shape of the solute molecule is not a determining factor. With phenyl-X solutes in aromatic solvents the interaction is more extensive and cannot be adequately accounted for in terms of a simple dipole model.

The molecular force field of benzene, and of aromatic molecules generally, has a pronounced directional character. The π -electron system in such molecules represents a relatively exposed region of electronic charge directed normal to the molecular plane. Accordingly, when a second molecular species interacts with benzene, the interaction will be primarily through the π -electrons, and in the resulting complex the interacting molecules will tend to have preferred mutual orientations. It turns out that nuclear magnetic resonance techniques provide us with a method of extraordinary sensitivity for studying systems of this kind. The reason for this is the large anisotropy in the magnetic susceptibility of aromatic molecules, also commonly referred to as the "ring current effect."² In order to illustrate how the ring current effect influences nuclear magnetic resonance measurements we consider a very simple model, shown in Fig. 1. In this model we regard the aromatic ring as a simple circular conducting loop. A magnetic field H_0 applied normal to this loop induces a circular current, which generates a secondary magnetic field opposed in direction to that of the applied field. We can approximate this very crudely by a dipole placed at the center of the ring. This dipole has magnetic lines of force as illustrated by the dotted lines. Suppose now we are measuring the proton resonance of the hydrogen atoms in benzene, only one of which is shown here. The component of the secondary field at this proton is in the same direction as the applied field, *i.e.*, it enhances the applied field H_0 . Therefore to bring this proton into resonance we will require an external field H which is less than H_0 , or, in

other words, the resonance is shifted to lower applied field. On the other hand protons which find themselves in positions immediately above or below the plane of the aromatic ring will have their resonances shifted to higher applied field. This is because here the component of the secondary field is opposed to that of the applied field and hence to bring such protons into resonance we have to apply a field H greater than H_0 . We have here considered a fixed orientation of the aromatic ring with respect to the external field. If the external field is applied parallel to the plane of the ring there will be no induced ring current and no resonance shifts. So even after averaging over all directions we will still observe a net effect as indicated.

A simple example of the kind of behavior discussed here is provided by the proton resonance of CHCl_3 contained in a dilute solution of benzene. This is illustrated in Fig. 2. When CHCl_3 is dissolved in cyclohexane, there will be no specific interaction with the solvent, other than relatively weak van der Waals and dipole interactions. For the present purpose we may regard the cyclohexane solvent as an inert medium and accordingly we arbitrarily assign the chloroform resonance in this case the value zero. In ether, which is an n-type donor, the chloroform hydrogen interacts by forming hydrogen bonds with the ether oxygen, giving rise to a shift of the chloroform proton resonance to lower applied field.³ This low-field shift is quite characteristic of all hydrogen atoms involved in hydrogen bonding with n-type donors. In benzene we observe the chloroform proton resonance shifted very much to higher field. We interpret this to mean that the chloroform is here also forming a

(1) Presented at the Prof. Hildebrand 80th Birthday Symposium at Berkeley, Calif., September 11th and 12, 1961.

(2) (a) L. Pauling, *J. Chem. Phys.*, **4**, 673 (1936); (b) J. A. Pople, *ibid.*, **24**, 1111 (1956).

(3) The proton resonance of the CHCl_2 in ether, as well as in benzene, was measured relative to the proton resonance of cyclohexane, a small amount of which was added to the solutions to serve as an internal reference.

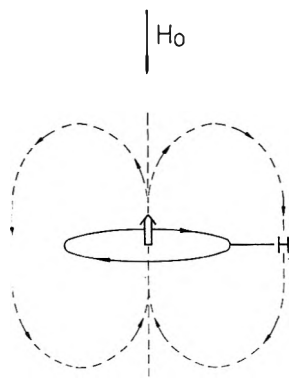


Figure 1.

weak hydrogen bond, the aromatic solvent functioning as a π -electron donor. Accordingly the hydrogen of the CHCl_3 is directed normal to the molecular plane of the aromatic solvent molecules and, because of the ring current effect, its resonance will be shifted very much to higher field. If the ring current effect did not exist we might have expected this hydrogen-bonding interaction to result in a small shift of the CHCl_3 resonance to lower field.

Another example involving a different type of interaction is illustrated by CH_3CN when dissolved in benzene (Fig. 3). If we dissolve a small amount of acetonitrile in neopentane we find the proton resonance of the acetonitrile to appear about 50 c./s. to the low field side of the proton resonance of the neopentane solvent. Again it may be assumed that neopentane is an inert solvent, and there will be no specific interaction of the acetonitrile with neopentane other than the relatively weak van der Waals interactions. If now we dissolve a small amount of acetonitrile in benzene and at the same time we add a small amount of neopentane, to serve as an internal reference signal, we now find the acetonitrile resonance on the high-field side of the neopentane reference. In other words in the benzene solution the acetonitrile resonance has been displaced to high field by 56.8 c./s. (at 60 Mc./s.). The most probable explanation of this is one which involves an induced dipole interaction with the benzene. Acetonitrile has a large dipole moment, the negative end of which is concentrated mainly in the N atom. This will be repelled by the π -electron distribution of the benzene and will tend to lie off the ring. Since benzene has a large polarizability in the plane of the ring, a dipole is induced as shown in Fig. 3, and the resulting attraction will tend to locate the CH_3 group of the acetonitrile over the aromatic ring. In this orientation the ring current effect will then cause a pronounced high-field shift of the acetonitrile proton resonance. Now if there were no specific interaction between benzene and acetonitrile involving preferred mutual orientations of these molecules, *i.e.*, if we had complete randomization of this system, both the acetonitrile and the reference neopentane molecules would experience the same environment due to the solvent benzene. To a first approximation both should be affected in the same way by the magnetic anisotropy of the benzene solvent. The observed high-field shift

for the acetonitrile resonance leads us to conclude there is a preferred mutual interaction between benzene and acetonitrile.

On the basis of previous work⁴ on solvent effects in proton resonance measurements the observed shift in acetonitrile in the present experiment⁵ may be regarded as made up of the following separate contributions

$$\delta(\text{benzene soln.}) - \delta(\text{neopentane soln.}) = \Delta\delta = \delta_a + \delta_w + \delta_E + \delta_c$$

Here δ_a is the shift due to the different magnetic environment of the neopentane and benzene solutions, *i.e.*, due to the magnetic anisotropy effects of the benzene solvent. The contribution δ_w is the shift arising from different van der Waals interaction of the solute with neopentane and with benzene. (Since the solutions employed were dilute, the solute concentration being 5 mole %, solute-solute interactions are negligible.) The term δ_E is the shift due to the "reaction field" effect.⁴ Finally δ_c is the shift due to specific molecular interaction or complex formation in the benzene solution. The terms δ_w , δ_E , and δ_c all arise from small perturbations of the electronic charge distribution of the solute molecule due to the electric fields of neighboring molecules. They are generally negative, that is, the proton resonance is shifted toward lower field. The term δ_a has a purely magnetic origin, and for aromatic solvents it is positive in sign.

In the systems being considered here the terms δ_w and δ_E are relatively small and may be neglected for our present purpose. If $\delta_c = 0$, implying complete molecular randomization, then in the present experiment δ_a should be zero. This is because, as indicated above, both the acetonitrile and neopentane solutes in benzene should experience the same magnetic environment. If $\delta_c \neq 0$, that is, if there is a specific interaction between acetonitrile and benzene causing preferred mutual orientations, then $\delta_a \neq 0$. Hence the quantity actually measured is $\Delta\delta = \delta_a + \delta_c$, and since for acetonitrile in benzene this is a large positive quantity, $\delta_a \gg \delta_c$. In other words small proton chemical shifts of solute molecules resulting from specific complex formation with benzene molecules are effectively "amplified" because of the large magnetic anisotropy of the solvent molecules.

At this point there is a further question to be examined. Acetonitrile is a linear molecule and benzene is disk-shaped. Is it possible that the apparent non-randomization, indicated by the proton resonance shifts, arises not so much from molecular complex formation, but from molecular shape effects? To investigate this question we have carried out similar experiments with a number of hydrocarbon solutes, three of which are rod-like, and two are planar. The results are shown in Table I. The observed values of $\Delta\delta$ are not significantly different from the estimated experimental error of the measurements, and may be

(4) A. D. Buckingham, T. Schaefer, and W. G. Schneider, *J. Chem. Phys.*, **32**, 1227 (1960).

(5) See also R. J. Abraham, *ibid.*, **34**, 1062 (1961); A. D. Buckingham, T. Schaefer, and W. G. Schneider, *ibid.*, **34**, 1064 (1961).

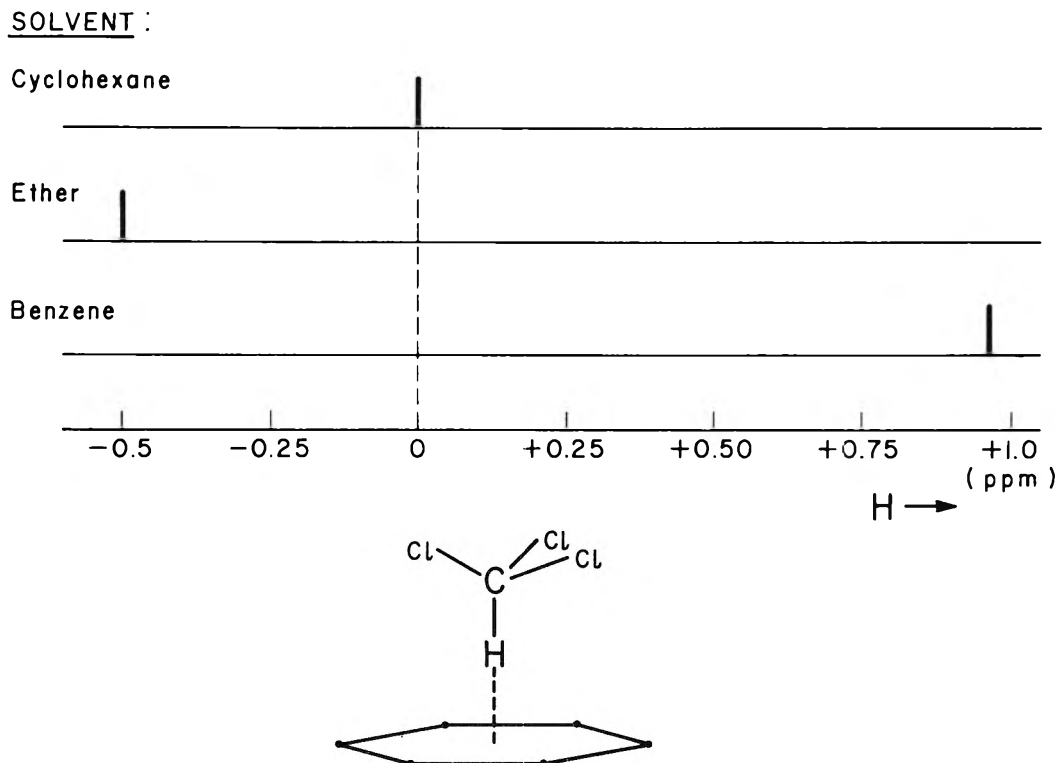



Fig. 2.— CHCl_3 proton magnetic resonance shifts (in 5 mole % solutions).

TABLE I
PROTON SHIFTS OF HYDROCARBON SOLUTES IN NEOPENTANE
AND BENZENE (5 MOLE % SOLUTIONS)^a
(In c./s. at 60 Mc./s. relative to internal neopentane
reference)

Solute	Solvent		$\Delta\delta$
	Neopentane	Benzene	
$\text{CH}_3\text{-CH}_3$	+4	+6	+2(±2)
$\text{CH}_3\text{-C}\equiv\text{C-CH}_3$	-41	-38	+3(±2)
$\text{H}_2\text{C=C=CH}_2$	-216.8	-215.9	+1(±1)
H-C=C-H	-263	-261	+2(±2)
	-363.2 ^b	-362.3 ^b	+1(±1)

^a The sign convention employed for the chemical shifts is that signals appearing at lower applied field than the reference signal are negative, and those at higher field (higher screening) are positive. ^b Average shifts of α and β protons.

taken as zero. It thus appears we can exclude molecular shape and evidently the significant property is the polar nature of the solute. If our crude dipole model of the interaction with benzene is valid, then we would expect that if we examined a series of polar CH_3X compounds, the measured shifts Δ should be simply proportional to the dipole moment of the CH_3X solute and its molecular volume. The molecular volume comes in because after rotational averaging this will determine the mean distance of approach to the benzene molecule. Figure 4 shows a plot of $\Delta\delta$ vs. μ/V for a number of solutes. There is a rough correlation as expected. Shown on the same plot is the corresponding point for CHCl_3 . This deviates widely from the correlation plot and this would tend to confirm our previous conclusion that

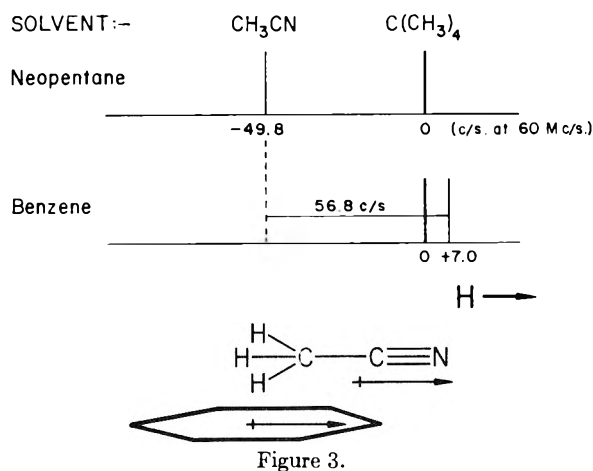


Figure 3.

in this case the interaction has a different origin and is not simply of the dipole type.

The individual proton shifts, listed in Table II, reveal a high degree of specificity in the interaction of certain solutes with benzene. Thus in propionitrile the CH_2 group, being adjacent to the polar CN group, has a higher $\Delta\delta$ value than the CH_3 group. This suggests that the CH_2 group tends to be located more nearly over the center of the aromatic ring than the CH_3 group. A high degree of specificity also is evident in dimethylformamide as a solute in benzene, the CH_3 group which is *trans* to the carbonyl group (labeled α) being preferentially located over the aromatic ring. This behavior of dimethylformamide has been reported previously by Hatton and Richards.⁶

Table III summarizes $\Delta\delta$ values for CH_3CN

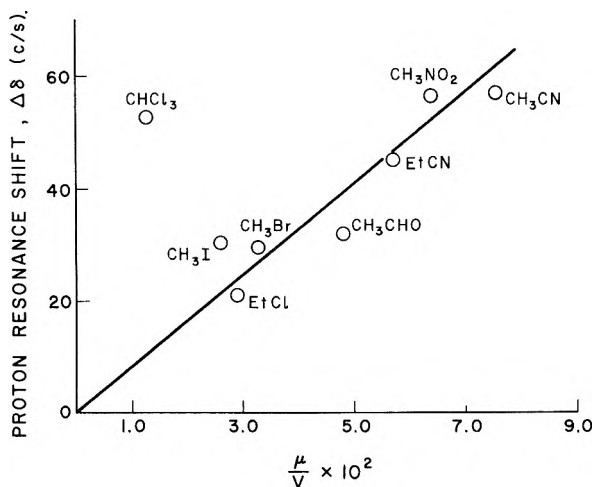


Figure 4.

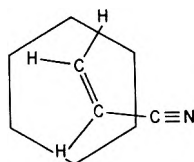


Figure 5.

TABLE II
PROTON SHIFTS OF ALKYL-X SOLUTES IN BENZENE
(5 MOLE % SOLUTIONS)

(In c./s. at 60 Mc./s. relative to internal neopentane reference)

Solute	Solvent		$\Delta\delta$
	Neopentane	Benzene	
$\text{CH}_3\text{C}\equiv\text{N}$	-49.8	+7.0	+56.8
$\text{CH}_3\text{CH}_2\text{C}\equiv\text{N}$	{ CH_3	+24.4	+40.0
	{ CH_2	-25.3	+49.7
$(\text{CH}_3)_3\text{C}-\text{C}\equiv\text{N}$	-21.0	+4.0	+25.0
CH_3NO_2	-188.7	-132.0	+56.7
$\text{CH}_3-\text{C}(=\text{O})-\text{H}$	{ CH_3	-31.6	+31.7
	{ CHO	-497.3	+27.3
$\text{CH}_3\text{CH}_2\text{Cl}$	{ CH_3	-8.0	+20.8
	{ CH_2	-127.0	+21.9
CH_3Br	-91.4	-61.8	+29.6
CH_3I	-63.9	-33.2	+30.7
$(\alpha)\text{CH}_3-\text{N}(\text{C}(\text{O})\text{H})-\text{C}(\text{O})-\text{H}$	{ $(\alpha)\text{CH}_3$	-67.0 ^a	+46.0
	{ $(\beta)\text{CH}_3$	-92.0 ^a	+17.1
	{ CHO	-412.0	+5.3

^a The assignment of methyl group proton signals follows that of ref. 6.

in several other solvents. In α -methyl-naphthalene the $\Delta\delta$ value is much larger than in benzene. This is because with two aromatic rings the shift to high field due to the ring current effect is much greater. The non-aromatic solvent butadiene causes only a very small shift.

Table IV summarizes the corresponding $\Delta\delta$ values for the three non-equivalent protons (labeled H_A , H_B , and H_C) of several polar vinyl-X solutes. Again a high degree of specificity is evident, the proton H_B which is *trans* to the X substituent tending to have the largest solvent shift in benzene. This may be interpreted as a greater tendency for this proton to be located nearer the center over

TABLE III
THE PROTON CHEMICAL SHIFT OF CH_3CN (5 MOLE %) IN
DIFFERENT SOLVENTS

Solvent	δ	$\Delta\delta$
Neopentane	-49.8
Benzene	+7.0	+56.8
<i>p</i> -Xylene	+2.5	+52.3
N-Dimethylaniline	-1.6	+48.2
N-Dimethyl- <i>p</i> -toluidine	-5.2	+44.6
α -Methylnaphthalene	+31.6	+81.4
1,3-Butadiene	-44.6	+5.2

the benzene ring. The assumption is again that the polar group tends to lie off the ring and the vinyl-X solute and the benzene solvent molecule prefer to have their molecular planes co-parallel, as illustrated in Fig. 5. The relative variation of the individual proton resonance shifts in vinyl bromide on dilution in benzene has been employed previously in a study of the proton resonance spectrum of vinyl bromide.⁷

TABLE IV
PROTON CHEMICAL SHIFTS OF VINYL-X COMPOUNDS IN
DILUTE (5 MOLE %) SOLUTION IN NEOPENTANE AND
BENZENE

(In c./s. measured at 60 Mc./s. relative to neopentane internal reference)

Solute	Solvent		$\Delta\delta$	
	Neopentane	Benzene		
$\text{H}_B-\text{C}(\text{H}_C)=\text{C}(\text{H}_A)-\text{CN}$	{ H_A	-306.5	-264.5	+42.0
	{ H_B	-293.6	-243.0	+50.6
	{ H_C	-269.4	-221.5	+47.9
$\text{H}_B-\text{C}(\text{H}_C)=\text{C}(\text{H}_A)-\text{NO}_2$	{ H_A	-330.4	-293.2	+37.2
	{ H_B	-281.8	-223.8	+58.0
	{ H_C	-364.3	-323.3	+41.0
$\text{H}_B-\text{C}(\text{H}_C)=\text{C}(\text{H}_A)-\text{Br}$	{ H_A	-286.6	-273.6	+13.0
	{ H_B	-292.6	-267.1	+25.5
	{ H_C	-238.0	-306.0	+22.0
$\text{H}_B-\text{C}(\text{H}_C)=\text{C}(\text{H}_A)-\text{C}(=\text{O})-\text{CH}_3$	{ H_A	-315.3	-303.7	+11.6
	{ H_B	-311.0	-291.9	+19.1
	{ H_C	-283.2	-259.4	+23.8
	{ CH_3	-70.7	-51.0	+20.0


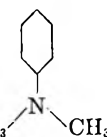
With phenyl-X solutes (Table V) the interaction with benzene is more complicated and the simple dipole model appears inadequate to account for the experimental results. The $\Delta\delta$ values for the *meta* and *para* protons in nitrobenzene solute are about twice as large as that for the *ortho* protons. Assuming the interacting molecules prefer a parallel and staggered configuration it may be assumed the benzene solvent molecule would avoid the NO_2 group in the solute molecule and would tend to "sit" over the opposite end, encompassing mainly the *meta* and *para* protons.⁸ However when the experiment is reversed, that is when benzene is employed as the solute and dissolved in an excess of nitrobenzene, we now find the benzene protons

(7) T. Schaefer and W. G. Schneider, *Can. J. Chem.*, **38**, 2066 (1960).

(8) In a previous study (T. Schaefer and W. G. Schneider, *J. Chem. Phys.*, **32**, 1218 (1960)) similar results were observed for *p*-methyl-nitrobenzene in benzene solution, the *meta* proton resonance being shifted to higher field to a much greater extent than the *ortho* proton resonance. It was suggested this was due to a preferential interaction of benzene solvent molecules with the *meta* protons, but the proposed nature of the interaction, assumed to be similar to that of CHCl_3 with benzene, appears untenable in the light of the present work.

to have a *negative* $\Delta\delta$ value. In other words, due to the nitrobenzene environment the benzene proton resonance is displaced to *lower field* by 13 c./s. If the interacting molecules tend to be parallel the benzene solute molecules would be expected also to experience a positive shift due to the ring current effect in the nitrobenzene solvent molecule. Negative $\Delta\delta$ values also are observed for the ring protons of *N,N*-dimethylaniline when the latter is dissolved in benzene. These values are not large but nonetheless significant. On the other hand, the CH_3 groups have positive shifts as in *N,N*-dimethylformamide. Since the molecular dipole moment of *N,N*-dimethylaniline is reversed from that of nitrobenzene, the behavior of the CH_3 resonances in the former is perhaps to be expected but the negative shifts of the ring protons remain unexplained.

TABLE V
PROTON SHIFTS OF AROMATIC SOLUTES IN 5 MOLE %
SOLUTIONS
(In c./s. relative to internal cyclohexane)

Solute	Solvent			$\Delta\delta$
	Cyclohexane	Benzene	Nitrobenzene	
	H_o	-403.1	-384.4	+18.7
	H_m	-358.8	-322.5	+36.3
	H_p	-366.3	-331.5	+34.8
Benzene		-346.3	-359.2	-12.9
	H_o	-310.3	-313.4	-3.1
	H_m	-338.7	-350.1	-11.4
	H_p	-309.4	-322.4	-13.0
	CH_3	-82.9	-68.0	+14.9

The inadequacy of the dipole model for aromatic solutes is further illustrated by the results for *p*-benzoquinone shown in Table VI. The ring protons of *p*-benzoquinone show a pronounced positive shift in benzene and α -methylnaphthalene solvents, yet *p*-benzoquinone has no molecular dipole moment. Additional experiments with other aromatic solutes and aromatic solvents provide further evidence that in these systems the interaction involves fairly extensive polarizations of both interacting molecules. Whether these can be more conveniently described in terms of other forms of interaction, as for example charge-transfer interaction, must await a more detailed study of such systems. On the other hand, the simple dipole-induced dipole model appears to account for the main features of the proton resonance results for the alkyl-X and vinyl-X solutes, and there appears little doubt that a specific interaction involving preferred mutual orientation with respect to the benzene solvent molecules does occur. The resulting complexes may be expected to have rather short mean lifetimes and to be relatively weak, presumably involving interaction energies of the order of kT . On this basis a pronounced temperature dependence of the proton resonance shifts may be anticipated. This remains to be confirmed experimentally.

TABLE VI
PROTON RESONANCE SHIFTS OF *p*-BENZOQUINONE
(5 MOLE % SOLUTIONS)
(In c./s. relative to internal cyclohexane)

Solvent	δ	$\Delta\delta$
Cyclohexane	-307.4
Benzene	-277.8	+29.6
α -Methylnaphthalene	-249.5	+57.9

A STUDY OF THE ADSORPTION OF CARBON MONOXIDE AND OXYGEN ON PLATINUM. SIGNIFICANCE OF THE "POLARIZATION CURVE"¹

BY S. GILMAN

General Electric Research Laboratory, Schenectady, New York

Received May 5, 1962

The adsorption of carbon monoxide on smooth platinum immersed in 1 *N* HClO_4 has been examined by means of linear potentiostatic pulses. Carbon monoxide adsorption was determined both in the presence and absence of dissolved gas. The extent and nature of saturation coverage was ascertained. The technique was further utilized to determine the extent of carbon monoxide and oxygen adsorption during a slow triangular potentiostatic sweep. Some of the characteristics of the current-voltage curves were interpreted with the aid of the adsorption data.

Introduction

The ambient temperature electrochemistry of carbon monoxide is of interest in connection with fuel cell technology.² Conclusions on the mechanism of oxidation of this gas on nickel and copper fuel cell anodes in aqueous potassium hydroxide

have been attempted on the basis of measured non-electrochemical surface conversion of carbon monoxide to formic acid.³ For platinum, only fuel-cell polarization data are available.⁴ Also, it has been observed that adsorbed carbon monoxide may be detected by means of an anodic galvanostatic pulse of long duration.⁵

In this first paper of a series, conditions for de-

(1) This work was made possible by the support of the Advanced Research Projects Agency (Order No. 247-61) through the United States Army Engineer Research and Development Laboratories under Contract Number DA-44-009-ENG-4853.

(2) E. Justi, "High Drain Hydrogen-Diffusion Electrodes Operating at Ambient Temperature and Low Pressure," Akad. Wiss., Mainz, 1959.

(3) G. Grüneberg, Technische Hochschule Braunschweig, Dissertation, 1958.

(4) L. Niedrach, this Laboratory, to be published.

(5) L. Niedrach, unpublished work.

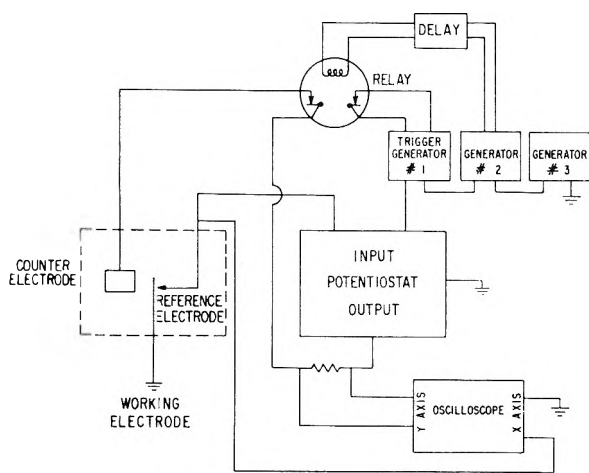


Fig. 1.—Circuit diagram.

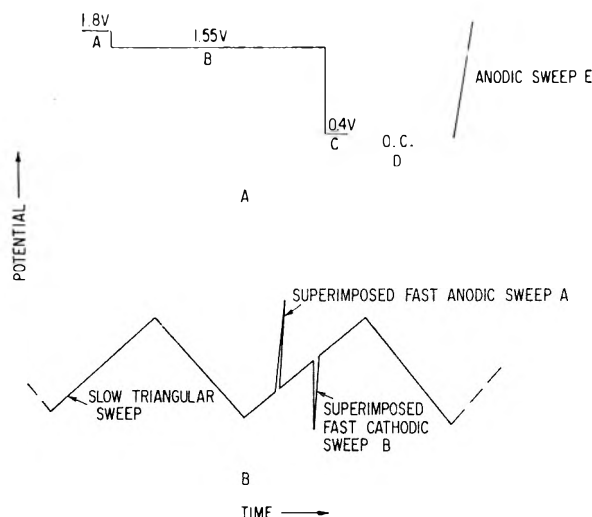


Fig. 2.—Signals used in the electrochemical study of CO adsorption: A, adsorption at open circuit; B, adsorption during a slow triangular sweep.

termination of adsorbed carbon monoxide by means of linear potential-time pulses are discussed. Also discussed is the application of the technique toward determination of the saturation coverage with carbon monoxide, and the adsorption of carbon monoxide and oxygen under the conditions of a slow linear potential-time sweep. Finally, the significance of the "polarization curve" is discussed in terms of the measured adsorptions.

Experimental

The all-Pyrex cell was patterned after that described by Breiter, *et al.*⁶ Stopcocks and gas inlet and outlet tubes were designed so that no leakage could occur from the water bath thermostated at 30°. The electrode consisted of a length of 0.020 in. C.P. Pt wire sealed in a soft-glass tube so as to expose 0.08 cm.² of the wire to the solution when the glass-metal seal was immersed beneath the liquid level. The lower end of the platinum wire was sealed in a soft-glass bead to accomplish cylindrical symmetry.

The counter-electrode and reference electrodes were platinum-platinum flags of 4 cm.² and 2 cm.², respectively. Both were kept immersed in perchloric acid solution. The reference electrode was kept in a rapidly-flowing stream of electrolytic grade hydrogen. The stopcock between the Luggin capillary and the reference electrode was kept shut

to prevent CO poisoning of the latter. The effective resistance between the electrode and the Luggin capillary tip was found to be approximately 0.25 ohm by measurement with a constant-current pulse. All potentials are reported against the reference hydrogen electrode in 1 *N* perchloric acid solution, with no correction being made for the capillary resistance, which contributes negligibly to the slow linear-potential sweeps.

A G.K. Heller Model GT 21 thyatron controlled stirring motor was used to power the all-glass mercury-seal stirrer.

The carbon monoxide used was Matheson C.P. grade and the hydrocarbon content was found to be less than 0.05% by mass spectrographic analysis. Perchloric acid was reagent grade. The distilled water was of 2-megohm specific resistivity. Tank argon was passed through a purification train consisting of a tube packed with hot copper, and two traps refrigerated with Dry Ice-ethanol, one trap containing activated charcoal.

The circuit employed in this work appears in Fig. 1. The potentiostat is a Wenking Breitband potentiostat (2 μ sec. rise time). Generator 1 is a custom built generator capable of generating a single fast triangular sweep. Generator 2 is a custom-built generator capable of generating a voltage step. Generator 3 is a Hewlett-Packard Model 202A signal generator, used to supply a continuous triangular voltage signal of speed $v = 0.04$ v./sec. The custom-built delay device is capable of triggering generator 2 and then, within a specified interval of time, activating the relay. The relay, in turn, can simultaneously (within a few μ sec) close the potentiostat circuit and trigger generator 1.

Figure 2 diagrams the two potential-time wave forms impressed upon the working electrode in this work. The signal diagrammed in Fig. 2A was used for determination of CO adsorption at open circuit. Generator 3 was eliminated from the circuit. Steps A, B, and C are produced by generator 2 with the relay contacts closed. Step D is produced when the relay contacts are opened by the delay device, and step E results when the relay again is closed by the delay device.

To obtain the signal diagrammed in Fig. 2B, generator 2, the delay device, and the relay are eliminated from the circuit. Generator 3 supplies the repetitive triangular sweep. The potential is followed on a Keithley electrometer placed in parallel with the *x*-axis of the oscilloscope. When the desired potential is reached, generator 1 is triggered manually, yielding either an anodic spike (A) or a cathodic spike (B). Two complete triangular sweeps were allowed to elapse after their superposition of an anodic or cathodic spike before another was impressed.

Current-voltage data were recorded on a Model 536 Tektronix oscilloscope using type D plug-in preamplifiers.

Results and Discussion

CO Adsorption Determined in the Presence of Dissolved CO.—The procedure used was similar to that employed in the investigation of methanol⁷ and served to bring the surface to a reproducibly clean state for adsorption and to assure reproducible extent of coverage. The solution first was saturated with CO by bubbling the gas through for more than 20 min. with the electrode at open circuit. The signal diagrammed in Fig. 2A then was applied. The details and significance of each step are as follows:

(A) Fifteen-second pretreatment step to remove oxidizable impurities, and to produce a layer of adsorbed oxygen which serves to block adsorption. CO is kept bubbling through the solution. Some molecular oxygen is evolved at a steady-state rate of approximately 1 ma./cm.².

(B) Potential step during which the oxygen layer formed in (A) is maintained, molecular oxygen from (A) is swept away, and the concentration of the adsorbate is brought to its bulk value. CO

(6) M. Breiter, K. Hoffmann, and C. Knorr, *Z. Elektrochem.*, **61**, 1168 (1957).

(7) (a) M. Breiter and S. Gilman, *J. Electrochem. Soc.*, **109**, 622 (1962); (b) S. Gilman and M. Breiter, *ibid.*, in press.

is kept bubbling through the solution for 0.5 min. The flow of gas then is stopped and the solution allowed to become quiescent for 1.5 min. No measurable current (less than $1 \mu\text{a./cm.}^2$) flows after the first second of pretreatment during this step.

(C) Reduction step. This step is of 10 msec. duration. During the first few msec. of this step, the surface layer of oxygen is reduced and adsorption of CO begins.

(D) Open-circuit adsorption step. CO is allowed to adsorb during the 1-min. duration of this step. Since the electrode is not part of a circuit, it serves simply as a freshly reduced surface, and the potential of the metal-electrolyte interface varies freely. Surface reaction products which might form and be consumed at any fixed potential are conserved and may later be determined.

(E) Anodic sweep. The open-circuit potential of the electrode is measured, and the d.c. level of the combined signal generators is set to the measured potential. When the relay is closed, the potentiostat circuit is closed and the linear sweep starts at the pre-set d.c. level. The current-voltage trace is recorded on the X-Y oscilloscope.

It was found that after step D, the voltage slowly drifted from 0.4 toward 0.1 v. (apparently due to extremely small hydrogen coverage). No species were detectable between the open-circuit potential and approximately 0.9 v. (except for small amounts of hydrogen when step D was prolonged for over 20 min.), and so the sweep has usually begun at 0.4 v. for simplicity.

Current-voltage traces were recorded for values of the anodic sweep speed, v , from 880 to 0.04 v./sec. Representative traces appear in Fig. 3. The dashed curves are experiments performed in the absence of CO, *i.e.*, with the solution saturated with argon. These "solvent corrections" include currents due to formation of an adsorbed oxygen layer and to charging of the double layer.⁸ To obtain the charge due to oxidation of CO, the dashed and solid curves are integrated to the potential where intersection occurs, E , (time, t_1). The integral for the dashed curve then is subtracted from that for the solid curve. The assumptions involved in this procedure are explored below.

Let Q_1 and Q_2 represent the integrated charge under the solid and dashed curves, respectively. Then

$$Q_1 = Q_{1C} + Q_{1(O)} + Q_{CO} + Q_{CO}^d \quad (1)$$

$$Q_2 = Q_{2C} + Q_{2(O)} \quad (2)$$

Q_{1C} = capacitance current in presence of CO, integrated from $t = 0$ to $t_1 = (E - 0.4)/v$

Q_{2C} = integrated capacitance current in absence of CO

$Q_{1(O)}$ = integrated oxygen adsorption current in presence of CO

$Q_{2(O)}$ = integrated oxygen adsorption current in absence of CO

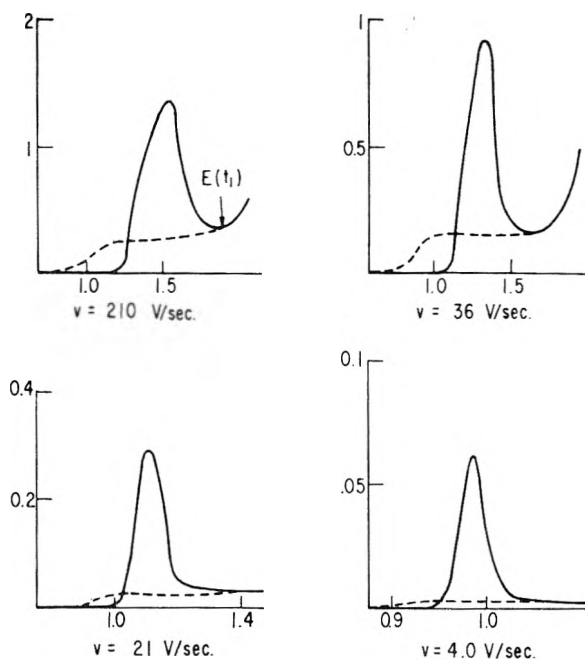


Fig. 3.—Anodic I - U curves for CO after 1 min. of adsorption (solid lines); dashed lines are for the same conditions in the absence of CO (argon-bubbling). Ordinate is current in amp./cm.² and abscissa is potential in volts.

Q_{CO} = charge due to oxidation of adsorbed CO present on the surface at $t = 0$

Q_{CO}^d = charge due to oxidation of CO which diffuses to the surface at $0 < t < t_1$.

$$\Delta Q = Q_1 - Q_2 \approx Q_{CO} + Q_{CO}^d \quad (3)$$

The validity of eq. 3 is based upon elimination of several terms in eq. 1 and 2 which is justified as follows:

(a) Q_{1C} and Q_{2C} , while not likely equal, are relatively small charges and are taken as equal. It has been estimated previously⁶ that the difference might cause as much as a 7% uncertainty in ΔQ .

(b) $Q_{1(O)} = Q_{2(O)}$ = total charge due to partial formation of an adsorbed oxygen film to time t_1 . This is implied by the coincidence of the solid and dashed curves beyond $t_1(E)$. For the 0.04 v./sec. sweep there is direct evidence given below for this equality at high potentials.

To separate Q_{CO} from Q_{CO}^d we must note that i_{CO}^d is supplied by diffusion and hence Q_{CO}^d must become insignificant compared with Q_{CO} for large values of v . ΔQ is plotted against v in Fig. 4, for $v = 1100$ to 3.6 v./sec. ΔQ is found to hold constant with an average value of 0.51 mcoulomb/cm.² and an average deviation of 6% and must represent Q_{CO} . Since reproducibility of ΔQ at $v = 210$ v./sec. was found better than 1%, it is not the variation in Q_{CO} but the inequality of Q_{1C} and Q_{2C} and various instrumental errors that determine the scatter. For values of v less than 3.6 v./sec., the contribution of Q_{CO}^d becomes increasingly evident. A sweep speed of 210 v./sec. was used for determining CO coverage in the remainder of the work.

To determine whether contribution of Q_{CO}^d to ΔQ might be predicted on the basis of simple theory,

(8) F. C. Will and C. A. Knorr, *Z. Elektrochem.*, **64**, 258 (1960).

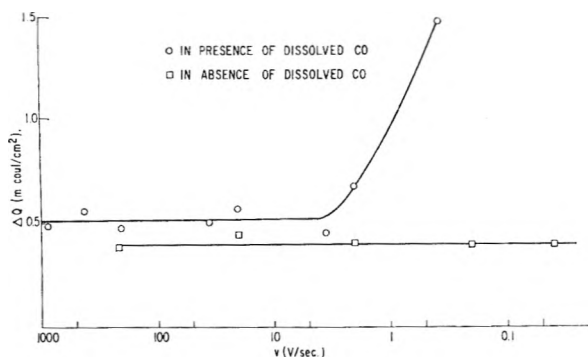


Fig. 4.—Integrated charge due to CO oxidation as a function of linear sweep speed.

let us calculate the *maximum* possible contribution of Q_{CO}^d to ΔQ during the linear sweep. Let us assume that before the application of the anodic sweep (step E, Fig. 2A) the concentration of dissolved CO near the electrode has returned to the bulk value, C_{CO} . Let us also assume that re-adsorption of CO (removed during the sweep) is limited only by semi-infinite linear diffusion. Then the rate of adsorption of oxidizable CO, expressed as a current density i_{ads} is⁹

$$i_{ads} = \frac{nFD_{CO}^{1/2} C_{CO}}{\pi^{1/2} t^{1/2}} \quad (4)$$

then

$$(Q_{CO}^d)_{max.} = \int_0^\tau i_{ads} dt = \frac{2nF\pi^{-1/2}D_{CO}^{1/2}C_{CO}\tau^{1/2}}{\pi^{1/2}} \quad (5)$$

Taking $n = 2$

D_{CO} = diffusion constant of CO = 3.1×10^{-5} cm.²/sec. (see below)

C_{CO} = bulk concn. of CO = 8.92×10^{-7} mole/cm.³¹⁰

We obtain

$$(Q_{CO}^d)_{max.} = 1.10\tau^{1/2} \text{ m.coulomb/cm.}^2 \quad (6)$$

τ is now the interval of time between first oxidation of CO and coincidence of the CO and "solvent curves" (point E on Fig. 3). At $v = 1100$ v./sec., the oxidation of CO occurs over a 1.0-v. range and τ has the value 1 msec. Using eq. 6, $(Q_{CO}^d)_{max.} = 0.04$ m.coulomb/cm.² or 8% of Q_{CO} . At $v = 21$ v./sec. or approximately $1/60$ the higher sweep speed, the oxidation of CO occurs over a 0.15 v. range and $\tau = 7.5$ msec. Therefore $(Q_{CO}^d)_{max.} = 0.096$ m.coulomb or 19% of Q_{CO} in this case. It immediately is apparent from the sample calculations that the factor which serves to limit $(Q_{CO}^d)_{max.}$ is the reduction in τ with decreasing sweep speed. The apparent constancy (6% average deviation) of ΔQ implies that additional factors operate to reduce Q_{CO}^d to 0 in that range of sweep

(9) H. A. Laitinen and I. M. Kolthoff, *J. Am. Chem. Soc.*, **61**, 3344 (1939).

(10) "Lange's Handbook of Chemistry," Tenth Edition, McGraw-Hill Book Co., Inc., New York, N. Y., 1961.

speeds. These factors might include: (1) Slow adsorption of CO at high coverages¹¹; (2) Immediate adsorption of oxygen on sites vacated by CO, preventing oxidation on those sites.

CO Saturation Coverage and Bonding.—It was demonstrated above that the coverage with CO after one minute's adsorption time could be reproducibly established and detected within a large range of sweep speeds. The completeness of CO adsorption was investigated by extending the adsorption time (open-circuit) to 10 min. No increase in Q_{CO} was observed.

By studying the adsorption of hydrogen electrolytically deposited at zero and full coverage with CO it is possible to define the CO coverage relative to hydrogen coverage, which in turn relates it to the true surface area. It also is possible to determine the extent to which the surface is not covered with CO. This in turn allows conclusions to be drawn on the nature of the CO-Pt bond. The saturation coverage of the surface with hydrogen, Q_H^S , was found to be 0.37 m.coulomb/cm.² by the method of Will and Knorr⁸ using a 2 v./sec. repetitive triangular sweep. Assuming $Q_H^S = 0.21$ m.coulomb/cm.² for a surface roughness of 1.0,⁸ the electrode used had a surface roughness of 1.8. Adsorption of CO was allowed to occur for 1 min. in the usual way, and a cathodic sweep (substituted for step E, Fig. 2A), $v = 6.0$ v./sec., was applied. The charge due to adsorption of hydrogen, Q_H , was 0.080 m.coulomb/cm.². The measured charges may be expressed as

$$Q_H^S = n_H S_H^S F \quad (7)$$

$$Q_H = n_H S_H F \quad (8)$$

where

$n_H = 1$ = no. of electrons required for oxidation of hydrogen atom

S_H^S = concn. of sites (in mmols/cm.²) available for hydrogen adsorption on the bare surface

S_H = concn. of sites available for hydrogen adsorption on the CO-covered surface

If we assume that S_H^S represents the total concentration of sites available for adsorption of both hydrogen and oxygen, then $S_H^S - S_H$ is the concentration of sites covered by CO. If we assume that one molecule of CO occupies one site, then

$$Q_{CO} = n_{CO} S_{CO} F \quad (9)$$

where

$n_{CO} = 2$ = no. of electrons required for oxidation of one CO molecule

S_{CO} = concn. of sites covered with CO.

If our assumption of one-site adsorption were correct then combining eq. 7-9

$$2(Q_H^S - Q_H) = Q_{CO} \quad (10)$$

(11) S. Gilman, *J. Phys. Chem.*, in press.

Actually, $2(Q_H^S - Q_H)$ has the value 0.58 mcoulomb/cm.² while Q_{CO} has the average value 0.51. The discrepancy could be due to experimental error, or to some two-site adsorption of CO. Evidence for some two-site adsorption of CO from the gas phase on supported platinum has been found by Eischens and Pliskin¹² using infrared techniques. On the other hand Lanyon and Trapnell¹³ report complete one-site adsorption of CO on evaporated Pt films. The possibility of occurrence of some two-site adsorption under our conditions will be more thoroughly explored in a future publication.¹¹

CO Adsorption Determined in the Absence of Dissolved CO.—Employing the usual pretreatment (steps A–C, Fig. 2B), the electrode was allowed to stand at open-circuit (step D, Fig. 2B) for 1 min. in the presence of dissolved CO. Argon then was bubbled vigorously through the cell for 9 min. to remove dissolved CO. The solution was allowed to stand quiet for 1.5 min. and a linear sweep was applied. Figure 4 reveals that ΔQ in the absence of dissolved CO is fairly constant through sweep speeds as low as 0.04 v./sec.

Referring to eq. 3, $\Delta Q \sim Q_{CO}$ over the entire frequency range since $Q_{CO}^d = 0$. The average value of Q_{CO} in the absence of dissolved CO is 0.42 mcoulomb/cm.², as compared with 0.51 mcoulomb/cm.² in the presence of dissolved CO. In Fig. 5, current-voltage traces obtained for the two different conditions are compared at two different values of the sweep speed. It is apparent that in the absence of dissolved CO not only is the area under the curve diminished but the shape and location of peaks also undergo change in comparison with the situation in the presence of dissolved CO. For $v = 4.0$ v./sec. the original peak at 1.02 v. is represented by a "shoulder" to the new peak appearing at 0.98 v. At $v = 36$ v./sec., the "shoulder" is not detectable except possibly as a broadening of the curve. There is, however, noticeable shift of the original peak at 1.35 to 1.26 v. No similar shifts are observed in comparable times at open circuit in the presence of dissolved CO, and as already indicated, the area under the curve undergoes increase (to saturation) rather than decrease.

The decrease in Q_{CO} in the absence of dissolved CO is logically attributed to desorption of CO. The shift in potentiostatic peak voltages also has been found to accompany decreasing initial coverages with CO.¹¹

Quasi-stationary Current-Voltage (Polarization) Curves. General.—CO was bubbled through the electrolyte with rapid mechanical stirring. A 0.04 v./sec. periodic triangular sweep was applied to the cell. The resulting current was found to increase regularly with rate of stirring but to remain constant and reproducible as the rate exceeded approximately 180 r.p.m. This is a result of transport being proportional to rotational speed raised to a small fractional power.¹⁴ The data in Fig. 6 correspond to approximately 200

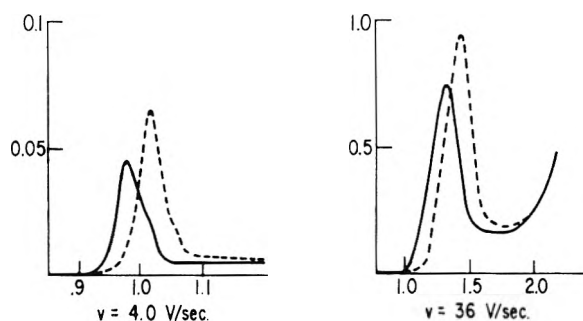


Fig. 5.—Anodic $I-U$ curves for adsorbed CO in the presence (dashed lines) and in the absence of CO (solid lines).

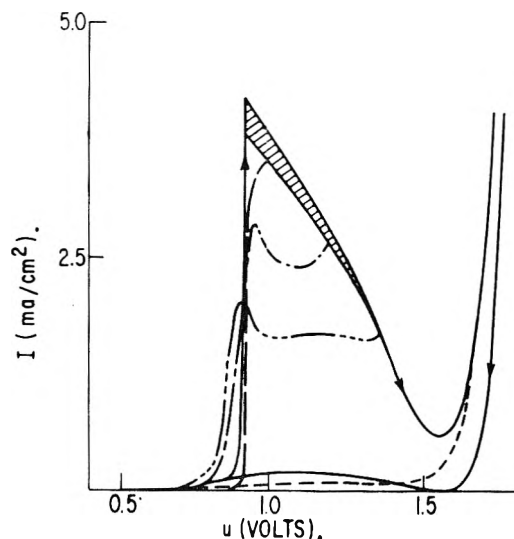


Fig. 6.—Quasi-stationary $I-U$ curves for CO with rapid mechanical stirring. Shaded region indicates oscillations during ascending sweep; $v = 0.04$ v./sec: ———, ascending to 1.8 v. and return; - - - -, ascending to 1.8 v., absence of CO; ———, descending from 1.0 v.; - - - -, descending from 1.2 v.; - - - -, descending from 1.4 v.

r.p.m. A curve is shown for the ascending sweep from 0.4 to 1.8 v. Curves are shown for descending sweeps from 1.8, 1.4, 1.2, and 1.0 v. During the ascending sweep virtually no current flows until a potential of approximately 0.91 v. is exceeded, when the current rises vertically. From 0.91 to 1.6 v. the current drops almost linearly with potential, and regular current oscillations are apparent. Above 1.6 v., the current rises again. During the descending sweep from 1.8 v., very little current is measured. During the descending sweeps from lower maximum potentials, the current remains fairly constant, and a "hysteresis effect" is noted, in that current flows at low values of potential during the descending sweeps where insignificantly small currents flowed during the ascending sweep. The current during the ascending sweep between 0.91 and 1.6 v. is much decreased in the absence of stirring. This fact, and the observed current oscillations in this range, may be taken as proof of (at least partial) current limitation by mass-transport, as in the case of the limiting-current region for the hydrogen anode.¹⁵ The features of the polarization curve may be more fully explained through measurement of CO and

(12) R. P. Eischens and W. Pliskin, *Advan. Catalysis*, **10**, 18 (1958).

(13) M. Lanyon and B. Trapnell, *Proc. Roy. Soc. (London)*, **A227**, 387 (1955).

(14) P. Delahay, "New Instrumental Methods in Electrochemistry," Interscience Publishers, Inc., New York, N. Y., 1954, p. 233.

(15) M. Becker and M. Breiter, *Z. Elektrochem.*, **60**, 1080 (1956).

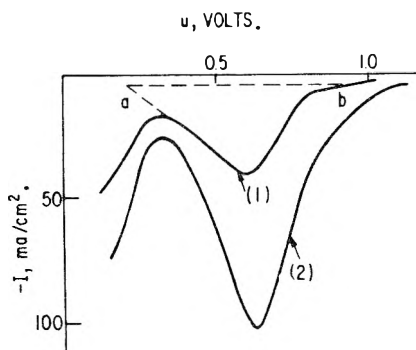


Fig. 7.— I - U traces obtained for the reduction of oxygen by means of a cathodic linear pulse (in presence of dissolved CO): trace (1), potential initially 0.90 v. during descending portion of triangular sweep; trace (2), potential initially 1.2 v. during descending portion of triangular sweep.

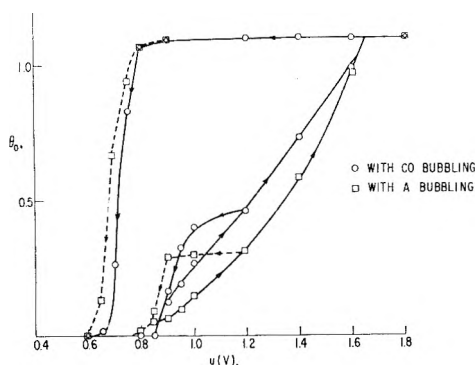


Fig. 8.—Fraction of surface covered with adsorbed oxygen during periodic triangular sweep (0.04 v./sec.) as a function of potential, U .

oxygen adsorption under the experimental conditions.

Oxygen Coverage.—Oxygen coverage was determined as a function of potential during the 0.04 v./sec. triangular sweep by the superposition of a 14 v./sec. cathodic sweep (step B, Fig. 2B). Cathodic reduction peaks similar to those obtained by Will and Knorr⁸ in nitrogen-saturated sulfuric acid were obtained (Fig. 7). The dashed lines serve as an approximate correction for double-layer capacitance and hydrogen-overlap (the latter becomes serious only at higher oxygen coverages). The charge due to oxygen-adsorption, Q_0 , was obtained by integration of the resulting closed curve from point a to point b.

Let us define the surface coverage with oxygen, θ_0

$$\theta_0 = Q_0/2Q_H^s \quad (11)$$

Equation 11 follows from the assumption that $2Q_H^s$ is equivalent to one monolayer of oxygen.¹⁶ Values of θ_0 are plotted in Fig. 8 for the slow ascending sweep to 1.8 v. and for the descending sweeps from 1.8 and 1.2 v. The experiments were conducted both in CO and in argon-saturated solutions.

As already has been observed for methanol^{7a} the oxygen coverage during the ascending sweep tends to be higher in the presence than in the absence of CO with coincidence achieved toward 1.6 v. when

(16) M. Breiter, C. A. Knorr, and W. Völkl, *Z. Elektrochem.*, **59**, 681 (1955).

approximately a monolayer of oxygen is formed. During the descending sweep from 1.8 v. the reduction of oxygen coverage occurs somewhat earlier on the potential axis in the presence than in the absence of CO. The fact that CO does not directly reduce the oxygen coverage until the approximate potential for electrolytic reduction is achieved may be taken as evidence that the direct (non-electrochemical) reduction of the adsorbed oxygen layer by CO is slow. The results of the descending sweep from 1.2 v. also show somewhat earlier reduction in the presence of CO.

CO Coverage.—CO coverage during the 0.04 v./sec. sweep was determined by superposition of a positive-going 210 v./sec. sweep at the desired potential (step A, Fig. 2B). Curves similar to that appearing in Fig. 3 were obtained for large coverages. However, referring to eq. 1 to 3 we must note that $Q_{1(O)}$ and $Q_{2(O)}$ are no longer necessarily equal since starting potentials may be above 0.8 volt. To correct for this

$$Q_{1(O)} + Q_{1(O)'} = Q_{2(O)} + Q_{2(O)'} \quad (12)$$

where $Q_{1(O)'}$ is the charge required for the partial oxygen coverage in the presence of CO at starting potential E' at which measurement is made. $Q_{2(O)'}$ is the charge required for the partial oxygen coverage in the absence of CO at starting potential, E' . All integrations are, as before, made to potential E and time t_1 and

$$t_1 = \frac{E - E'}{v} \quad (13)$$

Equation 12 again is based on the assumption that the total oxygen coverages are equal at time t_1 . Then assuming $Q_d^{CO} = 0$

$$\Delta Q \sim Q_{CO} + Q_{1(O)} - Q_{2(O)} = Q_{CO} + Q_{2(O)'} - Q_{1(O)'} \quad (14)$$

According to eq. 14 Q_{CO} may be found by correcting the experimental values of ΔQ with the aid of the oxygen coverages plotted in Fig. 8. This was done in preparing Fig. 9. In Fig. 9, $\theta_{CO} = Q_{CO}/2Q_H^s$ is plotted against potential during the slow linear sweep. During the ascending sweep the surface is 75% covered with CO up to approximately 0.90 v. A very steep drop in coverage then is observed over 10–20 mv. of potential, and then θ_{CO} remains 0 up to 1.8 v. During the descending sweep from 1.8 v. re-adsorption of CO occurs in the potential range 0.60–0.75 v. where adsorbed oxygen is being reduced (Fig. 8). During the descending sweep from 1.2 v., re-adsorption of CO commences at approximately 0.9 v.

Application of CO and Oxygen Adsorption Data to Polarization Curves.—It already has been demonstrated that the current which flows on ascent from 0.91 to 1.6 v. is at least partially transport-controlled. From Fig. 9 we see that there is no adsorbed CO on the surface in this potential range, and from Fig. 8 we see that the surface is gradually covered with a monolayer of oxygen, until at 1.6 v. the rising current may be ascribed to evolution of

molecular oxygen. In this range, therefore, molecular CO is brought to the surface by stirring and is oxidized before any accumulation of adsorbed CO is possible. Indirect oxidation by reaction with the adsorbed oxygen is judged improbable on the basis of the observation that adsorbed oxygen is not reduced by CO during the descending slow voltage sweeps.

The gradual decrease in current during the ascending sweep in the range from 0.91 to 1.6 v. may be ascribed either to: (1) physical masking of the surface by oxygen, reducing the effective geometric surface area, or (2) decrease in the rate constant for CO oxidation due to partial coverage with oxygen. Possibility (1) appears attractive here because of the very gradual decline in current as the oxygen coverage increases. However, for physical masking to occur, we might expect the passive film to develop in splotches considerably larger in diameter than the diffusion layer thickness (approximately 10^{-3} cm. in this case). There is no previous evidence for this being the case. Possibility (2) can clearly be invoked in methanol oxidation where only 10% coverage of the surface with oxygen causes drastic decrease in the methanol oxidation current.^{7b} This possibility is not so obvious here because of the gradual nature of the effect.

On a platinized electrode (roughness factor 100) the current was found to remain constant from 0.9 to oxygen evolution, resembling a true limiting current. Here the increase in surface area may be held responsible for off-setting the effect of either possibility (1) or (2) above, and no final judgment may be made on the basis of the available information.

To help explain the abrupt rise in current above 0.91 v. and the "hysteresis effect" during the descending sweep from 1.2 v., the current-voltage curve is plotted along the same potential abscissa as $\theta_F = 1 - \theta_{CO} - \theta_O$ in Fig. 10. During the ascending sweep θ_F has the value 0.25 until oxygen adsorption causes a dip near $U = 0.9$ v. The current does not increase from its almost negligible value until θ_F undergoes its own abrupt increase toward 1. At this point the surface coverage with CO is zero, and remains zero throughout the (partially) diffusion-controlled region. During the descending sweep from 1.2 v., θ_F remains fairly constant and so does the current. At 0.95 v., the current begins to drop, CO is readsorbed, and θ_F decreases. Current continues to flow during the descent from 0.91 to 0.85 v., in which range no current flowed during the ascending sweep. This additional current may be correlated with the higher values of θ_F which occur in this region of enhancement of I .

We conclude that large CO oxidation currents occur at low coverage in all cases. During the ascending sweep, the small initial oxidation of CO at 0.91 results in lower coverage, which in turn increases the rate of oxidation, leading to an "avalanche" effect, and hence an abrupt rise in current. During the descending sweep, when the electrochemical rate constant drops to a sufficiently low level, CO again tends to build up on the surface.

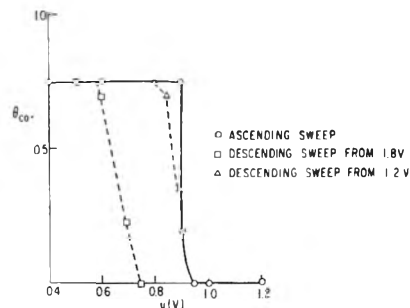


Fig. 9.—Fraction of surface covered with CO during periodic triangular sweep (0.04 v./sec.) as a function of potential, U .

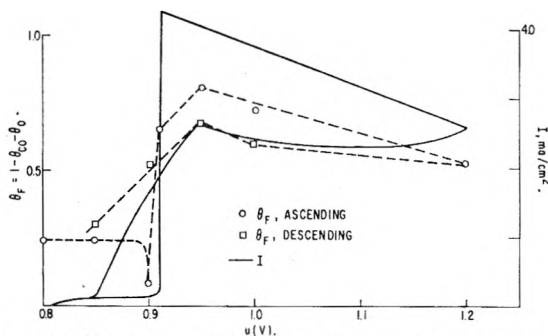


Fig. 10.—Comparison of current with free surface, θ_F , during 0.04 v./sec. triangular sweep to 1.2 volts.

This would cause an abrupt decrease in current, were it not for the fact that the readsorption is delayed (by diffusion¹¹), and the "hysteresis effect" is observed. The generalized conclusion is that high coverages with CO tend to poison its own electrochemical oxidation. There are at least two ways in which this may be accomplished: (1) The electrochemical rate constant for oxidation of adsorbed CO may decrease with increasing coverage. (2) The currents which flow at small, or zero, CO coverage may be considered as due to "unadsorbed" CO which is not tightly bound to the surface and for this reason is more easily oxidizable.

This subject will be investigated further and the results published in a future paper. Some early evidence already favors possibility (2).

The limiting current density for hydrogen measured under the conditions of our slow sweep may be written¹⁷

$$i_L' = \frac{2FD_{H_2}C_{H_2}}{\delta} \quad (15)$$

Writing a similar equation for CO

$$i_L = \frac{2FD_{CO}C_{CO}\theta_F}{\delta} \quad (16)$$

where θ_F serves to empirically correct for the decrease in current with decrease in θ_F . Taking $C_{H_2} = 7.55 \times 10^{-7}$ mole/cm.³, $C_{CO} = 8.92 \times 10^{-7}$ mole/cm.³,¹⁸ $i_L' = 5.5$ ma./cm.², $i_L = 4.0$ ma./cm.², and $\theta_F = 0.82$, then from eq. 15 and 16

(17) P. Delahay, "New Instrumental Methods in Electrochemistry," Interscience Publishers, Inc., New York, N. Y., 1954, p. 219.

(18) "Lange Handbook of Chemistry," Tenth Edition, McGraw-Hill Book Co., Inc., New York, N. Y., 1961.

$$\frac{D_{CO}}{D_{H_2}} = 0.75 \quad (17)$$

Taking $D_{H_2} = 4.1 \times 10^{-5}$ cm.²/sec. (25°, H₂O)¹⁹ the approximate value obtained for D_{CO} is 3.1×10^{-5} cm.²/sec.

The value of D_{CO} so obtained proves to be in

excellent agreement with that obtained under conditions of semi-infinite linear diffusion.¹¹

Acknowledgment.—The author wishes to thank J. T. Adamechick for his valuable assistance with the electronic instrumentation.

(19) G. Tammann and V. Jessen, *Z. anorg. allgem. Chem.*, **179**, 125 (1929).

THE CHEMISTRY OF XYLYLENES. XV. THE KINETICS OF FAST FLOW PYROLYSIS OF *p*-XYLENE

BY L. A. ERREDE AND F. DEMARIA

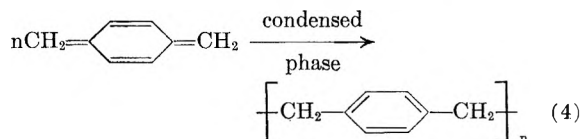
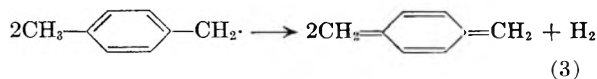
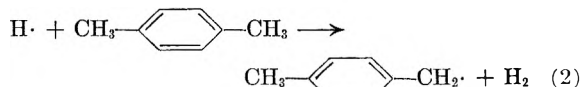
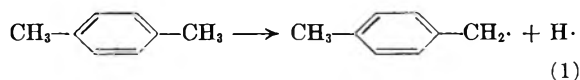
Contribution No. 233 from the Central Research Laboratories of the Minnesota Mining and Manufacturing Company,¹ St. Paul, Minn.

Received May 23, 1962

The fast flow pyrolysis of *p*-xylene was re-examined and the kinetics were followed by total analysis of the reaction products. Rate constants were determined for formation and subsequent destruction of *p*-methylbenzyl radicals and of toluene. These reactions are homogeneous and consequently unaffected by the type of surface in the pyrolysis system. The rate constant for formation of *p*-methylbenzyl radicals agrees with earlier results that were determined indirectly by analysis for H₂. Equations were developed that give the conversions of *p*-xylene to *p*-methylbenzyl radicals and to toluene in terms of the pyrolysis temperature and residence time. When compared at like residence times, the conversions calculated by use of these equations agree within experimental error with results observed by other investigators. These equations also were used to calculate the amount of *p*-methylbenzyl radicals available for gas phase synthesis *via* coupling with other radicals.

Introduction

When *p*-xylene is subjected to fast flow pyrolysis at low pressure, a mixture of products is obtained.² Most of the components of this mixture can be traced to a common intermediate, *p*-methylbenzyl radical, as outlined in Fig. 1. This intermediate is formed by thermal rupture of the C-H bond (eq. 1 and 2) as the gas stream travels through the pyrolysis zone of the flow system. Most of these radicals then are dehydrogenated catalytically as the pyrolyzate streams away from the furnace³ (eq. 3).



Side reactions comprise coupling of *p*-methylbenzyl radicals to give 1,2-di-*p*-tolylethane and *p*-ethyltoluene. If formed in the pyrolysis zone,

(1) This work was done in the laboratories of the M. W. Kellogg Company. The data were acquired by the Minnesota Mining and Manufacturing Company with the purchase of the Chemical Manufacturing Division of the M. W. Kellogg Company in March, 1957.

(2) L. A. Errede and J. P. Cassidy, *J. Am. Chem. Soc.*, **82**, 3653 (1960).

(3) L. A. Errede and J. P. Cassidy, Paper XVII, *J. Phys. Chem.*, in press.

these compounds can continue to react to give 4,4'-dimethylstilbene and *p*-methylstyrene. In addition the ditolylethane can rearrange to the *o*-methylidiphenylmethane, which in turn can be converted to the corresponding anthracene.² When the pyrolysis conditions are severe, cyclooctatetraene and styrene are produced in appreciable amounts, presumably *via* successive thermal rearrangements^{2,4} as indicated in Fig. 1. Demethylation is a major competing reaction that consumes *p*-xylene² and complicates the pyrolysis.

Solutions of *p*-xylene are prepared by collecting the *p*-xylene pyrolyzate in a solvent kept at -78° .⁵ When these solutions are warmed to room temperature, the accumulated *p*-xylene polymerizes rapidly to give insoluble poly-(*p*-xylene)⁵ easily separated by filtration. The other non-volatile but soluble products (low molecular weight polymer, the diarylethanes, the diarylmethanes, and the anthracenes) can be recovered from the mother liquor by evaporation to dryness.^{2,6}

It was shown² that 96–100% of the phenyl units metered to the pyrolysis system as *p*-xylene can be accounted for if the non-volatile products are weighed as "*p*-xylyl equivalents"² and the volatile components (*p*-xylene, toluene, styrene, and *p*-ethyltoluene) are determined by mass spectrometric analysis of an aliquot sample. Since all the reaction products containing phenyl units are formed *via* a common intermediate, *p*-methylbenzyl radical as shown in Fig. 1, the sum total moles of stable end products exclusive of toluene represents the number of moles of *p*-methylbenzyl radicals generated by pyrolysis of *p*-xylene.

(4) E. J. Prosen, W. H. Johnson, and F. D. Rossini, *J. Am. Chem. Soc.*, **69**, 2068 (1947).

(5) L. A. Errede and B. F. Landrum, *ibid.*, **79**, 4952 (1957).

(6) L. A. Errede, R. S. Gregorian, and J. M. Hoyt, *ibid.*, **82**, 5218 (1960).

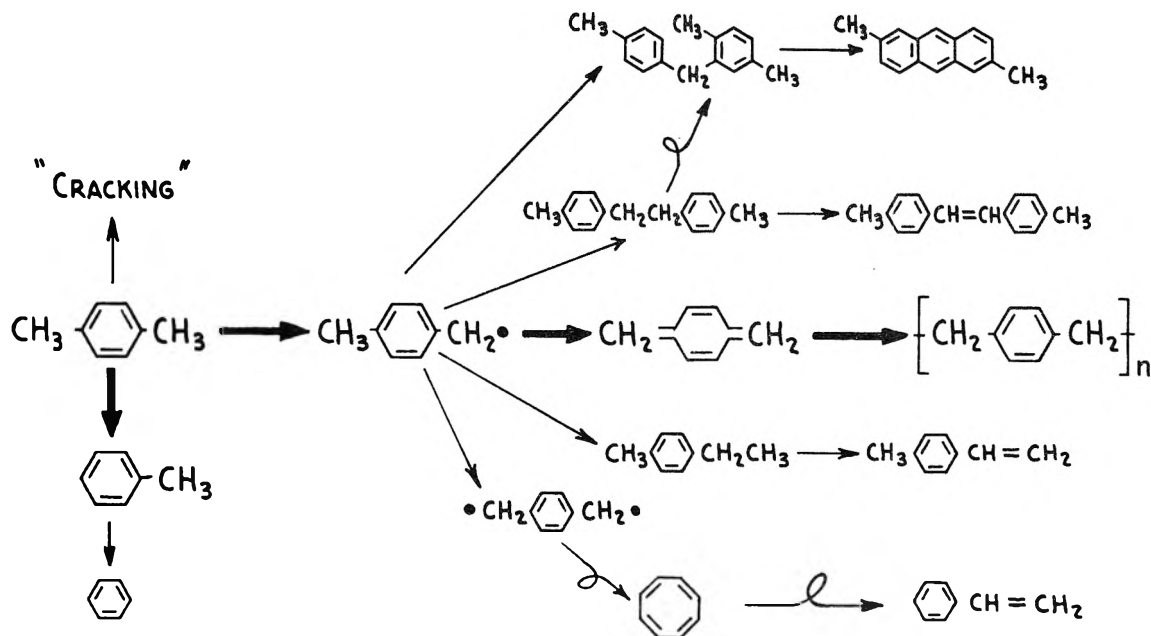
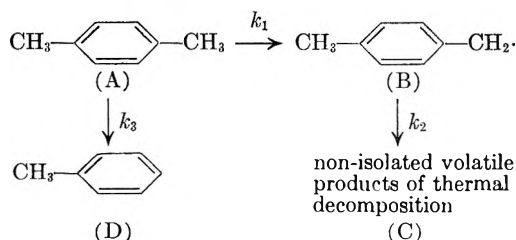


Fig. 1.—Reactions that account for the products isolated when *p*-xylene is subjected to fast flow pyrolysis at low pressure. Bold faced arrows indicate the main reaction paths and smaller arrows indicate less important side reactions.

These results suggested that the over-all pyrolysis kinetics could be followed by total analysis of the reaction products using a combination of gravimetric analysis for non-volatile products and mass spectrometric analysis for volatile products. It was of interest to compare these results with those reported by earlier workers^{7,8} who studied the pyrolysis of *p*-xylene indirectly by measuring the rate of hydrogen and methane formation.

Results and Discussion

Since most of the products of *p*-xylene pyrolysis can be traced to *p*-methylbenzyl radicals as shown in Fig. 1, the pyrolysis picture can be simplified for the purpose of the kinetic studies to the following indicated reactions



It was shown that k_1 and k_3 are first-order reactions.^{7,8} If one makes the assumption that k_2 is also a first-order reaction and that k_1 , k_2 , and k_3 are the only reactions of importance that consume *p*-xylene (A) and *p*-methylbenzyl radicals (B), to give toluene (D) and non-isolated volatile products of thermal decomposition (C), respectively, one then can write the rate equations

$$-\frac{dA}{dt} = k_1A + k_3A \quad (5)$$

(7) M. Szwarc, *J. Chem. Phys.*, **16**, 128 (1948).

(8) J. R. Schaeffgen, *J. Polymer Sci.*, **15**, 203 (1955).

$$\frac{dB}{dt} = k_1A - k_2B \quad (6)$$

$$\frac{dC}{dt} = k_2B \quad (7)$$

where the letters *A*, *B*, and *C* refer to the mole fraction of the components in question. Equation 5 can be integrated to give

$$A = A_0 e^{-(k_1+k_3)t} \quad (8)$$

Substitution of (8) into eq. 6 gives

$$\frac{dB}{dt} = k_1A_0 e^{-(k_1+k_3)t} - k_2B \quad (9)$$

Equation 9 is a linear equation of the first order and it can be shown that the integrated form of eq. 9 is

$$B = \frac{k_1A_0 e^{-k_2t}}{k_2 - (k_1 + k_3)} [e^{(k_2 - (k_1 + k_3))t} - 1] \quad (10)$$

If we let $K = k_1 + k_3$ and divide both sides by *t* one obtains

$$\frac{F}{t} = \frac{B/A_0}{t} = \frac{k_1 e^{-k_2t}}{k_2 - K} \left[\frac{e^{(k_2 - K)t} - 1}{t} \right] \quad (11)$$

where F^9 is the fraction of *p*-xylene converted to *p*-methylbenzyl radicals. Equation 11 can be rewritten as eq. 12.

(9) $F = \sum n_i/n_x$, where $\sum n_i$ is the moles of *p*-methylbenzyl radicals produced and isolated as "*p*-xyllyl equivalents," styrene, and *p*-ethyltoluene, and where n_x is the number of moles of *p*-xylene metered to the pyrolysis system.

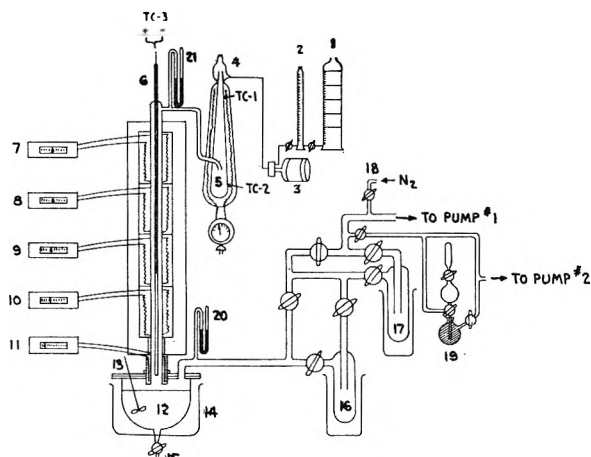


Fig. 2.—Pyrolysis system used for kinetic study of fast flow pyrolysis of *p*-xylene. Procedure and definition of numbered articles are given in the Experimental section.

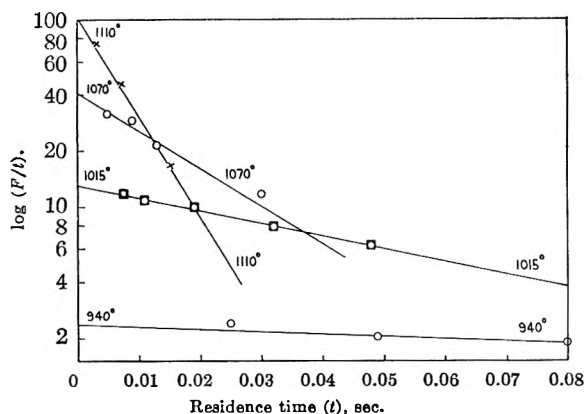


Fig. 3.—Plot showing log ratio of fractional conversion of *p*-xylene to *p*-methylbenzyl radicals (F) over residence time (t) as a function of residence time in seconds in a platinum lined Inconel tube.

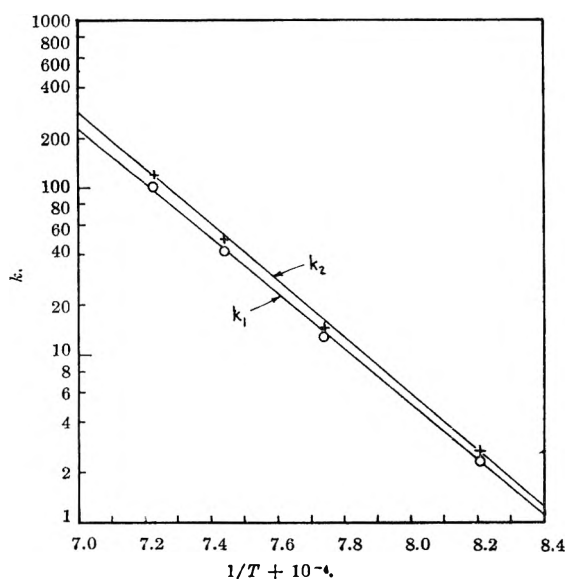


Fig. 4.—Arrhenius plot showing rate of formation of *p*-methylbenzyl radicals from *p*-xylene (k_1 , \odot) and rate of destruction of *p*-methylbenzyl radicals to give non-condensable gases (k_2 , \times) as a function of reciprocal of absolute temperature. Pyrolyses were carried out in a platinum lined Inconel tube.

$$\ln(F/t) = \ln k_1 - \ln(k_2 - K) - k_2 t + \ln \left[\frac{e^{(k_2 - K)t} - 1}{t} \right] \quad (12)$$

The last term of eq. 12 can be expressed in the form of a power series which, if divided by t and if the terms for $\ln(k_2 - K)$ are combined, gives eq. 13.

$$\ln(F/t) = \ln k_1 - k_2 t = \ln \left[1 + \frac{(k_2 - K)t}{2!} + \dots + \frac{[(k_2 - K)^{n-1} t^{n-1}]}{n!} \right] \quad (13)$$

When $k_2 - K$ is small the entire third term of eq. 13 converges to zero as t approaches zero and for pyrolysis temperatures below 1050° can be neglected when t is < 0.05 sec. Hence, eq. 13 reduces to its much simplified form, eq. 14, or to its alternate equivalent form, eq. 15.

$$\ln(F/t) = \ln k_1 - k_2 t \quad (14)$$

$$F = k_1 t e^{-k_2 t} \quad (15)$$

If $\log F/t$ is plotted as a function of t , the residence time, one should obtain a straight line. The intercept of this line at $t = 0$ gives the rate constant for *p*-methylbenzyl radical formation (k_1) and the slope gives the rate constant for subsequent thermal degradation of the aromatic nucleus (k_2).

The definition of residence time reported in earlier pyrolysis studies is sometimes rather arbitrary. Here residence time (t) is defined as the average time the gas molecules are at reaction temperature. This was calculated by means of eq. 16.

$$t = \frac{60dAP}{n(1+x)RT} \quad (\text{in seconds}) \quad (16)$$

where A is the cross-sectional area of the pyrolysis tube in cm^2 , d is the length of the pyrolysis zone in cm , P is the reaction pressure in mm , n is the *p*-xylene throughput in moles/min , x is the fraction of *p*-xylene converted to other products, R is the gas constant in $\text{cm}^3\text{-mm/mole-deg}$, and T is the weighted average reaction temperature in $^\circ\text{K}$. The pyrolysis zone (d) was defined arbitrarily as the distance through which the temperature of the gas stream was not less than 50° below its maximum, since it was observed that below this limit the relative contribution to total pyrolytic conversion is very small. The length of the pyrolysis zone was established by means of a sliding thermocouple in a central thermowell coaxial with the length of the pyrolysis tube.

Pyrolyses were carried out initially in the relatively small apparatus shown in Fig. 1 of ref. 5. This system later was modified as shown in Fig. 2 of this publication to permit better control of the pyrolysis conditions. The multiple unit furnace enabled us to vary the pyrolysis zone from 8 to 40 in. The pyrolysis tube was 6 ft. long and 1 in. i.d. It was fitted with a $5/16$ in. o.d. thermowell that extended the full length of the tube. The

temperature was measured internally by means of a movable platinum-rhodium thermocouple. Temperature profiles indicated a sharp rise of about 100°/in. to a thermal plateau where the temperature was constant within $\pm 2^\circ$. At the exit side of the furnace system, the temperature fell sharply (about 100°/in.) to about 500°. The length of the pyrolysis zone was taken as the distance through which the gas was not less than 50° below the maximum temperature. A weighted average was recorded as the pyrolysis temperature. The throughput of *p*-xylene, metered as a liquid by means of a Zenith feed pump, could be controlled within ± 0.001 mole/min. from 0.01 to 0.5 mole/min. The pressure within the pyrolysis tube was kept constant within ± 0.1 mm. The pyrolyzate was collected in 15 l. of heptane and about 700-g. aliquots were used for gravimetric analysis of the non-volatile products after polymerization of *p*-xylylene. The volatile products were determined by mass spectrometric analysis of a second aliquot sample of the mother liquor. The over-all results were reproducible within 1 or 2%. Pyrolysis studies were carried out at 940, 1015, 1070, and 1110° using a platinum-lined Inconel tube. The data are collected in Table I.

When the log conversion to *p*-methylbenzyl radicals (F) at a given temperature divided by the residence time (t) was plotted as a function of the residence time, straight lines were obtained in agreement with eq. 15 as shown in Fig. 3. Accordingly, the corresponding rate constants k_1 and k_2 were calculated from the intercept and slope, respectively, of each line. The Arrhenius relation, shown in Fig. 4, was obtained when $\log k$ was plotted as a function of the reciprocal of absolute temperature. Hence, k_1 and k_2 were calculated to be

$$k_1 = 9.3 \times 10^{13} \exp(-76/RT) \quad (17)$$

$$k_2 = 2.4 \times 10^{14} \exp(-78/RT) \quad (18)$$

Equation 17 is in good agreement with the corresponding rate constant reported by Szwarc,⁷ who followed the reaction indirectly by measuring the hydrogen formation.

Pyrolyses also were carried out in a quartz tube of the same dimensions as the platinum-lined Inconel tube and comparable results were obtained, as shown in Table II. Similarly, the conversion to non-volatile "*p*-xylyl equivalents" was not modified appreciably when pyrolysis was carried out in the presence of various metallic surfaces¹⁰ as indicated in Table III.

These results confirm the earlier observation of Szwarc,⁷ who reported that conversion of *p*-xylene to *p*-methylbenzyl radicals is a homogeneous gas phase reaction; consequently the conversion is independent of the type of pyrolysis surface. On the other hand, conversion of *p*-methylbenzyl radicals to *p*-xylylene is a heterogeneous reaction,³ but this affects only the distribution of products, not the over-all conversion to *p*-methylbenzyl radicals and daughter products.

When the log fraction of unreacted *p*-xylene

(10) The authors are indebted to R. M. Mantell for performing these experiments.

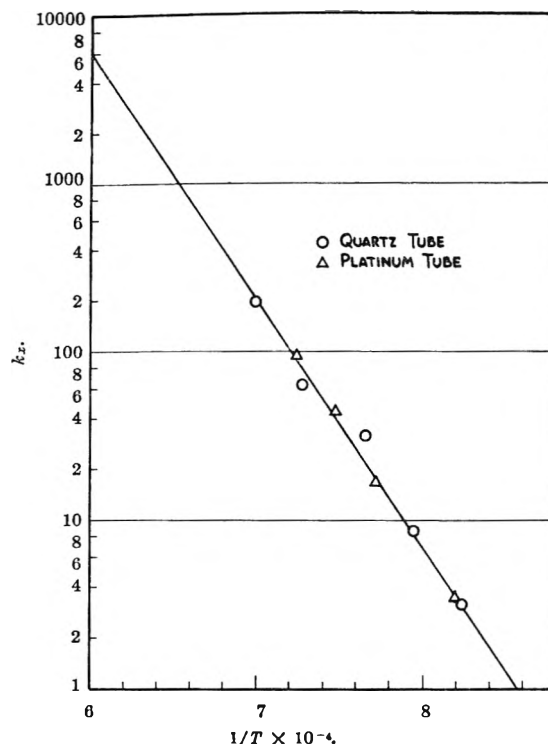


Fig. 5.—Rate of conversion of *p*-xylene to other products as a function of the reciprocal of the absolute temperature in a quartz tube \circ and in a platinum lined Inconel tube Δ .

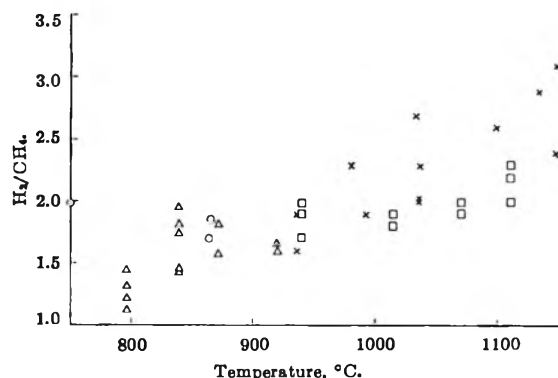


Fig. 6.—The ratio of H_2 to CH_4 produced as a function of the pyrolysis temperature: \circ , Szwarc's⁷ results; Δ , Schaeffer's⁸ results; \times , our data using a quartz pyrolysis tube; \square , our data using a platinum lined Inconel pyrolysis tube.

was plotted as a function of residence time at a given pyrolysis temperature, straight lines were obtained, indicating that the over-all pyrolytic disappearance of *p*-xylene is first order. The observed rate constants for conversion of *p*-xylene to other products in the platinum and the quartz reactors were plotted as a function of the reciprocal of the absolute temperature of reaction and a typical Arrhenius relationship was obtained in Fig. 5. Hence, the over-all rate constant for consumption of *p*-xylene to give total reaction products via several reaction paths was calculated to be

$$k_x = 2.9 \times 10^{18} \exp(-48 \text{ kcal.}/RT) \quad (19)$$

In this and previous studies^{7,8} it is noted that the ratio of H_2 to CH_4 produced is about 2/1. The ratio is independent of residence time but appears

TABLE I
FAST FLOW PYROLYSIS OF *p*-XYLENE IN A PLATINUM LINED INCONEL TUBE

Pyrolysis conditions		1110 ^g	1110	1070	1070	1070	1070	1010	1010	1010	1010	1010	940	940	940	940
Temp. (°C.)		1110 ^g	1110	1070	1070	1070	1070	1010	1010	1010	1010	1010	940	940	940	940
Residence time (sec.)		0.015 ^f	0.0070	0.030	0.013	0.0090	0.0048	0.032	0.019	0.011	0.0075	0.13	0.082	0.049	0.025	0.025
Product distribution ^a																
<i>p</i> -Xylene		.26	.55	.41	.58	.64	.79	.56	.64	.82	.87	.68	.75	.85	.91	.91
" <i>p</i> -Xylyl equivalents" ^b		.09	.24	.26	.24	.20	.13	.22	.20	.12	.09	.17	.16	.10	.06	.06
Calcd. ^c		(.29)	(.21)	(.24)	(.26)	(.22)	(.16)	(.22)	(.21)	(.17)	(.09)	(.17)	(.15)	(.10)	(.05)	(.05)
Toluene		.21	.13	.16	.14	.11	.07	.15	.11	.09	.06	.11	.09	.05	.02	.02
C ₈ H ₈ ^d		.09	.04	.07	.03	.04	.02	.05	.03	0	0	.04	0	0	0	0
C ₉ Aromatics ^e		.07	.04	.03	.01	.02	0	.03	.02	0	0	0	0	0	0	0
H ₂ /CH ₄		2.3 ^g	2.0	1.9	1.9	2.0	1.9	1.8	1.9	1.9	1.8	1.9	1.8	1.9	1.7	1.7
F/D ^f		1.3	2.5	2.4	2.2	2.0	2.4	2.0	2.3	2.0	2.2	1.9	1.8	2.0	3.0	3.0

^a Moles of product/mole of *p*-xylene metered to the system (about 10 moles of *p*-xylene used for each pyrolysis). ^b Isolated as polymerization products of *p*-xylylene, 1,2-di-*p*-tolylethane, diarylmethanes, and anthracenes. ^c Calculated by means of eq. 29-30 or by direct comparison with Fig. 9. ^d Mixture of cyclooctatetraene and styrene. ^e Mostly *p*-ethyltoluene. ^f F/D is ratio of (*p*-xylyl equivalents)/(toluene). ^g Large increase in proportion of ϵ cetylenes and olefins noted in gas sample.

TABLE II
FAST FLOW PYROLYSIS OF *p*-XYLENE IN A QUARTZ TUBE

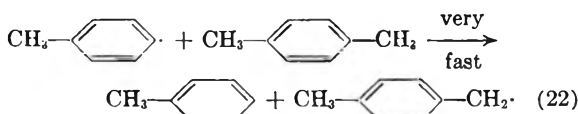
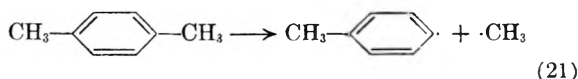
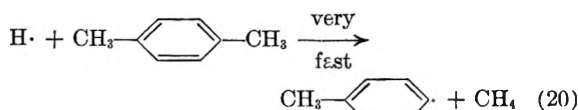
Pyrolysis conditions		1180	1140	1135	1135	1100	1065 ^f	1060	1040	1035	1035	1035	980	940	935
Temp. (°C.)		1180	1140	1135	1135	1100	1065 ^f	1060	1040	1035	1035	1035	980	940	935
Residence time (sec.)		0.017	0.0062	0.014	0.0043	0.040	0.004 ^f	0.021	0.0075	0.0084	0.0080	0.14	0.069	0.030	0.034
Product distribution ^a															
<i>p</i> -Xylene		.12	.32	.41	.77	.12	.76 ^f	.66	.80	.78	.78	.41	.54	.90	.91
" <i>p</i> -Xylyl equivalents" ^b		.34	.18	.30	.14	.29	.14 ^f	.23	.15	.17	.16	.22	.22	.07	.05
Calcd. ^c		(.27)	(.17)	(.27)	(.14)	(.21)	(.13)	(.26)	(.16)	(.17)	(.16)	(.15)	(.21)	(.07)	(.06)
Toluene		.18	.20	.14	.07	.22	.07 ^f	.08	.05	.05	.05	.21	.20	.03	.04
C ₈ H ₈ ^d		.12	.21	.07	0	.11	.02 ^f	.02	.06	.08	.08	.09	.04	0	0
C ₉ Aromatics ^e		.24	.09	.08	0	.26	.01 ^f	0	0	0	0	.07	0	0	0
H ₂ /CH ₄		3.2	2.4	1.8	2.8	2.6	2.3	2.0	2.0	1.9	2.3	1.6	1.9
F/D ^f		3.9	2.4	3.2	2.0	3.0	2.5 ^f	3.1	4.2	5.0	4.8	1.8	1.2	2.3	1.3

^a Moles of product/mole of *p*-xylene metered to the system (about 10 moles *p*-xylene used for each pyrolysis experiment). ^b Isolated as polymerization products of *p*-xylylene, 1,2-di-*p*-tolylethane, diarylmethanes, and anthracenes. ^c Calculated conversion by means of eq. 29-30 or Fig. 9. ^d Mixture of cyclooctatetraene and styrene. ^e Mostly *p*-ethyltoluene. ^f Experiment carried out using smaller pyrolysis unit. ^g F/D is the ratio of ("*p*-xylyl equivalents" + C₈H₈ + C₉ aromatics)/(toluene).

TABLE III
EFFECT OF PYROLYSIS SURFACE ON PYROLYSIS CONVERSION¹⁰

Pyrolysis tube packing Material	Pyrolysis Type	Pyrolysis conditions T, °C.	t (sec.)	% Conversion to non-volatile product	
				Expected	Observed
Copper	Gauze	1025	0.06	10	10
Iron	Gauze	1025	.06	10	8
Nickel	Wire	1010	.06	7	8
Nichrome	Wire	1010	.06	7	8
Platinum	Gauze	1010	.06	7	7
Silver	Wool	900	.06	Trace	Trace

to increase with increase in pyrolysis temperature as shown in Fig. 6. These observations can be accounted for by assuming toluene formation *via* reaction 20 as suggested by Szwarc⁷ or by reaction 21 as suggested by Schaeffgen.⁸



Toluene, formed by abstraction of a hydrogen atom from a neutral molecule (as indicated in reaction 22), is consumed in turn by thermal reactions analogous to those that convert *p*-xylene to daughter products as shown in Fig. 1. Equation 23 can be derived in a way analogous to that for conversion of *p*-xylene to *p*-methylbenzyl radicals.

$$D = k_3 t \exp(-k_4 t) \quad (23)$$

where D is the fraction of *p*-xylene isolated as toluene, k_3 is the rate constant for formation of toluene from *p*-xylene, k_4 is the over-all rate constant for consumption of toluene to give benzene and other degradation products, and t is the residence time. In accordance with eq. 23, straight lines are obtained when $\log D/t$ is plotted as a function of t as shown in Fig. 7; hence k_3 and k_4 were determined from the intercept and slope, respectively, for each line. Straight lines also are obtained when $\log k_3$ and $\log k_4$ are plotted as a function of the reciprocal of the absolute temperature as shown in Fig. 8. Consequently the rate expressions for k_3 and k_4 were calculated to be

$$k_3 = 9.3 \times 10^{12} \exp(72/RT) \quad (24)$$

$$k_4 = 3.4 \times 10^{14} \exp(80/RT) \quad (25)$$

The fraction of *p*-xylene isolatable as toluene calculated by means of eq. 24 and 25 agrees within experimental error with the data reported by Schaeffgen.⁸

The ratio of H_2 to CH_4 is about equal to the ratio of the fraction of *p*-xylene isolated as daughter products of *p*-methylbenzyl radicals (F) to the fraction of *p*-xylene isolated as toluene (D) as shown in Tables I and II. This agreement suggests that

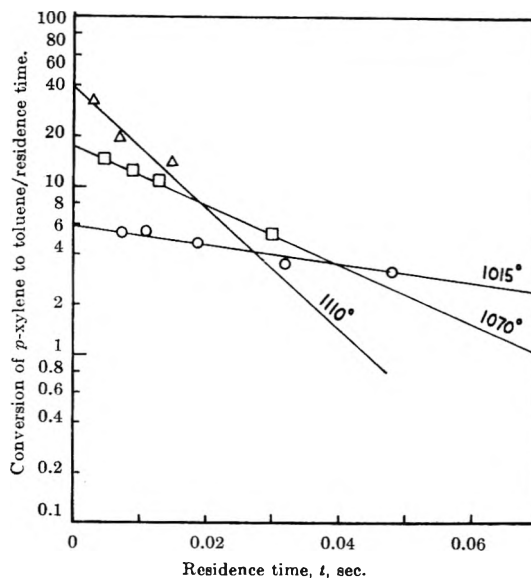


Fig. 7.—Plot showing log ratio and fractional conversion of *p*-xylene to toluene (D) over residence time (t) as a function of residence time in seconds.

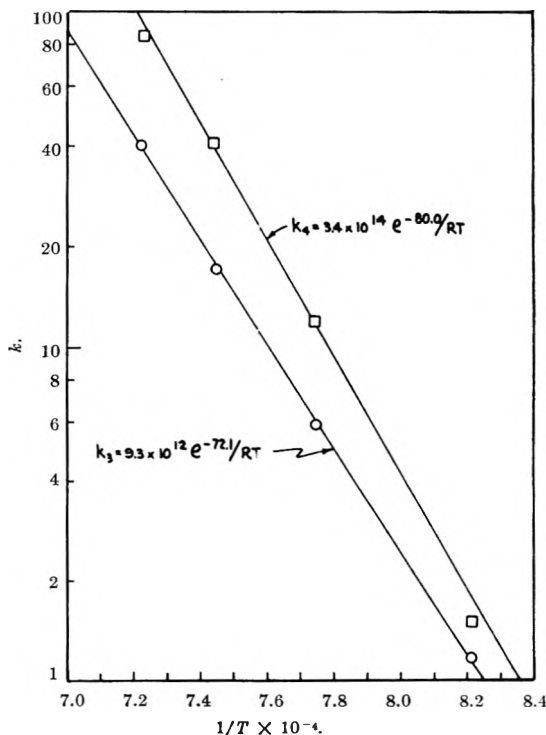


Fig. 8.—Arrhenius plot showing rate of formation of toluene (k_3 , \circ) from *p*-xylene and rate of destruction of toluene (k_4 , \square) as a function of reciprocal of absolute temperature.

formation of *p*-methylbenzyl radicals (eq. 1) and toluene (eq. 21) might occur *via* simultaneous reactions as postulated by Schaeffgen.⁸

The ratios of H_2/CH_4 and C/D , however should be dependent on residence time as indicated by eq. 26.

$$\log(C/D) = \log(k_1/k_3) - \left(\frac{k_4 - k_2}{2.3}\right)t = \log(\text{H}_2/\text{CH}_4) \quad (26)$$

It was observed that the ratios in question appear to be independent of the residence time. The contribution of residence time, however, is relatively small, and since other pyrolytic reactions such as cracking also are concurrent reactions, the small over-all effect of residence time might be masked within the range of experimental reproducibility.

On the other hand, Szwarc's mechanism is favored when one considers the relative bond dissociation energies for rupture of Ar-CH₃ and ArCH₂-H bonds. The former requires about 90 kcal.¹¹ and the latter about 75 kcal.¹¹ The present data as well as that of Szwarc⁷ and of Schaeffgen⁸ indicate that the activation energy for formation of toluene from xylene is from 72 to 82 kcal. This range is considerably lower than that required for direct thermal rupture of the Ar-CH₃ bond, indicating that some form of secondary reaction is responsible for toluene formation, perhaps as suggested by Szwarc. The observations reported thus far, however, are mutually inconsistent and suggest that more research in this area is necessary before one can accept with confidence the true mechanism for pyrolytic formation of toluene.

The highest conversion of *p*-xylene to non-volatile "p-xylyl equivalents" realized by earlier workers^{7,8,12-15} was about 26%. It was suggested by Corley, *et al.*,¹³ that even better results could be obtained if it were possible to carry out pyrolyses at relatively higher temperatures (<1150°) and correspondingly shorter residence times (<0.008 sec.). This possibility was investigated in our Laboratory using the small pyrolysis system shown in Fig. 1 of ref. 5.

It was established² that pyrolysis of *p*-xylene at 1065 ± 5° and 0.0041 ± 0.0003 sec. residence time in the pyrolysis zone of this apparatus affords a 14 ± 1% conversion to non-volatile "p-xylyl equivalents." Since this value represents about 90% of the *p*-methylbenzyl radicals generated by pyrolysis, simple gravimetric analysis appeared to be a convenient method for following the conversion of *p*-xylene to *p*-methylbenzyl radicals as a function of pyrolysis temperature and residence time. It was found that the reproducibility of the pyrolysis data was not sacrificed if one used only 100-cc. aliquots of the cold *p*-xylylene solution for determination of the "p-xylyl equivalents." This simplification enabled us to use the main portion of the monomer solution (4.5 l.) for elucidation of the chemistry of *p*-xylylene. Most of our pyrolyses were carried out at below 5 mm. pressure to ensure high efficiency in conversion to this monomer (about 70-80%).^{3,5,6}

In this way, data relating conversion of *p*-xylene to non-volatile "p-xylyl equivalents" (*F*) as a function of pyrolysis temperature (*T*) and residence time (*t*) were accumulated routinely over a period of many months. These data, collected prior to

our kinetic study already described, are summarized in Fig. 9, which is a two-dimensional projection on the *T*-*t* plane of the three-dimensional surface relating *F*, *T*, and *t*. The data are shown on a semilog scale to provide adequate detail on a small graph. The contour lines represent the best lines drawn through isoconversion points that are reproducible within ±1% with about 65% confidence. These isoconversion lines show the maximum conversion area in the form of a long ridge, the crest of which is indicated by the dotted line. The highest point of this ridge represents a maximum conversion of about 30-32%, realizable at about 1100-1150° and 0.020-0.025 sec. residence time. In general, those pyrolyzates in the area below 1050° and to the left of the ridge line were light amber and the polymer produced from these solutions was almost snow-white. In other areas, especially above 1050°, the pyrolyzates were dark amber to dark brown, indicating that considerable thermal degradation had occurred. The polymers produced from these solutions were amber in color. When exposed to ultraviolet light they appeared bright yellow or purple owing to absorbed 2-methylantracene or anthracene, respectively, depending on the severity of the pyrolysis condition.

Below 1050° the intersections of *c*-*t* planes, with the three-dimensional surface represented by Fig. 9, are a family of curves with maxima that increase with increase in temperature as shown in Fig. 10. The dotted lines for 850 and 800° were calculated by eq. 27 through 30 derived later and then checked by only one or two experiments; they do not represent examples of summary data and are included in Fig. 10 only to illustrate the trends.

These curves in Fig. 10 can be represented by

$$F' = Ate^{-Bt} \quad (27)$$

or

$$\log (F't) = \log A - (B/2.3)t \quad (28)$$

which are similar in form to eq. 14 and 15. Consistent with eq. 28, straight lines were obtained when $\log (F'/t)$ was plotted as a function of *t*. The constants *A* and *B* were obtained from the intercept and slope, respectively, of each line and the results were plotted in Fig. 11 as a function of the absolute temperature. Typical Arrhenius relationships are noted below 1040°, whereas above this temperature an inversion occurs and the slopes become positive. Apparently thermal degradation of the aromatic nucleus becomes significant above 1050° and this has an adverse effect on conversion to non-volatile "p-xylyl equivalents." Accordingly the conversion to *p*-xylylene is not increased appreciably above that already realized by Corley, *et al.*,¹³ when pyrolysis is carried out at higher temperatures and correspondingly shorter residence times as shown in Fig. 9.

The simplifying assumption that the non-volatile products represent >90% of the *p*-methylbenzyl radicals produced by fast flow pyrolysis is not valid above 1040°. Below this temperature, however, *A* and *B* are given by eq. 29 and 30.

(11) L. A. Errede, *J. Phys. Chem.*, **64**, 1031 (1960).

(12) R. N. Roper, private communication, 1953.

(13) R. S. Corley, H. C. Haas, M. W. Kane, and D. L. Livingston, *J. Polymer Sci.*, **13**, 137 (1954).

(14) M. H. Kaufman, H. F. Mark, and R. B. Mesrobian, *ibid.*, **13**, 3 (1954).

(15) L. A. Auspos, L. A. R. Hall, J. K. Hubbard, W. Kirk, Jr., J. R. Schaeffgen, and S. B. Speck, *ibid.*, **15**, 9 (1955).

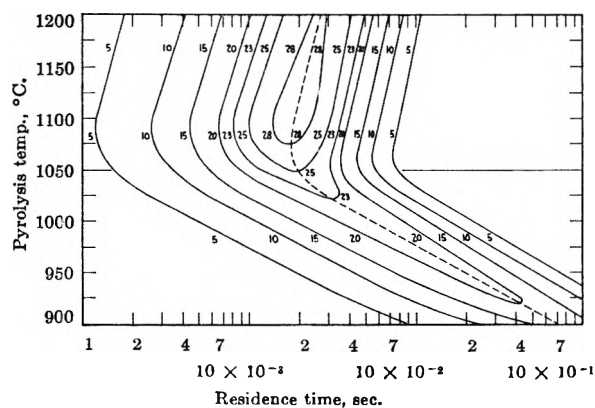


Fig. 9.—Yield contour plot for conversion of *p*-xylene to *p*-methylbenzyl radicals as a function of pyrolysis temperature and residence time. Data accumulated routinely over a period of many months using quartz pyrolysis system and simplified gravimetric procedure.

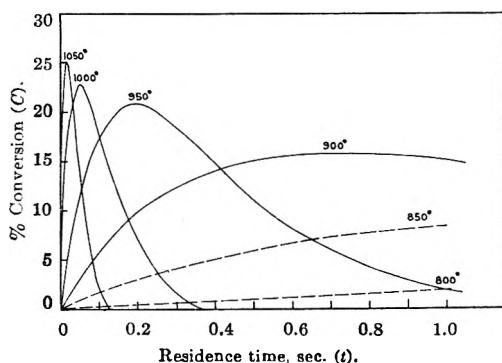


Fig. 10.—% conversion of *p*-xylene to *p*-methylbenzyl radicals as a function of residence time.

$$A = 2.61 \times 10^{15} \exp(-83.2/RT) \quad (29)$$

$$B = 8.45 \times 10^{14} \exp(-79.6/RT) \quad (30)$$

Equations 29 and 30 are reasonably close to the rate constants k_1 and k_2 given in eq. 17 and 18.

Although eq. 29 and 30 are not valid rate expressions, they can be used to check the data reported by earlier workers.¹²⁻¹⁵ These reported data for conversion of *p*-xylene to non-volatile "*p*-xylyl equivalents" at supposedly the same pyrolysis temperature and residence time are not in agreement from one laboratory to another. These differences appear to be manifestations of arbitrary ways for defining residence time. To compare some of the earlier data with our results, a correction factor was applied to the residence times reported from a given laboratory. Accordingly, the residence times reported by Corley, *et al.*,¹³ were divided by two, whereas those reported by Schaeffgen⁸ were used uncorrected. No residence time was reported by Kaufman, *et al.*,¹⁴ but this information could be calculated from the reported throughput of *p*-xylene, their description of the pyrolysis system, and the use of eq. 16 of this publication. Figure 12 shows the close agreement between these pyrolysis data and the corresponding data calculated by means of eq. 16, 27, and 28.

The universal reproducibility gave us confidence in the reliability of these equations; hence, they were used to determine the amount of *p*-methylbenzyl radicals available for reaction when con-

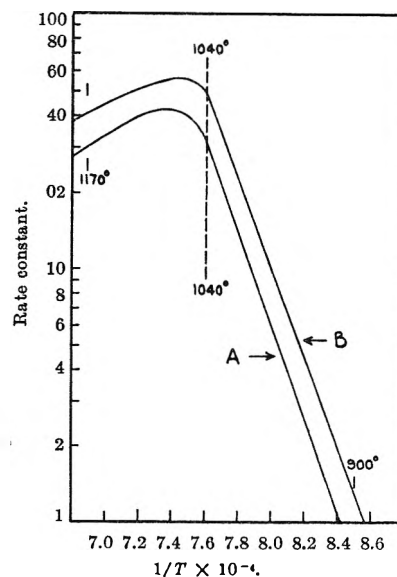


Fig. 11.—Plot showing the A and B terms of eq. 27 as a function of reciprocal of absolute temperature.

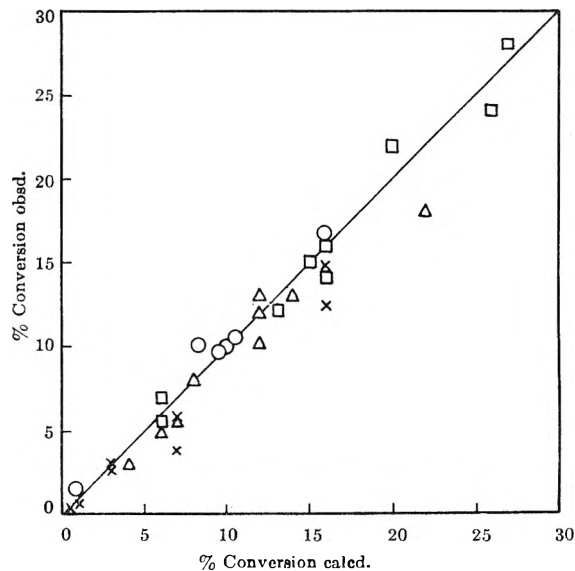


Fig. 12.—Comparison of calculated and observed per cent conversion of *p*-xylene to non-volatile "*p*-xylyl equivalents": \circ , data from Kaufman, *et al.*,¹⁴ residence time calculated on the basis of descriptive data; \times , data from Schaeffgen⁸; Δ , data from Corley, *et al.*,¹³ residence times reported were divided by two owing to arbitrary difference in defining length of pyrolysis zone; \square , data obtained by Errede and DeMaria using a larger pyrolysis system, shown in Fig. 2.

ventional methods of analysis were not applicable.¹⁶ The conversion and yields of monofunctional and difunctional derivatives of *p*-xylene produced *via* reaction of *p*-methylbenzyl radicals and/or *p*-xylylene with other radicals in gas phase were compared with the corresponding calculated amounts using these equations. Relatively good agreement was noted, as described in our other publications.^{3,16}

Experimental

Procedure for Gravimetric Determination of "*p*-Xylyl Equivalents."—The apparatus shown in Fig. 1 of ref. 5

(16) Paper XVI, L. A. Errede and J. P. Cassidy, *J. Phys. Chem.*, in press.

was used in this investigation. Fast flow pyrolysis of *p*-xylene at low pressure was carried out under predetermined reaction conditions according to the procedure described previously.⁵ The pyrolyzate was collected in a weighed 6-l. flask containing 4.5 l. of solvent, usually heptane, kept at -78° . After accumulation of about 0.5 mole of *p*-xylylene, pyrolysis was terminated and the internal pressure of the evacuated system was equalized to that of the atmosphere by addition of nitrogen. The monomer receiver (no. 7) was disengaged from the pyrolysis system and weighed. The reaction mixture was agitated vigorously to ensure uniform suspension of crystalline *p*-xylene and three aliquot samples were withdrawn by means of a prechilled 100-cc. rapid delivery pipet. The aliquots were added to weighed erlenmeyer flasks which then were warmed to room temperature. The flask again was weighed and the contents evaporated in a stream of nitrogen to constant weight at room temperature. A small amount of polymer (about 1–3 g.) always deposited in the form of a film on the unprotected surface of the monomer receiver (no. 7) above the level of the liquid. The weight of this film was added to the average total weight of non-volatile products calculated from the aliquot samples.

In this way, all of the cold *p*-xylylene solution, minus the aliquot samples, was available for elucidation of the chemistry of this pseudo-diradical as described in preceding publications.^{5,6}

Fast Flow Pyrolysis of *p*-Xylene.—The pyrolysis system was assembled as shown in Fig. 2. The *p*-xylene reservoir consisted of a modified 2-l. graduate (1) and a 50-l. buret (2) installed in a series so that the feed rate could be checked continuously during the pyrolysis. The *p*-xylene was fed to the evacuated system by means of Zenith feed pump (3) back pressured to 50 p.s.i. An overflow (4) fitted to a conical flask (5) kept at 100° at its top and 150° at its bottom served as the vaporizer for *p*-xylene. The pyrolysis tube was 6 ft. long and 1 in. i.d. It was fitted with a 6-ft. thermowell (6) $\frac{5}{8}$ in. o.d. which contained a 6-ft. movable platinum-rhodium thermocouple protected by a 18-in. Inconel sheath. Two pyrolysis tubes were used alternately. One was made of quartz and the other was made of Inconel lined internally with a 0.005 in. layer of platinum supported on a 0.025 in. layer of nickel. The pyrolysis furnace consisted of four 12-in. 4000-watt heating units made of coiled-coils of Kanthal wire. A smaller unit was used at the base of the furnace to heat the nozzle that protruded into the monomer condenser. Each heater was controlled by a Wheelco Capacitor unit (7–11). The monomer condenser was a kettle (12) 2 ft. in diameter and 15 in. deep, made of $\frac{1}{2}$ in. stainless steel. Its cover was fitted with a stirrer (13), pyrolysis nozzle inlet, solvent

inlet (not shown), and a gas outlet. The bottom was fitted with a Dry Ice–acetone cooling bath (14) through which extended a drain spout (15).

Two alternate 1-l. capacity traps (16 and 17) cooled with liquid air were used to collect any condensable product that escaped condensation in the Dry Ice trap. The system was evacuated by means of a 800 l./min. Beach-Russ pump (pump no. 1). The pressure was regulated by means of a continuous nitrogen bleed (18). A Toepfer pump (19) serviced by a regular 33 l./min. Welch pump (pump no. 2) was used to collect samples of the non-condensable gases. The pyrolysis pressure was recorded at the outlet (20) of the first condenser. The pressure at the top (21) of the pyrolysis tube was about 1 mm. higher than that recorded at the outlet. When not in use the pyrolysis system was filled with nitrogen. In general, pyrolyses were carried out as described below.

The system was evacuated and the heaters were adjusted to give the desired temperature over the desired length of pyrolysis zone. The cold traps were chilled to Dry Ice and liquid air temperature. Fifteen liters of heptane were metered through copper coils imbedded in the Dry Ice bath and then into the monomer condenser where the solvent was kept in circulatory motion by the motor-driven stirrer. The pressure was adjusted to the pre-selected value and *p*-xylene was metered through the Zenith feed pump at a predetermined rate to give the desired residence time, calculated as described in the Discussion. About 1060 g. (10 moles) of *p*-xylene was pyrolyzed in each run.

At the end of the pyrolysis, the solution produced in the Dry Ice cold trap was drained through the bottom of the condenser into a weighed receiver. Three weighed aliquots were taken (about 700 g. each) for gravimetric analysis. The remaining solution (about 2 l.) was used to elucidate the chemistry of *p*-xylylene as described previously.^{5,6,17–20} Less than 1% of the accumulated *p*-xylylene remained in the receiver as polymer.

The three aliquot samples were warmed to room temperature and the insoluble poly-(*p*-xylylene) produced thereby was separated by filtration. A 10-cc. sample of the mother liquor was taken for mass spectrometric analysis of the volatile components; the remainder was evaporated to constant weight. The weight of insoluble polymer and residue of soluble non-volatile products of pyrolysis and polymerization was taken as the weight of "*p*-xylyl equivalents" in the aliquot. The average of the three aliquots, which agreed within 1–2%, was recorded as the best value. The mass spectrometric analysis data for *p*-xylene, toluene, styrene, *p*-ethyltoluene, etc., were accurate within 10%. The data are collected in Tables I and II.

Gas samples were taken by means of the Toepfer pump in the usual way. The composition of the gas sample in mole % was determined by mass spectrometric analysis. The major components were H_2 and CH_4 with trace amounts of ethylene, propylene, acetylenes, and butenes. The ratios of H_2 and CH_4 are shown in Fig. 6.

(17) L. A. Errede and J. M. Hoyt, *J. Am. Chem. Soc.*, **82**, 436 (1960).

(18) L. A. Errede, J. M. Hoyt, and R. S. Gregorian, *ibid.*, **82**, 5224 (1960).

(19) L. A. Errede and W. A. Pearson, *ibid.*, **83**, 954 (1961).

(20) L. A. Errede and R. S. Gregorian, *J. Polymer Sci.*, **60**, 21 (1962).

γ -IRRADIATION OF SMALL MOLECULES AT 4 AND $77^{\circ}K$.¹

BY ROLAND E. FLORIN, DANIEL W. BROWN, AND LEO A. WALL

Polymer Chemistry Section, National Bureau of Standards, Washington, D. C.

Received May 31, 1962

The γ -irradiation of CH_4 , CF_4 , and SiF_4 was investigated by electron spin resonance both at 4 and $77^{\circ}K$. The influence of inert matrices of Xe also was studied and found to be useful in trapping radical species, particularly at $77^{\circ}K$. The electron spin resonance spectra for the radicals CH_3 and CF_3 were altered profoundly by both temperature and presence of the matrix, whereas that for SiF_3 was not. Spectra from several irradiated fluorocarbons also are reported.

1. Introduction

The atoms and radicals formed by irradiating small molecules are interesting as the simplest prototypes of radicals to be expected in irradiated polymers where identification is less certain.

(1) Based on work supported by the Aeronautical Research Laboratory, Wright Patterson Air Force Base, Ohio.

The main features of the e.s.r. spectrum of CH_3 are now well known.² There are four lines, resulting from hyperfine interaction of the odd electron with the three methyl hydrogen atoms. However, in

(2) (a) C. K. Jen, S. N. Foner, E. L. Cochran, and V. A. Bowers, *Phys. Rev.*, **112**, 1169 (1958); (b) L. A. Wall, D. W. Brown, and R. E. Florin, *J. Phys. Chem.*, **63**, 1762 (1959).

irradiated methane at 4°K., the lines are rather broad. Upon heating to 20°K., the lines are narrowed somewhat, presumably because greater freedom of rotational motion has decreased the line broadening effect of anisotropic hyperfine interaction in the polycrystalline medium; the line shape is also somewhat complicated. Unfortunately, the lifetime of radicals in irradiated pure methane at 77°K. is too short for observation by ordinary methods. To obtain radicals at relatively high temperatures, where greater freedom of motion and sharper lines could be expected, the use of xenon as a trapping matrix at 77°K. (m.p. 161°K.) appeared promising. In connection with current interest in fluorocarbon polymers, the simple fluorine-containing molecules CF_4 and SiF_4 , and others slightly more complicated, also were irradiated.

2. Experimental

The techniques have been described previously.^{2b} About 1 mmole of sample in the lower end of a high-purity silica tube 0.3 by 70 cm. was irradiated at 4 or 77°K. by a Co^{60} γ source giving approximately 5×10^6 r./hr. Before irradiation, mixing was ensured by allowing the sample to remain as vapor for several hours and rapidly condensing in the lower end of the tube. Samples to be used at 77°K. were melted and refrozen rapidly after the initial condensation. The detailed phase behavior of the solid mixtures is unknown. At 77°K., the volatility of CH_4 and CF_4 could have permitted redistribution of components during irradiation, although no gross changes were evident. Samples were observed with a Varian 4500 e.s.r. spectrometer, the cavity of which accommodated the lower tip of a dewar containing the sample in a bath of He, H_2 , O_2 , or CH_4 . Microwave frequency was near 9200 Mc. and power level in the cavity was in the range of 0.3 to 1 mw. A low-power bridge was used for some of the work at 4°K., and 100-kc. field modulation was used with some of the observations at 20°K. and in all work at 77°K. At 77°K., saturation usually was unappreciable at microwave power levels of 1 to 3 mw.; lower power levels than this usually were required at the lower temperatures.

3. Results and Discussion

Spectra of CH_3 and CF_3 at 77°K.—The e.s.r. spectrum of irradiated CH_4 is due to CH_3 and H at 4°K. and to CH_3 alone at 20°K. and in the Xe mixtures at 77°K. The different spectra are shown in Fig. 1. Undiluted CH_4 and CF_4 show no radicals at 77°K. Besides the regular spectrum, the usual sharp hydrogen atom lines of low integrated intensity, commonly observed in irradiations conducted in quartz at 77°K., were evident as well, even in irradiated SiF_4 and CF_4 .

Some specimens of CH_4 , observed at 4 or 20°K., after annealing at 20°K., and the CH_4 -rich Xe mixtures observed at 77°K., exhibit satellite peaks. For the 77°K. specimens, the most prominent positions, which are poorly defined, appear to be -26 and -9 gauss from the first peak, and $+9$ gauss from the fourth peak (Fig. 1B). There are further peaks at 20°K. (Fig. 1C).

These satellites may be due to multiple sites, CH_3 in a CH_4 matrix having slightly different spacing parameters from CH_3 in Xe. Another possible cause is a combination of anisotropic g-tensor and anisotropic hyperfine structure; the former can give rise to over-all dissymmetry, and the latter, with appropriate values of parameters, can give the appearance of as many as three derivative peaks in one actual line.^{3,4}

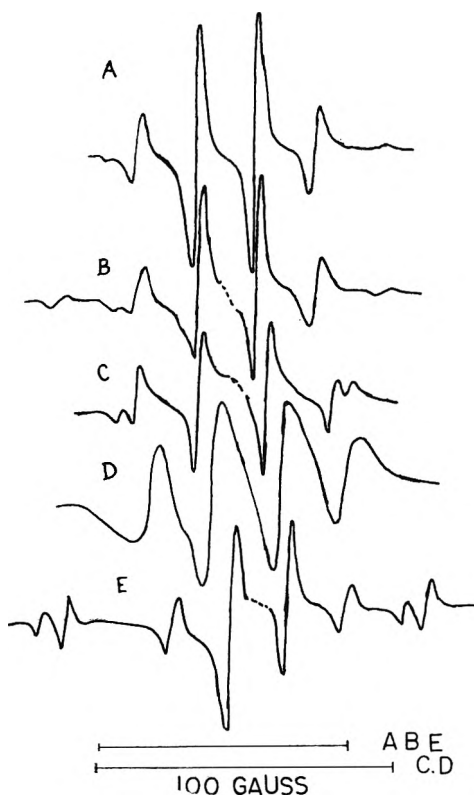


Fig. 1.—E.s.r. spectra of CH_3 and CF_3 : A, 23% CH_4 in Xe at 77°K.; B, 69% CH_4 in Xe, 77°K.; C, CH_4 at 20°K.; D, CH_4 at 4°K.; E, 15% CF_4 in Xe at 77°K.

The lines of the low CH_4 mixture (23% CH_4) at 77°K. are well separated even in the integral. The separation is poorer in the CH_4 -rich material; although the derivative peak widths differ but little, the width at half maximum absorption is about 20% greater in the 69% CH_4 mixture. The width at which the derivative attains half its maximum value is more easily measured, and is listed in Table I for various irradiated methane samples, along with the derivative peak width. In a sample cooled to 20°K., these width parameters are hardly greater than at 77°K., and in a sample irradiated at 4° and annealed at 20°K., they actually are less, but in both of these cases there is extra satellite line structure. The appreciably greater width of samples irradiated at 4 or 20°K. and kept without heating may be due mainly to these satellites. Rotational jumps presumably are frequent in an important number of sites at all temperatures and in all mixtures. There is no evidence for R...Xe hyperfine interaction similar to that seen in $\text{HI} + \text{Xe}^5$; either the wave-function of CH_3 does not mix with the electron wave function of xenon as well as is done by the S-function of H atoms, or rapid relaxation at 77°K. broadens such hyperfine structure beyond detection. In the latter case, xenon hyperfine structure fields might be detectable at 4°K.

(3) S. M. Blinder, *J. Chem. Phys.*, **33**, 743 (1960).

(4) E. L. Cochran, F. J. Adrian, and V. A. Bowers, "Anisotropic Hyperfine Interactions in the ESR Spectra of Alkyl Radicals," Paper presented at 138th National Meeting of the American Chemical Society, New York, N. Y., September, 1960.

(5) S. N. Foner, E. L. Cochran, V. A. Bowers, and C. K. Jen, *Phys. Rev. Letters*, **2**, 43 (1959).

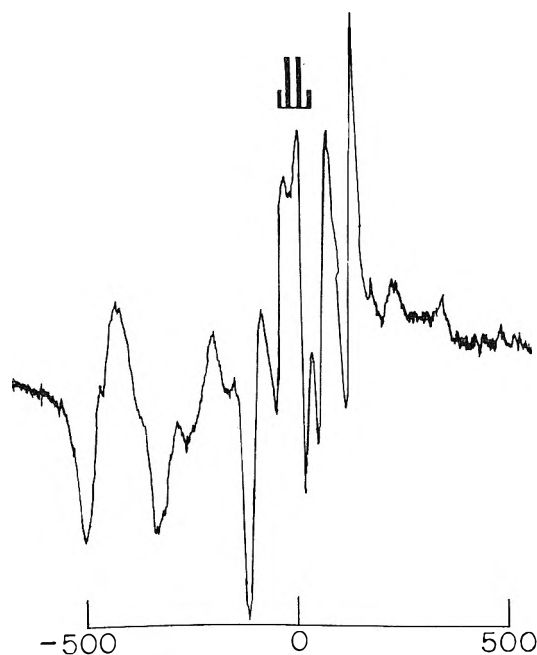


Fig. 2.—E.s.r. spectrum of CF_4 irradiated at 4°K . Lines of 77°K . spectrum, Fig. 1E, shown for comparison.

The main peaks of CF_3 , in $\text{CF}_4\text{-Xe}$ at 77°K ., almost coincide with those of CH_3 (Fig. 1E). The over-all spacing (peak 1 to peak 4) is only about 1 to 1.5 gauss less in CF_3 , and the g -value is 0.0003 ± 0.0010 unit less. The CF_3 spectrum also contains two pairs of faint sharp peaks outside the main spectrum, at -52 and -45 gauss from peak 1 and at $+24$ and $+33$ gauss from peak 4. They are not symmetrical about the center; in each pair the weaker member lies at the lower field. Together they account for less than 10% of the total absorption, and they are less subject to power saturation than the main system. They do not appear in irradiated empty quartz tubes, and may possibly be due to reaction products of the quartz surface with fluorine atoms or fluorocarbon radicals. In view of the recent discovery of XeF_4 [H. H. Claassen, H. Selig, and J. G. Malm, *J. Am. Chem. Soc.*, **84**, 3593 (1962)], the species Xe^{129}F should be considered.

Spectrum of Irradiated CF_4 at 4°K .—The spectrum of CF_4 irradiated at 4°K . (Fig. 2) is completely different from the 77°K . CF_3 spectrum (Fig. 1E), and has no obvious relation to a CF_3 radical. Ultraviolet-irradiated CF_3I is reported to give a somewhat similar spectrum, except for the low-field region.^{5a} Conceivably, the diffuse low-field peaks and the most intense sharp peak may be due to F atoms, for which an abnormal spectrum is plausible. It has been suggested in view of considerable negative evidence that halogen atoms generally will be undetectable because of rapid relaxation broadening.^{2a} In the gas, Radford⁶ finds intermediate-field conditions at usual fields and frequencies, with $g = 4/3$, a large hyperfine

(5a) F. J. Adrian, E. L. Cochran, V. A. Bowers, "ESR Studies of Inorganic Free Radicals in Photolytic Systems," Paper presented at the 142nd National Meeting of the American Chemical Society, Atlantic City, N. J., September, 1962.

(6) H. E. Radford, *Bull. Am. Phys. Soc.*, [2] **3**, 325 (1958).

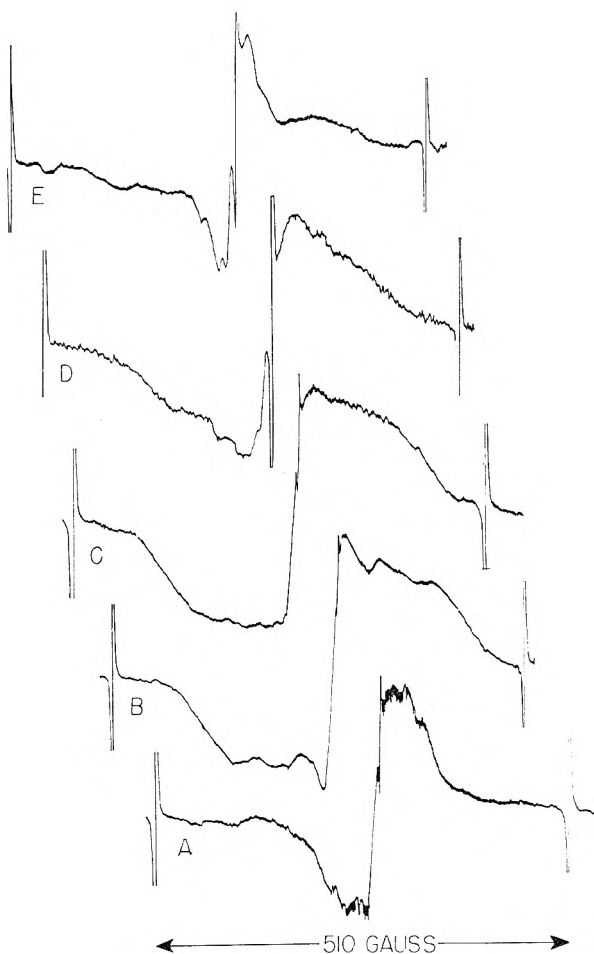


Fig. 3.—E.s.r. spectra of irradiated fluorocarbons at 77°K .: A, C_2F_4 ; B, C_3F_6 ; C, C_7F_{14} ; D, C_6F_6 ; E, C_7F_{16} .

coupling, and allowed and forbidden lines covering a wide range of magnetic fields. The V and V_t centers of irradiated LiF^7 have some slight bearing on the condition of F atoms in a condensed system, since they can be represented as F atoms coordinated with ions, (F^-F^-) and $(\text{F}^-\text{F}^-\text{F}^-)$, respectively. The hyperfine spacings in the latter are very large (400–1600 gauss), highly orientation-dependent, and unsymmetrical about $g = 2$.

In the present spectrum, if we provisionally exclude the low group of peaks and the very sharp peak at $+150$ gauss as due to F atoms, possibly the remaining sharp peaks at $+88$, $+28$, -35 , and -97 gauss could be attributed to non-rotating CF_3 with a very large anisotropic hyperfine interaction, and the more blunt peaks could be the extended tails of the typical anisotropic line shape.

Spectra of Irradiated Fluorocarbons.—In C_2F_4 , C_3F_6 , C_7F_{14} , C_6F_6 , and C_7F_{16} , the e.s.r. derivative curves (Fig. 3) are characterized by a relatively broad plateau, implying an absorption curve of approximately triangular shape. Less intense absorption occurs in a region 500 gauss wide. The saturated fluorocarbon C_7F_{16} exhibits a much sharper central region in addition to the plateau. Traces of structure are seen, but are inadequate for identi-

(7) M. H. Cohen, W. Kanzig, and T. O. Woodruff, *J. Phys. Chem. Solids*, **11**, 120 (1959).

fication. Table II shows, for various irradiated fluorocarbon spectra, the region at which substantial absorption begins.

TABLE I
PEAK WIDTHS IN E.S.R. SPECTRA OF IRRADIATED METHANE
AND CF₄

Sample and peak	Derivative peak width, gauss	Peak width "A," gauss ^a
CF ₄ + Xe (14%), 77°K.	5.5	10.5
CH ₄ + Xe (23%), 77°K.	5.5	10.7
CH ₄ + Xe (68%), 77°K.		
3rd	6.0	10.5
4th	5.6	13.0
CH ₄ + Xe (23%), 20°K.		
3rd	5.5	8.4
4th	5.3	11.2
CH ₄ , 4 or 20°K.		
3rd	6.2	16.2
4th	8.2	20.6
CH ₄ , 4°K., heated 20°K.		
3rd	4.2	8.5
4th, main line	4.2	7.7
4th, over-all	4.25	16.0

^a Separation between points at which derivative reaches half maximum value.

TABLE II
E.S.R. SPECTRA OF IRRADIATED FLUOROCARBONS

Material	Beginning of derivative plateau, gauss from center
C ₂ F ₄	- 74 to - 58
C ₄ F ₆	-186 to -132
C ₇ F ₁₄	-186 to -132
C ₆ F ₆	-168 to -118
C ₇ F ₁₆	-182 to -144
C ₇ F ₁₆ (central)	- 45

The spectra of C₃F₆ and C₇F₁₄ are quite similar; the plateau is more than twice as wide as in C₂F₄. The similarity may indicate similar numbers of interacting fluorine atoms, and the extra width over C₂F₄ may be a measure of the extra interacting atoms. The observed spectra may be due to more than one radical species present together, *e.g.*, CF₃CF₂· and CF₂=CF·; C₆F₆· and C₆F₇·; CF₃CF₂CF₂·, CF₃C=CF₂, CF₂=CFCF₂·, and numerous primary and secondary radicals from C₇F₁₆.

The spectrum of irradiated C₆F₆ has no obvious resemblance to that of irradiated C₆H₆, which consists of three fairly well separated groups of peaks and which has not yet been explained.⁸ The great breadth and poor line separation in all these solid fluorocarbons are in contrast to the well developed line structure of warm irradiated polytetrafluoroethylene, and to the close resemblance of proton and F¹⁹ splittings found in liquid solutions⁹ and in CF₄ + Xe. Little identification will be possible without spectra of pure known fluorocarbon radicals in liquid and solid media.

(8) N. Ya. Buben, I. I. Chkeidze, A. T. Koritzky, Yu. N. Molin, V. N. Shamshev, and V. Voevodsky, "ESR Investigations on Energy Transfer in Radiolysis of Organic Substances," Paper presented before the 5th International Symposium on Free Radicals, Uppsala, Sweden, July 6 and 7, 1961, Fig. 2a.

(9) D. H. Anderson, P. J. Frank, and H. S. Gutowsky, *J. Chem. Phys.*, **32**, 196 (1960).

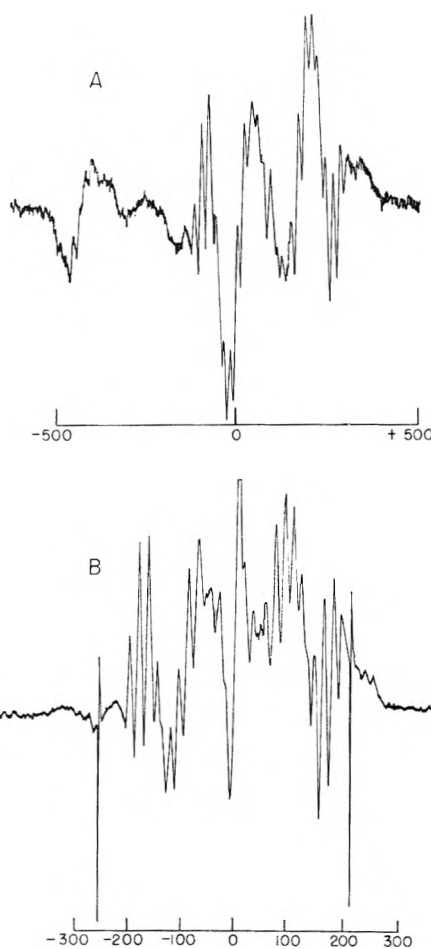


Fig. 4.—E.s.r. spectra of irradiated SiF₄: A, at 4°K.; B, at 77°K.

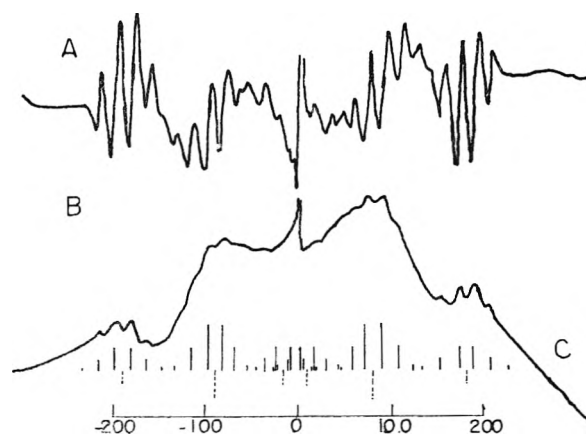


Fig. 5.—E.s.r. spectrum of irradiated SiF₄: A, derivative at 77°K.; B, integral at 77°K.; C, proposed line scheme.

Spectrum of Irradiated SiF₄.—Irradiated SiF₄ gave essentially the same spectrum at 4°, 77°, and 112°K., and in Xe mixtures (Fig. 4). The bewildering complexity is simplified somewhat by examining the integral (Fig. 5). At first sight, the envelope of the integral seems to display four groups of peaks with group intensity ratios 1:3:3:1, as required for SiF₃ with three equivalent F. However, the center spacing is too large, and there is proposed instead the more complicated scheme

at the bottom of Fig. 5. The distribution is developed from a large splitting of 176 gauss for one F, a smaller splitting of 100 gauss for each of the other two F atoms, and small nearest-neighbor interactions of 18 gauss with three or five equivalent F atoms on neighboring SiF₄ molecules. The faint lines around -286, +252, and ±426 gauss (Fig. 4B) are then the more prominent parts of an extension involving the Si²⁹ nucleus (abundance 5%, spin 1/2, magnetic moment -0.55477) with a very large splitting of 245 gauss. This scheme accounts for most of the visible lines. The failure of equivalence for all three F atoms is unexpected, but consistent with the possible electronic structures of atoms in the second row of the periodic table, where d-orbitals can be used. An example of such non-equivalence occurs in the stable molecule ClF₃,¹⁰ where analysis of the n.m.r. spectrum reveals one F different from the other two.

The presence of so many distinguishable lines suggests that the hyperfine interactions are predominantly isotropic and that the SiF₃ radicals are free to rotate at the lowest temperatures.

Yields and Stability.—The concentrations reached at several doses, and the radiation *G*-values, radicals per 100 e.v. of energy absorbed, are shown in Table III.

TABLE III
RADICAL CONCENTRATIONS AND RADIATION *G*-VALUES FOR IRRADIATED COMPOUNDS

Material	Temp., °K.	Dose, e.v./g. × 10 ⁻²⁰	Concn., radicals per g. × 10 ⁻¹⁸	<i>G</i> , radicals per 100 e.v.
CH ₄	4	28	26.2	0.9
CH ₄ + Xe (90)	77	6	0	.0
CH ₄ + Xe (68)	77	6.7	1.1	.17
CH ₄ + Xe (23)	77	14.0	0.9	.07
CH ₄ + Xe (21)	77	6.16	0.3	.05
CF ₄	4	9.15	4.1	.45
CF ₄ + Xe (90)	77	8.86	0.009	.001
CF ₄ + Xe (72)	77	8.48	.01	.001
CF ₄ + Xe (46)	77	7.9	.08	.01
CF ₄ + Xe (14)	77	6.16	.015	.002
CF ₄ + Xe (14)	77	14.1	.02	.0015
SiF ₄	4	9.15	3.8	.42
SiF ₄	77	7.01	3.1	.44
SiF ₄ + Xe (18)	77	6.17	0.9	.15
C ₂ F ₄	77	8.8	4.4	.5
C ₃ F ₆	77	8.8	12.2	1.4
C ₇ F ₁₄	77	8.8	4.3	0.5
C ₆ F ₆	77	7.01	2.1	.3
C ₇ F ₁₆	77	7.01	4.4	.6

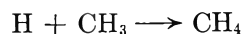
^a Figures in parentheses are mole % of substrate in xenon

The values for the CF₄ + Xe and CH₄ + Xe mixtures are liable to unusually large errors connected with sample dimensions. Most of the CH₄ and CF₄ mixtures decay to 40–70% of the initial concentration in 30 hr. at 77°K. and almost completely in a few hours at 90°K. Consideration of the decay rate and the time in the radiation source (38 hr. for 6.16 × 10²² e.v./g.) would lead to

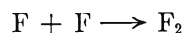
(10) D. F. Smith, *J. Chem. Phys.*, **21**, 609 (1953).

an estimated initial *G*-value 30 to 50% higher than the values in the table, assuming that the decay is second order and that one can apply the usual hyperbolic tangent formula without complications.

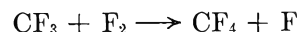
The *G*-values for CH₃ and CF₃ at 77°K. are much lower than at 4°K.; that for CF₄-Xe at 77°K. is especially low. These low values may be partly due to recombination with H and F atoms which would be rather mobile in molecular crystal matrices at 77°K. and evidently are not trapped. Nitrogen atoms, of dimensions comparable to F, are not trapped in Xe at 77°K.



A certain number of H atoms are removed by H + H combinations H + H → H₂, permitting the accumulation of CH₃. In CF₄ the corresponding combination



produces a species which is still reactive



unlike the H₂ from CH₄. This mechanism for the removal of CF₃ perhaps contributes to the very low observed yield at 77°K., although it does not prevent high yields of radicals from other fluorocarbons.

The efficiency of Xe as a trapping matrix at 77°K. presumably is connected with its higher m.p. and b.p. (m.p. 161°K., b.p. 166°K.; compared with CH₄ m.p. 89°K., b.p. 113°K., CF₄ m.p. 89°K., b.p. 145°K.). There is an appreciable radical yield even at the high CH₄ content, about 69 mole % CH₄, where the matrix may be considerably modified. In accounting for the relative independence of yield with respect to composition, it is uncertain at this time what roles are played by energy transfer from xenon to methane, and by concentration and nature of the trapping sites. Considerable mutual solubility of Xe and CH₄ may occur, for the molar volumes, estimated at 49 and 38 cm.³, respectively, are not too dissimilar.

The yields of radicals in irradiated SiF₄ are relatively independent of temperature and roughly proportional to concentration, and the radicals in it do not decay very rapidly even at 120°K.

The radical yields from the larger fluorocarbon molecules at 77°K. are comparable to those from CF₄ at 4°K.; that from C₆F₆ is the smallest in this group, but larger than the yield in the polymer (C₆F₅CHCH₂)_x.

The sample of C₂F₄ produced less than 1 mg. of polymer upon rapid warming, showing that the large concentrations of radicals existing at 77°K. predominantly disappeared by combination in preference to adding C₂F₄ units. This is in contrast to the nearly 100% conversion of C₂F₄ to polymer when irradiated to only 10¹⁸ e.v./g. at 193°K., at low dose rates.

MATRIX EFFECTS IN THE GASEOUS H ATOM-CONDENSED OLEFIN SYSTEM; SURFACE REACTION—OLEFIN DIFFUSION MODEL

BY RALPH KLEIN AND MILTON D. SCHEER

National Bureau of Standards, Washington 25, D. C.

Received June 4, 1962

The reaction between hydrogen atoms, produced in the gas phase, and a condensed film of an olefin depends markedly on the matrix. This matrix may be either the pure olefin or a mixture of the olefin with a diluent. The model consistent with the experimental data is one in which the H atom addition to the olefin occurs as a surface reaction. The olefin is replenished by diffusion from the interior. Two characteristic limiting processes may be distinguished. One involves a diffusion-controlled, and the other a chemical reaction-controlled rate. The reaction products, that is the monomer to the dimer alkane ratio, depend on the mobility of the alkyl radical formed on the surface.

The reaction between hydrogen atoms, generated on a hot tungsten filament, and olefin films condensed below 100°K., has been observed for a variety of terminal unsaturated hydrocarbons.^{1,2} Several features of this type of system led to a physical model consistent with the experimental observations.³ Hydrogen atoms were assumed to diffuse into the solid. They reacted by terminal addition to give secondary radicals which disproportionated and dimerized to give the stable end products.^{4,5} Diffusion of hydrogen atoms into the olefin layer appeared to explain the results obtained. Large differences in the rates of hydrogen atom pick-up by various olefins (the absence of reaction with *n*-hexene-1 and butene-2, as compared to propene and butene-1, for example) were ascribed to small differences in the activation energies. This was not in agreement with gas phase experiments, where the rates for H atom addition were approximately the same for a variety of olefins, including those with an internal double bond. However, the lower temperature rate measurements would reveal small differences in activation energy that would not have been evident in the higher temperature regions, particularly if the activation energy for the reaction were sufficiently small.

Several additional experiments with the hydrogen atom-solid olefin system have indicated that the previously postulated model requires modification. It has been found that the immobilizing effect of the matrix, whether it consists of the olefin alone or an admixture of the olefin with inerts, greatly affects the reaction rate as measured by either hydrogen pick-up or saturate formation. We have found that *n*-hexene-1 appears to be inert at 77°K. when present in 100% concentration, but shows considerable reaction with atomic hydrogen when diluted with propane, propene, or any other substances which substantially increase diffusion in the solid. The rate of hydrogen uptake by condensed 3-methyl-butene-1 under continuous exposure of the film to H atoms was rapid initially. The rate decreased in time. If the reaction was interrupted for a few minutes, the rate increased compared to that immediately before the interruption. Hydrogen atom diffusion into the solid cannot account for these observations, whereas reac-

tion of H atoms and olefin molecules at the surface of the solid, and replacement of the reactive molecules by diffusion from the interior, is in accord with these experiments.

The hydrogen atom diffusion model was suggested by the apparent linear dependence of the initial reaction rate³ on film thickness, and by complete conversion of the olefin.² It has now been shown that in a matrix where diffusion is slow (propene in 3-methylpentane, for example) complete conversion is unattainable. The linear dependence behavior with small film thickness is not compelling. Experimentally it is most difficult to determine initial rates for very thin films because the olefin concentration decreases very rapidly as the reaction proceeds even for very short times. There is also the experimental difficulty of making a uniformly coherent film for such thin films.

Experimental Results

The apparatus used has been described previously.⁶ Some modifications were made so that the hydrogen atom concentration could be maintained at a constant value. A reservoir volume was incorporated. This communicated with the reaction vessel through a precision type variable leak valve. The pressure was kept constant in the reaction vessel by matching the leak rate with the reaction rate during the course of the experiment. A calibrated thermocouple gage with a potentiometric recorder was used to measure the hydrogen depletion of the reservoir in time. The deposition process was found to be important for obtaining uniform, reproducible films. The procedure adopted consisted in immersing the flat bottom of the reaction vessel in the refrigerant. The appropriate mixture was metered through a throttle valve into the reaction vessel. The deposition rate used was such that the film thickness was increased about 1 μ /min.

The dependence of the rate of H atom addition and product yields of C₃ and C₄ olefins on dilution with various matrices is shown in Table I. The effect of the matrix is apparent. Matrices such as propane or butane at 77°K. give mixtures whose reaction rates vary linearly with olefin dilution. This is not true for diluents such as 3-methylpentane or *cis*-butene-2. Table II gives some experimental data for product analysis in systems of mixed olefins. The matrix affects not only the rate, but also the product distribution.

Figure 1 is a plot of the propane and hexane yields as a function of time when mixtures of propylene, *n*-hexene-1, and *n*-butane are deposited together in a film. The striking increase in rate upon dilution with *n*-butane demonstrates the marked matrix effect. Figures 2 and 3 give the hydrogen depleted (at constant hydrogen pressure and tungsten filament temperature) by very thick films of propylene deposited in *n*-butane and 3-methylpentane. It is seen that the *n*-butane environment gives a linear time dependence while the 3-methylpentane matrix shows a $t^{1/2}$ dependence.

(1) R. Klein and M. D. Scheer, *J. Am. Chem. Soc.*, **80**, 1007 (1958).(2) R. Klein and M. D. Scheer, *J. Phys. Chem.*, **62**, 1011 (1958).(3) R. Klein, M. D. Scheer, and J. G. Waller, *ibid.*, **64**, 1247 (1960).(4) M. D. Scheer and R. Klein, *ibid.*, **63**, 1517 (1959).(5) R. Klein and M. D. Scheer, *ibid.*, **65**, 324 (1961).(6) M. D. Scheer and R. Klein, *ibid.*, **65**, 375 (1961).

TABLE I

THE DEPENDENCE OF H ATOM ADDITION AND PRODUCT YIELDS OF THE C₃ AND C₄ OLEFINS ON DILUTION

Film thickness = 3 μ; film area = 80 cm.²; film T = 77°K., W ribbon T = 1800°K., P_{H₂} ≈ 150 μ; deposition rate ~ 50 μ/min.

Film compn.	Relative rates	Alkane ratios		Olefin isomerization yields C ₄ <i>trans</i> -Butene-2
		C ₃ /C ₄	C ₃ /C ₂	
Propylene	1.00	8
Propylene = 0.01 Butane	0.01	8
Butene-1	.80	..	18	2.5
Butene-1 = 0.01 Propane	.009	..	21	2.3
<i>cis</i> -Butene-2	.050	..	^a	>50
<i>cis</i> -Butene-2 = 0.1 Propane	.025	..	^a	5
<i>cis</i> -Butene-2 = 0.03 Propane	.015	..	^a	8
<i>cis</i> -Butene-2 = 0.01 Propane	.010	..	^a	15
Propylene = 0.40 3-Methylpentane	.010
Propylene = 0.33 3-Methylpentane	.002

^a C₃ is too small to measure relative to low C₄ yields.

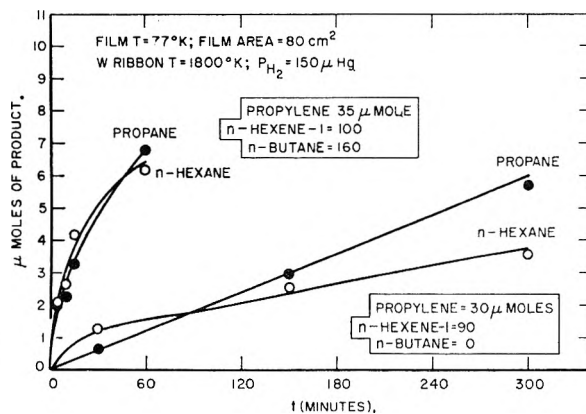


Fig. 1.—Matrix effect on rate of product formation.

Discussion

The rate of the H atom addition to olefins is strongly dependent on the diffusion of the reactive olefin in the matrix in which it is condensed. This correlation is clearly shown in the rate of hydrogen pick-up by propylene. When diluted with butane, a 30% propylene film shows a rate 100 times faster than the same concentration in 3-methylpentane. The latter has been widely used in matrix isolation experiments.⁷ A rule of thumb stated by Pimental³ is that reactive species cannot be preserved if the temperature of the matrix substance is higher than approximately $T_m/2$, where T_m is the melting point. This is supported by experiments on a variety of

(7) I. Norman and G. Porter, *Proc. Roy. Soc. (London)*, **A230**, 399 (1955).

(8) A. M. Bass and H. P. Broida, "Formation and Trapping of Free Radicals," Academic Press, New York, N. Y., 1960, Chapter 4.

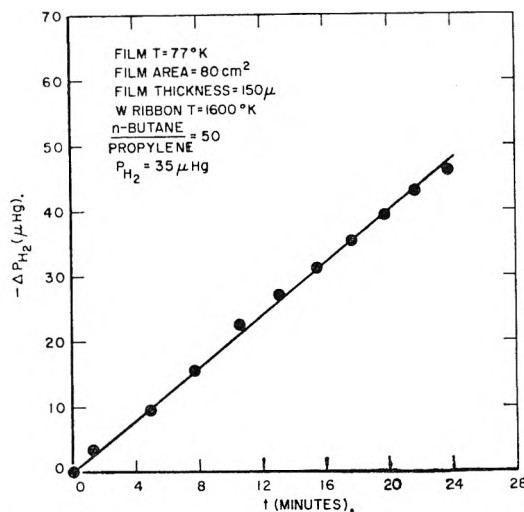


Fig. 2.—Time dependence of reaction with a non-rigid matrix.

matrices and a range of diffusing substances.⁸ The conclusion that a matrix containing olefin at temperatures more than half its melting point would show observable rates of H atom addition requires modification. In order to sustain the reaction, the olefin must be capable of diffusing through the matrix at a relatively rapid rate. In the matrix isolation experiments, diffusion must be inhibited over distances of the order of molecular diameters. For conveniently observable rates of hydrogen pick-up where reaction occurs on the surface and must be sustained by diffusion of reactive molecules from the interior, diffusion over hundreds of molecular diameters must occur in times of the order of several minutes. This requires temperatures well above $T_m/2$. This is illustrated by hexene-1 functioning as its own matrix. At 77°, $77/T_m = 0.6$, the rate is so low that the reaction as measured by decrease in hydrogen pressure is not observable. At 90°, $90/T_m = 0.7$, the rate is observable.

Additional evidence for diffusional processes in the hydrogen atom-condensed olefin reaction system is the formation of the dimer product of the alkyl radicals. It has been shown previously by isotope tracer studies that disproportionation as well as dimerization occurs.⁵ The constancy of the alkane ratios (C_n/C_{2n}) over a wide concentration range was interpreted as demonstrating the absence of the H atom addition to the radical. We have now found that this ratio can be greatly altered in favor of the monomer alkane in a matrix where the diffusion processes are slower. For a 100% propylene film, the propane/2,3-dimethylbutane ratio found in the products is 8. The same ratio is obtained with 1% propylene in butane (Table II). Ten per cent propylene in *cis*-butene-2 shows a C₃/C₈ ratio of 35. *cis*-Butene-2 at 77° provides a rigid environment. The diffusion processes are slowed considerably, diffusion is undoubtedly rate controlling, and some hydrogen atom addition to the alkyl radical occurs.

The interpretation of the absence or at least the small extent of the H atom addition to the alkyl radical in a non-isolating matrix⁵ is the short life-

TABLE II

PRODUCT RATIOS FOR H ATOM ADDITION TO MIXED C₃ AND C₄ OLEFIN FILMSFilm thickness = 5 μ; film area = 80 cm.²; film T = 77°K.; W ribbon T = 1800°K., P_{H₂} ≈ 150 μ; olefin conversion ≈ 20%; deposition rate ~ 50 μ per minute

Film composition	Alkane ratios				Olefin isomerization yields C ₄ (Butane) <i>trans</i> -Butene-2
	$\frac{C_3}{C_4}$	$\frac{C_3}{C_3 + 1/2C_1}$	$\frac{C_4}{C_3 + 1/2C_1}$	$\frac{C_7^2}{C_6C_8}$	
(1) $\frac{\text{Propylene}}{\text{Butene-1}} = 0.84$	1.0	8	18	3.7	2.3
(2) $\frac{\text{Propylene}}{\text{Butene-1}} = 0.80$ (Deposited separately; propylene on top)	1.1	10	20	3.5	2.0
(3) $\frac{\text{Propylene}}{\text{cis-Butene-2}} = 0.10$	0.2	35	100	3.4	2.8
(4) $\frac{\text{Propylene}}{\text{cis-Butene-2}} = 0.11$ (Deposited separately; propylene on top)	2.6	9	16	0.4	2.0
(5) Propylene: <i>cis</i> -butene-2: butene-1 1:9:1	0.1	>50	>50	3.2	2.5
(6) 3 olefins deposited separately in the above order and quantity	0.01	10	18	0.8	1.9

time of the radical on the surface. The olefin, and correspondingly the alkyl radical, diffuses readily. The alkyl radical, once formed on the surface by the reaction of the H atom with an olefin molecule, readily diffuses one or two molecular layers below the surface, and is removed from further exposure to the atomic hydrogen. However, the alkyl radical recombination and disproportionation reactions still may readily occur. With an immobilizing matrix, the diffusion of the radical is much slower, and the surface lifetime and exposure to H atoms is longer.

Some interesting results have been obtained with mixed olefins in rapidly deposited films (~100 μ/min.). Propylene and butene-1, when hydrogenated by H atoms at 77°K., give propane, butane, 2,3-dimethylbutane, (C₆), 3,4-dimethylhexane, (C₈), and 2,3-dimethylpentane, (C₇). If the propyl and butyl radicals are formed and recombine in a random manner, the ratio C₇²/C₆C₈ is expected to have a value equal to 4 on a purely statistical basis. Table II, 1, shows this to be the case. The departure of the ratio C₇²/C₆C₈ from the approximate value of 4 may be used as a measure of the uniformity of mixing of the condensed solid. An attempt was made to condense propylene on top of butene-1 to give a layered structure. This could never be achieved, as shown by Table II, 2. Even when the deposition was slow, extending over several hours (~0.1 μ/min.), the pseudo-equilibrium constant of about 4 was obtained. It must be concluded that the diffusion processes are quite rapid in propene-butene-1 mixtures at 77°K. Departures from the value of 4 were found when propylene was deposited on top of *cis*-butene-2. The situation can be interpreted by a hill and valley structure of the first deposited butene-2 film. The subsequent deposition of propylene might occur in the valleys, and, as the thickness was increased, present a surface of large patches of propylene, bound by areas of butene-2 or propylene-butene-2 mixtures. Here the C₇²/C₆C₈ ratio of 0.4 (4, Table II) or 0.8 (6, Table II) shows

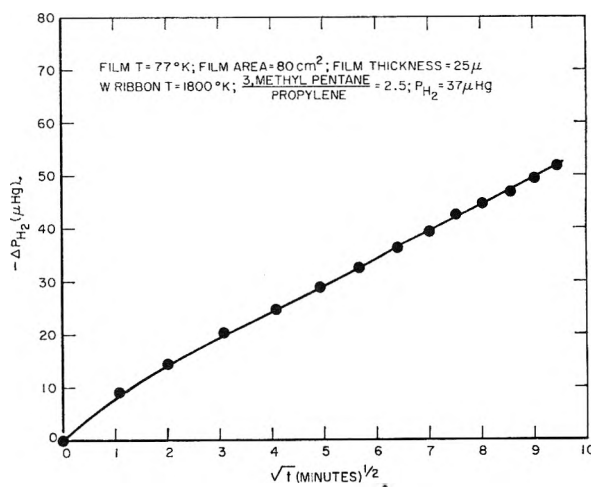


Fig. 3.—Time dependence of reaction with a rigid matrix.

a marked lack of uniformity of the surface layer. In 3, Table II, both the C₃/C₆ and C₄/C₈ ratios show large increases over that characteristic of loose matrices.

It was shown previously that the atom diffusion model leads to a hyperbolic tangent relationship between initial rate and film thickness, with the atom concentration being a maximum at the surface. Observations of the hydrogen pick-up on a given system may be made as a function of time. Comparison of these results with the model requires the solution of the equations

$$D \frac{\partial^2 H}{\partial x^2} - kH(Ol) = \frac{\partial H}{\partial t}$$

$$\frac{\partial(Ol)}{\partial t} = \frac{1}{2} kH(Ol)$$

$$\frac{dH_2}{dt} = -\frac{1}{2} \int_0^l kH(Ol) dx$$

where *H* and *Ol* represent H atom and olefin con-

centrations at a distance x from the base of the olefin slab. In this treatment, the olefin was not assumed to diffuse. From the above dH_2/dt could be calculated numerically with the appropriate boundary conditions. The analytical solution is not accessible but it is evident that for small olefin concentration, thin films, and high hydrogen atom concentration, first-order behavior for the total olefin depletion is to be expected. Although first-order behavior may be observed, such a limiting case is non-specific with regard to detailing the mechanism of the diffusion-reaction process. A model consistent with the data is one in which, in contrast to that proposed previously, the H atom addition reaction occurs on the surface. This implies that hydrogen atoms do not diffuse into the solid, and that for the reaction to proceed, olefin molecules in the interior must diffuse to the surface to replenish those which have reacted. Two cases may be considered. In the first, the olefin is a slab, the front surface of which is exposed to hydrogen atoms. The slab thickness is taken as l with $x = 0$ the back surface. The olefin, whose concentration at x is designated by C , conforms to the set of equations

$$\begin{aligned} D \frac{\partial^2 C}{\partial x^2} &= \frac{\partial C}{\partial t} \\ \frac{\partial C}{\partial x} &= 0 \text{ at } x = 0 \\ C &= C_0 \text{ at } t = 0 \\ D \frac{\partial C}{\partial x} &= kH_0C \text{ at } x = l \end{aligned}$$

The standard solution of this set is

$$C = \sum \frac{2C_0 \sin \alpha_i l}{\alpha_i l} \cos \alpha_i x e^{-D\alpha_i^2 t}$$

Where the α_i 's are the roots of

$$\tan \alpha_i l = \frac{kH_0}{D\alpha_i}$$

$$\frac{dC}{dt} = -kH_0C \text{ at } x = l, \text{ so that}$$

$$\frac{dC}{dt} = -\sum \frac{kH_0C_0}{\alpha_i l} \sin 2\alpha_i l e^{-D\alpha_i^2 t}$$

For small film thickness, large D , and small hydrogen atom concentration, the rate of hydrogen pick-up is approximately equal to kH_0C , where C under these conditions is uniform through the film. This result is not very informative. Unfortunately, the form of the solution for the general case is not amenable to a comparison of the experimental results without an independent measure of H_0 and D .

For a second case, the semi-infinite solid, closely approximated by thick deposits, is considered. The applicable equations are

$$D \frac{\partial^2 C}{\partial x^2} = \frac{\partial C}{\partial t}$$

$$D \frac{\partial C}{\partial x} = kH_0C \text{ at } x = 0$$

$$C = C_0 \text{ at } x = \infty$$

Only $C(0,t)$ is required, the quantity of interest being $kH_0C(0,t)$. The solution is well known and is

$$C(0,t) = C_0 e^{k^2 H_0^2 t / D} \operatorname{erfc}(kH_0 \sqrt{t/D})$$

It is to be noted that the diffusion of products has not been taken into account. This is of little consequence if the concentrations are dilute, or if the diffusion of the products in the matrix and their interaction with the surface is nearly the same as the reactants. Negligible error is introduced by considering D to be time independent. The rate of reaction is given by

$$\begin{aligned} \frac{dH_2}{dt} &= -\frac{kH_0C(0,t)}{2} \\ &= -\frac{kH_0C_0}{2} e^{k^2 H_0^2 t / D} \operatorname{erfc}(kH_0 \sqrt{t/D}) \end{aligned}$$

For short times,

$$\frac{dH_2}{dt} = -\frac{k}{2} H_0 C_0$$

If $kH_0 \sqrt{t/D}$ is large, then

$$\frac{dH_2}{dt} = -\frac{C_0}{2\sqrt{\pi}} \left[\left(\frac{D}{t} \right)^{1/2} - \frac{1}{2k^2 H_0^2} \left(\frac{D}{t} \right)^{3/2} + \dots + \right]$$

The moles of hydrogen reacted in time t is

$$\begin{aligned} \Delta H_2 &= \frac{kH_0C_0}{2} \int_0^t e^{k^2 H_0^2 t / D} \operatorname{erfc}(kH_0 \sqrt{t/D}) dt \\ &= \frac{C_0 D}{2kH_0} \left[e^{k^2 H_0^2 t / D} \operatorname{erfc} \left\{ kH_0 \left(\frac{t}{D} \right)^{1/2} \right\} - 1 \right] + \left(\frac{Dt}{\pi} \right)^{1/2} C_0 \end{aligned}$$

This expression reduces to

$$\left(\frac{Dt}{\pi} \right)^{1/2} C_0 \text{ for large values of } kH_0 \sqrt{t/D}$$

For small values of $kH_0 \sqrt{t/D}$ the ΔH_2 reduces to $kH_0C_0 t/2$, the limiting case for large diffusion coefficients.

The two limiting conditions are represented by the experimental results of Fig. 2 and Fig. 3. Figure 2 is illustrative of a matrix where the diffusional processes are rapid compared to the rate of reaction. The hydrogen depletion is linear in time. This is precisely what is expected, since the surface concentration of olefin will, for a semi-infinite solid, be maintained constant by the rapid diffusion of olefin from the interior. Here

the chemical reaction is rate controlling. Figure 3 shows the other limiting condition where the olefin diffusion process is rate controlling. The hydrogen uptake, after about 4 min., follows a square root of time dependence. By equating the slope of the linear portion of the curve to $(D/\pi)^{1/2}C_0$, a value for the diffusion coefficient $D = 1 \times 10^{-12}$ cm.²/sec. is derived. This refers to diffusion at 77°K. of propylene in a matrix of 3-methylpentane in a molar ratio of 1 to 2.5.

If the hydrogen atom-condensed olefin experiment is interrupted at some time \bar{t} , the olefin concentration at the surface will increase in time because of diffusion from the interior. The process will be strongly dependent on the diffusion coefficient of the olefin in the matrix. Calculation of the surface concentration with time after the H atom supply is stopped follows from

$$C(x, \bar{t}) = C_0 \left[\operatorname{erf} \frac{x}{2\sqrt{D\bar{t}}} + \exp \left(\frac{kH_0}{D} x + \frac{k^2 H_0^2}{D} \bar{t} \right) \operatorname{erfc} \left\{ \frac{x}{2\sqrt{D\bar{t}}} + kH_0 \sqrt{\bar{t}/D} \right\} \right]$$

and

$$C(0, t - \bar{t}) = \frac{C_0}{\sqrt{\pi D(t - \bar{t})}} \int_0^\infty \left[\operatorname{erf} \frac{x}{\sqrt{2D(t - \bar{t})}} + \exp \left(\frac{kH_0}{D} x + \frac{k^2 H_0^2}{D} (t - \bar{t}) \right) \operatorname{erfc} \left\{ \frac{x}{\sqrt{2D(t - \bar{t})}} + kH_0 \sqrt{t - \bar{t}/D} \right\} \exp \left(-\frac{x^2}{4D(t - \bar{t})} \right) \right] dx$$

The value of $C(0, t - \bar{t})$ increases from its value of $C(0, \bar{t})$. Thus the interruption experiments with 3-methylbutene-1 are understood, and furnish good

evidence for the "olefin diffusion with reaction on the surface" model.

Finally, it may be noted that the initial rate for the presently proposed model is directly proportional to the olefin concentration, that is

$$\left(\frac{dH_2}{dt} \right)_{\text{initial}} = -\frac{k}{2} H_0 C(0, 0)$$

The "H atom diffusion into the solid" model gives a rate proportional to the square root of the olefin concentration for thick films.³ The data² clearly support the present model in that initial rates for thick films are linear with olefin concentration.

It has now been established that the mechanism for the reaction between hydrogen atoms, generated in the gas phase, and a condensed reactant is one in which the reaction occurs on the surface. The surface concentration is maintained by diffusion in the condensed phase. The rate varies depending on the magnitude of the diffusion processes in the solid. If the diffusion is sufficiently small, the observed reaction rate may drop quickly to an immeasurably low value after the surface layer has been depleted. Thus the previously reported large differences in reactivity of various condensed olefins may be interpreted in terms of diffusion limiting processes. The interpretation of rates in terms of matrix effects and chemical reactivity now permits a quantitative examination of both the surface reactions and diffusion processes.

Acknowledgment.—We express our thanks to Richard Kelley, who participated in much of the experimental work. Charles Hill and V. J. DeCarlo contributed to some of the earlier experiments.

THE PHOTOLYSIS OF AZOMETHANE AT HIGHER PRESSURES: A SECOND ETHANE-PRODUCING REACTION

BY S. TOBY AND B. H. WEISS

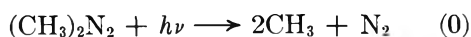
School of Chemistry, Rutgers University, New Brunswick, New Jersey

Received June 11, 1962

Azomethane was photolyzed from 25 to 150° in the pressure range 10 to 200 mm. At temperatures above 50° and pressures above 50 mm. the hitherto accepted mechanism breaks down. It is shown that the results can be explained by the postulation of an additional ethane-forming step. This reaction does not involve methyl radicals nor is it a simple unimolecular intramolecular split.

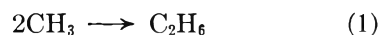
Introduction

The photolysis of azomethane (A) has been studied by Jones and Steacie¹ in the range 25 to 190° and by Toby² from -50 to +50°. The main features of the photolysis may be represented by



(1) M. H. Jones and E. W. R. Steacie, *J. Chem. Phys.*, **21**, 1018 (1953).

(2) S. Toby, *J. Am. Chem. Soc.*, **82**, 3822 (1960).



from which it follows that

$$R_{\text{CH}_4}/R_{\text{C}_2\text{H}_6}^{1/2}[\text{A}] = k_2/k_1^{1/2}$$

The quantity $R_{\text{CH}_4}/R_{\text{C}_2\text{H}_6}^{1/2}[\text{A}]$ (henceforth in this paper denoted by α , units l.^{1/2} mole^{-1/2} sec.^{-1/2}) thus should be independent of $[\text{A}]$. In Jones and Steacie's data,¹ however, there is a

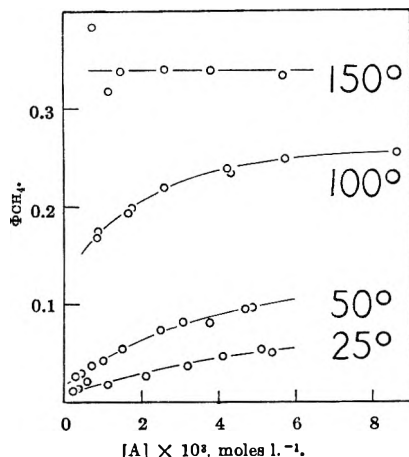


Fig. 1.—Quantum yield of methane as a function of azomethane concentration.

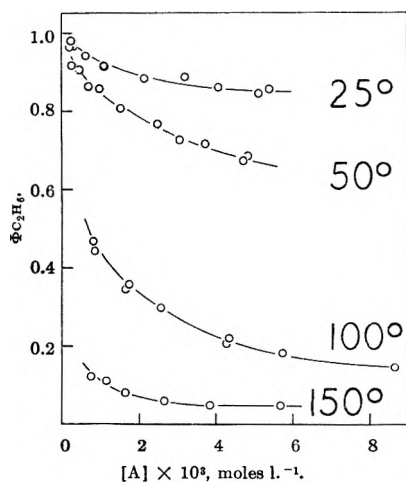


Fig. 2.—Quantum yield of ethane as a function of azomethane concentration.

distinct decrease in α as the azomethane pressure was increased from 10 to 100 mm. in experiments performed above 90°. Toby's experiments² were done over a smaller range of $[A]$ but as $[A]$ increased there was a decrease in α beyond the experimental error. Such an increase in α with decrease in $[A]$ could be accounted for by a third-body restriction of the recombination of methyl radicals. This has been observed in the photolysis of acetone in the range 150–250° by Kistiakowsky and Roberts³ and by Dodd and Steacie.⁴ However, the third-body effect they observed was at much lower pressures (of the order of a few mm., as predicted by Marcus⁵) than changes of α in the azomethane investigations. The third-body region should occur at even lower pressures as the temperature decreases because of the increased stability of the $C_2H_6^*$ complex. It therefore seemed unlikely that the change of α with $[A]$ was due to a third-body restriction, particularly since the azomethane and acetone molecules are so similar.

The present investigation was an attempt to

(3) G. B. Kistiakowsky and E. K. Roberts, *J. Chem. Phys.*, **21**, 1637 (1953).

(4) R. E. Dodd and E. W. R. Steacie, *Proc. Roy. Soc. (London)*, **A223**, 283 (1954).

(5) R. A. Marcus, *J. Chem. Phys.*, **20**, 364 (1952).

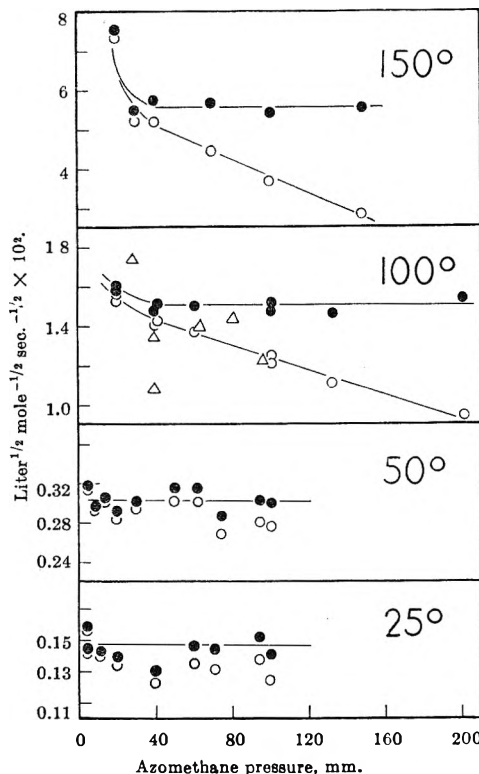


Fig. 3.—Variation of α and $k_2/k_1^{1/2}$ with azomethane pressure: O, α ; ●, $(RC_2H_5[A]^2/RC_2H_6^2 - k_b RN_2^2[A]^2/k_a^2 RC_2H_4)^{-1/2}$; Δ, α , data from Jones and Steacie.¹

investigate this anomaly further and offer a possible explanation.

Experimental

The apparatus and techniques used have been described previously.² The photolysis cell was immersed in a heated thermostated oil bath and over the range of 25 to 150° temperature control to within $\pm 0.15^\circ$ was obtained.

The Osram HBO-74 high-pressure mercury arc was powered by a constant wattage transformer (No. 77124, Sola Electric Co.) and the combination was found to give a very steady output. The light beam was made parallel with a quartz lens and filtered with a Corning 7-37 filter to give approximately monochromatic light at 3660 Å.

Results

The data obtained are plotted as Φ_{CH_4} and $\Phi_{C_2H_6}$ in Fig. 1 and 2, assuming Φ_{N_2} equals unity.¹ It will be seen that the values of Φ_{CH_4} and $\Phi_{C_2H_6}$ extrapolate to zero and unity, respectively, as $[A]$ approaches zero.

The variation of α with azomethane pressure is shown in Fig. 3 (open circles). As the azomethane pressure decreases from 150 to 50 mm., α increases by 70% at 150° and 30% at 100°. At 50 and 25° α remains approximately constant with pressure. Jones and Steacie's results¹ at 90° have been corrected to 100° and compared with the present data. In spite of the large scatter the agreement is good.

Thus at 100 and 150° there is a large change in α with $[A]$ at pressures far too high for third-body effects to be feasible.

Discussion

The results are consistent with the occurrence of other steps in the mechanism resulting in ethane formation. A possible scheme which is tentatively proposed is



These primary processes (which would still allow Φ_{N_2} to be unity) then are followed by reactions 1 and 2 as before.

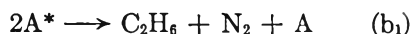
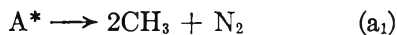
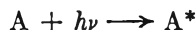
If we assume that the rate of reaction (b) is much less than that of (a) so that $k_a[\text{CH}_3\text{N}_2\text{---}] \gg k_b[\text{CH}_3\text{N}_2\text{---}]^2$ it follows that

$$R_{\text{C}_2\text{H}_6}[\text{A}]^2/R_{\text{CH}_4}^2 = k_b R_{\text{N}_2}^2[\text{A}]^2/k_a^2 R_{\text{CH}_4}^2 + k_1/k_2^2$$

A graph of $R_{\text{C}_2\text{H}_6}[\text{A}]^2/R_{\text{CH}_4}^2$ against $R_{\text{N}_2}^2[\text{A}]^2/R_{\text{CH}_4}^2$ is shown in Fig. 4. In spite of the scatter at the two lower temperatures, satisfactory linearity is obtained. There is evidence of deviations at azomethane pressures of 20 mm. at 150 and 100° and these departures from linearity occur at conditions where third-body effects on $R_{\text{C}_2\text{H}_6}$ would be expected to be noticeable. The slopes of the lines correspond to values of k_b/k_a^2 of $(3.1 \pm 0.1) \times 10^6$, $(6.4 \pm 0.3) \times 10^6$, $(1.6 \pm 0.6) \times 10^7$, and $(1 \pm 0.9) \times 10^7$ l. sec. mole⁻¹ at 150, 100, 50, and 25°, respectively. This suggests that if E_b is zero, then E_a is approximately 2 kcal. mole⁻¹.

Using these values of k_b/k_a^2 , one may correct for the effect of reaction (b) and so obtain values of $k_2/k_1^{1/2}$. These values are shown in Fig. 3, where the apparent change of $k_2/k_1^{1/2}$ with pressure at 150 and 100° vanishes except at the lowest pressures. The magnitude of the correction is slightly larger at 50 and 25° but produces little change in $k_2/k_1^{1/2}$ because at the lower temperatures $R_{\text{C}_2\text{H}_6}$ is much larger than R_{CH_4} . The percentage of nitrogen formed by reaction (b) compared to the total formed is given by $100(1 + k_a^2/2k_b R_{\text{N}_2})^{-1}$. This function increases with azomethane pressure increase and ranged from about 5% at the lower pressures to about 15% at the higher pressures with little temperature dependence.

The experimental data obtained do not distinguish between the proposed mechanism and an excited molecule mechanism such as



This latter mechanism seems to us inherently unlikely since the importance of reaction (b) increases with azomethane pressure, which argues against an excited molecule mechanism.

The formation of ethane by non-free radical processes cannot be ruled out entirely, however, in view

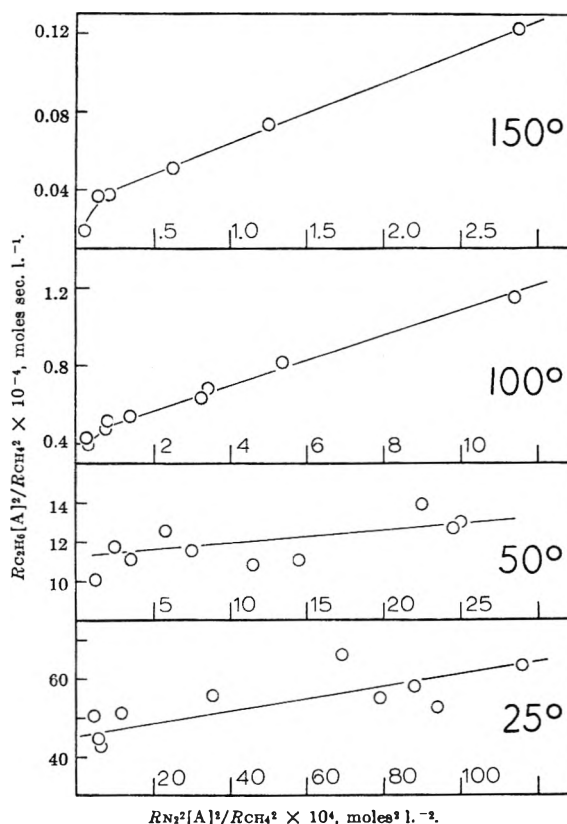


Fig. 4.—Variation of $R_{\text{C}_2\text{H}_6}[\text{A}]^2/R_{\text{CH}_4}^2$ with $R_{\text{N}_2}^2[\text{A}]^2/R_{\text{CH}_4}^2$.

of results obtained by the photolysis of azomethane in the presence of nitric oxide. Davis, Jahn, and Burton⁶ found that methane formation could be completely suppressed by the presence of nitric oxide, but that ethane formation, although decreased, was not reduced to zero. Calvert⁷ found no methane or ethane under comparable conditions but found³ some ethane in the nitric oxide-inhibited flash photolysis of azomethane. In view of the current controversy on the role of nitric oxide in radical scavenging⁹ no definite conclusion seems possible on the exact nature of the non-methyl ethane-producing step. The results, however, are not consistent with such sequences as $\text{A} + h\nu \rightarrow \text{A}^*$, $\text{A}^* \rightarrow 2\text{CH}_3 + \text{N}_2$, and $\text{A}^* \rightarrow \text{C}_2\text{H}_6 + \text{N}_2$ or $\text{A} + \text{A}^* \rightarrow \text{C}_2\text{H}_6 + \text{N}_2 + \text{A}$.

Acknowledgment.—The authors wish to thank the National Science Foundation for Grant G-14398, which supported this work.

(6) T. W. Davis, F. P. Jahn, and M. Burton, *J. Am. Chem. Soc.*, **60**, 10 (1938).

(7) J. G. Calvert, S. S. Thomas, and P. L. Hanst, *ibid.*, **82**, 1 (1960).

(8) W. C. Sleppy and J. G. Calvert, *ibid.*, **81**, 769 (1959).

(9) See, for example J. G. Larson and A. Kupermann, 141st National ACS Meeting, Washington, D. C., 1962, Abstracts 55 and 56, Physical Chemistry Division.

SOLVENTS HAVING HIGH DIELECTRIC CONSTANTS. X. SOLUTIONS OF ACETIC ACID AND ITS DERIVATIVES IN N-METHYLACETAMIDE AT 40^o1,2

BY L. R. DAWSON, J. W. VAUGHN, M. E. PRUITT, AND H. C. ECKSTROM

Department of Chemistry, University of Kentucky, Lexington, Kentucky

Received June 12, 1962

It has been shown that small quantities of acetic acid and/or acetates remain with persistent tenacity in N-methylacetamide (NMA) even after it is subjected to rather extensive purification processes. Probably this results from hydrogen bonding in which the impurity becomes an integral part of this highly structured solvent. In NMA having a specific conductance of $2-5 \times 10^{-8}$ ohm⁻¹ cm.⁻¹, the dissociation constant for acetic acid at 40° is approximately 7×10^{-8} ; in water at 40° it is 1.7×10^{-5} . Conductance data for potassium chloride, potassium acetate, monochloroacetic acid, and dichloroacetic acid in NMA have been obtained. Trichloroacetic acid forms a semicrystalline solvate at 30° but decomposes in the solution at higher temperatures.

Unpublished conductance data obtained in this Laboratory several years ago by McCreary³ gave evidence that acetic acid is only slightly dissociated in formamide. More recent exploratory conductance studies here⁴ have indicated that acetic acid is dissociated only very little in N-methylacetamide also in spite of its very high dielectric constant (165.5 at 40°), but that there is a strong affinity between the acetic acid and the solvent.

The object of the present investigation was to study the conductance behavior of solutions of acetic acid and some of its derivatives in N-methylacetamide (NMA) in an attempt to understand more about the solute-solvent relationships existing in this solvent medium, which has an unusually high dielectric constant.

Experimental

Apparatus and Procedure.—The equipment and the procedures used have been described previously.⁵⁻⁷

Solutes.—Glacial acetic acid was dried over P₂O₅ for 24 hr.; then it was refluxed over P₂O₅ for 5 hr., and finally distilled. From 1 l. of acetic acid, two 10-ml. portions were collected after 450 ml. had distilled over. The freezing point of these two portions was 16.6°.

Monochloroacetic and dichloroacetic acids were purified by a series of fractional distillations. Trichloroacetic acid was recrystallized several times from cyclohexane and dried over magnesium perchlorate in a vacuum desiccator.

Reagent grade potassium acetate was recrystallized three times from a 50-50 water-alcohol mixture, then dried to constant weight in a vacuum oven.

Solvent.—A stock solution of NMA was prepared as described previously.⁵ The quality of this solvent compared favorably with the solvent used in earlier studies. It had the following physical properties at 40°: conductivity, from $1-5 \times 10^{-7}$ ohm⁻¹ cm.⁻¹; density, 0.9420 g./ml.; viscosity, 0.03020 poise; dielectric constant, 165.5.

In an attempt to obtain the most accurate data possible and because of a suspicion that traces of a source of acetate ion might remain persistently in the solvent, the process of purifying the NMA was extended by several additional freezing cycles. During the freezing process, an internal heater assembly was placed inside the inner tube in the

apparatus described by Berger and Dawson.⁸ The heater assembly consists of a nichrome wire encased in a glass tube. Crystallization was allowed to proceed at room temperature while 3-7 v. was applied to the heater by means of a variable resistor. The voltage applied depended upon the temperature of the room and the purity of the NMA. After a period of from 5 to 9 days the remaining liquid was drawn off by suction. Throughout the fractional freezing cycles, the NMA was kept under an atmosphere of purified nitrogen. In this manner solvent having a conductivity less than 5×10^{-8} ohm⁻¹ cm.⁻¹ was produced.

Solutions.—The solutions were prepared on a weight basis with solution transfers being made in an atmosphere of nitrogen. The assumption was made that the density of each solution was the same as the density of the solvent for calculations of concentration on a volume basis.

Results

A plot of Λ vs. \sqrt{C} for solutions of acetic acid in highly purified NMA (specific conductance = $1-5 \times 10^{-8}$ ohm⁻¹ cm.⁻¹) at concentrations above 10^{-4} N is shown in Fig. 1. Figure 2 shows similar plots for solutions of potassium chloride and potassium acetate at concentrations greater than 2×10^{-5} N. Summaries of pertinent conductance data appear in Tables I-III. In Table I values for Λ are obtained using the adjusted solvent correction.

TABLE I

TYPICAL CONDUCTANCE DATA FOR ACETIC ACID IN NMA AT 40°

$C^{1/2} \times 10^2$	Λ	$C^{1/2} \times 10^2$	Λ
0.950	0.5258	4.175	0.1194
0.960	.5217	5.718	.0875
1.541	.3271	7.481	.0690
2.636	.1877	8.670	.0582

TABLE II

TYPICAL CONDUCTANCE DATA FOR POTASSIUM CHLORIDE IN NMA AT 40°

$C^{1/2} \times 10^2$	Λ	$C^{1/2} \times 10^2$	Λ
0.3935	20.02	1.4164	19.80
.6308	19.99	1.7963	19.74
.7721	19.96	2.7672	19.59
.8976	19.95	4.0598	19.42
1.1528	19.88	5.5062	19.15

In each case the conductance of the solution was corrected by subtracting the conductance of the solvent. This correction did not exceed 5% where

(8) C. Berger and L. R. Dawson, *Anal. Chem.*, **24**, 994 (1952).

(1) Taken from theses submitted by J. W. Vaughn and M. E. Pruitt.

(2) Financial support from the U. S. Atomic Energy Commission under Contract No. AT-(40-1)-2451 is gratefully acknowledged.

(3) W. J. McCreary, thesis, University of Kentucky, 1948.

(4) J. W. Vaughn, dissertation, University of Kentucky, 1959.

(5) L. R. Dawson, P. G. Sears, and R. H. Graves, *J. Am. Chem. Soc.*, **77**, 1986 (1955).

(6) L. R. Dawson, E. D. Wilhoit, and P. G. Sears, *ibid.*, **78**, 1569 (1956).

(7) L. R. Dawson, G. R. Lester, and P. G. Sears, *ibid.*, **80**, 4233 (1958).

TABLE III
TYPICAL CONDUCTANCE DATA FOR POTASSIUM ACETATE
IN NMA AT 40°

$C^{1/2} \times 10^2$	Λ	$C^{1/2} \times 10^2$	Λ
0.6501	18.00	2.253	17.92
0.7236	17.70	2.993	17.81
0.9774	17.98	4.179	17.65
1.344	17.96	5.493	17.48
1.615	17.93	6.502	17.33

the concentration of the solute was greater than $1 \times 10^{-4} N$.

Conductance curves for monochloroacetic and dichloroacetic acids are shown in Fig. 3. Trichloroacetic acid decomposes in NMA at 40°.

Discussion

The Kohlrausch plot shows that acetic acid behaves like a typical weak electrolyte in NMA. It seems to be much less dissociated than it is in water despite the very high dielectric constant of NMA.

The limiting equivalent conductance for acetic acid was calculated from available limiting ionic conductances⁹ and the conductance of potassium acetate determined in this investigation ($\lambda_0^{H^+} = 9.1$; $\lambda_0^{C_2H_3O_2^-} = 9.8$; Λ_0 for $HC_2H_3O_2 = 18.9$). Using the Ostwald dilution law, $1/\Lambda$ was plotted against CA in an attempt to obtain a straight line with the proper intercept, $1/\Lambda_0$. The experimental data were plotted with the normal solvent correction and with no solvent correction. Neither plot gave a straight line. By successive approximations an intermediate solvent correction was found which gave a straight line intercepting the ordinate at the proper value for $1/\Lambda_0$. Its value varied from 2.0×10^{-8} to 2.7×10^{-8} ohm⁻¹ cm.⁻¹ for different batches; in each case it was approximately one-half the measured conductance of the solvent. This was considered to be the "adjusted" solvent correction. Such a correction gave evidence that even in this solvent there remained a trace of acetic acid, the influence of which appeared at very low solute concentrations. Using the adjusted solvent correction and the Arrhenius theory of dissociation, a value of 7.3×10^{-8} was obtained for the dissociation constant. The dissociation constant for acetic acid in water at 40° is 1.70×10^{-5} .¹⁰ The dissociation constant for acetic acid in NMA is unexpectedly low in view of the great dissociating power resulting from the solvent's high dielectric constant; however, the relative strength of the solvent as an acid or a base must be considered. The acetate ion is more basic than NMA. Since the acetate ion is such a strong base, it holds the proton so tightly that the NMA is not effective in removing it. The acetic acid, therefore, is only slightly dissociated. Water molecules are more effective in separating protons from the acetate ion, making acetic acid a stronger electrolyte in aqueous solutions.

The persistence with which acetic acid remains in NMA throughout the purification cycles may be explained by its tendency to form hydrogen bonds

(9) E. D. Wilhoit, dissertation, University of Kentucky, 1956.

(10) H. S. Harned and R. W. Ehlers, *J. Am. Chem. Soc.*, **56**, 1042 (1934).

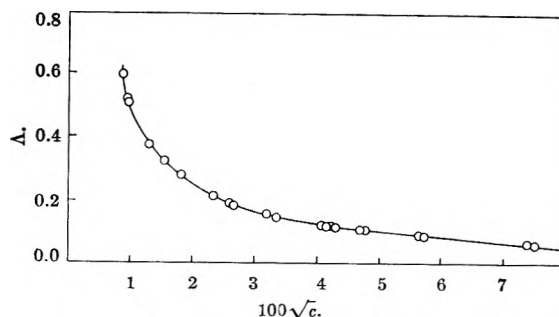


Fig. 1.—Equivalent conductance of acetic acid in NMA at 40°.

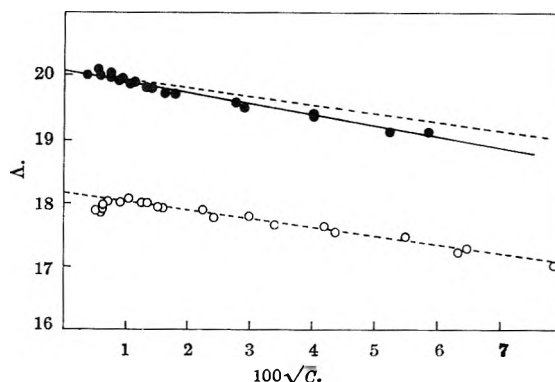


Fig. 2.—Equivalent conductances of potassium chloride (solid circles) and potassium acetate (open circles) in NMA at 40°. Dashed lines represent Onsager theoretical slopes.

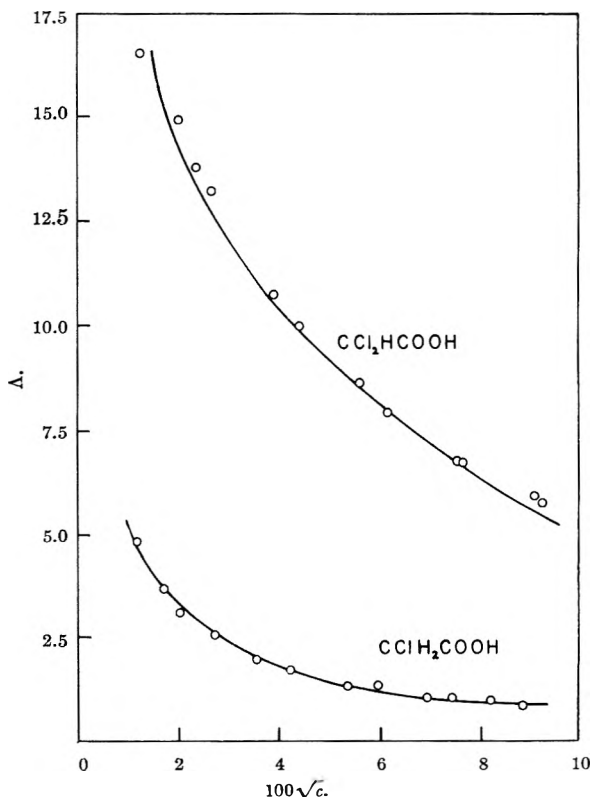


Fig. 3.—Equivalent conductances of monochloroacetic and dichloroacetic acids in NMA at 40°.

with NMA molecules, probably at the oxygen atoms. In this way acetic acid molecules become structural units in this highly structured solvent.

It has been shown experimentally that small amounts of acetic acid have negligible effects on the conducting properties of most uni-univalent or bi-univalent salts in NMA. Because of the solute ion common to that of the solvent impurity, the conductance plot for potassium acetate shows a slight maximum at very low concentrations where the normal solvent correction is used. Suppression of the ionization of the acetic acid impurity would make the proper solvent correction less than the normal value. This was shown above to be the case also where acetic acid was the solute under investigation. The limiting equivalent conductance of potassium acetate was determined by extrapolation by the method of least squares using data representing concentrations greater than 10^{-4} *N*. The plot reproduced the experimental slope and the limiting equivalent conductance obtained previously⁴ with less pure solvent ($\Lambda_0 = 18.2$).

A normal Kohlrausch plot was found (Fig. 2) for potassium chloride in the more highly purified NMA. The experimental slope and the limiting equivalent conductance were in good agreement with those obtained earlier⁵ using less pure NMA having a specific conductance of $2-5 \times 10^{-7}$ ohm⁻¹ cm.⁻¹. (Present: slope = -16.6 ; $\Lambda_0 = 20.1$. Earlier values: slope = -15.1 ; $\Lambda_0 = 20.1$.) Obviously, a small amount of acetic acid impurity in NMA has no measurable effect on the conductance of potassium chloride.

Monochloroacetic acid acts as a weak electrolyte in NMA, but it is stronger than acetic acid. The electronegative chlorine exerts an electron withdrawing effect making the carbonyl group more positive and the proton more easily lost to the solvent.

As would be expected, dichloroacetic acid is stronger than the monosubstituted acid. Trichloroacetic would be expected to be the strongest of the three substituted acids; however, it decomposes in NMA. Verhoek¹¹ has stated that this decomposition in various solvents involves the

trichloroacetate ion and proceeds as $\text{CCl}_3\text{COO}^- \rightarrow \text{CCl}_3^- + \text{CO}_2$. He proposed a mechanism which consists of three steps, the first of which is ionization of the acid. This is followed by dissociation of the ions and subsequent unimolecular decomposition of the trichloroacetate ion.

From our studies it appears that decomposition of the trichloroacetate ion in NMA proceeds *via* first-order kinetics as given by the expression

$$k = 1/t(2.303) \log a/a - x$$

The activation energy for decomposition in the temperature interval 40 to 50° was found to be 28.9 kcal./mole. This value for the activation energy is intermediate between Verhoek's values of 30.9 kcal./mole for the trichloroacetate ion in ethanol and 25.0 kcal./mole in aniline for the same temperature interval. The activation energies in these solvents appear to vary in the order of the expected differences in the extent of solvation of the trichloroacetate ion.

Mono- and dichloroacetic acids are stable in NMA and gave no indication of decomposition after standing for 12 hr. Apparently, three chlorine atoms on the α -carbon are necessary to weaken the carbon-carbon bond sufficiently to cause decomposition.

Stable solvates of hydrochloric acid with NMA having the formulas $\text{NMA} \cdot \text{HCl}$ and $(\text{NMA})_2 \cdot \text{HCl}$ have been reported by D'Alelio and Reid.¹² Compounds having the formulas $(\text{NMA})_2 \cdot \text{HCl}$ and $\text{NMA} \cdot \text{H}_2\text{SO}_4$ were prepared in this Laboratory by Berger.¹³ Solvates of acetic, monochloroacetic, and dichloroacetic acids could not be isolated. However when mixed in a one to one ratio with NMA, trichloroacetic acid reacts producing a white, hygroscopic, semicrystalline solvate which has the composition $\text{CCl}_3\text{COOH} \cdot \text{NMA}$. This reaction proceeds readily at 30°. At higher temperatures the acid decomposes with the evolution of chloroform.

(11) F. H. Verhoek, *J. Am. Chem. Soc.*, **56**, 571 (1934).

(12) G. F. D'Alelio and E. E. Reid, *ibid.*, **59**, 109 (1937).

(13) J. E. Berger, unpublished data, University of Kentucky, 1958.

ACID-BASE EQUILIBRIA IN CONCENTRATED SALT SOLUTIONS. I. POTENTIOMETRIC MEASUREMENTS, INDICATOR MEASUREMENTS, AND UNCHARGED BASES IN DILUTE ACID SOLUTIONS¹

BY DONALD ROSENTHAL² AND JAMES S. DWYER

Department of Chemistry, The University of Chicago, Chicago, Illinois

Received June 13, 1962

An acidity function, H_0 , was established in 4 and 8 *M* LiCl solutions containing small concentrations of strong acids. $\text{pMH} - H_0$ (where $\text{pMH} = -\log$ total strong acid concentration) was shown to be a constant for a given salt solution. $\text{pH}_{\text{G.E.}} - \text{pMH}$ (where $\text{pH}_{\text{G.E.}}$ is the pH measured using a cell with a glass indicator electrode and a saturated calomel reference electrode) also was found to be a constant for 4 and 8 *M* LiCl, 6 *M* NaClO₄, 6 *M* NaNO₃, and 4 *M* CaCl₂ solutions which contain dilute strong acid. Identical results were obtained in 4 and 8 *M* LiCl solutions where the hydrogen electrode was substituted for the glass electrode. The significance of $\text{pH}_{\text{G.E.}}$ and H_0 measurements is discussed. In dilute acid solutions of weak uncharged bases $K_{\text{BH}^+} = ([\text{B}][\text{total strong acid}]/[\text{BH}^+])Q_{\text{BH}^+}$ where K_{BH^+} is the thermodynamic dissociation constant of the acid BH^+ , and Q_{BH^+} is a constant for a particular base B and a particular salt solution. The values of $\text{pH}_{\text{G.E.}}$ and H_0 calculated using this equation are in good agreement with the experimental values obtained for aniline and 2-aminopyrimidine solutions containing dilute strong acids and concentrated salts.

Introduction

Some studies of acid-base equilibrium in concentrated salt solutions have previously been reported.³⁻⁶ Potentiometric^{3,4,6} and indicator^{5,6} measurements have been made on these solutions.

The present studies were initiated in an attempt to explain the quantitative aspects of the potentiometric and indicator results, and of acid-base equilibria in these solutions. This work extends the measurements to more concentrated solutions than were previously studied.^{3,4}

In this paper potentiometric and H_0 ⁵ measurements and acid-base equilibria in dilute acid solutions are discussed. Subsequent papers will consider charged bases in dilute acid solution, the situation in basic and concentrated acid solutions, reaction kinetics, and the practical aspects of acid-base titrations in these solutions.

The results obtained in this study are consistent with the hypothesis that the situation in acidified salt solution is formally similar to that in water, *e.g.*, the reaction $\text{BH}^+ \rightleftharpoons \text{B} + \text{H}^+$ can be written for an uncharged base, B, and its conjugate acid, BH^+ . Further, the quantitative aspects of equilibrium in these solutions can be accounted for using the equation

$$K_{\text{BH}^+} = ([\text{B}][\text{H}^+]/[\text{BH}^+])Q'_{\text{BH}^+} \quad (1)$$

where K_{BH^+} is the thermodynamic molar acid dissociation constant and $Q'_{\text{BH}^+} = f_{\text{B}}f_{\text{H}^+}/f_{\text{BH}^+}$ depends upon the nature and concentration of the salt and the nature of the base, B. Since undis-

sociated strong acid may be present (*e.g.*, HNO₃ in 6 *M* NaNO₃),⁷ it is desirable to use a somewhat more general form of eq. 1

$$K_{\text{BH}^+} = ([\text{B}][\text{total strong acid concentration}]/[\text{BH}^+])Q_{\text{BH}^+} \quad (2)$$

The following additional symbols are used in this and subsequent papers

$\text{pMH} = -\log$ of the total molar concn. of dissociated and undissociated strong acid

$\text{pH}_{\text{G.E.}}$ is the pH as determined with a pH meter using a glass electrode and a saturated calomel reference electrode

pH_{H} is the pH as determined using a hydrogen electrode and a saturated calomel reference electrode

$\text{p}a_{\text{H}^+} = -\log a_{\text{H}^+} = -\log f_{\text{H}^+}[\text{H}^+]$

a_{H^+} is the activity of hydrogen ion, and f_{H^+} is the molar activity coefficient

$H_0 = \text{p}K_{\text{BH}^+} - \log [\text{BH}^+]/[\text{B}] = \text{pMH} - \log Q_{\text{BH}^+} \quad (3)$

where B is one of a series of indicator bases (usually substituted anilines), the H_0 indicators⁵

a_{w} is the activity of water

Experimental

Reagents.—Baker Analyzed Reagent grade LiCl, Mallinckrodt Analytical Reagent grade NaNO₃ and anhydrous CaCl₂, and G. F. Smith anhydrous NaClO₄ were used. The maximum limits of impurities listed on the labels were small, except for the presence of magnesium and alkali salts in CaCl₂.

Fisher reagent grade aniline was purified by distillation. Matheson, Coleman and Bell 2-aminopyrimidine was recrystallized from benzene, then from absolute ethanol. The indicators were purified as described elsewhere.⁸

Solutions.—All solutions used in this study were prepared

(1) Taken in part from the Ph.D. research of James S. Dwyer. This work was supported by two grants from Research Corporation, principally in the form of Research Corporation fellowships for J. S. D. A portion of this work was presented at the 138th National Meeting of the American Chemical Society, New York, N. Y., September 12, 1960.

(2) Department of Chemistry, Clarkson College of Technology, Potsdam, N. Y.

(3) (a) H. S. Harned and B. B. Owen, "The Physical Chemistry of Electrolyte Solutions," Reinhold Publ. Corp., New York, N. Y., 1958, pp. 675-681; (b) M. Kilpatrick, *et al.*, *J. Am. Chem. Soc.*, **75**, 584, 586, 588 (1953).

(4) A. Ellila, *Ann. Acad. Sci. Fennicae, Ser. A, II*, No. 51 (1953); *Acta Chem. Scand.*, **8**, 1257 (1954).

(5) M. A. Paul and F. A. Long, *Chem. Rev.*, **57**, 1 (1957).

(6) F. E. Critchfield and J. B. Johnson, *Anal. Chem.*, **30**, 1247 (1958); **31**, 570 (1959).

(7) (a) T. F. Young, L. F. Moranville, and H. M. Smith in "The Structure of Electrolyte Solutions," W. J. Hamer, Ed., John Wiley and Sons, Inc., New York, N. Y., 1959, pp. 38-48; (b) A. A. Krawetz, Thesis, University of Chicago, 1955.

(8) D. Rosenthal and J. S. Dwyer, "The Acidity Function in Aqueous Concentrated Acid and Salt Solutions," *Can. J. Chem.*, in press (1963).

TABLE I
 MEASUREMENTS OF DILUTE HCl SOLUTIONS IN 4 M LiCl AT 25°

HCl concn., moles/l.	Indicator	H_0	pH _{G.E.} glass electrode	pH _H hydrogen electrode	pMH - H_0 = log Q_{BH^+}	pMH - pH _{G.E.}
4.98×10^{-3}	pNA ^a	1.237	1.36	1.35	1.066	0.94
7.97×10^{-3}	pNA	1.044	1.13	1.14	1.055	.96
1.00×10^{-2}	pNA	0.970	1.06	1.07	1.030	.94
2.99×10^{-2}	pNA	0.497	0.55		1.027	.97
7.97×10^{-2}	oNA	0.007	0.15		1.092	.94
					Av. = 1.054	0.95
					S.D. \bar{x} = 0.012	0.0063
					90% level = ± 0.026	± 0.013

^a pNA is *p*-nitroaniline; oNA is *o*-nitroaniline.

 TABLE II
 MEASUREMENTS OF DILUTE HCl SOLUTIONS IN 8 M LiCl AT 25°

HCl concn., moles/l.	Indicator ^a	H_0	pH _{G.E.} glass electrode	pH _H hydrogen electrode	pMH - H_0 (= log Q_{BH^+})	pMH - pH _{G.E.}
2.000×10^{-4b}			2.92			2.30 ^b
1.000×10^{-3}			0.79			2.30
1.996×10^{-3}			.44	0.44		2.30
3.997×10^{-3}			.11			2.31
4.98×10^{-3}	oNA	-0.194	.02	0.02	2.503 ^b	2.30
7.98×10^{-3}	oNA	-0.406	<0	-0.20	2.514	2.30 ^d
1.000×10^{-2}	oNA	-0.480			2.489	
2.99×10^{-2}	4Cl2NA	-0.967			2.493 ^c	
4.00×10^{-2}	4Cl2NA	-1.075			2.475	
4.98×10^{-2}	4Cl2NA	-1.177			2.481	
7.98×10^{-2}	4Cl2NA	-1.389			2.488	
					Av. = 2.492	2.30
					S.D. \bar{x} = 0.005	
					90% level = ± 0.010	

^a oNA is *o*-nitroaniline, 4Cl2NA is 4-chloro-2-nitroaniline. ^b In calculating pMH and pMH - pH_{G.E.} and pMH - H_0 a correction was applied because of the presence of basic impurities in the 8 M LiCl solutions (see Experimental). The average pMH - pH_{G.E.} value of 2.30 gave satisfactory results in all subsequent calculations. Without applying this correction an average log Q_{BH^+} value of 2.488 (S.D. \bar{x} = 0.004, 90% level 0.008) was obtained. ^c A value for log Q_{BH^+} of 2.468 was obtained with oNA. This value was not included in the average. It is believed not to be accurate because of the relatively large $[BH^+]/[B]$ ratio. ^d pMH - pH_H rather than pMH - pH_{G.E.} value used.

from stock solutions except for aniline. Aniline solutions were found to be unstable and the pure liquid reagent was stored under nitrogen.

The temperature was maintained at $25 \pm 0.5^\circ$. Final concentrations with respect to each of the salts were 4.000 and 8.000 M LiCl for Tables I, II, and III; 3.995 M and 7.990 M LiCl, 5.987 M NaClO₄, 5.989 M NaNO₃, and 4.013 M CaCl₂ for Table IV.

Estimates of total acid or basic impurities in the salt solution were obtained by dropwise titration using the expanded scale of the Beckman Model GS pH meter. The end point was taken to be the point at which the second derivative of pH_{G.E.} with respect to volume was zero. The estimates were: 9.6×10^{-6} M base for 4 M LiCl; 1.7×10^{-4} M base for 8 M LiCl; 3.8×10^{-5} M base for 6 M NaClO₄; 4.5×10^{-5} M acid for 6 M NaNO₃; and 1×10^{-3} M base for 4 M CaCl₂. Acidic or basic impurities were assumed to be negligible in all except the 4 M CaCl₂ and 8 M LiCl solutions. Corrections were applied for the 8 M LiCl solutions. Sufficient acid was added in the preparation of 4 M CaCl₂ to neutralize the basic impurity. The large amount of impurity in the CaCl₂ solution and its variability with time is believed to account for the somewhat larger errors associated with the CaCl₂ measurements.

Separate solutions were prepared for each of the per cent neutralized points in Tables III and IV.

Potentiometric Measurements.—pH_{G.E.} measurements in Tables I, II, and III were made with a Beckman Model G pH meter using the General Purpose glass electrode (shielded, 5 in.) and the Fiber Type calomel electrode (5 in.). Measurements in Table IV were made with a Beckman GS pH meter using a different set of Beckman electrodes of

the same type as above. The pH meter was standardized using standard buffer solutions^{8,9} having pH values close to the solutions being measured.

About five measurements were made on each solution. As a check that no drifting due to change in asymmetry or liquid junction potential had occurred, the pH of the reference solutions was checked before and after measurements were made.

Hydrogen electrode measurements (pH_H) were made by substituting a Hildebrand type electrode for the glass electrode, and proceeding as outlined above. Equilibration times were from 3 to 8 hr. for salt solutions. Most acid and non-reducible buffer solutions equilibrated within 0.5–1 hr.

Spectrophotometric Measurements.—Measurements were made using a Beckman DU spectrophotometer. The solutions and cells were maintained at $25 \pm 0.5^\circ$. In each instance the reference solution was identical in composition with the corresponding indicator solution except for the absence of the indicator. The wave length of maximum absorbance and the molar absorptivity of the basic form of the indicators were determined for each salt solution in which measurements were made. With the exception of *p*-aminoazobenzene (pAAB), the acid forms of the indicators used did not absorb at the base peak. Except as noted below details of the measurements and H_0 calculations were as described elsewhere.⁸

The conjugate acid of pAAB can exist in tautomeric ammonium (BH⁺) and azonium (HB⁺) forms.¹⁰ If f_{HB^+}/f_{BH^+} is constant for a range of acid concentrations in a given salt

(9) R. G. Bates, "Electrometric pH Determinations," John Wiley and Sons, Inc., New York, N. Y., 1954, p. 74.

TABLE III

COMPARISON OF CALCULATED AND EXPERIMENTAL VALUES OF $pH_{G.E.}$ AND H_0 OBTAINED IN THE NEUTRALIZATION OF 0.03 *M* ANILINE

% Neutralized	4 <i>M</i> LiCl				8 <i>M</i> LiCl					
	$pH_{G.E.}$		H_0		$pH_{G.E.}$		H_0			
	Exptl.	Calcd.	Exptl.	Calcd.	Exptl.	Calcd. ^a	Exptl.	Calcd.	Calcd. ^a	
20	5.15	5.12	4.965 A ^b	5.01	5.02	5.02	5.03	4.80 A ^b	4.83	4.84
40	4.68	4.69	4.56 A	4.59	4.60	4.60	4.60	4.41 A	4.41	4.41
50	4.51	4.52	4.405 A	4.41	4.42	4.42	4.42	4.23 A	4.23	4.23
80	3.90	3.91	3.80 A	3.81	3.83	3.82	3.83	3.64 A	3.63	3.64
89.73	3.60	3.58	3.45 A-pAAB	3.47	3.51	3.45	3.50	3.30 A ^c	3.29	3.31
94.95	3.28	3.26	3.17 pAAB ^d	3.16	3.20	3.15	3.19	2.95 pAAB ^e	2.96	3.00
98.95	2.74	2.76	2.63 pAAB	2.65	2.53	2.47	2.66	2.32 pAAB	2.28	2.46
100.0	2.59	2.55	2.44 pAAB	2.44	1.95 ^f	1.82	2.28	1.87 pAAB ^g	1.63	2.09
100.95	2.33	2.36	2.26 pAAB-mNA ^h	2.25	1.30	1.22	1.57	1.17 pNA	1.03	1.38
110	1.60	1.57	1.42 pNA	1.46	0.21	0.22	0.25	0.08 oNA ⁱ	0.03	0.06
120	1.30	1.27	1.19 pNA	1.17	<0	-0.08	-0.06	-0.22 oNA	-0.26	-0.25
140	0.99	0.97	0.91 pNA	0.87	<0	-0.38	-0.36	-0.54 4Cl2NA	-0.56	-0.55
$pMH - pH_{G.E.}$	0.95				2.30					
$pMH - H_0$	1.054				2.492					
$\log Q_{AH^+}$ ^j	0.868				2.127 (2.113) ^a					
K_{AH^+}/Q_{AH^+}	3.43×10^{-6}				1.89×10^{-7} (1.95×10^{-7}) ^a					

^a Calculated using corrected % neutralized obtained assuming 8 *M* LiCl contains 1.94×10^{-4} *N* strong basic impurities (see footnote *b*, Table II). The preceding column assumes very weak basic impurities. ^b Letters represent abbreviations for indicators used in H_0 measurements: A, aniline; pAAB, *p*-aminoazobenzene; pNA, *p*-nitroaniline; oNA, *o*-nitroaniline; 4Cl2NA, 4-chloro-2-nitroaniline. With aniline as the indicator H_0 values were calculated using eq. 12 to place the indicator on the H_0 scale. ^c An H_0 value of 3.18 was obtained for this solution with *p*-aminoazobenzene as the indicator and 3.38^k was obtained with mNA. ^d A value of 3.24 was obtained for this solution with 7×10^{-6} mNA. ^e A value of 3.14 was obtained with 7×10^{-6} *M* mNA. ^f An experimental value for $pH_{G.E.}$ of 1.89 was obtained at the inflection point in the neutralization in 8 *M* LiCl. ^g This value may not be very accurate because of the large value of $[BH^+]/[B]$. ^h A value of 2.33 was obtained for this solution with 1.5×10^{-4} mNA. A calculated correction of -0.06 due to the effect of the indicator was applied. ⁱ A value of 0.14 was obtained with pNA as the indicator. ^j $pK_{AH^+} = 4.597$ (R. A. Robinson and R. H. Stokes, "Electrolyte Solutions," Butterworths Publications, Ltd., London, 1959, p. 532, 30). The correction of 0.001 (-log density of water) is required to convert *pK* values from the molal to the molar scale. ^k This H_0 value may not be very accurate because of the relatively small value of $[BH^+]/[B]$.

TABLE IV

COMPARISON OF CALCULATED AND EXPERIMENTAL VALUES OF $pH_{G.E.}$ OBTAINED IN THE NEUTRALIZATION OF 0.03 *M* 2-AMINOPYRIMIDINE

% Neutralized	Water		4 <i>M</i> LiCl		8 <i>M</i> LiCl		6 <i>M</i> NaClO ₄		6 <i>M</i> NaNO ₃		4 <i>M</i> CaCl ₂	
	Exptl.	Calcd.	Exptl.	Calcd.	Exptl.	Calcd.	Exptl.	Calcd.	Exptl.	Calcd.	Exptl.	Calcd.
10	4.64	4.62	4.83	4.82	4.92	4.90	4.81	4.82	5.03	5.03	4.95	4.93
20	4.29	4.28	4.47	4.46	4.56	4.55	4.47	4.46	4.68	4.68	4.56	4.58
50	3.70	3.70	3.86	3.86	3.92	3.94	3.85	3.86	4.09	4.07	3.94	3.97
79.75	3.17	3.17	3.26	3.27	3.33	3.35	3.27	3.27	3.47	3.48	..	3.37
89.81	2.92	2.94	2.93	2.94	3.01	3.00	2.87	2.92	3.12	3.14	3.06	3.03
99.80	2.67	2.67	2.27	2.25	1.89	1.68	1.73	1.83	2.33	2.41	2.38	1.84
109.90	2.42	2.42	1.57	1.58	0.20	0.23	0.71	0.68	1.67	1.69	0.61	0.56
120	2.23	2.23	1.29	1.29	<0	-0.08	0.42	0.38	1.42	1.40	0.19	0.26
140	1.98	1.98	0.99	0.99	<0	-0.38	..	0.08	..	1.11	..	-0.04
$pMH - pH_{G.E.}$	$\log f_i$ ^a		0.93		2.30		1.84		0.817		1.967	
$\log Q_{PH^+}$ ^b	0		1.153		2.605		2.063		1.250		2.302	
$S.D_{\log Q_{PH^+}}$ ^c			0.0044		0.0094		0.003		0.0079		0.018	
K_{PH^+}/Q_{PH^+}	2.307×10^{-4}		1.62×10^{-5}		5.73×10^{-7}		2.00×10^{-6}		1.30×10^{-5}		1.15×10^{-6}	

^a Calculated using the expression $\log f_i = 0.5I^{1/2}/(1 + I^{1/2}) - 0.2I$ (see R. A. Robinson ref. 7a, p. 257). ^b $pK_{PH^+} = 3.637$. This represents an average pK_{PH^+} ($n = 5$, $S.D_{\bar{x}} = 0.0068$) obtained from the 10-89.81% neutralized $pH_{G.E.}$ measurements. A value of 3.54 has been reported previously (A. Albert, R. Goldacre, and J. Phillips, *J. Chem. Soc.*, 2246 (1948)).

^c $\log Q_{PH^+}$ values represent an average obtained from the 10-89.81% neutralized $pH_{G.E.}$ measurements, except in the case of NaClO₄, where the 89.81% value was omitted.

solution, it can be shown that the theoretical error in pAAB- H_0 values obtained by the usual method is $\log([BH^+] + [HB^+]/f_{HB^+}/f_{BH^+})/([BH^+] + [HB^+])$.^{11,12} From the data available, no good estimate of the error term can be made.

(10) G. E. Lewis, *Tetrahedron*, **10**, 129 (1960); M. T. Rogers, T. W. Campbell, and R. W. Maatman, *J. Am. Chem. Soc.*, **73**, 5122 (1951); W. R. Brode and G. M. Wyman, *ibid.*, **74**, 4641 (1952).

(11) Further complications due to the presence of *cis* and *trans* azo isomers and the activity of water in the equilibrium constant expression result in a similar but more complicated expression.¹²

(12) J. S. Dwyer, Thesis, University of Chicago.

However, the good agreement between calculated and experimental H_0 values and the 90 and 101% overlap values in 4 *M* LiCl (Table III) seem to indicate the error is small in 4 *M* LiCl. Similar good agreement is obtained in water. There is more uncertainty about the magnitude of the pAAB- H_0 error in 8 *M* LiCl, although the agreement between calculated and experimental values appears to be good.

Results

Potentiometric and H_0 Measurements in Dilute Solutions of HCl.—The results of potentiometric measurements using the glass electrode in 4

and 8 *M* LiCl solutions are summarized in Tables I and II. A second series of measurements in 4 and 8 *M* LiCl, 4 *M* CaCl₂, 6 *M* NaNO₃, and NaClO₄ also was performed.¹² In each instance, the pMH - pH_{G.E.} value obtained in a particular salt solution was a constant independent of pMH (e.g., see Tables I and II). Measurements made with different sets of electrodes on different pH meters gave essentially the same pMH - pH_{G.E.} values for 4 and 8 *M* LiCl solutions (0.95 in 4 *M* LiCl and 2.29 in 8 *M* LiCl for the second series). Estimates of pMH - pH_{G.E.} for the other salt solutions are given in Table IV.

The measurements made using the hydrogen electrode (Tables I and II) are in good agreement with the glass electrode measurements.¹³

These results demonstrate the meaningfulness of potentiometric measurements made with the glass electrode in concentrated salt solutions.¹⁴

Values of pMH - *H*₀ in 4 and 8 *M* LiCl are summarized in Tables I and II. The values of pMH - *H*₀ in 4 *M* LiCl over a wide range of HCl concentrations were not significantly different.⁶ The same is true for 8 *M* LiCl. This establishes an acidity function for these solutions.⁵

Neutralization of Aniline in LiCl Solutions.—To calculate pMH from eq. 2 and then the pH_{G.E.} and *H*₀ values obtained in the neutralization of aniline, it is necessary to have an estimate of K_{AH^+}/Q_{AH^+} . (The subscript AH⁺ refers to anilinium ion.) One method of obtaining such an estimate involves making pH_{G.E.} measurements in the aniline buffer region where [AH⁺]/[A] is known. pMH then is calculated by using the pMH - pH_{G.E.} values in Tables I and II. Log (K_{AH^+}/Q_{AH^+}) then can be calculated from the logarithmic form of eq. 2.

$$-\log (K_{AH^+}/Q_{AH^+}) = \text{pMH} + \log ([AH^+]/[A]) \quad (4)$$

Average values of $-\log (K_{AH^+}/Q_{AH^+})$ of 5.465 (*n* = 4, S.D._{x̄} = 0.012) in 4 *M* LiCl and 6.724 in 8 *M* LiCl (*n* = 4, S.D._{x̄} = 0.003) were obtained. Another method of estimating log (K_{AH^+}/Q_{AH^+}) involves using the expression

$$\log (K_{AH^+}/Q_{AH^+}) = \log ([BH^+]/[B]) - \log ([AH^+]/[A]) - (\text{p}K_{BH^+} + \log Q_{BH^+}) \quad (5)$$

which is derivable from eq. 2 and 4. The concentration ratios of conjugate acid to base for an *H*₀ indicator and aniline were determined spectrophoto-

(13) F. E. Critchfield measured pH with the glass and hydrogen electrodes of 0.025 *M* HCl solutions containing concentrated salts. The agreement between the two measurements was excellent. In the following listing of results, the value of pH_{G.E.} is followed by the value of pH_H in parentheses: 4 *M* LiCl, 0.66 (0.68); 4 *M* KCl, 1.20 (1.20); 4 *M* NaCl, 0.87 (0.85); 2.67 *M* CaCl₂, 0.49 (0.51); 2.67 *M* MgBr, 0.02 (0.02). The pMH - pH_{G.E.} value of 0.94 for 4 *M* LiCl obtained from these data is in good agreement with the values of Table I. S. Bruckenstein and I. M. Kolthoff obtained pH_{G.E.} and pH_H results which were not significantly different for 0.01 *M* acetic acid solutions, and for 0.05 *M* acetic acid-0.05 *M* sodium acetate solutions which were 1, 2, 3, 4, and 5 *M* in CaCl₂ (personal communications).

(14) W. H. Beck and W. F. K. Wynne Jones, *J. chim. phys.*, **49**, C98 (1952); M. Dole, *J. Am. Chem. Soc.*, **54**, 3095 (1932); D. A. MacInnes and D. Belcher, *ibid.*, **53**, 3322 (1931); D. Hubbard, E. H. Hamilton, and A. N. Finn, *J. Res. Natl. Bur. Std.*, **22**, 346 (1939).

metrically. A value of $-\log (K_{AH^+}/Q_{AH^+})$ of 5.46 was obtained for 4 *M* LiCl using the 89.73% neutralization data. In 8 *M* LiCl a value of 6.81 was obtained with mNA (6.61 with pAAB). The discrepancy between the values in 8 *M* LiCl may be due to deviations of *m*-nitroaniline and pAAB from "true" *H*₀ indicator behavior (see Experimental and Discussion). The spectrophotometric and calculated values of log [AH⁺]/[A] in the buffer region for 4 and 8 *M* LiCl were in good agreement. The values of K_{AH^+}/Q_{AH^+} obtained from the pH_{G.E.} measurements were believed to be more accurate and were used in the subsequent calculations.

Experimental and calculated pH_{G.E.} and *H*₀ results are presented in Table III. In 4 *M* and 8 *M* LiCl the differences between calculated and experimental values are comparable in magnitude to the error in the pH_{G.E.} and *H*₀ measurements, except near the 100% point in 8 *M* LiCl. At or near the 100% point solutions are poorly buffered, and pH_{G.E.} and *H*₀ values are significantly affected by acidic or basic impurities or small errors in the preparation of solutions.

It was necessary to correct for the basic impurity in the LiCl solution to obtain a consistent explanation of pH_{G.E.} measurements in 8 *M* solution (Table II). The magnitude of the effect of this impurity upon the pH_{G.E.} and *H*₀ values in the aniline titration depends upon the strength of the base. The columns in Table III marked with a superscript *a* contain the results of calculations based upon assuming a strong base. Results in the column preceding these are calculated assuming the base is very weak (or absent). The actual situation probably is between these extremes.

A minimal concentration of *H*₀ indicator was introduced into the aniline solutions. Calculation of the effect of pAAB (8 × 10⁻⁶ *M*) upon the 100% neutralized value in 8 *M* LiCl indicated a pH_{G.E.} change from 1.82 to 1.84. An error of one part per thousand in the titration in 8 *M* LiCl solutions is equivalent to an error in calculated pH_{G.E.} or *H*₀ value of 0.09 at the 100% neutralized point and of 0.04 at the 99 or 101% points. All such errors are of lesser importance in 4 *M* LiCl (10⁻⁵ *M* pAAB 0.01 at 100%, 1 part/1000 0.02 at 99, 100, or 101%).

Neutralization of 2-Aminopyrimidine (P).— K_{PH^+}/Q_{PH^+} values were obtained using pH_{G.E.} values in the buffer region, pMH - pH_{G.E.} values, and eq. 4. The K_{PH^+}/Q_{PH^+} estimates, pMH - pH_{G.E.} values, and experimental and calculated pH_{G.E.} values obtained in the neutralization of 2-aminopyrimidine are presented in Table IV. Differences between calculated and experimental results were comparable to errors in glass electrode measurements except for some of the 99.8% neutralized points. The larger error at 99.8% is presumably due to impurities and small errors in preparing solutions.

Discussion

$$\text{pMH} - \text{p}a\text{H} = \log f_{H^+} \quad (6)$$

Since the molar concentration of hydrogen ion is small compared to the concentration of salt, it is

not unreasonable that $\log f_{H^+}$ will be a constant for a given concentrated salt solution.¹⁵ Although $pMH - pH_{G.E.}$ and $pMH - paH$ are both constants, $paH \neq pH_{G.E.}$, but rather

$$paH = pH_{G.E.} + \frac{\Delta E_{L.J.}}{0.059} \quad (7)$$

at 25°, $\Delta E_{L.J.}$ is the difference between the saturated calomel electrode-concentrated salt solution liquid junction potential and the saturated calomel-reference (standardization) solution liquid junction potential. $\Delta E_{L.J.}$ is a constant where measurements are made using a particular concentrated salt and reference solution and a particular reference electrode.¹⁶

From eq. 3, for an H_0 indicator

$$pMH - H_0 = \log Q_{BH^+} \quad (8)$$

The H_0 scale established in Tables I and II is for uncharged bases whose $\log Q_{BH^+}$ values are 1.054 in 4 M LiCl and 2.492 in 8 M LiCl. Although substituted anilines are used to establish this scale, aniline (A) itself does not satisfy these requirements (see Table III). Assuming $\log Q_{BH^+}$ and $\log Q_{AH^+}$ can adequately be represented by

$$\log Q_i = B_i M - n \log a_w \quad (9)^{8,17}$$

and that n has the same value but B_i has different values for aniline and the H_0 indicators

$$\log Q_{BH^+} - \log Q_{AH^+} = (B_{BH^+} - B_{AH^+})M \quad (10)$$

in a solution M molar in LiCl. If

$$B_{BH^+}M = \log f_B f_{H^+} / f_{BH^+} \quad (11)$$

and similarly for aniline, then the difference in B_i terms (eq. 10) is due in part to differences between $\log f_B$ and $\log f_A$. $\log f_B = B_B M$,¹⁸ where B_B

(15) J. N. Brønsted, *Trans. Faraday Soc.*, **23**, 430 (1927).

(16) H. S. Harned, *J. Phys. Chem.*, **30**, 436 (1926); ref. 9, pp. 22-33, 40-45.

(17) K. N. Bascombe and R. P. Bell, *Discussions Faraday Soc.*, **24**, 158 (1957).

(18) F. A. Long and W. F. McDevit, *Chem. Rev.*, **51**, 119 (1952).

has a value of 0.105 for *p*-nitroaniline¹⁹ and 0.11 for 4-chloro-2-nitroaniline.¹² B_A (for aniline) has a value of 0.07.²⁰ Values for $B_{BH^+} - B_{AH^+}$ (eq. 10) of 0.046 in 4 M LiCl and 0.0455 in 8 M LiCl are obtained. These two values are not significantly different and their magnitude is not unreasonable ($B_B - B_A \sim 0.04$).

The requirements, which a series of indicators must possess to be satisfactory in establishing a self-consistent H_0 scale in concentrated salt solutions, are much more stringent than in concentrated acid solutions. This is because an indicator can be used over a much wider range of electrolyte (salt) concentration and a_w . As a result, the difference of $\log Q_{BH^+} - \log Q_{B'H^+}$ may not be constant (eq. 10) and may be quite different from the value in the acid solutions in which " pK_{BH^+} " was determined. For this reason, indicators quite similar in structure were used in establishing the acidity function, H_0 (Tables I and II) in LiCl solutions and where possible in the subsequent H_0 measurements (Table III).

Once an H_0 scale has been established, indicators (I) like aniline which conform to eq. 2 can be used as pseudo- H_0 indicators

$$H_0 = pK'_{IH^+} + (\log Q_{IH^+} - \log Q_{BH^+}) - \log ([IH^+]/[I]) = pK'_{IH^+} - \log ([IH^+]/[I]) \quad (12)^{21}$$

where pK'_{IH^+} is an "adjusted" pK . pK'_{IH^+} may be different for each salt concentration, but values of H_0 obtained with legitimate and pseudo- H_0 indicators will be self-consistent. Aniline was employed as a pseudo- H_0 indicator for some of the H_0 measurements in Table III.

(19) M. A. Paul, *J. Am. Chem. Soc.*, **76**, 3236 (1954). However, see ref. 5, p. 20.

(20) R. L. Bergen, Jr., and F. A. Long, *J. Phys. Chem.*, **60**, 1134 (1956). However, see S. Glasstone, J. Bridgman, and W. R. P. Hodgson, *J. Chem. Soc.*, 637 (1927).

(21) In evaluating H_0 and pK'_{IH^+} (actually pK'_{IH^+}) values in concentrated acid solutions, $\log Q_{IH^+} - \log Q_{BH^+}$ is assumed to be zero. Actually all that is necessary is that the difference is relatively constant over the range of indicator overlap (usually ca. one molar change in acid concentration).

THE STRUCTURE OF ACTIVE CENTERS IN COPPER CATALYST¹

BY ITURO UHARA, SADAQ YANAGIMOTO, KAZUO TANI, GIN-YA ADACHI, AND SHOSUKE TERATANI

Chemistry Department, Faculty of Science, Kobe University, Mikage, Kobe, Japan

Received June 18, 1962

On annealing cold-worked Cu, the release of strain energy and changes of various physical properties take place in a comparatively narrow temperature range (T_D) and they are attributed to the disappearance of dislocations. A sudden decrease in the catalytic activity of cold-worked Cu for Gattermann's reaction and dehydrogenation of ethanol was found to take place in T_D , too. Since the diminution of the surface area of the catalyst is negligible, it was concluded that the active center of Cu catalyst is the termination of dislocations at the surface of the metal. The generation of active centers under various circumstances is discussed.

I. Introduction

Little has been known with physical certainty concerning the structure of active centers in

(1) Read at the Annual Meeting of the Chemical Society of Japan held on April 4, 1960 and April 3, 1962.

heterogeneous catalysts since Taylor's proposal.² We established a method to estimate the structure of active centers in metallic catalysts, and found that the active centers of Cu catalyst for the de-

(2) H. S. Taylor, *Proc. Roy. Soc. (London)*, **A108**, 105 (1925).

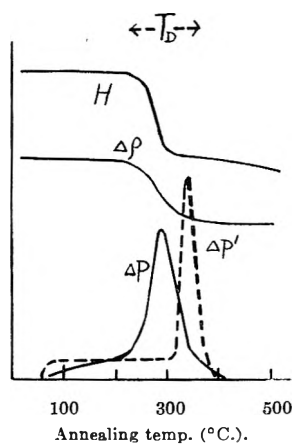


Fig. 1.—Changes of hardness (H), and extra-resistivity ($\Delta\rho$), and the rate of release of defect energy (ΔP) during annealing of Cu specimens (99.96%) deformed in torsion to $nd/l = 1.8$. $\Delta P'$ = the rate of release of energy of a specimen containing 0.35% As and 0.05% P (by Clarebrough, *et al.*).

composition of diazonium salt are the termination of dislocations at the surface,³ and that the active centers of Ni catalyst for various reactions are both the termination of dislocations and point defects at the surface.⁴ In this paper, details of the study on Cu catalyst and further extensions are reported.

In recent years, the behavior of lattice defects in cold-worked, irradiated, or quenched metals has been studied by measuring the rate of release of strain energy (ΔP), changes in density, extra-resistivity ($\Delta\rho$), and hardness (H) during annealing,⁵ some of which are shown in Fig. 1.

In a temperature range T_D a sudden change takes place in density, in $\Delta\rho$, and in H with the rapid release of defect energy and recrystallization. These phenomena are attributed to the disappearance of dislocations in the deformed metals, although the rearrangement of dislocations may take part in the changes in the lower range of T_D , too. Point defects produced in Cu by slight cold-working or irradiation at sub-zero temperatures disappear by annealing below room temperature and it seems unlikely that any appreciable concentration of vacancies and interstitials exists in the specimen of pure Cu used in the present work, especially in one annealed over 100°.⁶

As the concentration of lattice defects increases with the degree of cold-working, strong interaction among them lowers T_D considerably,^{5b} *e.g.*, the maximum of ΔP for 99.967% Cu is displaced from 390 to 270° as the degree of twisting (nd/l , where

(3) I. Uhara, S. Yanagimoto, K. Tani, and G. Adachi, *Nature*, **192**, 867 (1961).

(4) I. Uhara, Y. Numata, and Y. Kageyama, *J. Phys. Chem.*, **66**, 1374 (1962).

(5)(a) T. Suzuki, *Sci. Rep. Res. Inst. Tohoku Univ.*, **A1**, 55 (1949); L. M. Clarebrough, M. E. Hargreaves, and G. W. West, *Proc. Roy. Soc. (London)*, **A232**, 252 (1955); L. M. Clarebrough, M. E. Hargreaves, and M. H. Loretto, *Acta Met.* **6**, 725 (1958).

(b) L. M. Clarebrough, M. E. Hargreaves, D. Michell, and G. W. West, *Proc. Roy. Soc. (London)*, **A215**, 507 (1952); S. Boas, "Defects in Crystalline Solids," The Physical Society, London, 1955, p. 212.

(6) *Inst. Met.*, "Vacancies and other Point Defects in Metals and Alloys" (1958); J. A. Manintveld, *Nature*, **169**, 623 (1952); A. W. Overhauser, *Phys. Rev.*, **90**, 393 (1953).

n = the number of turns, d = diameter, and l = length) increases from 0.47 to 3.03, and the recovery in thermoelectric force (S) of cold-worked Cu occurs at 250–350°, 160–240°, and 120–240° for specimens under compression of 15, 57, and 90%, respectively.⁷

On the other hand, the existence of impurities (especially non-metallic) raises T_D remarkably, as shown in Fig. 1. Accordingly, for the purpose of studying the relation among catalytic activity, physical properties, and lattice defects, it is desirable to employ the identical specimen, or at least specimens of the same material and of the same degree of working (as small as possible to avoid confusion due to interaction among lattice defects). If we compare the catalytic activity of Cu specimens which have been cold-worked and annealed at various temperatures below or above T_D , some conclusion may be drawn concerning the relation between catalytic activity (or active centers) and dislocations.

II. Experimental

(A) **Decomposition of Diazonium Salt (Gattermann's Reaction).**—Pieces of Cu 99.96% pure (containing O = 0.036, S = 0.0011, and Pb = 0.0018%, etc.) wire, with a diameter of 2.60 mm., were twisted slowly to avoid temperature elevation to $nd/l = 1.0$ after complete annealing at 550°, and then annealed again in N_2 for 1 hr. at various temperatures. The specimens were cut into short pieces (cut ends were sealed with a mixture of beeswax and resin), washed with concentrated ammonia for 20 min. to remove the oxide layer, and then thrown into the reaction vessel. The total surface area of the catalyst before twisting was *ca.* 6.4 cm.²

Benzene diazonium chloride solution was prepared by adding pure $NaNO_2$ solution (5.8×10^{-3} mole) slowly into a well cooled mixture of newly distilled aniline (5.9×10^{-3} mole), water (2.5 cc.), and concentrated HCl (5.7×10^{-2} mole). The reaction vessel was shaken in a thermostat and the volume of N_2 (V cc. at NTP) evolved was measured with a gas buret filled with saturated NaCl solution, the reaction rate being compared by V in 20 min.

(B) **Dehydrogenation of Ethanol.**—Cu wire (not annealed) was twisted to $nd/l = 0.8$, and then annealed at various temperatures. Two l. of N_2 saturated with ethanol vapor at room temperature was carried on the catalyst in 4 hr. at 275°, where the decomposition of aldehyde can be avoided. The product was dissolved in water and the yield of CH_3CHO was determined colorimetrically with *m*-phenylenediamine.

(H).—Parallel to the study of the catalytic activity, the change in physical properties of cold-worked Cu during annealing was studied, *e.g.*, hardness (H) was measured with a micro-Vickers hardness tester employing the same specimens as in (A). As the specimens are small and the surface is roughened by twisting, fluctuations of the data are unavoidable, but the tendency of the change is apparent, as shown in Fig. 2.

(S).—It was clearly shown by Kishimoto⁷ that the measurement of the thermoelectric force (S) of cold-worked metals is an effective method to study the relation between lattice defects and the catalytic activity. It can be carried out easily with a small quantity of the material with considerable precision. His result for specimens of the same material as used in (A) and (B) against well annealed Cu wire is shown in Fig. 2.

III. Results

(A) **Decomposition of Diazonium Salt.**—The value of V consists of the rate of (i) natural decomposition, (ii) homogeneous decomposition catalyzed by cuprous ion dissolved from the metal, (iii) heterogeneous decomposition catalyzed by

(7) S. Kishimoto, *J. Phys. Chem.*, **66**, 2694 (1962).

the normal surface of Cu, and (iv) heterogeneous decomposition catalyzed by the active center at the surface. It was found that (ii) is almost constant irrespective of the annealing temperature and the surface area of the metal. The change of the surface area on annealing is considered to be negligible, because it was found that catalytically active Cu powder deposited from CuSO_4 solution by means of the reaction with Zn dust has almost the same adsorption capacity for methylene blue even after it is annealed at 500° and loses most of the active centers (3.3×10^{-7} and 3.1×10^{-7} mole are adsorbed by 1 g. of Cu before and after annealing, respectively).

The value of V for a specimen without dislocations (although a very small number of dislocations survive over T_D , their activity is negligibly small) which is, generally speaking, obtained by annealing at temperatures higher than T_D is the sum of (i), (ii), and (iii), and the decrease of V on removing Cu from the solution is the sum of (iii) and (iv) when reduced to the initial concentration of the solution, hence each value can be obtained separately. For example, (i) = 4.6, (ii) = 1.5, (iii) = 1.6, and (iv) = 8.3 cc. at 25° for a specimen annealed below T_D , although very exact values of V cannot be obtained owing to fluctuations of the activity, probably due to non-uniformity of cold-working and resulting distribution of lattice defects. The fraction of V , (iii) + (iv), which is ascribed to heterogeneous catalysis is shown in Fig. 2A together with H and S .

Considering the large effect of impurities and the degree of cold-working on the values of T_D , it may be that the sudden changes of H and S observed near 400° correspond to the changes observed in T_D in Fig. 1, and that the concurrent decrease in the catalytic activity is naturally ascribed to the disappearance of dislocations. Consequently, the active center of Cu catalyst for this reaction is concluded to be the termination of dislocation at the metal surface. About 60–85% of the heterogeneous decomposition of diazonium salt takes place at the active center (iv), and the rest at the normal metallic surface (iii). Analogous curves were obtained from measurements at 20, 30, and 35° , too, and approximate values of the energy of activation are as follows: (i) = 24, (ii) = 23, and (iv) = 33 kcal., but that of (iii) is not obtained owing to large fluctuations of data.

(B) **Dehydrogenation of Ethanol.**—As shown in Fig. 2B *ca.* 70% of the heterogeneous reaction occurs at the termination of dislocations.

Method of Preparation of Metals in Relation to their Catalytic Activity and Generation of Dislocations.—Utilizing the conclusion in III(A) it may be possible to detect dislocations in specimens prepared by various methods by measuring their catalytic activity and to gain some knowledge concerning the generation of dislocations in the metal.

(C) **Electrolytic Copper.**—Particles of 80–100 mesh were obtained by the electrolysis of a solution containing 10% CuSO_4 and 10% H_2SO_4 with various current densities, D_K amp./cm.². The specific area is almost constant irrespective of the

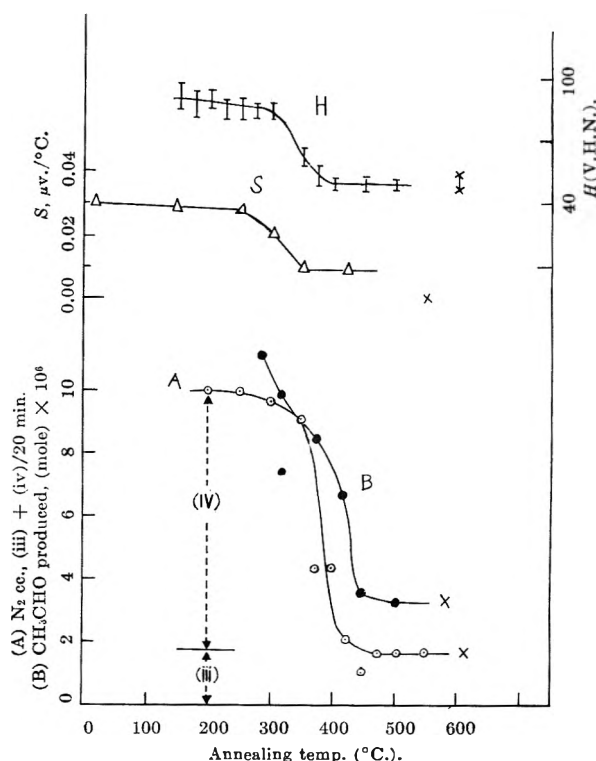


Fig. 2.—Hardness (H), thermoelectric force (S), $\mu\text{v./deg.}$, under 15% compression⁷ (for slighter working T_D will become somewhat higher), and catalytic activity of Cu (99.96%) cold-worked and annealed at various temperatures: (A) $\text{C}_6\text{H}_5\text{N}_2\text{Cl} = \text{C}_6\text{H}_5\text{Cl} + \text{N}_2$ at 25° ; (B) $\text{C}_2\text{H}_5\text{OH} = \text{H}_2 + \text{CH}_3\text{CHO}$ at 275° ; \times = values for specimens not cold-worked. The scale of H in the previous paper³ must be corrected as shown here.

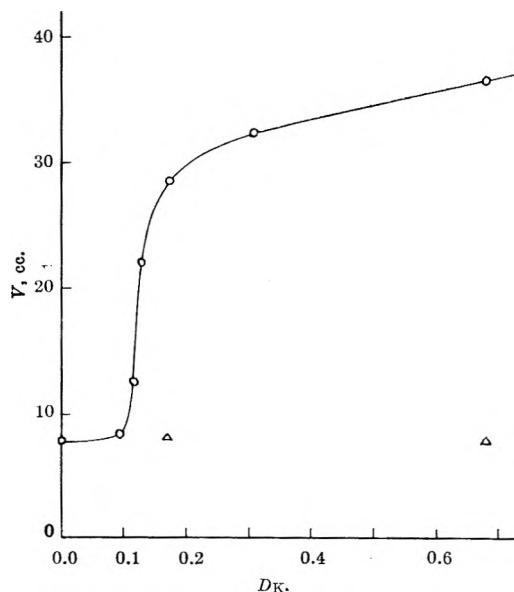


Fig. 3.—Catalytic activity for the decomposition of diazonium salt measured by the volume of N_2 evolved in 20 min. at 25° (V) of Cu specimens electrolytically deposited under the current density (D_K , amp./cm.²). Triangles show data for specimens after annealing at 500° .

magnitude of D_K and it also is unaffected by annealing at 500° as stated above. The rate of decomposition of diazonium chloride catalyzed by 0.1 g. of the specimens is given in Fig. 3. Since the activity of the specimens electrolyzed at lower D_K

is equal to that of the specimen completely annealed, it is concluded that dislocations are generated during electrolysis only when D_K is larger than 0.1 amp./cm.² and that the density of the dislocations, hence the degree of distortion in the metal, increases remarkably with D_K . It often was observed⁸ that in electrodeposited metals such as Cu and Ni inclusion of oxide, hydroxide, and other impurities and hardness of metals increase considerably with D_K . All of these facts can be attributed to the generation of dislocations which is caused by the lattice distortion due to the inclusion of impurities.

(D) **Chemically Deposited Copper.**—Cu powder usually used for Gattermann's synthesis is prepared by adding Zn dust in CuSO₄ solution. The catalytic activity of a 0.1-g. sample at 25° was (iii) 42.2 and (iv) 12.8 cc. in 20 min., the contribution of dislocations being 23%. Dislocations probably may be generated in an analogous manner as electrolysis under high current density.

(E) **Copper Reduced from Oxide Layer.**—Pieces of the same dimension as in II(A) were annealed, oxidized, and reduced at 300°. The

(8) M. Schlötter, *Discussions Faraday Soc.*, **31**, 1177 (1935); W. Blum and C. Kasper, *ibid.*, **31**, 1203 (1935).

induced catalytic activity (iv) at 27° was 0.9 and 0.5 cc. for specimens the oxide layer of which before reduction was 560 Å. thick and far thinner, respectively. This indicates the possibility of generating dislocations in a very thin layer on metals during a chemical change such as reduction.

(F) **Irradiation with Neutrons.**—Well annealed pieces were irradiated with neutrons and the resulting catalytic activity was investigated after the disappearance of the induced radioactivity.

Thermal neutrons/cm. ²	1–2 × 10 ¹⁶	1.5 × 10 ¹⁶
Induced activity, (iv), cc.	0	0.3 at 25°, 0.7 at 30°
(iii) =	1.6–1.0	

i.e., dislocations are generated although the efficiency is not high.

(G) **Irradiation with γ -Rays.**— γ -Rays of Co⁶⁰ amounting to 3.7 × 10⁸ r. were irradiated on a well annealed specimen, resulting in no generation of catalytic activity and dislocations.

Acknowledgment.—We wish to thank Dr. H. Wakeshima, Dr. H. Takegoshi, Dr. A. Saika, and Mr. S. Taniguchi for their kind advice and assistance. Our thanks also are due to the Ministry of Education in aid of this research.

STUDIES ON THERMOELECTRIC FORCE AND LATTICE DEFECTS AS ACTIVE CENTERS IN METALLIC CATALYSTS¹

BY SHOZO KISHIMOTO

Chemical Department, Science Faculty, Kobe University, Higashinada-ku, Kobe, Japan

Received June 19, 1962

Changes in thermoelectric force (S) by annealing were measured for copper and nickel cold-worked at room temperature. In the case of copper (90 ~ 15% compression), the changes in the region from 120 to 400° are attributed to the disappearance of dislocations (T_D). The changes for nickel (80% compression) occurred in two stages, one between 200 and 300° and the other above 400°. These are attributed to the disappearance of point defects (vacancies) (T_V) and dislocations (T_D), respectively. T_D was considerably shifted to lower temperatures, with increase in the degree of compression. The complete parallelism between changes in S and decreases in the catalytic activities of cold-worked copper and nickel during annealing was found. Consequently, it is concluded that the lattice defects at the surface play the part of active centers for various reactions and that the measurement of S is a convenient and effective means of identifying lattice defects with active centers.

Introduction

It was assumed by Taylor² that catalytic reactions take place at active sites only. There is much evidence that indicates the existence of active sites on the surface of catalyst, but few attempts have been made experimentally to determine their structure.

In the last decade, the behaviors of lattice defects in cold-worked, quenched, and irradiated metals have been studied by measuring the release of stored energy, changes in density, extra-resistivity, and hardness during annealing. Consequently, the structure and properties of defects have been elucidated.^{3–6}

It was proposed recently by Uhara and co-workers that lattice defects (point defects and dislocations) at the surface of metallic catalysts play the part of active centers for various reactions in the case of copper⁷ and nickel,⁸ in view of the fact that the disappearance temperature of vacancies (T_V) or dislocations (T_D) agrees with decreasing temperature of catalytic activities of cold-worked metals during annealing. Since T_D is markedly influenced by the impurities as well as by the degree and method of cold-working, it is desirable to make these comparisons with the same specimens.

It was found by Tammann⁹ in 1933 that the

(5) L. M. Clarebrough, M. E. Hargreaves, and G. W. West, *Acta Metal.*, **8**, 797 (1960).

(6) T. Broom and R. K. Ham, "Vacancies and other point defects in metal and alloys" (*Inst. of Metals Monograph 23*).

(7) I. Uhara, S. Yanagimoto, K. Tani, and G. Adachi, *Nature*, **192**, 867 (1961).

(8) I. Uhara, Y. Numata, H. Hamada, and Y. Kageyama, *J. Phys. Chem.*, **66**, 1374 (1962).

(9) G. Tammann and G. Bndel, *Ann. Physik.*, **16**, 120 (1933).

(1) Read at the Annual Meeting of the Chemical Society of Japan held on April 5, 1962.

(2) H. S. Taylor, *Proc. Roy. Soc. (London)*, **A108**, 105 (1925).

(3) L. M. Clarebrough, M. E. Hargreaves, and G. W. West, *ibid.*, **A232**, 252 (1955).

(4) (a) L. M. Clarebrough, M. E. Hargreaves, and G. W. West, *Acta Metal.*, **5**, 738 (1957); (b) *Phil. Mag.*, **1**, 528 (1956).

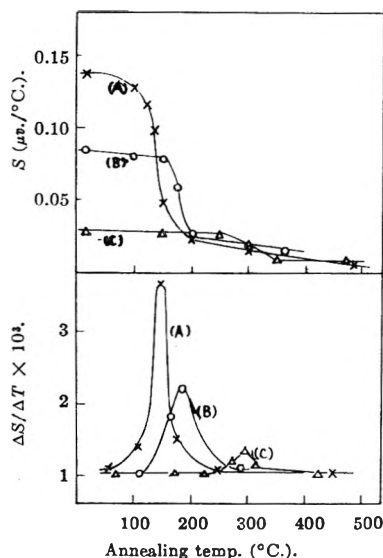


Fig. 1.—Changes in thermoelectric force (S) of cold-worked copper and their first difference by successive annealing 30 min. at each temperature: (A) 90% compression; (B) 57% compression; (C) 15% compression.

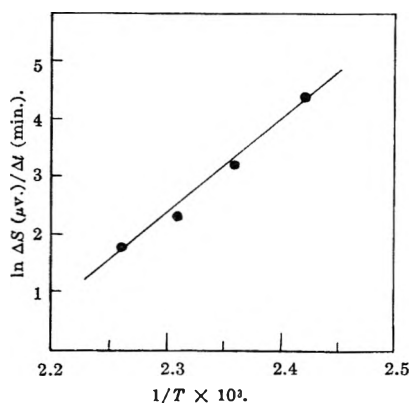


Fig. 2.—Determination of activation energy for the disappearance of lattice defects in cold-worked copper (90% compression).

thermoelectric force (S) of cold-worked metals is affected by annealing. Since then, however, little effort has been made to extend his work either theoretically or experimentally.^{10,11} We have found the complete parallelism between changes in S and decreases in the catalytic activity of cold-worked metals on annealing. It is suggested that the measurement of S is a more convenient and effective means for the purpose of identifying lattice defects with active centers than the measurement of the other physical properties mentioned above.

I. Thermoelectric Force (S) of Cold-Worked Metals

(1) **Experimental.**—Wires well annealed in the atmosphere of N_2 or H_2 at 600 or 900° were compressed at room temperature and S of cold-worked wire was measured against an annealed wire to 10^{-8} volt as a function of the temperature of the hot junction, the cold junction always being kept at room temperature in a thermostat. A linear relationship was found between S and the temperature difference at the junctions below 50°. In order to obtain the disappearance

(10) C. A. Domenicali and F. A. Otter, *Phys. Rev.*, **95**, 1134 (1954).

(11) T. L. L. Richards, S. F. Pugh, and H. J. Stokes, *Acta Metal.*, **4**, 75 (1956).

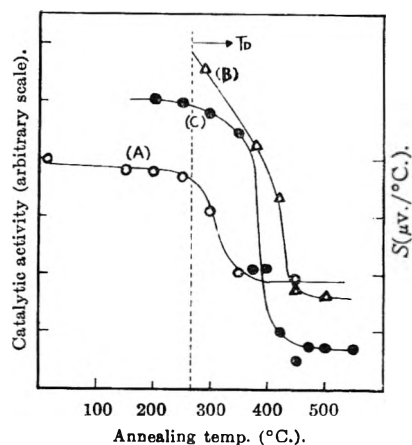


Fig. 3.—Changes in thermoelectric force and catalytic activities of cold-worked copper: (A) thermoelectric force (15% compression); (B) dehydrogenation of ethyl alcohol (Uhara and Teratani); (C) decomposition of diazonium salt (Uhara, Yanagimoto, Tani, and Adachi).

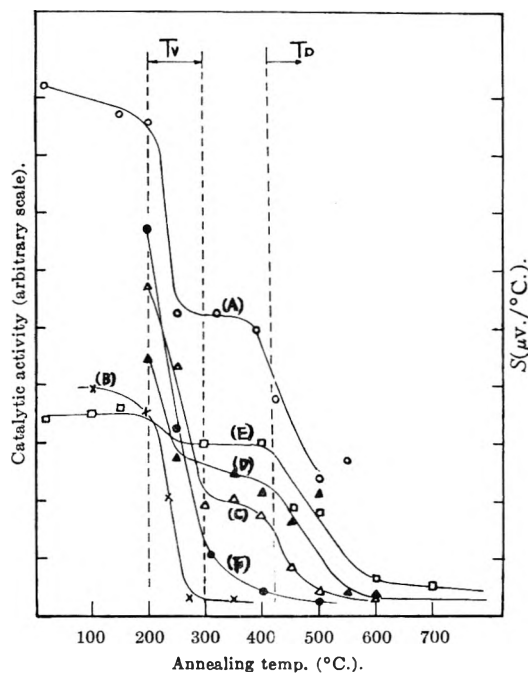


Fig. 4.—Changes in thermoelectric force and catalytic activities of cold-worked nickel: (A) thermoelectric force (80% compression); (B) hydrogenation of ethylene (Eckell); (C) p - o H_2 conversion (Uhara and Numata); (D) dehydrogenation of ethyl alcohol (Uhara and Numata); (E) hydrogenation of cinnamic acid (Uhara and Hamada); (F) p - o H_2 conversion (Cremer and Kerber).

range of defects, the cold-worked wire was annealed in N_2 or H_2 at various temperatures for a definite time (30 min.), and the changes in S were measured.

(2) **Results.** The changes in S of cold-worked copper (15, 57, and 90% compression) by annealing are shown in Fig. 1. As the degree of compression increases, the recovery temperatures of S (T_D) is shifted to lower temperatures. The peaks of $\Delta S/\Delta T$ curves were found at 300, 200, and 150°, respectively. In comparison with Clarebrough and his co-workers' results^{3,4} (measurements on stored energy, etc.), these phenomena are attributed to the disappearance of dislocations in cold-worked copper, because point defects disappear by annealing below room temperature. On the assumption

that S of cold-worked metals is proportional to the concentration of defects, the activation energy for the motion of dislocations (E_m) could be determined for a specimen of 90% compression. From the curve shown in Fig. 2, E_m is estimated to be 1.4 e.v. in the region between 140 and 200°, which agrees with the values obtained by Phillips¹² (1 ~ 2 e.v. at 200°).

The recovery curve for cold-worked nickel (80% compression) has two stages, one between 200 and 300° and the other above 400° as shown in Fig. 4A. According to Clarebrough and his co-workers,³⁻⁵ these are attributed to the disappearance of vacancies (T_v) and dislocations (T_D), respectively. Tammann reports that the changes in S occur only in the region from 150 to 350°.

II. Lattice Defects as Active Centers in Heterogeneous Catalysts

Uhara and his co-workers^{7,13} found that the activities of twisted copper for the decomposition of diazonium salt and dehydrogenation of ethyl alcohol considerably decrease by annealing at about 350°, as shown in Fig. 3. This temperature range coincides with the recovery temperature of S (Fig. 1) for a slightly cold-worked specimen (the compression is usually more severe working than twisting as shown by the comparison of induced catalytic activity).

In 1933, it was found by Eckell¹⁴ that the catalytic activity of nickel for the hydrogenation of ethylene was enhanced by a factor of 600 to 1000 after rolling. Since the activity is eliminated by annealing in the region from 200 to 300°, as shown in Fig. 4B, we may conclude that the active center

(12) V. A. Phillips, *J. Inst. Metals*, **81**, 185 (1952).

(13) I. Uhara, S. Yanagimoto, K. Tani, G. Adachi, and S. Teratani, *J. Phys. Chem.*, **66**, 2691 (1962).

(14) J. Eckell, *Z. Elektrochem.*, **39**, 433 (1933).

is some kind of point defect at the surface, contrary to Cratty and Granato's postulate¹⁵ ascribing the activity to dislocations.

Uhara, *et. al.*,⁸ found that the catalytic activities of cold-worked nickel for para-ortho (p-o) H₂ conversion, dehydrogenation of ethyl alcohol, and hydrogenation of cinnamic acid decrease suddenly in the two temperature ranges T_v and T_D , perfectly in parallel with the change in S as shown in Fig. 4C-4E, when the measurements were carried out with the same cold-worked specimens. Consequently, active centers in these catalysts may be both point defects and the termination of dislocations at the surface. According to Cremer and Kerber,¹⁶ the activity of nickel foil for p-o H₂ conversion was decreased by raising the temperature of annealing as shown in Fig. 4F. Since the foil was prepared by severe deformation, it is felt that T_D was shifted to lower temperatures, eventually overlapping T_v . Similarly, it is almost impossible to find the distinction between T_v and T_D for active centers in ordinary catalysts, which are prepared by chemical procedures and contain a large number of defects, as shown by X-ray studies.

The measurement of S of cold-worked metals can be carried out readily by a simple technique with a small quantity of the sample, and hence it offers a very convenient method for identifying lattice defects with active centers in metallic catalysts.

Studies on platinum catalysts will be reported in forthcoming papers.

Acknowledgment.—The author wishes to express sincere thanks to professor Uhara for his kind guidance and to Dr. Saika for his advice.

(15) L. E. Cratty and A. V. Granato, *J. Chem. Phys.*, **26**, 96 (1957).

(16) E. Cremer and R. Kerber, *Advan. Catalysis*, **7**, 82 (1955).

DISSOCIATION CONSTANT OF *t*-BUTYLAMMONIUM ION AND RELATED THERMODYNAMIC QUANTITIES FROM 5 TO 35°

BY HANNAH B. HETZER, R. A. ROBINSON, AND ROGER G. BATES

Solution Chemistry Section, National Bureau of Standards, Washington 25, D. C.

Received June 25, 1968

The acidic dissociation constant of *t*-butylammonium ion has been determined from 5 to 35° by e.m.f. measurements of hydrogen-silver bromide cells without liquid junction. At 25°, $-\log K_{bb} = 10.685$, and the temperature coefficient of the dissociation constant gives the values $\Delta H^0 = 60,070$ j. mole⁻¹ and $\Delta S^0 = -3.1$ j. mole⁻¹ deg.⁻¹. These thermodynamic constants are compared with the corresponding values for the acidic dissociation of the protonated forms of the aminoalcohols related structurally to *t*-butylamine.

Introduction

The relationship between basic strength and molecular structure has long been of interest.¹ Recent studies of the basic dissociation of the aminoalcohols have shed further light on the influence of structural factors in this class of com-

pounds. To this end, the dissociation constants for the three ethanol-ammonium ions were determined.²⁻⁴ In addition, the three structurally related substituted ammonium ions, namely, 2-ammonium-2-(hydroxymethyl)-1,3-propanediol,⁵ 2-ammonium-2-methyl-1,3-propanediol,^{6,7} and 2-

(1) See, for example, D. H. Everett and W. F. K. Wynne-Jones, *Proc. Roy. Soc. (London)*, **A177**, 499 (1941); A. G. Evans and S. D. Hamann, *Trans. Faraday Soc.*, **47**, 34 (1951); D. H. Everett and B. R. W. Pinsent, *Proc. Roy. Soc. (London)*, **A215**, 416 (1952); R. P. Bell, "The Proton in Chemistry," Cornell University Press, Ithaca, N. Y., 1959, chapter 5.

(2) Monoethanolammonium: R. G. Bates and G. D. Pinching, *J. Res. Natl. Bur. Std.*, **46**, 349 (1951).

(3) Diethanolammonium: V. E. Bower, R. A. Robinson, and R. G. Bates, *ibid.*, **66A**, 71 (1962).

(4) Triethanolammonium: R. G. Bates and G. F. Allen, *ibid.*, **64A**, 343 (1960).

TABLE I

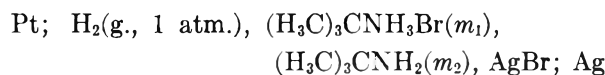
ELECTROMOTIVE FORCE OF THE CELL: Pt; H₂(g., 1 atm.) (H₃C)₃CNH₃Br(*m*₁), (H₃C)₃CNH₂(*m*₂), AgBr; Ag, FROM 5 TO 35° (IN V.)

<i>m</i> ₁	<i>m</i> ₂	5°	10°	15°	20°	25°	30°	35°
0.09065	0.04588	0.76420	0.76357	0.76271	0.76173	0.76058	0.75927	0.75783
.08043	.03945	.76562	.76502	.76427	.76331	.76226	.76101	.75960
.07316	.03702	.76843	.76787	.76711	.76620	.76504	.76381	.76243
.07081	.03536	.76900	.76833	.76756	.76665	.76555	.76435	.76293
.06422	.03150	.77016	.76959	.76884	.76793	.76686	.76567	.76433
.05890	.02942	.77243	.77196	.77126	.77039	.76935	.76820	.76690
.05350	.02708	.77449	.77404	.77335	.77248	.77148	.77033	.76900
.05037	.02516	.77543	.77504	.77434	.77351	.77255	.77143	.77014
.04724	.02359	.77678	.77641	.77573	.77494	.77405	.77295	.77171
.04256	.02126	.77887	.77846	.77782	.77708	.77625	.77518	.77396
.04045	.01983	.77927	.77893	.77834	.77763	.77681	.77586	.77462
.03592	.01818	.78231	.78207	.78149	.78081	.77996	.77896	.77784
.03374	.01655	.78277	.78252	.78199	.78132	.78049	.77950	.77837
.02421	.01225	.79022	.78999	.78959	.78901	.78838	.78753	.78654
.01293	.006341	.80205	.80203	.80181	.80149	.80096	.80042	.79925

ammonium-2-methyl-1-propanol⁷ have been studied. Data now have been obtained for the fourth member of this series, namely, the hydroxy-free parent compound, *t*-butylamine.

Experimental

Method and Procedure.—The electromotive force method used was essentially that previously employed in this Laboratory for studies of other volatile bases.⁸ Because of the considerable solubility of silver chloride in solutions containing *t*-butylamine, however, the silver-silver bromide electrode was substituted for the silver-silver chloride electrode. The cell used, therefore, is represented as



where *m* is molality.

The preparation of the standard solution of hydrobromic acid and of the silver-silver bromide electrodes has been described previously.⁹

A commercial preparation of *t*-butylamine was distilled (at approximately 25° and 400 mm.) through a spinning-band distillation column of the Piros-Glover type.¹⁰ The column had a rectifying section about 60 cm. in length and was rated at about 80 theoretical plates. Several fractions (about 17 in number) were analyzed by vapor-liquid chromatography, and the best were retained for use. The commercial amine gave a band believed to indicate the presence of a higher-boiling impurity, but the material used for the e.m.f. measurements showed no peak on the chromatogram except that for *t*-butylamine.

In order to correct the observed e.m.f. values to a pressure of 1 atm. of dry hydrogen, the partial pressure of the amine from 0.1 *M* and 0.05 *M* aqueous solutions was measured at 25, 40, 45, and 50° by a gas-transpiration method.¹¹ Henry's law appeared to be valid over this limited range of concentrations. The constant, $k = p/m$, for partial pressures in mm., was found to be approximately 20 at 25°, 64 at 40°, 82 at 45°, and 123 at 50°. Values of *k* at 30 and 35° were read

(5) R. G. Bates and H. B. Hetzer, *J. Phys. Chem.*, **65**, 667 (1961).

(6) H. B. Hetzer and R. G. Bates, *ibid.*, **66**, 308 (1962).

(7) B. A. Timini, thesis, University of Bristol, 1960; D. H. Everett, private communication.

(8) See, for example, R. G. Bates and G. D. Pinching, *J. Res. Natl. Bur. Std.*, **42**, 419 (1949).

(9) H. B. Hetzer, R. A. Robinson, and R. G. Bates, *J. Phys. Chem.*, **66**, 1423 (1962). This paper also gives the values of the standard e.m.f. of the cell which was used in deriving the dissociation constant from the e.m.f. data.

(10) The authors are indebted to Dr. R. T. Leslie and Mr. E. C. Kuehner for the distillation and for the vapor-liquid chromatographic analysis of the amine.

(11) See ref. 8.

TABLE II

VALUES OF $-\log K_{bh}$ AND $-\log K_b$ FROM 5 TO 35°

Temp., °C.	$-\log K_{bh}$	σ	$-\log K_b$
5	11.439	0.002	3.295
10	11.240	.001	3.295
15	11.048	.001	3.298
20	10.862	.001	3.305
25	10.685	.001	3.311
30	10.511	.001	3.322
35	10.341	.002	3.339

TABLE III

THERMODYNAMIC QUANTITIES FOR THE ACIDIC DISSOCIATION OF *t*-BUTYLAMMONIUM ION (BH⁺) FROM 5 TO 35°

<i>t</i> , °C.	ΔG° , j. mole ⁻¹	ΔH° , j. mole ⁻¹	ΔS° , j. deg. ⁻¹ mole ⁻¹
5	60,910	59,780	-4.1
10	60,930	59,850	-3.8
15	60,950	59,920	-3.6
20	60,970	59,990	-3.3
25	60,980	60,070	-3.1
30	61,000	60,140	-2.8
35	61,010	60,220	-2.6

from a plot of $\log k$ against $1/T$, where *T* was in °K. It was found necessary to take the vapor pressure of the amine into account only at 35° and for buffer solutions in which *m*₂ was 0.025 or greater. For other temperatures and concentrations, the pressure corrections calculated with and without the partial pressure of the amine agreed to within 0.02 mv., and the contribution of the amine to the total pressure was neglected accordingly. To reduce losses by volatilization, the ratio *m*₁/*m*₂ was kept at about 2 in all of the cell solutions.

Values of *K*_f, the stability constant for the diammine complex formed by silver ion and *t*-butylamine, were calculated from measurements of the solubility of silver chloride in 0.11 *M* and 0.07 *M* solutions of the amine. The results for $\log K_f$ were as follows: 8.78 (0°), 7.88 (25°), 7.12 (50°). The solubility product of silver chloride being 2,800 times greater than that of silver bromide (at 25°), it can be shown that the solubility of silver bromide in the buffer solutions would be too small to require corrections to the stoichiometric bromide concentration (*m*₁). Corrections to *m*₁ and *m*₂ for the dissociation of the amine were necessary, however, and were applied in the usual way. The molality of free amine in the stock solutions was determined by weight titration to the calculated equivalence point (5.9 in 0.05 *M* solution), detected by means of a glass electrode.

Because of the high volatility of the base, the e.m.f. decreased slowly with time. After the completion of a series

TABLE IV

COMPARISON OF THE THERMODYNAMIC QUANTITIES AT 25° FOR THE DISSOCIATION OF *t*-BUTYLAMMONIUM ION AND THREE STRUCTURALLY RELATED AMMONIUM ALCOHOLS

Base	Ref.	M.p. of amine, °C.	$-\log K_{bb}$	ΔG° , j. mole ⁻¹	ΔH° , j. mole ⁻¹	ΔS° , j. deg. ⁻¹ mole ⁻¹	ΔC_p° , j. deg. ⁻¹ mole ⁻¹
(CH ₂ OH) ₃ C·NH ₂	5	171	8.075	46,075	47,600	5.1	-64
(CH ₂ OH) ₂ C·NH ₂	6	111	8.801	50,238	49,860	-1.3	-45
	7	...	8.790	50,176	49,720	-1.5	-46
$\begin{array}{c} \text{CH}_3 \\ \\ \text{CH}_3 \\ \\ \text{CH}_2\text{OH}-\text{C}-\text{NH}_2 \\ \\ \text{CH}_3 \end{array}$	7	30-31	9.691	55,318	53,930	-4.6	-25
(CH ₃) ₃ C·NH ₂		-67.5	10.685	60,980	60,070	-3.1	15

of measurements, the e.m.f. of test cells without the triple saturator for the hydrogen gas was found to be about 1 mv. lower than at the beginning of the series, some 52 hr. earlier. The saturators were used accordingly for all of the measurements from which the dissociation constant was derived, but decreases of e.m.f. ranging from 0.25 to 0.5 mv., roughly proportional to elapsed time, still were observed. The e.m.f. values at temperatures other than 25° therefore were corrected to "zero time" in order to allow for loss of the amine through volatilization.¹¹ The largest correction is at 35°, where it amounts to 0.008 in ($-\log K_{bb}$); a correction of this small magnitude can be made with confidence.

Results

The corrected values of the e.m.f. of the cell are given in Table I. The calculation of the acidic dissociation constant, K_{bb} , of the *t*-butylammonium ion was made in the manner already described.^{5,6} A value of 0 for the ion-size parameter (α^*) gave straight-line plots of K_{bb}' as a function of ionic strength at each temperature. The intercepts were determined by the method of least squares. The values of $-\log K_{bb}$ and of $-\log K_b$ (the negative logarithm of the basic dissociation constant of *t*-butylamine) are collected in Table II; σ is the standard deviation of the intercept ($-\log K_{bb}$) at each temperature.

The following equations represent the "observed" data at the seven temperatures with a mean deviation of ± 0.001 unit

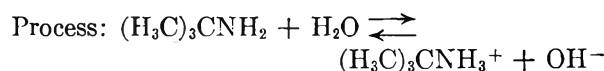
$$-\log K_{bb} = \frac{3021.63}{T} + 0.9376 - 0.001303T \quad (1)$$

$$-\log K_b = \frac{1477.29}{T} - 7.2023 + 0.018647T \quad (2)$$

The value of $-\log K_{bb} = 11.644$ at 0° (calculated by eq. 1) can be compared with 11.64 from the work

of Pearson and Williams¹²; 10.937 at 18° with 10.83 from the measurements of Girault-Vexlearschi¹³; 10.685 at 25° with 10.53 from the conductance data of Bredig.¹⁴

The thermodynamic quantities for the dissociation of *t*-butylammonium ion in the standard state were derived from the constants of eq. 1 and are listed in Table III. Only an approximate value of ΔC_p° can be calculated from data over a short temperature range, but eq. 1 gives $\Delta C_p^\circ = 15$ j. deg.⁻¹ mole⁻¹ at 25°. The following values pertain to the basic dissociation of *t*-butylamine at 25°



$$\Delta G^\circ = 18,910 \text{ j. mole}^{-1}$$

$$\Delta H^\circ = -3450 \text{ j. mole}^{-1}$$

$$\Delta S^\circ = -75.0 \text{ j. mole}^{-1} \text{ deg.}^{-1}$$

The thermodynamic quantities for the dissociation of *t*-butylammonium ion are compared in Table IV with the corresponding quantities for the protonated forms of the three aminoalcohols related structurally to *t*-butylamine. A small unexplained irregularity in the trend of ΔS° is apparent, but the change of entropy is generally in qualitative agreement with expectation, insofar as the effect of hydroxyl groups on the entropy of solvation is concerned. The melting points show that the successive introduction of hydroxyl into the methyl groups of the parent compound produces a considerable lowering of the volatility of the amine as well.

(12) R. G. Pearson and F. V. Williams, *J. Am. Chem. Soc.*, **76**, 258 (1954).

(13) G. Girault-Vexlearschi, *Bull. soc. chim. France*, 577 (1956).

(14) G. Bredig, *Z. physik. Chem.*, **13**, 289 (1894).

DIFFUSION OF RADIOACTIVELY TAGGED CETANE IN POLYISOBUTYLENE-CETANE MIXTURES AND IN THREE METHACRYLATE POLYMERS

BY ROBERT S. MOORE¹ AND JOHN D. FERRY

Department of Chemistry, University of Wisconsin, Madison, Wisconsin

Received July 9, 1962

The self-diffusion of cetane, using a radioactive tracer, has been measured in polyisobutylene-cetane solutions in the concentration range from 35 to 87% polymer, and the diffusion of radioactive cetane into pure polyisobutylene, poly-*n*-hexyl methacrylate, poly-*n*-octyl methacrylate, and poly-*n*-dodecyl methacrylate has been measured under conditions of very low cetane concentration. The temperatures ranged from 24 to 48°. Curve-matching methods were used to obtain diffusion coefficients without waiting for equilibrium to be reached. The apparent activation energy for self-diffusion of cetane increases monotonically with volume fraction of polymer (v_2) in the polyisobutylene-cetane system, with a sharp increase in slope near $v_2 = 0.6$. The values are essentially identical with the apparent activation energies for viscoelastic relaxation times of the polymer segments in the same solutions from $v_2 = 0.64$ to 1.00, determined from mechanical measurements. The friction coefficient ζ_1 for translation of cetane at 24° increases from $10^{-7.94}$ to $10^{-4.32}$ dyne-sec. cm.⁻¹ over the concentration range from pure cetane to pure polymer. Its concentration dependence is quite well described in terms of the Doolittle free volume concept by the theory of Fujita, with values of the free-volume parameters of both polymer and solvent in agreement with those derived from other sources. The friction coefficients for cetane in the methacrylate polymers, and their temperature dependences, are considerably smaller than the corresponding quantities for translatory motion of polymer segments derived from viscoelastic measurements using the modified Rouse theory. The differences are attributed qualitatively to effects of additional local free volume in the immediate vicinity of the diluent molecule, which may be important when the temperature is not too far above the glass transition temperature. The effective local free volume around the cetane molecule is estimated to be about 40% greater than the average free volume for the hexyl and octyl polymers, and 16% greater for the dodecyl.

Measurements of the diffusion of small molecules in very concentrated polymer solutions have provided information about molecular motions in such systems.² The frictional resistance to translatory motion of a diluent molecule can be determined and compared with the resistance to segmental motion in the polymer matrix as estimated from viscoelastic measurements.³

The interpretation of diffusion measurements is considerably simplified if the experiment corresponds to self-diffusion of one component in the mixture. This condition is fulfilled when a radioactive tracer is used and the chemical concentration is uniform through the system,⁴ and also in nuclear magnetic resonance measurements by the spin-echo method.⁵ The experiments reported here were performed with a tracer. The diffusion of radioactively tagged cetane (*n*-hexadecane) was followed in mixtures of polyisobutylene and cetane over a wide range of concentrations. In addition, diffusion into pure polyisobutylene and into three methacrylate polymers was studied under conditions closely approximating self-diffusion. The viscoelastic properties of the same polyisobutylene-cetane mixtures will be reported subsequently⁶; those of the methacrylate polymers have been published previously.⁷⁻⁹

Materials.—The polyisobutylene was obtained from Esso Research and Engineering Co. through the kindness of Dr. Ralph M. Hill. It was designated as type L-80 and is believed to have very little material with molecular weight

less than 0.5×10^6 . Its intrinsic viscosity in benzene at 24.0° was 1.02 dl./g., corresponding¹⁰ to a viscosity-average molecular weight of 1.5×10^6 . Its shear relaxation spectrum at the lower end of the transition zone, determined from dynamic measurements to be reported,⁶ was identical with that of the National Bureau of Standards polyisobutylene with weight-average molecular weight 1.56×10^6 , studied¹¹ in 1952. The presence of molecular weight distribution should not affect the diffusion of cetane so long as there are no polymer components of very low molecular weight.

The poly-*n*-hexyl methacrylate, poly-*n*-octyl methacrylate, and poly-*n*-dodecyl methacrylate were the same samples used in earlier investigations of mechanical properties.⁷⁻⁹ They were all rough fractions from which components of very low molecular weight had been removed, and their weight-average molecular weights were, respectively, 4.0, 3.6, and 0.95×10^6 .

Non-radioactive cetane, practical grade, was obtained from Matheson, Coleman and Bell, and radioactive 1-C^{14} cetane from Nuclear-Chicago Corporation. The latter was furnished in benzene solution at a specific activity of about 5 mc./mmole. The benzene was removed by aspiration in a specially designed device with a cold trap and the residue was diluted with ordinary cetane to a convenient level of activity (7.3 and 81 $\mu\text{c./g.}$, respectively, for the two types of diffusion experiments to be described below).

Solutions of polyisobutylene in ordinary cetane and in radioactive cetane with an activity level of the order of 2 $\mu\text{c./g.}$ of solution were made up over the concentration range of 35 to 87% polymer by weight. Santonox (Monsanto Chemical Co.) was added as an antioxidant, at a concentration corresponding to 0.5% of the polymer present. The maximum concentration which could be prepared by direct mixing with a very slowly rotating magnetic stirrer at 60° was 70%. Higher concentrations were achieved by slowly evaporating some cetane *in vacuo* from the samples before molding. In fact, such evacuation was applied to all except the 35 and 47% samples, to assist in removing bubbles and to adjust the polymer concentration to the desired values. In the twin disk method, in particular (see below), the concentrations of the two disks had to be matched accurately. The temperature during this evacuation was sufficiently high so that the diffusion of cetane through the sample would prevent development of significant concentration gradients. Further details of preparation of solutions

(1) United States Rubber Company Foundation Post Graduate Fellow in Physical and Engineering Science, 1961-1962.

(2) H. Fujita, *Advan. Polymer Sci.*, **3**, 1 (1961).

(3) J. D. Ferry and R. F. Landel, *Kolloid-Z.*, **148**, 1 (1956).

(4) R. J. Bearman, *J. Phys. Chem.*, **65**, 1961 (1961).

(5) D. C. Douglass and D. W. McCall, *ibid.*, **62**, 1102 (1958).

(6) J. R. Richards, K. Ninomiya, and J. D. Ferry, *ibid.*, in press.

(7) W. C. Child, Jr., and J. D. Ferry, *J. Colloid Sci.*, **12**, 389 (1957).

(8) W. Dannhauser, W. C. Child, Jr., and J. D. Ferry, *ibid.*, **13**, 103 (1958).

(9) S. F. Kurath, T. P. Yin, J. W. Berge, and J. D. Ferry, *ibid.*, **14**, 147 (1959).

(10) P. J. Flory, "Principles of Polymer Chemistry," Cornell Univ. Press, Ithaca, N. Y., 1953, p. 312.

(11) J. D. Ferry, L. D. Grandine, Jr., and E. R. Fitzgerald, *J. Appl. Phys.*, **24**, 911 (1953).

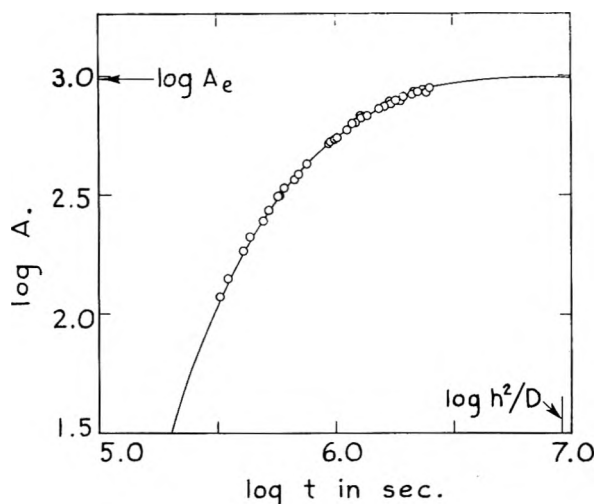


Fig. 1.—Activity in counts per min. plotted logarithmically vs. time, for the twin disk method. Points, experimental, for 87.4% polyisobutylene in cetane at 48.4°; curve, eq. 1 with origin located by arrows as indicated.

and precautions used in handling the radioactive material are given in an unpublished report.¹²

Method

Two geometrical arrangements were employed for the diffusion process. In the twin disk method, a molded disk prepared with ordinary cetane was carefully layered on a radioactive disk with the same concentration and dimensions, and the diffusion was followed by measuring the activity at the top, initially inert surface. The conditions here correspond strictly to self-diffusion.⁴ In the thin smear method, a single disk of pure polymer was joined to a very thin layer of radioactive cetane and the activity was measured at the opposite face. This, of course, is not self-diffusion but since the concentration of cetane after attainment of equilibrium was only 1 to 2%, the process represents cetane moving in essentially a very dilute solution, and in these circumstances the diffusion coefficient becomes identical with that for self-diffusion.⁴ For the methacrylate polymers, only this method was used.

The molded disks were all of 1-in. diameter; the thicknesses were 0.138 to 0.159 in. for the twin disk geometry, and 0.057 in. for the thin smear method. Inserts of aluminum foil in the mold facilitated removal and handling of the samples^{8,9}; all details of procedure were established with non-radioactive samples before processing radioactive material.¹²

During the course of diffusion, a period of hours to weeks, the disks were kept in vapor-tight aluminum cylinders with removable lids for intermittent activity measurements. The arrangement was similar to that used by Auerbach and Gehman¹³ except that a larger area, essentially all of the upper sample surface, was exposed to the Geiger counter when the lids were removed. For temperature control during diffusion, the cylinders were kept in a heavy aluminum box in an air thermostat or a large copper cylinder in a water bath.

For measurement of activity, a cylinder was opened and mounted in an aluminum counting platform which provided positive positioning under the mica window of a Geiger tube and was surrounded by a lead shield. The counts of the β particles were registered on a binary-counting scaler (Instrument Development Laboratories), usually for a 15-min. period. The elapsed time since the start of the diffusion experiment was taken as the middle of this interval. The background radiation was measured for a similar period. The Geiger tube was operated at 1400 v. and it was checked each day with an uncalibrated radiocarbon source (Tracer Lab., Inc., Model R-10). The counting equipment was generously lent by Professor John E. Willard.

Since the maximum range of the β particle in the polymer is about 0.035 cm. and the half-thickness for absorption can be taken as one-tenth of this,¹⁴ the activity (A) essentially measures the concentration of radioactive cetane at the upper surface of the sample. Specifically, for the twin disk method, 94% of the measured radiation comes from the upper 2% of the twin sample.

Twin Disk Method.—The diffusion equations may be formulated in terms of A , which is proportional to the concentration of radioactive cetane at the upper surface. This rises during the course of diffusion from zero to a value A_e at equilibrium which represents half the concentration originally present in the radioactive (lower) disk. The time dependence of A under the boundary conditions of the experiment can be expressed as¹⁵

$$A(t)/A_e = 1 - (4/\pi) [e^{-\pi^2\theta} - (1/3)e^{-9\pi^2\theta} + (1/5)e^{-25\pi^2\theta} + \dots] \quad (1)$$

where $\theta = D_1 t/h^2$, D_1 is the diffusion coefficient (in our system, the self-diffusion coefficient of cetane), and h the total thickness of the pair of disks. To determine D_1 from experimental data, it is not necessary to wait until equilibrium is reached to obtain A_e directly. Instead, a master logarithmic plot of $A(t)/A_e$ vs. θ from eq. 1 is matched to an experimental plot of $\log A(t)$ vs. $\log t$. The position of the origin of the theoretical plot on the experimental coordinate axes determines A_e and D_1/h^2 , respectively. An example is shown in Fig. 1. The precision of D_1 determined in this manner was ordinarily within about 5%.

Thin Smear Method.—In this procedure, a drop of radioactive cetane was placed on an aluminum insert at the bottom of the sample cylinder, allowed to spread uniformly, and, after weighing, frozen in the cold room. Radioactive cetane with the higher level of 81 $\mu\text{c./g.}$ was used for this purpose. The single disk of polymer then was placed on the thin layer of crystalline cetane and the assembly was allowed to warm to melt the latter. Careful precautions were necessary to prevent the cetane from climbing up the cylinder walls (the latter had to be coated with a thin layer of Carbowax, a low-molecular weight polyethylene oxide) and to achieve uniform contact between the cetane and polymer.

Since the initial ratio of cetane thickness (b) to polymer thickness (h) is very small, it can be shown¹² that the course of the diffusion except in its earliest stages is actually independent of the initial cetane thickness to a close approximation. The activity (in this case, proportional to the concentration of total cetane, as well as of radioactive cetane, at the top surface) again rises from zero to a value A_e which depends on the total amount of radioactivity present. When the diffusion equations¹⁵ are solved for these boundary conditions, the approximation $b/h \ll 1$ allows replacing $\sin m\pi b/h$ by its argument in a Fourier expansion where m is the summation index. The time dependence of A then can be expressed by the equation¹²

$$A(t)/A_e = 1 - 2[e^{-\pi^2\theta} - e^{-4\pi^2\theta} + e^{-9\pi^2\theta} + \dots] \quad (2)$$

where θ is defined as before. Equation 2 was evaluated numerically on a Bendix G-15 computer.¹⁶

From a logarithmic plot of A against t compared with a logarithmic master curve of $A(t)/A_e$ vs. θ , it was possible to determine D_1 from experimental data as before. An example is shown in Fig. 2.

The approximation that the activity measures the concentration of radioactive cetane at the upper sample surface is not quite so well fulfilled here because the sample is thinner. However, examination of this approximation together with that involving replacing the sine by its argument in the Fourier expansion leads to the conclusion that the error does not exceed 3% for $\log \theta = -1.2$ and diminishes quickly as time increases.

Values of D determined in this manner for diffusion of cetane into polymer are identified with D_1 and cited below as

(14) G. Friedlander and J. W. Kennedy, "Nuclear and Radiochemistry," John Wiley and Sons, New York, N. Y., 1959, pp. 197-198.

(15) J. Crank, "The Mathematics of Diffusion," Oxford, 1966.

(16) We are much indebted to Dr. Stuart E. Lovell for making these calculations. Numerical tables for eq. 1 and 2 are available on request.

(12) R. S. Moore, Ph.D. Thesis, University of Wisconsin, 1962.

(13) I. Auerbach, S. D. Gehman, W. R. Miller, and W. C. Kuryla, *J. Polymer Sci.*, **28**, 129 (1958).

corresponding to the pure polymer ($v_2 = 1.0$), even though the concentration is changing slightly during the diffusion process. The difference in $\log D$ between pure polymer and the equilibrium concentration ($v_2 = 0.98$ to 0.99) is of the order of 0.1, but the actual error probably is somewhat less, because during the early stages the cetane is advancing into essentially pure polymer. The twin disk and thin smear methods were compared for 35% polyisobutylene at 48.4° , and the values of $\log D_1$ agreed within 0.02.

Results and Discussion

Polyisobutylene Systems

Values of $\log D_1$ and $\log \zeta_1$ for polyisobutylene and its solutions are given in Table I for the range of concentrations and temperatures of 24, 40, and 48.4° . The friction coefficient for the cetane, ζ_1 , is calculated^{3,4} as kT/D_1 . Plots of $\log D_1$ against $1/T$ were linear within this narrow temperature range, and from their slopes the apparent heat of activation for diffusion, ΔH_D , was calculated and is listed in the last column of the Table.

Temperature Dependence.—In Fig. 3, ΔH_D is plotted vs. volume fraction of polymer, v_2 . The value of 3.90 kcal. for $v_2 = 0$ is actually the apparent heat of activation for viscous flow obtained from viscosity data for cetane.¹⁷ The figure also includes values of ΔH_a for viscoelastic relaxation times. These are derived from dynamic measurements⁶ near the boundary between the transition zone and plateau zone of the relaxation spectrum, and reflect the temperature dependence of the monomeric friction coefficient ζ_0 of the polymer. It is clear that the two friction coefficients have identical temperature dependence over the concentration range where the measurements overlap. This concordance appears to be characteristic of amorphous polymer systems which are far above their glass transition temperatures.³

The plot of ΔH_D vs. v_2 appears to change in slope abruptly at about $v_2 = 0.6$. A somewhat similar phenomenon is evident in the diffusion of trioctyl phosphate in polyvinyl chloride¹⁸ and acetone in polyvinyl acetate,¹⁹ although these investigations did not involve self-diffusion, and large thermodynamic corrections^{4,20} are needed to convert the apparent diffusion coefficient to a quantity equivalent to the self-diffusion coefficient. Whether there is really an abrupt break at $v_2 = 0.6$ is not certain. It could not be correlated with the onset of coupling entanglements²¹; for solutions of polyisobutylene with this molecular weight, entanglements exist at concentrations as low as $v_2 = 0.05$, as shown by the dependence of viscosity on molecular weight at constant concentration.²²

The apparent energy can be calculated from the free volume concept of Doolittle,^{23,24} which has

(17) American Petroleum Institute Project 44, "Selected Values of Properties of Hydrocarbons and Related Compounds," Carnegie Institute of Technology, Pittsburgh, Pa., 1953, p. 288.

(18) W. Knappe, *Z. angew. Phys.*, **6**, 97 (1954).

(19) A. T. Hutcheon, R. J. Kokes, J. L. Hoard, and F. A. Long, *J. Chem. Phys.*, **20**, 1232 (1952).

(20) M. J. Hayes and G. S. Park, *Trans. Faraday Soc.*, **52**, 959 (1956).

(21) T. G. Fox, S. Gratch, and L. Loshaek, in F. R. Eirich, "Rheology," Vol. I, Academic Press, New York, N. Y., 1956, Chapter 12.

(22) M. F. Johnson, W. W. Evans, I. Jordan, and J. D. Ferry, *J. Colloid Sci.*, **7**, 498 (1952).

(23) A. K. Doolittle, *J. Appl. Phys.*, **22**, 1471 (1951).

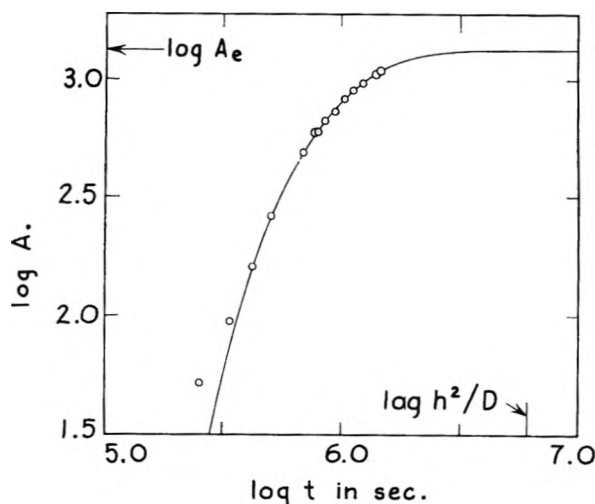


Fig. 2.—Activity in counts per min. plotted logarithmically vs. time, for the thin smear method. Points, experimental, for a thin smear of cetane on poly-*n*-hexyl methacrylate at 24° ; curve, eq. 2 with origin located by arrows as indicated.

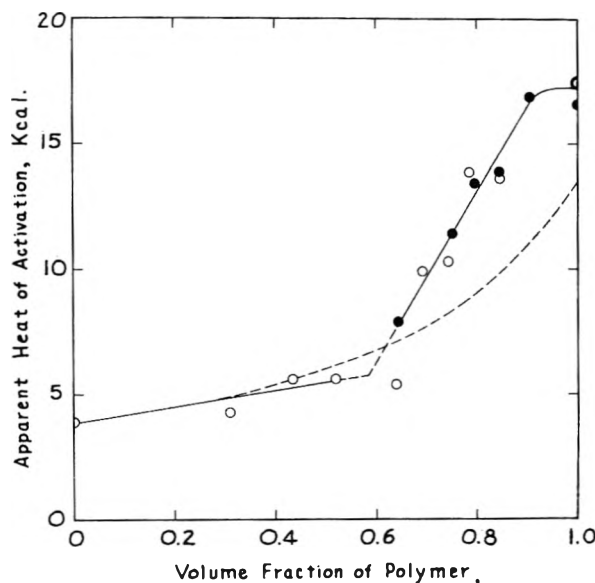


Fig. 3.—Apparent activation energy plotted vs. volume fraction of polymer in the system polyisobutylene-cetane. Open circles, for self-diffusion of cetane (Table I); black circles, for viscoelastic relaxation times,⁶ reflecting configurational changes of the polymer.

been applied to diffusion by Fujita.² If the temperature dependence of the diffusion process is controlled by free volume, the apparent activation energy at temperature T is given by

$$\Delta H_D(T) = B_d R T^2 \alpha_f / f^2 \quad (3)$$

where B_d is a numerical constant usually set equal to unity, f is the fractional free volume, and $\alpha_f = df/dT$. Since the experimental values of ΔH are the same for diffusion and viscoelastic measurements, we can take the parameters for the pure polymer from viscoelastic data,^{3,25} setting B_d

(24) J. D. Ferry, "Viscoelastic Properties of Polymers," John Wiley and Sons, New York, N. Y., 1961, pp. 225, 363.

(25) A later choice of parameters:²⁵ $\alpha_f = 2.5 \times 10^{-4}$ and $f_g = 0.026$, which give almost the same temperature dependence of viscoelastic

TABLE I

DIFFUSION COEFFICIENT AND FRICTION COEFFICIENTS FOR
CETANE IN POLYISOBUTYLENE SOLUTIONS

Wt. % polymer	v_2	$T, ^\circ\text{K.}$	$\log D_1$	$\log \zeta$	ΔH_D , kcal.
35.45	0.3182	297.1	-5.94	-7.45	
35.18	.3145	313.0	-5.77	-7.59	4.28
35.66	.3185	321.6	-5.70	-7.66	
35.13 ^a	.3139	321.6	-5.71	-7.64	
47.53	.4349	297.1	-6.20	-7.18	
47.20	.4304	313.0	-5.97	-7.40	5.58
47.20	.4297	321.6	-5.89	-7.47	
56.06	.5201	297.1	-6.39	-6.99	
56.09	.5194	313.1	-6.18	-7.18	5.65
56.30	.5206	321.5	-6.04	-7.31	
67.65 ^b	.6398	297.0	-6.71	-6.67	
			-6.77	-6.61	
67.01	.6319	313.0	-6.44	-6.92	5.38
67.07	.6319	321.6	-6.34	-7.02	
72.64	.6915	297.2	-7.08	-6.31	
72.09	.6870	313.0	-6.64	-6.72	9.97
72.58	.6905	321.5	-6.53	-6.83	
77.37	.7439	297.2	-7.32	-6.07	
76.75	.7362	313.0	-6.87	-6.50	10.32
77.46	.7434	321.4	-6.75	-6.60	
81.45	.7886	297.1	-7.71	-5.68	
80.77	.7802	313.0	-7.18	-6.18	13.92
81.02	.7825	321.5	-6.93	-6.42	
86.86	.8489	297.1	-7.92	-5.47	
86.71	.8466	313.0	-7.47	-5.90	13.62
87.38	.8537	321.6	-7.20	-6.15	
100.00 ^a	1.0000	297.2	-9.06	-4.32	
100.00	1.0000	313.2	-8.46	-4.90	17.46
100.00	1.0000	321.6	-8.01	-5.34	

^a By the thin smear method. ^b Large uncertainty because of low level of radioactivity.

$= 1$, $\alpha_f = 4.4 \times 10^{-4} \text{ deg.}^{-1}$, and $f = 0.031 + \alpha_f(T - T_g)$, where the glass transition temperature T_g is 202°K. It must be recognized, however, that the present temperature range is so far above T_g that the parameters of the WLF equation²⁴ determined in the usual manner may not be strictly applicable.

It has been customary² to assume that the fractional free volumes of polymer and diluent are additive. To calculate the values of α_f for the solutions we have assumed that this quantity also varies linearly with volume fraction. The fractional free volume of pure cetane, f_1 , was calculated¹² from the data of Doolittle²⁸ to be 0.210 at 313.2°K. , and α_f was determined from the same source as $8.55 \times 10^{-4} \text{ deg.}^{-1}$. By linear interpolation, α_f and f at 313° were obtained for the various solutions, and ΔH_D at 313° was calculated by eq. 3. The results, shown by the dashed line in Fig. 3, agree fairly well in the diluent-rich systems but are too low above $v_2 = 0.6$. Small adjustments in α_f and f would improve the agreement. Nevertheless,

properties in the range from T_g to $T_g + 100$, must be rejected; α_f cannot²⁷ be appreciably less than $\Delta\alpha$, the difference between the macroscopic thermal expansion coefficients above and below T_g , which for polyisobutylene is 4.5 to $5 \times 10^{-4} \text{ deg.}^{-1}$.

(26) Reference 24, p. 219.

(27) A. J. Kovacs, R. A. Stratton, and J. D. Ferry, *J. Phys. Chem.*, in press (Jan., 1963).

(28) A. K. Doolittle, *J. Appl. Phys.*, **23**, 236 (1952).

the free volume theory with linear additivity of f explains the concentration dependence of D_1 and ζ_1 rather well, as will be shown below.

Concentration Dependence.—In Fig. 4, $\log \zeta_1$ is plotted against v_2 at three temperatures. The figure includes values for pure cetane, estimated from the spin-echo measurements of Douglass and McCall⁵ on various n -paraffin hydrocarbons. The self-diffusion coefficient of cetane at 25° was interpolated from their data, and evaluated at the other temperatures by taking the value of 3.90 kcal. for ΔH_D . At 24.0 , 40.0 , and 48.4° , $\log D_1$ is, respectively, -5.440 , -5.284 , and -5.222 , whence ζ_1 is obtained as kT/D_1 .

The cetane friction coefficient increases monotonically by about three powers of ten over the complete concentration range. The slope of $\log \zeta_1$ appears to change most rapidly at about $v_2 = 0.6$, however, where the break appears in Fig. 3. Comparison of these values of ζ_1 with the monomeric friction coefficient of the polymer, ζ_0 , derived from viscoelastic measurements on some of the same solutions, will be discussed subsequently.⁶ For the pure polymer,²⁹ $\log \zeta_0$ at 25° is -4.35 , which is very close to $\log \zeta_1$ at 24° in Table I, although the sizes of the monomer unit and the cetane molecule are not exactly comparable.³⁰

To apply the free volume concept to the concentration dependence of the diffusion coefficient, Fujita^{2,32} has expressed the Doolittle relation in the form

$$D_T = RTA_d \exp(-B_d/f) \quad (4)$$

where A_d and B_d are constants assumed to be independent of both concentration and temperature; as before, we shall set B_d equal to unity. This treatment has in the past been applied to the "thermodynamic" diffusion coefficient with polymer-fixed frame of reference, D_T . However, it is evident from the relations among various diffusion coefficients discussed by McCall³³ and Fujita^{2,34} that in concentrated polymer solutions D_T actually is identical with D_1 . We therefore can treat D_1 in the same manner. At constant temperature, f again is assumed to be a linear function of the diluent volume fraction v_1

$$f(v_1, T) = f(0, T) + \beta(T)v_1 \quad (5)$$

where $\beta(T)$ is related to the free volume of the pure diluent as described below. The ratio of D_1 at v_1 to D_1 in the pure polymer is given then by

$$\ln [D_1/D_1(0)] = B_d\beta(T)v_1 / \{ [f(0, T)]^2 + \beta(T)f(0, T)v_1 \}$$

(29) Reference 24, p. 258.

(30) Surprisingly, the diffusion coefficients and friction coefficients of n -butane and n -pentane in polyisobutylene, extrapolated to zero concentration of penetrant from the measurements of Prager and Long,³¹ are closely similar in magnitude to ours for cetane, despite the considerable difference in molecular size. The dependence on the size of the penetrant molecule requires further study.

(31) S. Prager, E. Bagley, and F. A. Long, *J. Am. Chem. Soc.*, **75**, 1255 (1952).

(32) H. Fujita, A. Kishimoto, and K. Matsumoto, *Trans. Faraday Soc.*, **56**, 424 (1960).

(33) D. W. McCall and D. C. Douglass, to be published.

(34) H. Fujita, private communication.

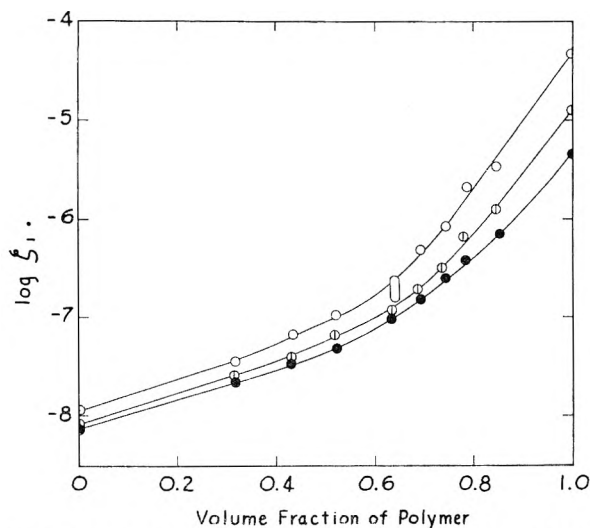


Fig. 4.—Log ζ_1 plotted vs. v_2 : open circles, 24.0°; slotted circles, 40.0°; black circles, 48.4°.

from which two linear test plots can be devised

$$1/\ln [D_1/D_1(0)] = f(0,T)B_d + [f(0,T)]^2/v_1B_d\beta(T) \quad (6)$$

$$v_1/\ln [D_1/D_1(0)] = [f(0,T)]^2/B_d\beta(T) + v_1f(0,T)/B_d \quad (7)$$

From the slope and intercept of either of these plots, the parameters $f(0,T)$ and $\beta(T)$ can be determined, provided $B_d = 1$.

In Fig. 5 and 6, data from Fig. 4 are plotted as the left sides of eq. 6 and 7 vs. $1/v_1$ and v_1 , respectively, including the data for pure cetane estimated as described above from the measurements of Douglass and McCall.⁵ The lines are drawn with the values of $f(0,T)$ and $\beta(T)$ listed in Table II. Since the two plots weight the individual points quite differently, the rather good coincidence with the lines in both figures represents a quite satisfactory fit to eq. 6 and 7.

TABLE II

FREE-VOLUME PARAMETERS FOR THE POLYISOBUTYLENE-CETANE SYSTEM

T , °K.	$\beta(T)$	$f(0,T)$	$f_2(T)$	$\gamma(T)$	$f_1(T)$
297.2	0.120	0.074	0.073	0.194	0.196
313.2	.141	.085	.080	.226	.210
321.6	.134	.092	.084	.226	.217

The parameter $f(0,T)$ obtained from this curve fitting should be equal to $f_2(T)$, the fractional free volume of the pure polymer, in accordance with eq. 5. It is compared in Table II with $f_2(T)$ calculated from f_g and α_f as given in the preceding section. The agreement in magnitude is quite good, although the temperature dependence of $f(0,T)$ is a little too great, reflecting the same discrepancy seen in Fig. 3 between observed and calculated values of ΔH .

The quantity $\beta(T) + f(0,T)$, denoted $\gamma(T)$ by Fujita, should be equal to $f_1(T)$ according to eq. 5. These quantities are compared in the last two columns of Table II, and the agreement is excellent. It may be concluded that the Fujita theory

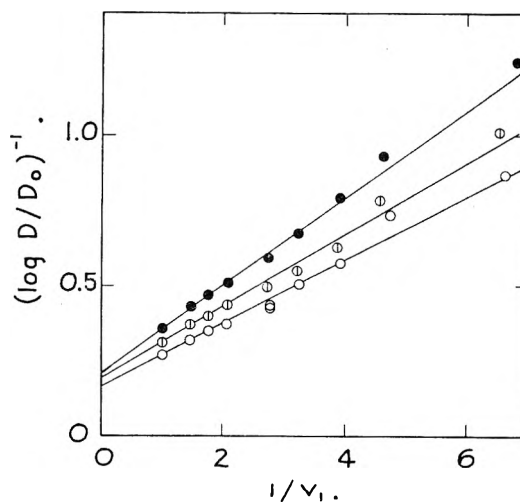


Fig. 5.—Test plot of eq. 6; lines drawn with parameters in Table II; key to experimental points same as in Fig. 4.

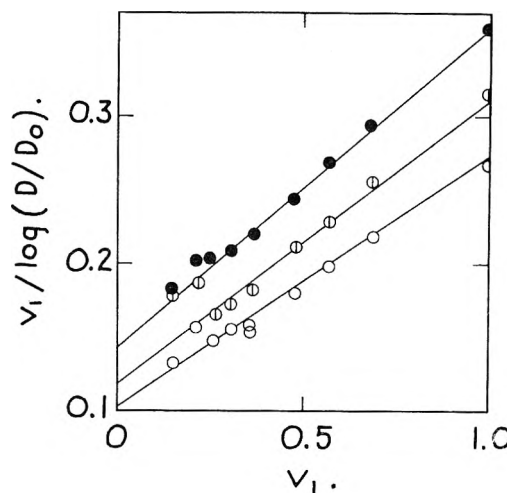


Fig. 6.—Test plot of eq. 7; lines drawn with parameters in Table II; key to experimental points same as in Fig. 4.

describes the concentration dependence of D_1 very well, even though the proportion of diluent covers a much wider range than in most systems to which it has been applied previously.²

Methacrylate Polymers

Values of $\log D_1$ and $\log \zeta_1$ for the three methacrylate polymers are given in Table III, together with some values of the apparent heat of activation for diffusion. It is evident that both the magnitude of the friction coefficient and the heat of activation

TABLE III

DIFFUSION COEFFICIENTS AND FRICTION COEFFICIENTS FOR CETANE IN METHACRYLATE POLYMERS

Polymer	T , °K.	$\log D_1$	$\log \zeta_1$	ΔH_D , kcal.
Hexyl	297.2	-8.45	-4.93	13.4
	313.2	-7.91	-5.45	
	321.6	-7.75	-5.60	
Octyl	297.2	-7.83	-5.56	11.9
	321.6	-7.16	-6.19	
Dodecyl	297.2	-7.66	-5.73	9.3
	321.6	-7.14	-6.22	

decrease with increasing side chain length of the polymer, as would be expected from comparison of the mobilities of the polymer backbones.⁷⁻⁹

However, a comparison of ζ_1 interpolated at 25° with ζ_0 at this temperature, and of ΔH_D with ΔH_a at 25° obtained from viscoelastic measurements through the modified Rouse theory,⁷⁻⁹ shows some striking differences (Table IV). As far as the size of the moving unit is concerned, the molecular weight of cetane, 226, is comparable in magnitude with the monomer molecular weights M_0 as listed in the table, which are the units on which ζ_0 is based. But in contrast with the polyisobutylene case where ζ_1 and ζ_0 are of similar magnitude and the ΔH values are identical, here ζ_1 is very much less than ζ_0 and ΔH_D is somewhat less than ΔH_a . Moreover, the ratio ζ_1/ζ_0 deviates farther from unity with decreasing side group length, becoming less than 10^{-4} for the hexyl polymer.

TABLE IV

COMPARISON OF FRICTION COEFFICIENTS OF CETANE AND POLYMER BACKBONE SEGMENTS IN METHACRYLATE POLYMERS AT 25°

	Polymer		
	Hexyl	Octyl	Dodecyl
M_0	170	198	254
$\log \zeta_1$	-4.96	-5.58	-5.75
$\log \zeta_0^a$	-0.75	-2.29	-4.69
$\log (\zeta_1/\zeta_0)$	-4.21	-3.29	-1.06
$T - T_g$, deg.	30	45	50
f_2	0.031	0.038	0.051
f_e	0.044	0.054	0.058
ΔH_a , ^b kcal.	36.8	30.2	24.9
ΔH_D (obsd.), kcal.	13.4	11.9	9.3
ΔH_D (calcd.), ^c kcal.	17.4	15.2	19.4

^a From ref. 7-9. ^b From differentiation of the WLF equation with the appropriate parameters for each polymer (ref. 24, p. 225). ^c From eq. 3 with f_e substituted for f .

Some similar comparisons from fragmentary data in the literature with large differences between ζ_1 and ζ_0 were attributed³ to excess local free volume in the immediate vicinity of the penetrant molecule, which is assumed to be increasingly important as the glass transition temperature is approached and the average free volume becomes scarce. This

interpretation is borne out by Table IV, since the ratio ζ_1/ζ_0 deviates farther from unity as $T - T_g$ and the fractional free volume f_2 diminish. For polyisobutylene at 25°, $T - T_g$ is 96° and f_2 is 0.073; the data of the preceding section indicate that by the time the average free volume reaches this magnitude, the effects of the excess local free volume disappear.

It is of interest to extend these qualitative considerations by estimating the effective free volume f_e which would correspond to the observed value of ζ_1 , as a measure of the local fractional free volume in the immediate vicinity of a diluent molecule. For this purpose, we obtain from eq. 4

$$\ln (\zeta_1/\zeta_0) = 1/f_2 - 1/f_e \quad (8)$$

where B has been set equal to unity and the difference in size between monomer unit and diluent molecule has been ignored. The values of f_e at 25°, given in Table IV, are of reasonable magnitude; for the hexyl and octyl polymers, f_e is about 40% greater than f_2 , and for the dodecyl, 16% greater.

Given f_e , one can estimate the apparent activation energy for diffusion from eq. 3, substituting f_e for f but assuming that α_f will be the same for the local as for the average free volume. The results are given in the last row of Table IV. Although they are still higher than the observed values of ΔH_D , they are in reasonable agreement for the hexyl and octyl polymers.

From the fragmentary data available, it appears that the effect of excess local free volume cannot be predicted from the magnitude of the average free volume alone. The details of molecular packing of the diluent with the polymer backbone and side groups must be involved.

Acknowledgments.—This work was supported in part by a grant from the National Science Foundation, and in part by the Research Committee of the Graduate School of the University of Wisconsin from funds supplied by the Wisconsin Alumni Research Foundation. We are indebted to Professors R. Byron Bird, L. J. Gosting, and H. Fujita for helpful discussions.

NOTES

STUDIES ON SOLUTIONS OF HIGH DIELECTRIC CONSTANT. PART I. PARTIAL MOLAL VOLUMES OF SOME UNIVALENT ELECTROLYTES IN FORMAMIDE AT 25°

BY RAM GOPAL AND RAMAY KUMAR SRIVASTAVA

Chemistry Department, Lucknow University, Lucknow, India

Received March 3, 1962

The study of partial molal volumes of electrolytes in aqueous solutions at infinite dilution, *i.e.*, \bar{V}_0 , has drawn the attention of a number of workers in re-

cent years¹ because of the knowledge it provides about ion-solvent interactions. The earlier studies of Fajans and Johnson² have been followed by those of Laidler and co-workers,³ Hepler,⁴ Benson,⁵ and Mukerji.⁶ These workers have investigated the partial molal volumes, \bar{V}_0 , of different electro-

(1) H. S. Harned and B. B. Owens, "Physical Chemistry of Electrolytic Solutions," Third Edition, Reinhold Publ. Corp., New York, N. Y., 1958, p. 358.

(2) K. Fajans and O. Johnson, *J. Am. Chem. Soc.*, **64**, 668 (1942).

(3) A. M. Couture and K. J. Laidler, *Can. J. Chem.*, **34**, 1209 (1956); **35**, 207 (1957).

(4) L. G. Hepler, *J. Phys. Chem.*, **61**, 1426 (1957).

(5) S. W. Benson, unpublished calculations.

(6) P. Mukerji, *J. Phys. Chem.*, **65**, 740, 744 (1961).

lytes, the individual ionic contributions to \bar{V}_0 , and the electrostriction effect (*i.e.*, the compression of the solvent molecules around the ions of the solute⁷). These studies have been confined to aqueous solutions. It is of interest to examine the behavior of electrolytes and ions in non-aqueous solvents from this point of view and so obtain a broader outlook about the ion-solvent interactions. Only a few attempts appear to have been made in this direction. The studies of Stark and Gilbert,⁸ Gibson and Kincaid,⁹ and of Butler and co-workers,¹⁰ may be mentioned in this connection. Unfortunately, the solvents used by these workers were of low dielectric constant (alcohols and glycol), where ionic association and ion-pair formation may complicate the interpretation of the data. We have, therefore, chosen solvents like formamide, methylformamide, and methylacetamide, all of which have a higher dielectric constant than that of water, for the study of partial molal volumes of different electrolytes. The present note reports some preliminary data on partial molal volumes of some uni-univalent electrolytes in formamide at 25°.

Experimental

The electrolytes used were all B.D.H. analytical grade and were recrystallized from conductivity water. Merck formamide (sp. cond. $\sim 10^{-4}$ mho) was recrystallized and distilled under reduced pressure (2 mm.). The product gave a conductance of the order of 10^{-5} mho. The pycnometers used were of more than 10-ml. capacity and their volumes were calibrated with the help of redistilled mercury. The thermostat was controlled to $\pm 0.02^\circ$. The volumes could be read on the graduated capillary side arm of the pycnometer to 0.0005 ml. The densities of solutions of different concentrations were determined in the usual manner and were believed to be correct up to the fifth decimal place and the apparent molal volumes \bar{V} in ml., calculated therefrom, up to the second decimal place. This is especially true at higher concentrations (lowest concentration used is about 0.15 *M*), from which extrapolations were made to obtain partial molal volumes at infinite dilutions, *i.e.*, \bar{V}_0 .

The densities obtained above were used to calculate the apparent molal volumes \bar{V} using the equation

$$\bar{V} = \frac{1000(d_0 - d)}{mdd_0} + \frac{M}{d}$$

where d is the density of the solution, d_0 that of formamide, m the molality, and M the molecular weight of the solute. The \bar{V} values at different concentrations were plotted against \sqrt{c} as required by the equation^{11,12} $\bar{V} = \bar{V}_0 + S_v\sqrt{c}$ (c = molar concn.). Extrapolation of the curves to infinite dilution gives \bar{V}_0 for different electrolytes and the slope gives S_v . Figure 1 gives the plots thus obtained in different cases.

Discussion

The values of \bar{V}_0 and S_v for different electrolytes, obtained from the procedure described earlier, are given in Table I. A comparison also is made to the corresponding values obtained in aqueous solvent.

From Table I it is clear that the \bar{V}_0 values in formamide are higher than the corresponding values

(7) T. J. Webb, *J. Am. Chem. Soc.*, **48**, 2589 (1926); D. M. Ritson and J. B. Hasted, *J. Chem. Phys.*, **16**, 11 (1948).

(8) J. B. Stark and F. C. Gilbert, *J. Am. Chem. Soc.*, **59**, 1818 (1937).

(9) R. E. Gibson and J. F. Kincaid, *ibid.*, **59**, 579 (1937).

(10) J. A. V. Butler, W. C. Vosborgh, and L. C. Connell, *J. Chem. Soc.*, 933 (1933).

(11) D. O. Masson, *Phil. Mag.*, **8** [7], 218 (1929).

(12) W. Geffeken, *Naturwissenschaften*, **19**, 221 (1931); *Z. physik. Chem.*, **A155**, 1 (1931).

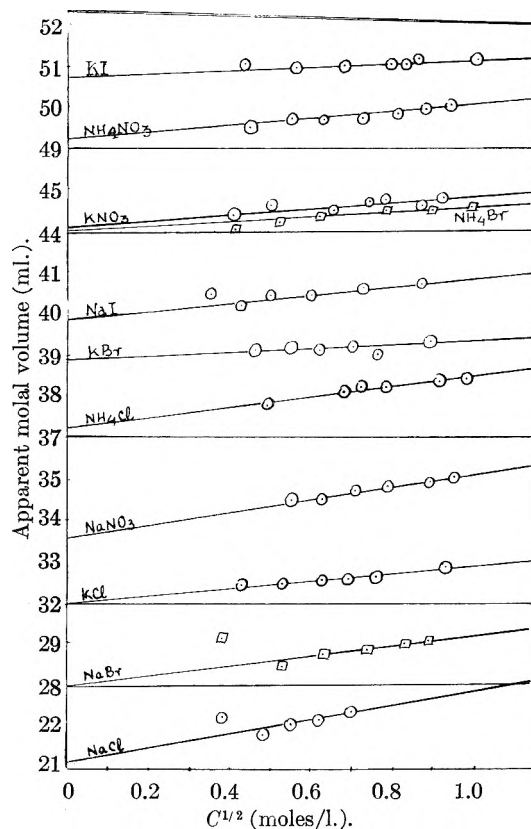


Fig. 1.—Apparent molal volumes of salts in formamide.

TABLE I
Temperature 25 \pm 0.02°

Electrolyte	\bar{V}_0 , ml.		S_v	
	In formamide	In water ^a	In formamide	In water ^a
KCl	32.00	26.52	0.88	2.327
KBr	38.90	33.73	.43	1.919
KI	50.75	45.36	.38	1.556
KNO ₃	44.10	38.18	.73	2.30
NaCl	21.10	16.40	1.60	2.133
NaBr	28.00	23.51	1.18	1.760
NaI	39.85	35.10	0.93	1.346
NaNO ₃	33.55	...	1.55	...
NH ₄ Cl	37.20	35.98	1.31	1.45
NH ₄ Br	44.05	...	0.50	...
NH ₄ NO ₃	49.24	47.56	0.83	0.97

^a See ref. 1.

TABLE II

$$\begin{aligned} \bar{V}_0(\text{KCl}) - \bar{V}_0(\text{NaCl}) &= 10.90 \text{ ml.} \\ \bar{V}_0(\text{KBr}) - \bar{V}_0(\text{NaBr}) &= 10.90 \text{ ml.} \\ \bar{V}_0(\text{KNO}_3) - \bar{V}_0(\text{NaNO}_3) &= 10.55 \text{ ml.} \\ \bar{V}_0(\text{KBr}) - \bar{V}_0(\text{KCl}) &= 6.90 \text{ ml.} \\ \bar{V}_0(\text{NaBr}) - \bar{V}_0(\text{NaCl}) &= 6.90 \text{ ml.} \\ \bar{V}_0(\text{NH}_4\text{Br}) - \bar{V}_0(\text{NH}_4\text{Cl}) &= 6.85 \text{ ml.} \\ \bar{V}_0(\text{NH}_4\text{Cl}) - \bar{V}_0(\text{NaCl}) &= 16.10 \text{ ml.} \\ \bar{V}_0(\text{NH}_4\text{Br}) - \bar{V}_0(\text{NaBr}) &= 16.05 \text{ ml.} \\ \bar{V}_0(\text{NH}_4\text{NO}_3) - \bar{V}_0(\text{NaNO}_3) &= 15.70 \text{ ml.} \\ \bar{V}_0(\text{KI}) - \bar{V}_0(\text{KBr}) &= 11.85 \text{ ml.} \\ \bar{V}_0(\text{NaI}) - \bar{V}_0(\text{NaBr}) &= 11.85 \text{ ml.} \end{aligned}$$

and so on.

in water. They are, however, additive, as in water. Table II makes this quite obvious.

Table I also shows that the values of S_V for different electrolytes in formamide are much smaller than the corresponding values in water.

A detailed examination of \bar{V}_0 and S_V for different electrolytes and of other related aspects of ion-solvent interaction will be taken up when more extensive data have been obtained.

R. K. S. is grateful to the Scientific Research Grants Committee, Uttar Pradesh Govt., for the financial support. Our thanks also are due to the Head of the Chemistry Department and the authorities of the Lucknow University for providing the necessary facilities.

SPECIFIC ADSORPTION OF ISOTHIOCYANATOCHROMIUM(III) COMPLEX IONS AT THE MERCURY-AQUEOUS SOLUTION INTERFACE

BY NOBUYUKI TANAKA, EISHIN KYUNO, GEN SATO, AND REITA TAMAMUSHI

Department of Chemistry, Faculty of Science, Tohoku University, Sendai, Japan

Received March 12, 1962

Only a few examples have been reported on the specific adsorption of inorganic cations at the mercury-aqueous solution interface. The specific adsorption of thallium(I) ion at the mercury-solution interface has been reported by several authors.¹⁻⁴ Laitinen and Randles reported that the anomalous faradaic impedance of a dropping mercury electrode in a solution of tris-(ethylene-diamine)-cobalt(II) and -cobalt(III) complex ions was attributed to the adsorption of these ions.⁵ Recently, specific adsorption of $[\text{Cr}(\text{NCS})_6]^{3-}$ ion at the mercury electrode surface was pointed out by Fischerová and Fischer from the measurement of capacity current.⁶

In the systematic investigation on the polarographic behavior of chromium(III) complex ions, we have noticed that some of them have an extraordinary adsorbability at the mercury-aqueous solution interface. These complexes were prepared and their electrocapillary curves were examined: $[\text{Cr}(\text{NH}_3)_6]\text{Cl}_3$, $[\text{CrCl}(\text{NH}_3)_5]\text{Cl}_2$, $[\text{Cr}(\text{ox})(\text{NH}_3)_5]\text{Cl} \cdot n\text{H}_2\text{O}$,⁷ $[\text{CrN}_3(\text{NH}_3)_5](\text{NO}_3)_2$, $[\text{Cr}(\text{en})_3]\text{Cl}_3 \cdot 3.5\text{H}_2\text{O}$, $[\text{Cr}(\text{NCS})(\text{NH}_3)_5]\text{Cl}_2$, *cis*- $[\text{Cr}(\text{NCS})_2(\text{NH}_3)_4]\text{Cl}$, *trans*- $[\text{Cr}(\text{NCS})_2(\text{en})_2]\text{Cl} \cdot 11.5\text{H}_2\text{O}$, *trans*- $[\text{Cr}(\text{NCS})_2(\text{pn})_2]\text{Cl} \cdot \text{H}_2\text{O}$,⁷ *trans*- $\text{NH}_4[\text{Cr}(\text{NCS})_4(\text{NH}_3)_2] \cdot 2/3\text{H}_2\text{O}$, and $\text{K}_3[\text{Cr}(\text{NCS})_6] \cdot 4\text{H}_2\text{O}$. Electrocapillary curves were obtained by the measurement of the drop-time of a dropping mercury electrode in a solution containing 1 mM complex ion, 0.1 M sodium acetate, 0.1 M acetic acid, 0.9 M potassium

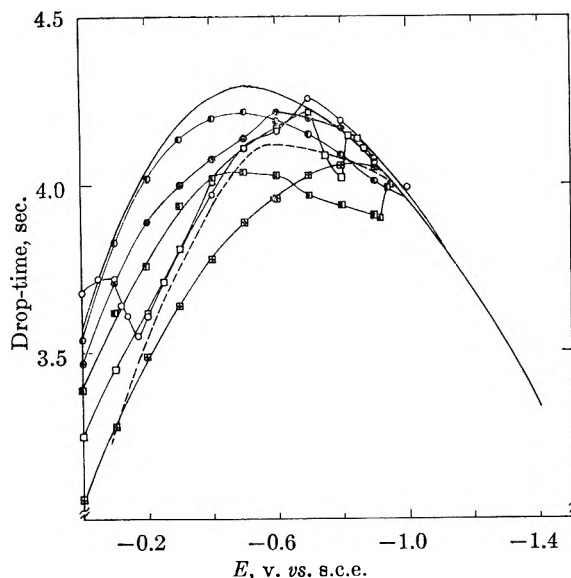


Fig. 1.—Electrocapillary curves of isothiocyanatochromium(III) complexes at 25°; supporting electrolyte, 0.1 M NaOAc + 0.1 M HOAc + 0.9 M KCl + 0.005% gelatin (for $\text{K}_3[\text{Cr}(\text{NCS})_6] \cdot 4\text{H}_2\text{O}$, 1 M KCl + 0.005% gelatin was used): \bullet —, *trans*- $[\text{Cr}(\text{NCS})_2(\text{pn})_2]\text{Cl} \cdot \text{H}_2\text{O}$; \oplus —, $[\text{Cr}(\text{NCS})(\text{NH}_3)_5]\text{Cl}_2$; \blacksquare —, *trans*- $[\text{Cr}(\text{NCS})_2(\text{en})_2]\text{Cl} \cdot \text{H}_2\text{O}$; \square —, *trans*- $\text{NH}_4[\text{Cr}(\text{NCS})_4(\text{NH}_3)_2] \cdot 2/3\text{H}_2\text{O}$; \ominus —, *cis*- $[\text{Cr}(\text{NCS})_2(\text{NH}_3)_4]\text{Cl}$; \circ —, $\text{K}_3[\text{Cr}(\text{NCS})_6] \cdot 4\text{H}_2\text{O}$ (1 M KCl + 0.005% gelatin); —, 0.1 M NaOAc + 0.1 M HOAc + 0.9 M KCl + 0.005% gelatin; —, 1 M KSCN + 0.005% gelatin.

chloride, and 0.005% gelatin, unless otherwise stated. In the case of $\text{K}_3[\text{Cr}(\text{NCS})_6]$, 1 M potassium chloride solution containing 0.005% gelatin was used as the supporting electrolyte. The first five complexes did not show any marked adsorbability under the experimental conditions, whereas the other complexes, which have NCS⁻ coordinated, exhibited remarkable effects on the drop-time as shown in Fig. 1. Their adsorbability must be attributed to the sulfur atom rather than to the nitrogen atom of the NCS⁻ ligand, because the azido complex ion was not adsorbed.

The structure of crystalline $\text{NH}_4[\text{Cr}(\text{NCS})_4(\text{NH}_3)_2] \cdot 2/3\text{H}_2\text{O}$ has been determined; the NCS⁻ ligands are coordinated to the central ion through the nitrogen atoms.^{8,9} The same structure has been assumed for $[\text{Cr}(\text{NCS})(\text{NH}_3)_5](\text{NO}_3)_2$ and *trans*- $[\text{Cr}(\text{NCS})_2(\text{en})_2]\text{Cl} \cdot 11.5\text{H}_2\text{O}$ in the solid state.¹⁰ On the other hand, Linhard, Siebert, and Weigel suggested that the NCS⁻ ligand of $[\text{Cr}(\text{NCS})(\text{NH}_3)_5]^{2+}$ ion is bonded with the sulfur atom from the absorption spectrum of its aqueous solution.¹¹ The present results, however, lead to the conclusion that these rhodanatochromium(III) complex ions may have the Cr(III)-NCS structure in aqueous solutions.

The extremely high adsorbability of these isothiocyanatochromium(III) complex ions may be realized when the electrocapillary curves of these com-

(1) A. Frumkin and A. Titievskaja, *Russ. J. Phys. Chem.*, **31**, 485 (1957).

(2) A. Frumkin and N. Poljanovskaja, *ibid.*, **32**, 157 (1958).

(3) A. Frumkin, "Surface Phenomena in Chemistry and Biology," Pergamon Press, London, 1958, p. 189.

(4) R. Tamamushi and N. Tanaka, *Z. physik. Chem. (Frankfurt)*, **28**, 158 (1961).

(5) H. A. Laitinen and J. E. B. Randles, *Trans. Faraday Soc.*, **51**, 54 (1955).

(6) E. Fischerová and O. Fischer, *Collection Czech. Chem. Commun.*, **26**, 2570 (1961).

(7) New compounds; the method of preparation for these compounds will be reported elsewhere.

(8) Y. Saito, Y. Takeuchi, and R. Pepinsky, *Z. Krist.*, **106**, 476 (1955).

(9) Y. Takeuchi and Y. Saito, *Bull. Chem. Soc. Japan.*, **30**, 319 (1957).

(10) J. Fujita, K. Nakamoto, and M. Kobayashi, *J. Am. Chem. Soc.*, **78**, 3295 (1956).

(11) M. Linhard, H. Siebert, and M. Weigel, *Z. anorg. allgem. Chem.*, **278**, 287 (1955).

plex ions are compared with that of potassium thiocyanate; 1 mM of these complex ions gave an effect on the drop-time comparable to that given by 1 M potassium thiocyanate (Fig. 1). Coördination of NCS⁻ ion to Cr(III) seems to increase the affinity of the sulfur atom in NCS⁻ ion to mercury.

The electrocapillary curves of [Cr(NCS)(NH₂)₅]²⁺, *cis*-[Cr(NCS)₂(NH₂)₄]⁺, and *trans*-[Cr(NCS)₂(en)₂]⁺ ions clearly indicate that these cations are strongly adsorbed in the positive branch of the electrocapillary curve. In this respect, they exhibit the character of capillary-active anions. The adsorbability of these complex ions seems to depend on the local charge distribution rather than on the total charge of the complex ion. Figure 1 also shows that *trans*-[Cr(NCS)₂(en)₂]⁺ ion has much higher adsorbability than *trans*-[Cr(NCS)₂(pn)₂]⁺ ion. This difference may be due to a kind of steric effect.

The current-potential curves of these complex ions also were obtained, which indicated clearly that anomalies on the electrocapillary curves are closely related to the reduction or oxidation of these complexes. The current-potential curve of *trans*-[Cr(NCS)₂(en)₂]⁺ ion showed a sudden increase in reduction current at -0.92 volt *vs.* s.c.e., where the electrocapillary curve shows an anomaly as seen in Fig. 1. On the current-potential curve of [Cr(NCS)₆]³⁻ ion a small anodic wave appeared at -0.15 volt *vs.* s.c.e.,⁶ where an anomalous change is observed also on the electrocapillary curve in Fig. 1. These relations suggest, in turn, that the adsorption of reacting species plays an important role in the electrode reactions.

The present results provide not only interesting examples of electrocapillary phenomena of inorganic ions, but also some important experimental data pertinent to the discussion of the structure of complex ions in solution and their electrode reactions.

Acknowledgment.—The authors thank the Japan Society for the Promotion of Science for the financial support granted for this research.

KINETICS OF REACTION BETWEEN NAPHTHALENE AND PICRIC ACID IN THE SOLID STATE

By R. P. RASTOGI,* PARMJIT S. BASSI,* AND S. J. CHADHA

Chemistry Department, Panjab University, Chandigarh, India

Received March 19, 1962

Reactions in the solid state are a class by themselves. Because of difficulties in analysis of the composition of the solid phase, studies have been confined mainly to those cases where the course of reaction could be followed by X-ray crystallographic methods or by measuring the amount of gas evolved in suitable reactions.¹ The present note describes a new technique for studying the kinetics of reaction between naphthalene and picric acid in the solid state by following the movement of the colored interface which apparently gives worthwhile results.

* Chemistry Department, Gorakhpur University, Gorakhpur, India.

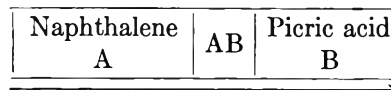
(1) S. W. Benson, "The Foundations of Chemical Kinetics," McGraw-Hill Book Co., Inc., New York, N. Y., 1960, p. 616.

However, the reaction under study may be controlled by vapor phase diffusion.

Naphthalene and picric acid were purified by sublimation *in vacuo* and fractional crystallization with ethanol, respectively. The melting points were 80.3 and 121.4°, respectively. The reaction in the solid state was studied in the following way.

Experimental

Clean thick-glass capillaries (5 in. long) with uniform diameters (internal 3 mm. and external 9 mm.) were taken. Finely ground naphthalene was introduced in the capillary with a clean metal rod from one side while picric acid was introduced from the other side in a similar manner and the position of the interface was noted. The capillaries were sealed from either side with a paste which hardened after some time. These capillaries were kept in air-thermostats maintained at suitable temperatures but below the eutectic temperature. The temperature fluctuations were of the order of ±1°. A scale was attached to these capillaries. The start of the reaction was indicated by a change in color at the naphthalene-picric acid boundary. The distance through which the boundary moved was noted at different time intervals. The induction period at room temperature was found to be only 7 to 10 min. It also was observed that picric acid did not diffuse through product layer whereas naphthalene did. This is schematically shown below.



In this case it appears that the phase-boundary processes are so rapid that equilibrium is established at the boundaries during the entire course of reaction. The diffusion in the product layer is alone rate determining as happens in the case of tarnishing reactions so that if ξ is the thickness of the diffusion layer²

$$\xi^2 = kt \quad (1)$$

where k is a certain constant and t is the time. Modification has been made in the above relationship to account for the heating at the interface due to poor thermal conductivities of the solids. For such a case it has been shown that

$$\xi^2 = 2k_i t \exp(-P\xi) \quad (2)$$

where

$$k_i = C \exp(-E/RT_{\max})$$

C = certain constant

E = energy of activation

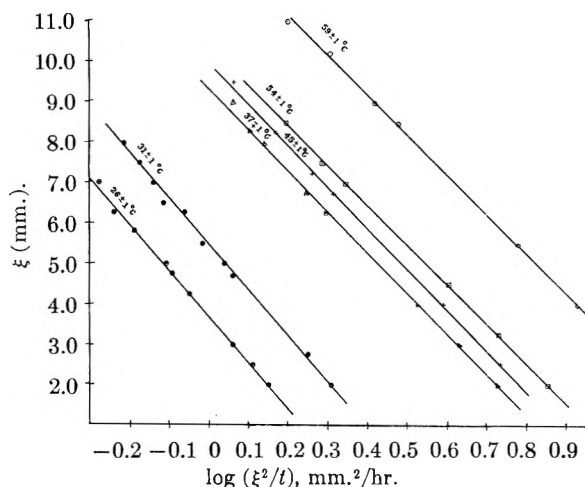
P = proportionality constant

T_{\max} = maximum temp. attained instantaneously in the mixture

In this derivation it is assumed that $T_i - T = k'\xi$ where k' is another constant so that $P = k'E/RT_i T$; T_i is the initial temperature and T is any temperature intermediate between T_i and T_{\max} . Equation 1 did not satisfy the data. For testing eq. 2 $\log \xi/t$ was plotted against ξ . Straight lines were obtained at all temperatures of observations, justifying the validity of eq. 2. This is shown in Fig. 1.

It is interesting to note that all the curves have approximately the same slope, indicating thereby that P has the same value, which should be the case. Further, with increase in the value of T_i , k_i also

(2) G. Chhn, *Chem. Rev.*, **42**, 527 (1948).

Fig. 1.—Estimation of k_i and p .

would increase. This is confirmed by the fact that the intercepts of the straight lines increase with rise in temperature. The values of k_i and P were determined by the method of least squares. These are given in Table I.

TABLE I
PARAMETERS OF EQUATION 2

Temp., °C.	k_i (mm. ² /hr.)	P (mm. ⁻²)
26 ± 1	1.08	0.206
31 ± 1	1.47	.205
37 ± 1	4.225	.218
45 ± 1	4.68	.223
54 ± 1	5.77	.234
59 ± 1	10.8	.225

If $T_i/T_{\max} \ll 1$, as appears to be the case, an approximate idea of the energy of activation of the reaction can be obtained by plotting $\log k_i$ against $1/T_i$. The energy of activation is found to be 14 kcal. The enthalpy and the entropy of activation would be of the order of 13 kcal. and -11 cal./deg./mole. The sign and magnitude of these quantities is not unexpected. It is premature to speculate on the mechanism of the reaction. Kinetic data show that the reaction is diffusion controlled. There is a possibility that in the present study the kinetics of diffusion of naphthalene in the gas phase through the porous reaction product is primarily involved. Further studies are in progress to investigate the nature of the diffusion mechanism.

Acknowledgment.—Thanks are due to Prof. F. C. Tompkins, F. R. S., for a critical reading of the manuscript. This work forms part of a project sponsored by the Indian Council of Scientific and Industrial Research.

DIPOLE MOMENT MEASUREMENTS OF O¹⁸-LABELED X=O COMPOUNDS

BY E. FISCHER, I. LAULICHT AND S. PINCHAS

The Weizmann Institute of Science, Rehovoth, Israel

Received June 12, 1962

The absorption intensity of the X=O¹⁸ (X = C, P, S) stretching bands seems to be generally significantly different from that of the correspond-

ing X=O¹⁶ absorptions.¹ The ultraviolet absorption intensity of a number of O¹⁸-labeled X=O compounds also appears to be measurably different from the parallel normal compounds.^{1d,2} Since the absorption intensity of molecules, both in the infrared and in the ultraviolet region of the spectrum, is a function of their respective transition dipole moment, this (unexpected)^{1b} change in the absorption intensity of X=O¹⁸ compounds made it interesting to measure their permanent dipole moment in comparison with that of the corresponding normal substances. Theoretically, however, the dipole moment of two isotopic modifications of the same compound should differ only very slightly, mainly as the result of the change in the zero-point energy of the molecules. The calculated dipole moment of HD is thus only³ 5.67×10^{-4} D. (as compared with zero for H₂).

No dipole moment measurements of O¹⁸-compounds seem to have been reported yet, although some comparative values for various pairs of normal and deuterated molecules were reported⁴ and the effect of Cl¹³ and S³⁴ on the moment was estimated⁵ in one case. It thus was observed that even for ammonia-*d*₃ the increase in the electric moment is only small⁴ (0.03 D.), although the relative difference in all three isotopic masses is here very high and in spite of the fact that X-H bonds show the largest anharmonicities⁶ (which are the main cause for the observed changes in the dipole moment of labeled compounds^{4f,d}).

The electric moment of the following pairs of X=O compounds therefore has been measured accurately: (a) normal and 90 atom % O¹⁸-benzophenone, (b) normal and 54 atom % O¹⁸-triphenylphosphine oxide, (c) normal and 90 atom % O¹⁸-diphenyl sulfoxide, and (d) normal and 69 atom % O¹⁸-N,N-dimethylbenzamide. Special care was taken to minimize the relative error by using identical methods of measurement as well as calculation for each pair of compounds.

Experimental Details

The measurement of the benzophenones was carried out in solution in 2,2,5-trimethylhexane, while the other compounds were dissolved in *p*-xylene. Both solvents were chosen because of their low vapor pressures, *p*-xylene being used because of its higher dissolving power. The physical constants at 30°, the specific polarizations p_0 , and the constants C_0 , defined by $C_0 = 3/(\epsilon_0 + 2)^2 d_0$, were:

	d_0	n_0	ϵ_0	C_0	p_0
Trimethylhexane	0.6995	1.3960	1.941	0.2762	0.3410
<i>p</i> -Xylene	0.8531	..	2.243	0.1953	0.3434

(1) (a) M. Halmann and S. Pinchas, *J. Chem. Soc.*, 1703 (1958); (b) 264 (1958); (c) S. Pinchas, D. Samuel, and M. Weiss-Brodsky, *ibid.*, 1688 (1961); (d) 2382 (1961); (e) 2666 (1961); (f) 3063 (1961); (g) in press.

(2) M. Halmann and S. Pinchas, *ibid.*, 1246 (1960).

(3) S. H. Blinder, *J. Chem. Phys.*, **35**, 974 (1961).

(4) (a) C. A. Burrus, *ibid.*, **28**, 427 (1958); (b) M. H. Sirvetz and R. E. Weston, *ibid.*, **21**, 898 (1953); (c) H. R. Johnson and M. W. P. Strandberg, *ibid.*, **20**, 687 (1952); (d) R. P. Bell and I. E. Coop, *Trans. Faraday Soc.*, **34**, 1209 (1938); (e) V. W. Laurie, *J. Chem. Phys.*, **26**, 1359 (1957); (f) J. M. A. De Bruyne and C. P. Smyth, *J. Am. Chem. Soc.*, **57**, 1203 (1935); (g) L. G. Groves and S. Sugden, *J. Chem. Soc.*, 971 (1935); (h) Von F. H. Mueller, *Physik. Z.*, **35**, 1009 (1934); (i) J. N. Shoolery, R. G. Shulman, and D. M. Yost, *J. Chem. Phys.*, **19**, 250 (1951).

(5) R. G. Shulman and C. H. Townes, *Phys. Rev.*, **77**, 500 (1950).

(6) G. Herzberg, "Infrared and Raman Spectra of Polyatomic Molecules," D. Van Nostrand Co., Inc., Princeton, N. J. 1945, p. 207.

TABLE I
DIELECTRIC INCREMENT, $\delta\epsilon$, AND DENSITY INCREMENT, δd , AT VARIOUS WEIGHT FRACTIONS, w , OF THE LIGHT AND HEAVY COMPOUNDS

Normal benzophenone	10^4w	5.5	10.8	15.95	26.7	36.65	45.85	54.5	72.1	98	187	282
	$10^4\delta\epsilon$	20.7	40.85	61.05	108.0	150.5	184.0	222.0	292.5
	$10^4\delta d$	26.0	49.5	75.6
90% O ¹⁸ -Benzophenone	10^4w	5.2	10.2	15.0	25.1	34.5	43.1	51.2	67.75	100	185	276
	$10^4\delta\epsilon$	20.5	41.4	60.3	98.0	134.5	169.0	203.8	272.6
	$10^4\delta d$	27.1	50	75.0
Normal triphenylphosphine oxide	10^4w	4.4	8.60	20.6	31.3	40.8	49.6	62.4	73.9	78.5	174.5	228
	$10^4\delta\epsilon$	33	70	160.0	245.0	318.0	384.5	485.5	572.0
	$10^4\delta d$	19.7	44.2	57.4
54% O ¹⁸ -Triphenylphosphine oxide	10^4w	4.3	8.4	20.05	30.5	39.75	48.3	60.8	71.8	76	228	..
	$10^4\delta\epsilon$	28.45	61.05	152.0	231.5	306.0	369.5	468.5	551.0
	$10^4\delta d$	19.8	59.0	..
Normal diphenyl sulfoxide	10^4w	4.5	8.88	21.2	32.25	42.05	51.05	64.3	75.95	85.5	190	..
	$10^4\delta\epsilon$	36	73.4	175.6	265.3	360.4	426.7	538.9	634.0
	$10^4\delta d$	21.9	47.9	..
90% O ¹⁸ -Diphenyl sulfoxide	10^4w	4.3	8.4	20.15	30.6	39.9	48.5	61.1	72.15	77	157	..
	$10^4\delta\epsilon$	35.5	72.5	174.7	256.3	334.8	405.6	508.7	601.8
	$10^4\delta d$	19.4	41.3	..
Normal N,N-dimethylbenzamide	10^4w	4.3	8.5	20.3	30.9	40.3	48.95	61.65	72.8	74.5
	$10^4\delta\epsilon$	40.1	79.3	194.1	296.4	391.2	468.1	598.4	706.5
	$10^4\delta d$	13.25
69% O ¹⁸ -N,N-dimethylbenzamide	10^4w	4.5	8.75	20.9	31.8	41.5	50.4	63.45	74.9	78	154	228
	$10^4\delta\epsilon$	40.9	82.7	195.5	302.0	395.0	482.0	609.0	717.5
	$10^4\delta d$	14.1	28.20	41.5

TABLE II

EMPIRICAL CONSTANTS, MOLAR POLARIZATIONS AND REFRACTIONS, AND DIPOLE MOMENTS FOR ISOTOPIC COMPOUND PAIRS

Compound	$C\alpha\epsilon_0$	β	P	R_D	$1.05R_D$	P_{or}	Moment	Moment (lit.)
Normal benzophenone	1.124	0.381	243.2	57.8	60.7	182.5	3.013 ± 0.015	2.95^a
90% O ¹⁸ -Benzophenone	1.110	.386	242.9	58.15	61.05	181.85	3.007 ± 0.015	..
Normal triphenylphosphine oxide	1.507	.296	486.2	..	96.0	390.2	4.403 ± 0.01	4.28^b
54% O ¹⁸ -Triphenylphosphine oxide	1.515	.300	490.2	..	(96.0)	394.2	4.425 ± 0.02	..
Normal Diphenyl sulfoxide	1.636	.299	379.3	61.2	64.3	315.0	3.954 ± 0.015	4.00^c
90% O ¹⁸ -Diphenyl sulfoxide	1.619	.302	379.0	(61.2)	(64.3)	314.7	3.951 ± 0.015	..
Normal N,N-dimethylbenzamide	1.892	.209	322.1	43.8 ^d	46.0	276.1	3.703 ± 0.015	..
69% O ¹⁸ -N,N-dimethylbenzamide	1.872	.213	322.6	(43.8)	(46.0)	276.6	3.705 ± 0.015	..

Solvent: for benzophenone, trimethylhexane; otherwise *p*-xylene.

^a M. J. Granier, *Compt. rend.*, **223**, 893 (1946). ^b G. M. Phillips, J. S. Hunter, and L. E. Sutton, *J. Chem. Soc.*, 146 (1945). ^c G. C. Hampson, R. H. Farmer, and L. E. Sutton, *Proc. Roy. Soc. (London)*, **A143**, 147 (1933). ^d Calculated from bond refractions, A. I. Vogel, *et al.*, *Chem. Ind. (London)*, 358 (1950).

For each compound four to five series of dielectric measurements were carried out, each series corresponding to eight solutions of different concentrations.

The normal and labeled compounds were synthesized as already described.^{1a,b,c,z} Each isotopic modification was synthesized and purified (by repeated recrystallizations) exactly in the same way as the other.

The experimental set-up for the measurement of the dielectric constant already has been described.⁷

Results

Characteristic results of one series of dielectric measurements for each compound are given in Table I in the form of dielectric increments $\delta\epsilon = \epsilon - \epsilon_0$ and density increments $\delta d = d - d_0$ as functions of the weight fraction w . (The subscript 0 denotes the solvent.) As usual, $\delta\epsilon$ and δd were found to be linear functions of w : $\delta\epsilon = \alpha\epsilon_0w$; $\delta d = \beta d_0w$. The slopes $C_0\alpha\epsilon_0$ found for all the series of each compound were averaged and the resulting value was used for the computation of its polarization at infinite dilution.^{7,8}

The resulting empirical constants and molar polarizations at infinite dilution P_∞ are given in the first three columns of Table II. In all cases

(7) E. D. Bergmann, A. Weizmann, and E. Fischer, *J. Am. Chem. Soc.*, **72**, 5009 (1950).

(8) B. Harris, R. G. W. Le Fèvre, and E. P. A. Sullivan, *J. Chem. Soc.*, 1622 (1953).

the sum of the atomic and electronic polarizations $P_a + P_e$ was taken to be $1.05R_D$, R_D denoting the molar refraction observed by previous authors for the normal compound. It was assumed that the molar refractions of the normal and labeled compounds are in all cases identical within the experimental error of the present method and this was proved experimentally for benzophenone. The dipole moment values of three out of the four normal compounds investigated were reported in the literature and are listed in Table II. Values for the corresponding R_D were taken from the same papers while the R_D for N,N-dimethylbenzamide was calculated from bond refraction data. The errors in the electric moments indicated in Table II are relative ones, calculated from the mean deviation of the results obtained for all the series of each compound.

The results thus indicate that the electric moments of O¹⁸-labeled benzophenone, diphenyl sulfoxide, and N,N-dimethylbenzamide are practically the same as those of the corresponding normal analogs, as can be expected from the small relative change in mass of the isotopic oxygen atom. The small difference in moment observed between the two isotopic modifications of triphenylphosphine

oxide (0.022 D.), although somewhat less than the combined experimental error (of the two values), still seems to be interesting.

The somewhat different values for the moment of the two isotopic benzophenones observed previously³ seem now to be due to insufficient purification of the measured samples.

Acknowledgments.—The authors thank Dr. D. Samuel and Mrs. M. Weiss-Brodway for the synthesis of all the samples and Mrs. N. Castel for technical assistance.

(9) Mentioned in a footnote to ref. 2.

INFLUENCE OF THE ALKALI METAL CATIONS ON THE REDUCTION OF IODATE ION ON MERCURY IN ALKALINE SOLUTION

BY AKIKO ARAMATA¹ AND PAUL DELAHAY

Coates Chemical Laboratory, Louisiana State University,
Baton Rouge 3, Louisiana

Received July 2, 1962

The influence of the nature of the cation in the double layer correction for electrode kinetics has been investigated mostly by Frumkin and his school² and, more recently, by Giersz and co-workers.³ The cations of the alkali metals have been primarily studied, though the influence of the alkaline earth cations has been examined in some instances. It generally is observed for reduction on a mercury electrode that the absolute value of the overvoltage, at a given current density and for given concentrations of reactant and supporting electrolyte, increases from Li⁺ to Cs⁺ for the reduction of cations and decreases from Li⁺ to Cs⁺ for the reduction of anions. This variation of overvoltage is explained (a) by specific adsorption of the heavier cations (especially Cs⁺) and (b) by the abnormally high hydration of Li⁺. Hence, the actual difference of potential across the diffuse double layer is somewhat different from the value calculated from the Gouy-Chapman theory. Application of the Brodowski-Strehlow theory⁴ of the diffuse double layer improves somewhat the agreement between theory and experiment but the two foregoing effects remain predominant.⁵ In all cases, to our knowledge, a monotonic variation of overvoltage was observed from Li⁺ to Cs⁺. Abnormal overvoltages were found in the course of this work for the reduction of iodate on mercury in alkaline solution in the presence of Li⁺. These results are described and interpreted.

Experimental

Experimental methods, which were quite conventional, were the same as in previous work.⁶ RbOH and CsOH were

(1) Graduate student since September, 1960.

(2) For a survey, see, e.g., R. Parsons, *Advan. Electrochem. Electrochem. Eng.*, **1**, 1 (1961).

(3) L. Gierst, private communication.

(4) H. Brodowski and H. Strehlow, *Z. Elektrochem.*, **63**, 262 (1959); **64**, 891 (1960).

(5) E. A. Maznichenko, B. B. Damaskin, and Z. A. Iofa, *Dokl. Akad. Nauk SSSR*, **138**, 1377 (1961).

(6) (a) K. Asada, P. Delahay, and A. K. Sundaram, *J. Am. Chem. Soc.*, **83**, 3396 (1961); (b) P. Delahay and A. Aramata, *J. Phys. Chem.*, **66**, 2208 (1962).

prepared by electrolysis of the chloride solutions on a mercury cathode and subsequent decomposition of the amalgam.

Description and Discussion of Results

Tafel plots were parallel in the range 25 to 500 $\mu\text{a. cm.}^{-2}$ for the solutions of Table I and yielded $\alpha n_a = 0.76 \pm 0.02$ (α , transfer coefficient; n_a , number of electrons in the activation step). Results were interpreted according to the corrected Tafel plot^{6a}

$$\ln I + \frac{zF}{RT} \Delta\varphi = \ln I^0 + \frac{\alpha n_a F}{RT} E_e - \frac{\alpha n_a E}{RT} (E - \Delta\varphi) \quad (1)$$

where I is the current density, I^0 the exchange current density, E the electrode potential, E_e the equilibrium electrode potential, $\Delta\varphi$ the difference of potential across the diffuse double layer from the plane of closest approach to solution, z the ionic valence (with sign) of the reduced species (iodate), and F , R , and T are as usual. Values of $\Delta\varphi$ were computed from the Gouy-Chapman (G. C.) and Brodowski-Strehlow (B. S.) theories.⁷ Correction for ionic association in the bulk of the solution was made⁸ for LiOH but was neglected for NaOH and the other hydroxides and metal iodates.^{6b}

TABLE I

	—0.02 M MOH—			0.02 M MOH + 0.1 M MCl ^a		
	$-(E - \Delta\varphi)_{G.C.}^{d,e}$ mv.	$-(E - \Delta\varphi)_{B.S.}^{e,f}$ mv.	$-(E - \Delta\varphi)_{B.S.}^{e,f}$ mv.	$-(E - \Delta\varphi)_{G.C.}$ mv.	$-(E - \Delta\varphi)_{B.S.}$ mv.	
Li	192	57	49	148	90	80
Na	229	92	78	159	98	84
K	247	101	96	106 ^d	108 ^a	..
Rb	222	78	72	152	92	84
Cs	197	54	49	103	37	26

^a Except for KCl which was 0.4 M. ^b All values of E and $E - \Delta\varphi$ are referred to the hydrogen electrode in the same electrolyte, but without IO₃⁻, as for the reduction of IO₃⁻. ^c Values of E for $I = 10^2 \mu\text{a. cm.}^{-2}$. ^d G. C. = Gouy-Chapman theory. ^e B. S. = Brodowski-Strehlow theory. ^f Values of $E - \Delta\varphi$ for $\log I - (F\Delta\varphi/2.3RT) = 4$ (I in $\mu\text{a. cm.}^{-2}$).

The corrected Tafel plots were parallel (Fig. 1) and yielded for the G. C. theory $\alpha n_a = 0.90 \pm 0.03$ except for the 0.1 M CsCl solution, for which $\alpha n_a = 0.96$. The B. S. theory yielded the same average value of αn_a except for the 0.1 M CsCl solution, for which $\alpha n_a = 0.98$. The same trend in the variation of $E - \Delta\varphi$ for the alkali metal cations, for a given value of $\log I - (F\Delta\varphi/2.3RT)$, was observed by correction either by the G. C. theory or the B. S. theory (Table I). The corrected Tafel plots of Fig. 1 are almost independent of the cation concentration for K⁺ and Na⁺.

(7) (a) Radii of solvated ions needed in the B. S. theory were taken from C. B. Monk, "Electrolytic Dissociation," Academic Press, Inc., New York, N. Y., 1961, p. 271. Thus $r = 2.50, 2.17, 1.75, 1.53$, and 1.47 \AA. from Li⁺ to Cs⁺. (b) Dielectric constants needed in the B. S. theory: $\epsilon = 77.5$.

(8) Association constants were taken from J. Bjerrum, G. Schwarzenbach, and L. G. Sillén, "Stability Constants, Part II," The Chemical Society, London, 1958. $\log K = 0.18$ and -0.57 for LiOH and NaOH, respectively. Association for iodate is quite negligible for KIO₃ ($\log K = -0.23$) and probably for the iodates of the other alkali metals.

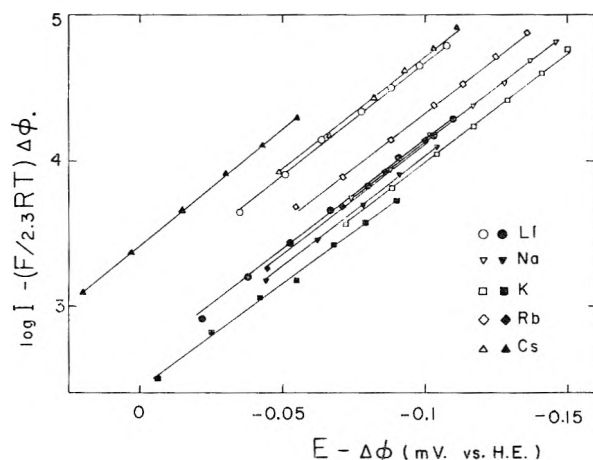


Fig. 1.—Corrected Tafel plot for the reduction of 5 mM MIO_3 at 25° on mercury in 0.02 M MOH (open symbols) and 5 mM MIO_3 in 0.02 M MOH and 0.1 M MCl (solid symbols; except for KCl, which was 0.4 M); I in $\mu\text{a. cm.}^{-2}$.

There is a shift toward lower values of $|E - \Delta\phi|$ with increasing concentration for Rb^+ and especially for Cs^+ . This observation is in agreement with previous work^{2,3} on the reduction of other anions and is accounted for by specific cation adsorption. The position of the two lines for Li^+ in Fig. 1, however, is abnormal, since they correspond to lower values of $|E - \Delta\phi|$ than for Na^+ and K^+ . A monotonic increase of $|E - \Delta\phi|$ from Cs^+ to Li^+ would be expected from previous work^{2,3} on other anions. Such an abnormal behavior of Li^+ also was observed recently by Gierst³ in the polarographic reduction of IO_3^- . It was suggested by this author that addition of Li^+ to IO_3^- affects in some way the hydration shell of that ion and renders reduction easier. The strong hydration of Li^+ ion and probably IO_3^- ($\lambda^0 = 40.8 \text{ ohm}^{-1} \text{ cm.}^2$ for 9 IO_3^-) seems to support this view. Less strongly hydrated ions (BrO_3^- , $\text{S}_2\text{O}_8^{2-}$) do not exhibit this abnormal behavior. Investigation of the influence of Li^+ on the kinetics of the purely chemical reduction of IO_3^- would be of interest in this connection.

Acknowledgment.—This investigation was supported by the Office of Naval Research. We are indebted to Dr. L. Gierst, University of Brussels, for discussion of this work.

(9) R. Parsons, "Handbook of Electrochemical Constants," Academic Press, Inc., New York, N. Y., 1959, p. 85.

FREEZING POINT DEPRESSIONS IN SODIUM FLUORIDE. II. EFFECT OF TETRAVALENT FLUORIDES¹

BY STANLEY CANTOR AND TERRY S. CARLTON²

*Oak Ridge National Laboratory,³ P. O. Box X, Oak Ridge, Tennessee
Received July 2, 1962*

The objectives of these studies and the usefulness

(1) Presented before the Southeastern Regional Meeting, American Chemical Society, Birmingham, Ala., Nov., 1960.

(2) Summer employee, Oak Ridge National Laboratory, June–Sept., 1960.

(3) Operated for the United States Atomic Energy Commission by Union Carbide Corporation.

of NaF as a high temperature cryoscopic medium were discussed in a previous publication.⁴

For fixed alkaline earth fluoride concentration it was found⁴ that the smaller the alkaline earth cation radius the greater was the negative deviation from ideal solution behavior for NaF. In this particular investigation it was of interest to test whether this trend in solution behavior also applied to tetravalent fluorides. The tetravalent fluorides were chosen because their cations have electric field strengths that are considerably greater than those of any alkaline earth cation.

Experimental

Apparatus, procedures, and NaF purification used in this investigation were outlined in a previous publication.⁴

UF_4 (Mallinckrodt) was purified by hydrofluorination at 650°. Adsorbed HF was flushed away with a helium stream while the sample cooled. This product was found to contain 100 p.p.m. oxygen when analyzed by the KBrF_4 technique.⁵ Spectroscopic analysis indicated the only other impurity that exceeded 50 p.p.m. was Ni, 70 p.p.m. Commercial ThF_4 (made by National Lead Company) was recrystallized from slowly cooled melts from which clear crystalline portions were selected. The melt was contained in graphite and protected by a helium atmosphere. Analyses of the clear portions showed 370 p.p.m. oxygen, 300 p.p.m. Ca, and none of the rare earth elements in excess of 800 p.p.m. ZrF_4 was obtained at Oak Ridge National Laboratory and further purified by sublimation at 720° under vacuum. Translucent crystals were selected from the sublimate. Spectrochemical analyses showed these impurities in p.p.m.: Hf, 40; Si, 200; Al, less than 100; Fe, less than 100; Ni, less than 300. HfF_4 was produced by treating HfO_2 (from Wah Chang Corp., Albany, Oregon) with NH_4HF_2 , at 250°, in a graphite vessel. Unreacted NH_4HF_2 and sorbed HF were driven off by heating at 600° under continuous helium flush. The HfF_4 was further purified in the manner indicated for ZrF_4 . Clearer portions of the sublimate were found to contain 500 p.p.m. Al and 570 p.p.m. Zr. Other impurities determined by spectroscopic means did not exceed 200 p.p.m.

Microscopic examination of the purified tetravalent fluorides indicated the absence of inclusions with higher indices of refraction except for ThF_4 . In general, such inclusions are associated with the presence of oxides.⁶ In the case of ThF_4 , the inclusions occupied very little volume in the crystal, and the subsequent oxygen analysis (given above) showed a negligible oxide content.

Results and Discussion

Freezing Points of NaF With One Tetravalent Fluoride Solute.—The temperatures at which NaF began precipitating from solution are given in Table Ia. The excess partial molal free energies of solution of NaF, $(\bar{F} - F^0)_{\text{NaF}}$, were calculated from these temperatures and are shown in Fig. 1. The thermochemical quantities used for these calculations are the same as those previously given (for NaF: melting point = 1268.0°K., heat of fusion = 8017 cal., $C_p(\text{liquid}) - C_p(\text{solid}) = 6.00 - 3.88 \times 10^{-3}T$).⁴ As expected, the excess free energies with ZrF_4 and HfF_4 solutes were identical within experimental error. All deviations from ideality were negative.

At the same concentration, the excess partial molal free energies of solution of NaF with these tetravalent fluoride solutes were lower than with alkaline earth fluoride solutes (see Fig. 1). These observed differences are consistent with the

(4) S. Cantor, *J. Phys. Chem.*, **65**, 2208 (1961).

(5) G. Goldberg, A. S. Meyer, Jr., and J. C. White, *Anal. Chem.*, **32**, 314 (1960).

(6) C. J. Barton, H. A. Friedman, W. R. Grimes, H. Insley, R. E. Moore, and R. E. Thoma, *J. Am. Ceram. Soc.*, **41**, [2] 63 (1958).

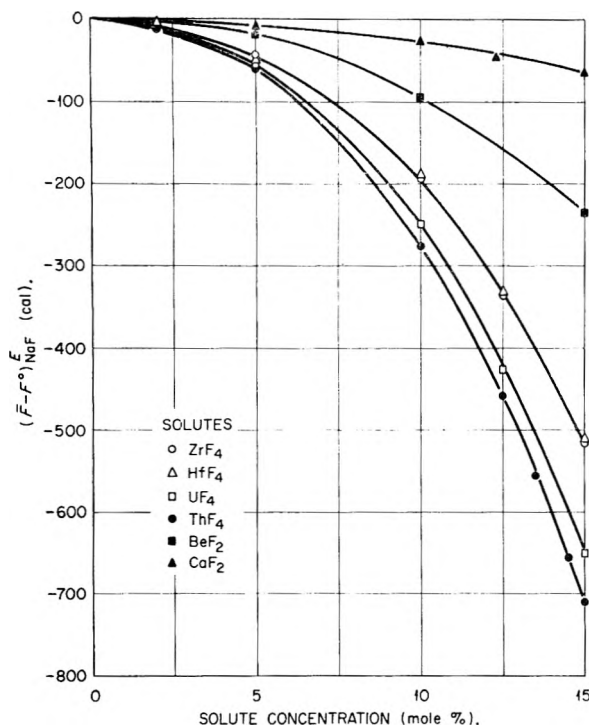


Fig. 1.—Excess partial molal free energy of solution of NaF vs. mole fraction of solute.

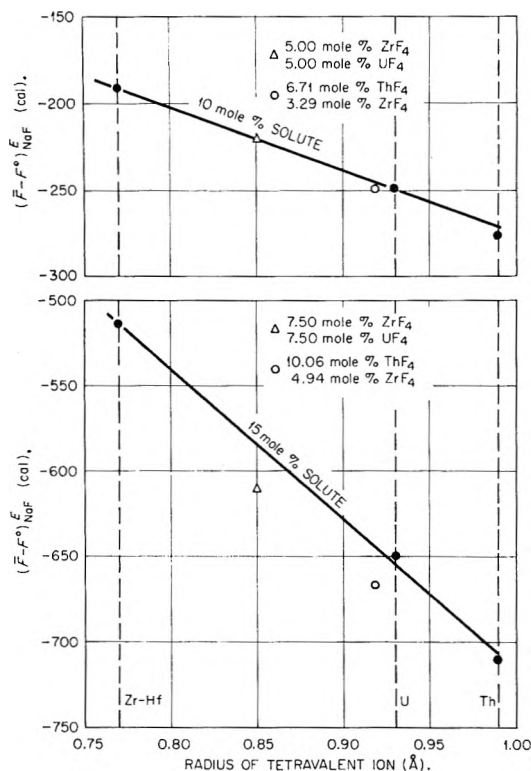


Fig. 2.—Excess partial molal free energy of solution of NaF in NaF-MF₄ systems as a function of solute ionic radius.

plausible assumption that the solutes and solvent are ionic. The tetravalent cations, with electric fields greater than those of any alkaline earth cations, have greater attraction for fluoride ions;

TABLE Ia
OBSERVED FREEZING POINTS OF NaF CONTAINING MF₄ SOLUTES

Mole fraction NaF	F.p. of NaF, °C.			
	ZrF ₄	HfF ₄	ThF ₄	UF ₄
1.000	995.0	995.0	995.0	995.0
0.980	...	985.0	985.0	985.6
.979	985.4
.950	968.4	967.0	966.0	966.7
.900	924.3	924.8	911.4	915.6
.875	892.7	892.7	873.0	878.2
.865	854.1	...
.855	834.8	...
.850	854.0	854.4	824.0	833.5

TABLE Ib
OBSERVED FREEZING POINTS OF NaF CONTAINING TWO MF₄ SOLUTES

NaF	Mole fraction			F.p. of NaF, °C.
	ZrF ₄	ThF ₄	UF ₄	
0.900	0.0500	0.0500	920.1
.900	.0329	0.0671	915.4
.850	.07500750	839.7
.850	.0494	.1006	830.7

consequently, the establishment of long-range order for NaF (crystallization) is more difficult.

The trend of the liquidus temperatures (and free energies of solution) of NaF within the series of tetravalent solutes is opposite to that observed for the alkaline earth fluorides. At fixed concentration, the larger the tetravalent cation radius, the greater were the deviations from ideal solution behavior. At first sight, this trend appears to contradict the explanation as given, *i.e.*, ZrF₄ and HfF₄ would have been expected to yield the lowest liquidus temperatures for NaF because Zr⁴⁺ and Hf⁴⁺ have the strongest electric field strengths. However, the existence of very strong electric field strength for these cations provides a hypothesis for this seemingly anomalous trend. In these solutions the number of nearest-neighbor fluorides to the tetravalent ions is probably large, perhaps eight or greater. (In crystalline ZrF₄ and UF₄ the cations are known^{7,8} to be eight-coordinated.) Assuming that in solution there are at least eight coordinated fluoride ions around each M⁴⁺ ion, then the sizes of the tetravalent cations impose significant steric consequences if all the ions are spherical. In the case of Zr⁴⁺ eight spherical fluoride ions cannot be in contact with the cation simultaneously. The U⁴⁺ cation could be in contact with eight fluoride ions provided the coordinated fluoride ions had a regular Archimedean antiprism arrangement, while Th⁴⁺ is large enough to contact eight fluoride ions arranged cubically. If the number of nearest-neighbor fluorides averages eight or more, those coordinated anions not in contact with the tetravalent cation should be less tenaciously held and therefore more "available"

(7) R. D. Burbank and F. N. Bensey, Jr., "The Crystal Structure of ZrF₄," Report No. K-1280, Union Carbide Nuclear Company, Oct. 31, 1956.

(8) R. D. Burbank, "The Crystal Structure of UF₄," Report No. K-769, Union Carbide Nuclear Company, June 6, 1951.

to sodium ions for crystallization. In short, steric effects probably operate in these melts in a direction opposite to the expected coulombic effects. Apparently these steric effects are directly related to the size of the solute cation. The nature of the relationship between the excess partial molal free energy of solution of NaF and the tetravalent cation radius⁹ is shown in Fig. 2. Similar plots were obtained for concentrations other than 10 and 15 mole % where melts contained one MF₄ solute.

Freezing Points of NaF with Two Tetravalent Fluoride Solutes.—To test whether the linear relationship indicated by Fig. 2 holds when two tetravalent fluorides are in solution, the liquidus temperatures of four samples were measured. Microscopic examination of these samples after cooling showed crystalline NaF to be the primary precipitating phase.

The compositions and liquidus temperatures of the solutions are given in Table Ib. The derived excess partial molal free energies of solution of NaF *vs.* tetravalent cation radius are plotted in

(9) W. H. Zachariasen, "Crystal Chemistry of the 5f Elements," "The Actinide Elements," G. T. Seaborg and J. J. Katz, Ed., McGraw-Hill Book Co., New York, N. Y., 1954, pp. 775-776.

Fig. 2. The radius for the solute pair was taken as the concentration-weighted arithmetic average of the two cations, *i.e.*

$$R_{1,2} = \frac{N_1}{N_1 + N_2} R_1 + \frac{N_2}{N_1 + N_2} R_2$$

where N is mole fraction.

Seemingly, for melts containing these components in the concentration ranges 0-15 mole % MF₄, the radius of the solute(s) cation(s) is the key variable in setting the liquidus temperature of NaF. At higher concentration (15 mole % MF₄ with two solutes), two tetravalent cations appeared to have a synergistic effect for fluoride attraction, *i.e.*, the partial molal excess free energies of mixing of NaF were somewhat lower than expected. The reasons for these lower free energies are presently not understood.

Acknowledgments.—The authors wish to thank Mr. Clayton F. Weaver for performing some of the petrographic examinations and the Analytical Chemistry Division of Oak Ridge National Laboratory for performing spectrochemical and oxygen analyses.

COMMUNICATIONS TO THE EDITOR

EXTENDED CALCULATIONS OF THE ELECTRON AFFINITIES OF POLY- NUCLEAR AROMATIC HYDROCARBONS BY THE LCAO-MO ω -TECHNIQUE

Sir:

Recently Ehrenson¹ has derived and discussed closed equations for the calculation of ionization potentials and electron affinities of organic compounds using the ω -technique in the LCAO-MO approximation. Previously, Streitwieser^{2,3} had made successful correlations between experimental ionization potentials and those calculated from the semi-empirical ω -technique. In the ω method, the coulomb integral (α) is assumed to be linearly related to the charge density (q) within the Hückel MO approximation through the parameter ω .⁴ Normally, an iterative process is used where the Hückel MO values of α and q are used to calculate new values of α and q . This process is repeated until the value of α becomes self-consistent. However, Ehrenson has shown that an approximation to the iterative results for electron affinities of alternant aromatic hydrocarbons may be had by using the expression

$$A = -\alpha^0 - \left(m_{\bar{N}} - \frac{\eta + 1}{\eta} \omega \right) \beta^0 \quad (1)$$

In this equation, A is the electron affinity, $\alpha^0 = -9.878$ e.v., $\beta^0 = -2.110$ e.v., $m_{\bar{N}}$ is the coefficient of the highest occupied level of the anion as given by Hückel theory, η is the number of π -electrons in the neutral molecule, and ω is given some constant value.

Wentworth and Becker⁵ have recently completed measurements of the electron affinities of several aromatic hydrocarbons using a gas chromatographic technique. Also Hoyland and Goodman⁶ have recently published SCF calculations of electron affinities of several aromatic compounds. Ehrenson noted that the calculated electron affinities using $\omega = 1.4$ did not correlate well with those of Hush and Pople⁷ or the limited and questionable experimental values. However, Ehrenson did suggest that the use of $\omega = 3.8$ gave more meaningful results. We wish to pursue this correlation further with the aid of new experimental and theoretical data.

In Table I we give the experimental electron affinities for the alternant aromatic hydrocarbons⁵ and the values calculated by using eq. 1 for various values of ω . We have included the electron affinities calculated by using $\omega = 1.40, 3.80,$ and 3.73 . The value of $\omega = 1.4$ is the one which is preferred by Streitwieser. This value also was used by Ehren-

(1) S. Ehrenson, *J. Phys. Chem.*, **66**, 706, 712 (1962).

(2) A. Streitwieser, Jr., and P. M. Nair, *Tetrahedron*, **5**, 149 (1959).

(3) A. Streitwieser, Jr., *J. Am. Chem. Soc.*, **82**, 4123 (1960).

(4) See ref. 1 for further details.

(5) W. E. Wentworth and Ralph S. Becker, *J. Am. Chem. Soc.*, **84**, 4263 (1962).

(6) J. R. Hoyland and L. Goodman, *J. Chem. Phys.*, **36**, 21 (1962).

(7) N. S. Hush and J. A. Pople, *Trans. Faraday Soc.*, **51**, 600 (1955).

TABLE I
 ELECTRON AFFINITIES

Compound	Exptl. (e.v.)	Calculated (e.v.)			SCF ^a
		$\omega = 1.4$	$\omega = 3.80$	$\omega = 3.73$	
Benzene	...	4.32	-1.59	-1.42	-1.40 ± 0.2
Naphthalene	...	5.33	-0.25	-0.08	-0.20 ± .2
Anthracene	0.42	5.84	0.42	0.58	0.61 ± .2
Naphthacene	...	6.14	.79	.95	...
Pentacene	...	6.33	1.04	1.19	...
Phenanthrene	.20	5.44	0.01	0.17	.25 ± .2
3,4-Benzophenanthrene	.33	5.56	.21	.37	...
Chrysene	.33	5.66	.31	.47	...
Benzanthracene	.46	5.81	.46	.61	...
Pyrene	.39	5.80	.42	.57	.55 ± .2
Triphenylene	.14	5.32	-0.03	.12	...
Pentaphene	...	5.87	0.58	.73	...
Picene	...	5.73	.44	.59	...
Perylene	...	6.04	.73	.88	...
1,2-3,4-Dibenzanthracene	...	5.74	.43	.58	...
1,2-5,6-Dibenzanthracene	...	5.79	.50	.65	...
1,2-7,8-Dibenzanthracene	...	5.75	.46	.62	...
3,4-5,6-Dibenzo-phenanthrene	...	5.66	.37	.52	...
1,12-Benzo- perylene	...	5.87	.57	.73	...
Coronene	...	5.66	.39	.54	...
Biphenylene	...	5.74	.26	.42	...

^a Error estimated by J. R. Hoyland in a private communication to R. S. B.

son in his very successful calculation of ionization potentials using an approximation similar to that of eq. 1. We also have included the SCF calculated values of Hoyland and Goodman.⁶ As noted by Ehrenson, the electron affinities calculated using $\omega = 1.4$ are significantly larger than the theoretical or experimental values. However, if $\omega = 3.80$ is used, then a better correlation between the ω -technique values and either the experimental or theoretical values is noted. Ehrenson used $\omega = 3.8$ on the basis of the value of ω which would give graphite an electron affinity of 4.39 e.v. (work function of the crystal) - 2.53 e.v. (correction from crystal to vapor).⁸ In fact, our agreement with experiment or SCF theory is excellent except for phenanthrene, 3,4-benzophenanthrene, and triphenylene. For these compounds, it appears that $\omega = 3.73$ gives much greater agreement with experiment.

Ehrenson has noted that the ω -technique introduces a correction for π -electron repulsion and σ -electron rearrangement which is omitted in the Hückel MO method. Hoyland and Goodman⁶ also have emphasized the importance of these factors as well as reminimization of the negatively charged state. The necessity of using $\omega = 3.73$ for the three compounds mentioned above may be caused by varying π and σ -deformation within the series of aromatic compounds which are reflected in a varying value of ω . Table I also includes calculated values of electron affinities of several alternant aromatic hydrocarbons for which the necessary

Hückel results were available. It is suggested that future calculations of electron affinities of alternant aromatic hydrocarbons using the ω -technique employ the value $\omega = 3.77$ until additional experimental work dictates an alternative value. This procedure should give very good approximations to the electron affinities where such may be required, *e.g.*, in charge transfer studies. We should point out that the very good agreement between the calculated and experimental values for these compounds provides a further confirmation of the validity of the recent experimental values determined by Wentworth and Becker.⁵ We wish to thank Dr. W. E. Wentworth for helpful discussion.

(9) National Science Foundation Coöperative Predoctoral Fellow 1962/1963. On leave from Texaco Research Laboratories, Bellaire, Texas.

DEPARTMENT OF CHEMISTRY
UNIVERSITY OF HOUSTON
HOUSTON, TEXAS

DONALD R. SCOTT⁹
RALPH S. BECKER

RECEIVED OCTOBER 10, 1962

ISOPROPYLBENZENE CONVERSION ON PRE-IRRADIATED SILICA-ALUMINA

Sir:

In γ -irradiation of isopropylbenzene adsorbed on microporous silica-alumina (400 m.²/g.), $G(\text{benzene})$ was observed to be greater than one at electron fractions of isopropylbenzene, F , ranging from 0.0107 down to 0.00106 and to fall to $G(\text{benzene}) = 0.40$ at $F = 0.00046$.¹ These results were interpreted as indicative of energy transfer from the solid to the adsorbed isopropylbenzene. Further, the persistence of such a high yield as $G(\text{benzene}) = 1.13$ to such a low electron fraction as $F = 0.00106$, at which presumably 99.9% of the radiation energy is initially absorbed in the solid and which corresponds to about 0.6% surface coverage, suggested that transfer of energy is rapid relative to the decay time of the responsible transfer entity produced by radiation in the solid. Additional evidence now has been obtained in support of these interpretations.

Using the same chemicals and procedures as previously reported,¹ the following experiments were performed in which about 30 g. of silica-alumina (400 m.²/g.) was irradiated to a dose of 5.3×10^{21} e.v. at 36° in the absence of isopropylbenzene, and then about 0.2 g. of isopropylbenzene was introduced to the pre-irradiated solid and products were recovered.

1. Irradiation imparted a very dark, essentially black, color to the solid. No gas was obtained from the solid. With liquid nitrogen on the reaction cell which had been attached to a vacuum line, isopropylbenzene was distilled onto the dark solid after it had stood for 2 hr. at room temperature following irradiation. The cell with contents then was brought to room temperature, and the uppermost beads of solid were observed to be partially decolorized. The beads appeared white on the periphery first with dark centers, and decolorization proceeded inward to the bead centers. At the same

(8) D. R. Kearns and M. Ca'via, *J. Chem. Phys.*, **34**, 2028 (1961).

(1) R. R. Hentz, *J. Phys. Chem.*, **66**, 1625 (1962).

time decolorization proceeded down the column of beads in the reaction cell and appeared to be essentially complete in 3-4 hr. The decolorization process apparently is governed by isopropylbenzene diffusion. (Kohn² has observed similar phenomena in decolorization of irradiated silica, silica-alumina, and alumina by hydrogen, ethylene, water vapor, and ammonia.) Cell and contents stood overnight and products were removed. Only total gas and benzene could be measured with reasonable accuracy: $F = 0.0070$; $G(\text{total gas}) = 0.011$; $G(\text{benzene}) = 0.42$.

2. The cell with irradiated solid was kept in liquid nitrogen from the termination of irradiation to introduction of isopropylbenzene: $F = 0.0067$; $G(\text{total gas}) = 0.012$; $G(\text{benzene}) = 0.42$. After product recovery the cell with decolorized solid was opened to the vacuum line and pumped overnight at 10^{-5} - 10^{-6} mm. Another 0.2-g. portion of pure isopropylbenzene was introduced to give $F = 0.0068$ and allowed to stand overnight on the solid. There was no detectable product formation or isopropylbenzene decomposition.

3. Isopropylbenzene was allowed to distil onto irradiated solid which was at room temperature (this process required only 10 min.). Decolorization proceeded much more uniformly over the whole solid in this case, although the rate still was slightly more rapid in the uppermost beads than in the lowest. Complete decolorization required about 3 hr.: $F = 0.0070$; $G(\text{total gas}) = 0.009$; $G(\text{benzene}) = 0.43$.

4. Irradiated solid was maintained at 100° for four hours. The solid remained quite dark, but some bleaching did occur. Isopropylbenzene then was introduced as in the third experiment, and decolorization proceeded in the same fashion: $F = 0.0068$; $G(\text{total gas}) = 0.001$; $G(\text{benzene}) = 0.33$. Thus, a 10-fold decrease in gas yield and a 21% decrease in benzene yield occurred as a result of the 4 hr. at 100° . Since complete deactivation of the solid was observed in experiment 2, the deactivation could not have been due to the product recovery procedure (4 hr. at 100°)¹ but must have been due to the prior contact with isopropylbenzene.

5. Irradiated solid was stored in the sealed reaction cell for 1 year at room temperature prior to introduction of isopropylbenzene. Darkness of the solid after the year's storage had definitely decreased to a shade judged roughly equivalent to a dose one-fourth of that originally received: $F = 0.0072$; $G(\text{total gas}) = 0.0045$; $G(\text{benzene}) = 0.41$.

Under conditions comparable with these experiments, irradiation of isopropylbenzene adsorbed on the solid gave $G(\text{benzene}) = 1.05$ and $G(\text{total gas}) = 0.219$. The gas was 95% hydrogen.¹

These experiments demonstrate the longevity at room temperature of certain benzene-producing "excited states of the solid" formed by irradiation. (The general expression "excited states of the solid" is used in the absence of definitive evidence for the mechanism of energy storage in the solid. It is considered probable that the long-lived excited

states responsible for benzene formation are trapped electrons and/or concomitant positive holes.¹) Further, these experiments suggest that benzene formation involves energy transfer from "excited states of the solid" which are destroyed thereby. If one molecule of benzene is produced per "excited state," then $G(\text{benzene}) = 0.42$ gives 7×10^{17} excitations per gram of solid. The approximately 20-fold lower $G(\text{total gas})$ in these experiments is consistent with the previously proposed mechanism for hydrogen formation¹ in that hydrogen atoms formed on irradiation of the solid would be recaptured at surface sites in the absence of adsorbed isopropylbenzene. The results of experiment 5 suggest that although gas formation on contact of isopropylbenzene with the pre-irradiated solid may be associated with visible "excited states," benzene formation is not but probably involves "excited states" which absorb in the ultraviolet. Dose-effect and other studies are in progress to determine the nature and concentration of defects responsible for the energy storage and to explain the 40% lower $G(\text{benzene})$ as compared with that in simultaneous irradiation of solid and adsorbed isopropylbenzene.

To the author's knowledge these experiments constitute the first conclusive demonstration of a chemical conversion due to transfer of energy stored in a solid (without destruction of the solid^{3,4}) by exposure to high-energy ionizing radiation.

(3) T. Westermark and B. Grapengiesser, *Arkiv Kemi*, **17**, 139 (1961).

(4) T. Westermark, N. Biesert, and B. Grapengiesser, *ibid.*, **17**, 151 (1961).

SOCONY MOBIL OIL COMPANY, INC. ROBERT R. HENTZ
RESEARCH DEPARTMENT
PRINCETON, NEW JERSEY

RECEIVED SEPTEMBER 21, 1962

ELECTRONIC PARAMAGNETIC RESONANCE OF MANGANOUS ION IN CALCIUM PYROPHOSPHATE AND CALCIUM FLUORIDE

Sir:

Kasai¹ recently published electronic paramagnetic resonance (e.p.r.) spectra of divalent manganese in calcium fluorophosphate (fluorapatite) and calcium compounds used in the synthesis of the fluorophosphate. We believe that the e.p.r. spectra shown in the publication are incorrect for divalent manganese in calcium pyrophosphate and in calcium fluoride.

We have prepared polycrystalline alpha calcium pyrophosphate and beta calcium pyrophosphate by pyrolysis of dibasic calcium orthophosphate, CaHPO_4 , at 1200 and 1050°, respectively.² The chemical identity and crystalline form of the pyrophosphates were confirmed by the weight loss during preparation, X-ray diffraction analysis, and measurement of the refractive indices. Manganese was introduced in the atomic proportion, $\text{Mn}/\text{Ca} = 10^{-3}$, by slurring the CaHPO_4 in

(1) P. H. Kasai, *J. Phys. Chem.*, **66**, 674 (1962).

(2) A. O. McIntosh and W. L. Jablonski, *Anal. Chem.*, **28**, 1424 (1956).

(2) H. W. Kohn, *Nature*, **184**, 630 (1959).

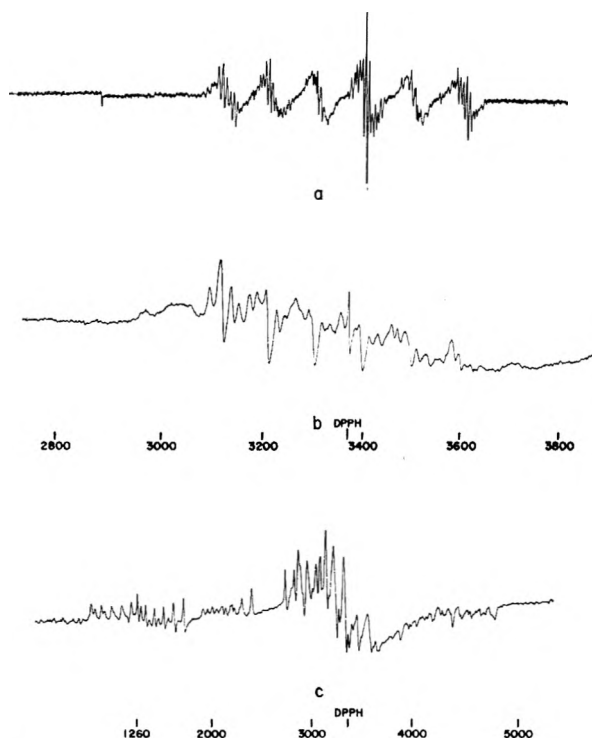


Fig. 1.—E.p.r. spectra of Mn^{+2} in polycrystalline substances: (a) CaF_2 , (b) $\beta-Ca_2P_2O_7$, and (c) $\alpha-Ca_2P_2O_7$.

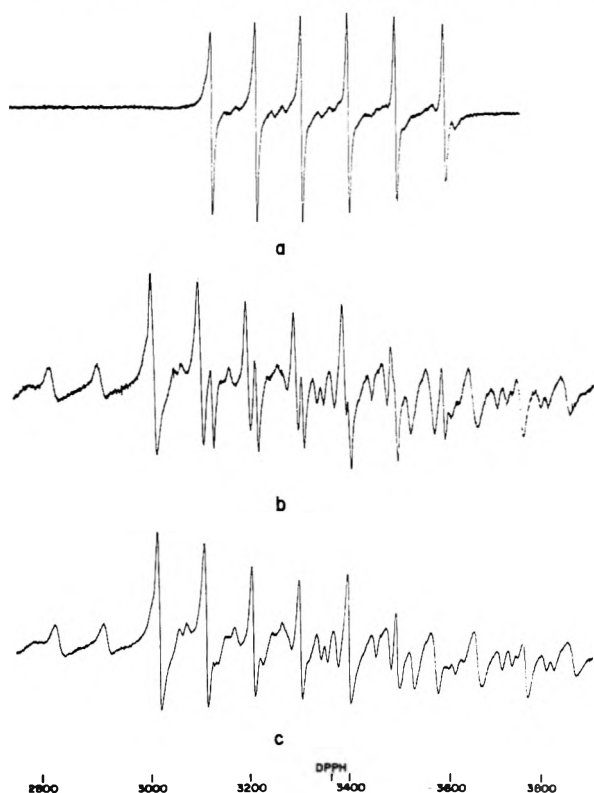


Fig. 2.—E.p.r. spectra of Mn^{+2} in polycrystalline substances: (a) CaO , (b) mixture of CaO and $Ca_5F(PO_4)_3$, and (c) $Ca_5F(PO_4)_3$.

acetone to which an aqueous solution of a manganese salt (acetate, nitrate, or sulfate) had been added, then drying. A second method which

gave the same e.p.r. spectra involved introducing manganese into pre-formed pyrophosphates by the same procedure and then firing at the above temperatures.

The same method was used to introduce manganese into phosphor grade calcium fluoride and into calcium oxide prepared by ignition of phosphor grade calcium carbonate at 1000° . The manganese was fired into these samples at 1050° . The Mn/Ca ratio was 10^{-4} in CaF_2 and 10^{-3} in CaO . The e.p.r. spectra of Mn^{+2} in the two pyrophosphates and calcium fluoride are given in Fig. 1 and in calcium oxide in Fig. 2.

Comparing these spectra with Kasai's, it is seen that (a) Kasai's spectrum of $CaF_2 + MnSO_4$ is identical with our spectrum of $\beta-Ca_2P_2O_7 : 2 \times 10^{-3} Mn$, Fig. 1(b); and (b) his spectrum of $Ca_2P_2O_7 + MnSO_4$ resembles neither of our pyrophosphates, but rather it appears to be the spectrum of Mn^{+2} in CaO , Fig. 2(a). Our spectrum of Mn^{+2} in polycrystalline CaF_2 , a large number of sharp lines superimposed on six broad lines, Fig. 1(a), appears to be consistent with the results of Baker, Bleaney, and Hayes³ for the e.p.r. of Mn^{+2} in a single crystal of CaF_2 . They found that each Mn^{+2} line, of which there are normally 30, is further split into nine components by hyperfine interaction between the Mn^{+2} ion and eight nearest-neighbor fluorine nuclei.

A re-interpretation of Kasai's experiment investigating the behavior of manganese during the course of reaction to form fluorapatite based on our identification of his reactants follows. Manganese first diffuses into calcium oxide, which then reacts in formation of the apatite. In support of our interpretation, we present in Fig. 2(b) a composite spectrum of calcium fluorapatite, $Ca_5F(PO_4)_3 : 1.5 \times 10^{-3} Mn$, and calcium oxide, $CaO : 10^{-3} Mn$, made by introducing both materials simultaneously into the resonant cavity. It matches exactly Kasai's curve for his fluorapatite mixture after 10 min. of firing at 1150° . Further substantiation for our interpretation was obtained from time-temperature studies on the rate of manganese diffusion into calcium oxide and beta calcium pyrophosphate. We found that manganese diffused much more rapidly into CaO than into $\beta-Ca_2P_2O_7$ at temperatures between 900 and 1150° .

(3) J. M. Baker, B. Bleaney, and W. Hayes, *Proc. Roy. Soc. (London)*, **A247**, 141 (1958).

LAMP DIVISION
GENERAL ELECTRIC COMPANY
LIGHTING RESEARCH AND
DEVELOPMENT OPERATION
LAMP RESEARCH LABORATORY
CLEVELAND, OHIO

R. L. HICKOK
J. A. PARODI
W. G. SEGELKEN

RECEIVED OCTOBER 22, 1962

THE EFFECT OF THE IONIZATION OF WATER ON DIFFUSIONAL BEHAVIOR IN DILUTE AQUEOUS ELECTROLYTES

Sir:

If one ion of a binary salt is radioactively tagged and an aqueous solution of the salt is allowed to

diffuse into pure water, we would normally expect to obtain the binary salt diffusion coefficient by measuring the movement of radioactivity. The restriction of electroneutrality ensures that each tagged ion is accompanied by its oppositely charged counterpart.

However, it has been pointed out recently¹ that if, in such a system, the salt concentration was reduced to the order of $10^{-7} M$, then a different diffusional behavior might be observed. At this order of dilution, the concentration of salt and that of the ions resulting from the ionization of water become comparable. We now have an effective multicomponent system in which coupling can occur between the various species of ions so that the measured diffusion coefficients will contain contributions from cross-term coefficients. Due to the high mobilities of H^+ and OH^- ions, the effect should be quite pronounced and may be detectable at considerably higher concentrations than $10^{-7} M$. If the concentration of salt is reduced to a sufficiently low value, we might also expect to measure the trace-ion diffusion coefficient of the tagged ion in the above system. In this case it is a trace species in a uniform electrolyte of H^+ and OH^- ions of much higher concentration.

In this Laboratory we have been calibrating open-ended capillaries by allowing fairly dilute tagged salt solutions to diffuse into pure water. It is imperative to know the concentration above which the assumption is valid that the binary salt diffusion coefficients are being measured. The effect also is of considerable interest for its own sake and therefore we have undertaken the exploratory studies reported below.

The two salts used in these experiments were sodium chloride and magnesium bromide. "Carrier-free" $^{22}NaCl$ was purified by selective elution through a cation ion-exchange column. $Mg^{82}Br_2$ was made by adding AnalaR HBr to "Specpure" MgO and then irradiating in the high neutron flux of the Lucas Heights Reactor, Sutherland, N.S.W. The specific activity obtained was of the order of 7 curies/g. of bromine. Solutions were made up approximately by weight and then successively diluted, all concentrations being checked by conductivity measurements. The water used in these studies was purified first by distillation and then by passage through an Elgastat de-ionizer at a rapid flow rate. Its specific conductance was 8.4×10^{-7} mho/cm. For the diffusion measurements a simple open-ended technique was used,² the capillaries being of Perspex to minimize absorption.

The diffusion coefficients obtained in this work are given in Table I. The measured coefficients are integral ones and for the purposes of this survey, the approximation has been made that they are equal to the differential coefficients at half the solution concentration. To demonstrate the incidence of the effect, these values are compared to salt diffusion coefficients calculated by the

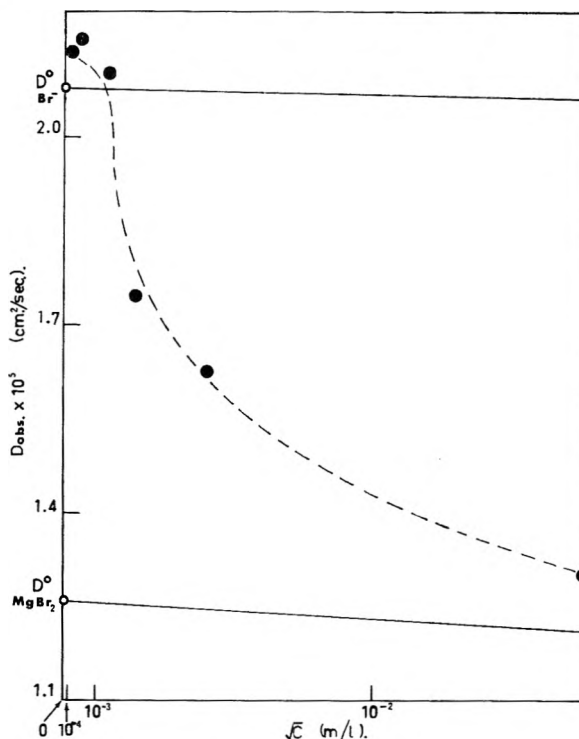


Figure 1.

Onsager and Fuoss limiting equation.³ The precision of the measurements is from 1 to 2%.

TABLE I

Salt	C, mole/l.	$D_{obsd.} \times 10^5$, cm. ² /sec.	$D_{calcd.} \times 10^5$, cm. ² /sec.
NaCl	2×10^{-5}	1.51	1.61
	9×10^{-6}	1.54	1.60
	5×10^{-4}	1.58	1.59
MgBr ₂	2×10^{-3}	1.58	1.58
	3×10^{-8}	2.13	1.26
	3×10^{-7}	2.16	1.26
	2×10^{-6}	2.10	1.25
	5×10^{-6}	1.75	1.25
	2×10^{-5}	1.62	1.24
	2.9×10^{-4}	1.30	1.21
2.83×10^{-3}	1.14	1.15	

From Table I, the change-over from binary to mixed diffusion is clearly seen for both salts. In the case of NaCl, the presence of some inactive carrier made it impracticable to use concentrations below $10^{-5} M$. Consequently only the beginnings of the transition to the trace-ion coefficient can be seen. For $MgBr_2$, however, which was chosen because of the large numerical difference between the values of binary and trace coefficients and for the high specific activity obtainable, the change-over as illustrated in Fig. 1 is quite striking. In both cases the effect commences at about $10^{-4} M$ and in the $MgBr_2$ case the rate of change is a maximum at $\sim 4 \times 10^{-6} M$. The surprisingly high

(1) L. A. Woolf, D. G. Miller, and L. J. Gosting, *J. Am. Chem. Soc.*, **84**, 317 (1962).

(2) R. Mills, *ibid.*, **77**, 6116 (1955).

(3) L. Onsager and R. M. Fuoss, *J. Phys. Chem.*, **36**, 2689 (1932).

concentration at which the effect becomes noticeable is undoubtedly related to the high mobilities of H^+ and OH^- ions.

Further studies would require greater control of water purity and a more refined diffusion technique to increase precision. It is of interest to speculate whether the shape of the curve in the transitional

region would give information about the cross-term coefficients which are required to describe multicomponent diffusion.

RESEARCH SCHOOL OF PHYSICAL SCIENCES
AUSTRALIAN NATIONAL UNIVERSITY
CANBERRA, A. C. T., AUSTRALIA

R. MILLS

RECEIVED NOVEMBER 9, 1962

ADDITIONS AND CORRECTIONS

1960, Vol. 64

W. A. T. Macey. The Physical Properties of Certain Organic Fluorides.

Page 254. The author wishes to note that the experimental work was largely carried out at the Woolwich Polytechnic in 1953-1957 and some work described was a part of a thesis approved for the award of the Ph.D. degree by the University of London.—W. A. T. MACEY.

1961, Vol. 65

Edward P. Egan, Jr., and Basil B. Luff. Heat of Solution of Orthophosphoric Acid.

Page 524. In column 1, 4th line from bottom, for “-2913” read “-2931”; the correct value appears in Table II.—EDWARD P. EGAN, JR.

Joshua Jortner, Rapahel Levine, Michael Ottolenghi, and Gabriel Stein. The Photochemistry of the Iodide Ion in Aqueous Solution.

Page 1233. In the legend to Fig. 1, J should be equal to 9.7×10^{-7} einstein l^{-1} sec. $^{-1}$; in Fig. 1 and 6 the unit of $[I_2]$ concentration should read 10^6 mole l^{-1} .

Page 1234. In Fig. 3 the unit of $(d[I_2]/dt)_0$ should read 10^6 mole $^{-1}$ l^{-1} sec. $^{-1}$.

Page 1237. The left side of eq. X should read $(d[I_2]/dt)_0$ instead of $d[I_2]_t/dt$. The last equation on the page should read

$$k_{11} = k_{11}^b + k_{11}^a K_e/[I^-]$$

Page 1238. The first equation on the page should read

$$k_{12} = k_{12}^b + k_{12}^a K_e/[I^-]$$

The calculation of the quantum yields and rate constant ratios presented in the paper was carried out using the correct data.—GABRIEL STEIN.

R. J. Thorn and G. H. Winslow. Correction of the Potassium Vapor Pressure Equation by Use of the Second Virial Coefficient.

Page 1297. The constant term in the equation obtained by reworking the data of Makansi, *et al.* (ref. 8 of the paper) is 4.127 rather than 4.927. The equation given for $\log p$ (total) in the Abstract is preferred over the one in the Summary.—GEORGE H. WINSLOW.

L. S. Bartell and D. Churchill. Polarimetric Determination of Absorption Spectra of Thin Films on Metal. I. Interpretation of Optical Data.

Page 2243. In eq. 5 k' should read κ' . The absorption index, κ' , is related to the absorption coefficient, k' , by $k' = n'\kappa'$. The symbol $\cos \phi$ in eq. 8 should be replaced by $\tan \phi$.

Page 2244. The constant c should read $c = (4\pi/\lambda) \sin \phi \tan \phi$.—L. S. BARTELL.

A. G. Buyers. A Study of the Rate of Isotopic Exchange for Zn^{65} in Molten Zinc-Zinc Chloride Systems at 433-681°.

Page 2256. The authors of ref. 5 should read L. E. Wallin and A. Lunden.—A. G. BUYERS.

Stuart E. Lovell and John D. Ferry. Influence of Molecular Weight Distribution of Viscoelastic Properties of Poly-

mers as Expressed by the Rouse and Zimm Theories.

Page 2275. In the second line below eq. 3, “thermal” should read “terminal.”—JOHN D. FERRY.

1962, Vol. 66

Paul H. Kasai. Electron Paramagnetic Resonance Study of Mn^{++} Ion in Polycrystalline Calcium Fluorophosphate.

Page 674. Re-examination of our original samples by X-ray proves that the figure captions given to Fig. 4 were incorrect and should be changed to (a) $CaCO_3 + MnSO_4$, (b) $Ca_2P_2O_7 + MnSO_4$, (c) $CaF_2 + MnSO_4$.

This change, of course, leads to a revision in the interpretation of the behavior of Mn^{++} ions during the reaction, as pointed out by Hickok, *et al.*¹ It also was learned that the sharp sextet observed in the spectrum (c) of Fig. 4 is due to Mn^{++} ion in CaO impurity in CaF_2 .² The author wishes to express his thanks to Drs. Hickok, Parodi, and Segelken for pointing out the mistake.

(1) R. L. Hickok, J. A. Parodi, and W. G. Segelken, *J. Phys. Chem.*, **66**, 2715 (1962).

(2) R. L. Hickok, J. A. Parodi, and W. G. Segelken, private communication.

R. C. Millikan. Non-equilibrium Soot Formation in Premixed Flames.

Page 798. My attention has kindly been directed by C. P. Fenimore to an arithmetic error in the constant terms of eq. 9, 10, and 12. In eq. 9 and 10 the constant terms should be 4.37, not 5.41 as given. In eq. 12 the constant term should read 9.54. These changes do not affect the reasoning or conclusions of the paper, for they were concerned solely with the temperature-dependent terms of these equations. However, if one wishes to go beyond that and ask what is the ratio of pre-exponential factors for the competing reactions, a reasonable answer is now obtainable from the corrected equations.—ROGER C. MILLIKAN.

Charles M. Apt, Frederick F. Margosian, Ivan Simon, Jay H. Vreeland, and Raymond M. Fuoss. Pressure Dependence of Electrolytic Conductance in Toluene.

Page 1211. Equation (1) should read

$$\Lambda c^{1/2} = \Lambda_0 K_A^{-1/2} + (\lambda_0/K_A^{1/2} k_3) c$$

RAYMOND M. FUOSS

J. B. Ott, J. R. Goates, and A. H. Budge. Solid-Liquid Phase Equilibria and Solid Compound Formation in Mixtures of Aromatic Compounds with Carbon Tetrachloride.

Page 1389. The references to the formation of a compound between CCl_4 and *p*-xylene should read 1 and 7 instead of 1 and 6. The names in ref. 7 should read C. J. Egan and R. V. Luthy.

In addition the authors failed to mention that C. J. Egan and R. V. Luthy [*Ind. Eng. Chem.*, **47**, 250 (1955)] found a 1:1 compound between CCl_4 and pseudocumene, and did not find compounds in the CCl_4 -*o*-xylene and CCl_4 -*m*-xylene systems. Our results are in agreement with this earlier work.—J. B. OTT AND J. R. GOATES.

Author Index to Volume 66, 1962

- ABRAHAMSON, E. W. See Dawson, W., 2542
- ACRIVOS, J. V., AND FITZGERALD, K. S. Temperature dependence of the Knight shift of the sodium-ammonia system. 1693
- ADACHI, G. See Uhara, I., 2691
- ADISESH, S. R. See Brown, G. H., 2426
- AGARWALA, U., ANBAR, M., AND TAUBE, H. Tracer studies on the oxidation of lead(II) by hydrogen peroxide. 1421
- AHEARN, A. J., AND THURMOND, C. D. Mass spectrographic detection of molecular species in group III-V compounds. 575
- AHLBURG, H., AND CAINES, R. Cubic cadmium sulfide. 185
- AHRENS, R. W. γ -Irradiation of aqueous solutions of Fe(II)-hydrazine. 2108
- AIKENS, D. A. See Rogers, D. W., 1582
- ALBERTY, R. A. See Erickson, L. E., 1702; Fleck, G. M., 1678
- ALBRECHT, A. C. See Kalantar, A. H., 2279; Meyer, W. C., 1168
- ALDER, B. J. See Kobatake, Y., 645
- ALEI, M. The reaction between uranium hydride and ammonia at room temperature. 145
- ALEXANDER, A. E. See Brooks, J. H., 1851; Hibberd, G. E., 1854; Tuddenham, R. F., 1839
- ALLAN, E. A., AND REEVES, L. W. The use of the chemical shift parameter for study of intramolecular hydrogen bonds. 613
- ALLEN, A. O. See Czapski, 262
- ALLEN, G. F., ROBINSON, R. A., AND BOWER, V. E. The ionization constant of *p*-nitrophenol from 0 to 60°. 171
- ALLEN, L. C., AND KARO, A. M. Electronic structure of simple molecules. 2329
- ALLEN, T. L., AND SHULL, H. Electron pairs in the beryllium atom. 2281
- ALLEY, S. K. See Andersen, D. L., 621
- ALLISON, J. B. See Scott, D. R., 561
- ALLRED, A. L. See Creswell, C. J., 1469
- ALTMAN, H. W. See Rubin, T., 266, 948
- ANBAR, M. See Agarwala, U., 1421
- ANDER, P. See Strauss, U. P., 2235
- ANDERSEN, D. L., SMITH, R. A., MYERS, D. B., ALLEY, S. K., WILLIAMSON, A. G., AND SCOTT, R. L. Thermodynamic study of the system 1-hydro-*n*-perfluoroheptane + acetone. 621
- ANDERSON, A. R. A calorimetric determination of the oxidation yield of the Fricke dosimeter at high dose rates of electrons. 180
- ANDERSON, A. R., AND HART, E. J. Radiation chemistry of water with pulsed high intensity electron beams. 70
- ANDERSON, D. K., AND BABB, A. L. Mutual diffusion in non-ideal liquid mixtures. III. Methyl ethyl ketone-carbon tetrachloride and acetic acid-carbon tetrachloride. 899
- ANDERSON, J. R., AND BAKER, B. G. The adsorption of xenon and hydrogen on evaporated films of tungsten and nickel. 482
- ANDERSON, L. L., AND KAHN, M. Arsenic(III)-arsenic(V) exchange reaction in HCl solutions. 886
- ANDERSON, N. G. The zonal ultracentrifuge. A new instrument for fractionating mixtures of particles. 1984
- ANDERSON, R. B. See Sultz, J. F., 501
- APPELMAN, E. H., AND SULLIVAN, J. C. Kinetics of the vanadium(III)-neptunium(V) reaction in perchlorate solutions. 442
- APT, C. M., MARGOSIAN, F. F., SIMON, I., VREELAND, J. H., AND FUOSS, R. M. Pressure dependence of electrolytic conductance in toluene. 1210
- ARAMATA, A., AND DELAHAY, P. Influence of the alkali metal cations on the reduction of iodate ion on mercury in alkaline solution. 2710
- ARAMATA, A. See Delahay, P., 1194, 2208
- ARCAND, G. M., AND CARROLL, W. R. Extraction of sodium thiocyanate from aqueous solutions by tributyl phosphate. 1014
- ARGERSINGER, W. J., JR. See Leifer, L., 1321
- ART, E. W. See Walsh, P. N., 1546
- ATEN, C. F., JR. See Chiltz, G., 1426
- ATKINSON, G., AND YOKOI, M. High-field conductance of polyvalent electrolytes. I. Apparatus and experimental techniques: the Wien effect in some 2-2 and 3-3 electrolytes. 1520
- ATLAS, S. M. See Schick, M. J., 1326
- AUSLOOS, P. See Rebbert, R. E., 2253
- AUSTIN, J. M., AND MAIR, A. D. The standard enthalpy of formation of complex sulfate ions in water. I. HSO_4^- , LiSO_4^- , NaSO_4^- 519
- AWAD, S. A. Poisoning effect of telluride ions on hydrogen evolution and cathodic formation of hydrogen ditelluride. 890
- BABB, A. L. See Anderson, D. K., 899
- BACHRACH, H. L. See Trautman, R., 1976
- BACK, R. A., AND MUI, J. Y. P. The reactions of active nitrogen with N^{15}O and N_2^{15} 1362
- BAES, C. F., JR. An isopiestic investigation of di-(2-ethylhexyl)-phosphoric acid (DPA) and tri-*n*-octylphosphine oxide (TPO) in *n*-octane. 1629
- BAILEY, S. D. See Kortum, G., 2439
- BAK, T. A. See Frisch, H. L., 2101
- BAKER, B. G. See Anderson, J. R., 482
- BALDWIN, R. L. See LaBar, F. E., 1952
- BANERJEE, S. See Chandra, A. K., 952
- BANKS, E. See Mayer, I. P., 693
- BARD, A. J., AND MAYELL, J. S. Secondary reactions in controlled potential coulometry. II. Secondary electrode reactions. 2173
- BARHAM, D. C. See Whittaker, A. G., 354
- BARNETT, L. See Peller, L., 680
- BARTELL, E. F. See Reitzner, B., 421
- BARTELL, L. S. See Sutula, C. L., 1010
- BARTON, H. J. See Tombalakian, A. S., 1006
- BASCOM, W. D., AND SINGLETERRY, C. R. The effect of polar-non-polar solutes on the water wettability of solid surfaces submerged in oil. 236
- BASILA, M. R. An infrared study of a silica-alumina surface. 2223
- BASILA, M. R. See Saier, E. L., 232
- BASSI, P. S. See Rastogi, R. P., 2707
- BATES, R. G. See Hetzer, H. B., 308, 1423, 2696; Wolford, R. K., 1496
- BAUER, S. H. See Chiltz, G., 1426; Tsang, W., 282
- BEAMS, J. W. See Hexner, F. E., 1948
- BEARMAN, R. J. Ratio of self-diffusion coefficients in liquid argon-krypton mixtures. 379
- BEARMAN, R. J. The polarographic diffusion coefficient. 2072
- BEATTIE, I. R., AND WEBSTER, M. The base strengths of 2,2'-bipyridyl and 1,10-phenanthroline. 115
- BEATTY, A. M. J. See Heidt, L. J., 336
- BECKER, R. S. See Scott, D. R., 2713
- BECHER, P. Non-ionic surface-active compounds. VI. Determination of critical micelle concentration by a spectral dye method. 374
- BEEVERS, R. B. The ultraviolet spectrum of polyacrylonitrile and the identification of ketene-imine structures. 1271
- BELL, J. A. See Linschitz, H., 2574
- BELL, W. E., TAGAMI, M., AND MERTEN, U. The rhodium-chlorine system at high temperature. 490
- BENNETT, L. E., AND SHEPPARD, J. C. The kinetics of the iron(II)aq-cobalt(III)aq reaction. 1275
- BERENDS, W., AND POSTHUMA, J. Energy transfer in aqueous solution. 2547
- BERG, W. T. See Scott, D. W., 911
- BERKENBLIT, M. See Reisman, A., 2210
- BERMAN, E. Photochromic spiropyrans. 2275

- BERMAN, N. S., AND MCKETTA, J. J. The thermodynamic properties of 2-butanol. 1444
- BERNETT, M. K., JARVIS, N. L., AND ZISMAN, W. A. Surface activity of fluorinated organic compounds at organic liquid-air interfaces. Part IV. Effect of structure and homology. 328
- BERNETT, M. K., AND ZISMAN, W. A. Wetting Properties of acrylic and methacrylic polymers containing fluorinated side chains. 1207
- BESTEN, I. E. D., FOX, P. G., AND SELWOOD, P. W. The mechanism of chemisorption: carbon monoxide and carbon dioxide on nickel. 450
- BEVAN, R. B., JR. See Busey, R. H., 82
- BIELSKI, B. H. J., AND SAITO, E. The activation energy for the disproportionation of the HO₂ radical in acid solutions. 2266
- BIELSKI, B. H. J. See Black, G. W., 1203
- BILLICK, I. H. The variation of the sedimentation coefficient with pressure and concentration. 565
- BILLICK, I. H. Velocity sedimentation studies on pressure and concentration dependent systems. 1941
- BIRELY, J. H., AND CHESICK, J. P. The kinetics of the thermal decomposition of [2,2,1]bicycloheptadiene. 568
- BIRNBOIM, M. H., AND DE MALLIE, R. B., JR. Viscoelastic properties of dilute polystyrene solutions and verification of the Zimm theory. 536
- BISHOP, C. A., AND TONG, L. K. J. The kinetics of the keto-enol tautomerism of benzoylacetanilide. 1034
- BISWAS, A. B. See Deo, A. V., 1361
- BLACK, G. W., AND BIELSKI, B. H. J. The radiation-induced oxidation of 4-*t*-butylpyrocatechol in aqueous solutions. 1203
- BLANDER, M. See Manning, D. L., 2069
- BLANK, M. Monolayer permeability and the properties of natural membranes. 1911
- BLATZ, L. A. The use of a cation-exchange resin to study the cerous and sulfate ion complexes. 160
- BLAUER, G., AND LINSCHITZ, H. Flash-excitation of acridine orange in acidic and basic solvents. 453
- BLOMGREN, G. E. Theories of fused salt solutions. 1500
- BLUME, H. See Schulte-Frohlinde, D., 2486
- BLYHOLDER, G., AND BOWEN, D. O. Infrared spectra of sulfur compounds absorbed on silica-supported nickel. 1288
- BLYHOLDER, G., AND NEFF, L. D. Infrared spectra of CO, CO₂, O₂, and H₂O adsorbed on silica-supported iron. 1464
- BLYHOLDER, G., AND NEFF, L. D. Infrared study of the interaction of carbon monoxide and hydrogen on silica-supported iron. 1664
- BLYHOLDER, G., AND RICHARDSON, E. A. Infrared and volumetric data on the adsorption of ammonia, water, and other gases on activated iron(III) oxide. 2597
- BODANSZKY, A., AND KAUFMANN, W. The apparent molar volume of sodium hydroxide at infinite dilution and the volume change accompanying the ionization of water. 177
- BOLEN, R. J. See Dwiggins, C. W., Jr., 574
- BOND, W. D. Thermogravimetric study of the kinetics of the reduction of cupric oxide by hydrogen. 1573
- BOROWITZ, J. L. The relative volatilities of the system H₂O¹⁷-H₂O¹⁶. 1412
- BORYTA, D. A. See Markowitz, M. M., 358, 1477
- BOSTON, C. R., AND SMITH, G. P. Spectra of dilute solutions of bismuth metal in molten bismuth trihalides. I. Evidence for two solute species in the system bismuth-bismuth trichloride. 1178
- BOTTEI, R. S., AND LAUBENGAYER, A. W. The dipole moment and magnetic susceptibility of decaborane. 1449
- BOWEN, D. O. See Blyholder, G., 1288
- BOWEN, E. J., HOLDER, N. J., AND WOODGER, G. B. Hydrogen bonding of excited states. 2491
- BOWER, V. E. See Allen, G. F., 171
- BOYD, G. E., GRAHAM, E. W., AND LARSON, Q. V. Recoil reactions with high intensity slow neutron sources. IV. The radiolysis of crystalline alkali metal bromates with γ -rays. 300
- BOYD, G. E. See Lindenbaum, S., 1383
- BOYLE, R. D. See Hexner, P. E., 1948
- BRACKETT, E. B. See Brackett, T. E., 1542
- BRACKETT, T. E., AND BRACKETT, E. B. Binding energies of the gaseous alkaline earth halides. 1542
- BRADOW, R. L. See Milligan, B., 2118
- BRADY, L. E. See Hamilton, J. F., 2384
- BRASSINE, W. F. See Larese, R. J., 897
- BRATED, R. C., AND NELSON, A. K. Molar refractions of aqueous solutions of some condensed phosphates. 377
- BRAUN, W., RAJBENBACH, L., AND EIRICH, F. R. Peroxide decomposition and cage effect. 1591
- BRAUNSTEIN, J. See Manning, D. L., 2069
- BREDIG, M. A. See Bronstein, H. R., 44; Dworkin, S., 572, 1201
- BREESE, S. S., JR. See Trautman, R., 1976
- BRICHARD, R. See Fripiat, J. J., 805
- BRIDGES, J. M., RYMER, G. T., AND MACIVER, D. S. The mechanism of potassium promotion of chromia-alumina dehydrogenation catalysts. 871
- BROCK, J. R. Investigation of a first-order slip-flow continuum analysis: the thermal force. 1763
- BRODALE, G. E., AND GIAUQUE, W. F. The freezing point-solubility curve of aqueous sodium hydroxide in the region near the anhydrous-monohydrate eutectic. 2051
- BRODALE, G. E. See Valentine, R. H., 392
- BRODERICK, E. See Sandler, S. R., 404
- BRONSTEIN, H. R., DWORKIN, A. S., AND BREDIG, M. A. The electrical conductivity of solutions of metals in their molten halides. III. Cerium-cerium trichloride. 44
- BRONSTEIN, H. R. See Dworkin, A. S., 572, 1201
- BROOKS, J. H., AND ALEXANDER, A. E. Spreading and collapse phenomena in the fatty alcohol series. 1851
- BROWN, D. W., FLORIN, R. E., AND WALL, L. A. Formation and decay of atoms and small free radicals at low temperatures. 2602
- BROWN, D. W. See Florin, R. E., 2672
- BROWN, F. C. Electronic properties and band structure of the silver halides. 2368
- BROWN, G. H., ADISESH, S. R., AND TAYLOR, J. E. Kinetic studies of phototropic reactions. I. Evidence for an ion-pair intermediate in the reaction of methyl violet with cyanide ion. 2426
- BROWN, G. H. See Venkatesetty, H. V., 2075
- BROWN, M. S. See Margerum, J. D., 2434
- BROWNE, J. C. See Matsen, F. A., 2332
- BROWNSTEIN, S., BYWATER, S., AND WORSFOLD, D. J. Proton resonance spectra and tacticity of polystyrene and deuteriopolystyrenes. 2067
- BRUCKENSTEIN, S., AND MUKHERJEE, L. M. Equilibria in ethylenediamine. II. Hydrogen electrode studies of some acids and sodium salts. 2228
- BRUNAUER, S. See Kantro, D. L., 1804
- BRUYN, DE, P. L. See Parks, G. A., 967
- BUDGE, A. H. See Ott, J. B., 1387
- BURCHARD, J. K., AND TOOR, H. L. Diffusion in an ideal mixture of three completely miscible nonelectrolytic liquids—toluene, chlorobenzene, bromobenzene. 2015
- BURKARDT, L. A. The system 2,4,6-trinitrotoluene-1,3,5-trinitrobenzene. 1196
- BURRELL, E. J., JR. The reactions of nitric oxide in irradiated cyclohexane. 401
- BURTON, M. See Mellows, F. W., 2164
- BURWELL, R. L., JR. See Newham, J., 1431, 1438
- BUTLER, W. L. See Hendricks, S. B., 2550
- BUSEY, R. H., DEARMAN, H. H., AND BEVAN, R. B., JR. The heat capacity of potassium hexachlororhenate(IV) from 7 to 320°K. Anomalies near 12, 76, 103, and 111°K. Entropy and free energy functions. Solubility and heat of solution of K₂ReCl₆. Entropy of the hexachlororhenate ion. 82
- BUYERS, A. G. The hydrolytic degradation of sodium triphosphate. 939
- BYWATER, S. See Brownstein, S., 2067
- CAFASSO, F. A., FEDER, H. M., AND JOHNSON, I. Partition of solutes between liquid metals. I. The aluminum-cadmium system. 1028
- CAHILL, J. A., AND KIRSHENBAUM, A. D. The density of liquid copper from its melting point (1356°K.) to 2500°K. and an estimate of its critical constants. 1080

- CAINES, R. See Ahlburg, H., 185
- CALLIS, J. W. See Clampitt, G. H., 201
- CALVIN, M. See Engelsma, G., 2517; Millich, F., 1070
- CANADY, W. J. See Larese, R. J., 897
- CANTOR, S., AND CARLTON, T. S. Freezing point depressions in sodium fluoride. II. Effect of tetravalent fluorides. 2711
- CARDELL, R. R., JR. See Watson, J. H. L., 1757
- CARLTON, T. S. See Cantor, S., 2711
- CARNALL, W. T., GRUEN, D. M., AND MCBETH, R. L. The near infrared transitions of the trivalent lanthanides in solution. I. Praseodymium(III), neodymium(III), samarium(III), and europium(III) ions. 2159
- CARROLL, B., AND CHEUNG, H. C. On the interaction of dyes and polysaccharides. 2585
- CARROLL, W. R. See Arcand, G. M., 1014
- CARTER, H. T. See Shereshfsky, J. L., 1846
- CARTER, J. L. See Lucchesi, P. J., 1451
- CEFOLA, M., TAYLOR, R. C., GENTILE, P. S., AND CELIANO, A. V. Coordination compounds. III. Chelate compounds of the uranyl ion with hydroxy, mercapto, and amino acids. 790
- CELIANO, A. V. Chemistry of coordination compounds. IV. Enol stability of β -diketones and the rate of formation of monoenolatocopper(II) ions. 1132
- CELIANO, A. V. See Cefola, M., 790
- CHABEREK, S. See Shepp, A., 2563
- CHADHA, S. L. See Rastogi, R. P., 2707
- CHANDRA, A. K. Ultraviolet absorption spectra of *o*-, *m*-, and *p*-nitrobenzoic acids. 562
- CHANDRA, A. K., AND BANERJEE, S. Equilibrium constant of a hydrogen bonding system: phenol-pyridine. 952
- CHANG, S.-S., AND WESTRUM, E. F., JR. Heat capacities and thermodynamic properties of globular molecules. III. Two methyl-substituted polythiaadamantanes. 524
- CHANTOONI, M. K., JR. See Kolthoff, I. M., 1675
- CHAPMAN, I. D. See Elmer, T. H., 1517
- CHEN, T.-H., AND JOHNSON, E. R. The effect of pressure on radiolysis of potassium nitrate. 2068
- CHEN, T.-H., AND JOHNSON, E. R. Mechanism of the decomposition of inorganic nitrates. 2249
- CHESICK, J. P. See Birely, J. H., 568
- CHESICK, J. J. A criticism of heat immersional wetting practice. 762
- CHESICK, J. J. See Srinivasan, G., 1819; Wightman, J. P., 1217
- CHEUNG, H. C. See Carroll, B., 2585
- CHILD, W. C., JR. See Knopp, J. A., 1513
- CHILTZ, G., ATEN, C. F., JR., AND BAUER, S. H. Rate of decomposition of azomethane in a shock tube. 1426
- CHIPMAN, J. See Gleiser, M., 1539
- CHOI, E. I. See Edwards, J. O., 1212
- CHOI, J. S., AND MOORE, W. J. Diffusion of nickel in single crystals of nickel oxide. 1308
- CHOI, Q. W. See Kolthoff, I. M., 1233
- CHOI, S. U., AND WILLARD, J. E. The radiolysis of chloro-, bromo-, and iodobenzenes with cobalt-60 γ -rays. 1041
- CHOPPIN, G. R. See Dinius, R. H., 268
- CHOW, N., AND WILSON, D. J. Intermolecular energy transfer in gas reactions. 242
- CHOWDHURY, M. Absorption maxima of some molecular complexes. 353
- CHRISTENSEN, J. J., AND IZATT, R. M. Thermodynamics of proton dissociation in dilute aqueous solution. II. Heats of proton dissociation from ribonucleotides and related compounds determined by a thermometric titration procedure. 1030
- CHRISTENSEN, J. J. See Izatt, R. M., 359
- CHRISTIAN, S. D., AND DHARMAWARDHANA, M. W. C. A new method for the determination of self-association constants of carboxylic acids in solution. 1187
- CHRISTODOYLEAS, N. D. See McGlynn, S. P., 2499
- CHU, B. See Debye, P., 1021
- CIRIC, J., AND GRAYDON, W. F. Ion-exchange membranes. IV. Univalent cation transfer rates. 1549
- CLAMPITT, G. H., AND CALLIS, J. W. Photochemical isomerization of cinnamic acid in aqueous solutions. 201
- CLARK, L. W. Comparative studies on the decarboxylation of picolinic acid and malonic acid in the molten state and in solution. 125
- CLARK, L. W. The kinetics of the decarboxylation of cinnamalmalonic acid in aromatic amines. 836
- CLARK, L. W. The kinetics of the decarboxylation of oxanilic acid in ethers and in the molten state. 1543
- CLEVER, H. L., AND REEVES, R. M. Precise measurements with glass electrodes: The activity coefficients of hydrochloric acid at 65°. 2268
- COBBLE, J. W. See McDonald, J. E., 791
- COCHRAN, C. N., AND FOSTER, L. M. The stability of silica. 380
- COCKERELL, L., AND WALTON, H. F. Metal-amine complexes in ion exchange. II. 2-Aminoethanol and ethylenediamine complexes. 75
- COETZEE, J. F., AND PADMANABHAN, G. R. Properties of bases in acetonitrile as solvent. II. The autoprotolysis constant of acetonitrile. 1708
- COETZEE, J. F. See Munev, W. S., 89
- COHEN, I., ECONOMOU, P., AND LIBACKYJ, A. Critical phenomenon in aqueous solutions of long chain quaternary ammonium salts. IV. Hyamine 1622-iodine complex systems. 1829
- COHEN, M. D., AND SCHMIDT, G. M. J. Photochromy and thermochromy of anils. 2442
- COLCLEUGH, D. W., AND GRAYDON, W. F. The kinetics of hydrogen peroxide formation during the dissolution of polycrystalline copper. 1370
- COLWELL, J. H., AND HALSEY, G. D., JR. Vapor pressure studies of sulfur trioxide and the water-sulfur trioxide system. 2179
- COLWELL, J. H., AND HALSEY, G. D., JR. The properties of α -sulfur trioxide. 2182
- CONNOLLY, J. F. Ideality of *n*-butane:isobutane solutions. 1082
- CONSTABARIS, G. See Sams, J. R., Jr., 2154
- COOK, C. M., JR. The heat of vaporization and the heat of fusion of ferric chloride. 219
- COOPER, A. R., JR., AND KINGERY, W. D. Kinetics of solution in high viscosity liquids: sodium chloride-glycerol. 665
- COOPER, W. Photovoltaic effect of silver bromide. 857
- COUCH, J. P. See Matijević, E., 111
- COUSINS, L. R. See Saier, E. L., 232
- CRABLE, G. F., AND KEARNS, G. L. Effect of substituent groups on the ionization potentials of benzenes. 436
- CRACCO, F. See Dole, M., 193
- CREETH, J. M. Studies of the transport properties of the system thallosulfate-water. II. Sedimentation coefficients at 25°; a test of the "Svedberg equation" at finite concentration. 1228
- CRESWELL, C. J., AND ALLRED, A. L. Thermodynamic constants for hydrogen bond formation in the chloroform-benzene-cyclohexane system. 1469
- CROFT, T. S., AND HANRAHAN, R. J. Iodine production in the γ -radiolysis of cyclohexane-alkyl iodide solutions. 2188
- CROSBY, G. A., WHAN, R. E., AND FREEMAN, J. J. Spectroscopic studies of rare earth chelates. 2493
- CUBICCIOTTI, D. The bismuth-sulfur phase diagram. 1205
- CUNNINGHAM, J. Radiation chemistry of ionic solids. II. Free radicals detected in irradiated potassium nitrate by electron paramagnetic resonance. 779
- CZANDERNA, A. W. See Wieder, H., 816
- CZAPSKI, G., AND ALLEN, A. O. The reducing radicals produced in water radiolysis: Solutions of oxygen-hydrogen peroxide-hydrogen ion. 262
- CZAPSKI, G., AND SCHWARZ, H. A. The nature of the reducing radical in water radiolysis. 471
- DADAPE, V. V. See Dreger, L. H., 1556
- DAHLEN, J. V. See Thompson, H. B., 1634
- DAIGRE, G. W. See McGlynn, S. P., 2499
- DANIELS, M. Photochemically-induced oxidation of arsenite: evidence for the existence of arsenic(IV). 1473
- DANIELS, M. The radiation chemistry of arsenite. Part II. Oxygen-free solution. 1475

- DANON, F., AND PITZER, K. S. Corresponding states theory for argon and xenon. 583
- DARBY, W. See Galasso, F., 131, 1318
- DAVIDSON, A. W. See Leifer, L., 1321
- DAVIES, T., GOLDSMITH, P. L., RAVENS, D. A. S., AND WARD, I. M. The kinetics of the hydrolysis of polyethylene terephthalate film. 175
- DAVIS, R. E. Displacement reactions at the sulfur atom. III. The reaction of cyanide with thiosulfate. 956
- DAWSON, L. R., VAUGHN, J. W., PRUITT, M. E., AND ECKSTROM, H. C. Solvents having high dielectric constants. X. Solutions of acetic acid and its derivatives in *N*-methylacetamide at 40°. 2684
- DAWSON, W., AND ABRAHAMSON, E. W. Population and decay of the lowest triplet state in polyenes with conjugated heteroatoms: retinene. 2542
- DAY, G. F., AND HULTGREN, R. Thermodynamics of the gold-nickel system. 1532
- DEAN, S. W., JR. See Michaels, A. S., 1790
- DEARMAN, H. H. See Busey, R. H., 82
- DEBYE, P., AND CHU, B. Spectrophotometry and light scattering on supported platinum. 1021
- DECARLO, V., AND GRIFFING, V. An SCF-LCAO-MO study of H₂⁺ and H₂. 845
- DELAHAY, P. Coulostatic method for the kinetic study of fast electrode processes. I. Theory. 2204
- DELAHAY, P., AND ARAMATA, A. Ionic association and correlation between double layer structure and electrode kinetics. 1194
- DELAHAY, P., AND ARAMATA, A. Coulostatic method for the kinetic study of fast electrode processes. II. Experimental results. 2208
- DELAHAY, P., AND MOHLNER, D. M. Rate equation for adsorption of a neutral substance at a metal-electrolyte interface. 959
- DELAHAY, P. See Aramata, A., 2710; Imai, H., 1108, 1683
- DE MALLIE, R. B., JR., BIRNBOIM, M. H., FREDERICK, J. E., TSCHOEGL, N. W., AND FERRY, J. D. Viscoelastic properties of dilute polystyrene solutions and verification of the Zimm theory. 536
- DEMARCO, J. See Markham, M. C., 932
- DEMARIA, F. See Errede, L. A., 2664
- DEO, A. V., KULKARNI, S. B., GHARPUREY, M. K., AND BISWAS, A. B. Rate of spreading and equilibrium spreading pressure of the monolayers of *n*-fatty alcohols and *n*-alkoxy ethanols. 1361
- DEUTSCH, S., AND KRIEGER, K. A. Free radicals from the decomposition of toluene and butene-1. 1569
- DEWAR, M. J. S., AND SABELLI, N. L. The split *p*-orbital (s.p.o.) method. III. Relationship to other m.o. treatments and application to benzene, butadiene, and naphthalene. 2310
- DEŽELIC, G., AND KRATOCHVIL, J. P. Influence of sodium chloride on light scattering by colloidal silica. 1377
- DHARMAWARDHANA, M. W. C. See Christian, S. D., 1187
- DI CARLO, E. N., AND SMYTH, C. P. Microwave absorption and molecular structure in liquids. XLVII. The dielectric relaxation of quinoline, isoquinoline, and several monosubstituted biphenyls in a very viscous solvent. 1105
- DI CARLO, E. N. See Horrocks, W. D., Jr., 186
- DINIUS, R. H., AND CHOPPIN, G. R. N.m.r. study of the ionization of aryl sulfonic acids. 268
- DINTZIS, F. R. See Gill, S. J., 2046
- DIORIO, A. F., MANDELKERN, L., AND LIPPINCOTT, E. R. Polymorphism in fibrous polypeptides: α - β transformation in naturally occurring keratin. 2096
- DIORIO, A. F. See Mandelkern, K., 375
- DIRAIMONDO, J. C. See McMasters, D. L., 249
- DOBIN, C. See Oster, G. K., 2511
- DOEPKER, R. D., AND MAINS, G. J. Photolysis of diethyl ketone in perfluorodimethylcyclobutane. 690
- DOLE, M., AND CRACCO, F. Radiation chemistry of polyethylene. V. Hydrogen isotope exchange studies. 193
- DORER, F. H. See Stern, J. H., 97
- DORFMAN, L. M. See Sauer, M. C., Jr., 322
- DOUGHERTY, P. H. See LaValle, J. E., 2403
- DOUSLIN, D. R. See Good, W. D., 958; Scott, D. W., 1334
- DRATZ, E. A. See Ramette, R. W., 527
- DREGER, L. H., DADAPE, V. V., AND MARGRAVE, J. L. Sublimation and decomposition studies on boron nitride and aluminum nitride. 1556
- DUBY, P. See Kellogg, H. H., 191
- DUDLEY, D. See Forster, L. S., 838
- DUECKER, H. C., AND HALLER, W. Determination of the dissociation equilibria of water by a conductance method. 225
- DUELL, P. M., AND LAMBERT, J. L. Complex structures in aqueous binary salt solutions. 1299
- DUKE, F. R., AND SHUTE, E. A. The catalytic decomposition of bromate in fused alkali nitrates. 2114
- DUNLAP, R. D., AND SCOTT, R. L. Internal pressures of perfluoro-*n*-hexane, *n*-hexane, and their mixtures. 631
- DUNLAP, R. D. See Scott, R. L., 639; Tripp, T. B., 635
- DWIGGINS, C. W., JR., AND BOLEN, R. J. Ultracentrifugal determination of the micellar character of non-ionic detergent solutions. III. 574
- DWORKIN, A. S., BRONSTEIN, H. R., AND BREDIG, M. A. Miscibility of metals with salts. VI. Lithium-lithium halide systems. 572
- DWORKIN, A. S., BRONSTEIN, H. R., AND BREDIG, M. A. The electrical conductivity of solutions of metals in their molten halides. V. Praseodymium-praseodymium trichloride. 1201
- DWORKIN, A. S. See Bronstein, H. R., 44
- DWYER, J. S. See Rosenthal, D., 2687
- DYE, J. L. See Karl, D. J., 477, 550
- DYNE, P. J. The mechanism of the unimolecular yield of hydrogen in the radiolysis of liquid cyclohexane. 767
- DZHIGIT, O. M., KISELEV, A. V., AND MUTTIK, G. G. The measurement of heats of adsorption of *n*-pentane and ether by Zeolite Type 5A by means of an isothermal constant heat exchange calorimeter. 2127
- EBERLY, P. E., JR. High temperature adsorption studies on various ion-exchanged forms of Zeolites A and X. 812
- EBERSON, L. See Thompson, H. B., 1634
- ECKSTROM, H. C. See Dawson, L. R., 2684
- ECONOMOU, P. See Cohen, I., 1829
- EDEN, C., AND FEILCHENFELD, H. The destruction of the aluminum-carbon bond in aluminum alkyls by carbon tetrachloride. 1354
- EDWARDS, J. O., IBNE-RASA, K. M., CHOI, E. I., AND RICE, C. L. Kinetic deuterium isotope effect in the nitrosation of aniline. The deuterium isotope effect on three equilibrium constants. 1212
- EDWARDS, R. K., AND VELECKIS, E. Thermodynamic properties and phase relations in the system hydrogen-hafnium. 1657
- EHRENSON, S. A closed form analysis of the LCAO-MO ω -technique. I. Ionization potentials and electron affinities. 706
- EHRENSON, S. A closed form analysis of the LCAO-MO ω -technique. II. Mechanics of the technique. 712
- EIRICH, R. F. See Braun, W., 1591; Kwei, K. P. S., 828; Schick, M. J., 1326; Schmidt, W., 1907
- ELIEZER, I. See Marcus, Y., 1661
- ELLISON, A. H. Surface pressure-area properties of organic monolayers on mercury. 1867
- ELLISON, F. O. Some applications of semi-empirical valence bond theory to small molecules. 2294
- ELMER, T. H., CHAPMAN, I. D., AND NORDBERG, M. E. Changes in length and infrared transmittance during thermal dehydration of porous glass at temperatures up to 1200°. 1517
- ELMORE, K. L. See Farr, T. D., 315
- EMMETT, P. H., LIVINGSTON, R., ZELDES, H., AND KOKES, R. J. Formation of hydrogen atoms in irradiated catalysts. 921
- ENGELHARDT, E. H. See Pohl, H. A., 2085
- ENGELSMAN, G., YAMAMOTO, A., MARKHAM, E., AND CALVIN, M. The effect of light on oxidation and reduction reactions involving phthalocyanine and etioporphyrin I manganese complexes. 2517

- ERICKSON, L. E., AND ALBERTY, R. A. Evidence from nuclear magnetic resonance for malate complexes of alkali metal cations. 1702
- ERREDE, L. A., AND DEMARIA, F. The chemistry of xylylenes. XV. The kinetics of fast flow pyrolysis of *p*-xylene. 2664
- ESTOK, G. K., AND SOOD, S. P. Electric moments from extrapolated mixed solvent data. IV. Amides and thioamides. 1372
- ESVAL, O. E., AND TYREE, S. Y., JR. The activity coefficients of ammonium perchlorate in water at 25°. 940
- EVERHARD, M. E., AND GROSS, P. M., JR. Solubilities of some strong electrolytes in the hydrogen peroxide-water system. II. Rubidium and cesium nitrates. 548
- EVERHARD, M. E., GROSS, P. M., JR., AND TURNER, J. W. Properties of electrolytes in hydrogen peroxide-water solutions. I. Solvation of alkali nitrates. 923
- EYRING, H. See Henderson, D., 1128; Woodbury, H. A., 551
- FAELENS, P. A., AND TAVERNIER, B. H. On the mechanism of the antifogging and sensitizing action of noble metal salts on photographic emulsion. 2411
- FAKTOR, M. M. Standard free energy of formation of monogermene. 1003
- FARNSWORTH, H. E. See Shooter, D., 222
- FARR, T. D., AND ELMORE, K. L. System CaO-P₂O₅-HF-H₂O: Thermodynamic properties. 315
- FARR, T. D., TARBUTTON, G., AND LEWIS, H. T., JR. System CaO-P₂O₅-HF-H₂O: Equilibrium at 25 and 50°. 318
- FATT, I. A modified diffusion time-lag. 760
- FAUCHER, J. A., AND KEGELES, G. Flotation equilibrium in the ultracentrifuge. 1945
- FEDER, H. M. See Cafasso, F. A., 1028; Velecki, E., 362; Wise, S. S., 381
- FEICHTMAYR, F. See Scheibe, G., 2449
- FEIGENBLATT, F. See Mayer, I., 1737
- FEILCHENFELD, H. See Eden, C., 1354
- FEITELSON, J. Electrostatic interactions between simple ions and highly swollen polyelectrolyte gels. Selectivity in the alkali ion series. 1295
- FELIX, D. See Henderson, D., 1128
- FERRY, G. V., AND GILL, S. J. Transference studies of sodium polyacrylate under steady-state electrolysis. 999
- FERRY, G. V. See Gill, S. J., 995
- FERRY, J. D. See De Mallie, R. B., Jr., 536; Markovitz, H., 1567; Moore, R. S., 2699; Morton, S. D., 1639
- FIELDING, W., AND PRITCHARD, E. O. The reactions of phenyl radicals in the gas phase and the carbon-hydrogen dissociation energy in benzene. 821
- FINKE, H. L. See Scott, D. W., 1334
- FISCHER, E., LAULICHT, I., AND PINCHAS, S. Dipole moment measurements of O¹⁸-labeled X=O compounds. 2708
- FISCHER, E. See Gabor, G., 2478; Heiligman-Rim, F., 2465, 2470; Malkin, S., 2432
- FISHER, F. H. The effect of pressure on the equilibrium of magnesium sulfate. 1607
- FISHER, S. See Kunin, R., 2275
- FLANAGAN, T. B. The effects of reactor irradiation on the subsequent thermal decomposition of lead styphnate. 416
- FLANAGAN, T. B., AND KIM, C. H. The effect of irradiation upon the kinetics of an endothermic solid reaction. The dehydration of manganous oxalate dihydrate. 926
- FLECK, G. M., AND ALBERTY, R. A. Kinetics of the reaction of pyridoxal and alanine. 1678
- FLEISCHER, D., AND FREISER, H. The heats of solution of nickel and copper dimethylglyoximes. 389
- FLORIN, R. E., BROWN, D. W., AND WALL, L. A. γ -Irradiation of small molecules at 4 and 77°K. 2672
- FLORIN, R. E. See Brown, D. W., 2602
- FORSLIND, E. See Svanson, S.-E., 174
- FOSTER, L. S., AND DUDLEY, D. The luminescence of fluorescein dyes. 838
- FORT, T., JR. Adsorption and boundary friction on polymer surfaces. 1136
- FOSTER, L. M. See Cochran, C. N., 380
- FOWKES, F. M. Determination of interfacial tensions, contact angles, and dispersion forces in surfaces by assuming additivity of intermolecular interactions in surfaces. 382
- FOWKES, F. M. Ideal two-dimensional solutions. II. A new isotherm for soluble and "gaseous" monolayers. 385
- FOWKES, F. M. The micelle phase of calcium dodecylphenylthale sulfonate in *n*-decane. 1843
- FOWKES, F. M. Ideal two-dimensional solutions. III. Penetration of hydrocarbons in monolayers. 1863
- FOX, P. G. See Besten, I. E. D., 450
- FOX, T. G. See Markovitz, H., 1567
- FRANKEL, S. P., AND MYSLS, K. J. On the "dimpling" during the approach of two interfaces. 190
- FREDERICK, J. E. See De Mallie, R. B., Jr., 536
- FREEMAN, J. J. See Crosby, G. A., 2493
- FREISER, H. See Fleischer, D., 389; Honaker, C. B., 127
- FREUND, H. See Varga, L. P., 21, 187
- FRIAUF, R. J. Ionic transport processes in the silver halides. 2380
- FRIEDMAN, H. L. Electrolyte solutions that unmix to form two liquid phases. Solutions in benzene and in diethyl ether. 1595
- FRIPIAT, J. J., GASTUCHE, M. C., AND BRICHARD, R. Surface heterogeneity in silica gel from kinetics of isotopic exchange OH-OD. 805
- FRIPIAT, J. J., AND UYTTERHOEVEN, J. Hydroxyl content in silica gel "aerosil". 800
- FRISCH, H. L., BAK, T. A., AND WEBSTER, E. R. Corresponding state treatment of chemical kinetic data—solvent effects. 2101
- FRISCH, H. L., AND STILLINGER, F. H. On the adsorption of polyelectrolytes at planar dielectric substrates. 823
- FROSC, C. J., AND THURMOND, C. D. The pressure of Ga₂O over gallium-Ga₂O₃ mixtures. 877
- FUJISHIRO, R., AND HILDEBRAND, J. H. The liquid-liquid solubility of cyclohexane and perfluorotributylamine at 25°. 573
- FUJITA, H., INAGAKI, H., KOTAKA, T., AND UTIYAMA, H. Application of the Archibald ultracentrifugal method for the study of dilute polymer solutions. I. Theory and some preliminary data on the system polystyrene-methyl ethyl ketone. 4
- FUJITA, H., AND MAEKAWA, E. Viscosity behavior of the system polymethyl acrylate and diethyl phthalate over the complete range of composition. 1053
- FUOSS, R. M., AND ONSAGER, L. The conductance of symmetrical electrolytes. I. Potential of total force. 1722
- FUOSS, R. M. See Apt, C. M., 1210; Kunze, R. W., 930; Lind, J. E., Jr., 1727, 1749
- GABOR, G., AND FISCHER, E. Tautomerism and geometrical isomerism in arylazophenols and naphthols. Part II. 2-Phenylazo-3-naphthol. The effect of internal hydrogen bonds on photoisomerization. Part I. 2478
- GABRYSH, A. F. See Woodbury, H. A., 551
- GALASSO, F., AND DARBY, W. Ordering of the octahedrally coordinated cation position in the perovskite structure. 131
- GALASSO, F., AND DARBY, W. Preparation, structure, and properties of K₂NbO₃F. 1318
- GALE, L. H., GORDON, B. E., STEINBERG, G., AND WAGNER, C. D. Radiolysis of toluene: Mechanism of formation of benzyl radicals. 1538
- GALLEGOS, E. J., AND KISER, R. W. Electron impact spectroscopy of the four- and five-membered, saturated heterocyclic compounds containing nitrogen, oxygen, and sulfur. 136
- GALLEGOS, E. J. See Kiser, R. W., 947
- GANT, P. L. See Yang, K., 1619
- GARVIN, D. See Gladney, H. M., 1560
- GASTUCHE, M. C. See Fripiat, J. J., 805
- GEERS, M. G. See Wosten, W. J., 1252
- GENTILE, P. S. See Cefola, M., 790
- GERSHFELD, N. L. Film penetration and adsorption. 838

- The effect of veratrine and procaine on the desorption kinetics of monolayers of mono-octadecyl phosphate. 1923
- GERSHON, A. A. See Ray, J. D., 1750
- GESKE, D. H. Evidence for the formation of biphenyl by intramolecular dimerization in the electrooxidation of tetraphenylborate ion. 1743
- GESSER, H. See Zabolotny, E. R., 408, 854
- GHARPUNEY, M. H. See Deo, A. V., 1361
- GIAQUINTO, C. See Mackham, M. C., 932
- GIAUQUE, W. F. See Brodale, G. E., 2051; Murch, L. E., 2052; Papadopoulos, M. N., 2049; Valentine, R. H., 392
- GIBERSON, R. C. Oxygen diffusion and reaction during γ -irradiation of polyethylene. 463
- GIL-AV, E., AND HERLING, J. Determination of the stability constants of complexes by gas chromatography. 1208
- GILKERSON, W. R. The dielectric constant and conductance of ion pairs: An extension of Onsager's field effect to relaxation of ion pairs in an alternating field. 669
- GILL, S. J., AND DINTZIS, F. R. Strain birefringence of a solution of rod-shaped molecules. 2046
- GILL, S. J., AND FERRY, G. V. Ion exchange kinetics of polyelectrolytes under steady-state electrolysis across a porous frit. 995
- GILL, S. J. See Ferry, G. V., 999
- GILLESPIE, T., AND WILEY, R. M. On the determination of London-van der Waals constants from suspension and emulsion viscosity and surface energy data. 1077
- GILMAN, S. A study of the adsorption of carbon monoxide and oxygen on platinum. Significance of the "polarization curve". 2657
- GLADNEY, H. M., AND GARVIN, D. Oxidation-reduction analysis of cryogenically stable products of dissociated water vapor. 1560
- GLASNER, A. See Mayer, I., 1737
- GLEDHILL, R. J. Particle-size distribution determination by turbidimetry. 458
- GLEISER, M., AND CHIPMAN, J. Free energy of formation of molybdenum oxide and carbide. 1539
- GLEMZA, R., AND KOKES, R. J. Transient species in oxygen take-up by zinc oxide. 566
- GLEW, D. N. Aqueous solubility and the gas-hydrates. The methane-water system. 605
- GOATES, J. R., SNOW, R. L., AND OTT, J. B. A test of generalized quasi-lattice theory. Calculations of thermodynamic properties of solutions of alcohols in aromatic hydrocarbons. 1301
- GOATES, J. R. See Ott, J. B., 1387
- GOLD, D. H., AND GREGOR, H. P. Metal-polyelectrolyte complexes. IX. The poly-N-ethylene-glycine-copper(II) complex. 246
- GOLDSMITH, P. L. See Davies, T., 175
- GOLUB, M. A. Intermolecular energy transfer in polyethylene-polybutadiene blends during γ -irradiation. 1202
- GONSER, U. Recoil-free γ -ray transition of Fe^{57} in blood component hemin. 564
- GOOD, W. D. The heat of formation of silica. 380
- GOOD, W. D., DOUSLIN, D. R., AND McCULLOUGH, J. P. 1,2-Bis-difluoroamino-4-methylpentane: Heats of combustion, formation, and vaporization; and vapor pressure. 958
- GOOD, W. D., LACINA, J. L., SCOTT, D. W., AND McCULLOUGH, J. P. Combustion calorimetry of organic fluorine compounds. The heats of combustion and formation of the difluorobenzenes, 4-fluorotoluene, and *m*-trifluorotoluic acid. 1529
- GOODRICH, F. C. On the damping of water waves by monomolecular films. 1858
- GOPAL, R., AND SRIVASTAVA, R. K. Studies on solutions of high dielectric constants. Part I. Partial molal volumes of some uni-univalent electrolytes in formamide at 25°. 2704
- GORDON, A. S., AND SMITH, S. R. A study of the photolysis of cyclohexane and acetone. I. Some reactions of the cyclohexyl radical. 521
- GORDON, B. E. See Gale, L. H., 1538
- GORDON, J. E. Proton magnetic resonance and infrared spectra of some ion-exchange resin-solvent systems. 1150
- GORDON, J. E., AND JOHNSON, S. L. Ionization constant of 2,2'-dihydroxybiphenyl in light and heavy water. 534
- GORING, D. A. I. See Sitaramaiah, G., 1364
- GOULD, E. S. See Hopkins, T. E., 733
- GOYA, H., WAUGH, J. L. T., AND ZEITLIN, H. The color of mercuric iodide on alumina. 1206
- GRAHAM, D. Activation of metal hydrogenation catalysts by irradiation. 510
- GRAHAM, D. Physical adsorption on low energy solids. I. Adsorption of carbon tetrafluoride, argon, and nitrogen on polytetrafluoroethylene. 1815
- GRAHAM, E. W. See Boyd, G. E., 300
- GRANTHAM, L. F., AND MOSER, H. C. Radiation induced exchange of phosphorus in the PCl_3 - POCl_3 system. 863
- GRAYDON, W. F. See Ciric, M., 1549; Colcleugh, D. W., 1370; Tombalikian, A. S., 1006
- GREENBERG, E., SETTLE, J. L., AND HUBBARD, W. N. Fluorine bomb calorimetry. IV. The heats of formation of titanium and hafnium tetrafluorides. 1345
- GREENLER, R. G. An infrared investigation of xanthate adsorption by lead sulfide. 879
- GREGOR, H. P. See Gold, D. H., 246
- GREGOR, L. V. The heat capacity of cuprous oxide from 2.8 to 21°K. 1645
- GREGORY, N. W. See Hammer, R. R., 1705
- GREYSON, J. Transfer free energies for some measurements of ion exchange membrane potentials. 2218
- GRIFFING, V. See DeCarlo, V., 845
- GROENWEGHE, L. C. D., MAIER, L., AND MOEDRITZER, K. Nuclear magnetic resonance studies of the P^{31} nucleus in phosphorus compounds. 901
- GROOT, R. C. See Vold, R. D., 1969
- GROSS, P. M., JR. See Everhard, M. E., 548, 923
- GROSSE, A. V. See McGonigal, P. J., 737
- GRUBER, H. L. Chemisorption studies on supported platinum. 48
- GRUEN, D. M., AND McBETH, R. L. Absorption spectra of the II, III, IV, and V oxidation states of vanadium in LiCl-KCl eutectic. Octahedral-tetrahedral transformations of V(II) and V(III). 57
- GRUEN, D. M. See Carnall, W. T., 2159; Ibersen, E., 65
- GULYAS, E. See Katzin, L. I., 494
- GUPTA, R. P. Study of molecular motion in some isoprenes and butadienes. 1
- GUPTA, R. P. Electron spin resonance investigation on neutron irradiated polypropylene. 849
- GÜSTEN, H. See Schulte-Frohlinde, D., 2486
- GUT, R. See Ibersen, E., 65
- GUTHRIE, G. B. See Scott, D. W., 911
- HACKERMAN, N. See Wade, W. H., 1823
- HADA, H. See Tamura, M., 559
- HALL, P. G., AND TOMPKINS, F. C. Adsorption of water vapor on potassium chloride films. 2206
- HALL, W. F. See Hildenbrand, D. L., 754
- HALL, W. K. See Leftin, H. P., 1457
- HALLER, W. See Duecker, H. C., 225
- HALSEY, G. D., JR. See Colwell, J. H., 2179, 2182; Sams, J. R., Jr., 2154
- HAMADA, H. See Uhara, I., 1374
- HAMANN, S. D. The influence of pressure on the formation of micelles in aqueous solutions of sodium dodecyl sulfate. 1359
- HAMILL, W. H. See Nash, J. R., 1097
- HAMILTON, J. F., AND BRADY, L. E. The role of mobile silver ions in latent-image formation. 2299
- HAMMER, R. R., AND GREGORY, N. W. An effusion study of the simultaneous vaporization and decomposition of solid iron(III) chloride. 1705
- HAMMOND, G. S., AND LEERMAKERS, P. A. Mechanisms of photoreactions in solution. X. Relative efficiencies of various quenchers in photoreduction of benzophenone. 1148
- HAMMOND, G. S., TURRO, N. J., AND LEERMAKERS, P. A. The mechanisms of photoreactions in solution. IX. Energy transfer from the triplet states of aldehydes and ketones to unsaturated compounds. 1144
- HANCOCK, C. K. See Rapoport, M., 1752

- HANRAHAN, R. J. See Croft, T. S., 2188
- HANSEN, R. L. The acid dissociation of γ -butyrolactam in water at 25°..... 369
- HANSEN, R. S. Thermodynamics of interfaces between condensed phases..... 410
- HANSON, R. C. Hall mobility of holes in silver bromide..... 2376
- HARDWICK, R. Kinetic studies of the thionine-iron system. II..... 349
- HARDWICK, R. See Margerum, J. D., 2434
- HARDWICK, T. J. The reactivity of hydrogen atoms in the liquid phase. II. The reaction with some organic solutes..... 117
- HARDWICK, T. J. The reactivity of hydrogen atoms in the liquid phase. III. The reactions with olefins..... 291
- HARDWICK, T. J. The radiolysis of saturated hydrocarbons..... 1611
- HARDWICK, T. J. Charge transfer in the radiolysis of organic liquids. I. Evidence from hydrogen gas yields..... 2132
- HARDWICK, T. J. The reactivity of hydrogen atoms in the liquid phase. IV. The reaction with some halogenated compounds..... 2246
- HARNED, H. S. A rule for the calculation of the activity coefficients of salts in organic solvent-water mixtures..... 589
- HARRINGTON, G. W., AND TIEN, H. T. A reference electrode for certain molten salt solutions..... 173
- HARRIS, J. See Leussing, D. L., 1544
- HARRIS, R. K. Variations in the coupling constant between C and directly-bonded fluorine..... 768
- HART, E. J. See Anderson, A. P., 70
- HASEGAWA, H. Spectroscopic studies on the color reaction of acid clay with amines. II. The reaction with aromatic tertiary amines..... 834
- HATCHARD, C. G. See Parker, C. A., 2506
- HAYASHI, S. See Tamura, M., 559
- HAYNES, J. M. Use of krypton for surface area measurements..... 182
- HEALY, T. W., AND LAMER, V. K. The adsorption-flocculation reactions of a polymer with an aqueous colloidal dispersion..... 1835
- HEER, DE, J. A refined alternant molecular orbital treatment of the ground state of benzene..... 2288
- HEICKLEN, J. See Johnston, H. S., 532
- HEIDT, L. J., MULLIN, M. G., MARTIN, W. B., JR., AND BEATTY, A. M. J. Gross and net quantum yields at 2537 Å. of ferrous to ferric in aqueous sulfuric acid and the accompanying reduction of water to gaseous hydrogen..... 336
- HEIJDE, H. B. VAN DER, AND WAGNER, C. D. Radiolysis of liquid 1,5-hexadiene..... 1746
- HEILIGMAN-RIM, R., HIRSHBERG, Y., AND FISCHER, E. Photochromism in spiropyrans. Part IV. Evidence for the existence of several forms of the colored modification..... 2465
- HEILIGMAN-RIM, R., HIRSHBERG, Y., AND FISCHER, E. Photochromism in spiropyrans. Part V. On the mechanism of phototransformation..... 2470
- HEINE, R. F. Some effects of ionizing radiation on fluorocarbon liquids..... 2116
- HELFFERICH, F. Ion-exchange kinetics. III. Experimental test of the theory of particle-diffusion controlled ion exchange..... 39
- HELLER, W., AND TABIBIAN, R. Experimental investigations on the light scattering of colloidal spheres. IV. Scattering ratio..... 2059
- HELLER, W. See Watson, J. H. L., 1757
- HENDERSON, D., EYRING, H., AND FELIX, D. The significant structure theory of liquid hydrogen in its various ortho-para and isotopic forms..... 1128
- HENDRICKS, S. B., BUTLER, W. L., AND SEGELMAN, H. W. A reversible photoreaction regulating plant growth..... 2550
- HENSHALL, T. See March, D. M., 840
- HENTZ, R. R. γ -Irradiation of isopropylbenzene..... 1622
- HENTZ, R. R. Irradiation of isopropylbenzene adsorbed on microporous silica-alumina..... 1625
- HENTZ, R. R. Isopropylbenzene conversion on pre-irradiated silica-alumina..... 2714
- HERCULES, D. M. See Surash, J. J., 1602
- HERLEY, P. J. See Prout, E. G., 961
- HERLING, J. See Gil-Av, E., 1208
- HERNDON, J. R. See Hopkins, T. E., 733
- HERRMANN, K. W. Non-ionic-cationic micellar properties of dimethyldeoxyamine oxide..... 295
- HETZER, H. B., AND BATES, R. G. Dissociation constant of 2-ammonium-2-methyl-1,3-propanediol in water from 0 to 50° and related thermodynamic quantities..... 308
- HETZER, H. B., ROBINSON, R. A., AND BATES, R. G. Standard electromotive force of the cell H₂; HBr(m), AgBr; Ag from 0 to 50°..... 1423
- HETZER, H. B., ROBINSON, R. A., AND BATES, R. G. Dissociation constant of *t*-butylammonium ion and related thermodynamic quantities from 5 to 35°..... 2696
- HEXNER, P. E., BOYLE, R. D., AND BEAMS, J. W. Molecular weight determinations with a magnetically supported ultracentrifuge..... 1948
- HIBBERD, G. E., AND ALEXANDER, A. E. Hydrogen bonding in monomolecular films: the strength of the keto-imino hydrogen bond in aqueous media..... 1854
- HICKOK, R. L., PARODI, J. A., AND SEGELKEN, W. G. Electronic paramagnetic resonance of manganous ion in calcium pyrophosphate and calcium fluoride..... 2715
- HIKINO, T. See Uhara, I., 1374
- HILDEBRAND, J. H. See Fujishiro, R., 573
- HILDEBRAND, D. L., AND HALL, W. F. The vapor pressure and heat of sublimation of gold..... 754
- HILLER, M. A. See Mackey, J. D., 311
- HINTON, J. F., AND JOHNSTON, F. J. Kinetics of chlorine exchange between chloride and ethyl chloroacetate..... 1368
- HIRAYAMA, C. The vapor pressure of germanium telluride..... 1563
- HIRSCHBERG, Y. See Heiligman-Rim, R., 2465, 2470
- HIRT, T. J., AND WIGHTMAN, J. P. Mass spectrum of carbon suboxide..... 1756
- HOBROCK, B. G., AND KISER, R. W. Electron impact spectroscopy of tetramethylgermanium, trimethylsilane, and dimethylmercury..... 155
- HOBROCK, B. G., AND KISER, R. W. Electron impact spectroscopy of propylene sulfide..... 1551
- HOBROCK, B. G., AND KISER, R. W. Electron impact spectroscopy of sulfur compounds. I. 2-Thiabutane, 2-thiapentane, and 2,3-dithiabutane..... 1648
- HOBROCK, B. G. See Kiser, R. W., 957, 1214; Shenkel, R. C., 2074
- HOBSON, M. C. See Leftin, H. P., 1214
- HOFER, L. J. E. See Shultz, J. F., 501
- HOLCOMB, D. N., AND VAN HOLDE, K. E. Ultracentrifugal and viscometric studies of the reversible thermal denaturation of ribonuclease..... 1999
- HOLDER, N. J. See Bowen, E. J., 2491
- HOLM, R. D. See Popov, A. I., 158
- HOLROYD, R. A. Ethylene as a scavenger in the radiolysis of liquid cyclopentane..... 730
- HONAKER, C. B., AND FREISER, H. Kinetics of extraction of zinc dithizonate..... 127
- HONG, J. M. Adaptation of lattice vacancy theory to gas adsorption phenomena..... 1305
- HOODLESS, I. M., AND MORRISON, J. A. Ionic transport and the crystallographic transition in cesium chloride..... 557
- HOPKINS, T. E., PASTERNAK, R. A., GOULD, E. S., AND HERNDON, J. R. X-Ray diffraction study of arsenic trisulfide-iodine glasses..... 733
- HORROCKS, W. D., JR., AND DiCARLO, E. N. The dielectric constant and loss of iron pentacarbonyl at microwave frequencies..... 186
- HOSSENLOPP, I. A. See Scott, D. W., 911, 1334
- HOTCHKISS, D. R. See Tiers, G. V. D., 560
- Hsu, R. See Wen, W., 1353
- HUBBARD, W. N. See Greenberg, E., 1345; Scott, D. W., 1334; Wise, S. S., 381
- HUGGINS, C. M. See Lupinski, J. H., 2218
- HULTGREN, R. See Day, G. F., 1532
- HUMMEL, R. L., AND RUEDENBERG, K. Electronic spectra of catcondensed and percondensed aromatic hydrocarbons..... 2334
- HUNTER, R. J. The calculation of ζ -potential from mobility measurements..... 1367
- HURST, P., SKIRROW, G., TIPPER, C. F. H., AND

- WHIM, B. P. Activation energies of gas-phase oxidations. 191
- HUTCHINSON, E. See Shinoda, K. 577
- IBERSON, E., GUT, R., AND GRUEN, D. M. The nickel chloride-cesium chloride phase diagram. Tetrahedral NiCl_4^- ion in the new compound Cs_3NiCl_5 65
- IBNE-RASA, K. M. See Edwards, J. O., 1212
- IFFT, J. B., AND VINOGRAD, J. The buoyant behavior of bovine serum mercaptalbumin in salt solutions at equilibrium in the ultracentrifuge. I. The protein concentration distribution by schlieren optics and the net hydration in CsCl solutions. 1990
- IMAI, H. Faradaic rectification and electrode processes. IV. 1744
- IMAI, H., AND DELAHAY, P. Faradaic rectification and electrode processes. III. Experimental methods for high frequencies and application to the discharge of mercurous ion. 1108
- IMAI, H., AND DELAHAY, P. Kinetics of discharge of the alkali metals on their amalgams as studied by faradaic rectification. 1683
- INAGAKI, H. See Fujita, H., 4
- INOUE, Y., AND FERRIN, D. D. Kinetics of the reversible hydration of 2-hydroxypteridine. 1689
- IRANI, R. R., AND MOEDRITZER, K. Metal complexing by phosphorus compounds. VI. Acidity constants and calcium and magnesium complexing by mono- and polymethylene diphosphonates. 1349
- ISIRIKYAN, A. A., AND KISELEV, A. V. Adsorption isotherms of nitrogen, benzene, and *n*-hexane and the heats of adsorption of benzene and *n*-hexane on graphitized carbon blacks. II. Adsorption of graphitized channel blacks. 205
- ISIRIKYAN, A. A., AND KISELEV, A. V. Adsorption isotherms of nitrogen, benzene, and *n*-hexane and the heats of adsorption of benzene and *n*-hexane on graphitized carbon blacks. III. The thermodynamic characteristics of adsorption equilibria. 210
- IZATT, R. M., AND CHRISTENSEN, J. J. Thermodynamics of proton dissociation in dilute aqueous solution. I. Equilibrium constants for the stepwise dissociation of protons from protonated adenine, adenosine, ribose-5-phosphate, and adoxinediphosphate. 359
- IZATT, R. M. See Christensen, J. J., 1030
- JACOBS, P. W. M., TOMPKINS, F. C., AND VERNEKER, V. R. P. The photochemical decomposition of barium azide. 1113
- JACOBSEN, E., AND SCHRODER, K. Polarography of some metal complexes with triethylenetetramine. 134
- JACOBSON, H. Preparation and properties of a variable charge ion-exchange membrane. 570
- JAMES, T. H. Some views on the mechanism of development. 2416
- JANSEN, P. W. J. See Spitsbergen, U., 2273
- JARNAGIN, R. C. See Thaxton, G. D., 2461
- JARVIS, N. L. See Burnett, M. K., 328
- JAYNE, J. See Leussing, D. L., 426
- JOHNSON, E. R. Effect of intensity on the radiation induced decomposition of inorganic nitrates. 755
- JOHNSON, E. R. See Chen, T.-H., 2068, 2249
- JOHNSON, H. W., JR. See Pitts, J. N., Jr., 2456
- JOHNSON, I. See Cafasso, F. A., 1028; Velecki, E., 362
- JOHNSON, J. F. See Porter, R. S., 1826
- JOHNSON, S. See Rudd, D. W., 351
- JOHNSON, S. L. See Gordon, J. E., 534
- JOHNSTON, F. J. Kinetics of chlorine exchange between chloride and chloroacetate ion. 1719
- JOHNSTON, F. J. See Hinton, J. F., 1368
- JOHNSTON, H. L. See Rubin, T., 266, 948
- JOHNSTON, H. S., AND HEICKLEN, J. Tunnelling corrections for unsymmetrical Eckart potential energy barriers. 532
- JONES, L. H. See McMasters, D. L., 249
- JORTNER, J., OTTOLENGHI, M., AND STEIN, G. Cage effects and scavenging mechanisms in the photochemistry of the iodide ion in aqueous solutions. 2029
- JORTNER, J., OTTOLENGHI, M., AND STEIN, G. The effect of nitrous oxide and the nature of intermediates in the photochemistry of the iodide ion in aqueous solution. 2037
- JORTNER, J., OTTOLENGHI, M., AND STEIN, G. The effect of oxygen on the photochemistry of the iodide ion in aqueous solutions. 2042
- JORTNER, J., AND RABANI, J. The decomposition of chloroacetic acid in aqueous solutions by atomic hydrogen. I. Comparison with radical chemical data. 2078
- JORTNER, J., AND RABANI, J. The decomposition of chloroacetic acid in aqueous solutions by atomic hydrogen. II. Reaction mechanism in alkaline solutions. 2081
- JORTNER, J., AND STEIN, G. The photochemical evolution of hydrogen from aqueous solutions of ferrous ions. Part I. The reaction mechanism at low pH. 1258
- JORTNER, J., AND STEIN, G. The photochemical evolution of hydrogen from aqueous solutions of ferrous ions. Part II. Effect of changing pH. 1264
- JORTNER, J., AND STEIN, G. Deuterium isotope effects in the photochemical evolution of hydrogen from aqueous ferrous solutions. 2200
- JOYNER, P. A. See Olsen, D. A., 883
- KAGEYAMA, Y. See Uhara, I., 1374
- KAHN, M. See Anderson, L. L., 886
- KAIL, J. A. E., SAUER, J. A., AND WOODWARD, A. E. Proton magnetic resonance of some synthetic polypeptides. 1292
- KAKIUCHI, H. See Meehan, E. J., 1238
- KALANTAR, A. H., AND ALBRECHT, A. C. Concerning the primary absorption act in a one-electron photo-oxidation in a rigid medium. 2279
- KANAAN, A. S. See Margrave, J. L., 1200
- KANDA, F. A. See Wang, F. E., 2138, 2142
- KANTRO, D. L., BRUNAUER, S., AND WEISE, C. H. Development of surface in the hydration of calcium silicates. II. Extension of investigations to earlier and later stages of hydration. 1804
- KARG, G. See Oster, G., 2514
- KARL, D. J., AND DYE, J. I. The effect of the exponential distribution function on the electrophoretic contribution to the conductance of 1-1 electrolytes. 477
- KARL, D. J., AND DYE, J. L. The transference number and activity coefficient of tris-(ethylenediamine)-cobalt(III) chloride in water at 25°. 550
- KARN, F. S. See Shultz, J. F., 501
- KARO, A. M. See Allen, L. C., 2329
- KASAI, P. H. Electron paramagnetic resonance study of Mn^{++} ion in polycrystalline calcium fluorophosphate. 674
- KATZ, J. L. See Powers, B. F., 103
- KATZIN, L. I., AND GULYAS, E. Effects of electrolytes on rotatory dispersion of aqueous tartrate solutions. 494
- KATZIN, L. I. See Schug, K., 907
- KAUFMAN, J. J. The effect of substitution on the ionization potentials of free radicals and molecules. IV. $\delta\kappa$ Values for alcohols, ethers, thiols, and sulfides. 2269
- KAUFMAN, J. V. R. See Reitzner, B., 421
- KAUZMANN, W. See Bodanszky, A., 177
- KAY, R. L. See Vidulich, G. A., 383
- KEARNS, G. L. See Crable, G. F., 436
- KEGELES, G. See Faucher, J. A., 1945; Kim, H., 1960
- KELLOGG, H. H., AND DUBY, P. An improved method of transport number measurement in pure fused salts. 191
- KELLY, P. W. See Ramette, R. W., 527
- KERKER, M. See Matijević, E., 111, 1799
- KERR, G. T. Confirmation of the nature of cation depopulation in synthetic crystalline zeolites. 2271
- KESAVULU, V., AND TAYLOR, H. A. Effect of light on hydrogen chemisorption on zinc oxide. 54
- KETELAAR, J. A. A. See Versteeg, J. M. P. J., 216
- KHAN, M. M. T., AND MARTELL, A. E. Metal chelates of adenosine triphosphate. 10
- KIM, C. H. See Flanagan, T. B., 926
- KIM, H., PATEL, B. S., AND KEGELES, G. Interference optical studies of restricted diffusion. 1960
- KING, A. J. See Wang, F. E., 2138, 2142

- KINGERY, W. D. See Copper, A. R., Jr., 665
- KIRCH, A. D., AND PORTER, G. B. Kinetics of excited molecules. III. Photooxidation of acetone. 556
- KIRSCHENBAUM, A. D. See Cahill, J. A., 1080; McGonigal, P. J., 737
- KISELEV, A. V. See Dzhigit, O. M., 2127; Isirikyan, A. A., 205, 210
- KISER, R. W., AND GALLEGOS, E. J. A technique for the rapid determination of ionization and appearance potentials. 947
- KISER, R. W., AND HOBROCK, B. G. The ionization potentials of cyclopropyl radical and cyclopropyl cyanide. 957
- KISER, R. W., AND HOBROCK, B. G. The ionization potential of hydrogen disulfide (H_2S_2). 1214
- KISER, R. W. See Gallegos, E. J., 136; Hobrock, B. G., 155, 1551, 1648; Lapp, T. W., 152, 1730; Shenkel, R. C., 2074; Wada, Y., 1652
- KISHIMOTO, S. Studies on thermoelectric force and lattice defects as active centers in metallic catalysts. 2694
- KISSINGER, L. W. See Ungnade, H. E., 2643
- KITAHARA, A., KOBAYASHI, T., AND TACHIBANA, T. Light scattering study of solvent effect on micelle formation of aerosol OT. 363
- KLEIN, E. The theory of the photographic sensitivity. 2407
- KLEIN, R., AND SCHEER, M. D. Matrix effect in the gaseous H atom-condensed olefin system; surface reaction-olefin diffusion model. 2677
- KLEPPA, O. J. Calorimetric investigations of liquid solutions of the alkaline earth nitrates in the alkali nitrates. 1668
- KLEPPA, O. J. See Powers, B. F., 103
- KLOTZ, P. See Newman, L., 2262
- KNOPP, J. A., LINNELL, W. S., AND CHILD, W. C., JR. The thermodynamics of the thermal decomposition of acid in the liquid phase. 1513
- KOBATAKE, Y., AND ALDER, B. J. Cell potentials and gas solubility theory. 645
- KOBAYASHI, T. See Itahara, A., 363
- KODAMA, M. See Miura, M., 252
- KOHN, H. W. Deuterium exchange on silica gel initiated by cobalt-60 irradiation. 1017
- KOHN, H. W. Surface carbonium ions produced by irradiating silica gel. 1185
- KOKES, R. J. The influence of chemisorption of oxygen on the electron spin resonance of zinc oxide. 99
- KOKES, R. J. See Emmett, P. H., 921; Glemza, R., 566
- KOLTHOFF, I. M., AND CHANTOONI, M. K., JR. The stability constant of the $H_2SO_4 \cdot HSO_4^-$ ion and its mobility in acetonitrile. 1675
- KOLTHOFF, I. M., MEEHAN, E. J., TSAO, M. S., AND CHOI, Q. W. Oxidation of *n*-octyl mercaptan by ferricyanide in acetone-water solution. 1233
- KOLTHOFF, I. M. See Meehan, E. J., 1238
- KORAL, M. See LuValle, J. E., 2403
- KORST, W. L. The crystal structure of $NiZrH_3$ 370
- KORTUM, G., KORTUM-SEILER, M., AND BAILEY, S. D. Optical properties of 2-(2',4'-dinitrobenzyl)-pyridine in the adsorbed state. 2439
- KORTUM-SEILER, M. See Kortum, G., 2439
- KOSKI, W. S. See Perkins, W. C., 474
- KOTA, T. See Fujita, H., 4
- KRATOCHVIL, J. P. See Dezelic, Gj., 1377
- KRAUS, D. L., AND PETROCELLI, A. W. The thermal decomposition of rubidium superoxide. 1225
- KRIEGER, K. A. See Deutsch, S., 1569
- KRISHNA PILLAI, M. G. Microwave spectrum of formaldoxime. 179
- KROGH-MOE, J. See Svanson, S.-E., 174
- KULKARNI, S. B. See Deo, A. V., 1361
- KUMMER, J. T. Ortho-para-hydrogen conversion by metal surfaces at 21°K. 1715
- KUNIN, R., AND FISHER, S. Effect of cross-linking on the properties of carboxylic polymers. II. Apparent dissociation constants as a function of the exchanging monovalent cation. 2275
- KUNZE, R. W., AND FUOSS, R. M. Conductance of the alkali halides. III. The isotopic lithium chlorides. 930
- KURZ, J. L. See Markham, M. C., 932
- KURZ, J. L. Effects of micellization on the kinetics of the hydrolysis of monoalkyl sulfates. 2239
- KUWANA, T. See Pitts, J. N., Jr., 2456
- KWEI, K. P., AND KWEI, T. K. The sorption of organic vapors by polyolefins. 2146
- KWEI, K. P. S., AND EIRICH, F. R. Chain transfer constant of vinylpyrrolidone with dextran. 828
- KWEI, T. K. See Kwei, K. P., 2146
- KYUNO, E. See Tanaka, N., 2706
- LABAR, F. E., AND BALDWIN, R. L. A study by interference optics of sedimentation in short columns. 1952
- LABOWITZ, L. C. Water-rich equilibria in the system $CH_3COONa-CH_3COOH-H_2O$ 1197
- LACINA, J. L. See Good, W. D., 1529
- LAL, K. C. See Srivastava, H. N., 1739
- LAMBERT, J. L. See Duell, P. M., 1299
- LA MER, V. K. The solubility behavior of hydroxylapatite. 973
- LA MER, V. K. See Healy, T. W., 1835
- LA PAGLIA, S. R., AND ROQUITE, B. C. The luminescence of cyclopentanone. 1739
- LAPP, T. W., AND KISER, R. W. Carbon-14-containing compounds produced by the pile neutron irradiation of cyanoguanidine. 152
- LAPP, T. W., AND KISER, R. W. Radio-carbon labeled compounds produced by the neutron irradiation of crystalline acetamide. 1730
- LARESE, R. J., ROBINSON, D. A., BRASSINE, W. F., AND CANADY, W. J. High speed stirring techniques in solubility studies: A critical appraisal and application to hippuric acid esters. 897
- LARSON, Q. V. See Boyd, G. E., 300
- LAUBENGAYER, A. W. See Bottei, R. S., 1449
- LAULICHT, I. See Fischer, E., 2708
- LAYER, H., AND SLIFKIN, L. Studies of point defects in silver chloride. 2396
- LEE, C. L., SMID, J., AND SZWARC, M. The mechanism of formation of living α -methylstyrene dimer and tetramer. 904
- LEE, E. K. C., AND ROWLAND, F. S. The reactions of recoil tritium atoms with cyclopropane platinum chloride. 2622
- LEE, W. G., AND MILLER, S. I. The secondary isotope rate effect in the iodide debromination of *sym*-tetrabromoethane and *sym*-tetrabromoethane- d_2 655
- LEERMAKERS, P. A. See Hammond, G. S., 1144, 1148
- LEFTIN, H. P., AND HALL, W. K. Electronic spectra of olefins adsorbed on silica-alumina catalysts. 1457
- LEFTIN, H. P., HOBSON, M. C., AND LEIGH, J. S. The effect of gases on the electron spin resonance spectrum of chemisorbed diphenylethylene. 1214
- LEIDER, M. See Nathans, M. W., 2012
- LEIFER, A. See Noble, W. J., 1188; LuValle, J. E., 2403
- LEIFER, I., ARGERSINGER, W. J., JR., AND DAVIDSON, A. W. Activity coefficients in mixed aqueous cadmium chloride-hydrogen chloride solutions at 25° by the electromotive force method. 1321
- LEIGH, J. S. See Leftin, H. P., 1214
- LELAND, T. W., JR. See Lunsford, J. H., 2591
- LEUSSING, D. L., HARRIS, J., AND WOOD, P. The effect of electrolytes on the solution chromatropism of bis-(*meso*-2,3-diaminobutane)-nickel(II) ions. 1544
- LEUSSING, D. L., AND JAYNE, J. Mononuclear and polynuclear complex formation between iron(II) and 2,3-dimercapto-1-propanol. 426
- LEVITT, L. S. The viscosity of liquids from the half-time of rise in a fine vertical capillary. 1748
- LEVY, J. B. The thermal decomposition of perchloric acid vapor. 1092
- LEWIS, G. P., AND RUETSCHI, P. The dependence of the electrolytic hydrogen deuterium separation factor on the electrode potential. 1487
- LEWIS, H. T., JR. See Farr, T. D., 318
- LEWIS, P. H. Perturbations of the nickel metal K X-ray absorption edge due to small crystal size and hydrogen chemisorption. 105
- LI, J. C. M. Caratheodory's principle and the

- thermokinetic potential in irreversible thermodynamics. 1414
- LIBACKYJ, A. See Cohen, I., 1829
- LIETZKE, M. H., AND STOUGHTON, R. W. The calculation of activity coefficients from osmotic coefficient data. 508
- LIETZKE, M. H., AND STOUGHTON, R. W. The thermodynamics of aqueous electrolyte mixtures at elevated temperatures. The solubility of silver sulfate in KNO_3 - K_2SO_4 , K_2SO_4 - MgSO_4 , and K_2SO_4 - H_2SO_4 mixtures. 2264
- LIFSHITZ, A., AND PERLMUTTER-HAYMAN, B. The kinetics of the hydrolysis of chlorine. III. The reaction in the presence of various bases, and a discussion of the mechanism. 701
- LIND, J. E., JR., AND FUOSS, R. M. Conductance of the alkali halides. IV. Rubidium bromide in dioxane-water mixtures. 1727
- LIND, J. E., JR., AND FUOSS, R. M. Conductance of 2-2 electrolytes with multiple charge sites. 1749
- LINDENBAUM, S., AND BOYD, G. E. Liquid amine and ion-exchange resin absorption of bromide ion from aqueous salt solutions; variation with aqueous electrolyte activities. 1383
- LINDGREN, F. T., NICHOLS, A. V., UPHAM, F. T., AND WILLS, R. D. Subfractionation of the S_i 20-10^s lipoproteins in a swinging bucket rotor. 2007
- LINDLEY, R. P. See McMasters, D. L., 249
- LINDSAY, W. T., JR. Equivalent conductance and ionic association in aqueous thallos hydroxide solutions at 25°. 1341
- LINNELL, R. H. See Wimette, H. J., 546
- LINNELL, W. S. See Knopp, J. A., 1513
- LINSCHITZ, H., STEEL, C., AND BELL, J. A. The uncatalyzed decay of anthracene and porphyrin triplets in fluid solvents. 2574
- LINSCHITZ, H. See Blauer, G., 453; Steel, C., 2577
- LIPPERT, E., AND LÜDER, W. Photochemical *cis-trans* isomerization of *p*-dimethylaminocinnamic acid nitrile. 2430
- LIPPINCOTT, E. R. See Diorio, A. F., 2096
- LIU, C. H. Electrode potentials in molten lithium sulfate-potassium sulfate eutectic. 164
- LIVINGSTON, R., AND STOCKMAN, D. A further study of the phototropy of chlorophyll in solution. 2533
- LIVINGSTON, R. See Emmett, P. H., 921
- LONG, F. A. See McDougall, A. O., 429
- LOSHAEEK, S. See Sandler, S. R., 404
- LOUGHRAN, E. D. See Ungnade, H. E., 2643
- LUBELL, M. S. See Mazelsky, R., 1408
- LUCCHESI, P. J., CARTER, J. L., AND YATES, D. J. C. An infrared study of the chemisorption of ethylene on aluminum oxide. 1451
- LÜDER, W. See Lippert, E., 2430
- LUDLUM, D. B., WARNER, R. C., AND SMITH, H. W. The diffusion of thiourea in water at 25°. 1540
- LUKENS, H. R., JR., MEISENHEIMER, R. G., AND WILSON, J. N. An isotopic exchange method for measuring the surface area of supported transition metal sulfides. 469
- LUNDELL, O. R. See Stephenson, C. C., 787
- LUNSFORD, J. H., AND LELAND, T. W., JR. Effects of neutron and ultraviolet irradiation on the catalytic activity of magnesium oxide. 2591
- LUPINSKI, J. H., AND HUGGINS, C. M. The charge transfer complex between β -carotene and iodine. I. Synthesis and optical spectra. 2221
- LUVALLE, J. E., LEIFER, A., DOUGHERTY, P. H., AND KORAL, M. Investigation of spectral sensitization. I. Some properties of sensitizing and desensitizing dyes. 2403
- LUVALLE, J. See Noble, W. J., 1188
- LUZ, Z. See Sheinblatt, M., 1535; Silver, B., 1356
- LYKOS, P. G. The present status of π -electron calculations. 2324
- MACIVER, D. S. See Bridges, J. M., 871; O'Reilly, D. E., 276
- MACKEY, J. L., HILLER, M. A., AND POWELL, J. E. Rare earth chelate stability constants of some aminopolycarboxylic acids. 311
- MACNEIL, R. See Shepp, A., 2563
- MACQUEEN, J. T. See Rice, O. K., 625
- MACZUK, J. See Schwan, H. P., 2626
- MAEKAWA, E. See Fujita, H., 1053
- MAIER, L. See Groenweghe, L. C. D., 901
- MAINS, G. J. See Doepker, R. D., 690
- MAIR, A. D. See Austin, J. M., 519
- MAKI, A. G., AND PLYLER, E. K. Formation constant of the 1:1 pyridine-iodine complex. 766
- MALCOLM, G. N., AND RITCHE, G. L. D. The thermal pressure coefficient and the entropy of melting at constant volume of polyethylene oxide. 852
- MALIK, W. U., AND SIDDIQI, F. A. Studies on the sol-gel transformation of the ferro- and ferricyanides of some metals. Part III. Gelation in chromic ferrocyanide. 356
- MALIK, W. U., AND SIDDIQI, F. A. Studies on the sol-gel transformation of the ferro- and ferricyanides of some metals. Part IV. Variation in viscosity and hydrogen ion concentration during the gelation of chromic ferrocyanide. 357
- MALKIN, S., AND FISCHER, E. Temperature dependence of photoisomerization. Part II. Quantum yields of *cis-trans* isomerization in azo compounds. 2482
- MANDELKERN, L., MEYER, W. T., AND DIORIO, A. F. Effect of monomeric reagents on the melting (contraction) and recrystallization of fibrous proteins. 375
- MANDELKERN, L. See Diorio, A. F., 2096; McIntyre, D., 1932
- MANNING, D. L., BRAUNSTEIN, J., AND BLANDER, M. Association constants of silver(I) and chloride ions in molten potassium nitrate. 2069
- MARCH, D. M., AND HENSHALL, T. The kinetics of cyclization of some 2,2'-diphenic acids in sulfuric acid. 840
- MARCUS, Y., AND ELIEZER, I. Mercury(II) halide mixed complexes in solution. V. Comparison of calculated and experimental stability constants. 1661
- MARGERUM, D. W., AND ZABIN, B. A. Coordination kinetics by ion exchange. 2214
- MARGERUM, J. D., MILLER, L. J., SAITO, E., BROWN, M. S., MOSHER, H. S., AND HARDWICK, R. Phototropism of *ortho*-nitrobenzyl derivatives. 2434
- MARGOSIAN, F. F. See Apt, C. M., 1210
- MARGRAVE, J. L. The heat of formation of $\text{BF}_3(\text{g})$ 1209
- MARGRAVE, J. L., KANAAN, A. S., AND PEASE, D. C. The heat of formation of difluorosilylene. 1200
- MARGRAVE, J. L. See Dreger, L. H., 1556; Mezaki, R., 1713; Wise, S. S., 381
- MARKHAM, E. See Engelsma, G., 2517
- MARKHAM, M. C., KURIAKOSE, J. C., DEMARCO, J., AND GIAQUINTO, C. Effects of amides on photochemical processes at zinc oxide surfaces. 932
- MARKOVITZ, H., FOX, T. G., AND FERRY, J. D. Calculations of entanglement coupling spacings in linear polymers. 1567
- MARKOWITZ, M. M., AND BORYTA, D. A. Retardation of the thermal decomposition of lithium perchlorate. 358
- MARKOWITZ, M. M., AND BORYTA, D. A. The determination of sublimation equilibria by differential thermal analysis. 1477
- MARTELL, A. E. See Khan, M. M. T., 10; Nakamoto, K., 346
- MARTIN, R. J. See Schug, J. C., 1554
- MARTIN, W. B., JR. See Heidt, L. J., 336
- MASON, E. A. See Stevens, N. J., Jr., 2613
- MATHAI, K. G., AND RABINOWITZ, E. Studies of the thionine-ferrous iron reaction in a heterogeneous system. 663
- MATHAI, K. G., AND RABINOWITZ, E. The chlorophyll-sensitized photoreduction of thionine by ascorbic acid. 954
- MATHAI, K. G. See Matijević, E., 1799
- MATHESON, R. A. The conductances of dilute aqueous cadmium perchlorate solution at 25°. 439
- MATIJEVIĆ, E., COUGH, J. P., AND KERKER, M. Detection of metal ion hydrolysis by coagulation. IV. Zinc. 111
- MATIJEVIĆ, E., MATHAI, K. G., AND KERKER, M. Detection of metal ion hydrolysis by coagulation. V. Zirconium. 1799
- MATSEN, F. A., AND BROWNE, J. C. In defense of

- the use of atomic orbital configuration wave functions for small molecules. 2332
- MAUZERALL, D. The photoreduction of uroporphyrin: Effect of pH on the reaction with EDTA. 2531
- MAYELL, J. S. See Bard, A. J., 2169
- MAYER, I., STEINBERG, M., FEIGENBLATT, F., AND GLASNER, A. The preparation of some rare earth formates and their crystal structures. 1737
- MAYER, I. P., BANKS, E., AND POST, B. Rare earth disilicides. 693
- MAYER, J. E. Heat capacity and open and closed ensemble averages. 589
- MAZELSKY, R., AND LUBELL, M. S. Solid solution study of some post-transition metal tellurides of the rock salt structural type. 1408
- MCANDREW, R., AND WHEELER, R. The recombination of atomic hydrogen in propane flame gases. 229
- MCBETH, R. L. See Carnall, W. T., 2159; Gruen, D. M., 57
- MCCARTHY, J. L. See Ratkowsky, D. A., 516
- MCCULLOUGH, J. D., AND ZIMMERMANN, I. C. Thermodynamic studies of the iodine complexes of *s*-trithiane, thiacyclohexane, and thiacyclopentane in carbon tetrachloride solution. 1198
- MCCULLOUGH, J. P. See Good, W. D., 958, 1529; Scott, D. W., 911, 1334
- MCDONALD, J. E., AND COBBLE, J. W. The heats of combustion of ReS_2 and Re_2S_7 and the thermodynamic functions for transition metal sulfides. 791
- MCDUGALL, A. O., AND LONG, F. A. Relative hydrogen bonding of deuterium. II. Acid ionization constants in H_2O and D_2O 429
- MCGLOTHLIN, R. E. See Zingaro, R. A., 2579
- MCGLYNN, S. P., REYNOLDS, M. J., DAIGRE, G. W., AND CRISTODOYLEAS, N. D. The external heavy-atom spin orbital coupling effect. III. Phosphorescence spectra and lifetimes of externally perturbed naphthalenes. 2499
- MCGONIGAL, P. J. A generalized relation between reduced density and temperature for liquids with special reference to liquid metals. 1686
- MCGONIGAL, P. J., KIRSHENBAUM, A. D., AND GROSSE, A. V. The liquid temperature range, density, and critical constants of magnesium. 737
- MCGONIGAL, P. J. See Sandler, S. R., 166
- MCINTYRE, D., WIMS, A., WILLIAMS, L. C., AND MANDELKERN, L. Conformation and frictional properties of polystyrene in dilute solutions. 1932
- MCKETTA, J. J. See Berman, N. S., 1444
- MCKINLEY, J. D. Translational energy accommodation in the nickel-chlorine surface reaction. 554
- MCMASTER, D. L., DIRAIMONDO, J. C., JONES, L. H., LINDLEY, R. P., AND ZELTMANN, E. W. The polarographic determination of the formation constant of the oxalate complexes of copper(II) and cadmium(II) in light and heavy water. 249
- MCNEAL, R. J. See Storms, E. K., 1401
- MCQUARRIE, D. A. Theory of fused salts. 1508
- MEAD, T. E. Heats of neutralization and relative strengths of amines in benzene. 2149
- MEEHAN, E. J., KOLTHOFF, I. M., AND KAKIUCHI, H. Reaction between ferricyanide and 2-mercaptoethanol. 1238
- MEEHAN, E. J. See Kolthoff, I. M., 1233
- MEISENHEIMER, R. G. See Lukeas, H. R., Jr., 469
- MELLOWS, F. W., AND BURTON, M. A kinetic study of telomer production from chloroform-ethylene mixtures initiated by cobalt-60 γ -radiation. 2164
- MERTEN, U. See Bell, W. E., 490
- MESSERLY, J. F. See Scott, D. W., 911, 1334
- METZ, F. I., SERVOS, W. C., AND WELSH, F. E. Photochromic behavior of sydnone. 2446
- MEYER, W. C., AND ALBRECHT, A. C. A quantitative study of a one-electron photooxidation in a rigid medium. 1168
- MEYER, W. K. See Rogers, M. T., 1397
- MEYER, W. T. See Mandelkern, L., 375
- MEYERS, E. A. See Rapoport, M., 1752; Zingaro, R. A., 2579
- MEYERSTEIN, D., AND TREININ, A. The relation between lyotropic and spectroscopic properties of anions in solution. 446
- MEZAKI, R., AND MARGRAVE, J. L. Thermodynamic properties of inorganic substances. IV. The high temperature heat contents of TeO_2 and Na_2TeO_4 1713
- MICHAELS, A. S., AND DEAN, S. W., JR. Contact angle relationships on silica aquagel surfaces. 1790
- MICHAELSEN, J. D. See Rice, F. O., 1535
- MILLER, J. G. See Verderame, F. D., 2185
- MILLER, L. J. See Margerum, J. D., 2434
- MILLER, S. I. Models for isotope rate effects in displacement, dissociation, elimination, and addition reactions. 978
- MILLER, S. I. See Lee, W. G., 655
- MILLICH, F., AND CALVIN, M. Coacervation of salts of polyvinylsulfonic acid as induced by heavy metal ions. 1070
- MILLIGAN, B., AND BRADOW, R. L. Photochemical interchange of halogens in aromatic compounds. II. Temperature dependence of some substituent effects. 2118
- MILLIKAN, R. C. Non-equilibrium soot formation in premixed flames. 794
- MILLS, R. The effect of the ionization of water on diffusional behavior in dilute aqueous electrolytes. 2716
- MINEO, J. See Reisman, A., 1181
- MITCHELL, J. W. Some aspects of the theory of photographic sensitivity. 2359
- MIURA, M., OTANI, S., KODAMA, M., AND SHINAGAWA, K. Effect of several phosphates on the crystallization and crystal habit of strontium sulfate. 252
- MOBERLY, W. H. Shock tube study of hydrazine decomposition. 366
- MOEDRITZER, K. See Groenweghe, L. C. D., 901; Irani, R. R., 1349
- MOHLNER, D. M. Thermodynamic treatment of the electrocapillary curve for reversible electrodes and properties of the double layer. 724
- MOHLNER, D. M. See Delahay, P., 959
- MOORE, G. E., SMITH, H. A., AND TAYLOR, E. H. Catalytic reactions on semiconductors: hydrogen-deuterium exchange and formic acid decomposition on chemically doped germanium. 1241
- MOORE, L. P. See Studier, M. H., 133
- MOORE, R. S., AND FERRY, J. D. Diffusion of radioactively tagged cetane in polyisobutylene-cetane mixtures and in three methacrylate polymers. 2699
- MOORE, W. J. See Choi, J. S., 1308
- MORIMOTO, Y. See Nakamoto, K., 346
- MORREY, J. R. Fused salt spectrophotometry. III. Isosbestic points generated by variation in temperature. 2169
- MORRISON, J. A. See Hoodless, I. M., 557
- MORTON, S. D., AND FERRY, J. D. Dynamic mechanical properties of polyvinyl chloride gels. 1639
- MOSER, H. C., AND SHORES, R. D. Reactions of tritium atoms with frozen cyclopropane. 2272
- MOSER, H. C. See Grantham, L. F., 863
- MOSHER, H. S. See Margerum, J. D., 2434
- MUI, J. Y. P. See Back, R. A., 1362
- MUKERJEE, P. The nature of the binding of counterions on charged colloids and macromolecules. 943
- MUKERJEE, P. The thermodynamics of micelle formation in association colloids. 1375
- MUKERJEE, P. The partial specific volume and the density of micelles of association colloidal electrolytes. 1733
- MUKHERJEE, L. M. See Bruckenstein, S., 2228
- MULLIKEN, R. S. π -Delocalization in butadiene and cyanogen. 2306
- MULLIN, M. G. See Heidt, L. J., 336
- MUNEY, W. S., AND COETZEE, J. F. Properties of bases in acetonitrile as solvent. I. Conductivity of nitrogen bases. 89
- MUNSON, R. A. The role of adsorption in constant current transition time studies—the hydrogen electrode. 727
- MURAMATSU, M., AND SOBOTKA, H. Molecular weight, limiting area, and flexibility of unimolecular layers of serum albumin and its derivatives. 1918
- MURCH, L. E., AND GIAUQUE, W. F. The thermodynamic properties of sodium hydroxide and its monohydrate. Heat capacities to low temperatures. Heats of solution. 2052
- MUTTIK, G. G. See Dzहित, O. M., 2127

- MYERS, D. B. See Andersen, D. L., 621
 MYSELS, K. J. See Frankel, S. P., 190
- NACHTRIEB, N. H. Magnetic susceptibility of some liquid metals, molten salts, and their solutions. 1163
 NAITO, K., AND SUZUKI, T. The mechanism of the extraction of several proton acids by tri-*n*-butyl phosphate. 983
 NAITO, K., AND SUZUKI, T. The mechanism of the extraction of several uranyl salts by tri-*n*-butyl phosphate. 989
 NAKAMOTO, K., MORIMOTO, Y., AND MARTELL, A. E. Infrared spectra of metal chelate compounds. V. Effect of substituents on the infrared spectra of metal acetylacetonates. 346
 NARTEN, A. Separation factors in the NO-NOBr system. 1189
 NASH, J. R., AND HAMILL, W. H. The effect of hydrogen iodide on the radiolysis of cyclohexane-*d*₁₂. 1097
 NATHANS, M. W., AND LEIDER, M. Studies on bismuth alloys. I. Liquidus curves of the bismuth-copper, bismuth-silver, and bismuth-gold systems. 2012
 NEFF, L. D. See Blyholder, G., 1464, 1664
 NELSON, A. K. See Brasted, R. C., 377
 NELSON, H. M. The infrared spectrum of methyl chloride in stannic chloride and antimony pentachloride solution. 1380
 NÉMETHY, G., AND SCHERAGA, H. A. The structure of water and hydrophobic bonding in proteins. III. The thermodynamic properties of hydrophobic bonds in proteins. 1773
 NEWHAM, J., AND BURWELL, R. L., JR. The hydrogenolysis of dicyclopropylmethane on platinum catalysts. 1431
 NEWHAM, J., AND BURWELL, R. L., JR. The hydrogenolysis of dicyclopropylmethane on nickel catalysts. 1438
 NEWMAN, L., AND KLOTZ, P. A secondary interaction of tri-*n*-octylamine with hydrochloric acid and thenoyltrifluoroacetone. 2262
 NICHOL, J. C. Intermittent current effects in free electrophoresis. 830
 NICHOLS, A. V. See Lindgren, F. T., 2007
 NICHOLS, E. See Shereshefsky, J. L., 1846
 NIGHTINGALE, E. R., JR. Viscosity of aqueous solutions. III. Tetramethylammonium bromide and the role of the tetraalkylammonium ions. 894
 NOBLE, LE, W. J., LUVALLE, J., AND LEIFER, A. The strength of butyric and *o*-toluic acids. 1188
 NOGUCHI, J. See Tamura, M., 559
 NORDBERG, M. E. See Elmer, T. H., 1517
 NOTLEY, N. T. Polyfunctional addition polymerization (theory and experiment). 1577
 NOYES, R. M. Some conditions for validity of statistical thermodynamic treatments of reaction kinetics. 1058
 NUMATA, Y. See Uhara, I., 1374
- ODAJIMA, A, SAUER, J. A., AND WOODWARD, A. E. Proton magnetic resonance of some normal paraffins and polyethylene. 718
 OLIVIER, J. P. See Ross, S., 696
 OLSEN, D. A., JOYNER, P. A., AND OLSON, M. D. The sliding of liquid drops on solid surfaces. 883
 OLSON, M. D. See Olsen, D. A., 883
 OLVER, J. W., AND ROSS, J. W., JR. Catalytic polarographic currents for the reduction of vanadium(III) in the presence of vanadium(IV). 1699
 ONSAGER, L. See Fuoss, R. M., 1722
 OPP, D. A. See Pohl, H. A., 2121
 O'REILLY, D. E., AND MACIVER, D. S. Electron paramagnetic resonance absorption of chromia-alumina catalysts. 276
 OSTER, G., OSTER, G. K., AND KARG, G. Extremely long-lived intermediate in photochemical reactions of dyes in non-viscous media. 2514
 OSTER, G., AND WASSERMAN, M. Photo-induced binding of fluorescein dyes to zinc oxide. 1536
 OSTER, G. See Oster, G. K., 2511
 OSTER, G. K., OSTER, G., AND DOBIN, C. Stepwise photoreversible dye systems. 2511
 OSTER, G. K. See Oster, G., 2514
- OSTERYOUNG, R. A. See Topol, L. E., 1587; Van Norman, J. D., 1565
 OTANI, S. See Miura, M., 252
 OTT, J. B., GOATES, J. R., AND BUDGE, A. H. Solid-liquid phase equilibria and solid compound formation in mixtures of aromatic compounds with carbon tetrachloride. 1387
 OTT, J. B. See Goates, J. R., 1301
 OTTOLENGHI, M. See Jortner, J., 2029, 2037, 2042
- PADMANABHAN, G. R. See Coetzee, J. F., 1708
 PAPADOPOULOS, M. N., AND GIAUQUE, W. F. The low temperature heat capacity and entropy of mercurous sulfate to 300°K. 2049
 PARFITT, G. D., AND SMITH, A. L. Conductivity of sodium dodecyl sulfate solutions below the critical micelle concentration. 942
 PARKER, C. A., AND HATCHARD, C. G. Triplet-singlet emission in fluid solution. 2506
 PARKS, G. A., AND BRUYN, DE, P. L. The zero point of charge of oxides. 967
 PARODI, J. See Hickok, R. L., 2715
 PASSCHIER, A. A. See Stern, J. H., 752
 PASTERNAK, R. A. See Hopkins, T. E., 733
 PATEL, B. S. See Kim, H., 1960
 PAUL, A. D. The chloride and bromide complexing of scandium(III) and yttrium(III) in aqueous solution. 1248
 PAULY, H. See Schwan, H. P., 2626
 PAYNE, D. H., AND WESTRUM, E. F., JR. Heat capacities and thermodynamic properties of globular molecules. IV. Pentaerythritol chloride, bromide, and iodide from 6 to 300°K. 748
 PEASE, D. C. See Margrave, J. L., 1200
 PEBLER, A., AND WALLACE, W. E. Crystal structures of some lanthanide hydrides. 148
 PELLER, L. On enzyme catalyzed equilibrium polymerizations. II. Growth on a branched chain primer and copolymerization. 685
 PELLER, L., AND BARNETT, L. On enzyme catalyzed equilibrium polymerizations. I. Linear polymers by direct reaction and through primer initiation. 680
 PERKINS, W. C., AND KOSKI, W. S. N¹⁵-labeled products from C¹²(d,n) reaction in alcohols. 474
 PERLMUTTER-HAYMAN, B. See Lifshitz, A., 701
 PERRIN, D. D. See Inoue, Y., 1689
 PETRAKIS, L. Lattice energy and stability of chromium monohalides. 433
 PETROCELLI, A. W. See Kraus, D. L., 1225
 PICKETT, L. W. See Vars, R., 1754
 PIEROTTI, R. A. Multilayers of argon and nitrogen on hexagonal boron nitride. 1810
 PINCHAS, S. See Fischer, E., 2708
 PITTS, J. N., JR., JOHNSON, H. W., JR., AND KUWANA, T. Structural effects in the photochemical processes of ketones in solution. 2456
 PITZER, K. S. See Acrivos, J. V., 1693; Danon, F., 583
 PLUMB, R. C. Oxide-coated electrodes. I. Aluminum in acid solutions. 866
 PLYLER, E. K. See Maki, A. G., 766
 POHL, H. A., AND ENGELHARDT, E. H. Synthesis and characterization of some highly conjugated semiconducting polymers. 2085
 POHL, H. A., AND OPP, D. A. The nature of semiconduction in some acene quinone radical polymers. 2121
 POHL, H. A., AND ZABUSKY, H. H. Stereospecificity and dielectric properties of polar polymers. 1390
 POPOV, A. I., AND HOLM, R. D. Electric moments of metrazole and some related tetrazoles. 158
 POPOVYCH, O. Acid-base equilibria between bromophenol blue and selected N-heterocyclics in non-aqueous solvents. 915
 PORTER, G. B. See Kirk, A. D., 556
 PORTER, R. F., AND SMITH, D. H. Heat of reaction of fluorine with graphite. 1562
 PORTER, R. S., AND JOHNSON, J. F. Orientation of nematic mesophases. 1826
 POST, B. See Mayer, I. P., 693
 POSTHUMA, J. See Berends, W., 2547
 POWELL, J. E. See Mackey, J. L., 311
 POWERS, B. F., KATZ, J. L., AND KLEPPA, O. J. The

- volume change on mixing in some binary liquid alkali nitrates. 103
- PRAUSNITZ, J. M. Solubility thermodynamics in chemical engineering. 640
- PREVORSEK, D. C. The structure of *N*-mono- and *N,N'*-disubstituted amidines. 769
- PRITCHARD, H. O. The dissociation of diatomic molecules and the recombination of atoms. 2111
- PRITCHARD, H. O. See Fielding, W., 821
- PROUT, E. G., AND HERLEY, P. J. The thermal decomposition of irradiated permanganates. 961
- PRUITT, M. E. See Dawson, L. R., 2684
- RABANI, J. On the reactivity of hydrogen atoms in aqueous solutions. 361
- RABANI, J. See Jortner, J., 2078, 2081
- RABINOWITZ, E. Reversible photochemical reactions of chlorophyll in photosynthesis. 2537
- RABINOWITZ, E. See Mathai, K. G., 663, 954
- RAJENBACH, L. See Braun, W., 1591
- RAMASUBRAMANIAN, N., AND YEDDANAPALLI, L. M. Kinetics of hydrogen chemisorption on nickel-magnesia catalysts. 1222
- RAMETTE, R. W., DRATZ, E. A., AND KELLY, P. W. Acid-base equilibria of methyl red. 527
- RANSOM, L. D. See Yosim, S. J., 28
- RAPOPORT, M., HANCOCK, C. K., AND MEYERS, E. A. Hammett correlations for the solubility of gaseous hydrogen chloride in certain aromatic systems. 1752
- RASTOGI, R. P., BASSI, P. S., AND CHADHA, S. L. Kinetics of reaction between naphthalene and picric acid in the solid state. 2707
- RATKOWSKY, D. A., AND MCCARTHY, J. L. Spectrophotometric evaluation of activity coefficients in aqueous solutions of sulfur dioxide. 516
- RAVENS, D. A. S. See Davies, T., 175
- RAY, J. D., AND GERSHON, A. A. The heat of formation of gaseous methyl nitrite. 1750
- READ, S. M. See Svrbely, W. J., 658
- REBBERT, R. E., AND AUSLOOS, P. The photolysis and radiolysis of $\text{CH}_3\text{N}_2\text{CH}_3$ and $\text{CH}_3\text{N}_2\text{CH}_3\text{-CD}_2\text{N}_2\text{CD}_3$ mixtures. 2253
- REDLICH, O. Generalized coordinates and forces. 585
- REEVES, L. W. See Allan, E. A., 613
- REEVES, R. M. See Clever, H. L., 2268
- REHFELD, S. J. Stability of emulsions to ultracentrifugation: discontinuity at the critical micelle concentration. 1966
- REID, R. C. See Stevens, N. J., Jr., 2613
- REILLEY, C. N. See Rogers, D. W., 1582
- REISMAN, A. Compound repetition in oxide systems. Solid phases in the systems $\text{Li}_2\text{O-Ta}_2\text{O}_5$ and $\text{Na}_2\text{O-Ta}_2\text{O}_5$ 15
- REISMAN, A., BERKENBLIT, M., AND WITZEN, M. Non-stoichiometry in cadmium selenide and equilibria in the system cadmium-selenium. 2210
- REISMAN, A., AND MINEO, J. Compound repetition in oxide-oxide interactions: the systems $\text{Li}_2\text{O-V}_2\text{O}_5$ 1181
- REITZNER, B., KAUFMAN, J. V. R., AND BARTELL, E. F. Thermal decomposition of silver-coated α -lead azide. 421
- REYERSON, L. H. See Solbakken, A., 365
- REYNOLDS, M. J. See McGlynn, S. P., 2499
- RICE, C. L. See Edwards, J. O., 1212
- RICE, F. O., AND MICHAELSEN, J. D. Methylene and diphenylmethylene. 1535
- RICE, O. K., AND MACQUEEN, J. T. The effect of an impurity on the phase transition in a binary liquid system. II. 625
- RICHARDSON, E. A. See Blyholder, G., 2597
- RITCHIE, G. L. D. See Malcolm, G. N., 852
- ROBERTS, R. W. Decomposition of *n*-propane and *n*-butane on clean rhodium films. 1742
- ROBERTSON, R. F. See Sitaramaiah, G., 1364
- ROBINSON, D. A. See Lares, R. J., 897
- ROBINSON, P. L. See Shereshefsky, J. L., 1846
- ROBINSON, R. A., AND STOKES, R. H. Activity coefficients of mannitol and potassium chloride in mixed aqueous solutions at 25°. 506
- ROBINSON, R. A. See Allen, G. F., 171; Hetzer, H. B., 1423, 2696
- ROGERS, D. W., AIKENS, D. A., AND REILLEY, C. N. The kinetics of exchange of copper(II) between ethylenediaminetetraacetic acid and Eriochrome Blue Black R. 1582
- ROGERS, M. T., AND MEYER, W. K. Molecular complexes of some interhalogen compounds. 1397
- ROGERS, M. T., AND WOODBREY, J. C. A proton magnetic resonance study of hindered internal rotation in some substituted *N,N*-dimethylamides. 540
- ROGERS, R. N. See Zinn, J., 2646
- ROHRER, J. C., AND SINFELT, J. H. A micro-reactor study of some reactions of C_2 hydrocarbons over alumina. 950
- ROHRER, J. C., AND SINFELT, J. H. Catalytic hydrogenolysis of benzene and toluene. 1190
- ROHRER, J. C., AND SINFELT, J. H. Interaction of hydrocarbons with $\text{Pt-Al}_2\text{O}_3$ in the presence of hydrogen and helium. 1193
- ROHRER, J. C., AND SINFELT, J. H. Catalytic isomerization of 2-pentene. 2070
- ROHRER, J. C. See Sinfelt, J. H., 1559
- ROQUITTE, B. C. See La Paglia, S. R., 1739
- ROSANO, H. L., SCHIFF, H., AND SCHULMAN, J. H. Molecular interactions between phospholipids and salts at air and liquid-liquid interfaces. 1928
- ROSENBLATT, G. M. The composition of antimony vapor. 2259
- ROSENTHAL, D., AND DWYER, J. S. Acid-base equilibria in concentrated salt solutions. I. Potentiometric measurements, indicator measurements, and uncharged bases in dilute acid solutions. 2687
- ROSS, J. W., JR. See Olver, J. W., 1699
- ROSS, S., SAELENS, J. K., AND OLIVIER, J. P. On physical adsorption. XVIII. Limiting isosteric heats of adsorption of gases on graphitized carbon by the chromatographic method. 696
- ROWLAND, F. S. See Lee, E. K. C., 2622
- RUBIN, T., JOHNSTON, H. L., AND ALTMAN, H. W. The thermal expansion of lead. 266
- RUBIN, T., JOHNSTON, H. L., AND ALTMAN, H. W. The thermal expansion of potassium chloride. 948
- RUDD, D. W., VOSE, D. W., AND JOHNSON, S. The permeability of niobium to hydrogen. 351
- RUEDENBERG, K. See Hummel, R. L., 2334
- RUETSCHI, P. See Lewis, G. P., 1487
- RYMER, G. T. See Bridges, J. M., 871
- SABELLI, N. L. See Dewar, M. J. S., 2310
- SAELENS, J. D. See Ross, S., 696
- SAIER, E. L., COUSINS, L. R., AND BASILA, M. R. The doublet nature of the aldehydic C-H stretching vibration. 232
- SAITO, E. See Bielski, B. H. J., 2266; Margerum, J. D., 2434
- SALLACH, R. A. See Yosim, S. J., 28
- SAMS, J. R., JR., CONSTABARIS, G., AND HALSEY, G. D., JR. Adsorption of argon on graphitized entropies of adsorption. 2154
- SAMUEL, A. H. Theory of radiation chemistry. V. Generalized spur diffusion model. 242
- SANDLER, S. R., LOSHAEK, S., BRODERICK, E., AND TSOU, K. C. 1,3,5-Triaryl-2-pyrazolines as wave length shifters in scintillation plastics. 404
- SANDLER, S. R., MCGONIGAL, P. J., AND TSOU, K. C. Correlation of the relative pulse height of organic scintillators with polarity and resonance effects. 166
- SATŌ, G. See Tanaka, N., 2706
- SAUER, J. A. See Odajima, A., 718
- SAUER, J. S. See Kail, J. A. E., 1292
- SAUER, M. C., JR., AND DORFMAN, L. M. The radiolysis of ethylene: Details of the formation of decomposition products. 322
- SAXENA, S. C., AND TAYLOR, T. I. Enrichment of oxygen-18 by the chemical exchange of nitric oxide with nitric acid solutions. 1480
- SCATCHARD, G. The Gibbs adsorption isotherm. 618
- SCHAEER, M. D. See Klein, R., 2677
- SCHWEIBE, G., AND FEICHTMAYER, F. The phototropy of tetrachloro-*o*-dihydro-naphthalene as a reversible photochemical reaction. 2449
- SCHERAGA, H. A. See Némethy, G., 1773
- SCHICK, M. J., ATLAS, S. M., AND EIRICH, F. R. Micellar structure of non-ionic detergents. 1326

- SCHIESER, D. W. See Tuck, L. D., 937
- SCHIFF, H. See Rosano, H. L., 1928
- SCHISSEL, P. O., AND TRUISON, O. C. Mass spectro-metric study of the vaporization of the titanium-boron system. 1492
- SCHMIDT, G. M. J. See Cohen, M. D., 2442
- SCHMIDT, J. G., AND TRIMBLE, R. F. The stability constants of the mono- and dipyrzazine-silver complexes. 1063
- SCHMIDT, W., AND EIRICH, F. R. Adsorption of a copolymer polyelectrolyte. 1907
- SCHNEIDER, W. G. Directed solute-solvent interactions in benzene solutions. 2653
- SCHRÖDER, K. See Jacobsen, E., 134
- SCHUG, J. C., AND MARTIN, R. J. Proton chemical shifts in pi complexes. 1554
- SCHUG, K., AND KATZIN, L. I. A Raman spectral study of some gallium(III) chloride systems. 907
- SCHULMAN, J. H. See Rosano, H. L., 1928
- SCHULTE-FROHLINDE, D., BLUME, H., AND GÜSTEN, H. Photochemical *cis-trans* isomerization of substituted stilbenes. 2486
- SCHWAGER, I. See Streitwieser, A., Jr., 2316
- SCHWAN, H. P., SCHWARZ, G., MACZUK, J., AND PAULY, H. On the low-frequency dielectric dispersion of colloidal particles in electrolyte solution. 2626
- SCHWARTZ, W. F. See Soulen, J. R., 2066
- SCHWARZ, G. A theory of the low-frequency dielectric dispersion of colloidal particles in electrolyte solution. 2636
- SCHWARZ, G. See Schwan, H. P., 2626
- SCHWARZ, H. A. A determination of some rate constants for radical processes in the radiation chemistry of water. 255
- SCHWARZ, H. A. See Czapski, G., 471
- SCOTT, D. R., AND ALLISON, J. B. Solvent glasses for low temperature spectroscopic studies. 561
- SCOTT, D. R., AND BECKER, R. S. Extended calculations of the electron affinities of polynuclear aromatic hydrocarbons by the LCAO-MO ω -technique. 2713
- SCOTT, D. W., DOUSLIN, D. R., FINKE, H. L., HUBBARD, W. N., MESSERLY, J. F., HOSSENLOPP, I. A., AND McCULLOUGH, J. P. 2-Methyl-2-butanethiol: chemical thermodynamic properties and rotational isomerism. 1334
- SCOTT, D. W., GUTHRIE, G. B., MESSERLY, J. F., TODD, S. S., BERG, W. T., HOSSENLOPP, I. A., AND McCULLOUGH, J. P. Toluene: Thermodynamic properties, molecular vibrations, and internal rotation. 911
- SCOTT, D. W. See Good, W. D., 1529; Waddington, G., 1074
- SCOTT, R. L., AND DUNLAP, R. D. On the determination of second virial coefficients. 639
- SCOTT, R. L. See Andersen, D. L., 621; Dunlap, R. D., 631
- SEARLES, S., JR. See Tamres, M., 1099
- SEGELKEN, W. G. See Hickok, R. L., 2715
- SELLER, B. C. See Slabaugh, W. H., 396
- SELTZER, S. See Weston, R. E., Jr., 2192
- SELWOOD, P. W. See Besten, I. E. D., 450
- SERVOSS, W. C. See Metz, F. I., 2446
- SETTLE, J. L. See Greenberg, E., 1345
- SEWARD, R. P. Hydrazinium bromide as a solvent. 1125
- SHAFFRIN, E. G., AND ZISMAN, W. A. Effect of progressive fluorination of a fatty acid on the wettability of its adsorbed monolayer. 740
- SHARMA, M. N. See Srivastava, H. M., 1739
- SHEINBLAT, M., AND LUZ, Z. Hydrogen exchange in benzyl mercaptan studied by nuclear magnetic resonance. 1535
- SHENKEL, R. C., HOBROCK, B. G., AND KISER, R. W. The ionization potential of (iso)thiocyanic acid. 2074
- SHEPP, A., CHABERER, S., AND MACNEIL, R. Thionine-sensitized photopolymerization of acrylamide. 2563
- SHEPPARD, J. C. See Bennett, L. E., 1275
- SHERESHNEFSKY, J. L., CARTER, H. T., NICHOLS, E., AND ROBINSON, P. L. Monolayers of myristyl and cetyl esters of oxalic, malonic, succinic, glutaric, adipic, and pimelic acids. 1846
- SHINAGAWA, K. See Miura, M., 252
- SHINODA, K., AND HUTCHINSON, E. Pseudo-phase separation model for thermodynamic calculations on micellar solutions. 577
- SHOOTER, D., AND FARNSWORTH, H. E. A search for hydrogen-deuterium exchange on clean germanium surfaces. 222
- SHORES, R. D. See Moser, H. C., 2272
- SHULL, H. The nature of the two-electron chemical bond. II. The heteropolar case. 2320
- SHULL, H. See Allen, T. L., 2281
- SHULTZ, J. F., HOFER, L. J. E., KARN, F. S., AND ANDERSON, R. B. Studies of the Fischer-Tropsch synthesis. Prepoisoning of iron catalysts by sulfur compounds. 501
- SHUTE, E. A. See Duke, F. R., 2114
- SIDDIQI, F. A. See Malik, W. U., 356, 357
- SIEGELMAN, H. W. See Hendricks, S. B., 2550
- SILBERBERG, A. The adsorption of flexible macromolecules. Part I. The isolated macromolecule at a plane interface. 1872
- SILBERBERG, A. The adsorption of flexible macromolecules. Part II. The shape of the adsorbed molecule; the adsorption isotherm, surface tension, and pressure. 1884
- SILVER, B., AND LUZ, Z. Oxidation of phosphorous acid. 1356
- SIMON, I. See Apt, C. M., 1210
- SINANOĞLU, O. Some aspects of the quantum theory of atoms, molecules, and their interactions. 2283
- SINFELT, J. H., AND ROHRER, J. C. Cracking of hydrocarbons over a promoted alumina catalyst. 1559
- SINFELT, J. H. See Rohrer, J. C., 950, 1190, 1193, 2070
- SINGLETERRY, C. R. See Bascom, W. D., 236
- SINISTRÌ, C. Transport numbers in pure fused salts. 1600
- SITARAMAIAH, G., ROBERTSON, R. F., AND GORING, D. A. I. Charge and configurational effects in the concentration dependence of sedimentation of sodium carboxymethylcellulose. 1364
- SKIRROW, G. See Hurst, P., 191
- SLAUBAUGH, W. H., AND SEILER, B. C. Interactions of ammonia with graphite oxide. 396
- SLICK, P. I. See Wirth, H. E., 2277
- SLIFKIN, L. See Layer, H., 2396
- SLOTH, E. N. See Studier, M. H., 133
- SMID, J. See Lee, C. L., 904
- SMITH, A. L. See Parfitt, G. D., 942
- SMITH, C. S., AND SPITZER, D. P. A simple method of measuring liquid interfacial tensions, especially at high temperatures, with measurements of the surface tension of tellurium. 946
- SMITH, D. H. See Porter, R. F., 1562
- SMITH, E. B., AND WALKLEY, J. The thermodynamic properties of gases in solution. I. The partial molal volume. 597
- SMITH, G. P. See Boston, C. R., 1178
- SMITH, H. A. See Moore, G. E., 1241
- SMITH, H. W. See Ludlum, D. B., 1540
- SMITH, J. C. See Waddington, G., 1074
- SMITH, R. A. See Andersen, D. L., 621
- SMITH, S. R. See Gordon, A. S., 521
- SMYTH, C. P. See DiCarlo, E. N., 1105
- SNOW, R. L. See Goates, J. R., 1301
- SNYDER, L. C. A simple molecular orbital study of aromatic molecules and ions having orbitally degenerate ground states. 2299
- SOBOTKA, H. See Muramatsu, M., 1918
- SOLBAKKEN, A., AND REYERSON, L. H. The chemisorption of nitric oxide by alumina gel at 0°. 365
- SOOD, S. P. See Estok, G. K., 1372
- SOULEN, J. R., AND SCHWARTZ, W. F. Infrared spectrum of nitril perchlorate. 2066
- SPITSBERGEN, U., AND JANSEN, P. W. J. High temperature disproportionation of lower vanadium oxides reacting with barium oxide. 2273
- SPITZER, D. P. Intercrystalline energies in the alkali halides. 31
- SPITZER, D. P. See Smith, C. S., 946
- SRINIVASAN, G., CHESSICK, J. J., AND ZETTMLOYER, A. C. Adsorption studies on metals. XI. Water on *n*-type germanium powders. 1819
- SRIVASTAVA, H. N., LAL, K. C., AND SHARMA, M. N.

- Relaxation times and "averaged mutual viscosities" of some aliphatic ketones. 1739
- SRIVASTAVA, R. K. See Gopal, R., 2704
- STEEL, C., AND LINSCHITZ, H. The catalysis of anthracene triplet decay by copper complexes. 2577
- STEEL, C. See Linschitz, H., 2574
- STEGMEYER, H. On the mechanism of photochemical *cis-trans* isomerization. 2555
- STEIN, G. See Jortner, J., 1258, 1264, 2029, 2037, 2042, 2200
- STEIN, L. Heats of formation of bromine fluorides. 288
- STEINBERG, G. See Gale, L. H., 1538
- STEINBERG, M. See Mayer, I., 1737
- STEPHENSON, C. C., AND LUNDELL, O. R. The heat capacity of diammonium dicadmium sulfate from 15 to 300°K. 787
- STERN, J. H., AND DORER, F. H. Standard heats of formation of 2,2-dimethoxypropane (I), and 2,2-diethoxypropane (I). Group additivity theory and calculated heats of formation of five ketals. 97
- STERN, J. H., AND PASSCHLER, A. A. The heats of formation of triiodide and iodate ions. 752
- STERN, K. H. Oxidation of metals in molten salts. Silver in sodium chloride. 1311
- STEVENS, N. J., JR., MASON, E. A., AND REID, R. C. The effect of electron irradiation prior to reaction on the activity of a semiconductor catalyst. 2613
- STEWART, A. C. See Wolf, C. J., 1119
- STILLINGER, F. H. See Frisch, H. L., 823
- STOCKMAN, D. See Livingston, R., 2533
- STOKES, R. H. See Robinson, R. A., 506
- STORMS, E. K., AND MCNEAL, R. J. The vanadium-vanadium carbide system. 1401
- STOUGHTON, R. W. See Lietzke, M. H., 508, 2264
- STRAUSS, U. P., AND ANDER, P. Molecular dimensions and interactions of lithium polyphosphate in aqueous lithium bromide solutions. 2235
- STREITWIESER, A., JR. A molecular orbital study of the effect of methyl groups on ionization potentials. 368
- STREITWIESER, A., JR., AND SCHWAGER, I. A molecular orbital study of the polarographic reduction in dimethylformamide of unsubstituted and methyl-substituted aromatic hydrocarbons. 2316
- STRONG, R. L. The presence of transient charge-transfer complexes in halogen atom recombination and photohalogenation processes. 2423
- STUDIER, M. H. Gaseous oxides of rhenium. 189
- STUDIER, M. H., SLOTH, E. N., AND MOORE, L. P. The chemistry of uranium in surface ionization sources. 133
- SULLIVAN, J. C. See Appleman, E. H., 442; Zielen, A. J., 1065
- SUNDHEIM, B. R. See Windwer, S., 1254
- SURASH, J. J., AND HERCULES, D. M. Studies on photo-induced electrode potentials. 1602
- SURYANARAYANA, M. Ultrasonic determination of reaction rates in magnesium sulfate and manganese sulfate solutions. 360
- SURYARAMAN, M. G., AND WALTON, H. F. Metal-amine complexes in ion exchange. III. Diamine complexes of silver(I) and nickel(II). 78
- SUTULA, C. L., AND BARTELL, L. S. Structure and molecular orientation in multimolecular films of long-chain *n*-hydrocarbon derivatives. 1010
- SUZUKI, T. See Naito, K., 983, 989
- SVANSON, S.-E., FORSLIND, E., AND KROGH-MOE, J. Nuclear magnetic resonance study of boron coordination in potassium borate glasses. 174
- SVIRBELY, W. J., AND READ, S. M. The thermodynamic properties of liquid ternary zinc, indium, and gallium solutions. 658
- SZWARC, M. See Lee, C. L., 904
- TABIBIAN, R. See Heller, W., 2059
- TACHIBANA, T. See Kobayashi, T., 363
- TAGAMI, M. See Bell, W. E., 490
- TAMAMUSHI, R. See Tanaka, N., 2706
- TAMRES, M., AND SEARLES, S., JR. The iodine complexes of some saturated cyclic sulfides. 1099
- TAMURA, M., HADA, H., NOGUCHI, J., AND HAYASHI, S. Infrared spectra of some photographic stabilizers absorbed on silver bromide. 550
- TANAKA, N., KYUNO, E., SATO, G., AND TAMAMUSHI, R. Specific adsorption of isothiocyanatochromium(III) complex ions at the mercury-aqueous solution interface. 2706
- TANI, K. See Uhara, I., 2691
- TARBUTTON, G. See Farr, T. D., 318
- TAUBE, H. See Agarwala, U., 1421
- TAVERNIER, B. H. See Faelens, P. A., 2411
- TAYLOR, E. H. See Moore, G. E., 1241
- TAYLOR, H. A. See Kesavulu, V., 54
- TAYLOR, J. E. See Brown, G. H., 2426
- TAYLOR, R. C. See Cefola, M., 790
- TAYLOR, T. I. See Saxena, S. C., 1480
- TERATANI, S. See Uhara, I., 2691
- THARP, A. G. The structure of lanthanum family silicides. 758
- THAXTON, G. D., AND JARNAGIN, R. C. Band structure and transport of holes and electrons in homologs of anthracene. 2461
- THOMPSON, H. B., EBERSON, L., AND DAHLEN, J. V. Electric moments of substituted succinic acids. The low electric moment of succinic acid. 1634
- THORP, J. M. The dielectric behavior of vapors adsorbed on porous solids. 1086
- THURMOND, C. D. See Ahearn, A. J., 575; Frosch, C. J., 877
- TIEN, H. T. See Harrington, G. W., 173
- TIERS, G. V. D. Fluorine n.m.r. spectroscopy. VI. Fluorocarbon sulfides. 764
- TIERS, G. V. D. Fluorine n.m.r. spectroscopy. VIII. Coupling constants in normal and isotopic C₂F₈. 945
- TIERS, G. V. D. Fluorine nuclear magnetic resonance spectroscopy. IX. *cis*- and *trans*-2-chloroheptafluorobutene-2. The assignment of shielding values and spin-spin coupling constants in fluorolefin spectra. 1192
- TIERS, G. V. D., AND HOTCHKISS, D. R. Proton n.m.r. spectroscopy. XIV. Accurate measurement of the spectral position of the formyl peak of *p*-anisaldehyde, useful for checking the calibration of n.m.r. spectrometers. 560
- TIPPER, C. F. H. See Hurst, P., 191
- TOBY, S., AND WEISS, B. H. The photolysis of azomethane at higher pressures: a second ethane-producing reaction. 2681
- TODD, S. S. See Scott, D. W., 911
- TOENISKOETTER, R. H. See Wolf, C. J., 1526
- TOMBALAKIAN, A. S., BARTON, H. J., AND GRAYDON, W. F. Electroosmotic water transport across ion-exchange membranes. 1006
- TOMPKINS, F. C. See Hall, P. G., 2260; Jacobs, P. W. M., 1113
- TONG, L. K. J. See Bishop, C. A., 1034
- TOOR, H. L. See Burchard, J. K., 2015
- TOPOL, L. E., AND OSTERYOUNG, R. A. Electromotive force, polarographic, and chronopotentiometric studies in molten bismuth-bismuth tribromide solutions. 1587
- TOPOL, L. E. See Yosim, S. J., 28
- TRAUTMAN, R., BREESE, S. S., JR., AND BACHRACH, H. L. Preparative ultracentrifugation of foot-and-mouth disease virus through immiscible fluid interfaces into a cesium chloride density gradient. 1976
- TREININ, A. See Meyerstein, D., 446
- TRIMBLE, R. F. See Schmidt, J. G., 1063
- TRIPP, L. A. See Vars, R., 1754
- TRIPP, T. B., AND DUNLAP, R. D. Second virial coefficients for the systems: *n*-butane + perfluoro-*n*-butane and dimethyl ether + 1-hydroperfluoropropane. 635
- TRULSON, O. C. See Schissel, P. O., 1492
- TSANG, W., BAUER, S. H., AND WAELEBROECK, F. Kinetics of the production of C₂ during the pyrolysis of ethylene. 282
- TSAO, M. S. See Kolthoff, I. M., 1233
- TSCHOEGL, N. W. See De Mallie, R. B., Jr., 536
- TSCHUIKOW-ROUX, E. Thermodynamic properties of nitril fluoride. 1636
- TSOU, K. C. See Sandler, S. R., 166, 404
- TUCK, L. D., AND SCHIESER, D. W. Electron spin resonance of some nitrogen-containing aromatic free radicals. 937
- TUDDENHAM, R. F., AND ALEXANDER, A. E. The

- effect of pressure on micelle formation in soap solutions.....
- TURNBULL, D. On the relation between crystallization rate and liquid structure..... 609
- TURNER, J. W. See Everhard, M. E., 923
- TURRO, N. J. See Hammond, G. S., 1144
- TUUL, J. A. A study of adsorption of various gases at 300°K..... 1736
- TYREE, S. Y., JR. See Esvál, O. E., 940
- UHARA, I., HIKINO, T., NUMATA, Y., HAMADA, H., AND KAGEYAMA, Y. The structure of active centers in nickel catalyst..... 1374
- UHARA, I., YANAGIMOTO, S., TANI, K., ADACHI, G., AND TERATANI, S. The structure of active centers in copper catalyst..... 2691
- UNGNÄDE, H. E., LOUGHRAN, E. D., AND KISSINGER, L. W. Hydrogen bonding in β -nitrol alcohols. II. Association in solution..... 2643
- UPHAM, F. T. See Lindgren, F. T., 2007
- UTYAMA, H. See Fujita, H., 4
- UYTTERHOEVEN, J. See Fripiat, J. J., 800
- VALENTINE, R. H., BRODALE, G. E., AND GIAUQUE, W. F. Trifluoromethane: entropy, low temperature heat capacity, heats of fusion and vaporization, and vapor pressure..... 392
- VAN HOLDE, K. E. See Holcomb, D. N., 1999
- VAN NORMAN, J. D., AND OSTERYOUING, R. A. A spectrophotometric method for determination of formation constants of lead halide complexes in fused sodium nitrate-potassium nitrate..... 1565
- VARGA, L. P., AND FREUND, H. The formation constants of the tantalum fluoride system. I. Potentiometric and anion exchange studies—evidence for species of coordination number nine..... 21
- VARGA, L. P., AND FREUND, H. The formation constants of the tantalum fluoride system. II. Tantalum electrode potential studies..... 187
- VARS, R., TRIPP, L. A., AND PICKETT, L. W. Molecular complexes of tetracyanoethylene with tetrahydrofuran, tetrahydropyran, and *p*-dioxane..... 1754
- VAUGHN, J. W. See Dawson, L. R., 2684
- VELECKIS, E., FEDER, H. M., AND JOHNSON, I. Decomposition pressure of UCl_{11} 362
- VELECKIS, E. See Edwards, R. K., 1657
- VENKATASETTY, H. V., AND BROWN, G. A study of the conductance behavior of lithium and ammonium iodides in *n*-butanol..... 2075
- VERDERAME, F. D., AND MILLER, J. G. The electric moments of organic peroxides. III. Peresters..... 2185
- VERNEKER, V. R. P. See Jacobs, P. W. M., 1113
- VERSTEGEN, J. M. P. J., AND KETELAAR, J. A. A. The distribution of sulfuric acid between water and kerosene solutions of tri-*n*-octylamine and tri-*n*-hexylamine..... 216
- VIDULICH, G. A., AND KAY, R. L. The dielectric constants of water between 0° and 40°..... 383
- VINOGRAD, J. See Ifft, J. B., 1990
- VOEKS, J. F. Concerning a so-called check on the initial deviation from Newtonian flow of polymer solutions..... 176
- VOET, A. The dielectric constant of emulsions of the water-in-oil type..... 2259
- VOLD, R. D., AND GROOT, R. C. An ultracentrifugal method for the quantitative determination of emulsion stability..... 1969
- VOSE, D. W. See Rudd, D. W., 351
- VREELAND, J. H. See Apt, C. M., 1210
- WADA, Y., AND KISER, R. W. Electron impact spectroscopy of some substituted oxiranes..... 1652
- WADDINGTON, G., SMITH, J. C., WILLIAMSON, K. D., AND SCOTT, D. W. Carbon disulfide as a reference substance for vapor-flow calorimetry; the chemical thermodynamic properties..... 1074
- WADE, W. H., AND HACKERMAN, N. Heats of immersion. VII. The immersion of silica, alumina, and titania in hexane—variation with particle size and outgassing temperature..... 1823
- WÄELBROECK, F. See Tsang, W., 282
- WAGNER, C. D. Radiation-polymerization of ethylene: evidence for ion-molecule condensation..... 1158
- WAGNER, C. D. See Gale, L. H., 1538; Heijde, H. B. van der, 1746
- WALEM, M. Particle size distribution in rubber latex..... 1768
- WALKLEY, J. See Smith, E. B., 597
- WALL, L. A. See Brown, D. W., 2602; Florin, R. E., 2672
- WALLACE, W. E. See Pebler, A., 148
- WALSH, P. N., ART, E. W., AND WHITE, D. The heat capacity of the silver chalcogenides, $Ag_{1.99}S$, $Ag_{1.99}Se$, and $Ag_{1.98}Te$ from 16 to 300°K..... 1546
- WALTON, H. F. See Cockerell, L., 75; Suryaraman, M. G., 78
- WANG, F. E., KANDA, F. A., AND KING, A. J. The lithium-strontium equilibrium system..... 2138
- WANG, F. E., KING, A. J., AND KANDA, F. A. The crystal structure of Sr_2Li_{23} and Sr_3Li_2 2142
- WARD, I. M. See Davies, T., 175
- WARE, W. R. Oxygen quenching of fluorescence in solution: An experimental study of the diffusion process..... 455
- WARNER, R. C. See Ludlum, D. B., 1540
- WASSERMAN, M. See Oster, G., 1536
- WATSON, J. H. L., CARDELL, R. R., JR., AND HELLER, B. The internal structure of colloidal crystals of β -FeOOH and remarks on their assemblies in Schiller layers..... 1757
- WAUGH, J. L. T. See Goya, H., 1206
- WEBSTER, E. R. See Frisch, H. L., 2101
- WEBSTER, M. See Beattie, I. R., 115
- WEISE, C. H. See Kantro, D. L., 1804
- WEISS, B. H. See Toby, S., 2681
- WELLINGTON, C. A. The thermal isomerization of vinylcyclopropane..... 1671
- WELSH, F. E. See Metz, F. I., 2446
- WEN, W., AND HSU, R. Effect of dimerization upon the α -phosphorescence of acriflavine in glucose glass..... 1353
- WENDT, R. P. Studies of isothermal diffusion at 25° in the system water-sodium sulfate-sulfuric acid and tests of the Onsager relation..... 1279
- WENDT, R. P. The density gradient and gravitational stability during free diffusion in three-component systems..... 1740
- WEST, W. Some recent trends in the theory of spectral sensitization..... 2398
- WESTON, R. E., JR., AND SELTZER, S. The secondary deuterium isotope effect in the pyrolysis of dimethylmercury..... 2192
- WESTRUM, E. F., JR. See Chang, S.-S., 524; Payne, D. H., 748
- WETTERMARK, G. Light-induced isomerization of *o*-nitrotoluene in water solution..... 2560
- WHALEN, J. W. Heats of immersion. II. Silica-benzene and silica-cyclohexane..... 511
- WHAN, R. E. See Crosby, G. A., 2493
- WHEELER, R. See McAndrew, R., 229
- WHIM, B. P. See Hurst, P., 191
- WHITE, D. See Walsh, P. N., 1546
- WHITTAKER, A. G., AND BARHAM, D. C. A phase diagram study of the system ammonium nitrate-ammonium perchlorate..... 354
- WIEDER, H., AND CZANDERNA, A. W. The oxidation of copper films to $CuO_{0.67}$ 816
- WIGHTMAN, J. P., AND CHESSICK, J. J. Non-soap greases. V. The influence of *n*-heptyl derivatives on silica-non-polar liquid gel stability..... 1217
- WIGHTMAN, J. P. See Hirt, T. J., 1756
- WILEY, R. M. See Gillespie, T., 1077
- WILKINSON, F. Transfer of triplet state energy and the chemistry of excited states..... 2569
- WILLARD, J. E. See Choi, S. U., 1041; Young, A. H., 271
- WILLIAMS, L. C. See McIntyre, D., 1932
- WILLIAMS, R. R., JR. Low energy electron irradiation of methane..... 372
- WILLIAMSON, A. G. See Andersen, D. L., 621
- WILLIAMSON, K. D. See Waddington, G., 1074
- WILLS, R. D. See Linden, F. T., 2007
- WILSON, A. S., AND WOGMAN, N. A. The affinity of hydrohalic acids for tri-*n*-octylamine..... 1552
- WILSON, D. J. See Chow, N., 342
- WILSON, J. N. See Lukens, H. R., Jr., 469
- WIMETTE, H. J., AND LINNELL, R. H. Thermodynamics of H-bonding pyrrole-pyridines..... 546

- WIMS, A. See McIntyre, D., 1932
- WINDWER, S., AND SUNDHEIM, B. R. Solutions of alkali metals in ethylenediamine. 1254
- WINKLER, C. A. See Wright, A. N., 1747
- WIRTH, H. E., AND SLICK, P. I. The relative basicities of ethers. 2277
- WISE, H. See Wood, B. J., 1049
- WISE, S. S., MARGRAVE, J. L., FEDER, H. M., AND HUBBARD, W. N. The heat of formation of silica and silicon tetrafluoride. 381
- WITZEN, M. See Reisman, A., 2210
- WOGMAN, N. A. See Wilson, A. S., 1552
- WOLF, C. J., AND STEWART, A. C. Radiation chemistry of octamethylcyclotetrasiloxane. 1119
- WOLF, C. J., AND TOENISKOETTER, R. H. The γ -ray radiolysis of methyl substituted borazoles. 1526
- WOLFORD, R. K., AND BATES, R. G. Kinetics of the hydrolysis of acetal in N-methylpropionamide-water and N,N-dimethylformamide-water solvents at 20, 25, 30, and 40°. 1496
- WOOD, B. J., AND WISE, H. The kinetics of hydrogen atom recombination on Pyrex glass and fused quartz. 1049
- WOOD, P. See Leussing, D. L., 1544
- WOOD, S. E. The energy-temperature-volume surface for a single component system. 600
- WOODBREY, J. C. See Rogers, M. T., 540
- WOODBURY, H. A., EYRING, H., AND GABRYSH, A. F. Thermoluminescence of golden sapphire and fused borax seeded with Ni, Mg, and UO₃. 551
- WOODGER, G. B. See Bowen, E. J., 2491
- WOODWARD, A. E. See Kail, J. A. E., 1292; Odajima, A., 718
- WORSFOLD, D. J. See Brownstein, S., 2067
- WOSTEN, W. J., AND GEERS, M. G. The vapor pressure of zinc selenide. 1252
- WRIGHT, A. N., AND WINKLER, C. A. Nitric oxide decomposition induced by excited nitrogen molecules in active nitrogen. 1747
- WRIGHT, F. J. Gas-phase oxidation of *o*-xylene. 2023
- YAMAMOTO, A. See Engelsma, G., 2517
- YANAGIMOTO, S. See Uhara, I., 2691
- YANG, K., AND GANT, P. L. Reactions initiated by β -decay of tritium. IV. Decay and β -labeling. 1619
- YATES, D. J. C. See Lucchesi, P. J., 1451
- YEDDANAPALLI, L. M. See Ramasubramanian, N., 1222
- YOKOI, M. See Atkinson, G., 1520
- YOSIM, S. J., RANSOM, L. D., SALLACH, R. A., AND TOPOL, L. E. The bismuth-bismuth tribromide and bismuth-bismuth triiodide systems. 28
- YOUNG, A. H., AND WILLARD, J. E. Radiolytic and photochemical decomposition and exchange in liquid and gaseous CCl₃Br. 271
- YOUNT, R. A. Adsorption and dielectric studies of the alumina-ethyl chloride system at 35°. 326
- ZABIN, B. A. See Margerum, D. W., 2214
- ZABOLOTNY, E. R., AND GESSER, H. The reaction of active nitrogen with ammonia at -196°. 408
- ZABOLOTNY, E. R., AND GESSER, H. The reaction of active nitrogen with simple hydrocarbons. 854
- ZABUSKY, H. H. See Pohl, H. A., 1390
- ZEITLIN, H. See Goya, H., 1206
- ZELDES, H. See Emmett, P. H., 921
- ZELTMANN, E. W. See McMasters, D. L., 249
- ZETTLEMOYER, A. G. See Srinivasan, G., 1819
- ZIELEN, A. J., AND SULLIVAN, J. C. Effects of solution composition on the potentials of the couples: Np(V-VI), Fe(II-III), Hg(0-I), and Hg(I-II). 1065
- ZIMMERMANN, I. C. See McCullough, J. D., 1198
- ZINGARO, R. A., MCGLOTHLIN, R. E., AND MEYERS, E. A. Phosphine oxide, sulfide, and selenide complexes with halogens: visible and ultraviolet studies. 2579
- ZINN, J., AND ROGERS, R. N. Thermal initiation of explosives. 1412
- ZISMAN, W. A. See Bennett, M. K., 328, 1207; Shatrin, E. G., 740

Subject Index to Volume 66, 1962

- Acepleiadylene, molecular orbital study of polarographic reduction in dimethylformamide of 2316
 Acetal, hydrolysis of, in amide-water solvents 1496
 Acetamide, radiocarbon-labeled compounds produced by neutron irradiation of crystalline 1730
 Acetanilide, benzoyl-, rate of keto-enol tautomerism of 1034
 Acetic acid, diffusivities and viscosities of system with CCl_4 , 899; system with sodium acetate and water, 1197; thermal decomposition of, in liquid phase, 1513; solutions of high dielectric constant of, and its derivatives in *N*-methyl-acetamide 2684
 Acetone, photolysis, 521; photooxidation, 556; thermodynamic data for, -1-hydro-*n*-perfluorohexane system 621
 Acetonitrile, binary systems of, with *n*-butylamine, diethylamine, pyrrolidine, 1,1-dimethylguanidine, 1,3-diphenylguanidine, and triethylamine, conductivities of, 89; conductivities of bases dissolved in, 89; autoprotolysis constant of 1708
 Acetylacetone, hexafluoro- and trifluoro-, infrared spectra of complexes with Cu(II) and Ni(II) 346
 Acetylene, reaction of, with active N 854
 Acids, fluorination effect on wettability of adsorbed monolayers of fatty, 740; dilute solns. of, in concentrated salt solns., potentiometric measurements, indicator measurements, and uncharged bases in 2687
 Acridine, H bonding and quantum yields of fluorescence of 2491
 Acridine orange, flash excitation of, in acidic and basic solvents 453
 Acriflavine, effect of dimerization on α -phosphorescence of, in glucose glass 1353
 Acrylamide, thionine-sensitized photopolymerization of 2563
 Acrylates, polyethyl, stereospecificity and dielectric properties of 1390
 Acrylic polymers, containing fluorinated side chains, wetting properties of 1207
 Activation energies, of gas-phase oxidations, 191; of disproportionation of the HO_2 radical in acid solutions 2266
 Activity coefficients, of mannitol and KCl in mixed aq. solns., 506; calculation from osmotic coefficient data of, 508; in aq. solns. of SO_2 , spectrophotometric evaluation of, 516; of tris-(ethylenediamine)-cobalt(III) chloride in water, 550; of salts in organic solvent-water mixtures, 589; of NH_4ClO_4 in water, 940; of $\text{CdCl}_2\text{-HCl-H}_2\text{O}$ system, 1321; of HCl measured with glass electrodes 2268
 Adamantanes, methyl-substituted polythia-, heat capacities, entropies, and free energy functions of 524
 Addition reaction rate, isotope effects in 978
 Adenine, protonated, equilibrium constants for stepwise dissociation of protons from 359
 Adenosine, protonated, equilibrium constants for stepwise dissociation of protons from 359
 Adenosine diphosphate, protonated, equilibrium constants for stepwise dissociation of protons from 359
 Adenosine triphosphate, stability constants of metal chelates of 10
 Adipic acid, cetyl ester of, monolayers of 1846
 Adsorption, effect of light on, of H on ZnO, 54; of ethyl chloride on alumina, dielectric studies of, 326; of NO by alumina gel, 365; of CO and CO_2 on Ni, 450; heats of, of gases on graphitized C, 696; in constant current transition time studies of the H electrode, 727; of xanthate by PbS, 879; of a neutral substance at a metal-electrolyte interface, 959; on polymer surfaces, 1136; of gases and lattice vacancy theory, 1305; of ethylene on Al_2O_3 , 1451; of gases, 1736; of CF_4 , Ar, and N on polytetrafluoroethylene, 1815; of water on *n*-type Ge powders, 1819; of isolated flexible macromolecules at a plane interface, 1872; of flexible molecules: shape of adsorbed molecule, 1884; of a copolymer polyelectrolyte, 1907; of films, 1923; of Ar in graphitized carbon black; surface area and heats and entropies of adsorption, 2154; of water vapor on KCl films, 2260; of isothiocyanatochromium(III) complex ions at the Hg-aq. soln. interface 2706
 Adsorption equilibria, thermodynamics of 210
 Adsorption free energy, of polyelectrolytes at a dielectric interface 823
 Adsorption isotherm, Gibbs, 618; of flexible adsorbed macromolecules 1884
 Aerosil silica gel, hydroxyl content in 800
 Aerosol OT, micelle formation of, solvent effect on 363
 Alanine, rate of pyridoxal reaction with 1678
 Alcohols, heats and excess free energies of mixing of, in aromatic hydrocarbon systems, 1301; *n*-fatty, monolayers of, rate of spreading and equilibrium spreading pressure of, 1361; fatty, spreading and collapse of monolayers of, 1851; ionization potentials of, 2269; β -nitro, H bonds in monomeric and associated 2643
 Aldehyde, C-H stretching vibration, doublet nature of 232
 Alkali ions, electrostatic interactions between, and highly swollen polyelectrolyte gels 1295
 Alkali metals, intercrystalline energies of halides of, 31; nitrate binary liquid systems, volume change of, 103; solutions in ethylenediamine, 1254; discharge rate of, on their amalgams, 1683; influence of, cations on reduction of iodate ion on Hg in alkaline soln. 2710
 Alkaline earth, binding energies of gaseous halides, 1542; alkali nitrate liquid solns. of nitrates of 1668
 Alumina, γ -irradiated, formation of H in, 921; Aluminum, electron paramagnetic resonance absorption of chromia-, catalysts, 276; adsorption and dielectric studies of the system ethyl chloride-, 326; adsorption of NO by, gel, 365; mechanism of K promotion of chromia-, dehydrogenation catalysts, 871; variation with particle size and outgassing temperature of heat of immersion in hexane, 1823; infrared study of a silica-, surface 2223
 Aluminum, potentials of oxide-coated electrodes of, in acid solns., 866; partition of liquid metals in Al-Cd system, 1028; destruction of Al-C bond in aluminum alkyls by CCl_4 , 1354; sublimation and decomposition of AlN 1556
 Amalgams, rate of alkali metals discharge on 1683
 Amides, stabilization by, of H_2O_2 produced at irradiated ZnO surfaces, 932; electric moments of 1372
 Amidines, *N*-mono- and *N,N*-disubstituted, structure of 769
 Amine, complexes with metals, in ion exchange, 75, 78; system amine sulfate-bisulfate, 216; color reaction of aromatic tertiary, with acid clay, 834; heats of neutralization and relative strengths of, in benzene 2149
 Amino acids, poly-*L*- α -, proton magnetic resonances of 1292
 2-Aminoethanol, complexes of, with Ag, Ni(II), and Cu(II), stability in a cation-exchange resin and in aq. soln. 75
 Ammonia, reaction of, with uranium hydride at room temperature, 145; interactions with graphite oxide, 396; reaction of active N with, 408; temperature dependence of Knight shift of Na-NH₃ system, 1693; adsorption of, on activated $\alpha\text{-Fe}_2\text{O}_3$ 2597
 Ammonium compounds, phase diagram of the system $\text{NH}_4\text{NO}_3\text{-NH}_4\text{ClO}_4$, 354; heat capacity of $(\text{NH}_4)_2\text{Cd}_2(\text{SO}_4)_3$, 787; viscosity of tetramethylammonium bromide in aq. soln., 894; activity coefficients of NH_4ClO_4 in water, 940; conductance of NH_4I in *n*-butanol, 2075; dissociation constant

- and related thermodynamic quantities of *t*-butylammonium ion 2696
- Amylodextrins, interaction with methylene blue and congo red 2585
- Amylose, and amylose hydrolyzates, interaction with methylene blue and congo red 2585
- Angle of repose, of liquid drops on solid surfaces 883
- Aniline, nitrosation of, D isotope effect in 1212
- Anils, photochromy and thermochromy of 2442
- Anions, lyotropic and spectroscopic properties of dissolved 446
- Anisaldazine, orientation of mesophase of 1826
- p*-Anisaldehyde, calibration standard for n.m.r. spectrometers 560
- Anisole, phase diagram for system with CCl₄ and solid compound formation in, 1387; *p*-azoxy-, orientation of mesophase of 1826
- Anthracene, absorption maxima of complexes with organic compounds, 353; band structure and transport of holes and electrons in homologs of, 2461; uncatalyzed decay of, triplets in fluid solvents, 2574; triplet decay of, catalyzed by Cu complex compounds with ethylenediamine, pyridine, and *o*-phenanthroline 2577
- Antifogging, mechanism of, action of noble metal salts on photographic emulsion 2411
- Antimony, SbCl₅-methyl chloride addition compounds, 1380; pseudo-binary systems of, with Bi, Pb, Te, Tl, and Sn, 1408; composition of Sb vapor 2259
- Appearance potentials, determination of 947
- Area, surface, determination by an isotopic method of supported transition metal sulfides, 469; limiting, of unimolecular layers of bovine serum albumin and its derivatives 1918
- Argon, coefficients of self-diffusion of Ar-Kr liquid mixtures, 379; corresponding states theory for, 583; multilayers on hexagonal BN, 1810; adsorption on polytetrafluoroethylene, 1815; adsorption of, on graphitized carbon black; surface area and heats and entropies of adsorption 2154
- Arsenic, structure of As₂S₃-I glasses, 733; As(III)-As(V) exchange reaction in HCl solns., 886; photochemically induced oxidation of arsenite, and evidence for As(IV), 1473; X-ray irradiation of arsenite in O-free solution 1475
- Ascorbic acid, chlorophyll-sensitized photoreduction by, of thionine 954
- Association constants, of Ag(I) and chloride ions in molten KNO₃ 2069
- Atomic orbital, use of, configuration wave functions for LiH and He₂⁺ 2332
- Autoprotolysis constant, of acetonitrile 1708
- Azetidine, electron impact spectroscopy of 136
- Azobenzene, temperature effect on quantum yields of *cis*⇌*trans* photoisomerization of 2482
- Azomethane, pyrolysis of, in a shock tube, 1426; photolysis and radiolysis of, 2253; photolysis of, with production of ethane 2681
- Azulene, molecular orbital study of the polarographic reduction of 2316
- Barium, ordering of the octahedrally coordinated cation position in ternary systems of Ba and Nb with rare earth, In, or Fe oxides, 131; rate of photochemical decomposition of Ba(N₃)₂, 1113; liquid soln. of Ba(NO₃)₂ in NaNO₃, KNO₃, RbNO₃, and CsNO₃, 1668; high-temperature disproportionation of lower V oxides reacting with BaO 2273
- Bases, nitrogen, dissolved in acetonitrile, conductivities of 89
- Benzamide, *N,N*-dimethyl-, dipole moments of O¹⁸ labeled 2708
- Benzene, adsorption on graphitized C black, 205, 210; effect of substituent groups on ionization potentials of, 436; heat of immersion of silica in, 511; C-H bond dissociation energy in, 521; dielectric behavior of vapors of, adsorbed on alumina and silica gel, 1086; catalytic hydrogenolysis of, 1190; phase diagram for system with CCl₄ and solid compound formation in, 1387; H bond formation in system with chloroform and cyclohexane, 1469; Ag complex of, proton chemical shift in, 1554; refined alternant molecular orbital treatment of the ground state of, 2288; split *p*-orbital treatment of, and relationship to other molecular orbital treatments, 2310; transient charge-transfer complexes in halogen atom recombination and photohalogenation processes, 2423; directed solute-solvent interactions in, solns. 2653
- Benzene, chloro-, bromo-, iodo-, γ -ray-induced radiolysis of, 1041; 1,3,5-trinitro-, system with 2,4,6-trinitrotoluene, 1196; heats of combustion and formation of, difluoro-, 1529; γ -irradiation of isopropyl-, 1622; γ -irradiation of isopropyl-, adsorbed on microporous silica-alumina, 1625; isothermal diffusion in an ideal mixture of chloro-, bromo-, with toluene, 2015; hexamethyl-, transient charge-transfer complexes in halogen atom recombination and photohalogenation processes, 2423; isopropyl-, conversion on silica-alumina preirradiated with γ -rays 2714
- Benzoic acid, surface pressure-area properties of monolayers on Hg 1867
- Benzophenone, photoreduction of, efficiencies of various quenchers in, 1148; dipole moments of O¹⁸ labeled 2708
- Benzoylacetone, hexafluoro- and trifluoro-, infrared spectra of complexes with Cu(II) and Ni(II) 346
- Benzyl radicals, formation of, in toluene radiolysis by electrons 1538
- Beryllium, electron pairs in, 2281; applications of semi-empirical valence bond theory to BeH 2294
- Binding energies, of gaseous alkaline earth halides 1542
- Biphenyl, absorption maxima of, complexes with organic compounds, 353; ionization constant of 2,2'-dihydroxy-, in light and heavy water, 534; dielectric constant of monosubstituted, in a viscous solvent, 1105; formation of, by intramolecular dimerization in the electrooxidation of tetraphenylborate ion 1743
- Biphenylene, molecular orbital study of polarographic reduction in dimethylformamide of, and 2,3-benzo- 2316
- 2,2'-Bipyridyl, base strength 115
- Birefringence, of a solution of rod-shaped molecules 2046
- Bismuth, phase diagrams of systems of, with BiBr₃ and BiI₃, 28; magnetic susceptibility of Bi-BiCl₃ molten system, 1163; absorption spectra of and solute species in Bi-BiCl₃ liquid system, 1178; phase diagram of the system Bi-S, 1205; pseudo-binary systems of, with Sb, Pb, Te, Tl, and Sn, 1408; electromotive force, polarographic, and chronopotentiometric studies in molten Bi-BiBr₃ solns., 1587; liquidus curves of binary alloys with Cu, Ag, and Au 2012
- Bonds, hydrophobic, in proteins, 1773; nature of the two-electron chemical; the heteropolar case 2320
- Boron, coordination in potassium borate glasses, 174; thermoluminescence of fused borax seeded with Ni, Mg, and UO₂, 551; heat of formation of BF₃, 1209; dipole moment and magnetic susceptibility of decaborane, 1449; vaporization of the Ti-B system, 1492; γ -ray radiolysis of methyl-substituted borazoles, 1526; sublimation and decomposition of BN, 1556; biphenyl formation by intramolecular dimerization in electrooxidation of tetraphenylborate ion, 1743; Ar and N multilayers on hexagonal BN, 1810; applications of semi-empirical valence bond theory to BH 2294
- Bromine, exchange between, and CCl₄Br, 271; heats of formation of bromine fluorides, 288; radiolysis of bromates with γ -rays, 300; secondary isotope rate effect in iodide-promoted removal from *sym*-tetrabromoethane, 655; bromide complexing of Sc(III) and Y(III) in aq. soln., 1248; variation with aq. electrolyte activities of, absorption of bromide ion by tri-*n*-octylamine and strong-base anion exchange resin, 1383; molecular complex compounds of IBr with dioxane and pyridine derivatives, 1397; catalytic decomposition of bromate in fused alkali nitrates, 2114; transient charge-transfer complexes in Br recombination and photohalogenation processes 2423

- Bromophenol blue, acid-base equilibria between, and some N-heterocyclics in non-aq. solvents 915
- Butadiene, molecular motion in, I; π -electron delocalization in, 2306; split p-orbital treatment of, and relationship to other molecular orbital treatments 2310
- n*-Butane, second virial coefficients for system with perfluoro-*n*-butane, 635; gas compressibilities and virial coefficients of system with isobutane, 1082; thermal decomposition of, on Rh 1742
- Butane, perfluoro-*n*-, second virial coefficients for, -*n*-butane system, 635; bis-(*meso*-2,3-diamino)-, electrolyte effect on ions of Ni complex of, 1544; 2-thia- and 2,3-dithia-, electron impact spectroscopy of 1648
- Butanethiol, 2-methyl-2-, chemical thermodynamic properties and rotational isomerism of 1334
- 2-Butanol, vapor heat capacity and latent heat of vaporization of 1444
- Butanone, system with polystyrene, 4; diffusivities and viscosities of system with CCl₄ 899
- Butene-1, free radicals from thermal decomposition of 1569
- Butene-2, *cis*- and *trans*-chloroheptafluoro-, coupling between CF₃ and F groups of 1192
- 1-Butene, 3,4-epoxy-, electron impact spectroscopy of 1652
- cis*-2-Butene, proton chemical shift in Ag complex of 1554
- Butylamine, perfluorotri-, solubility in cyclohexane 573
- n*-Butylamine, conductivity of acetonitrile-, system 89
- Butyric acid, strength of 1188
- γ -Butyrolactam, acid dissociation in water 369
- Cadmium, polarography of complex of, with triethylenetetramine, 134; cubic crystals of CdS, 185; formation constants of complexes with oxalate in light and heavy water, 249; decomposition pressure of UCd₁₁, 362; conductances of perchlorate aq. solns. of, 439; heat capacity of (NH₄)₂Cd₂(SO₄)₃, 787; partition of liquid metals in Al-Cd system, 1028; magnetic susceptibility of Cd-CdCl₂ molten system, 1163; activity coefficients of CdCl₂-HCl-H₂O system, 1321; non-stoichiometry in CdSe and equilibria in the system Cd-Se 2210
- Cage effect, of peroxide, 1591; in aq. iodide ion photochemistry 2029
- Calcium, thermodynamic data for system CaO-P₂O₅-HF-H₂O, 315; phase equilibria in system CaO-P₂O₅-HF-H₂O, 318; electron paramagnetic resonance study of Mn²⁺ in polycrystalline calcium fluorophosphate, 674; complexing of, by methylene diphosphonates, 1349; development of surface in hydration of Ca₃SiO₈, 1804; micelle phase of calcium dinonylnaphthalene sulfonate in *n*-decane, 1843; reaction with cephalin at air and liquid-liquid interfaces 1928
- Calorimeter, isothermal constant heat exchange 2127
- Carathodory's principle, and the thermokinetic potential in irreversible thermodynamics 1414
- Carbon, heats of adsorption of benzene and *n*-hexane on graphitized, black, 205; doublet nature of stretching vibration of C-H bond, 232; production during the pyrolysis of ethylene of diatomic, 282; limiting isosteric heats of adsorption of gases on graphitized, 696; non-equilibrium soot formation in premixed ethylene-air flames, 794; dissociation energy of C-H bond in benzene, 821; adsorption of Ar on graphitized C black; surface area and heats and entropies of adsorption 2154
- Carbon, C¹³, coupling constant between, and directly-bonded F, 768; effect on coupling constants of C₂Cl₆ 945
- Carbon, C¹⁴, compounds containing, produced by neutron irradiation of cyanoguanidine, 152; in compounds produced by neutron irradiation of crystalline acetamide 1730
- Carbon compounds, adsorption of CO on Pt-on-alumina catalysts, 48; radiolytic and photochemical decomposition and exchange in liquid and gaseous CCl₄Br, 271; graphite oxide interactions with ammonia, 396; CO and CO₂ adsorption in Ni, 450; diffusivities and viscosities of CCl₄-butanone and CCl₄-acetic acid systems, 899; CS₂ standard for vapor-flow calorimetry and CS₂ heat capacity, 1074; destruction of Al-C bond in aluminum alkyls by CCl₄, 1354; phase diagrams for and solid compounds formation in CCl₄ binary systems with benzene, toluene, pseudocumene, and anisole, 1387; infrared spectrum of CO and CO₂ adsorbed on silica-supported Fe, 1464; interaction of CO and H on silica-supported Fe, 1664; mass spectrum of C₃O₂, 1756; adsorption of CF₄ on polytetrafluoroethylene, 1815; adsorption of CO on Pt; significance of the "polarization curve," 2657; γ -irradiation of CF₄ 2672
- Carbonium ions, produced by γ -irradiation of adsorbates on silica gel 1185
- Carboxylic acids, determination of self-association constants of, in soln. 1187
- β -Carotene, charge transfer complex between, and I; synthesis and optical spectra 2221
- Cation, transfer rates of, through ion-exchange membranes, 1549; nature of, depopulation in synthetic crystalline zeolites, 2271; apparent dissociation constants as a function of the exchanging monovalent, of carboxylic polymers 2275
- Cell potentials, and gas solubility theory 645
- Cephalin, reaction with Ca at air and liquid-liquid interfaces 1928
- Cerium, electrical conductivity of Ce-CeCl₃ system, 44; association constants of, with sulfate ions, 160; partition of, in liquid Al-Cd system, 1028; preparation and crystal structure of Ce formate 1737
- Cesium, the system NaF-Te-CsCl, 31; phase diagram of Ni-CsCl system, and Cs₃NiCl₆, 65; volume change of CsNO₃-NaNO₃ liquid system, 103; γ -ray radiolysis of CsBrO₃, 300; solubility of CsNO₃ in aq. H₂O₂, 548; ionic transport and crystallographic transition in CsCl, 557; effect of intensity on radiation-induced decomposition of CsNO₃, 755; thermal decomposition of γ -ray irradiated CsMnO₄, 961; solutions in ethylenediamine, 1254; malate complex of, 1702; CsCl in the ultracentrifugative preparation of foot-and-mouth virus, 1976; solns. of CsCl in ultracentrifugation of bovine serum mercaptalbumin 1990
- Cetane, diffusion of radioactively tagged, in polyisobutylene-cetane mixtures and in three methacrylate polymers 2699
- Cetyl esters, of dicarboxylic acids, monolayers of 1846
- Chain transfer constant, of vinylpyrrolidone with dextran 828
- Charge transfer, in radiolysis of organic liquids; evidence from H gas yields 2132
- Charge transfer complex, between β -carotene and I; synthesis and optical spectra 2221
- Chelates, stability constants of metallic, of adenosine triphosphate 10
- Chlorine, system with Rh at high temperature, 490; translational energy accommodation in the Ni-Cl surface reaction, 554; velocity of, hydrolysis in presence of various bases, 701; chloride complexing of Sc(III) and Y(III) in aq. soln., 1248; molecular complex compounds of ICl₃ and ICl with dioxane and pyridine derivatives, 1397; exchange rate of, between chloride and chloroacetate ions, 1719; infrared spectrum of NO₂ClO₄, 2066; association constants of chloride ions in molten KNO₃ 2069
- Chlorine, Cl³⁶, exchange between NaCl³⁶ and ethyl chloroacetate 1368
- Chloroacetic acid, decomposition in aq. soln. by atomic H; comparison with radiation chemical data, 2078; reaction mechanism in alkaline solns. 2081
- Chloroform, H bond formation in system with benzene and cyclohexane, 1469; rate of telomer production from mixtures with ethylene initiated by Co⁶⁰ γ -radiation 2164
- Chlorophyll, in photoreduction of thionine by ascorbic acid, 954; phototropy of, in soln. in anaerobic ethyl acetate, methanol, pyridine, cyclohexanol, and castor oil solutions, 2533; reversible photochemical reactions of, in photosynthesis 2537
- Chromatography, gas, in determination of stability constants of complexes 1208
- Chromium, electron paramagnetic resonance absorption of chromia-alumina catalysts, 276; gelation

- in chromic ferrocyanide, 356; viscosity and hydrogen ion concentrations during gelation in chromic ferrocyanide, 357; lattice energy and stability of monohalides, 433; mechanism of K promotion of chromia-alumina dehydrogenation catalysts, 871; adsorption of isothiocyanatochromium(III) complex ions at the Hg-aq. soln. interface. 2706
- Chromotropism, electrolyte effect on, of bis-(*meso*-2,3-diaminobutane)-Ni(II) ions. 1544
- Chronopotentiometry, of Bi-BiBr₃ molten solns. 1587
- Chrysene, absorption maxima of complexes with organic compounds. 353
- Cinnamic acid, photochemical isomerization in aq. solns. 201
- Cinnamic acid nitrile, *p*-dimethylamino-, photochemical *cis-trans* isomerization of. 2430
- Clay, color reaction of, with aromatic tertiary amines. 834
- Coacervation, of polyvinylsulfonic acid salts induced by heavy metal ions. 1070
- Cobalt, polarography of complex of, with triethylenetetramine, 134; transference number and activity coefficient of tris(ethylenediamine)-Co(III) in water, 550; oxidation of Fe(II) by Co(III) in aq. soln. 1275
- Colloids, binding of counterions on charged, 943; micelle formation in, 1375; low-frequency dielectric dispersion of spherical colloidal particles in electrolyte soln., 2626; theory of low-frequency dielectric dispersion of colloidal particles in electrolyte soln. 2636
- Complexes, determination by gas chromatography of stability constants of. 1208
- Complexing, of calcium and magnesium, by methylene diphosphonates. 1349
- Conductance, electrical, of the system Ce-CeCl₃, 44; for determination of disocn. equilibria of water, 225; of dilute aq. cadmium perchlorate solns., 439; effect of exponential distribution function on electrophoretic contribution to, of electrolytes, 477; of ion pairs in an alternating field, 669; of isotopic Li chlorides, 930; of sodium dodecyl sulfate solns. below the critical micelle concentration, 942; electric, of the system Pr-PrCl₃, 1201; dependence on pressure of, of toluene, 1210; equivalent, and ionic association in aq. TlOH solns., 1341; of polyvalent electrolytes, 1520; of symmetrical electrolytes, 1722; of RbBr in dioxane-water mixtures, 1727; of 2-2 electrolytes with multiple charge sites, 1749; of LiI and NH₄I in *n*-butanol. 2075
- Congo red, interaction with carboxylated starches, amylose, amylose hydrolysates, and amyloextrins. 2585
- Contact angles, in surfaces, determination of. 382
- Contraction, of fibrous proteins, effect of monomeric reagents on. 375
- Copper, stability in a cation-exchange resin and an aq. soln. of complexes of Cu(II) with 2-aminoethanol and ethylenediamine, 75; polarography of complex of, with triethylenetetramine, 134; electrode potentials of Cu(II)-Cu(I) and Cu(I)-Cu(0) in molten Li₂SO₄-K₂SO₄ eutectic, 164; complex of Cu(II) with poly-N-ethyleneglycine, 246; formation constants of complexes of Cu(II) with oxalate in light and heavy water, 249; infrared spectra of complexes of Cu(II) with hexafluoro- and trifluoroacetylacetone, benzoylacetone, and dibenzoylmethane, 346; heat of solution of Cu dimethylglyoxime, 389; oxidation of, to CuO_{0.67}, 816; density and critical constants of liquid, 1080; rate of reaction of Cu(II) with β -diketones, 1132; rate of formation of H₂O₂ during dissolution of polycrystalline, 1370; rate of reduction of Cu(O) by H, 1573; rate of exchange of Cu(II) between ethylenediaminetetraacetic acid and Eriochrome Blue Black R, 1582; heat capacity of Cu₂O, 1645; liquidus curves of Bi-Cu system, 2012; complex compounds with ethylenediamine, pyridine, and *o*-phenanthroline, in catalyzed anthracene triple decay, 2577; structure of active centers in, 2691; thermoelectric force and lattice defects as active centers in metallic. 2694
- Corresponding state treatment, of chemical kinetic solvent effects. 2101
- Coulometry, secondary electrode reactions in controlled potential. 2173
- Counterions, binding of, on charged colloids and macromolecules. 943
- Coupling, in linear polymers. 1567
- Coupling constant, of carbon-13 with directly-bonded fluorine, 768; in normal and isotopic C₃H₈. 945
- Cracking, of hydrocarbons over a promoted alumina catalyst. 1559
- Critical micelle concentration, determination, 374; discontinuity of, during ultracentrifugation of emulsions. 1966
- Crotonic acid, adsorption on anatase of, copolymer with vinyl acetate. 1907
- Crystallization, of fibrous proteins, effect of monomeric reagents on. 375
- Crystallization rate, relation between, and liquid structure. 609
- Cyanide, reaction of, with thiosulfate, 956; ion-pair intermediate in the phototropic reaction of CN⁻ with methyl violet. 2426
- Cyanogen, π -electron delocalization in. 2306
- Cyclization, rate of, of 2,2'-diphenic acids in sulfuric acid. 840
- Cyclobutadiene, molecular orbital study of C₄H₄ and C₄H₄⁺, which have orbitally degenerate ground states, 2299; tetraphenyl-, molecular orbital study of C₄(C₆H₅)₄ and C₄(C₆H₅)₄⁺, which have orbitally degenerate ground states. 2299
- Cycloheptadiene, [2,2,1]bi-, rate of thermal decomposition of. 568
- Cyclohexane, reaction of NO with electron-irradiated, 401; heat of immersion of silica in, 511; photolysis, 521; solubility in perfluorotributylamine, 573; H yield in radiolysis of, 767; H bond formation in system with benzene and chloroform. 1469
- Cyclohexane-*d*₁₂, effect of HI on γ -radiolysis of. 1097
- Cyclohexene, Ag complex of, proton chemical shift in. 1554
- Cyclohexyl radical, reactions. 521
- Cyclooctatetraene, molecular orbital study of C₈H₈ and C₈H₈⁻, which have orbitally degenerate ground states. 2299
- Cyclopentane, radiolysis of, ethylene scavenger in. 730
- Cyclopentanone, luminescence of. 1739
- Cyclopropane, reactions of T atoms with frozen, 2272; reactions with recoil T atoms of complex compound with PtCl₂. 2622
- Cyclopropyl radical, ionization potential of. 957
- Decarboxylation, rate of, of cinnamalmalonic acid in aromatic amines, 836; rate of, of oxanilic acid in ethers and in the molten state. 1543
- Decomposition, of BN and AlN, 1556; thermal, of FeCl₃, 1705; mechanism of, radiation-induced, of inorganic nitrates. 2249
- Dehydration, of porous glass. 1517
- Dehydrogenation, mechanism of K promotion of chromia-alumina catalyst. 871
- Density, temperature relation with, of liquid metals. 1686
- Density gradient, and gravitational stability during free diffusion in three-component systems. 1740
- Desorption, effect of veratrine and procaine on, of monoctadecyl phosphate monolayers. 1923
- Detergent, micellar character in solution of non-ionic, 574; pseudo-phase separation model for micellar, solns., 577; micellar structure of non-ionic, in aq. solns. 1326
- Deuterium, H bonding of, 429; OH-OD exchange in silica gel, 805; exchange with methane and H on silica gel initiated by γ -radiation, 1017; structure theory of liquid, in its ortho-para forms, 1128; isotope effect in nitrosation of aniline and on equilibrium constants, 1212; exchange with H on chemically doped Ge, 1241; dependence of electrolytic H-D separation factor on electrode potential, 1487; secondary D isotope effect in pyrolysis of dimethylmercury, 2192; isotope effects in photochemical evolution of H from aq. ferrous solns., 2200; formation and decay of atoms and small free radicals by γ -irradiation of solid. 2602

- Deuteron, activation of metal hydrogenation catalysts by 510
- Development, mechanism of photographic 2416
- Dextran, chain transfer constant of, with vinylpyrrolidone 828
- Dielectric behavior, of adsorbed vapors of water and benzene 1086
- Dielectric constant, and loss of iron pentacarbonyl at microwave frequencies, 186; and loss of the alumina-ethyl chloride system, 326; of water, 383; of ion pairs in an alternating field, 669; of quinoline, isoquinoline, and monosubstituted biphenyls in a viscous solvent, 1105; of emulsions of the water-in-oil type, 2259; of solns. of acetic acid and its derivatives in *N*-methylacetamide 2684
- Dielectric dispersion, low-frequency, of spherical colloidal particles in electrolyte soln., 2626; theory of low-frequency, of colloidal particles in electrolyte soln. 2636
- Dielectric interface, adsorption free energy of polyelectrolytes at 823
- Dielectric properties, of polyvinyl isobutyl ethers, polyethyl acrylates, and poly-*p*-chlorostyrenes 1390
- Dielectric relaxation, of quinoline, isoquinoline, and monosubstituted biphenyls in a viscous solvent 1105
- Diethylamine, conductivity of acetonitrile-, system 89
- Diethyl phthalate, viscosity of system with polymethyl acrylate 1053
- Differential thermal analysis, sublimation equilibria determination by 1477
- Diffusion, in non-ideal liquid mixtures, 899; isothermal, in the system $H_2O-Na_2SO_4-H_2SO_4$ and tests of the Onsager reciprocal relation, 1279; of Ni in NiO single crystals, 1308; of thiourea in water, 1540; density gradient and gravitational stability during, in three-component systems, 1740; interference optical studies of restricted, 1960; isothermal, in an ideal mixture of toluene, chlorobenzene, and bromobenzene 2015
- Diffusion coefficients, in liquid Ar-Kr mixtures, 379; time-lag measurement of, 760; polarographic 2072
- Diffusional behavior, in dilute aqueous electrolytes, effect of ionization of water on 2716
- β -Diketones, rate of reaction with Cu(II), and enol stability of 1132
- Dimerization, effect of, on α -phosphorescence of acriflavine in glucose glass, 1353; intramolecular, in the electrooxidation of tetraphenylborate ion with biphenyl formation 1743
- N,N*-Dimethylamides, proton magnetic resonance study of hindered internal rotation in 540
- Dimethyldodecylamine oxide, non-ionic-cationic micellar properties of 295
- Dimethylglyoximes, nickel and copper, heats of solution of 389
- 1,1-Dimethylguanidine, conductivity of acetonitrile-, system 89
- Dimpling, during the approach of two interfaces 190
- Dioxane, complex compounds of, with iodine halides 1397
- p*-Dioxane, molecular complex with tetracyanoethylene 1754
- 2,2'-Diphenic acids, rate of cyclization of, in H_2SO_4 840
- 1,3-Diphenylguanidine, conductivity of acetonitrile-, system 89
- Diphenylmethane, stabilization of 1535
- Diphenyl sulfoxide, dipole moments of O^{18} -labeled 2708
- Dipole moment, of decaborane, 1449; of O^{18} -labeled $X=O$ compounds 2708
- Dispersion, rotatory, of aqueous tartrate solutions, effects of electrolytes on 494
- Dispersion forces, determination of, in surfaces 382
- Displacement reaction rate, isotope effects in 978
- Dissociation, of diatomic molecules and the recombination of atoms 2111
- Dissociation constant, of 2-ammonium-2-methylpropanediol-1,3 in water, and related thermodynamic quantities, 308; a function of the exchanging monovalent cation of carboxylic polymers, 2275; and related thermodynamic quantities of *t*-butylammonium ion 2696
- Dissociation energy, C-H bond in benzene 821
- Dissociation equilibria, of water 225
- Dissociation reaction rate, isotope effects in 978
- Distillation, extractive, in chemical engineering 640
- Drops, sliding of liquid, on solid surfaces 833
- Dyes, fluorescein, luminescence of, 838; fluorescein, photo-induced binding of, to ZnO, 1536; spectral sensitizing and desensitizing 2403
- Dysprosium hydride, crystal structure 148
- Eckart potential energy barriers, tunnelling corrections for unsymmetrical 532
- Electric moments, of amides and thioamides, 1372; of substituted succinic acids, 1634; of *t*-butyl esters of long-chain aliphatic peracids and of *t*-butyl perbenzoate 2185
- Electrode, reference, for molten salt solutions, 173; thermodynamic treatment of electrocapillary curve for reversible, and properties of double layer, 724; oxide-coated, in acid solutions 866
- Electrode double layer, and ionic association 1194
- Electrode potential, effect on electrolytic H-D separation factor, 1487; photo-induced 1602
- Electrode processes, and faradaic rectification, 1108; faradaic rectification and, 1744; fast, theory of coulstatic method for rate study of, 2204; fast, experimental results 2208
- Electrode reactions, secondary, in controlled potential coulometry 2173
- Electrolytes, effect of exponential distribution function on electrophoretic contribution to conductance of, 477; effects on rotatory dispersion of aqueous tartrate solutions of, 494; photovoltaic effect of, AgBr systems, 857; conductance of polyvalent, 1520; effect on soln. chromatropism of bis-(*meso*-2,3-diaminobutane)-Ni(II) ions, 1544; phase unmixing in benzene and diethyl ether solns. of, 1595; conductance of symmetrical, 1722; partial specific volume and micelle density of association colloidal, 1733; conductance of, with multiple charge sites 1749
- Electromotive force, of the cell Pt; $H_2(g, 1 \text{ atm.}), HBr(m), AgBr; Ag, 1423$; of Bi-BiBr₃ molten solns. π -Electron, distribution in ground, double, and triplet states 2324
- Electron affinities, LCAO-MO ω -technique determination of, 706; extended calculations of, of polynuclear aromatic hydrocarbons by the LCAO-MO ω -technique 2713
- Electron irradiation, of methane 372
- Electron paramagnetic resonance, of Mn^{++} in polycrystalline calcium fluorophosphate, 674; free radicals detected by, of γ -irradiated potassium nitrate, 779; of manganese ion in calcium pyrophosphate and calcium fluoride 2715
- Electron spin resonance, of ZnO with adsorbed O, 99; of neutron-irradiated polypropylene, 849; of some N-containing aromatic free radicals, 937; spectrum, effect of gases on, of diphenylethylene adsorbed in alumina-silica 1214
- Electroösmosis, of water across ion-exchange membranes 1006
- Electrooxidation, biphenyl formation by intramolecular dimerization in, of tetraphenyl borate ion 1743
- Electrophoresis, intermittent current effects in 830
- Elimination reaction rate, isotope effects in 978
- Emulsions, stability to ultracentrifugation of, and discontinuity at the critical micelle concentration, 1966; determination by an ultracentrifugal method of stability of, 1969; dielectric constant of water-in-oil 2259
- Energy, one-component system, -temperature-volume surface for 600
- Energy accommodation, translational, in the Ni-Cl surface reaction 554
- Energy transfer, intermolecular, in gas reactions, 342; intermolecular, in polyethylene-polybutadiene system during γ -irradiation, 1202; in aq. soln. 2547
- Entanglement, in linear polymers 1567
- Enthalpy, of FNO₂ reactions, 1636; in photochemical aromatic halogen interchange 2118
- Enthalpy of formation, of HSO_4^- , $LiSO_4^-$, and $NaSO_4^-$ ions in water 519
- Entropy, of potassium hexachlororhenate(IV) and of the hexachlororhenate(IV) ion, 82; of trifluoromethane, 392; of methyl-substituted polythiadamantanes, 524; of pentaerythrityl halides, 748:

- of melting at constant volume of polyethylene oxide, 852; of FNO_2 reactions, 1636; of Hg_2SO_4 , 2049; in photochemical aromatic halogen interchange, 2118; of adsorption of Ar on carbon black.. 2154
- Enzymes, phosphorolytic, in polysaccharide and polyribonucleotide synthesis, 680; catalysis of equilibrium polymerizations by, 680..... 685
- Eosin, triplet-singlet luminescence from, in ethanol and glycerol solution..... 2506
- Epibromohydrin, electron impact spectroscopy of... 1652
- Epichlorohydrin, electron impact spectroscopy of... 1652
- Equilibria, acid-base, between bromophenol blue and some N-heterocyclics in non-aq. solvents..... 915
- Equilibrium constant, of phenol-pyridine system, 952; D isotope effects on, 1212; of FNO_2 reactions..... 1636
- Erbium hydride, crystal structure..... 148
- Eriochrome Blue Black R, Cu(II) exchange between, and ethylenediaminetetraacetic acid..... 1582
- Ethane, 1,2-bis-[2-di-(carboxymethyl)-aminoethoxy]-, stability constants of complexes with rare earths, 311; *sym*-tetrabromc-, secondary isotope rate effect in iodide-promoted debromination of, 655; reaction of, with active nitrogen, 854; formation of, in photolysis of azomethane..... 2681
- Ethanol, 2-amino-, complexes with Ag, Ni(II), and Cu(II), stability in a cation-exchange resin and in aq. soln., 75; N^{13} -labeled products from deutron irradiated, 474; 2-mercapto-, oxidation by $\text{K}_3\text{Fe}(\text{CN})_6$, 1238; *n*-alkoxy, rate of spreading and equilibrium spreading pressure of monolayers of, 1361; adsorption of, on activated $\alpha\text{-Fe}_2\text{O}_3$ 2597
- Ether, 2,2'-bis-[di-(carboxymethyl)-amino]-diethyl, stability constants of complexes with rare earths, 311; dimethyl, second virial coefficients for, -1-hydroperfluoropropane system, 635; polyvinyl isobutyl, stereospecificity and dielectric properties of, 1390; diethyl, heat of adsorption by zeolite, 2127; ionization potentials of, 2269; relative basicities of, 2277; adsorption of ethyl, on activated $\alpha\text{-Fe}_2\text{O}_3$ 2597
- Ethyl chloride, adsorption and dielectric studies of the system alumina..... 326
- Ethyl chloroacetate, rate of chlorine exchange with sodium chloride- Cl^{34} 1368
- Ethylene, velocity of production of diatomic carbon molecules during pyrolysis of, 282; decomposition products from radiolysis of γ -rays and electrons, 322; scavenger in liquid cyclopentane radiolysis, 730; non-equilibrium soot formation in premixed ethylene-air flames, 794; 1,2-dichloro-, *cis* \rightleftharpoons *trans* isomerization of, 1144; ion-molecule condensation in polymerization of, by ionizing radiation, 1158; diphenyl-, effect of gases on electron spin resonance spectrum of, adsorbed on alumina-silica, 1214; adsorption of, on aluminum oxide, 1451; tetracyano-, molecular complexes of, with tetrahydrofuran, tetrahydropyran, and *p*-dioxane, 1754; polytetrafluoro-, adsorption on, of CF_4 , Ar, and N, 1815; rate of telomer production from mixtures with chloroform initiated by Co^{60} γ -radiation..... 2164
- Ethylenediamine, complexes with Ni(II), Cu(II), and Zn, stability in a cation-exchange resin and in aq. soln., 75; complexes with Ag, stability in a cation-exchange resin and in aq. soln., 78; solutions of alkali metals, 1254; H electrode equilibrium studies of some acids and Na salts in, 2228; complex compound with Cu in catalyzed anthracene triplet decay..... 2577
- Ethylenediaminetetraacetic acid, Cu(II) exchange between, and Eriochrome Blue Black R..... 1582
- Ethylene terephthalate, polymer hydrolysis kinetics. 175
- Etioporphyrin I, effect of light on oxidation and reduction reactions of, complex compounds with Mn(II), Mn(III), Mn(IV), Fe(III), and Co(III)... 2517
- Europium, near infrared transitions of Eu(III) in soln. in molten $\text{LiNO}_3\text{-KNO}_3$ eutectic..... 2159
- Eutectic, freezing point-solubility curve of, of $\text{NaOH-NaOH}\cdot\text{H}_2\text{O}$ 2051
- Exchange reaction, between As(III) and As(V) in HCl soln..... 886
- Excited states, transfer of triplet state energy and the chemistry of..... 2569
- Explosives, thermal initiation of..... 2646
- Faradaic rectification, in alkali metal discharge on amalgams, 1683; and electrode processes..... 1744
- Ferricyanide, oxidation of 2-mercaptoethanol by $\text{K}_3\text{Fe}(\text{CN})_6$ 1238
- Field effect, extension of, of Onsager, to relaxation of ion pairs in an alternating field..... 669
- Films, structure and molecular orientation in, of long-chain *n*-hydrocarbon derivatives, 1010; H bonding in monomolecular, 1854; damping of water waves by monomolecular, 1858; penetration and adsorption of..... 1923
- Fischer-Tropsch synthesis..... 501
- Flames, of premixed ethylene-air, non-equilibrium soot formation in..... 794
- Flexibility, of unimolecular layers of bovine serum albumin and its derivatives..... 1918
- Flotation equilibrium, in the ultracentrifuge..... 1945
- Fluorescein dyes, luminescence of, 838; photo-induced binding of, to ZnO , 1536; halogenated, extremely long-lived intermediates in photochemical reactions of, in tertiary amines..... 2514
- Fluorescence quenching, by oxygen of dissolved aromatic hydrocarbons..... 455
- Fluorine, heats of formation of bromine fluorides, 288; effect on wettability of adsorbed monolayers of heptadecanoic acids of fluorination, 740; spectroscopy of F compounds, 764, 945; coupling constant between C^{13} and directly-bonded, 768; n.m.r. spectroscopy of, 1192; preparation, structure, and properties of $\text{K}_2\text{NbO}_3\text{F}$, 1318; molecular complex compounds of IF_6 with dioxane and pyridine derivatives, 1397; calorimetry of, in organic compounds, 1529; heat of reaction of, with graphite, 1562; thermodynamic properties of FNO_2 , 1636; effect of tetravalent fluorides on freezing point depressions in NaF..... 2711
- Fluorocarbons, effect of γ -radiation on..... 2116
- Fluoroolefin spectra, assignment of shielding values and spin-spin coupling constants in..... 1192
- Forces, definition of generalized..... 585
- Formaldoxime, microwave spectrum of..... 179
- Formamide, partial molal volumes of some univalent electrolytes in, solns. of high dielectric constant..... 2704
- Formates, rare earth, preparation and crystal structures of..... 1737
- Formation constant, of the 1:1 pyridine-iodine complex, 766; determination of, of lead halide complexes in fused $\text{NaNO}_3\text{-KNO}_3$ 1565
- Formic acid, radiation chemistry of, 70; decomposition on chemically doped Ge..... 1241
- Free energy, of potassium hexachlororhenate(IV), 82; of methyl-substituted polythiaadamantanes, 524; adsorption, of polyelectrolytes at dielectric interface, 823; of formation of GeH_4 monomer, 1003; excess, of mixing of alcohols with aromatic hydrocarbons, 1301; of formation of MoO_2 and " Mo_2C ," 1539; of FNO_2 reactions, 1636; transfer, for some univalent chlorides from H_2O to D_2O from measurements of ion exchange membrane potentials..... 2218
- Free radicals, electron spin resonance of aromatic N-containing, 937; from the thermal decomposition of toluene and butene-1, 1569; formation and decay of, by γ -radiation on solid H_2 , D_2 , N_2 , and CH_4 ... 2602
- Freezing point, of $\text{NaOH-NaOH}\cdot\text{H}_2\text{O}$ eutectic..... 2051
- Freezing point depression, effect of tetravalent fluorides on, in NaF..... 2711
- Fricke dosimeter, oxidation yield of, at high dose rates of electrons..... 180
- Friction, on polymer surfaces..... 1136
- Furan, tetrahydro-, molecular complex with tetracyanoethylene..... 1754
- Gadolinium formate, preparation and crystal structure of..... 1737
- Gallium, molecular species in Ga phosphide and Ga arsenide, 575; thermodynamic data for liquid ternary Zn-In-Ga solns., 658; pressure of Ga_2O over Ga_2O_3 mixtures and heat of formation of Ga_2O , 877; Raman-spectral study of molecular species in diisopropyl ether-aq. extraction systems containing GaCl_3 907
- Gas adsorption, limiting isosteric heats of, on

- graphitized carbon, 696; and lattice vacancy theory..... 1305
- Gas solubility theory, cell potentials and..... 645
- Gases, partial molal volume of dissolved, 597; adsorption of..... 1736
- Generalized coordinations, definition..... 585
- Germanium, electron impact spectroscopy of Ge tetramethyl, 155; H isotope exchange on surfaces of, 222; standard free energy of formation of GeH₄ monomer, 1003; H-D exchange and formic acid decomposition on chemically doped, 1241; vapor pressure of GeTe, 1563; water adsorption on *n*-type..... 1819
- Gibbs adsorption isotherm..... 618
- Glass, boron coordination in potassium borate, 174; solvent for low-temperature spectroscopy, 561; changes in length and infrared transmittance during thermal dehydration of porous..... 1517
- Glucose, addition to a limit dextrin of glycogen..... 685
- Glutaric acid, cetyl ester of, monolayers of..... 1846
- Glycerol, rate of solution of NaCl crystals in..... 665
- Glycine, poly-*N*-ethylene-, complex with Cu(II)..... 246
- Glycogen, limit dextrin of, addition of glucose to..... 685
- Gold, vapor pressure and heat of sublimation of, 754; thermodynamic data for Au-Ni system, 1532; liquidus curves of Bi-Au system, 2012; mechanism of antifogging and sensitizing action of Au salts on photographic emulsion..... 2411
- Graphite, heat of reaction with F..... 1562
- Greases, influence of *n*-heptyl derivatives of non-soap, on silica-non-polar liquid gel stability..... 1217
- Guanidine, cyano-, neutron irradiated, C-14-containing compounds produced from..... 152
- Hafnium, heat of formation of HfF₄, 1345; thermodynamic properties and phase relations in the H-Hf system..... 1657
- Hammett correlations, for solubility of HCl in aromatic systems..... 1752
- Heat capacity, of potassium hexachlororhenate(IV), 82; of trifluoromethane, 392; of methyl-substituted polythiaadamantanes, 524; and open and closed ensemble averages, 591; of pentaerythritol halides, 748; of (NH₄)₂Cd₂(SO₄)₂, 787; of CS₂ vapor, 1074; of 2-butanol vapor, 1444; of Ag₂S, Ag₂Se, and Ag₂Te, 1546; of Cu₂O, 1645; of TeO₂ and Na₂TeO₄, 1713; of Hg₂SO₄, 2049; of NaOH and NaOH·H₂O..... 2052
- Heat of adsorption, of benzene and *n*-hexane on graphitized C black, 205, 210; isosteric, of gases on graphitized C, 696; on zeolites, 812; measurement of, of *n*-pentane and ether by zeolite by means of an isothermal constant heat exchange calorimeter, 2127; of Ar on C black..... 2154
- Heat of combustion, of ReS₂ and Re₂S₇, 791; of 1,2-bis-difluoroamino-4-methyl pentane, 958; of difluorobenzenes, 4-fluorotoluene, and *m*-trifluorotoluic acid..... 1529
- Heat of dilution, of perchloric acid, lithium perchlorate, and sodium perchlorate in water..... 519
- Heat of dissociation, of protons from ribonucleotides and related compounds..... 1030
- Heat of formation, of bromine fluorides, 288; of silica, 380, 381; of SiF₄, 381; of triiodide and iodate ions, 752; of Ga₂O, 877; of 1,2-bis-difluoroamino-4-methylpentane, 958; of SiF₂, 1200; of BF₂, 1209; of TiF₄ and HfF₄, 1345; of difluorobenzenes, 4-fluorotoluene, and *m*-trifluorotoluic acid, 1529; of gaseous methyl nitrite..... 1750
- Heat of fusion, of FeCl₃, 219; of trifluoromethane, 392; of TeO₂..... 1713
- Heat of immersion, of silica in benzene and cyclohexane, 511; variation with particle size and outgassing temperature of, of silica, alumina, and titania in hexane..... 1823
- Heats of mixing, of alcohols with aromatic hydrocarbons..... 1301
- Heats of neutralization, and relative strengths of amines in benzene..... 2149
- Heat of reaction, of F with graphite..... 1562
- Heat of solution, of potassium hexachlororhenate(IV), 82; of nickel and copper dimethylglyoximes, 389; of NaOH and NaOH·H₂O..... 2052
- Heat of sublimation, of gold..... 754
- Heat of vaporization, of FeCl₃, 219; of trifluoromethane, 392; of 1,2-bis-difluoroamino-4-methylpentane..... 958
- Heat of wetting, determination of..... 762
- Helium, atomic orbital configuration wave functions for He₂⁺..... 2332
- α -Hematite, zero point of charge of..... 967
- Hemin, recoil-free γ -ray transition of iron-57 in..... 564
- Heptadecanoic acids, fluorination effect on wettability of adsorbed monolayers of..... 740
- Heptane, 1-hydro-*n*-perfluoro-, thermodynamic data for -acetone system..... 621
- Heterocyclic compounds, acid-base equilibria between, and bromophenol blue in non-aqueous solvents..... 915
- 1,5-Hexadiene, radiolysis of..... 1746
- Hexane, adsorption on graphitized C black, 205, 210; internal pressures of, -perfluoro-*n*-hexane system, 631; thiacyclo-, complex with I, 1198; effect of particle size and outgassing temperature on heats of immersion in, of silica, alumina, and titania..... 1823
- Hippuric acid esters, solubility of..... 897
- Holes, Hall mobility of, in AgBr..... 2376
- Holmium hydride, crystal structure..... 148
- Hyamine 1622, I compds. with..... 1829
- Hydration, reversible, of 2-hydroxypteridine, 1689; development of surface in, of Ca₃SiO₅..... 1804
- Hydrazine, complexes with Ni(II), stability in a cation-exchange resin and in aq. soln., 78; shock tube study of homogeneous decomposition of, 366; inhibition of γ -induced oxidation of aq. solns. of Fe(II) by..... 2108
- Hydrazinium bromide, as a solvent..... 1125
- Hydrocarbons, reaction of Pt-C₅ over alumina catalysts, 950; interaction of Pt-alumina catalyst with, in the presence of H and He, 1193; heats and excess free energies of mixing with alcohols, 1301; cracking of, over a promoted alumina catalyst, 1559; radiolysis of saturated, 1611; penetration of monolayers by, 1863; electronic spectra of catacondensed and pericondensed aromatic, 2334; extended calculations of electron affinities of polynuclear aromatic, by the LCAO-MO ω -technique..... 2713
- Hydrogen, adsorption on Pt-on-alumina catalysts, 48; effect of light on chemisorption of H on ZnO, 54; K X-ray absorption edge of H adsorbed on Ni metal, 105; reactivity of H atoms with org. solutes, 117; effect of adsorbed H on crystal structures of Pr, Nd, and Sm hydrides, 148; isotope exchange in γ -irradiated polyethylene, 193; isotope exchange on Ge surfaces, 222; recombination in propane flame gases of atomic, 229; doublet nature of stretching vibration of H-C bond, 232; reactivity with olefins of atoms of, 291; quantum yields of H from photochemical reduction of water, 336; transport through Ni, 351; reactivity of H atoms in aq. solns., 361; crystal structure of NiZrH₂, 370; bonding of D, 429; adsorption on W and Ni films, 482; OH-OD exchange in silica gel, 805; dissociation energy of C-H bond in benzene, 821; SCF-LCAO-MO study of H₂⁺ and H₂, 845; poisoning by telluride ions of evolution of H from Te cathodes, 890; formation of H in γ -irradiated silica gel, alumina, and silica-alumina catalysts, 921; bonding, in phenol-pyridine system, 952; γ -ray-initiated exchange with D on silica gel, 1017; rate of recombination of H atoms on Pyrex glass and fused quartz, 1049; structure theory of liquid H in its ortho-para and isotopic forms, 1128; rate of adsorption on Ni-magnesia catalysts, 1222; exchange with D on chemically doped Ge, 1241; evolution from photolysis of aq. ferrous solns. at low pH, 1258, 1264; dependence of the electrolytic H-D separation factor on the electrode potential, 1487; n.m.r. study of H exchange in benzyl mercaptan, 1535; thermodynamic properties and phase relations in the H-Hf system, 1657; CO reaction with H on silica-supported Fe, 1664; rate of CuO reduction by, 1673; ortho-para conversion of H by Cu, Ni, Fe, Au, Cu-Ni, Fe-Au, oxidized Ni, and oxidized Fe surfaces, 1715; decomposition of chloroacetic acid in aq. soln. by atomic H; comparison with radiation chemical data, 2078;

- reaction mechanism in alkaline solns., 2081; from radiolysis of organic liquids, 2, 32; D isotope effects in photochemical evolution of H from aq. ferrous solns., 2200; reactivity of H atoms in the liquid phase; reaction with halogenated compounds, 2246; applications of semi-empirical valence bond theory to H₂, LiH, BeH, and BH, 2294; atomic orbital configuration wave functions for LiH, 2332; formation and decay of atoms and small free radicals by γ -irradiation of solid, 2602; matrix effects in reaction of gaseous H with a condensed olefin; surface reaction—olefin diffusion model. . . . 2677
- Hydrogen bonding, in pyrrole-pyridines system, 546; in monomolecular films; strength of the keto-imino H bond in aq. media, 1854; of excited states. . 2491
- Hydrogen bonds, chemical shift of protons and intramolecular, 613; formation of, in the chloroform-benzene-cyclohexane system, 1469; effect of, on photoisomerization of 2-phenylazo-3-naphthol, 2478; in associated and monomeric β -nitro alcohols. 2643
- Hydrogen chloride, activity coefficients of CdCl₂-HCl-H₂O system, 1321; solubility in aromatic systems of, 1752; activity coefficients of, measured with glass electrodes. 2268
- Hydrogen disulfide, ionization potential of. 1214
- Hydrogen electrode, adsorption in constant current transition time studies of, 727; equilibrium studies of some acids and Na salts in ethylenediamine. . . 2228
- Hydrogen fluoride, thermodynamic data for system CaO-P₂O₅-HF-H₂O, 315; phase equilibria in system CaO-P₂O₅-HF-H₂O. 318
- Hydrogen iodide, effect on γ -radiolysis of cyclohexane-d₁₂ of. 1097
- Hydrogen peroxide, radiation chemistry of, 70; aq., RbNO₃ and CsNO₃ solubility in, 548; partial pressure of H₂O₂ and H₂O in alkali nitrate-H₂O₂-H₂O system, 923; stabilization of, by amides, 932; rate of formation of, during dissolution of polycrystalline Cu, 1370; Pb(II) oxidation by. 1421
- Hydrogen sulfide, infrared spectrum of, adsorbed on silica-supported Ni, 1288; adsorption of, on activated α -Fe₂O₃. 2597
- Hydrogenolysis, catalytic, of benzene and toluene, 1190; of dicyclopropylmethane on Pt catalysts, 1431; of dicyclopropylmethane on Ni catalyst. . . . 1438
- Hydrohalic acids, affinity of, for tri-*n*-octylamine. . . 1552
- Hydrolysis, mechanism of, of chlorine in the presence of various bases, 701; of acetal in amide-water solvents, 1496; of Zr ion, detection by coagulation, 1799; effects of micellization on the rate of, of monoalkyl sulfate. 2239
- Hydroperoxo, activation energy for the disproportionation of the HO₂ radical in acid solutions. 2266
- o*-Hydroxybenzophenone, spectroscopic study of complex compounds of, with La³⁺, Pr³⁺, Sm³⁺, Eu³⁺, and Ge³⁺. 2493
- Hydroxylapatite, solubility in water and physiological salt soln. of. 973
- Indium, ordering of the octahedrally coordinated cation position in the system In-Nb-Ba oxides, 131; thermodynamic data for liquid ternary Zn-In-Ga solns. 658
- Interfaces, dimpling during approaching, 190; measurement of properties of, between condensed phases, 410; rate of adsorption of a neutral substance at metal-electrolyte, 959; molecular interactions between phospholipids and salts at air and liquid-liquid. 1928
- Interfacial tensions, determination of in surfaces, 382; measurement of liquid. 946
- Iodine, structure of As₂S₃-I glasses, 733; heat of formation of iodate ions, 752; formation constant of 1:1 complex with pyridine, 766; complex compounds with saturated cyclic sulfides, 1099; complexes with *sym*-trithiane, thiacyclohexane, and thiacyclopentane in CCl₄ soln., 1198; molecular complex compounds of ICl₃, IF₅, ICl, and IBr with dioxane and pyridine derivatives, 1397; Hyamine 1622 complex with, 1829; cage effects and scavenging mechanisms in the photochemistry of aq. iodide ion, 2029; effect of N₂O and nature of intermediates in the photochemistry of aq. iodide ion, 2037; effect of O in the photochemistry of aq. iodide ion, 2042; conductance of LiI and NH₄I in *n*-butanol, 2075; production in the γ -radiolysis of cyclohexane-alkyl iodide solns., 2188; charge transfer complex between β -carotene and I; synthesis and optical spectra, 2221; transient charge-transfer complexes in I recombination and photohalogenation processes, 2423; visible and ultraviolet studies of complex compounds of I, IBr, or ICl with phosphine oxide, sulfide, and selenide, 2579; influence of alkali metal cations on the reduction of iodate ion on Hg in alkaline soln. . . . 2710
- Ion exchange, velocity of particle-diffusion controlled, 39; metal-amine complexes in, 75, 78; of polyelectrolytes under steady-state electrolysis across a porous frit, 995; in study of fast coordination reactions in soln. 2214
- Ion-exchange membrane, variable-charge, 570; water transport across, under electroosmosis, 1006; univalent cation transfer rates in, 1549; transfer free energies for some univalent chlorides from H₂O to D₂O from measurements of, potentials. 2218
- Ion transport, in AgCl and AgBr, 2380; role of, in latent-image formation. 2384
- Ionic association, and electrode double layer. 1194
- Ionic transport, and crystallographic transition in cesium chloride. 557
- Ionization, of aryl sulfonic acids, n.m.r. study of, 268; of water, effect on diffusional behavior in dilute aqueous electrolytes. 2716
- Ionization constants, acid, in H₂O and D₂O, 429; of 2,2'-dihydroxybiphenyl in light and heavy water. . . 534
- Ionization potentials, effect of methyl groups on, 368; effect of substituent groups on, of benzenes, 436; LCAO-MO ω -technique determination of, 706; LCAO-MO ω -technique determination of, of cyclic polyenes, 712; determination of, 947; of cyclopropyl radical and cyclopropyl cyanide, 957; of H₂S₂, 1214; in isothiocyanic acid, 2074; δ_K values for alcohols, ethers, thiols, and sulfides. 2269
- Iron, radiation chemistry of FeSO₄ in aq. soln., 70; ordering of the octahedrally coordinated cation position in the system Fe-Nb-Ba oxides, 131; dielectric constant and loss at microwave frequencies of Fe pentacarbonyl, 186; heat of vaporization and heat of fusion of FeCl₃, 219; quantum yields of photochemical oxidation of Fe(II) to Fe(III) sulfate, 336; reaction velocity studies of Fe-thionine system, 349; 2,3-dimercapto-1-propanol complexes with Fe(II), 426; catalysts for Fischer-Tropsch synthesis, prepoisoning by S compounds, 501; recoil-free γ -ray transition of Fe⁵⁷ in hemin, 564; thionine reaction with Fe(II) in a heterogeneous system, 663; zero point of charge of Fe₂O₃, 967; potential of Fe(II-III) couple, 1065; H from photolysis of ferrous aq. solns. at low pH, 1258, 1264; oxidation of Fe(II) by Co(III) in aq. soln., 1275; vaporization and decomposition of solid FeCl₃, 1705; internal structure and assemblies in Schiller layers of colloidal crystals of β -FeOOH, 1757; hydrazine-inhibited oxidation of Fe(II) in aq. soln., 2108; D isotope effects in photochemical evolution of H from aq. ferrous solns., 2200; infrared and volumetric data on adsorption of ammonia, water, and other gases on activated Fe₂O₃. . . 2597
- Isobutane, gas compressibilities and virial coefficients of system with *n*-butane. 1082
- Isomerism, geometrical, in arylazophenols and naphthols; effect of internal H bonds on photoisomerization of 2-phenylazo-3-naphthol. 2478
- Isomerization, see also *Photoisomerization*; photochemical, of cinnamic acid in aq. solns., 201; *cis* \rightleftharpoons *trans*, of piperylenes, 1,2-dichloroethylenes, and 2-pentenes, 1144; thermal, of vinylcyclopropane, 1671; catalytic, of 2-pentene, 2070; photochemical *cis*-*trans*, of *p*-dimethylaminocinnamic acid nitrile, 2430; photochemical *cis* \rightleftharpoons *trans*, of substituted stilbenes. 2486
- Isoprenes, molecular motion in. 1
- Isoquinoline, dielectric relaxation of, in a viscous solvent. 1105

- Isosbestic points, generated by variations in temperature of fused salts. 2169
- Isotherm, for soluble and "gaseous" monolayers. 385
- Isothiocyanates, adsorption of isothiocyanatochromium(III) complex ions at the Hg-aq. soln. interface. 2706
- Isothiocyanic acid, ionization potential of. 2074
- Isotope effect, in the nitrosation of aniline, 1212; secondary, in the iodide-promoted debromination of *sym*-tetrabromoethane and *syn*-tetrabromoethane-*d*₂, 655; in displacement, dissociation, elimination, and addition reactions. 978
- Keratin, polymorphism in fibrous polypeptides; $\alpha \rightleftharpoons \beta$ transformation in naturally occurring. 2096
- Ketals, heats of formation. 97
- Ketones, relaxation times and viscosities of aliphatic, 1739; structural effects in the photochemical processes of aromatic, in solution. 2456
- Knight shift, temperature dependence of, of the NaNH_2 system. 1693
- Krypton, surface area measurements with, 182; coefficients of self-diffusion of Ar-Kr liquid mixtures. 379
- Lanthanide, hydride, crystal structures, 148; crystal structure and lattice constants of, disilicides, 693; near-infrared transitions of Pr(III), Nd(III), Sm(III), and Eu(III) in soln. in molten $\text{LiNO}_3\text{-KNO}_3$ eutectic. 2159
- Lanthanum, structure of silicides, 758; partition of, in liquid Al-Cd system. 1028
- Latent heat of vaporization, of 2-butanol. 1444
- Latex, particle size distribution in rubber. 1768
- Lattice energy, of chromium monohalides. 433
- Lattice vacancy theory, adaptation to gas adsorption phenomena. 1305
- Lauric acid, surface pressure-area properties of, monolayers on Hg. 1867
- Layers, unimolecular, of bovine serum albumin and its derivatives. 1918
- LCAO-MO ω -technique, closed form analysis of, 706, 712; mechanism of. 712
- Lead, polarography of complex with triethylenetetramine, 134; thermal expansion coefficient, 266; effects of neutron irradiation on thermal decomposition of lead styphnate, 416; thermal decomposition of Ag-coated α -Pb azide, 421; effect of intensity on radiation-induced decomposition of $\text{Pb}(\text{NO}_3)_2$, 755; xanthate adsorption by PbS, 879; pseudo-binary systems of, with Sb, Bi, Te, Tl, and Sn, 1408; oxidation of Pb(II) by H_2O_2 , 1421; formation constants of complexes of Pb halides. 1565
- Light scattering, by catalyst-supported platinum, 1021; NaCl influence on, by colloidal silica, 1377; by colloidal spheres. 2059
- Lipoproteins, subfractionation of. 2007
- Liquid crystals, orientation of, of *p*-azoxyanisole and anisaldazine. 1826
- Liquid structure, relation between, and crystallization rate. 609
- Lithium, solid phases in the system $\text{Li}_2\text{O-Ta}_2\text{O}_5$, 15; volume change of $\text{LiNO}_3\text{-NaNO}_3$ liquid system, 103; electrode potentials in molten eutectic of $\text{Li}_2\text{SO}_4\text{-K}_2\text{SO}_4$, 164; radiolysis with γ -rays of LiBrO_3 , 300; retardation of thermal decomposition of LiClO_4 , 358; heat of dilution in water of LiClO_4 , 519; Li-Li halide systems, 572; partial pressure of H_2O_2 and H_2O in $\text{LiNO}_3\text{-H}_2\text{O}_2\text{-H}_2\text{O}$ system, 923; conductance of isotopic chlorides, 930; thermal decomposition of γ -ray-irradiated LiMnO_4 , 961; compound repetition in $\text{Li}_2\text{O-V}_2\text{O}_5$ system, 1181; solutions in ethylenediamine, 1254; complex structures of ThCl_4 and LiCl , 1299; malate complex of, 1702; conductance of LiI in *n*-butanol, 2075; Li-Sr equilibrium system, 2138; crystal structure of $\text{Sr}_6\text{Li}_{23}$ and Sr_3Li_2 , 2142; molecular dimensions and interactions of Li polyphosphate in aq. LiBr solns., 2235; applications of semi-empirical valence bond theory to LiH , 2294; atomic orbital configuration wave functions for LiH 2332
- London-van der Waals constants, determination of, from suspension and emulsion viscosity and surface energy data. 1077
- Luminescence, of fluorescein dyes, 838; of cyclopentanone, 1739; triplet-singlet emission from solns. of eosin and proflavine hydrochloride in ethanol or glycerol. 2506
- Lutetium, crystal structure of hydride. 148
- Macromolecules, charged, binding of counterions on, 943; adsorption of isolated flexible, at a plane interface, 1872; adsorbed, shape of the molecule, adsorption isotherm, surface tension, and pressure. 1884
- Magnesium, reaction velocities in MgSO_4 solns., 360; liquid temperature range, density, and critical constants of, 737; rate of H adsorption in Ni-MgO catalysts, 1222; complexing of, by methylene diphosphonates, 1349; effect of pressure on equilibrium of aq. solns. of MgSO_4 and MgCl_2 , 1607; effects of neutron and ultraviolet irradiation on the catalytic activity of MgO. 2591
- Magnetic susceptibility, of liquid metals, molten salts, and their solutions, 1163; of decaborane. 1449
- Maleic anhydride, absorption maxima of complexes with organic compounds. 353
- Malic acid, alkali metal complexes of. 1702
- Malonic acid, decarboxylation in the molten state and in solution, 125; cinnamal-, decarboxylation rate of, in aromatic amines, 836; monolayers of cetyl esters of. 1846
- Manganese, reaction velocities in manganous sulfate solutions, 360; electron paramagnetic resonance study of Mn^{++} in polycrystalline calcium fluorophosphate, 674; effect of neutron irradiation on rate of dehydration of manganous oxalate dihydrate, 926; thermal decomposition of γ -ray irradiated permanganates, 961; effect of light on oxidation and reduction reactions involving phthalocyanine and etioporphyrin I-Mn complex compounds, 2517; electronic paramagnetic resonance of Mn^{++} in calcium pyrophosphate and calcium fluoride. 2715
- Mannitol, activity coefficients of, -KCl aq. solns. 506
- Mass spectrum, of C_3O_2 1756
- Melting, effect of monomeric reagents on, of fibrous proteins. 375
- Membranes, monolayer permeability and properties of natural. 1911
- Mercaptan, *n*-octyl-, ferricyanide oxidation of, in acetone-water soln., 1233; methyl and ethyl, infrared spectra of, adsorbed on silica-supported Ni, 1288; *t*-amyl, chemical thermodynamic properties and rotational isomerism of, 1334; benzyl, nuclear magnetic resonance study of H exchange in. 1535
- Mercury, electron impact spectroscopy of Hg dimethyl, 155; potentials of Hg(0-I) and Hg(I-II) couples, 1065; discharge of Hg(I) on Hg, 1108; color of HgI_2 adsorbed on alumina, 1206; stability constants of Hg(II) halide ternary complexes in soln., 1661; heat capacity and entropy of Hg_2SO_4 , 2049; secondary D isotope effect in pyrolysis of dimethylmercury. 2192
- Merocyanines, mechanism of phototransformation to spiropyrans. 2470
- Mesitylene, transient charge-transfer complexes in halogen atom recombination and photohalogenation processes. 2423
- Mesophases, orientation of nematic. 1826
- Methacrylic polymers, wetting properties of, containing fluorinated side chains, 1207; diffusion of radioactively tagged cetane in. 2699
- Methane, dibenzoyl-, hexafluoro- and trifluoro-, complexes with Cu(II) and Ni(II), infrared spectra of, 346; electron irradiation of, 372; N^{13} -labeled products from deuteron-irradiated, 474; hydrate in aq. soln., 605; solubility of, hydrates in water, 605; reaction of, with active N, 854; γ -ray-induced exchange with D on silica gel, 1017; dicyclopropyl-, hydrogenolysis of, on Pt catalysts, 1431; dicyclopropyl-, hydrogenolysis of, on Ni catalysts, 1438; trifluoro-, thermodynamic constants of, 392; formation and decay of atoms and small free radicals by γ -irradiation of solid, 2602; γ -irradiation of. 2672
- Methanol, deuteron-irradiated, N^{13} -labeled products from. 474
- Methyl chloride, infrared spectrum of, in SnCl_4 and

- SbCl₃ soln., and addn. compds. with SnCl₄ and SbCl₅ 1380
- Methyl groups, effect on ionization potentials of 368
- Methyl nitrite, heat of formation of gaseous 1750
- Methyl red, acid-base equilibria of 527
- Methyl violet, ion-pair intermediate in the phototropic reaction of, with cyanide ion 2426
- N-Methylacetamide, solutions of high dielectric constant in 2684
- Methylene, stabilization of 1535
- Methylene blue, interaction with carboxylated amylose, amylose hydrolysates, and amyloextrins 2585
- α -Methylstyrene, mechanism of formation of living dimer and tetramer of 904
- Metrazoles, electric moments of 158
- Micelle, determination of critical concentration, 374; density of association colloidal electrolytes, 1733; of Ca dinonylnaphthalene sulfonate in *n*-decane, 1843; effect of pressure on formation in sodium dodecyl sulfate aq. solns., 1359; formation in association colloids, 1375; pressure effect on formation in soap solutions 1839
- Microwave absorption, and molecular structure in liquids 1105
- Mobility, of the H₂SO₄-HSO₄⁻ ion in acetonitrile 1675
- Molal volume, partial, of gases in solution 597
- Molar volume, partial, of some uni-univalent electrolytes in formamide solns. of high dielectric constant 2704
- Molecular complexes, of tetracyanoethylene with tetrahydrofuran, tetrahydropyran, and *p*-dioxane . . 1754
- Molecular dissociation, and the recombination of atoms 2111
- Molecular motion, in some isoprenes and butadienes 1
- Molecular orbital, study of the effect of methyl groups on ionization potentials, 368; of the ground state of benzene, 2288; study of aromatic molecules and ions having orbitally degenerate ground states, 2299; split *p*-, relation to other molecular orbital treatments and application to benzene, butadiene, and naphthalene, 2310; study of polarographic reduction in dimethylformamide of unsubstituted and methyl-substituted aromatic hydrocarbons 2316
- Molecular weight, of unimolecular layers of bovine serum albumin and its derivatives, 1918; determination of, with an ultracentrifuge 1948
- Molecules, birefringence of a solution of rod-shaped, 2046; electronic structure of simple 2329
- Molybdenum, free energy of formation of MoO₃ and "Mo₂C" 1539
- Monolayers, isotherm for soluble and "gaseous," 385; effect of fluorination on adsorbed, of fluorinated heptadecanoic acids, 740; rate of spreading and equilibrium spreading pressure of, of *n*-fatty alcohols and *n*-alkoxy ethanols, 1361; of myristyl and cetyl esters of dicarboxylic acids, 1846; hydrocarbon penetration in, 1863; surface pressure-area properties of organic, on Hg, 1867; permeability of, and properties of natural membranes 1911
- Myristyl esters, of dicarboxylic acids, monolayers of 1846
- Naphthalene, absorption maxima of complexes with organic compounds, 353; split *p*-orbital treatment of, and relation to other molecular orbital treatments, 2310; tetrachloroketodihydro-, phototropy of, as a reversible photochemical reaction, 2449; band structure and transport of holes and electrons in, 2461; 1-monohalogenated, phosphorescence spectra and decay times of externally perturbed, 2499; phosphorescence spectra and decay times of externally perturbed, 2499; rate of solid-state reaction with picric acid 2707
- 1-Naphthoic acid, surface pressure-area properties of, monolayers on Hg 1867
- Naphthol, 2-phenylazo-3-, effect of internal H bond on photoisomerization of 2478
- Neodymium, hydride crystal structure, 148; preparation and crystal structure of Nd formate, 1737; near infrared transitions of Nd(III) in soln. in molten LiNO₃-KNO₃ eutectic 2159
- Neptunium, reaction velocity in perchlorate solns. of V(III)-Np(V), 442; potential of Np(V-VI) couple 1065
- Neutron, effect of irradiation on subsequent lead styphnate thermal decomposition, 416; activation of metal hydrogenation catalysts by, 510; e.s.r. investigation on irradiated polypropylene 849
- Neutron magnetic resonance spectroscopy, of C₃F₈ 945
- Nickel, phase diagram of Ni-Cs chlorides system, and tetrahedral NiCl₄⁻ ion in Cs₂NiCl₆, 65; stability of complexes of Ni(II) with 2-aminoethanol and ethylenediamine in a cation-exchange resin and in aq. soln., 75; stability in a cation-exchange resin and in aq. soln. of complexes of Ni(II) with hydrazine, 78; K X-ray absorption edge perturbations due to small crystal size and hydrogen chemisorption on Ni metal, 105; polarography of complex of, with triethylenetetramine, 134; infrared spectra of complexes of Ni(II) with hexafluoro- and trifluoroacetylacetone, benzoylacetone, and dibenzoylmethane, 346; crystal structure of NiZrH₃, 370; heat of solution of Ni dimethylglyoxime, 389; adsorption of CO and CO₂ by, 450; adsorption of Xe and H on evaporated films of, 482; high-energy irradiation activation of hydrogenation catalysts, 510; translational energy accommodation in the Ni-Cl surface reaction, 554; rate of H adsorption on Ni-MgO catalysts, 1222; infrared spectra of S compounds adsorbed on silica-supported, 1288; diffusion of, in NiO single crystals, 1308; structure of active centers in Ni catalyst, 1374; thermodynamic data for Au-Ni system, 1532; electrolyte effect on ions of bis-(*meso*-2,3-diaminobutane) complex of Ni(II), 1544; rate of formation of Ni(II)-EDTA, 2214; thermoelectric force and lattice defects as active centers in metallic 2694
- Niobium, ordering of the octahedrally coordinated cation position in ternary systems of Ba and Nb with rare earth, In, or Fe oxides, 131; permeability to H, 351; preparation, structure, and properties of K₂NbO₅F 1318
- Nitric acid, O¹⁸ enrichment in the NO-HNO₃ system 1480
- o*-, *m*-, and *p*-Nitrobenzoic acids, ultraviolet absorption spectra of 562
- o*-Nitrobenzyl derivatives, phototropism of 2434
- Nitrogen, electron impact spectroscopy of saturated heterocyclic compounds of, 136; adsorption on graphitized C black 205, 210; ammonia reaction with active, 408; effect of intensity on radiation-induced decomposition of inorganic nitrates, 755; reactions of active, with methane, ethane, and acetylene, 854; separation factors in NO-NOBr system, 1189; active N reactions with N¹⁶O and N₂¹⁵, 1362; O¹⁸ enrichment in the NO-HNO₃ system, 1480; thermodynamic properties of FNO₂, 1636; NO decomposition induced by excited N molecules in active, 1747; multilayers on hexagonal BN, 1810; adsorption on polytetrafluoroethylene, 1815; infrared spectrum of NO₂ClO₄, 2066; mechanism of the radiation-induced decomposition of inorganic nitrates, 2249; formation and decay of atoms and small free radicals by γ -irradiation of solid 2602
- Nitrogen, N¹³, labeled compounds from deuteron irradiation of methane, methanol, and ethanol 474
- Nitrogen, N¹⁵, reaction with active N 1362
- Nitrogen oxide, adsorption of NO by alumina gel, 365; reaction of electron-irradiated cyclohexane with NO, 401; reaction of nitrosocyclohexane with NO, 401; effect of N₂O in aq. iodide ion photochemistry 2037
- Nitrosocyclohexane, dimerization of, and reaction of NO with 401
- o*-Nitrotoluene, photoisomerization of, in aq. soln 2560
- Nuclear magnetic resonance, study of the ionization of aryl sulfonic acids, 260; spectroscopy of fluorocarbon sulfides, 764; of P³¹ in P compounds 901
- Nucleoside diphosphates, equilibrium copolymerization of 685
- n*-Octacosane, surface pressure-area properties of monolayers on Hg 1867
- tri-*n*-Octylamine, variation with aq. electrolyte activities of absorption of bromide ion from aq. salt solns. by, 1383; affinity of hydrohalic acids for, 1552; secondary reaction of, with HCl and thenoyltrifluoroacetone 2262

- Oil, interfacial tension with water on solid surfaces... 236
- Olefin, stability constants of complexes with Ag ions in ethylene glycol soln., 1208; electronic spectra of, adsorbed on silica-alumina catalysts, 1457; condensed, matrix effects in the reaction with gaseous H; surface reaction—olefin diffusion model... 2677
- Onsager reciprocal relation, tests of... 1279
- Orientation, molecular, in multimolecular films of long-chain *n*-hydrocarbon derivatives, 1010; of nematic mesophases... 1826
- Osmotic coefficient, activity coefficient calculation from... 508
- Oxalate, formation constants of complexes with Cu(II) and Cd(II) in light and heavy water... 249
- Oxalic acid, monolayers of myristyl and cetyl esters of 1846
- Oxanilic acid, decarboxylation rate of, in ethers and in the molten state... 1543
- Oxides, zero point of charge of... 967
- Oxiranes, substituted, electron impact spectroscopy of 1652
- Oxygen, adsorption on Pt-on-alumina catalysts, 48; adsorbed on ZnO, effect on electron spin resonance, 99; electron impact spectroscopy of saturated heterocyclic compounds containing, 136; quenching of fluorescence of dissolved aromatic hydrocarbons, 455; diffusion and reaction during γ -irradiation of polyethylene, 463; transient species in O adsorption by ZnO, 566; infrared spectrum of O adsorbed on silica-supported Fe, 1464; effect in aq. iodide ion photochemistry, 2042; adsorption on Pt; significance of the "polarization curve"... 2657
- Oxygen, O¹⁸, enrichment of by chemical exchange of NO with HNO₃ solutions... 1480
- Palladium, electrode potentials of Pd(II)-Pd(0) in molten Li₂SO₄-K₂SO₄ eutectic, 164; high-energy irradiation activation of hydrogenation catalysts, 510; partition of, in liquid Al-Cd system... 1028
- Paraffins, proton magnetic resonance of... 718
- Partial specific volume, of association colloidal electrolytes... 1733
- Particle size distribution, determination by turbidimetry... 458
- Penetration, of films... 1923
- Pentacene, band structure and transport of holes and electrons in... 2461
- Pentaerythryl, halides, heat capacities and entropies of... 748
- Pentane, 1,2-bis-difluoroamino-4-methyl-, heats of combustion, formation, and vaporization of, and vapor pressure of, 958; thiacyclo-, complex with I, 1198; 2-thia-, electron impact spectroscopy of, 1648; heat of adsorption by zeolite... 2127
- Pentanone, photolysis in perfluorodimethylcyclobutane soln... 690
- 2-Pentene, *cis*⇌*trans* isomerization of, 1144; catalytic isomerization of... 2070
- Peptides, polymorphism in fibrous; α ⇌ β transformation in naturally occurring keratin... 2096
- Peracids, electric moments of *t*-butyl esters of... 2185
- Perchloric acid, heat of dilution in water, 519; thermal decomposition of vapor... 1092
- Permeability, of a monolayer and properties of natural membranes... 1911
- Perovskite structure, ordering of the octahedrally coordinated cation position in... 131
- Peroxide, decomposition and cage effect, 1591; electric moments of organic... 2185
- Phases, measurement of properties of plane interfaces between condensed... 410
- Phase transitions, impurity effect on, in a binary liquid system... 625
- Phase separation, in electrolyte solns. in benzene and diethyl ether... 1595
- Phenanthrene, absorption maxima of complexes with organic compounds... 353
- 1,10-Phenanthroline, base strength... 115
- o*-Phenanthroline, complex compound with Cu in catalyzed anthracene triplet decay... 1334
- Phenol, *p*-nitro-, ionization constant, 171; intramolecular H bonds in, 613; equilibrium constant of system with pyridine... 952
- Phenosafranin, complex compound with polymethacrylic acid, stepwise photoreversion of... 2511
- Phenyl radicals, gas-phase reactions of... 821
- p*-Phenylenediamine, N,N,N',N'-tetramethyl-, photooxidation of... 1168
- Phosphine oxide, tri-*n*-octyl-, isopiestic investigation of, in *n*-octane soln., 1629; triphenyl-, dipole moments of O¹⁸-labeled... 2708
- Phospholipids, molecular interactions between, and salts at air and liquid-liquid interfaces... 1928
- α -Phosphorescence, effect of dimerization on, of acriflavine in glucose glass... 1353
- Phosphorescence spectra, and lifetimes of externally perturbed naphthalenes... 2499
- Phosphoric acid, di-(2-ethylhexyl)-, isopiestic investigation of, in *n*-octane soln... 1629
- Phosphorous acid, oxidation of... 1356
- Phosphorus, effect of phosphates on SrSO₄ crystallization and crystal habit, 252; thermodynamic data for the system CaO-P₂O₅-HF-H₂O, 315; phase equilibria in the system CaO-P₂O₅-HF-H₂O, 318; molar refractions of aq. solns. of condensed phosphates, 377; radiation induced exchange of, in the PCl₃-POCl₃ system, 863; n.m.r. of P³¹ in P compounds, 901; extraction of acids by tri-*n*-butyl phosphate and acid complexes of, 983; mechanism of the extraction of uranyl salts by tri-*n*-butyl phosphate, and complex compound formation, 989; extraction of aq. NaSCN by tributyl phosphate, 1014; acidity constants and Ca and Mg complexing by methylene diphosphonates, 1349; effect of veratrine and procaine on desorption of monolayers of mono-octadecyl phosphate, 1923; visible and ultraviolet studies of complex compounds of phosphine oxide, sulfide, and selenide with I, IBr, or ICl... 2579
- Photochemical processes, reversible (Symp.) 2423-2579
- Photochemistry, of oxidation of Fe(II) to Fe(III) sulfate and accompanying reduction of water to H₂, 336; photochemical reaction, in gases, intermolecular energy transfer in, 342; at irradiated ZnO surfaces, 932; of arsenite oxidation, 1473; cage effects and scavenging mechanisms in, of the iodide ion in aq. solns., 2029; effect of N₂O and the nature of intermediates in, of the iodide ion in aq. soln., 2037; effect of O on, of aq. iodide ion, 2042; interchange of halogens in aromatic compounds; temperature dependence of some substituent effects, 2118; D isotope effects in the photochemical evolution of H from aq. ferrous solns., 2200; phototropy of tetrachloroketodihydronaphthalene as a reversible photochemical reaction, 2449; structural effects in the, of aromatic ketones in soln., 2456; *cis*⇌*trans* isomerization of substituted stilbenes, 2486; extremely long-lived intermediates in, of dyes in non-viscous media, 2514; of phthalocyanine Mn and metal derivatives of porphyrins, 2517; reversible photochemical reactions of chlorophyll in photosynthesis... 2537
- Photochromism, of spiropyrans, 2275; of anils, 2442; of sydnone, 2446; effect of temperature and solvent on spectrum of colored photochromic spiropyrans, 2465; mechanism of phototransformation spiropyran⇌merocyanine... 2470
- Photographic processes (Symposium)... 2359-2422
- Photographic sensitivity, Mitchell theory of... 2359
- Photoisomerization, see also *Isomerization*; effect of internal hydrogen bonds on, of 2-phenylazo-3-naphthol, 2478; temperature dependence of, and quantum yields of *cis*⇌*trans* isomerizations in azo compounds, 2482; mechanism of *cis*⇌*trans*, 2555; of *o*-nitrotoluene in aq. soln... 2560
- Photolysis of CCl₄Br, 271; of cyclohexane and acetone, 521; of diethyl ketone in perfluorodimethylcyclobutane soln., 690; of aq. ferrous solns. at low pH, 1258, 1264; of azomethane and CH₃N₂CH₃-CD₃N₂CD₃ mixtures, 2253; of halogenated fluorescein dyes in the presence of tertiary amines, 2514; of azomethane at higher pressures with production of ethane... 2681
- Photooxidation, of acetone, 556; in a rigid medium, 1168; primary absorption act in one-electron, in a rigid medium... 2279
- Photopolymerization, thionine-sensitized, of acrylamide... 2563

- Photoreactions, mechanisms of, in soln., 1144, 1148; of phytochrome which regulates plant growth 2550
- Photoreduction, chlorophyll-sensitized, of thionine by ascorbic acid, 954; of uroporphyrin to dihydroporphyrin; effect of pH on the reaction with EDTA 2531
- Photoreversion, stepwise, of phenosafranin-polymethacrylic acid complex compound 2511
- Photosynthesis, reversible photochemical reactions of chlorophyll in 2537
- Phototropy, rate studies of, and evidence for an ion-pair intermediate in the reaction of methyl violet with cyanide ion, 2426; of *ortho*-nitrobenzyl derivatives, 2434; of tetrachloroketodihydronaphthalene as a reversible photochemical reaction, 2449; of chlorophyll in soln. in anaerobic ethyl acetate, methanol, pyridine, cyclohexanol, and castor oil solutions 2533
- Photovoltaic effect, of silver bromide-electrolyte systems 857
- Phthalic acid, absorption maxima of complexes with organic compounds 353
- Phthalic anhydride, absorption maxima of complexes with organic compounds 353
- Phthalimide, complexes with organic compounds, absorption maxima of 353
- Phthalocyanine, effect of light on oxidation and reduction reactions of complex compounds with Mn 2517
- Phytochrome, reversible photoreaction of, which regulates plant growth 2550
- Picolinic acid, decarboxylation 125
- Picric acid, rate of solid-state reaction with naphthalene 2707
- Pimaricin, photodecomposition of, sensitized by riboflavin and lumichrome in aq. soln. 2547
- Pimelic acid, monolayers of cetyl ester of 1846
- Piperylenes, *cis* \rightleftharpoons *trans* isomerization of 1144
- Platinum, adsorption of H, O, and CO on Pt-on-alumina catalysts, 48; high-energy irradiation activation of hydrogenation catalysts, 510; spectrophotometry and light scattering by catalyst-supported, 1021; interaction of hydrocarbons with Pt-alumina catalyst in the presence of H and He, 1193; reactions of recoil T atoms with cyclopropane compound with PtCl₂, 1407; adsorption of CO and O₂ by, and significance of the "polarization curve" 2657
- Polarity, correlation with organic scintillator pulse height 166
- Polarization curve, significance of, in the adsorption of CO and O₂ on Pt 2657
- Polarographic diffusion coefficient 2072
- Polarography, of triethylenetetramine complexes with Cd, Cu, Pb, Zn, Ni, and Co, 134; of Bi-BiBr₃ molten solns. 1587
- Polyacrylate, sodium, transference of, under steady-state electrolysis 999
- Polyacrylonitrile, ultraviolet spectrum 1271
- Polybutadiene, intermolecular energy transfer in, -polyethylene system during γ -irradiation 1202
- Polyelectrolyte gels, electrostatic interactions between simple ions and highly swollen 1295
- Polyelectrolytes, adsorption free energy of, at a dielectric interface, 823; ion exchange rate of, under steady-state electrolysis across a porous frit, 995; adsorption of copolymer 1907
- Polyenes, cyclic, LCAO-MO ω -technique determination of ionization potentials of 712
- Polyethylene, radiation chemistry of γ -irradiated, 193; oxygen diffusion in and reaction with γ -irradiated, 463; proton magnetic resonance of, 718; intermolecular energy transfer in, -polybutadiene system during γ -irradiation 1202
- Polyethylene oxide, thermal pressure coefficient and entropy of melting at constant volume of 852
- Polyisobutylene, diffusion of radioactively tagged cetane in 1424
- Polymerizations, equilibrium, enzyme-catalyzed, 680, 685; γ -ray-induced, of octamethylcyclotetrasiloxane, 1119; polyfunctional addition 1577
- Polymers, initial deviation from Newtonian flow of solutions, 176; adsorption and boundary friction on surfaces of, 1136; wetting properties of acrylic and methacrylic, containing fluorinated side chains, 1207; entanglement coupling spacings in linear, 1567; adsorption-flocculation reactions with an aq. colloidal dispersion of, 1835; synthesis and characterization of some highly conjugated semiconducting, 2085; nature of semiconduction in some acene quinone radical, 2121; apparent dissociation constants as a function of the exchanging monovalent cation of carboxylic 2275
- Polymethacrylic acid, stepwise photoreversion of complex compound with phenosafranin 2511
- Polymethyl acrylate, viscosity of system with diethyl phthalate 1053
- Polymorphism, in fibrous polypeptides; $\alpha \rightleftharpoons \beta$ transformation in naturally occurring keratin 2096
- Polyolefins, sorption of organic vapors by 2146
- Polypeptides, proton magnetic resonances of synthetic 1292
- Polypropylene, neutron-irradiated, e.s.r. of 849
- Polysaccharide, synthesis by phosphorolytic enzymes, 680; interaction with methylene blue and congo red 2585
- Polystyrene, system with methyl ethyl ketone, 4; viscoelastic properties of solutions, 536; conformation and frictional properties of, in dilute solns., 1932; light scattering by, latex, 2059; proton resonance spectra and tacticity of deuterio- 2067
- Polyvinyl chloride gels, dynamic mechanical properties of 1639
- Polyvinylsulfonic acid salts, coacervation of, induced by heavy metal ions 1070
- Polyvinyltoluene, light scattering by, latex 2059
- Porphyryns, see also *Etioporphyrin I*; uncatalyzed decay of, triplets in fluid solvents 2574
- Potassium, heat capacity, entropy, free energy, solubility, and heat of soln. of K₂ReCl₆, 82; electrode potentials in molten eutectic of K₂SO₄-Li₂SO₄, 164; B coordination in borate glasses, 174; radiolysis with γ -rays of KBrO₃, 300; mechanism of promotion of chromia-alumina dehydrogenation catalysts by, 871; solutions in ethylenediamine, 1254; preparation, structure, and properties of K₂NbO₃F, 1318; pressure effect on equilibrium of aq. solns. of K₂SO₄, 1607; malate complex of 1702
- Potassium chloride, activity coefficients of mannitol-aq. solns., 506; thermal expansion of, 948; complex structures in aq. solns. of ThCl₄ and, 1299; pressure effect on equilibrium of aq. solns., 1607; adsorption of water vapor on, films 2260
- Potassium nitrate, volume change of KNO₃-NaN₃ liquid system, 103; effect of intensity on radiation-induced decomposition of, 755; free radicals in γ -irradiated, detected by electron paramagnetic resonance, 779; partial pressure of H₂O₂ and H₂O in KNO₃-H₂O₂-H₂O system, 923; liquid soln. in, of Sr(NO₃)₂ and Ba(NO₃)₂, 1668; effect of pressure on γ -radiolysis of, 2068; association constants of Ag(I) and chloride ions in molten, 2069; catalytic decomposition of bromate in fused, 2114; ζ -potential, calculation from mobility measurements 1367
- Potential energy barriers, tunnelling corrections for unsymmetrical Eckart 532
- Potentials, of oxide-coated Al electrodes in acid solns., 866; determination of ionization and appearance, 947; of Np(V-VI), Fe(II-III), Hg(0-I), and Hg(I-II) couples, 1065; photoinduced electrode, 1602; of total force 1722
- Praseodymium, hydride crystal structure, 148; partition of, in liquid Al-Cd system, 1028; electrical conductivity of the Pr-PrCl₃ system, 1201; preparation and crystal structure of Pr formate, 1737; near-infrared transitions of Pr(III) in soln. in molten LiNO₃-KNO₃ eutectic 2159
- Procaine, effect on desorption of mono-octadecyl phosphate monolayers 1923
- Proflavine hydrochloride, triplet-singlet luminescence from, in ethanol and glycerol soln. 2506
- Propane, 2,2-dimethoxy- and 2,2-diethoxy-, heats of formation of, 97; atomic H recombination in, flame gases, 229; 1-hydroperfluoro-, second virial coefficients for, -dimethyl ether system, 635; perfluoro-, coupling constants in normal and isotopic, 945; reaction with T initiated by β -decay, 1619; 1,2-epoxy-3-methoxy-, electron impact spectroscopy of,

- 1652; vinylcyclo-, thermal isomerization of, 1671; thermal decomposition of, on Rh. 1742
- 1,3-Propanediamine, stability in a cation-exchange resin and in aq. soln. of complexes with Ag. 78
- Propanediol-1,3, 2-ammonium-2-methyl-, dissociation constant of, in water. 308
- 1-Propanol, 2,3-dimercapto-, -iron(II) complexes. 426
- Propylene sulfide, electron impact spectroscopy of. 1551
- Proteins, effect of monomeric reagents on the melting (contraction) and recrystallization of fibrous, 375; structure of water and hydrophobic bonding in. 1773
- Protons, chemical shift of, in intramolecular H bonds, 613; dissociation in dilute aq. soln., 1030; chemical shifts in aq. Ag ion complexes of cyclohexene, *cis*-2-butene, benzene, and toluene. 1554
- Proton dissociation, equilibrium constants for, from protonated adenine, adenosine, ribose-5-phosphate, and adenosinediphosphate in dil. aq. soln. 359
- Proton magnetic resonance, of normal paraffin and polyethylene, 718; of ion-exchange resin-solvent systems, 1150; of benzene solutions. 2653
- Proton resonance spectra, of polystyrene and deuteriopolystyrenes. 2067
- Pseudocumene, phase diagram for system with CCl₄ and solid compound formation in. 1387
- Pteridine, 2-hydroxy-, reversible hydration rate of. 1689
- Pyran, tetrahydro-, molecular complex with tetracyanoethylene. 1754
- Pyrazine, stability constants of complexes with Ag. 1063
- 2-Pyrazolines, 1,3,5-triaryl-, as wave length shifters in scintillation plastics. 404
- Pyrene, absorption maxima of complexes with organic compounds. 353
- Pyridine, H bonding in, -pyrrole system, 546; formation constant of 1:1 complex with I, 766; equilibrium constant of system with phenol, 952; complex compounds of, derivatives with I halides, 1397; 2-(2',4'-dinitrobenzyl)-, optical properties of, in the adsorbed state, 2439; complex compound with Cu, in catalyzed anthracene triplet decay. 2577
- Pyridoxal, rate of alanine reaction with. 1678
- Pyrocatechol, 4-*t*-butyl-, γ -radiation-induced oxidation of. 1203
- Pyrollidine, electron impact spectroscopy of. 136
- Pyrolysis, of azomethane in a shock tube, 1426; secondary D isotope effect in the, of dimethylmercury. 2192
- Pyrrole, H bonding in, -pyridines system, 546; 1-*n*-butyl-, thermal isomerization and decomposition of. 1245
- Pyrrrolidine, conductivity of -acetonitrile system. 89
- Quantum efficiency, of *cis* \rightleftharpoons *trans* photoisomerization in azo compounds. 2482
- Quantum mechanics, applications of, to chemistry (Symposium). 2281-2359
- Quantum theory, of atoms, molecules, and their interactions. 2283
- Quantum yields, of oxidation of Fe(II) to Fe(III) sulfate and accompanying reduction of water to H. 336
- Quinoline, dielectric relaxation of, in a viscous solvent. 1105
- Radiation chemistry, theory of, generalized spur diffusion model, 242; rate constants for radical processes in water, 255; of ionic solids. 779
- Radical processes, rate constants for, in water radiation chemistry. 255
- Radiolysis, reducing radicals produced in, of water, 262; of CCl₃Br, 271; of crystalline alkali metal bromates with γ -rays, 300; with slow neutron sources, 300; decomposition products from, of ethylene with γ -rays and electrons, 322; reducing radical in, of water, 471; ethylene scavenger in, of liquid cyclopentane, 730; "unimolecular" yield of hydrogen from, of cyclohexane, 767; γ -ray-induced, of chlorobenzene, bromobenzene, and iodobenzene, 1041; effect of hydrogen iodide on, of cyclohexane-d₁₂, 1097; of octamethylcyclotetrasiloxane, 1119; γ -ray, of methyl-substituted borazoles, 1526; of toluene by electrons, 1538; of saturated hydrocarbons, 1611; of 1,5-hexadiene, 1746; charge transfer in the, of organic liquids; evidence from H gas yields, 2132; I production in the γ -ray, of cyclohexane-alkyl iodide solns., 2188; of azomethane and CH₃N₂CH₃-CD₃N₂CD₃ mixtures. 2253
- Rare earths, ordering of the octahedrally coordinated cation position in the system of, with Ba and Nb oxides, 131; stability constants of complexes of, with 1,2-bis-[2-di-(carboxymethyl)-aminoethoxy]ethane and 2,2'-bis-[di-(carboxymethyl)-amino]-diethyl ether, 311; crystal structure and lattice constants of, disilicides, 693; preparation and crystal structure of, formates, 1737; spectroscopic studies of complex compounds with *o*-hydroxybenzophenone. 2493
- X-Ray, activation of metal hydrogenation catalysts by, 510; arsenite irradiation by, in O-free soln. 1475
- Reaction velocity, of uranium hydride with ammonia at room temperature, 145; of hydrolysis of polyethylene terephthalate film, 175; of production of C₂ molecules during the pyrolysis of ethylene, 282; of thionine-iron system, 349; of LiClO₄ thermal decomposition, 358; in MgSO₄ and manganous sulfate solns., 360; of H atoms in aq. and formic acid solns., 361; shock tube study of, of hydrazine homogeneous decomposition, 366; of NO with electron-irradiated cyclohexane and with nitrosocyclohexane, 401; of thermal decomposition of previously neutron-irradiated lead styphnate, 416; of vanadium(III) with neptunium(V) in perchlorate solns., 442; of dissolved aromatic hydrocarbon fluorescence quenching by O, 455; of acetone photooxidation, 556; of [2,2,1]bicycloheptadiene thermal decomposition, 568; of Cl hydrolysis in the presence of various bases, 701; of cinnamalmalonic acid decarboxylation in aromatic amines, 836; of 2,2'-diphenic acids cyclization in H₂SO₄, 840; effect of neutron irradiation on, of manganous oxalate dihydrate dehydration, 926; isotope effects in, 978; of keto-enol equilibration in benzoylacetonilide, 1034; of H atom recombination on Pyrex glass in fused quartz, 1049; validity of statistical thermodynamic treatments of, 1058; of barium azide photochemical decomposition, 1113; of Cu(II) with β -diketones, 1132; of D isotope effect in aniline nitrosation, 1212; of *n*-octyl mercaptan oxidation by ferricyanide in acetone-water soln., 1233; of Fe(II) oxidation by Co(III) in aq. soln., 1275; of Ag oxidation in molten NaCl, 1311; of Cl exchange between NaCl³⁶ and ethyl chloroacetate, 1368; of H₂O₂ formation during dissolution of polycrystalline Cu, 1370; of azomethane pyrolysis in a shock tube, 1426; of acetal hydrolysis in amide-water solvents, 1496; of decarboxylation of oxanilic acid in ethers and in the molten state, 1543; of CuO reduction by H, 1573; of Cu(II) exchange between ethylenediaminetetraacetic acid and Eriochrome Blue Black R, 1582; of vinylcyclopropane thermal isomerization, 1671; of pyridoxal and alanine, 1678; of 2-hydroxypteridine reversible hydration, 1689; of Cl exchange between chloride and chloroacetate ions, 1719; corresponding state treatment of chemical kinetic data; solvent effects, 2101; of telomer production from chloroform-ethylene mixtures initiated by Co⁶⁰ γ -radiation, 2164; of secondary D isotope effect in the pyrolysis of dimethylmercury, 2192; of fast electrode processes; theory of coulometric method for, 2204; of fast electrode processes; experimental results, 2208; of fast coordination reactions in soln. studied by ion exchange, 2214; effects of micellization on, of hydrolysis of monoalkyl sulfates, 2239; of flash photolysis of I in benzene, toluene, *o*- and *p*-xylene, mesitylene, and hexamethylbenzene, and of Br in benzene, 2423; ion-pair intermediate in the phototropic reaction of methyl violet with cyanide ion, 2426; of uncatalyzed decay of anthracene and porphyrin triplets in fluid solvents, 2574; of fast-flow pyrolysis of *p*-xylene, 2664; between naphthalene and picric acid in the solid state. 2707
- Reactivity, of H atoms with org. solutes, 117; of H atoms with olefins. 291
- Rectification, faradaic, and electrode processes. 1108
- Reduction, polarographic, of V(III) in the presence of V(IV). 1699
- Relaxation, of ion pairs in an alternating field. 669

- Relaxation times, of aliphatic ketones 1739
- Resin, ion-exchange, -solvent systems, proton magnetic resonance and infrared spectra of, 1150; variation with aq. electrolyte activities of absorption of bromide ion from aq. salt solns. by 1383
- Resonance, correlation with organic scintillator pulse height 166
- Retinene, population and decay of the lowest triplet state in 2542
- Rhenium, heat capacity, entropy, free energy, solubility, and heat of solution of K_2ReCl_6 , 82; gaseous oxides of, 189; heats of combustion of ReS_2 and Re_2S_7 ; and the thermodynamic functions for transition metal sulfides 791
- Rhodium, electrode potentials of $Rh(III)-Rh(0)$ in molten $Li_2SO_4-K_2SO_4$ eutectic, 164; system with chlorine at high temperature, 490; thermal decomposition of *n*-propane and *n*-butane on 1742
- Ribonuclease, sedimentation velocity and viscosity data for reversible thermal denaturation of 1999
- Ribonucleotide, phosphorolytic enzyme synthesis of linear polymers of, 680; heats of proton dissociation from 1030
- Ribose-5-phosphate, protonated, equilibrium constants for stepwise dissociation of protons from 359
- Rubber latex, particle size distribution in 1768
- Rubidium, volume change of $RbNO_3-NaNO_3$ liquid system, 103; γ -ray radiolysis of $RbBrO_3$, 300; solubility of $RbNO_3$ in aq. H_2O_2 , 548; partial pressure of H_2O_2 and H_2O in $RbNO_3-H_2O_2-H_2O$ system, 923; thermal decomposition of RbO_2 , 1225; solutions in ethylenediamine, 1254; liquid soln. in $RbNO_3$ of $Sr(NO_3)_2$ and $Ba(NO_3)_2$, 1668; malate complex of, 1702; conductance of $RbBr$ in dioxane-water mixtures 1727
- Salts, transport number measurement in fused, 191; activity coefficients of, in organic solvent-water mixtures, 589; theories of fused, 1500; theory of fused, 1508; transport numbers in fused, 1600; spectrophotometry of fused 2169
- Salt solutions, acid-base equilibria in concentrated, containing dilute acids 2687
- Samarium, hydride crystal structure, 148; preparation and crystal structure of Sm formate, 1737; near-infrared transitions of Sm(III) in soln. in molten $LiNO_3-KNO_3$ eutectic 2159
- Sapphire, thermoluminescence of golden, seeded with nickel, magnesium, and uranium trioxide 551
- Scandium, chloride and bromide complexing of Sc(III) in aq. soln. 1248
- Scavenging, mechanisms of, in aq. iodide ion photochemistry 2029
- Schiller layers, in β -FeOOH colloidal crystals 1757
- Scintillation plastics, 1,3,5-triazyl-2-pyrazolines as wave length shifters in 404
- Scintillator, pulse height correlation with polarity and resonance effects 166
- Sebacic acid, surface pressure-area properties of monolayers on Hg 1867
- Sedimentation, see also *Ultracentrifuge*; charge and configurational effects in the concentration dependence of, of sodium carboxymethylcellulose, 1364; rate of, in pressure- and concentration-dependent systems (polystyrene), 1941; interference optical study of, in short columns 1952
- Sedimentation coefficient, variation of, with pressure and concentration, 565; of thalious sulfate-water system 1228
- Selenium, non-stoichiometry in CdSe and equilibria in the system Cd-Se 2210
- Self-association constants, of carboxylic acids in soln., determination of 1187
- Semiconduction, nature of, in some acene quinone radical polymers 2121
- Semiconductors, catalytic reactions on, 1241; synthesis and characterization of some highly conjugated semiconducting polymers, 2085; effect of electron irradiation prior to reaction on the activity of a, catalyst 2613
- Sensitivity, photographic, Mitchell theory of, 2359; theory of photographic 2407
- Sensitization, theory of spectral, 2398; properties of sensitizing and desensitizing dyes, 2403; action of noble metal salts on photographic emulsion 2411
- Serum albumin, molecular weight, limiting area, and flexibility of unimolecular layers of bovine, and its derivatives 1918
- Serum mercaptalbumin, bovine, concentration distribution and hydration in CsCl solutions in an ultracentrifuge 1990
- Silane, electron impact spectroscopy of trimethyl- 155
- Silica, stability of, 380; heat of formation, 380, 381; heat of immersion in benzene and cyclohexane, 511; NaCl effect on light scattering by colloidal, 1377; variation with particle size and outgassing temperature of heat of immersion in hexane, 1823; infrared study of a silica-alumina surface 2223
- Silica gel, hydroxyl content (Aerosil), 800; surface heterogeneity in, from rate of isotopic exchange OH-OD, 805; formation of H in γ -irradiated, 921; influence of *n*-heptyl derivatives on, -non-polar liquid stability, 1217; contact angle relation on surfaces of, 1790; heat of formation of SiF_4 , 381; crystal structure and lattice constants of silicides of lanthanides and actinides, 693; structure of lanthanum silicides, 758; heat of formation of SiF_2 , 1200; γ -irradiation of SiF_4 2672
- Siloxane, octamethylcyclotetra-, γ -ray-induced decomposition and polymerization of 1119
- Silver, stability in a cation-exchange resin and in aq. soln. of complexes with 2-aminoethanol, 75; stability in a cation-exchange resin and in aq. soln. of complexes with ethylenediamine and 1,3-propanediamine, 78; electrode potentials of Ag(I) and Ag(0) in molten $Li_2SO_4-K_2SO_4$ eutectic, 164; thermal decomposition of Ag-coated α -Pb azide, 421; infrared spectra of photographic stabilizers adsorbed on AgBr, 559; photovoltaic effect of AgBr electrolyte systems, 857; stability constants of complexes with pyrazine, 1063; stability constants of complexes with olefins in ethylene glycol solns., 1208; oxidation in molten NaCl, 1311; heat capacity of Ag_2S , Ag_2Se , and Ag_2Te , 1546; proton chemical shifts in complexes of, with cyclohexane, *cis*-2-butene, benzene, and toluene, 1554; liquidus curves-Ag system, 2012; association constants of Ag ions in molten KNO_3 , 2069; solubility of Ag_2SO_4 in $KNO_3-K_2SO_4$, $K_2SO_4-MgSO_4$, and $K_2SO_4-H_2SO_4$ mixtures, 2264; electronic properties and band structure of AgCl and AgBr, 2368; Hall mobility of holes in AgBr, 2376; ionic transport processes in AgCl and AgBr, 2380; role of mobile Ag ions in latent-image formation, 2384; point defects in AgCl, 2396; mechanism of the antifogging and sensitizing action of Ag salts on photographic emulsion 2411
- Slip-flow coefficients, first-order, derived from thermal force data 1763
- Soaps, pressure effect on micelle formation in solutions of 1839
- Sodium, solid phases in the system $Na_2O-Ta_2O_5$, 15; grain boundary energy of NaF; the system NaF-Te-CsCl, 31; apparent molar volume of NaOH, 177; radiolysis with γ -rays of NaBrO₃, 300; molar refractions of aq. solns. of $Na_4P_2O_7$, $Na_5P_3O_{11}$, $Na_7P_3O_9$, and $Na_4P_2O_7$, 377; heat of dilution in water of NaClO₄, 519; hydrolytic degradation of sodium triphosphate, 939; conductivity of solns. of sodium dodecyl sulfate below the critical micelle concentration, 942; thermal decomposition of γ -ray irradiated NaMnO₄, 961; transference of sodium polyacrylate under steady-state electrolysis, 999; extraction of NaSCN from aq. solns. by tributyl phosphate, 1014; magnetic susceptibility of Na-NaCl and Na-NaBr liquid systems, 1163; sodium acetate-acetic acid-water system, 1197; solutions in ethylenediamine, 1254; isothermal diffusion in $Na_2SO_4-H_2SO_4-H_2O$ system, and tests of the Onsager reciprocal relation, 1279; effect of pressure on micelle formation in aq. solns. of sodium dodecyl sulfate, 1359; charge and configurational effects in concentration dependence of sedimentation of sodium carboxymethylcellulose, 1364; temperature dependence of Knight shift of Na-NH₃ system, 1693; malate complex of, 1702; heat content of Na_2TeO_4 ,

- 1713; freezing point-solubility curve of aq. NaOH in the region near the anhydrous-monohydrate eutectic, 2051; heat capacities and heats of solution of NaOH and NaOH·H₂O, 2052; effect of tetravalent fluorides on freezing point depressions in NaF
- Sodium chloride, rate of solution of, crystals in glycerol, 665; complex structures in aq. solns. of ThCl₄ and 1299; Ag oxidation in molten, 1311; rate of Cl exchange between NaCl³⁶ and ethyl chloroacetate, 1368; influence on light scattering by colloidal silica, 1377; pressure effect on equilibrium of aq. solns. 2711
- Sodium nitrate, binary liquid systems of, with Li, K, Rb, and Cs nitrates, volume change of, 103; effect of intensity on radiation-induced decomposition of, 755; partial pressure of H₂O₂ and H₂O in NaNO₃-H₂O₂-H₂O system, 923; liquid soln. of Sr(NO₃)₂ and Ba(NO₃)₂ in, 1668; catalytic decomposition of bromate in fused. 1607
- Solids, radiation chemistry of ionic. 2114
- Solubility, in chemical engineering, 640; high-speed techniques in studies of, application to hippuric acid esters, 897; of HCl in aromatic systems, 1752; of NaOH-NaOH·H₂O eutectic, 2051; of Ag₂SO₄ in KNO₃-K₂SO₄, K₂SO₄-MgSO₄, and K₂SO₄-H₂SO₄ mixtures. 779
- Solutes, polar-non-polar, effect on the water wettability of solid surfaces submerged in oil. 2264
- Solutions, isotherm for ideal two-dimensional, 385; solid, for low-temperature spectroscopy, 561; micellar, pseudo-phase separation model for, 577; ideal two-dimensional. 236
- Sorption, of organic vapors by polyolefins. 1863
- Spectra, absorption, of four oxidation states of V in LiCl-KCl eutectic, 57; infrared, of photographic stabilizers adsorbed on AgBr, 559; ultraviolet, of *o*-, *m*-, and *p*-nitrobenzoic acids, 562; electronic, of catacondensed and pericondensed aromatic hydrocarbons. 2146
- Spectrometer, calibration standard for neutron magnetic resonance. 2334
- Spectrophotometry, of fused salts. 560
- Spin orbital, external heavy-atom, and orbital coupling effect in the phosphorescence spectra and lifetimes of externally perturbed naphthalenes. 2169
- Spiropyrans, photochromic, 2275; effect of temperature and solvent on the spectrum of photochromic colored, 2465; mechanism of phototransformation to merocyanines. 2499
- Spreading, of fatty alcohol monolayers. 2470
- Spreading pressure, and rate, of monolayers of *n*-fatty alcohols and *n*-alkoxy ethanols. 1851
- Stability, gravitational, and density gradient during free diffusion in three-component systems. 1361
- Stability constants, of complexes between rare earths and aminopolycarboxylic acids, 311; of uranyl nitrate complexes with monobasic and dibasic acids, 790; of dipyrzine-Ag complexes, 1063; determination by gas chromatography of, of complexes, 1208; of Hg(II) halide ternary complexes in soln., 1661; of the H₂SO₄-HSO₄⁻ ion in acetonitrile. 1675
- Starches, carboxylated, interaction with methylene blue and congo red. 2585
- Stearic acid, surface pressure-area properties of monolayers on Hg. 1867
- Stearyl alcohol, surface pressure-area properties of monolayers on Hg. 1867
- Stereospecificity, of polyvinyl isobutyl ethers, polythyl acrylates, and poly-*p*-chlorostyrenes. 1390
- Stilbenes, photochemical *cis-trans* isomerization of substituted. 2486
- Strontium, effect of phosphates on crystallization and crystal habit of SrSO₄, 252; liquid soln. of Sr(NO₃)₂ in NaNO₃, KNO₃, RbNO₃, and CsNO₃, 1668; Li-Sr equilibrium system, 2138; crystal structure of Sr₂Li₂₃ and Sr₃Li₂. 2142
- Structure, effect on surface activity of fluorinated organic compounds at organic liquid-air interfaces. 328
- Styrene, poly-, system with methyl ethyl ketone, 4; poly-*p*-chloro-, stereospecificity and dielectric properties of. 1390
- Sublimation, determination of equilibria by differential thermal analysis, 1477; of BN and AlN. 1556
- Succinic acid, monolayers of cetyl ester of, 1846; electric moments of substituted. 1634
- Sulfate ions, association constants of, with Ce(III) ions. 160
- Sulfonic acids, aryl, n.m.r. study of ionization of. 268
- Sulfur, electron impact spectroscopy of saturated heterocyclic compounds of, 136; cubic crystals of CdS, 185; prepoisoning of iron catalysts for the Fischer-Tropsch synthesis by S compounds, 501; spectrophotometric evaluation of activity coefficients of SO₂ aq. solns., 516; structure of As₂S₃-I glasses, 733; n.m.r. spectrum of fluorocarbon sulfides, 764; displacement reactions at, 956; complexes of saturated cyclic sulfides with I, 1099; phase diagram of the system Bi-S, 1205; electron impact spectroscopy of compounds, 1648; vapor pressure studies of γ - and β -SO₂ and the H₂O-SO₂ system, 2179; properties of α -SO₂, 2182; ionization potentials of sulfides. 2269
- Sulfur, S²⁵, for surface area determination of supported transition metal sulfides. 469
- Sulfuric acid, distribution between water and kerosene solutions of tri-*n*-octylamine and tri-*n*-hexylamine, 216; isothermal diffusion in the H₂SO₄-Na₂SO₄-H₂O system and tests of the Onsager reciprocal relation, 1279; stability constant and mobility of H₂SO₄-HSO₄⁻ ion. 1675
- Surface activity, effect of structure and homology on, of fluorinated organic compounds at organic liquid-air interfaces. 328
- Surface area, measurements with Kr, 182; of graphitized C black. 2154
- Surface pressure, of flexible adsorbed macromolecules. 1884
- Surface reaction, matrix effects in the reaction of gaseous H with a condensed olefin film; surface reaction-olefin diffusion model. 2677
- Surface tension, of Te, 946; of flexible adsorbed macromolecules. 1884
- Surfaces, interfacial tension, contact angle, and dispersion force determination in, 382; heterogeneity in silica gel determined from rate of isotopic exchange OH-OD, 805; sliding of liquid drops on solid, 883; adsorption and boundary friction on polymer, 1136; contact angle relations on silica gel, 1790; infrared study of a silica-alumina. 2223
- Svedberg equation, test of, at finite concentration. 1228
- Sydnones, photochromic behavior of. 2446
- Tacticity, of polystyrene and deuteriopolystyrenes. 2067
- Tantalum, solid phases in binary systems of Ta₂O₅ with Li₂O and Na₂O, 15; formation constants and species of coordination number nine in Ta fluoride system, 21; formation constants of Ta-F system and Ta electrode potentials. 187
- Tartrate, effects of electrolytes on rotatory dispersion of aq. solns. of. 494
- Tautomerism, keto-enol, of benzoylacetanilide, 1034; in arylazophenols and naphthols; effect of internal H bonds on photoisomerization of 2-phenylazo-3-naphthol. 2478
- Tellurium, the system NaF-Te-CsCl, 31; poisoning by telluride ions of H evolution at Te cathodes and cathodic formation of H₂Te₂, 890; surface tension, 946; pseudo-binary systems of, with Sb, Bi, Pb, Tl, and Sn, 1408; vapor pressure of GeTe, 1563; heat content and heat of fusion of TeO₂. 1713
- Telomer, rate of production from chloroform-ethylene mixtures initiated by Co⁶⁰ γ -radiation. 2164
- Temperature, one-component system, energy-volume surface for, 600; density relation with, of liquid metals. 1686
- Terbium hydride, crystal structure. 148
- Tetracene, band structure and transport of holes and electrons in. 2461
- Tetrahydrofuran, electron impact spectroscopy of. 136
- Tetrahydrothiophene, electron impact spectroscopy of. 136
- Tetrazole, 1-cyclohexyl-5-methyl-, electric moment of. 158
- Thallium, sedimentation coefficients of the system

- $\text{Ti}_2\text{SO}_4\text{-H}_2\text{O}$; test of the "Svedberg equation" at finite concentration, 1228; equivalent conductance and ionic association in aq. TiOH solns., 1341; pseudo-binary systems of, with Sb, Bi, Te, Sn, and Pb. 1408
- Thenoyltrifluoroacetone, secondary reaction of, with HCl and tri-*n*-octylamine. 2262
- Thermal expansion, of Pb, 266; of KCl. 948
- Thermal force, on aerosol particles, from first-order slip-flow continuum analysis. 1763
- Thermal pressure coefficient, of polyethylene oxide. 852
- Thermochromy, of anils. 2442
- Thermodynamics, irreversible, Caratheodory's principle and the thermokinetic potential in. 1414
- Thermokinetic potential, and Caratheodory's principle in irreversible thermodynamics. 1414
- Thermoluminescence, of golden sapphire and fused borax seeded with Ni, Mg, and UO_2 551
- Thioamides, electric moments of. 1372
- Thiols, ionization potentials of. 2269
- Thionine, reaction velocity study of system with Fe, 349; reaction with Fe(II) in a heterogeneous system, 663; chlorophyll-sensitized photoreduction of, by ascorbic acid, 954; photopolymerization of acrylamide sensitized by. 2563
- Thiophene, infrared spectrum of, adsorbed on silica-supported Ni. 1288
- Thiosulfate, reaction of, with cyanide. 956
- Thiourea, diffusion of, in water. 1540
- Thorium, complex structures in ThCl_4 aq. solns. containing LiCl, NaCl, or KCl. 1299
- Thulium hydride, crystal structure. 148
- Tin, SnCl_4 -methyl chloride addition compounds, 1380; pseudo-binary systems of, with Sb, Bi, Pb, Te, and Tl. 1408
- Titanium, heat of formation of TiF_4 , 1345; vaporization of the Ti-B system, 1492; variation with particle size and outgassing temperature of heat of immersion of titania in hexane. 1823
- Toluene, thermodynamic properties, molecular vibrations, and internal rotation of. 911; catalytic hydrogenolysis of, 1190; 2,4,6-trinitro-, -1,3,5-trinitrobenzene system, 1196; electrolytic conductance of, dependence on pressure of, 1210; phase diagram for system with CCl_4 and solid compound formation in, 1387; 4-fluoro-, heats of combustion and formation of, 1529; electron radiolysis of, 1538; proton chemical shift in Ag complex of, 1554; free radicals from the thermal decomposition of, 1569; isothermal diffusion in an ideal mixture of, with chlorobenzene and bromobenzene, 2015; transient charge-transfer complexes in halogen atom recombination and photohalogenation processes. 2423
- Toluic acid, heats of combustion and formation of *m*-trifluoro-, 1529; strength of *c*-. 1188
- Transference number, of tris-(ethylenediamine)-cobalt(III) chloride in water. 550
- Transition metal sulfides, thermochemical data for. 791
- Transport number, in pure fused salts, 191. 1600
- Triethylamine, conductivity of acetonitrile-, system. 89
- Triethylenetetramine, complexes with Cd, Cu, Pb, Zn, Ni, and Co, polarography of. 134
- Trimethylene oxide and sulfide, electron impact spectroscopy of. 136
- Triplet state energy, transfer of, and the chemistry of excited states. 2569
- sym*-Trithiane, complex with I. 1198
- Tritium, reaction initiated with propane by β -decay of, 1619; reaction of T atoms with frozen cyclopropane, 2272; reactions of recoil T atoms with cyclopropane- PtCl_2 2622
- Tungsten, adsorption of Xe and H on evaporated films of. 482
- Ultracentrifugation, stability of emulsions to, and discontinuity at the critical micelle concentration, 1966; for the determination of emulsion stability, 1969; of foot-and-mouth virus through immiscible fluid interfaces into a CsCl density gradient. 1976
- Ultracentrifuge, flotation equilibrium in, 1945; molecular weight determination with, 1948; zonal, for fractionating mixtures of particles, 1984; behavior of bovine serum mercaptalbumin in, 1990; studies of reversible thermal denaturation of ribonuclease. 1999
- Uranium, behavior in surface ionization sources, 133; reaction of, hydride with ammonia at room temperature, 145; decomposition pressure of UCd_{11} , 362; uranyl ion complex compounds with hydroxy, mercapto, and amino acids, 790; mechanism of extraction of uranyl salts by tri-*n*-butyl phosphate and complex compound formation, 989; partition of, in liquid Al-Cd system. 1028
- Uroporphyrin, effect of pH on the photoreduction of, to dihydroporphyrin with EDTA. 2531
- Valence bond theory, applications of semi-empirical, to small diatomic molecules. 2294
- Vanadium, absorption spectra in four oxidation states, 57; octahedral-tetrahedral transformations of, in LiCl-KCl eutectic, 57; reaction velocity in perchlorate solns. of V(III)-Np(V), 442; compound repetition in $\text{Li}_2\text{O-V}_2\text{O}_5$ system, 1181; phase diagram of the system V-VC, 1401; reduction by catalytic polarographic currents of V(III) in presence of V(IV), 1699; high-temperature disproportionation of lower V oxides reacting with BaO. 2273
- Vaporization, in the Ti-B system, 1492; of solid FeCl_3 1705
- Vapor pressure, of trifluoromethane, 392; of Au, 754; of 1,2-bis-difluoroamino-4-methylpentane, 958; of ZnSe, 1252; of GeTe, 1563; of γ - and β - SO_3 and the $\text{H}_2\text{O-SO}_3$ system. 2179
- Veratrine, effect on desorption of monoöctadecyl phosphate monolayers. 1923
- Vinyl acetate, adsorption on anatase of, copolymer with crotonic acid. 1907
- Vinylcyclopropane, thermal isomerization of. 1671
- Vinylpyrrolidone, chain transfer constant of, with dextran. 828
- Virial coefficients, second, for the systems *n*-butane-perfluoro-*n*-butane and *d*-methyl ether-1-hydroperfluoropropane, 635; determination of second, 639; of *n*-butane-isobutane system. 1082
- Virus, preparative ultracentrifugation of foot-and-mouth disease, through immiscible fluid interfaces into a CsCl density gradient. 1976
- Viscoelastic properties, of dilute polystyrene solutions. 536
- Viscosities, variation during gelation of, of chromic ferrocyanide, 357; of tetramethylammonium bromide in aq. soln., 894; of polymethyl acrylate-diethylphthalate system, 1053; of aliphatic ketones, 1739; determination of liquid, by half-time of rise in a vertical capillary, 1748; of polystyrene in dilute solns. 1932
- Volatility, of H_2O^{17} and H_2O^{16} 1412
- Volume, one-component system, -energy-temperature surface for. 600
- Water, radiation chemistry of, 70; volume change accompanying ionization of, 177; dissociation equilibria determination, 225; interfacial tension with oil on solid surfaces, 236; effect of polar-nonpolar solutes on wettability by, of solid surfaces submerged in oil, 236; rate constants for radical processes in radiation chemistry of, 255; reducing radicals produced in radiolysis of, 262; thermodynamic data for the system $\text{CaO-P}_2\text{O}_5\text{-HF-H}_2\text{O}$, 315; phase equilibria in the system $\text{CaO-P}_2\text{O}_5\text{-HF-H}_2\text{O}$, 318; quantum yields of, in photochemical reduction to H, 336; dielectric constant of, 383; reducing radical in radiolysis of, 471; light and heavy, 2,2'-dihydroxybiphenyl ionization constants in, 534; solubility of methane hydrates in, 605; partial pressure of H_2O_2 and H_2O in alkali nitrate- $\text{H}_2\text{O}_2\text{-H}_2\text{O}$ system, 923; electroosmosis of, across ion-exchange membranes, 1006; dielectric behavior of vapors of, adsorbed on alumina, 1086; system with acetic acid and sodium acetate, 1197; volatility of $\text{H}_2\text{O}^{17}\text{-H}_2\text{O}^{16}$, 1412; infrared spectrum of, adsorbed on silica-supported Fe, 1464; oxidation-reduction analysis of cryogenically stable

- products of dissociated vapor, 1560; adsorption on *n*-type Ge powders, 1819; vapor pressure studies of the H₂O-SO₃ system, 2179; adsorption of vapor on KCl films, 2260; adsorption of vapor on activated α -Fe₂O₃..... 2597
- Wave length shift, in scintillation plastics by 1,3,5-triaryl-2-pyrazolines..... 404
- Waves, damping by monomolecular films..... 1858
- Wetting properties, of acrylic and methacrylic polymers containing fluorinated side chains..... 1207
- Wien effect, in polyvalent electrolytes..... 1520
- Xanthate, adsorption of, by PbS..... 879
- Xenon, adsorption on W and Ni films, 482; corresponding states theory for..... 583
- Xylene, gas-phase oxidation of *o*-, 2023; transient charge-transfer complexes in halogen atom recombination and photohalogenation processes of *o*- and *p*-, 2423; rate of pyrolysis of *p*-, in fast flow.... 2664
- Yttrium, hydride crystal structure, 148; chloride and bromide complexing of Y(III) in aq. soln..... 1248
- Zeolites, heats of adsorption on ion-exchanged forms, 812; nature of cation depopulation in synthetic crystalline..... 2271
- Zimm theory, of viscoelastic properties of polymer solutions, verification of..... 536
- Zinc, effect of light on adsorption of H by ZnO, 54; stability in a cation-exchange resin and in aq. soln. of complexes with ethylenediamine, 75; electron spin resonance of ZnO with adsorbed O, 99; hydrolysis of Zn ion by coagulation, 111; extraction velocity of Zn dithizonate, 127; polarography of complex of Zn with triethylenetetramine, 134; transient species in O adsorption by ZnO, 566; thermodynamic data for liquid ternary Zn-In-Ga solns., 658; amide effect on photochemical processes at irradiated surfaces of ZnO, 932; vapor pressure of ZnSe, 1252; photoinduced binding of fluorescein dyes to ZnO..... 1536
- Zirconium, crystal structure of NiZrH₃, 370; detection by coagulation of hydrolysis..... 1799

No. **36** in the
**ADVANCES IN
CHEMISTRY
SERIES**

Free Radicals in Inorganic Chemistry

These 17 papers presented before the Symposium on Inorganic Free Radicals and Free Radicals in Inorganic Chemistry were sponsored by the Division of Inorganic Chemistry at the 142nd ACS Meeting in Atlantic City in September 1962. They constitute the latest findings in this fast-developing area.

In very recent years inorganic free radicals particularly have been intensively and productively studied. Already they are proven or postulated intermediates in a variety of synthetic inorganic processes.

The papers in this volume do not exhaust the subject of free inorganic radicals, but they aim rather to give a status report on what is believed will be an extremely active field of chemical investigation over the next few years. One of the best known inorganic free radicals, NO_2 , is discussed in detail, as is also one of the most recently discovered, NF_2 . Thus, this book contains not only historical background material necessary to workers in inorganic free radical chemistry but also reports of recent research of the utmost timeliness and significance.

175 pages.

Paper bound.

Price: \$7.00

Order from:

Special Issues Sales/American Chemical Society/1155 Sixteenth Street, N. W./Washington 6, D. C.

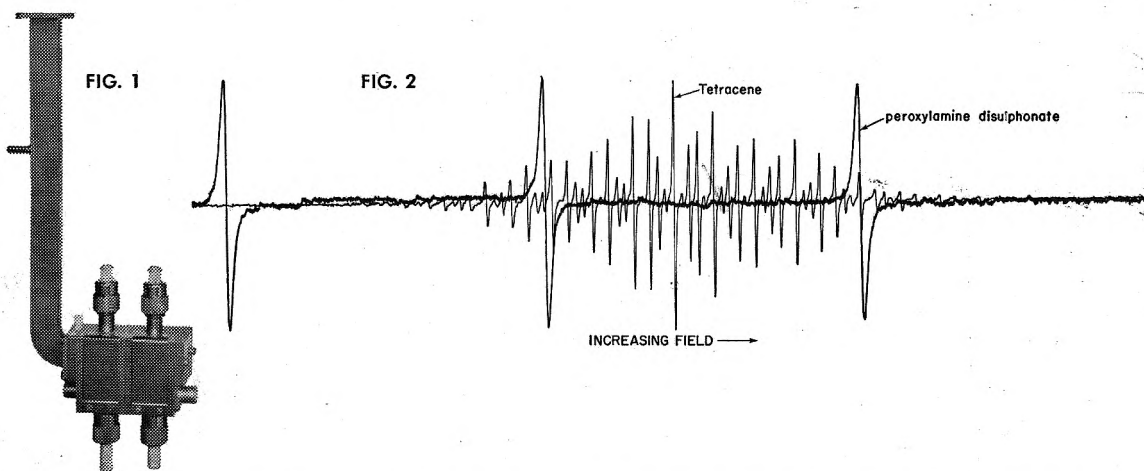
PRECISION MEASUREMENTS IN EPR

[ELECTRON PARAMAGNETIC RESONANCE]

Precise determinations of g -values, spin concentrations, and hyperfine splittings in EPR are both difficult and time consuming. A new development at Varian, the V-4532 Dual Sample Cavity, designed as an accessory for the V-4502 EPR Spectrometer system, overcomes these problems. It allows simultaneous and independent detection of the resonances of two samples which are in the same microwave cavity, and may be used for reliable comparison of a standard and an unknown sample.

EXAMPLE

The g -Value of Peroxyle Amine Disulphonate



The Varian EPR Spectrometer contains two independent systems for modulation, amplification and phase detection, one at 100 kcps and one at audio frequencies (400 cps). The V-4532 Dual Sample Cavity (Fig. 1) operates in the TE_{104} mode, permits insertion of two samples, and utilizes two pairs of modulation coils, with one pair excited at 100 kcps and the other at 400 cps. Effectively, each sample "sees" the modulation field from only its pair of coils. The Varian G-22A Dual Channel Recorder provides a convenient recorder display of the simultaneous and independent signals from the two samples.

Figure 2 illustrates the superposition of the spectrum of peroxyle amine disulphonate (EPR at Work #1) and tetracene positive ion (EPR at Work #21). Bloise, Brown, and Maling¹ have measured the g -value of tetracene to a high degree of accuracy using an NMR fluxmeter, transfer oscillator and frequency counter. They report 2.00250 ± 0.00003 . This provides a convenient standard to determine the g -value of peroxyle amine disulphonate.

The expression used to calculate the unknown g -value is:

$$g = 2.00250 \left(1 - \frac{\Delta H}{H} \right)$$

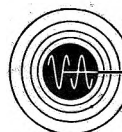
Here ΔH is the shift of the unknown resonance field with respect to tetracene, and is positive for a shift to higher fields. It may be determined from known hyperfine splittings. The field at which the center line of tetracene resonates, H , may be calculated from the tetracene g -value and knowledge of the microwave frequency. (Wavemeter accuracy is sufficient.) One must initially calibrate the V-4532 Dual Sample Cavity by placing identical samples in each channel to determine the difference in magnetic field at the two sample positions.

Using the outlined technique, a g -value for peroxyle amine disulphonate of 2.00550 ± 0.00005 has been obtained.

This comparison technique can be applied equally well for the determination of hyperfine splittings and spin concentrations.

(1) M. S. Bloise, Jr., H. W. Brown, and J. E. Maling, *Free Radicals in Biological Systems* (Academic Press, New York, 1961) p. 121.

For literature which fully explains the 100 kc EPR Spectrometer and its application to basic and applied research in physics, chemistry, biology, and medicine, write the Instrument Division.



VARIAN associates
PALO ALTO 52, CALIFORNIA